20th Symposium of the New Zealand Geotechnical Society

Napier 2017

Convenor's Introduction

The 20th New Zealand Geomechanics Symposium was held in Napier, the Art Deco capital of the world. On behalf of the Symposium Committee and NZGS I was delighted to welcome the keynote lecturers Emeritus Professor John Atkinson, Ruth Allington, Professor David Petley and Professor Michael Pender. We were honoured to have them share their knowledge with us.

Geotechnical work involves risk and uncertainty, and this is reflected in the symposium theme **what in earth is going on;** *balancing risk, reward regulation and reality*. The theme is reflected in our keynote presenters, who are all adept and experienced at the reality of balancing risk and reward in geotechnical work. We also focussed on the effects of the Kaikoura Earthquake in Wellington, and the implications for the profession of the extensive damage this event caused. The technical stream of the symposium was rounded out by our session reporters, who summarised and discuss more than 70 papers presented in these proceedings.

I wish to acknowledge the financial support which was afforded by the Symposium sponsors and exhibitors. Symposia like this cannot happen without the support these organisations offer, and we thank them for this, with particular thanks to our Principal Sponsors Brian Perry and Tonkin + Taylor.

Finally, the Organising Committee comprising Guy Cassidy, Ross Roberts, Gavin Alexander, David Milner, Tom Bunny and Safia Moniz have contributed a huge amount of energy and time over the past two years. Their commitment and work, ably assisted by Angie Rawlinson and Amanda Blakey, have enabled this symposium to occur. I would like to publicly and warmly thank each of them for the outstanding contributions made.

Pierre Malan
Symposium Convenor

Sponsors

NZGS 2017
WHAT IN EARTH IS GOING ON?
BALANCING RISK, REWARD, REGULATION AND REALITY

The NZGS Symposium could not take place without the generous support of our sponsors. We would like to extend our thanks to all our sponsors, and in particular our Principal and Associate sponsors.

Principal sponsors

BPC BRIAN PERRY CIVIL

Tonkin+Taylor

Associate sponsors

GRIFFITHS DRILLING
RESULT DRIVEN GEOTECHNICAL SPECIALISTS

OPUS

Proceedings sponsor

Beca

Session Reporters

WHAT IN EARTH IS GOING ON?
BALANCING RISK, REWARD, REGULATION AND REALITY

The New Zealand Geotechnical Society would like to thank our session reporters for the significant contribution they made to this Symposium

Session 1

Themes: Communicating and managing risk, Standards, guidelines and regulation

- **Gabriele Chiaro**
- **Hayden Bowen**

Session 2

Theme: Natural hazards and resilience

- **Kaley Crawford-Flett**
- **Phil Clayton**

Session 3

Theme: Innovative tools and techniques

- **Liam Wotherspoon**
- **Martin Larisch**

Session 4

Themes: Best practice in design and construction & Putting theory into practice

- **Marlene Villeneuve**
- **Nick Wharmby**

Reviewers

The New Zealand Geotechnical Society would like to thank the following reviewers for the arduous task of undertaking reviews of the papers presented in these proceedings:

Gavin Alexander
Clive Anderson
Kevin Anderson
Nick Barounis
Dick Beetham
Hayden Bowen
Professor Andrew Chan
Dr CY Chin
Phil Clayton
Neil Crampton
Dr Ching Dai
Geoffrey Farquhar
Debbie Fellows
Stuart Finlan
Sian France
Marcus Gibson
Evan Giles
Eleni Gkeli
Sally Hargraves
Bernard Hegan
Vassilis Houssiadas
David Jennings
Dr Claudia Kayser
Dr Richard Kelly
Dr George Kouretzis
Dr Nathan McKenzie
Ian McPherson
Dr Zarnaz Mehryar
Dr Alexei Murashev
Dr Marianne Halloran
Wataru Okada
Assoc Prof Rolando Orense
Stuart Palmer
Charlie Price
Ken Read
Stuart Read
Dr Bruce Riddolls
Nicola Ridgley
Phil Robins
John Seward
Dr Merrick Taylor
Alan Thorp
Susan Tilsley
John Underhill
Harry Wahab
Ann Williams
Simon Woodward
Cam Wylie
Dr Ryan Yan
Dr Saman Zargarbashi

Non-linear soil mechanics

J H Atkinson
City University of London, UK.
j.h.atkinson@city.ac.uk

Keywords: strength, stiffness, power law, laboratory testing, settlement

ABSTRACT

Routine effective stress analyses for failure of geotechnical structures use a linear Mohr-Coulomb envelope and routine analyses for ground movements use linear elasticity with constant Young's Modulus E' or one-dimensional modulus M'. Observations of soil behaviour show that strength and stiffness are non-linear and so the conventional simplifications do not match these basic observations. Measurements from several different soils show that their strengths can be represented by a simple power law similar to the familiar Hoek-Brown model for rock strength. For soft soil, stiffness for analyses of settlements of embankments may be approximated as linear. For stiff soil which is highly non-linear, a value of E' for analyses of settlements of foundations may be approximated to $E'_0/3$ where E'_0 is the stiffness at very small strain.

1 SOIL STRENGTH

1.1 Conventional Linear Mohr-Coulomb Soil Strength Envelope

A linear relationship between the limiting shear *force* and normal *force* is attributed to Coulomb (1773) as discussed by Heyman (1972). Following the development of analysis of stress by Mohr the original Coulomb relationship was recast in stresses and this is the familiar Mohr-Coulomb strength criterion. In the original Mohr-Coulomb strength criterion stresses were total stresses and the relationship was mostly applied to unsaturated compacted fills. Terzaghi (1936) extended the original Mohr-Coulomb criterion to effective stresses and this is now the conventional criterion for soil strength.

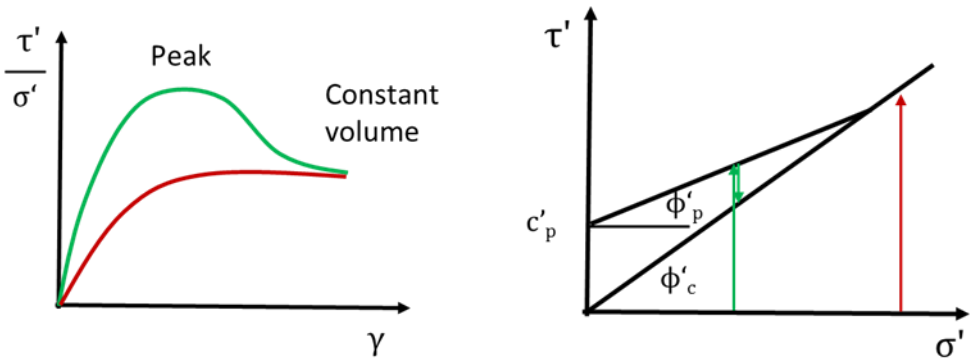

(a) (b)

Figure 1: Mohr-Coulomb linear soil strength envelopes

In Figure 1(a) a typical stress –strain curve for soil has a peak strength at a strain of the order of 1% and a smaller constant volume or critical state strength at a strain of the order of 10%. (Clay soils may also have a lower residual strength after very large deformations on a slip plane.) It is well established that all these strengths increase with effective normal stress and they are

conventionally described by linear relationships as shown in Figure 1(b) so the peak strength is given by

$$\tau'_p = c'_p + \sigma' \tan\phi'_p \qquad 1$$

and the constant volume or critical state strength is given by

$$\tau'_c = \sigma' \tan\phi'_c \qquad 2$$

It is also well established that at sufficiently large normal stresses soils do not have a peak strength only a constant volume strength so the peak and constant volume failure envelopes must meet as shown in Figure 1(b). The stress paths in Figure 1(b) correspond to the stress ratio strain curves Figure 1(a).

In conventional geotechnical engineering practice the linear Mohr-Coulomb strength envelope is used for routine analyses of ultimate limit states with a factor of safety of about 1.3 and it is used for routine assessment of serviceability limit states with a load factor of about 3.

1.2 Peak strength of soil

Figure 2 shows a set of Mohr circles for the stresses at the peak state and the constant volume, critical state of samples of London Clay (Atkinson and Crabb 1997). The constant volume envelope shown by double lines is linear with parameters c' = 0 and $\phi'_c = 22^0$. The circles for the peak states have a curved envelope which passes through or very close to the origin. It should be noted that the stresses in the samples with the lowest stresses were only a few kiloPascals requiring very careful experimental techniques.

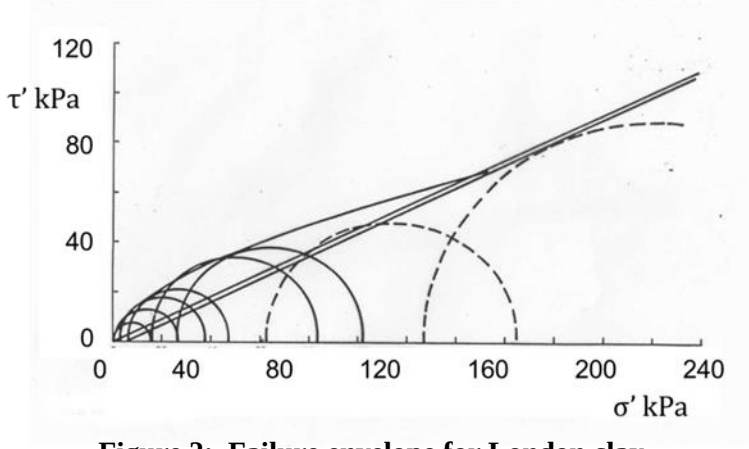

Figure 2: Failure envelope for London clay

Figure 3(a) illustrates the features of the peak envelope from Figure 2. The effective stress strength is negligible when the effective normal stress is zero at the point O. It is impossible to make a stable vertical slope in dry sand. In plastic clays the strength at zero effective normal stress may not be exactly zero but careful experiments show that it is very small and only a few kiloPascals (Atkinson 2007). At relative large effective normal stresses beyond the point Y soils have no peak strength only a constant volume strength. Between O and Y there is a peak strength at P which is larger than the constant volume linear strength envelope. It is impossible for a linear peak strength envelope to join the points O – P - Y.

It is worth recalling that Coulomb developed the linear relationship for unsaturated compacted fill in military earthworks (Heyman 1972). For such soils, and in total stresses, there is a substantial strength at zero total stress. Although the relationship between strength and total normal stress may not be exactly linear the original Mohr-Coulomb total stress relationship is not obviously incorrect for unsaturated soils. It was when the original total stress linear criterion was

converted to effective stress by Terzaghi (1936) that it no longer correctly represented observed behaviour of saturated soil.

1.3 Non-linear soil strength

A convenient formulation for the non-linear peak envelope in Figure 3(a) is a simple power law such as

$$\tau'_p = A\sigma'^b \qquad 3.$$

where A and b are parameters that depend on the soil grains and on the critical stress σ'_y. This simple power law is similar to the basic formulation of the Hoek-Brown (1980) criterion commonly used to describe the strength of rock. A similar power law was found by Atkinson (2007) for peak strengths of several overconsolidated clays.

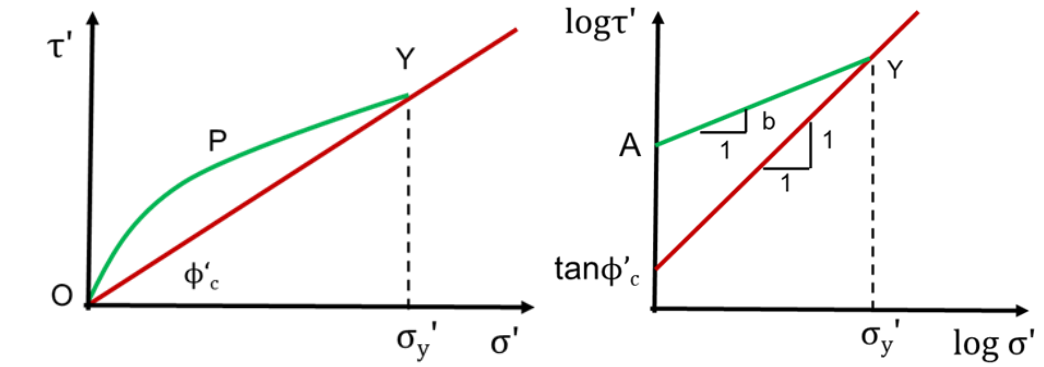

(a) (b)

Figure 3: Non-linear soil strength envelopes

When the stresses are converted to logarithms equation 3 becomes

$$\log\tau'_p = \log A + b\log\sigma' \qquad 4$$

which gives a log-linear envelope as shown in Figure 3(b). Figures 4(a) to (d) show peak and constant volume strengths of some fine and coarse grained soils.

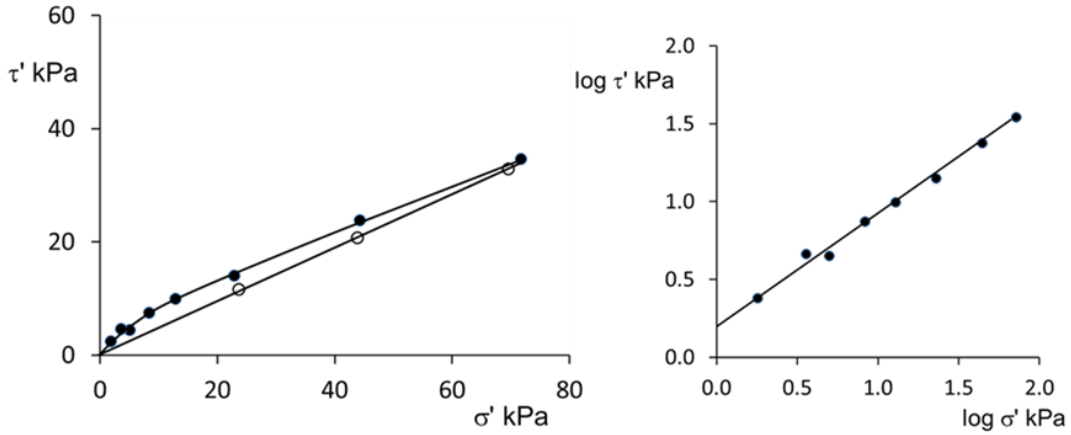

(a) Kaolin clay

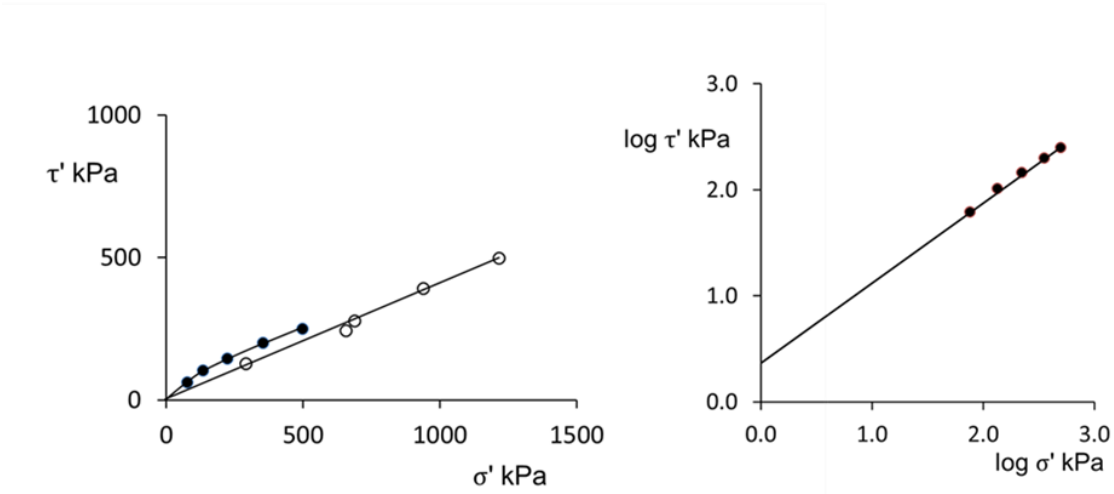

(b) Glacial till

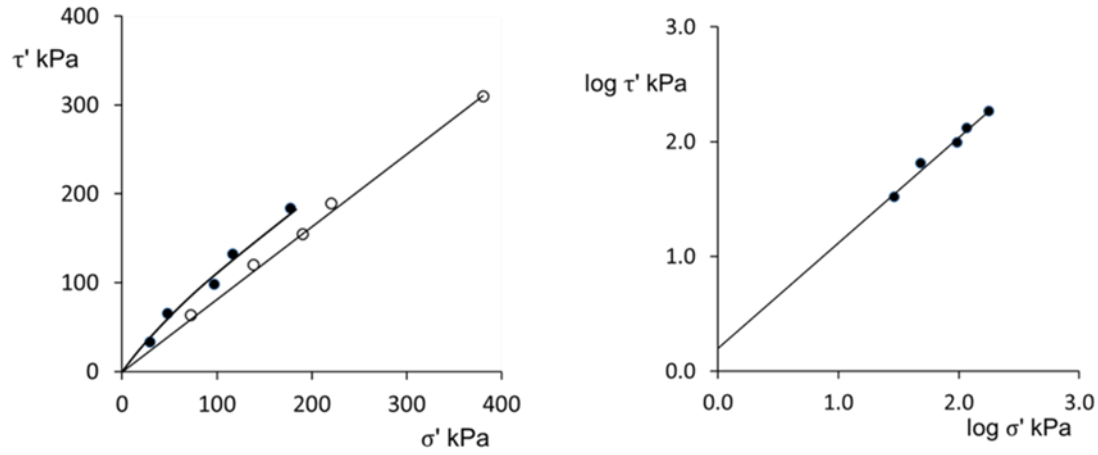

(c) Carbonate sand

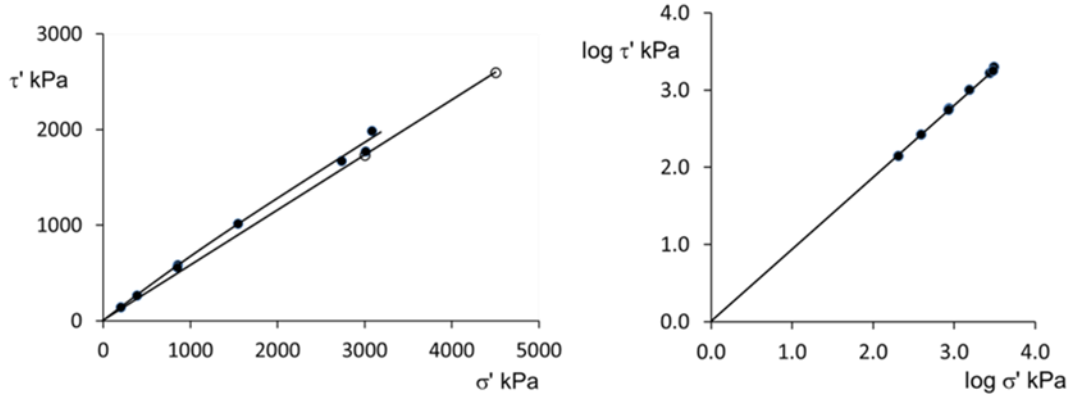

(d) Quartz sand

Figure 4: Peak and constant volume strengths of soil

In the left hand diagrams in Figure 4 the constant volume critical state strengths are linear with arithmetic scales and conform to equation 2. In the right hand diagrams the peak state strengths are linear with logarithmic scales and conform to equation 4. Values for the parameters A and b in equation 4 and the constant volume friction angle ϕ'_c in equation 2 are summarised in Table 1.

Table 1: Values for parameters in Figures 4

Soil	A	b	ϕ'_c
Kaolin clay	1.6	0.72	25
Glacial till	2.8	0.72	22
Carbonate sand	2.0	0.83	39
Quartz sand	1.0	0.93	30

The data in Figures 4 show that the peak strength envelopes of several coarse and fine grained soils are non-linear. They all pass through or very close to the origin. These envelopes can be described by the simple power law in eqn 5 with the parameters given in Table 1. The large strain, constant volume, strengths of these soils are linear and are described by eqn 2 with zero cohesion and friction angles ϕ'_c given in Table 1.

1.4 Errors using a linear Mohr-Coulomb envelope

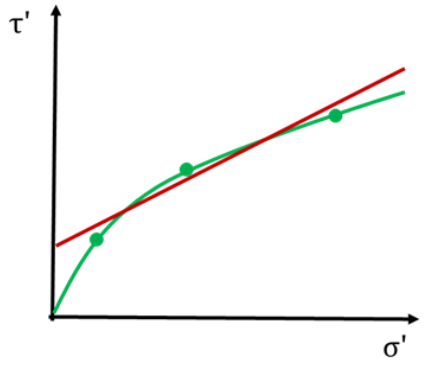

Figure 5: Fitting a linear envelope.

Figure 5 illustrates the errors implicit in the linear Mohr-Coulomb envelope. There are three data points obtained from a set of three triaxial or shear tests that define a non-linear failure curve and a linear Mohr-Coulomb envelope has been fitted through them. There is a mid-range of stress for which the soil strength is greater than that given by the linear Mohr-Coulomb criterion but at larger and smaller stresses the linear envelope is above the true curved envelope and it is unsafe. At small stresses relevant to stability of shallow landslides the errors using the linear Mohr-Coulomb envelope can be considerable (Atkinson, 2007, Atkinson and Crabb 1991).

2 SOIL STIFFNESS

2.1 Linear and non-linear stiffness

Stiffness is the relationship between changes of stress and changes of strain and stiffness modulus is the gradient of a stress- strain curve. These may be shear stress and strain giving a shear modulus G' or mean stress and volumetric strain giving a bulk modulus K' or a one-dimensional modulus M'. Figure 6(a) illustrates a general non-linear stress – strain curve. The stiffness at a point may be described as a tangent modulus $\delta\sigma'/\delta\varepsilon$ or as a secant modulus $\Delta\sigma'/\Delta\varepsilon$.

Materials may be elastic or in-elastic and the criterion is what happens during a loading – unloading cycle. Elastic materials are conservative so (by definition) stress-strain curves for

loading followed by unloading must be identical so no work is dissipated over the cycle as illustrated in Figure 6(b). Figure 6(c) illustrates the behaviour of a material that is linear but inelastic; the area within the loading – unloading loop is a measure of the work dissipated.

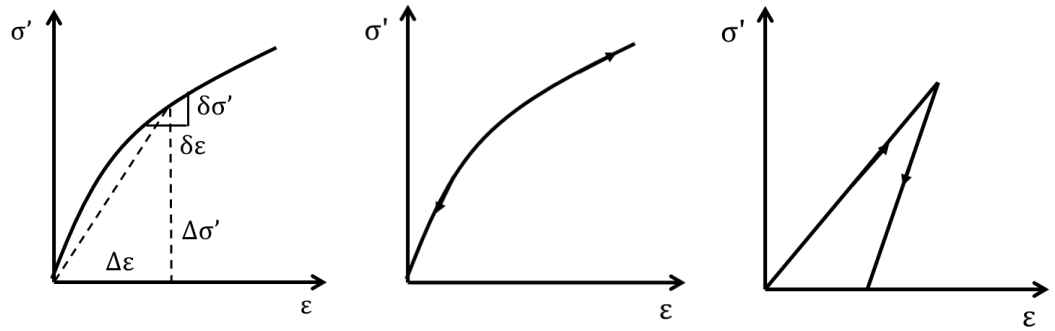

(a) Increments (b) Non-linear elastic (c) Linear inelastic

Figure 6: Material stiffness.

2.2 Conventional linear soil stiffness

Fig 7(a) illustrates a typical stress – strain curve of soil in a drained shear test with an unloading – reloading cycle. The stress – strain curve for a drained triaxial test would be similar. The gradient is the shear modulus G' and for a triaxial test it is Young's modulus E'. Fig 7(b) illustrates a typical stress – strain curve of soil in isotropic compression with an unloading – reloading cycle. The curve for one-dimensional compression would be similar. The gradient of the isotropic loading stress – strain curve is the bulk modulus K' and for one-dimensional loading it is M' = $1/m_v$ where m_v is the 1D compressibility.

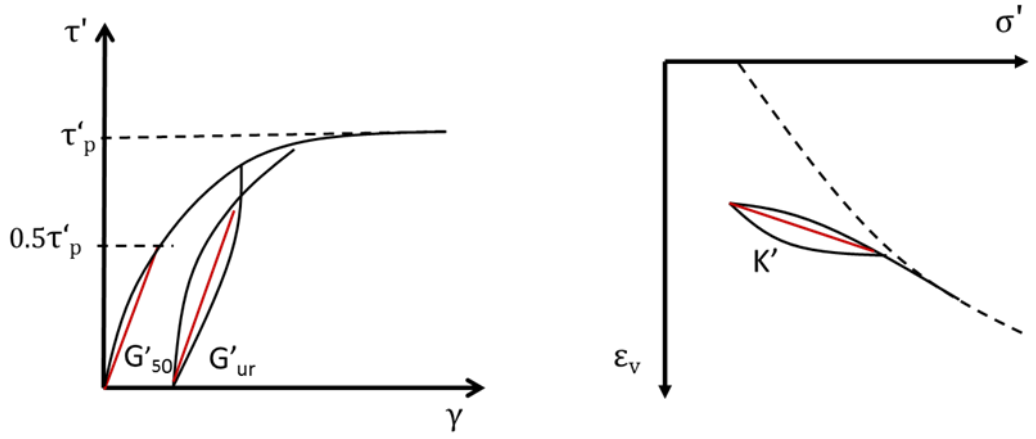

(a) (b)

Figure 7: Typical stress – strain curves for soil

In conventional practice ground movements are calculated assuming the soil to be linear with a single value for stiffness. There are several ways in which the value of stiffness is determined and the red lines illustrate some of these.

2.3 Non-linear soil stiffness and settlements of foundations

For any of the loading or unloading stress – strain curves shown in Figure 7 the stiffness decays with strain from the start of the loading or unloading stage. The decay of stiffness with strain is well-established (Atkinson 2000) and a typical stiffness decay curve is illustrated in Figure 8. The strains vary over several orders of magnitude from very small strain (<0.001%) to large strain (>1%). Different experimental techniques are required to measure soil stiffness over different ranges of strain as illustrated in Figure 8.

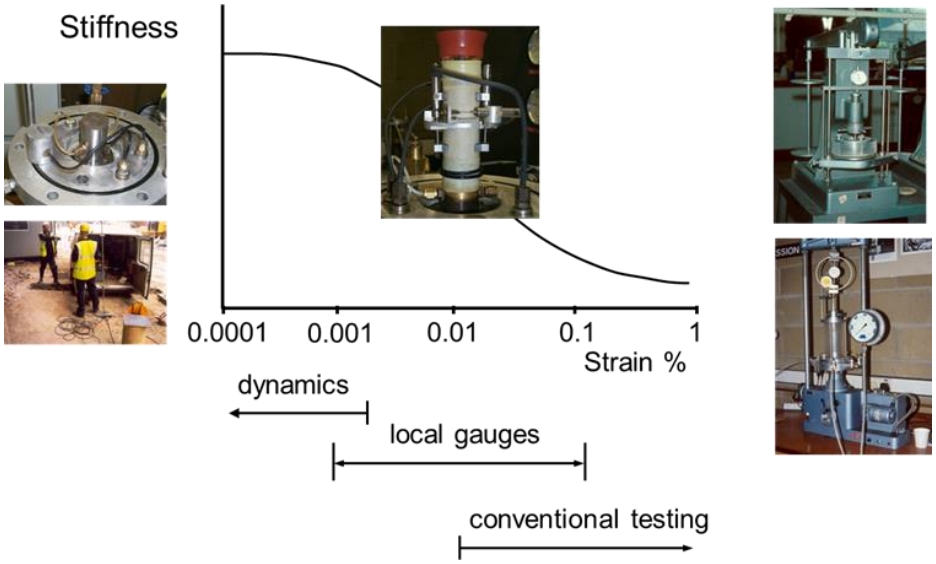

Figure 8: Measurement of soil stiffness

In conventional triaxial or oedometer tests there several sources of error in measurement of strain and it is impossible to obtain reliable measurements smaller than about 0.01%. To measure smaller strains it is necessary to use local gauges attached to the sample but these are limited to strains of about 0.001%. Soil stiffness at very small strain less than about 0.001% may be found from measurements of shear wave velocity in the ground or in laboratory samples.

2.4 Calculation of settlements of foundations

Some soils in the ground are heavily overconsolidated and are relatively stiff while other soils are lightly overconsolidated and are relatively soft. Analyses of settlements on soft soil should be treated differently from analyses of settlements on stiff soil. In practice there are two general cases and these are illustrated in Fig 9.

Buildings and embankments apply similar bearing pressures, typically 100 to 200kPa. An embankment can tolerate relatively large settlements of 100mm or more and can be built on soft soil. If the depth of soft soil is 10m the strains are of the order of 1%. Most buildings can tolerate only relatively small settlements of the order of 10mm and for a foundation 10m wide the mean strains are of the order of 0.1%. Shallow foundations can only be built on stiff soil so buildings on soft soil are most often on piled foundations.

The strains resulting from the same loading $\Delta\sigma'$ are illustrated in Fig 9(c) and the corresponding stiffness decay curves are illustrated in Fig 9(d). The initial state of the soft soil is close to the normal consolidation line so the embankment loading moves the state from lightly overconsolidated to normally consolidated. The initial state of the stiff soil is far from the normal consolidation line and the state remains overconsolidated throughout the foundation loading.

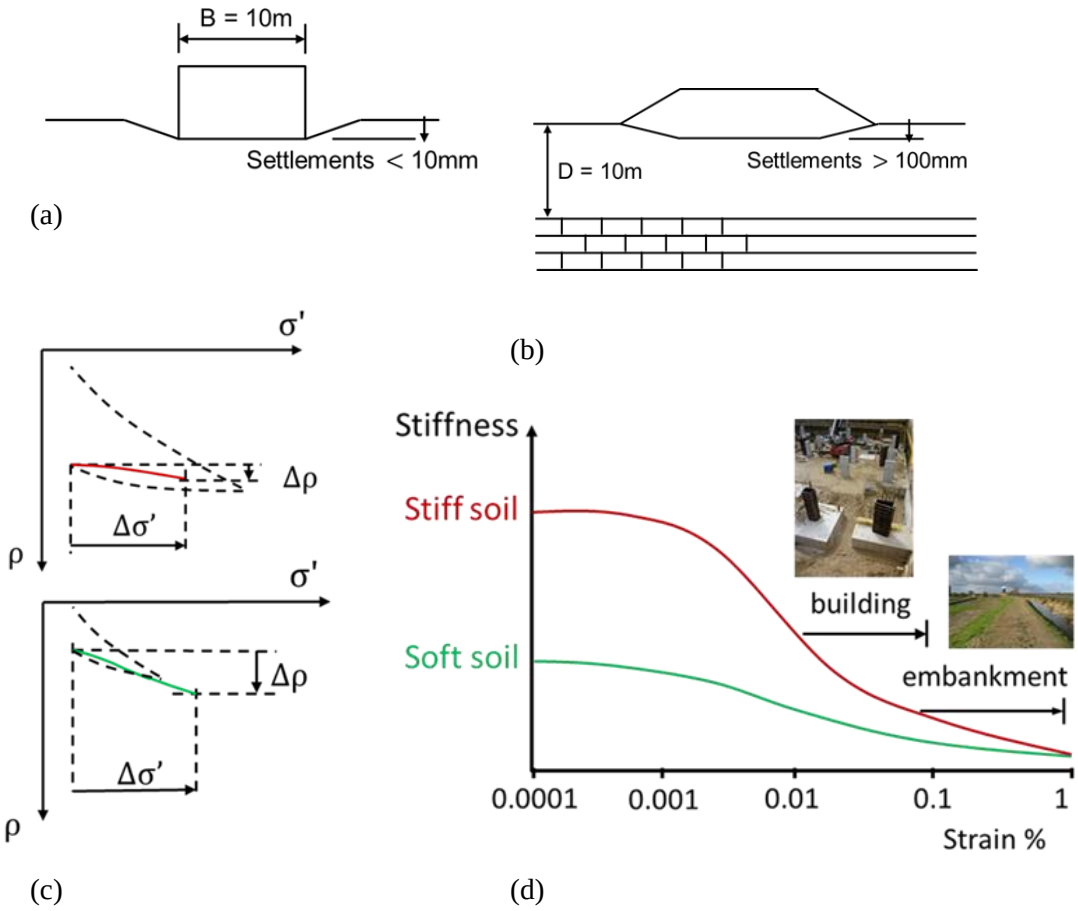

Figure 9: Settlement of structures on stiff and soft soil

Figure 10 illustrates an embankment on a layer of soft soil of limited thickness. The deformations approximate to one-dimensional. The soil state moves from an initial lightly overconsolidated state and ends at a normally consolidated state. Over this range the stress – strain can reasonably be approximate as linear with gradient M'

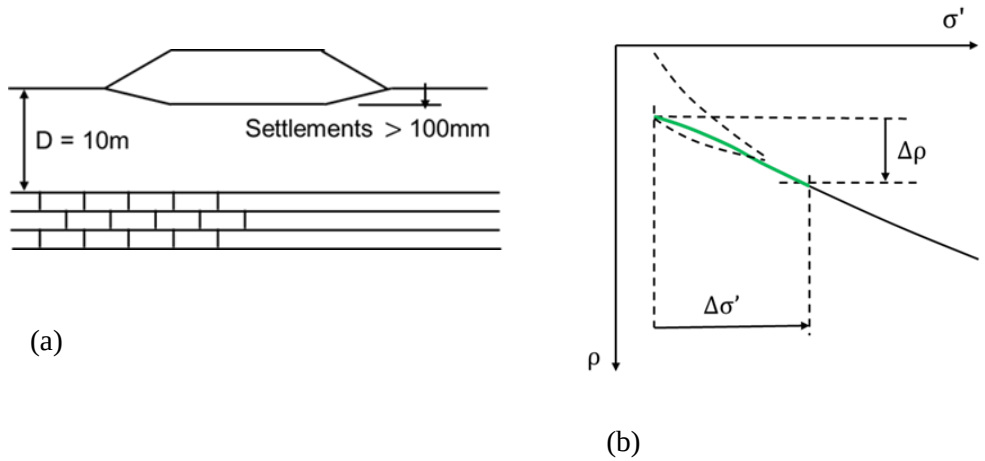

Figure 10: Settlement of an embankment on soft soil

Figure 11(a) shows a foundation on stiff soil and Figure 11(b) shows the load –settlement curve. The state remains inside the normal consolidation line and the soil remains overconsolidated. A

typical design would require settlements less than 10mm and for a foundation 10m wide this is a strain of about 0.1%. A typical stiffness – strain decay curve for stiff soil is illustrated in Figure 11(c). For very small strain less than about 0.001% the stiffness is approximately constant. For larger strains the stiffness decays and becomes very small as the soil fails. As a simplification, sufficient for routine foundation design, the decay of stiffness with log strain can be taken as linear as shown in Figure 11(d).

Values for E'_0 the stiffness at very small strains less than about 0.001% can be found from routine measurements of shear wave velocity either in situ or from tests on laboratory samples. (Atkinson 2000). Stiff soils typically reach a state of failure with very small stiffness at strains approximately 1%. From Figure 11(d) the stiffness for simple design of a foundation on stiff soil can be taken as $E'_o/3$ corresponding to settlements $\Delta\rho/B$ of 0.1%.

In routine ground engineering practice the errors implicit in these simplifications are often no greater than the uncertainties in determining the ground conditions and soil parameters from routine in situ or laboratory tests.

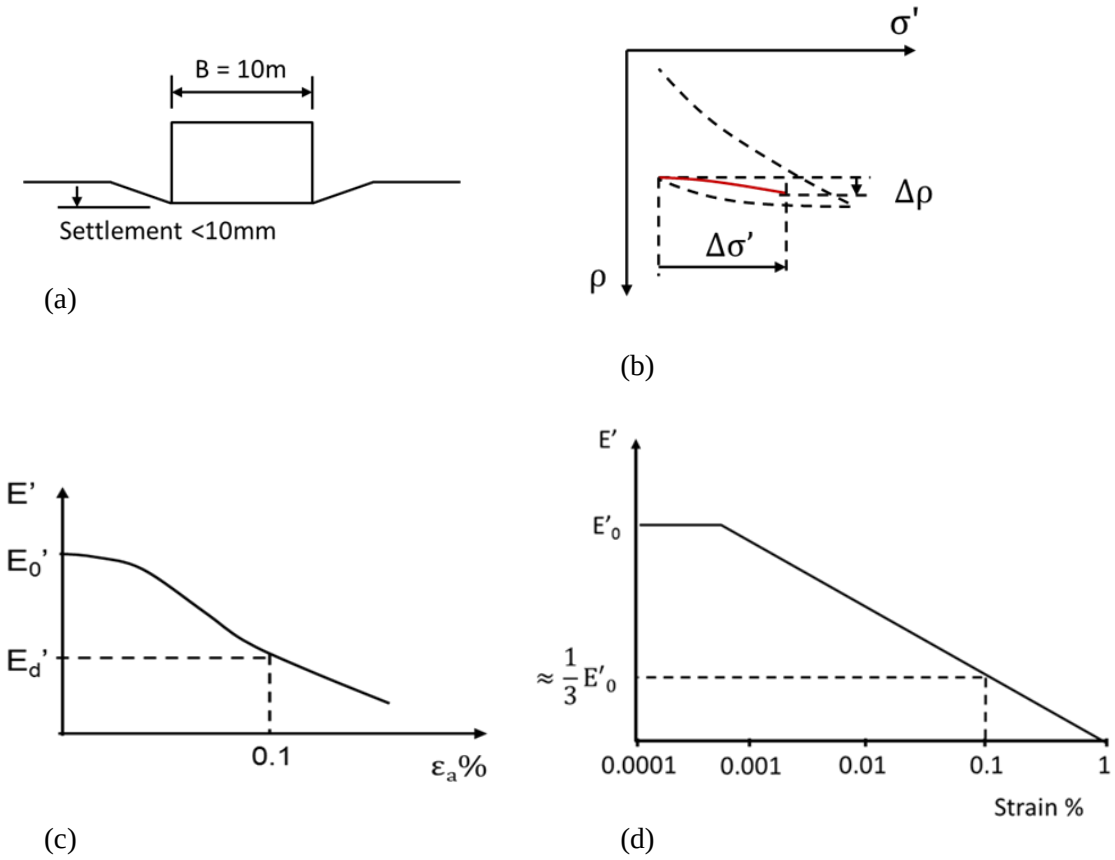

Figure 11: Settlement of a foundation on stiff soil

3 SUMMARY

In routine ground engineering practice soil strength is described by a linear Mohr-Coulomb criterion and stress-strain behaviour is linear. Neither of these approximations adequately represent the general features of soil behaviour.

Peak strengths of a variety or soils measured over range of normal stresses can be described by a simple power law given by equation 3 which is similar to the Hoek-Brown failure criterion for rocks.

The stress-strain behaviour of stiff soil is highly non-linear and stiffness decays rapidly with strain. A reasonable approximation is to take a design stiffness as $E'_o/3$ corresponding to a strain of about 0.1%.

Strains below an embankment on soft soil are commonly of the order of 1% as the soil state moves from lightly overconsolidated to normally consolidated. Over this range the stress-strain behaviour approximates to linear with one-dimensional stiffness M'.

REFERENCES

Atkinson, J.H. (2000) 40th Rankine Lecture: Non-linear stiffness in routine design. *Geotechnique*; Vol. 50, No, 5, pp. 487-508

Atkinson, J.H. (2007) Peak strength of overconsolidated clays, *Geotechnique*, 57(2), 127-135.

Atkinson, J.H. and Crabb, G.I. (1991) Determination of Soil Strength Parameters for the Analysis of Highway Slope Failure. *Proc. I.C.E. Int Conf. on Slope Stability Engineering Developments and Applications*. Paper No 2, pp. 11-16.

Coulomb, C. A. (1773) Essai sur une application des regles de maximis et minimis a quelques problemes de statique relatifs a l'architecture. *Mem. Div. Sav. Acad*, Paris, Vol 7 pp 343-382

Heyman, J. (1972) *Coulomb's Memoir on Statics*. Cambridge University Press.

Hoek E. and Brown E. T. (1980) *Underground Excavations in Rock*, p. 527. London, Inst Min Metall.

Terzaghi, K. (1936) The shearing resistance of saturated soil and the angle between the planes of shear. *Proc. 1st Int. Conf. Soil Mech and Foundn Engng*, Vol 1, pp 54-56, Harvard Mass.

Understanding patterns of movement for slow moving landslides

D N Petley
Vice-Chancellors Office, University of Sheffield, UK.
d.n.petley@sheffield.ac.uk (Corresponding author)

J M Carey
GNS Science, Wellington, NZ
j.carey@gns.cri.nz

K-Y Ng
Ove Arup & Partners (HK) Ltd, Hong Kong
angel.ng@arup.com

C I Massey
GNS Science, Wellington, NZ
c.massey@gns.cri.nz

M J Froude
Department of Geography, University of Sheffield, UK
m.froude@sheffield.ac.uk

Keywords: landslide, movement, deformation, pore water pressure, strain rate, creep

ABSTRACT

The movement of many landslides is controlled by the force imbalance associated with a reduction in shear resistance caused by a decrease in normal effective stress as pore water pressures increase. This basic premise might lead to an assumption that the movement rate has a simple relationship with the pore water pressure / normal stress state, but previously studies have shown marked differences in this relationship according to whether pore water pressures are rising or falling. This paper reviews examples from the literature in which high resolution monitoring allows the relationship between the movement rate and the pore water pressure / normal effective stress state to be determined. We show that a variety of relationships exist between these parameters with the key determinant appearing to be the peak movement rate of the landslide during the movement event in question. We propose that the key factor is whether the yield stress is exceeded. If so, rate and state friction may dominate; if not then creep decay may be critical.

1 INTRODUCTION

Landslides are a pervasive hazard on the surface of the earth, responsible for an average of up to 14,000 fatalities per annum (Petley 2012). Triggered primarily by one or more of the effects of precipitation, seismic shaking or slope alteration by humans, landslides also induce substantial socio-economic impacts on society. In many cases these effects are magnified by a lack of insurance cover, resulting from both their socio-economic setting (the majority of loss-inducing landslides occur in comparatively poor countries across Asia and Latin America) and by an unwillingness by insurance companies to provide cover for mass movement hazards in most territories. The latter results from a perceived poor understanding of the geographic distribution of landslide hazard, and the difficulties of determining potential levels of consequential loss. The effects are to increase the impact of landslide hazards relative to other natural hazards.

Whilst the majority of human casualties are associated high velocity landslides, and in particular debris flows, mudflows and soil/rock avalanches, slow moving landslides can cause high levels of financial loss, and, in some cases, loss of life. Thus, understanding these landslides remains a priority. The simple mechanics of these landslides is well-understood in terms of the role of elevated pore fluid pressure leading to a reduction in normal effective stress, and thus failure, and the development of strain, when the yield strength is exceeded. However, observed patterns of movement are more complex than this simple relationship would imply, and are important in terms of understanding, and forecasting, future behaviour for any slow moving landslide. In this paper, the relationship between pore fluid pressure and the rate of movement of landslides is reviewed, demonstrating complex patterns that have hitherto not been fully understood. Interestingly, glaciers display similar behaviour, and a number of hypotheses have been proposed to explain these mechanics across the two types of mass movement. The viability of these models for landslides is examined, and a new framework is proposed to account for the observed complex behaviour in landslide systems.

2 PATTERNS OF MOVEMENT OF SLOW MOVING LANDSLIDES

2.1 A review of landslide movement patterns

It is well established that the movement rate in a slope has a non-linear relationship with pore water pressure (e.g. Bertini, et al, 1984; Gonzalez et al. 2008). In general, once movement has commenced small increments of additional pore water pressure lead to successively greater increases in movement rate; the relationship between pore water pressure and movement rate is sometimes characterised as being exponential. This has sometimes been characterised with a viscosity modification to the Mohr-Columb failure criterion, with some success in predicting the moment patterns of flow type landslides. These models predict a movement rate for any given value of pore water pressure in the landslide, regardless of the dynamic state of that pore water pressure. Of course in reality, factors such as the geometry of the landslide play a key role. Thus, for example, in a rotational landslide the mass becomes increasingly stable as strain accumulates, such that the relationship between strain rate and pore water pressure will change as movement develops (primarily because the static stress state will change). However, in a large landslide this changing relationship will require large strains to become significant.

Some landslides show a simple relationship between pore water pressure and rate of movement in monitoring data. Thus, for example, monitoring of the Vallcebre landslide in the Eastern Pyrenees of Spain showed a simple, non-linear relationship between velocity and the depth of ground water (i.e. the shear surface pore water pressure) (Corominas et al. 1999; Fig. 1). In such cases the movement rate of the landslide can be predicted for any groundwater level.

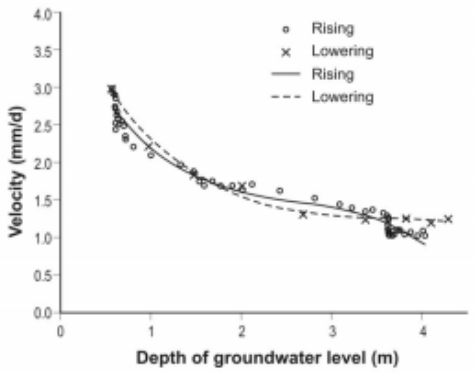

Figure 1: Patterns of movement of the Vellcebre landslide. Data from Corominas et al. (1999). Figure from Massey (2010)

Interestingly, however, there are a number of documented cases in which this relationship has proven to be more complex than might be expected, even when geometric factors have been taken into consideration. In particular, many landslides show a different movement response when pore water pressure is increasing in comparison to when pore water pressure is falling. But, surprisingly, there is no consistent relationship. The following sections provide some examples. Unfortunately though, there is a surprising paucity of published examples in which monitoring data is of sufficient quality to allow this relationship to be examined in detail.

2.2 La Valette landslide, France

La Valette landslide is located close to Saint-Pons in the Barcelonnette basin, in the Alpes-de-Haute-Provence region of France. Movement began in March 1982 as a reactivation of a pre-existing landslide (Van Asch et al. 2007). The landslide consists of an upper rotational slide that transitions into a mudflow as the displaced blocks degrade. It is large – the estimated volume is about 3.5 x 10^6 m^3, the length is about 2 km and the shear surface depth is 25 to 35 m in the central part of the mudflow. The landslide moves at variable rates, with a total displacement rate of about 1 to 2 m per annum.

La Valette landslide is extensively monitored due to the threat that it poses to the community at the foot of the slope. Van Asch et al. (2007) presented monitoring data for the landslide during a phase of increased pore water (Fig. 2). As expected they found a non-linear relationship (hysteresis) between movement rate and groundwater level, but perhaps less predictably they also found that the movement rate when the ground water was increasing was substantially different from that when groundwater level was declining. In this case a rising groundwater level was associated with a higher movement rate than was the case with a falling groundwater level. This was found to be consistent across two substantial periods of movement. This behaviour appears to be a complex version of strain hardening, in which resistance to movement increases with deformation. In this paper we refer to this style of relationship between movement rate and pore water pressure as strain hardening behaviour. Note however that this is a more complex style of behaviour than is normally ascribed to strain hardening as the increased resistance appears to develop at the point at which pore water pressures start to fall, but not before.

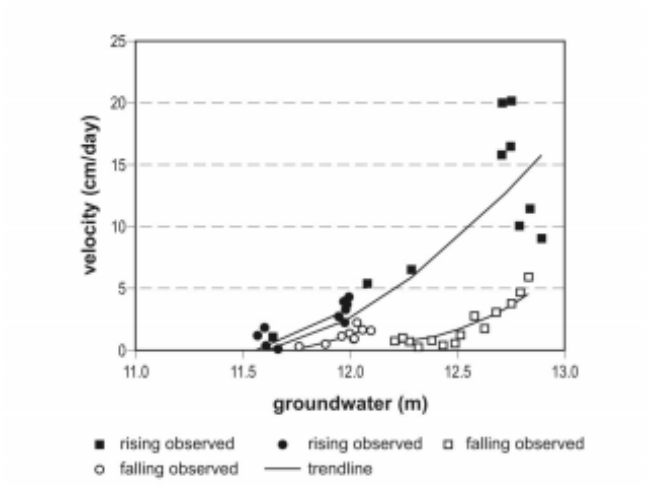

Figure 2: The relationship between velocity and groundwater level (depth above the shear surface) for La Vallette landslide. Data from Van Asch et al. (2007), figure from Massey (2010)

Similar behaviour has been seen in other landslides. Thus for example, Bertini et al. (1986) saw strain hardening behaviour at the Fasio San Martino landslide in Central Italy.

2.3 A reactivated landslide in central Japan

Matsuura et al. (2008) monitored both pore water pressures and landslide displacement in an unnamed reactivated landslide in weathered mudstone and silty sandstone in central Japan. This landslide was about 400 m long and 50 to 70 m wide. Movement occurred in response to increased pore water pressures driven by both precipitation and snowmelt. The basal shear surface, which was at a depth of 4 to 7 m, lay in highly weathered tuff. This was a comparatively fast moving landslide – rates of up to 50 mm per day were recorded – and between 9th September and 3rd December 1992 the landslide moved a total of about 1290 mm. During phases of increased rates of displacement the landslide displayed a strong pattern of hysteresis in the relationship with pore water pressure, but in the opposite sense to that displayed by La Valette (Fig 3). In this case displacement rates were comparatively slow as pore water pressure increased, and more rapid as it decreased. Particularly interesting is the observation that the landslide continued to accelerate even as pore water pressure started to fall. We term this a strain weakening behaviour, in which the landslide shows increased susceptibility to movement as strain develops, although once again the pattern of behaviour may be more complex than simple strain weakening would imply. In the case of the unnamed C. Japan landslide, this strain weakening behaviour was displayed in several movement periods. Matsuura et al. (2008) were not able to explain this behaviour, but suggested that it might be controlled by the geometry of the landslide:

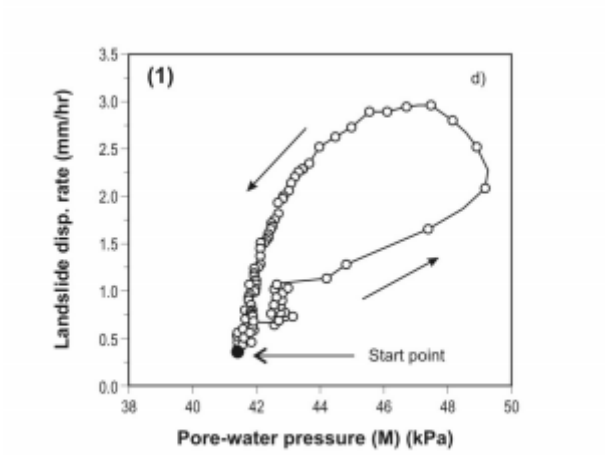

Figure 3: The relationship between the landslide displacement rate and the pore water pressure for the C. Japan landslide. Data from Matsuura et al. (2008),

"One reason for this may be that some aspects of landslide kinematics are controlled by the inclination of the sliding surface and the interaction between the moving body and side in the surrounding stable ground."

It is unclear as to how this mechanism would operate in a landslide of this type.

2.4 The behaviour of the Kualiangzi landslide in China

The Kualiangzi landslide on the margin of the Sichuan Basin of central China is a deep-seated translational bedrock landslide in interbedded mudstones and sandstones (Xu et al. 2016). This landslide is very large, with a width of about 1,100 metres and a length of up to 390 m, with an estimated volume of about 25.5 million m^3. Movement occurs on an inclined shear surface in weathered mudstone located an average of 50 m below the surface. At the rear of the landslide there is an exceptionally large tension trough.

Xu et al. (2016) monitored movement on the landslide through 2013, finding that the displacement rate of the landslide increased in response to precipitation. Analysis of the movement of the

landslide record suggests that it broadly shows the strain hardening type of behaviour (Figure 4). Interestingly, the two movement events represent different failure regimes – in the case of the first movement event, the calculated factor of safety of the landslide did not drop below unity. In the second movement event this was the case (Xu et al. 2016 suggested that it reached about Fs=0.93). Nonetheless in both cases the landslide showed the strain hardening style of behaviour.

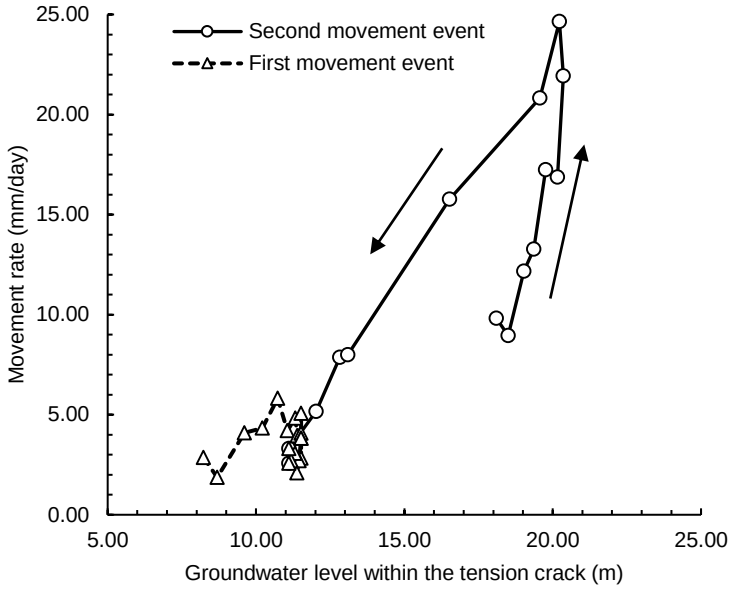

Figure 4: The relationship between the movement rate and the groundwater level in the Kualiangzi landslide, after Xu et al. (2016)

2.5 The behaviour of the Ventnor landslide in southern England

Amongst many other studies (e.g. Hutchinson and Bromhead 2002), Carey (2011) investigated the behaviour of the large (700 hectare), slow moving landslide complex upon which the town of Ventnor is built in the Isle of Wight in southern Britain. This is a complex landslide, involving differential block movement and the opening of grabens, on a very deep (>100 metre) shear surface (Hutchinson and Bromhead 2002). Movement rates are very low however, with peak velocities below 1 mm / day. This very large landslide has been extensively monitored, in particular in the area of a large graben structure that is developing at the crown of the landslide. At this location, both pore water pressure and displacement have been measured at various times.

A notable movement event occurred in the winter of the year 2000 in response to a prolonged and unusually wet period of weather. In this case, the strain weakening style of behaviour was clearly observed (Fig. 5), with movement rates being considerably higher on the falling limb than when pore water pressures were increasing.

2.6 The response of glaciers

Interestingly, it has long been observed that some glaciers also show hysteresis in movement in response to stress changes (Iken et al. 1983 for example). Shallow glaciers are in many ways landslides of ice, with sliding occurring either on a bedrock – ice interface or through deformation of a layer of till between the ice and the bedrock. An advantage of glacers is the relative ease with which the basal processes can be investigated (certainly in comparison with landslides), as it is sometimes possible to access the basal region. Considerable work has been undertaken to understand their dynamics.

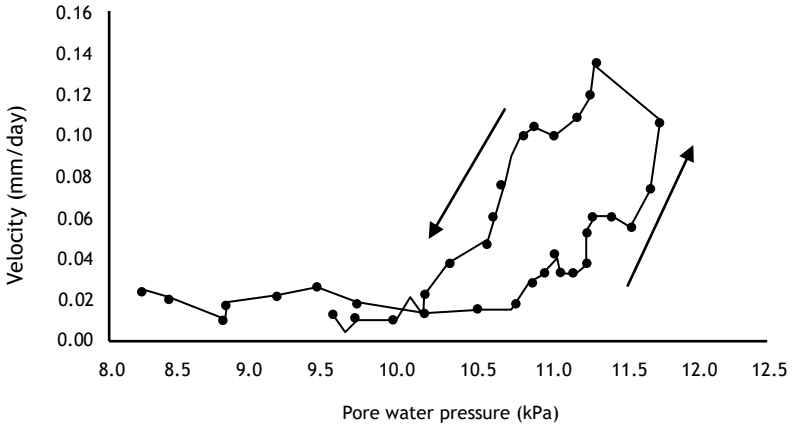

Figure 5: The relationship between landslide velocity and pore water pressure for the Ventnor landslide, after Carey (2011)

Basal tills show creep like behaviour below the yield strength, and a combination of creep and stick-slip behaviour (representing periods in which the effective normal stress reduces sufficiently to ensure that the macroscopic yield strength is lower than the externally imposed shear stress) results in a stepped movement pattern, in common with landslides. A key finding in till dominated systems is that creep rates often decay rapidly under constant stress forcing, once the initial perturbation that caused the movement to start has passed. Thus, till deformation provides a potential mechanism to explain this behaviour; creep rates have been observed to increase so long as normal effective stress is increasing, but decline under constant stress conditions. In a real system this would generate the strain hardening style of behaviour.

Glaciers examined by Damsgaard et al. (2016) shows this behaviour, with slow increases in velocity during phases of increasing pore water pressure, but rapid reductions in movement rate when pore water pressures peak. The authors point out that behaviour that is similar to that of glaciers is seen in landslides, and hence argue that the styles of deformation are directly analogous.

2.7 Insights into landslide response to pore water pressure change from laboratory testing

Most laboratory testing of landslide materials does not provide insight into the response of materials to changes in normal effective stress. The vast majority of geotechnical tests use a non-representative stress path, in which deformation is driven by changing shear stress under conditions of constant strain rate. In drained tests, normal effective stress is not permitted to change; in undrained tests pore water pressure can be generated, but only as a response to the application of shear stress. To investigate the behaviour described above requires the use of the field stress path, sometimes termed the pore pressure reinflation (PPR) test (see Petley *et al.* 2005), in which normal and total effective stress are kept constant, and pore water pressure is varied. The PPR test is most commonly undertaken within triaxial or stress path equipment, which makes it simple to capture the pore water pressure increase phase, but challenging to deal with the subsequent reduction in pore water pressure conditions. Nonetheless this equipment can provide considerable insight.

Ng (2007) undertook a large suite of PPR tests on undisturbed residual soil samples from Lantau Island in Hong Kong. Some of these experiments involved a step-wise increase in pore water pressure (and thus a reduction in normal effective stress) with axial stress and confining pressure held constant, initially at less than the yield stress, but ultimately exceeding it. Fig. 6 shows the development of strain rate in two tests, for one of which pore water pressure was increased in steps of 10 kPa, once per hour, whilst in the other pore water pressure was increased constantly

(ramped) at 10 kPa per hour. In the ramped test the strain rate increased exponentially with increasing pore water pressure (i.e. decreasing effective stress state). However, in the stepped test the strain rate initially increased at a rate substantially higher than that of the other test, but which subsequently declined. This initially high and then declining creep rate is a manifestation of the creep decay mechanism. This behaviour, which was seen consistently in the tests of Ng (2007), is similar to that observed in the till deformation of glaciers.

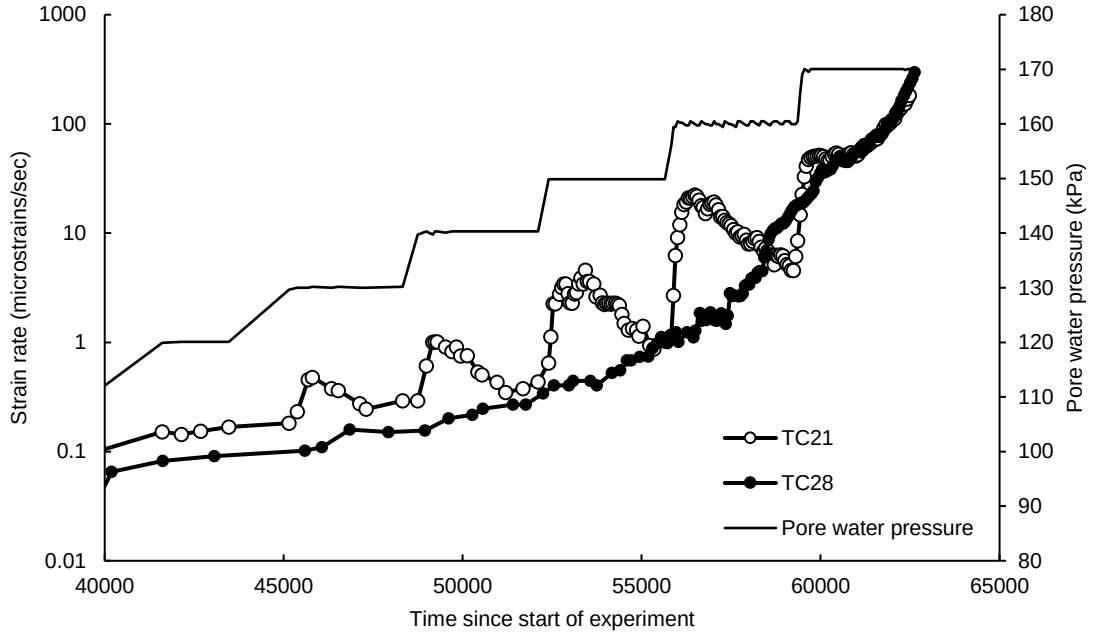

Figure 6: PPR experiment results for residual soil samples from Lantau, Hong Kong, after Ng (2008). Sample TC21 was subjected to increases in pore water pressure in 10 kPa steps (illustrated on the graph), whilst for sample TC28 porewater pressure was increased at the same average rate, but at a constant rate

The initiation of final failure in these tests was also interesting. After the final pore water pressure step the stepped test sample (TC28) showed an initial increase in strain rate (Fig. 7), which then declined before increasing again, with the sample then proceeding to full failure. This appears to be evidence that the final failure event is associated with damage accumulation, as postulated by Petley et al. (2002). Interestingly, Carey and Petley (2014) saw similar behaviour, with final failure being observed in a long term creep test in which no change in effective stress state occurred.

3 DISCUSSION

From the examples described above, and from others in the literature (Table 1), is clear from a range of landslides that different patterns of movement can be seen in response to changes in pore water pressure. In all cases the relationship between movement rate and pore water pressure is exponential once FoS≤1, but for some landslides the relationship may be considered to be strain hardening, in others strain weakening, whilst in a small number the behaviour may be strain neutral, or the response to pore water changes is weak (e.g. Taihape and Utiku). In none of the studies outlined above was a clear explanation given for the response observed. In all cases in which there were multiple movement events the landslide showed consistent behaviour. Thus, in each case it appears to be a fundamental property of the landslide in question.

The strain hardening style of behaviour has also been observed in glaciers moving through deformation of a basal till. Damsgaard et al. (2016) noted the similarity in behaviour seen between glaciers and some landslides. In the case of the glaciers that they modelled, creep was a distributed mechanism whilst slip involved some degree of strain localisation. Whilst a creep decay mechanism was observed, this applied below the critical shear stress. Interestingly, Damsgaard et al. (2016) also note that above the yield strength the rheology of the systems becomes rate independent. This view does not seem to be supported by the monitoring data for the landslides.

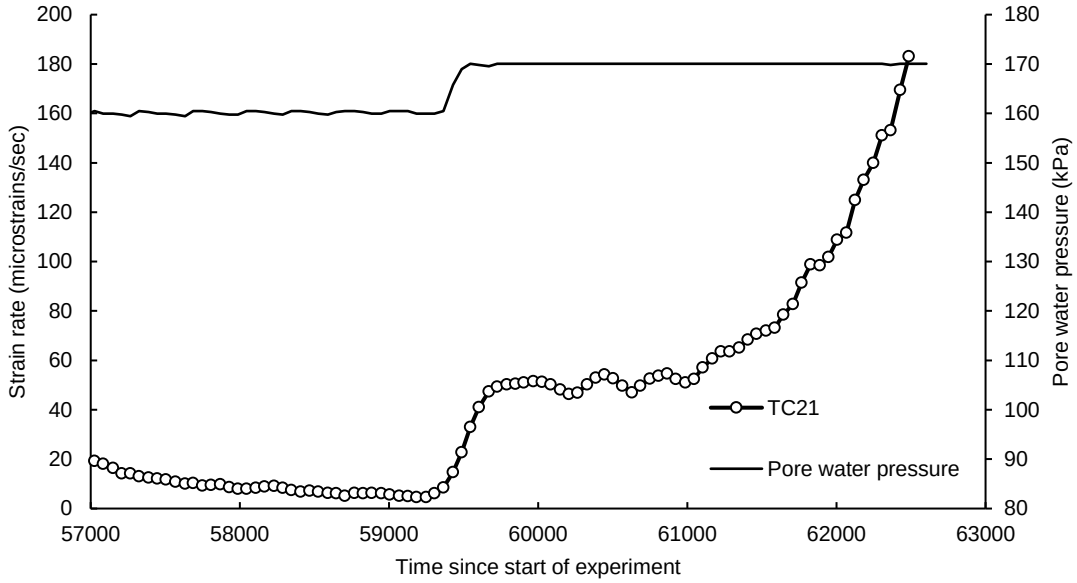

Figure 7: Detail of the last phase of the experiment on sample TC21, after Ng (2008).

Van Asch et al. (2017) described the strain weakening style of behaviour as a lower intrinsic viscosity and lower dependency on excess pore water pressure when the pore water pressure is rising. They noted that intrinsic viscosity is not necessarily a constant value, but recognised that a decrease in viscosity after pore water pressures have peaked is hard to explain. They propose that this may be an effect of the size of the landslide body, with different parts of the mass experiencing extension and compression at different times. This may explain a complex response to fluctuations in pore water pressure at any point in the landslide.

The various landslides for which there is adequate monitoring data to determine hysteresis behaviour in response to changes in pore water pressure are listed in Table 1 in order of peak movement rate. No obvious relationship between the pattern of movement described in the paper and landslide type or material can be seen, but there does appear to be a general relationship in terms of movement rate. On the whole (but not in every case), landslides with high movement rates show a strain weakening pattern (typically >20 mm / day), whilst those with low movement rates (typically <10 mm/day) show the strain hardening pattern. The exception to the latter is the Ventnor landslide, but note that this movement record is from the graben structure at the crown of the landslide, where the stress regime and deformation pattern may be highly complex.

This behaviour may be explainable by considering the deformation state. We hypothesise that slow rates of landslide deformation in these systems are typically occurring within the creep domain, where the dominant mechanism is plastic deformation through interparticle movement. In this domain, the creep decay mechanism suggests that under constant stress states the creep rate will decline; this behaviour is also seen in the experiments of Ng (1999) and in the behaviour of glaciers. Given this creep decay mechanism, it is inevitable that a reduction in pore water pressure will induce a dramatic reduction in the rate of movement.

Table 1: A summary of the landslide movement records analysed in this paper

Name	Landslide type	Basal material	Peak movement rate (mm/day)	Pattern	Reference
La Valette	Translational mudflow	Weathered soil	200	SH	Van Asch et al. (2007)
Purbeck	Mudslide	Weathered clay	60	SW	Allison and Brunsden (1990)
C. Japan	Translational rockslide	Mudstone /silt	50	SW	Matsuura et al. (2008)
Kualiangxi	Translational rockslide	Clay	25	SW	Xu et al. (2016)
Slumgullion	Earthflow	Clay-rich debris	10	Neutral/SH	Schulz et al. (2009)
Utiku	Translational rockslide	Weathered clay	3.0	SH (? Role of pore water)	Massey et al. (2013)
Vallcebre	Translational rockslide	Colluvium	1.5	Neutral	Corominas et al. (1999)
Fasio San Martino	Earthflow	Clay-rich siltstone	0.4	SH	Bertini et al. (1986)
Taihape	Translational rockslide	Weathered clay	0.1	SH (? Role of pore water)	Massey et al. (2016)
Ventnor	Rotational rockslide	Weathered clay	0.1	Neutral / SW	Carey (2011)

On the other hand, the more rapid movement rates, and those associated with faster glacial movement, are associated with the strain weakening mechanism. In this case, Dansgaard et al. (2016) note that in glaciers and landslides this may well be associated with a localisation process that occurs once the yield stress has been exceeded. We propose that the key mechanism here is a rate dependent friction law that allows resistance to movement to change once movement has been initiated. Such a rate-dependent friction process, in which friction reduces with increasing movement rate, as outlined in Handwerger et al. (2016) would generate a strain weakening pattern of movement. On the other hand, a state and rate dependent friction law could also allow the development of strain hardening behaviour under the right circumstances.

As a consequence, the different styles of behaviour seen in landslides in response to changes in pore water pressure, and thus to the normal effective stress state, is probably related to two different processes. Below the yield stress, creep mechanisms dominate. In this case, the creep decay mechanism is critical, in particular when pore water pressures start to fall. In these circumstances, creep rate rapidly declines, causing the strain hardening style of behaviour to be displayed. On the other hand, above the yield stress rate and state dependent friction dominates, allowing both strain weakening and strain hardening styles of behaviour to be shown. In both cases, behaviour may be modified by local conditions associated with the geometry of the landslide, such as curvature of the shear surface and stress transfer between blocks.

4 CONCLUSIONS

Through a review of the literature we have shown that the relationship between pore water pressure / normal effective stress and the rate of movement of landslides is complex. Beyond the yield stress the movement rate generally has an exponential relationship with normal effective stress. However, it is also clear that the rate of movement may be different between increasing and decreasing pore water pressure states. We have demonstrated that during phases of slow movement landslides tend to show a strain hardening style of behaviour, whilst rapidly moving

slide tend to show the strain weakening style. We suggest that this may be associated with the presence of two different mechanisms – below the yield stress creep mechanisms dominate, and thus the effects of creep decay mean that strain hardening is likely. On the other hand, above the yield stress, rate and state dependent friction becomes important, meaning that both the strain weakening and strain hardening styles of behaviour can be shown, depending on the frictional properties of the basal material.

REFERENCES

Allison, R.J. and Brunsden, D. (1990) Some mudslide movement patterns. *Earth Surface Processes and Landforms*, **15** (4), 297–311.

Bertini, T., Cugusi, E., D'Elia, B., et al. (1986) Lenti Movimenti di Versante nell'Abruzzo Adriatico: caratteri e criteri di stabilizzazione. *Proceedings XVI Convegno Nazionale Di Geotecnica*, Bologna, 1, 91–100.

Carey, J.M. (2011) *The Progressive Development and Post-failure Behaviour of Deep-seated Landslide Complexes*. Doctoral thesis, Durham University.

Carey, J., & Petley, D.N. (2014) Progressive shear-surface development in cohesive materials; implications for landslide behaviour. *Engineering Geology* 177, 54-65.

Corominas, J., Moya, J., Ledesma, et al (1999) *Monitoring of the Vallcebre landslide, Eastern Pyrenees, Spain*. In N. Yagi, T. Yamagami and J.-C. Jiang (eds.), Slope Stability Engineering, A.A. Balkema, Rotterdam, 1239–1244.

Damsgaard, A., Egholm, D.L., Been, L.H. et al. (2016) Ice flow dynamics forced by water pressure variations in subglacial granular beds. *Geophysical Research Letters* **43** (23) 12,165 - 12,173.

Gonzalez, D.A., Ledesma, A. And Corominas. (2008) The viscous component in slow moving landslides: A practical case. In: Chen et al. (Editors) *Landslides and Engineered Slopes*, Taylor and Francis Group: London. pp. 237-242.

Handwerger, A.L., Rempel, A.W., Skarbek, R.M et al. (2016) Rate-weakening friction characterizes both slow sliding and catastrophic failure of landslides. *Proceedings of the National Academy of Sciences*, **113** (37), 10281-6.

Hutchinson, J.N. and Bromhead, E.N. 2002. Keynote Paper: Isle of Wight landslides. In: R.G McInnes and J Jakeways (Editors), *Instability Planning and Management: Seeking Sustainable Solutions to Ground Movement Problems*. Thomas Telford: London, pp. 3-70.

Iken, A., Rothlisberger, H., Flotron A. et al. (1983) The uplift of Unteraargletscher at the beginning of the melt season – a consequence of water storage at the bed? *Journal of Glaciology* **29** (101), 28–47.

Massey, C., Petley, D.N. and McSaveney, M. (2013) Patterns of movement in reactivated landslides. *Engineering Geology* **159** 1-19.

Massey, C.I., Petley, D.N., McSaveney, et al. (2016). Basal sliding and plastic deformation of a slow, reactivated landslide in New Zealand. *Engineering Geology* **208** 11-28.

Matsuura, S., Asano, S. and Okamoto, T. (2008) Relationship between rain and/or meltwater, pore-water pressure and displacement of a reactivated landslide. *Engineering Geology* **101** (1–2), 49-59.

Ng, K-Y. (2007) *Mechanisms of shallow rainfall-induced landslides in residual soils in humid tropical environments*. Doctoral thesis, Durham University.

Petley, D.N., Bulmer, M.H.K., & Murphy, W. (2002) Patterns of movement in rotational and translational landslides. *Geology* **30** (8) 719–722.

Petley, D.N., Higuchi, T., Petley, D.J., et al. (2005) The development of progressive landslide failure in cohesive materials. *Geology*, **33** (3): 201-204

Petley, D.N. (2012) Global patterns of loss of life from landslides. *Geology* **40** (10), 927-930.

Schulz, W.H., McKenna, J.P., Kibler, J.D et al. (2009) Relations between hydrology and velocity of a continuously moving landslide – evidence of a pore-pressure feedback regarding landslide motion? *Landslides*, **6**, 181-90.

Van Asch, Th.W.J., Van Beek, L.P.H. & Bogaard, T. (2007) Problems in predicting the mobility of slow-moving landslides. *Engineering Geology* **91**, 46-55.

Xu, Q., Liu, H., Ran, J. et al. (2016) Field monitoring of groundwater responses to heavy rainfalls and the early warning of the Kualiangzi landslide in Sichuan Basin, southwestern China. *Landslide*s **13** 1555-1570.

Yong, I. & Clayton, P.B. (2017)
Application of Soil Specific Correction Factors for Liquefaction Assessment: Case Study in Waikato Soils for the Hamilton Section of the Waikato Expressway.
Proc. 20th NZGS Geotechnical Symposium. Eds. GJ Alexander & CY Chin, Napier

Application of soil specific correction factors for liquefaction assessment: case study in Waikato soils for the Hamilton section of the Waikato expressway

Irene Yong
Geotechnical Engineer, Beca Auckland, NZ
irene.yongz@beca.com

Philip Clayton
Technical Director, Beca Auckland, NZ.
philip.clayton@beca.com (Corresponding author)

Keywords: Fines Correction, Ic Cutoff, Liquefaction, Hamilton Ash, Waikato.

ABSTRACT

The four-lane, 21.8 kilometre long, Hamilton Section of the Waikato Expressway is the largest roading project undertaken in this region's history and one of the larger projects currently being undertaken in New Zealand. Many of the seventeen expressway bridges in the Hamilton Section are underlain by Pleistocene soils assessed as having a high liquefaction potential. Typically the soils encountered are volcanic in origin either as primary tephra deposits or reworked volcanically derived material. A number of researchers have noted the potential for misclassification of such soils by the CPT, therefore it was decided to undertake co-located borehole/SCPT/SDMT and laboratory classification testing for use in conjunction with a site wide geologic model to develop soil specific correction factors for use in liquefaction assessment. Soil specific correction factors were investigated for the Ic sand like/clay like cut-off (B&I 2014) and the fines content (Cfc). The specific correction factors derived are presented along with examples from the project showing the consequence, some of which are significant, of adopting soil specific correlations. Given the widespread occurrence of some of the soils considered e.g. Hamilton Ash, within the Waikato and Bay of Plenty region, the authors suggest that the database of testing presented in this study could be readily supplemented by results from other sites and the proposed soil specific correction/correlations extended.

1 INTRODUCTION

This paper presents a case study of the development of site specific CPT derived soil behaviour/composition correlations within volcanogenic sediments of the Waikato Region of the north island of New Zealand. Two correlations are considered:

a) Soil Behaviour Index (Ic) to fines content (FC) and;

b) Soil behaviour Index (Ic) to Plasticity Index (Ip) as a proxy of liquefaction susceptibility

These two correlations are key to the assessment of liquefaction susceptibility and so the authors have chosen to investigate how they may vary from the norm in volcanogenic sediments, in particular those containing pumice (NZ Geotechnical Society, 2010).

This study uses data sourced from the extensive investigation undertaken for the Hamilton Section of the Waikato Expressway, a recently designed 21.8km long highway project including 17

bridges. The project area lies in the centre of the Hamilton Basin, a large alluvial plain approximately 40km wide by 90km long.

Many of the soil types encountered in this study are widespread across the region. In the future the authors would like to extend the database by incorporating suitable investigation data from elsewhere within the Waikato and Bay of Plenty region, where similar soils are known to exist.

2 GEOLOGY & SEISMICITY OF AREA

The Hamilton Basin can generally be divided into two geological terranes, the Hamilton Hills and the Lowlands. The Hamilton basin was infilled with sediments derived from volcanic activity within the Taupo Volcanic Zone, located approximately 100 km southeast of Hamilton, during the Quaternary period (last 2 Million years). Most of the basin is a broad alluvial floodplain (lowland) with widely spaced rounded hills (Hamilton Hills) that protrude some 20 m to 70 m above the plain surface. Most of the primary (airfall and pyroclastic deposits) and reworked (alluvial fans and lacustrine) soils in this region are rhyolitic in composition sourced from volcanic events within the Taupo Volcanic Zone, located approximately 100 km southeast of Hamilton. The soils contain significant amounts of volcanic glass, pumice, other rhyolitic lithic gravels, as well as crystalline minerals.

2.1 Hamilton Hills

The Hamilton Hills comprise older volcanic ignimbrites mantled by volcanic airfall deposits whose upper surface forms a characteristic stiff to very stiff orange-brown weathered silt-clay crust (Hamilton Ash Formation). These hills comprise a sequence of at least three distal ignimbrites (pyroclastic density currents) deposited approximately 1 to 1.2 Million years ago interfingered with alluvium. The hills have since been eroded by the ancestral Waikato River into a series of rounded hills and valleys, which in turn deposited reworked volcanic sediments. Subsequently the hills were mantled by ash fall beds known as the Kauroa and Hamilton Ash Formations and undifferentiated younger tephra beds (cover beds). The surfaces of the Hamilton Hills have been deeply weathered with the highly reactive volcanic glass fragments altering to sensitive clay minerals such as allophane and halloysite (Moon et al, 2015).

2.2 Lowlands

The Lowlands are the valleys between the Hamilton Hills that have been infilled with younger (late Quaternary, last 25,000 yrs) alluvial sediments of the Piako Subgroup. The Lowlands typically have a very gently tilting (south to north) topographic surface, known as the Hinuera Surface. Deposits underlying the surface are known as Hinuera Formation. Interfingering with the thick and often pumice rich sand beds are silt layers comprising silicic fragments (volcanic glass with limited weathering) as well as silty/sandy and occasionally organic alluvium.

3 LIQUEFACTION SUSCEPTIBILITY

3.1 Potential for Misclassification

A number of researchers have reported concerns with the use of liquefaction assessment procedures based on penetrometer testing in rhyolitic (or specifically pumiceous) soils as the structure, shape and composition of the sediment varies significantly from the more typical alluvial sediments derived from sedimentary rocks which form the basis for empirically derived liquefaction assessment tools.

Murashev et al (2014) stated in NZTA research Report 553 that conventional interpretation (i.e. penetrometer tests such as SPT and CPT) are less effective in assessing liquefaction resistance in pumice soils. Numerous researchers also have concluded that penetration tests can underestimate liquefaction resistance in pumice soils. Clayton et.al (2017), Murashev et al (2014), Clayton & Johnson (2013). Orense & Pender M. (2013)

The referenced works generally refer to the potential for underestimation of the relative densities and hence liquefaction resistance in rhyolitic soils. Should this be the case then it follows that there may be the potential for CPT tests to also misclassify such soils.

3.2 Assessment of Susceptibility

Soil response to earthquake shaking and hence liquefaction potential has been widely related to soil plasticity. Idriss and Boulanger (2006, 8, 14) suggests that all soils may be divided, based on their plasticity index into the following categories:

a) *Sand like* - soil that may be subject to classical cyclic liquefaction if sufficiently loose and*;*

b) *Clay like* - soil not subject to classical liquefaction, but may be subject to cyclic softening if sufficiently soft.

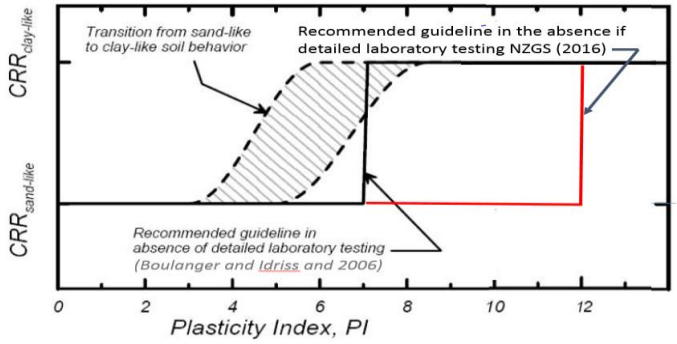

Figure 1: Sand-like & clay-like behaviour modified from Boulander & Idriss (2006).

It is generally not viable for practitioners to directly determine the plasticity index and hence expected behaviour of every variation of soil within each profile, particularly in the complex interbedded sequences often encountered within the Hamilton Basin. Instead a correlation between the Cone Penetrometer Test (CPT) derived Soil Behaviour Index (Ic) and Plasticity Index (PI) is utilised to identify the soil susceptibility. The Ic value that corresponds to the boundary between sand like and clay like soil is termed the Ic cutoff, and typically assigned a value of 2.6, as originally proposed by Robertson and Wride (1998).

Idriss and Boulanger (2014) recommend site specific sampling and testing for major projects to evaluate the sensitivity of Ic cut-off in liquefaction assessments. The authors of this study concur, particularly within volcanically derived soils, as the correlations used have been originate primarily from testing soils derived from weathering and erosion of rocks (lithic soils).
Ideally the Ic cutoff would be established on a site and soil specific basis by undertaking side by side CPT testing (for Ic) and undisturbed sampling, with dynamic testing then undertaken on the undisturbed samples. However difficulties in obtaining truly undisturbed samples and the costs associated with undertaking the large number of tests necessary to generate a statistically valid site specific correlation are prohibitive even for substantial infrastructure projects.

An alternative is to undertake side by side CPT testing and disturbed sampling (for Atterberg testing). This approach allows the generation of a site specific Ic to PI correlation and validation (or correction) of the Ic Cutoff. In the Authors view this is particularly important in the volcanogenic soils of the Waikato and Bay of Plenty region as these soils can differ in their behaviour when subject to penetrometer tests compared to soils composed of hard lithic grains (Clayton & Johnson, 2013).

3.3 Assessment of Fines Content

Another necessary input to the liquefaction analysis is the fines content (FC). Liquefaction potential is noted to decrease with increasing fines content for a given penetration resistance, and this effect is accounted for by applying a fines correction factor. In a similar manner to the PI cut-off, correlation between fines content (FC) to CPT Ic is used to allow fines correction to be applied in analyses, without the need for closely spaced laboratory grading tests.

As noted above Rhyolitic soils may respond differently compared lithic soils and existing correlations may be less reliable. Idriss and Boulanger (2014) recommend the calibration of the fines correction curve fitting parameter CFC for any CPT-based liquefaction triggering evaluation. Calibration within the project has been achieved by undertaking paired CPT testing and borehole sampling across a wide range of soils followed by regressing Ic against FC.

4 IC CUT-OFF

4.1 Soil Behaviour Index, Ic Cut-off

Paired BH and CPT were undertaken and samples selected, specifically targeting soils of relatively consistent properties within the sample depth range and generally with an Ic in the range of 2.0 to 2.6 as this was expected to be the zone where the Ic cutoff was expected to occur.

Atterburg tests were undertaken on the selected samples and the representative Ic of the sample zone assessed. The resulting PI is then plotted against Ic and compare against the Robertson & Wride (1998) cut-off value of 2.6 and the (conservatively) adopted PI cutoff line of 12. Fig 2 below presents a plot of PI against Ic based on available laboratory testing results for all soils with the exception of Units 1a, 2b, 2d, 3b and 6 which were not sampled.

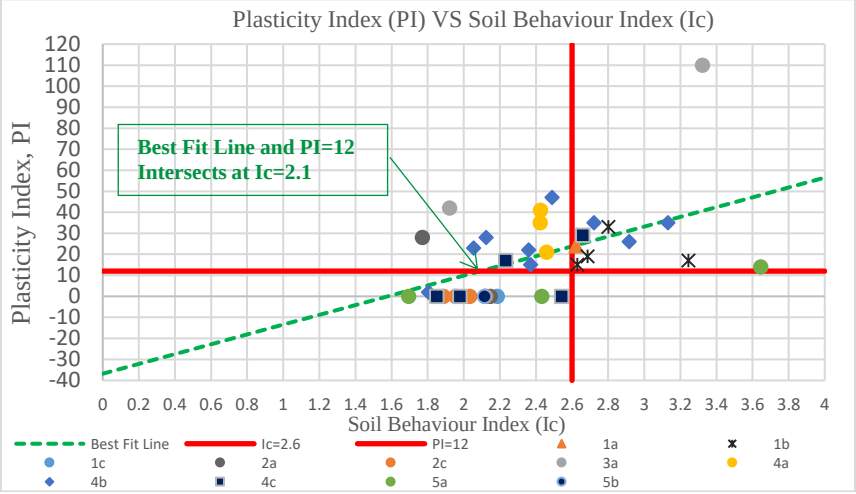

Figure 2: Plasticity Index (PI) VS Soil Behaviour Index (Ic) for all soils

In terms of design, in these soils the default Ic cutoff value of 2.6 appears conservative, compounding the already conservative adoption of an PI cutoff of 12 (refer fig 1). Considering the above results there is some justification to apply a revised Ic cutoff for all the soils encountered of 2.2, however the paucity of results for some units lead the authors to focus on deriving Ic for selected soils at this stage. During this stage of the project we chose to focus on Unit 4 which includes the Hamilton ash (a widely distributed and readily recognisable unit), associated tephra's and contemporaneous ignimbrite sands.

4.2 Individual Sub-unit Results

Figure 3 below presents the laboratory result for Hamilton Ash Formation, Tephra and Ignimbrite.

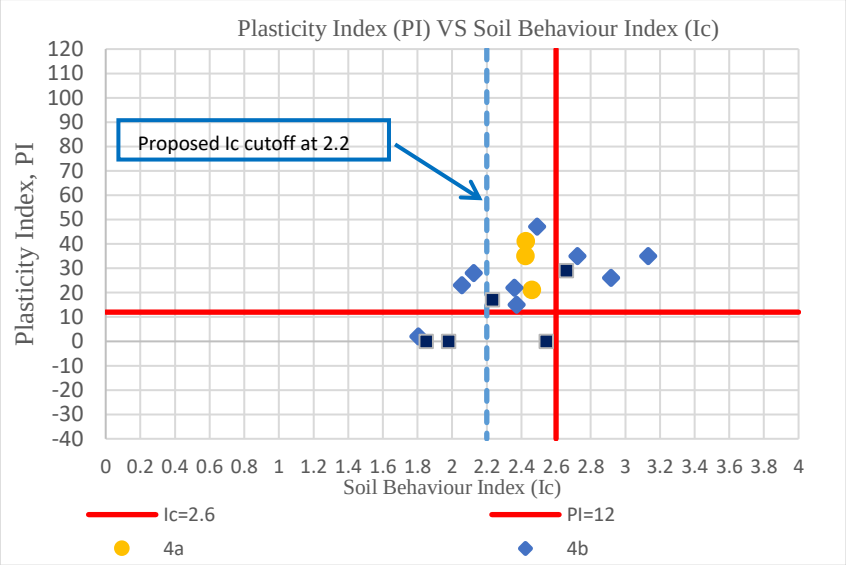

Figure 3: Plasticity Index (PI) VS Soil Behaviour Index (Ic) for Hamilton Ash (Unit4A), Tephra (Unit 4B) & Ignimbrite (Unit 4C)

- Hamilton Ash (Unit 4A), based on PI result is clay-like and that it is not susceptible to liquefaction. However, CPT based assessment showed Ic less than 2.6.
- Tephra (Unit 4B), referring to Figure 3, most of the laboratory results for unit 4B typically have PI more than 12, while Ic is typically less than 2.6.
- Ignimbrite (Unit 4C), shows a mix of plasticity index and Ic.

4.3 Proposed Ic Cutoff

The combined results of tests undertaken in Unit 4 supported the adoption of an Ic cutoff of 2.2 for Hamilton Ash and associated tephra deposits within the project (refer fig 3). Following additional tests elsewhere in the Waikato/Bay of Plenty area it may be possible to apply this revised cutoff wherever these units occur.

5 FINES CORRECTION

The second correlation highlighted in this paper relates to the fines content assumed in liquefaction analyses based on correlation to Ic. Idriss and Boulanger (2014) recommend the calibration of the correlation by adjusting the fines correction curve fitting parameter CFC. CFC is calibrated to site specific data by regressing Ic against FC using the following equation: Ic = [(FC+137) / 80] – CFC.

5.1 Fines Correction, C_{FC}

Grading tests were undertaken to determine a Fines Content (FC) on the same samples as discussed in 2.1. The FC is then converted to an equivalent Ic value using the equation: Ic = [(FC+137) / 80] – CFC. Initially Ic as determined from the CPT is compared against the equivalent Ic determined from FC. Where a mismatch is found, the curve fitting parameter CFC is varied until a match is achieved. With the scatter of the results (Ic to FC has significant inherent scatter as noted below) and the general applicability of FC correction across all soils it was decided to derive a CFC for all soils, rather than attempting to define a CFC for individual units.

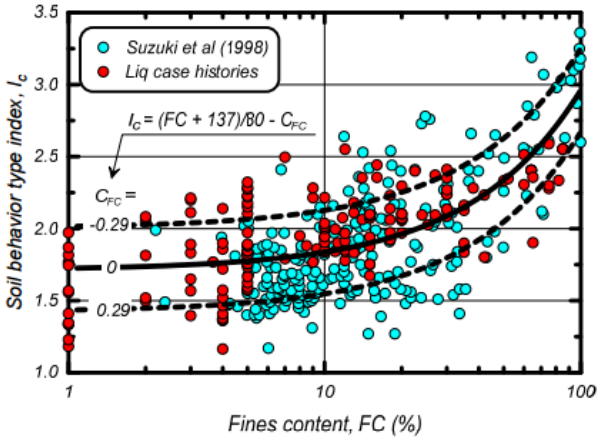

Figure 4: Recommended correlation between Ic and FC (Idris and Boulanger 2014)

5.2 Determination of Site Specific C_{FC}

Figure 6 shows a comparison between fines content (FC) from lab testing versus the estimated FC from CPT. Fig 7 utilises a CFC of zero (the nominal value) and the underestimation of fines content is clearly apparent.

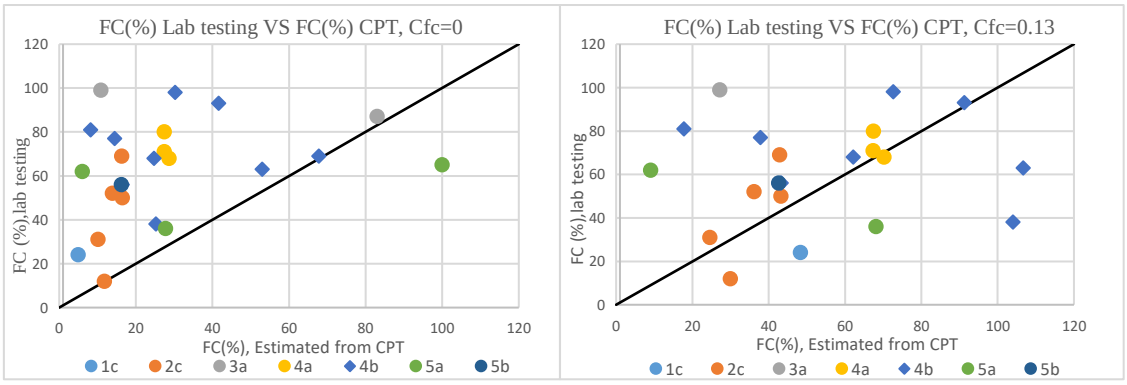

Figure 5 & Figure 6: Fines Content (Laboratory data) VS Fines Content Estimated Fines Content from CPT, CFC=0, CFC=0.13

Fig 6 Utilises a CFC of 0.13 for a much improved correlation. A site wide fines content correction factor (CFC) of 0.13 was therefore adopted for the project. The skew from the nominal correlation (of around half a standard deviation) is within the range suggested for sensitivity analysis by Idriss and Boulanger (2014). The application of the Cfc = 0.13 increases the fines content considered in liquefaction analysis resulting in a modest increase in FOS liq.

6 DISCUSSIONS

Liquefaction assessment using the Simplified Method requires the consideration of both susceptibility and triggering potential. There are significant unknowns relating to these two aspects for soils of rhyolitic origin. This aspect is discussed further in Clayton et al. (2017). Two aspects of the CPT based simplified method Ic/Ip and Ic/FC correlations are considered in detail.

Based on the Ic to PI plot in Fig 2, the use of an Ic cutoff of 2.6 appears (overly) conservative in many of the soils encountered in this investigation and that this leads to incorrect assumptions about the liquefaction potential of low plasticity weathered tephra/ash deposits. Sufficient testing was undertaken on the Hamilton section of the Waikato Expressway that the authors (and project designers) considered justified in reducing the Ic cutoff of selected soils. This lead to a significant reduction in the inferred extent of liquefaction on the project.

The author's hypothesis is that the structure and grain composition of Rhyolitic volcanic soil common in this area of New Zealand result in a correlation between Ic and PI that differ from what might be found in soils composed of hard lithic grains. Ideally the refinement in the use of CPT testing for liquefaction assessment undertaken on this project could be extended in a number of other ways to avoid overly conservative assessment of liquefaction potential in such soils:

- Additional test data could be compiled from other paired investigation test points and laboratory testing within these units - which are present and readily recognised across much of the Waikato and Bay of Plenty. This data could be used to investigate if the lower Ic cutoff is applicable to these soils on other sites.
- Additional test data could be compiled and analysed for other soils of rhyolitic origin, for example in pumiceoeus alluvium and ignimbrites.
- Dynamic testing could be undertaken on undisturbed samples to examine the validity of the assumed PI cutoff in these soils to complete the connection between Ic and soil susceptibility.

In conjunction with testing and a revision of the Ic cutoff for liquefaction susceptibility the Ic to fines content correlation was reviewed. Adjustment of the curve fitting parameter Cfc to achieve a better match between measured and correlated fines content across the site has lead to a site wide increase in fines correction and removal of unnecessary conservatism in the FOSliq. In a similar manner as for the Ic cutoff additional test data could be compiled from other paired investigation test points and laboratory testing within these soils that occur across much of the Waikato and Bay of Plenty. This data could be used to investigate if the site specific Cfc is applicable to these soils on other sites.

7 CONCLUSIONS

A number of paired CPT/BH investigations have been undertaken through a range of rhyolitic soils on the Hamilton Section of the Waikato Expressway, as part of the NZ Transport Agency's Waikato Expressway Project. Investigation points were paired to allow (among other things) the investigation of default CPT (Ic) to Fines Content (FC) and Plasticity Index (PI) correlations. Clear trends were identified which justified adopting a revised Ic cutoff of 2.2 for soil units related to the Hamilton Ash within the Hamilton Expressway project.

Further research is required to extend results among similar soils that commonly occur in the Waikato and Bay of Plenty. Further research is also suggested in reviewing the plasticity index (PI) cutoff used in liquefaction analysis to differentiate between sand like and clay like soil for rhyolitic soils.

A site specific fines content (FC) to soil behaviour index (Ic) curve fitting parameter (Cfc) was also derived for the project. A Cfc of 0.13 was derived by matching measured and correlated FC. The use of this site specific correction factor results in the removal of a source of unnecessary conservatism in liquefaction assessment on the project through a generally increased fines correction.

8 ACKNOWLEDGEMENTS

The authors wish to thank the New Zealand Transport Agency for their permission to publish this paper and in particular the valuable contributions from Stuart Finlan. The authors would also like to acknowledge The City Edge Alliance, the Project Geotechnical Steering Group and Beca colleagues who contributed to this project.

REFERENCES

Boulanger, R. W., & Idriss, I. M. (2006) Liquefaction Susceptibility Criteria for Silts and Clays. *Journal of Geotechnical and Geoenvironmental Engg*., ASCE 132:11, 1413-1424.

Boulanger R.W. & Idriss, I.M. (2007) Evaluation of Cyclic Softening in Silts and Clays. *Journal of Geotechnical and Geoenvironmental Engineering* 133(6), 641 – 652.

Boulanger R.W. & Idriss, I.M. (2014) *Soil liquefaction during earthquakes: CPT and SPT based Liquefaction Triggering Procedures*. University of California Davis, report No UCD/CGM 14/01.

Clayton & Johnson (2013) *Liquefaction Resistance and Possible Aging Effects in Selected Pleistocene Soils of the Upper North Island.*

Clayton, P.J., Yong, I., Green, R.A., Bastin, S.H., (2017). Case study in the use of paleoliquefaction techniques to investigate liquefaction potential of Waikato soils for the Hamilton section of the Waikato expressway. *Proceedings 29th NZGS Geotechnical Symposium.* Eds. GJ Alexander & CY Chin, Napier.

McCraw (2011) *The wandering river: landforms and geological history of the Hamilton basin.* Lower Hutt: Geoscience Society of New Zealand.

Moon, V.G., Lowe D.J., Cunningham M.J., Wyatt J., Churchman G.J., de Lange W.P., Mörz T., Kreiter S., Kluger M.O., Jorat M.E. (2015) *Sensitive pyroclastic- derived halloysitic soils in northern New Zealand: interplay of microstructure, minerals, and geomechanics.* Pp. 3–21.

Murashev et al (2014) *The Development of Design Guidance for Bridges in New Zealand for Liquefaction and Lateral Spreading Effects.*

Orense, R. & Pender, M. (2013) Liquefaction characteristics of crushable pumice sand. *Proc. 18th Intern. Conf. on Soil Mechanics and Geotechnical Engineering, Paris, France.*

NZ Geotechnical Society (2010) *Geotechnical Earthquake Engineering Practice – Module 1: Guidelines for the identification, assessment and mitigation of liquefaction hazards.*

A methodology for examining soil-water characteristics of loess and loess-derived soils on Banks Peninsula, New Zealand.

K Yates
Department of Geological Sciences, University of Canterbury, NZ.
Kathering.yates@pg.canterbury.ac.nz (Corresponding author)

C Fenton
Department of Geological Sciences, University of Canterbury, NZ.
clark.fenton@canterbury.ac.nz

Keywords: loess, slope stability, soil suction, microstructure

ABSTRACT

Loess and loess-derived soils cover much of Canterbury, from the foothills of the Southern Alps to the Pacific Coast. These soils are of variable thickness, ranging from several metres up to 40m at the base of slopes on Banks Peninsula. In many areas primary, air-fall loess has been reworked by slope processes to form a loess colluvium. These soils are comprised predominantly of silt but can contain up to 45 % clay, giving rise to low plasticity clay behaviour. Loess and loess-derived soils are relatively dense, and can form vertical exposures. Dry densities are typically between 1.6 t/m3 and 1.8 t/m3, hence these soils do not display collapse behaviour common to other loess deposits around the World. Across Canterbury these soils display high dry strength but weaken rapidly with small increases in moisture content. Periodic wetting leads to a variety of slope failures related to internal erosion (tunnel gullying) and rapid loss of shear strength (debris flows and soil slides). In this paper, we present a methodology to investigate the effects of soil microstructure and soil suction on the shear strength and stability of loess soils in Akaroa Harbour.

1 INTRODUCTION

Loess and loess-derived soils, collectively termed loess deposits, greater than 1m thick cover approximately 10% of the South Island, New Zealand (Figure 1). Often considered a problematic soil, slope failures related to internal erosion and rapid loss of shear strength can occur within loess deposits. When dry, an in situ loess soil mass can stand vertically, and its strength and stability is often controlled by vertical discontinuities. However, upon small (2 – 3%) increases in moisture content, the shear strength of the soil matrix can weaken rapidly. The mechanics of this behaviour, in terms of the relative contributions of soil suction and inter-particle bonding to overall soil strength, is not well understood for loess deposits in Canterbury. Furthermore, the current understanding of the geotechnical shear strength of Canterbury loess deposits is based on a relatively small number of studies with limited geographic coverage.

As it is considered likely that the shear strength of the soil is controlled by a combination of the soil microstructure and negative pore pressures, understanding these mechanics is important for developing further understanding of the behaviour of loess slopes. This is the focus of current research which aims to inform future development in loess covered areas, and will improve the understanding of the behaviour of loess with respect to how changes in moisture content affect shear strength. The purpose of this paper is to outline the methodology of ongoing research by the University of Canterbury.

2 CANTERBURY LOESS DEPOSITS

Loess in Canterbury, New Zealand, is a yellowish brown windblown deposit with predominantly silt-sized grains. Sand content typically comprises fine, angular particles and, along with clay content, varies depending on location and degree of reworking. New Zealand loess has been formed from aeolian transportation and deposition of glacially derived rock flour. Deposition of these deposits has occurred primarily during the Late Pleistocene and Post Glacial (Holocene) (Bell et al., 1986; Bell and Trangmar, 1987; Bruce, 1973; Griffiths, 1973; Ives, 1973; Raeside, 1964; Sparrow, 1948). In Canterbury, the primary parent rock for loess is greywacke (Torlesse Group).

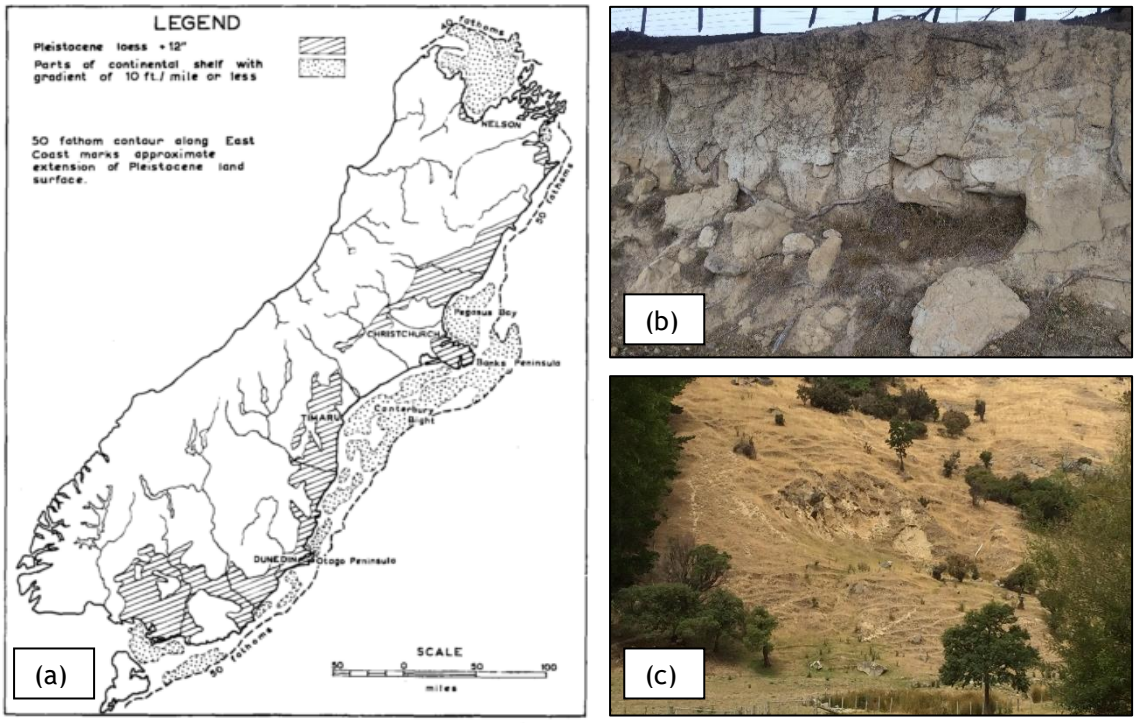

Figure 1: (a) distribution of loess >30cm thick in the south island (Raeside, 1964); (b) loess cutting with vertical discontinuities and large blocks released from the slope, Chorlton Rd, Okains Bay, Banks Peninsula; and (c) shallow slope instability in loess slope, Okains Bay

Loess greater than 1m thick covers approximately 10% of the South Island. The thickest deposits reach up to 40m thick, with the thickest deposits typically occurring at the base of slopes as colluvial aprons (Bell and Trangmar, 1987). Typically loess deposits overlie Pliocene age Cannington Gravels and Timaru Basalt in South Canterbury, and Miocene age volcanics in Banks Peninsula (Tonkin et al., 1974). Depending on location, loess deposits in Canterbury have been divided into 2 to 4 stratigraphic units separated by either colluvial layers or paleosols (Almond et al., 2007; Griffiths, 1973; Ives, 1973; Tonkin et al., 1974).

Two main groups of loess deposits are recognised in Canterbury: In situ (Primary air-fall) loess and loess colluvium. In situ loess refers to loess that has been formed from aeolian deposition, i.e., loess sensu stricto, and shows no evidence of reworking. In situ loess in Canterbury is predominantly quartzofelspathic silt, with minor amounts of accessory minerals and clay (generally illite and vermiculite) (Griffiths, 1973; Raeside, 1964).

Loess colluvium refers to materials that have been formed from the reworking of in situ loess by slope processes. It is also a quartzofelspathic silt or fine sand, but may also contain (volcanic) rock fragments (Bell and Trangmar, 1987). Loess colluvium generally has a lower bulk density,

and greater permeability than in situ loess (Bell and Trangmar, 1987). Loess colluvium deposits are often discontinuous and variable in thickness, indicating episodic deposition (Bell and Trangmar, 1987).

When dry, the strength and stability of in situ loess is controlled by discontinuities in the soil mass. Cuttings within loess can stand vertically (Figure 2), however, the shear strength of the soil matrix can weaken rapidly upon small (2% - 3%) increases in moisture content (Hughes, 2002; Jowett, 1995; McDowell, 1989). This, and susceptibility to clay dispersion and erosion, can make loess subject to instability on slopes, particularly during and after intense rainfall events (Alley, 1966; Bell et al., 1986; Bell and Trangmar, 1987; Hutchinson, 1975). Wetting of the soil mass leads to a variety of slope failures related to internal erosion (tunnel gullying) and rapid loss of shear strength (debris flows and soil slides).

Our current understanding of the geotechnical characteristics of Canterbury loess deposits is based on a relatively small number of studies with limited geographic extent. In particular, the influence of soil microstructure and the relative contributions of soil suction and inter-particle bonding to overall soil strength are not well understood. As it is considered likely that the shear strength of the soil is controlled by a combination of both, examining the soil microstructure and the role of negative pore pressures in the loess deposits is the focus of ongoing research.

3 PROJECT OBJECTIVES

The primary purpose of this research is to examine soil suction and soil microstructure, and how they contribute to the shear strength and stability of loess and loess-derived soils in Canterbury, New Zealand. In particular:

1. How do loess slopes respond to rainfall in terms of pore water pressure, matric suction, water content and lateral deformation (if any), and what are the implications for slope performance and instability?
2. What is the impact of changes on pore water pressures on the shear strength of the loess?
3. What are the characteristics of the loess microstructure (including particle shape, angularity, particle size, clay bonding, location and consistency of clays within microstructure), and how does the application of moisture change this structure?
4. How does microstructure and soil suction contribute to the shear strength of loess?

Research will be conducted using a combination of field monitoring and laboratory testing techniques to allow both detailed observation of shear strength characteristics and global examination of these mechanisms in situ. The results of this research will inform future development in loess covered areas, and will improve the understanding of the behaviour of loess deposits with respect to changes in moisture content and shear strength.

4 FIELD INSTRUMENTATION

The field component of this research includes installation of subsurface sensors in a loess slope for a six month period over winter, spring and summer. Subsurface instrumentation will gather data on water content and soil suction during rainfall events. A similar approach has been used to investigate loess in China (Ng et al., 2003; Tsai and Wang, 2011; Xu et al., 2012, 2011; Zhou, 2012; Zhou et al., 2014). These data will allow analysis of the fundamental mechanics of rainfall-induced slope failures in loess in terms of its behaviour as a partially saturated soil.

4.1 Site Description

The field instrumentation will be installed in a grassed loess slope in Takamatua, Akaroa Harbour (Figure 2). The area to be instrumented is a north-facing 20° slope, approximately 90m

in elevation. The site has been selected because it is isolated from stock and easily accessible for equipment installation. Preliminary subsurface investigations indicate that the site comprises approximately 1.5m of loess colluvium overlying primary in situ loess of an unknown thickness. No ground water was observed within the upper 2.5m of the loess profile. However the moisture content of the loess colluvium was slightly higher than the in situ loess (between 19 – 22% for the loess colluvium, and 19 – 20% for in situ loess). Shallow slope instabilities are observed near the site. Hummocky, uneven ground is located upslope, and downslope of the site several erosion features have been observed in road cuttings.

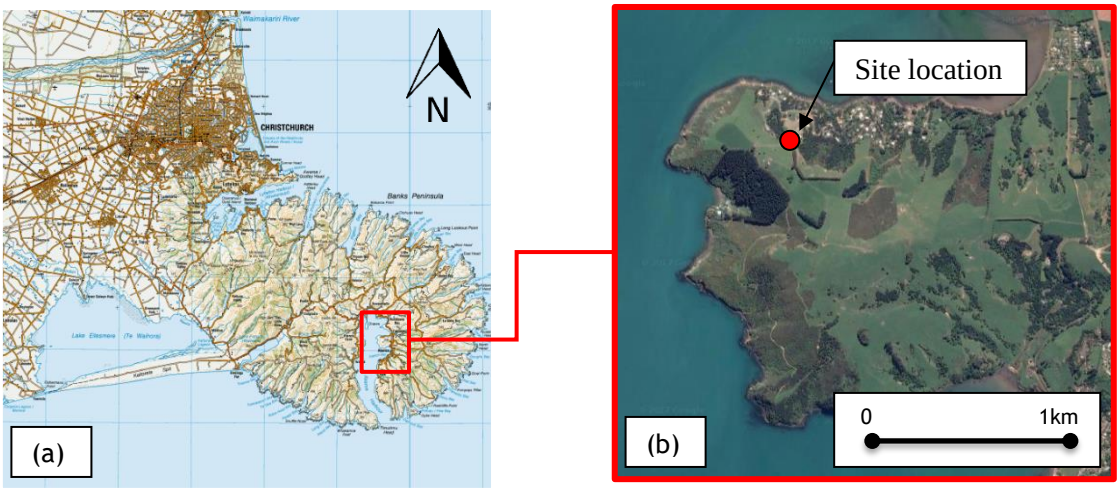

Figure 2: Site location for field instrumentation, (a) Topographic map of Banks Peninsula, (source: https://www.topomap.co.nz/ 1:250 000 Topographic map, accessed 6 March 2017) (b) Aerial image of Takamatua, (source: https://mapviewer.canterburymaps.govt.nz/ accessed 6 March 2017)

To enable the application of the results of the field monitoring to the surrounding Akaroa Harbour region, a detailed stratigraphy of loess in the area will be developed by mapping road cuttings at various sites. The purpose of this is to develop a regional geotechnical ground model incorporating lateral and stratigraphic variations in the loess soils geotechnical properties.

4.2 Instrumentation

The field instrumentation (Table 1) will be installed by hand auguring to the required installation depth. A 'dummy' frame will be pushed into moistened loess to form an indentation within the soil mass for the sensors to be installed. Once in the ground, the augur holes will be back filled. Back fill will be compacted to original field density to reduce the risk of preferential drainage.

Table 1: Sensors to be installed

Sensor type	Make	Quantity	Depths	Data collected
CS-616	Campbell Scientific	12	0.5m, 1.5m, 2.5m	Volumetric water content (%)
MPS-6	Decagon	12	0.5m, 1.5m, 2.5m	Soil suction (kPa)
Rain Gauge		1	Surface	Rainfall intensity (mm/min)

Data will be collected using a Campbell Scientific CR1000 data logger. Sensors will be installed in four arrays across the site (Figure 3). In each array there will be three CS-616 and three MPS-6 sensors. These sensors will be installed at three varying depths to capture progression of the wetting front during and after rainfall events. The data logger and rain gauge will be installed at the centre of the site.

Surface movement (if any) will be recorded by visual inspection and repeated real time kinematic GPS survey undertaken after each major rainfall event. Additional meteorological data, including temperature, sunshine hours, and barometric pressure near the site will be acquired from the NIWA database. Once the period of data collection has ceased, sensors will be removed by machine excavation. During this time samples will be obtained for laboratory testing. Further samples will be obtained from cuttings near the site for additional laboratory testing and Scanning Electron Microscopy (SEM) analysis.

Figure 3: Field monitoring site at Takamatua showing the location of the *in situ* instrument arrays. Site slopes towards the north.

Collectively, these data will allow comparison between the volumetric water content and the soil suction, and inform our understanding of the response of loess deposits to the infiltration of rain. Furthermore, these data can contribute to the soil water characteristic curve for the soil and present an in situ example of how rain infiltrates loess in the Akaroa Harbour area. Due to the known susceptibility of the loess in this area to moisture driven slope instability, it is important to gather such information to better understand the stability of slopes in these materials.

5 LABORATORY TESTING

Laboratory testing will be undertaken to examine the shear strength of the loess, and the relative contribution of microstructure and soil suction to the strength of the soil. The laboratory programme involves three components: investigation of index properties, triaxial testing, and the development of soil-water characteristic curves (Table 2). Undisturbed samples will be obtained by block sampling from existing exposures and from excavation at the instrumentation site in Takamatua.

Triaxial tests will be undertaken using a GDS motorised cell apparatus (Figure 4) to examine the soil strength behaviour in a laboratory setting. Testing will be undertaken at various moisture contents, including those recorded in situ at Takamatua. Correlation with soil suction during the tests will be obtained by the use of a soil water characteristic curve which will be developed during laboratory testing by means of the filter paper method and pressure plate test. This method allows the observation of soil suction in the absence of an unsaturated triaxial apparatus and direct measurement of soil suction during testing.

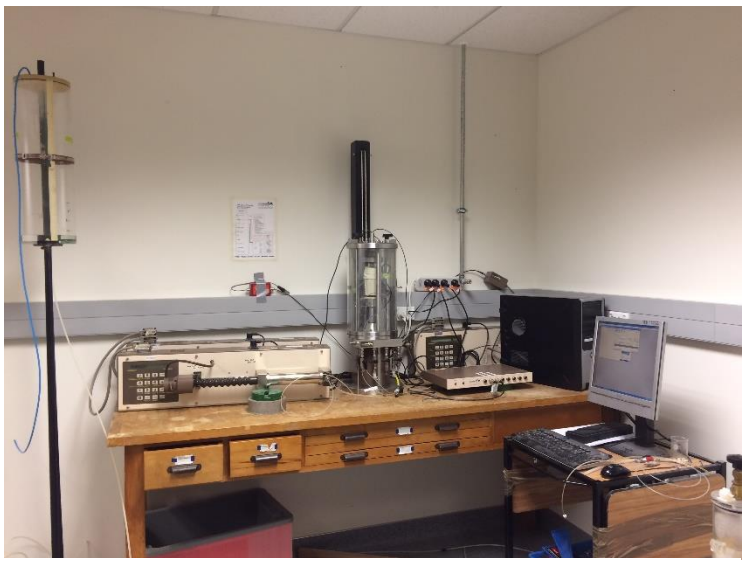

Figure 4: GDS triaxial cell

Triaxial testing will be undertaken on both undisturbed and remoulded *in situ* loess and loess colluvium to examine the influence of soil microstructure on the shear strength. In addition, pre- and post-failure samples will examined by Scanning Electron Microscopy (SEM) to investigate the role of inter-particle bonding during shearing. To examine the anisotropy of the soil mass, two orientations of *in situ* loess samples will tested using the triaxial apparatus. These orientations include sample alignment so that principle stress is normal to grain arrangement, and alignment so the principle stress is 45° to grain arrangement.

Table 2: Laboratory testing schedule

Category	Test	Purpose
Geotechnical index testing	Atterberg Limits	Examine relationship between particle size grading, clay mineralisation and plasticity of loess
	Particle size distribution and clay content (hydrometer method)	
	Clay mineralogy (XRD testing)	
	Moisture content (at start and end of field trials)	Examine change in gravimetric water content throughout field trials
	Dry density	Inform relationships between density and other geotechnical characteristics
	Specific Gravity	Characterisation & calculate initial void ratio
	Oedometer Test (stress history)	Examine consolidation state and infer impacts of stress state on soil consolidation Examine the possibility of collapse failure in loess
Soil water characteristics	Soil-water characteristic curve test (SWCC)	Determine the soil-water characteristic curve for both drying and wetting of the loess.
Triaxial testing on *in situ* and remoulded loess	Isotropically Consolidated drained test (ICD) and Isotropically Consolidated undrained test (ICU) (Monotonic loading)	Examine stress-strain relationship, volumetric change, dilatancy, pore water pressure, critical state line and stress paths for loess
	Anisotropically Consolidated drained test (ACD) and Anisotropically Consolidated undrained test (ACU)	Examine the influence of slope effects on the shear strength of loess

Category	Test	Purpose
	(Monotonic loading)	
	Constant deviator stress test (CQS)	Simulate the stress paths of saturated soil in a loess slope with a rise in groundwater level. Keep deviator stress constant but increase pwp.

6 PROJECT OUTPUTS

The primary purpose and output for this research is to develop a better understanding of soil-water characteristics of loess and loess-derived soils in Canterbury, New Zealand. This is achieved by examining the interaction between soil suction and volumetric water content in both a field and laboratory setting. By correlating field measurements with laboratory shear strength testing we can better understand how loess slopes respond to rainfall and the implication of this to slope performance and instability.

The outputs of this research include:

- Field observations on the behaviour of a loess slope in terms of soil suction and volumetric water content, subject to seasonal rainfall.
- Shear strength data from a range of moisture contents.
- Microscopic imaging of the soil microstructure of loess.
- Definition of the soil water characteristic curve for loess in Canterbury.

Because the current understanding of the soil microstructure of loess at this time is limited, SEM imaging will inform our understanding of the soil matrix characteristics (including particle shape, angularity, particle size, clay bonding, location and consistency of clays within microstructure). Using these data, we will be able to develop a better understanding of the performance of loess slopes for engineering design of cut slopes, foundations, and management of slope failures. Furthermore, this information will be able to inform land development and assessment of the slope failure susceptibility.

7 CONCLUSIONS

Loess deposits are widespread in Canterbury, New Zealand. Due to the susceptibility of loess slopes to failure during rainfall events, the relationship between shear strength and moisture content is important to understand. As a consequence, a proposed methodology for researching this has been outlined in this paper. By examining the interaction between soil suction and volumetric water content in both a field and laboratory setting, the shear strength of loess can be better understood. Data gathered during subsurface field instrumentation in Banks Peninsula will inform on how loess slopes respond to rainfall, and inform on the implication of this to slope performance and instability.

8 ACKNOWLEDGMENTS

Current research of Canterbury loess (Yates) is supported by Environment Canterbury and a University of Canterbury PhD scholarship.

REFERENCES

Alley, P.J., 1966. Cashmere Hills Loess. *New Zeal. Eng*. 424.

Almond, P.C., Shanhun, F.L., Rieser, U., Shulmeister, J., 2007. An OSL, radiocarbon and tephra isochron-based chronology for Birdlings Flat loess at Ahuriri Quarry, Banks Peninsula, Canterbury, *New Zealand. Quat. Geochronol*. 2, 4–8.

doi:10.1016/j.quageo.2006.06.002

Bell, D., Glassey, P.J., Yetton, M.D., 1986. Chemical stabilisation of dispersive loessical soils, Banks Peninsula, Canterbury, New Zealand, in: *5th International IAEG Congress*. Buenos Aires, pp. 2193–2208.

Bell, D., Trangmar, B., 1987. Regolith materials and erosion processes on the Port Hills, Christchurch, New Zealand, in: *5th International Conference & Field Workshop on Landslides*. Christchurch, pp. 93–105.

Bruce, J.G., 1973. Loessial deposits in southern South Island, with a definition of Stewarts Claim Formation. *New Zeal. J. Geol. Geophys.* 16, 533–548. doi:10.1080/00288306.1973.10431376

Griffiths, E., 1973. Loess of Banks Peninsula. *New Zeal. J. Geol. Geophys*. 16, 657–675. doi:10.1080/00288306.1973.10431388

Hughes, T.J., 2002. A Detailed Study of Banks Peninsula Shear Strength. MSc Thesis, Department of Geological Sciences, University of Canterbury.

Hutchinson, G., 1975. Akaroa Harbour suffers extensive earth movements. *Soil Water* 12, 6–7.

Ives, D., 1973. Nature and distribution of loess in Canterbury, New Zealand. *New Zeal. J. Geol. Geophys*. 16, 587–610. doi:10.1080/00288306.1973.10431382

Jowett, T.W.D., 1995. An investigation of the geotechnical properties of loess from Canterbury and Marlborough. MSc Thesis, Department of Geological Sciences, University of Canterbury.

McDowell, B.J., 1989. Site Investigations for Residential Development on the Port Hills, Christchurch. MSc Thesis, Department of Geological Sciences, University of Canterbury.

Ng, C.W.., Zhan, L.T., Bao, C.G., Fredlund, D.G., Ong, B.W., 2003. Performance of an unsaturated expansive soil slope subjected to artificial rainfall infiltration 53, 143–157.

Raeside, J.D., 1964. Loess Deposits of the South Island, New Zealand, and Soils Formed on them. *New Zeal. J. Geol. Geophys.* 7, 811–838. doi:10.1080/00288306.1964.10428132

Sparrow, C., 1948. Loess Deposits of Banks Peninsula. Unpublished MA Thesis, University of New Zealand.

Tonkin, P.J., Runge, E., Ives, D., 1974. A Study of Late Pleistocene Loess Deposits, South Canterbury, New Zealand. *Quat. Res.* 4, 217–231.

Tsai, T.L., Wang, J.K., 2011. Examination of influences of rainfall patterns on shallow landslides due to dissipation of matric suction. *Environ. Earth Sci.* 63, 65–75. doi:10.1007/s12665-010-0669-1

Xu, L., Dai, F.C., Gong, Q.M., Tham, L.G., Min, H., 2012. Irrigation-induced loess flow failure in Heifangtai Platform, North-West China. *Environ. Earth Sci.* 66, 1707–1713. doi:10.1007/s12665-011-0950-y

Xu, L., Dai, F.C., Tham, L.G., Tu, X.B., Min, H., Zhou, Y.F., Wu, C.X., Xu, K., 2011. Field testing of irrigation effects on the stability of a cliff edge in loess, North-west China. *Eng. Geol.* 120, 10–17. doi:10.1016/j.enggeo.2011.03.007

Zhou, Y., 2012. *Study on Landslides in Loess Slope Due to Infiltration*. University of Hong Kong.

Zhou, Y.F., Tham, L.G., Yan, W.M., Dai, F.C., Xu, L., 2014. Laboratory study on soil behavior in loess slope subjected to infiltration. *Eng. Geol.* 183, 31–38. doi:10.1016/j.enggeo.2014.09.010

Anchor load test results in Wellington soil and rock

A R Wightman
ENGEO Ltd, Wellington, NZ
awightman@engeo.co.nz

Keywords: anchor, load test, bond capacity, stiffness

ABSTRACT

Vertical and horizontal ground anchors are used frequently in Wellington. This study presents summaries of the results of tension tests of ground anchors across 33 sites in Wellington. The study includes ground anchors in soil and in rock, and both sacrificial and production anchor tests. Results of limit bond stress and stiffness are presented for several weathering grades of greywacke rock, and for several categories of soil. Suggestions for preliminary design values of limit bond stress and stiffness are provided for several soil and rock categories.

1 INTRODUCTION

Vertical ground anchors are used frequently in the Wellington region to increase the structural capacity of existing buildings or to support new buildings. Horizontal ground anchors are used to provide support to retaining walls and/or as horizontal support to buildings sited on steep terrain.

Anchors comprise drilled holes, typically of 100mm to 200mm diameter and of 6m to 15m length, comprising a steel bar in their centre, with an annulus of grout. They can be installed with a gravity grout ("drill and drop") technique, whereby the hole is drilled (with or without casing), the bar is installed and the grout is installed, typically from the base via a grout tube. Alternatively, the hole can be drilled with a sacrificial drilling bit on the bar, and a weak grout used during drilling. Once complete, a thick grout is injected into the hollow bar which then flows out through holes in the bar. These are referred to as injection grouted anchors.

The vast majority of the anchors in this study are gravity grouted as this is the most commonly used technique in Wellington. Anchors can be tensioned, or can be left un-tensioned, the latter sometimes referred to as "passive anchors" or "soil nails". This paper makes no distinction between tensioned and un-tensioned, calling both "anchors". Some anchors contain steel tendons, but all the anchors included in this study contained bar only.

2 SCOPE OF STUDY

Load testing of anchors is routinely carried out in Wellington, as the costs are relatively low, and the information obtained is of significant value to the designer. In particular, the designer, knowing that load testing will be carried out, can make a design assumption that is less conservative than if no load testing were planned.

This paper presents a summary of the load tests carried out in tension on anchors installed within the Wellington region, extending from the city's southern suburbs, as far north as Pauatahanui, and as far north-east as central Lower Hutt. 124 tests across 33 sites are included, with the majority of the tests within Wellington's central business district and inner suburbs.

Underlying most of the region is greywacke rock, and this is the natural target stratum for anchoring where it is close to the surface. Overlying the rock on the hills is colluvial soil, typically silt and gravel, which can be an adequate layer for anchoring to low loads. On the flat ground lie deep expanses of alluvial soils, and these often contain dense sand and/or gravel layers which are satisfactory anchoring strata. The load test data presented here cover all the geological units discussed above.

There are typically two general types of load tests carried out – sacrificial and production. Sacrificial tests are carried out on anchors installed solely for the purpose of testing, and the testing continues until either the bond has failed, the steel has reached yield (or near it) or the reaction system has reached capacity. Several cycles of loading are typically applied in sacrificial tests. Production tests are carried out as checks on anchors intended for use in the structure. They typically are tested to a load somewhat above the design load, with few cycles to avoid damaging the bond. Production tests are typically more numerous than sacrificial tests, and therefore make up the majority of tests (about 60%) in this study.

3 TEST RESULTS

Test results are presented in Table 1 for greywacke and in Table 2 for soils. Mean values are given for strength and stiffness, with a lower quartile also provided for sample sizes of 8 or more. For strength, bond stress (i.e. applied load divided by bonded area) and load per bonded length data are provided.

For greywacke, analyses were carried out for each grade of weathering, with a distinct increase in strength and stiffness seen from CW to HW. The data did not display a significant difference in strength between HW, HW/MW and MW, hence the values for these designations are lumped together and presented alongside the separate results for HW and MW. MW did however show a distinct increase in stiffness from HW. The data for HW/MW were too inconclusive to warrant their own data column.

Stiffness values are presented as bulk stiffness – that is, the load divided by the deflection of the bar at the anchor head. Anchor stiffness is a function of both the elastic stretch in the bar and the slip that occurs between the grout and the ground. The data below indicate that the bulk stiffness of anchors increases markedly with increasing ground quality, suggesting that grout to ground slip may be the governing element of overall anchor stiffness.

Table 1: Greywacke parameters

119/212 (8) denotes a lower quartile of 119, a mean of 212 and a sample size of 8. Lower quartile values are only presented for sample sizes of 8 or more.

	CW	CW/HW	HW	MW	Combined HW, HW/MW and MW
Number of sites	2	2	10	3	15
Number of tests	8	4	32	15	56
Range of bonded lengths (m)	3.5 – 4	2 – 3	2 - 8	1 – 14	1 – 14
Average bonded length (m)	3.8	2.75	3.8	7.4	4.8
Range of grout diameters (mm)	100 – 150	100 – 135	100 - 200	100 – 200	100 – 200
Maximum load achieved (kN)	315	439	1500	2200	2200

	CW	CW/HW	HW	MW	Combined HW, HW/MW and MW
Average bond stress achieved (kPa), not necessarily limit stress	119	214	437	329	410
Bond stress at limit (kPa)	-/136 (5)	-/170 (3)	-/459 (6)	NR	269/537 (9)
Bond stress at 25mm displacement (kPa)	-/153 (2)	-/207 (1)	366/515 (10)	-/228 (5)	246/474 (17)
Load per bonded length at limit (kN/m)	-/56 (5)	-/86 (3)	-/194 (6)	NR	128/242 (9)
Load per bonded length at 25mm displacement (kN/m)	-/54 (2)	-/85 (1)	167/244 (10)	-/144 (5)	154/234 (17)
Stiffness (kN/mm)	8/11 (8)	-/19 (3)	23/36 (32)	33/55 (15)	24/43 (56)

For soils, the division into categories was more subjective and several grouping combinations were possible. The groupings presented below represent the most useful and consistent reporting in the author's opinion.

Table 2: Soil parameters

	D-VD gravel and sand	MD-D sand and silty sand	St-VSt silt/clay with some gravel content	F-H Silt
Number of sites	6	3	1	7
Number of tests	22	4	15	13
Range of bonded lengths (m)	4.5 – 10.1	6.0 – 12.5	3 – 5	2 – 7
Average bonded length (m)	6.7	10.75	4	5.3
Range of grout diameters (mm)	100 – 220	150 – 200	100	75 – 150
Maximum load achieved (kN)	2700	730	575	272
Average bond stress achieved (kPa), not necessarily limit stress	210	123	218	79
Bond stress at limit (kPa)	-/303 (3)	NA	-/271 (1)	-/79 (5)
Bond stress at 25mm displacement (kPa)	119/212 (8)	-/98 (2)	-/363 (5)	-/56 (5)
Load per bonded length at limit (kN/m)	-/167 (3)	NA	-/85 (1)	-/31 (5)
Load per bonded length at 25mm displacement (kN/m)	75/115 (8)	-/54 (2)	-/114 (5)	-/20 (5)
Stiffness (kN/mm)	29/36 (21)	-/29 (4)	13/16 (15)	4/7 (11)

Notes on the tables:

CW – Completely weathered; HW – Highly weathered; MW – Moderately weathered
VD – Very dense; D – Dense; MD – Medium Dense
F – Firm; St – Stiff; VSt – Very stiff; H – Hard
NR – Not reliable, there were only two tests in MW that reached their limit, and they were significantly different values.
NA – Not applicable – none of the tests reached the apparent bond limit.
Stiffness was calculated as (max load) / (max deflection), unless the deflection exceeded 25mm, in which case it was calculated as (load at 25mm deflection) / 25mm

Most of the groups showed a wide variability in the limit bond stresses. The HW greywacke group showed the most variability, with limit bond stresses varying from 51 to 1009 kPa. The second lowest limit value was 170 kPa. It is suspected that the two lowest values are both from errors during drilling or grouting, rather than variability in the ground conditions. The range in anchor stiffness values within groups was similarly wide.

One site (on The Terrace) represents 60% of the data for highly weathered greywacke 54% of the data for all greywacke. There is therefore a possible over-reliance on the one site, although the values from this site do not differ greatly from typical numbers for other sites.

4 COMPARISON WITH MEMORIAL PARK DATA

In a separate study, Christie et al (2015) reported on sacrificial anchor load tests for Memorial Park in Wellington. The programme included load tests on ten injection grouted anchors and five gravity grouted anchors, with tests carried out in soil and rock. Grout diameters ranged from 100 – 180 mm.

All rock anchors extended into CW greywacke, with peak bond stress values of 172 – 283 kPa reported, somewhat higher than the mean limit bond stress values in Table 1. Peak bond stresses in soils varied from 130 kPa in Upper Pleistocene Alluvium (clayey gravelly silt), 155 – 292 kPa in Lower Pleistocene Alluvium (clay silt sand and gravel mixtures) and 110 – 183 kPa in Colluvium / Residual Soil (clay silt sand and gravel mixtures).

Christie et al do not specifically report the densities of the various soil layers, so comparison with the figures in Table 2 is challenging. The average peak bond stress value reported in soil by Christie is 181 kPa, with all soil layers containing gravels, which shows a degree of consistently with the D-VD gravel and sand column of Table 2.

5 COMPARISON OF INJECTION GROUTED VERSUS GRAVITY GROUTED

Christie et al reported results on injection grouted and gravity grouted anchors in Lower Pleistocene Alluvium at Memorial Park. Injection grouted anchors had a peak bond stress of 155 to 260 kPa, and gravity grouted anchors a peak bond stress of 196 to 292 kPa, indicating that gravity grouted anchors had a slightly higher strength.

At a site in central Wellington, forming part of the current study, with the bonded length in MD – VD sands and gravels, an injection grouted anchor (described by the contractor as “installed under grout flush”) had a peak bond stress of 360 kPa with a stiffness of 29 kN/mm. The limit bond strength was not clearly reached. A gravity grouted anchor at the same site, but installed by a different contractor, reached limit bond stress at 185 kPa, with a stiffness of 20 kN/mm. Thus, at this site, the injection grouted anchors had a much greater strength and slightly greater stiffness,

although this could be at least partially a reflection of the difference in technique between contractors.

6 CONCLUSIONS

6.1 Preliminary bond capacities

Taking into account the results of this study, and that of Christie et al, the following tentative recommendations for preliminary design of ground anchors in Wellington are presented. As the variability amongst the soil or rock categories is substantial, load testing should be carried out on site to confirm the design values. When using these (or any) values, increases in total anchor strength for bonded lengths beyond 6m or 8m may not be achieved.

The values chosen are intended to represent a range approximating the lower quartile to the mean. It is considered that designing for the lowest recorded value in each group is unreasonably conservative, as these may be a result of drilling or grouting errors. Such errors could of course occur in any given job, but it is hoped that any such errors are detected by project quality assurance, in particular load testing on production anchors.

Table 3: Suggested preliminary bond capacities

Material	Preliminary ultimate bond capacity (kPa)
CW greywacke	110 – 150
HW/MW greywacke	300 – 500
D-VD gravel and sand	150 – 230
MD-D sand and silty sand	90 – 150
F-H silt	50 – 80

6.2 Stiffness

In some cases, particularly in the strengthening of existing structures containing brittle elements, deflection may the governing criterion in design. For example, deflections of more than 10mm or 15mm may not be acceptable, in which case an understanding of stiffness of proposed anchors becomes important. In such cases, use of the stiffness values in the bottom row of Tables 1 and 2 could be considered for preliminary design. As discussed in Section 3, the values reported are bulk stiffness values, so could be too high if used for anchors with long unbonded lengths.

As nearly all anchors in the study returned a stiffness value, there is more data for stiffness than for strength, and hence the lower quartiles and averages in Tables 1 and 2 are considered likely to be more reliable. However, the range within categories is high, so stiffness values should also be checked by site-specific load testing.

6.3 Injection Grouting

On the small sample size in the study and presented by Christie et al, it is inconclusive as to whether injection grouting provides a stronger bond than gravity grouting in Wellington soils.

6.4 New Zealand Geotechnical Database

The knowledge of bond capacity within the geotechnical community could be advanced by allowing anchor load test results to be uploaded to the New Zealand Geotechnical Database. It is suggested that uploaded information should include a log of the ground conditions, whether the

anchor was horizontal or vertical, the steel used, the free length, the bonded length, the grout diameter and a table showing the load cycles, with deflections and duration of load at each load increment.

7 ACKNOWLEDGEMENTS

Thanks to my colleagues Ollie Van Rooyen and Neil Charters for their reviews of the text.

REFERENCES

Christie, E.B., Van Rooyen, O., Meiring, C. & Symmans, B. (2015) Ground anchor testing in Wellington soils and weathered Greywacke. *Proceedings of the 12th Australia New Zealand Conference on Geomechanics*

Groundwater control using slurry cut off walls in acidic soils

N J Wharmby
March Construction, Auckland, NZ.
nwharmby@marchcon.co.nz (Corresponding author)

J-L Gorinas
GHD Consultants, Auckland, NZ
Jean-Luc.Gorinas@ghd.com

Keywords: Groundwater, Cut off wall, Acidic soils, Peat, Slurry walls.

ABSTRACT

To facilitate the development of residential area a major upgrade of the storm water management system was required using open channels and flow attenuation ponds. The area is underlain by soft alluvial soils comprising organic silts, clays and peat. The high groundwater level and compressible soils makes the area susceptible to long-term settlement if the general groundwater level is reduced. With storm water channels extending to 3m below groundwater level some form of cut off wall was required to prevent significant groundwater drawdown and associated settlements.

Following an optioneering phase the use of a slurry cut off wall was considered the most appropriate given the site conditions and identified risks. Whilst uncommon in NZ there is significant worldwide use of the method for groundwater or leachate migration control. A slurry wall is excavated under self-hardening cement bentonite slurry; the soil is fully replaced by the slurry. A specific mix design is developed based upon the material sources to ensure that it has the fluid properties required for installation and the hardened properties to provide an effective long-term low permeability barrier.

The paper covers the following aspects of the slurry cut off wall methodology:

- Project requirements
- Material selection
- Laboratory trials and mix development in France
- Site establishment
- Site controls and verification
- Project challenges and solutions
- Project learnings

1 PROJECT REQUIREMENTS & BACKGROUND

A new 2.3 km long stormwater conveyance corridor was required to facilitate the development of a 164 hectare rural catchment. Zoning of the land allowed for significant residential development, however the lack of stormwater infrastructure restricted growth prior to the implementation of this project.

The stormwater conveyance corridor varies in width from 20 to 50 m and includes:

- A series of open water bodies / wetlands maintained by weirs
- Riparian planting alongside the channel, with specimen trees throughout the corridor
- Shared paths, boardwalks and play areas along the corridor
- High level pedestrian bridges / crossings
- Trafficable culvert crossings

The area is underlain by soft alluvial soils comprising organic silts, clays and peat. The high groundwater level and compressible soils makes the area susceptible to long-term settlement if the general groundwater level is reduced. The depth of the stormwater channel varies with a maximum depth of approximately 3m below groundwater level. To reduce the extent and magnitude of groundwater drawdown, and potential settlement, some form of mitigation was required. A number of options were considered including lining the channel, piping a length of the channel or installing an in-ground cut-off barrier. An in-ground cut-off barrier was the preferred option for managing groundwater drawdown related effects of the channel

1.1 Ground Conditions

The geology in the area based on the 1:250,000 geological maps include Recent Alluvium and Puketoka Formation Alluvium comprising soft peats, organic silts and sands. In the eastern area of the catchment, residually weathered East Coast Bays Formation are mapped, comprising stiff clays and silts and clays of the Waitemata Group. Soils and rock of the Auckland Volcanic Group are also present near the site. The detailed geotechnical investigation undertaken by GHD in 2014/15 confirmed this sequence.

For the stormwater conveyance channel design and mitigation measures the alluvial deposits are most influential. These comprise amorphous, fibrous and spongy peat material with interbedded organic cohesive soils and locally non-organic silts and clays, thin beds of rhyolitic ash and locally extensive pockets of wood, kauri stumps and large tree trunks.

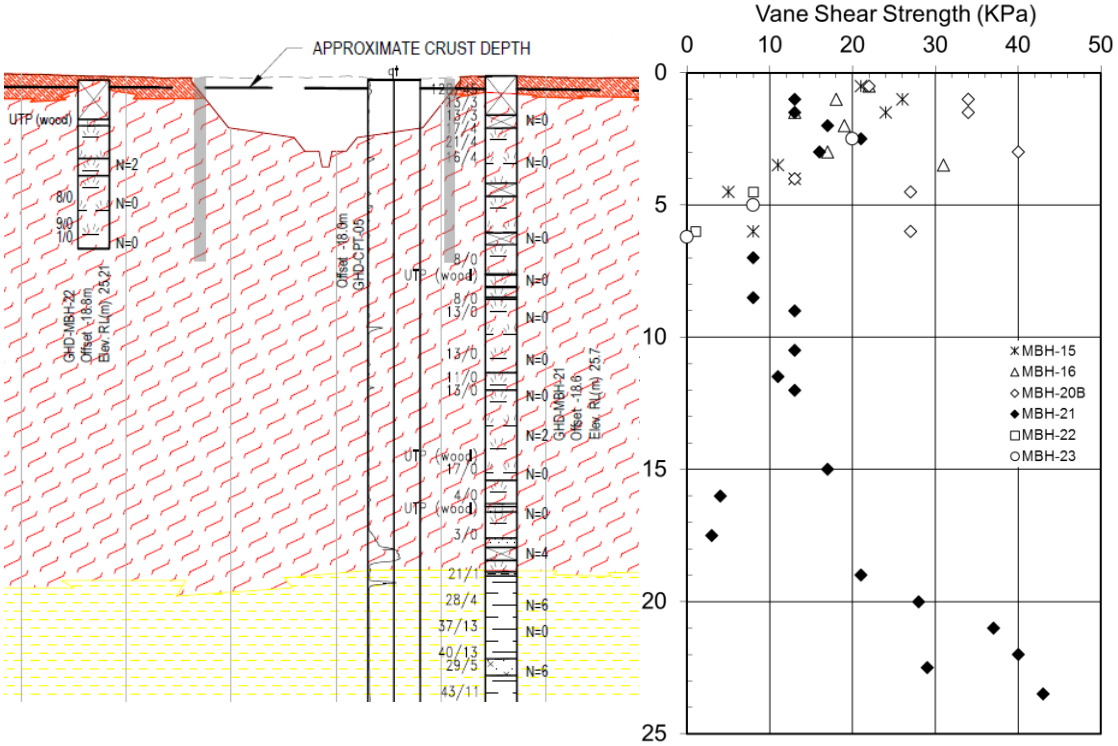

Figure 1: Typical Geotechnical Section and Vane Shear Strength Profile

There are rhyolitic ash layers, with a consistent 100 mm to 500 mm thick layer encountered in many investigation locations at around 1.0 – 1.5 m depth. Thinner lenses were found incorporated into peat deposits which were associated with carbonaceous bands above and below suggesting combustion. This and some of the large logs and stumps found in the sequence may be due to past eruption events.

Peat deposits were encountered in all investigation locations extending from near surface to between 2.2 m and 21 m depth. Peat deposits generally thinned out to the southeast with thickest deposits identified at the northern end of the northern channel alignment. Associated soil and ground water chemistry tests indicated acidic conditions with a pH as low as 4.2

1.2 Hydrogeological Conditions

The deep groundwater movement in the wider Takanini-Drury area is strongly influenced by the presence of large scale structural faulting within the basement Greywacke (and Waitemata Group) rock which effectively compartmentalise the regional groundwater flow system. The site location lies to the east of the inferred Drury Fault line which influences deep groundwater flows. That said, it is the shallow groundwater system resides within the recent Tauranga Group alluvial sediments that will potentially be affected by the stormwater channel. The groundwater flow direction is from east to west with groundwater draining into the Manukau Harbour inlet via the McLennan wetland. Hydraulic gradients are generally fairly flat.

Depths to groundwater in the shallow unconfined aquifer system range from 0.6 m in the eastern part of the subject site to 1.0 m to 1.5 m near Cosgrave Road and are >1.5 m depth in the south western part of the site near Grove Road. A strong relationship between site topography and groundwater levels is noted to exist with groundwater encountered at shallower depths in the eastern part of the site where the ground surface is flatter. In the west, the depth to groundwater increases with proximity to McLennan Park and drains towards the ponds.

The vertical permeability of the peat was estimated as between 1x10-4 m/s to 1x10-6 m/s, while the horizontal permeability was estimated between 1x10-5 m/s to 1x10-7 m/s. These values were confirmed via a long-term pumping test of the groundwater and analysis of the resulting dewatering curve.

1.3 Cut off Wall Requirements

Groundwater flow modelling of the stormwater channel section was performed using the derived soil parameters to understand the drawdown profile resulting when the stormwater channel was in steady state low flow conditions. The potential impact extended to over 100m away from the channel that would result in unacceptable long term settlement. Sensitivity analysis considering the location and depth of the cut off wall lead to the selection of a 7m deep wall located within the batter of the channel with a permeability, k = 1x10-8 m/s.

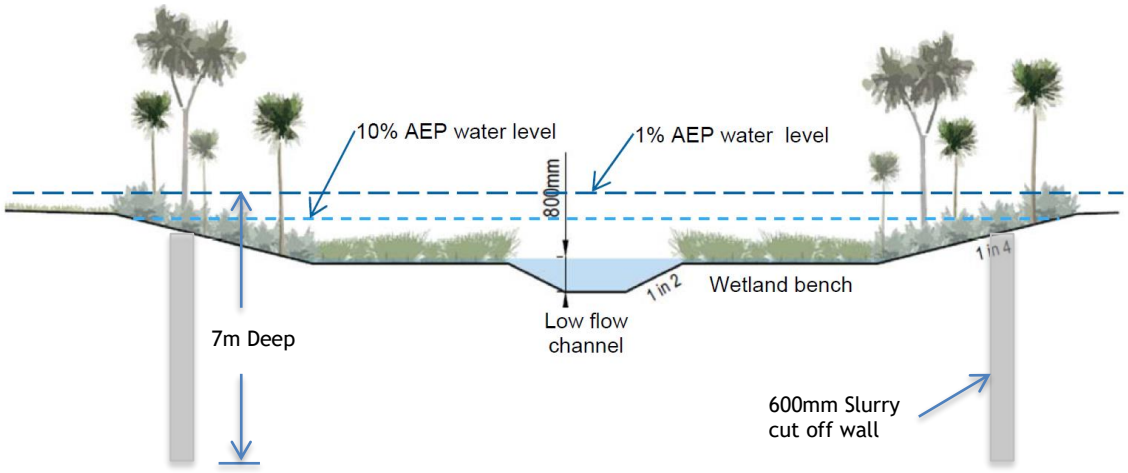

Figure 2: Typical channel section with slurry cut off wall

2 OPTIONEERING

A ground water cut off can be formed by a number of different construction methodologies including concrete panels, secant piles, sheet piles, soil mix walls and slurry walls. Whilst cost is the primary driver it is the final cost to complete the works to the desired performance criterion that must be evaluated taking into account the associated risks.

The most efficient installation solution needs to consider how the ground conditions will affect the installation and the impact on the long term properties of the cut off wall. At this site the primary physical factors are:

- soft organic soils
- high ground water level
- acidic soils
- potential buried timber obstruction

Table 1 provides a list of potential options with comparative evaluation against cost and other risk factors.

Table 1: Option evaluation - primary risk and cost

Construction Methodology	Permeability	Durability	Soil Acidity	Obstructions	Cost
Diaphragm or Secant pile walls (Cased / CFA)	Multiple cold joints ✓✓	Concrete mix design to standards ✓✓✓	Replacement methodology ✓✓✓	Coring ✓ Impact on sequencing ×	$$$$$
Soil Mixing (DSM / CSM, Trenchmix©)	Homogeneity of soil mix & cold joints ××	Binder selection & dispersion ✓×	Effect on binder reactivity ××	Impact on mixing and homogeneity ××	$$$$
Sheet Piling - lightweight steel	Sheet pile joint / clutch treatment	Sacrificial thickness ✓	Corrosion ××	Installation and material / clutch damage	$$
- Mandrel - driven GRP	✓	✓✓	✓✓	×××	$$$
Slurry Wall	Mix design & Verifiable ✓✓✓	Mix design and material selection ✓✓✓	Replacement methodology ✓✓	Coring but effect on soft organic soils ✓	$$$

In terms of providing a reliable cut off wall solution the diaphragm wall or secant pile wall using appropriate materials would be the most robust solution as it represent a soil replacement method but has the highest cost. The use of deep soil mixing provides a potentially cheaper methodology because it uses the soil to form the structure but relies on the effective dispersion and reaction of a binder and the soil. An earlier trial on the site highlighted that the acidity, organic matter and timber adversely affect the reactivity and dispersion of the binder which compromised the quality of the cut off formed. This leads to a strong preference to adopt a replacement methodology.

If the basic cost was the selection criterion for a replacement method, the use of a thin wall steel sheet piles would be the obvious choice. The acidic conditions make the long-term performance questionable leading to consideration of alternative mandrel-driven GRP sheet pile options. However, large timber obstructions are known to be present in the area; these represent a significant installation risk. Apart from the programme and material wastage issues the primary risk is associated with potential damage / de-clutching which ultimately affects the integrity of the cut off wall.

A slurry wall using appropriate materials and self-hardening mix design can meet the long-term cut off wall requirements as it is a replacement methodology. The obstructions can be removed by the excavator with the fluid slurry to maintaining a stable trench. The obstruction risk associated with this methodology is primarily the additional time and slurry consumption.

3 SLURRY WALL METHODOLOGY

Soletanche Bachy have used of slurry walls to provide low permeability cut off walls around the world typically to contain plumes of contamination or contain leachate from landfill sites. The method involves the excavation, removal and replacement of the soil with self-hardening slurry to form the trench. The nature of the landfill, soil or other material that the trench is constructed through generally has no impact on the strength and permeability of the slurry. The excavation under the full pressure of the fluid slurry serves to support the trench and prevent the ingress of groundwater resulting in no contamination and delivery of a full replacement methodology. When hardened and below the water table the slurry is of low density with a permeability in the order of 1 x 10-8 m/s. Above the water table the slurry can desiccate without appropriate cover / capping.

3.1 Quality control of slurry wall

Apart from the basic slurry trench geometry, the slurry wall quality control is focussed on the slurry material so generally the following is implemented:

a) The design of the slurry mix is undertaken in the laboratory to test the interaction of the mix-water, cement, bentonite and other cement replacement materials.
b) Quality control of the slurry is via batching records and tests carried out to evaluate fluid properties (primarily density, pH and viscosity) for mix consistency.
c) Wet sampling from different depths in the trench is used to form specimens and facilitate strength and permeability testing as required.

3.2 Slurry wall materials

The soil chemistry and in this particular case the pH = 4.2 – 4.5 needs to be considered for long-term durability; General Purpose (GP) OPC is not sufficient based upon the Soletanche Bachy experience of forming slurry cut off walls in acidic soils with a pH in the range of 3.0 – 5.0. Blended cement with 60% GGBS was recommended based upon the following:

a) Where soil / water pH < 4 durability is an issue and a membrane advocated.
b) Where soil / water pH is in the range 4.0 – 4.5 the use of OPC / GGBS blended cements are required, adding a further element, PFA, blend can increase overall durability.
c) The GGBS replacement reduces the strength development of the slurry.

Around the world GGBS and PFA by-products are widely used to reduce cost at cementitious replacement levels of between 30 – 90%. The use of these blended materials has many affects including reduced heat of hydration and improved durability in concrete. However, these materials are not readily available in New Zealand resulting in the use of Duracem, an imported Holcim blended cement.

4 SLURRY TRIALS IN FRANCE

A slurry wall has not been used in such conditions in New Zealand to form a long-term groundwater cut off. The use of the imported cement and bentonite makes a robust mix design trial essential to provide confidence in the site batched product. It is also worth noting that test results are not available for 28 days which impacts the programme and means a significant volume of slurry is produced at an industrial level prior to QC results being obtained.

Soletanche Bachy has a research and development laboratory in Paris, France that has testing facilities and experts in the geotechnical and associated geo-materials field. The ability to draw on this international experience is invaluable to minimise learning curves when applying new technology. The laboratory testing programme was based upon the approach used on similar

successfully delivered grout, slurry and soil mixing projects; comparison of the fluid and hardened properties with similar mixes is also possible as can be seen in Figure 2.

All materials were sampled and sent to the laboratory in Paris. The testing regime implemented based upon the following objectives:

- Fluid properties - Viscosity: 32 < MVF < 50 s
  - Stability: Bleeding @3h < 5%
- Long-term - Permeability: k = 1 E-08 m/s
  - Strength: UCS @ 28 days > 1.5 MPa

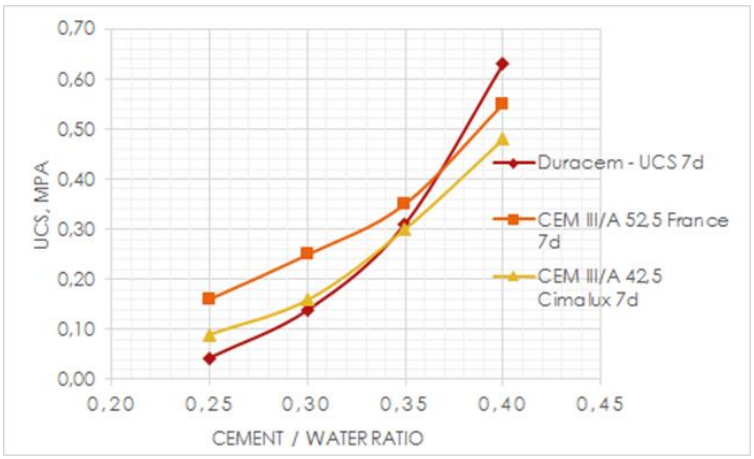

Figure 3: Cement reactivity comparison from other Soletanche Bachy projects

A series of mixes were prepared to understand the sensitivity of the fluid and hardened properties of the slurry constituents. It is worth noting that the samples prepared for permeability testing use disposable crystal plastic moulds to ensure representative results. The long-term permeability was the critical parameter but it is important to recognise that this test is time consuming to perform and hence the use of strength represents a good early quality control guide.

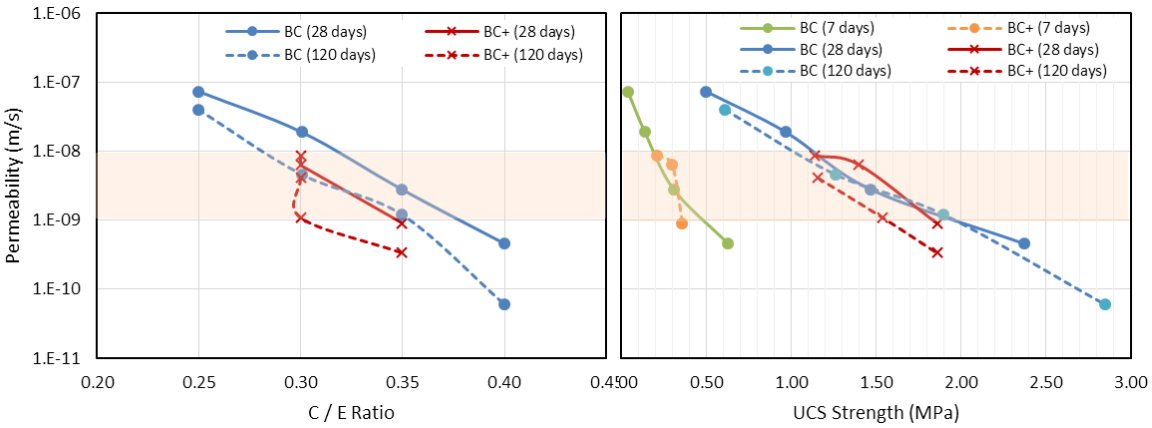

Figure 4: Laboratory trial summary permeability and strength results

The selected mix design needs to consider that the laboratory trials represent very accurate batching and efficient mixing. Industrial batching and mixing will result in more variability. Furthermore, the impact of the excavation process and potential contamination by soil or groundwater whilst excavation through the slurry needs to be considered. To provide some margin an order of magnitude in the target permeability it is normally considered appropriate.

5 SLURRY WALL INSTALLATION

The slurry batching plant was set up with automated mixer, bentonite mixer, bentonite hydration tanks, cement silos and slurry reticulation. The mixing process is shown schematically in Figure 5. Excavation was performed with a long-reach excavator.

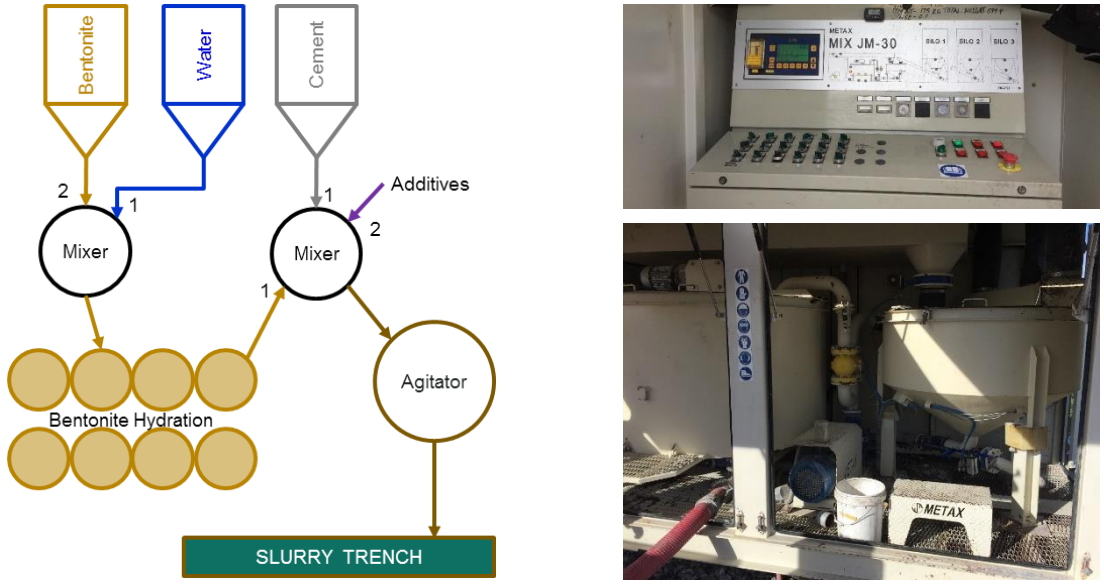

Figure 5: Mixing methodology

5.1 Monitoring of the slurry production

During the initial stages of slurry production intensive sampling and testing was adopted to facilitate training, allow benchmarks to be established with the site team and to ensure site batched material was in line with the laboratory trials. The fluid properties of the bentonite slurry pre & post hydration were tested to optimise production mixing and hydration time. The fluid properties of self-hardening cement bentonite mix were visually monitored as "instantaneous" quality control to ensure consistency of the mix; density, pH, viscosity and bleed tests were recorded. For strength and permeability testing four samples were made for each, sufficient for 7, 28 and 56 day testing.

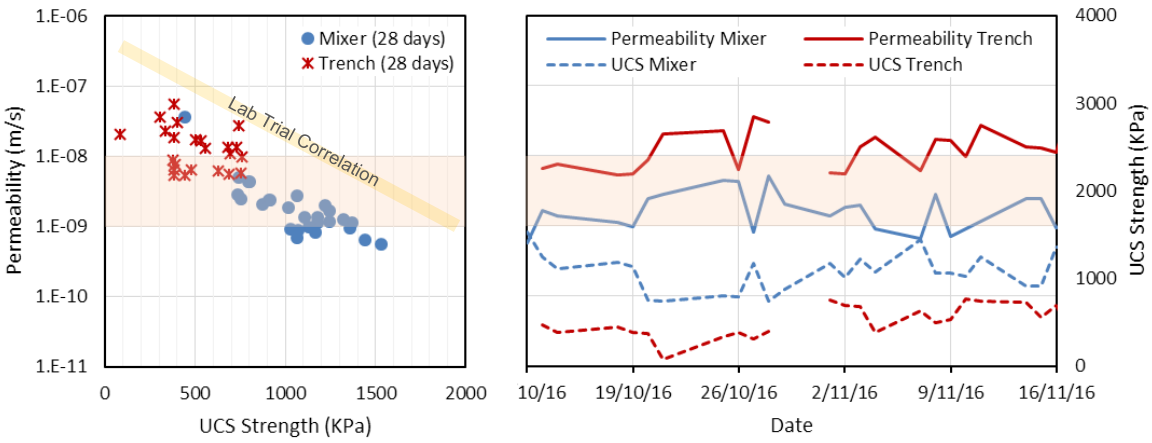

Figure 6: Industrial permeability and strength results

As can be seen from Figure 6 there is a reasonably good correlation between strength and permeability albeit offset from the laboratory trial data. It is also evident that the results from the

mixer are better than those from the trench in terms of strength and permeability at a test age of 28 days.

5.2 Obstructions in soft organic deposits

The primary issue on the site was the extensive buried timber obstructions typically encountered between 2m and 4m depth. These tree trunks were in some cases up to 2m in diameter and several metres in length. From a design perspective it was not acceptable to leave these obstructions encapsulated in the slurry wall as future excavation or degradation would compromise the integrity of the slurry cut off wall. Following a probing exercise, it was possible to re-align the wall around some of the obstructions where the site delineation and development extents permitted. Where this was not possible coring was carried out to cut and remove the obstruction; using light weight plant given the low bearing capacity crust / working platform.

Figure 7: Slurry wall installation and obstruction removal

6 LESSON LEARNT

The acidic ground conditions and obstructions at the site make the installation of a permanent cut off wall challenging which provides a number of key points of learning, namely:

1. As part of a global company with appropriate connections it is possible to find potential solutions to address similar challenges; in this case slurry cut off walls in acidic soils.
2. Well planned laboratory mix trials using the actual materials are essential to develop a robust mix design; noting the difference between laboratory and industrial processes.
3. Variability of the fluid properties of bentonite, above API minimum standards, can impact slurry mixing; monitoring fluid properties is a good quality control mechanism.
4. The slurry sampling from the trench needs to be representative.
5. The removal of obstructions in a low strength high water content soil matrix will cause loss of structure and strength reduction; this disturbance can result in slurry wall contamination requiring pre-treatment.

7 CONCLUSIONS

A cut off wall has been successfully implemented in the prevailing acidic ground conditions using a cement bentonite slurry wall. This outcome is due to the collaboration between Auckland Council (Client), GHD (Designer) and March Construction (Contractor) with the technical support of the Soletanche Bachy laboratory. It is fair to say that the obstructions were a particularly challenging but solutions were developed to locate and overcome these and as a result a further phase of work is underway

Numerical simulation of inclined piles in liquefiable soils

Y Wang & R P Orense
Department of Civil and Environmental Engineering, University of Auckland, NZ.
ywan833@aucklanduni.ac.nz (Corresponding author)

Keywords: inclined pile; liquefaction; OpenSees; soil-pile interaction

ABSTRACT

A three-dimensional finite element model (3D FEM) has been developed in OpenSees to investigate the seismic response of inclined piles in liquefiable sand. The spring interface method is compared with the no interface approach in which pile and soil are bonded directly together to shed light on the effects of soil-pile interaction. By employing a Pressure-Dependent Multi-Yield surface material (PDMY02) model for the saturated sand, the seismic behaviour of sand under liquefaction is taken into consideration. By verifying modelled results with corresponding case studies on vertical pile in liquefied ground, the proposed modelling method is shown to be suitable for the simulation with acceptable accuracy. Based on the proposed model with inclined piles, a series of numerical analyses is conducted to examine the influence of raked angle and liquefaction on the seismic response of the model. It is concluded that pile inclination could be beneficial in reducing the lateral displacement of the superstructure but results in increasing pile shear forces. It is recommended that inclined piles are designed to accommodate these additional shear demands.

1 INTRODUCTION

Inclined piles are believed to be able to resist higher lateral loadings than vertical piles by transferring part of the lateral force into the axial direction. On one hand, evidences have revealed that the inclined piles designed properly may be beneficial for both the superstructure and piles themselves. For example, Berrill et al. (2001) investigated the Landing bridge in New Zealand after the 1987 Edgecumbe earthquake and found the effective impact of raked piles against lateral spreading. On the other hand, there are several frequently mentioned drawbacks resulting in the discouragement of the use of inclined piles in the seismic design of foundations. These drawbacks include residual bending moment due to soil consolidation (pre-earthquake) and settlement (post-earthquake), large kinematic force at the pile-cap connection, reduction in bending capacity due to the tensile axial forces and undesirable rotation on the cap supported by non-symmetrical batter piles (Gerolymos et al., 2008).

The beneficial or detrimental role of inclined piles on the dynamic behaviour of the superstructure and foundation is still not well established, despite numerous research carried out by means of laboratory tests and numerical investigations. Most of the laboratory experiments have been performed on dry sand or clay (Li et al., 2016; Subramanian & Boominathan, 2016). Only a few experiments focused on the seismic response of inclined piles in liquefiable soil (Dash & Bhattacharya, 2015; McManus et al., 2005). Numerical methods found in literature are mainly based on FEM methodology with different implementations, including sophisticated FEM models, coupled boundary element and FEM models and simplified non-linear system of springs and dashpots based on Winkler's assumptions. However, in most of the numerical simulations, the soil is modelled as elastic material for simplication (Ghorbani et al., 2014; Goit & Saitoh, 2013).

This paper discusses a series of 3D FEM analyses which were carried out through the platform of OpenSees (Open System for Earthquake Engineering Simulation), a freely available software

sponsored by PEER (Mazzoni et al., 2007). The seismic behaviour of liquefiable soil was taken into consideration by an appropriate constitutive soil model. A nonlinear spring soil-pile interface was adopted and compared with the no interface method in which the pile nodes were directly tied with the soil nodes. The numerical model was firstly verified by modelling a vertical pile and compared with experimental data. The model was then adopted for modelling inclined piles. By changing the raked angle of the pile (0°-20°), a parametric analysis was finally conducted to investigate the seismic response of the system.

2 VERTICAL SINGLE PILE ANALYSIS

2.1 Model description

In order to verify the numerical method, a vertical single pile was modelled and the results were compared with a centrifuge experiment (CSP3-J) from Wilson (1998). The prototype partial model layout is shown in Figure 1a. In the test, an aluminum pipe with an outer diameter of 670 mm and wall thickness of 19 mm was installed into the layered Nevada sand. The pile toe was about 3.9 m above the base and the pile head was about 3.8 m above the ground surface. The relative densities of the soil in liquefiable and non-liquefiable layers were about 55% and 80%, respectively. A superstructure weighing 49.1 ton was put on the pile head and the 1995 Kobe earthquake acceleration record (Figure 1b) was scaled to 0.22 g as the input motion.

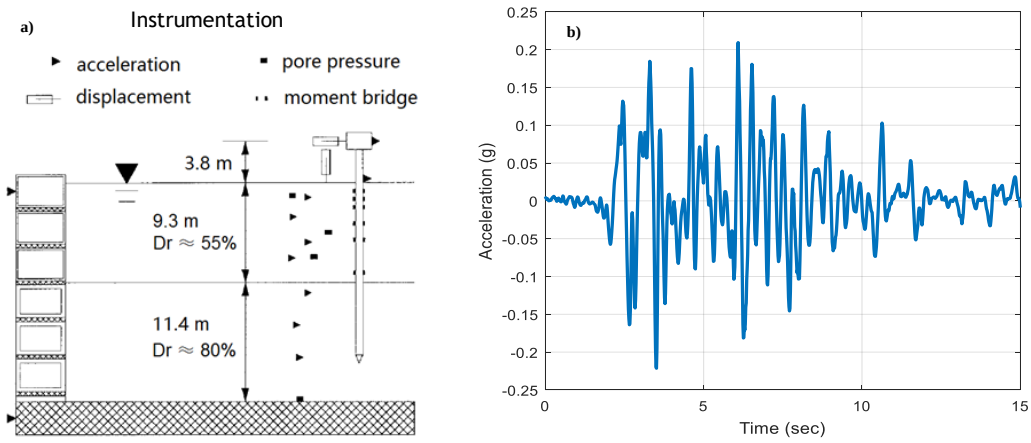

Figure 1: a) Partial model layout (Wilson 1998); and b) 1995 Kobe earthquake motion used in the centrifuge test and numerical modelling

Because of symmetry, only half of the model (32.0 m × 6.0 m × 20.7 m) was simulated as shown in Figure 2a. The horizontal black line in the soil represents the interface of the two soil layers. The saturated soil was modelled using 8-node BrickUP elements (element size varied) implemented with the PDMY02 material (Yang et al., 2003). The properties of the Nevada sand (Table 1) were derived from Choobbasti & Zahmatkesh (2016) and Karimi (2016). The bottom of the model was fixed in all three directions and nodes at the same depth on the left and right sides were tied together in the *x*-direction to simulate the free-field condition. For the front and back boundaries, translational displacements in the *y*-direction were not allowed. Moreover, water could drain from the ground surface only. Displacement-based beam elements were adopted to simulate the pile which was considered as an elastic material.

Based on Cheng & Jeremić (2009), a series of stiff elastic beam elements (rigid links) was used as "connections" between pile and soil nodes as illustrated in Figure 2b. Pile nodes and rigid link nodes were bonded in all six degrees of freedom (DOFs) (u_i and θ_i), and only the three translational DOFs (u_i) of the rigid link nodes were tied with soil nodes. These rigid links also prevent the soil opening from collapsing. For the nonlinear spring interface method, zero-length elements implemented with *p-y* and *t-z* spring materials were inserted between the rigid links and

the surrounding soil. Another zero-length element with *q-z* spring material was inserted between the pile toe node and the subjacent soil node. Due to liquefaction effects, the spring parameters were further modified by the coefficients of subgrade reaction from Boulanger et al. (2003).

The FE analyses were carried out in three loading stages: 1) self-weight loading, 2) pile installation loading and 3) seismic loading. The first stage was the consolidation process of the saturated level ground. During the second stage, a soil column at the model centre was excavated and the pile was then installed into the soil opening. A superstructure load was then added on the pile head followed by a static loading analysis. Finally, a seismic analysis was carried out by accelerating the model along the *x*-direction. There were also several seconds to rest the model after the loading.

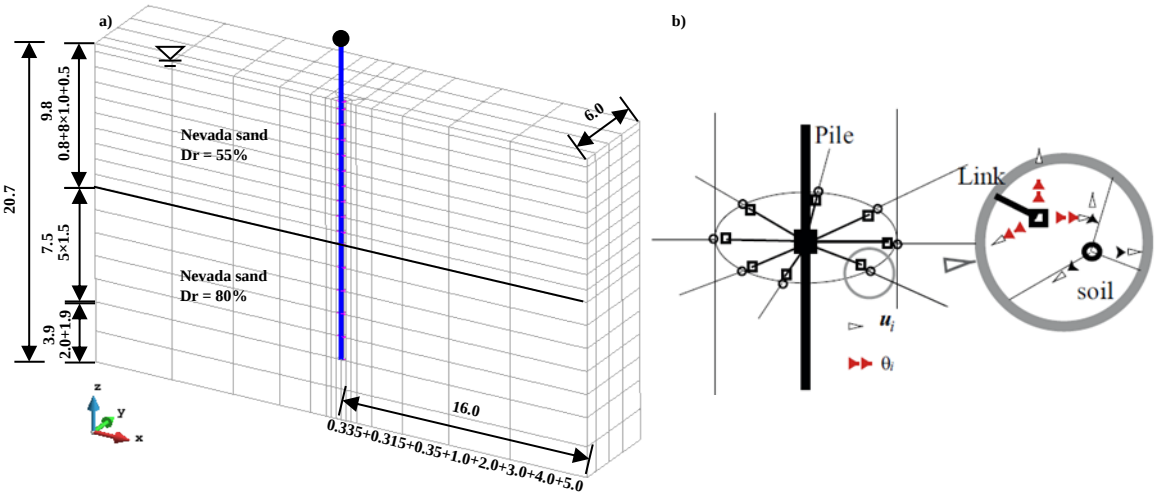

Figure 2: a) Model mesh; and b) Coupling of pile-soil nodes (Cheng & Jeremić 2009)

Table 1: Properties of Nevada sand used in the analysis

Model parameters	Nevada Sand	
Relative density D_r (%)	55	80
Reference effective confining pressure P_r' (kPa)	101	101
Reference shear modulus G_r (MPa)	63.0	88.4
Reference bulk modulus B_r (MPa)	168.2	236.0
Peak shear strain γ_{max}	0.1	0.1
Pressure dependency coefficient d	0.5	0.5
Friction angle φ_f (°)	33.5	36.5
Phase transformation angle φ_{PT} (°)	25.5	26.0
Contraction coefficients (c_1, c_2, c_3)	0.046, 3.42, 0.23	0.018, 1.48, 0.145
Dilation coefficients (d_1, d_2, d_3)	0.064, 3.0, 0.0	0.195, 3.0, 0.0
Number of yield surface	20	20
Liquefaction induced strain constants (liq_1, liq_2)	1.0, 0.0	1.0, 0.0
Void ratio e	0.685	0.618
Saturated unit weight ρ (ton/m^3)	1.98	2.03
Permeability coefficient k (m/s)	4.0×10^{-5}	2.5×10^{-5}

2.2 Verification of the numerical model

Figure 3 shows the comparison of the excess pore water pressure (EPWP) at the far-field between the numerical analysis (left and right boundaries of the model) and the centrifuge experiment at depths of 4.5 m and 7.0 m, which are approximately at the middle and bottom of the liquefiable layer, respectively. As results of numerical models with and without interface are the same, only one curve for the numerical model is plotted in the figure. The peak EPWP was well simulated at

depth of 4.5 m, but the simulation result has higher values at depth of 7.0 m. It is also evident that the simulation results showed the EPWP dissipated faster than that in the experiment. According to some researchers (e.g., Shahir et al., 2014), the permeability of the soil will increase during the liquefaction process and a variable permeability coefficient function should be adopted. This might be one of the reasons for the difference. However, the simulation does depict the accumulation process and the spikes well.

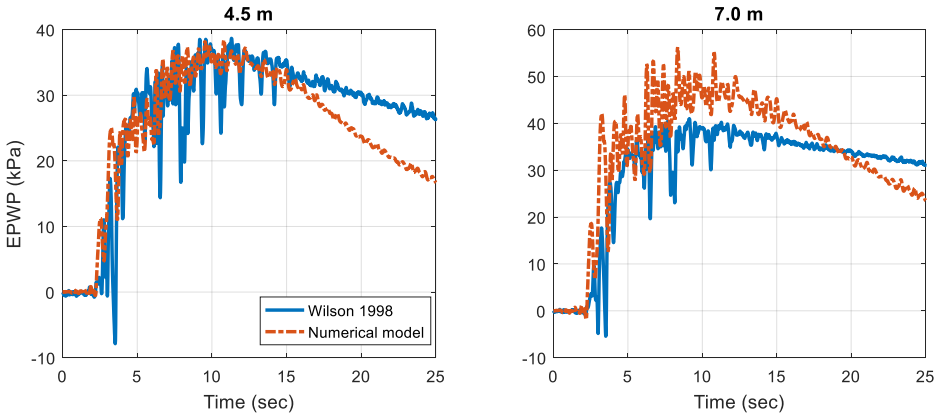

Figure 3: Free-field EPWP time history at different depths

The response of the pile at 2.0 m below the ground surface is shown in Figure 4 in which *p* and *y* represent the lateral reaction on the pile and the relative lateral displacement between the pile and soil, respectively. Good agreements can be detected between the experiment and simulation up to about 5 seconds after which the simulation response becomes smaller compared to the actual results. As shown in Figure 3, the increase in EPWP is found to be one of the reasons for this situation. This indicates that the adopted parameters or the performance of the PDMY02 material describing the liquefaction-induced deformation of the soil needs further enhancement. However, since the *p*-*y* relationship and the general trend of the response are satisfactory, this material was continued to be used in the next stage of the analysis.

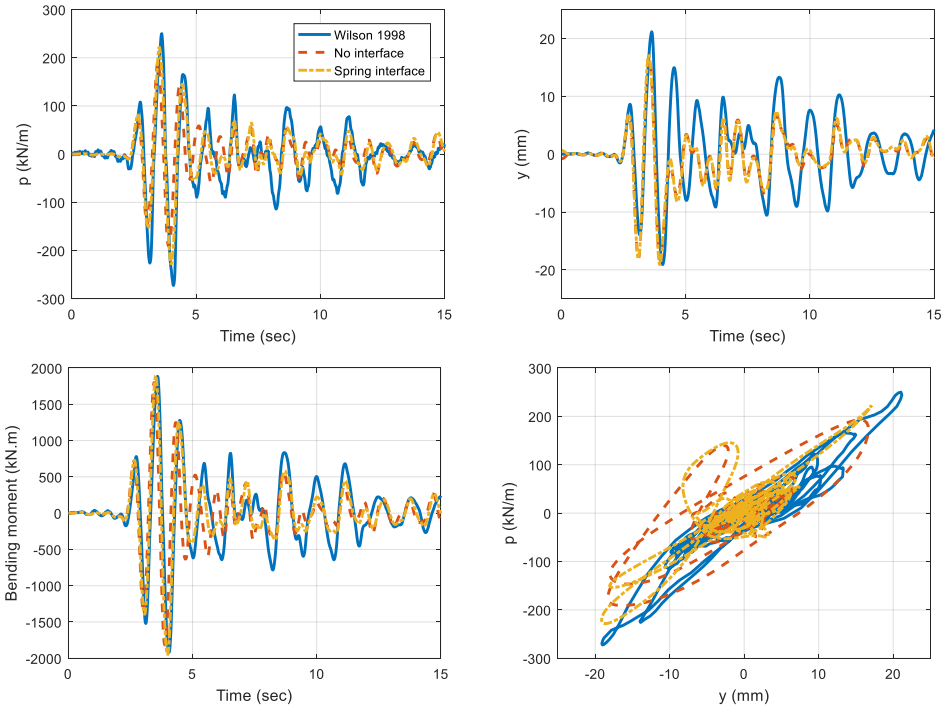

Figure 4: Dynamic response of vertical pile

Comparing the no-interface method with the spring interface method, one can observe that the difference between results is negligible. Neglecting the possible slippage or gapping on the soil-pile interface also seems to be the most common numerical approach emphasizing the soil-pile interaction problem (Zhang et al., 2017). Therefore, considering the advantages of simplicity and time-saving, the no-interface method was applied in the inclined pile analysis.

3 INCLINED PILE ANALYSIS

3.1 Model description

The same simulation method was applied in the inclined pile analysis, including the three-stage loading, coupling of pile-soil nodes and boundary conditions. Figure 5 depicts the meshing of the model and the inclined pile foundation with a raked angle θ = 10°. The model includes a soil block (36.0 m × 6.0 m × 15.0 m), two piles with the same inclination, a cap (3.0 m × 1.5 m × 1.0 m) and a column (4.0 m in length). The pile toe was 3.0 m above the model base and thicknesses of the liquefiable and non-liquefiable soil layers were 6.0 m and 9.0 m, respectively. In order to exclude the effects of soil-cap interaction, the cap was placed 1.0 m above the ground surface. A superstructure mass of 100 ton was added on top of the column. The diameter of the piles was set to 0.5 m for the sake of simplicity and the distance between the pile heads was 1.5 m (thrice the diameter). Material properties of the pile and Nevada sand were the same as the previous simulation. The cap and the column were elastic and had the same properties with the pile. By changing the raked angle (θ = 0°, 5°, 10°, 15° and 20°), a series of numerical simulations was conducted. It is worth mentioning that the 0° raked angle signifies that piles are vertical and the vertical length of piles is 13.0 m and independent from the raked angle.

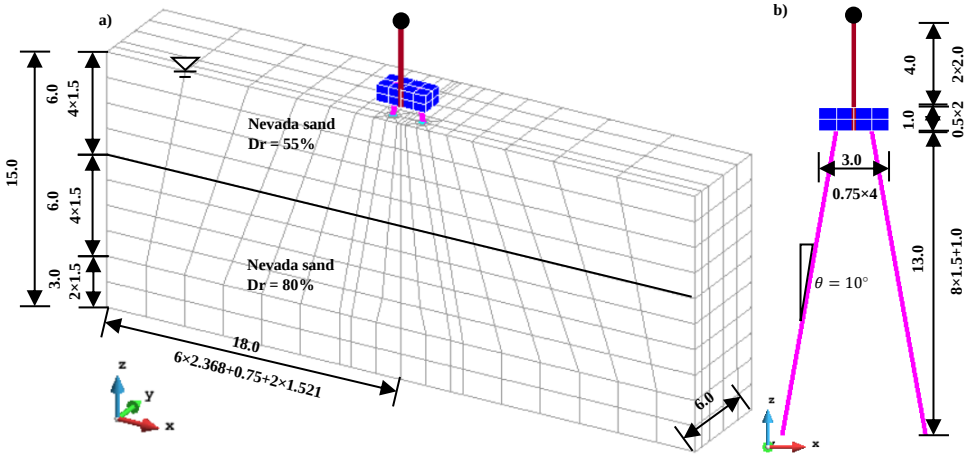

Figure 5: Inclined pile foundation model ($\theta = 10°$).

3.2 Comparison of results

The seismic response of the pile cap is shown in Figure 6a-d. With the increase of the inclination, the acceleration response of the cap (*Sa*) increases slightly at a period lower than 0.2 second (low period) and decreases at higher period as shown in Figure 6b. However, the horizontal displacement response of the pile is different with this investigation. As seen in Figure 6d, the response displacement *Sd* drops significantly as the inclination increase from 0° to 5° and then gradually decreases with the inclination. The reason may be that the inclined piles have enhanced the lateral resistance of the soil-pile-cap system. This indicates that the inclination of the pile may result in higher seismic acceleration or force on the cap but will be beneficial to reduce the lateral displacement. Similar conclusions can be obtained from the seismic response of the superstructure.

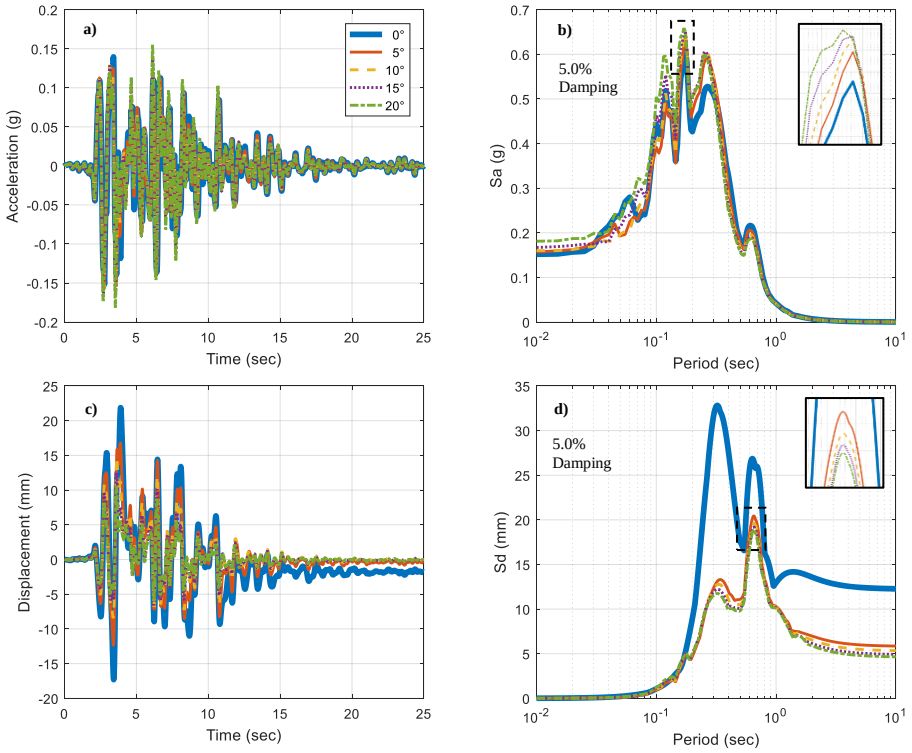

Figure 6: Seismic response of the cap

Figure 7a illustrates the EPWP development in the soil immediately adjacent to the pile at 3.0 m depth (the middle of the liquefiable layer). It is obvious that the pile inclination only results in slight fluctuations of the EPWP and has negligible effects on the developing process. Similar results can be obtained at other depths. Differences between the responses of the two piles are found to be ignorable which could be due to the fair symmetry of the input motion. Therefore, only results of the left pile are presented in the following figures. As demonstrated by Figure 7b, the inclination seems to reduce the maximum bending moment of the pile at around 3.0 m depth, the middle of the liquefiable layer; however, amplification can be observed near the pile head. With the increase of the inclination, a significant decrease in maximum positive axial force and increase of maximum shear force along the pile can be found in Figure 8. The presence of an initial shear force on inclined piles may be one of the reasons. As seen from Figure 9, piles with higher inclination angles suffer from higher soil resistance at the pile toe. Even though the inclination induces higher maximum pile displacement along most of the pile (below about 2.0 m), a reduction in the lateral displacement of the pile head can be observed.

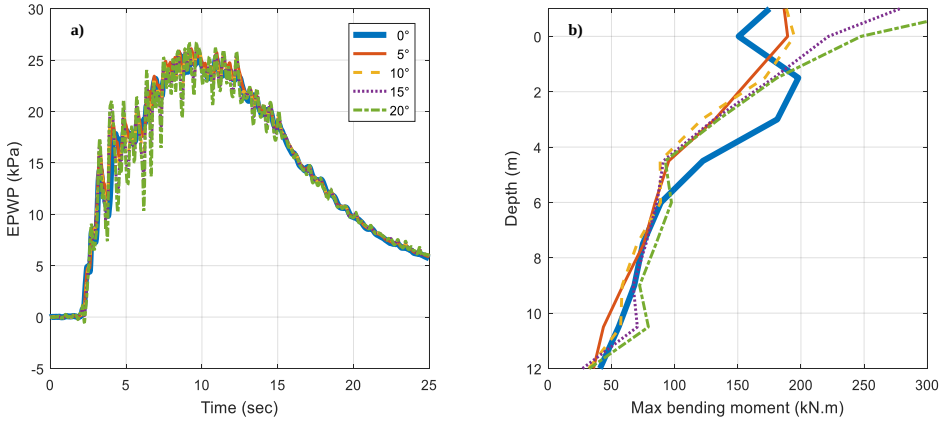

Figure 7: a) EPWP adjacent to the pile (3.0 m); and b) Max bending moment of the pile

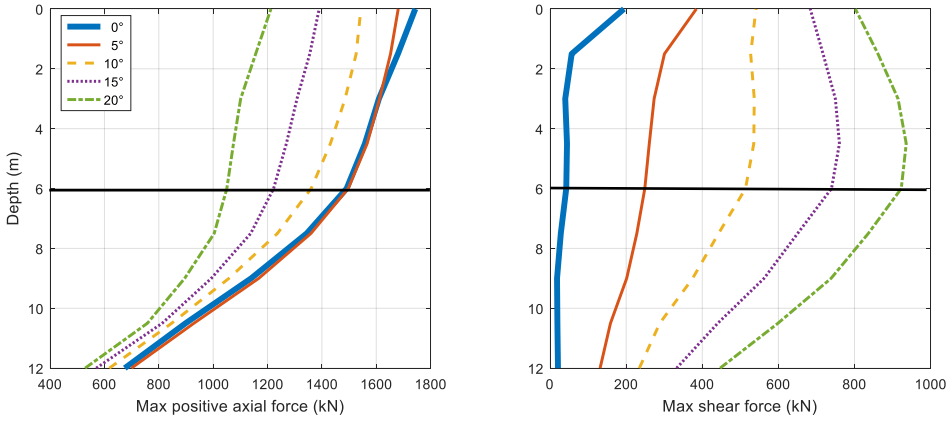

Figure 8: Max positive axial and shear force along the pile

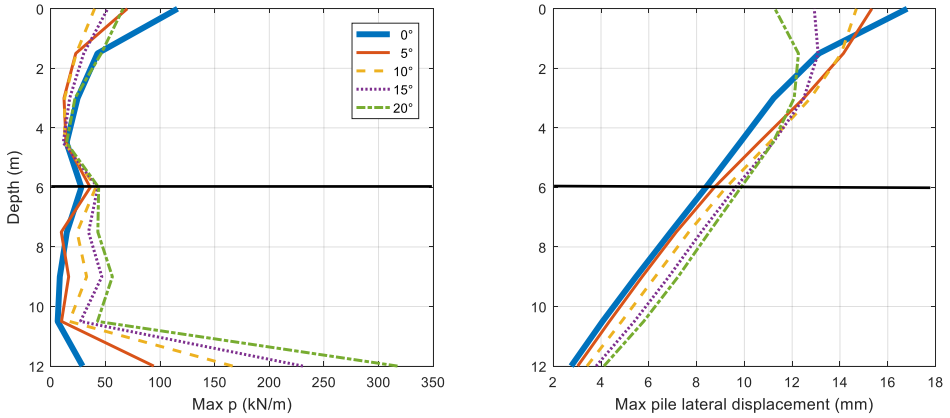

Figure 9: Max *p* and lateral displacement along the pile

4 CONCLUSIONS

To investigate the dynamic response of inclined piles in liquefiable soil, a comprehensive 3D FEM model has been developed using OpenSees. Spring interface method and no interface approach were compared with each other to detect the effects of soil-pile interaction. Results show that the difference between these two methods is negligible, at least for the model considered in this study. The influence of raked angles was then explored through the inclined pile analysis in which the no interface method was implemented. The pile inclination was found to be detrimental in inducing higher seismic force on the cap and superstructure and higher shear force along the pile. However, it played a beneficial role in reducing the lateral displacement of the above structures. Therefore, inclined piles are supposed to be designed with higher shear strength when used in the engineering practice. Otherwise, a combination of vertical and inclined piles with proper raked angle could be an alternative approach. This aspect may need further explorations for more details.

REFERENCES

Berrill, J. B. et al. (2001) Case study of lateral spreading forces on a piled foundation. *Géotechnique, 51*(6), 501–517.

Boulanger, R. W. et al. (2003) Pile foundations in liquefied and laterally spreading ground during earthquakes: centrifuge experiments & analyses. *Report No. UCD/CGM-03/01, Department of Civil and Environmental Engineering, UC Davis,*

205pp.

Cheng, Z., & Jeremić, B. (2009) Numerical modeling and simulation of pile in liquefiable soil. *Soil Dynamics and Earthquake Engineering*, *29*(11–12), 1405–1416.

Choobbasti, A. J., & Zahmatkesh, A. (2016) Computation of degradation factors of p-y curves in liquefiable soils for analysis of piles using three-dimensional finite-element model. *Soil Dynamics and Earthquake Engineering*, *89*, 61–74.

Dash, S. R., & Bhattacharya, S. (2015) Pore water pressure generation and dissipation near to pile and far-field in liquefiable soils. *International Journal of GEOMATE*, *9*(2), 1454–1459.

Gerolymos, N. et al. (2008) Evidence of beneficial role of inclined piles: Observations and summary of numerical analyses. *Bulletin of Earthquake Engineering*, *6*(4), 705–722.

Ghorbani, A. et al. (2014) Comprehensive three dimensional finite element analysis, parametric study and sensitivity analysis on the seismic performance of soil-micropile-superstructure interaction. *Soil Dynamics and Earthquake Engineering*, *58*, 21–36.

Goit, C. S., & Saitoh, M. (2013) Model tests and numerical analyses on horizontal impedance functions of inclined single piles embedded in cohesionless soil. *Earthquake Engineering and Engineering Vibration*, *12*(1), 143–154.

Karimi, Z. (2016) Seismic performance of shallow-founded structures on liquefiable ground An experimental and numerical study. *PhD Thesis*, University of Kurdistan.

Li, Z. et al. (2016) Centrifuge modeling of batter pile foundations under sinusoidal dynamic excitation. *Bulletin of Earthquake Engineering*, *14*(3), 673–697.

Mazzoni, S. et al. (2007) OpenSees command language manual. *Pacific Earthquake Engineering Research (PEER) Center*, 451.

McManus, K. et al. (2005) Inclined reinforcement to prevent soil liquefaction. In *Proceedings of the Annual NZSEE Technical Conference*, 523–533.

Shahir, H. et al (2014) Employing a variable permeability model in numerical simulation of saturated sand behavior under earthquake loading. *Computers and Geotechnics*, *55*, 211–223.

Subramanian, R. M., & Boominathan, A. (2016) Dynamic experimental studies on lateral behaviour of batter piles in soft clay. *International Journal of Geotechnical Engineering*, *10*(4), 317–327.

Wilson, D. W. (1998) Soil-pile-superstructure interaction in liquefying sand and soft clay. *PhD Thesis*, University of California, Davis.

Yang, Z. et al. (2003) Computational model for cyclic mobility and associated shear deformation. *Journal of Geotechnical and Geoenvironmental Engineering*, *129*(12), 1119–1127.

Zhang, L. et al. (2017) Seismic response of pile-raft-clay system subjected to a long-duration earthquake: centrifuge test and finite element analysis. *Soil Dynamics and Earthquake Engineering*, *92*, 488–502.

Liquefaction assessment for an urban roading project in the Bay of Plenty

H Wahab
Beca Ltd, Tauranga, NZ.
harry.wahab@beca.com

P J Clayton
Beca Ltd, Auckland, NZ.
philip.clayton@beca.com (Corresponding author)

Keywords: volcanic soils, aging, liquefaction, shear wave velocity

ABSTRACT

The NZ Transport Agency Baypark to Bayfair link upgrade project will provide improvements to two key intersections on State Highway 2 in the east of urban Tauranga in the Bay of Plenty. The project will be constructed in an area which is susceptible to liquefaction and cyclic strain softening. The ground conditions comprise Holocene beach deposit sands overlying swamp deposits, underlain by Pleistocene age volcanically derived alluvium. Preliminary analyses using CPT based methods indicated potential widespread liquefaction (and associated effects) in a 1/2500 APE event. This represented a significant risk to the project and it was recognised that a robust and considered assessment of the liquefaction hazard was necessary. This paper describes the investigation techniques used and the approach taken to undertake that assessment. The assessment was based on an extensive investigation programme comprising boreholes, Cone Penetration Tests (CPTs), seismic CPTs, seismic Dilatometer tests, downhole (Geonor) Shear Vane tests and laboratory testing. The investigation highlighted the importance of, and difficulties with, obtaining good quality data in the field. Both CPT and shear wave velocity based methods were used in the liquefaction assessment with a particular emphasis on the liquefaction potential of the Pleistocene aged soils. Findings from the liquefaction assessment showed good agreement with other recent liquefaction studies carried out within volcanic soils in the central North Island.

1 INTRODUCTION

The NZ Transport Agency Baypark to Bayfair link upgrade project will provide improvements to the Te Maunga intersection at Baypark and to the Maunganui Road/Girven Road intersection at Bayfair, in Tauranga, Bay of Plenty. The project lies at the northern terminus of the Tauranga Eastern Link (TEL) which was completed in 2015. The TEL is located to the east of Tauranga and is a key freight route for transporting goods from the Eastern Bay of Plenty agricultural and forestry areas to the Port of Tauranga and wider markets.

The project layout is shown in Figure 1. The project features a 3 span flyover at the Maunganui/Girven intersection and 2 single span bridges at the Te Maunga intersection, with significant lengths of MSE type approach embankment. The estimated project cost is $100m.

The project will be constructed in an area which is susceptible to liquefaction and cyclic strain softening. Seismic stability of the up to 8m high approach embankments and abutments under the various design events was a key consideration. Preliminary analyses indicated that liquefaction could be initiated in events with an Annual Probability of Exceedance (APE) of as little as around 1/100 (equivalent to a Minor earthquake), with widespread liquefaction (and associated effects) indicated in a 1/2500 APE (Design earthquake) event. This represented a significant risk to the project.

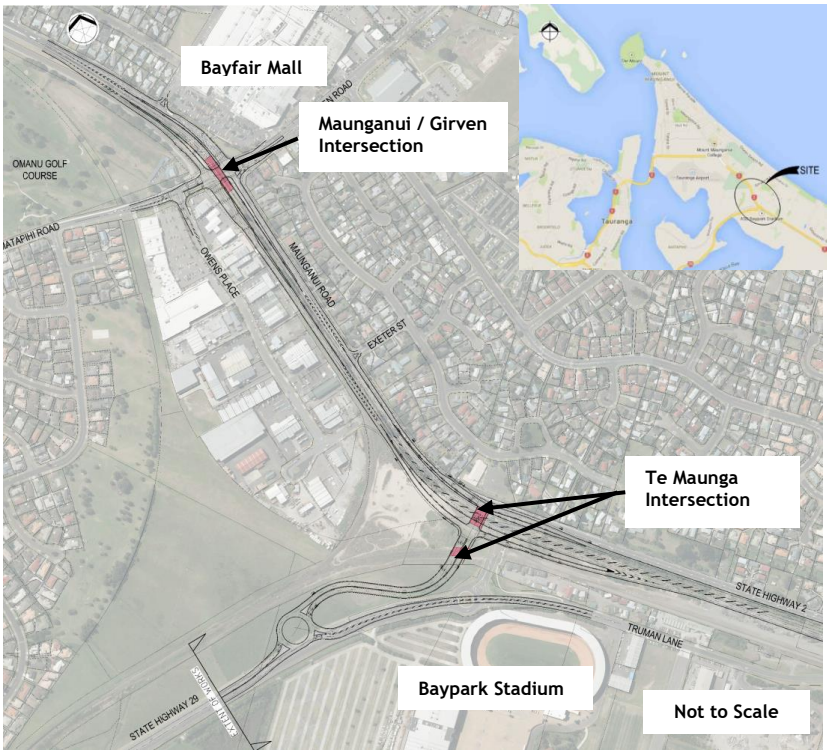

Figure 1: Project layout plan

2 GEOLOGY, GROUNDWATER AND SEISMICITY

2.1 Geology

The site is relatively flat and sits between the coastal barrier system at Omanu Beach to the northeast and the Matapihi peninsula to the southwest. The Tauranga Harbour and associated estuarine environment extends to the south of the site at Rangataua Bay. The city of Tauranga is located almost completely within the Tauranga Basin, a Pleistocene to Holocene (about 2 million years to the present) tectonic sedimentary basin up to 150m thick (Briggs et al, 1996). The basement of the Tauranga Basin consists of variably welded ignimbrites of Upper Tertiary age.

Deposits infilling this basin are termed Tauranga Group and consist of a basal Pleistocene sequence and an upper Holocene unit. The Pleistocene sequence comprises mainly alluvial deposits interbedded with unwelded ignimbrites and tephras, and is commonly referred to as the Matua Subgroup. The Holocene sediments include estuarine (swamp), alluvial, beach and dune deposits. The most recent geological map covering the area (Leonard et al, 2010) shows that the low lying areas of Tauranga and Mount Maunganui, where the site is located, are underlain by Beach Deposits and Swamp Deposits. The Matapihi peninsula, close to the southwest limit of the site, is underlain by the Matua Subgroup. These three units were of particular significance to the study and are described below in stratigraphic order:

2.1.1 Holocene beach deposits

The beach deposits are composed mainly of sands with little fines. Most of these deposits consist of loose to medium dense, fine to coarse-grained sands, composed largely of quartz and, subordinately, of shells and pumice. Trace silt was frequently observed, whilst minor pumice gravel occurs locally.

The sands extend across the whole site with relatively uniform thickness, to depths of about 10m below ground level (bgl). In the southeastern part of the site, a dense to very dense bed of gravelly sands was encountered at the base of the beach deposits. A number of Cone Penetration Tests (CPTs) refused on this bed.

2.1.2 Holocene swamp deposits

The swamp deposits consist of a sedimentary package of clays and silts interbedded with lenses/beds of sands. These deposits are estuarine in nature but the "swamp deposits" terminology was adopted to follow the QMAP series units. The swamp deposits occur throughout much of the site, immediately below the beach deposits, from a depth of about 10m bgl. Apart from the edges where the unit thins out, the thickness of the swamp deposits is reasonably regular, varying between 4 and 8m. The swamp deposits were classified into cohesive and granular sub-units. The cohesive sub-unit was typically described as a soft to firm sensitive clayey silt of high plasticity, the granular sub-unit as loose to medium dense sands with some silt.

2.1.3 Matua Subgroup

This Pleistocene deposit is composed mainly of loose to dense silty sand alluvium and is occasionally pumiceous. In addition to the sands, beds or lenses of fine-grained soils are frequently distributed throughout the unit and are interpreted as likely tephras.

A cross section that presents the typical geology of the site is shown in Figure 2.

2.2 Groundwater

The groundwater level is typically encountered at around 2.5m bgl across much of the site.

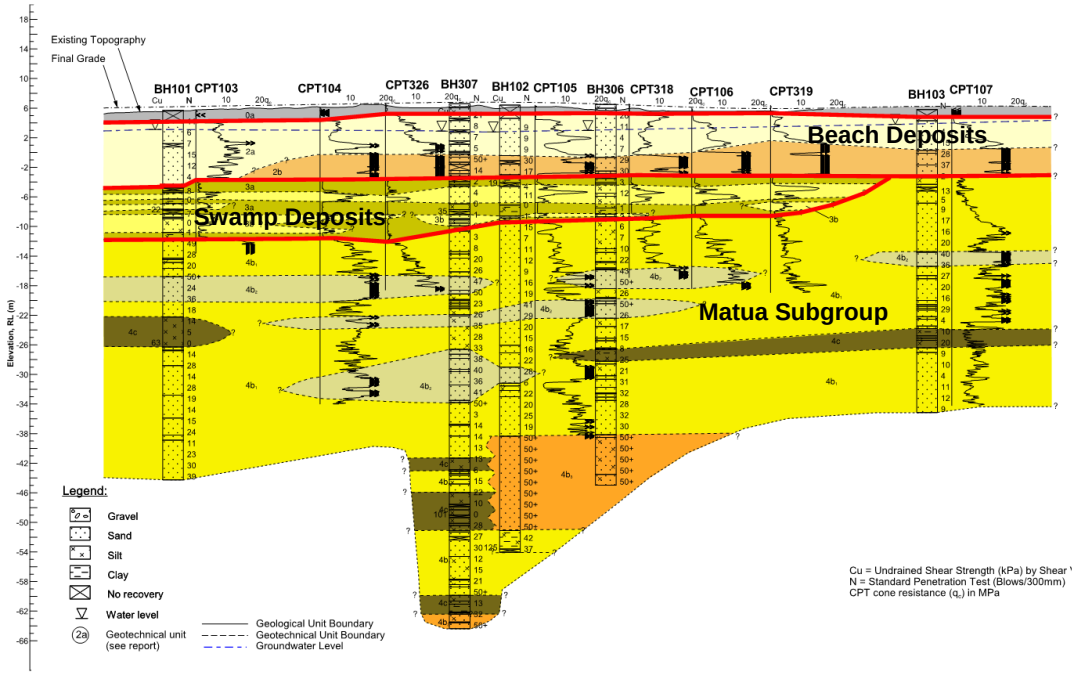

Figure 2: Typical geological section

2.3 Seismicity

The Tauranga area is located to the north of the Taupo Volcanic Zone (TVZ) and to the east of the Hauraki Rift. Active faults associated with both the TVZ and the Hauraki Rift occur in the

region. However no active faults are known to exist within a 20km radius from the site (New Zealand Active Faults Database, 2015). The closest faults to the site are the Kerepehi Fault (38km to WSW) and, possibly, some offshore faults close to Motiti Island (22km to ENE).

The Peak Ground Accelerations (PGAs) and corresponding Representative Magnitudes recommended in the Site specific Seismic Hazard Assessment (SSHA) were used as inputs to the detailed liquefaction assessment (refer Table 1).

Table 1: SSHA Peak Ground Acceleration & corresponding Representative Magnitudes

Design Event	Annual Probability of Exceedance (APE)	PGA (g)	Representative Magnitude
Minor / Operational Continuity	1/100	0.15	5.9
Design Level	1/2500	0.42	5.7
MCE	-	0.46	6.9

Note. MCE = Maximum Considered Earthquake

3 LIQUEFACTION ASSESSMENT CHALLENGES

.

3.1 Pleistocene age volcanogenic soils

A number of researchers and recent studies (refer Clayton et al, 2017) have highlighted challenges with undertaking liquefaction assessment in volcanically derived soils of the central North Island of New Zealand. It is widely considered that conventional penetrometer based liquefaction assessment methods in these soils can over predict liquefaction triggering in these unusual soils. The over-prediction is thought to result from the presence of crushable pumice grains and/or age effects. Where particle crushing occurs during a static Cone Penetration Test (CPT) the relative density of a soil can be under-estimated. Older deposits (such as the Pleistocene age Matua Subgroup) are considered to exhibit some cementation which are only partially recognised using large strain investigation techniques such as a CPT. Shear wave velocity based liquefaction assessment methods have been suggested as being more appropriate for such soils – refer to Clayton et al (2017) for further discussion.

3.2 Residual shear strength

Correlations associated with conventional penetrometer based methods may under-estimate the undrained and residual shear strength of young sensitive soils, such as the Holocene swamp deposits. This can result in the resistance to cyclic strain softening being under-estimated. Cyclic strain softening was an important consideration for stability given the extent of embankments on the project.

4 INVESTIGATION METHODS

4.1 Shear wave velocity

Paired seismic CPT (sCPT) and seismic Dilatometer (sDMT) direct push tests were carried out to provide down-hole shear wave velocity (Vs) data at five key locations. This enabled a comparison to be made between pseudo interval and true interval methods and gave confidence in the quality of the data obtained. Figure 3 shows the typical setup for the sCPT and sDMT testing.

Some challenges had been experienced with obtaining good quality shear wave velocity data during the initial investigations, particularly in locations where there was significant background noise, such as near the East Coast Main Trunk (ECMT) nearby. Within this investigation close collaboration between the consultant, the investigation contractor (Perry Geotech Ltd) and their

specialist geophysics supplier (Baziw Consulting Engineers Ltd) was found to be beneficial as rapid evaluation and interpretation of test results allowed changes in investigation scope to suit conditions identified and evaluation of data reliability allowed interpretation to place appropriate levels of confidence on results.

Figure 3: sCPT / sDMT field testing

The approach followed, for obtaining good quality data with the sCPTs, was to establish suitable controls during data acquisition. The Vs data was captured using specialist software (SC3-DAC Pro™) that allowed field checking of the data during acquisition. For example, the operator was able to check the signal to noise ratio as the data was acquired and assess the quality of the data 'on the fly'. If poor quality data was acquired then the test could be repeated at that depth, until an acceptable data quality was achieved, before advancing the CPT probe further. Another control put in place was to observe potential sources of interference during testing, e.g. from heavy vehicles on the highway or trains passing nearby. Testing could be halted, repeated or rescheduled if necessary.

Tests using the sCPT were undertaken at 1.0m intervals typically, reducing to 0.5m intervals as the soil profile transitioned into the top of the Matua Subgroup. This was done to provide a clear indication of the Vs profile through the transition. Seismic readings were obtained at 0.5m intervals using the sDMT.

4.2 Geonor vane testing

Down-hole Geonor vane testing was carried out at five locations at various depths to obtain direct measurements of the peak and residual shear strength of the Holocene swamp deposits. The testing was carried out by Perry Geotech Ltd using an electronic Geonor vane. The vane test locations were paired with an existing CPT, to enable the required test depths within the target cohesive materials to be identified, and to allow calibration of N_{kt} and evaluation of sleeve friction (fs) as a measure of remoulded shear strength for the site soils.

5 ANALYSIS OF RESULTS

5.1 Comparison of shear wave velocity

5.1.1 Velocity Comparison

Comparison was undertaken of co-located Vs and correlated Vs from CPT testing. sDMT (true interval) and sCPT (pseudo interval) results correlate well with the exception of a zone approximately corresponding with the dense/weakly cemented zone at the base of the beach deposits and the top of the swamp deposits, in this zone limitations in the quality of data is apparent (402 to 404) indicated by the averaging of results (constant velocity/depth over >0.5m).

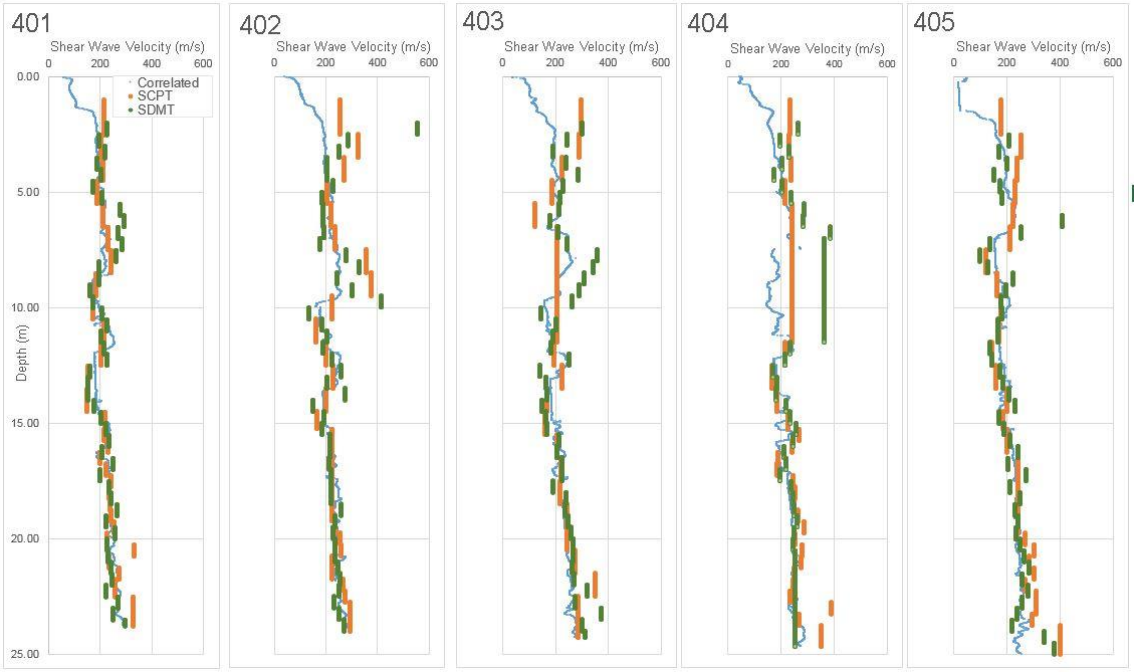

Figure 4: Comparison of co-located CPT derived and sDMT derived shear wave velocities

5.1.2 Liquefaction potential comparison

The measured and correlated Vs profile presented in Figure 4 are then utilised to prepare FOSliq under ULS shaking for further comparison in Figure 5. The nonlinear relationship between CRR and Vs is illustrated by the significantly greater apparent variation in the test results. Another noteworthy aspect of the plots in Figure 5 is the significantly higher FOSliq indicated by the Vs based analysis compared to the CPT based analysis in the older soils, particularly Matua Subgroup (typically around a depth of 15m).

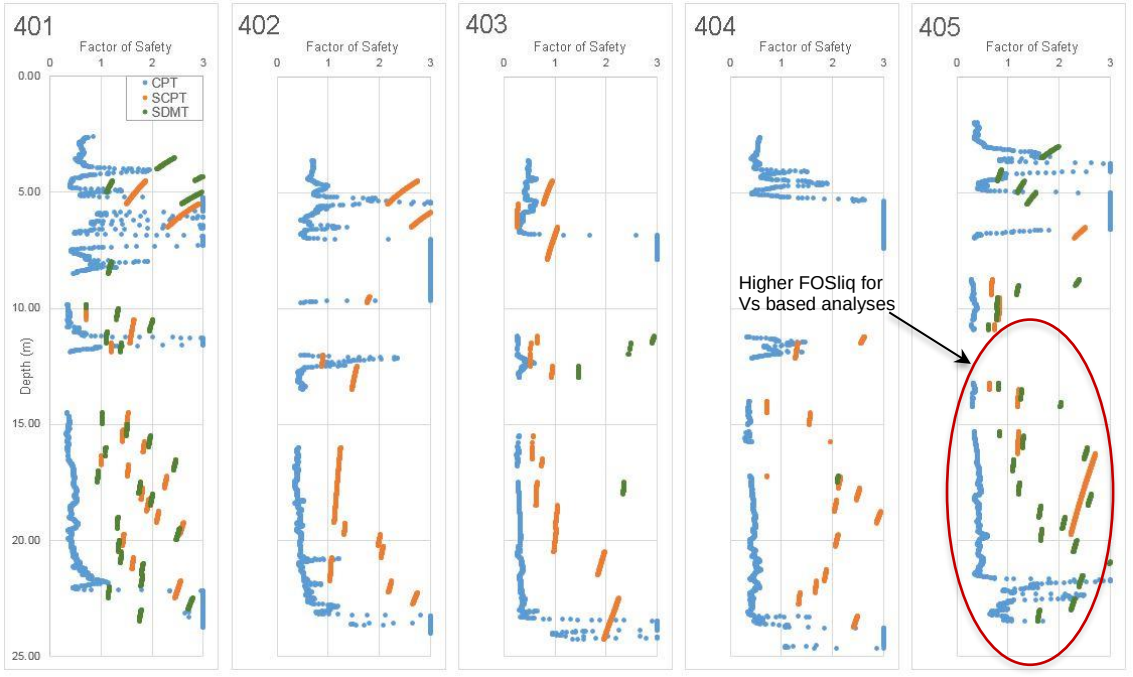

Figure 5: Comparison of CPT, Vs (sCPT) and Vs (sDMT) FOSliq for co-located tests

5.2 Comparison of shear strengths

Comparison was also made of peak and residual Cu measured from vane tests against peak Cu derived by correlation to CPT (CuNkt), (CuNk) and residual Cu based on CPT sleeve friction (Figure 6A and 6B). Correlated peak/residual Cu would commonly be applied while assessing the potential for and consequences of cyclic softening.

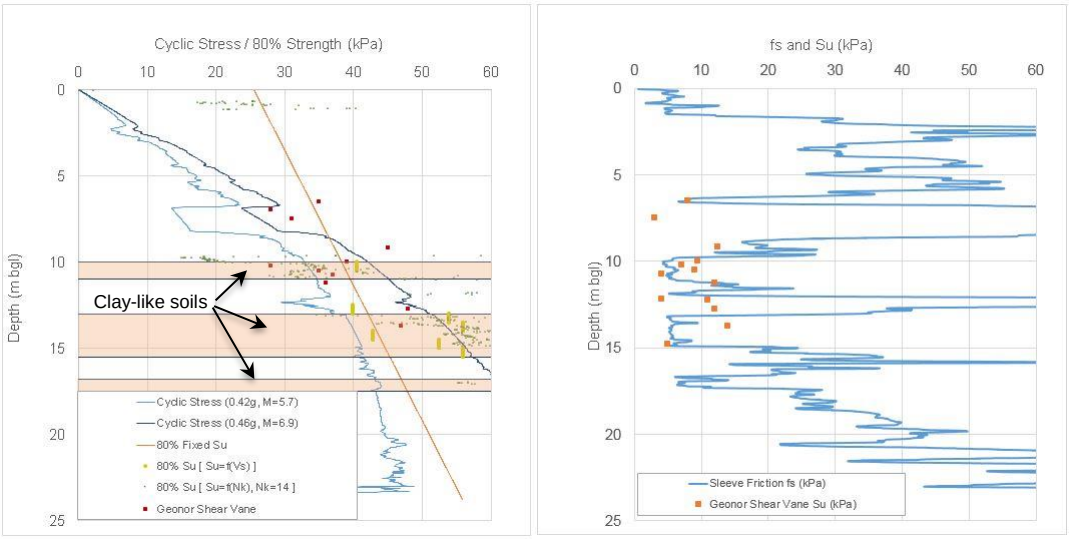

Figure 6A and 6B: Depth vs measured and correlated strength.

6 DISCUSSION

6.1 Shear wave velocity testing

The execution of a number of side by side Vs and CPT tests has allowed comparison of both true and pseudo interval downhole Vs measurements and the correlated Vs from CPT. In general very good correlations were present between all three, with two exceptions:

- sDMT (true interval) and SCPT (pseudo interval) results correlate well with the exception of a zone corresponding with the dense/weakly cemented sands at the base of the beach deposits and the top of the swamp deposits. Limitations in the quality of data is apparent (esp 402 to 404) indicated by the averaging of results (constant velocity/depth over >0.5m). This is likely associated with the large velocity contrast and inverted velocity profile between the base of the beach deposits and the swamp deposits.
- The ratio between measured and estimated (from CPT) Vs (MEVR) was noted to be greater at depth, in particular within the Matua Subgroup. This is likely associated with age related effects (or less likely, particle crushing).

The above findings have a number of implications for design. Firstly that shear wave velocity measurement can provide consistent results independent of method, but that care is required to assess the quality of data prior to application. To that end contractors undertaking investigation and practitioners utilising Vs testing should communicate about the level of uncertainty in individual test results, including flagging areas of uncertainty such as where data must be averaged over a greater interval or where there is a large difference between polarised results. Secondly, higher MEVR are noted within older deposits in this location, in particular the Matua Subgroup, indicative of comparatively higher age related liquefaction resistance not identified in the penetrometer based (CPT) liquefaction assessment.

Although the CPT derived Vs correlation used showed good agreement with the Vs measurements in this instance, in the authors' experience elsewhere there is typically a bias with the particular correlation that results in correlated Vs higher than measured. This bias is reflected in the variance shown in FOSliq (Vs/qc) in Figure 5.

6.2 Shear Strength

Comparison of measured and correlated peak and residual undrained shear strength determined utilising correlations of Cu (peak) = qt *Nkt and Cu (residual) = fs based on Robertson (2015) were found to show good agreement with shear strength as measured using a large vane test (LVT). This finding validates the ongoing use of CPT based cyclic softening assessment.

7 CONCLUSIONS

The execution of five sets of side by side true and pseudo interval Vs and paired CPT tests through Holocene and Pleistocene alluvial and airfall deposits has allowed comparison of both Vs from two different methods and CPT. This comparison has lead to the following conclusions:

- Downhole Vs testing, either true or pseudo interval, can give good repeatability of results.
- Under certain ground conditions, in this case likely associated with an inverted velocity profile, shear wave test results may be less reliable/more challenging to interpret.
- An appreciation for reliability of data can be gathered from close attention to the difference between polarised results and where velocity is averaged over an interval.
- Consistent with observations from a number of other studies (Clayton et,al (2017), Clayton & Johnson (2013)) measured to estimated velocity ratio (MEVR) is typically higher in older deposits (in this case the c. 1.8Ma to 0.1Ma Matua Subgroup) indicating age related liquefaction resistance is not identified by CPT based assessments.

LVT were also carried out to validate CPT based correlation to peak and residual undrained shear strength. These tests identified a good correlation between correlations of qt and fs to peak and residual shear strength for use in assessing the risk, and consequences of cyclic softening.

8 ACKNOWLEDGEMENTS

The authors wish to thank the New Zealand Transport Agency for their permission to publish this paper. The authors would also like to acknowledge Perry Geotech Ltd, Kim de Graaf and the many Beca colleagues who contributed to this project.

REFERENCES

Briggs, R. M., Hall, G. J., Harmsworth, G. R., Hollis, A. G., Houghton, B. F., Hughes, G. R. Morgan, M. D. and Whitbread-Edwards, A. R. (1996) *Geology of the Tauranga Area: Sheet U14 1:50,000*. IGNS.

Clayton, P.J., Johnson, J., T. (2013) Liquefaction Resistance and Possible Aging Effects in Selected Pleistocene Soils of the Upper North Island *Proc. 19th NZGS Geotechnical Symposium. Queenstown*.

Clayton, P.J., Wong, I., Wotherspoon, L. (2017) Case study in the use of shear wave velocity techniques to investigate liquefaction potential of Waikato soils for the Hamilton section of the Waikato expressway. *Proceedings 20th NZGS Geotechnical Symposium.* Eds. GJ Alexander & CY Chin, Napier.

Leonard, G.S.; Begg, J.G.; Wilson, C.J.N. (compilers) (2010) *Geology of the Rotorua area*. Institute of geological & Nuclear Sciences 1:250,000 geological map 5. 1 sheet + 102p. Lower Hutt, New Zealand. GNS Science.

Robertson P.K., Cabal K.L. (2015) *Guide to Cone Penetration Testing for Geotechnical Engineering*. Gregg drilling. 6th edition July 2015.

New Zealand Active Faults Database (2015) http://data.gns.cri.nz/af/ - Accessed November 2015

Using Tunnel Boring Machine Penetration Tests to Quantify Performance in Hard Rock

M C Villeneuve
Department of Geological Sciences, University of Canterbury, New Zealand.
marlene.villeneuve@canterbury.ac.nz (Corresponding author)

Keywords: penetration rate, geological characteristics, grinding, chipping, face stability

ABSTRACT

Tunnel boring machine (TBM) penetration tests entail incrementally increasing TBM thrust from full stop to maximum speed and recording the penetration rate either at set thrust levels or at set times. TBM penetration test data can be analysed by plotting the penetration rate (distance/revolution) against the net cutter thrust (force per cutter) over the full range of thrust levels in the test, called the penetration-thrust graph. This research shows that the transition from excavation dominated by grinding to excavation dominated by chipping can be observed in penetration-thrust graphs. Correlating penetration test data to the geological and geomechanical characteristics of rock masses through which a penetration test is conducted provides the ability to reveal the efficiency of the chipping process in response to changing geological conditions. By analysing penetration test data from projects in the Swiss Alps, and published data from Singapore, this research shows that the strength of the rock is an important control on how much net cutter thrust is required to transition from grinding to chipping. It also shows that the geological characteristics of a rock will determine how efficiently chipping occurs once it has begun. In particular, geological characteristics that lead to efficient fracture propagation, such as fabric and mica content, will lead to efficient chipping. These findings will enable a better correlation between TBM performance and geological conditions for use in TBM design, as a basis for contractual payments where penetration rate dominates the excavation cycle and in further academic investigations into the TBM excavation process.

1 INTRODUCTION

During hard rock tunnel boring machine excavation, a cutter first creates a crushed zone at the cutter-rock interface and the stresses from the thrust of the cutter are transmitted through this crushed zone into the adjacent undamaged rock (Figure 1). The induced stresses and dilation within the crushed zone cause extensile fracturing of the rock away from the crushed zone. Eventually, fractures generated by subsequent cutter passes extend either to the rock surface or to fractures propagating from adjoining kerfs and coalesce to form chips. This occurs at different cutter thrust magnitudes for different rock types. If the cutter thrust necessary for tensile fracture propagation is not achieved, due to excessively high cutter thrust requirements or an underpowered TBM, then only grinding at the crushed zone occurs. Grinding produces fines, rather than chips, leading to much lower penetration rate. Chipping is a more efficient excavation process because generating chips through tensile fracturing is much more efficient than the formation of fines in the crushed zone (Teale, 1964; Snowdon et al., 1982; Bruland, 1998; Gertsch et al., 2007; Yin et al., 2014). The formation of chips by the chipping process is, therefore, critical for achieving high penetration rates.

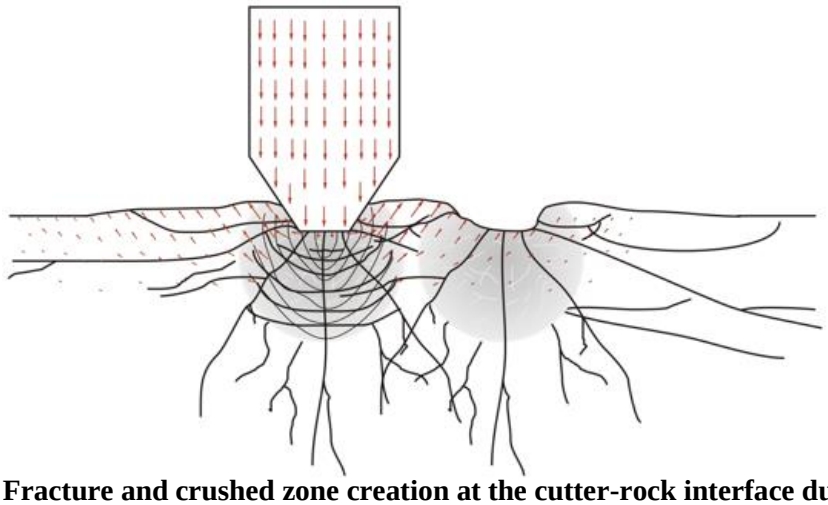

Figure 1: Fracture and crushed zone creation at the cutter-rock interface during TBM excavation (modified from Villeneuve, 2008).

This research demonstrates what TBM penetration testing can show about the excavation process. Based on work by Villeneuve (2008, 2017) and Frenzel et al. (2012), penetration tests are defined and index values are demonstrated for TBM performance analysis. Geological characteristics are linked to the chipping process identified with the penetration tests. TBM operational data and results from penetration tests are analysed to provide feedback about whether excavation is occurring efficiently through chipping or inefficiently through grinding.

2 PENETRATION TESTS

Villeneuve (2017) performed a total of 16 penetration tests in three different rock units in the Swiss Alps: schist (Figure 2), granite (Figure 3) and gneiss (Figure 4). Figure 4 also includes data for marble and granite from Yin et al. (2014) and Gong et al. (2007). The tests in the Swiss Alps were undertaken using three Herrenknecht hard rock gripper TBMs with a diameter range of 8.83-9.58 m. All TBMs utilised 432 mm diameter cutters with 90 mm spacing on centre. During normal TBM start-up only a few data points at low penetration rates were recorded by the data acquisition system (DAS) due to the sampling interval (typically 1/10 s). In order to capture sufficient data through the full range of penetration rates, penetration tests were adopted (Villeneuve, 2008; later described in detail in Frenzel et al., 2012), and conducted by gradually increasing the TBM thrust from full stop to the maximum thrust over a period of 8-10 min. The cutterhead rotational speed (RPM) was kept constant during these tests, typically ranging from 5.5 rpm to 6.2 rpm, and was selected based on the face condition (i.e. it would be higher in stable face conditions than in blocky face conditions). Depending on the operator, RPM and rock type, the length of tunnel tested is approximately 30-200 mm.

The penetration rate (mm/rev) was used in Villeneuve (2017), rather than speed (mm/min), because this removes the effect of RPM and allows comparison of test results from different strokes. The thrust value obtained from the DAS is gross thrust, which is the amount of force exerted by the thrust pistons. This thrust incorporates friction on the TBM head, which is independent of cutting processes occurring at the tunnel face. The net cutter thrust is used, which is the gross thrust minus the frictional losses, divided by the number of cutters, to allow comparison of test results from different locations and different TBMs. The friction contribution to gross thrust is estimated by averaging the gross thrust required to reverse and advance the TBM cutterhead (i.e. moving the cutterhead when it is not touching the rock at the face, usually during cutter changes). Gross thrust also includes impacts of TBM stiffness and losses in the hydraulic systems, but these should remain constant for any TBM.

Villeneuve (2008) showed that penetration curves highlight (Figure 5): (1) the minimum thrust required to begin advancing the TBM; (2) initial penetration behaviour dominated by grinding (creating fines); (3) the change from grinding to chipping (creating chips), called the critical thrust (Robbins, 1970), located at the inflection point; (4) the chipping efficiency, represented by the slope of the line past the inflection point; and (5) the point of steady-state penetration.

The steady-state penetration rate is limited by TBM design parameters, which define performance limits. The penetration limit is a function of muck conveyance, bucket design, cutter wear and maximum head revolution speed (Frenzel et al., 2012). The torque limit provides the transition from the penetration limit to the maximum thrust (Frenzel et al., 2008), which is a function of the rotational speed and is controlled by the maximum torque capacity. The thrust limit is controlled by cutter type, maximum thrust capacity and TBM head design. The penetration limit for the TBMs used in this investigation is ~11 mm/rev (Villeneuve, 2017). The torque limit for the TBMs in this study is ~30% of the maximum torque capacity (Villeneuve, 2017). The maximum net thrust on 432 mm cutters is ~250-267 kN (Frenzel et al., 2008; Maidl et al., 2008).

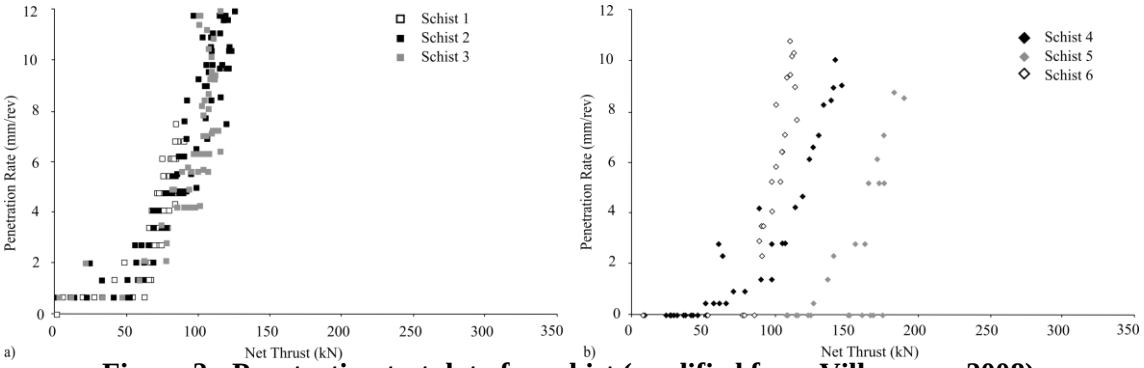

Figure 2: Penetration test data for schist (modified from Villeneuve, 2008).

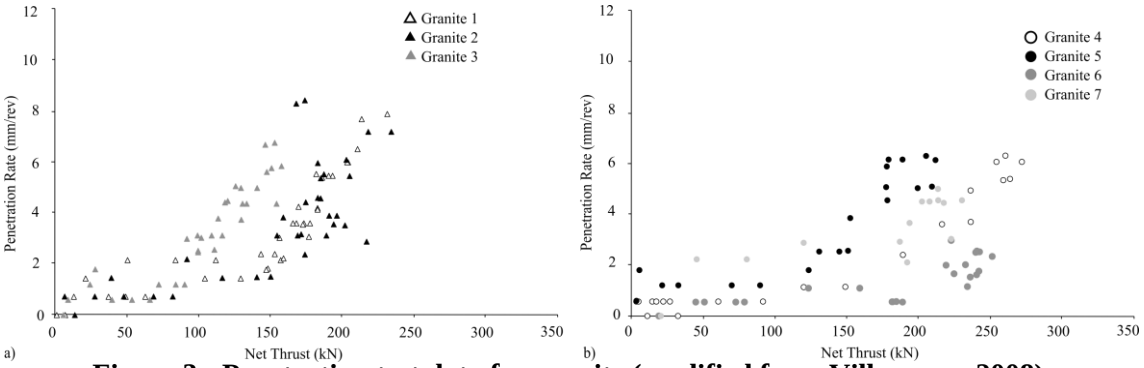

Figure 3: Penetration test data for granite (modified from Villeneuve, 2008).

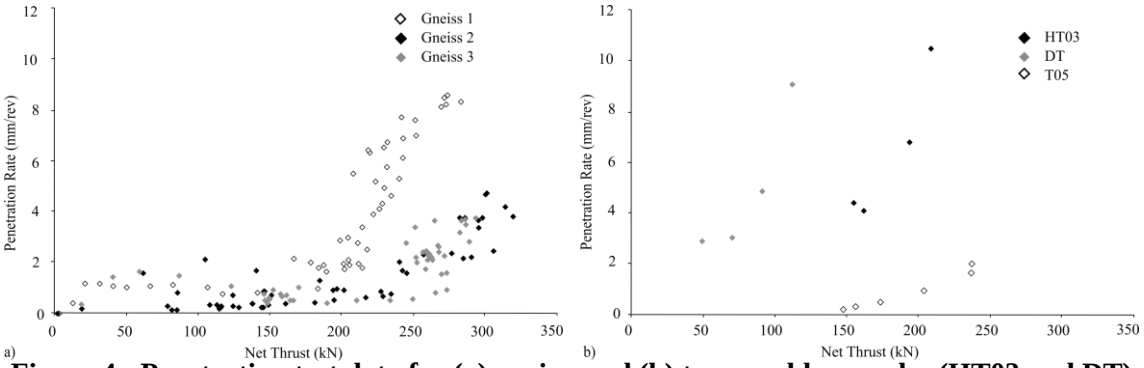

Figure 4: Penetration test data for (a) gneiss, and (b) two marble samples (HT03 and DT) tested in Yin et al. (2014) and one granite sample (T05) from Gong et al. (2007) (modified from Villeneuve, 2008).

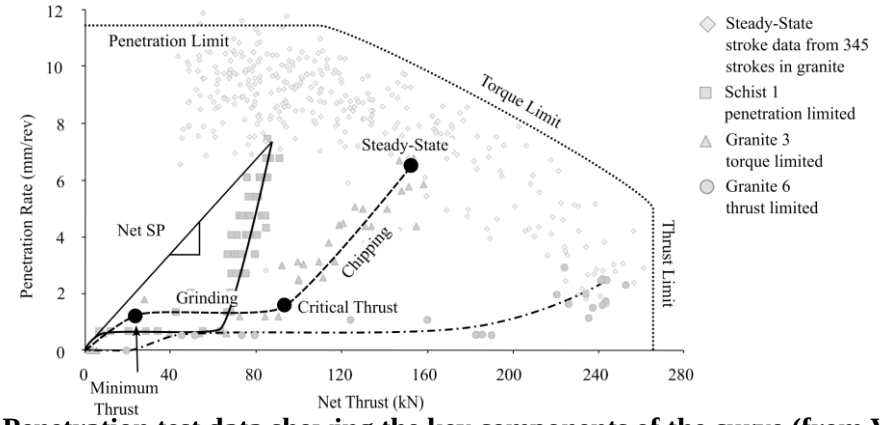

Figure 5: Penetration test data showing the key components of the curve (from Villeneuve, 2017).

3 PENETRATION TEST ANALYSIS

The minimum thrust and grinding portion of the penetration curve will depend on the resistance of the rock to crushing (Villeneuve, 2017). The critical thrust point and the slope of the curve during chipping (as discussed in Samuel and Seow (1984), Zhang et al. (2003) and Gehring (2009)), are related to rock strength and brittleness, mineralogy and fabric (Villeneuve et al., 2007, 2012; Villeneuve, 2008), and stress at the tunnel face (Yin et al., 2014). The location of the critical thrust and the slope and length of the curve beyond the critical thrust point are representative of the 100-200 mm thickness of rock over which the test is performed. Performing the test in different lithologies will produce different curves, which can be related back to the geological conditions.

The UCS values for the schist and granite in which the penetration tests were conducted show a strong relationship with critical thrust (Figure 6). The variance in these data likely results from fractures (pre-existing or stress-induced) in the face and variability at the metre scale in the rock strength. This shows that, while UCS can be used to identify rocks that are at risk of poor excavation performance, penetration tests are required to identify the actual point at which chipping occurs.

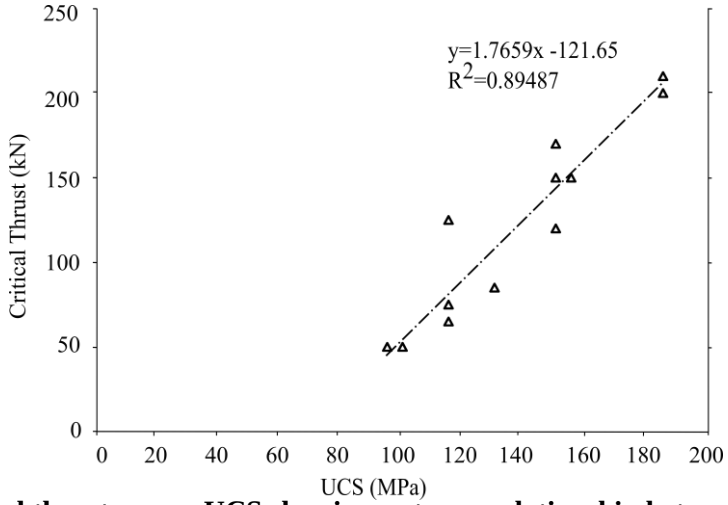

Figure 6: Critical thrust versus UCS showing a strong relationship between rock strength and thrust at transition from grinding to chipping.

The penetration curves in the schist, gneiss and granite are grouped in Figure 7 according to the dominant excavation mode. The curves for Schists 4 and 5 have the lowest strength (115 MPa (Villeneuve, 2017)) and low critical thrust, with chipping-dominated excavation. The curves for

Granites 2, 5 and 7 have moderate strength between 150-185 MPa (Villeneuve, 2017) and tend to have a critical thrust between 100 kN and 200 kN (Figure 7). The curves above the critical thrust are torque limited, showing that chipping was occurring, but not very efficiently. The curves with critical thrust above 200 kN (Granites 4 and 6, T05, and Gneiss 2 and 3 in Figure 7) are very short with shallow slope, and are limited by the cutter thrust. The high critical thrust shows that minimal chipping is occurring due to high strength (Granite 4 = 150 MPa, Granite 6 = 185 MPa and T05 = 175 MPa (Villeneuve, 2017)), with excavation dominated by grinding.

The critical thrust and the slope of the penetration curve above the critical thrust are key indicators of cutter efficiency, which are controlled by the strength (Figure 6) and ease of propagation of newly initiated fractures. Geological characteristics play an important role in both the strength and the ability to propagate fractures (Villeneuve, 2017). An easy transition to tensile fracturing processes (chipping) occurs in Schist 4 (Figure 8), which has a well-defined micaceous (40%) cleavage that facilitates fracture propagation (Villeneuve et al., 2012). A less efficient transition to tensile fracturing, and thus less chipping, occurs in Granite 2 (Figure 8), which has a poorly defined micaceous (15%) schistosity. Grinding occurs in Granite 6 (Figure 8), which has very low mica content (5%) and no foliation. As demonstrated by Granites 2 and 6, geological characteristics, such as fabric and mica content, are especially important for rocks with moderate to high critical thrust, where the ability to propagate fractures can make a large difference in the resulting penetration rate (i.e. torque limited rather than thrust limited).

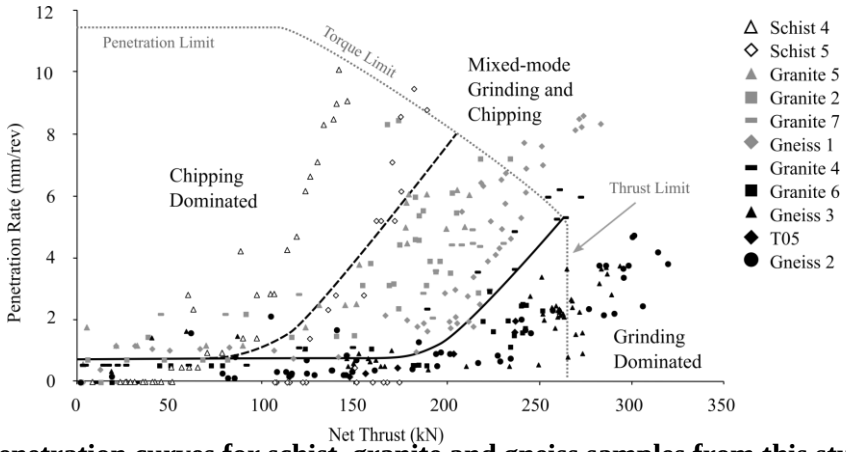

Figure 7: Penetration curves for schist, granite and gneiss samples from this study and one granite sample from Gong et al. (2007) excavated under stable face conditions overlaid by the performance limits from Fig. 5 (from Villeneuve, 2017).

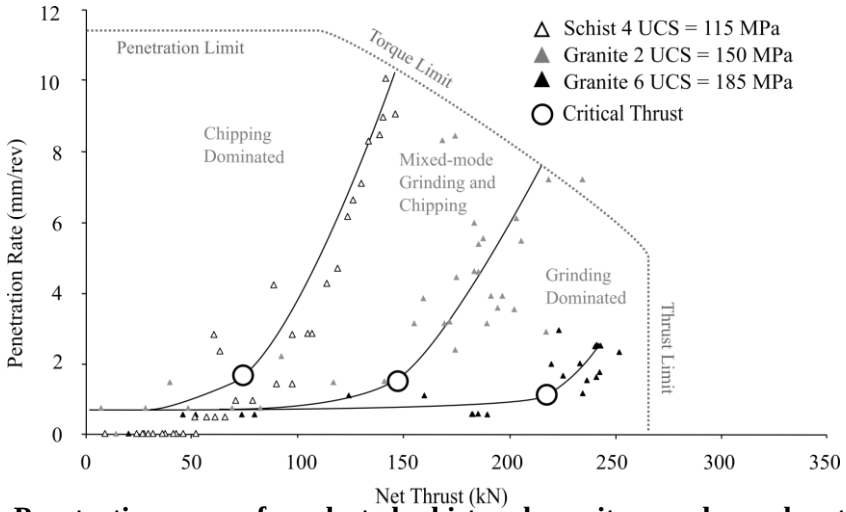

Figure 7: Penetration curves for selected schist and granite samples under stable face conditions showing the location of critical thrust overlaid by the performance limits from Figure 5, and excavation types from Figure 7 (from Villeneuve, 2017).

4 DISCUSSION

The penetration graphs in Figures 2-4 show that the transition from grinding to chipping does not consistently occur at 1 mm/rev. Manual analysis is required to determine the inflection point for critical thrust. Depending on the quality of the penetration test data, in particular the density of data points defining the start-up curve, it is not always possible to identify the critical thrust (e.g. Figure 4b). For this reason, a precision of 5 kN was selected for critical thrust for the tests in this study (Villeneuve, 2017), in Yin et al. (2014) and in Gong et al. (2007). Considering the ease with which the critical thrust can be obtained with good penetration test data it provides an easy method to identify the transition from grinding to chipping.

The findings from this research can be used to provide guidance to aid in drawing up contract documents and selecting the method by which TBM performance will be used for payment and progress assessment, depending on the anticipated geomechanical and geological conditions. During construction, penetration tests can be used to provide guidance to TBM operators regarding thrust application. In a rock type similar to Granite 6, which tends to be excavated via the grinding process, very little gain in penetration rate can be achieved by applying higher thrust, and wear and cutter damage could be minimised by lowering the thrust without substantially reducing penetration rate. Chipping-dominated excavation may never be achieved in these rock types with very high strength, even if cutter thrust limits were increased, as the process will remain too energy intensive due to the high fracture initiation threshold and the poor fracture propagation in these rocks.

5 CONCLUSIONS

This research focused on the determination of the impact of intact rock characteristics at the tunnel face on the rock cutting process. It was demonstrated that TBM penetration tests can provide a measure of TBM performance. Critical thrust can provide an understanding of the transition from grinding to chipping.

Penetration test data were used to categorise penetration-thrust graphs according to TBM operational constraints and the excavation performance from grinding-dominated, through mixed-mode grinding and chipping, to chipping-dominated. Using these categorised graphs, it was shown that rocks with higher strength tend to be excavated through the grinding-dominated process. For massive rock masses with significantly high strength, over 175 MPa in this study, only minor gains in penetration rate can be achieved through increased thrust because the critical thrust approaches the cutter thrust limit of 267 kN for commonly used 432 mm (17 inch) cutters. Penetration testing can help TBM operators identify whether additional thrust is warranted in individual rocks masses with low penetration rates during excavation.

This research has also shown that geological characteristics, in addition to rock strength, play an important role in both the chipping process and stress-induced face instability. Under similar stress conditions, rocks with well-defined fabric, oriented oblique to the tunnel face were easier to excavate than rocks without fabric or fabric oriented perpendicular to the face.

The penetration test methodology can be used for further investigation into the rock cutting process, to aid in developing better penetration rate prediction tools, and as a measure of TBM performance for tunnelling contract management during excavation. We have shown that our methodologies provide repeatable results using data from Gong et al. (2007) and Yin et al. (2014). For these data to be comparable across projects, a consistent testing methodology should be used, for example the methodology set out in Gong et al. (2007) or in Frenzel et al. (2012).

6 ACKNOWLEDGEMENTS

This work was supported by Herrenknecht AG, a Postgraduate Scholarship from the Natural Science and Engineering Research Council (NSERC) of Canada and the Golder Associates (Canada) Visitor Programme to the Queen's Geo-Engineering Centre. Murer-Strabag and Tunnel Alp Transit consortia are also thanked for their in-kind support during penetration testing and data collection.

REFERENCES

Frenzel C, Galler R, Käsling H, Villeneuve M. (2012) Penetration tests for TBMs and their practical application. *Geomechanics and Tunnelling* 5(5): 557–66.

Frenzel C, Käsling H, Thuro K. (2008) Factors influencing disc cutter wear. *Geomechanics and Tunnelling* 1(1): 55–60.

Gehring K. (2009) The influence of TBM design and machine features on performance and tool wear in rock. *Geomechanics and Tunnelling* 2(2): 140–55.

Gertsch R, Gertsch L, Rostami J. (2007) Disc cutting tests in Colorado Red Granite: Implications for TBM performance prediction. *International Journal of Rock Mechanics and Mining Sciences* 44(2): 238–46.

Gong QM, Zhao J, Jiang YS. (2007) In situ TBM penetration tests and rock mass boreability analysis in hard rock tunnels. *Tunnelling and Underground Space Technology* 22(3): 303–16.

Maidl B, Schmid L, Ritz W, Herrenknecht M. (2008) *Hardrock tunnel boring machines*. Berlin: Ersnt & Sohn Verlag

Samuel AE, Seow LP. (1984) Disc force measurement on a full-face tunnelling machine. *International Journal of Rock Mechanics and Mining Sciences & Geomechanics* Abstracts 21(2): 83–96.

Snowdon, R.A., Ryley, M.D, and Temporal, J. (1982) A study of disc cutting in selected British rocks. *International Journal of Rock Mechanics and Mining Sciences & Geomechanics* Abstracts 19(3): 107–21.

Teale R. The mechanical excavation of rock – experiments with roller cutters. (1964) *International Journal of Rock Mechanics and Mining Sciences* 1(1): 63–78.

Villeneuve MC, Diederichs MS, Kaiser PK, Frenzel C. (2007) Geomechanical characterisation of massive rock for deep TBM tunnelling. In: Eberhardt E, Stead D, Morrison T, editors. Rock Mechanics: Meeting Society's Challenges and Demands, *Proceedings of the 1st Canada-US Rock Mechanics Symposium*. CRC Press; p. 1131–9.

Villeneuve MC. (2008) Examination of geological influence on machine excavation of highly stressed tunnels in massive hard rock. *PhD Thesis*. Kingston, Canada: Queen's University

Villeneuve MC, Diederichs MS, Kaiser PK. (2012) Effects of grain scale heterogeneity on rock strength and the chipping process. *International Journal of Geomechanics* 12(6): 632–47.

Villeneuve MC. (2017) Hard rock tunnel boring machine penetration tests as an indicator of chipping process efficiency. *International Journal of Rock Mechanics and Geotechnical Engineering*, in press.

Yin LJ, Gong QM, Zhao J. (2014) Study on rock mass boreability by TBM penetration test under different in situ stress conditions. *Tunnelling and Underground Space Technology* 43: 413–25.

Zhang ZX, Kou SQ, Tan XC, Lindqvist PA. (2003) In-situ measurement of cutter forces on boring machine at Äspö Hard Rock Laboratory. Part I. Laboratory calibration and in-situ measurements. *Rock Mechanics and Rock Engineering* 36(1): 39–61.

Soakage and the Building Code

M D Trigger
AECOM New Zealand Limited.
mike.trigger@aecom.com (Corresponding author)

Keywords: Soakage testing, Building Code, E1, Natural Hazards

ABSTRACT

Soakage to ground is often used as a method of managing stormwater runoff generated by development. The New Zealand Building Code compliance document E1 is the only national guideline that provides methods for determining the soil soakage rate and the size of the related system. Several other guidelines exist locally and many engineers do not use the method in E1. Once stormwater is discharged to ground there is often little consideration given to the effects on other properties. This paper explores the variation between the methods and whether the method in E1 complies with the New Zealand Building Code.

1 INTRODUCTION

Effective stormwater management is essential for managing flooding and ponding in the built environment. Soakage to ground is promoted as preferable to assist in groundwater recharge, and in some areas, it also prevents saltwater intrusion.

Based on my experience processing resource and building consents at two councils, many designers did not use the New Zealand Building Code Verification Method E1/VM1 (MBIE, 1992) to determine soakage rates or design soakage systems. The few designers that do use E1/VM1 reported much higher soakage rates and designed substantially smaller systems. Frequently little thought was given to the long-term performance or operation and maintenance of the system. Their design fees are less and their system costs less to construct. The market dictates that they are preferred.

By comparing requirements and soakage test results from E1/VM1 with other guidelines this paper looks at whether soakage systems, in particular, those designed using E1/VM1 can reliably meet the objectives, functional requirements and performance criteria of the New Zealand Building Code.

2 SYSTEM FAILURES

During my first experience at a council, several soakage systems for roads that had been vested to the Council were not functioning well during normal rainfall. The effects of the failures were flooding and erosion. The following patterns were identified in the designs:

- The use of E1/VM1 to determine the soakage rate
- Adopting an average value due to the tail on the soakage curve
- Designing the soakage system using base and side wall areas in combination with using the an averaged E1/VM1 soakage rate
- Testing in summer without consideration to winter groundwater levels
- Testing undertaken in soils that would be excavated during the works

Similar patterns were identified in consents lodged at the second Council that I worked for.

3 REGULATORY REVIEW

3.1 The New Zealand Building Act 2004

The New Zealand Building Act 2004 (BA04) defines building work as works associated with the construction of a building and includes site works (BA04-S7). A stormwater soakage system to service stormwater runoff from the development of a site is therefore building work. All building work must comply with the building code regardless of whether a consent is required for that work (BA04-S17) but there is no requirement to achieve performance criteria that is additional to or more restrictive than the performance criteria described in the building code (BA04-S18). The Building Code is Schedule 1 of the Building Regulations 1992. Clause E1 contains the requirements for surface water. Clause E1 is repeated in Table 1:

Table 1 - Clause E1 of the Building Code

Objective	
E1.1	*The objective of this provision is to:* *(a) safeguard people from injury or illness, and other property from damage, caused by surface water, and* *(b) protect the outfalls of drainage systems.*
Functional requirement	
E1.2	*Buildings and sitework shall be constructed in a way that protects people and other property from the adverse effects of surface water.*
Performance	
E1.3.1	*Except as otherwise required under the Resource Management Act 1991 for the protection of other property, surface water, resulting from an event having a 10% probability of occurring annually and which is collected or concentrated by buildings or sitework, shall be disposed of in a way that avoids the likelihood of damage or nuisance to other property.*
E1.3.2	*Surface water, resulting from an event having a 2% probability of occurring annually, shall not enter buildings.* *Performance E1.3.2 shall apply only to housing, communal residential and communal non-residential buildings.*
E1.3.3	*Drainage systems for the disposal of surface water shall be constructed to:* *(a) convey surface water to an appropriate outfall using gravity flow where possible,* *(b) avoid the likelihood of blockages,* *(c) avoid the likelihood of leakage, penetration by roots, or the entry of ground water where pipes or lined channels are used,* *(d) provide reasonable access for maintenance and clearing blockages,* *(e) avoid the likelihood of damage to any outfall, in a manner acceptable to the network utility operator, and* *(f) avoid the likelihood of damage from superimposed loads or normal ground movements.*

An outfall in relation to a surface water disposal system *"may include a natural watercourse, kerb and channel, or a soakage system"* (MBIE, 1992).

3.2 The Resource Management Act 1991

Clause E1.3.1 of the Building Code allows for a more onerous design storm to be required under the Resource Management Act 1991 (RMA91). RMA91-S76 allows territorial authorities (city and district councils) to include rules in a District Plan to achieve the objectives and policies of the plan, and any rule in a District Plan is thereby given the force and effect of a regulation under RMA91. The section goes on to state:

(2A) Rules may be made under this section, for the protection of other property (as defined in section 7 of the Building Act 2004) from the effects of surface water, which require persons undertaking building work to achieve performance criteria additional to, or more restrictive than, those specified in the building code as defined in section 7 of the Building Act 2004.
(3) In making a rule, the territorial authority shall have regard to the actual or potential effect on the environment of activities including, in particular, any adverse effect.

3.3 Discussion

From the regulatory review, it is apparent that a soakage system associated with a building is building works and must comply with The Building Act 2004 and The Building Code. While the Building Code sets out the minimum requirements that a soakage system must achieve, territorial authorities can include rules in a District Plan that require designs to achieve a higher standard of protection.

4 NATURAL HAZARDS ASSOCIATED WITH SOAKAGE

A Building Consent Authority (BCA) must refuse a building consent if the land on which the building work is to be carried out is subject to or is likely to be subject to one or more natural hazards or the building work is likely to accelerate, worsen, or result in a natural hazard on that land or any other property (BA04-S71-1). Property includes, land, buildings and goods. Other property is any land or buildings, or part of any land or buildings, that are not held under the same allotment or the same ownership, including roads (BA04-S7). BA04-S71 defines five natural hazards, four of which can be affected by the use or lack of use of soakage systems; erosion, subsidence, inundation, and slippage.

4.1 Erosion

If a soakage system fails and/or water does not enter it due to blockages, the resulting runoff can contribute to surface erosion. Soakage can also contribute to subsurface erosion such as piping or tomo development in susceptible soils, such as recent volcanic soils or loess.

4.2 Subsidence

If soakage is not adopted in areas where compressible soils are present, there is potential for lowering of groundwater table(s). This results in an increase in effective stress and can induce or accelerate settlement of the compressible soils. Where peat soils are present, shrinkage due to oxidation may also occur due to changes in the groundwater regime.

4.3 Inundation

There are three types of inundation that can be affected by the performance of a soakage system: flooding, overland flow and ponding. Soakage systems that are under designed may result in ponding within the property but in many instances, there will be overland flow towards other property. If the other property is a road there may or may not be capacity to receive the additional runoff without flooding.

Prior to development, a proportion of the rainfall infiltrates into the ground from the surface, the remainder runs off as sheet flow or is concentrated by topography into overland flow paths that eventually form streams and rivers. On a rural property in a large undeveloped catchment, the change in runoff characteristics as a result of an underperforming soakage system serving a new dwelling is unlikely to significantly alter the drainage characteristics. As development intensifies, the cumulative effects require consideration. In the urban environment if multiple soakage

systems do not perform as designed the runoff volume will be greater. When this is coupled with the reduction in permeable surfaces, there is potential to increase the overland flow volume, depth and velocity. If the flow is impounded, then the depth and extent of ponding or flooding will increase. It is now more common for councils with urban centres to undertake flood hazard modelling for the 1% or 2% Annual Exceedance Probability (AEP) storm. At risk areas, can now be quickly identified by council staff.

The performance criteria of the E1.3.1 (refer **Table 1**) requires design for the storm event having a 10% AEP, except when otherwise required by the Resource Management Act. If the modelling identifies low return period flooding and systems are designed to a lesser standard, then there is potential that flooding is made worse by designing to the requirement in E1.3.1. Many engineers also consider the critical storm duration. E1/VM1 considers only the 60-minute storm. The critical storm duration is often more than 60 minutes and therefore systems designed for the 60-minute storm are more prone to failure. While District Plans can require the higher standard than E1.3.1 there are variations between Councils.

4.4 Slippage

When soakage is used as a primary outfall, both the rainfall that would naturally runoff in the greenfield situation, and the rainfall that would have infiltrated through the soil matrix are collected by the stormwater management system. The rainfall is then injected into the soil profile at a depth. As a result, there is more stormwater going into the ground, in a concentrated location and the natural attenuation is bypassed. If the singular or cumulative effects are sufficient, either a loss of matric suction in partially saturated soils, or an increase in pore water pressure in saturated soils can occur. Both can result in land slippage.

4.5 Discussion

The natural hazards associated with stormwater soakage are not likely to be isolated to the property, as the excess water may affect other property through overland flow and contributing to ponding or existing flood hazards. Changes in groundwater flows because of soakage may also result in slippage, subsidence and erosion on other property.

5 SUITABILITY FOR SOAKAGE

The designer needs to address if the location is suitable for soakage. Landfill sites; flood areas; valley floors where there may be groundwater inflows; access for maintenance; clearance from buildings and services and slope stability all require consideration (NZWERF, 2004). Once the intended location has been assessed, an investigation is necessary to confirm if the subsurface conditions are suitable for soakage. This should consider the depth of the permeable materials, extent and depth of impermeable materials, the winter water table level and likely effects of water table rise, both short term and long term (NZWERF, 2004).

E1/VM1 Section 9.0.1 simply states that the *"suitability of the natural ground to receive and dispose of the water without causing damage or nuisance to neighbouring property shall be demonstrated to the satisfaction of the Territorial Authority".* E1/VM1 also includes a comment that it does not address the suitability for soakage, however Section 9.0.2 of E1/VM1 contains a prescriptive soakage test. E1/VM1 used the term neighbouring property which is not defined in either BA04 or MBIE, 1992. The Oxford Dictionary defines neighbouring as *next to* or *very near another place*. BA04 and Clause E1 of the Building Code use the term Other Property which is more encompassing and not necessarily limited by proximity.

By not addressing suitability for soakage E1/VM1 is incomplete. It also appears to set a lower standard than required in the Building Code with respect to the protection of other property.

6 SOAKAGE TEST METHODS

Table 2 compares the falling head soakage tests method in E1/VM1 with three other guidelines from the upper North Island. The other guidelines are for Auckland Council (Auckland Council, 2013), Matamata Piako Distict Council (Aurecon NZ Ltd, 2010) and Cambridge North (Tonkin & Taylor Ltd, 2004).

Table 2 - Soakage Test Methods

	NZBC E1/VM1	Auckland	Matamata Piako	Cambridge North
Test diameter	100-150 mm	100 to 150 mm	100 to 150 mm	100 mm
Depth	Intended depth of the soakhole	Intended depth of the soakhole	Intended depth of the soakhole	≥ intended depth of soakage
Number of tests	Not specified	1 per 50 m^2 of soakage device	Varies	Minimum 2 in area of system
Groundwater	If encountered take as depth of the soakhole	Oct-May then water table taken 1 m higher than observed.	0.5 m above winter groundwater and 1 m above summer groundwater	Not addressed
Pre-soak requirement	4 hours unless drains completely in a short time	4 hours winter. 17 hours in summer.	4 hours unless completely drains in < than 5 minutes. If < 5 minutes refill & retest 5 times.	Fill and allow to drain, then repeat.
Completion	Almost empty or 4 hours - use shortest	Water level is 250 mm from base or 4 hours. If quick draining repeat several times	Between 200 and 300 mm from the base	250 mm from base then repeat
Interpretation	The soakage rate in mm/hr is determined from the minimum slope of the curve. If there is a marked decrease the lower rates may be discarded and value closer to the average can be used	Use the minimum slope to determine litres/m^2/min using worksheet provided	Use the average wetted perimeter and volume of water lost at each time step to determine litres/min/m^2. Take the average value and half it for design	Use lower quartile to calculate soakage rate in m/sec using wetted perimeter and volume lost
Comments		Also has a constant head method		
Sizing of system	Use base area only	Use base + half side wall area	Design charts	Not provided

7 COMPARATIVE TESTING

To compare the various methods, several soakage tests were repeated on a Hamilton site in August 2016 and May 2017. The soil profile consisted of 250 mm topsoil overlying stiff clayey silt to 900 mm. Below 900 mm, medium dense to dense sand was present to the base of the 1.9 m deep test hole. In August 2016, the groundwater table was measured at 2.2 m depth. In May, the groundwater was measured in the original test hole at 1.5 m, so a second test hole was augured 2

m away to 1.4 m depth. Wet sieve samples tested by an IANZ accredited laboratory show the sand is primarily a medium sand with less than 15% fines. The test conditions are summarised in **Table 3**. The soakage rate was calculated using the methods in **Table 2** along with Horslev's method. Constant head calculations were undertaken at the completion of the 4-hour pre-soak. The soakage test data is presented graphically in **Figure 1** and the calculated results are presented in **Table 4**.

Table 3 - Soakage Test Conditions

Test Number	Date	Depth to base / groundwater (m)	Presoak	Time to Drain (min)
1	20 August 2016	1.95 / 2.20	No presoak	26
2	20 August 2016		Immediate refill after Test 1	33
3	20 August 2016		Immediate refill after Test 2	44
4	21 August 2016		4 Hour presoak	174
5	13 May 2017	1.35 / 1.52	No Presoak	145
6	13 May 2017		Immediate refill after Test 5	159
7	14 May 2017		4 Hour presoak	330

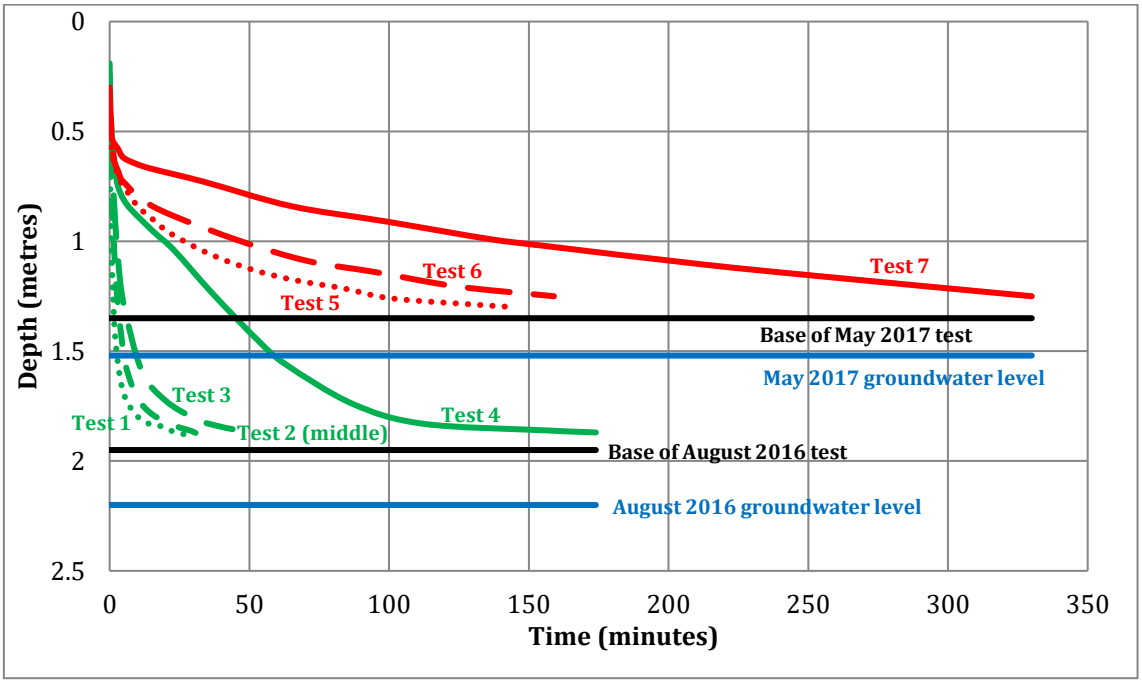

Figure 1 – Soakage test results

E1/VM1 uses mm/hour or distance/time as it is a simple observed drop over time. The other methods all use volume lost/time/surface area. As volume is m^3 and area is m^2 this reduces to m. The time component can be adjusted to suit. Therefore 300 litres/hour/m^2 is 0.3m^3/hour/m^2 which reduces to 0.3 m/hour or 300 mm/hour. On this basis, the results are comparable.

7.1 Discussion of results

Unsurprisingly the graphical results show decreasing soakage rates with each subsequent test, however the degree of the change with the 4-hour pre-soak was not expected. The volume of water used in the pre-soak was approximately 380 litres in one test and 520 litres in the other test. Considering a 1 hour 50-year storm in Hamilton will generate approximately 490 litres of water

from 10 square metres, the volume of water used in the pre-soak seems disproportionately large to the scale of the test. It is unlikely a full size system would be soaked with 40 to 50 times its volume prior to the design storm occurring. Wetting would be progressive as the hole fills and infiltration occurs during the storm.

Table 4 - Soakage test results – Specified rate in bold

	Test Results in litres/m^2/hour or mm/hour							
	1		**2**		**3**		**4**	
	Min.	**Avg.**	**Min.**	**Avg.**	**Min.**	**Avg.**	**Min.**	**Avg.**
NZBC E1/VM1	**100**	14965	**248**	14435	**164**	12435	**32**	3428
Auckland	**17**	372	**46**	302	**29**	220	**7**	62
Matamata Piako	14	**358**	39	**293**	25	**215**	5	**60**
Cambridge North	16	**440**	43	**359**	27	**265**	6	**74**
Horslev	19	427	53	346	34	253	8	70
Constant head								244
	5		**6**		**7**			
	Min.	**Avg.**	**Min.**	**Avg.**	**Min.**	**Avg.**		
NZBC E1/VM1	**56**	4317	**77**	7110	**72**	1738		
Auckland	**13**	126	**10**	170	**5**	45		
Matamata Piako	11	**122**	9	**166**	5	**44**		
Cambridge North	12	**148**	10	**203**	6	**54**		
Horslev	15	144	11	195	6	52		
Constant head						338		

The minimum in **Table 4** was the true minimum from the time steps. E1/VM1 does allow the lower values to be discarded and a value closer to the average to be used if there is a marked decrease. For Test 4 the average over the mid-part (0.96m to 1.74m) is approximately 700mm/hour. E1/VM1 doesn't include the side area in the calculation of the soakage rate or the calculation of the soakage system. It also does not include any means of preventing loss through the side walls of the soakage test. The effect of this is shown in **Table 5** where the sidewall surface area in a small-scale test has a much greater proportion of the total soakage area regardless of the water depth. If there is only 0.03 m of water in the test hole, the side wall is the dominant part of the soakage area. For example the average of the tail, (last 5 result increments) on Test 1 is 758mm/hour using E1/VM1. As all soakage tests have a tail, the loose wording in E1 allows un-conservative rates dominated by sidewall soakage to be used.

Table 5 - Surface area ratios of small scale tests and full size soakage tests

	0.1 m diameter test hole			**1.2 m diameter porous soak hole**		
Water depth	**Side wall surface area**	**Base area**	**Ratio - Side / Base**	**Side wall surface area**	**Base area**	**Ratio - Side / Base**
m	**m2**	**m2**		**m2**	**m2**	
0.02	0.006	0.008	0.8	0.08	1.13	0.07
0.03	0.009	0.008	1.2	0.11	1.13	0.1
0.1	0.031	0.008	4	0.38	1.13	0.33
0.2	0.063	0.008	8	0.75	1.13	0.67
0.5	0.157	0.008	20	1.88	1.13	1.67
1	0.314	0.008	40	3.77	1.13	3.33

The averages presented were calculated using all the time steps in the data. This gives a higher weighting to the parts of the test with more data, normally at the commencement of the test, with

greater head. This explains why Test 6 has faster rates than Test 5, even though the curve indicates it should be less. If a single line calculation is undertaken the results are typically much lower, for example using only the first and last data points on Test 6 the MPDC rate is 52 litres/m^2/hour. The latter values may also be more representative of steady state saturated conditions. Averages need to be more considered, with outliers removed, and consider the soakage zone. The Auckland Council method appears to be overconservative by requiring the minimum rate of the curve to be used with a prescribed calculation. Several councils require that the test rate is halved in the design (as a factor of safety), while Auckland does not require this, the rate would still be considerably less than the other methods.

The soils in the comparative testing were strongly layered and it is reasonable to assume that the soakage was occurring preferentially through the sand layer. None of the methods used to calculate the soakage rate consider the effects of strongly stratified soils. This may be acceptable as this is also likely to occur in a full-size system, however further research could be done in this area to confirm if scale effects need to be accounted for.

8 CONCLUSIONS

Soakage testing is highly subjective to the method used, the test conditions and the interpretation of the data. As E1/VM1 does not include information on the suitability for soakage, there is potential for soakage systems to cause, accelerate or worsen several types of natural hazards on other property. E1/VM1 did not require the winter water table to be established and testing in summer can result in a reduced storage capacity leading to failure. E1/VM1 does not include any information on the location or the operation and maintenance requirements that the designer needs to address and therefore it does not meet E1.3.3 of the Building Code. Based on the unconservative soakage test rate, failure to address suitability of soakage, groundwater conditions and operation and maintenance requirements, it is concluded that the soakage test and design method in E1/VM1 does not meet the requirements of the Building Code Clause E1. Clause E1 of the Building Code is out of date for modern urban intensification. The level of protection to other property should be reviewed and bought into line with current best practice nationally and internationally. It is recommended that the soakage test and design methods are removed from E1/VM1 and replaced with a New Zealand Standard for On-site Stormwater Management: Soakage and Attenuation. This should be consistently adopted by Councils.

Further research is recommended into the effects of layered soils and the proximity of groundwater to the soakage test, suitable pre-soak times, scale effects, interpretation of the test results and a suitable factor of safety.

REFERENCES

Auckland Council. (2013) *Stormwater Disposal via Soakage in the Auckland Region*. Auckland: Auckland Council.

Aurecon NZ Ltd. (2010) *Soakage Design Procedures and Guidelines.* Te Aroha: Matamata Piako District Council.

MBIE. (1992) *Acceptable Solutions and Verification Methods For New Zealand Building Code Clause E1 Surface Water* (10 ed.). (MBIE, Ed.) Wellington: Ministry of Business, Innovation and Employment.

NZWERF. (2004) *On-site Stormwater Management Guideline.* Wellington: New Zealand Water Environment Research Foundation.

Tonkin & Taylor Ltd (2004). *Cambridge North Residential Zone Guidelines for On-site Stormwater Soakage.* Te Awamutu: Waipa District Council.

Observations from reviewing consent applications

M D Trigger
AECOM New Zealand Limited.
mike.trigger@aecom.com (Corresponding author)

Keywords: Producer statements, retaining walls, siteworks, liquefaction

ABSTRACT

Building control authorities use producer statements throughout the building consent and certification process. When it comes to geotechnical matters, acceptance of a producer statement may not be a reliable indication that the works comply with the building code. There is often a lack of consideration to site works and compliance with the building code beyond the envelope of the main building. Building practices have changed and flat sites are now desired, timber retaining is preferred, but are their long term consequences? Although the geotechnical earthquake engineering modules have been released, it is not a simple matter to implement them. This paper discusses some of the challenges that councils face with geotechnical matters and suggests some enhancements.

1 INTRODUCTION

At two stages of my career I have worked for different councils processing geotechnical and civil engineering reports and designs that have accompanied resource consents and building consents. Working at councils provides access to information and examples of where things have gone wrong and you work to prevent it recurring in the future. Councils are not companies and may be caught up in litigation years after the design firm has been disestablished, so it is therefore important to reduce the risk of legacy issues developing. This paper provides a snapshot of some of my experiences at both councils, and includes some comments based on my dealings with other councils when representing clients.

2 GEOTECHNICAL REPORTING DURING SUBDIVISION

During the land development process, several geotechnical reports are often provided to councils. The first is to demonstrate the suitability of the land for the proposed development. The purpose of this report is to address natural hazards and demonstrate to councils that the land can be developed to meet the requirements of the Resource Management Act and District Plan.

If the site is to be modified then a geotechnical design report is often needed. The purpose of this report should be to confirm the suitability of the proposed landform and provide any specific assessments needed to support the detailed design of the subdivision and landform. This is a detailed design stage, however it is not always completed and I have had experiences where the development works have been approved without the input recommended in the suitability report. In these cases we have had to tell the clients that we need to satisfy ourselves that the works are suitable before we can supervise them, and in some instances modify the works and have the new design approved by the council.

The final report for each stage of a development should be a Geotechnical Completion Report or GCR. This report summarises the works undertaken and provides the recommendations for the building consent phase. Some GCRs provide recommendations for additional investigation and assessment. Other GCRs state that buildings can be built in accordance with NZS3604, provide an ultimate bearing capacity or recommend liquefaction resistant foundation design. In my experience some councils have issued building consents without requiring the subsequent

assessment that was recommended by the GCR, or validating that the assessment has addressed the issues flagged in the GCR. When this occurs the council exposes itself to liability should any issue arise in the future.

Sometimes the GCR for new sections on sloping land states that the site is suitable for standard foundations in accordance with NZS3604. The recommendation has often been provided on the basis of a test between 1.5 and 2 metres deep. While the GCR is technically correct that the site is suitable for *some types of foundations* in accordance with NZS3604 it does not address construction of the single level concrete floor.

3 SLOPE STABILITY

Both of the councils I worked at have areas where the topography and geology is prone to deep seated instability and flow failures have previously occurred. One of the councils had zoned a significant area of steep unstable land for lifestyle sections with a minimum size of 5000m^2. I was frequently provided with geotechnical reports with 2 metre deep hand augers and statements such as "the slope is less than 25 degrees and considered stable". On more than one occasion while undertaking my site check or checking the aerial photos in the GIS system, I identified active or past instability. There was no mention of the wider geomorphology or recognition of the geohazards in documents that were described as geotechnical reports. While a house was under construction on one of these sites, a deep seated slip occurred metres from the house that resulted in a flow that had enough momentum to travel 5-6 metres up the adjacent ridge. Fortunately I had not been involved in either the subdivision or building consent process for that site.

Having a suitable geotechnical report is no guarantee that the recommendations will be followed. I once reviewed a building consent for a house adjacent to the crest a steep 35 m high slope. The house was entirely located downslope of the established building restriction line. The consent included an engineer designed raft and a PS1 (Producer Statement – Design) that was issued subject to confirmation of ground conditions. The engineer had signed the plans showing where the house was in relation to the building restriction line. On another site where most of a debris protection bund was removed to create a building platform, the engineer who provided the PS1 did not considering the purpose of the bund and the impact forces that could occur. In a third example for a house on a slope, the engineer who provided the PS1 designed piles to extend through deep fill and an underlying buried topsoil layer, to be founded with only 300mm embedment into the natural soil. No assessment or calculations were provided for the possible lateral forces on the piles.

4 PRODUCER STATEMENTS

An engineer must provide sufficient information with an application to satisfy the council on reasonable grounds that the proposed works would comply with the Building Code if the works are completed in accordance with the plans and specifications that accompanied the application (BA04 - S49). Many councils request PS1s at the time consent is lodged. At the end of the building process PS4s (Producer Statement - Construction Review) may also be requested.

IPENZ, 2014 refers to the recommended practice when producer statements are used to support building consent applications:

> *"… a BCA (Building Consent Authority) that relies wholly on a producer statement, without providing some level of assessment, audit or review of the work, is not taking reasonable steps to satisfy itself as to the design or construction's adequacy. BCAs should also satisfy themselves, on reasonable grounds, that the author of the producer statement is suitably competent to have carried out the work described."*

Multiple determinations also refer to the role of the producer statement as part of the documentation, however the BCA still had sole responsibility to determine that the documents and built work complied with the building code.

In Section 3, I provided three examples where the designs did not have sufficient information to demonstrate compliance with the building code and yet PS1s were issued. Unfortunately this is common.

Many engineers also supply PS4's without any additional information or a summary providing the basis for issuing the PS4. I have seen PS4s for retaining walls that were later shown to be factually incorrect. PS4s issued for earthfills have not had test records or the testing used incorrect methods. Earthfills are building works if associated with a building (BA04 - S7 & S8) and must comply with Clause B1 of the Building Code (BA04 - S17),

In some instances, supporting information has been requested and not supplied, even though record keeping is very important and councils need to be the keeper of records. One company told a council they don't keep testing records and provide their recommendations on site. Years down the track when someone wants to know what has happened, the companies involved may no longer exist, but the councils will (in one form or another).

5 COMMERCIAL BUILDING FOUNDATIONS

It is common for structural engineers to supply producer statements for commercial buildings assuming ground conditions are in accordance with NZS3604 or an ultimate bearing capacity of 300kPa subject to on-site verification. BA04-S49 requires that it is reasonable to accept that construction in accordance with the ***plans submitted*** will comply with the building code. The B1 compliance document states that 300kPa can be assumed if testing with a Scala Penetrometer indicates 5/blows per 100mm to a depth equal to twice the width of the foundation. This is seldom established and commercial buildings often have large pads, which would require testing deeper than most structural engineers would undertake during construction. Where sedimentary soils are present the ground conditions can also be variable horizontally and vertically.

Several buildings have required the foundations to be redesigned following requests for assessment by a geotechnical engineer. One of the more extreme examples I have been involved with was a 2-storey office building that had a shallow investigation by the designer of shallow pad foundations. The investigations showed saturated loose sand and organic soil to the base of the testing. I requested a geotechnical peer review. The reviewer required several drill holes and CPT tests to be undertaken with the resulting report recommending a raft foundation for liquefaction and settlement mitigation. When the designer only increased the size of the pads I requested the geotechnical engineer sign the plans. A new design for a raft was subsequently supplied.

6 SITE WORKS

Site works associated with the construction of a building are building works (BA04 – S7 & S8) and all building works must comply with the building code, (BA04 - 17). Of interest in this section are provisions B1.2 and B1.3 of the building code which requires buildings and sitework to withstand the combination of loads that they are likely to experience and have a low probability of rupturing, becoming unstable, losing equilibrium or collapsing during construction or alteration and throughout their lives.

In the past, buildings were designed to fit the land. Free-standing garages, basements and upper floor garages are common sights in the hilly older suburbs of many cities. Today, single level concrete floor construction makes up the vast majority of new buildings within greenfield subdivisions. Most building companies do not have standard plans offering split level buildings,

basements or pole construction. As a result, the building company will need to undertake further earthworks to create the level site that they need. This will often involve the construction of retaining walls on or near boundaries.

Many architectural designers misrepresent the site works on plans. The elevations tend to show the site to be level and they do not extend the ground beyond the boundaries. Contours or levels on plans frequently do not match subdivision as built contours. Those that got it right would have deep excavations adjacent to boundaries to construct retaining walls or large fills. It wasn't just the designers; many engineers gave no thought to the stability of cuts during construction. Although some soils will often stand vertically unsupported for some time, there have been cases where other property was adversely affected by temporary works in these soils.

Fills for single house sites are frequently poorly controlled. Engineers have certified deep fills that went beyond building restrictions lines imposed by a geotechnical engineer without any additional assessment. Cohesive fills have been tested with a Scala penetrometer, or only tested in the upper metre. I have seen cases where building inspectors could push their 'T' probes up to the handle in "tested" fill. When we began requesting earthworks specifications that showed compliance with NZS4431, a number of structural and civil firms were unable to show that they had an understanding of soil compaction and current practice.

Scala penetrometer testing is presented in a variety of non-standard ways. It is not uncommon to see Scala penetrometer testing presented as a bearing capacity with depth or a California Bearing Ratio with depth, without the site data. One engineer was generally presenting penetration per 10 blows but on some data lines they indicated a different number of blows. Once I had confirmed with them what the document was showing I needed to make a check sheet for the council staff so that they could readily confirm that the test results provided reasonable grounds to be accepted as good ground, as described in NZS3604.

7 RETAINING WALLS

Retaining walls are buildings (BA04 - S7 & S8), although not all retaining walls require a building consent (BA04 - Schedule 1). Regardless of whether a building consent is required; they must comply with the building code (BA04 - S17). It has been common place to show some retaining walls on plans as "landscaping walls"

For a wall to be a landscaping wall, there needs to be no surcharge throughout the life of the wall. I also think it is also reasonable that for any retaining wall that is shown on plans that a council approves to have sufficient information to show how it complies with the Building Code, as the council is confirming that the documents comply with the building code when the plans are approved, and at the end of the process the building works are signed off with a Code of Compliance Certificate (CCC). If the applicant does not want to demonstrate that the wall complies with the Building Code, they need to show how they can develop the site without the need for the wall, and build their non-compliant wall once they have received their (CCC).

7.1 Timber pole retaining walls

The most common type of retaining wall is the timber pole retaining wall. At both councils, compliance of a retaining wall with the building code was assessed by the Building Consent Officer (BCO). The wall was accepted as compliant if there was design by an engineer with a PS1 and the BCO recorded "PS-1 from XX CPEng No. YY".

The first retaining wall design I reviewed for a council was designed by a CPEng and it had an accompanying set of calculations, a PS1 producer statement and a hand sketch of the wall. The wall appeared undersized and an independent calculation check indicated that the wall poles were at least 2 sizes too small and embedment was not sufficient. The documentation was also

insufficient to demonstrate compliance with the building code. The omissions and errors are listed in **Table 1**.

Table 1 - Timber pole retaining wall design omissions / errors

No geotechnical investigation*	No design description of the site and boundary conditions*	Did not allow for sloping ground above and below the walls
No comment on seismic requirements*	Did not consider long term drained soil failure*	Increased the undrained shear strength for the highest wall height without explanation
Bending moment taken at ground level*	Superseded timber bending strength used*	Multiple calculation errors
Global stability not addressed*	Missing elevations of the walls*	Safety in design not considered*

*Denotes items that were commonly omitted by designers

The sketch detail was basic and didn't include the key assumptions from the design calculations such as the rail span and strength grade, the treatment of timber wasn't specified and drainage was simply referred to as free draining backfill. By not supplying a reasonable detail that was consistent with the design, there was not sufficient grounds to accept that it would comply with B1 and B2 when built.

It soon became apparent that it was common practice for structural and civil engineers to present a set of calculations with a PS1 without any reasonable supporting documentation. The PS1 would often state ground assumed to be as per NZS3604, and more than often the wall was designed from the plans and the engineer had not been to the site or verified the topography.

In contrast designs received from geotechnical engineers always included a site investigation, a design summary and generally addressed the other matters. This leads to the question *what do the structural engineers know about highly variable soil and ground water conditions that the geotechnical specialists don't?*

Some firms gave inspection schedules that only required them to inspect the holes to issue a PS4 or recommended that Council inspect the wall. They were taking aggressive design approaches such ignoring groundwater, adopting the maximum pole taper, requiring rails to be strength tested timber and have multiple spans. In my opinion, a building inspector is unlikely to see these and is even more unlikely to understand the basis of the design based on a rudimentary detail and several pages of calculations.

7.2 Stacked or terraced retaining walls

If multiple building companies are developing sites within a subdivision it is likely that they don't know what is happening on the adjacent site until it happens. This has led to consents being issued for retaining walls that are influenced by other retaining walls which then needed to be dealt with during the construction phase. There are at least two ways that this can be prevented. Retaining walls can be constructed as part of subdivisional work, so single walls are built near the boundaries that are suitable for the future building consents. Alternatively, the BCA needs to keep records of the levels shown on plans that are already in the system or approved.

Terraced retaining walls are also problematic as there is no code or design note for how to assess the force interactions. Some engineers can present reasonable interpretations while others simply try to ignore it.

7.3 Masonry retaining walls

Masonry walls are often designed by structural engineers using the vertical bearing capacity from a geotechnical completion report or an assumed bearing capacity if there is no GCR. From the bearing capacity equation in B1/VM4, the associated worked example and more recently Module 6 (MBIE, 2017) it is apparent that load inclination factors adversely affect the bearing capacity. There is normally no specific check on the bearing capacity. Several design firms did not check sliding until requested and free standing walls are routinely not checked for global stability.

7.4 Pool retaining walls

Pools are often submitted with generic producer statements and assumed ground conditions. One pool company uses an engineer in Australia and the site assumptions relate to expansive soil conditions. Council building inspectors are very unlikely to understand the Australian expansive soil references. Pools are big investments. In my opinion generic producer statements that are not based on site specific ground conditions should not be accepted.

7.5 Potential legacy issues

In my opinion, the prevalence of timber retaining walls to create level building sites may well be the next "leaky building crisis". The preferred construction material is soft pine that has been chemically treated to prevent rot. The H5 treated timber poles are rated for structural ground contact with a design life of 50 years. The lagging between the poles is routinely constructed with H4 timber as permitted by NZS3603. It is not clear how the lagging (or poles) on a 4-metre-high retaining wall supporting someone else's property can be adequately replaced without a large excavation extending into that property. More concerning is that on many properties it will not be possible to access the walls with the machinery necessary to replace them. Strengthening work such as soil anchors may also not be possible.

Another point to ponder is whether a retaining wall that is constructed as part of a subdivision with a design life of 50 years remains suitable to support a building if the consent for the building is lodged 10 years later.

8 SECTION 72

One of the requirements of both the councils I worked for is the identified building sites shown on subdivision plans can have a building consent issued without reference to S72 of the Building Act 2004 (BA04). There are varying interpretations within councils and also between different councils, as to how S72 should be applied and in what situations. New titles have been created on land that floods or is prone to settlement, without imposing consent notices informing the buyers that a S72 would be required.

An interesting example of how S72 can be interpreted is a house that cantilevers over a building restriction line. The house has been mitigated yet the land under the house and towards the slope crest has been assessed as potentially subject to a natural hazard. Some believe the house is supported on stable ground and S72 is not applicable. Alternatively, EQC considers the land within 8 metres of the dwelling as contiguous with the dwelling and would cover a claim on that land.

Should S72 be applicable for a palisade wall within a zone of instability? The wall is designed to protect the upslope land. The ground downslope of the wall remains unstable and it's possible that strengthening works would be required once the land in front slips. The same could also be true for a house that is piled beyond the building restriction line.

9 LIQUEFACTION

Taylor, 2012 discussed a historical environment in Christchurch where developers, relied on engineers, engineers needed to keep costs down to win work and would do the minimum to get it through council. This meant that if the council didn't ask for liquefaction to be assessed it wasn't undertaken and the cycle continued.

In 2016, Modules 2 and 3 of the geotechnical earthquake engineering series were released (MBIE, 2016a and 2016b). The intent was to standardise the assessment requirements nationally. Despite the modules, it is still common for engineers to prepare geotechnical reports in areas where liquefaction assessment should be undertaken, without doing an assessment. When a council started to ask for liquefaction to be addressed, the majority of geotechnical engineers supported this approach. Building designers, structural and civil engineers protested. One rang MBIE several months after the modules were published and was told that the guidelines were for Canterbury only. Complainants focused on time delays and additional cost, not the long term resilience of the community, costs of displacement and repair nor the risk exposure to the organisation by issuing building consents in an area with a mapped hazard.

10 PRESSURES ON COUNCIL STAFF

Councils have statutory time frames that need to be met for resource consents and building consents. This is a key audit metric in a BCA's accreditation. At both councils; resource consents and building consents submitted were lacking supporting information or with inadequate supporting information. By the time they are reviewed and information is requested, the majority of the days have lapsed. This applies pressure in responding to further information received.

In some instances, designs take several iterations between council and the designers. As they solve one issue, they create another. Significant staff time is tied up dealing with consents that are not in a state that can be approved. This can entail emails, phone calls and meetings. Some applicants or their representatives automatically escalate matters to elected members or senior management. Complaints often focus on timeframes and costs. Again this impedes the ability of staff to focus on the good consents as their time is spent justifying decisions to several layers of management.

While councils can use peer reviews, their use is contentious. The applicant or their agent complains that they have already used a "highly qualified member of IPENZ". They object to the additional costs and delays. The peer reviewer then ends up having the same discussions as council with the originator and having to resolve the design. When a council has had a number of such reviews they lose confidence in the designer. While complaints can be lodged with IPENZ they are time consuming to resolve and in the interim council can't advise the public against the use of the engineer. They therefore have to continue to accept their work when submitted and review it for compliance.

11 BUILDING CONTROL OFFICERS

Building Control Officers (BCO's) and inspectors have a history of focusing on "the building". The interaction of building works outside of the main building envelope is often not assessed by the BCO. However, the compliance of the building works also requires that the following building code clauses are addressed, safe and functional access for vehicles and persons (Clause D1), site works (Clause B1), retaining walls (Clauses B1 and B2), on-site stormwater management (Clause E1) and on-site wastewater management (Clause G13). In my experience these are not things that BCOs and inspectors are trained to assess.

Both councils I was involved with used had historically used Project Information Memorandum Officers (PIM officers) that sat outside of the BCA to review geotechnical and environmental

engineering. The PIM officers did not have an engineering background, and their primary function was to confirm that producer statements had been supplied or would be supplied. This is inconsistent with the requirements of the Building Act and IPENZ, 2014.

12 CONCLUSIONS

There are a number of good engineers supplying a high standard of work. Unfortunately the market dictates that the cheaper engineers, who will undertake geotechnical design without investigation and provide minimal supervision, will undertake the greater portion of the work, particularly in the residential building market.

In my opinion councils and the wider industry would be assisted if the following suggestions were adopted by MBIE, IPENZ and NZGS:

- Review extent that producer statements are relied on and how BCA's determine if the works referred to in a producer statement comply with the building code. This should be undertaken as part of the BCA's compliance audits.
- Develop a mandatory competency standard for anyone who assesses the compliance of site works and geotechnical information. The standards would also include the triggers for specialist review.
- Further development of Module 6 for the design of residential retaining walls including minimum investigation and documentation requirements, durability requirements and safety in design considerations.
- Development of a design methodology for the design of terraced timber pole retaining walls.
- Promote greater integration between geotechnical and structural disciplines with an IPENZ practice note on the design of foundations. Include geotechnical review of the final design.
- Develop guidance on the use of S72 of the Building Act, with examples of when it should and should not be applied.
- Recognise the recommendations of the Earthquake geotechnical engineering practice Modules 1 to 6 in the building code.

REFERENCES

Building Act 2004 (BA04) New Zealand Government.

Institute of Professional Engineers of New Zealand (2014) Practice Note No 1 *Guidelines on Producer Statement.*

Ministry of Business, Innovation & Development (2016a) New Zealand Geotechnical Society (NZGS). *Earthquake Geotechnical Engineering Practice, Module 2: Geotechnical investigations for earthquake engineering*.

Ministry of Business, Innovation & Development (2016b) New Zealand Geotechnical Society (NZGS). *Earthquake Geotechnical Engineering Practice, Module 3: Identification, assessment and mitigation of liquefaction hazards*.

Ministry of Business, Innovation & Development (2017) New Zealand Geotechnical Society (NZGS). *Earthquake Geotechnical Engineering Practice, Module 6: Earthquake resistant retaining wall design*.

Taylor M., (2012) Geohazard Mitigation in New Zealand – In search of a normative and informative balance. *New Zealand Geomechanics News*.

Resin injection as a ground improvement method

N Traylen
Geotech Consulting Ltd, Christchurch, NZ
ntraylen@geotech.co.nz (Corresponding author)

T Hnat
Mainmark Ground Engineering Ltd, Christchurch, NZ
thnat@mainmark.com

R Wentz
Wentz-Pacific Ltd, Napier, NZ
rwentz@wp-geo.co.nz

L Wotherspoon
University of Auckland, Auckland, NZ
l.wotherspoon@auckland.ac.nz

S van Ballegooy
Tonkin + Taylor, Auckland, NZ
SVanBallegooy@tonkintaylor.co.nz

R Deller
Mainmark Ground Engineering Ltd, Christchurch, NZ
rdeller@mainmark.com

Keywords: ground improvement, liquefaction mitigation, resin

ABSTRACT

There are few practical methods currently available for liquefaction mitigation beneath existing structures, despite a growing demand for this due to a significant number of structures being targeted for seismic upgrading. One such method that is viable for liquefaction mitigation beneath existing structures is the injection of expanding resin. This method densifies soils (of suitable composition) and thus increases liquefaction resistance (i.e. increases the relative density and therefore the cyclic resistance ratio of the soils), as well as improves the composite stiffness of the ground.

This paper describes the results of a controlled study that has been carried out into the efficacy of this ground improvement technique. In the study, three test sites in the Christchurch 'Red Zone' were selected for the construction of resin-injected test panels. The soils were assessed using Cone Penetrometer Test (CPT), cross-hole geophysical testing, and dilatometer testing (DMT), to examine the effects the injected materials have had on the density and stiffness of the soils, and therefore their likely liquefaction performance.

The results of the study show that significant improvements in soil density, stiffness and strength were achieved, demonstrating that resin injection is a viable ground improvement method.

1 INTRODUCTION

Injection into the ground of expanding resin mixtures (at relatively shallow depths) has long been used for the level correction of buildings. The injection and expansion process also compacts or densifies the ground, and therefore this process has potential uses in liquefaction mitigation projects, or other applications where ground densification is required.

The aim of this study was to examine on a formal basis whether resin injection is a viable form of ground improvement, primarily for liquefaction mitigation. This has been achieved through a series of trial injection panels, where pre-injection and post-injection soil density and stiffness have been compared by cone penetration testing (CPT), geophysical testing (Vs and Vp testing), dilatometer testing (DMT) and plate load testing (PLT).

2 SOIL IMPROVEMENT MECHANISM

With this technology liquefaction mitigation primarily occurs from densification of the soil by an aggressively expanding polyurethane resin product (although other secondary effects such as improvement in composite stiffness, cementation, etc are also present). With this method, injection tubes are driven into the ground at regular intervals, and at each injection point an injection nozzle is attached to the injection tube. Multipart materials are mixed at specific pressures and temperatures at the nozzle; the live composite material ('resin') is then pumped to the base of the tube, where it enters the soil matrix. Either 'top down' or 'bottom up' methods can be employed. In a typical 'bottom up' installation the tube is withdrawn either in set stages with set volumes of material injected at each stage, or it is withdrawn slowly on a continuous basis with set volumes of material being injected per unit length that the tube is withdrawn.

The low viscosity resin is injected at controlled pressures and penetrates the soil mass along pre-existing planes of weakness or through fracturing of the soil mass. The resin also permeates the soil mass to a limited extent depending on the porosity of the soil. The resin mix chemically reacts soon after injection (at controllable 'rise' times). The material expands rapidly to many times its original volume and changes from a fluid form to an (inert) solid one. Depending on soil density, confinement pressure, and the resin material selected, the expansion volume can be in the order of 5 – 15 times the injected volume (or more if required). The looser the soil, the greater the expansion for a given resin mix. The expansion of the injected material results in compaction of the adjacent soils, due to new material being introduced into a relatively constant soil volume. The resin injection process has been observed to result in a 'veining' of material distributed through the soil mass as dykes, sills or networks of sheets or plates, typically tens of millimetres thick (refer to Figure 1).

Figure 1. Hand-exhumed resin veins (left) and hydro-exhumed resin veins (right).

3 BACKGROUND AND RECENT USE

Ground strengthening by polymer injection has been previously used in Turkey (Erdemgil et al. 2007). Liquefaction mitigation by Resin Injection in New Zealand has been examined in some detail on two recent occasions. A preliminary trial was carried out as part of the 2013 EQC Ground Improvement Trials, and resin injection was also used on a 5400m2 commercial building rehabilitation project in 2015/2016.

3.1 EQC ground improvement trials, 2013

In 2013 a series of ground improvement trials were undertaken in Christchurch by EQC (in press) to examine the performance of various forms of ground improvement, including a preliminary examination of resin injection. The resin injection panel that was tested showed an increase in liquefaction resistance by a number of mechanisms: (i) the overall density of the soil increased, as measured by CPT tip resistance, (ii) shear wave velocity testing showed that the composite stiffness of the improved soil block increased, (iii) the cyclic strains in the soils during shaking were decreased, as measure during vibroseis T-Rex testing, and (iv) pore pressure response during shaking was significantly decreased. The result of these effects was that the ground surface settlements during subsequent blasting trials were also much reduced.

3.2 Commercial shopping centre

Three adjoining large format retail buildings that had suffered liquefaction-related settlement damage in the Canterbury Earthquake Sequence (up to 160mm differential settlement across the 5400m2 combined building footprint) were relevelled, repaired, and upgraded in 2015/2106. The first stage of the remediation works consisted of liquefaction mitigation by densification and stiffening of the underlying shallower soils by Mainmark Ground Engineering Ltd, using their TeretekTM resin injection methodology.

The resin injections resulted in increases in qc1ncs (i.e. the clean sand equivalent of the corrected CPT tip resistance) in the order of 40%, and decreases in calculated settlements in the treated zones of 40-80% at 100-year return periods of shaking (Traylen et al. 2016, Hnat et al. 2017).The project therefore demonstrated that resin injection is a viable technology for ground improvement, and is particularly useful for liquefaction mitigation or ground densification beneath existing structures. Furthermore, the low level of intrusion required to carry out the process was a particular advantage for this operation, as the three retail outlets (including a large supermarket) were able to continue trading uninterrupted through the busy Christmas trading period.

4 RED ZONE SITE SELECTION AND CHARACTERISATION

The 2013 EQC ground improvement trials were carried out in Christchurch in the abandoned 'Red Zone' of Avondale and Bexley. This land is some of the worst affected from the Canterbury earthquakes (due to liquefaction damage). The sites used in this study (Table 1) were adjacent to the areas used in the EQC trial process - they were selected to avoid areas which had been affected by the installation of other ground improvement methods and instruments, and also to avoid areas affected by liquefaction-inducing blasting trials that were carried out in the 2013 study.

Table 1. Trial Sites

Site	Soils	CPT q_c	Water Table	
			Measured*	GNS**
3 – Breezes Rd, Avondale	Silty sands and some silts overlying clean sands at 4.5m depth.	2-5 MPa in the upper 3m; 11 MPa to 5m depth; 5 to 11 MPa to 8m depth.	1.1 – 1.2m	1.1m
4 – Ardrossan St, Avondale	Silty sands and sandy silts overlying clean sands at 2.5m depth.	2-3 MPa in the upper 3-4m; 10 - 12 MPa down to 7m; 5 to 10 MPa to 8m depth.	1.1 – 1.25m	1.1m
6 – Onepu St, Bexley	A predominantly sandy site	Increasing from 2-4 MPa at 1m depth to 10-12 MPa at 4m depth; 7-11 Mpa to 5m depth; 10 -14 MPa to 8m depth.	0.65 – 0.85m	0.8m

* measured Sept – Nov 2016 ** van Ballegooy et al (2014)

5 TEST PANEL LAYOUTS AND TESTING REGIME

Each of the 8m x 8m test panels was set out with a 1.2m triangular grid of resin injection points (Figure 2). The tests were CPT, direct-push crosshole (Vs/Vp), dilatometer ('DMT') and plate load tests ('PLT'). Borehole drilling and laboratory testing was also carried out to determine soils fines contents.

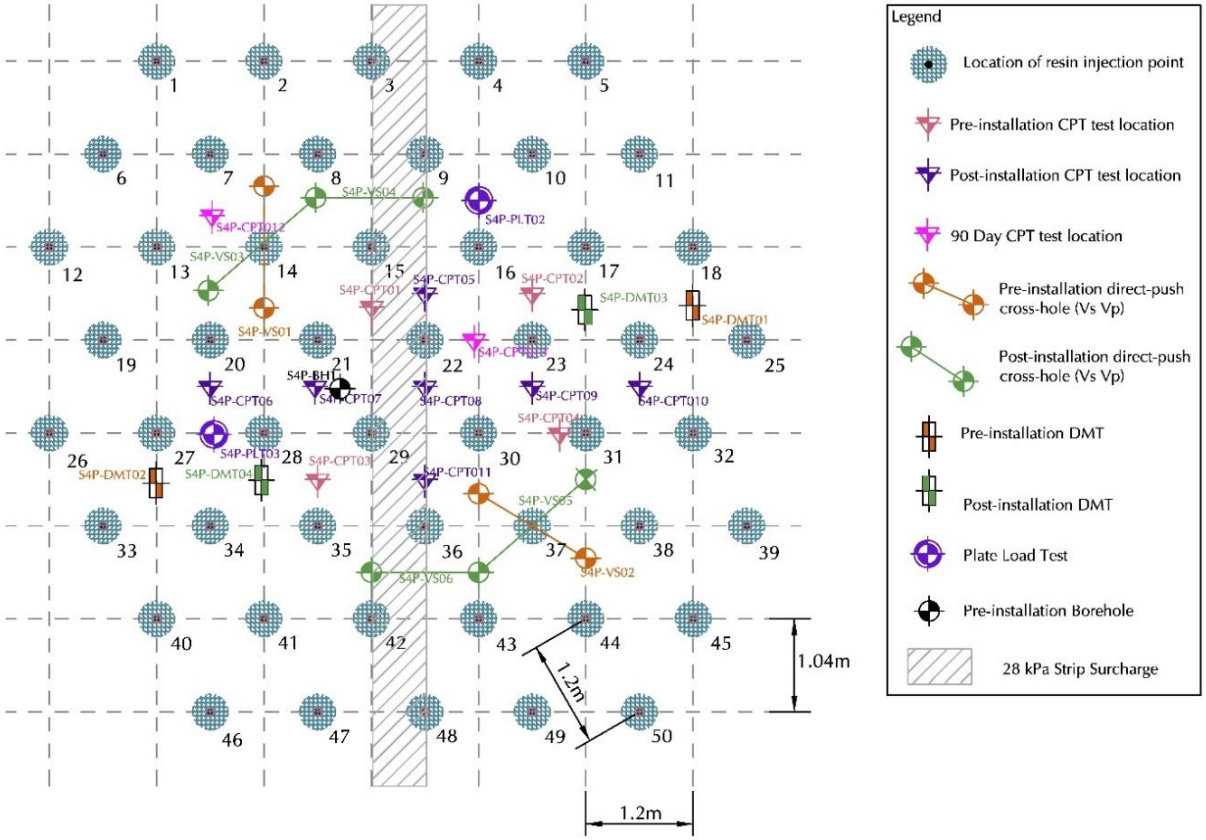

Figure 2 Site 4 installation and testing layout

Table 2. Pre- and post-injection testing

Test	Number carried out at each panel	
	Pre-injection	Post-Injection
CPT	4	7
Direct-push Crosshole (Vs/Vp)	2	4
Dilatometer tests	2	2
Plate load tests	2	2
Borehole	1	-
Fines Content Lab test	3-4	-
Plasticity Index Lab test	0-2	-

Plywood was laid on the ground (over compacted gravel) and then concrete blocks were laid to give a 14 kPa surface load. Steel plate was placed over the blocks to provide a stable working platform. Additional blocks were then laid to superimpose a 28 kPa strip footing load. Pilot holes were drilled and cored through the steel plate, concrete blocks, and plywood to allow the installation of the grout tubes into the ground. The surcharge loads were selected to model both a 2-level unreinforced masonry building ('URM'), as well as a large format commercial building. In each case an assumed 10 kPa floor load was used. Analysis demonstrated that the concrete blocks, along with an additional 28 kPa 'footing' strip load created foundation / floor surcharge stresses generally in the mid-range of those for the modelled buildings.

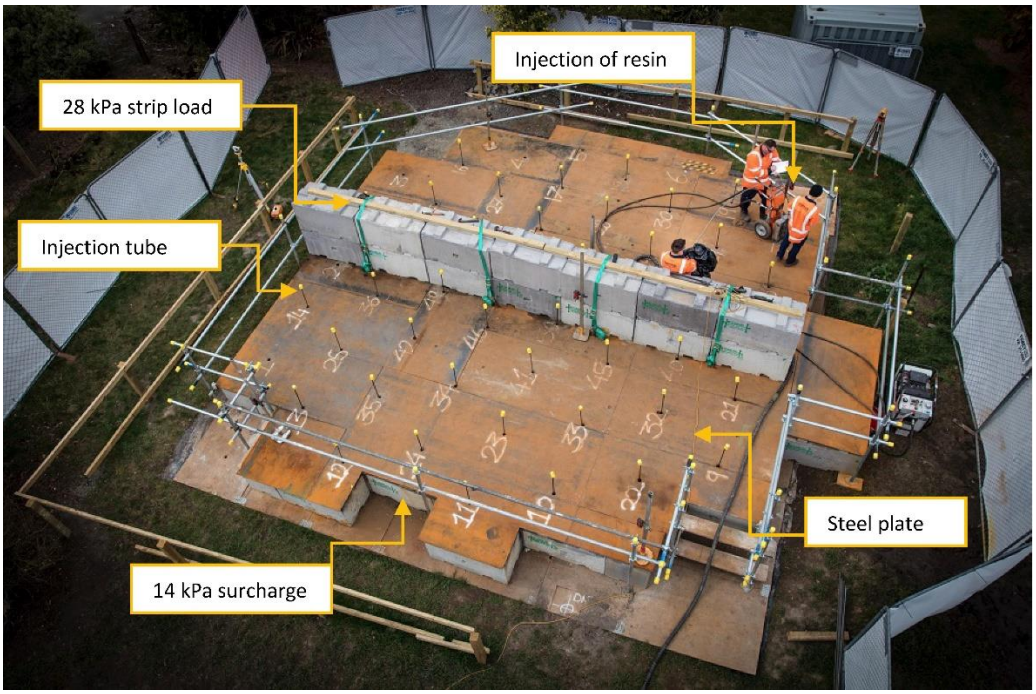

Figure 3 Site 3 aerial view of trial panel resin injection

The ground was treated with injected resin by first applying a 'capping layer' at 0.5 – 1.5m, and then injecting from 6m depth upwards on a 'bottom up' basis. After a period of at least two weeks the concrete blocks were removed, and post injection testing was carried out. One of the panels was partially exhumed to expose the resin veins in the ground (see Figure 1 in Section 2).

Ground heave was observed, averaging 40 to 70mm (σ = 30mm) across the three sites – however there was no attempt made to control ground heave in this case, as there were no adverse consequences from this (70% of the lift was created during the injection of the capping layer in the upper 1 to 1.5m of the ground profile). Ground heave and general surface disturbance using resin injection was observed to be noticeably less than that for other technologies such as stone columns or driven piles. Some controlled ground heave can be beneficial in cases where a building also requires level correction. In other cases, allowances need to be made so that the building can accommodate some changes in final floor level. For heavy buildings, or on sites where the soils are only being treated below 2m depth, significant ground heave may not occur at all.

6 RESULTS

There is a clear trend of increased soil densities and stiffness at all sites, with the level of increase varying with soil characteristics. Improvements in the soils are noticeable up to a metre below the base of treatment. Table 3 provides a summary of results across all three sites.

Table 3 Averaged increases in parameters within the treatment zones

Site	q_c	q_{c1Ncs}	D_R	Vs	K_D	k^*
3	88%	68%	32%	35%	47%	57%
4	81%	64%	34%	43%	74%	90%
6	101%	76%	27%	51%	150%	52%

*Modulus of Subgrade Reaction

CPT qc increased on average 80 - 100%, or about 4 - 12 MPa. This corresponds to increases in relative density (Dr) in the order of 30%. Modulus of Subgrade Reaction (k) increased 50 to 90% (from plate load tests). Shear wave velocities (Vs) increased on average 40% - 50 to 75 m/s at Sites 3 and 4, and 75 to 100 m/s at Site 6 (demonstrating an approximate doubling of soil shear

stiffness). Dilatometer testing showed an increase in horizontal stress index KD of 50-150%. Given the observed increases in CPT qc, static bearing capacities for shallow foundations also increased, and potential for static settlements decreased. (Schmertmann, 1970, 1978).

The averaged results from all site investigation methods at Site 3 are presented in Figure 4. (Similar trends were evident at Site 4 and better results at Site 6, but these have been omitted here due to space constraints for this paper).

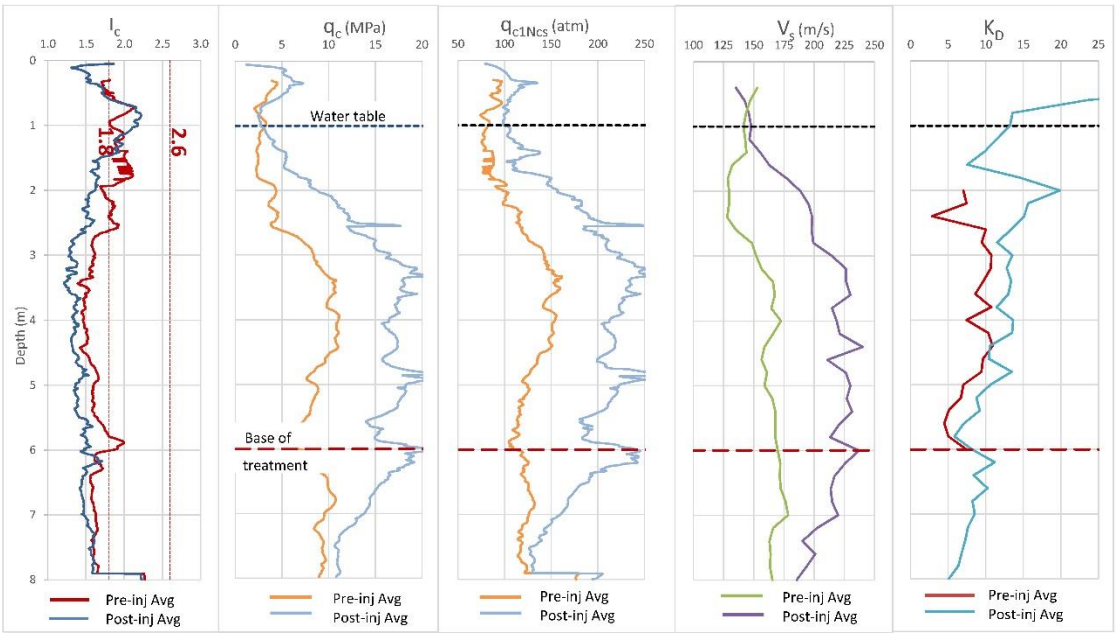

Figure 4 Average test results at Site 3

Figure 5 below provides a summary of qc1Ncs at each site pre- and post-improvement. There is variability in the change in these values at each site through the different soil types; on average, there is a 65 - 75% increase - approximately 50 atm at Sites 3 and 4, and 100 atm at Site 6.

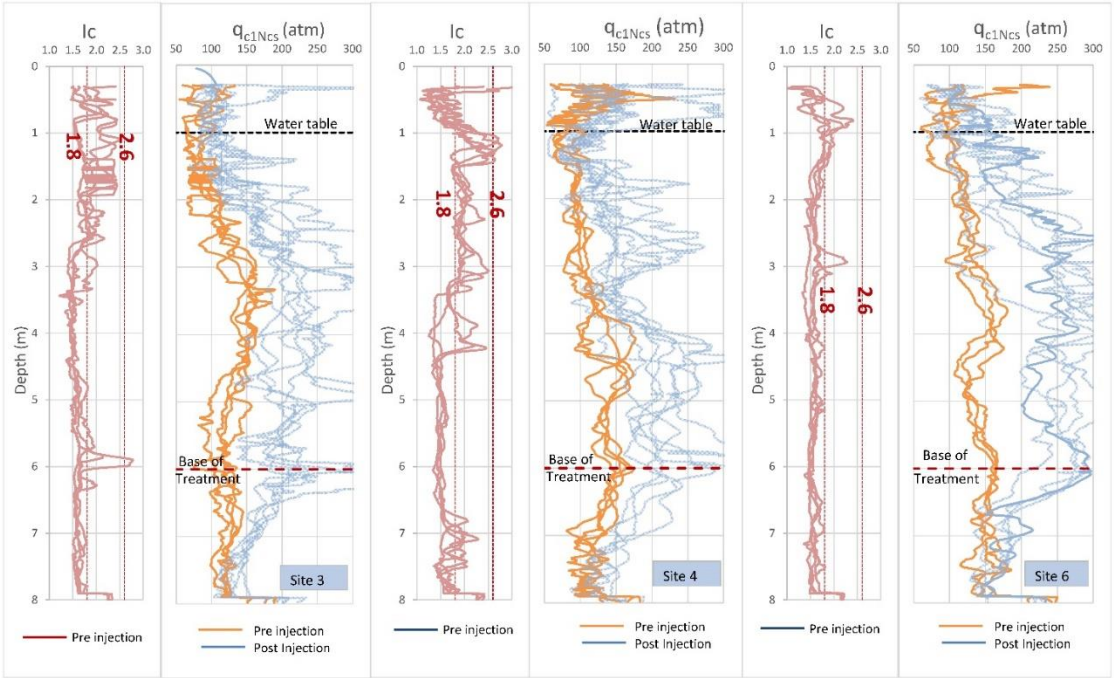

Figure 5 Pre- and post-injection q_{c1Ncs} data

6.1 Calculated liquefaction settlements & liquefaction severity number (LSN)

The CPT data was analysed for liquefaction triggering potential, (Boulanger & Idriss, 2014), and free-field settlements (Zhang et al. 2002). The results for Site 3 are presented in Figures 6 and 7 below, with a selection of return period events for Christchurch highlighted. Considerable reductions in settlements and liquefaction severity number, LSN (van Ballegooy et al., 2014b) are indicated. At the 25-year return period there is a reduction in these values of 90%; as the return period goes out to 500 years this reduction is still over 70%. Across all three sites, calculated liquefaction settlements and LSN values have reduced by 50 – 80%. The implied surface damage potential for these sites from liquefaction is therefore significantly reduced.

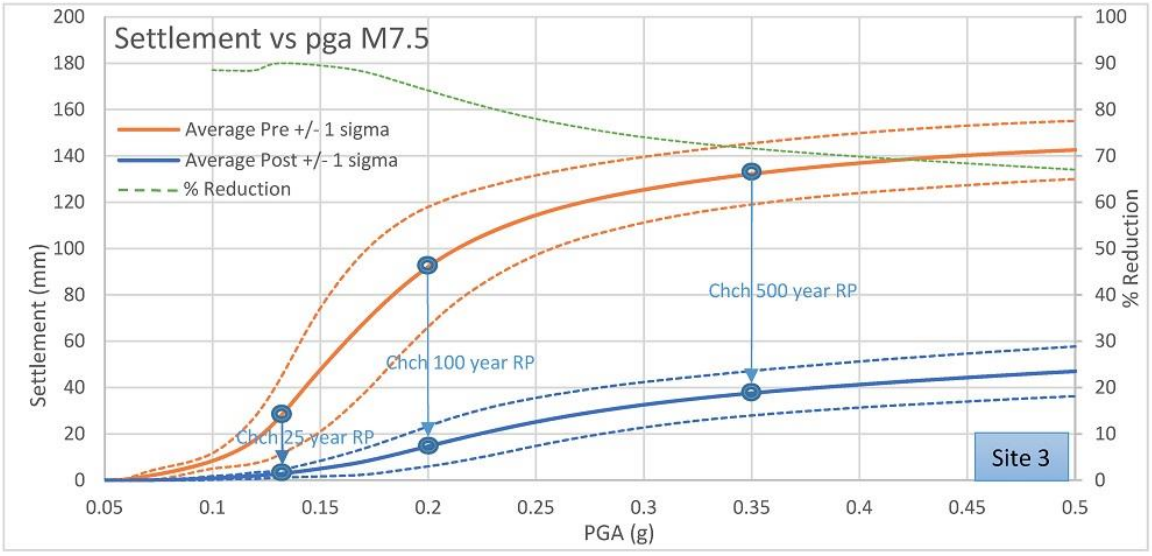

Figure 6 Free-field settlements pre- and post-improvement (Site 3)

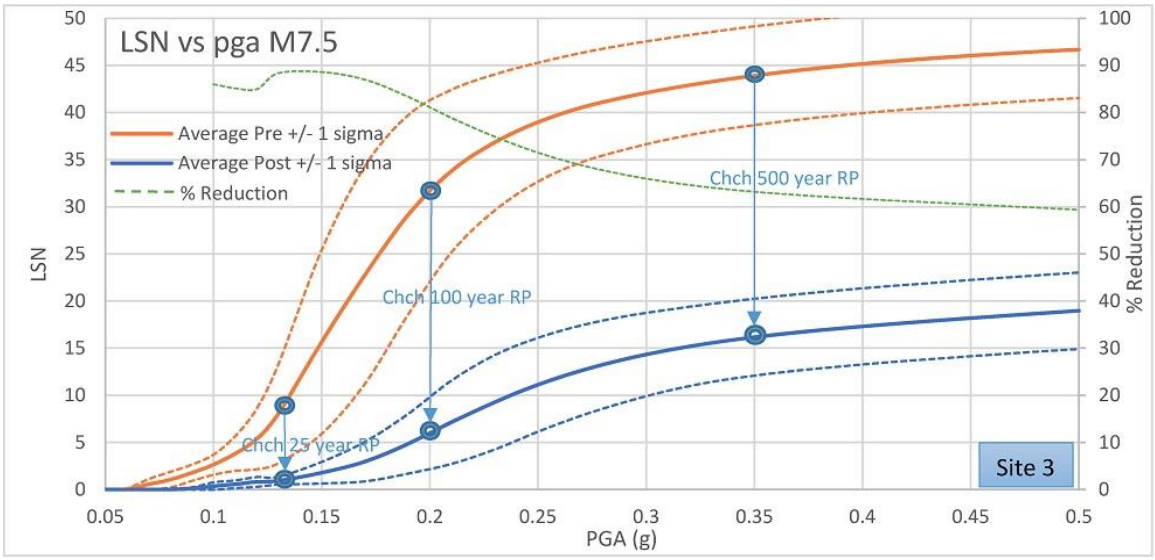

Figure 7 Calculated LSN pre- and post-improvement (Site 3)

7 CONCLUSIONS

The results of the study demonstrate that resin injection can be an effective ground improvement method for mitigation of liquefaction potential, and also for increasing foundation bearing capacities in sandy soils (including the siltier sands – e.g., sandy soils with CPT IC values up to about 2.0). Significant improvements in soil density and stiffness have been demonstrated. It has been noted that decreasing fines content, and increasing confining pressures, lead to better

densification effects in treated soils. While the fines content of a soil deposit may constrain the applicability of this technology at any particular site, confining pressures can often be applied through the use of portable kentledge if necessary.

This trial, and commercial application of the technology have shown that the resin injection ground improvement methodology can be successfully applied for liquefaction mitigation or bearing capacity enhancement to cleared sites as well as to ground beneath existing buildings, structures, and infrastructure assets (for which there are currently few viable options).

A more comprehensive research report on these trials (Traylen, 2017) is available on the NZGS website.

8 ACKNOWLEDGEMENTS

This research project was jointly funded by Mainmark Ground Engineering (NZ) Ltd (Mainmark), EQC and MBIE. Mainmark also provided all equipment, materials, and site management for the project. We thank all parties for providing both the research funding, as well as the data for this paper.

REFERENCES

Boulanger, R.W. & Idriss, I.M. 2014. CPT and SPT based Liquefaction Triggering Procedures. *Report No UCD/CGM-14/01 Dept of Civil & Environmental Engineering, College of Engineering, University of California at Davis.*

Erdemgil, M., Saglam, S., Bakir, B. 2007. Utilization of Highly Expansive Polymer Injection to Mitigate Seismic Foundation Failure for Existing Structures. *Proc. 8th Pacific Conference on Earthquake Engineering.*

EQC (in prep). Ground Improvement Trials Report.

Hnat, H., Traylen, N., Wentz, R, van Ballegooy, S., 2017. Resin Injection for Seismic Liquefaction Mitigation Beneath Existing Commercial Buildings in Christchurch. *NZSEE Conference 27-29 April 2017, Wellington NZ.*

Schmertmann, J.H. 1970. Static Cone to Compute Static Settlement Over Sand. *Journal of Soil Mechanics and Foundation Design, ASCE*, Vol 96, SM3.

Schmertmann, J.H. 1978. Guidelines for Cone Penetration Test: Performance and Design. *FHWA-TS-78-209 report, US Dept of Transportation.*

Traylen, N., van Ballegooy, S., Wentz, R. 2016. Liquefaction Mitigation beneath Existing Structures Using Polyurethane Grout Injection. *NZSEE Conference 1-3 April 2016 Christchurch NZ.*

Traylen, N., 2017. Resin Injection Ground Improvement Research Trials. *Research Report.* www.nzgs.org/library/resin-injection-ground-improvement-research-trials/

van Ballegooy, S., Cox, S. C., Thurlow, C., Rutter, H. K., Reynolds, T., Harrington, G., Fraser, J., Smith, T. 2014 (a). Median water table elevation in Christchurch and surrounding area after the 4 September 2010 Darfield Earthquake: Version 2, *GNS Science Report 2014/18, April 2014*.

van Ballegooy, S., Malan, P., Lacrosse, V., Jacka, M., Cubrinovski, M., Bray, J. D., O'Rourke, T. D., Crawford S. A., Cowan, H. 2014 (b). Assessment of liquefaction-induced land damage for residential Christchurch. *Earthquake Spectra, February 2014*, 30 (1), 31-55.

Wotherspoon, L.M., Cox, B.R., Stokoe, K.H., Ashfield D.J., Phillips, R.A. (2015) Utilising direct-push crosshole testing to assess the effectiveness of soil stiffening caused by installation of stone columns and Rammed Aggregate Piers. *6th International Conference on Earthquake Geotechnical Engineering 1-4 November 2015 Christchurch NZ.*

Zhang, G., Robertson, P., & Brachman, R. 2002. Estimating liquefaction-induced ground settlements from CPT for level ground. *Canadian Geotechnical Journal*, 39(5), 1168-1180.

Observation of horizontal movement of a vertical soil nail retaining wall in firm to very stiff soil

S Tjokro
Tonkin & Taylor Ltd, Auckland, NZ
STjokro@tonkintaylor.co.nz

Keywords: soil nail, horizontal displacement, monitoring, retaining wall, soil shrink-swell

ABSTRACT

Soil nailing is a common type of construction for retaining walls. For retaining wall structures with "passive" nails, mobilisation of the nails is required in order to retain the ground. An approximately 400 m long vertical soil nail retaining wall of up to 7.5 m height has recently been completed at the NZ Transport Agency's Waterview Connection Project in Auckland, New Zealand. The soil nails comprise inclined glass-fibre reinforced plastic (GRP) bars, drilled and grouted in predominantly firm to very stiff Tauranga Group alluvium and East Coast Bays Formation residual soil. The nails are connected to a vertical reinforced shotcrete facing, constructed in a top-down sequence. The wall and retained ground surface have been monitored for movements during and after construction using survey markers and in-ground inclinometers. This paper presents the results of the monitoring, including observation of movement associated with soil shrink and swell. The paper also discusses how the results are compared with the design prediction, as well as movements observed from bored pile retaining walls of similar retained height and ground condition in other parts of the project.

1 INTRODUCTION

A new retaining wall has recently been completed along the southern edge of the recently re-aligned Great North Road westbound off-ramp at the NZ Transport Agency's Waterview Connection Project in Auckland, New Zealand. The Great North Road westbound off-ramp was required to be re-aligned to allow for a geometrically acceptable connection to be established between the existing State Highway 16 (SH 16) and the new Great North Road Interchange. The re-alignment works involved removal of the existing cantilevered post and panel retaining wall, and the excavation and construction of a new retaining wall to support the new alignment.

The new retaining wall consists of three types of wall structure:

1) Cantilevered reinforced concrete bored pile wall structure, which forms about twenty percent of the retaining wall, mainly within the eastern section.
2) Carrington Road overbridge retention, which is a retention system provided by the existing Carrington Road bridge south abutment columns.
3) Soil nail wall, which makes up the majority of the retaining wall and the focus of this paper.

Figure 1 below shows the aerial view of the completed retaining wall.

Figure 1: Aerial view of the Great North Road westbound off-ramp new retaining wall

The soil nail wall structure was monitored for movement, more extensively than the other wall structure types, during and after construction. This was because, besides the soil nail wall forming the majority of the retaining wall, the "passive" nails within the wall structure are required to mobilise to achieve the resistance required to retain the ground. Therefore, it was essential to monitor the soil nail wall movements to confirm that the wall has achieved the intended performance as predicted in the design.

This paper focuses on the results of the soil nail retaining wall monitoring results, in particular with respect to the wall horizontal movements, and provides discussion of the observations made from the monitoring outcome.

2 SOIL NAIL RETAINING WALL DESCRIPTION

The soil nail retaining wall section is approximately 400 m long in total; approximately 260 m long to the west of the Carrington overbridge and 140 m long to the east of the Carrington overbridge. The western soil nail wall has a maximum retained height of approximately 7.5m, and the eastern soil nail wall has a maximum retained height of 3.8 m. The nails comprise BluGeo Powerthread K60 glass-fibre reinforced plastic (GRP) 25 mm diameter solid bar, with associated glass-fibre nail plates, nuts and stainless steel couplers. The nail lengths vary from 5 m to 15 m long and the spacings vary from 0.8 m to 1.3 m depending on the ground condition and the retained height. The nails are placed and grouted into 150 mm diameter holes on a triangular grid.

The construction of the soil nail retaining wall was undertaken in a top-down sequence. The excavation and nail installation were carried out row by row, with the excavated face and nail heads shotcreted immediately upon completing the nail installation on each row. Following completion of the shotcrete and excavation works for the entire retaining wall, precast concrete panels were placed in front of the completed retaining wall. Bored drains, strip drains and weep holes were also installed within the retaining wall to maintain a drained retaining wall condition.

One of the typical sections of the soil nail retaining wall is illustrated in Figure 2 below.

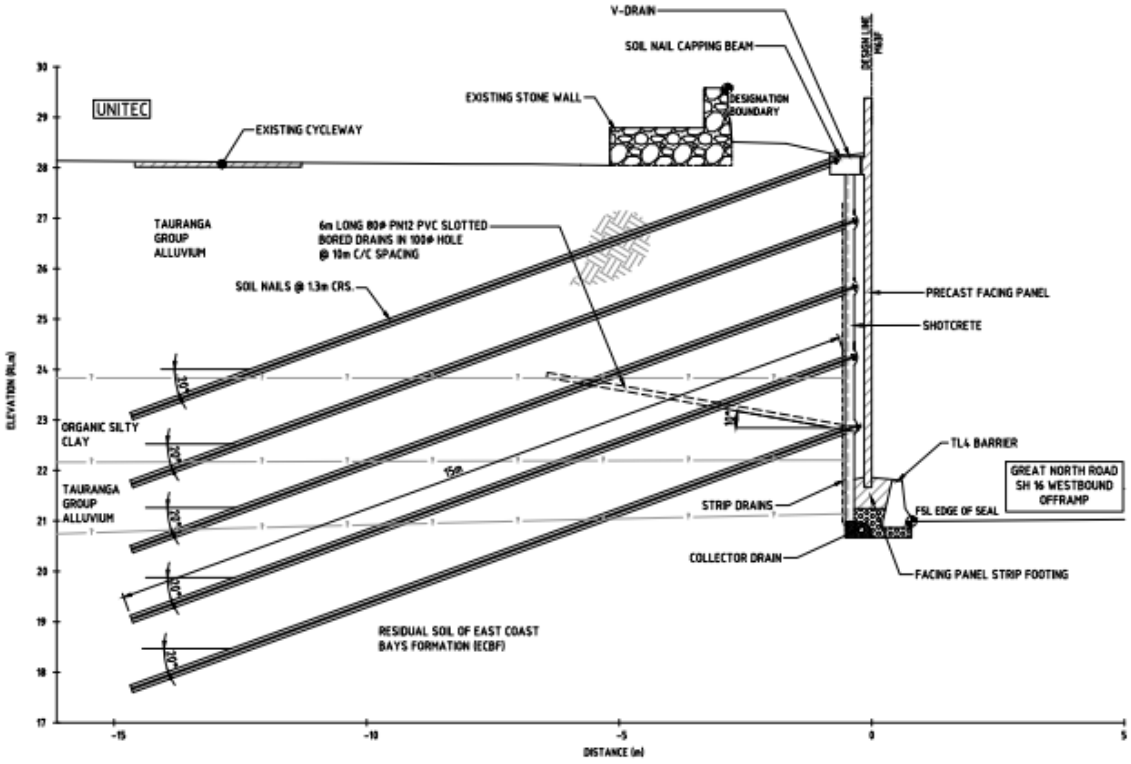

Figure 2: A typical section of soil nail retaining wall with 15 m long nails at 1.3 m spacing

3 GEOLOGY AND GEOTECHNICAL DESIGN PARAMETERS

The site is generally underlain by Tauranga Group alluvium ('alluvium') overlying East Coast Bays Formation (ECBF) residual soil ('residual soil'). The alluvium layer is approximately 5 m thick at the western end of the retaining wall increasing to about 10 m thick at the eastern end of the retaining wall. It generally comprises stiff, silty clay and clayey silt. A layer of firm silty clay with some organics of about 1 to 2 m thickness was also identified within the alluvium. The alluvium was assessed to be overconsolidated with an over consolidation ratio (OCR) of approximately 2. The residual soil is typically a stiff to very stiff clayey silt.

The geotechnical design parameters for the retaining wall design were developed and assessed based on in situ testing, laboratory testing and back analysis of historical surficial slope movement. The following parameters were adopted for the alluvium and the residual soil:

Table 1: Geotechnical design parameters adopted in the retaining wall design

Geological Unit	Unit Weight (kN/m^3)	Effective cohesion (kPa)	Effective friction angle (degrees)	Drained Young's Modulus, E' (MPa)
Tauranga Group Alluvium – stiff silty clay or clayey silt	18.5	5	29	15
Tauranga Group Alluvium – firm clay with organics	17	3	26	10
Residual ECBF soil	18.5	5	30	20

4 ASSESSMENT OF SOIL NAIL WALL MOVEMENT DURING DESIGN

During the design stage, the horizontal movements of the soil nail retaining wall were assessed using the following methods:

1) An empirical correlation from Clouterre (1991) as recommended by CIRIA C637 (2005) guideline; and
2) A finite element analysis using the computer software SIGMA/W.

Using the Clouterre (1991) empirical correlation, it was calculated that the retaining wall could move up to 25 mm horizontally. However, the finite element analysis calculated a horizontal movement of up to 100 mm at the end of construction, which is significantly greater than the Clouterre (1991) approach. Figure 3 below shows a plot of the calculated horizontal displacement along the retained height of the soil nail retaining wall. The plot was produced from the finite element analysis which was carried out at the assessed critical location.

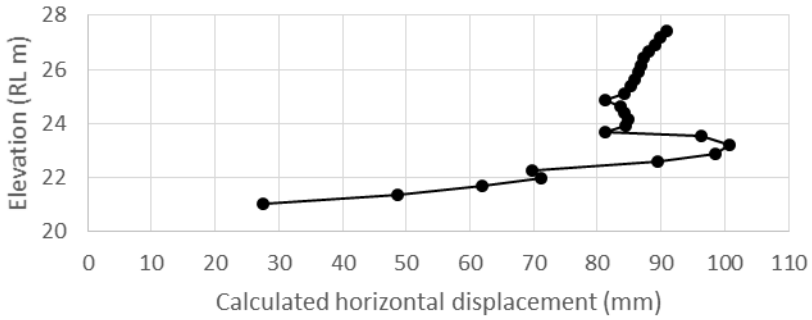

Figure 3: Plot of the calculated horizontal displacement of the soil nail retaining wall from the SIGMA/W analysis at the assessed critical location

It was also assessed in the plot above that the maximum horizontal movement could occur at the wall mid-height (i.e. bulging of the wall). In the case of Figure 3, the maximum horizontal movement was assessed to be influenced by the organic silty clay layer.

5 MONITORING INSTRUMENTS

During and after construction, the soil nail retaining wall was monitored for movements. The following instrumentation was installed on the retaining wall or within close proximity to the retaining wall:

1) Three in-ground inclinometers:

    a. Two inclinometers were located at the section of the soil nail retaining wall to the west of the Carrington Road overbridge. The inclinometers were installed approximately 2 m upslope of the retaining wall design line prior to construction of the wall. One inclinometer was situated at the assessed critical location. The other one was situated at the location of the highest retained height. It was assessed that the critical location was not at the location of the highest retained height, but was rather driven by the underlying ground condition.

    b. One inclinometer was located at the section of the soil nail retaining wall to the east of the Carrington Road overbridge, approximately 3 m upslope of the retaining wall design line. The inclinometer was a pre-existing instrument, which was installed when the cantilevered post and panel retaining wall was constructed

in the early 1990's. Following a check by an instrumentation technician, it was found that the instrument was still functioning. Therefore, it was decided to utilise the pre-existing inclinometer to monitor the eastern section of the soil nail retaining wall.

2) Approximately seventy survey markers were installed on the soil nail retaining wall as well as on the ground above the retaining wall. The soil nail retaining wall survey markers were installed on the capping beam at the top of the wall and on the surface of the shotcrete at approximately mid-height. They were spaced at approximately 20 m along the wall alignment. When the facing panels were installed, the survey markers located on the shotcrete were moved to the surface of the facing panels, placed at similar height. Additionally, survey markers were also placed on the ground surface of the park in the UNITEC complex above the western section of the soil nail retaining wall. The survey markers were installed in three rows at approximately 5 m, 10 m and 20 m away from the retaining wall capping beam. The survey markers were spaced at approximately 5 m in the direction parallel to the wall alignment within each row.

The monitoring was carried out from the start of the construction and continued for approximately 2.5 years. The inclinometer readings were generally taken weekly for the first 2 years, and then reduced to bi-weekly in the last 6 months of monitoring period. The survey marker readings were generally taken weekly for most of the monitoring period. However, not all survey markers were measured for the entire monitoring period. Only the ones that were deemed critical were kept and measured weekly until the monitoring period was concluded.

6 OBSERVED MOVEMENTS FROM THE MONITORING RESULTS

The measured movements of the soil nail retaining wall from the inclinometer are summarised in plots presented in Figure 4 and 5 below. The presented measured movements were taken from the inclinometer located at the assessed critical location of the retaining wall, as it showed the most movements among the installed inclinometers.

Figure 4 below provides the measured horizontal movement along the wall depth from the reading of the inclinometer on the last day of the monitoring on 23 November 2016.

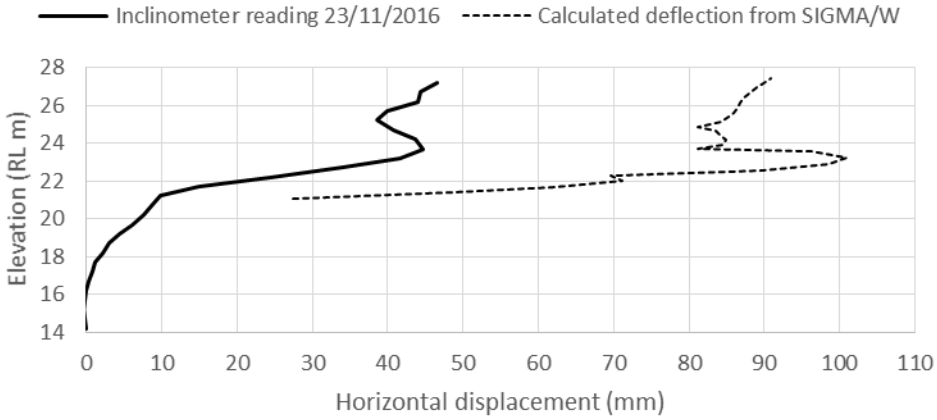

Figure 4: Inclinometer reading on 23 November 2016 at the assessed critical location

It can be observed from the inclinometer plot above that the measured deflection shape is generally in agreement with the predicted deflection from the finite element analysis.

Figure 5 below shows the readings from the inclinometer located at the assessed critical location, which were taken from the start of the wall construction to the conclusion of the inclinometer monitoring period on 23 November 2016. The plot is showing readings at three different elevations, RL 27.2 m which is the top of the wall, RL 23.2 m which is at the location of the organic silty clay layer and RL 21.2 m which is the bottom of the wall.

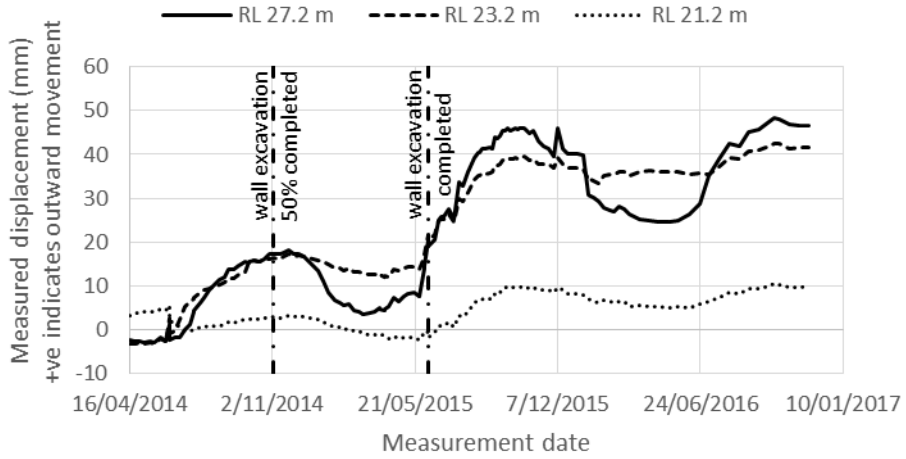

Figure 5: Inclinometer readings at the assessed critical location

Figure 6 below provides a summary of the horizontal movement readings from selected wall capping beam survey markers, which are located over the highest section and the assessed critical location of the soil nail retaining wall. The readings were taken from the start of the wall excavation to the conclusion of the survey monitoring period on 28 November 2016. It should be noted that the wall movement readings presented in Figure 6 below also contain a few inferred readings due to the survey markers being destroyed and re-established a number of times during construction. As observed in the plot below, the survey marker readings were in general agreement with the inclinometer readings.

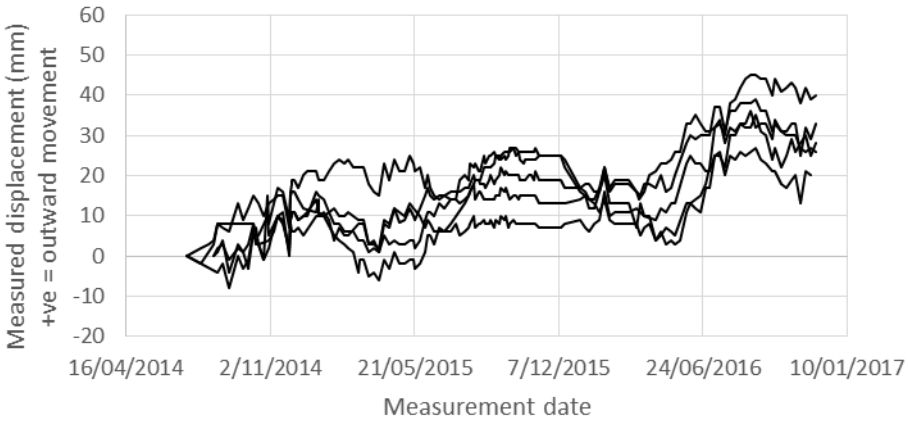

Figure 6: Summary of the top of wall survey marker readings at the assessed critical location

Survey markers located at the mid-height of wall were not observed to pick up as much movement compared to the top of the wall ones during the monitoring period.

Both the inclinometer and survey marker readings show that the magnitude of the wall horizontal movement calculated by the finite element analysis appears to be overestimated. This may have been influenced by a rather conservative soil stiffness parameters used for the analysis. However, Clouterre (1991) approach appears to have underestimated the movement magnitude. Therefore, careful consideration should be given when assessing the wall movements, in particular if there is any structure or object that is sensitive to movement above the wall. In the case of the Great North Road westbound off-ramp retaining wall, no sensitive structure nor object is present above the wall. Nonetheless, it is still essential to assess the wall movement to provide a measure on whether the soil nail retaining wall has or has not performed as expected on the field.

Furthermore, both the inclinometer and survey marker readings on Figure 5 and 6 also show that the soil nail retaining wall is responding to the seasonal shrink and swell movement of the soil. Up to 30 mm of horizontal movement was observed between the 'trough' (dry period) and the 'peak' (wet period). The inclinometer readings on Figure 5 also suggest the soil shrink-swell effect is mainly experienced by the soil in the near surface. No soil shrink-swell movement was observed in the survey markers located at the mid-height of wall. These findings show that designer should be mindful of the effect of soil shrink-swell to the soil nail retaining wall.

As an additional note, the soil shrink and swell movements were also picked up by the survey markers installed on the park ground inside the UNITEC complex. Figure 7 below provides a summary of the observed vertical movements of the ground surface due to the seasonal shrink and swell of soil. The survey makers observed up to 75 mm of settlement during the dry period.

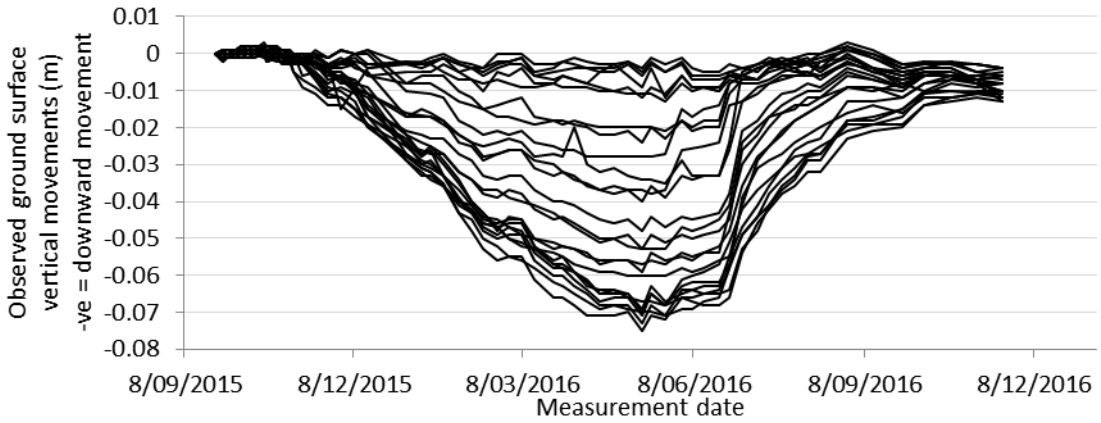

Figure 7: Recorded vertical movement of the ground surface in the park inside the UNITEC complex

7 COMPARISON WITH BORED PILE RETAINING WALL

Directly opposite to the Great North Road westbound off-ramp retaining wall, along the northern edge of the SH 16 eastbound, a new retaining wall ('north retaining wall') has also recently been completed as part of the Waterview Connection Project. The north retaining wall has a similar retained height, and was constructed in a similar geological condition to the Great North Road westbound off-ramp retaining wall. But the majority of the north retaining wall was a bored pile retaining wall. A part of the bored pile retaining wall was cantilevered, and another part was tied-back with ground anchors. As a comparison, Figure 8 below provides a summary of the horizontal movement readings from survey markers installed on the retaining wall. It can be observed from the plots that the bored pile retaining wall did not experience as much horizontal movement or the soil shrink-swell effect comparatively to the soil nail retaining wall.

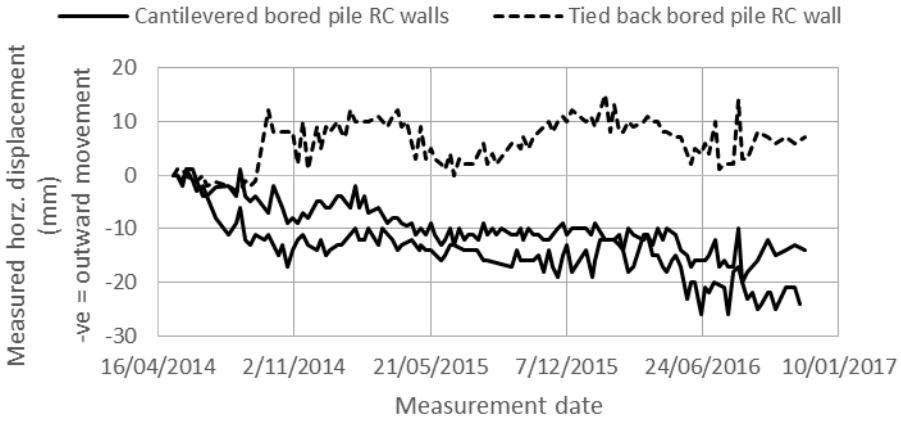

Figure 8: Survey marker readings from the new bored pile retaining wall along the northern edge of the SH 16 eastbound

8 CONCLUSION

Soil nail retaining wall relies on the mobilisation of the "passive" nails to develop the resisting forces for retaining the ground behind it. Therefore, it is recommended that the movement of the soil nail retaining wall be assessed during the design stage to provide a measure on whether the soil nail retaining wall has or has not performed as expected on the field. It may also be essential to assess the movements using more than one approach, e.g. an empirical correlation approach accompanied by finite element or finite difference analyses.

Soil nail retaining walls can also be subject to seasonal soil shrink and swell movements. In the case of the Great North Road westbound off-ramp retaining wall, where the site is generally underlain by Tauranga Group alluvium overlying East Coast Bays Formation (ECBF) residual soil, up to 30 mm of horizontal movement was observed between the 'trough' (dry period) and 'peak' (wet period).

For retaining walls with structures or objects that are sensitive to movement above the wall, it may be wise that other types of retaining wall, such as bored pile retaining wall, be considered to allow for better control to movements.

9 ACKNOWLEDGEMENTS

The writer would like to acknowledge the Well-Connected Alliance (WCA) for permission to publish our findings.

REFERENCES

GEO-SLOPE International Ltd (2012) *GeoStudio SIGMA/W Stress-deformation Analysis*. Calgary, Canada.

Phear, A., Dew, C., Ozsoy, B., Whamby, N. J., Judge, J. & Barley, A. D. (2005) *CIRIA C637 Soil Nailing – Best Practice Guidance*. CIRIA. London, UK.

Schlosser, F. et al (1991) *Recommendations Clouterre 1991. Soil Nailing Recommendations – 1991 For Designing, Calculating, Constructing and Inspecting Earth Support System Using Soil Nailing*. French National Research Project Clouterre. English translation by Federal Highway Administration, FHWA-SA-93-026. Washington D. C., USA.

Providing resilience in a Wellington waterfront development

E Stocks
Tonkin & Taylor Ltd, Wellington
estocks@tonkintaylor.co.nz (Corresponding author)

A Riman
Tonkin & Taylor Ltd, Wellington
ariman@tonkintaylor.co.nz

S Palmer
Tonkin & Taylor Ltd, Wellington
spalmer@tonkintaylor.co.nz

Keywords: ground improvement, liquefaction, lateral spread, CFA

ABSTRACT

Wellington's waterfront is in demand for new developments due to its proximity to the central business district, infrastructure, and harbour. This area can be impacted on by several hazards like earthquake shaking, liquefaction and lateral spread, see level rise and tsunami (tsunami not considered in this paper). The waterfront was reclaimed in a number of stages beginning in the 1850s, mainly by end tipping of weathered gravels. Liquefaction and lateral spread of these gravels as a consequence of a strong earthquake shaking event is likely to occur as was observed in the recent M7.8 Kaikōura earthquake in November 2016. This paper presents a case study of a five-storey building currently being constructed on the Wellington waterfront. To mitigate the impact from some of the natural hazards and to provide a resilient structure various foundation and ground improvement systems were considered. An in-ground cellular foundation solution was selected. This solution offers: liquefaction mitigation, shear resistance to resist lateral spread beneath the building, foundations for the new structure, temporary basement walls and effective cut-off of ground-water flow during construction. The foundation selection process, features and associated risks are discussed in this paper.

1 INTRODUCTION

Since the 2011 Canterbury earthquakes and 2016 Kaikōura earthquake, 'resilience' is one of the main focuses while designing foundations and substructures on sites prone to liquefaction and lateral spread such as the Wellington waterfront.

A five storey building with a basement is currently being constructed on the Wellington waterfront. While the waterfront provides unique location and amenity advantages for developments, the ground conditions are very challenging and complex.

The building design includes base isolation to prevent the building's superstructure from absorbing earthquake energy, with ground improvement to support the base isolation system and provide a high level of resilience to earthquake damage.

This paper discusses the foundation options considered for this complex site, the basis of selecting the in-ground cellular foundation solution and its features and associated risks and hazards.

2 PROJECT INFORMATION

2.1 Proposed development

A five storey building with a basement beneath approximately 90% of the building footprint is currently being constructed on the Wellington waterfront (refer Figure 1 for site location). The building owner wanted to provide a high level of resilience under an extreme earthquake event, including a lower potential for damage in a severe event than a normal office building.

The building design includes base isolation to provide high seismic performance by reducing the extent to which the building's superstructure absorbs earthquake energy. To support the base isolation system and ensure this high seismic performance, ground improvement was needed to reduce liquefaction and lateral spread.

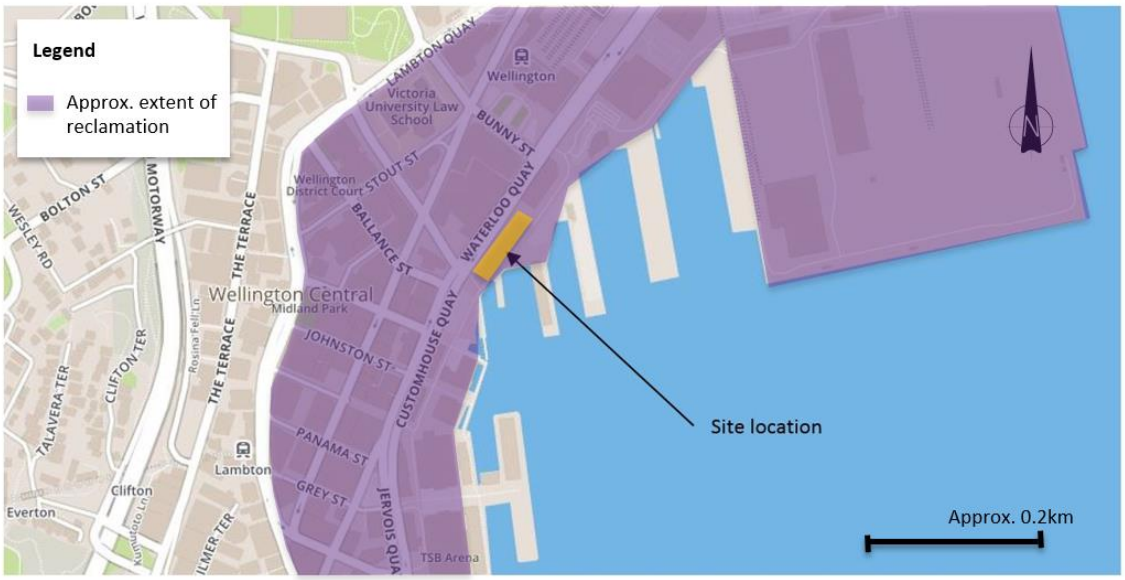

Figure 1. Site plan

2.2 Specific site conditions

The site is on reclaimed land on the Wellington Harbour foreshore. The reclamation fill is underlain by thin layer of recent marine deposits and Pleistocene alluvial deposits, which infilled the steeply graded valley (Begg & Johnston, 2000). Changes in sea level built up the alluvial deposits in layers of gravel, sand and silt. Greywacke bedrock underlies the alluvial deposits at more than 100m below existing ground level.

The original shoreline, which ran along Lambton Quay, is approximately 300m west of the site (refer Figure 1). Prior to 1876, the reclamation fills extended up to Waterloo Quay (Semmens et al. 2010). The land beneath the site was reclaimed in the early 1900s. As illustrated in Figure 2, a mass concrete seawall was constructed immediately to the south-east of the site which formed the edge of that reclamation. It is likely that the reclamation was formed by tipping materials excavated during roading and other construction work, predominately silty sandy gravels. In the early 1970s, a reclamation southeast of the site was constructed, supported by a sheet pile wall to the east and rock revetment to the south.

2.3 Seismic shaking hazard and liquefaction risk

The seismic subsoil class for the site is considered to be 'Class D – Deep or Soft Soil Sites' in accordance with NZS 1170.5:2004 (Standards New Zealand, 2004). An Ultimate Limit State (ULS) of 2500 year return period has been considered. Peak Ground Acceleration (PGA) of 0.62g and a corresponding earthquake magnitude of M_w 7.1 was derived from NZTA Bridge Manual (NZTA, 2016) following the recommendation in recent geotechnical guideline (NZGS, 2016).

Liquefaction occurs when excess pore pressures are generated in loose, saturated, generally cohesionless soil (sands and non-plastic silts) during earthquake shaking. This causes the soil to undergo a partial to complete loss of shear strength. Such a loss of shear strength can result in settlement, bearing capacity failure and / or horizontal movement of the soil mass. Liquefaction of gravels within reclamation fills has also been observed following the earthquake in Kobe, Japan in 1995 (Cubrinovski & Ishihara, 2003; Hara et al. 2004; Hara et al. 2012), and the recent earthquake in Kaikōura in 2016 which greatly affected Wellington port land (Cubrinovski et al. 2017).

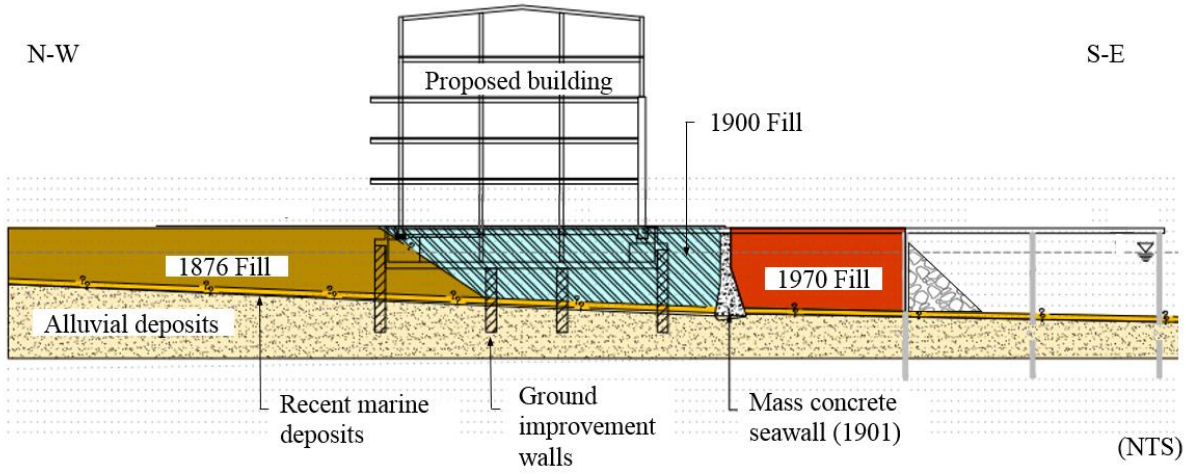

Figure 2. Cross section of reclamation fill and proposed development

Soils which are susceptible to liquefaction require a certain level of earthquake shaking (trigger) to cause them to liquefy. Analysis using the method proposed by Boulanger and Idriss (Boulanger & Idriss, 2014) concluded that as a consequence of a 150 year return period earthquake event (PGA 0.2g, magnitude M_w 7.1) liquefaction could occur within the reclamation fill and zones of liquefaction could occur within the marginal marine deposits. Due to the dense nature of the alluvium and the age of the deposit (Pleistocene >12000 years old) it was concluded that liquefaction of these soils is not likely but cannot be discounted as a consequence of severe earthquake shaking (>200 year return period).

Following the recent earthquake in Kaikōura, the site experienced greater level of shaking (PGA 0.23g, magnitude M_w 7.8). No liquefaction effects were observed at this level of shaking, however this cannot rule out the potential for liquefaction to occur under stronger shaking.

Liquefaction induced lateral spread is a movement of ground toward the free edge (i.e. sea) as a result of shearing of weak liquefied ground under seismic and / or gravity forces. It could be expected to occur in a series of scollops extending back from the reclamation edge with the magnitude of total displacement reducing with distance from the reclamation edge. As a consequence of a 500 year return period earthquake event (PGA 0.35g, magnitude M_w 7.1) lateral spread is expected.

2.4 Design objectives

The design objectives for the in-ground works were to:

- Retain life safety for a 2500 year event and limit building damage for a 1000 year event;
- Mitigate liquefaction beneath the building footprint and associated differential settlement of the building;
- Distribute building loads with depth and provide a relatively stiff base to found the building on;
- Provide adequate bearing capacity to support the building compression loads;
- Provide resistance to building seismic uplift loads;
- Mitigate basement buoyancy effects in the event of liquefaction and due to sea level rise over the lifespan of the building;
- Mitigate lateral spread potential beneath the building footprint and resist base shear from the structure;
- Provide lateral support to the basement excavation during construction; and
- Provide a cut off to groundwater to aid dewatering during construction.

2.5 Foundation options considered

At the concept design stage a broad range of foundation options were identified and discussed by the project team (the owner, the structural engineer and the geotechnical engineer).

- Option 1: Grid of gravel columns for ground improvement with bored belled piles to resist high, concentrated compression and tension loads;
- Option 2: Bored belled piles to resist tension, compression and lateral loads;
- Option 3: A deep foundation system comprising a grid of in-ground walls of secant deep soil mixing (DSM) or continuous flight auger (CFA). The in-ground walls extend through weak and potentially liquefiable reclamation fill and upper alluvium to support the building loads in the competent lower alluvium. Anchor piles at specific locations provide resistance to tension loads; and
- Option 4: Ground improvement comprising a cellular grid of in-ground walls to mitigate liquefaction of the reclamation fill and spread the building loads over the upper alluvial deposits. The in-ground walls created by secant DSM or CFA columns on which a concrete raft foundation is constructed. Anchor piles at specific locations provide resistance to tension loads.

The relative advantages and disadvantages of each option were considered. An option evaluation was undertaken in conjunction with the project team, and the robust system of CFA in-ground walls as a ground improvement system (Option 4) was identified as the preferred foundation option. A geotechnical risk register was developed and was updated throughout the design process.

The CFA construction method was selected over the DSM method due to the variable nature of the reclamation fill and the upper alluvium, which could compromise the effectiveness of the DSM method (i.e., DSM might not be able to achieve consistent cementation). The layout of the in-ground walls and a cross section is shown in Figures 3 and 4.

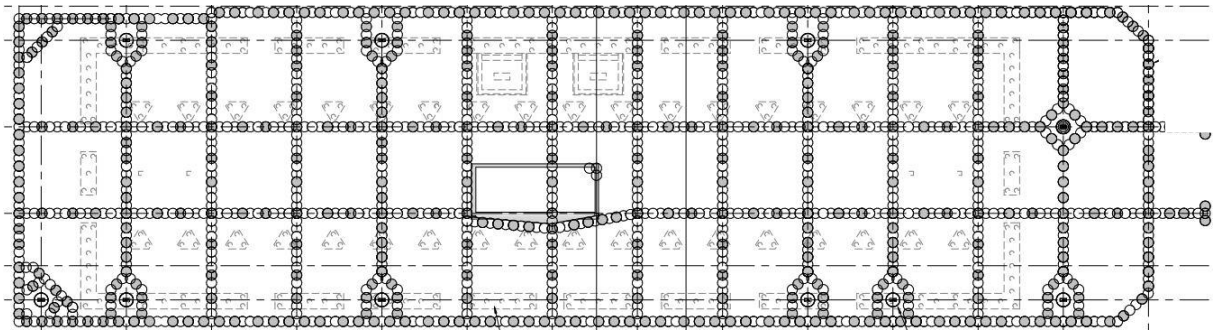

Figure 3. Plan of CFA in-ground walls foundation system

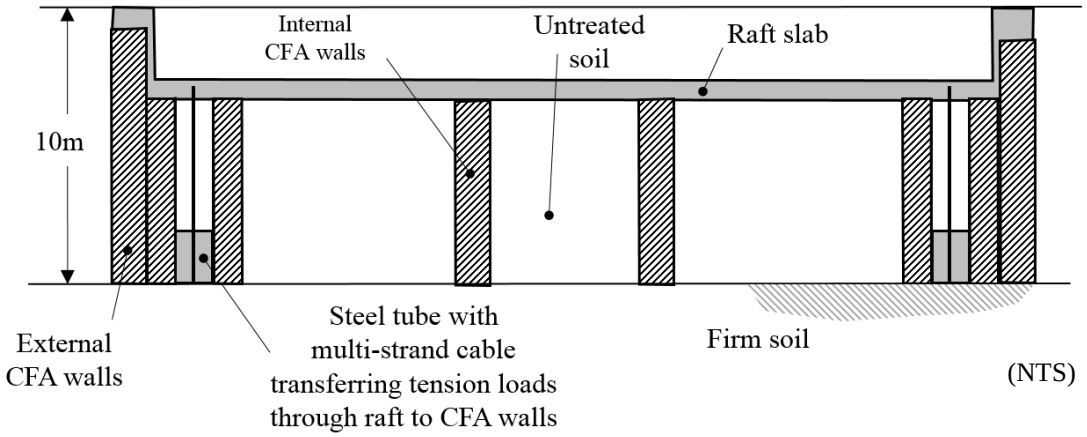

Figure 4. Cross section of CFA in-ground walls foundation system

3 CFA GROUND IMPROVEMENT

The CFA ground improvement meets all the design objectives listed in Section 2.4. In this section, we discuss in particular how this foundation system mitigates liquefaction and lateral spread, and resists uplift loads. An understanding of soil-structure interaction was achieved through collaborative approach between the project's structural and geotechnical engineers (Stocks et al. 2017).

3.1 Description of CFA ground improvement

At the Wellington waterfront site the ground improvement was constructed with secant CFA piles. Using hit one and miss one approach at the perimeter wall the unreinforced "soft" piles were formed first using lower strength concrete. The remaining piles were standard reinforced concrete "hard" piles constructed to overlap the "soft" pile by minimum 20% on both sides. The face of the piles following excavation is presented in Figure 5. The perimeter CFA piles created both a cut-off wall and a temporary basement retaining wall.

During construction the wall provided satisfactory performance of cutting of water flow. Ongoing groundwater monitoring outside the perimeter wall and movement monitoring at the top of the wall indicated little to no change during the construction period.

Figure 5. Hard and soft piles following basement excavation

Once the perimeter was completed, dewatering and bulk-excavation (to basement level) was carried out. The interior, cellular walls were then augered and cast from the excavated level, typically with a ratio of two "soft" piles to one "hard" pile.

At each tension pile location a ring of CFA piles was formed to help distribute the concentrated loads.

3.2 Mitigation of liquefaction

The cellular structure of in-ground walls mitigates liquefaction within the cells by:

- Resisting cyclic shear stresses from earthquake shaking to reduce cyclic shear strains in the soils within the cells to a level which mitigates their liquefaction; and
- Providing a barrier against the migration of high pore-water pressure from surrounding liquefied unimproved ground.

The layout of the in-ground walls to was developed using the method of Nguyen (Nguyen et al. 2013). The centre-to-centre spacing is typically 7.5m with maximum spacing up to 10.5m at selected locations.

The CFA ground improvement was designed to reduce the dynamic shear stresses and strains imposed on the enclosed saturated soils. This was expected to reduce the rate at which excess pore water pressures accumulate within the enclosed soil during severe earthquake shaking.
The lateral stability analysis did not rely on any shear resistance from the potentially-liquefiable marine deposits as the CFA piles were keyed into the underlying alluvial deposits, which are predominantly non-liquefiable.

Based on available research (e.g. Bradley et al. 2013), even though excess pore pressures develop to varying degrees within the enclosed soil, the lattice acts to limit loss of shear stiffness and significantly reduce the maximum shear strain, settlement and horizontal displacement.

3.3 Mitigation of lateral spread

Without ground improvement, lateral spread of the ground beneath building could be expected in a 500 year seismic event and is possible in lesser events. The improved ground is assessed to have adequate shear capacity to resist lateral spread beneath the building including kinematic / displacement loads from the ground landward of the proposed building, and including base shear from the building. The lateral spread assessment assumed the following:

- 65% of the peak building base shear;
- 100% of the lateral spreading load acting on the landward side; and
- Loss of support on the seaward side due to mass concrete seawall failure.

3.4 Buoyancy

The basement and structure has been designed for ground water pressure equivalent to water at ground level to account for possible sea level rise scenarios. The buoyancy forces were resisted by a combination of the following:

- Weight of the CFA walls;
- Weight of confined soils (friction on the CFA walls); and
- Weight of the superstructure.

3.5 Uplift resistance

Seismic uplift resistance is provided by connecting the secondary reinforced CFA piles with the substructure beams and basement walls. The seismic loads were resisted by the weight and shear resistance of ground improvement. Uplift resistance has been assessed considering:

- Buoyant weight of CFA piles;
- Lesser of shear resistance of soil against CFA piles and the buoyant weight of wedge of soil against CFA piles;
- Shear strength of potentially liquefiable soils is ignored. Soils outside the CFA system and over the bottom 1m of the CFA system were assumed to liquefy (The assumption that the Pleistocene Alluvial deposits will globally liquefy is rather conservative. In reality, due to the nature of these deposits and the reinforcement provided by the lattice, liquefaction is not expected except in some localised lenses, which is also unlikely); and
- Strength reduction factor of 0.5 on soil / CFA shear strength and 0.9 on soil / CFA pile weights.

3.6 Stiffness and bearing capacity

The gravity and serviceability limit state (SLS 1) loading cases did not require a detailed soil-structure interaction analysis. The improved ground was behaving as a relatively rigid block compared to the bearing pressures imposed by the substructure. The concentrated loads/ pressures were not high enough to unduly stress the improved CFA block. The loading stresses transferred to the bottom of the CFA block were less than 10% of the overburden pressure and resulted in minor differential settlements.

For the ultimate limit state (ULS) loading case, most of the soil-structure interaction analysis was carried out to design a substructure that would transfer large earthquake loads to the ground in a distribution that would not unduly stress the CFA improved block. Numerical analysis was undertaken in conjunction with the structural engineer to satisfy this design objective. Details of the soils-structure interaction analysis are provided in a separate paper (Stocks et al. 2017).

4 CONCLUSIONS

Nowadays, ‘resilience’ is one of the main focuses while designing foundations and substructures on sites prone to liquefaction and lateral spread such as the Wellington waterfront.

For the new development at the Wellington waterfront, the consideration of geotechnical hazards were taken into account from concept design stage through to construction. Understanding of the geotechnical hazards and their influence on seismic performance of foundations and the substructure was very important. For this project, it was achieved by collaboratively working together with the owner, the structural and geotechnical engineers and the contractor. The owner’s objectives for the building included a high level of resilience under an extreme earthquake event (2500 year seismic event) and a low level of damage in a severe event (1000 year seismic event).

A cellular ground improvement of CFA piles met these objectives and dealt with the geotechnical hazards by providing a stiff raft of soil-concrete composite. This solution offered: liquefaction mitigation, shear resistance to resist lateral spread beneath the building, foundations for the new structure, temporary basement walls, and effective cut-off of ground-water flow during construction.

5 ACKNOWLEDGEMENTS

The authors wish to express their great appreciation to Mike Jacka from Tonkin and Taylor Ltd for his support during the writing of this paper.

REFERENCES

Begg, J. G. & Johnston, M. R. (2000) *Geology of the Wellington area. 1: 250 000 Geological Map 10*. Lower Hutt, New Zealand. Institute of Geological and Nuclear Sciences Ltd.

Boulanger, R.W. & Idriss, I.M. (2014) *CPT and SPT based liquefaction triggering procedures*. Report No. UCD/CGM-14/01, Center for Geotechnical Modeling, Department of Civil and Environmental Engineering, University of California, Davis, CA.

Bradley B.A. et al (2013) Effect of lattice-shaped ground improvement geometry on seismic response of liquefiable soil deposits via 3-D seismic effective stress analysis. *Soil Dynamics and Earthquake Engineering,* 48.

Cubrinovski, M. & Ishihara, K. (2003) Liquefaction-induced ground deformation and damage to piles in the 1995 Kobe Earthquake. *International Conference on Skopje Earthquake - 40 years of European earthquake engineering SE40EEE, Skopje-Ohrid, Macedonia.*

Cubrinovski, M et al (2017) Liquefaction effects and associated damages observed at the Wellington CentrePort from the 1026 Kaikōura earthquake. *New Zealand Society for Earthquake Engineering Bulletin*, vol. 50, No. 2.

Hara T. et al (2004) Undrained strength of gravelly soils with different particle gradations. *13th World Conference on Earthquake Engineering, Vancouver, Canada.*

Hara T. et al (2012) Liquefaction characteristic of intermediate soil including gravel. *15th World Conference on Earthquake Engineering, Lisboa, Portugal.*

Nguyen, T.V. et al (2013) Design of DSM grids for liquefaction remediation. *Journal of Geotechnical and Geoenvironmental Engineering*, 139(11).

NZGS (2016) *Earthquake geotechnical engineering practice. Module 1: Overview of the guidelines*. Rev 0, Wellington, New Zealand

NZTA (2016) *Bridge Manual SP/M/022*. Third Edition, Wellington, New Zealand

Semmens, S. et al (2011) NZS 1170.5: 2004 site sub soil classification of Wellington city. *Proceedings of the ninth Pacific conference on earthquake engineering, Auckland, New Zealand.*

Standards New Zealand (2004). *NZS 1170.5:2004 Structural Design Actions - Earthquake Actions. Section 3 - Site Hazard Spectra*, Standards New Zealand.

Stocks E. et al (2017) In-ground cellular structure as a foundation system. *2017 NZSEE Annual Technical Conference and 15th World Conference on Seismic Isolation, Energy Dissipation and Active Vibration Control of Structures, Wellington, New Zealand*

Unravelling Fault Structures of the Hamilton Basin

F. Spinardi
School of Science, University of Waikato, Private Bag 3105, Hamilton 3240, New Zealand
fspinardi027@gmail.com (Corresponding author)

B. R. Campbell
School of Science, University of Waikato, Private Bag 3105, Hamilton 3240, New Zealand
brc16@students.waikato.ac.nz

V. G. Moon
School of Science, University of Waikato, Private Bag 3105, Hamilton 3240, New Zealand
vicki.moon@waikato.ac.nz

A. Pittari
School of Science, University of Waikato, Private Bag 3105, Hamilton 3240, New Zealand
adrian.pittari@waikato.ac.nz

B. R. S. Fox
School of Science, University of Waikato, Private Bag 3105, Hamilton 3240, New Zealand
beth.fox@waikato.ac.nz

W. P. de Lange
School of Science, University of Waikato, Private Bag 3105, Hamilton 3240, New Zealand
willem.delange@waikato.ac.nz

Keywords: faults, tectonic geomorphology, Hamilton Basin

ABSTRACT

Geological and geomorphological mapping provide evidence for three complex fault zones in the Hamilton Basin, an area with no previously mapped surface fault traces. Rectangular drainage patterns, stream knickpoints, and linear ridge and drainage systems all point to structural control on the path of the Waikato River and its tributary gullies. Exposed fault traces indicate significant splintering of fault planes on encountering the soft sediments and tephras infilling the basin; hence fault zones are wide and characterised by multiple traces forming a complex ridge geomorphology. Steeply dipping normal faults are observed, with relative uplift to the north, indicating a north-south extensional environment. So far, no definitive evidence for movement more recent than 350 ka has been identified.

1 INTRODUCTION

Recently faulted tephras were identified in an excavation during subdivision development in northern Hamilton City; analysis of a high-resolution digital elevation model (DEM) derived from LiDAR showed the trace of this fault running SW-NE across the Hamilton Basin. Prior to this discovery, no faults had been reported within surficial sediments in the Hamilton Basin. Hence, we embarked on a multi-method approach to better characterise the structure within the Hamilton Basin; particularly in terms of identifying structures developed in the Pleistocene and younger sediments that infill the basin. Our work involves geological and geomorphological mapping, re-assessment of publicly available geophysical data such as gravity, aeromagnetic, and seismic reflection surveys, and new shallow geophysical measurements. This paper presents aspects of our recent geological and geomorphic assessment of the structure of the basin.

2 BACKGROUND SETTING

The Hamilton Basin is a depression confined by the Hakarimata-Taupiri Ranges to the north, the Pakaroa Ranges and Maungakawa Hills to the east, and the Alexandra Volcanics and the Kawhia Syncline to the west. The surficial geology of the Hamilton Basin consists mainly of primary and reworked non-welded ignimbrites (Puketoka and Karapiro Formations) and tephras of the Pleistocene Walton Subgroup, overlain by a Late Pleistocene, low-angle alluvial fan deposit of reworked volcaniclastic sediments known as the Hinuera Formation (Edbrooke and Begg, 2005; McCraw 2011). Previous geological research of the Hamilton Basin concluded that the only faults affecting the basin were the non-active Waipa Fault inferred along the Junction Magnetic Anomaly (JMA) in the west, and the active Kerepehi Fault in the adjoining Hauraki Basin to the east. An additional E-W trending fault, the Taupiri Fault, was proposed by Kirk (1991) separating the Hakarimata-Taupiri Ranges from the Hamilton Basin. Information regarding movement on the Waipa Fault in this region is limited, with some evidence suggesting activity during the early Paleogene and possibly even into the Oligocene (Kear et al, 1978; King, 2000). Currently, seismic hazards within the Hamilton Basin, as defined by the National Seismic Hazard Model (Stirling et al., 2010), are considered to be relatively low due to the absence of known active faults.

3 METHODS

Tectonic geomorphology is key to understanding the structural history of soft-sediment filled basins. With the use of LiDAR data provided by the Waikato Regional Council the geomorphology of the basin is easily examined. The Waikato River in particular, is an important geomorphic tool as rivers act as linear structures that contain features such as terraces, floodplains, and channels that give insight into temporal changes associated with land movements (Schumm et al., 2000; Burbank & Anderson, 2012). Using a combination of LiDAR data, river geomorphology, and sidescan and multibeam images of the riverbed (Wood, 2006) we have examined tectonic geomorphic signatures within the Hamilton Basin.

Standard geological mapping techniques were employed to map riverbank geology, using foot access where feasible, and boat surveys from the Narrows Bridge (37° 50’ 30.7” S, 175° 20’ 54.2”) to the old Horotiu Bridge (37° 41’ 52.1” S, 175° 12’ 19.9” E) for all other sites. Sites exposed by development of the Hamilton Bypass section of the Waikato Expressway were also surveyed, notably a large cutting at Kay Road on the northern margin of Hamilton City (37°42’40” S, 175°15’25” E). In all cases, landform and outcrop photographs, sketches, stratigraphic logs, and measurements were taken, including dips and dip directions where relevant. Fault plane orientations were recorded using mobile application GeoID and location parameters were recorded using Garmin GPS. Samples were collected from areas where lithology could not readily be determined in the field and used for preparation of thin sections and Scanning Electron Microscope (SEM) samples.

4 RESULTS

4.1 River geomorphology and geology

Figure 1A presents a DEM of the Hamilton City area derived from the LiDAR data. The Waikato River runs diagonally through the map from the lower right to upper left corners. It can be seen that the river undertakes a series of sharp bends, notably near Stubbs Road at the southern boundary of Hamilton (location B); in central Hamilton City near Lake Rotoroa (location E); at Day’s Park in northern Hamilton (location D); and a smaller one near Flagstaff in northern Hamilton (location F). This rectangular drainage system is accompanied by a pattern at three of these bend locations (locations B, D & F) where the upriver areas show aggradation and the downriver areas show degradation through entrenchment (Figure 1A). The aggradational zones

are evidenced by broad embayments with well-developed terraces and a more sinuous channel, while the degradational zones are evidenced by a more incised channel with knickpoints, narrow terraces, and abandoned higher level channels. Multibeam data reveals an abrupt change in the riverbed nearby each of these sharp bends whereby the upriver side contains a resistant material and the downriver side more erodible material, resulting in the formation of knickpoints along the river's profile (Figure 1B). These sharp bends are accompanied by linear ridges crossing the river, or tributary drainage systems (gullies) entering the river. The three sites (B, D & F) will be discussed in more detail in following sections.

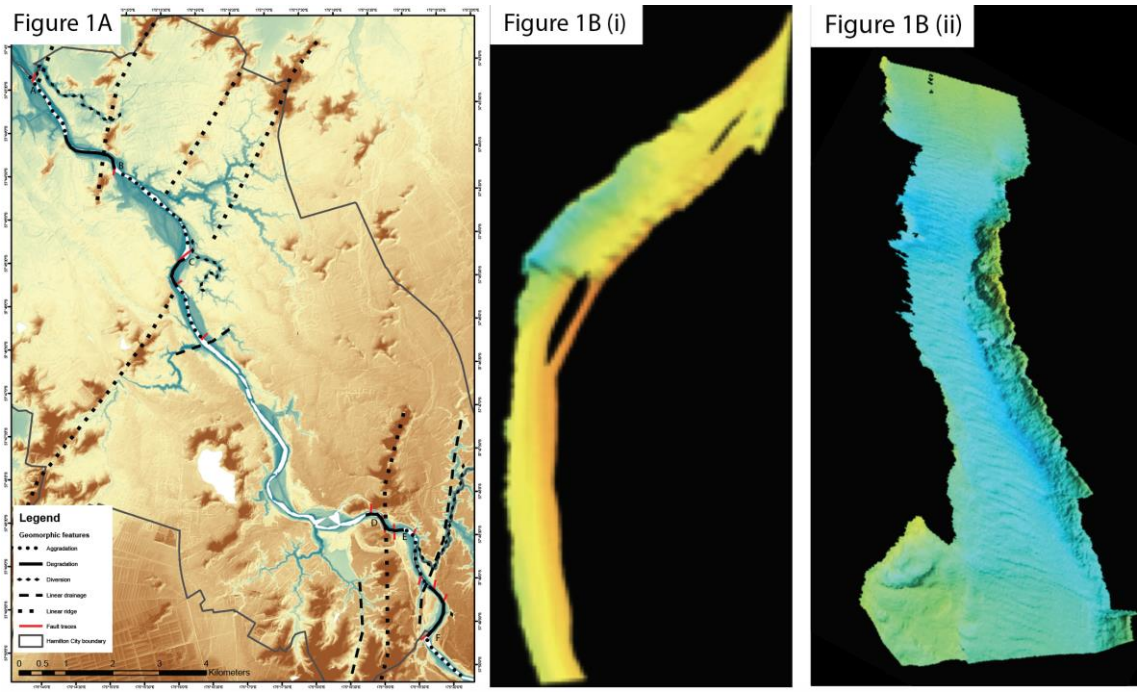

Figure 1. (A) LiDAR DEM of the Hamilton Basin from the Narrows, Tamahere to Horotiu with marked tectonic geomorphic features found within the basin. Letters A-G indicate areas referred to in the text. (B) Sidescan and multibeam images of seafloor at (i) Stubbs Road (site B) and (ii) Day's Park (site D).

A geological strip map along the Waikato River is shown in Figure 2. Ignimbrites are readily identified in outcrops near Stubbs Road (location B) and the Hamilton Gardens. Between these two sites, stratigraphic relationships between the ignimbrites and surrounding materials are indicative of faulted contacts, but only one directly identifiable fault exposure was recognised near Stubbs Road. Other materials of Walton Subgroup age are plotted as "Undifferentiated Pleistocene Sediments"; thin sections suggest that most of these are reworked pyroclastic materials, probably with very minimal local reworking from the weak ignimbrite deposits. Surprisingly little clearly identifiable Hinuera Formation sediments were exposed along the riverbanks in the area shown in Fig. 1B, though this is likely a function of vegetation and development patterns. As the Hinuera Formation forms shallow-angle (compared with other materials) slopes with unconsolidated sediment, vegetation growth on this material is extensive and hence obscures direct observation of the geology. Hinuera Formation is mapped in Hamilton City on the eastern bank of the river from Cobham Bridge to the Claudelands Bridge. It likely comprises considerably more of the riverbanks through the city portion of the map.

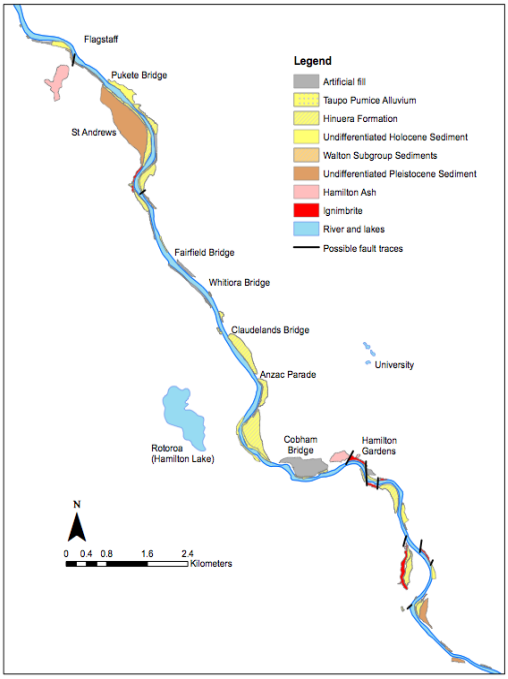

Figure 2. Geological map along the Waikato River, Hamilton City

Figure 3. Exposed fault trace near Rototuna, Hamilton City.

4.2 Rototuna cutting

The site initially identified at Rototuna (location G, 37°43’24” S, 175°16’40” E) is a fault zone exposed in the wall of an excavation (Figure 3). The zone is approximately 4 m wide, comprising 4 main strands of the fault trace, with several smaller strands linking between them, and has a total vertical offset across the zone of approximately 0.5 m. Normal (extensional) movement occurs across this zone, with dips on the strands ranging from 51 – 84°. The 4 apparent main strands have an average dip direction of 089° (strike 356°), while the 2 measurable minor strands have a dip direction of 351° (strike 081°). Unfortunately, the top layers of the stratigraphy were removed during excavation, so limited stratigraphic information is available to date the movement of this fault. The white layers at the top of the cutting, which are clearly displaced by the fault movement, are tentatively identified as K12/K13 (Kauroa ash sequence) of approximately 1.23 million years ago. Soil infilling down the fault traces is identified as part of the Hamilton Ash sequence, being amongst the younger portion due to the strong brown colouration (the oldest Hamilton Ash units are pale coloured). This suggests that the fault movement is within the last 250 ka, but this is not definitive.

4.3 Kay Road exposure

Recent cuttings created as part of the Hamilton Bypass portion of the Waikato Expressway development have exposed a complex fault zone in the hill section at Kay Road (location A) on the northern boundary of Hamilton City (37°42’40” S, 175°15’25” E). This site consists of a deep cutting through a hill (Figure 4), with the cutting running approximately normal to the strike of the ridgeline. Thus two exposures exist, one on each side of the cutting. Exposure of the cutting on the western face consists of an approximately 85 m long by 35 m high embankment, while the exposure on the eastern face is approximately 70 m long by 30 m high. Images of both the East and west faces are depicted in Figure 4 below.

These cuttings expose a complex fault zone with numerous steeply dipping normal faults, together with apparently lower angle linking strands. Relatively few fault planes are found within the the

lower lying Walton Subgroup. An average observed dip of 57.3° was recorded for these faults, with an average dip direction of 191° (NNE) . Many more faults are observable within the overlying Kauroa Ash beds, suggesting splintering of the faults as they encountered the weaker tephric marterials. Displacement of a golden silt unit is immediately apparent, with a throw of 2.72 m observed. This throw was constant throughout the area, and occurred on both exposures of the unit within the field area. Faults within the Kauroa beds have an average dip of 73° and dip direction of 55°, trending across a NE-SW plane. The distinctive Rangitawa Tephra at the base of the Hamilton Ashes is undisturbed throughout the entirety of the Kay Road site, and no evidence for offset of this unit was found. It is, therefore, thought that faulting of these units is confined to a time sometime between deposition of the Walton Sub-group 1.8 Ma - 0.5 Ma, and deposition of the Rangitawa tephra 350 ka. These faults are thus inferred to be inactive.

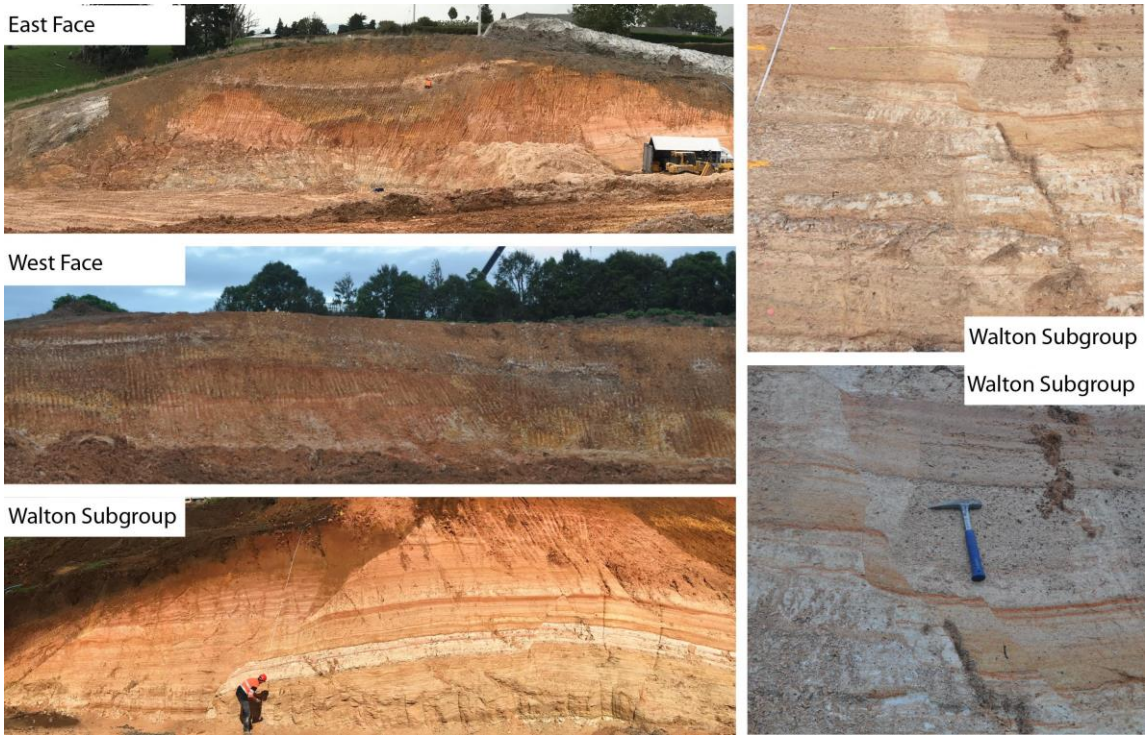

Figure 4. Exposures at Kay Road. Eastern face, western face and Walton Subgroup exposures depicted above. Pictured right is faulting within the Walton Subgroup.

4.4 Stubbs Road

At Stubbs Road (37° 49’ 38” S 175° 19’ 34” E) the geomorphology consists of a north – south trending set of hills, which disappear into peat swamps to the north and south. The Waikato River appears to turn sharply to the northeast at Stubbs Rd, and more gently to the northwest closer to Hamilton City (Figure 5A). There are terraces flanking the river on the upstream side approaching the bend. While some continue around the bend, the pattern of terraces appears to be disrupted. Above the river on the western bank there is a deep channel (50-100 m wide) that initially follows the alignment of the upstream river channel, before turning towards the north. This has been interpreted as an abandoned river channel. A gully system containing a small stream enters the river at the sharp bend, and the system generally aligns with the river channel downstream of the bend (Figure 5A). The gullies in the Hamilton Basin have previously been considered to be formed in random locations by headward erosion within relatively homogenous materials (Schofield, 1965). However, the relationship between the gully system and the other features at Stubbs Rd suggests that at least some of the gully/stream systems within the Hamilton Basin are influenced by non-homogenous materials affected by faulting, resulting in stream locations that

reflect underlying structures, either through exploiting weaker materials or by the effect of buried topography on groudwater flow concentration.

One measurable fault alignment was observable on the western bank of the river at 37°49'39.0"S, 175°19'35.2"E, as shown in Figure 5B. This fault offset shallow-dipping sedimentary beds at the base of the sequence, and was marked by ductile deformation of a pale yellow clay layer, together with ironstaining on the fault surface. Measured apparent vertical offset at this site was 43 mm and fault orientation was 85/047 (dip/dip direction, °T).

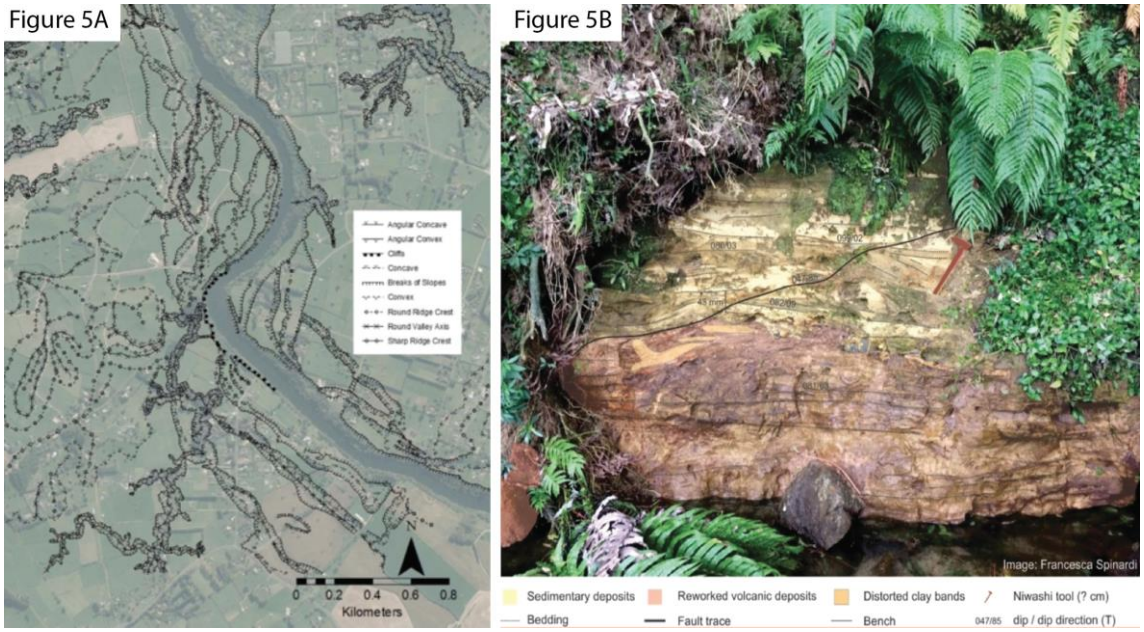

Figure 5. (A) Geomorphic map of Stubbs Road area (location A). (B) Annotated image of small exposed fault in riverbanks near Stubbs Road. Map courtesy Mike Cummins.

5 DISCUSSION

The Kay Road site provides an excellent window into the structure of fault zones within the Hamilton Basin. The zone shows complex deformation, with multiple, steeply-dipping, normal fault strands contributing to overall uplift of the hills in this area (uplift to north, downdrop to south). As the faults propagate into and through the weak materials in the basin, they appear to splinter: several relatively simple faults in the lower sedimentary units present as a complex pattern of intersecting fault traces in the upper tephra beds. Consequently, in identifying faults in this region it is important to recognise that we are unlikely to be seeing a single, well-defined fault trace, and total vertical offset is likely distributed over a number of different strands.

For fault zones where no exposure of displaced strata is available, we are forced to rely on more circumstantial geomorphic evidence. There are many process that contribute to the formation of river channels, but certain patterns are characteristics of tectonic regions, such as rectangular drainage patterns, deflection of the river channel, and changes in channel profile with accompanying knickpoints and associated areas of degradation/aggradation (Schumm et al., 2000; Burbank and Anderson, 2012). Within the Hamilton Basin the Waikato River displays a rectangular drainage pattern suggesting an influence of discontinuities on the river's path, combined with morphological features indicative of episodic disruption of the drainage system. Rivers that are oriented perpendicular to the strike of a normal fault will experience changes in their channel types where areas of uplift cause the river to entrench itself, and areas of down-drop cause aggradation due to the river seeking to rebuild to its baseline (Schumm et al., 2000).

Degradational areas contain knickpoints along river profiles and often display steep river slopes due to entrenchment. Areas of aggradation on the other hand contain shallower and broader channels that are either braided or more sinuous (Schumm et al., 2000). Such patterns are observed at the locations where fault zones were inferred from other evidence. The multibeam, sidescan and seismic survey data provide additional evidence, where knickpoints and discontinuities are present at each sharp bend (Figure 1). It is possible that during an earthquake the Waikato River became blocked by displacement of the footwall, causing the river to either be slowed or dammed and the creating regions of aggradation. Over time the river would have eroded a new path through the footwall creating a region of degradation. Alternatively the River has encountered these resistant zones as it entrenched following deposition of the Hinuera Formation.

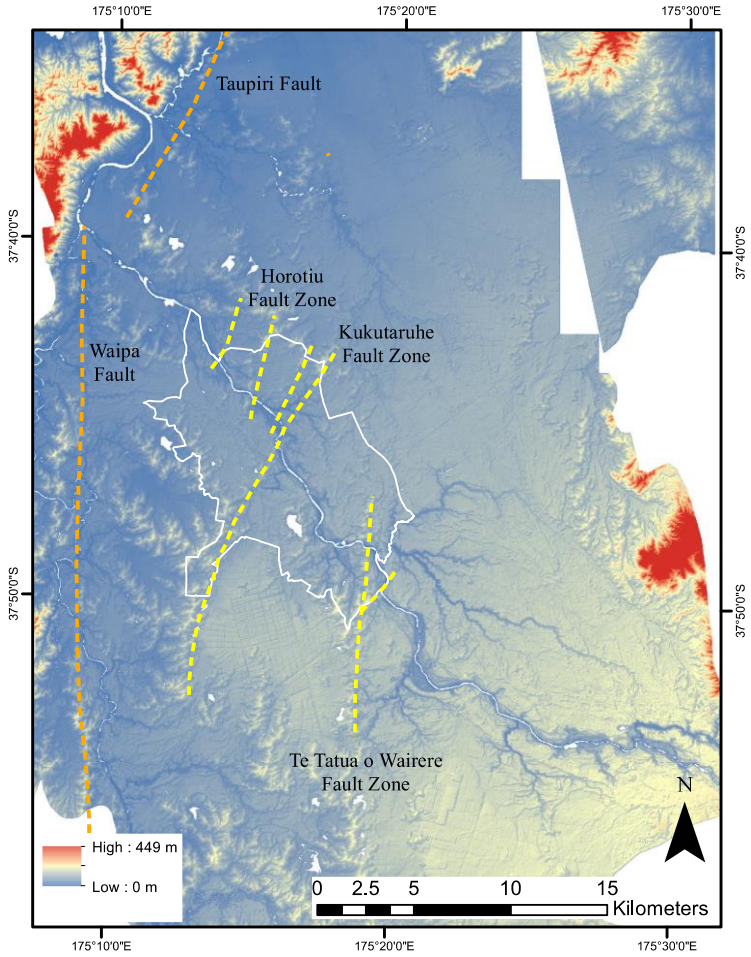

Figure 6. Map of inferred fault zones recognised from surface exposures and geological mapping of the Waikato River. White outline is Hamilton City.

Based on the available data, we infer three main fault zones running southwest – northeast across the Hamilton Basin (Figure 6). We are using informal names for these and they are: Te Tatua o Wairere Fault Zone, extending from Stubbs Road northward through Hammond Park and the Hamilton Gardens and following the ridge through the University; Kukutaruhe Fault Zone, following the ridge from Te Awamutu through to Rototuna, and including the Rototuna and Kay Road exposures; and Horotiu Fault Zone, less well evidenced, near Horotiu. These are zones and display considerable splay in their traces, making for complex geomorphology. The faults that we have observed are dominantly steeply dipping normal faults, indicating formation in an extensional regime. Generally they are uplifted to the north.

6 CONCLUSION

The Hamilton Basin is considered an area of low seismic risk as no surface fault traces have previously been recognised in the basin. Our recent mapping has revealed several sites where complex fault traces can be identified, and geomorphic features which allow these traces to beextended across the basin. Hence, we now infer that the Hamilton Basin has a system of normal faulting indicating a north-south extensional regime, with relative uplift to the north. Assessment of the timing of the events is difficult due to limited exposure, but from the actual exposures discussed here, there is no definitive evidence for movement on these faults post-dating the ~350,000 year old Rangitawa Tephra at the base of the Hamilton Ashes. Further work is proposed to better define age and frequency of events.

REFERENCES

Burbank, D., & Anderson, R. (2012) *Tectonic geomorphology* (2nd ed.). Chichester, West Sussex; Hoboken, N.J.: J. Wiley & Sons.

Edbrooke, S. & Begg, J. (2005) *Waikato* (Institute of Geological & Nuclear Sciences Limited. Institute of Geological & Nuclear Sciences 1:250 000 geological map; 4). Lower Hutt, N.Z.: Institute of Geological & Nuclear Sciences.

Kear, D., Schofield, J., & Couper, R. (1978) *Geology of the Ngaruawahia subdivision (New Zealand Geological Survey.* Bulletin; 88). Wellington: New Zealand, Dept. of Scientific and Industrial Research.

King, P. (2000) Tectonic reconstructions of New Zealand: 40 Ma to the Present. *New Zealand Journal of Geology and Geophysics* 43(4), 611-638.

Kirk, P. A. (1991) Waipa Fault and the tectonic rotation of Hakarimata-Taupiri block. New Zealand Geological Survey Record 43: 81-84. Wellington, Department of Scientific and Industrial Research

McCraw, J. (2011) *The wandering river: Landforms and geological history of the Hamilton Basin* (Guidebook (Geoscience Society of New Zealand); no. 16). Lower, Hutt, N.Z.: Geoscience Society of New Zealand.

Schumm, S., Dumont, J., & Holbrook, J. (2000) *Active tectonics and alluvial rivers*. Cambridge, UK; New York, NY: Cambridge University Press.

Stirling, M.W., McVerry, G.H., Gerstenberger, M.C., Litchfield, N.J., Van Dissen, R.J.; Berryman, K.R., Barnes, P., Wallace, L.M., Villamor, P, Langridge, R.M., Lamarche, G., Nodder, S.; Reyners, M.E., Bradley, B., Rhoades, D.A., Smith, W.D., Nicol, A., Pettinga, J., Clark, K.J., Jacobs, K., 2012 National Seismic Hazard Model for New Zealand: 2010 Update. *Bulletin of the Seismological Society of America*, Issue 102(4): Pp. 1514-1542. Doi: 10.1785/0120110170

Wood, A. P. (2006) Morphodynamic Channel and Stability of the Waikato River: Karapiro to Nagruawahia Reach (Doctoral dissertation, University of Waikato).

Field tests on shallow foundations on stiff clay: moment-rotation response and damping

R S Salimath
Tonkin & Taylor Ltd, Auckland, NZ
rsalimath@tonkintaylor.co.nz.

M J Pender
Department of Civil & Environmental Engineering, University of Auckland, NZ.
m.pender@auckland.ac.nz (Corresponding author)

L S Hogan
Department of Civil & Environmental Engineering, University of Auckland, NZ.
l.hogan@auckland.ac.nz

L M Wotherspoon
Department of Civil & Environmental Engineering, University of Auckland, NZ.
l.wotherspoon@auckland.ac.nz

Keywords: shallow foundation, moment-rotation curve, snap-back tests, damping

ABSTRACT

The moment-rotation response of shallow foundations is inherently nonlinear being controlled by the "elastic" stiffness at small rotations and the moment capacity of the foundation at larger rotations. Simple elastic soil structure interaction (SSI) does not model this rotational response and elastic radiation damping is very small for rocking response. The purpose of this paper is to report on shallow foundation field tests at a site in Silverdale which complement earlier tests done at a site in Albany. In these tests the foundations were subject to bi-directional loading so that the response was first measured by loading in one direction and then loading in the opposite direction. Initially, two-way slow cyclic loading was applied to the foundations with gradually increasing maximum moments until the moment capacity of the foundation was found. After this bi-directional snap-back testing was done, with the snap-back release from progressively increasing moments. The pull-back parts of these tests confirm the nature of the moment-rotation curves for the foundations and the measured curves are compared with those derived from nonlinear finite element modelling with PLAXIS 3D. The snap-back parts of the tests confirm that the damping in the first few half cycles of response is large, that the damping is amplitude dependent and decreases as the motion decays. The paper details the process for obtaining the damping values and discusses how this behaviour influences shallow foundation behaviour.

1 INTRODUCTION

The moment-rotation response of shallow foundations subjected to rocking is highly non-linear, a consequence of partial detachment of the footing edges and subsequent reattachment during cyclic loading. This reduction in contact area of the footing during rocking may result in reduction of actions applied to the superstructure which influences the seismic performance of the structure. Kelly (2009) explained that much of the NZ multi-storey building stock does not have adequate weight to resist the overturning moment that may occur during earthquakes and in such cases initiation of rocking can be beneficial as it limits the actions transmitted to the superstructure. Various researchers over the years have studied the possible benefits of rocking and how it may be incorporated into the design of shallow foundations under earthquake excitation. In order to achieve this it is important to estimate the amount damping that occurs during the rocking process as well as the change in stiffness that occurs with the foundation rotation.

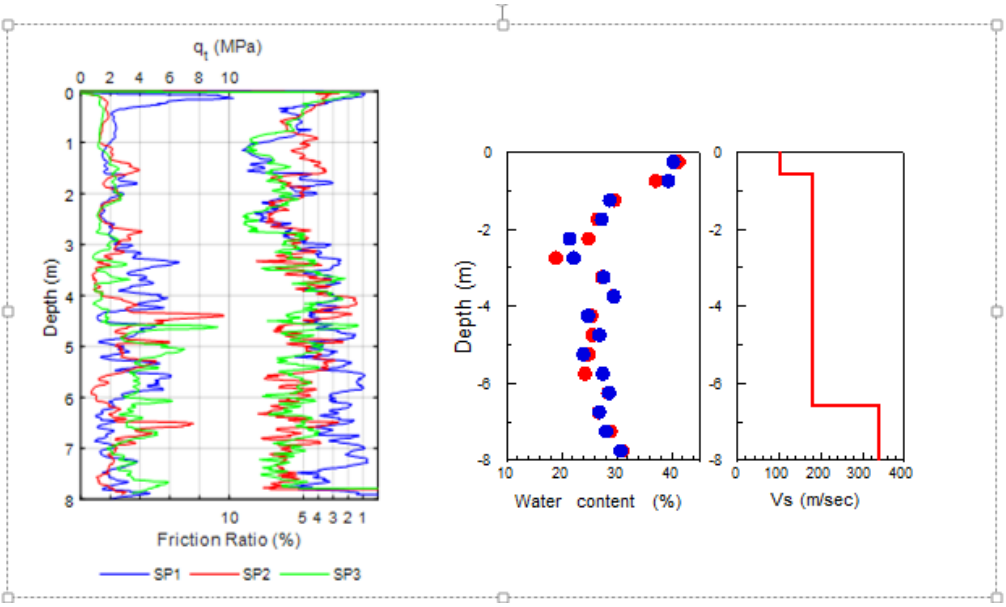

Figure 1: CPT data (left) and water content and shear wave velocity profiles (right

Algie (2011) carried out several large scale field tests on embedded strip footings (L/B = 5 and D_f/B = 1) to study the rocking and dynamic response of shallow foundations on stiff clay. In addition to this he also undertook some finite element modelling using ABAQUS (Simulia 2010) to study the nonlinear moment-rotation response of the footings. This paper presents results from the snap-back experiments performed as a follow-up to Algie's testing. One of the key features of this testing program was that separate snap-back tests were performed with moment about the shorter and longer axis. Our finite element studies showed, using PLAXIS 3D (Plaxis BV. 2012), that rectangular footings exhibit different rotational stiffness depending on the axis about which the moment is applied. This paper discusses the experimental set-up and static moment-rotation response obtained from slow-cyclic and snap-back tests. The damping values obtained for both of the test footing configurations are presented and their influence of design of rocking shallow foundations is discussed.

2 EXPERIMENTAL PROGRAMME

2.1 Site description

The tests were carried out on a site located in Silverdale, north of Auckland. The soil properties at the site showed that the ground is comprised of stiff to very stiff residual clay with the ground water table at approximately 1m below the ground surface. Geotechnical investigation was undertaken at the test location which comprised of CPT's and seismic dilatometer (SDMT) tests. Shear wave velocity profiles, using geophysical methods (MASW), were obtained after the foundation load tests were completed. Some of the CPT results along with the water content and wave velocity profile are shown in Figure 1. As seen from CPT data, stiff silty clay (cone resistance greater than 2 MPa) was encountered up to a depth of around 6m from the ground surface. The shear wave velocity profile reveals that the shear modulus of the soil increases with depth. The tests were performed at three different locations within the site. The ground surface was levelled at the test locations so that the footing can rest on a horizontal surface.

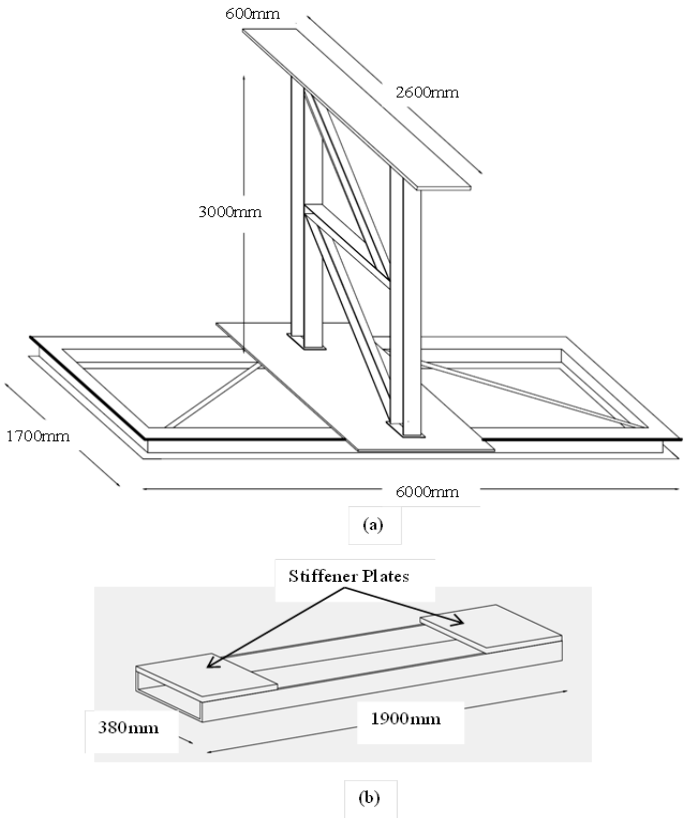

Figure 2: (a) Steel frame assembly for the experimental rig; (b) PFC380 channel sections with stiffeners used as footings

Figure 3: Experimental set-up assembled on site for snap-back test

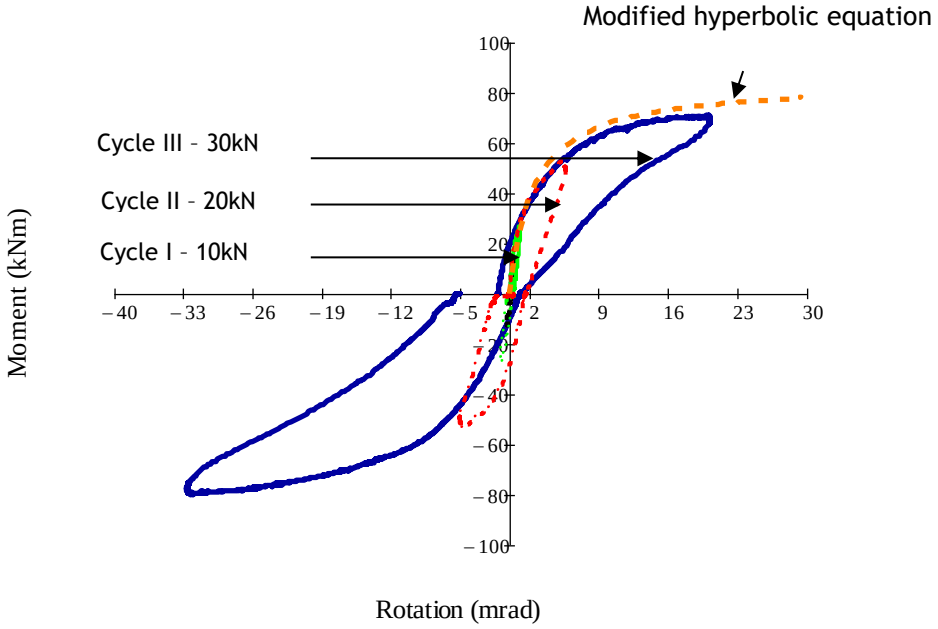

Figure 4: Hysteresis moment-rotation curves from slow-cyclic tests

Figure 5: Partial detachment of the footing with the underlying soil

2.2 Experimental set-up for slow cyclic and snap-back tests

The structural details and dimensions of the test assembly used for the experiments are shown in Figure 2a and 2b. The test assembly consists of two frames consisting of 200UC46.2 and 100UC14.8 sections. The two frames were bolted to each other with the 6m long frame resting horizontally flat on the ground. Two PFC380 channel sections (Fig 2b) were used as footings and were bolted to the underside of the 6m frame. The entire test structure was pulled and snapped in North-south direction only but two different test footing configurations were used so that moment can be applied about the short axis (configuration 1) and long axis (configuration 2) of the footings separately. The experimental set-up assembled on site for snap-back testing with moment about the short axis is shown in Figure 3. The rotation of the footing was measured using inclinometers and LVDT's placed at either ends of the footing. Accelerometers were installed at different heights to measure the acceleration and force time history during the snap-back tests. Draw wires were used to measure any horizontal displacement of the test structure during rocking. The test structure was pulled horizontally and both slow cyclic and snap-back tests were performed at pullback forces ranging from 5kN to 30kN.

2.3 Test procedure

The experimental program comprised of slow-cyclic and snap-back tests. The test structural assembly was the same for all the tests performed except that for snap-back test two different footing configurations were used. For slow cyclic tests, the test structure was pulled in horizontal direction (Figure 3) until the desired load is achieved and then slowly released. The initial pullback phase is the same for snap-back tests but instead of slow release the test structure is snapped using a quick-release mechanism, so that the structure rocks in the axis of the applied moment. The rotation-time and settlement-time history data recorded during the snap-back tests is used to estimate the magnitude of damping that occurs during rocking.

3 EXPERIMENTAL RESULTS

3.1 Slow-cyclic tests

The field experiments carried out for this study comprised of slow-cyclic and snap-back tests on two strip footings (L/B = 5). The hysteresis moment-rotation curves from the slow cyclic tests are shown in Figure 4. The tests were performed at pullback forces of 5kN, 10kN, 20kN and 30kN. For 10kN case, since the applied moment is very small (M/M_{ult} = 0.23, where, M_{ult} = ultimate moment capacity of the footing), the footing rotation is small and the moment-rotation plot is elastic. At a load of 30kN, the moment-rotation response is highly nonlinear and large plastic displacements are induced. There is also partial loss of contact between the footing and the underlying soil at this stage as seen in Figure 5. The theoretical moment-rotation curve obtained from the hyperbolic equation, modified to account for the footing shape, fits the experimental response well which confirms that nonlinear moment-rotation response of shallow foundations is hyperbolic in nature.

3.2 Snap-back test results

Unlike slow-cyclic tests, the snap-back tests were performed for two different footing configurations at three different locations on the site. For each configuration, snap-back releases were performed at different pull-back forces. Figure 6 shows the moment-rotation response of the footing during pull-back phase prior to the snap-back release for footing configuration 1. Also superimposed on the experimental results is the moment-rotation response from modified hyperbolic equation. From the curves it is evident that with every snap there is some degradation of rotational stiffness. The initial small strain rotational stiffness from the experimental curves was compared with theoretical stiffness predicted using Gazetas (1991) solutions. The comparison shows that the small strain rotational stiffness from the experimental curves is around 22-28% of the theoretical stiffness. The degradation of the rotational stiffness can be a result of rounding of soil surface under the footing due to footing rocking during snap-back. Pender (2015) concluded that degradation of rotational stiffness with increase in moment implied that it unlikely that ultimate moment capacity of the footing will ever be mobilized even at large PGA values. The rocking response of the footing is affected by both material and geometric (footing L/B ratio) nonlinearities.

Finite element studies carried out as part of this research showed that a rectangular footing exhibited higher rotational stiffness when moment is applied about the longer axis (configuration 2). Figure 7 has a comparison of the moment-rotation response of footings (L/B=5) obtained from pull-back phase of field experiments and that from finite element analysis. The finite element results are seen to converge with those from the field tests, which affirms that non-linear moment-rotation response of footings predicted from Plaxis3D is reliable. However, Plaxis holds the stiffness along the first part of the moment-rotation curve constant, a consequence of the way in which soil model stiffness is defined in the software.

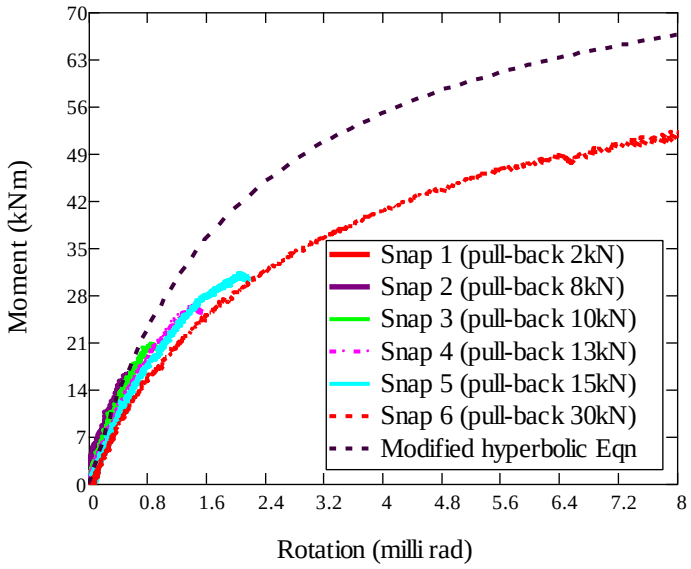

Figure 6: Moment-rotation curves from pull-back phases for snap-back tests with moment about the short axis (configuration 1)

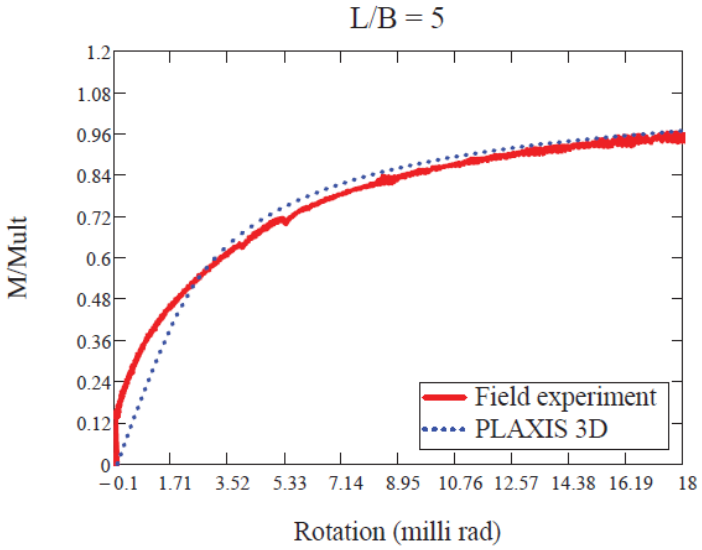

Figure 7: Comparison of moment-rotation curves from field experiments and PLAXIS 3D

3.3 Damping

One of the primary objectives of performing these snap-back tests was to estimate the amount damping that occurs during foundation rocking. The value of damping is very critical is assessing the enhanced seismic performance of rocking shallow foundations. Algie (2011), based on his snap-back experiments, concluded that the damping is significant when the footing rotation is greater than 0.6 milliradians. Pender (2014) concluded that foundation response is governed by the large damping that occurs in the first cycle of the response. Various methods are presented for estimation of damping in the past literature. Unlike dynamic loading, during snap-back test the natural frequency varies with cycles and hence, for this research, logarithmic decrement method (Chopra 2007) was used to evaluate damping. Figure 8 shows the rotation-time response obtained from snap-back tests for moment about the short axis. Damping ratio was estimated for each peak of the rotation time plot and the results are presented in Figure 9. The plots confirm that large damping occurs in the first cycle of the response, the magnitude of the damping is greater for snap-back from 30kN because the larger footing rotation at the time of snap. Thus the larger the

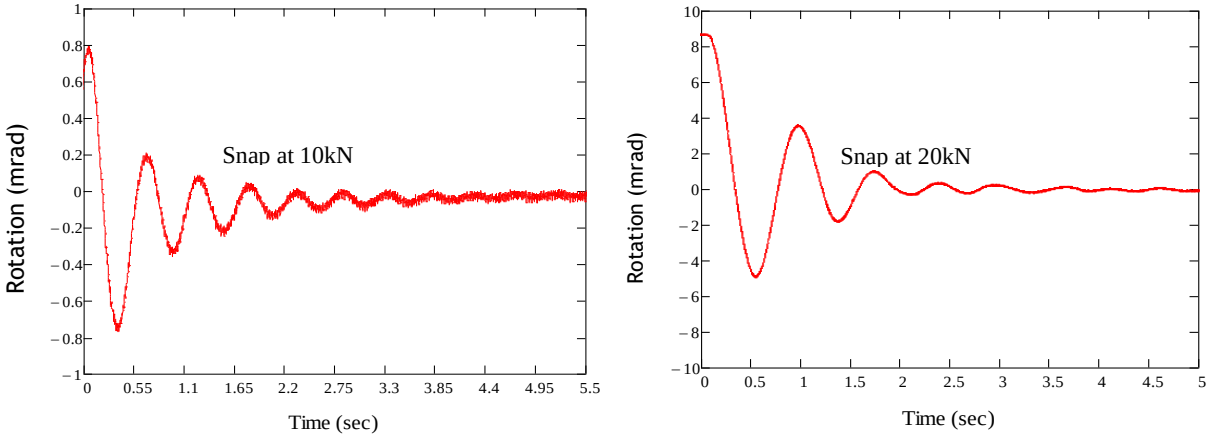

Figure 8: Comparison of rotation-time plots for snap-back tests with snap at 10kN and 20kN, with moment applied about short axis

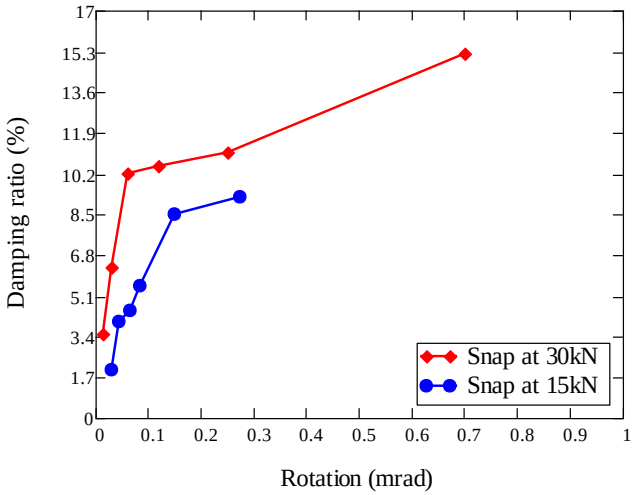

Figure 9: Variation of damping ratio vs footing rotation at each impact for snap at 15kN and 30kN

footing rotation at snap release the greater is the energy dissipation in the first rocking cycle and hence the initial damping value is larger. An additional factor which is important for foundation performance is the residual rotation when the motion ceases. The results in Figure 8 show that for rotations up to at least 10 milli-radians (about half a degree) at pull-back there is negligible residual rotation. This is very critical in seismic performance of rocking foundations, because significant residual rotation of the foundation means that tall structures have an easily perceived lean. The field test results show that even modest foundation rotation at snap-back results in good damping performance with negligible residual rotation. Figure 9 shows how the damping varies during successive cycles of response. More discussion of these matters is given by Salimath (2017) and Pender et al. (2017).

4 CONCLUSIONS

The following conclusions are reached:

- The test results show that, for the fixed static bearing strength factor of safety at which the tests were done, the moment-rotation response of shallow foundations resting on clay is highly nonlinear and hyperbolic in nature, Figures 4, 6 & 7;

- A contributing factor to the nonlinearity of the moment-rotation curve is the reducing area of contact as the moment applied to the foundation increases, Figure 5;
- Extensive finite element modelling has confirmed this conclusion for cyclic loading from other static factors of safety;
- With the increase in moment at each snap there is degradation of rotational stiffness of the footing. The magnitude of decrease in rotational stiffness also depends on the initial static factor of safety of the footing;
- The small strain rotational stiffness obtained from experimental moment-rotation curves was around 28% of the theoretical rotational stiffness (based on the shear wave velocity of the soil);
- The foundation moment-rotation curve obtained during the pull-back phase of the field tests can be modelled quite closely with PLAXIS 3D, Figure 7;
- When footing rotation at snap-back is larger, the number of impacts in the rotation-time plot is less which implies that the energy dissipation in the first few rocking cycles is high, Figure 8;
- Damping ratio is higher for the first rocking cycle, the magnitude also depends on the footing rotation at snap-back, Figure 9.

REFERENCES

Algie, T. B., Pender, M. J. and Orense, R. P. (2010) Large scale field tests of rocking foundations on an Auckland residual soil, In: *Soil Foundation Structure Interaction* (R Orense, N Chouw, and M Pender (eds.)), CRC Press / Balkema, The Netherlands, pp. 57- 65.

Algie, T. B. (2011) Nonlinear Rotational Behaviour of Shallow Foundations on Cohesive Soil, Ph D thesis, University of Auckland.

Chopra, A.K. (2007) *Dynamics of Structures, Theory and Application of Earthquake Engineering*, third edition. Pearson Education, Inc.

Gazetas, G. (1991) Foundation Vibrations. In: *Foundation Engineering Handbook*, H. Y. Fang, Ed. Van Nostrand, pp. 553-593.

Hakhamaneshi, M., and Kutter, B.L. (2016) Effect of footing shape and embedment on the settlement, recentering and energy dissipation of shallow footings subjected to rocking. *Journal of Geotechnical and Geoenvironmental Engineering*, Vol 12.

Pender M.J. (2014) "Integrated design of structure-foundation systems: the current situation and emerging challenges". Keynote address: *Proceedings of NZSEE Conference*, Auckland, New Zealand.

Pender, M.J., Algie, T.B., Storie, L.B., and Salimath, R.S. (2017) One dimensional moment-rotation macro-element for performance based design of shallow foundations. Paper 332, *PBD III Earthquake Geotechnical Engineering conference*, Vancouver.

Plaxis BV. PLAXIS 3D (2012) Reference Manual. Delft, Netherlands.

Salimath, R (2017) Experimental and finite element study of moment-rotation response of shallow foundations on clay, PhD thesis, University of Auckland.

Simulia (2010) ABAQUS 6.8-EF2. Dessault Systemes.

Is there a potassium-based solution to sensitive soil slipping within the Bay of Plenty?

T. Robertson
School of Science, University of Waikato, Private Bag 3105, Hamilton, NZ
robertson.tom0@gmail.com

V. G. Moon
School of Science, University of Waikato, Private Bag 3105, Hamilton, NZ
vicki.moon@waikato.ac.nz

D. J. Lowe
School of Science, University of Waikato, Private Bag 3105, Hamilton, NZ
david.lowe@waikato.ac.nz

Key words: halloysite, sensitive soil, triaxial, Atterberg limits, potassium

ABSTRACT

Landslides are common in sensitive, weathered pyroclastic soils in the Bay of Plenty (BOP). The clay mineralogy of these soils is dominated by halloysite, an inactive 1:1 clay mineral. Manipulation of cation content within the pore water of sensitive soils has been shown to improve *in situ* soil strength in illite-dominated soils in Norway. We present results of laboratory tests on the impact of altering cation status of a sensitive soil from the base of a large landslide at Omokoroa near Tauranga, BOP. Addition of KCl and KOH both reduced the liquid limit of the soil, a negative effect. In contrast, addition of K_2CO_3 caused an increase in the plasticity index of soil pastes. Soaking intact samples in K_2CO_3 for three weeks resulted in a considerable increase in peak stress in effective stress triaxial testing. These early results suggest that mitigation of sensitive soil landslides through increasing peak strength by addition of appropriate salts to the soil profile may be an option for mitigation of landslides in sensitive BOP soils.

1 INTRODUCTION

Sensitive soils are found across the globe, and have widely been identified as a significant contributor to slope instability. Most notably, sensitive soils can cause large, retrogressive landslides, resulting in serious hazards to infrastructure, the local environment, and human life (Quinn et al., 2011). Sensitivity is recognised as a considerable loss in strength on remoulding and is defined as the ratio of undisturbed to remoulded strength at the same moisture content. Young, clay-rich deposits from a variety of marine, lacustrine, and pyroclastic (tephra) environments have been reported as being sensitive (Rosenqvist, 1977; Torrance, 1983; Kluger et al., 2017). In New Zealand some of the most damaging sensitive soils are located within Bay of Plenty (BOP), eastern North Island. These soils are encompassed within altered Quaternary rhyolitic tephra deposits and reworked derivatives, and a key component is the presence in them of the clay mineral halloysite (Moon et al., 2015).

Recent reports from Norway indicate that a long-standing experiment has proven successful in the prevention of sliding within a sensitive soil landslide. Columns of potassium chloride installed in the glacially-derived sensitive soils (illite dominated) for a period of 30 years have produced improvements in peak undisturbed soil strength to the point that movement of the slide had been reduced to nil (Moum *et al.*, 1970; Torrance, 2014; Helle *et al.*, 2015). As a result, we postulate that the methodologies used by the researchers in Norway could be applied to the soils of BOP

with the ultimate goal of locally increasing peak shear strength in the soils. However, the clays differ in our tephra-derived soils from those of Norway (halloysite cf. illite), and the clay-cation interactions will be different. Hence, the aim of this paper is to investigate suitable salts that might be used to mitigate landsliding in the sensitive soils of BOP. We evaluate the most appropriate salt and the impacts its addition has on Atterberg limits and on peak strength under laboratory test conditions.

2 HALLOYSITE

Halloysite is a dioctahedral 1:1 clay mineral belonging to the kaolin sub-group (Joussein *et al.*, 2005; Churchman *et al.,* 2016). It is commonly formed in altered volcanic and tephra deposits, and within New Zealand these deposits are generally rhyolitic with the halloysite formed from rapid, low temperature alteration mainly of volcanic glass and also feldspar (Churchman and Lowe, 2012). Halloysite has a basal spacing of 7.2Å (dehydrated form) and 10.1Å (hydrated form), with the larger basal spacing deriving from the presence of interlayer H_2O ('water') between sets of octahedral (aluminol) and tetrahedral (silanol) sheets within the clay. The H_2O present within the clay is found in two forms: 'hole' water which solely interacts with the silanol sheet through forming hydrogen bonds with the oxygen of the silanol sheet; and 'associated' water which interacts with both the hole water and the hydroxyl groups on the aluminol sheet. This associated water acts as a bridge between the various sheets, and forms the intercalated water giving the increased basal spacing (Joussein *et al.*, 2005; Churchman *et al.*, 2016; Ferrante *et al*., 2017).

Interactions between halloysite and various cations have been explored in the literature and indicate that surface interactions between halloysite and cations may be responsible for the bonding between clay minerals *in situ.* As a consequence, the manipulation of the cation content should produce results similar to those observed in Norway, though the cation and salt utilised may not be the same. Based on the literature, we suggest the ideal potential choices are narrowed to potassium salts: potassium chloride (KCl), potassium hydroxide (KOH), and potassium carbonate (K_2CO_3).

3 METHODS

Soils were sampled from a layer of sensitive soil within the Pahoia Tephra sequence at the base of the Bramley Drive landslide, Omokoroa. Kluger *et al*. (2017) describe details of the profile, sampling site, and sampling procedure. For our study, 12 sample pipes (50 mm inside diameter) were pushed into a prepared horizontal platform, dug out, and wrapped carefully to avoid moisture loss. Approximately 4 kg of bulk soil was additionally collected for Atterberg limit testing.

Atterberg limits were determined on soil pastes following standard methods (ISO/TS 17892-12:2004(E)) using a drop-cone penetrometer to determine liquid limit, and rolled threads for plastic limit. Initially soil from the site was re-moulded into a large homogenous paste with distilled water as the mixing medium. Atterberg limits were first tested on this baseline untreated paste. Next, equal-size portions of the homogenous paste were used in Atterberg limit testing, with the difference between these and the initial baseline being the use of a salt solution instead of distilled water to change the moisture contents of the sample. For each treatment, the pH of the soil mixture was measured by placing the probe directly into the mixed soil paste as outlined by Torrance (1999). Salts used for treatments were KCl, KOH, and K_2CO_3.

Treatment of soil cores prior to triaxial testing was achieved via submersion in a K_2CO_3 solution at 2 mol L^{-1} strength and the initial electrical conductivity of the solution was measured before cores were placed in sealed plastic containers. Approximately 2.5 litres of solution were placed in each container, 4 soil cores were added to each, and the conductivity of the solution again

measured. The containers were sealed and placed in a dark room kept at a controlled temperature between 15 and 18 °C. The cores were treated for a period of 4 weeks.

Effective stress triaxial testing was undertaken following British Standard BS1377-8:1990. Samples were saturated to $B \geq 0.95$, then consolidated to effective confining stresses of 200, 280 and 355 kN m^{-2} to reflect *in situ* stresses. Testing rates varied between 0.5 mm min^{-1} to 0.524 mm min^{-1} depending on consolidation characteristics. During testing, measurements were made every 30 seconds until 20% of axial strain was reached.

4 RESULTS

4.1 Atterberg limits

Atterberg limit results are presented in Table 1. Baseline results for liquid limit and plasticity index are in keeping with data for other halloysite-rich soils from New Zealand; the plastic limit determined here is higher than other determinations on New Zealand soils, but within the ranges described by Wesley (1973) for Indonesian soils rich in halloysite. As anticipated, the liquid and plastic limits are high, because of the interlayer H_2O within halloysite, but the plasticity index is moderate to low and the soil is thus not active.

Table 1. Atterberg limit test results. Published ranges of results for New Zealand halloysite-rich soils mixed with distilled water are from Moon (2016).

Treatment	Liquid limit (%)	Plastic limit (%)	Plasticity index (%)	Activity	pH
Distilled water	92	78	14	1.1	4.8
KCl	79	74	5	0.3	4.4
KOH	83	72	11	0.7	8.7
K_2CO_3	93	73	20	1.1	10.1
K_2CO_3 (after 1 month)	92	72	20	1.1	10.1
Published ranges	42-99	29-67	10-46		

Surprisingly, KCl and KOH both reduced the liquid limit of the soil, whereas the plastic limit was reduced slightly for all treatments. As a result, the plasticity indexes of the soils treated with KCl and KOH are reduced markedly, the opposite of the desired effect, resulting in a reduced activity. In contrast, K2CO3 did not impact the liquid limit, but gave a reduction in plastic limit similar to that associated with the other treatments, resulting in a slightly increased plasticity index. Leaving the K2CO3 treated soil for a month and retesting showed no further change in Atterberg limits.

The pH measurements on the pastes made for Atterberg testing (Table 1) showed that the soil is characteristically acidic, with a pH of 4.8. Of all treatments only the K2CO3 raised the pH significantly enough to cause the soil to become basic (10.1), whereas KOH neutralised the soil (8.7) and KCl lowered the pH to 4.4.

4.2 Conductivity

The conductivity of the solute in which the soil cores were immersed was measured once a week following first immersion of the cores in the solutions. This was done to give an indication of the potential ion uptake by the soil. Over the first week there was a rapid uptake of ions from the solute to the soil for both sets of cores as overall conductivity dropped by approximately 50%; this rate of uptake continued over the second week of soaking (Figure 1). Little ion uptake appeared to be occurring after two weeks' immersion, as shown by the flattening out of the curves. Two curve appear as these plot the conductivities of two separate treatments that occurred simultaneously on the soil cores.

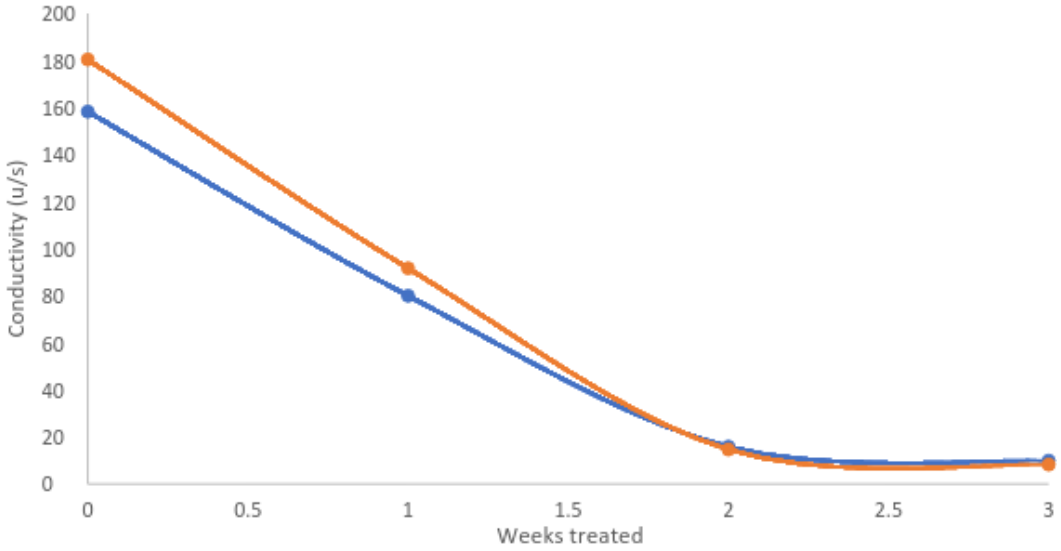

Figure 1: Graph displaying changing conductivity of solute during soil core treatment over time of treatment.

4.3 Triaxial testing

Table 2 details the key results from triaxial testing for both untreated (Un1-3) samples (saturated in distilled water), and treated (Tr1-3) samples which were immersed in K2CO3 solution for 3 weeks. Note that although samples were run to full extent of 20% of axial strain during testing, a malfunction with the data logger resulted in data being collected only for the first 10% of axial strain.

Table 2. Triaxial test conditions and results. ε = axial strain at point of failure, q = peak shear strength, and u = pore water pressure.

Sample	Confining Pressure (kPa)	ε failure (%)	q failure (kPa)	u failure (kPa)	Strain Softening (%)
Un1	205	6.48	151	50	12
Un2	280	1.53	227	174	35
Un3	355	1.09	313	195	41
Tr1	205	0.78	343	123	24
Tr2	280	0.9	424	153	32
Tr3	355	1.11	386	170	25

Figure 2 displays the deviator stress and pore water pressures measured during triaxial testing for both treated and untreated samples. It can be observed that for all confining pressures the peak shear strength of the treated samples is noticeably higher than that of the untreated samples. Indeed, even the lowest confining pressure of treated samples (Tr1, 205 kPa) exhibits a higher peak deviator stress than the untreated counterpart at highest confining pressure (Un3, 355 kPa). It is also worth noting the low variability of pore pressures, with the pore pressures of both 355 kN m-2 samples displaying similar values of pore pressure as shear strain increased.

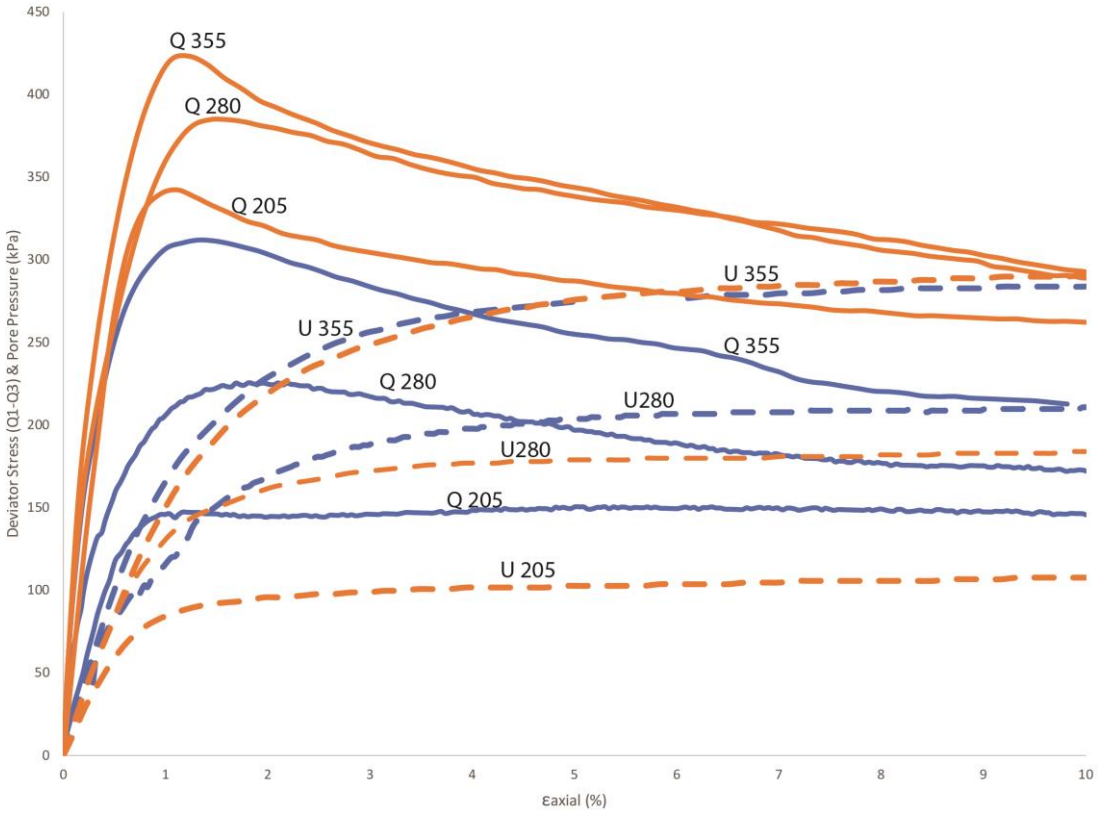

Figure 2. Graph displaying deviator stress (Q) and pore water pressure change (U) versus axial strain whether treated (orange) or untreated (blue)

Post-failure strain softening during testing is exhibited by all materials. Strain softening for untreated samples all showed an increase as confining pressure increased, whereas treated soil cores showed an inverse with a reduction in strain softening between the higher two confining pressures from 32% to 25%. Overall, strain softening tended to be less for the treated samples than for untreated samples (Table 2).

Stress path (p'/q') plots in the untreated soil cores showed a deviation to the left, indicating that slight contraction has occurred in the soil (Figure 3A). In contrast, for the treated soils, all curves deviate sharply to the left, thus indicating very clear contractive behaviour as the plots track down the critical state line.

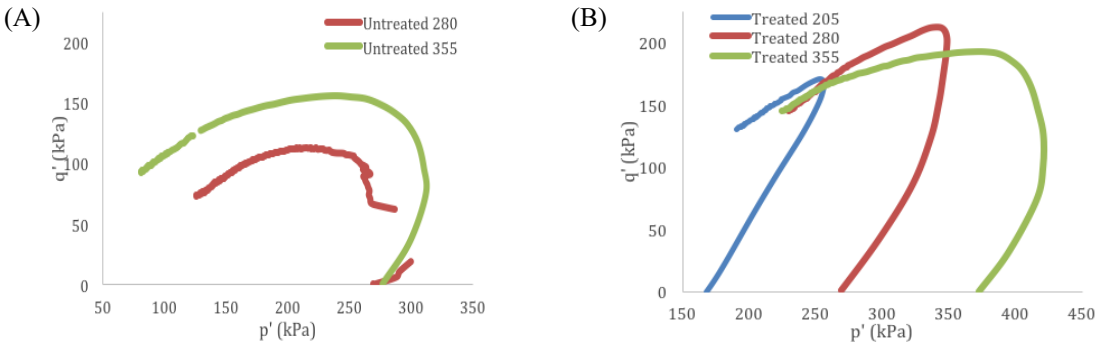

Figure 3. p' q' plots showing contraction of soil samples following failure at each confining pressure. (A) untreated samples, (B) treated samples.

5 DISCUSSION

Treatment with both KOH and KCl caused drops in the liquid limit, an unexpected result. Our hypothesis to explain this observation relates to the soil pH and the resulting reaction between the clay surface within the remoulded paste and the introduced salt solution. Theng & Wells (1995) undertook rheological tests on pastes of pure halloysite materials from various sites in New Zealand. They noted that for tubular and lath-type halloysite morphologies, the Bingham yield stress was strongly influenced by pH. They attributed this to charges on the crystal edges associated with protonation/deprotonation of exposed Al ions. At the point of zero charge (PZC) the edge surface is essentially uncharged; at pH values below the PZC the edges will be positively charged while at pH values above the PZC the edges will be negatively charged. For the samples evaluated by Theng & Wells (1995), the PZC occurred at a pH of approximately 6. The natural pH value for our soils (measured in distilled water) is acidic (pH 4.8). When KCl is introduced, dissociation of the salt means that the chloride ion forms a conjugate acid of hydrochloric acid (HCl), resulting in a lowered pH (4.4). While an overall positive edge charge might be expected to lead to enhanced interactions between edge surfaces and negatively-charged face surfaces of the halloysite minerals, in practice the interactions are mediated by cations within the pore fluid. We infer that due to the overall positive nature of the clay edges, the significant increase in K^+ ions within the soil media results in a net dispersive effect within the soil, causing the observed drop in the liquid limit.

In contrast, treatment with K_2CO_3 resulted in a slight decrease in plastic limit, and an unchanged or slightly increased liquid limit (Table 1). Addition of K_2CO_3 caused a significant rise in pH (10.1), lifting the pH to well above the PZC identified by Theng & Wells (1995). Thus the edge charges on the clay minerals will be negative, and the abundant K^+ ions are able to mediate a relatively strong attraction between negatively charged edge and face surfaces of the clay minerals. Unexpectedly, addition of KOH did not show the same impact, with liquid and plastic limits both depressed by this treatment, despite the pH rising above the likely PZC of the clay. We propose that this finding is due to the strongly amphoteric nature of the Al groups on the octahedral sheet edge resulting in bonding with the anionic OH^- groups as opposed to bonding with K^+ ions, resulting in a loss of overall strength in the soil paste.

A possible reason why K_2CO_3 worked as opposed to the KOH could potentially lie within the likelihood of the salt to readily intercalate into the crystal lattice structure of the halloysite itself. As stated above, halloysite has two forms of bonded water within its structure: hole H_2O, and associated H_2O (Ferrante et al., 2017), with each H_2O layer influencing a different bonding characteristic of the clay. In case of the K_2CO_3 treatment, the salt may potentially have an influence on both the hole H_2O and associated H_2O within the clay. Previous studies examining the introduction of K_2CO_3 to clay pastes indicated that K_2CO_3 will readily intercalate into the halloysite structure, as indicated by an increase in basal spacing following treatment with K_2CO_3 (Garrett & Walker, 1959). Intercalating the K_2CO_3 into the structure increases the structural strength as the K^+ ions actively form ionic bonds with the amphoteric aluminol groups on two separate octahedral clay sheets, with the potassium ion essentially forming an ionic bridge between the two sheets. This intercalation may contribute to the overall increase in peak shear strength of the soil seen in triaxial testing.

Core samples clearly took up ions readily over the 4-week soaking period and reached an equilibrium condition. This condition means either that ion exchange ceased when the ions in the solution were no longer able to overcome the thickness of the diffuse layer present on the surface of the clay, or that soil and solute are in an equilibrium with all negatively charged surfaces bonded with the K^+ ions present in the solution (Wada, 1959). We conclude from this equilibrium situation that the solute concentration was adequate, and that tested samples would display any possible impact of salt manipulation.

Following treatment and triaxial testing, it is evident that the presence of K2CO3 within the soil cores has had an active effect on the shear strength of the soil with the shear strength raised across all three confining pressures that were used. We infer that the increased bonding associated with surface charge effects at elevated pH in an environment with abundant K+ ions is the primary cause of the increased peak strength. Pore water pressures are relatively unaffected, indicating that the pore structure of the material is unchanged, and hence pore water pressure development is similar in the treated and untreated samples. Consequently, pore water pressure gradients are less able to break down the structure of the more strongly bonded materials.

6 CONCLUSIONS

Our studies suggest that mitigation of sensitive soil landslides through increasing peak strength using methods similar to those of Moum et al. (1970) and Helle et al. (2015) is a very real and plausible option for sensitive Bay of Plenty soils. Further studies into the effects of soil treatment need to be conducted across a wider range of confining pressures and treatment times, and the potential impacts of using such a method in practice on the environment and wider eco-system need to be investigated.

7 ACKNOWLEDGEMENTS

We thank the New Zealand Geotechnical Society and the University of Waikato for scholarship support for Tom Robertson. The Western Bay of Plenty District Council is thanked for site access. An anonymous reviewer is thanked for useful comments.

REFERENCES

BS 1377-2 (1990) *Methods of test for soils for civil engineering purposes.*

Churchman, G.J., Lowe, D.J. (2012) *Alteration, formation, and occurrence of minerals in soils*. In: Huang, P.M.; Li, Y.; Sumner, M.E. (eds) Handbook of Soil Sciences. 2nd edition. Vol. 1. CRC Press, Boca Raton, FL, pp.20.1-20.72.

Churchman, G.J., Pasbakhsh, P., Lowe, D.J., Theng, B.K.G. (2016) *Unique but diverse: some observations on the formation, structure, and morphology of halloysite*. Clay Minerals, 51, 395-416.

Ferrante, F., Armata, N., Cavallaro, G., & Lazzara, G. (2017) Adsorption studies of molecules on the halloysite surfaces: A computational and experimental investigation. *The Journal of Physical Chemistry* C, 121(5), 2951-2958.

Garrett, W., & Walker, G. (1959). The cation-exchange capacity of hydrated halloysite and the formation of halloysite-salt complexes. *Clay Minerals*, 4(22), 75-80.

ISO/TS 17892-12 (2004) *Geotechnical investigation and testing—Laboratory testing of soil—Part 12: Determination of Atterberg limits*

Helle, T. E., Nordal, S., Aagaard, P., & Lied, O. K. (2015*)* Long-term effect of potassium chloride treatment on improving the soil behavior of highly sensitive clay—Ulvensplitten, Norway. *Canadian Geotechnical Journal*, 53(3), 410-422.

Joussein, E., Petit, S., Churchman, J., Theng, B., Righi, D., & Delvaux, B. (2005) Halloysite clay minerals–a review. *Clay Minerals*, 40(4), 383-426.

Kluger, M. O., Moon, V. G., Kreiter, S., Lowe, D. J., Churchman, G. J., Hepp, D. A., . . . Mörz, T. (2017) A new attraction-detachment model for explaining flow sliding in clay-rich tephras. *Geology*, 45(2), 131-134.

Locat, J., & St-Gelais, D. (2014) *Nature of Sensitive Clays from Québec. Landslides in Sensitive Clays* (pp. 25-37): Springer.

Moon, V. (2016) Halloysite behaving badly: geomechanics and slope behaviour of halloysite-rich soils. *Clay Minerals*. 51(3), 517-528.

Moum, J., Sopp, O., & Loken, T. (1970) Stabilization of undisturbed quick clay by salt wells. *Norwegian Geotechnical Institute Publ.*

Rosenqvist, I. T. (1977) A general theory for quick clay properties. Paper presented at the *Proc. Third European Clay Conference, Oslo.*

Skemption, A., & Northey, R. (1952) The sensitivity of clays. *Géotechnique*, 3(1), 30-53.

Smalley, I., Ross, C. W., & Whitton, J. (1980) Clays from New Zealand support the inactive particle theory of soil sensitivity. *Nature*, 288(5791), 576-577.

Soma, M., Churchman, G., & Iheng, B. (1992) X-ray photoelectron spectroscopic analysis of halloysites with different composition and particle morphology. *Clay Minerals*, 27, 413-413.

Theng, B., & Wells, N. (1995) The flow characteristics of halloysite suspensions. *Clay Minerals*, 30(2), 99-106.

Torrance, J. K. (2014) *Chemistry, sensitivity and quick-clay landslide amelioration. Landslides in Sensitive Clays* (pp. 15-24): Springer.

Wada, K. (1959) Oriented penetration of ionic compounds between the silicate layers of halloysite. *American Mineralogist*, 44(1-2), 153-165.

Wesley L. (1973) Some basic engineering properties of halloysite and allophane clays in Java, Indonesia. *Géotechnique*, 23, 471−494.

Preliminary assessment of the acid sulphate soils hazard in the Auckland region

R C Roberts
Auckland Council, Auckland, NZ
ross.c.roberts@gmail.com (Corresponding author)

J McConchie
GHD, Auckland, NZ
Jade.McConchie@ghd.com

Keywords: Acid sulphate soils, Auckland

ABSTRACT

Acid Sulphate Soils have recently been encountered on projects in Whangarei and Auckland. These naturally occurring soils are rich in sulphide minerals that have the potential to cause changes in soil and water chemistry when they oxidise. This oxidation process occurs naturally but may be induced by human activities including excavations and groundwater drawdown. These changes include acid generation which can lead to significant harm to flora and fauna. Discharges of affected water have been linked to major fish kills and can also lead to sub-lethal effects, such as red spot disease in fish. It can cause the rapid decay of concrete and metal structures, resulting in significant maintenance costs and failure risks.

The presence of Acid Sulphate Soils is well documented overseas but is less well reported in New Zealand, and little research has been done into the extent and implications of these soils here. The lack of readily available information about the distribution of Acid Sulphate Soils makes it challenging for New Zealand regulators, infrastructure owners and designers to take these potentially damaging conditions into account in a consistent and effective way.

This paper presents the findings of a study in the Auckland Region commissioned by Auckland Council to assess the potential spatial distribution of acid sulphate soils. It is intended to provide a baseline for future research, and to inform current land development projects so that the potential risk can be considered during investigation, design and construction.

1 INTRODUCTION

1.1 Formation and distribution of acid sulphate soils

Acid sulphate soils (commonly abbreviated to ASS) are naturally occurring soils and sediments which contain sulphide minerals that have the potential to cause water and soil to acidify when they oxidise. Acid sulphate soils are a common occurrence in many parts of the world. They are known to occur throughout Australia and have been regulated there for many years. Their effects are usually more severe in warmer climates, such as northern and eastern Australia, but they are known to exist and have significant effects in cooler climates such as Tasmania. Northern New Zealand, including Auckland, has many characteristics that imply there is a high potential for acid sulphate soils.

These naturally occurring soils are commonly found in coastal and near-coastal sediments (Dear et al., 2014) that were inundated during the last interglacial period when sea levels were high (about 10,000 years ago). The sulphides prevalent in acid sulphate soil landscapes are formed in waterlogged soils and sediments by bacteria which reduce the naturally occurring sulphate in

water to form sulphides. This occurs in anaerobic aquatic environments and most frequently in warm, calm, marine environments which are high in organic matter (Macdonald, et al., 2002). Typical examples are shown in Figure 1. These conditions predominantly occur in areas similar to wave-protected mangroves, saltmarshes, outer barrier tidal lakes, and backswamps. The sulphides produced by the reducing bacteria form insoluble fine grained metal sulphides (commonly pyrite) that precipitate out of solution.

Figure 1: Examples of potential acid sulphate soils

Acid sulphate soils are stable while they remain in a waterlogged state as this limits oxidation. When exposed to oxygen the sulphides become unstable and oxidise, producing sulphuric acid and mobile metal ions.

Exposure of acid sulphate soils to oxygen commonly occurs when the watertable is lowered, or when the soil is disturbed by excavation. The aeration and ripening of these soils can be significantly enhanced through extensive artificial drainage of landscapes containing acid sulphate soil (Dent, 1986).

1.2 Significance of acid sulphate soils

Acid generation from the oxidation of iron sulphides can result in the change of soil pH to less than 4 (Wilson, 1995). Very low pH conditions can have deleterious effects on flora and fauna (Sammut et al., 1993). An example of such effects is the oxidation of pyritic sediments in Gwelup, Western Australia, which led to adverse effects on the ecology due to acidification and arsenic enrichment of the groundwater. These changes in groundwater chemistry can persist in the long-term and can lead to the water becoming unsuitable for use or consumption (Appleyard et al, 2006). The Richmond River in New South Wales, Australia has experienced numerous leaching events of acidified water enriched with metals being discharged from acid sulphate soils. These discharges have been linked to major fish kills and can also lead to sub-lethal effects, such as red spot disease in fish (Corfield, 2000).

The sulphuric acid generated by the oxidation of pyritic minerals is highly corrosive and can cause corrosion of concrete structures. Acid attacks concrete by dissolving both hydrated and unhydrated cement compounds as well as calcareous aggregates, evidenced by the loss of cement paste and aggregate from the matrix. If the steel in reinforced concrete becomes exposed to the acidic conditions, rust staining, cracking and spalling may also occur. The cement can decalcify, expand and crack, which can weaken the overall integrity of the concrete structures, in particular, structural foundations, bridge abutments, pipes, pavements and other concrete elements that are in contact with acidic soil and/or groundwater. This risk is of particular relevance to infrastructure that is designed to have a long life expectancy.

In 2014 Whangarei District Council identified problems with buried pipe work in a development in Ruakaka as concrete within the storm water system had begun to suffer chemical corrosion. Investigations into the cause of the corrosion identified the presence of acid sulphate soils. Extensive earthworks and lowering of the water table occurred during development. The continual draining of the site through subsoil drains caused sulphides in the soils to react with oxygen and release sulphuric acid. The acid then corroded the concrete pipes (Whangarei District Council, 2017). The local press have reported that this has resulted in a claim by Whangarei District Council in the order of $8 million against the designer and contractor (NZ Herald, 2016).

Although oxidation of iron sulphides may occur within a localised area, affected water may impact the surrounding areas some distance away from the original site. Acids and metals mobilised in soil leachate are usually transported episodically in concentrated slugs, usually after high rainfall events. As a result, leachate that is normally within acceptable limits may exceed these limits under episodic release conditions.

There is little awareness of acid sulphate soils in New Zealand, potentially because the infrastructure is relatively modern and the effects of acid sulphate soils have not been observed, and because development is only now being forced into lower quality land. Limited research has been done into the extent and implications of acid sulphate soils in New Zealand. Key pieces of research include the assessments of acid sulphate soils occurrence in Auckland and other northern parts of New Zealand in the 1970s and 1980s (Dent, 1980, 1986 and Metson et al, 1977).

The lack of readily available information about the potential distribution of acid sulphate soils makes it challenging for New Zealand regulators, infrastructure owners and designers to take these potentially damaging conditions into account in a consistent and effective way.

2 OBJECTIVES

A joint study was undertaken in 2016 by GHD and Auckland Council to provide information on the likelihood of acid sulphate soils occurring in the Auckland region to inform planners and developers of the potential risks.

3 METHODOLOGY

A desktop mapping exercise was undertaken using multi-criteria analysis to identify areas of the Auckland region that represent the greatest risk in terms of acid sulphate soils occurrence.

The desktop spatial assessment process began with the identification of the inputs (such as geology or soil maps) which inform the acid sulphate soils probability of occurrence. Based on a review of local and international literature these inputs were then divided into classes (such as geological units or soil types). Each class was given a rating of high, medium, low, or negligible based upon the probability of acid sulphate soil occurrence within that particular class based on a literature review.

A ground truthing exercise was then undertaken to validate and adjust the ratings identified in the desk study. This was targeted at key geological inputs, as described later. Finally, the ratings were overlain in GIS to produce a map of the results (Figure 2).

3.1 Map inputs

A summary of map inputs is provided here. For full details please refer to the Auckland Council Technical Report 2017/001 (currently in publication and due out later in 2017). An explanation of the function of primary and secondary inputs is provided in Section 3.3.

Primary Input	**Rationale and source**
Geology	Should give a reliable indicator of soil type. The published geological units adopted were assessed on considerations including the environment in which they were formed (e.g. marine or sulphur rich sediments, presence and type of organics) and laboratory results obtained during the ground truthing assessment. Swamp deposits and peat bogs were given a high rating, and alluvial/colluvial deposits were given a medium rating. See the Auckland Council Technical Report for the full list. (Source: GNS QMap)
Elevation	Provides an excellent indication of areas likely to contain marine and sulphur rich sediments, higher watertables, swamp environments and peat environments at low elevations which are all associated with acid sulphate soils. The elevation classes adopted were based on likely historical sea level taking into account geological uplift. (Source: Auckland Council LiDAR based Digital Elevation Model)
Wetlands	Can provide an environment in which acid sulphate soils may form and persist. (Source: Auckland Council GIS. This was adopted from the two layers available which were created by Auckland Council and the Department of Conservation)
Landcover	Vegetation provides an indication of soil types and conditions due to the characteristic tolerances or preferences of certain species such as mangrove, rush, and coastal shrubs. (Source: Landcare Research New Zealand)
Auckland Council generalised soil types	Gives an approximate indication of soil types including those that could indicate a present or historic environment in which acid sulphate soils could have been produced and persisted. The alluvial soils layer was deemed to add some value to the soil classification input. (Source: Auckland Council GIS)
Secondary Input	**Rationale and source**
Fundamental soil layers New Zealand soil classification	Soil classification was adopted as it provides an indication of soil types (such as those affiliated with marine sediments) the soil chemical properties such as acidity, sulphur content and anaerobic conditions. (Source: Landcare Research New Zealand)
Fundamental soil layers New Zealand pH	A measure of acidity and alkalinity and therefore can help inform where acid sulphate soils may occur. (Source: Landcare Research New Zealand)

3.2 Ground truthing

Ground truthing involved the collection of samples from each input class (such as geological units or soil types) to provide quantitative data to validate the ratings which are given to each input class during the desktop assessment. This is intended to reduce the level of conservatism adopted

during the desktop assessment and multi-criteria analysis, and to produce results which are more representative of field conditions.

This ground truthing assessment involved a targeted intrusive investigation across the Auckland region to validate key geological inputs. Locations for investigation were selected to provide a representative geographical distribution across the areas of the Auckland region identified as containing swamp deposits and peat bogs, alluvial/colluvial deposits, or beach deposits.

Soil samples were collected from three depths at each location (at target depths of 0.5 m, 1.0 m and 2.0 m below ground level), with two selected for field pH testing (90 samples in total) and one sample for full Suspended Peroxide Oxidation Combined Acidity and Sulphur (SPOCAS) analysis (45 samples in total) in accordance with ISO 14388-3:2014.

The pH results showed that nine of the 90 samples were highly acidic soils (pH <5). Two samples are considered to be Actual Acid Sulphate Soils because the pH was less than 4.

The SPOCAS analysis suggested that there is a high potential for acid generation in many of the sediments sampled. In 29 of the 45 samples analysed, the Titratable Peroxide Acidity (TPA) results were above the action criteria of 18 mol H^+ / t, with the highest TPA reported being 4,080 mol H^+ / t.

The three geological classes that were checked (swamp deposits and peat bogs, alluvial/colluvial deposits, and beach deposits) showed diverse responses to laboratory testing and were easily distinguished into three unique risk ratings based upon the results.

The swamp deposits and peat bogs geological input consistently returned high potential acid sulphate soils laboratory results. The desktop likelihood rating of high probability of acid sulphate soils occurring in these areas was retained.

The alluvial/colluvial deposits were the most extensive and geographically diverse of the geological inputs tested. This input also had the greatest variation in laboratory results with acid generation results at both the very high and very low ends of the spectrum. The high results were often associated with areas where other inputs were overlapping with the geological input. For example, many of the high acid generating samples were taken from areas where the geology input layer also intersected areas of low pH, high risk soil, wetland, or areas of low elevation. This complexity reflects that the geological classification was not the sole input contributing to the potential for acid generation in these areas. The presence of peat in this layer consistently returned high potential acid sulphate soil laboratory results and should be seen as an indicator for acid sulphate soils within this input. The result is that the alluvial/colluvial layer remained a medium risk. This is because even though high acid generation results were sometimes associated with this unit, these high risk areas were captured by other inputs and to classify the entirely of the input as high would not be representative of the other conditions observed. It should be noted that when the alluvial/colluvial layer is in the vicinity of another high or medium risk input, the likelihood of having acid sulphate soils appears to be greatly increased.

The ground truthing of the beach deposits input predominantly yielded a low to negligible risk of acid sulphate soil. However, some results showed the potential for acid generation at low to medium levels. Due to this variability and the majority of the results being of low risk, the decision was made to retain the beach deposits input class at a low probability of acid sulphate soils.

3.3 Rating calculation

The rating for each location was based on the highest primary input rating. This approach meant that an area with one high probability class (e.g., the presence of mangroves) and six low probability classes would be mapped as a high probability of occurrence. The decision to adopt

this approach was based upon the fact that one high probability of occurrence rating was considered to be more of concern than a large number of medium probabilities of occurrence.

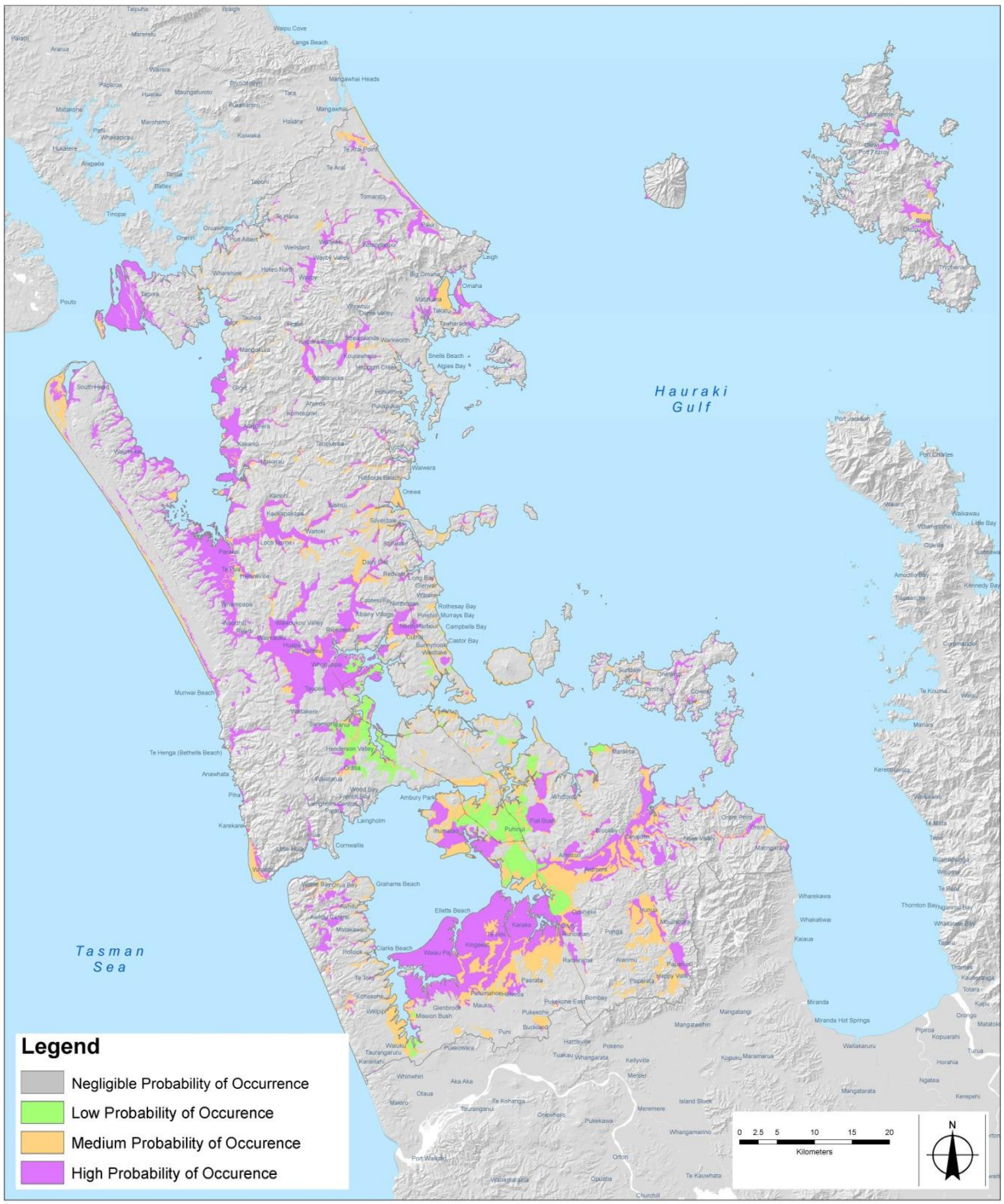

Figure 2: Preliminary map of the potential for acid sulphate soils in the Auckland Region

Where the secondary input rating was higher than the primary input rating, this rating was applied only in areas where the primary input rating suggested there was greater than negligible probability of occurrence. A site with a high probability rating in a secondary input would only show as high on the map in areas where one of the primary inputs also showed a probability of occurrence higher than negligible. This approach prevented sites being identified as having

potential for acid sulphate soils when the less reliable secondary factors were the only factors indicating a potential problem.

4 LIMITATIONS

The geology ground truthing assessment established that the desktop study weighting applied to the three geological classes appears to be reasonable. It does, however, raise questions around the approach for mapping the potential acid sulphate soil risk when multiple controlling factors are overlapping one another.

Limitations associated with the accuracy of the desktop study inputs were discovered on multiple occasions during the geology ground truthing investigations. These ranged from the incorrect mapping of areas to the lack of historic wetlands information and region-wide geomorphological maps. The effects of these limitations were diverse, with the lack of historic wetland extent data being an issue that may be most important. Current and historic wetlands appeared to be consistently associated with high potential of acid sulphate soil occurrence; however, due to the lack of data, these assumptions were based on field observations and aerial imagery.

While ground truthing has been carried out on three of the geology classes, results from this intrusive investigation are likely to be influenced by other controlling factors in some locations. These factors, such as unidentified historic wetlands or geomorphology, may either have not been captured in the adopted inputs or the inputs may not have been sufficiently accurate.

No assessment has been made of the potential for soils of volcanic origin to generate acid. It is assumed that the sub-aerial nature of our volcanics, combined with their non-acidic parent geology, would result in a low risk of acid generation.

This assessment considers the risk of there being acid sulphate soils present but does not consider whether those acid sulphate soils are problematic or not. For example, if the rate of reaction of slow, or the site conditions are right, then there may not be significant detrimental effects.

5 CONCLUSIONS

The acid sulphate soils probability map provides an indication of the relative likelihood of occurrence in the Auckland region. It will assist planners and developers in taking acid sulphate soils into consideration when assessing land capacity for development.

Ground truthing has been conducted on three classes (swamp deposits and peat bogs, alluvial/colluvial deposits, and beach deposits) within the geology input. Only two samples were found to be Actual Acid Sulphate Soils (pH is less than 4.0). However, a large number of the locations assessed were identified as Potential Acid Sulphate Soils with a very high potential for acid generation if disturbed or if groundwater levels fall.

The map produced by this study is based on a desktop study and limited ground truthing, and is therefore only appropriate for use as high level guidance. It intended to be updated as new field data becomes available. The authors request that test results (particularly Field pH, Chromium Reducible Sulphur and SPOCAS) are uploaded to the NZ Geotechnical Database and sent to ross.roberts@aucklandcouncil.govt.nz to be incorporated in future revisions of the map.

As a result of the variable quality of the input parameters a very simple approach to assessing the likelihood of occurrence was used. It is hoped that as more laboratory data becomes available, and better information sources are produced (including the GNS Urban Mapping Project), that a

more rigorous statistical correlation can be developed that will significantly improve the quality of the assessment presented in this paper.

REFERENCES

Appleyard, S. J., Angeloni, J., & Watkins, R. (2006) Arsenic-rich groundwater in an urban area experiencing drought and increasing population density, Perth, Australia. *Applied Geochemistry* 21, 83-97.

Corfield, J. (2000) The effects of acid sulphate run-off on a subtidal estuarine macrobenthic community in the Richmond River, NSW, Australia. *ICES Journal of Marine Science:* Journal du Conseil, 57 (5), 1517-1523.

Dear, S-E, Ahern, C. R., O'Brien, L. E., McElnea, A. E., Dobos, S. K., Moore, N. G. and Watling, K. M. (2014) *Queensland Acid Sulfate Soil Technical Manual: Soil Management Guideline*. Brisbane: Department of Science, Information Technology, Innovation, and the Arts, Queensland Government

Dent, D. (1980) Acid sulphate soils: Morphology and prediction. *Journal of Soil Science*, 87-99.

Dent, D. (1986) *Acid sulphate soils: A baseline for research and development*. International Institute for Land Reclamation and Improvement ILRI, Wageningen, The Netherlands.

Macdonald, B., Smith, J., Melville, M., & White, I. (2002) *Acid sulfate soil research in Australia*. Beijing: Science Press.

Metson, A. J., Janica, G. E., Cox, J. E., & Gibbs, D. B. (1977) The problem of acid sulphate soils with examples from north Auckland, New Zealand. *New Zealand Journal of Science* (20), 371-394.

NZ Herald, (2016) $1.3m to replace manholes: Ratepayers to foot bill. http://www.nzherald.co.nz/northern-advocate/news/article.cfm?c_id=1503450&objectid=11622279. Retrieved June 2017.

Sammut, J., White, I., & Melville, M. (1996) Acidification of an estuarine tributary in eastern Australia due to the drainage of acid sulfate soils. *Marine Freshwater Research*, 669-684.

Whangarei District Council, 2017. Building information > Property Information > Acid Sulphate Soil. http://www.wdc.govt.nz/BuildingandProperty/Property-Information/Pages/Acid-Sulphate-Soil.aspx. Retrieved June 2017.

Wilson, B. (1995) *Soil and hydrological relations to drainage from sugarcane of acid sulfate soils*. Australia: University of New South Wales.

A ground investigation specification for New Zealand

R C Roberts
Auckland Council, Auckland, NZ
ross.c.roberts@gmail.com (Corresponding author)

T Fairclough
Tonkin + Taylor, Christchurch, NZ
TFairclough@tonkintaylor.co.nz

S Hargraves
Terra Firma Engineering, Nelson, NZ
sally@tfel.co.nz

G Cassidy
ENGEO, Wellington, NZ
GCassidy@Engeo.co.nz

H Wahab
Beca Ltd, Tauranga, NZ
Harry.Wahab@beca.com

M Stannard
Ministry of Business Innovation and Employment, Wellington, NZ
Mike.Stannard@mbie.govt.nz

Keywords: ground investigation, specification, procurement

ABSTRACT

Until 2017 there was no standard template in New Zealand to assist in the specification and procurement of ground investigations, and so consequently specifications varied significantly from project to project and between organisations. This caused numerous problems: (1) Long project specific specifications were unlikely to be fully read by tenderers (at least within the tender period) while short specifications were unlikely to capture all the appropriate details. (2) Time was wasted writing a fresh specification for each project, adding to costs. (3) There was inconsistent pricing within and between tenders due to the lack of clarity on scope. (4) Inconsistent or unread specifications resulted in confusion about the scope of work, including expectations and practices about the quality standards required, leading to unexpected variations or rework on site.

This paper describes the development of a New Zealand standard specification template. This specification is the fruit of a collaborative process involving major clients, large and small consultants, and ground investigation contractors. It is a free to use, ready-to-go pack of documents which is suitable for small, medium and large projects of any complexity. It is designed to be easy to use, to simplify the procurement process, and to be customisable to suit the specific requirements for more complex projects.

This paper describes how the use of this specification and advice will benefit all parties.

1 THE NEED FOR A STANDARD SPECIFICATION AND GUIDANCE

Until 2017 there was no standard template in New Zealand for the specification and procurement of ground investigation work, so specifications varied significantly from project to project and between organisations. This variation meant that:

- Long specifications were unlikely to be fully read and understood by tenderers (at least within the tender period)
- Short specifications were unlikely to capture all the appropriate details.

This has resulted in a number of problems:

(1) Time was wasted writing a fresh specification for each project, adding to costs.
(2) There was inconsistent pricing within and between tenders due to the lack of clarity on scope
(3) There was confusion about the scope of work, including expectations and practices about the quality standards required, leading to variations or rework on site.

A standard specification, such as the one commonly used in the UK (AGS, 2012) can resolve many of these issues. Procurement of ground investigations should become quicker and more consistent. Once widely used the contents become familiar to all parties, giving a shared understanding of the project scope without the need for lengthy and detailed study of the specification. By setting a realistic benchmark for quality, clients can be confident that – with appropriate supervision – they are getting what they expect, and tenderers can be confident that they will not have to cut corners to have a chance of winning tenders.

2 THE NEED FOR PROCUREMENT GUIDANCE

Client organisations often report difficulty in procuring geotechnical services. Problems are perceived within the investigation process around large cost variations as the ground investigation proceeds, frequently associated with the difficulty of specifying ground investigation requirements. Later in the design and construction phase, problems are common when unforeseen ground conditions lead to construction cost over-runs which are often attributed to failings in the ground investigation.

2.1 Under-scoped ground investigations

Unforeseen ground conditions often have a significant impact on the success of construction projects. The extent of unforeseen conditions and the resultant capital cost increases are commonly linked to an under investment in ground investigation. International research shows a strong correlation exists between low spend on ground investigation and high capital cost over-runs (Figure 1).

Figure 1. Impact of ground investigation expenditure on UK highways contract cost over-runs (Mott MacDonald and Soil Mechanics, 1994)

This under investment occurs for a number of reasons including:

- Clients are awarding tenders for geotechnical services on lowest price conforming, not best value.
- Site investigation scope is being constrained by inappropriate procurement methods.

Clients also systematically over-estimate the amount they actually spend on ground investigation. Some examples of actual ground investigation costs from the UK are presented in Table 1, along with information based on surveys asking how much the client believed they spent. It is worth noting that all parties spent significantly less on ground investigations than they assumed.

The numbers presented in the table are not intended as a guide to the appropriate spend on future projects as they are based on historical spends regardless of outcome. Many of these projects are to likely have gone over-budget as a result of unforeseen ground conditions.

Table 1: Funding of site investigation as a percentage of total project costs (adapted from ICE, Inadequate Site Investigation, Table 2, 1991)

Consumer	**Amount consumer believed they spent on Ground Investigation (% CAPEX)**	**Amount consumer actually spent on Ground Investigation as calculated by researchers (% CAPEX)**
Government authorities	2.20	**0.29**
Manufacturing / commerce	0.76	**0.22**
Civil engineering contractors	0.85	**0.23**
Developers / builders	0.72	**0.11**
Architects	0.29	**0.14**
Multidisciplinary consultants	0.92	**0.23**
Civil engineers	1.94	**0.29**
Structural engineers	0.23	**0.16**
Average	0.99	**0.21**

While a specification cannot resolve problems with under-scoped ground investigations, guidance documents associated with technical specifications can be used to set improved benchmarks and raise awareness of the potential pitfalls and problems.

2.2 Ground investigation procurement and management challenges

2.2.1 Pre-determined scopes of work

In an attempt to create a fair and comparable tendering process for ground investigation work it has become common in New Zealand to provide a pre-determined scope of investigation to be priced.

Although the aim of this approach to provide comparable tenders is laudable, it often fails in practice. Tenderers are aware that they are being engaged as technical experts to re-scope the investigation as they judge necessary and that therefore they can (and should) change the scope to meet the actual project needs. It then becomes a simple process to work out what the 'minimum acceptable' scope for the investigation might be. By under-pricing aspects of the tender that they expect to later remove from the scope they can submit a lower price and increase their chances of winning. The client's desire for a fair tender process has been subverted. In addition, such a reduced scope is unlikely to optimally manage the client's risk and will result in more conservative design assumptions and therefore expensive construction. The client will get a lower cost investigation but a higher overall project cost and greater risk of variations during construction.

By partially locking consultants in to a pre-determined scope this approach also significantly limits the opportunities for the application of in-depth local knowledge, innovation and risk-sharing.

2.2.2 Tendering on price

It is standard practice to include price as a scoring attribute when tendering ground investigation work, with weightings commonly between 40% and 100% of the total criteria.

A ground investigation serves two primary purposes:

(1) Providing data for analysis and design
(2) Reducing uncertainty about ground conditions to reduce construction cost variations (i.e. control of risk).

Procurement approaches which focus on the cost of the geotechnical investigation, risk pushing the scope of investigations down as part of the competitive tender. Such 'minimum scope' investigations might achieve the first goal of a site investigation (to provide information for design) but are unlikely to meet the second goal (reducing project risk) and are therefore likely to lead to significant increases in construction cost.

3 DEVELOPMENT OF THE NEW ZEALAND GROUND INVESTIGATION SPECIFICATION

As a result of the problems described above the need for a standard specification with supporting procurement guidance was identified.

3.1 Governance

A Governance Group was set up to oversee the project. This group was tasked with providing leadership and governance oversight to the working group, agreeing the scope of the guidance/specification, and coordinating reviews on behalf of their respective organisations.

A Working Group was established to prepare the guidance in line with best practice under the oversight of the Governance Group. The membership for both groups is presented in Table 2.

Table 2: Governance and Working Group Membership

Governance Group	
Name	**Representing**
Sarah Sinclair	Auckland Council
Mike Stannard	MBIE
Stuart Finlan	NZ Transport Agency
Chris Beasley	Auckland Transport
Tony Fairclough	EQC & NZGS
Jean de Villiers	Watercare
Steve Faulkner	NZ Drillers Federation
Marco Holtrigter	CETANZ CPT
Ross Roberts	Auckland Council

Working Group	
Name	**Representing**
Ross Roberts	Auckland Council
Harry Wahab (Beca)	MBIE
Gilles Seve	MBIE
Stuart Finlan	NZ Transport Agency
Sally Hargraves	TerraFirma Engineering
Guy Cassidy	ENGEO Limited
Tony Fairclough	Tonkin & Taylor
Stephen Grace	Watercare
Steve Faulkner	NZ Drillers Federation
Marco Holtrigter	CETANZ CPT

The membership of these groups was designed to bring in a broad range of skills, and to include representation from key clients, large and small consultancies, and contractors. In addition to these core members, specialist input was sought as needed from technical experts.

3.2 Aims of the specification

The Governance Group set the key desired outcomes of the specification and associated guidance documents as:

a) Consistent, transparent and repeatable site investigation tendering by client organisations (limited to the technical aspects and excluding contractual and tendering terms) that is accepted by the building and infrastructure industries as a de facto standard.
b) Consistency of pricing by site investigation suppliers.
c) A clear understanding of the quality standards expected in ground investigation works by suppliers of ground investigation services. These quality standards align with best international practice.
d) The collection of ground investigation data in a format that can easily be stored in an electronic database.
e) A clear understanding of the required minimum standards for health and safety practices associated with the ground investigation works.
f) A document that can easily be up or down scaled depending on the nature and complexity of the project and the level of information required or contractors that need to be engaged.
g) Alignment with the MBIE/NZGS Module 2.
h) A bill of quantities with basis of payment and methods of measurement.

Activities considered out of scope were:

a) Site investigation activities beyond collection and collation of factual data (eg geotechnical interpretation, desk studies, design)

b) Specialist activities which are not conducive to a standardised approach or which are developing quickly so would be prevented from future improvements by a standardised specification (e.g. geological mapping, some geophysical methods).

3.3 Reviews and industry consultation

After internal reviews within the organisations represented in the Governance Group, a draft specification was released on the NZGS website for industry review in April 2016. Feedback was received over the six month consultation period from 26 individuals and 9 companies (Worksafe NZ, Tonkin & Taylor, Opus, DataTran, Beca, Perry Geotech, ENGEO and NZ Transport Agency). This feedback was incorporated into a new revision of the specification, which was issued in final status as Revision 0 in April 2017.

It is anticipated that as the document is used in practice, further revisions will be required. To streamline the collection of this feedback an online survey has been set up to allow easy tracking and compilation of feedback from multiple sources.

4 STRUCTURE OF THE SPECIFICATION

The specification comprises four compatible volumes that, when used together, are intended to enable an appropriate quality of ground investigation and a simpler, clearer and more consistent tendering process. Of these only Volume 1 would be used on all projects.

4.1 Volume 0: Commentary, introduction and guidance

This volume provides general advice regarding the correct application and intended use of the specification and the procurement of geotechnical services. It does not form part of the specification, although the specification is intended to be read in conjunction with this document.

It also provides (as appendices) a set of standard templates and guidance which may be useful in improving the consistency of ground investigation practice but do not form a part of the specification. These templates include:

- Standpipe piezometer installation instruction sheets / as-built records
- CPT data records
- Permit to dig

Each of these templates is considered appropriate for use on many projects, but will be superseded by project or client specific versions. This allows the consultants involved to use their own preferred templates where they already exist or where they are more appropriate for the project and site requirements.

4.2 Volume 1: Master specification

The master specification comprises a series of unambiguously worded clauses which are intended as minimum requirements to meet current standards and comply with established good practice. These minimum requirements have been set for the geotechnical investigation techniques which are most commonly used in New Zealand. It is implicit that only the sections relevant to the specific investigation being undertaken are applied to a particular project.

The specification is fixed in content and scope. Project specific requirements, including identification of which sections of the specification are relevant to that project, are defined in Volume 2 (the project specific requirements). This way the specification can be scaled to suit a range of project sizes.

4.3 Volume 2: Project Specific Requirements

The project specific requirements document is a template in MS Word format designed to be completed by the client and geotechnical professional to give details on which aspects of the specification will apply to the project, and any changes to the standard wording. Clients may choose to create their own versions of this document to suit their specific procurement and technical requirements.

4.4 Volume 3: Bill of Quantities

An example Bill of Quantities, together with a preamble which defines payment terms, is provided in spreadsheet format for ease of use. This is designed to be compatible with the specification and allow easy management of a ground investigation by defining consistent payment and measurement methods. It is also the preferred tool to clearly define the scope of work to the consultant or contractor. Some parties may choose to use the specification alone with their own alternative method of measurement.

5 CONCLUSIONS

The New Zealand Ground Investigation Specification provides an easy-to-use set of minimum requirements to meet current standards and comply with established good practice for commonly used ground investigation practices in New Zealand in a cost effective and consistent manner.

It also advises on best practice guidance for procuring good-quality site investigation and streamlines the procurement and investigation management to improve the efficiency of ground investigations.

It is based around good practice with New Zealand specific content to suit our specific requirements and expectations. It has been endorsed by the New Zealand Geotechnical Society, the New Zealand Drillers Federation, EQC, the NZ Transport Agency, the Ministry for Business Innovation and Employment, Auckland Council, Auckland Transport and Watercare.

6 ACKNOWLEDGEMENTS

The authors would like to thank the sponsors of this project (Auckland Council, MBIE, Auckland Transport and EQC). We would also like to express our gratitude to all the technical experts who generously gave their time and expertise, and the many individuals who gave valuable and detailed feedback during the consultation:

Paul Burton, Tom Grace, Ian Haycock, Carole Lee, Jane Sherrard, Sam Woodford, Shane Strode-Penny, Kevin Hind, Eleni Gkeli, Darrel Oosterberg, Christine Parkes, Dave Dennison, Steve Cooke, Doug Mason, Ella Boam, Jon English, Helen Davies, Robert Bond, Ken Read, Roger High, Lisa Bond, Reagan Knapp, Brian Tracey, Ross Paterson, Phillip Falconer, Paul Carter, Greg Haldane, Ann Neill, Martin Gribble, John Donbavand, Illya Kautai and Andrew Spittal.

None of this would have been possible without your support.

REFERENCES

AGS, (2012) *UK Specification for Ground Investigation.* Second edition. ICE Publishing, London.

Institution of Civil Engineers, (1991) *Inadequate site investigation; a report on inadequate site and ground investigations leading to construction delays and additional costs*. Thomas Telford Publishing, London.

MBIE, (2016) *Practice Advisory 17: Well planned ground investigations can save costs*. 30 June 2016. ISBN: 978-0-947497-63-7. https://www.building.govt.nz/building-code-compliance/b-stability/b1-structure/practice-advisory-17/

Mott MacDonald and Soil Mechanics, (1994) *Study of the Efficiency of Site Investigation Practices*. Transport Research Laboratory, Workingham, TRRL Project Report 60.

Volcanic hazard from the Auckland Volcanic Field

G S Leonard
GNS Science
g.leonard@gns.cri.nz

R C Roberts
Auckland Council
ross.c.roberts@gmail.com (Corresponding author)

Keywords: Auckland Volcanic Field, volcanic hazard, eruption rates

ABSTRACT

The Auckland Volcanic Field, which last erupted ~600 years ago, is a late Quaternary monogenetic basaltic volcanic field of approximately 500 km^2. A recent study (Leonard et al., 2017) has improved the accuracy of eruption dates for 23 of the eruptive centres. Previously only 12 of the 53 had been reliably dated. This new data illustrates a complex episodic eruption history with large variations in the eruption volumes and changes in the rate of eruptions over time. Such non-uniformity shows that averaging the number of eruptions over the lifespan of the field to give a mean eruption rate is overly simplistic. In particular, the rate of volcanism in the Auckland Volcanic Field has increased since 60 ka, suggesting that the field is still in its infancy.

This paper summarises the findings of this research and considers the implications for the future development of Auckland.

1 INTRODUCTION

Auckland is the largest city in New Zealand. Recent strong population growth is expected to continue, and according to the 2006 Census projections the population will reach 1.93 million by 2031, a 25% increase over current numbers (Statistics New Zealand, 2012).

As a result of its location and geological setting Auckland is exposed to a number of natural hazards including volcanic eruption. As the population grows the exposure to these natural hazards will increase. A priority within the Auckland Plan is to 'build resilience to natural hazards'. Understanding the likelihood of future eruptions is critical to accurately assessing these risks and building resilience.

1.1 The Auckland Volcanic Field

Auckland lies on an active basaltic volcanic field that contains at least 50 volcanoes (the exact number depends on the definition of 'volcano'). It sits on continental crust approximately 400 km west of the Hikurangi trench, where the Pacific Plate is being actively subducted below the Australian Plate, and approximately 200 km west of the active volcanic arc.

Approximately 3 km^3 of material has been erupted periodically over the last 200,000 years, covering a total area of approximately 100 km^2. Most of the erupted material is olivine basalt, although there are significant deposits of associated material including scoria cones, ash and lapilli mantles, and tuff-ring deposits.

The Auckland Volcanic Field volcanoes are normally considered to be monogenetic (each volcano usually only erupts once with further eruptions occurring at a new location). There is

debate about whether the volcanoes are truly monogenetic because of evidence for multiple events of contrasting chemistry from essentially the same centre (particularly Rangitoto: Needham et al., 2011; Linnell et al., 2016). The field as a whole is not monogenetic as it comprises many volcanic centres.

To the south of the AVF are older basalt volcanic fields; in turn, the South Auckland Volcanic Field, active from 1.6 to 0.5 Ma (Briggs et al., 1994) and the Ngatutura and Alexandra fields, active from ca. 2.7-1.5 Ma (Briggs et al., 1989). The South Auckland Volcanic Field may represent a precursor field to the AVF, but there is a distinct 300 ka hiatus in eruption ages, and a > 10 km gap between the closest vents, implying that they represent separate volcanic fields (Le Corvec et al., 2013).

Based on a comparison of centre numbers, eruptive volume estimates, geochemical evolution, and age ranges between the AVF and the South Auckland Volcanic Field, Allen and Smith (1994) proposed that the AVF is likely still in its infancy.

2 AGE OF THE AUCKLAND VOLCANIC FIELD

Previous estimates of the earliest volcanic eruption in the Auckland Volcanic Field have been up to 250,000 years ago; the most recent volcanic eruption, which was witnessed by Māori living on Motutapu Island, occurred approximately 600 years ago and produced Rangitoto.

2.1 Challenges in dating the Auckland Volcanic Field

The AVF is typical of basaltic volcanic fields, with spatially scattered vents erupting infrequently and relatively small volumes of magma in single eruptions (Connor and Conway, 2000). Unlike in polygenetic volcanoes, the wide dispersal of vents within volcanic fields means that often there are limited overlapping field relationships amongst deposits on which to base chronostratigraphic frameworks (Leonard et al, 2017).

For basaltic fields like the AVF where stratigraphic successions are ambiguous and thus relative sequencing of eruptive histories are difficult, the ability to directly date young basalts by radiometric methods is essential. Accurate dating allows a chronostratigraphic framework to be developed, which underpins all aspects of hazard and frequency forecasting.

Young basaltic rocks are difficult to directly date radiometrically. Their lack of zircon precludes U-series or U-Pb dating, and their low radiogenic argon have often precluded reliable K-Ar or $^{40}Ar/^{39}Ar$ dating. Historically, many studies have used conventional K-Ar dating, but these ages can be inaccurate due to excess argon issues (e.g. McDougall et al., 1969). Improvements in $^{40}Ar/^{39}Ar$ analytical techniques, coupled with ultrasensitive rare-gas mass spectrometers, have surplanted the K-Ar method (e.g. Fleck et al., 2014).

Lindsay et al. (2011) reviewed previous age data for the AVF and assessed these for reliability and consistency, rating only eleven centres as reasonably reliably and accurately dated. The youngest centres are constrained by ^{14}C dating, but many of the older ages were at the limits of the technique when analysed, and are now considered anomalous.

2.2 New results for the Auckland Volcanic Field

A recent study (Leonard et al., 2017) has improved the accuracy of eruption dates for 23 of the eruptive centres. Fifteen of the 23 new analyses are younger than 60 ka, but the remaining eight older analyses are particularly important because most of these eruptive centres had no previous age control. In total nine of the 23 new centres analysed had no previous ages associated with them. The full age data is presented in Leonard et al., 2017, and summarised in Figure 1.

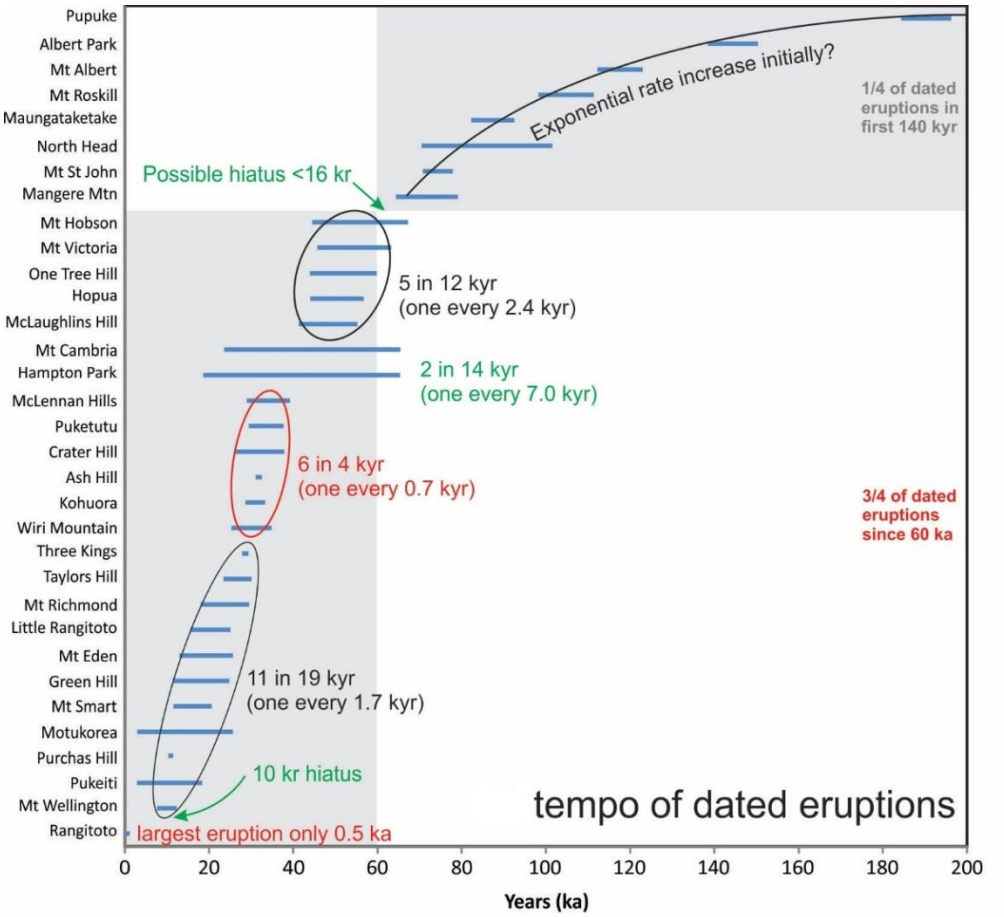

Figure 1: AVF volcanoes ordered in eruptive sequence by their ages, showing only volcanoes with radiometric dates, with annotation describing the complex tempo of post 60 ka eruptions (after Leonard, 2017)

3 IMPLICATIONS OF AGE DATA FOR BEHAVIOUR OF THE AVF

3.1 Frequency of eruptions

The gaps between eruptions (repose periods) have ranged from approximately 50 to 10,000 years. A simplistic approach of averaging the 53 volcanoes across the 193 ka history gives an average rate of one eruption every 3,600 years. Overall increases in eruptive frequency and volume over time have previously been proposed by Allen and Smith (1994) and Kerszturi et al. (2013), respectively. The new data (Leonard et al, 2017) show that at least 26 AVF centres have erupted since 60 ka, supporting the previous assumptions that there is a hinge point in AVF behaviour around that time. Different eruption frequency distributions can be suggested for the overall AVF depending on the ages adopted for the 20 volcanoes that remain undated. Two end-member approaches are presented in Figure 2, illustrating the range of possible eruption rates:

1. Approach 1: Assume a minimum eruption rate since 60 ka. In this approach all volcanoes with a documented maximum age from stratigraphy or geomorphology (see Lindsay et al., 2011) are assigned that age. Undated volcanoes are placed in the period prior to 60 ka. This yields an eruption rate of one per 2.6 kyr for the last 60 ka.

2. Approach 2: Assume a maximum eruption rate since 60 ka. In this approach all volcanoes with a documented minimum age from stratigraphy or geomorphology (Lindsay et al., 2011) are assigned that age. Undated volcanoes are placed within the last 60 ka. This yields an eruption rate of one per 1.5 kyr for the last 60 ka.

The real post-60 ka eruption tempo lies somewhere between these two end members (one per 2.6 - 1.5 kyr) but, regardless, has increased markedly compared to the rate prior to 60 ka (one per 13-5.2 kyr). Whether the increase in rate has been a gradual change or a sharp shift requires the remaining 20 undated volcanoes to be dated, coupled with more precise ages and absolute sequencing for those already dated.

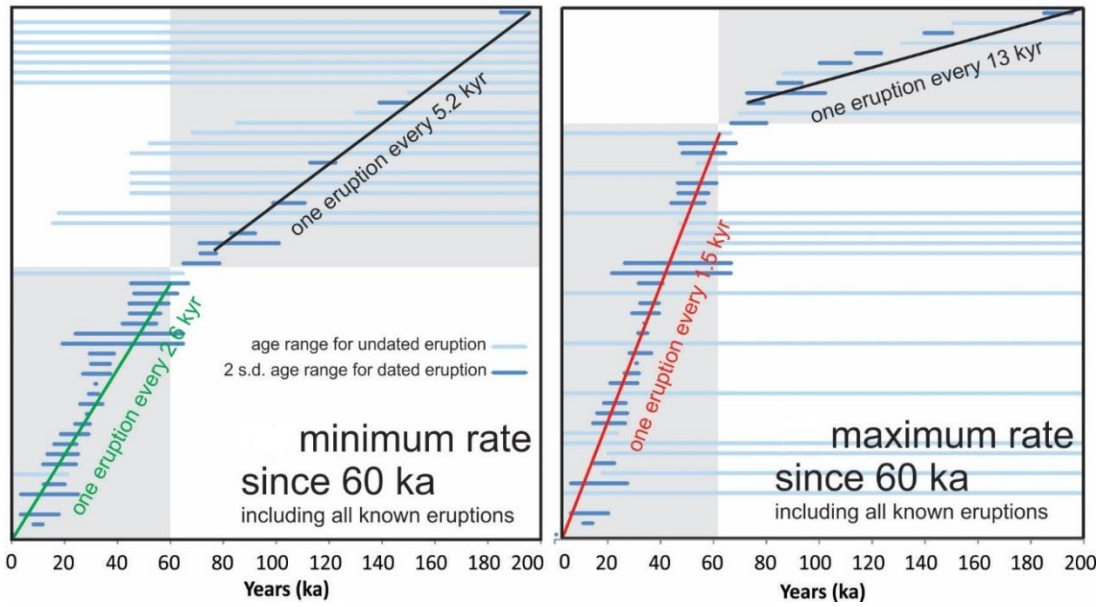

Figure 2: Volcanoes ordered in eruptive sequence by age, showing those with radiometric dates in bold (after Leonard, 2017). Radiometric ages depicted as 2SD error bars. LEFT: Approach 1 (minimum recent rate). RIGHT: Approach 2 (maximum recent rate).

3.2 Location of eruptions

The oldest five eruptions from the AVF show a spatial progression from north to south (Fig. 3) from 193 to 105 ka. After this period, the progression of ages appears to be random, but this may also reflect the fact that the age errors for the volcanoes overlap more in the younger $^{40}Ar/^{39}Ar$ data.

3.3 Volume and style of eruptions

The total Dense Rock Equivalent (DRE) volume for dated volcanoes is 1.5 km^3 (Kereszturi et al., 2013). This represents 96% of the total volume erupted in the AVF, so volume can be reckoned well from these dated centres. When plotted against dates there is no clear trend in eruption volume over time, but the five largest dated eruptions have occurred since 60 ka and the two largest eruptions (One Tree Hill, Rangitoto 2) have occurred following two long repose periods, as also noted by Kereszturi et al. (2013). However, another identified long repose period was followed by a relatively small volume eruption (Mt Hobson).

Most of the dated predominantly phreatomagmatic eruptions (producing little or no scoria cone or lava flow volume) have occurred post 60 ka. Only two eruptions so far have had volumes between 0.1 and 1 km^3 so forecasts of the largest size are limited by the number of events of this magnitude to extrapolate from. The magnitude-frequency relationship for the Auckland eruption sequence (Figure 4) shows variation over five orders of magnitude, but with the majority of the 53 eruptions between 0.001 and 0.03 km^3.

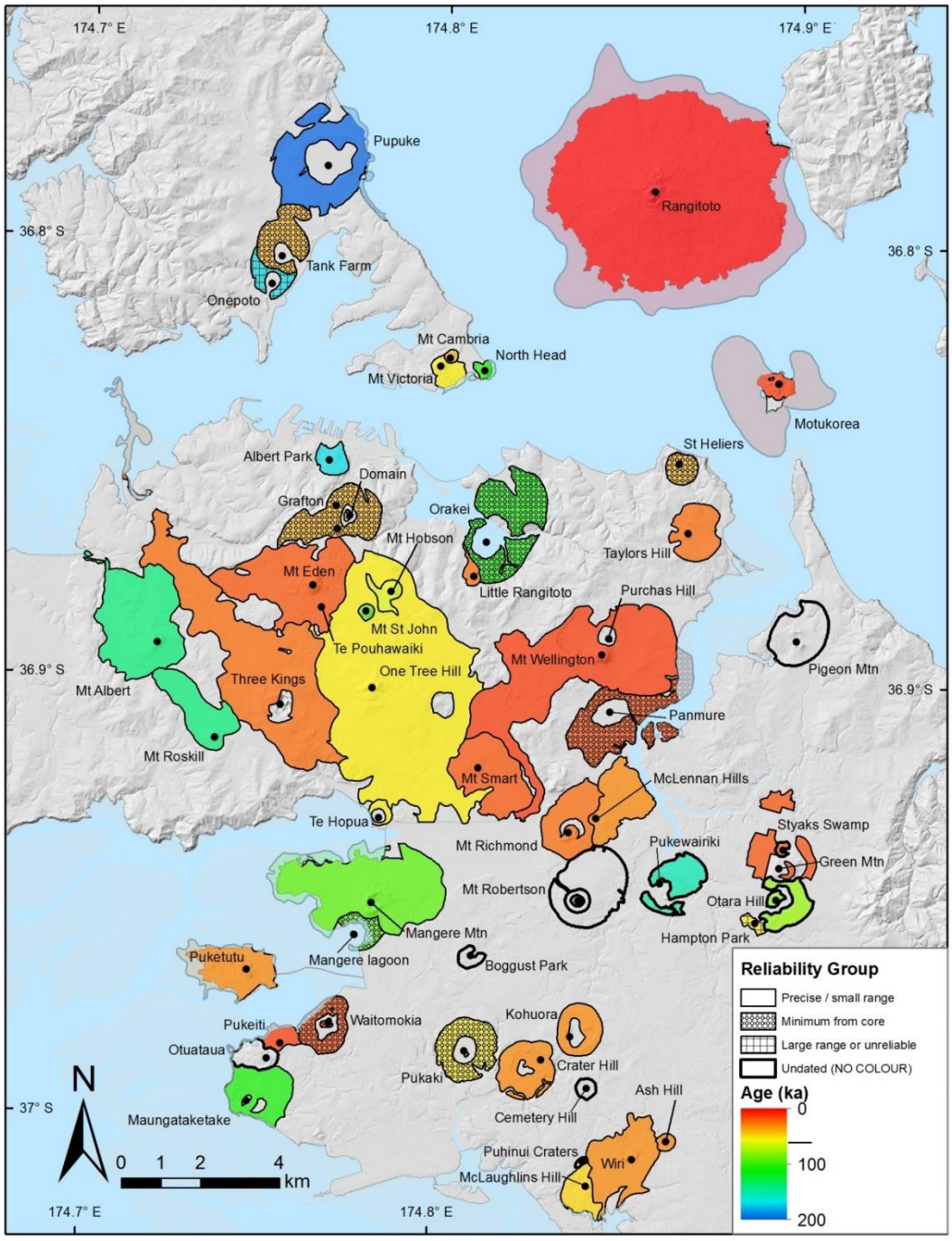

Figure 3: The volcanic deposits of the Auckland Volcanic Field centres, coloured by their interpreted ages. Hatching indicates grouped age reliability (after Leonard et al, 2017).

It should be noted that magmatic volume is not the most relevant hazard metric for phreatic eruptions, where the threat is posed by explosive but primarily non-magmatic fragments. However, it still may be of value in assessing the potential area of damage for loss estimation for scoria and lava.

4 THE RANGITOTO PARADOX

The most recent eruption in the AVF was unusual. It was much larger than any previous eruption (up to nearly four times larger than the next largest: Kereszturi et al., 2013) and it is one of only

two eruptions that exhibits a sub-alkaline basaltic geochemical signature, along with Pupuke, the oldest dated volcanic centre (Needham et al., 2011; McGee et al., 2013).

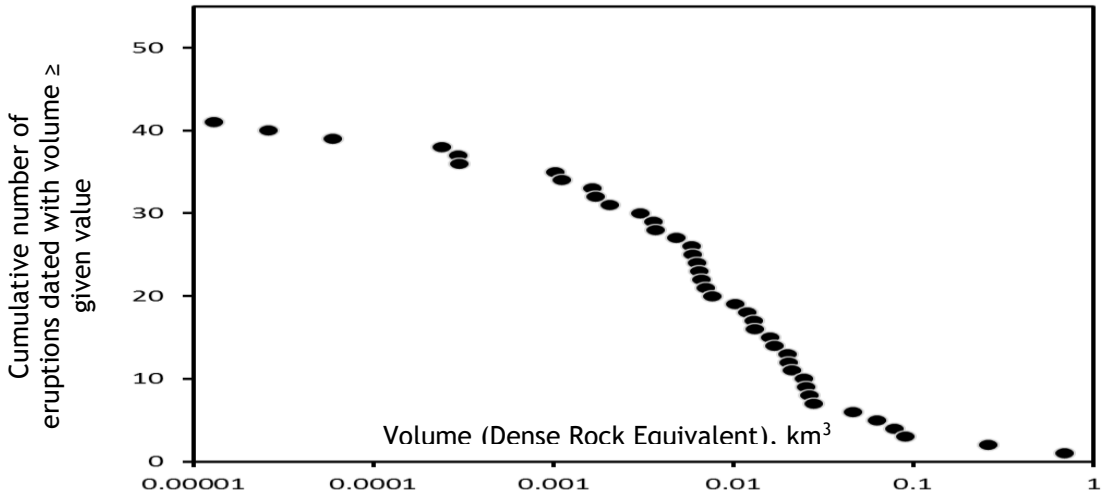

Figure 4: Magnitude-frequency plot for all radiometrically dated eruptions from the AVF (volumes from Kereszturi et al., 2013).

The combined Rangitoto episodes were preceded by one of the two longest repose periods in the AVF since 72 ka (Lindsay et al., 201 1; Needham et al., 2011). However, the other apparently long repose was followed by a relatively small volume eruption (Mt Hobson). There are other eruptives buried within Rangitoto that may be older than 600 years ago (Linnell et al., 2016) – research is ongoing. Spatially, the Rangitoto eruptions do not appear to follow any temporal trends within the wider field, highlighted by their proximity to the oldest centre (Pupuke).

5 REDUCING THE RISK

Although a future eruption in Auckland would be relatively small, its effects would be devastating to the economy of New Zealand (Lindsay, 2010). Hazard avoidance through land use planning is generally not feasible given the population size, and extent of economic and urban development (Becker et al, 2010). Most societal effort to mitigate the risk is put into contingency planning (e.g. evacuation). However, some of the risks can be reduced with careful planning and engineering. Lava flow susceptibility can be assessed (e.g. Kereszturi et al, 2012), and buried services within these zones kept at a depth that would limit damage to them as the flow passes over. Critical infrastructure diverted away from at-risk zones, or be designed to be bypassed or relocated. Buildings can be designed to resist loadings from volcanic ash, and to provide filtered air to reduce the impact of ash on the people inside.

6 CONCLUSIONS

Prior to Leonard et al. (2017), 12 volcanoes in the AVF were well dated. With the addition of 23 new ages this has been increased to 35 out of the 53 known volcanoes. This new data shows that since 60 ka the average rate of eruption has been between one every 1.5 and 2.6 kyr.

The use of a single frequency rate may be misleading for forecasting future events. Repose periods have ranged from ca. 50 to 10,000 years, volumes from ca. 0.001 km^3 to 0.7 km^3, and vent locations are distributed with no clear trend. There are thus no grounds on which the duration of the current repose period or the site of the next eruption can be forecast. The fact that the most recent eruption episode (ca. 600 years ago) was anomalous, i.e. included an eruption nearly four

times larger than any previous eruptions in the field, erupted magma of a different chemistry, and occurred after an unusual 10 ka hiatus, highlights the difficulty in forecasting.

Given these difficulties it is not currently realistic to reduce the risk to Auckland by changing the location of proposed development within the city. However, the new range of frequency rates and illustrations of clustering and pauses proposed by Leonard et al (2017) can provide a useful starting point for the assessment of relative risk when compared with other natural hazards. The long-term frequency of Auckland eruptions is probably similar to mega-tsunami, but less regular. However, the location of the next eruption is unknown within the field. This makes it very hard to land-use plan for eruptions, but it is very important to contingency plan for them. This includes considerations for emergency management, and design of infrastructure and urban growth to limit vulnerability and pinch points.

Geotechnical professionals are well placed to advise developers and infrastructure owners on the volcanic hazard in Auckland, and to propose engineering options to reduce the vulnerability of our society. The assessment of the likelihood of eruption presented in this paper can be used as a basis for building a business case to engineer more resilient infrastructure and buildings.

7 ACKNOWLEDGEMENTS

This work is based on research undertaken through the DEVORA project (Determining Volcanic Risk in Auckland) funded by the NZ Earthquake Commission, the Ministry of Business, Innovation and Employment, and Auckland Council.

REFERENCES

Allen, S.R., Smith, I.E.M., (1994) *Eruption styles and volcanic hazard in the Auckland Volcanic Field, New Zealand*. Geoscience Reports of Shizuoka University 20, 5-14.

Auckland Civil Defence and Emergency Management (2016) *Auckland Civil Defence and Emergency Management Group Plan 2016-2021*. http://www.aucklandcivildefence.org.nz/about-us/our-group-plan-2016-2021/

Becker, J.S., Saunders, W.S.A., Robertson, C.M., Leonard, G.S., Johnston, D.M., (2010) A synthesis of challenges and opportunities for reducing volcanic risk through land use planning in New Zealand. *Australasian Journal of Disaster and Trauma Studies* 2010-1. ISSN: 1174-4707

Briggs, R.M., Itaya, T., Lowe, D.J., Keane, A.J., (1989) Ages of the Pliocene-Pleistocene Alexandra and Ngatutura Volcanics, western North Island, New Zealand, and some geological implications. *New Zealand Journal of Geology and Geophysics* 32,417-427.

Briggs, R.M., Okada, T., Itaya, T., Shibuya, H., Smith, I.E.M., (1994) K-Ar ages, paleomagnetism, and geochemistry of the South Auckland volcanic field, North Island, New Zealand. *New Zealand Journal of Geology and Geophysics* 37, 143-153.

Cassata, W.S., Singer, B.S., Cassidy, J., (2008) Laschamp and Mono Lake geomagnetic excursions recorded in New Zealand. *Earth and Planetary Science Letters* 268, 76-88.

Connor, C.B., Conway, F.M., (2000) Basaltic volcanic fields. In: Sigurdsson, H. et al. (Eds)., *Encyclopedia of Volcanoes*. San Diego, Academic Press, pp. 331-343.

Fleck, R.J., Turrin, B.D., Sawyer, D.A., Warren, R.G., Champion, D.E., Hudson, M.R., Minor, S.A., (1996) Age and character of basaltic rocks of the Yucca Mountain region, southern Nevada. *Journal of Geophysical Research* 101, 8205-8227.

Hayward, B., Murdoch, Graeme, & Maitland, G. (2011) *Volcanoes of Auckland - The essential guide*. Auckland: Auckland University Press.

Kereszturi, G., Proctor, J., Cronin, S.J., Németh, K., Bebbington, M., Lindsay, J., (2012) LiDAR-based quantification of lava flow susceptibility in the City of Auckland (New Zealand). *Remote Sensing of Environment* 125, pp198-213.

Kereszturi, G., Nemeth, K., Cronin, S.J., Agustin-Flores, J., Smith, I.E.M, Lindsay, J., (2013) A model for calculating eruptive volumes for monogenetic volcanoes - implication for the Quaternary Auckland Volcanic Field, New Zealand. *Journal of Volcanology and Geothermal Research* 266, 16-33.

Le Corvec, N., Bebbington, M.S., Lindsay, J.M., McGee, L.E., (2013) Age, distance, and geochemical evolution within a monogenetic volcanic field: Analyzing patterns in the Auckland Volcanic Field eruption sequence. *Geochemistry, Geophysics, Geosystems*, 14,3648-3665.

Leonard G, Calvert A, Hopkins J, Wilson C, Smid E, Lindsay J, and Champion D (2017) High-precision 40Ar/39Ar dating of Quaternary basalts from Auckland Volcanic Field, New Zealand, with implications for eruption rates and paleomagnetic correlations. *Bulletin of Volcanology*.

Lindsay, J.M., (2010) Volcanoes in the big smoke: A review of hazard and risk in the Auckland Volcanic Field. In *Geologically Active* – Williams et al. (eds). ISBN 978-0-415-60034-7

Lindsay, J.M., Leonard, G.S., Smid, E.R., Hayward, B.W., (2011) Age of the Auckland Volcanic Field: a review of existing data. *New Zealand Journal of Geology and Geophysics* 54, 379-401.

Linnell, T., Shane, P., Smith, I., Augustinus, P., Cronin, S., Lindsay, J., Mass, R., (2016) Long-lived shield volcanisom within a monogenetic basaltic field: The conundrum of Rangitoto volcano, New Zealand. *Geological Society of America Bulletin* 128, 1160-1172.

McDougall I., Polach, H.A., Stipp, J.J., (1969) Excess radiogenic argon in young subaerial basalts from the Auckland volcanic field, New Zealand. *Geochimica et Cosmochimica Acta* 33, 1485-1520.

Needham, A.J., Lindsay, J.M., Smith, I.E.M., Augustinus, P., Shane, P.A., (2011) Sequential eruption of alkaline and sub-alkaline magmas from a small monogenetic volcano in the Auckland Volcanic Field, New Zealand. Jou*rnal of Volcanology and Geothermal Research* 201 , 126-142.

Statistics New Zealand, (2012) *Subnational Population Projections: 2006 base to 2031, October 2012 update*. Retrieved on 15 March 2014 from: http://www.stats.govt.nz/browse_for_stats/population/estimates_and_projections/SubnationalPopulationProjections_HOTP0631UpdateOct12.aspx

Post earthquake rockfall protection resilience for a lifeline transmission pylon in Christchurch

J P Riding
GHD Ltd, Christchurch, NZ. (Corresponding author) Member NZGS, Affiliate IPENZ
julia.riding@ghd.com

D J Woods
GHD Ltd, Christchurch, NZ
darren.woods@ghd.com

Keywords: rockfall, resilience, lifeline structure, geotechnical engineering

ABSTRACT

Following the 2010 to 2012 Canterbury Earthquake Sequence, a number a lifeline structures were noted to be at risk from damage from rockfall. An electrical transmission pylon, serving as a lifeline to a coastal suburban community of approximately 5000 residents, had been hit by rockfall triggered during the earthquakes. Due to the pylon design, damage had been limited and the structure was fit to remain in operation. The structure was assessed to have a high risk of damage in future rockfall events. Rebuilding of the structure to provide resilience was considered uneconomic. It was therefore decided that to maintain security of supply to the electrical network, rock protection measures would be used instead to safe guard against possible future damage.

The pylon is situated on steeply sloping terrain approximately 75 m above sea level. Outcrops of Port Hills volcanic rocks are located approximately 180 m upslope of the pylon. The slope beneath the rock outcrops comprises predominately loess colluvium (reworked windblown silt) with scattered rock at the near surface along with boulders from previous rockfall events.

This paper describes the process of assessing and designing resilient rock fall protection to a lifeline structure. Work has included:

- Rockfall modelling
- Rockfall protection optioneering
- Removal of source material
- Design of rock fall protection fence

The assessments and modelling resulted in the construction of a rockfall protection fence.

1 INTRODUCTION

The Canterbury Earthquake Sequence (CES), between 2010 and 2012, caused rockfall events on the Port Hills damaging residential properties and infrastructure. While some infrastructure such as roads were closed due to risk to life some structures such as lifeline infrastructure (e.g. overhead power, telecommunications etc.) had to continue to operate. This paper describes the process of providing protection to a lifeline structure to provide resilience against future rockfall events.

1.1 Background

During the CES a transmission pylon on the Heathcote to Barnett Park sub transmission tower line was damaged by multiple rock strikes. This created a significant risk to the electricity supply to Sumner, Redcliffs and the surrounding area.

The pylon is situated on sloping terrain approximately 75 m above sea level, see Figure 1. Outcrops of volcanic rocks from the Lyttleton Volcanic Group are located approximately 180 m upslope of the pylon.

The slope beneath the rock outcrops comprise predominately loess colluvium (reworked windblown silt) with scattered outcrops of exposed rock at the near surface and boulders from previous rockfall events.

Figure 1: Transmission pylon prior to works

Figure 2: Examples of rock damage to pylon

2 INVESTIGATION

2.1 Field Mapping

Field mapping was undertaken by GHD staff to map and quantify; the number, type / size of fallen boulders as well as, potential source boulders from both rock outcrops and the slope around the pylon. Bounce height data at the pylon location was measured from impact marks on the pylon, see Figure 2.

Field mapping, see Figures 3 to 5, identified two types of potential rockfall boulders:

1. Boulders formed by defects in the bluffs (i.e. not yet released);
2. Boulders that had previously released from a bluff onto the slope below and were now supported by soil.

Figure 3: Precarious source rocks identified during walkover

Figure 4: Looking upslope with pylon to the left.

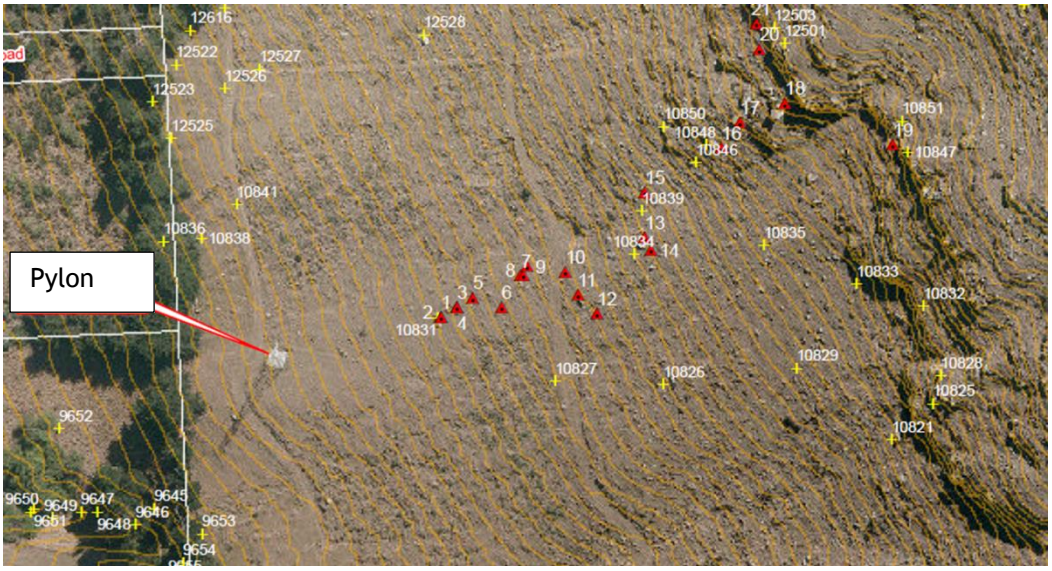

Figure 5: Mapped precarious boulders

3 RISK ASSESSMENT

3.1 Rockfall Modelling

Existing rockfall data collected by GNS Sciences (GNS) and the Port Hills Geotechnical Group (PHGG) following the earthquakes of the CES was obtained from Christchurch City Council (CCC). This data comprised the details and locations of mapped boulders that had moved in the CES and several attributes logged during field mapping of fallen boulders. Volumes of individual boulders were calculated by using a volume reduction factor of 30% to take into account the boulders shape. The mass was calculated using a boulder unit weight of 27 kN/m^3 as per GNS Science Consultancy Report CR2011/311.

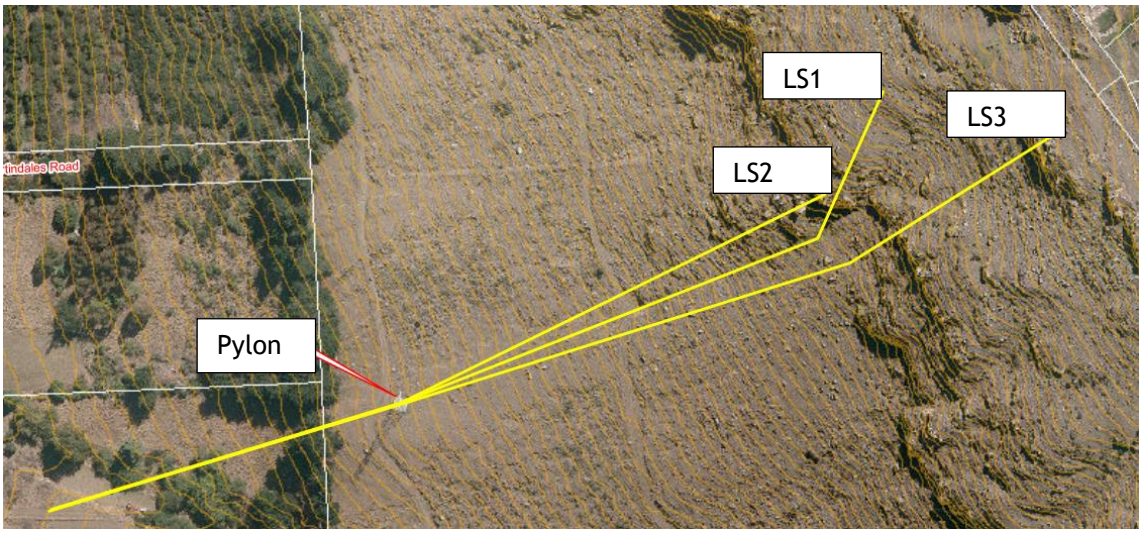

Figure 6: Boulder Runouts For Selected Sources

2-Dimensional rockfall modelling was undertaken using the rockfall modelling software RocFallTM (by Rocscience).

The rockfall modelling process, project settings and initial material parameters, were undertaken / selected in accordance with Appendix F (Rockfall Modelling Methodology for Field Verification) of GNS Science Consultancy Report CR2011/311.

Three transects (LS1 to LS3) were run downslope from the bluffs through the pylon, see Figure 6. Two boulder sizes were considered for the modelling of potential rockfall risk:

1. The 95 percentile boulder from the data collected during GHD's field assessment was 85,000 kg. This was revised to 7,300 kg following boulder deconstruction works undertaken subsequent to the field mapping.
2. The GNS Port Hills 95 percentile boulder size of 8,250 kg.

The GNS Port Hills 95 percentile boulder size was used for the modelling. This was considered the most conservative boulder size and removes any potential bias created by a limited field survey.

Through back analysis, the GNS guideline material parameters were modified to achieve similar bounce heights to those observed on the pylon. Run out distances from the modified parameters ran further than the furthest boulder recorded in the GNS dataset. However this boulder and all other boulders in the area appear to have been stopped prematurely by vegetation. From field mapping of potential boulders, a Super Ellipse^4 (5:6) boulder shape was used in the modelling due to the somewhat tabular nature of the boulders.
The rockfall modelling results are provided in Table 1.

Table 1: Rockfall model input parameters and results

Layout	Transect 1	Transect 2	Transect 4
Boulder Mass (kg)	8250	8250	8250
Pylon Location on Section (m)	235	186	283
No. Boulders Past Pylon	191	561	248
Max Runout Distance (m past Pylon)	77	86	95
Bounce Height at Pylon (m)	1.11	0.7	1.1
Total Kinetic Energy at Pylon (kJ)	646	516	584

The results were in line with observed data captured during the field inspection.

4 MITIGATION OPTIONS DISCUSSION

A variety of mitigation options to reduce the rockfall risk were considered with different advantages and disadvantages and cost implications and are discussed in the following sections.

4.1 Deconstruction and scaling of potential boulders

Deconstruction and scaling of individual boulders can be used as a targeted approach to eliminate high risk boulders. As the quantity of potential boulders increases this method becomes less economical. The method can be used to target specific large boulders and those that have a higher probability of detachment. This option results in a solution that does not produce a fixed asset that requires maintenance but would require ongoing re-assessment. In this case, it was considered uneconomical to deconstruct all potential boulders and completely remove the hazards. In addition, the incorrect deconstruction of boulders could trigger further weathering, instability and rockfall. Boulder No. 16 was identified as needing deconstruction immediately, as it posed an immediate significant risk. It was estimated that a further five large boulders (>24,000 kg) and several smaller boulders would require varying degrees of source treatment at some stage in the

future, as the soil support may erode and cause instability. This work was subsequently carried out by Solutions 2 Access Ltd.

4.2 Rock bolting of potential boulders

Rock bolting can be used as a targeted approach to reduce the probability of detachment of high risk boulders. This method is only suitable where boulders are supported by near surface bedrock for rock bolt installation, which was not the case in this situation. In addition rock bolts would become an asset with a limited lifespan and would require ongoing maintenance.

4.3 Reinforced concrete support/buttress of potential boulders

A reinforced concrete support or buttress of the boulder can be used as a targeted approach to reduce the probability of detachment of high risk boulders. However, this method can become uneconomical to treat many potential boulders and completely reduce the hazard. In this instance it was not suitable for all boulders due to the steep underlying terrain. Also it would become an asset with a limited lifespan that will require ongoing checking and maintenance.

4.4 Rockfall netting mesh/drapery system

A rockfall netting of mesh or a drapery system can cover large areas with suitable anchor points typically installed in rock. This method arrests boulder fall and prevents roll and bounce of boulders hitting the structure. The netting becomes an asset with a limited lifespan that requires maintenance and removal of rocks that fall within the mesh. It was not considered suitable due to the sheer scale of the area requiring cover.

4.5 Earth or Rock Embankment

Earth embankments are able to divert and catch large volumes of rock and can absorb impacts from boulders with large energies. This technique is also relatively easily repaired and cleared out after each large event. It can also be ‘greened’ to reduce the visual effect. However, it requires significant earthworks which can destabilise the slope if not undertaken carefully.

4.6 Concrete Deflection Barrier

Concrete deflection barriers are able to divert and catch large volumes of rock and withstand multiple boulder strikes. However they require deep embedment into the slope and may act as a dam, causing detrimental effect to water flows. This type of barrier in such a location was also considered to not to be aesthetically pleasing. It would require greater excavation and earthworks, and thus have greater environmental impact than a rockfall protection fence.

4.7 Rockfall Catch Fence/ Barrier System

A rockfall fence does not require significant earthworks and the structure can be small and targeted. Theses fences can withstand over two strikes from boulders. A fence will have to be emptied following boulder strike and will require ongoing maintenance.

5 SELECTED SOLUTION - PROTECTION TO STRUCTURE

5.1 Design Approach

Installation of a rockfall catch fence was recommended in conjunction with source treatment. A catch fence is considered an appropriate protection structure as total kinetic energies are within the limits of rockfall catch fence design and bounce heights are relatively low (~1 m) at the pylon. A rockfall catch fence required the least amount of earthworks and the modelled total kinetic energy (at the pylon) for the 95 percentile boulder is within its capability. Modelled bounce heights and observed bounce heights are approximately 1 m above ground level, indicating a 2 m

high rockfall catch fence is a realistic and feasible height. As the source treatment had been undertaken on the larger boulders, this significantly reduced the demand on the rockfall catch fence. In addition, construction of a rockfall catch fence directly upslope of the pylon minimised the length of the fence required.

The design approach needed to include consideration of the planning and consent process. As the pylon is located on land owned by the CCC, consultation was necessary to determine a mutually agreeable design.

5.2 Investigation

A 15 m deep machine borehole was drilled by McMillan Drilling to understand the depth of Loess and volcanic rock, and to provide soil and rock parameters for the design of the rockfall barrier anchoring and foundations. The investigation found up to 15 m of stiff Loess, with no bedrock encountered.

5.3 Detailed Design

The total kinetic energy of 95th percentile boulder strike was in the range of 600 to 800 KJ. Using a factor of safety of two, a catch fence with a maximum impact energy level of 1500KJ was identified as the most appropriate protection structure for this project. The proposed fence was designed to be 30 m wide, with post spacings of 10 m and with post heights of 4 m. The post height of 4 m was chosen to account for a conservative bounce height of 2 m, with a factor of safety of two. The embedment of the piles / anchors was based on the presence of weak loess soils and in consultation with Geofabrics. Allowing for a factor of safety of two the anchors are adequate for an 800 KJ boulder strike. The anchor type and length were specifically designed for the site.

6 CONSTRUCTION

The rockfall protection fence was constructed by Solutions 2 Access Ltd with a rockfall protection fence provided by Geofabrics. Figure 7 shows the site during construction. Figure 8 shows the completed fence.

Figure 7: Construction

Figure 8: Completed fence

7 CONCLUSIONS

A transmission power pylon had been struck by multiple boulder rolls following earthquakes of the Canterbury Earthquake Sequence (2010 -2012).

A field assessment of the area upslope of the pylon identified many potential boulders which could present future risk to the pylon (a lifeline structure). The potential boulders varied in both size and risk posed to the pylon. From this data set, a 95th percentile boulder was able to be determined and applied to 2-Dimensional rockfall modelling. The modelling was undertaken to determine parameters for the design of potential rockfall mitigation techniques. The modelling results indicated the bounce height to be low (<2 m), which agrees with observations of previous boulder strikes on the pylon. The calculated total kinetic energy of a 95th percentile boulder strike was in the range of 600 to 800 kJ.

There are a variety of rockfall protection techniques that could broadly be classified into two types; source treatment and protection structures. These were considered and a combined approach using both source treatment of the larger boulders as well as construction of a rockfall protection structure. The construction of the rockfall protection fence reduces the risk of boulder strike to the pylon. To date a small amount of rock has been caught by the fence, see Figure 8.

8 ACKNOWLEDGEMENTS

Eric Ewe - Geofabrics New Zealand Ltd
Martin Freemen - Solutions 2 Access Ltd
Jeff Price – Orion New Zealand Ltd
Richard Wise – McMillan Drilling Ltd

REFERENCES

Massey, C.I.; McSaveney, M.J.; Heron, D.; Lukovic, B. (2012a) *Canterbury Earthquakes 2010/11 Port-Hills Slope Stability: Pilot study for assessing life-safety risk from rockfalls (boulder rolls).* GNS Science Consultancy Report 2011/311.

Rocscience Version 5, RocFallTM

Use of UAVs and photogrammetry to reduce uncertainty in bulk earthwork calculations

T Revell
Aurecon, Christchurch, NZ
Tom.Revell@aurecongroup.com (Corresponding author)

Z Pletz
Aurecon, Christchurch, NZ
Zoe.pletz@aurecongroup.com

C Mangos
Aurecon, Christchurch, NZ
Charles.Mangos@aurecongroup.com

Keywords: UAV, photogrammetry, bulk earthworks, volumetric calculation

ABSTRACT

The application of Unmanned Aerial Vehicles (UAVs) and photogrammetry for bulk earthwork calculations is a recent development for ground engineering in New Zealand. The approach developed on the Deans Head Land Remediation Project has proven to be an innovative solution increasing workflow efficiency to calculate and reduce uncertainty during bulk earthworks.

Following the 2010-2011 Christchurch Earthquake Sequence, Deans Head and Shag Rock Reserve, located near the suburb of Sumner, Christchurch, suffered significant land damage. Subsequently, Shag Rock Reserve was inaccessible to the public and Deans Head was assessed as being in the highest relative landslide hazard category with a potential risk to life and/or cause significant lifeline damage.

This paper presents the application of UAV and photogrammetry technology, outlining the 'Fly-Model-Analyse' workflow to generate accurate change models on the Deans Head Land Remediation Project. UAV and photogrammetry methods are compared with traditional methods for volumetric calculations, such as LiDAR, ground surveys and truck count estimates. The associated emerging technologies to enhance its application for ground engineering and some of these progressions and future uses are explored.

1 INTRODUCTION

1.1 Outline

The recent advancement of UAVs and photogrammetry applications has enabled the project team to develop a workflow process to reduce the uncertainty in bulk earthwork calculations. Traditional methods including truck count for volume estimates and ground surveys were taken into account during project establishment however considered time consuming and labour intensive and more importantly placed staff into high risk areas. An alternative method that is safer, quicker and allowed third party verification was required by key stakeholders to meet their regular reporting requirements.

A proficient workflow system was created using UAVs and photogrammetry to calculate key volumes that were required every fortnight on the project. Increasing project efficiency reduced personnel working in high risk and complex, steeply inclined slope with heavy earthworks machinery.

1.2 Background

Following the 2010-2011 Canterbury Earthquake Sequences, significant land, property and infrastructure damage was observed south of Christchurch at the foot hills of the Port Hills (GNS Science, 2013). Located near the suburb of Sumner, Deans Head and Shag Rock Reserve were badly affected by the severe ground shaking, resulting in collapse of the 80m high volcanic cliffs above Shag Rock Reserve and dense ground cracking across the steep Deans Head hillside area.

Following the Canterbury earthquakes, GNS Science (Massey et al., 2014) identified numerous mass movement areas in the Port Hills. Identified as a Class I mass movement area, the Deans Head area extends approximately 8,300m2 in size and contained an estimated 53,300m3 of soil (loess) material that could be mobilised as an earth/debris flow likely to have debris runouts which could cause damage to critical infrastructure, lead to loss or disruption of services and/or loss of life. Based on recorded surface movements and slope displacements across the site area, the landslide direction has been modelled in a northwest direction in relation to the site with trigger mechanisms rain related. Located on a steep sloping hillside, Deans Head has an average slope angle between 25° to 30°. Deans Head and Shag Rock Reserve site locations are presented in Figure 1 including the Deans Head indicative landslide direction.

Figure 1: Deans Head and Shag Rock Reserve site areas in relation to Main Road. Indicative movement direction shown in red arrows (LINZ, 2011 and Aurecon, 2015).

Deemed as an unacceptable risk to road users, local and central government agencies aimed to remove all the mass movement hazard material (soil) to rock level, with a portion of material placed in Shag Rock Reserve to construct a rockfall protection bund. Bulk earthworks removal formed part of the overall Deans Head Land Remediation Project (New Zealand Government, 2016a, 2016b).

Tracking key milestones and earthwork progress during the project was a critical requirement for stakeholders in the early detection of potential cost overruns. With a limited number of historical ground investigations completed across the site area, final volume values deviating from initial estimates could have had financial implications for the overall project. Although allowed for in project contingencies, if overruns can be foreseen earlier, the better.

In a challenging site setting, developing UAV applications and workflows improved project efficiencies during the Deans Head Land Remediation Project. The ability to obtain aerial imagery quickly, reduced personnel and heavy earthmoving machinery interaction while operating in a common work area on the ground. Undertaking repeat surveys regularly allowed the project team to track contractor progress claims for bulk earthworks on a site with geological uncertainties.

2 APPLICATION OF UAVS

2.1 Previous Use

The applications of UAVs has significantly grown in recent years, driven by the availability and affordability of recreational and pro-consumer UAVs. The improvements in camera specifications fitted to UAVs has enabled visual imagery to be collected from a different perspective and at a fraction of the cost of a commercial helicopter. The terminology for "drones" is plentiful including; Unmanned Aerial Vehicles (UAV), Remotely Piloted Aerial Systems (RPAS), and Unmanned Aerial Systems (UAS). For continuity throughout this paper we use the term 'UAV' to cover all aerial systems.

Initially UAVs were used in the Port Hills for visual inspections using the high resolution photographs and high-definition video. These inspections focused on cliff edge deterioration and unstable boulder inspections, where access was limited and/or hazardous.

We developed this visual monitoring to incorporate the simple technique of cliff edge tell-tales or extensometers. During cliff face scaling works, abseil teams installed wooden stakes positioned horizontally across significant ground cracks, see Figure 2. These tell-tales could then be observed periodically using UAVs to visually compare imagery and detect ground movement. This technique reduced personnel accessing close to the cliff edge. Combining UAV technology and tell-tale monitoring simplified work streams and increased monitoring frequency in hazardous locations.

Figure 2: Comparison from UAV images of tell-tale monitoring at Shag Rock Reserve (Aurecon, 2016a).

2.2 UAV Volumetric Measurements

Identified during project establishment, volumetric calculations were required fortnightly during the 9 month earthworks programme to track milestones and verify contractor claims. To accurately calculate material removed and remaining on site, a unique and innovative workflow was developed using UAV and photogrammetry capabilities which was termed 'FMA' (Fly-Model-Analyse). From start to finish, the FMA process could be completed in approximately 24 hours.

This workflow comprises three key steps;

1. ***Fly*** - A UAV is flown over the site to capture high-resolution images. The flights were flown manually as flight automation is unable to account for complex 3D environment and gradual slope changes. The images were captured using a single camera and variations in flight altitude,

flight direction and camera angle, which enabled the the project team to obtain the required overlap and array of images for detailed photogrammetry modelling.

2. ***Model*** – The images captured are processed through multiple photogrammetry software, including Autodesk ReCap360, which transforms the 2D images into a 3D point cloud. Ground Control Points (GCPs) are included during the modelling phase. These points are captured using RTK-GPS survey.

3. ***Analyse*** – The 3D point cloud is then converted into a Digital Terrain Model (DTM), using software such as Autodesk ReMake. This data can then be used for a number of analysis functions including rockfall simulations, slope stability analysis and volumetric calculations.

The FMA workflow produced a DTM (3D model) that could be compared to previous models to identify topography changes, see Figure 3. With each new DTM the team were able to compare the mesh layers and calculate the difference between the current excavated surface and the previous ground surface to estimate the volume of material that has been removed between DTMs. Earth removal rates could then be calculated and tracked for project management purposes.

In addition, by comparing the latest DTM with the design surface the project team were able to forecast the amount of remaining soil to be removed. This was critical in key milestone decisions and sequencing works with site won material for the construction of mitigation works in Shag Rock Reserve.

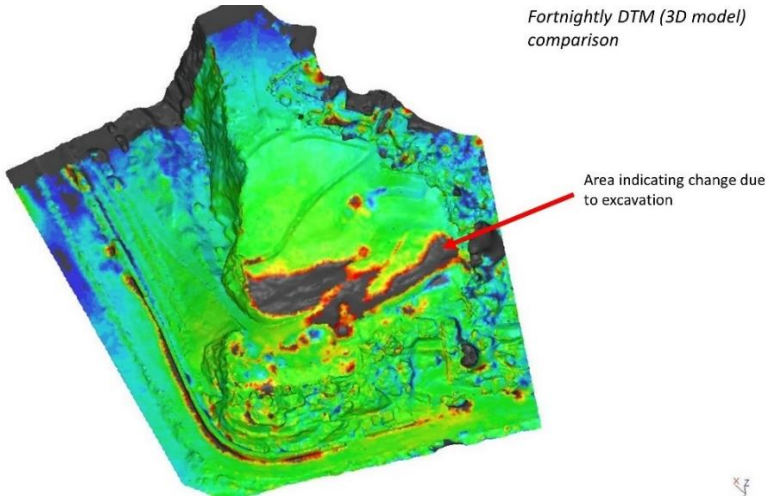

Figure 3: Fortnightly 3D terrain model comparison of Deans Head, green and blue signifying no significant change and black signifying vertical change due to excavation (Aurecon, 2016b).

Reducing DTM uncertainty or margin of error improves model reliability. We defined our error or uncertainty through the measurement of accuracy and resolution.

The level of accuracy is measured as the distance between the identified control points within the DTM to the corresponding known ground control points (GCPs) to provide difference in the x,y,z planes. During baseline establishment, this measurement started at 300mm, but was reduced to less than 50mm with the improvement of flight paths, ground control point locations and camera angles.

The resolution indicates the level of detail that is captured in relation to the ground surface. The ground sampling distance measures the distance between each pixel, which is represented as a point within the 3D point cloud. This measurement also relates to the amount of ground that each point (or pixel) represents. This measurement started at around 25mm and was reduced to less than 10mm using improved camera sensors and flight paths.

Increasing the level of accuracy and resolution decreased the margin of error or uncertainty for each DTM. On a larger site, such as Deans Head with an area of 8,300m2, reducing the margin of error was crucial in reducing potential volume errors. With the improvements in model accuracy and resolution, the uncertainties for earthwork volumes reduced from approximately ±2,300m³ to ±500m³ (Aurecon, 2016c).

3 DISCUSSION

3.1 Comparison between UAV and traditional methods

Traditional methods for earthwork volume calculations were investigated during project establishment and comprised of three main categories;

1. ***LiDAR*** – an aerial based system that provides accurate and high resolution data. The system normally requires piloted aircraft to fly-over the area, which can be expensive and challenging dependent on the size of the site. Capture of LiDAR data was impractical to achieve on a fortnightly basis.

2. ***Ground Survey*** – this includes laser scanning, theodolites and RTK GPS. These data capture techniques provide highly detailed and very accurate measurements. However GPS units and theodolites can be restricted in the number of total points captured across the site, which reduces the overall resolution. Laser scanning can be expensive and with complex terrain requires several set-up locations to achieve appropriate view angles, this become impractical across a working site with moving plant. Data capture with theodolite and GPS systems would need to consist of a grid style pattern (such as 0.5m by 0.5m) across the site and this was impractical due to the scale of the site and the resolution required to pick up the extremely variable terrain.

3. ***Contractor Estimations*** – a method most commonly used to calculate volume removed for bulk earthwork projects. The contractor provides the material that is excavated and/or trucked off-site. These estimated quantities are calculated based on the number of trucks, and the approximate known load of each truck. This form of volume calculation can have errors associated with larger volumes such as there may be one to two excavator buckets difference per load; generally the greater the number of trucks, the larger the error. Truck volume counts are difficult to verify and a weigh station would be costly to install.

On review at the beginning of the project, the above methods were deemed to be time consuming and labour intensive, and an alternative method using UAVs combined with photogrammetry was selected. Through recent advances in UAV and photogrammetry technology, good coverage and resolution was achieved on the project. Accuracy was improved by incorporating an increased number of ground control points to improve data quality.

The repeated collection of UAV derived photogrammetry models which formed our DTMs reduced the overall uncertainty of the underlying design (rock) surface, and enabled the project team to forecast and refine estimates of the remaining material to be removed. By building in these forecasted models along with refining the original estimates, the comparison between our forecasted removal estimates and actual volume removed calculation was on target and within ±110m3 of the 53,300 m³ to be removed (Aurecon, 2016c).

4 EMERGING TECHNOLOGIES

There are a number of emerging technologies that can be used to improve image capture and accuracy and resolution of the photogrammetry derived digital terrain models. These emerging technologies include;

- ***Operating Applications*** - There are several operation applications that have the ability to automate flight paths. Currently many of these applications do not allow for sloping and complex terrain. Automated flight path applications that adjust for variation in altitude would be beneficial, and improve efficiencies by removing the need to "over-fly" an area to ensure consistent data. Current automated volume calculation applications appear to struggle with complex terrain, as they are focused on stockpile estimates on flat surfaces compared to variations within complex terrain models.

- ***GPS Improvement*** – Continuing improvements in the on-board GPS technology for UAVs will improve the accuracy of the known location of each image captured. This improved accuracy will feed into improved accuracy of the 3D point clouds to create the DTMs. Improvement in GPS will also allow more accurate refinement of predefined automated flight paths for improved consistency between models.

- ***LiDAR*** – Current UAV LiDAR is available for a high cost, and the weight of the attachment requires a larger UAV requiring more restrictive operating procedures. As the LiDAR attachments develop and reduce in cost and size, they will become more applicable to smaller UAVs. This will allow for better resolution and accuracy of the digital terrain models, with the advantage of a reduction in "noise" from vegetation.

An advancing stream of emerging technologies is currently being developed that focuses on the stakeholders interaction with the DTMs using virtual reality (VR) and augmented reality (AR). Virtual Reality includes the use of headsets such as the Oculus Rift or HTC Vive to immerse the user into a virtual model of the DTM, enabling them to interact and explore the virtual environment. Augmented Reality requires devices such as the Microsoft HoloLens, which merges the digital terrain model with the real world, enabling users to view a blend of virtual and real world environments, see Figure 4.

During the Deans Head project, the team harnessed both VR and AR technologies to enable clients, contractors and engineers to discuss particular hurdles during the earthworks phase and logistical problems as well as final design. The AR technology provided project engineers with an opportunity to refine and visually check the proposed design surface. Health and safety hazards could be clearly communicated to stakeholders on an interactive level, facilitating engaging discussions prior to site visits.

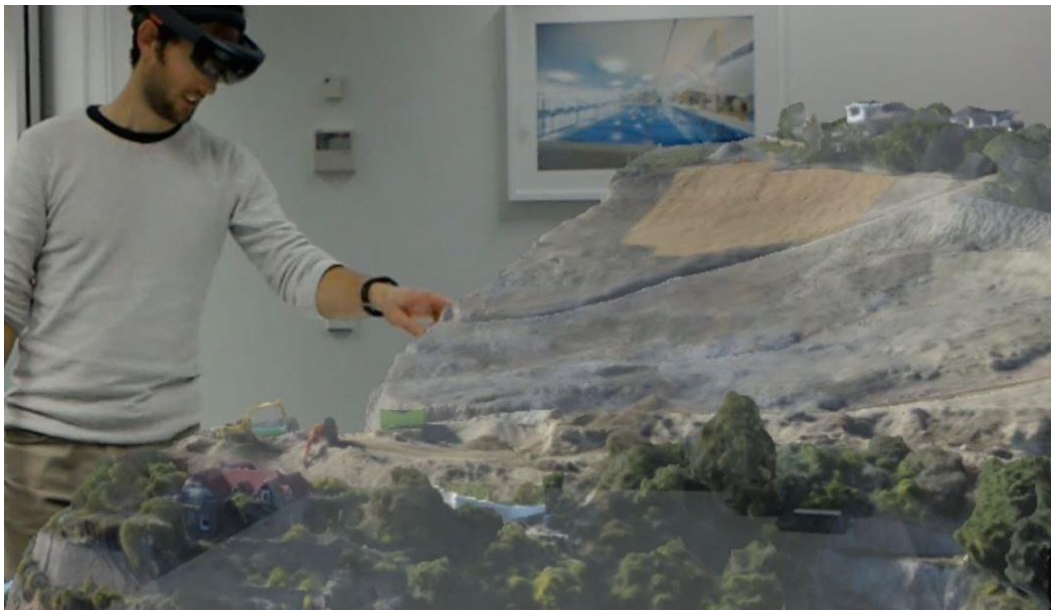

Figure 4: Deans Head viewed through the Microsoft HoloLens (Aurecon, 2016b).

5 FUTURE USES

There are a number of opportunities for the use of complex terrain photogrammetry models built from UAV derived imagery. The majority of industries are using UAVs to improve the efficiency of their operations, monitor sites and improve health and safety. The engineering industry is now forging ahead with the use of photogrammetry. Based on the recent developments in emerging technologies the use of workflows such as the FMA will likely develop several different work streams including;

- ***Environmental Management*** – The FMA process enables volume calculations to be used in a variety of ways, and due to the short turnaround period for the process, derived change models can be used for short and long term predications for erosion or sediment accumulation of rivers, beaches, slopes and exposed cliff faces. The UAV enables the FMA process to be used in inaccessible areas, using remotely placed ground control points, which could enable the monitoring of forests for their progressive growth and density increase. The information collected and recorded can be used to anticipate areas prone to erosion and enable decision makers to prioritise areas that may require additional remediation and slope stabilisation.

- ***Natural Disasters Response –*** following an earthquake or significant rainfall event, the FMA process could be used in an initial response to quantify the volume of debris flows or landslide material transported downslope and potentially covering road or rail infrastructure. This can provide emergency response crews with information critical to identifying the extent of the damage and enable recovery teams to repair the infrastructure.

- ***Infrastructure*** – The DTMs created through the FMA process can be used to measure any movement or settlement along road, rail and bridge embankments. As the FMA process can be undertaken within 24 hours, the process could be used on a scheduled type basis during construction and life cycle of the asset to improve the performance and safety for asset users.

- ***Underground engineering –*** Tunnelling and mining operations are associated with varying levels of geological uncertainty dependent on the stage and scale of the project. Comprehensive survey techniques are normally undertaken during the established and monitoring phase, these techniques include InSAR, Laser Scanning and prism based monitoring. The UAV-based FMA process can be beneficial in the concept phase and provide the initial information which detailed DTMs for planning purposes. The DTMs can be coupled with geological models to create 3D complex terrain models for planning and concept design. The low cost and timeliness of the FMA process makes it efficient to complete during the pre-feasibility stage of a project.

There are a number of future uses that are being developed outside of the engineering sector, and as these develop they may become transferrable for use. As the applications are explored and technologies improve the uses of UAVs and process such as the FMA will expand.

6 CONCLUSIONS

The application of UAV and photogrammetry technology through the Fly-Model-Analyse (FMA) workflow has been successful in the volumetric calculation of bulk earthworks during the Deans Head Land Remediation Project. UAV and photogrammetry methods have generated accurate models which are cost effective, timely and repeatable. These methods are comparable to traditional methods such as LiDAR, ground surveys and truck count estimates. UAV technology has reduced personnel working in high risk rockfall areas and interacting on the ground with heavy earth moving machinery.

UAV and photogrammetry is a new and evolving technology for ground engineering. There are a number of emerging technologies under development to improve image capture and the accuracy and resolution of photogrammetry derived digital terrain models. Some of these technologies include the

development of automated flight paths, improved on-board GPS and low cost LiDAR which will allow UAV and photogrammetry applications to become more affordable and practical. The inclusion of VR and AR developments into this workflow process enables the data to be interrogated in a more immersive environment, and can facilitate stakeholder and contractors collaboration.

There are a number of applications for UAV and photogrammetry technology. UAV surveys are repeatable and can be compared for periodic monitoring and erosional surface management such as around lakes, beaches and slopes. Other future uses include quantify damage extent caused by landslides and earth debris flows and assessments following natural disaster events.

7 ACKNOWLEDGEMENTS

We would like to acknowledge Land Information New Zealand (LINZ) and Aurecon for allowing the team to use the Deans Head Land Remediation project as a case study for this paper.

REFERENCES

Aurecon (2015) *Monitoring photographs of Deans Head* (unpublished).

Aurecon (2016a) *Monitoring photographs of Shag Rock Reserve* (unpublished).

Aurecon (2016b) *Deans Head Fortnightly DTM comparison* (unpublished).

Aurecon (2016c) *UAV volume comparisons for Deans Head bulk earthworks* (unpublished).

GNS Science (2013) *Vulnerability Assessment of Christchurch Building in Canterbury Earthquakes.* GNS Science Report 2013/20 (www.GNS.cri.nz).

Land Information New Zealand (2011) *NZ Topo 50-BX24*. Edition 1.02 Published 2011.

Massey C. I, Della Pasqua F., Taig. T, Lukovic. B., Ries. W. and Heron D. (2014) *GNS Canterbury Earthquakes 2010/11 Port Hills Slope Stability: Risk assessment for Deans Head*. GNS Science Consultancy Report 2014/77.

New Zealand Government. (2016a, June) Demolitions and clearances. Retrieved from Land Information New Zealand: http://www.linz.govt.nz/crown-property/types-crown-property/christchurch-residential-red-zone/demolitions-and-clearances

New Zealand Government. (2016b, June) *Red Zone information*. Retrieved from Canterbury Earthquake Recovery Authority: http://cera.govt.nz/land-information/red-zone

Autodesk ReCap360 (2016) v3.0, 2008 Autodesk, Inc.

Autodesk ReMake (2017) v1.8, 2008 Autodesk, Inc.

Bluff Road Coromandel: Rockfall Risk Management, Public Perception and Influence

C G C Hughes
Opus International Consultants, Auckland, NZ
Chris.Hughes@opus.co.nz (Corresponding author)

K J Read
Opus International Consultants, Hamilton, NZ*.
KenR@cmwgeosciences.com

(*now with CMW Geosciences, Hamilton, NZ.)

Keywords: risk management, rockfall, public perception, public influence.

ABSTRACT

Bluff Road is a low use, single lane, coastal road linking two beach resorts on the north east coast of the Coromandel Peninsula. It is a popular pedestrian short cut between the two beaches, is the access way to attractive fishing marks and provides important options for access to a number of properties.

At one location, close to the western end of the road, the road is overhung by a steep rock bluff at a point where it is partly formed on reclaimed land and supported by retaining structures. Following significant rockfalls and erosion damage in the years since Cyclone Wilma in 2011 a detailed assessment of possible remedial works to improve the safety and resilience was instigated.

Remedial works comprising blasting, scaling, bolting and a passive netting scheme commenced in late 2015. During this work further significant rockfalls occurred, promoted by previously unseen fractures. Following further risk and cost benefit assessment the decision was made to close the affected section of the road. This meant the popular recreational route for pedestrians and cyclists was no longer available and that the Matarangi fire service had a potential additional 11km route to reach the east end of Rings Beach.

Throughout 2016 the public repeatedly removed fences, barriers and warning signs erected to warn of the high risk of rockfalls and prevent access.

In this paper we describe the history of the site, the works carried out and discuss issues around rockfall risks, road closure and public perception of risk.

1 INTRODUCTION

Bluff Road is a low use, single lane, coastal road linking two beach resorts on the northeast coast of the Coromandel Peninsula, Figure 1. It is a popular pedestrian short cut between the two beaches, is the access way to attractive fishing marks and provides important options for private and emergency access to several properties.

At one location close to the western end of the road, the road is overhung by a near vertical 20m high bluff of variably weathered and hydrothermally altered andesite, that is also locally sheared and closely fractured, Figure 2. Three major discontinuity sets are present. Two of them, dipping out of the face at angles of between 30 and 50° and a second dipping out of the face at 70 to 80° promoted planar and toppling failure respectively. The third, near vertical set, has a strike at

almost 90° to the face and act as release planes for block failures. Weathering and hydrothermal alteration has particularly picked out the vertical discontinuities trending into the face, which are locally concentrated and may be localised fault or shear zones. The published geological information indicates these to be the Matarangi Andesite of the Coromandel Group of Miocene age (New Zealand Geological Survey 1976).

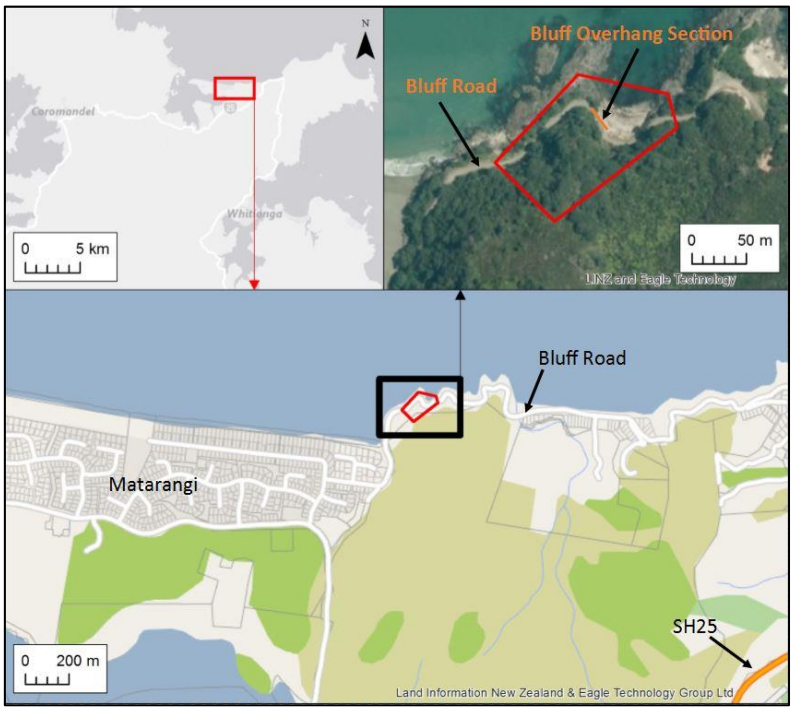

Figure 1: Site location

Figure 2: Views of Bluff Road section of concern showing overhang, fracturing and weathering/alteration

The section of road of concern has had a history of rockfalls coupled with coastal erosion which necessitated regular clearance and maintenance of the road. Following erosion and rockfalls associated with cyclone Wilma in early 2011 Thames Coromandel District Council (TCDC) set in train regular inspections and monitoring of the road and rock face.

Minor rock falls continued, typically following severe weather and were generally individual cobble to boulder sized block falls. Thames Coromandel District Council (TCDC) subsequently engaged Opus International Consultants (Opus) to carry-out stability and risk assessments for possible remedial works.

2 LANDSIDE RISK MANAGEMENT

Subsequent work generally followed the framework for landslide risk management as set out in the Australian Geomechanics Society (2007) guidelines. Hazard analysis (rockfall characterisation, frequency assessment), consequence analysis, risk assessment and finally risk management (risk mitigation options) activities were all carried out

Hazard Analysis: Site inspections and reporting in April 2011, November 2014 and a more detailed assessment of the site in March 2015 all found that the overhanging section clearly had unfavourable discontinuity orientations with respect to rock slope stability. The failure modes that appeared to be kinematically possible across the Bluff were planar, wedge and toppling.

There was a section at the east end of the overhang where three distinct blocks were visible and where if these were to fail the rockfall volumes could be significant (>10m^3), Figure 3.

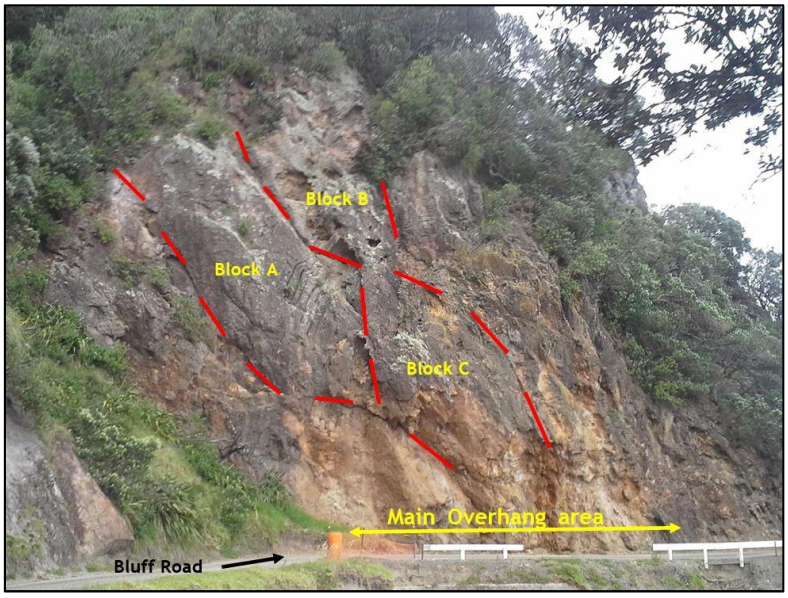

Figure 3: Potential failure masses observed in 2014.

At that time, we considered there was a high likelihood of small rock blocks (up to 0.5m diameter) continuing to fall onto the road. However we also considered that there was a high likelihood of a large volume (>10m^3) planar / wedge type rockslide that would block the road, sourced from any of, or all the blocks A to C shown on Figure 3.

Risk Assessment: The road was used by as little as five vehicles a day and a small number of pedestrians. With the greatest likelihood of failure occurring during or shortly after extreme weather events, the risk to life and limb was therefore considered low. However the road has a strategic importance of enabling emergency access to adjacent properties from two different directions, and this played a relatively greater role in the risk assessment by Thames Coromandel District Council.

Risk Management: An assessment was carried out for 4 treatment options and a 'do nothing' option, using the NZTA "Risk Management Process Manual" as a basis (Transit New Zealand, 2004). The criteria used and outcomes are given on Tables 1 and Table 2 below. Table 1 was generated for the bolt and mesh option (treated risk), similar tables were generated for the other options considered.

Table 1: Risk matrix for mesh and bolt option

Ref	OPTIONS AND RISK: The risk: What can happen and how can it happen?		Qualitative Risk Analysis			Risk Evaluation		Risk Score	Risk Priority	Threat Rank
		Threat or Opportunity	How likely is the event?	Consequence Rating	What are the consequences of the event?	Likelihood Rating	Consequence Rating			
E	**OPTION E: Rock bolting + Rock mesh**									
E1	**RISK 1 : Risk to Walkers**									
E1.1	Direct rockfall impact on member(s)of the public.	Threat	Rare	Major	Liklihood reduced as bolting and mesh will be designed to mitigate the risk such that impact on public would likely be negligible.	1	70	70	High Threat	2
E2	**RISK 2 : Risk to Road Users**									
E2.1	Direct rockfall impact on vehicle.	Threat	Rare	Major	Liklihood reduced as bolting and mesh will be designed to mitigate the risk such that impact on public would likely be negligible.	1	70	70	High Threat	2
E2.2	Vehicle accident due to rockfall debris in road / road blockage	Threat	Rare	Medium	Liklihood reduced as bolting and mesh will be designed to mitigate the risk such that impact on public would likely be negligible.	1	40	40	Moderate Threat	5
E3	**RISK 3 : Risk to Road Asset / Contractors in clean up**									
E3.1	Road blockage and damage to downhill side.	Threat	Unusual	Minor	Likely damage not exceeding $100k.	2	10	20	Low Threat	6
E3.2	Risk to contractors in the clear up of debris on road from rockfall event	Threat	Rare	Major	Digger drivers and contractors on site potentially at risk, especially if not carefully managed. Reasonable to assume measures can be put in place to manage risk during construction.	1	70	70	High Threat	2
E4	**RISK 4 : Reputation Risks**									
E4.1	Client and Opus image damaged due to costs and insurance / claims made	Threat	Unusual	Medium	Lower liklihood than blasting option.,	2	40	80	High Threat	1

Table 2: Summary of outcomes

Option	Very high threats	High threats	Weighted Score
"Do nothing"	1	4	18
Close the Road	0	1	5
Move Road Over Seaward	0	5	17
Scaling Works	0	5	17
Rock bolting / mesh works	0	4	15

The scoring reflected that whilst remedial work reduced the likelihood of key threats being realised the consequences of these were still very serious. It also reflected the responsibility felt by all parties to protect the public, and the client and consultant reputation risks around this.

Closing the road was considered by the client and the public to be a move of last resort, Other options such as a retreat of the cliff face, a rock block bolting and active mesh system and a rockfall protection structure were ruled out on environmental, cost or cultural grounds. Work was subsequently commenced to remove the overhang and improve safety by a combination of a passive mesh system secured to the rock face by bolt anchors.

2 SITE WORK

Work commenced in November 2015 to remove blocks B and C plus a section of material to the right of these blocks (Figure 3). This work was to consist of scaling and blasting to remove approximately 350m^3 of rock and the installation of 350 m^2 of passive mesh held in place by bolt anchors at the top and bottom of the slope. Scaling and blasting was completed prior to the Christmas holiday shutdown after which the placement of mesh was to be carried out. As works were not complete the road was temporarily closed over his period with signage and fencing erected.

A significant rock-fall occurred after heavy rain on the 25th of December (Figure 4). It is unclear if this was also related in part to the effects of the work, such as blasting and stress relief opening fractures.

Figure 4: Rockfall of 25 December 2015.

3 POST SITE WORK RISK AND RISK TAKING

A review of the discontinuity and weathering profile exposed after the December 2015 rockfall concluded that previously unknown discontinuities and deeper weathering and alteration of the rock mass indicated there was a greater risk of ongoing and potentially large volume rockfalls than previously understood.

Significant additional costs would be incurred to continue and the decision was made to discontinue work and close the road. The community was informed and barriers and signs erected to prevent pedestrian access. Rockfall debris was left in place to deter vehicle access. There is a footpath over the bluff that allows alternative pedestrian access.

However, over the next year the fences and barriers were repeatedly cut and broken down by members of the public seeking to use the road as a short cut between the two communities and to popular fishing and diving marks (Figure 5 and 6).

Figure 5: Vandalised fencing

Figure 6: Footpath past debris

This was despite clearly hazardous conditions, as exhibited by wide open fractures, isolated fallen blocks (Figure 7 and 8), signage / barriers and warnings in the press.

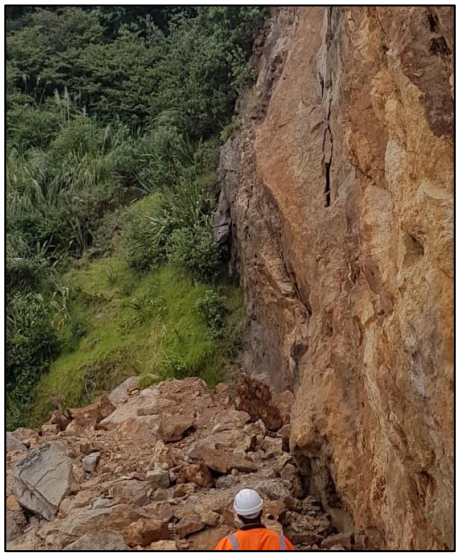

Figure 7: Open fractures above path

Figure 8: Fallen blocks on footpath

During site inspections by Opus and Council staff, members of the public would typically linger by the fences and barriers until they thought they could pass through unobserved.

4 DISCUSSION AND UPDATE

We used a well tried procedure to weigh factors in our decision making which, though still appearing to give a significant risk, did after consideration of factors beyond and behind the scoring system point to meshing and bolting as the preferred option.

The technical risk of finding more unknown and unfavourable discontinuities together with deeper weathering and alteration forced a rethink and change of policy to close the road. This was a decision that should have eliminated the risk, and elimination is always seen as the preferred option over mitigation.

As engineering geologists and geotechnical engineers, we make almost daily assessments of risk, assessing hazards, likelihoods and consequences. We are used to the concept and application of 'Factors of Safety' and basing our engineering and policy decisions on these.

However in this case, it is clear that certain members of the public did not agree to the 'no risk' option as evidenced through their actions at the site. Threats of prosecution, publicity (Figure 9) and signs warning of the danger (Figure 10) were ineffective and ignored, as was the actual occurrence of further rockfalls following road closure.


Road remains closed

The Thames District council has warned those ignoring the signs that Bluff Road between Matarangi and Rings Beach risk their own safety. The roads have been closed to the public due to safety concerns around slips and anyone trying to remove protective fences is likely to be prosecuted.

Figure 9: Regional Newspaper Article (Waikato Times)**Figure 10: Signage during site work**

Despite the continued rockfalls and clear evidence of danger, even families with young children are willing to take a risk if it will save them a 10-minute detour over the hill instead of around it. Ignoring the signage and barriers infers that the public made their own assessment of risk every time they use the road.

At the time of preparing this paper work was starting for a second phase of scaling and removal of the remaining hazardous block(s) and to install a passive mesh retention system so the road can be re-opened as a public footpath. It will remain closed to all but emergency vehicles.

5 CONCLUSIONS

We consider that two lessons can be drawn from this project.

The first is that there is always a risk that conditions exposed in a rock face do not fully reflect those behind it. In this case deeper weathering and alteration of the rock together with the presence of significant unfavourable discontinuities not exposed on the rock face meant that the scope of work to achieve an acceptable degree of safety increased to a point where it was concluded that it was no longer cost effective to continue mitigation works.

Reliance on engineering geological mapping of the exposed rock, with acknowledgement of possible variation, led to the bolt and mesh solution adopted. However unknown and unfavourable discontinuities together with more pervasive alteration than anticipated forced a reconsideration and change in risk management policy.

The second was confirmation that the perception of an acceptable level of risk is very dependent on the view of the beholder and what they stand to lose or gain. In this case the rockfall assessment procedure identified the mechanisms of rockfall, likelihood and threat, and concluded that these were significant. The management of those risks, threats and consequences fell to the Council who are responsible for the protection of the public and ensuring their safety as far as possible on the Council roads. Councils and Engineers have to act in what they consider to be the best interests of the public, and seek cost effective ways of achieving those aims. In this case road closure was adopted but not accepted by the public that it was intended to protect.

What the authors have taken from this is that you cannot underestimate the willingness of people to put themselves at risk if they consider the advantage gained (even minor) outweighs the likelihood of an adverse and unacceptable outcome.

6 ACKNOWLEDGEMENTS

The authors wish to thank Thames Coromandel District Council for their permission to prepare this paper.

REFERENCES

Australian Geomechanics Society (2007) Practice Note Guideline for Landslide Susceptibility, Hazard and Risk Zoning for Land Use Planning. *Australian Geomechanics*, Vol42 No1 March 2007.

New Zealand Geological Survey (1976) *Geological Map Sheet N40, Northern Coromandel*. 1:63,360 scale.

Transit New Zealand (2004) *Risk Management Process Manual*. AC/Man/1, Version 3.

Waikato Times, 30th December 2016.

Counterfort drains – design, installation and long-term performance in soils of Greater Auckland

S L Price
Riley Consultants Ltd, Auckland, NZ
sprice@riley.co.nz (Corresponding author)

N R Fitch
Riley Consultants Ltd, Auckland, NZ
nfitch@riley.co.nz

Keywords: counterfort drains, buttress drains, trench drains, long-term drain performance

ABSTRACT

Counterfort drains provide a method of improving slope stability by controlling groundwater levels via subsurface drainage; they can provide significant improvement to stability at moderate cost. Published information on the design, initial effectiveness and, importantly, the long-term performance of such drainage is limited, particularly in New Zealand soils. In the current and near future regulatory environment, the long-term performance and associated maintenance requirements of counterfort drains are a key aspect in evaluation of their suitability to a particular site and the level of risk acceptable to the designer, landowner, and territorial authority.

This paper provides comment on the design, installation, and maintenance of counterfort drains in the upper North Island, and observations of short-term measured groundwater levels following drain installation against design expectations from previous published information (e.g. Fitch 1990). Assessment is also made of long-term drainage performance based on monitoring at several sites, with regular monitoring at one site for 17 years, which shows ongoing satisfactory performance in Waitemata Group and Northland Allochthon soils.

1 INTRODUCTION

Counterfort drains, also known as buttress or trench drains, provide a method for improving slope stability through controlling groundwater pressures by subsurface drainage. They typically comprise trenches up to 6m depth, with a perforated pipe at the base, backfilled with suitable free-draining material. Where appropriately designed and constructed, they can provide significant improvement to site stability at moderate cost. However, with deep excavations in often marginally stable ground, construction difficulties are not uncommon.

Published geotechnical-specific information on design, initial effectiveness and, importantly, long-term performance is limited, particularly in New Zealand soils. Short to long-term monitoring by Riley Consultants Ltd (RILEY) of several sites in the greater Auckland area, through which counterfort drains have been installed, allows an assessment of design, effectiveness and performance comparison to be made with previous published information on counterfort drain performance in Auckland soil (Fitch 1990).

The long-term performance and associated maintenance requirements of counterfort drains is a key aspect in evaluating their suitability to a particular site and the level of risk acceptable to the designer, land owner, and territorial authority.

The following information is primarily suitable for residual fine-grained soils, derived from weathering of Waitemata Group deposits and Mangakahia Complex soils of the Northland Allochthon.

2 STABILITY IMPROVEMENT CONCEPT AND SETOUT

Site stability can be improved by reducing or maintaining satisfactorily low pore water pressures on a potential failure surface. This can be achieved by providing a high permeability preferential pathway to encourage groundwater flow from the surrounding soil. Counterfort drains present a significant surface area for drainage to occur (compared with bored drains or wells) and are typically constructed at regular spacings parallel to the slope gradient.

Counterfort drains can reduce groundwater from normal seasonal levels and storm peaks, whilst maintaining these lower levels (Cornforth 2005). Given the size of counterfort drains relative to many other drainage types, along with suitable design and construction, long-term performance with minimal degradation and maintenance is possible.

Whilst counterfort drains are typically constructed parallel or sub-parallel to the slope gradient (i.e. orthogonal to slope contour), they can be constructed across the slope as 'interceptor drains', often at or near the landslip headscarp to intercept subsurface groundwater flow into the affected area. Interceptor drains can be extremely effective in draining a slip feature (Cornforth 2005) and provide enhanced shear resistance across the failure surface. However, excavation across the slope can remove support from above and potentially compromise stability below due to reduction in compressional or tensile restraint, and possibly increase water ingression if not designed and constructed correctly. Due to the risks inherent with interceptor drains, these are rarely seen on current stability improvement works in the greater Auckland area, with conventional counterfort drains orthogonal to contour preferred.

Counterfort drains are most suitable for relatively shallow slips typically up to 6m depth, where trench excavation can reach the primary failure surface. Deeper drains are possible, however, these often require major earthmoving and have significant collapse risks. Counterfort drains are also most effective in gentle and moderate dipping slopes where instability can be driven by relatively large groundwater pressures, thus the drains can have a significant effect.

The depth of influence for counterfort drains can be extended below the base by bored drains (e.g. gravel-filled wells or wick drains) from the base of the trenches down to identified surfaces or zones with elevated groundwater pressures, which will drive the water upward into the trench.

3 TYPICAL DETAIL

Counterfort drain typical detail, as specified by RILEY, has changed little over the past 25 years. A cross section is presented in Figure 1. Key changes include the 110mm Novaflo pipe, now specified as 'heavy wall', and a Transit New Zealand F/2 drainage metal specified compared with a previous scoria material from Three Kings Quarry.

With counterfort drains in the Auckland area often excavated through fine-grained soils there is a risk of soil migration into the drainage medium leading to eventual clogging and significant reduction in the drain performance. To minimise the chance of this occurring, an all-passing drainage medium with significant fines content (sand) is required. Gap-graded materials, such as 20/40 are not specified and are liable to rejection on-site due to their poor filter suitability.

Use of a high-quality drainage aggregate with sufficient fines content to act as a suitable filter negates the need for a filter fabric wrap within the trench or wrapping the Novaflo, although if the contractor wishes to use a filter sock on the perforated collection pipe this is allowed (design criteria are available relating to the required hole size to prevent excess ingress of fines fraction of the drainage material). This approach avoids unnecessary risk with time involved placing a filter cloth in trench excavation of dubious stability.

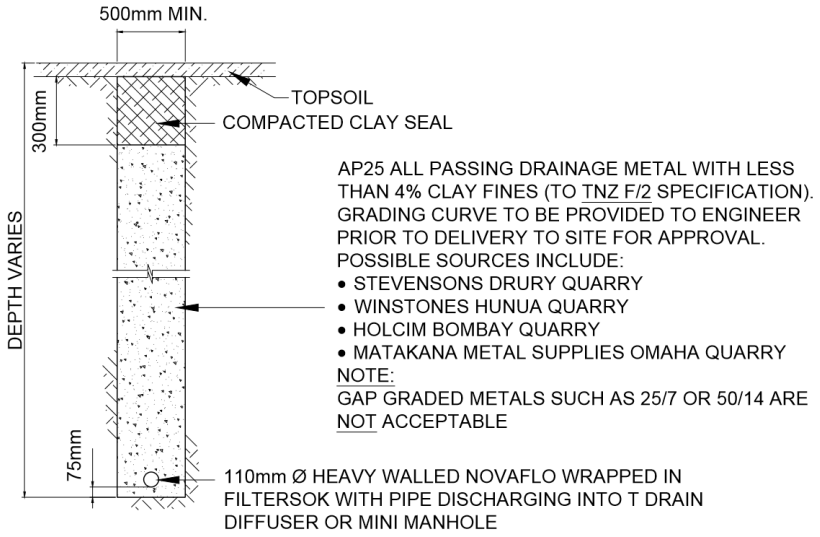

Figure 1: Current typical counterfort drain detail adopted by RILEY

4 DESIGN

4.1 Theory

Drainage design based on theoretical evaluation can be found in several published papers around the world (e.g., Hutchinson 1977, Stanic 1984, and Bromhead 1992) to determine drainage spacing and effective groundwater drawdown. These semi-empirical methods are still in use today (e.g. Cornforth 2005 and MacDonald et al 2012). Following monitoring of counterfort drain performance on two road cuts in England, it was recommended for design allowance of peak water levels 1.5m above the theoretical curve of Hutchinson (MacDonald et al 2012). These methods often assume infinite slope-type situations, homogeneity of the soils, and isotropy. In some cases, estimates of vertical and horizontal permeability are required along with soil porosity. Often these values are not available to the designer, but can be estimated, however, fissuring in Auckland soils can make permeability estimates problematic.

Experience shows there is little justification in a precise mathematical solution because of the wide differences possible between idealised assumptions and actual field conditions (Fitch 1990). A notable recommendation of Stanic (1984) is that the ratio between drain spacings and their depth below the original groundwater level should not be more than 4:1 (e.g. if the drains penetrate 5m below the pre-drain groundwater level they should not be spaced more than 20m apart).

A key design target is to intercept the assessed principal failure surface, if possible, to directly relieve water pressure on this surface. Often the surface will be acting as an aquitard and excavation to and through the surface will tap groundwater pressure.

4.2 Practical experience

Based on empirical evidence gathered by these authors, for residual Waitemata Group soils, and other fine-grained soils in the Auckland area, we consider the figures in Table 1 provide a reasonable approximation for drain performance. Monitoring to date has shown the predicted average depths to groundwater of Fitch (1990) to be accurate, noting these are average depths and peak water levels can rise higher.

Table 1: Predicted average depth to groundwater following counterfort drain construction based on measured performance in greater Auckland soils (modified from Fitch 1990)

Drain depth (m)	Drain Spacing (m)	Approximate average depth to groundwater level* (m)
2	5	1.5
2	10	1.0
4	10	3.0
4	15	2.5
5	15	3.0
5	20	2.5
6	15	4.0
6	20	3.5

* Depths to groundwater are averages, and can be higher at the midpoint between the drains. For brief a period during storm events, groundwater can rise approximately 1m above stated levels.

Groundwater levels up to 1.5m above theoretical were measured between counterfort drains on a road cut in England however, instability did not result This is believed to be a result of direct drainage of the failure surface and possible reinforcing effect of the drains (MacDonald et al 2012).

4.3 Other Considerations in Design

In the subdivisional situation, attention needs to be paid to the location of future building platforms, as deep drains can significantly affect foundation design and construction of future structures spanning over or in proximity to the drains, and also allow access for drain maintenance. Often, if lot boundaries are close enough and suitably orientated, the drains are aligned with boundaries. Location of the drains on boundaries can present issues with respect to ownership and fence construction, thus careful consideration is required.

5 CONSTRUCTION

With drains typically excavated below the groundwater table they are usually built in an uphill direction from the outfall. Due to contractor preference, sometimes these are undertaken in a downslope direction, with, in the authors' experience, mixed results.

Only a short length of trench should be open at any one time, with equipment and materials co-ordinated to prevent delays. This will reduce the risk of cave-ins occurring, however, during deeper excavations without support, such collapse will likely occur and the contractor should be made aware of this and take appropriate safety precautions. Methods to minimise the risk of collapse are hydraulic propping, trench shields, and the use of multiple excavators, all with cost implications and not always successful. As personnel need not enter the excavation, the safety responses are typically not to the same level as for excavations requiring manned entry.

Where groundwater levels are high and soils are potentially susceptible to collapse, counterfort drain construction can be problematic with collapse into the trench and insufficient time to properly backfill. This can result in ground being improperly backfilled, resulting in non-specific design foundations for future structures. To reduce this risk, initial dewatering can be undertaken by less hazardous methods, such as bored drains, directional drains, and well point drainage, with counterfort drain construction then undertaken during the summer earthworks period.

It is important to undertake regular inspection from the surface of the exposed trench side walls during excavation to evaluate whether the encountered ground conditions are consistent with that expected, and whether the design requires modification to intercept potential aquifers. Due to the nature of the construction, this may require an engineer's representative to be on-site for significant periods of time.

TNZ F/2 drainage metal is only produced at a few of the quarries that service the Auckland area and is often relatively expensive, thus there is often pressure from contractors to use a more readily available and cheaper aggregate. Gap-graded drainage metals should be avoided, with all-passing materials preferred, however, none of the usual products are ideal as they are either too coarse (with respect to retention criteria) or contain too many fines (silt and clay). The selection of a suitable drainage aggregate should be site-specific to the expected ground conditions. As a general guideline, fines (75µm or less) should be <5% with the D15 suitable for the excavated soils.

To avoid issues with the forming of wells from the base of trenches in potentially unstable counterfort drain excavations, wells can be drilled first and connected by later counterfort drain construction.

6 HISTORIC MONITORING OF COUNTERFORT DRAIN PERFORMANCE

The long-term performance of counterfort drainage, along with practical maintenance requirements, is key to acceptance as long-term solutions by designers, landowners, and territorial authorities. Recently, territorial authorities have rarely required long-term or even short-term monitoring of drainage performance to prove acceptable performance, provided the design engineer can demonstrate the drainage will produce an acceptable result based upon site-specific assessment and performance in similar sites in the past. However, concerns have recently been raised in some materials (e.g. Northland Allochthon) whether counterfort drains alone are sufficient. Presented below are performance results for counterfort drains from sites in Waitemata Group and Mangakahia Group soils. It is important the monitoring period before and after drain installation be as long as possible to record the response to a range of rainfall events.

Groundwater levels are usually monitored by standpipes or piezometers installed in separate hand or machine auger boreholes. Vandalism, and damage from mowing equipment or construction is a problem for long-term monitoring sites. It is important that a device is installed in the piezometers to record maximum groundwater levels as these often occur within a 24 hour period of a storm event, when it is unlikely someone will be on-site.

6.1 Orewa – Waitemata Group soils

Monitoring has been undertaken at a site on Waitemata Group soils in Orewa since 1999 in response to ground movement that occurred in 1998, following earlier movement in 1979. Monitoring has mostly been hand dipping at regular intervals, however, higher frequency monitoring was undertaken along with installation of maximum water level recorders to verify monitoring results immediately prior to, during, and following the counterfort drain construction in 2001. The inferred depth of failure was 5m to 6m, beyond practical construction depth in these collapsible soils, however, loose sandy horizons with elevated groundwater pressures were noted between 3m and 5m and targeted for drainage. The target of the installation was to improve stability of the land to reduce risk to the land owner, rather than development. Figure 2 presents a summary of long-term monitoring results from 1999 to 2016.

High frequency piezometer monitoring indicates groundwater levels rise within 24 hours of any significant rainfall event. Whilst long-term groundwater levels are generally below 3m, water levels do spike in response to heavy rainfall, rising to between 1m and 3m of ground surface

producing an evaluated FoS of approximately 1.3 for the site under transient storm conditions. No obvious reduction in performance of the counterfort drains has been detected over 15 years of operation.

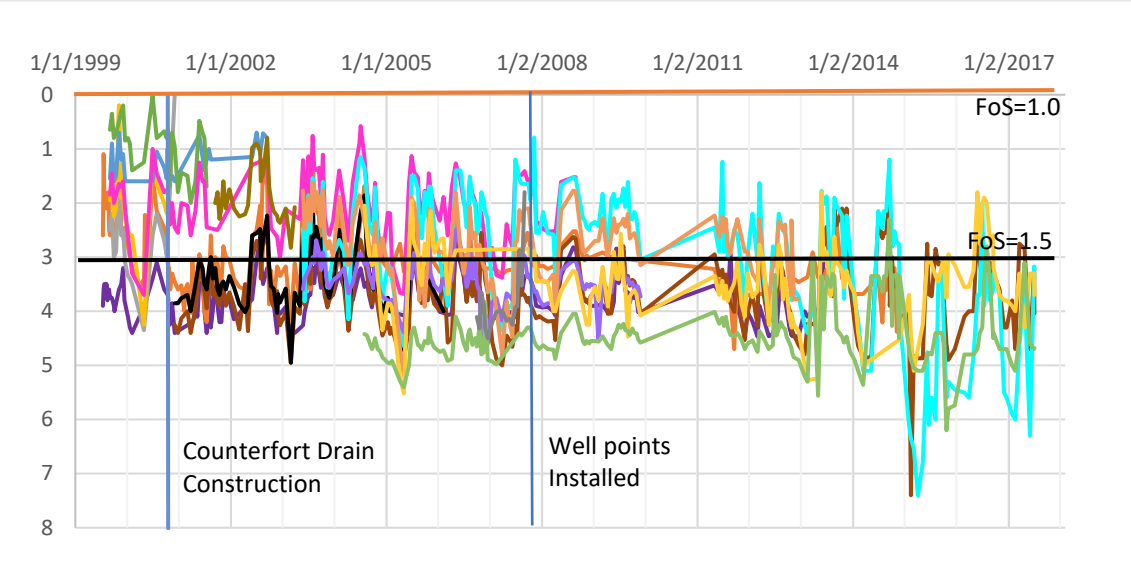

Figure 2: Summary of recorded groundwater level results from multiple piezometers across the site, prior and following counterfort drain construction from 1999 to 2017 in Waitemata Group soils, Orewa, Auckland

6.2 Hillsborough – Waitemata Group soils

Counterfort drains were excavated through weak and saturated ground between 4m to 5m depth and 10m spacing. Groundwater level monitoring was undertaken over a period of approximately 10 months; results are presented in Figure 3. Groundwater levels were maintained at a sufficient depth to achieve a minimum Factor of Safety (FoS) of 1.5 and was discussed in Fitch (1990).

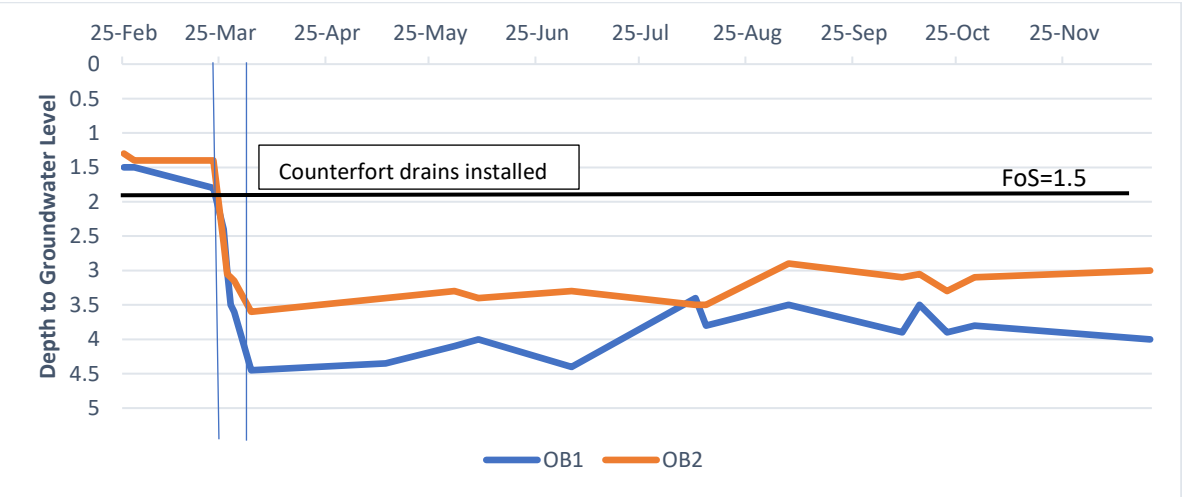

Figure 3: Summary of groundwater level results prior, during and following counterfort drain installation in Waitemata Group soils, Hillsborough, Auckland

There have been permanent dwellings constructed on the stabilised ground for a period of 27 years. A recent review, whilst not feasible to replicate the above data, indicates satisfactory land stability performance.

6.3 Waipu – Mangakahia Group, Northland Allochthon

Investigations for a proposed residential subdivision in Waipu (Northland) encountered Northland Allochthon sheared mudstones and weathered products (Mangakahia Group) subject to inferred ancient instability and evaluated as having an inadequate FoS for residential development under extreme conditions. Localised artesian water pressures were encountered above the soil-rock interface. Proof of concept was undertaken with trial counterfort drain installation in 2003 to maximum 4m depth, penetrating the soil-rock interface. Results of groundwater monitoring immediately prior and post-drain construction are presented in Figure 4. Following this trial, a more extensive array of counterfort drains was constructed.

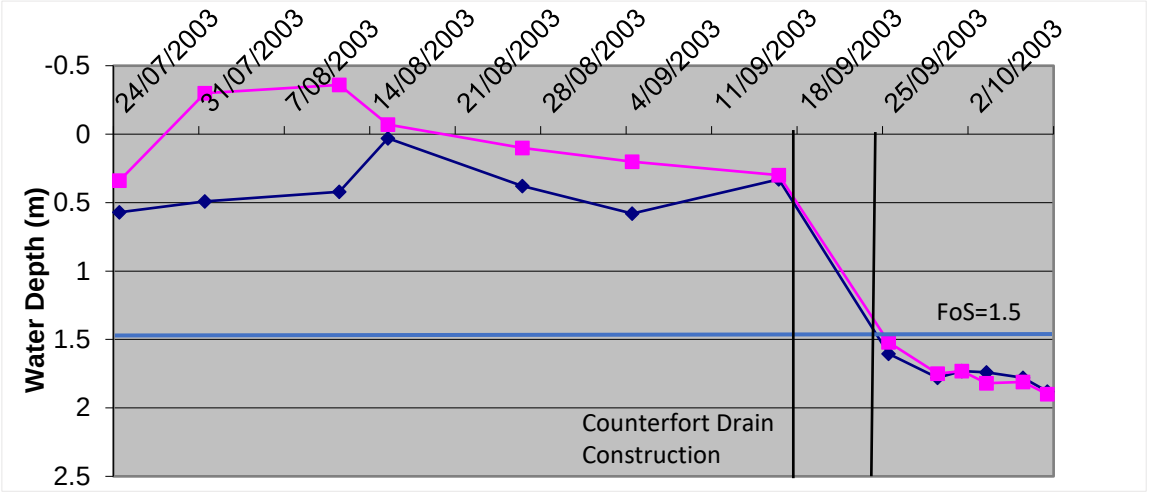

Figure 4: Summary of recorded groundwater levels prior, during, and following counterfort drain construction in Northland Allochthon materials, Waipu, Northland

The trial drain performance was reviewed in 2015 with installation of electronic logged piezometers. The recorded water levels in HA2 were relatively uniform, possibly indicating an issue with the piezometer or lack of penetration to water-bearing strata. However, this piezometer was constructed identical to the previous two in 2003 and also HA4 at the same time (which provided responses). In addition, HA2 extended to rock with groundwater typically encountered perched above the rock on a clay surface. Consequently, it is considered the monitoring results indicate satisfactory long-term performance of the drains. Results are presented in Figure 5.

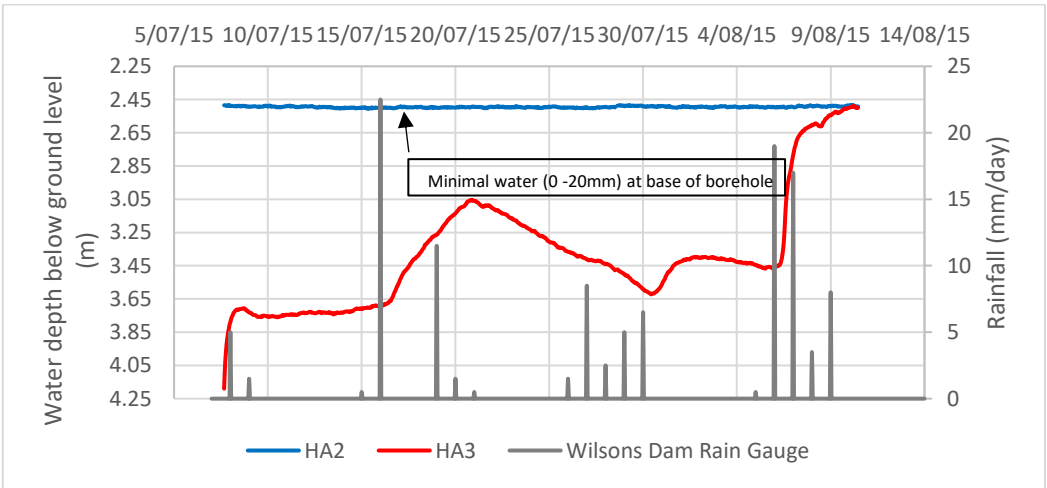

Figure 5: Summary of recorded groundwater levels during winter 2015 with HA2 (blue) within the influence zone of the drains and HA3 (red) outside the assessed key influence zone (some 20m from the nearest drain)

7 MAINTENANCE

Counterfort drains are considered relatively minimal maintenance items if constructed as outlined. The inclusion of a flushing point at the upstream end of the drain along with access from the outlet allows flushing of the drains, which is recommended on a five-yearly basis. However, with respect to the monitoring results presented in this paper, no flushing of the drains or any other regular maintenance has been undertaken.

8 CONCLUSIONS

Counterfort drains are a proven effective method to achieve slope stability improvement on sites with high groundwater levels. Typically, counterfort drains are most suitable to sites of gentle to moderate slopes, with perched groundwater and failure surfaces within 5m of ground surface. Drain spacing and depth is best assessed by a combination of analysis and practical experience. Precise mathematical solutions are not justified due to likely wide differences between idealised and actual field conditions. The drains should penetrate the failure surface.

Long-term monitoring at three sites, two in Waitemata Group soils and the third on Northland Allochthon, indicate no obvious deterioration in counterfort drain performance over the monitoring period (up to 15 years) where drains are constructed consistent with the typical design provided using a filter material similar to the TNZ F/2 envelope. Average groundwater levels as per design expectations have been recorded.

Required maintenance of well-constructed counterfort drains is minimal, however, flushing is recommended on a five-yearly basis.

REFERENCES

Bromhead, E.N. (1992). The Stability of Slopes, 2nd Edition. 242p; Taylor & Francis, London, New York.

Cornforth, D.H. (2005). Landslides in Practice – Investigation, Analysis and Remedial/ Preventative Options in Soils, John Wiley & Sons Inc, Hoboken.

Fitch, N. R. (1990). Ground Stabilisation with Counterfort Drains – Design, Installation and Monitoring of Drawdown Performance. *Proceedings NZ Geomechanics Society*, 16 1(G), 97-101.

Hutchison, J.N. (1977). Assessment of Corrective Measures in Relation to Geological Conditions and Types of Slope Movement. *Bulletin of the International Association of Engineering Geology.* No. 16:131-155, Springer, Berlin Heidelberg.

Stanic, B. (1984). Influence of Drainage Trenches on Slope Stability. *Journal of Geotechnical Engineering,* 110(11):1624-1636; American Society of Civil Engineers, Reston.

McDonald, G.J., Vooght, A.R., and Parkin, S. (2012). The use of deep counterfort drains as an effective method of stabilizing cuttings constructed in overconsolidated clays. *Earthworks in Europe*. Geological Society, London, p.115-124.

Elastic soil-structure interaction – is it worth the effort?

M J Pender
Department of Civil & Environmental Engineering, University of Auckland, NZ.
m.pender@auckland.ac.nz (Corresponding author)

Keywords: Shallow foundation, multi-storey buildings, soil-structure-interaction, SSI, cohesionless soil, EQ response spectrum, single degree of freedom model, SDOF.

ABSTRACT

It is widely acknowledged that soil-structure interaction (SSI) has an important effect on foundation performance during earthquake loading. The standard way of handling this is to assume elastic behaviour of the soil beneath and around the foundation. For shallow foundation response there are three dimensionless parameters which indicate the effect of SSI. These are functions of six properties of the structure-foundation system: the shear wave velocity and density of the foundation soil, the natural frequency of the fixed base structure, the height of the structure, the mass of the structure, and the dimensions of the foundation. However, elastic soil behaviour occurs only at very small shear strains. For realistic foundation proportions the effect of elastic soil-structure-interaction (SSI) is frequently quite small and so the response of the foundation is only marginally different from the fixed base response; the purpose of the paper is demonstrate this. The paper explains that real foundation designs involve larger shear strains than those for elastic behaviour over a substantial volume of soil beneath the foundation and so to achieve enhanced foundation performance from interaction with the soil below it is important to consider nonlinear soil behaviour. Nonlinear soil behaviour is approximated using a reduced shear modulus, the effect of such reduction is discussed.

1 INTRODUCTION

It is widely acknowledged that soil-structure interaction (SSI) has an important effect on foundation performance during earthquake loading. The standard way of handling this is to assume elastic behaviour of the soil beneath and around the foundation. Consideration of an earthquake design response spectrum, such as that shown in Figure 1, illustrates how SSI induced period lengthening of the system may reduce structural design actions if the periods concerned are located along the falling branch of the design spectrum.

Wolf (1985) and others have shown that there are three dimensionless parameters which indicate the significance of elastic SSI. These are functions of six properties of the structure-foundation system: the shear wave velocity of the foundation soil, the density of the foundation soil, the natural frequency of the fixed base structure, the mass of the structure, the height of the structure, and the dimensions of the foundation. The dimensionless quantities are the stiffness ratio (SR), the slenderness ratio (HR) and the mass ratio (MR):

$$SR = \frac{\omega_e h_e}{V_s} \qquad HR = \frac{h_e}{a} \qquad MR = \frac{M_e}{\rho a^3} \tag{1}$$

where: M_e is the mass of the structure supported on the foundation, a is the radius of a circle having the same area as the foundation, h_e is the height above foundation level of the centroid of the structural mass, ρ is the density of the soil, V_s is the shear wave velocity of the soil, and ω_s

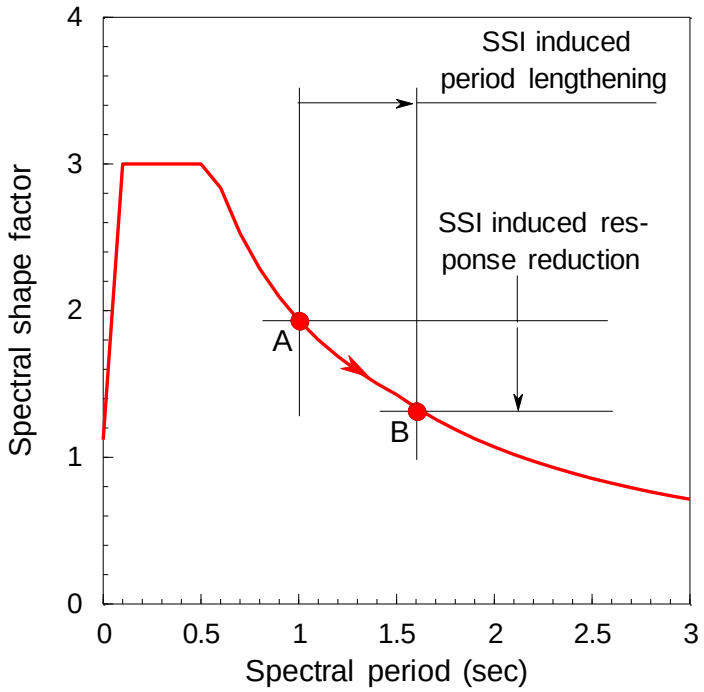

Figure 1: Potential beneficial effect of soil-structure interaction when the period of the fixed base structure is located along the falling branch of a design spectrum

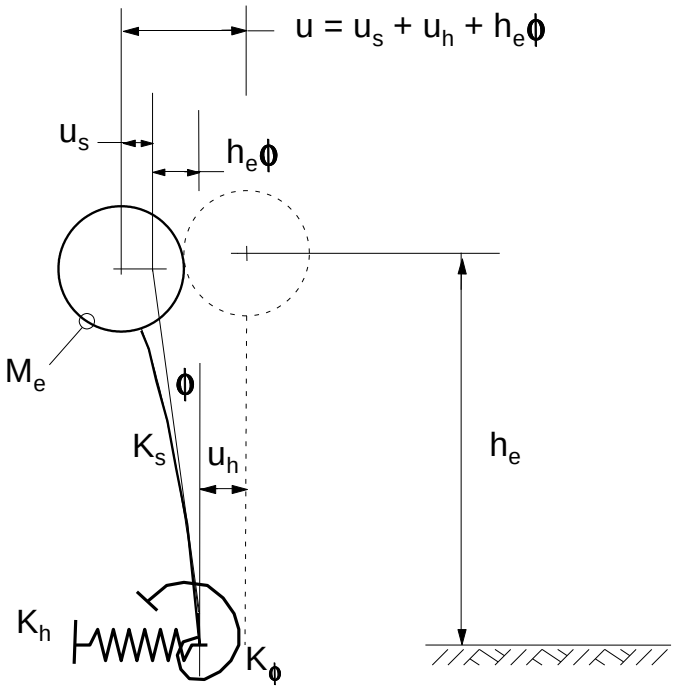

Figure 2: Single degree of freedom (SDOF) model of a structure-foundation system with a concentrated mass, M_e located h_e above the foundation, and three springs (K_s, K_h and K_ϕ)

is the natural frequency (radians/second) of the fixed base structure. Note that the shear wave velocity is a property of the soil at very small (ie elastic) shear strains.

The stiffness ratio compares the elastic stiffness of the fixed base structure to the elastic properties of the foundation soil. The slenderness ratio is a geometric parameter comparing structural and foundation dimensions. The mass ratio can be thought of as the mass of the structure in relation

Table 1: Soil layer properties 4 m beneath the ground surface

Soil density state	Shear wave velocity (V_s) (m/sec)	Density (ρ) (tonnes/m^3)	Small strain shear modulus (G_o) (MPa)
Loose (L)	160	1.70	44
Medium (M)	210	1.85	82
Dense (D)	250	2.00	125

to the mass of a volume of soil beneath the foundation which contributes to the foundation stiffness; as this ratio decreases the inertia of the foundation soil becomes more significant.

Frequently, a single degree of freedom (SDOF) model is used to represent to the first mode response of a structural system. Such a model is shown in Figure 2 in which a concentrated mass M_e represents the mass of the structure; a column, height h_e, represents the lateral stiffness, K_s, of the structure; a spring, stiffness K_h, represents the lateral stiffness of the foundation; and a spring, stiffness K_ϕ, represents the rotational stiffness of the foundation. Figure 2 shows how the lateral displacement of the mass consists of three components: the bending of the structural column, h_e times the rotation of the foundation, and the lateral displacement of the foundation. The natural frequency of such a model (readily established with a pushover analysis) is given by:

$$\omega_e^2 = \frac{\omega_s^2}{1 + \frac{K_s}{K_h} + \frac{K_s h_e^{\,2}}{K_\phi}} \qquad T_e = \frac{2\pi}{\omega_e} \tag{2}$$

where: ω_e and ω_s are respectively the natural frequencies of the elastic structure-foundation system and the fixed base structure (radians / second),
T_e is the period of the elastic structure-foundation system,
K_s is the flexural stiffness (elastic) of the column supporting the SDOF mass,
K_h is the elastic lateral stiffness of the foundation,
K_ϕ is the elastic rotational stiffness of the foundation,
and h_e is the height above foundation level of the SDOF lumped mass (M_e).

When an SDOF model is developed for a structure having uniform dimensions and distribution of mass with height, it is found from structural dynamics that the first mode frequency is obtained by setting M_e to about 70% of the total mass of the structure and h_e to about 70% of the height of the structure, Chopra (1995).

The purpose of this paper is to present the results of a small parametric study of the effect of shallow foundation soil-structure interaction when the structure and foundation behave elastically. Three sets of parameter values are explored. First, the building plan dimensions: 8x8 m, 16x16 m and 32x32 m. Second, building heights: 2, 4, 8, 12, 16 and 20 storeys and one level of basement the base slab of which forms a rigid raft foundation. The storey height is 3.5 m and the depth to the underside of the basement depth is 4 m. Third, the soil: a deep layer of loose, medium, and dense cohesionless sand or gravel with a horizontal ground surface.

The 32 m square plan dimension is representative of many multi-storey buildings, the 16 m square plan dimension is suggestive of a slim structure on a constrained site. The unlikely 8 m square plan dimension is used here to illustrate the effect of structural stiffness.

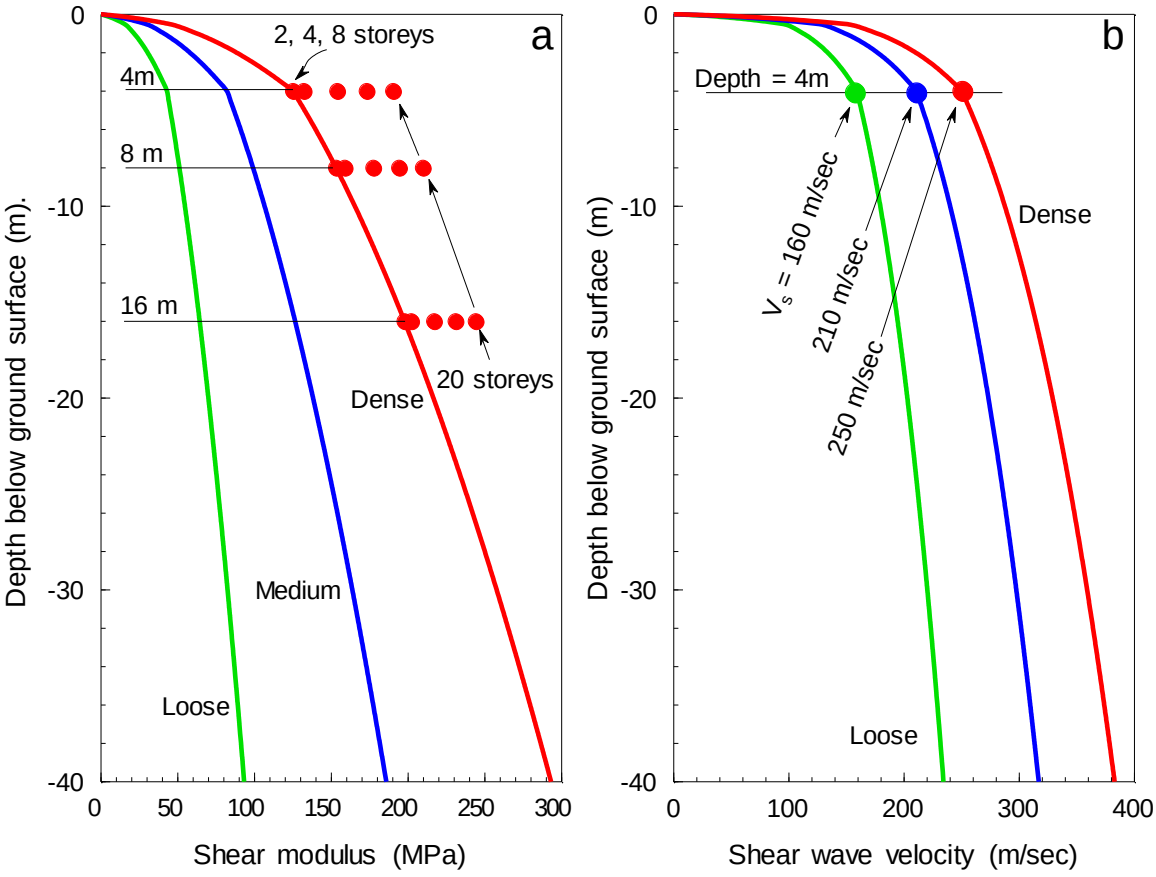

Figure 3: Small strain shear modulus and shear wave velocity variation with depth: (a) shear modulus profiles including the contribution from building weight to the dense profile modulus at depths of 4, 8 and 16 m, (b) level ground shear wave velocity profiles

2 SOIL PROFILE

The soil properties are specified with the shear wave velocity and density at a depth of 4 m. The deep sand/gravel layer is assumed to have permeability such that the response of the foundation is drained (that is there is no consideration of liquefaction of the cohesionless soil). The water table is at a depth of 4 m below the ground surface. Three sets of values are used to represent loose, medium, and dense soils. Property values are shown in Table 1 for a depth 4 m beneath the ground surface. Having the shear wave velocity and density at a depth of 4 m the small strain shear modulus is obtained from ρV_s^2. It is well known that soil moduli are a function of the square root of mean effective stress, Ishihara (1995). Thus, the shear wave velocity is a function of the fourth root of the mean effective stress. As the effective stress increases with depth below the ground surface, the shear wave velocity and small strain shear modulus will also increase with depth. The calculated distributions, anchored to the shear wave velocity values at a depth of 4 m for the loose, medium, and dense soil deposits, are shown in Figure 3b.

3 FOUNDATION AND STRUCTURE STIFFNESS VALUES

Referring to Figure 2 and equation 2, it is apparent that we need the fixed base natural frequency of each structure (ω_s), the flexural stiffness of column supporting the mass (K_s), the lateral stiffness of the foundation (K_h), and the rotational stiffness of the foundation (K_ϕ). Once we have these we can use equation 2 to calculate the natural frequency and from there the natural period of the elastic structure-foundation system.

First, the mass of the structures is obtained by assuming a uniform floor loading of 8 kPa (includes permanent and imposed loads).

Second, an equation which gives ω_s comes from the commentary to NZS1170.5 (SANZ 2005) where relationships are given for a range of structural types, all of which are a function of the height of the building. For the calculations discussed herein the period for eccentrically braced steel frame structures is used (1170.5 also gives similar equations for other structural forms):

$$T = 0.06h^{0.75} \qquad \omega_s = \frac{2\pi}{T} \tag{3}$$

where: T is the fixed base structural period (seconds), and h the height of the structure (metres).

Third, the lateral and rotational stiffnesses of the foundation are required. The square root modulus distributions in Figure 3a apply for the soil beneath a horizontal ground surface. The soil beneath the building foundation has additional stresses due to the weight of the structure so the soil modulus distribution will be complicated, varying both with depth and lateral extent. Herein one point beneath the foundation is used to give a representative value of the modulus of the soil for the whole foundation. Schmertmann (1970) proposed that during settlement of a shallow foundation on sand the maximum vertical strain occurs at a depth of half the foundation width. Burland and Burbidge (1985) found that the depth of influence for the settlement of shallow foundations on sand and gravel is a little more than half the foundation width. Using these ideas as guidance, it was decided to use the soil modulus at a depth of half the foundation width beneath the centre of the foundation as a representative value when estimating the foundation horizontal and rotational stiffnesses – this is the reason for the horizontal lines marking depths of 4, 8 and 16 m in Figure 3a. Additionally it is necessary to allow for the increase in vertical stress in the soil beneath the foundation because of the weight of the buildings. Assuming that the weight of the building is applied to the foundation as a uniform vertical pressure, the increase in vertical stress beneath the centre of a square foundation at a depth of half the width is very close to the applied pressure, Harr (1966). With this information the representative soil modulus beneath the foundation can be updated and it is now a function of the number of building storeys, as shown in Figure 3a for the dense profile (similar behaviour was calculated for the loose and medium profiles). The lateral and rotational stiffnesses of the foundation were calculated using the equations given by Gazetas (1991) which account for the shape of the foundation and the effect of embedment. Similar stiffness expressions are given in the NIST (2012) document.

4 RESULTS

Having the stiffness values for the structures and the foundations we can estimate what benefits will be obtained from SSI effects. The first step is to use equation (2) to obtain the period of the structure-foundation system incorporating SSI effects. Next the Spectral Shape Factor curves in NZS1170.5:2004 (SANZ 2004) are used to get comparative values of the earthquake design spectral accelerations (these curves are associated with a notional damping coefficient value of 5%). The ordinate in the NZS1170.5 curves gives a value which is multiplied by a hazard factor, a return period factor, and a near-fault factor to give the earthquake design spectral acceleration at a specific site location. But, for the work reported in this paper, comparing values for the spectral shape factor is adequate. Referring to Figure 1, comparison of the points marked A and B is used to obtain the SSI period lengthening and the reduction in the spectral shape factor. These changes are normalised with respect to the values associated with point A. Figure 4 shows the period elongation, expressed as a ratio of the value at point A, in moving from point A to B in Figure 1. Figure 5 has a similar plot, but this time the ratio given is that of the spectral shape coefficient values for the NZS 1170.5 Shallow ground curve. In both Figures 4 and 5 there is a reduction in the spectral shape coefficient because the fixed base structural period is positioned along the falling branch of the spectral shape coefficient curve.

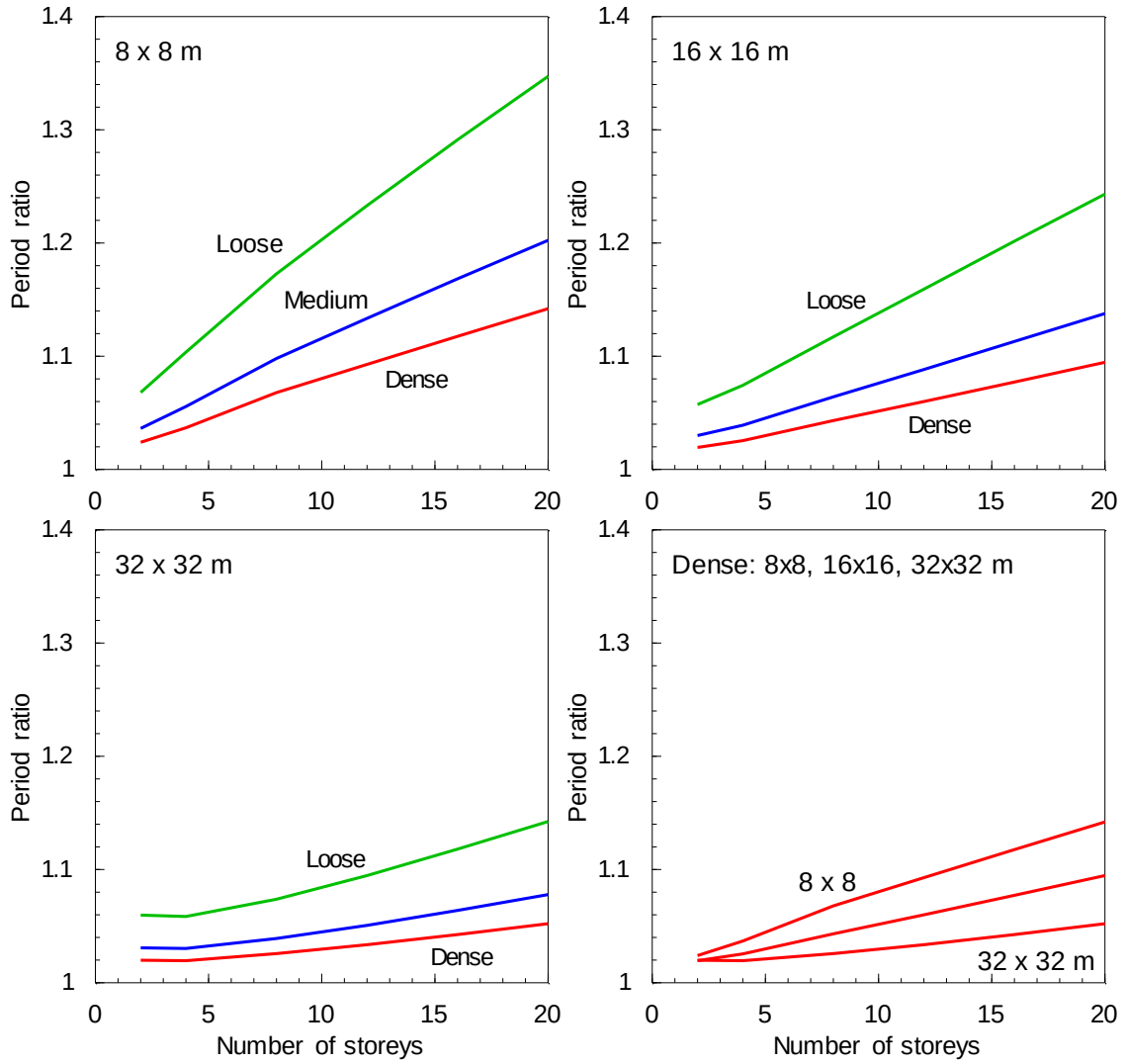

Figure 4: SSI induced period lengthening, expressed as a ratio of the SSI period to the fixed base period, for the various building configurations and ground conditions

5 DISCUSSION

Unsurprisingly the various parts of Figures 4 and 5 show that the loose soil deposit (V_s = 160 m/sec) has the greatest period elongation and reduction in spectral shape coefficient. It is apparent that, for the medium and dense soil conditions, the period lengthening is significantly less. Again, unsurprisingly, the smallest foundation demonstrates the largest SSI modifications to response.

We will limit our considerations to the buildings with 16 and 32 m square plan dimensions as an 8 m square tower 20 storeys in height is not a serious building configuration (but might be part of a guyed chimney or radio mast). A 32 m square tower would be representative of many typical buildings and 16 m square tower perhaps representative of the slim end of the range of typical structures. Furthermore, it is unlikely that a shallow foundation on loose sand would be considered for a tall building. Thus we are left with 16 and 32 m square building plan dimensions with shallow foundations on medium and dense soil. For these configurations Figures 4 and 5 show that even for the tallest buildings, elastic soil-structure interaction has only a minor contribution to the performance of the structure-foundation system.

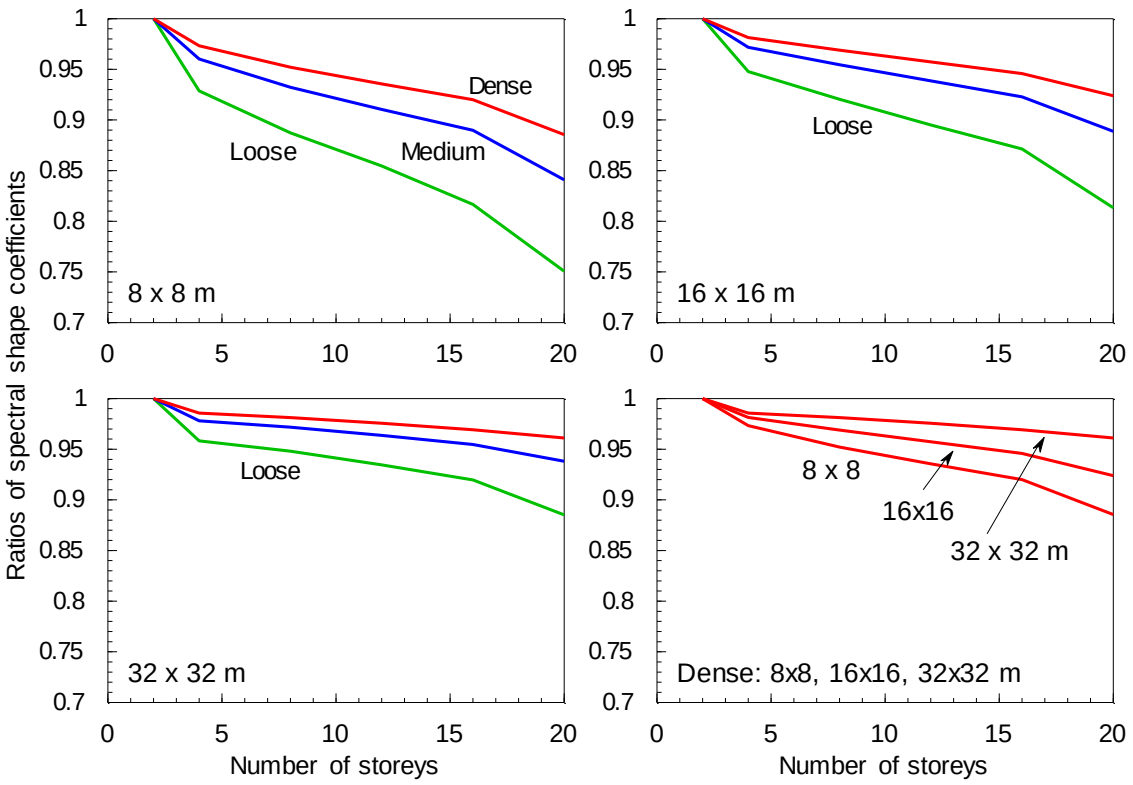

Figure 5: SSI induced reduction in the spectral shape coefficient, expressed as a ratio spectral shape coefficients from NZS1170.5 shallow site condition, for the various building configurations and ground conditions

Figures 4 and 5 were derived for the Shallow soil spectral shape coefficient curve in NZS1170.5, similar conclusions are reached when the Deep soil curve is used.

However, it is expected that soil beneath a shallow foundation will not remain elastic during a design earthquake and nonlinear deformation will take place with an effective reduction in the soil modulus. Table 4.1 in Part V of Eurocode 8 (BSI 2005) gives suggestions for this reduction with respect to the earthquake peak ground acceleration. For a PGA of about 0.3g it is suggested that an equivalent modulus about one third of the small strain value be used. Referring to Table 1 it is apparent that such a reduction would reduce the small strain stiffness of the dense soil to about the value for the loose material. Looking again at the lines for loose behaviour in Figures 4 and 5 it is apparent that nonlinear soil behaviour might provide a 15 to 20% reduction in foundation actions when tall 16 and 32 m square structures are subject to a modest earthquake.

Evaluating, and plotting against number of storeys, the values for the three dimensionless parameters given in equation (1), no additional insight is obtained. The values of all three parameters increase as the number of storeys increases. The structures with the 8 m square plan dimension with foundations on loose soil having the largest values for all three parameters, and the 32 m square plan dimension buildings with foundations on dense soil having the smallest values.

An important factor not considered above is the effect of damping on soil-structure interaction. Increasing damping, caused by hysteretic soil deformation, will move the design spectrum in Figure 1 downwards, so providing an additional mechanism to reduce design actions. Elastic radiation damping is small for foundation rotational deformation modes, the main foundation deformation mechanism for tall structures on shallow foundations, and so nonlinear soil deformation is important. Part V of Eurocode suggests a hysteretic damping coefficient value of

about 10% when the ground around the foundation is subject to a PGA of about 0.3g. Recent work on nonlinear moment-rotation behaviour of shallow foundations illustrates how rocking (that is cyclic loss of contact at the foundation edges during the earthquake loading) further reduces foundation actions (Pender el al. 2017a and b).

6 CONCLUSIONS

The calculations reported herein show that elastic soil-structure interaction is of negligible benefit for buildings on shallow foundations in medium and dense cohesionless soils, Figures 4 and 5. Thus the answer to the rhetorical question at the end of the title of this paper is negative.

To achieve a soil-structure interaction related improvement in building performance during earthquakes, nonlinear behaviour of the zone of soil around and beneath the foundation is needed to reduce the stiffness of the soil and provide hysteretic damping.

Part V of Eurocode 8 provides guidance for reducing soil stiffness and increasing hysteretic damping as earthquake peak ground acceleration increases. This provides an approximate simplified way to handle the complexities of the nonlinear cyclic stress-strain behaviour of soil.

REFERENCES

BSI (2005). BS EN 1998-1:2005: Eurocode 8: Design of structures for earthquake resistance – Part V: Foundations, retaining structures and geotechnical aspects. British Standards Institution, London, UK.

Burland, J. B. and Burbidge, M. C. (1985). Settlement of foundations on sand and gravel. *Proc. ICE,* Part 1, pp. 1325-1381.

Chopra, A. K. (1995). *Dynamics of Structures*. Prentice-Hall, New Jersey.

Gazetas, G. (1991). Foundation vibrations, in *Foundation Engineering Handbook*, 2nd. edition, H-Y Fang editor, Van Nostrand Reinhold, pp. 553-593.

Harr, M. E. (1966). *Foundations of theoretical soil mechanics*. MGraw-Hill, New York.

Ishihara, K. (!996). *Soil behaviour in earthquake geotechnics*. Oxford Engineering Science, Oxford, UK.

NIST (2012). *Soil-structure interaction for building structures*. NIST GCR 12-917-21, National Institute of Standards and Technology, Gaithersberg, Maryland.

Pender, M. J., Algie, T. B., Storie, L. B. and Salimath, R. (2017a). One dimensional moment-rotation macro-element for performance based design of shallow foundations. *Proceedings Performance Based Design III* (PBDIII), Vancouver.

Pender, M. J., Algie, T. B., Storie, L. B. and Salimath, R. (2017b). One dimensional shallow foundation macro-element. In: *Developments in Earthquake Geotechnics*, S. Iai ed. Springer, Singapore.

SANZ (2004).NZS 1170.5: 2004. *Structural Design Actions Part 5: Earthquake Actions* – New Zealand. Standards New Zealand, Wellington.

Schmertmann, J. H. (1970). Static cone to compute static settlement over sand. *Proc. ASCE,* Jnl. Soil Mechanics Div., Vol. 96 SM3, pp. 1011-1043.

Wolf, J. P. (1985). *Dynamic Soil-Structure Interaction*. Prentice Hall, New Jersey.

A risk based assessment to rockfall mitigation

C J Parkes
Opus International Consultants, Christchurch, New Zealand.
Christine.parkes@opus.co.nz (Corresponding author)

Keywords: rockfall, risk, mitigation

ABSTRACT

The Health and Safety at Work Act (2015) requires companies to provide safe working environments for its staff. In response to this, our client sought to identify effective mitigation solutions for a rockfall hazard above an operational access road. The slope consists of a near vertical, 15 m high, cutting into a steep (~35°) natural slope. Below the cut face there is a single lane access road, with the natural slope continuing below. Groundwater seepage near the top of the cut face has resulted in ongoing rockfall, presenting a hazard to staff using the access road. Previous geotechnical assessments had recommended large scale earthworks to reshape the cutting to remove the hazard. This paper presents an alternative risk management approach developed by Opus, identifying the most appropriate mitigation solution. The current level of risk was evaluated (using the AGS Landslide Risk Management Guidelines), and compared with industry standards to determine an acceptable level of life safety risk. By evaluating the relative cost and risk reduction achieved for feasible mitigation solutions, a proportional cost and acceptable risk based solution was identified. This paper focuses on how the rockfall risk was effectively assessed, managed and communicated with our client.

1 INTRODUCTION

Opus International Consultants Ltd (Opus) were engaged to undertake a site inspection, risk assessment and recommend mitigation options for an active rockfall site on an operational access road near Waipara in North Canterbury (refer to Figure 1).

Figure 1: Site location map (Source: LINZ data service)

The access road was constructed in c.2003, by cutting into a steep (35°) slope. This created a sub-vertical cutting, up to 15 m high along a 100 m section of the road. A 20 m section of the

cutting has been prone to ongoing rockfalls, prompting the client to seek specialist advice. A geotechnical appraisal was undertaken at the site in 2015, identifying several possible mitigation options including shotcrete/anchoring, large scale bench/battering of the slope and a local realignment. Until the hazard was appropriately mitigated, a spotter was being used to manage the risk. The client approached Opus in 2016 to review the site and the previous appraisal, and to provide a solution appropriate for the volume of traffic that uses the access road.

2 SITE DETAILS

2.1 Site Geology and Geomorphology

The existing cut batter is near the toe of a steep natural slope that extends a further 50 m upslope. The batter is up to 15 m high and cut at approximately 80° (refer to Figure 2). It is intersected by several gullies over its 100 m length. The site is underlain by Kowai Formation consisting of conglomerates, siltstones, sandstones and mudstones near the base of a local syncline structure (Forsyth et al, 2008). The material exposed in the cut face is interbedded very weak SILTSTONE and SANDSTONE beds, ranging from a few centimetres to up to a metre thick with sub horizontal bedding.

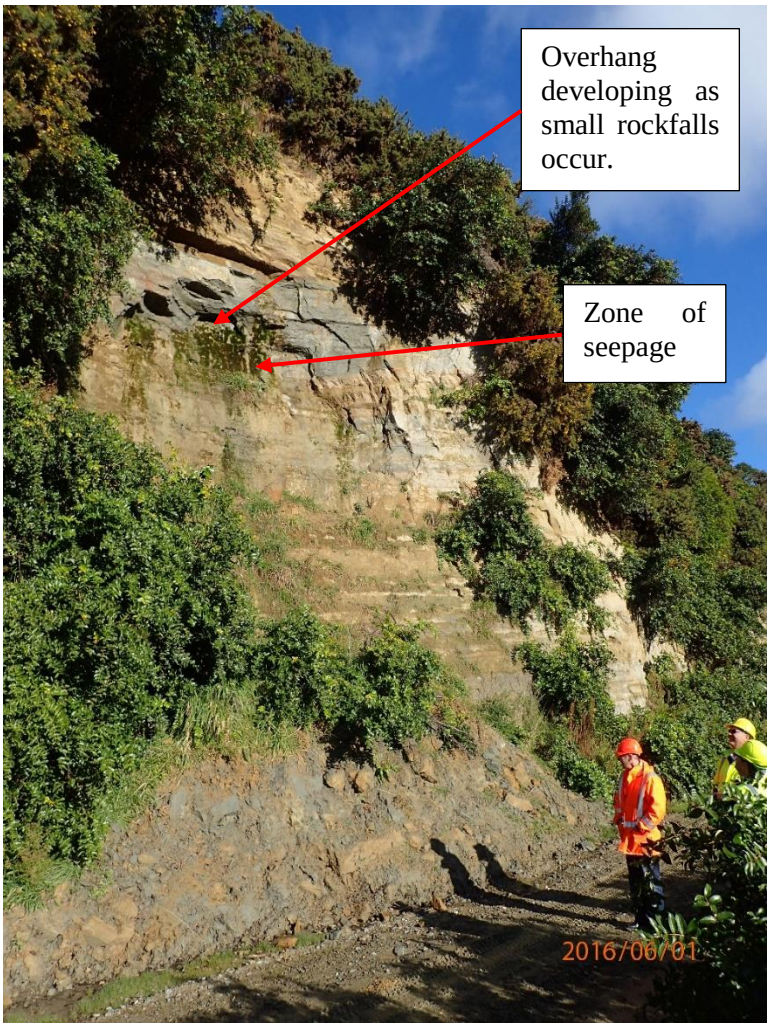

Figure 2: Cut face as inspected in 2016

2.2 Failure History

The full length of the cutting is prone to isolated rockfalls, however a section of cut approximately 20 m in length has a higher frequency of rockfalls, and occasional larger batter failures. The client indicated that small rockfalls (< 2 m^3 in volume) occur 1 – 2 times per annum. A larger event occurred in 2010 which inundated the full width of the access road (refer to Figure 3).

2.3 Site observations

The current area of cut batter instability is approximately 20 m in length. At the base of the cut, the access road is single lane and is approximately 4 m in width. Any available catch zone (approximately 1 to 1.5 m wide) has been inundated with rockfall debris (refer to Figure 2). On the downhill (north) side of the road, there is a berm of fill material (up to 2 m high) that is likely stockpiled rockfall debris from historical events.

Individual rock blocks of typically 100 mm to 200 mm size were observed at the base of the slope. Thicker bedding further up the slope will likely result in larger blocks being dislodged (as is evident in Figure 3).

Seepage was observed at several points in the lower 10 m of the cut face. The source of seepage was not identified during the walkover inspection.

Figure 3: Slip in 2010, debris extending over the access road

3 FAILURE MECHANISM

Weathering of material at the face being exacerbated by seepage is the inferred mechanism for small rockfalls. Subsequent undermining of upper portions of the slope then eventually results in

a larger failure (refer Figure 3). The face is expected to continue unravelling via regular small rockfalls and intermittent larger rockfalls.

4 RISK ASSESSMENT

Risk to life is assessed by estimating the probability of an event occurring (i.e. rockfall), the probability that someone is present when it occurs and the expected consequence. There is no worldwide standard for tolerable risk limits, which vary depending on the country and risk context. Australian Geomechanics Society Landslide Risk Management Guidelines (AGS, 2007d) suggest the upper limit for tolerable loss of life risk for the Person Most At Risk (PMAR) is 1×10^{-4} per annum (i.e. greater than 1 death every 10,000 years). Where the assessed risk of loss of life is greater, mitigation is required to reduce the risk to below this level. Below this threshold, the risk falls into an ALARP (As Low As Reasonably Practicable) zone, whereby steps should be implemented to reduce the risk where it is practical to do so. Christchurch City Council adopted similar levels for tolerable risk when assessing risk to life from rockfall following the Canterbury Earthquakes.

A semi-quantitative risk assessment was initially undertaken for the site using the New South Wales (NSW) Roads and Maritime Services Slope Risk Analysis methodology (Roads and Maritime Services, 2014). This method analyses the risk for a potential failure at the site using a series of ratings which are then combined through a matrix to determine an ARL (Assessed Risk Level) for each failure type. The highest ranking that can be achieved is an ARL1, which requires mitigation works to be undertaken to reduce the risk. ARL2 rankings are placed on a priority remediation list. The lowest ranking is an ARL5 which is associated with negligible risk (AGS, 2007d).

Using the NSW methodology, the following parameters/assumptions were used to assess the risk rankings for our site:

- The AADT for the road is 4 vehicles per day;
- The vehicle operational speed is approximately 40 km/h;
- A large rockfall (similar to the 2010 event) is expected approximately once every 5 to 10 years;
- A medium sized rockfall (maximum dimension 0.5 m, volume < 2 m^3) occurs annually; and,
- A small rockfall (individual blocks up to 0.3 m diameter) occurs annually.

The risk assessment evaluated both the risk of a fatality from (i) a vehicle hitting the fallen debris and (ii) a vehicle being hit by falling debris. The various scenarios evaluated to a maximum ARL3 rating. Work by Opus to assign a quantitative minimum, maximum and average values to each ARL band in the NSW Risk methodology (Likelihood, Temporal, Vulnerability and Consequence) indicates that the annualised risk level for each ARL3 event sits between 1×10^{-7} and 1×10^{-4}

The assessed risk was further verified using published quantitative methods (Bunce et al, 1997) which indicated an annualised risk of 2×10^{-6} for an individual rockfall event.

In order to determine the total annual risk for the site, the risks for each scenario were summed. The total risk for loss of life from rockfall to the PMAR is estimated to be in the order of 1×10^{-5} (which equates to 1 death per 100,000 years). This falls below the threshold of unacceptable risk, but remains within the ALARP zone. A summary of the assessed risk is presented in Table 1.

Rockfall Scenario		NSW Method	Bunce Methodology
Large	**Car Hits Debris**	ARL4	4.2×10^{-07}
	Debris Hits Car	ARL3	4.5×10^{-06}
Medium	**Car Hits Debris**	ARL3	1.0×10^{-07}
	Debris Hits Car	ARL3	2.3×10^{-06}
Small	**Car Hits Debris**	ARL3	1.0×10^{-07}
	Debris Hits Car	ARL3	2.3E x 10^{-06}
TOTAL			**9.6×10^{-06}**

Table 1: Evaluated risk for loss of life from rockfall

It is important to note that the economic consequences of rockfall (e.g. road closures) were deemed to be insignificant by the client and were not further evaluated.

5 MITIGATION EVALUATION

Several mitigation options were considered to reduce the rockfall risk, including those in the earlier appraisal and options suggested by the client. The client's preferred solution was a minor road realignment, as these works could be undertaken without specialised plant. Other options evaluated were: the use of a spotter (current practice); regular slope monitoring and risk management; low cost improvements such as installing horizontal drains or trimming the batter face and higher cost improvements such as installing a mesh drape or earthworks to remove the hazard.

In order to determine if the mitigation cost is warranted given the level of risk, the capital cost vs reduction in risk were evaluated for each option. This information was used to determine the Cost Effectiveness (with respect to life saved) and Disproportionality Ratios (using simplified methodology from Bowles, 2003).

Cost Effectiveness is a measure of life safety risk reduction (or cost per statistical life saved, CSLS) which is the equal to the annualised cost of the risk reduction measure divided by the annualised risk reduction achieved by the measure. Bowles proposed an Adjusted CSLS (ACSLS) for ALARP evaluations which also considers the economic benefit for each risk reduction measure (refer to equation 1).

$$ACSLS = (c-b_E)/r_L \quad (1)$$

Where:
c = Annualised Cost of Risk Reduction Measures
b_E = Annualised Economic Benefit of Risk Reduction Measures
= Economic Loss x Reduction in Probability of Loss of Life
r_L = Annualised Life Safety Risk Reduction for Risk Reduction Measure
= Estimated Number of Fatalities x Reduction in Probability of Loss of Life

The Disproportionality Ratio is a method proposed by HSE (Health and Safety Executive) to estimate the degree of disproportionality for a risk reduction measure in line with ALARP principles (Bowles, 2003). The ratio considers ACSLS and the Value of Preventing a Fatality (VPF) (refer to equation 2). Typically ratios of between 1 and 10 are considered to be at appropriate levels for ALARP principles (refer to Figure from Bowles (2003) in Appendix).

$$\text{Disproportionality Ratio, } R = ACSLS/VPF \quad (2)$$

For each mitigation measure Cost Effectiveness and Disproportionality was determined and compared against guideline values (refer to Table in Appendix) to determine the level of justification. For this assessment VPF was set at $4.1M which is similar to the Ministry of Transport's Value of Statistical Life (Ministry of Transport, 2015).

The evaluation identified that the current measure of risk reduction (using a spotter to observe traffic under the cutting) is associated with a high annual cost and minimal risk reduction. The cost effectiveness corresponds to a "Poor" ALARP justification rating and a disproportionality ratio greater than 50. Even low cost capital improvements (Options 3 to 5, $10,000 - $30,000) with an order of magnitude risk reduction (including the clients preferred solution) had "Moderate" ALARP justification rating and disproportionality ratios greater than 30.

Option 2 consisting of Slope Monitoring and Risk Management has an associated "Strong" ALARP Justification rating and disproportionality ratio of 10.

The earthworks option to bench and batter the slope has a "Poor" ALARP justification and very high disproportionality ratio. A summary of the options considered and associated Cost Effectiveness and Disproportionality is presented in Table 2.

	Option	Cost Estimate	Risk Reduction	Cost Effectiveness ($/life)	Disproportionality Ratio
1	Current practice – use of a spotter	~$18k	0.5 an order of magnitude	210M Poor Justification	52
2	Slope Monitoring and Management	~4k	0.5 an order of magnitude	40M Strong Justification	10
3	Install slope drainage	~$13k	1 order of magnitude	150M Moderate Justification	37
4	Trim the overhang	~$15k	1 order of magnitude	175M Moderate Justification	43
5	Minor road realignment	~$30k	1 order of magnitude	195M Moderate Justification	48
6	Install a mesh drape to slope	~$80k	1 order of magnitude	530M Poor Justification	129
7	Bench and Batter slope	~$300k	2 orders of magnitude	1800M Poor Justification	442

Table 2: Summary of Mitigation Option Evaluation

6 RISK MANAGEMENT

Findings were presented to the client, with a follow up meeting to further discuss the potential risk mitigation options. Based on the risk assessment and mitigation option evaluation, the client adopted Option 2 for the site, engaging our help to develop an appropriate monitoring and risk management plan for the site. This included:

- A sign in/sign out process for vehicles using the road;
- Visual inspection of the rockfall site prior to passing underneath;
- Maintaining a record of rockfalls;
- Monthly photograph of the site and review;
- Annual review of site changes and associated risk level; and
- Engage a specialist for review should any significant change occur.

7 CONCLUSIONS

An earlier geotechnical appraisal at a known rockfall site identified that road realignment or large scale earthworks to bench and batter the slope would provide rockfall risk reduction by either eliminating the hazard or minimising the probability of debris reaching the access road. Opus were engaged to review the site and previous appraisal, and recommend a solution appropriate for the traffic volume on the road.

Using NSW Slope Risk Analysis methodology a risk rating of ARL3 was determined for the site. This was further verified using quantitative methods which estimated the total annualised risk for loss of life from rockfall to be 1×10^{-5} for the PMAR. This sits below the threshold of unacceptable risk and in the ALARP zone.

To order to determine an appropriate mitigation solution for the level of risk, Cost Effectiveness and Disproportionality Ratios were calculated for each mitigation option. This identified that a low cost solution such as *slope monitoring and risk management* was appropriate an in line with ALARP principles for risk mitigation. This option was adopted by the client.

This method is considered applicable for assessing ALARP measures with respect to life safety and may not be applicable where there are significant other consequences from rockfall (e.g. closure of critical routes).

REFERENCES

AGS (2007c) Practice Note Guidelines for Landslide Risk Management 2007. *Australian Geomechanics* Vol 42 No 1 March 2007.

AGS (2007d) Commentary on Practice Note Guidelines for Landslide Risk Management 2007. *Australian Geomechanics* Vol 42 No 1 March 2007.

Bowles, D.S. (2003) ALARP Evaluation: Using Cost Effectiveness and Disproportionality to Justify Risk Reduction. *ANCOLD 2003 Conference on Dams.*

Bunce C.M. et al. (1997) Assessment of the hazard from rockfall on a highway. *Canadian Geotechnical Journal* 34: 344-356.

Forsyth, P.J.; et al. (compilers) (2008) *Geology of the Christchurch Area.* Institute of Geological Sciences (GNS) 1:250000 geological map 16. 1 sheet + 67p.

Ministry of Transport (2015) *Social Cost of Road Crashes and Injuries* Overview of 2016 Report. http://www.transport.govt.nz/research/roadcrashstatistics/thesocialcostoroadcrashesandinjuries/report-overview/

Roads and Maritime Service (2014) *Guide to Slope Risk Analysis*, Version 4. NSW Government, Roads and Maritime Services.

APPENDIX

Extract from
Bowles, D.S. (2003) *ALARP Evaluation: Using Cost Effectiveness and Disproportionality to Justify Risk Reduction.* ANCOLD 2003 Conference on Dams.

Table 2. ALARP Justification Ratings (Illustrative Example Only) (Bowles and Anderson 2003)

ALARP Justification Rating	Range of Cost-per-statistical-life saved (AUSM/life)	
	Greater than or equal to	Less than
Very Strong		5
Strong	5	50
Moderate	50	200
Poor	200	

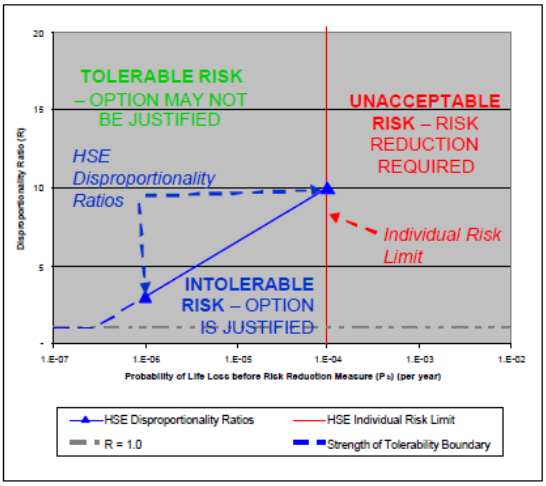

Figure 1. Plot of HSE Guidance for Evaluation of Disproportionality Ratio

Experimental study on the self-healing effect of laponite on the liquefaction resistance of sand

G S Pardo Tobar and R P Orense
Department of Civil and Environmental Engineering, University of Auckland, NZ
gpar659@aucklanduni.ac.nz (Corresponding author)

Keywords: earthquake, liquefaction, cyclic simple shear, countermeasure, nano-material

ABSTRACT

Currently, there is an increasing interest in providing more sustainable solutions for mitigating liquefaction and interdisciplinary work has started to introduce the use of nano-materials for this purpose. These materials have some advantages when compared with traditional techniques. For instance, they could be injected at low pressures or delivered into the natural ground water flow to treat a target area through passive remediation, which leads to less carbon emission production compared with normal grouting. In addition, after they gel, the nano-materials can provide increased shear strength and cohesion. This study focuses on the application of laponite, a synthetic nano-clay with the same structure as natural clays. Laponite suspensions have thinning behaviour characteristic in which its viscosity decreases with increase in shearing rate while keeping its gel properties. Moreover, after the shearing load is removed, the suspension recovers its viscosity in a self-healing process. In this study, the shear resistance of laponite suspension is studied by rheological measurements and the effect of the addition of 1% laponite (by weight) on the liquefaction resistance of the host sand is evaluated through cyclic simple shear tests. Results indicate that the number of cycles required to reach liquefaction is increased considerably for low shear stress conditions. In addition, by re-testing samples that have undergone liquefaction, the ability of the mixture to "heal" after liquefaction is confirmed. The results reaffirm the potential of laponite as an environmentally-friendly material for ground remediation purposes.

1 INTRODUCTION

To provide more sustainable solutions to mitigate soil liquefaction, interdisciplinary work has started to introduce nano-materials for soil remediation. Some of them, e.g. colloidal silica, bentonite and laponite, have been proven to be effective in increasing the liquefaction resistance of soils.

Colloidal silica is a chemical grout than can provide cementation and can restrain shear strain occurrence (e.g. Gallagher and Mitchell, 2002; Gallagher et al, 2007). Some researchers have performed cyclic triaxial tests (Gallagher and Mitchell, 2002), resonant column tests (Spencer et al., 2007), and centrifuge model tests (Conlee et al., 2012) and they found that colloidal silica suspensions injected into clean sand can increase the shear modulus and reduce strain deformation. These tests have reported that 10% by weight of colloidal silica suspension is enough to reduce the susceptibility to liquefaction. Colloidal silica seems to be very promising in passive site remediation application near existing structures.

On the other hand, laponite and bentonite are nano-clays that can modify the pore fluid (e.g Rugg et al., 2011; El Mohtar et al., 2013; Santagata et al., 2015; Ochoa-Cornejo et al., 2016) i.e. convert it to a solid-like fluid and delay the generation of excess pore water pressure. Bentonite and laponite suspensions make use of the hypothesis that highly plastic clays increase the resistance to liquefaction (Santagata et al., 2015).

Laponite has received attention in recent years due to its thixotropic properties that make it promising in mitigating liquefaction. Figure 1 schematically describes this phenomenon. Laponite's thixotropic behaviour is related to the flat-disc shape of its crystal (Figure 1 a, b) and its chemical composition that naturally makes its surface to be negatively charged and its edges positively charged (Barnes, 1997). When dry, its particles conglomerate with each other and form an aggregate of silt/clay size. In suspension, the particles disperse and arrange themselves in a kind of house-of-cards formation (Figure 1 c), and with time, this formation become stronger. Under very small strain, laponite suspension forms a gel that behaves like an elastic solid. When the applied shear stress is larger than a threshold value (or yield shear stress), i.e. $\tau \geq \tau_{ys}$, the network breaks and the material flows with a decreased viscosity (Figure 1 d, e). When the shear stress is supressed and the suspension goes back to rest, the structure is recovered and the resistance to flow increases again (Barnes, 1997). This is an indicator of a self-healing material that can be stable to resist new cyclic shear stress episode.

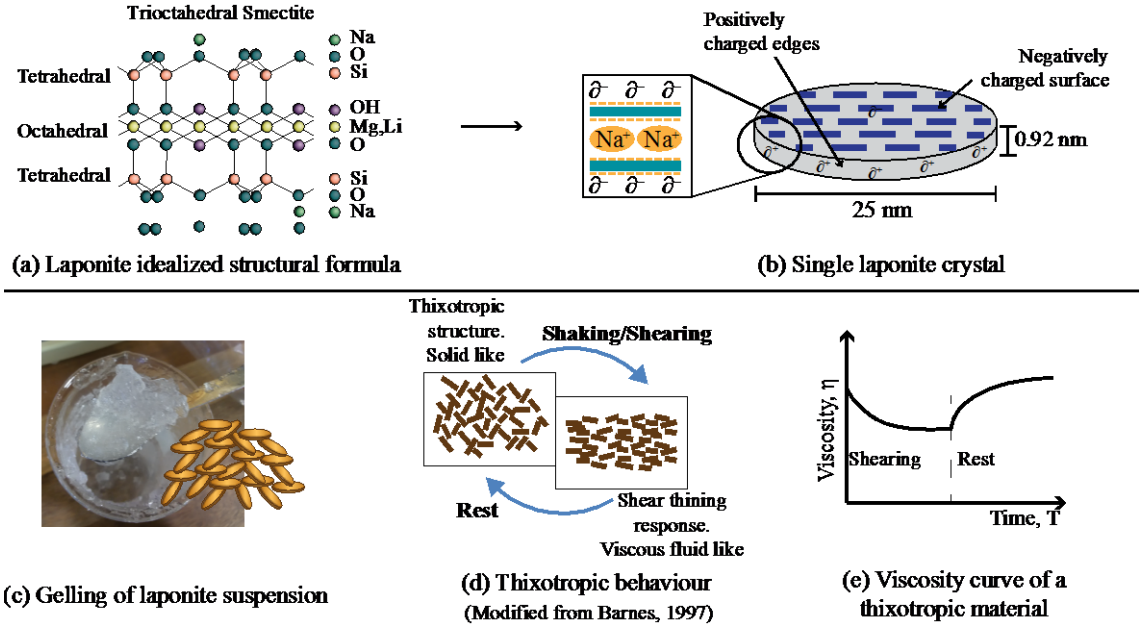

Figure 1: Scheme of thixotropic behaviour on laponite suspensions

Some researchers have studied this material and its potential to mitigate liquefaction. Ochoa-Cornejo et al. (2014) performed cyclic triaxial tests to study its effect on clean Ottawa sand, and they found that 1% laponite by dry mass of sand could increase the number of cycles to liquefaction from about 100 to 600 under similar shear stress. Santagata et al. (2015) performed dynamic oscillatory measurements to compare bentonite with laponite suspensions, and resonant column tests to study their effect on pure Ottawa sand's dynamic properties. They observed that sand mixed with 3.25% laponite suspensions had similar dynamic response to one with 10% bentonite. However, this material is still in evaluation stage and more research is needed to define its applicability in mitigating liquefaction.

In this study, the effect of adding 1% laponite to pure sand (by weight) is evaluated through cyclic simple shear tests and rheological characterization. The main objective is to assess the self-healing capacity of this material and its contribution to the liquefaction resistance of the host sand.

2 MATERIALS USED AND METHODOLOGY

2.1 Test materials

The host sand used in this study is the Mercer sand, sourced from the Waikato River. Figure 2 shows the grain size distribution of this material. It is a very uniform soil (coefficient of uniformity, C_U=2.1). To assess liquefaction, this material has been studied in loose condition.

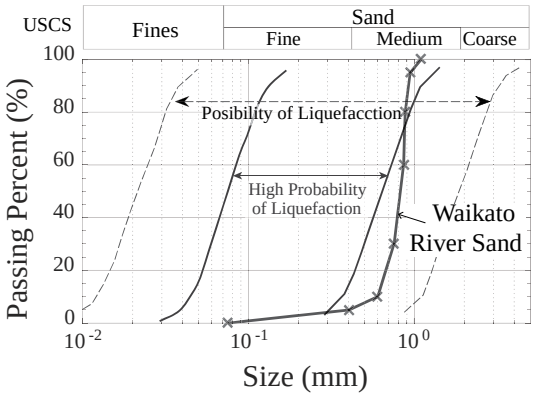

Figure 2: Grain size distribution curve of the host sand

On the other hand, laponite is a synthetic nano-clay with a structure similar to natural clays. It possesses no hazard to humans or to the environment. Laponite has a wide range of application, for example, it is usually used in cosmetics, as surface coatings, in some environmental applications as a barrier to trap gasses or contaminants, as well as in biomedical applications (e.g. Kwak, 2010; Tritschler et al., 2016).

In this study, Laponite RD was used, which is a general purpose rheology modifier. When a rheology modifier is dispersed in a fluid, it changes the way in which this fluid deforms when a shear load is applied. In this case, laponite changes the way the water flows when the cyclic loads are applied. To quantify the flow characteristic of laponite suspensions, rheological measurements were performed to measure the shear resistance of laponite suspension and to evaluate the gelling process. In addition, to study the effect of laponite on the liquefaction resistance of sand, undrained cyclic simple shear tests were performed.

2.2 Methodology

The soil samples were prepared by a modified slurry deposition method (Ishihara et al., 1978; Khalili and Wijewickreme, 2008). This method is useful in preparing highly gap-graded samples or, in this case, in preparing uniform sample consisting of granular material and nano-clay in saturated conditions. This method is very replicable and samples with a sand skeleton void ratio of e_{sk}=0.7581 can be prepared, with less than ±2% of variation. The laponite treatment was fixed at 1% by weight of sand. Then, the amount of water required to have 100% saturation was computed, leading to a laponite concentration by weight of water as 3.4%.

The procedure to prepare the samples is illustrated in Figure 3. First, laponite suspension with a concentration of 3.4% was prepared by pouring the laponite powder in deaired-deionized water, and mixed with magnetic stirrer for 20 minutes at about 1100 rpm. Then, enough suspension was poured into the dry soil, and the mixture was stirred until a uniform slurry was produced. The remaining suspension was poured into the simple shear base, and the slurry previously prepared was poured inside the mould with a spoon (Figure 3c). In some cases, gentle tamping was applied to fit the sample within the target volume. Finally, the excess amount was removed and collected

in a container to compute the amount of treatment, which varied from 0.99% to 1.15% of laponite by weight of sand.

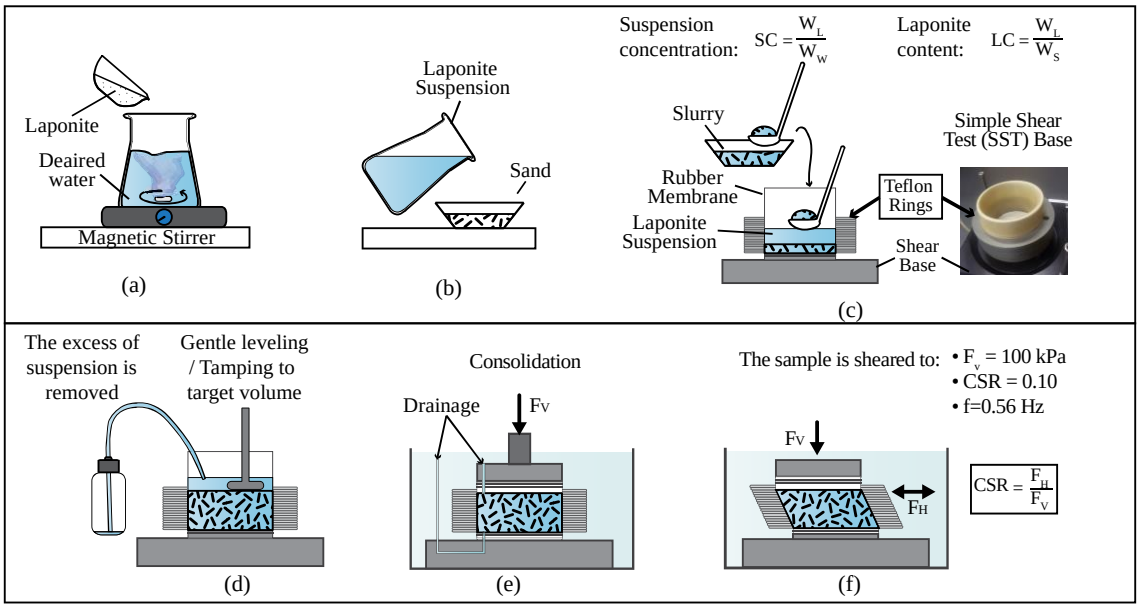

Figure 3: Sample preparation for specimens tested on CSST

2.3 Rheological measurements

Suspensions of 3.4% laponite by weight in water were prepared as described above (Figure 3a) and stored in a sealed container. The rheology tests were performed using a Physica UDS 200 rheometer with a cone-plate measuring device (Figure 4a). To avoid errors due to evaporation, the tests were conducted to last no more than 1 hour, and only a small portion of the suspension was used at each time with the rest of the batch stored in the sealed container. The first tests were performed almost immediately after the suspension was prepared, and then the tests were repeated with different specimens from the same suspension every 10 hours for 2 weeks.

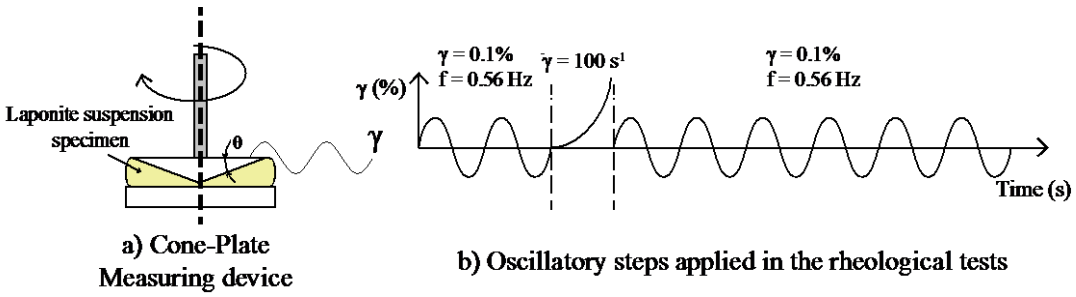

Figure 4: Rheological measurements

Each test consisted of 3 steps (Figure 4b). In the first step, small strain amplitude oscillations (γ=0.1%) were applied at a constant frequency 0.56 Hz. The purpose of this step is to assess the current shear strength of the sample, so it did not last for more than 10 minutes. In the second step, a high shear rotation $\dot{\gamma}$=100 s^{-1} was applied, with the purpose of breaking the internal structure of the developing gel. Finally, the sample was allowed to recover under small strain oscillations γ=0.1% at f=0.56 Hz, and the recovery was evaluated in terms of the time required to reach the same shear resistance that the sample had at the beginning of the test (i.e. in Step 1).

2.4 Cyclic Simple Shear Tests (CSST)

Specimens with a diameter of 63 mm, and height of 24 mm were tested in cyclic simple shear machine. To study the capability of laponite to recover, sand samples treated with laponite were tested in three phases, as depicted in Figure 5. First, the samples were consolidated with vertical load of σ'_{v0}=100 kPa (Figure 3e) for 72 hours. This was followed by the cyclic shearing stage, in which the cyclic shear stress ratio (CSR=τ / σ'_{v0}) was kept constant at 0.1. These two steps were repeated two more times (Phases 2 and 3).

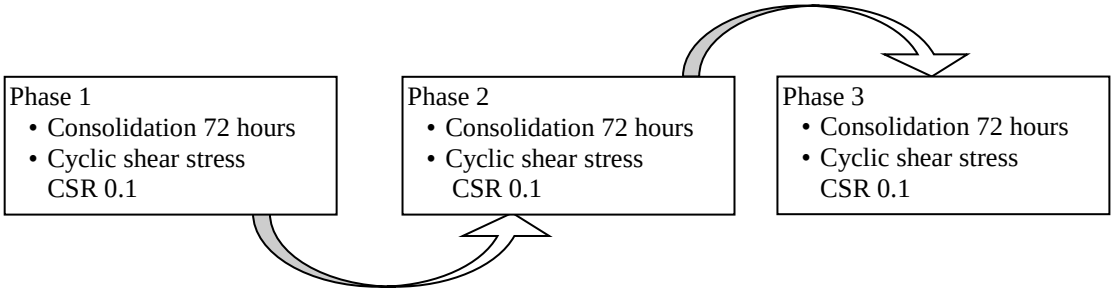

Figure 5: Scheme of the phases in testing laponite-treated sand samples

The sand skeleton void ratio at the beginning of each phase was computed, and pure sand samples were prepared with similar void ratios and compared with the response of laponite samples at each phase. The pure sand samples were consolidated for about 2-3 hours and then tested at CSR=0.1.

3 RESULTS AND DISCUSSION

3.1 Rheological measurement results

Figure 6a shows the shear modulus of the suspension versus the elapsed time since it was first prepared. From this result, it can be observed that at least 72 hours are required for the gel to have at least 80% of its final shear strength. This observation is consistent with those obtained by other researchers (e.g. El Howayek, 2011; Santagata et al., 2014; Ochoa-Cornejo et al., 2016).

On the other hand, Figure 6b shows the results only from the recovery step (described in Section 2.3). The markers' colour is proportional to the elapsed time since the suspension was first prepared. The results indicate that after enough time has elapsed (T_e >*3.5* h), the recovery time is almost instantaneous, i.e. within minutes, the shear strength has recovered. Consistent with Figure 6a, for samples just prepared, the time to reach a steady value is about 72 hours.

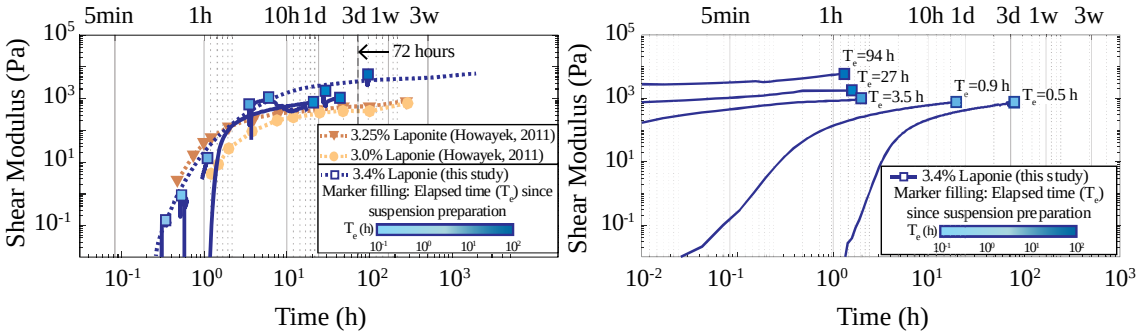

Figure 6: Time effect on laponite suspensions: (a) elapsed time since suspension preparation; and (b) recovery step

3.2 CSST results

Figure 7 shows the results from cyclic simple shear test for *CSR*=0.1, in terms of increase in excess pore water pressure ratio and double amplitude shear strain development. In the figure, the size of the marker is proportional to the relative density after consolidation, while the colour of the marker is related with to the time that elapsed since the sample was first prepared, i.e. white colour for less than 3 hours and black colour for more than 216 hours. The first column represents the first phase of the tests in which the samples were prepared with a skeleton void ratio of e_{sk}=0.758±0.015. The samples treated with laponite shows a gradual development in pore water pressure ratio until the 10th cycle, afterward the rate of development of pore water pressure increases, reaching liquefaction (i.e. r_u≈1) just a little later than the pure sand samples. Columns 2 and 3 show the results of re-testing Laponite samples two times after liquefaction. The initial void ratio before consolidation was estimated to be e_{sk}=0.710±0.015 and e_{sk}=0.681±0.003, respectively, for Phases 2 and 3. These samples were compared with pure sand specimens prepared with similar void ratios and the effect of time and self-healing is clear in the graphs.

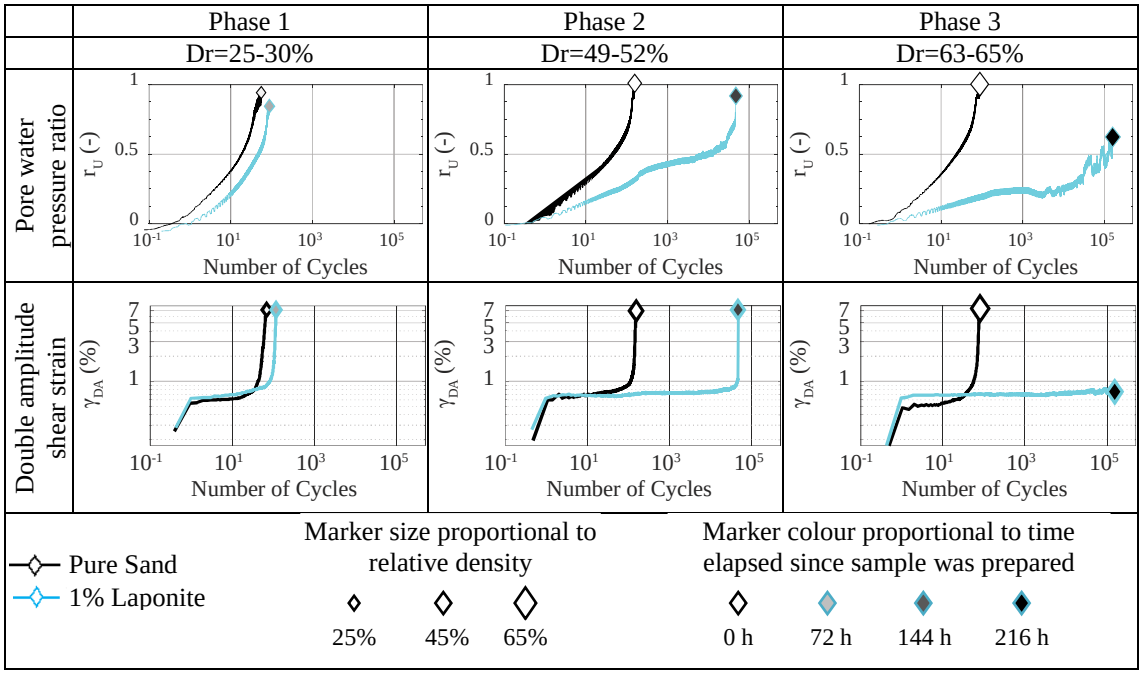

Figure 7: CSST results for *CSR*=0.1

These results are consistent with the rheology results shown in Figure 6, in which laponite suspension recovered very fast (within an hour), and the suspension continued to gain shear strength with time. Thus, in Phase 2, the number of cycles required for liquefaction to occur increased by about three orders of magnitude with the treatment; in Phase 3, the sample underwent more than 10^5 cycles with shear strain less than 1%. Moreover, during Phase 3, the excess pore water pressure oscillated more at the end of the test, possibly indicating that the sample was recovering while the test was in progress.

4 CONCLUSIONS

This paper presented the results of rheologic measurements on laponite suspensions and cyclic simple shear tests on laponite-mixed sands at *CSR*=0.1, in which the self-healing characteristic of laponite was confirmed. The results from the rheometer tests indicated that at least 72 hours are required after the suspension has been prepared for the fluid to provide enough resistance and to

behave as a gel; after that period, if shear stress was applied, the suspension yielded, but it recovered within one hour. These results were consistent with what was obtained in the cyclic simple shear tests, where the same sample was subjected to 3 phases of consolidation and cyclic shear application. Even though the void ratio of the sample decreased after each phase, the improvement was considerable when compared with pure sand samples with similar relative density. Therefore, the samples did not only recover, and being capable to resist a new set of cyclic stresses, it endured even more cycles because the laponite suspensions continued to harden.

These results indicated that with only 1% of laponite by weight of sand, it was possible to increase considerably the liquefaction resistance of pure sand. However, the results of CSST suggested that more than 72 hours may be required for effective treatment. After a sufficient time had elapsed after the sample preparation (more than 144 hours), the sample underwent more than three orders of magnitude of cyclic loading application than pure sand samples with similar relative density to liquefy. However, given the thinning behaviour of laponite suspension (i.e. decrease viscosity with increase in shear), such effectiveness observed for CSR=0.1 many not occur for higher CSR; more tests are currently planned to study the response at different levels of CSR, and different elapsed times and relative densities.

Laponite is currently being used in preliminary stages as a soil stabilizer, but the results presented in this paper reaffirmed their potential for ground remediation purposes. In practice, laponite could be injected or deposited in the ground and allowed to flow in passive remediation, where it could provide a more environmentally-friendly alternative to stabilize the soil since it poses no hazard to people and environment, and could help reduce carbon emission.

REFERENCES

Barnes, H. A. (1997) 'Thixotropy - A review', *Journal of Non-Newtonian Fluid Mechanics*, 70(97), pp. 1–33.

Conlee, C. T. Gallagher, P. M., Boulanger, R. W. and Kamai, R. (2012) 'Centrifuge modeling for liquefaction mitigation using colloidal silica stabilizer', *Journal of Geotechnical and Geoenvironmental Engineering*, 138(11), pp. 1334–1345.

Gallagher, P. M. and Mitchell, J. K. (2002) 'Influence of colloidal silica grout on liquefaction potential and cyclic undrained behavior of loose sand', *Soil Dynamics and Earthquake Engineering*, 22, pp. 1017–1026.

Gallagher, P. M., Pamuk, A. and Abdoun, T. (2007) 'Stabilization of liquefiable soils using colloidal silica grout', *Journal of Materials in Civil Engineering*, 19(1), pp. 33–40.

Ishihara, K., Sodekawa, M. and Tanaka, Y. (1978) 'Effects of overconsolidation on liquefaction characteristics of sands containing fines', *Dynamic Geotechnical Testing*. ASTM International, pp. 246–264.

Khalili, A. and Wijewickreme, D. (2008) 'New slurry displacement method for reconstitution of highly gap-graded specimens for laboratory element testing', *Geotechnical Testing Journal*, 31(5), pp. 424–432.

Kwak, J. (2010) 'Layered silicate particles filled polymer nanocomposite for barrier applications', *PhD Thesis*, University of Florida.

El Mohtar, C. S., Bobet, A., Santagata, M. C., Drnevich, V. P. and Johnston, C. T. (2013). 'Liquefaction mitigation using bentonite suspensions', *Journal of Geotechnical and Geoenvironmental Engineering*, 139(August), pp. 1369–1380.

El Howayek, A. (2011) 'Characterization, rheology and microstructure of laponite suspensions', *Master Thesis*, Purdue University.

Ochoa-Cornejo, F. Bobet, A., Santagata, M. and Johnston, C. and Sinfield, J. (2014) 'Liquefaction 50 years after Anchorage 1964: How nanoparticles could help prevent it', *Proceedings of the 10th National Conference in Earthquake Engineering*.

Ochoa-Cornejo, F. Bobet, A., Johnston, C., Santagata, M. and Sinfield, J. (2016) 'Cyclic behavior and pore pressure generation in sands with laponite, a super-plastic nanoparticle', *Soil Dynamics and Earthquake Engineering*, 88, pp. 265–279.

Rugg, D. A. Yoon, J., Hwang, H. and El Mohtar, C.S. (2011) 'Undrained shearing properties of sand permeated with bentonite suspension for static liquefaction mitigation', *ASCE Proceedings of the Geofrontiers.* Dallas, Texas, pp. 677–686.

Santagata, M. C. Clarke, J.P., Bobet, A., Drnevich, V. P., El Mohtar, C.S., Huang, P.T. and Johnston, C. T. (2014) 'Rheology of concentrated bentonite dispersions treated with sodium pyrophosphate for application in mitigating earthquake-induced liquefaction', *Applied Clay Science*. Elsevier B.V., 99(9), pp. 24–34.

Santagata, M. C. Bobet, A., El Howayek, Ochoa-Cornejo, F., Sinfield, J.V. and Johnston, C. T. (2015) 'Building a nanostructure in the pore fluid of granular soils', *Geomechanics from Micro to Macro.* Edited by K. Soga et al. CRC Press, pp. 1377–1382.

Spencer, L., Rix, G. J. and Gallagher, P. M. (2007) 'Dynamic properties of colloidal silica gel and sand mixtures', *4th International Conference on Earthquake Geotechnical Engineering*, (1324).

Tritschler, U., Zlotnikov, I., Fratzl P., Schlaad, H., Grüner S. and Cölfen H. (2016) 'Gas barrier properties of bio-inspired Laponite – LC polymer hybrid films', *Bioinspiration & Biomimetics*. IOP Publishing, 11.

Anzac Cliffs –Geotechnical aspects of cliff stabilisation works

S R Orgias
Riley Consultants Ltd, NZ
sorgias@riley.co.nz (Corresponding author)

D R Tate
Riley Consultants Ltd, NZ
dtate@riley.co.nz

S Pranjoto
Riley Consultants Ltd, NZ
spranjoto@riley.co.nz

Keywords: Anzac Cliffs, slope stabilisation, fill buttress

ABSTRACT

The Anzac Cliffs project involves two main elements: reshaping of the steep cliff, and realignment of the Manawatu River away from the cliff. The realignment of the river below Anzac Cliff was the last major development of the Lower Manawatu Scheme, City Reach Project. The project included the realignment of a 460m section of the Manawatu River opposite Anzac Park. The reshaping works were undertaken to stabilise the 50m high Anzac Cliffs adjacent to the river. The remedial works addressed the ongoing erosion of the unstable cliff by the Manawatu River.

Hazards associated with the project include direct river erosion undermining the lower cliff, and ongoing instability of cliff-face materials. The construction of foundations for a fill buttress within the active river channel and below the unstable cliff provided significant challenges, particularly due to the presence of liquefiable materials in its formation.

This paper provides a review of hazards associated with the project; sets out geotechnical investigations and analysis undertaken; and describes the development of the detailed design for the cliff stabilisation works. A review of construction and monitoring techniques for both the foundation treatment and compaction of granular and earth fill materials is presented, together with an outline of the management of numerous considerable technical and safety risks.

1 INTRODUCTION

The proposed Anzac Cliff residential subdivision is sited above the southern true left bank of the Manawatu River, some 3.5km south-east of Palmerston North City Centre (Figure 1). The north-eastern portion of the subdivision was bound by an approximately 50m high cliff that was subject to large-scale ongoing river erosion. The rapid erosion of this section of the cliff became a concern to various stakeholders with regard to the additional sediment load it added to the river, and the potential adverse effects that its altered course would have on the existing river protection works on the opposite northern bank. In April 2006 works to realign this section of the river back to its 1992 course were incorporated into the City Reach Project, a major works programme to upgrade the lower Manawatu River Scheme that protects Palmerston North from flooding.

Due to the unstable nature of the land along the site's north-eastern boundary, under the Palmerston North City District Plan, any building development within this portion of the proposed subdivision was a prohibited activity. It was identified that the proposed realignment of the river allowed for engineering works to be undertaken that would stabilise the land, making more of the site suitable for residential development. This led to a Plan Change that became operative in November 2011.

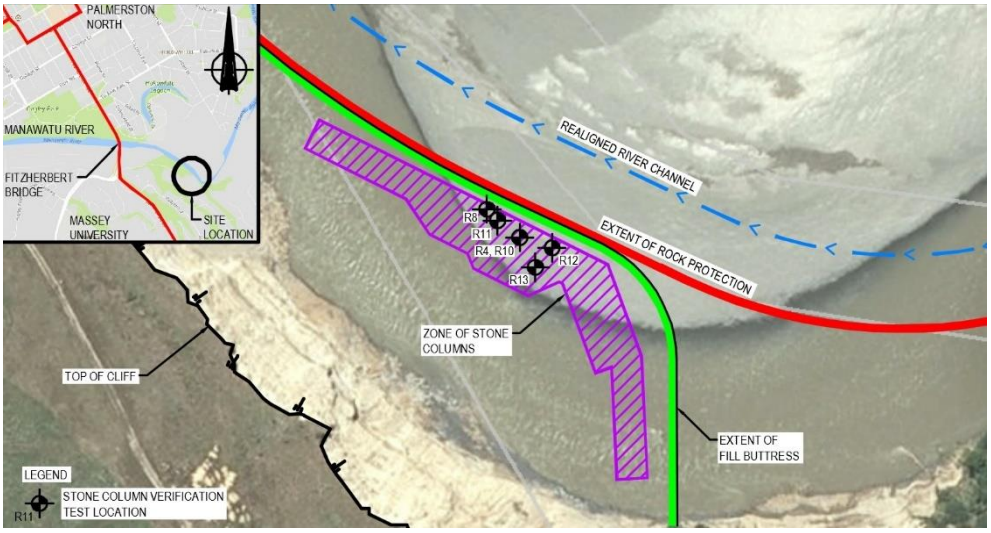

Figure 1: Location of machine holes for stone column verification testing, extent of stone columns, erosion protection and stabilisation works (additional borehole and test pit locations omitted for clarity)

The involvement of Riley Consultants Ltd (RILEY) with the project began in 2007 with the provision of a feasibility assessment of stabilisation works for the subdivision for HFH Properties Ltd (previously PBM Landco Ltd), and later with the development of a detailed design and definition of stable areas suitable for residential development, with Kevin O'Connor & Associates Ltd carrying out civil engineering, survey, and planning aspects. RILEY provided ongoing geotechnical consultancy input during construction, including monitoring of buttress filling.

The project consisted of the realignment of the river channel and construction of rock protection for the toe of the slope (undertaken by Horizons Regional Council (Horizons)). The buttressing and stabilisation of the cliff above the protection works was undertaken by HFH Properties Ltd. Stabilisation works included lowering the cliff crest by some 11m and construction of an approximately 38m high fill buttress along the north-eastern edge of the site. Foundation improvement works for the buttress fill included the installation of extensive stone columns and heavy compaction of the overlying ground. Earthworks consisted of cut to fill of approximately 300,000m³ over an area of 4.6ha. Fill material for the buttress was obtained from the excavation necessary to create the realigned river channel, and excavation of the top of the cliff.

2 INVESTIGATION

The initial feasibility study project undertaken by RILEY in 2007 was based on our knowledge of the area, visual assessment of the site and adjacent areas, and a review of available nearby subsurface information. The site had the advantage that the cliff materials were well-exposed over the majority of the cliff face (Figure 2). Subsurface investigation works at the base of the cliff were limited by access constraints to the gravel banks on the opposite side of the river to the cliff. In January 2008 two machine holes were drilled on the gravel banks adjacent to the true right northern side of the river, with a further two holes drilled along the gravel banks in August 2012 (Figure 2) in order to identify any constraints with respect to foundations of the proposed large fill buttress supporting the reshaped cliff.

Additional holes, drilled in August 2014, formed the basis for a verification trial for the stone columns prior to their construction. A series of test pits were also excavated in the gravel beach to assess the grading of material, along with four landward above the cliff to assess the suitability of the proposed fill materials. Samples recovered from standard penetration tests (SPT) split

spoon samples, and bulk samples taken from test pits, were logged, assessed for their intended purpose, and tested in the laboratory. Further machine holes and SPT tests were carried out to assess the effectiveness of foundation improvement works.

Figure 2: Composite of photographs taken from the opposite true right northern river bank during 2008 feasibility study

3 GEOLOGICAL MODEL

The Anzac Cliffs, along with the adjacent Waicola and Strand Cliffs, have formed as a result of down cutting of the Manawatu River into a coastal terrace formed during the previous interglacial period around 100,000 years ago (Lee & Begg 2002). These sand, silt, and interbedded sandy gravel horizons were visible in the cliff face and capped by loess. At the base of the cliff an erosion-resistant rock platform, interpreted to be of Pliocene Age, was exposed. The sandstone horizon is very weak in engineering terms, but is considered more erosion-resistant than the cliff materials above (Figure 3).

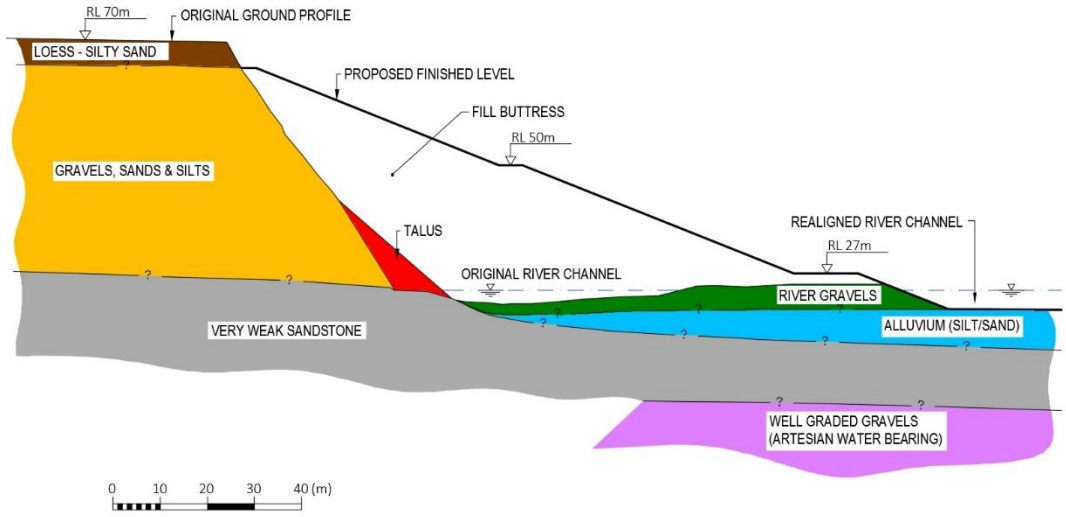

Figure 3: Simplified geological cross section showing original and finished ground profiles

4 BUTTRESS FILL DESIGN

4.1 Buttress fill foundation design

An assessment of the liquefaction risk to the project was carried out for the cliff materials, engineered fill, and foundations. Neither the in-situ cliff materials nor the engineered fill buttress were considered to be significant hazards. The cliff itself has a fundamentally low groundwater level, although minor seeps indicating perched water tables have been observed. Groundwater levels assumed for slope stability analysis purposes are shown in Figure 4. Buttress fill consists

of material compacted to engineered standards, with groundwater controlled by subsurface drainage. The more potentially hazardous location was assessed to be within the foundations of the fill buttress. Loss of support here due to widespread liquefaction could lead to large-scale lateral spreading, gross settlement and, in extreme cases, excess lateral movement of the entire cliff. Slope stability analysis was utilised for design of the fill slopes; this included an assessment and identification of where stability was assessed to be marginal below the buttress toe (Figure 4).

Modelling of the required ground improvement work was carried out utilising selected parameters and the slope computer program Slide, to meet the project criteria of no more than 500mm deformation in a 0.43g maximum design earthquake (MDE). The residual shear strengths for potentially liquefiable layers were selected based on correlations with SPT testing (Idriss and Boulanger 2008). Analysis indicating an 8m to 18m width of stone column treatment for different fill buttress heights could achieve the requirements of a static post liquefaction FoS of 1.2, from a FoS of less than 1.0 without stone columns. The finalised geometry of the stone column layout is based on these calculations, with extrapolation based on judgement. The design utilised a 15% replacement value of imported crushed gravels for the columns (Figures 1 and 4).

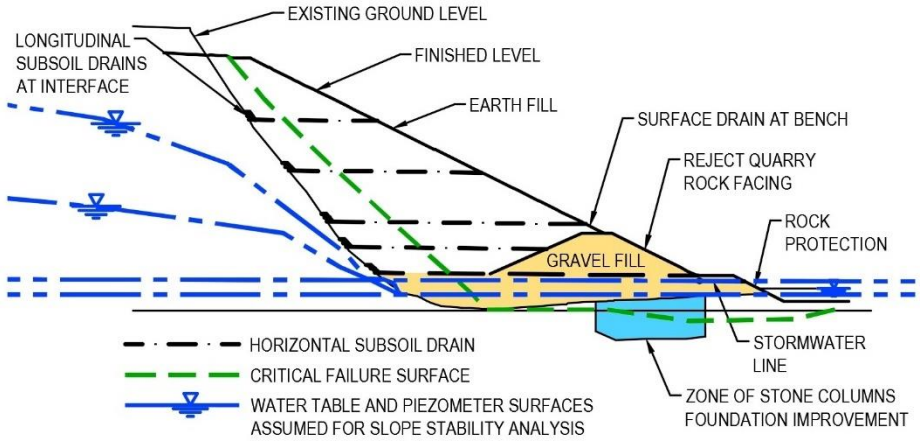

Figure 4: Cross section showing zone of stone columns, subsurface drainage, groundwater levels assumed for analysis, and critical failure surface from slope stability analysis

4.2 Buttress fill slope design

The buttress fill is a composite of gravel sourced from the river and finer largely cohesive earthfill material excavated from the cliff. The river gravels and terrace deposits have significantly different engineering properties. The base of the buttress within the area of potential flooding (below RL 27.0m) utilised compacted river-run gravel. The bulk of the fill buttress consists of silts, sands, and clayey soils.

It is an assumption of the design that in extreme rainfall and/or flooding of the toe by the Manawatu River, complete saturation over the full height of the buttress fill is an unrealistic scenario. The buttress fill may not be free-draining, and thus, a comprehensive system of subsurface drainage was incorporated into the design. A series of horizontal subsurface drains were constructed at four levels within the buttress (Figure 4). These form an important part of the design, providing the control of seepage and water pressures within the less permeable parts of the fill. They consist of horizontal trenched blanket drains along the interface with the in-situ cliff materials. These outlet by a number of horizontal strip drains to the face of the fill buttress. Drains were constructed using heavy-walled perforated polyethylene pipe surrounded by F/2 filter material, assessed to be filter compatible with the finest soils (Fell et al 2015).

Slope stability analysis was carried out using the computer program Slide and selected regression models to estimate permanent displacements in the MDE (Jibson, 2007). These displacements were calculated at the proposed building setback line for the subdivision. Slope stability analyses was carried out using parameters assessed to be attainable for the fill material, and parameters derived from back analysis of previous failures for the cliff materials.

5 RIVER REALIGNMENT WORKS

Works by Horizons to return the river to its 1992 alignment began towards the end of 2014 with approximately 250,000m³ of rock transported across the river to form the rock-lined gravel bank to protect the base of the slope from ongoing river erosion. This work was undertaken concurrently with the installation of the second production run of stone columns requiring a high degree of co-ordination between works within the shared area.

6 BUTTRESS CONSTRUCTION

6.1 Foundation improvement works

Construction of the stone columns was undertaken by Brian Perry Civil. It involved managing the challenges and mitigating the safety risks associated with working within an active river environment with constantly changing river levels, including flood events. The work, as with the majority of the construction, was restricted to favourable conditions during summer months.

A pre-trial for the stone columns was carried out over the period 13 May to 19 May 2014. A trial was necessary as the feasibility of the entire project depended on foundation improvement being demonstrated. Stone columns were installed utilising a wet top-feed method. Testing comprised split spoon SPTs undertaken at near continuous 0.5m intervals of depth within the areas of interest, along with the geotechnical logging of recovered samples. The installation of the stone columns and test drilling proved challenging due to rising water levels and the extremely permeable nature of the river gravels. For the pre-trial and main production runs a level platform, approximately 800mm below original ground level, was excavated to just above groundwater level. The initial trial comprised 12 stone columns centred on a borehole, chosen because it had encountered the most potentially liquefiable soils. SPT tests undertaken following installation indicated significant strength improvements, although at shallow depths from 3m to 4m limited improvement was noted. The test run was followed by the installation of 157 production columns, with an alteration in methodology to provide more vibration at the upper zone of the columns. These were installed, generally to the expected depth or slightly deeper, with no major difficulties experienced, and only one column unable to reach target depth, either due to a boulder or, more likely, a log or tree stump.

Further validation testing consisting of boreholes with SPT testing was carried out following installation of the columns with very significant strength improvements were recorded (Figures 1 and 5). As expected, there was a variability in the strength improvements, which is considered to be related to variability in material type, with the best response noted in the clean sands and gravels, and lesser improvements in silty sands. Figure 5 shows the calculated FoS of 1 against liquefaction based on correlations between relative density and liquefaction trigger values (Boulanger & Idriss, 2014). Due to the nature of the materials and significant scatter for the SPT results, the liquefiable layer was characterised based on the 66 percentile (i.e. 66% of values are greater than the design value) (Idriss and Boulanger, 2008).

The second stage of stone column installation commenced in December 2014 following works to divert the river (Figure 6). This involved the installation of a 3,899m total length of stone columns, with individual columns varying between 6.3m and 7.3m depth. River levels were a constant ongoing threat to progress, with a flood on 10 December raising water level about 2m

above the site of the column installation. Verification of the stone columns was completed with seven boreholes drilled that indicated satisfactory increases in SPT N values had been achieved.

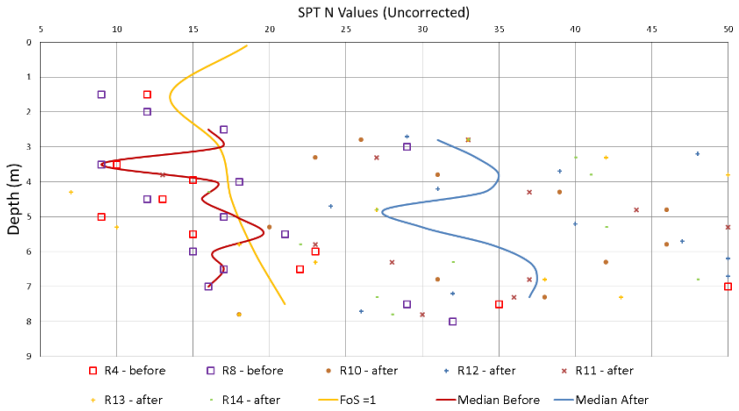

Figure 5: SPT N tests from boreholes measured before (plotted as squares), and after installation of stone columns installation (liquefaction trigger values (FoS=1), and median before and after SPT N lines shown)

6.2 Buttress fill slope construction

Earthworks for the buttress fill, undertaken by Goodmans Contractors Ltd, began in January 2015, and were completed in May 2017. This followed the completion of the realignment works by Horizons. Filling began with the placement of on-site river-run material above the rock buttress to RL 27.0m. Access to the fill area was initially limited to fording the river; later in the project access was created from the top of the cliff. The challenging constraints of the site provided significant hazards during construction. The contractor was required to develop construction methodologies to mitigate the risk of working beneath an unstable cliff, which included the removal of talus, excavation of the cliff, compaction of fill, installation of blanket and strip drains, and working in an active river bed.

Figures 6: Looking south towards stone column installation, (9 December 2014)
Figure 7: Looking north towards later filling operations (20 April 2016)

The design of the buttress fill assumed that any unsuitable materials within the now stranded river channel at the base of the cliff were excavated and the channel built-up with compacted river gravels. Although the high flow velocity of the river had prevented the deposition of fine-grained potentially liquefiable materials, compaction within the river channel posed specific challenges. Due to the very high permeability of both the natural river gravels and fill materials, the

groundwater level within the construction area reflected the current river level. The dewatering of sections of the channel excavation was problematic. These works were also being undertaken at the base of an unstable cliff. This meant that fill within the now stranded channel required a large thickness of loose granular material to be placed to a level above groundwater level, and compacted using heavy compaction equipment.

Above the foundation buttress, fill was sourced from material cut from the upper 11m of the cliff and terrace area, as well as the loose talus material at the cliff base. As the talus material was wet of the required moisture content for compaction, it was temporarily stockpiled on a high stand area, upstream of the buttress, until there was sufficient area to blend and condition this material. The material was then pushed from the upper terrace as part of the down-cutting of the cliff (Figure 7). Towards the upper portion of the buttress slope filling utilised materials with greater sand content, and care was taken by the contractor to stockpile finer-grained silt and clay material for the outside edge to help minimise surface erosion.

The variability of material encountered in the cliff meant that compaction test results needed to be closely monitored and testing criteria adjusted to reflect the materials. To ensure fill materials achieved the design criteria, ongoing standard compaction proctor tests to determine maximum dry density, were compared to materials tested in the field. Field tests consisted of Scala penetrometer, shear vane, and nuclear density meter (NDM) with oven-measured water contents. Testing of materials on the same site ranging from clay to sand highlighted the importance of selecting the correct targets for dry density, and field tests for different materials. The more sandy soils have typically shown a higher maximum dry density with a lower optimum water content, and the opposite for more clayey soils (Figure 8). Monitoring involved an ongoing review of field and laboratory test data and regular site visits, including documentation of fill material and ground conditions. Information and feedback shared between the laboratory, consultant, and contractor was required to ensure varying materials were conditioned to an acceptable water content.

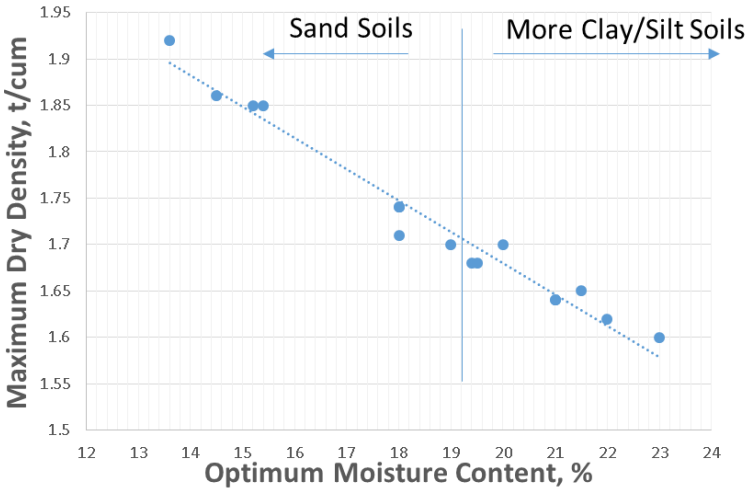

Figure 8: Range of maximum dry density vs optimum moisture content for buttress fill from laboratory proctor tests

Shallow-seated slumps were observed to occur on these steep cliff slopes where concentrations of surface water occurred. Surface collector drains were installed at the intermediate bench with a piped outlet to the cliff base (Figures 4 and 9). The reshaped slope is proposed to be vegetated to minimise surface water infiltration in the long term and also bind the surficial soils, reducing the risk of rill erosion on the face. To monitor the performance of the fill slope, a series of survey points were set up that are subject to ongoing monitoring for horizontal and vertical movement. To date the slope's overall performance is within expectations (Figure 9).

Figure 9: Photograph of completed realignment and cliff stabilisation works

7 CONCLUSIONS

The Anzac Cliffs project included detailed slope stability, liquefaction assessment, and modelling to facilitate the design of large-scale remedial works for the cliff, carried out within the active river channel of the Manawatu River. The works to realign the river, combined with the works to treat the buttress foundations and stabilise the slopes, have effectively stopped the erosion of the cliff, allowing the development of a proposed additional 36 residential lots.

Geotechnical assessment and modelling was used to identify the required scope of physical works to remediate the stability and liquefaction hazard, including defining a suitable building setback for the proposed residential subdivision. The initial model was developed further based on ongoing subsurface investigation work, testing, and the practical construction limitations encountered during construction.

The project demonstrates that large-scale works can be successfully undertaken in hazardous active environments provided ongoing monitoring, testing, and modelling manage the risk, and are combined to further develop the design as required.

REFERENCES

Boulanger, R. Idriss, I. (2014) *CPT and SPT Based Liquefaction Triggering Procedures.* Center for Geotechnical Modelling, Department of Civil and Environmental Engineering, University of California, Davis, California. Report No. UCD/CGM-14/01

Fell, R., et al. (2015) *Geotechnical Engineering of Dams, 2nd edition*. CRC Press/Balkema.

Idriss, I. and Boulanger, R. (2008) *Soil Liquefaction during Earthquake*. EERI Publication, Monograph MNO-12, Earthquake Engineering Research Institute, Oakland.

Jibson, R. (2007) Regression models for estimating coseismic landslide displacement. *Engineering Geology* 91 (2007) 209-218. Elsevier B. V.

Lee, J. Begg, J. (Compilers) (2002) *Geology of the Wairarapa Area. Institute of Geological and Nuclear Sciences 1:250 000 Geological Map 11*. Institute of Geological and Nuclear Sciences Limited.

Comparison of the post-liquefaction behaviour of hard-grained and crushable pumice sands

R P Orense, M S Asadi
Department of Civil & Environmental Engineering, University of Auckland, NZ
r.orense@auckland.ac.nz (Corresponding author)

M Rouholamin
School of Civil Engineering and Surveying, University of Portsmouth, UK

S. Bhattacharya
Department of Civil and Environmental Engineering, University of Surrey, UK

Keywords: earthquake, post-liquefaction, hard-grained sands, crushable sands, triaxial test

ABSTRACT

While the factors affecting the liquefaction resistance of sands have been studied by many researchers, their behaviour post liquefaction needs further examination. More specifically, understanding the effects of various parameters on the stress-strain relation of sands during the post-liquefaction stage is important not only for the purpose of assessing the magnitude of ground deformations induced by liquefaction, but also in investigating the impact of these deformations on buried structures, such as pipelines and pile foundations. In this paper, the post-liquefaction stress-strain behaviour of both hard-grained (silica) and crushable (pumice) sands is examined and attempts are made to express the stress-strain relation using a bilinear model which can be defined in terms of three parameters: initial shear modulus (G_1), shear modulus at recovery (G_2), and dilation shear strain (γ_{dil}) when the soil starts to dilate during post-liquefaction state. For hard-grained sands, it is observed that the three parameters are dependent on the initial relative density (D_r), i.e. with the increase in D_r, G_1 and G_2 would increase while γ_{dil} would decrease. On the other hand, test results on pumiceous sand show that, regardless of D_r, the value of $G_1$is larger while that of G_2 and γ_{dil} are smaller compared to those of a hard-grained sand. This can be attributed, partly at least, to crushing of the particles and their high angularity which induce interlocking between them when monotonically sheared.

1 INTRODUCTION

Past severe earthquakes have shown that failures and large flow slides happened after the cessation of shaking (e.g., Seed et al., 1975; Hamada, 1992). These deformations are typically triggered by earthquakes in liquefiable saturated sandy soils near river banks and quay walls, when horizontal ground movements and lateral spreading occurred after being subjected to seismic shaking. They can also be initiated in slopes and embankments where initial driving shear stresses existed. Such delayed failures and large ground movements are actually the result of a drastic reduction or even complete loss in the shear strength of saturated sand.

One of the key information required to estimate earthquake-induced displacement is the post-liquefaction stress-strain response of sand. Specifically, sand response, when it undergoes movements under states of zero effective stress, is needed when modeling the spatial effect of liquefaction underneath a given structure. In addition to estimating the magnitude of liquefaction-induced ground movements (lateral spreading, settlements and other associated ground deformations), post-liquefaction stress-strain response of sand is also required in estimating the *p-y* curve for analysing soil-structure interaction (i.e. using Winkler method).

However, there is a little research done to date in terms of understanding the post-liquefaction response of sand. Yasuda et al. (1995) carried out a series of multi-stage soil element tests on Toyoura sand at different relative densities. Vaid and Thomas (1995) carried out a similar test procedure on Fraser River sand with different relative densities and effective confining stress. In these works, the soil samples were made to liquefy first by applying cyclic loading followed by monotonic shearing under a certain constant strain rate. The results indicated that the liquefied sand showed nearly zero stiffness up to a particular level of strain, after which the soil resistance increased dramatically with strain. Focusing on the effect of axial strain, relative density and effective confining pressure on the post-liquefaction behaviour of sands, Sitharam et al. (2009) carried out cyclic triaxial tests on Ahmadabad sand (India) while Shamoto et al. (1997), Hyodo et al. (1998), and Kokusho et al. (2004) carried out similar studies. The main conclusion is that the undrained stress-strain response of post-liquefaction sand is dependent on the relative density of the sand while the effect of initial confining pressure is insignificant. However, no attempt has been made to incorporate this into a stress-strain model for liquefied sand.

The post-liquefaction stress-strain behaviour of sandy soils is generally of interest; however, that of other local soils, such as the highly crushable pumiceous sands (in the North Island of New Zealand) need to be equally addressed because many engineering projects are constructed in areas underlain by these deposits. A question that arises is whether the post-liquefaction stress-strain behaviour of crushable pumiceous soils is similar to those of hard-grained sands.

This paper presents the results of two independent but similar researches: (1) Phase 1 involved a series of multi-stage cyclic triaxial tests on different hard-grained sandy soils – two commercially available sands and two natural sands; and (2) Phase 2 comprised multi-stage cyclic triaxial tests on crushable natural pumiceous sands and hard-grained Toyoura sand. These tests were conducted with the aim of investigating the effect of relative density on the post-liquefaction stress-strain behaviour of both hard-grained and crushable soils.

2 MATERIALS AND EXPERIMENTAL METHOD

2.1 Phase 1 sand samples

Phase 1 of the research was conducted at SAGE (Surrey Advanced Geotechnical Engineering) Laboratory at the University of Surrey, U.K. Four types of sand were used to carry out the experimental investigation; two commercially available sands, Redhill-110 sand (UK) and Silica sand No. 8 (Japan), which are typically used in laboratory studies; and two natural sands from India, Assam sand and Ganga sand. Table 1 lists their index properties based on ASTM standards while Figure 1(a) shows their grain size distribution curves. Note that all four sands have uniform grain size distribution and low fines content. Also indicated in the figure is the range of grain size distributions of sands which are deemed to be liquefiable or highly liquefiable, as stipulated in the port and harbour facilities design code (PHRI, 1997).

2.2 Phase 2 sand samples

Phase 2 of the research was performed at the Geomechanics Laboratory of the University of Auckland. The materials used were natural pumiceous soils obtained from three different sites in the Waikato basin; these are referred to herein as NP1, NP2 and NP3 samples and obtained at depths of 1.5m, 2m and 4.5m, respectively, using block sampling. Details of the locations are discussed by Asadi et al. (2017). For the purpose of comparison, another set of tests was performed on Toyoura sand, known as hard-grained, sub-angular material and commonly used in Japan. The Japanese standard method was followed to measure the index properties of the materials and the results are also summarised in Table 1. The corresponding grain size distribution curves are shown in Figure 1(b). The Scanning Electron Microscope (SEM) images of pumice and Toyoura sands are illustrated in Figure 2 where the distinct feature of pumice can be clearly distinguished.

Table 1: Index properties of the materials used

	Sand name	Specific gravity, G_s	Mean diameter, D_{50} (mm)	Maximum void ratio, e_{max}	Minimum void ratio, e_{min}
Phase 1	Redhill-110 (UK)	2.65	0.18	1.04	0.61
	Silica sand No. 8 (Japan)	2.65	0.16	1.38	0.80
	Assam sand (India)	2.68	0.30	0.96	0.62
	Ganga sand (India)	2.67	0.35	1.00	0.85
Phase 2	NP1 (NZ)	2.53	0.60	0.99	0.65
	NP2 (NZ)	2.50	0.17	1.33	0.82
	NP3 (NZ)	2.54	0.24	1.74	1.04
	Toyoura sand (Japan)	2.66	0.21	0.89	0.61

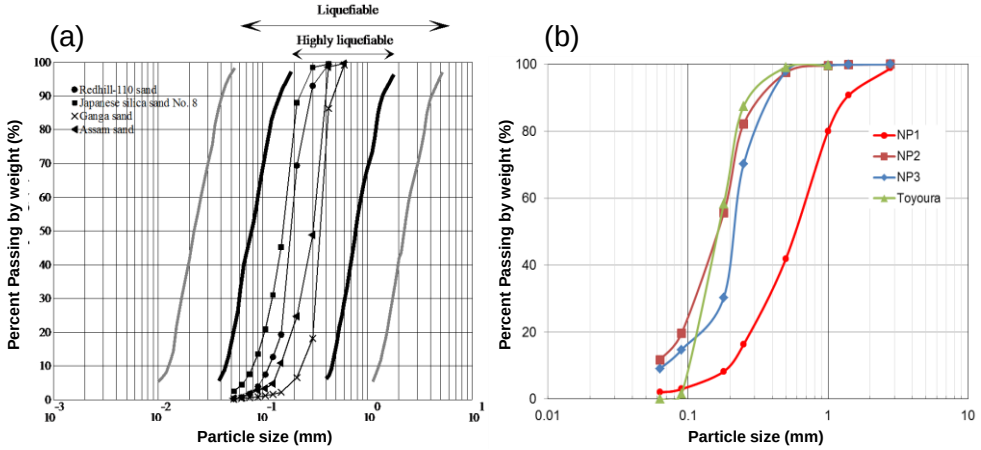

Figure 1: Particle size distribution curves: (a) Phase 1 materials; (b) Phase 2 materials.

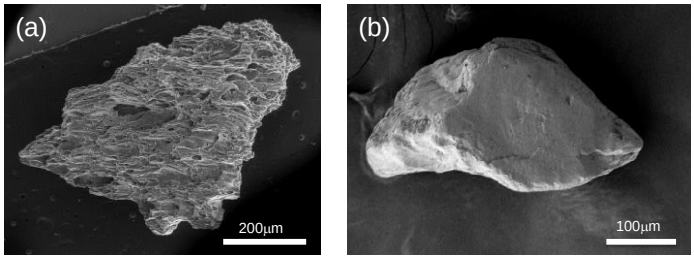

Figure 2: SEM images of particles: (a) pumice sand; (b) Toyoura sand.

2.3 Multi-stage undrained triaxial tests

In both phases of the research, several series of advanced soil testing (i.e. multi-stage soil element test) using cyclic triaxial apparatus were performed. In Phase 1, the 100mm diameter and 200mm high specimens were prepared using the dry pluviation method. In Phase 2, moist tamping was used to avoid segregation of the lighter pumiceous materials during preparation of the 63mm diameter and 126mm high specimens. The specimens were saturated with high back pressure, resulting in B-values in excess of 0.95. They were then isotropically consolidated in order to obtain the target effective confining pressure (σ'_c). Undrained stress-controlled sinusoidal cyclic loading with frequency of 0.1Hz was initially applied in order to liquefy the soil sample, with the amplitude of the cyclic load varied for the cases investigated. This cyclic load was stopped when the onset of liquefaction was recorded. In Phase 1, the onset of liquefaction was considered as the condition of: (a) zero effective stress for loose to medium dense condition, and (b) development of 5% double amplitude axial strain for dense condition. The latter was considered in all tests in Phase 2. Once the specimen liquefied, strain-controlled monotonic load was then applied under undrained condition to obtain the stress-strain curve of the liquefied sand keeping the drainage valve closed. The monotonic load was applied at a rate of 0.1% axial strain per minute. Such

multi-stage tests were conducted under different conditions of initial relative densities (D_r=30-80%), effective confining pressure (σ'_c=50-150 kPa), and applied cyclic deviator stress (σ_d=20-50 kPa) in order to have different levels of Cyclic Stress Ratio (*CSR*).

3 RESULTS AND DISCUSSION

3.1 Phase 1

Typical results of the undrained cyclic triaxial tests are shown in Figure 3. Figure 3(a) corresponds to those for medium-dense Redhill-110 sand samples (D_r=50%) which was isotropically consolidated under σ'_c=100 kPa and cyclically sheared with σ_d=30 kPa. As seen from the figure, the development of axial strain in the sample is slow during the early part of cyclic loading; then large axial strain is mobilised and the sample liquefied at nearly 10 cycles. With the generation of the excess pore water pressure, the effective stress decreases; consequently, the axial strain in the soil increases. Figure 3(b) displays the results for medium dense Assam sand under similar initial effective confining pressure and amplitude of cyclic deviator stress. The sand liquefied after around 23 cycles with the development of 5% double amplitude axial strain. The condition of momentary zero effective stress was also observed.

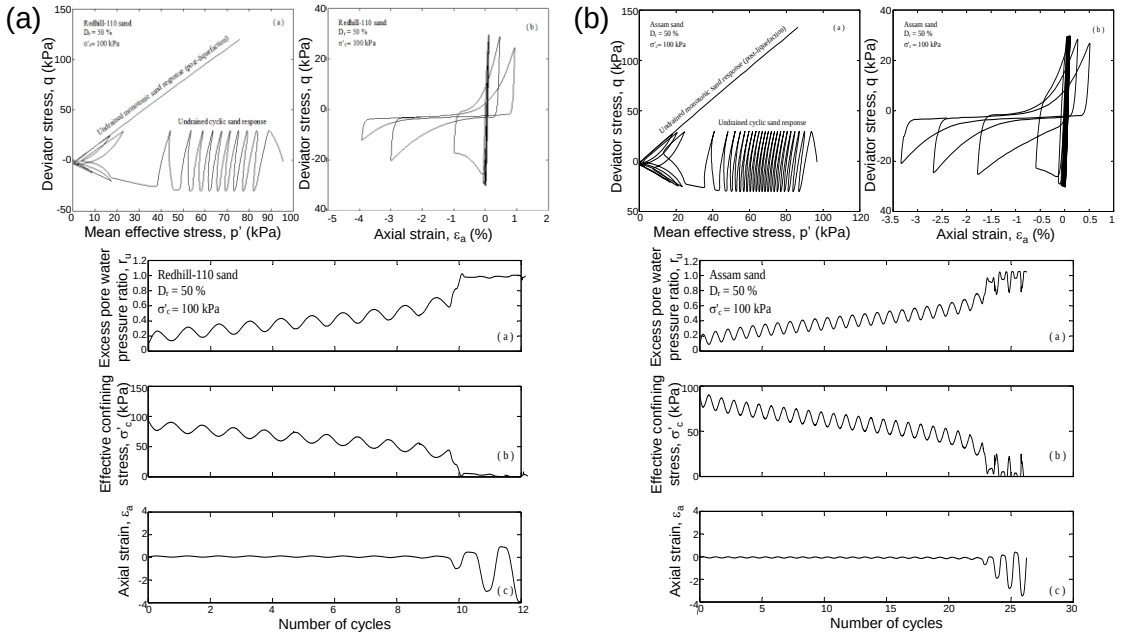

Figure 3: Typical results of the cyclic stage in Phase 1: (a) Redhill-110 sand; and (b) Assam sand.

Figure 4 shows the post-liquefaction response of two types of sands for the same level of *CSR*, in terms of variation of deviator stress and excess pore water pressure ratio with axial strain. From the figures, it can be seen that when the undrained monotonic load is applied to a liquefied specimen, it shows very small stiffness at the beginning of the loading until a certain level of axial strain is reached. After that, the resistance increases dramatically due to dilatancy induced by particle rearrangement. From the test results, it was observed that the axial strain at which such increase in resistance occurs depends on the initial density of the sand. Details of the results for the other sands are discussed by Rouholamin et al. (2017).

Looking at a typical deviator stress-axial strain curve post liquefaction, depicted in Figure 5(a), it is observed that the stiffness of the sand is almost negligible during the initial stage of monotonic loading; with continuous straining, the strength is recovered when a certain level of axial strain is reached. For better understanding of the response, the axial strain-deviator stress curve is

converted to a shear strain-shear stress curve (see Figure 5(b)). Essentially, it can be seen that the shear stress-shear strain curve can be modelled as bilinear, and represented by three parameters: the slope G_1 corresponding to the initial shear modulus (i.e. at the beginning of the loading); the slope G_2, representing the shear modulus during recovery stage; and γ_{dil}, the shear strain when the excess pore water pressure starts to significantly decrease (or when the shear stress increases remarkably) due to dilatancy. In this paper, the shear strain γ_{dil} is determined as the intersection of two tangent lines in the excess pore water pressure ratio versus shear strain curve (see Figure 5(f)). From the results of tests on all four types of sands, it would appear that each of these parameters is a function of the initial relative density of the sands.

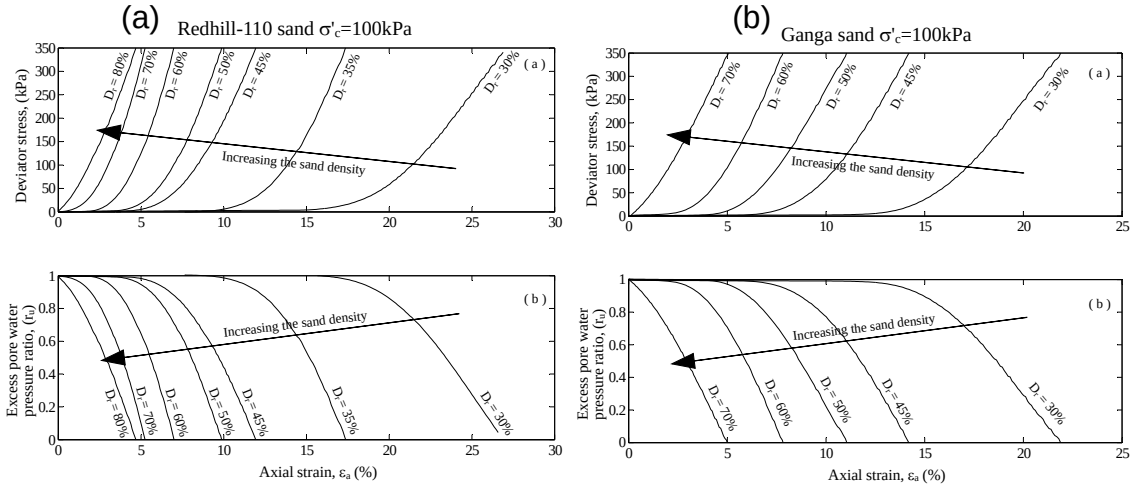

Figure 4: Typical post-liquefaction monotonic response for *CSR*=0.15 in Phase 1: (a) Redhill-110 sand; and (b) Ganga sand.

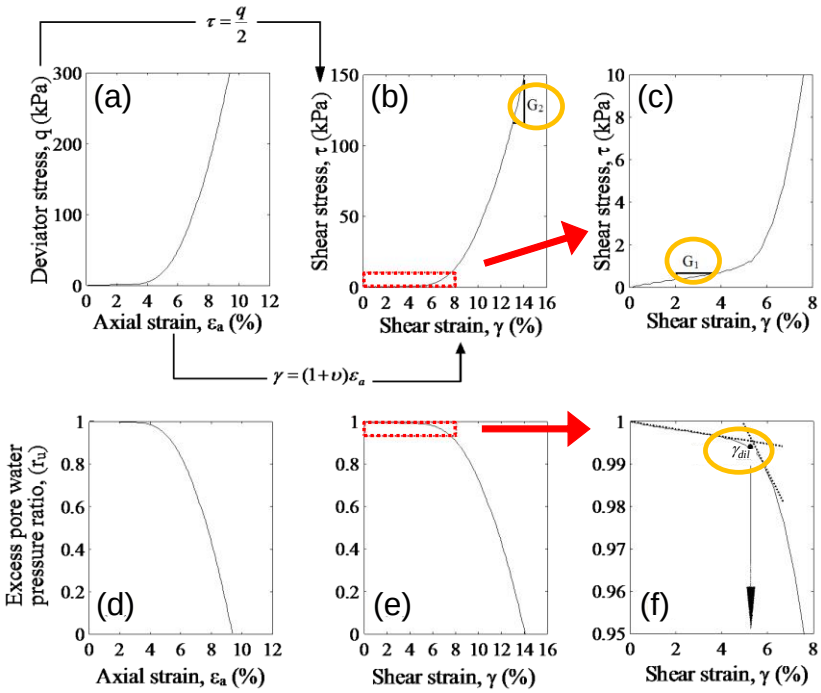

Figure 5: Schematic diagram showing the post-liquefaction stress-strain and excess pore water pressure ratio in normal and magnified situation: (a) axial strain vs deviator stress; (b) shear strain vs shear stress; (c) magnified shear strain-shear stress curve; (d) axial strain vs excess pore water pressure ratio; (e) shear strain vs excess pore water pressure ratio; and (f) magnified shear strain vs excess pore water pressure ratio.

Collating the values corresponding to the slopes G_1 and G_2, as well as the shear strain, γ_{dil}, for all the test results on four different sands, they are then correlated to the initial density of the specimen D_r; the results are shown in Figure 6. While there is a significant scatter, each of these parameters can be said to be a function of the relative density of the sands. Thus, if D_r of sand in-situ is estimated empirically (e.g. from penetration resistance or any other means), the three post-liquefaction parameters can be approximated and the post-liquefaction undrained response can be defined.

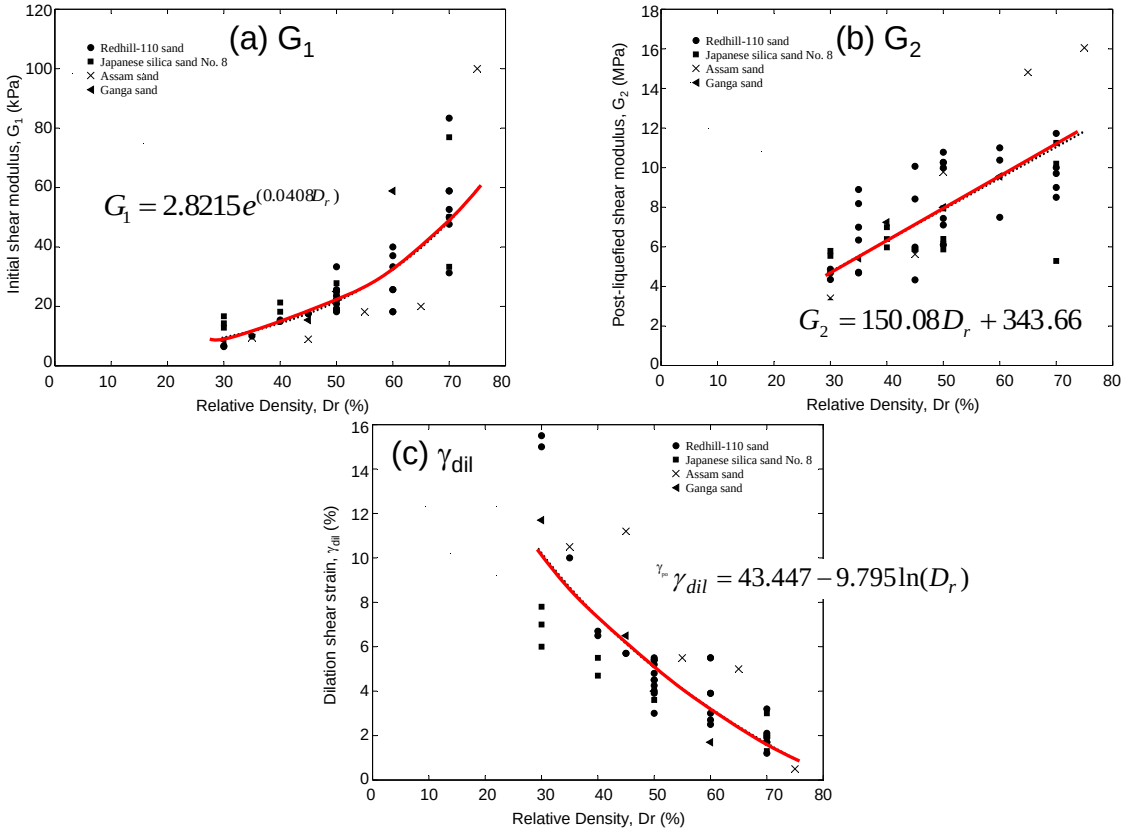

Figure 6: Variation of: (a) G_1; (b) G_2; and (c) γ_{dil} with respect to D_r for σ'_c=100 kPa.

3.2 Phase 2

A similar series of tests was performed on reconstituted natural pumiceous deposits and Toyoura sand. While it is obvious that the cyclic and post-cyclic response of Toyoura sand would be similar to those of the hard-grained sands used in Phase 1 and discussed above, the general behaviour of pumiceous sand appears to be relatively similar. A typical undrained behaviour (NP2 sample as a representative of the materials tested) is shown in Figure 7 for loose condition under σ'_c=100 kPa and *CSR*=0.22 when the soil was induced to liquefy (i.e. the attainment of 5% double amplitude axial strain). Application of monotonic load results in some deformation with almost zero stiffness; however, once a certain threshold strain is reached, the specimen dilates and the excess pore water pressure drops accompanied by an increase in shear stress.

While the general response of liquefied pumiceous sand to undrained loading is generally similar to that of liquefied Toyoura sand, detailed investigation showed subtle differences. Figure 8 illustrates the effect of relative density on the post-liquefaction behaviour of the two sands. Based on the results of several tests, the following are the main observations made:

- The post-liquefaction behaviour of Toyoura sand is affected more by D_r when compared to pumiceous sand;

- For similar D_r, the initial shear modulus, G_1, of pumiceous sand is higher while its shear modulus at recovery, G_2, is lower than those of Toyoura sand; and
- The region corresponding to negligible shear strength and, consequently, the magnitude of γ_{dil} are smaller for pumiceous sand, indicating that the pumiceous sand recovers its stiffness at considerably lower strain compared to Toyoura sand.

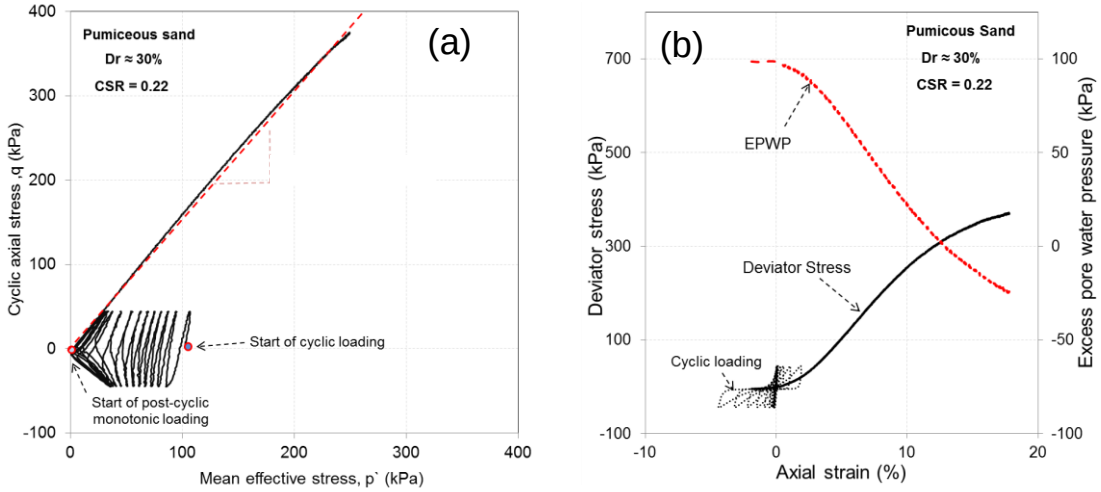

Figure 7: Typical response of loose (D_r≈30%) pumiceous sand (NP2): (a) effective stress path; (b) variation of deviator stress and EPWP with axial strain

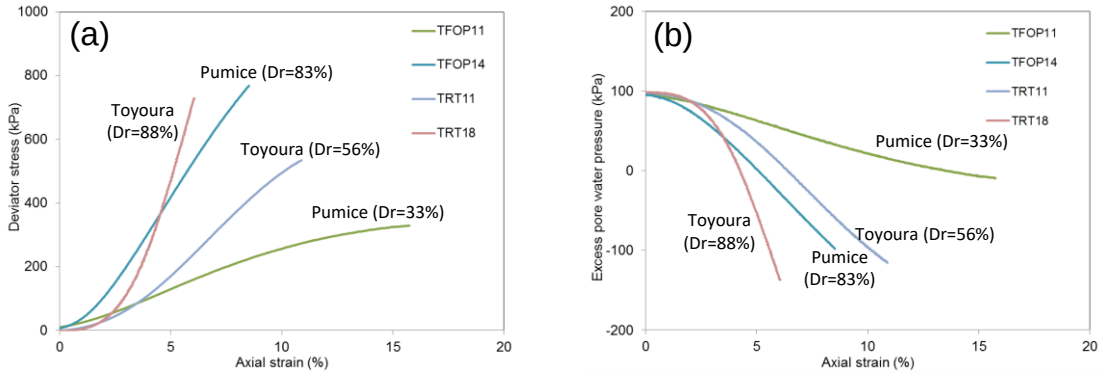

Figure 8: Comparison of the post-liquefaction undrained behaviour of Toyoura sand and NP2 pumiceous sand: (a) stress-strain relation; and (b) pore water pressure response.

The different behaviour of liquefied pumiceous and Toyoura sands under the application of monotonic loading may be attributed to the different ways by which the fabric changes during cyclic loading. Based on laboratory tests performed by Asadi et al. (2017), pumice particles are easily crushed during shearing; the crushing and the inherently high angularity of pumice particles, as observed through SEM image analyses, induce interlocking between them when sheared; thus, they recover their stiffness at considerably lower strain than Toyoura sand.

4 CONCLUDING REMARKS

The stress-strain behaviour of liquefied sand can be modelled as a bilinear curve which is defined in terms of three parameters: initial shear modulus (G_1); shear modulus at recovery (G_2); and dilation shear strain (γ_{dil}). Each of these parameters is a function of the initial relative density of the sand. Thus, if the in-situ relative density of sand is estimated empirically (e.g. from penetration resistance or any other means), the three post-liquefaction parameters can be approximated and the in-situ post-liquefaction undrained behaviour can be defined.

Crushable pumiceous sands appeared not to follow the behaviour of hard-grained sand. Previous research indicated that particle crushing occurred during cyclic and monotonic phases and this contributed to the formation of more stable soil skeleton and, coupled with the high angularity of the particles, induced interlocking during shearing.

5 ACKNOWLEDGEMENT

The Phase 1 research reported in this paper was based on work conducted while the first author was on Research & Study Leave at the University of Surrey, U.K. Phase 2 was done at the Geomechanics Laboratory, University of Auckland, with the help of M.B. Asadi. The authors would like to acknowledge the assistance of all those involved in both research.

REFERENCES

Asadi, M.S., Asadi, M.B., Orense, R.P., Pender, M.J., Jacobs, E. (2017). "Undrained cyclic and post-liquefaction behaviour of natural pumiceous soils," *3rd International Conference on Performance-based Design in Earthquake Geotechnical Engineering (PBD-III)*, Vancouver, BC, Canada, Paper 334, 7pp.

Hamada M. (1992) *Case Studies of Liquefaction and Lifeline Performance during Past Earthquakes, Vol. 1, Japanese Case Studies*, National Center for Earthquake Engineering Research, State Univ. of New York, Buffalo, N.Y.

Kokusho T, Hara T & Hiraoka R. (2004) Undrained shear strength of granular soils with different particle gradation. *J. Geotech. Eng. Div*., ASCE, 130(6), 621-629.

Hyodo M, Hyde AFL & Aramaki N. (1998) Liquefaction of crushable soils. *Geotechnique*, 48(4), 527-543.

Port and Harbour Research Institute (1997) *Handbook of Liquefaction Remediation in Reclaimed Lands*, Balkema.

Rouholamin M, Bhattacharya S & Orense R. (2017) Effect of initial relative density on the post-liquefaction behaviour of sand. *Soil Dynamics and Earthquake Engineering*, 97, 25-36.

Seed H B, Makdisi F, Idriss IM & Lee KL. (1975) The slides in the San Fernando Dams during the earthquake of February 9, 1971. *J. Geotech. Eng. Div*., ASCE, 101(7), 651-688.

Shamoto Y, Zhang JM & Goto S. (1997) Mechanism of large post-liquefaction deformation in saturated sand. *Soils and Foundations*, 37(2), 71-80.

Sitharam TG, Vinod JS & Ravishankar BV. (2009) Post-liquefaction undrained monotonic behaviour of sands: experiments and DEM simulations. *Geotechnique*, 59(9), 739-749.

Vaid Y & Thomas J. (1995) Liquefaction and post liquefaction behavior of sand. *J. Geotech. Eng. Div*., ASCE, 121(2), 163-173.

Yasuda S, Yoshida N, Masuda T, Nagase H, Mine K & Kiku H. (1995) Stress-strain relationships of liquefied sands. *International Conferences on Recent Advances in Geotechnical Earthquake Engineering and Soil Dynamics*, St. Louis, Missouri, 295-298.

Orense R.P., Wotherspoon, L.M., Pender, M.J., van Ballegooy, S., Cubrinovski, M. (2017)
Applicability of field-based methods for evaluating liquefaction potential of pumiceous deposits
Proc. 20th NZGS Geotechnical Symposium. Eds. GJ Alexander & CY Chin, Napier

Applicability of field-based empirical methods for evaluating liquefaction potential of pumiceous deposits

R P Orense, L M Wotherspoon and M J Pender
Department of Civil & Environmental Engineering, University of Auckland, NZ
r.orense@auckland.ac.nz (Corresponding author)

S Van Ballegooy
Tonkin & Taylor Ltd., Auckland, NZ

M Cubrinovski
Department of Civil & Natural Resources Engineering, University of Canterbury, NZ

Keywords: earthquake, liquefaction, pumiceous deposits, field testing, empirical methods

ABSTRACT

Pumice materials, which are problematic from an engineering viewpoint, are widespread in many parts of the North Island. Following the 2010-2011 Christchurch earthquakes, a clear understanding of their properties under earthquake loading is necessary. For example, the 1987 Edgecumbe earthquake showed evidence of localised liquefaction of sands of volcanic origin. To elucidate on this, research was undertaken to investigate whether existing empirical field-based methods to evaluate liquefaction potential of sands, which were originally developed for hard-grained soils, are applicable to crushable pumice deposits. For this purpose, two sites were selected where liquefaction have been observed following the Edgecumbe earthquake. Test site #1 was located adjacent to the Whakatane Sewage Pump station, while Test site #2 was opposite the Edgecumbe substation. Manifestations of soil liquefaction, such as sand boils and ejected materials, have been reported at both sites. Field tests, including cone penetration tests (CPT), shear-wave velocity profiling through seismic CPT, and screw driving sounding (SDS) tests were performed at the sites. Then, considering estimated peak ground accelerations (PGAs) at the sites based on recorded motions following the 1987 earthquake and possible range of ground water table locations, liquefaction evaluation was conducted at the sites using available empirical chart-based approaches. The applicability of the current field-based empirical approaches in assessing the liquefaction potential of pumiceous deposits was then scrutinised vis-à-vis the observed liquefaction manifestation at the target sites.

1 INTRODUCTION

The 2010-2011 Christchurch earthquakes have highlighted the impact of soil liquefaction and associated phenomena to the built environment. A cursory review of the current state of research on soil liquefaction showed that nearly all the work on this topic has been directed towards understanding the properties of hard-grained (quartz) sands; very little research has been done on the dynamic characteristics of volcanically-derived sands.

However, it is known that New Zealand's active geologic past has resulted in widespread deposits of volcanic soils throughout the country. The M_L=6.3 1987 Edgecumbe earthquake, for example, showed localized patches of liquefaction of sands of volcanic origin across the Rangitaiki Plains (Pender & Robertson 1987). Pumice deposits are found in several areas of the North Island. Although they do not cover wide areas, their concentration in river valleys and flood plains means they tend to coincide with areas of considerable human activity and development. Thus, they are frequently encountered in engineering projects and their evaluation is a matter of considerable geotechnical interest.

Previous research by Wesley et al. (1999) showed that the penetration resistance (q_c) values obtained from cone penetration tests (CPT) on pumice sand were only marginally influenced by the density of the material. The reason for this behaviour is possibly because the stresses imposed by the penetrometer are so severe that particle breakage forms a new material and that the properties of this are nearly independent of the initial state of the sand. Thus, conventional relationships between q_c value and relative density, D_r, which in turn is correlated with liquefaction resistance, appear to be not valid for these soils. In addition, research results reported by Orense et al. (2012) and Orense and Pender (2013) indicated that penetration-based approaches, such as cone penetration tests and seismic dilatometer tests, underestimated the value of liquefaction resistance of the pumice deposits, confirming that any procedure where the liquefaction resistance is correlated with relative density will not work on pumiceous deposits. The same research showed that empirical method based on shear wave velocity seemed to produce good correlation with liquefaction resistance of pumiceous soils.

Admittedly, the above observations were obtained from limited number of test data and such conclusions have not been well-validated. With many consultants and practitioners constantly asking for advice on how to evaluate the liquefaction susceptibility of pumice deposits, there is indeed a need to clarify and address this issue.

This paper presents the results of recent investigation on the evaluation of liquefaction triggering of in-situ pumice deposits through field testing at two sites where liquefaction have been observed following the 1987 Edgecumbe earthquake. Using field-obtained data, attempts were made to explain the occurrence/non-occurrence of liquefaction at the target sites following the earthquake using available empirical chart-based approaches. The applicability of the current field-based empirical approaches in assessing the liquefaction triggering of pumiceous deposit was then scrutinised vis-à-vis the observed liquefaction characteristics of pumice sands.

2 SELECTED TEST SITES AND FIELD TESTING

Two sites where liquefaction had been observed during the 1987 Edgecumbe Earthquake were selected in this research. Test site #1 was located adjacent to the Whakatane Sewage Pump station, while Test site #2 was opposite the Edgecumbe substation (see Figure 1). Manifestations of soil liquefaction, such as sand boils and ejected materials, have been reported at both sites (Pender & Robertson 1987).

At both sites, borehole sampling, cone penetration test (CPT), seismic cone penetration test (sCPT), and screw driving sounding (SDS) were performed (see Figure 2). SDS is a new in-situ method that has recently been developed in Japan, where a rod is drilled into the ground at several loading steps at the same time as the rod is being continuously rotated. Details of this test are reported elsewhere (e.g., Orense et al. 2013.) The SDS test is fast, the machine is small in size and the implementation is relatively cheap, compared to other in-situ testing methods.

Boreholes from the two tests sites indicate the presence of fine to coarse sand layers intermittently mixed with pumice. At site #1, the presence of pumice sands were visible between 0.5-7m, while at site #2, pumice was mixed with fine to medium sand from 0.5-6.2m. The ground water table was located at about 2m from the surface at both sites.

The results of the field tests are shown in Figures 3 and 4 for site #1 and site #2, respectively. At site #1, the cone tip resistance was about q_c=4 MPa up to a depth of 5m and it increased to about q_c=8 MPa up to a depth of 10m. The soil behaviour type (SBT), derived from CPT data, indicated alternating layers of sand and silt mixtures up to a depth of 5m, and predominantly sand up to a depth of 12m. The shear wave velocity profile showed V_s ranging from 90-120 m/s up to a depth of 5m, after which V_s increased with depth, reaching 170 m/s at depth of 11m. During the SDS test, several parameters were measured every 25cm; these include torque, load,

(a) (b)

Figure 1: Target sites for the study: (a) Test site #1 near Whakatane Sewage Pump station; and (b) Test site #2 near Edgecumbe substation. Yellow hatched zones are the regions where liquefaction had been observed based on literature.

(a) (b)

Figure 2: Field testing at Target site #1: (a) CPT and sCPT; and (b) SDS test.

speed of penetration, depth of penetration and friction on the rod. An important parameter derived was the specific energy of penetration, E_s, representing the sum of the contribution of the torque and applied load for every load step normalised by the volume of penetration (Mirjafari et al. 2016). At site #1, E_s <25 N-mm/mm^3 up to a depth of 10m, below which stiff layer with E_s<50 N-mm/mm^3 existed.

At site #2, q_c was generally <8MPa, except at depths of 3.0-3.5m and >6.5m; V_s generally varied between 110-170 m/s. SDS indicated E_s< 30 N-mm/mm^3, except at depths of 3.0-3.5m and >6.5m. From all tests, a hard layer was apparent at depth of approximately 7m, where q_c >20 MPa, V_s >160 m/s, and Es>70 N-mm/mm^3; all tests were terminated at this depth.

3 EVALUATION OF LIQUEFACTION TRIGGERING

For the purpose of evaluating the liquefaction triggering at both sites during the Edgecumbe earthquake, six simplified empirical methods were employed: 3 CPT-based methods – i.e. those proposed by Boulanger and Idriss (2014), Robertson and Cabal (2012) and Moss et al. (2006); two V_s-based methods – i.e. those proposed by Andrus and Stokoe (2000) and Kayen et al. (2013); and the SDS-based method proposed by Mirjafari et al. (2016). Per the analyses of Mellsop (2016), the Edgecumbe earthquake, with moment magnitude M_W=6.5, induced the following peak ground accelerations (PGA): 0.29g in site #1 and 0.53g in site #2.

In terms of ground water table (GWT), Pender et al. (1987) reported the following: "*the earthquake occurred at the end of the summer and after a long period of dry weather. Most of the deposits underlying the Rangitaiki Plains are saturated, with the water table ranging from near surface in the coastal margin, to about 3 m below ground level in the Te Teko area. (In Edgecumbe), the top of the soil profile is a layer of about 3m thickness which is very loose, (and) at the time of the earthquake, the water table was probably towards the bottom of this*

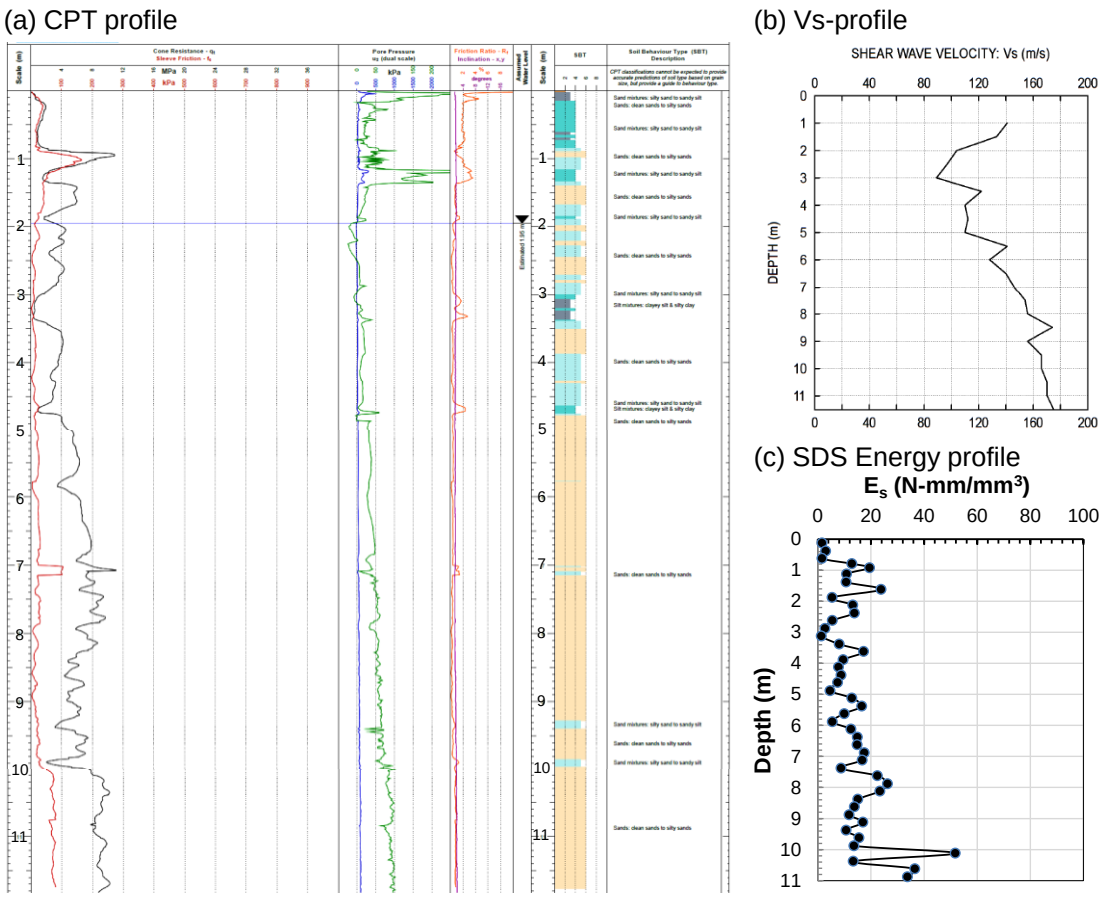

Figure 3: Results of field testing at site #1.

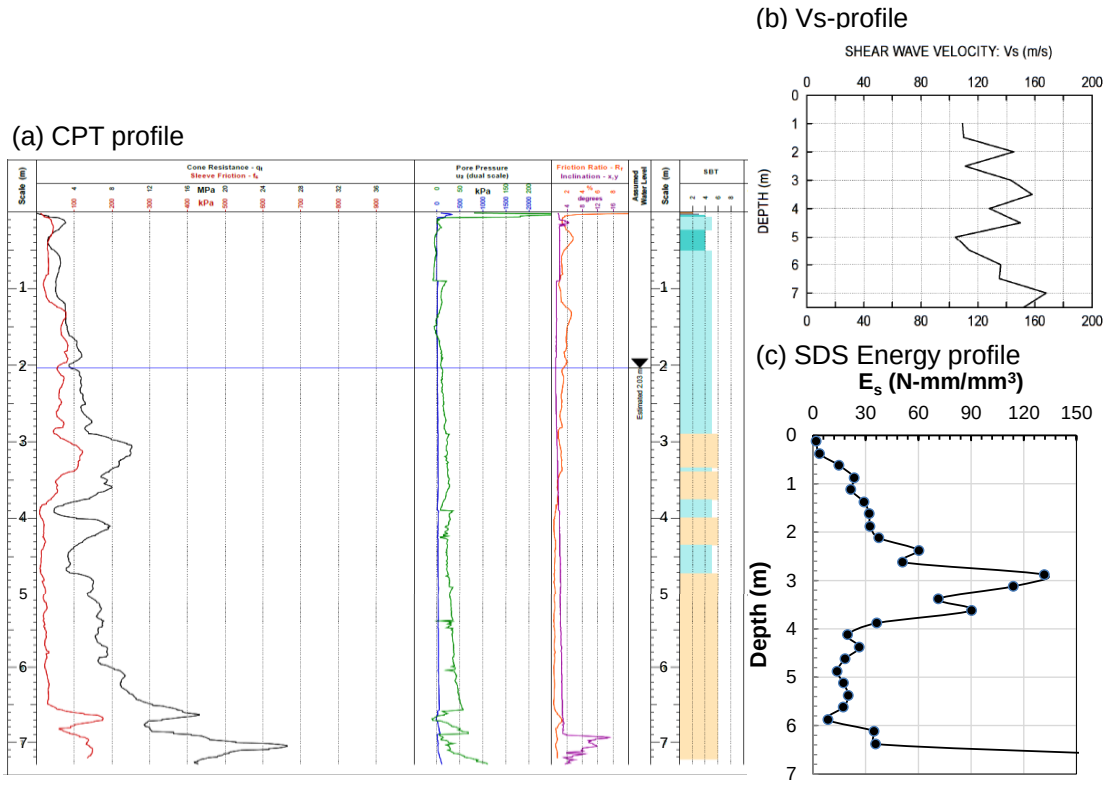

Figure 4: Results of field testing at site #2.

layer over much of the plains." Thus, for the purpose of the analyses, the GWT location was assumed at: 1m, 2m and 3m from the ground surface for site #1, and 2m, 3m and 4m for site #2.

Considering the input parameters mentioned above, liquefaction assessment was conducted using the 6 simplified methods. Results for site #1 considering GWT=2m are shown in Figure 5, while Figure 6 illustrates the results for site #2 with GWT=3m. In the figures, the depth profile of the cyclic stress ratio (*CSR*) and cyclic resistance ratio (*CRR*) are plotted, and the shaded regions represent the pumiceous zones which are deemed to have liquefied (i.e. $CRR \leq CSR$).

Based on the results, it is clear that at site #1 where field testing has been done up to a depth of 11.5m, all the methods considered would predict liquefaction of pumiceous deposits (between the depth ranging from the location of the water table up to 7m depth). Similarly, at site #2, all methods would predict pumice liquefaction between GWT up to 7m depth. Similar results were obtained for the other GWT locations. Thus, it would appear that for the sites selected, all empirical methods were able to predict the occurrence of liquefaction of the pumice layers. Note that at both sites, it would appear that the *CSR* induced by the earthquake was almost twice that of the liquefaction resistance of the soil, *CRR* (i.e. factor of safety, $F_L \approx 0.5$).

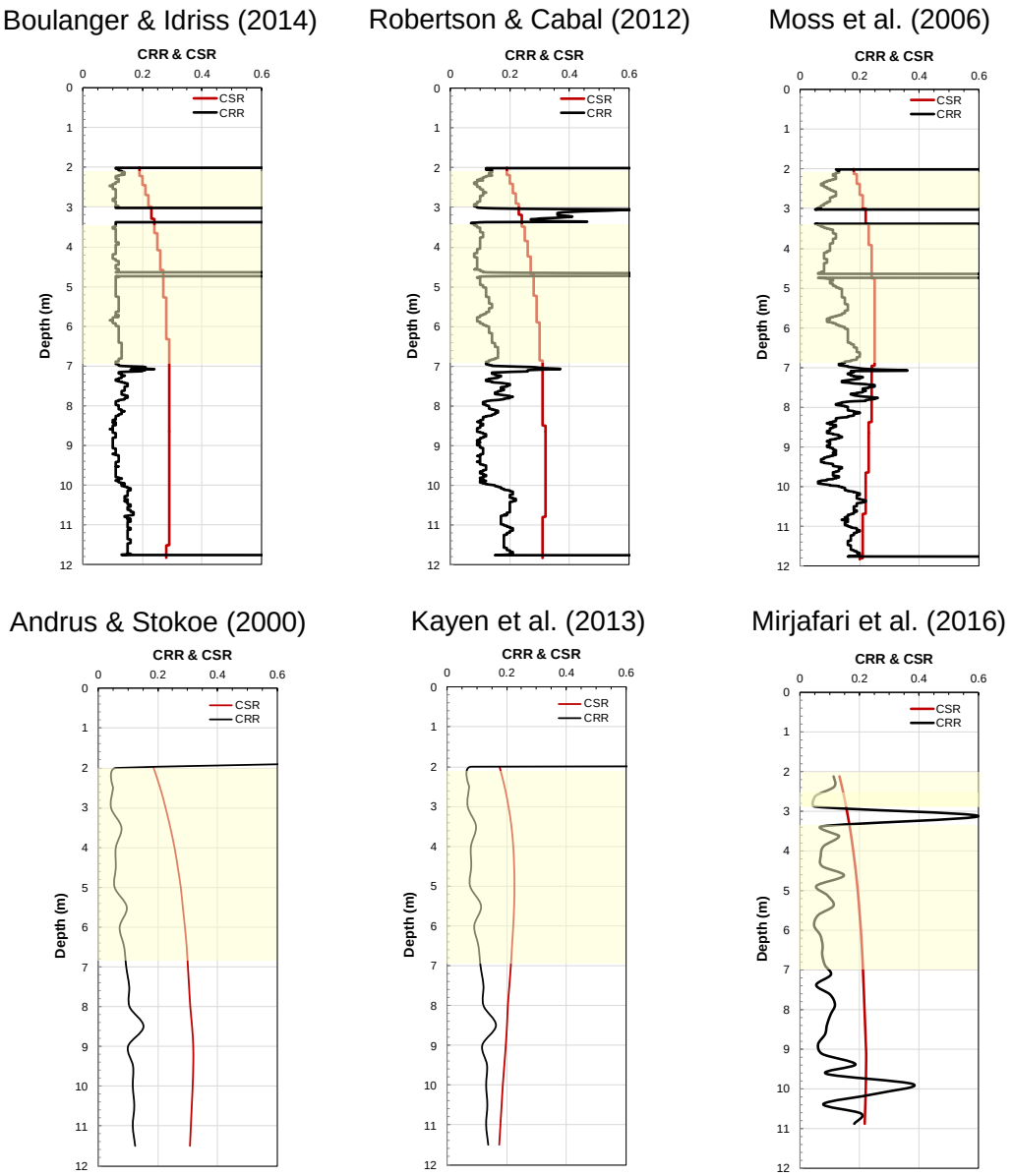

Figure 5: Liquefaction triggering results for site #1, with GWT=2.0m.

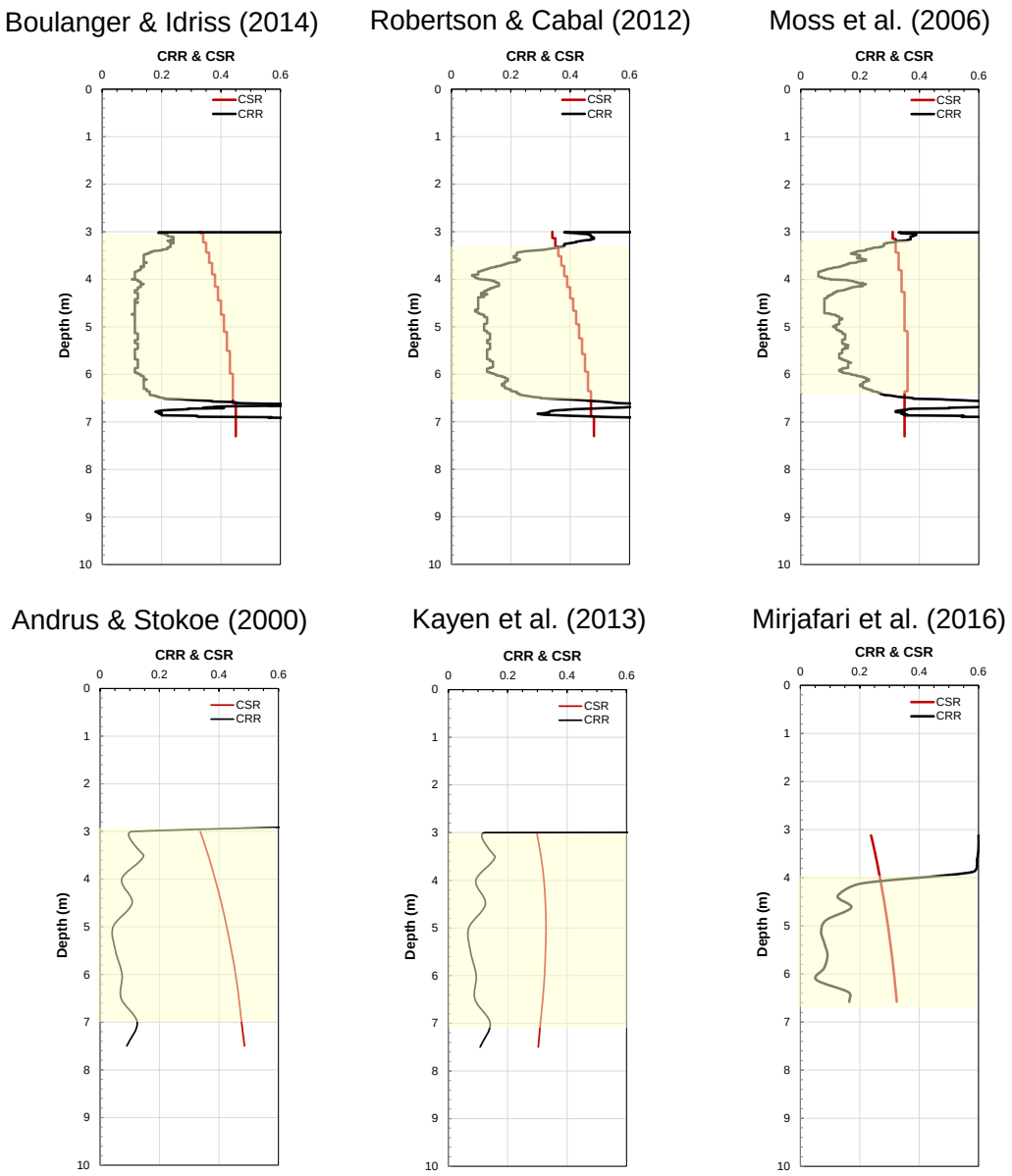

Figure 6: Liquefaction triggering results for site #2, with GWT=3.0m.

As mentioned earlier, borehole logs were taken at both sites and, in addition, undisturbed samples were obtained at site #1. Careful inspection of the obtained samples seems to indicate that the pumice contents at these sites were not as significant as initially reported in the literature (e.g. Pender et al. 2007). Figure 7 shows some of the samples obtained, where the pumiceous layers, depicted as white lenses, are not that many. Unfortunately, there are no reliable methods developed to date to quantify the pumice contents of soil deposits, so the authors cannot provide exact values except for visual inspection. As such, the current empirical methods developed for hard-grained sands seem to work well for these two sites.

4 CONCLUDING REMARKS

In order to investigate whether existing empirical field-based methods to evaluate liquefaction potential of sands, which were originally developed for hard-grained soils, are applicable to crushable pumice deposits, two sites were selected where liquefaction had been observed following the Edgecumbe earthquake. Manifestations of soil liquefaction, such as sand boils and

Figure 7: Samples of soils taken at site #1. White-coloured layers are pumiceous, while dark-coloured ones are hard-grained sands.

ejected materials, have been reported at both sites. Field tests, including cone penetration tests (CPT), shear-wave velocity profiling through seismic CPT, and screw driving sounding (SDS) tests were performed at the sites. Then, considering estimated peak ground accelerations (PGAs) at the site based on recorded motions following the 1987 earthquake and possible range of ground water table locations, liquefaction evaluation was conducted at the sites using available empirical chart-based approaches.

Using empirical methods, site #1 showed that all methods considered would predict liquefaction of pumice at depth ranging from the location of the water table up to the maximum depth. Similar results were obtained site #2. These results were consistent with the observed manifestation of liquefaction at the sites. Subsequent sampling showed that both sites have less pumice contents and, considering the large *CSR* at the sites, the current empirical methods appeared to predict well the liquefaction triggering at these deposits. Another reason may be the significant PGAs estimated at both sites.

From the results of this research, future work will focus on comparison of the liquefaction resistance of pumiceous sites in the Waikato region obtained in the laboratory (through undrained cyclic tests on high-quality samples) with those estimated from field-based parameters.

5 ACKNOWLEDGMENTS

The support of Whakatane District Council, AECOM and GNS Science in determining the target test sites is gratefully acknowledged. The assistance of Dr. Y Mirjafari and Mr B Asadi in conducting the calculations is also acknowledged. This project was supported by QuakeCoRE, a New Zealand Tertiary Education Commission-funded Centre. This is QuakeCoRE Publication Number 0201.

REFERENCES

Andrus RD & Stokoe KH II. (2000) Liquefaction resistance of soils from shear-wave velocity. *J. Geotech. Geoenviron. Eng.*, 126(11), 1015–1025.

Boulanger RW & Idriss IM. (2014) CPT and SPT based liquefaction triggering procedures. *Report No. UCD/CGM-14/01*, Center for Geotechnical Modeling, Department of Civil and Environmental Engineering, University of California, Davis, CA, 134 pp.

Kayen RE, Moss RES, Thompson EM, Seed RB, Cetin KO, Der Kiureghian A, Tanaka Y & Tokimatsu K. (2013) Shear-wave velocity–based probabilistic and deterministic assessment of seismic soil liquefaction Potential. *J. Geotech. Geoenviron. Eng*, 139(3), 407-419.

Mirjafari Y, Orense RP & Suemasa N. (2016) Soil classification and liquefaction evaluation using Screw Driving Sounding. *Proc., 5th International Conference on Geotechnical and Geophysical site Characterisation*, Gold Coast, Australia, 5-9 September 2016, 6pp.

Moss RES, Seed RB, Kayen RE, Stewart JP, Der Kiureghian A & Cetin KO. (2006) CPT-based probabilistic and deterministic assessment of in situ seismic soil liquefaction potential. *J. Geotech. Geoenviron. Eng*, 132(8), 1032-1051.

Mellsop, N. (2016) Personal communication.

Orense RP, Pender MJ & O'Sullivan A. (2012) Liquefaction characteristics of pumice sands. *Final Report of EQC Project 10/589*, 131pp.

Orense RP & Pender MJ. (2013) Liquefaction characteristics of crushable pumice sand." *Proc. 18th International Conference on Soil Mechanics and Geotechnical Engineering*, Paris, 4pp.

Orense R, Mirjafari Y & Suemasa N. (2013) Geotechnical site characterisation using Screw driving sounding method. *Proc. New Zealand-Japan Workshop on Soil Liquefaction during Recent Large-scale Earthquakes*, Auckland, NZ, 11-20.

Pender MJ, Robertson TW, eds. (1987) Edgecumbe Earthquake: Reconnaissance Report. *Bulletin of the New Zealand National Society For Earthquake Engineering*, 20 (3), 201-249.

Robertson PK & Cabal KL. (2012) *Guide to Cone Penetration Testing for Geotechnical Engineering*, 5th edition, Gregg Drilling & Testing, 131pp.

Wesley LD, Meyer VM, Pronjoto S, Pender MJ, Larkin TJ & Duske GC. (1999) Engineering properties of pumice sand. *Proc. 8th Australia-NZ Conference on Geomechanics*, Hobart, Vol. 2, 901 – 908.

Electro-osmosis stabilisation of slopes

M Naghibi & R P Orense
Department of Civil & Environmental Engineering, University of Auckland, NZ
mnag216@aucklanduni.ac.nz (Corresponding author)

H Abuel-Naga
School of Engineering and Mathematical Sciences, La Trobe University, AU
h.aboel-naga@latrobe.edu.au

Keywords: electro-osmosis, consolidation, slope stabilisation, field test, laboratory test

ABSTRACT

Slope failure is a major concern in New Zealand roads. Applying conventional slope stabilisation techniques, such as slope repair, benching, wire netting and soil nailing, is not always practical due to financial and environmental concerns. Electro-osmosis (EO) consolidation technique can provide engineers with a low impact and economical solution for that purpose. EO induces water movement in the fine-grained soil body due to external electric potential gradient (voltage) by establishing a net water flow toward the cathode and creating negative pore water pressure that produces soil consolidation. The external electric potential gradient is normally applied by means of conductive electrodes which can be laid horizontally for slope stabilisation. In this paper, a systematic review of EO consolidation case histories and large-scale experiments have been presented with the aim of establishing an initial cost-effective design framework for EO consolidation scheme in slopes. The hydraulic permeability, electrical resistivity and EO permeability of soil have been identified as factors controlling the shear strength improvement, EO efficiency and power consumption. In addition, depending on soil and system properties, up to approximately 300% increase in shear strength has been achieved.

1 INTRODUCTION

Some parts of New Zealand are covered by fine-grained soils, such as Oamaru clay loam in Southland, Waikato silty clay and Taranaki/Manawatu humic clay. In many cases, these soils need to be improved for the purpose of slope stabilisation and structural support. The traditional preloading consolidation method is one of the effective ground improvement techniques; however, it is time consuming and is not applicable in all cases. For instance, this technique cannot be used to enhance slope stability. In fact, slope failure often occurs because of pre-loading and the effect of other factors, including pore water increases, ground water flow and seasonal climate changes. Several ground improvement and repair methods for slopes are available, such as changing slope geometry and using stabilising piles, though their feasibility depends on site situation and project budget. Hence, there is a need to find a method for slopes that could overcome most of the limitations of the conventional methods.

Electro-osmosis (EO) is one of the efficient techniques in geotechnical engineering that could be used for this purpose. In many situations, because of the limitation related to load application and environmental and financial constraints, this technique is identified as a unique option (Bjerrum et al. 1967). Simply put, EO works in the following way: generally, under the influence of an electric potential, the cations within the body of saturated soil mass are drawn to the cathode and the anions to the anode. Ions carry their water of hydration and exert a viscous drag on the water around them. When the soil is subjected to direct current (DC), electric potential gradient induces a net water flow toward the cathode and creates negative pore water pressure that produces soil consolidation (Mitchell and Soga 2005). This method has been proven as a low impact,

environmentally-friendly and cost-effective technique. In addition, EO could consolidate the soil without clearing trees in forested areas (Jones et al. 2011). The characteristics of electrodes, properties of the soil, level and duration of applied potential difference and power consumption control the improved soil behaviour (Mimic et. al. 2001; Jeyakanthan 2011). Unfortunately, lack of knowledge in the field of electro-hydro-mechanical (EHM) behaviour of EO-treated soils, power consumption and, consequently, cost of the EO ground improvement technique restricts the applicability of this method. In addition, although the laboratory-scale understanding of EHM behaviour of the soil has improved recently, case histories of electro-osmosis consolidation in large-scale play a significant role in understanding the in-situ EHM behaviour. Therefore, to have a thorough understanding of EO consolidation effects and efficiency, laboratory and field scale tests should be studied simultaneously.

In this paper, the application of EO consolidation for slope stabilisation purposes in laboratory and field scale is investigated. In addition, the post-treated soil behaviour is studied in order to propose a more efficient EO consolidation set up and to determine the feasibility of EO system on slopes.

2 ELECTRO-OSMOSIS SYSTEM PROPERTIES AND APPLICATIONS

Generally, the electric field is applied by means of installing electrodes in the body of the soil in various directions. Based on electrode alignments, the application of electro-osmosis consolidation can be categorised into two general cases; (1) ground improvement applications and (2) slope stabilisation. As shown in Figure 1, for ground improvement purposes the electrodes are usually laid in vertical alignment.

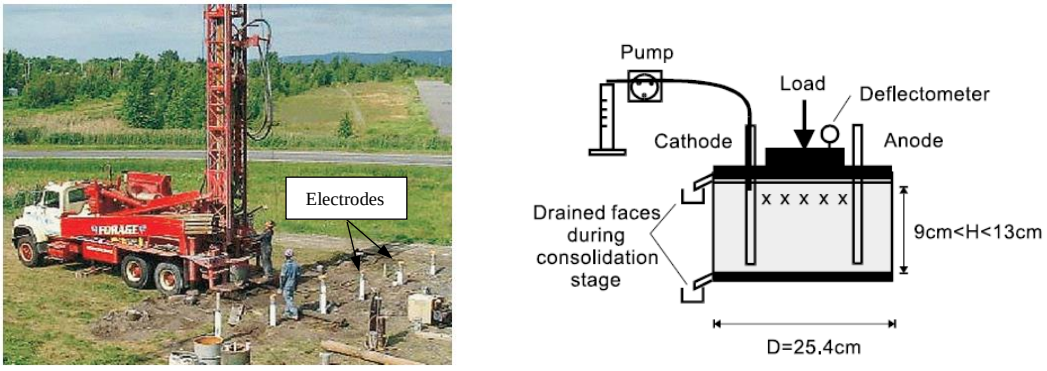

(a) **(b)**

Figure 1: Electro-osmosis ground improvement tests: (a) field test (Burnotte et al., 2004); and (b) laboratory test (Lefebvre and Burnotte, 2002)

Therefore, to accurately model the EO consolidation, the laboratory apparatus should be designed to accommodate the electrodes vertically in the testing cell (Figure 1b). However, in case of slope stability the electrodes are installed in horizontal alignment as shown in Figure 2. In addition, a self-climbing rig can be used to install electrodes on the slopes with no deforestation, as shown in Figure 2a. In such a case, the metallic electrodes can also be maintained in place to confine the soil and provide further improvement after EO treatment. Therefore, to accurately model the EO slope stability application in the laboratory, the electrodes should be installed in horizontal direction, as shown in Figure 3.

In addition to the electrodes alignment, electro-osmosis system properties consisting of level of applied electrical difference (V), electrode length (L) and electrode spacing (S), govern the behaviour of post-treated soil and economics of the EO improvement project. Therefore, depending on level of required treatment, the system properties and cost of the project can be estimated.

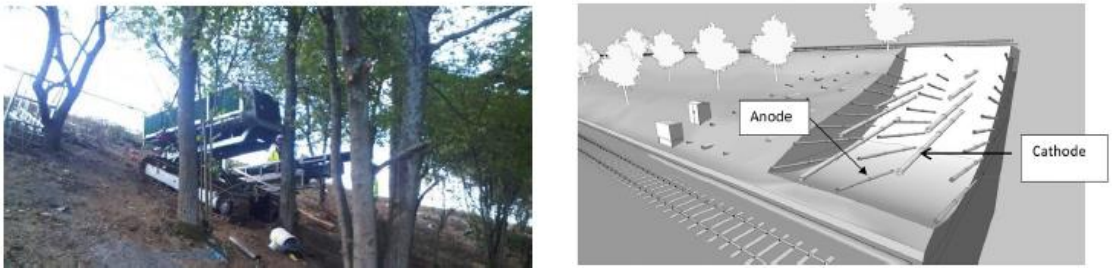

(a) self-climbing rig to install electrodes **(b) electrode alignment in slopes**

Figure 2: EO slope stabilisation (Lamont-Black et al., 2016)

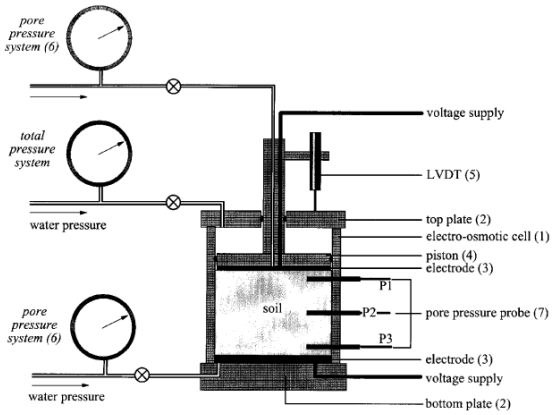

Figure 3: Typical laboratory EO cell for slope stabilisation application (Hamir et al., 2001)

3 BEHAVIOUR OF POST-TREATED SOIL

The properties of the EO system govern the characteristics of post-treated soil. Generally, the effect of system properties on post-treated soil behaviour is verified using post-treated soil response namely improvement depth (*ID*), undrained shear strength (S_u) of post-treated ground and soil settlement. In addition, the cost of a project depends on the level of power consumption which is governed by the electrical resistivity of soil. In terms of slope stability, *ID*, S_u and economics of the EO project are crucial factors which need to be fully investigated.

3.1 Improvement depth

Basically, *ID* is defined as a depth below which the shear strength of soil remains unchanged. Measurement of *ID* is not practical in laboratory tests as the specimen length is usually limited. Therefore, case histories have been used to accurately measure *ID*. In addition, results from vertical and horizontal alignment can be used to measure *ID*. A number of case histories, with various electrode materials, levels of *V/S* and improvement durations, show the *ID* to be exactly equal to the length of electrodes (Lo et al. 1991b; Ou et al. 2009). However, in case of quick clay of Norway, *ID* = 7m has been reported for 9m long steel electrodes (Bjerrum et al. 1967) while *ID* = 7m has been observed in soft Montreal clay with 5m long steel electrodes (Burnotte et al. 2004). The discrepancy observed in these cases can be attributed to the electrode diameter, *D*. Looking at the results, *D/L*=0.02 and *D/L*=0.4 correspond to *ID/L*=0.75 and *ID/L*=1.4, respectively. It should be noted that *D/L*=0.1 with acceptable level of *V/S* leads to *ID/L*=1 in EO system with metallic electrodes (Lo et al. 1991a; Ou et al. 2009). Therefore, by selecting *D/L* > 0.1 the treatment length *L* can be expected.

3.2 Shear strength of post-treated soil

Generally, a vane shear test is used to measure the shear strength of the pre/post-treated soil in the field and in the laboratory. For normally consolidated soil, the shear strength can be estimated

using the soil's preconsolidation pressure, as explained in Equation (1) (Bjerrum et al. 1967; Burnotte et al. 2004; Jeyakanthan et al. 2011):

$$C_u = \alpha_u \, \sigma'_p \tag{1}$$

where C_u is the undrained shear strength of the soil, σ'_p denotes preconsolidation pressure of the soil and α_u is the shear strength ratio. In addition, application of an electric potential gradient generates maximum negative porewater pressure at the anode side which is considered as the maximum generated preconsolidation pressure in the treated soil. Therefore, the level of increase in shear strength in post-treated soil can be computed as:

$$\Delta C_u = \alpha_u \, u_{max} \tag{2}$$

where u_{max} is maximum generated pore water pressure during EO consolidation, which is usually estimated based on an EO governing equation:

$$\partial^2 u_e/\partial y^2 + (k_e \gamma_w/k_h) \times \partial^2 V/\partial y^2 = (1/C_v) \times \partial u_e/\partial t \tag{3}$$

where k_e and k_h are the EO and hydraulic permeability, respectively. These parameters can be measured from an EO consolidation test similar to that shown in Figures 1 and 2. u_e and C_v denote the developed pore water pressure and coefficient of consolidation, respectively. By solving Equation (3), u_e can be found as:

$$u_e = - (k_e \gamma_w/k_h) \times V_x \tag{4}$$

Considering V= 0 at the cathode and V= V_{max} at the anode side, the maximum negative pore water pressure occurs in the anode side and no pore water pressure develops in the cathode. Therefore, maximum pore water pressure is:

$$u_{max} = - (k_e \gamma_w/k_h) \times V_{max} \tag{5}$$

It should be noted that the distribution of voltage across the electrodes is considered linear in majority of previous research. However, as the electrical resistivity of soil varies during consolidation, a linear voltage distribution cannot provide the most accurate results for calculation of maximum developed pore water pressure. Figure 4 shows the level of shear strength observed in the laboratory and field trials before and after EO consolidation. A list of utilised laboratory and field trials are provided in Table 1. Lo et al. (1991a) applied electric field intensity of 0.29 - 0.39 V/cm to Leda clay and an increase of 113.6 - 172.7% in average shear strength was observed. However, a maximum of 50.8% increase in average shear strength was reported in the field with similar electric intensity (0.1 - 0.4 V/cm).

Table 1: Properties of EO systems used in experimental tests

Test ID	Ave. Pore pressure developed (kPa)	Initial shear strength (kPa)	Final shear strength (kPa)	Reference
L-1	-75	11	30	Lo et al. (1991a)
F-1	-44.5*	18.2	27.4	Lo et al. (1991b)
L-2a	-101*	47	76	Lefebvre & Burnotte (2002)
L-2b	-98*	29	57	Lefebvre & Burnotte (2002)
L-2c	-263*	48	123	Lefebvre & Burnotte (2002)
F-2	-135*	30	60	Burnotte et al. (2004)
L-3	93	30	57.9	Win et al. (2001)
F-3	10	30	46	Chew et al. (2004)

*estimated by the authors based on Equations (1) – (3)

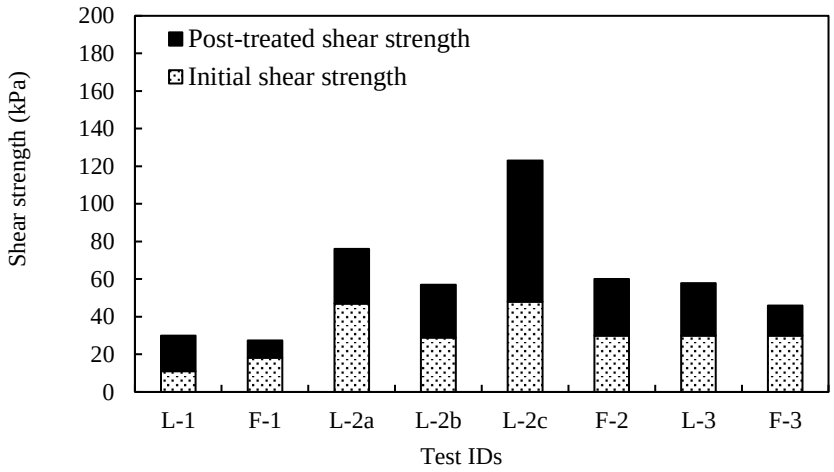

Figure 4: Comparison between measured initial and post-treated shear strength in laboratory and field trials

Lefebvre and Burnotte (2002) tested one specimen with σ'_p=175 kPa using the conventional method (test L-2a) and two other specimens with σ'_p=105 and 175 kPa using a treated EO system (tests L-2b & c). The average initial shear strengths of the soil with σ'_p=105 and 175 kPa were 29 kPa (test L-2b) and 47-48 kPa (tests L-2a & c), respectively. The post-treatment shear strengths of the specimen in test L-2b, L-2c and L-2a were reported to be 57, 123 and 76 kPa, respectively. Burnotte et al. (2004) reported 30 kPa for the initial shear strength of the soil in the field, which has been improved to an average of 60 kPa. A major improvement in shear strength has been observed in the anode vicinity. In the case of the Singapore marine clay, a maximum of approximately 50% shear strength increase was reported by Chew et al. (2004) in the field. However, Win et al. (2001) extracted a sample of similar clay from a depth of 17-17.8m (more or less similar to Chew et al. 2004) and tested it in the laboratory. Approximately σ'_p= 93 kPa achievement has been observed at the end of the EO process. Based on the results less deviation has been observed when the same electrode alignment is used in field and laboratory trials considering a more or less similar EO system. This fact signifies the importance of electrode alignment in estimation of EO system applicability in laboratory.

3.3 EO efficiency and power consumption

By definition, the EO efficiency is the amount of transported water per unit charge that passes through the soil. Thus, if efficiency is denoted by *e*, then:

$$Q = e\, I \tag{6}$$

where Q and I are water discharge and electrical current respectively. Based on Casagrande's relationship:

$$Q = k_e\, i_e\, A \tag{7}$$

where

$$i_e = V/L \tag{8}$$

Hence,

$$Q = k_e\, A \times (V/L) = e\, I \tag{9}$$

and

$$e = k_e \times (VA/IL) \tag{10}$$

This can be simplified to

$$e = \rho\, k_e \tag{11}$$

The electrical resistivity, ρ, of clays varies between 1 to 100Ω.m whereas k_e ranges from 1×10^{-8} to 1×10^{-9}. Therefore, the maximum theoretical efficiency is 1×10^{-6} m^3/C where C is unit charge (coulomb). To represent the EO efficiency of each type of soils as a percentage and for more convenient comparison, the EO efficiency has been normalised by the maximum theoretical efficiency (1×10^{-6} m^3/C), which is assumed to correspond to 100% efficiency. Based on this definition, the isochrone for EO efficiency has been generated and shown in Figure 5 with dotted lines. Percentage of efficiency (e%) has been defined as:

$$e\% = (e/e_{max})\times100\% \tag{12}$$

The EO efficiency for various tested materials is also shown in the figure. For all tested materials at low salinity levels, e% varies in a narrow range of 4 - 12%. In addition, the softer the soil, the higher the EO efficiency is. Soils which are categorised as soft show e% = 10 -12%; however, all tested stiff clays show e% = 4 - 10%. Therefore, by determining either one of the parameters ρ or k_e, the other one can be estimated based on Figure 5.

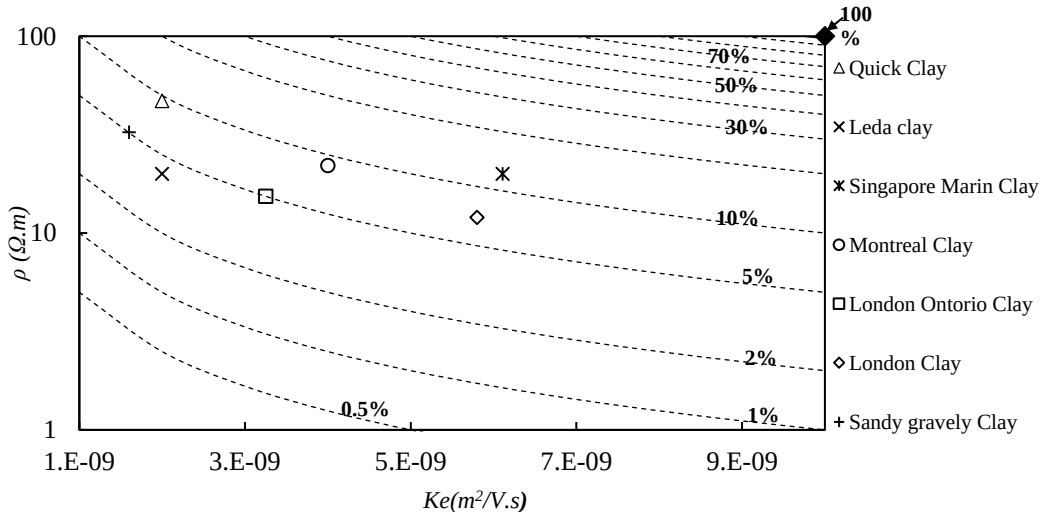

Figure 5: EO efficiency in various clays

Knowing the required level of improvement and accurate determination of EO efficiency leads to an estimation of the required voltage which holds a great importance in estimation of consumed power. In addition to the level of applied voltages, the level of power consumption depends on electrical response of soil to applied voltage (current). Based on Ohm's law, the level of power consumption in the EO system can be estimated as:

$$P = V^2/R \tag{13}$$

where R is soil resistance. To extend the estimated power consumption to the field, P is normalised by the volume of treated soil. Therefore:

$$P/vol = V_L^{\,2}/\rho \tag{14}$$

where V_L is electric field intensity which is defined as V/L (V/m) and *vol* denotes the volume of treated soil. In addition, based on experimental results in laboratory scale, approximately 40% of the applied potential will be lost in the soil-electrode vicinity due to loose soil-electrode connection and chemical processes. This potential loss should be considered in Equation (14). Therefore, considering 40% potential loss at soil-electrode interface, knowing the electrical resistivity of soil and applied electrical potential gradient, the level of power consumption can be estimated by Equation (14). Figure 6 shows the calculated power consumption based on the Ohm's rule considering the potential loss at the soil-electrode interface. Each dotted line shows specific level of power consumption in kW/m^3. For comparison, the consumed power of available field trials is also shown. In the majority of the field trials, the field-measured consumed power indicates a higher level of power rather than that shown for calculated power consumption. These results show more than 40% of potential loss in the field rather than that observed in the laboratory tests. In other words, the level of potential losses observed in the field is much higher than those measured in the laboratory. The reasons for this difference can be attributed to the lack of voltage calibration in the laboratory, short term measurement of voltage drops and perfect contact of soil-electrode in horizontal electrode configuration in the laboratory.

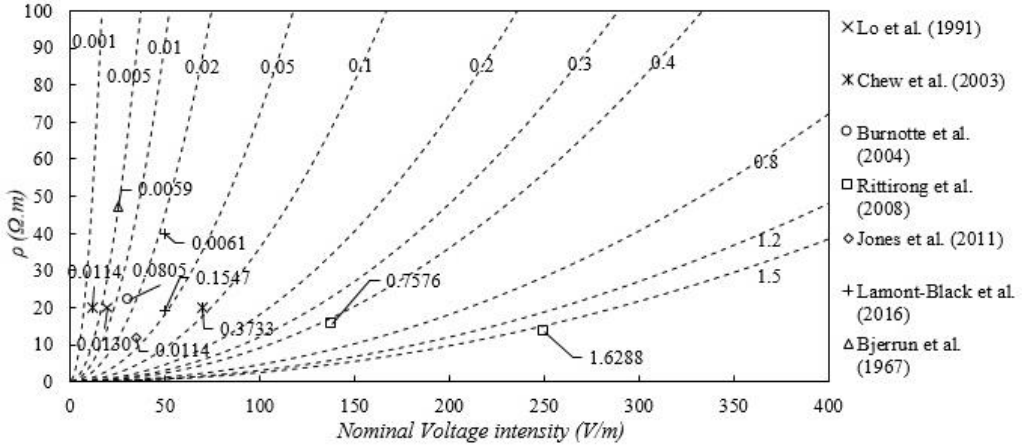

Figure 6: EO power consumption in various clays

4 CONCLUSIONS

EO consolidation can be used as a low-impact, environmental-friendly technique to stabilise slopes. A number of successful field tests had been carried out using voltage gradient of approximately 0.1 to 0.4 V/cm. Depending on soil types and electrode spacing, up to 300% increase in shear strength of the soil had been reported compared to the initial shear strength. In addition, in the case of an electrode dimension of $D/L > 0.1$ the effects of soil improvement have been observed up to a length equal to the electrode length (L). The efficiency of EO technique has been compared with the maximum theoretical efficiency and efficiency between 4 - 12% had been measured for various clays. In addition, the EO efficiency of soil implies the level of power consumption for a specific EO project from which the cost of a project can be estimated.

REFERENCES

Bjerrum, L., Moum, J. and Eide, O. (1967) Application of electro-osmosis to a foundation problem in a Norwegian quick clay. *Geotechnique,* 17(3): 214-235.

Burnotte, F., Lefebvre, G. and Grondin G. (2004) A case record of electroosmotic consolidation of soft clay with improved soil-electrode contact, *Canadian Geotechnical Journal*, 41(6): 1038-1053.

Chew, S.H., Karunaratne, G.P., Kuma, V.M., Lim, L.H., Toh, M.L. and Hee, A.M. (2004) A field trial for soft clay consolidation using electric vertical drains, *Geotextile and Geomembranes*, 22(1-2): 17-35.

Hamir, R. B., Jones, C. J. F. P. and Clarke, S. (2001) Electrically conductive geosynthetics for consolidation and reinforced soil. *Geotextile and Geomembranes*, 19(8), 455-482.

Jeyakanthan, V., Gnanendran, C.T., and Lo, S.-C.R. (2011) Laboratory assessment of electro-osmotic stabilization of soft clay, *Canadian Geotechnical Journal*, 48(12): 1788-1802.

Jones, C.J.F.P., Lamont-Black, J. and Glendinning, S. (2011) Electrokinetic geosynthetics in hydraulic applications. *Geotextile and Geomembranes*, 29(4): 381-390.

Lamont-Black, J., Jones, C.J.F.P. and Alder, D. (2016) Electrokinetic strengthening of slopes - Case history. *Geotextile and Geomembranes*, 44(3): 319-331.

Lefebvre, G. and Burnotte, F. (2002) Improvement of electroosmotic consolidation of soft clays by minimizing power loss at electrodes, *Canadian Geotechnical Journal*, 39(2): 399-408.

Lo, K.Y., Inculet I.I. and Ho, K.S. (1991a) Electroosmotic strengthening of soft sensitive clay, *Canadian Geotechnical Journal*, 28(1): 62-73.

Lo, K.Y., Ho, K.S. and Inculet I.I. (1991b) Field test of electroosmotic strengthening of soft sensitive clay, *Canadian Geotechnical Journal*, 28(1): 74-83.

Mimic, S., Shang, J.Q., Lo, K.Y., Lee, Y.N. and Lee, S.W. (2001) Electrokinetic strengthening of a marine sediment using intermittent current. *Canadian Geotechnical Journal*, 38(2), 287-302.

Mitchell, J.K., and Soga, K. (2005) *Fundamentals of Soil Behaviour*, John Wiley and Sons Press

Ou, C., Chien, S. and Chang, H. (2009) Soil improvement using electroosmosis with the injection of chemical solutions: field tests. *Can. Geotech. J.*, 46(6), 727-733.

Win, B.M., Choa, V. and Zeng X.Q. (2001) Laboratory investigation on electro-osmosis properties of Singapore clay, *Soils and Foundations*, 41(5): 15-23.

Keepa, C., Adhikari, G., Murashev, A., Cubrinovski, M. & Lloyd, N. (2017)
NZ Transport Agency's Detailed Design Guidance for Piled Bridges at Sites Prone to Liquefaction and Lateral Spreading
Proc. 20th NZGS Geotechnical Symposium. Eds. GJ Alexander & CY Chin, Napier

NZ Transport Agency's Detailed Design Guidance for Piled Bridges at Sites Prone to Liquefaction and Lateral Spreading

C Keepa
Opus International Consultants, NZ
Campbell.Keepa@opus.co.nz

G Adhikari
Opus International Consultants, NZ
Gopal.Adhikari@opus.co.nz

A K Murashev
Opus International Consultants, NZ
Alexei.Murashev@opus.co.nz

M Cubrinovski
University of Canterbury, NZ
misko.cubrinovski@canterbury.ac.nz

J N Lloyd
New Zealand Transport Agency, NZ
Nigel.Lloyd@nzta.govt.nz

Keywords: bridge, pseudo-static analysis, pile foundation, liquefaction, lateral spreading, displacement based method, performance based design, earthquake engineering

ABSTRACT

This paper presents a summary of an example of application of pseudo-static analysis in the design of a bridge on a site prone to liquefaction. The example is one of the outcomes from Stage 2 of a research project commissioned by the NZ Transport Agency (NZTA) to develop a comprehensive design guidance for piled bridges for liquefaction and lateral spreading effects. The Stage 1 report, published on the NZTA website in 2014, provides the key design recommendations for bridges located on sites prone to liquefaction and lateral spreading. The Stage 2 report gives detailed procedures for geotechnical field and laboratory testing, liquefaction evaluation methods and examples for two bridge sites, detailed description of recommended procedures for pseudo-static analysis (including flow charts for the design process), overview of dynamic analysis methods and detailed design examples for two bridges. The design requirements and guidelines given in Stage 1 report are to be incorporated in the NZ Transport Agency's Bridge Manual and disseminated to the wider New Zealand engineering community. A summary of the Stage 2 report is given and the design procedure for the design of two bridges for liquefaction and lateral spreading effects is described in detail.

1 INTRODUCTION

There are many case histories worldwide where extensive damage to piled bridges has been observed due to excessive lateral ground displacements and subsidence associated with liquefaction. A variety of methods is available in the literature for the evaluation of the performance of piled bridges on sites susceptible to liquefaction. With a goal of developing a unified approach consistent with the concept of Performance Based Earthquake Engineering (PBEE), the NZ Transport Agency commissioned a research project towards the development of

guidelines for the design and assessment of piled bridges at sites prone to liquefaction and lateral spreading in New Zealand. The first stage of this work has culminated in the NZTA Research Report 553 (2014). This report provides recommendations on pseudo-static analysis procedures to assess the effects of liquefaction and lateral spreading in the design of pile foundations for bridges. These recommendations have recently been incorporated in the 3rd edition of the New Zealand Transport Agency's Bridge Manual (2016).

The objective of the second stage is to provide practical examples of the use of the recommended procedures for the investigation and assessment of liquefaction and the assessment and design of piled bridges on sites with liquefiable soils. The project team comprised Opus Consultants, University of Canterbury (Prof. Misko Cubrinovski and Dr Jennifer Haskell) and Dr John Wood. Two practical examples are presented in Stage 2 report to demonstrate the Pseudo-Static Analysis (PSA) procedure. The first example illustrates performance evaluation of an existing bridge, ANZAC bridge, a 4-span reinforced concrete bridge crossing the Avon River in Christchurch. The bridge was severely affected by liquefaction and lateral spreading in the September 2010 M7.1 Darfield Earthquake and the February 2011 M6.2 Christchurch Earthquake. The second example demonstrates design of a new 2-span bridge at a grade separated intersection over the four-lane expressway north of Christchurch. This example is summarised in this paper.

2 ANALYSIS FRAMEWORK

The PSA procedures described in NZTA research report 553 (Murashev, 2014) are intended to provide a simplified yet accurate enough analysis tool for routine design or performance evaluation of pile foundations of a bridge. Among various PSA methods described, the displacement based approach developed by Cubrinovski is recommended in the Stage 2 report. In this approach, ground displacements are applied to the piles through bi-linear soil springs. This is consistent with the PBEE framework.

Being a simplified static procedure, three separate sets of analyses are required to capture the peak responses of piles during an earthquake, as recommended in NZTA research report 553 (Murashev et. al., 2014) and in the Bridge Manual (2013). The phases considered in the PSA are:

- Pre-liquefaction.
- Cyclic liquefaction.
- Lateral spreading.

The design is an iterative process that starts with an assumed layout and sizing of the load resisting elements followed by analysis of the piled system using the procedure outlined in Murashev et al. (2014) and then adjustments to the structure and re-analysis until the design meets the performance requirements. The Stage 2 report provides detailed guidance on the analysis procedure and how different parameters are estimated.

3 SITE AND STRUCTURE DESCRIPTION

This example demonstrates the use of the recommended analysis procedure in the design of a new bridge constructed as part of a new expressway between Christchurch and Kaiapoi. The bridge is part of a grade separated intersection taking a two lane local road over a new four lane expressway. The site is a relatively flat site. Approaches to the 53 m long bridge are formed with earth embankments up to 8 m high with spill through slopes at the abutments. The site geology consists of deep alluvial and marine deposits with loose sands and soft organic silt deposits in the upper 9.5 m of the ground profile. The site is within 20 km of the faults that caused the M7.1 Darfield and the M6.3 Christchurch Earthquakes in 2010 and 2011 and experienced peak ground accelerations estimated to be between 0.16 g and 0.22 g in these two events.

The superstructure, as shown in Figure 1, comprises two equal spans (2x26.50m) 16 no, 900mm deep single hollow core units seated on elastomeric bearing strips at the pier and connected integrally to the abutment cap. The foundation system comprises 3 no of 1200mm diameter concrete piles at the pier and 5 no of 900mm diameter concrete piles at each abutment. The pier piles are 24m long and the piles at each abutment are 30m long.

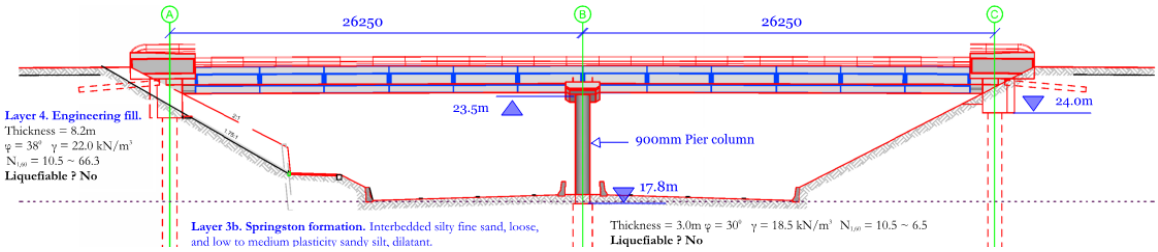

Figure 1: Longitudinal section of the bridge with idealised soil profile

4 GROUND CONDITIONS AND SEISMICITY

Ground conditions beneath the bridge and embankments have been assessed from 7 cone penetrometers, two including shear wave measurement and 4 fully cored boreholes. The site is underlain by 9.5 m of interbedded and laterally variable alluvial sand and silt over bank and flood channel deposits of the Springston Formation. Underlying the Springston Formation, from a depth of 9.5 m is the Christchurch Formation which extends to a depth of about 23 m and overlies the Riccarton Gravels. The Christchurch Formation comprises beach and dune sand deposits along with undifferentiated estuarine, lagoon and coastal swamp deposits of gravel, sand, silt, clay, shell and peat. The Riccarton Gravels, encountered from a depth of about 23 m comprise sandy and silty coarse gravel glacial outwash deposits interbedded with occasional layers of stiff to hard silt. The Riccarton Gravels are part of a series of Pliocene-Pleistocene marine sediments that are estimated to extend to a depth of about 580 m and are underlain by the Kowhai formation sediments.

As this is a local road bridge, a 1000 y return period was approved by the NZTA for the Ultimate Limit State (ULS) design. The site is classified as a Class D, Deep Soil site in accordance with NZS 1170.5. Using the method recommended by the Bridge Manual, the calculated peak ground acceleration for a 1000 y earthquake is 0.35 g. The effective earthquake magnitude for a 1000 year return period is M6.25 for northern Christchurch.

5 LIQUEFACTION AND LATERAL SPREADING

The propensity for significant excess porewater pressures or liquefaction to be generated in a ULS earthquake have been assessed using the empirical method by Boulanger and Idriss (2014). The fines content of each layer was estimated from i_c using the relationship proposed by Boulanger and Idriss calibrated to the measured fines content in sieve analyses. Results of the triggering analysis are shown in Figure 3. Observations following the CES indicated that the simplified methods over-predicted the extent of liquefaction at some sites with thinly layered soils. Possible reasons for this are discussed in the stage 2 report. The level of over-prediction of the thinly interbedded soils were evaluated in a qualitative sense with reference to observations of the site performance in the Canterbury Earthquake Sequence (CES). The layer of sand and low plasticity silt between depths of 3.3 m and 6 m below ground level is anticipated to liquefy at ULS earthquake.

Free field vertical and horizontal ground displacement profiles for the cyclic liquefaction case and the lateral spreading case have been calculated using the methods described in the stage 2 report and are shown in Figure 2. Cyclic ground displacements of non-liquefied soils have been estimated by integrating peak shear strains determined using the cyclic stress ratio and soil's secant shear modulus.

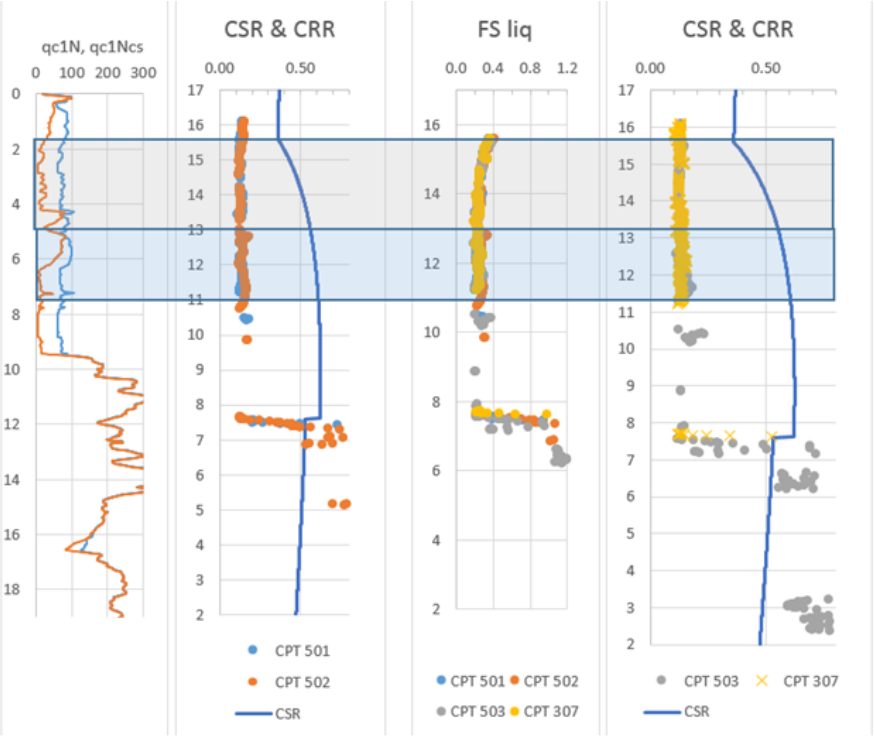

Figure 2: Results of Liquefaction Assessment for ULS

In estimating the free field lateral spread displacements, consideration has been given of the continuous crust overlying the liquefiable soils providing some resistance to spreading, the limited width of soil embankment driving lateral spreading and observations of spreading of the Chaneys Road approach embankments in the Canterbury Earthquake Sequence. We have assumed that permanent horizontal ground displacement of the soils below a depth of 9.5 m, (the base of the soft organic soils) will be negligible as a stability analysis shows that the relatively strong and stiff medium dense sands will constrain spreading to the soils above this layer. With the lack of simplified methods available to estimate permanent horizontal displacement of the soft organics, non-liquefied soils and the embankment fill at the abutments, permanent horizontal ground displacements in these layers have been estimated by multiplying the maximum cyclic ground displacement by a factor.

6 BRIDGE PILE ANALYSIS

The bridge was designed in accordance with the Displacement Based Design (DBD) method as given in the draft Section 5 of the Bridge Manual (2013). Analysis is carried out using a 3D model of the whole bridge in SAP2000. The piles are modelled using beam elements with nonlinear soil springs, to represent the vertical and lateral response of the surrounding soil.

At the beginning of the seismic design phase, the main lateral load resisting elements of the bridge, namely, the pier columns and piles, and the abutment piles, were modelled using their elastic effective member stiffness accounting for the degradation due to cracking. Geometric nonlinearity was included to capture the effect of large displacement demands on the piles, especially for the lateral spreading phase. Once the location of the plastic hinges are known,

further analysis including inelasticity with plastic hinges inserted in the elements at appropriate locations is undertaken. This allows the actual rotation demand in the hinges under a ULS or Major event to be evaluated and the remaining rotational capacity and likely post-earthquake repair requirements to be assessed.

Three types of soil springs were employed to simulate the lateral and vertical responses of the surrounding soil. The lateral soil resistance was modelled using the p-y springs. T-z springs represented the skin friction along the pile shaft and a q-z spring simulated the end bearing response of each pile. All springs were assumed uncoupled, i.e., the response of one spring depends only on the respective soil deformation at the spring location and is not influenced by the response of other springs at the same node. The passive resistance behind the abutment backwall was modelled using a row of soil springs using a simplified bi-linear curve. Soil springs and ultimate pressures were calculated using the methods prescribed in the NZTA research report 553 and the Stage 2 report. The analysis model developed in SAP2000 is presented in Figure 3.

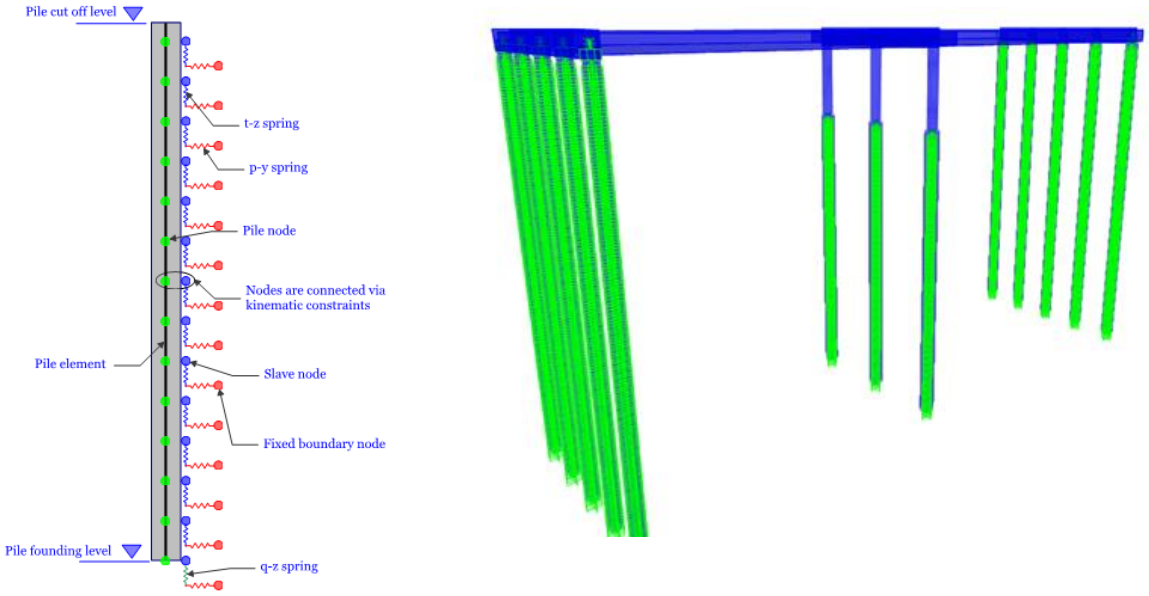

Figure 3: Idealised pile model and isometric view of complete ridge model in SAP2000

The peak pile response is then calculated from a pseudo-static analysis for each of the three phases representing the ground response during an earthquake, namely:

- Phase 1, cyclic phase without liquefaction (Pre-liquefaction phase)
- Phase 2, cyclic phase considering liquefaction and cyclic displacement of soils.
- Phase 3, lateral spreading phase including effects of liquefaction and lateral spreading on the pile foundations and bridge structure.

The main issue with the whole bridge model is how the kinematic loads are applied to different supports (e.g. piers and abutments) in each phase. In Phase 2, being a transient phase, the direction of kinematic displacements is not intuitive. Peak ground displacements at the opposing abutments could be in the same direction or opposing directions and may not occur concurrently at each support. In phase 3 there could be some permanent ground displacement at the pier and possibly differing extent of displacement at the abutments from differences in the ground conditions and asymmetry of the earthquake loading. There is no general consensus about how to consider different peak ground displacements at different supports together with the inertial demands from the superstructure in a pseudo-static analysis. Therefore, a significant amount of engineering judgement, as well as parametric analyses of the whole bridge model is required to envelope all

the possible design cases. The scenarios considered for the three phases in the analysis of the over-bridge in this example are shown in Figure 4.

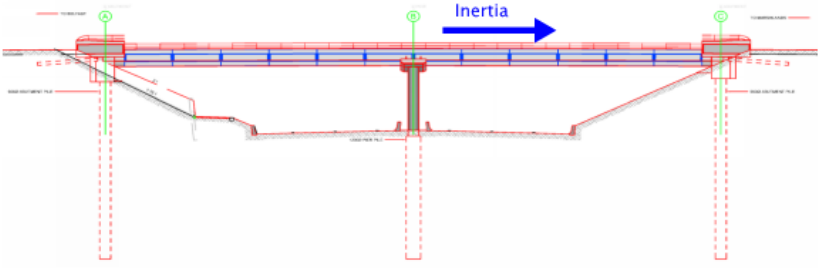

Phase 1. Pre-liquefaction.
Effective stiffness for lateral load resisting elements and standard soil springs

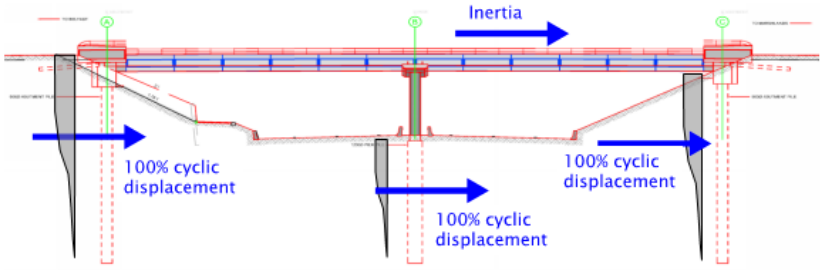

Phase 2a. Cyclic Phase.
Effective stiffness for lateral load resisting elements and liquefaction compatible soil springs

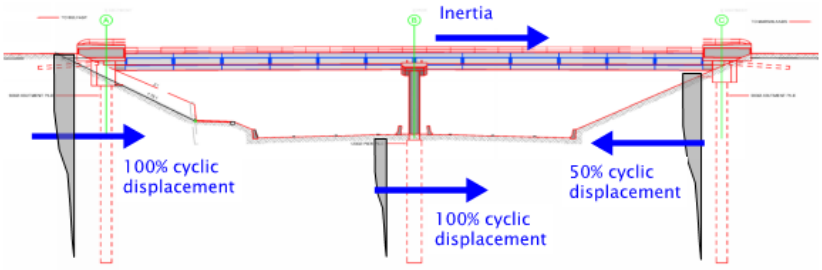

Phase 2b. Cyclic Phase.
Effective stiffness for lateral load resisting elements and liquefaction compatible soil springs

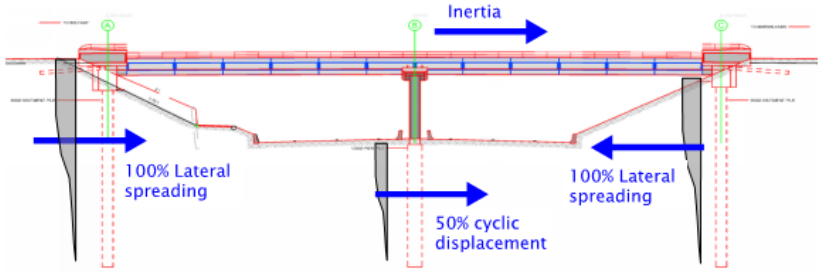

Phase 3a. Lateral spreading Phase.
Effective stiffness for lateral load resisting elements and lateral spreading compatible soil springs

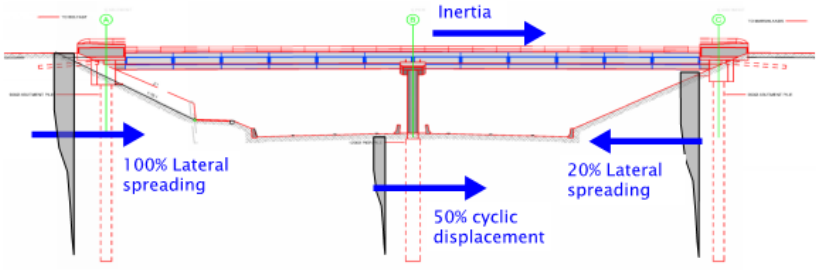

Phase 3b. Lateral spreading Phase.
Effective stiffness for lateral load resisting elements and lateral spreading compatible soil springs

Figure 4: Kinematic Load Scenarios for each Phase in Pseudo-Static Analysis

Another issue is how to impose the inertial demands from the superstructure in combination with the kinematic loading. Being a nonlinear analysis, the principle of superposition is not applicable. The sequence of application can affect the location that hinges form and significantly affect the calculated system response. In this example, both loadings are applied to the model together gradually.

Inertial demands can be applied in the model in two ways. The first is via application of a force, which is determined from multiplying the bridge mass by the spectral acceleration at the first fundamental period. The second is by application of the spectral displacement corresponding to the same fundamental period. In a linear elastic system both approaches yield the same results. However, for a nonlinear system, the results can vary significantly. In this example, three cases were considered for each design phase:

- Case 1. No inertial demands from the superstructure.
- Case 2. Inertial demands applied as a displacement.
- Case 3. Inertial demands applied as a force.

The calculated sub-structure displacements and bending moments from the whole bridge analysis in the bridge longitudinal direction for the three phases including the sub-phases are shown in Figure 5 with inertia loads applied as a displacement (Case 2). Bending moments and displacements for Phase 2a with the inertia applied as a force (Case 3) are also shown on Figure 5 to depict the differences that can occur from the different ways that the inertia can be applied in the analysis. Figure 5 shows bending demands on the pier piles are critical in the cyclic liquefaction phase. At the abutment piles, bending is critical in the lateral spreading phase, Phase 3 with hinging occurring at the top of the piles, below the abutment beam.

A parametric sensitivity analysis is an important part of the PSA process. The bridge response was found to be sensitive to the magnitude of free field horizontal ground displacement and the passive resistance of the embankment fill.

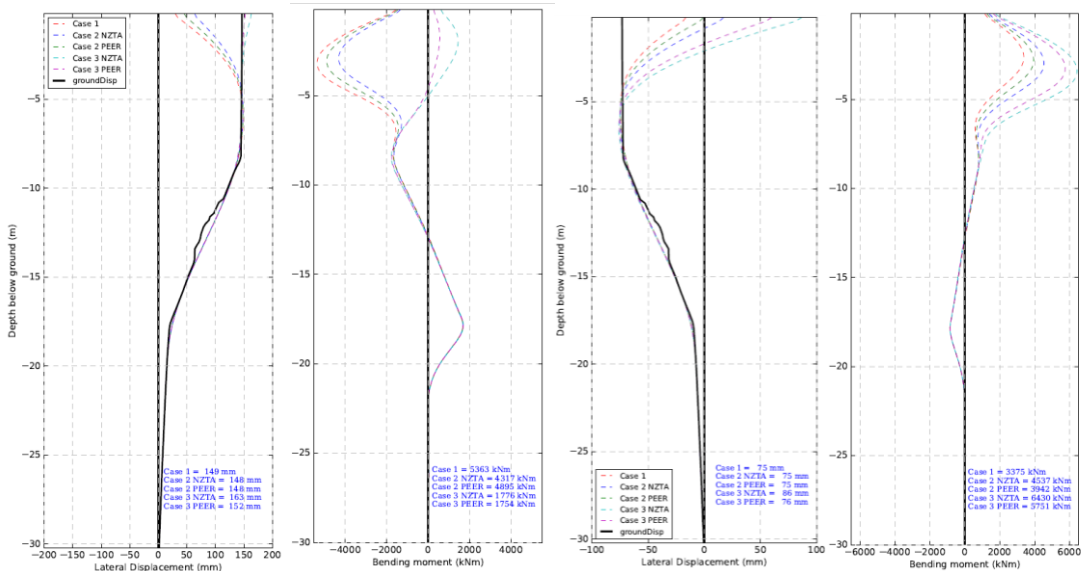

Figure 5: Displacements and Bending Moments for Abutment Pile (left) and Pier Pile (right) from Pseudo-Static Bridge Analysis

7 CONCLUSIONS

With a goal of developing a consistent approach to the analysis and design of bridges on liquefiable sites, the NZ Transport Agency commissioned a research project towards the

development of guidelines for the design and assessment of piled bridges at sites prone to liquefaction and lateral spreading in New Zealand. The report for the second stage of this project provides practical examples of the use of the recommended pseudo-static analysis framework for the design of typical bridges on sites susceptible to liquefaction and lateral spreading in New Zealand.

This paper describes an example of the application of the pseudo-static method in the analysis of an over bridge with approach embankments on a relatively flat liquefiable site. The example highlights some of the challenges when applying the recommended methods, the need for parametric studies and sound engineering judgement to envelope the response and gain a good understanding of the likely seismic performance of the bridge.

8 ACKNOWLEDGEMENTS

The funding for the project was provided by NZTA. Contributions of Mr Dejan Novakov (Opus International Consultants) and Dr Jennifer Haskell (University of Canterbury) are acknowledged. Dr John Wood is thanked for his review of the design guidance.

REFERENCES

Boulanger R.W. and Idriss, I.M. (2014). CPT and SPT Based Liquefaction Triggering Procedures, Report No. UCD/CMG–14/01, Dept. of Civil & Environmental Engineering, University of California at Davis.

Cubrinovski, M., Ishihara, K. and Poulos, H. (2009). Pseudostatic analysis of piles subjected to lateral spreading. Special Issue, *Bulletin of NZ Society for Earthq. Engrg*., 42(1), 28-38.

Murashev, A. K., Kirkcaldie, D. K., Keepa, C. and Lloyd, J. N. (2014) Proposed amendments to geotechnical requirements of NZTA Bridge manual. *Proceedings of 19th New Zealand Geotechnical Society Geotechnical Symposium,* Queenstown, NZ.

New Zealand Transport Agency (2013) *Bridge Manual* - Chapter 6 site stability, foundations, earthworks and retaining walls. New Zealand Transport agency. Wellington, New Zealand.

Murashev, A. K., Keepa, C., Orense, R. P., Scott, J.W., Seve, G. (2017)
National Design Guidelines for Ground Improvement of Soils prone to Liquefaction
Proc. 20th NZGS Geotechnical Symposium. Eds. GJ Alexander & CY Chin, Napier

National Design Guidelines for Ground Improvement of Soils Prone to Liquefaction

A K Murashev
Opus International Consultants Limited, NZ
Alexei.Murashev@opus.co.nz

C Keepa
Opus International Consultants Limited, NZ
Campbell.Keepa@opus.co.nz

R P Orense
University of Auckland, NZ
r.orense@auckland.ac.nz

J W Scott, G Seve
Ministry of Business, Innovation & Employment, NZ
John.Scott@mbie.govt.nz

Keywords: ground improvement, liquefaction, lateral spreading, dynamic compaction stone columns

ABSTRACT

One of the Canterbury Earthquake Royal Commission recommendations was that "ground improvement should be considered as part of the foundation system of a building and reliability factors included in the design procedures" and that "the Ministry of Business, Innovation and Employment should consider the desirability of preparing national guidelines specifying design procedures for ground improvement, to provide more uniformity in approach and outcomes". Opus International Consultants Limited (Opus) was engaged by MBIE to lead the preparation of the national ground improvement design guidelines - Module 5 (the Guidelines). The project team also included MBIE, EQC, University of Auckland, University of Canterbury, University of Southern California, University of California – Berkeley, Tokyo Denki University as well as a number of NZ consultants and ground improvement contractors. The Guidelines are based on the latest research and observations of the performance of ground improvement in earthquakes in New Zealand and internationally. The Guidelines were published for public comment in May 2017. The Guidelines identify the key issues that need to be addressed in the design and construction of ground improvement to mitigate the effects of liquefaction, cyclic softening and lateral spreading effects on buildings and provide a framework for resolving these issues through design and construction. In this paper, a summary of the Guidelines is given and complex design issues are discussed.

1 INTRODUCTION

International experience has shown that buildings founded on sites that would otherwise be liquefiable can perform well, where well-engineered, robust ground improvement has been carried out. The experience in Christchurch during the Canterbury earthquake sequence was more varied, noting that the ground shaking, in some areas, was more intense than that allowed for in design. The Canterbury Earthquake Royal Commission (CERC) recommended consideration be given to the preparation of national guidelines to improve uniformity in the design approach and outcomes.

The Guidelines are Module 5 in the MBIE / NZGS guidance series of geotechnical Modules that have been developed by MBIE and NZGS with support from NZ and international consultants, contractors and universities (MBIE, 2016a). The Guidelines cover the design of ground improvement and support the Canterbury Earthquake Royal Commission recommendations to prepare national guidelines specifying design procedures for ground improvement, to provide more uniformity in approach and outcomes. Opus was engaged by MBIE to lead the preparation of the Guidelines. The project team also included MBIE, EQC, University of Auckland, University of Canterbury, University of Southern California, University of California – Berkeley, Tokyo Denki University as well as a number of NZ consultants and ground improvement contractors.

The Guidelines identify the key issues that need to be addressed in the design and construction of ground improvement to mitigate the effects of liquefaction, cyclic softening and lateral spreading effects on buildings and provide a framework for resolving these issues through design and construction. A wide range of ground improvement techniques are available to mitigate the effects of liquefaction and many of these are briefly described in the Guidelines, including techniques that have not been used extensively in New Zealand to date. There is no attempt to provide a comprehensive discussion of all available liquefaction countermeasures in the Guidelines; rather, only commonly used methods in New Zealand are outlined in detail. A bibliography is provided that gives greater depth on specific topics and aspects of ground improvement and practitioners and constructors are encouraged to read these where relevant.

The objective of the document is to provide concise, practical advice and simplified procedures for the design of ground improvement by qualified, experienced engineers based on the latest research and observations of the performance of ground improvement in earthquakes in New Zealand and internationally. The Guidelines should also help to improve design consistency in New Zealand. The key issues covered by the Guidelines are summarised in this paper.

2 LIQUEFACTION CONSIDERATIONS

Where appropriate, the Guidelines refer to other MBIE modules. The topic of planning and undertaking site investigations for the purpose of characterising site geotechnical conditions and for the evaluation of liquefaction is discussed in Module 2 (MBIE, 2016b) and further in Module 3 (MBIE, 2016c) . Module 4 (MBIE, 2016d) gives guidance on the development of ground models and the selection of engineering soil properties for the design of foundations. The effectiveness of many ground improvement techniques is highly dependent on the fines content of the soils and the variability of the ground conditions to be treated. A comprehensive investigation should be undertaken to assess soil conditions and in particular, the fines content, location and extent of silt and clay layers at a site. Penetration testing undertaken as part of the site investigation also forms the basis for assessing the degree of treatment achieved. As discussed in Module 3, there is a high degree of uncertainty in the relationship between fines content and the soil behaviour index, I_c, calculated from cone penetration tests (CPT) and therefore fines content calculated from I_c should be calibrated against laboratory measured fines content and field descriptions of soils. Detailed recommendations on site investigations for assessment of liquefaction are given in Module 2. Guidance on the identification and assessment of liquefaction, and liquefaction induced ground deformation is provided in Module 3.

The seismic behaviour of a building on liquefiable ground is affected by the depth and stiffness of the structural foundation, magnitude of contact pressure, seismic response of the structure and soil, the thickness and properties of liquefiable soil layers and the non-liquefiable crust, the intensity of ground motion and many other factors.

There are a number of ways liquefaction can affect a building and its connecting infrastructure, including:

- Reduced bearing capacity due to the associated reduction in soil strength;
- Subsidence associated with shear deformation, cyclic ratcheting, lateral spreading and ground re-levelling, and reconsolidation;
- Surface ejection of soil and water (sand boils) from beneath or around foundations;
- Heave of ground bearing floor slabs and buoyancy of buried pipes, tanks, chambers and basements;
- Horizontal displacement and stretching of the footprint and foundation with lateral spreading;
- Kinematic bending of piles with horizontal ground displacements; and
- Pile down-drag (negative skin friction) caused by ground subsidence.

The degree to which these effects relate to a particular site and structure, depends on the site specific ground conditions and the details of the structural system. Detailed discussion on the effects of liquefaction on buildings is given in Module 4.

3 GROUND IMPROVEMENT PRINCIPLES

The Guidelines discuss five principal methods employed to improve the ground and increase its resistance to liquefaction: replacement, densification, solidification, reinforcement, and drainage. Ground improvement methods normally utilise one or a combination of these mechanisms to improve the ground's resistance to liquefaction and improve seismic performance. A secondary mechanism of some techniques is the potential improvement of the soil's resistance to liquefaction triggering by an increase in the lateral stress within the soil and thus changing its initial state. This mechanism cannot be easily verified in the field and may not greatly reduce the effects of liquefaction should it be triggered. Until further research gives a better understanding of its effectiveness at mitigating liquefaction and ways to confidently verify that the increase in lateral stress is achieved in the field, this mechanism should not be depended on in design.

4 SEISMIC RESPONSE OF BUILDINGS SUPPORTED ON IMPROVED GROUND

Ground improvement can greatly increase the stiffness of the soil profile. It is well understood that the stiffness of the soil has a marked effect on seismic ground motions at the surface. Stiffening the soil can amplify accelerations at the surface but decrease displacements. In many cases, ground improvement will not fully eliminate the effects of liquefaction. Settlement of buildings with shallow foundations supported on improved ground will result from shear and volumetric changes within the improved zone and in the soils surrounding or underlying the improved zone. The prevalent mode of deformation depends on the ground improvement method adopted, its size and stiffness; the size, weight and stiffness of the structure (and the distribution of weight and stiffness) and the extent of the liquefiable soil beneath the improved zone.

Except for methods that completely solidify or replace the liquefiable soils with stiff (cemented) low permeability materials, subsidence can develop from shear deformation in the improved ground under loading from the building. This is often more pronounced at the perimeter of structures, particularly for tall and heavy structures that can exert large loads on perimeter foundations. The magnitude of subsidence can be exacerbated by softening of the improved soils with cyclic shearing, the associated development of excess pore water pressure and the migration of excess pore water pressures from the surrounding liquefied soil into the improved zone. Reconsolidation of soils in the improved zone as excess pore-pressures dissipate will cause additional subsidence. Lattice and columnar reinforcement elements can be subjected to considerable bending, shear and axial stresses. With partial depth of improvement, settlement and tilting of the improved ground overall can develop from shear induced deformation in the liquefied soil beneath the improved zone, reconsolidation of the liquefied soils as pore water pressures dissipate and ratcheting effects during earthquakes, similar to the mechanisms of

settlement for shallow foundations on liquefaction prone sites as described in Module 4. Ground improvement in areas of lateral spreading can experience large compression and tension stresses from dynamic and kinematic forces imposed on it by the surrounding spreading ground. This can cause horizontal displacement, stretching and shear deformation of the zone of ground improvement.

5 PERFORMANCE REQUIREMENTS

The general philosophy for the design of ground improvement is to eliminate liquefaction and lateral spreading or mitigate their effects to the extent needed to meet the design performance criteria for the structure. In this context, the effectiveness of ground improvement should be assessed within the performance-based design framework by estimating the reduction of effects of liquefaction in relation to a no-improvement case, and by assessing the seismic response in relation to specific performance objectives for earthquake loads associated with different return periods. Qualitative effects of ground improvement on the dynamic response of foundation soils, structure and soil-structure system should be also considered in this evaluation. Such relatively rigorous performance requirements imply the need for adequate standards for design, construction control and verification of the effectiveness of ground improvement.

Performance criteria for the acceptable damage, settlement and differential settlement for each damage state should be developed collaboratively between the owner/developer, structural engineer and geotechnical specialist to get an overall system that meets regulatory (minimum) requirements and the expectations of the owner/developer.

It is often not economic, nor required in a regulatory sense, to completely eliminate liquefaction beneath buildings with ground improvement. Apart from methods that completely solidify or replace all liquefiable soils with non-liquefiable material, excess pore water pressures can develop within the zone of improvement. The frequency of earthquake at which these aspects start to have a significant effect on the amenity of the structure should be discussed and agreed with the owner/developer. Consideration should be given to the resilience of the ground treatment and the overall response should be ductile. The weight and stiffness of the structure and its foundations; the type, extent, and stiffness of the ground improvement; the ground conditions, characteristics of earthquake shaking and the extent of liquefaction triggered in an earthquake, all affect seismic performance. In assessing seismic performance and resilience, the uncertainties in these parameters and the interaction between the superstructure, connecting infrastructure, foundation, improved ground and native soil need to be considered holistically. The high degree of uncertainty in many of the parameters affecting seismic response implies the need to assess the sensitivity of the system response to each parameter and apply an appropriate level of redundancy in the design. Sensitivity assessment should be undertaken as part of any ground improvement design and discussed within the foundation options and design reports.

Improved structural measures can be incorporated to reduce damage susceptibility due to liquefaction, improve resilience and reduce or eliminate the need for ground improvement. These can comprise:

- Use of robust mats or a stiff grid of intersecting ground beams instead of stand-alone footings.
- Making above ground structural elements or connections between structures flexible and ductile to cope with total and differential settlements or lateral spread.
- Constructing foundation systems that seismically isolate the building from the ground and allow it to be re-levelled.
- Pile foundations to competent ground that is not underlain by liquefiable soils to prevent bearing failure and mitigate settlement and uplift (buoyancy).

- Control of ground deformation and structural performance by structural measures (rigidity of the structure, rigid rafts, sheet piles to confine liquefiable material, geogrids, base isolation of structures).

6 DESIGN OF GROUND IMPROVEMENT

Engineering assessment, consideration and design process for ground improvement can be summarised as follows:

- Determine performance requirements for the building and its foundation system (refer to the NZ Building Code, NZS1170, Module 1 and Module 4 and NZSEE Assessment and Improvement of the Structural Performance of Buildings in Earthquakes).
- Assess site conditions, ground conditions and geohazards including seismicity and susceptibility to liquefaction and lateral spreading (refer to Modules 1, 2 and 3). Where existing geotechnical information is insufficient, a geotechnical investigation should be carried out (refer to Module 2).
- Assess if liquefaction will be triggered, severity of liquefaction and the free field effects of liquefaction at the site (refer to Module 3).
- Assess the lateral spreading hazard at the site and the potential for differential lateral displacement across the building footprint.
- Assess the effects of liquefaction on the structure (with shallow or pile foundations and no ground improvement) and compare with the performance criteria. Consider whether there are readily available structural options to reduce susceptibility to damage from liquefaction. Where reasonable structural options alone are not sufficient to satisfy the performance requirements, consider ground improvement options.
- Select suitable methods for ground improvement.
- Design the extent (depth and size in plan) of improvement needed to meet design objectives. Consider soil-ground improvement-structure interaction. Early engagement between the structural and geotechnical engineers, and where practicable constructors, will enable a more efficient and holistic assessment of ground improvement and foundation options (also refer to Module 4).
- Design the size and arrangement of the ground improvement; determine material requirements, e.g. unconfined compressive strength of soil-cement mixture.
- The usual goal of ground improvement is to eliminate liquefaction. However ground improvement does not necessarily need to eliminate liquefaction within the improved zone but should control and mitigate the effects of liquefaction, and meet the performance criteria.
- Determine quality control (QC) and quality assurance (QA) requirements. In many cases a ground improvement trial will be required to confirm design assumptions and QA methods and optimise the design.

Full depth improvement is unlikely to be economic for sites underlain by deep liquefiable deposits and partial depth improvement can often give acceptable performance by reducing the magnitude of settlement. Assessment of nearly 60,000 lightweight single family dwellings in Christchurch following the Canterbury Earthquake Sequence clearly showed that less structural damage occurred in liquefaction prone areas containing an intact relatively stiff non-liquefying crust that was at least 3 m thick. From case history studies, Hausler and Sitar (2001) noted that one of the reasons why unacceptable performance was noted in the majority of ground improvement cases they investigated was due to inadequate remediation zone depth. Centrifuge studies on this topic (Liu and Dorby, 1997; Hausler 2002) came to a similar conclusion. Figure 1 shows the plot of normalised foundation settlement (i.e. foundation settlement divided by the total thickness of liquefiable layer) vs normalised improvement depth (i.e. thickness of improved soil divided by the total thickness of liquefiable layer) from case studies and centrifuge tests. The case studies

and centrifuge tests indicate a marked increase in settlement for treatment depths that are less than 50% of the thickness of the liquefiable layer.

The required lateral distance or width of soil improvement outside the perimeter of the structure is determined by the zone that controls the stability and deformation of the structure, even if liquefaction occurs over a wide area.

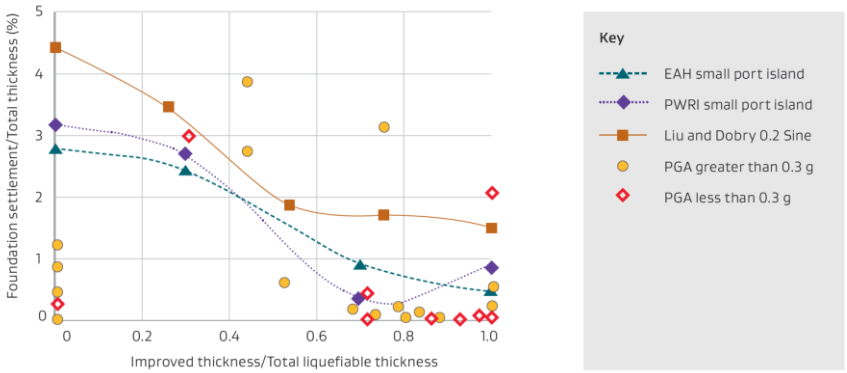

Figure 1: Normalised building settlement vs normalised improvement depth (Liu and Dorby 1997, Hausler 2001, 2002)

Factors that need to be considered when determining the lateral extent of improvement include:

- stresses applied to the improved ground by the building during earthquake shaking. Compressional and shear stresses near the edge of structures can fluctuate greatly and may have a larger zone of influence compared to static stresses, especially for tall and slender structures.
- strength and stiffness of the improved ground and the potential for a reduction in strength and stiffness due to excess pore pressures generated in the surrounding liquefied soil migrating laterally into the improved zone during and after shaking.

Model tests and analysis of ground improved by densification over the full depth of liquefiable soils indicate that in the soils bounded by the square ABCD (Figure 2), the pore water pressure ratio, r_u is often greater than 0.5 (Iai et al, 1988).

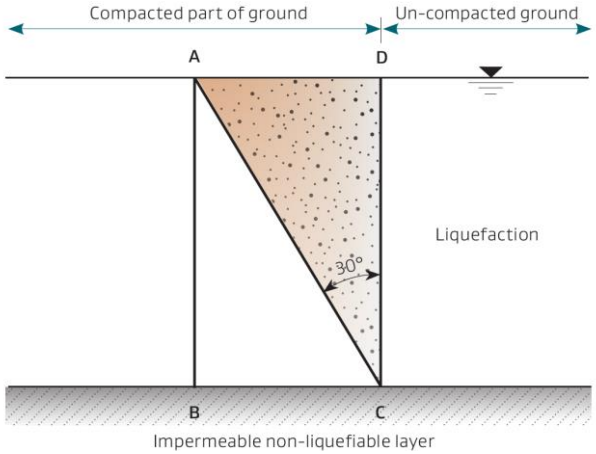

Figure 2: Area of softening in ground improved by densification (ACD) due to pore water pressure migration (after Iai et al, 1988)

The triangular area ACD exhibits particularly unstable behaviour and hence, this part should be treated as liquefied in the design of ground improvement that utilises densification techniques. As

a result, it is common practice to continue densification improvement to a distance of at least half of the depth of the improved zone from the edge of the structure.

It is sometimes not possible to extend improvement the recommended distance beyond a structure because of the presence of other structures, property boundaries, or utilities. In these cases, it may be possible to cantilever the foundation over the area of ground improvement affected by lateral migration of pore water pressure. Lattice ground improvement structures and other ground improvement methods that solidify or constrain the lateral deformation of soil beneath the foundation typically do not need to extend far beyond the foot print of the building.

Damage to structures may be especially severe where they are subjected to lateral spreading in conjunction with liquefaction. Strategies to mitigate lateral spreading and its effects at building sites include:

- Construction of structural walls separate from the building. These could be soldier pile walls tied back to anchor piles that cantilever from non-liquefiable soils or caissons founded on non-liquefiable ground.
- Using a buttress of ground improvement on the down slope side of the building but separate from the building foundations. This is may be desirable for piled structures in laterally spreading zones as the greater stiffness and strength of the improved soils could place larger kinematic loads on the piles and increase structural inertia.
- Improving the ground under the structure to mitigate lateral spreading as well as provide a suitable platform for the building.
- A combination of these treatments except that ground improvement should extend under the entire footprint of the building or not at all to avoid high contrasts in stiffness beneath the building that could cause differential subsidence and increase torsional response.

The Guidelines give design recommendations for the following ground improvement methods: replacement, densification (dynamic compaction, vibro-compaction, stone columns, compaction piles, compaction grouting, resin injection), solidification (soil mixing, jet grouting, permeation grouting), reinforcement (lattice intersecting walls, grid of stiff vertical columns) and drainage.

7 QUALITY CONTROL

The Guidelines give recommendations on design verification, quality control and quality assurance procedures, and emphasise the importance of interaction between structural and geotechnical designers. Where the structural and the geotechnical designers work together, the integration of structural and geotechnical design solutions to meet the performance requirements for the building in mitigating the effects of liquefaction and lateral spreading normally results in the most cost-effective design outcomes. The interaction between the structural and the geotechnical designers should also continue through the construction phase, as some adjustments to the structural design may be required depending on the achieved level of ground improvement.

8 CONCLUSION

The national ground improvement design guidelines -Module 5 have been prepared and issued for public comment. The Guidelines identify the key issues that need to be addressed in the design and construction of ground improvement to mitigate the effects of liquefaction, cyclic softening and lateral spreading effects on buildings and provide a consistent framework for resolving these issues through design and construction in New Zealand.

9 ACKNOWLEDGEMENTS

The funding for the project was provided by MBIE. Contributions of Prof Misko Cubrinovski, Dr Kevin McManus, Messrs Stuart Palmer, Nick Traylen, Phil Clayton, Tony Fairclough and Nick Wharmby are acknowledged. Prof Jonathan Bray, Prof Geffrey Martin and Prof Susumu Yasuda are thanked for their review of the draft Guidelines.

REFERENCES

Hausler, E.A. and Sitar, N. (2001) Performance of soil improvement techniques in earthquakes. *Fourth International Conference on Recent Advances in Geotechnical Earthquake Engineering and Soil Dynamics*, San Diego, CA, Paper 10.15.

Hausler, E. A. (2002) Influence of ground improvement on settlement and liquefaction: a study based on field case history evidence and dynamic geotechnical centrifuge tests, *PhD Thesis*, University of California, Berkley, 364

Iai, S., Noda, S. and Tsuchida, H. (1988) Basic consideration for designing the area of the ground compaction as a remedial measure against liquefaction. *Proc., U.S.-Japan Joint Workshop on Remedial Measures for Liquefiable Soils*, U.S.-Japan Panel on Wind and Seismic Effects, UJNR, Jackson, Wyoming, May 11-13.

Liu, L and Dobry, R. (1997) Seismic response of shallow foundation on liquefiable sand, *Journal of Geotechnical and Geoenvironmental Engineering*, 123(6): 557–567.

Ministry of Business, Innovation and Employment (2016a) *Earthquake Geotechnical Engineering Practice – Module 1: Overview of the Guidelines.*

Ministry of Business, Innovation and Employment (2016b) *Earthquake Geotechnical Engineering Practice – Module 2: Geotechnical Investigations for Earthquake Engineering.*

Ministry of Business, Innovation and Employment (2016c) *Earthquake geotechnical Engineering Practice – Module 3: Identification, Assessment and Mitigation of Liquefaction Hazards.*

Ministry of Business, Innovation and Employment (2016d) *Earthquake Geotechnical Engineering Practice – Module 4: Earthquake Resistant Foundation Design.*

Ministry of Business, Innovation and Employment (2017) *Earthquake Geotechnical Engineering Practice – Module 5: Ground Improvement of Soils Prone to Liquefaction*, draft for public comment.

Sensitive pyroclastic soils in the Bay of Plenty, New Zealand: microstructure to failure mechanisms

V.G. Moon
School of Science, University of Waikato, Private Bag 3105, Hamilton 3240, New Zealand
vicki.moon@waikato.ac.nz (Corresponding author)

P.R. Mills
Coffey Geotechnics, Tauranga, New Zealand
pip.mills@outlook.co.nz

M.O Kluger
MARUM–Center for Marine Environmental Sciences, University of Bremen, Germany
mkluger@marum.de

D.J. Lowe
School of Science, University of Waikato, Private Bag 3105, Hamilton 3240, New Zealand
david.lowe@waikato.ac.nz

G.J. Churchman
School of Agriculture, Food and Wine, University of Adelaide, Adelaide, SA 5005, Australia
jock.churchman@adelaide.edu.au

W.P. de Lange
School of Science, University of Waikato, Private Bag 3105, Hamilton 3240, New Zealand
willem.delange@waikato.ac.nz

D.A. Hepp
MARUM–Center for Marine Environmental Sciences, University of Bremen, Germany
dhepp@marum.de

S. Kreiter
MARUM–Center for Marine Environmental Sciences, University of Bremen, Germany
skreiter@uni-bremen.de

T. Mörz
MARUM–Center for Marine Environmental Sciences, University of Bremen, Germany
tmoerz@uni-bremen.de

Keywords: sensitive soil; tephra; halloysite; microstructure

ABSTRACT

Sensitive soils derived from weathered rhyolitic pyroclastic materials are associated with many landslides in the Bay of Plenty. Undrained, consolidated static triaxial tests show contractive p'-q' plots, strain-softening stress-strain behaviour coupled with rising pore water pressures, shear band formation after peak strength, and considerable strain softening. Cyclic triaxial tests confirm brittle failure and extensive softening of the soil. Pore pressure gradients developed during shearing initiate collapse of clay microstructures into shear zones; further excess pore pressure generation in the shear zone leads to progressive failure. Halloysite, a low-activity clay mineral, is associated with sensitive layers within the pyroclastic sequences. Mushroom cap–shaped spheroidal halloysite results in weak short-range interactions between exposed clay surfaces on incomplete spheroids. This weak bonding allows disassociation of clay aggregates during slope failure, leading to strain softening and the development of flow post-failure.

1 INTRODUCTION

Overnight on 5/6 April 2017 Omokoroa Peninsula in Tauranga Harbour experienced a major landslide event along the coastal cliff margins following the passage of extratropical Cyclone Debbie during the night of 4/5 April. A second large rainfall event, extratropical Cyclone Cook, followed 9 days later on the evening of the 14th April, resulting in a further series of landslides. Altogether, some 18 landslides, many of which comprise complex zones of multiple failures, occurred in two distinct phases (5/6 and 14 April). These landslides clearly cluster into two distinct types (Figure 1): translational slides that extend the full height of the cliffs and denude a considerable length of the cliff face, but only extend a few metres back into the cliff; and flow-slides based in sensitive (ratio of undisturbed/remoulded strength > 4) soil layers that are often well above the mean sea level and which extend up to tens of metres back into the face. The geomorphology shows that these sensitive soil failures are common on the Omokoroa peninsula, and indeed in other parts of Tauranga and the wider Bay of Plenty. We have been undertaking research on the nature and causes of sensitivity in these materials for some time. This paper presents a synthesis of our current understanding of these soils and their behaviour.

(A) (B)

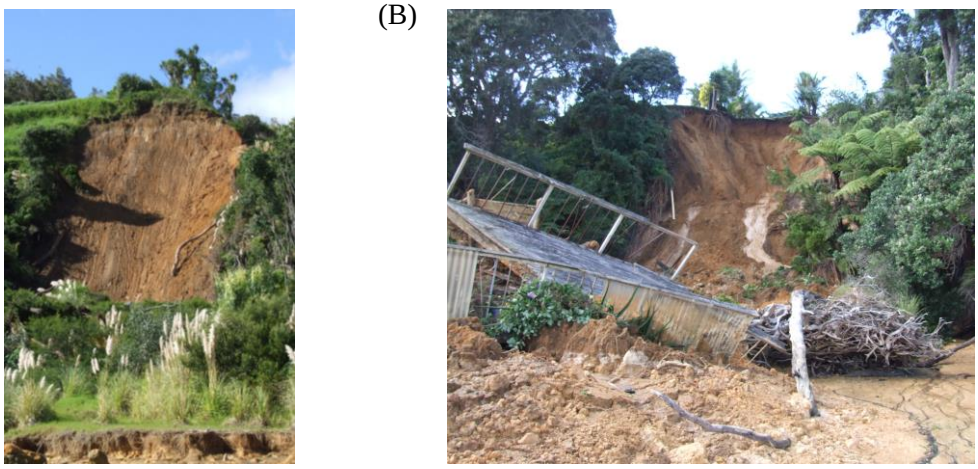

Figure 1. Translational (A) and flow-slide (B) landslides initiated following the passage of Cyclone Debbie on 4/5 April 2017. Although translational failures can denude large areas of the slope, flow-slides cause greater excursion into the slope and hence pose greater risk.

2 STUDY SITE

While we have examined and sampled several sites around Tauranga, the data presented here are derived from a landslide at Bramley Drive, Omokoroa. This landslide is situated on the coastal margin of Omokoroa Peninsula approximately 12 km north of Tauranga City. The coastal bluffs at the site are 33 m above high tide, and the landslide debris protrudes onto the intertidal sand flats. The initial failures occurred in early August 1979 and resulted in ~ 30 m retreat of the cliff over a length along the cliffs of ~ 60 m; a distinctive ledge was apparent in the failure at approximately 24 m below the original ground surface, and the debris flowed rapidly to a distance some 150 m from the cliff (Gulliver and Houghton, 1980). The scarp remained essentially stable for just over 30 years until 2011 and 2012 when several smaller reactivations resulted in a further ~ 10 m retreat. A steep (50 - 60°) scarp some 24 m high is now exposed, along with an eroded debris zone approximately 130 m in extent.

Three key sequences of material are exposed in the landslide scarp (Kluger *et al*., 2017): recent eruptives including the Rotoehu Ash (~ 50,000 years) and younger materials with the modern soil developed on late Quaternary tephras; the rhyolitic Hamilton Ash sequence (~0.05 – 0.35 Ma) derived from Taupo Volcanic Zone eruptives; and the Pahoia Tephras (0.35 – 2.18 Ma). The Pahoia Tephras are a complex unit within the wider Matua Subgroup. Whilst some layers are

definitely tephra-fall deposits, the unit contains many reworked, weakly-consolidated pyroclastic materials of rhyolitic origin as well as partially to non-welded pyroclastic flow deposits (ignimbrites); it is this Pahoia Tephra sequence that contains the sensitive soils associated with landsliding throughout the Tauranga region.

3 HALLOYSITE

We have identified halloysite as the key clay mineral in the pyroclastic sequence comprising the Pahoia Tephra sequence in the Bay of Plenty (Kluger *et al.*, 2017). Halloysite is a product of weathering mainly of volcanic glass (± plagioclase feldspars) in an environment with abundant Si in the pore water. In particular, in high-Si rhyolitic eruption products, such as the ignimbrites and tephra-fall beds derived from eruptions in the Taupo Volcanic Zone, especially under conditions of impeded drainage, halloysite is a common alteration product. Halloysite is a 1:1 kaolin-subgroup clay mineral with one silanol sheet for each aluminol sheet. This structure is similar to that of kaolinite but halloysite contains additional interlayer H_2O (water).

Halloysite-rich soils formed in weathered tephras characteristically have very low bulk densities and associated high porosities (Table 1). Many authors report small pore spaces, and natural moisture contents are high as the soils remain close to fully saturated in normal field conditions due to the capillary effects of small pores. Liquid and plastic limits tend to be relatively high, yet conversely, plasticity indexes are low: halloysite-rich soils typically plot below, but parallel to, the A-line as "high compressibility silts" (Wesley, 1973). High limit values are to be expected from the H_2O molecules included in the structural formula for hydrated halloysite, but the low plasticity indicates that the water is in positions that does not lubricate contacts between clay minerals or enhance chemical and electrostatic surface interactions. Thus the low plasticity is a reflection of the relatively low cation exchange capacity (CEC) of halloysite, and is reflected in a low activity. Despite a low activity (shrink/swell capacity) halloysite minerals can dehydrate, resulting in shrinkage. This dehydration is irreversible under ambient environmental conditions, and hence swelling is unlikely to be a problem. Low plasticity index and very high field moisture contents leads to characteristically very high liquidity indexes.

Table 1: Ranges of physical properties of halloysite-rich soils (after Moon, 2016).

parameter	symbol	unit	range
dry bulk density	ρ_{dry}	kg m^{-3}	480-1080
porosity	η	%	33-71
field moisture content	w_{field}	%	31-160
saturation		%	91-109
coefficient of permeability	k	$*10^{-9}$ ms^{-1}	1-111
plastic limit	PL	%	18-75
liquid limit	LL	%	34-110
plasticity index	PI	%	10-48
liquidity index	LI		0.3-2.4
peak cohesion	c, c'	kN m^{-2}	0-70
peak friction angle	ϕ, ϕ'	°	21-56
residual cohesion	c, c'	kN m^{-2}	0-13
residual friction angle	ϕ, ϕ'	°	9-34.2
sensitivity	S_t		5-140

Strength parameters for undisturbed samples show characteristically low cohesion, reflecting the low CEC, but high friction angles which are generally attributed to irregular morphologies of halloysite clay minerals. Typical values of residual cohesion are very low, whereas the residual friction angle ranges from 15 to 35°. Thus, relatively high friction angles may be retained after remoulding. This is not always the case however, and in some instances considerable loss in frictional resistance is observed. As these halloysite-rich soils have formed *in situ* without any previously elevated overburden stresses, they remain normally consolidated.

The morphology of halloysite clays is highly variable, and the interactions between clay mineral surfaces are strongly influenced by the morphology. Typically, halloysite crystals are considered to be tubular: a mismatch between the sizes of the silanol and aluminol sheets that is exacerbated by interlayer water which weakens inter-layer forces, allows rolling of clay layers. This characteristic is the subject of considerable research into halloysite nanoparticles as vectors for drug delivery or as components in polymers. However, it has long been recognised that halloysite also occurs in other forms, in particular small spheres. Smalley *et al*. (1980) recognised spherical halloysite as a key component of the sensitive soils at the base of the landslide at Bramley Drive, and suggested that limited particle interactions across the surfaces of the spheres contributed to the sensitivity of the materials.

Recently we have recognised two more morphologies of halloysite in Bay of Plenty sensitive soils: books (Cunningham *et al.*, 2016) and mushroom-caps (Kluger *et al*., 2017). The book morphology (Figure 2A) mimics a common morphology of kaolinite, and may have been responsible for mis-identification of halloysite clays in the Bay of Plenty in previous work. The mushroom-cap morphology (Figure 2B) is recognised from the same location at Bramley Drive as the spheres described by Smalley et al. (1980). With improved SEM technology, we identify these spheres as incomplete: individual halloysite spheroids are typically ~250–400 nm in diameter with openings ~80–160 nm in diameter on one side, giving the "mushroom-cap" appearance. We infer that the spheroids observed are composed of concentrically stacked 1:1 layers, reminiscent of the structure of an onion. A complete silanol layer, as comprises the outer sphere surface, carries a net negative charge. In the openings, ends of both silanol and aluminol sheets are exposed, giving a neutral or weakly positive overall charge. Electrostatic or van der Waals forces lead to attraction between the negatively charged convex surfaces of the silanol sheets and the weak positive charges of the concave openings, allowing the individual minerals to aggregate into a network of connected particles in the undisturbed state (Figure 2C). The attractions are short-range however, and detachment by remoulding allows a disaggregation, giving the material a low remoulded strength. While the various halloysite morphologies occur mixed throughout the profile; the mushroom-caps are most abundant in the highly sensitive layers, whereas tubular halloysite is more abundant in the upper, less sensitive materials.

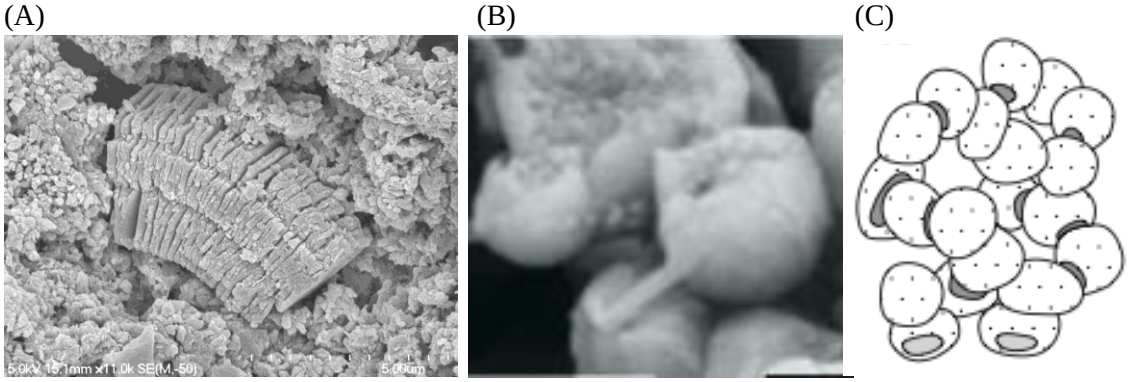

Figure 2. Scanning electron micrographs of (A) book and (B) mushroom-cap morphologies of halloysite. (C) Inferred framework network of mushroom cap clay minerals. Image credits: (A) Helen Turner, (B) and (C) from Kluger et al. (2017).

4 STATIC RESPONSE

Undrained effective triaxial tests were undertaken on samples collected from a sensitive layer near the base of the landslide scarp at Bramley Drive (Mills and Moon, 2016). Tests were undertaken on three 48 mm diameter thin-walled core samples collected from a horizontal bench dug into the headwall of the landslide at a depth of 19 m below the original ground level. The bench was dug out to 1.5 m behind the exposed headwall so that samples were beyond the depth affected by surface weathering effects. Cores were wrapped for transport and storage, and the

samples were stored in their tubes in sealed chambers until immediately before testing. Testing followed standard NZ procedures (NZS4402 (1986)), with the exception of the rate of stress application where a high rate of 0.5 mm min^{-1} was chosen following the model of Gylland *et al.* (2013). B values greater than 95 % were achieved during saturation, and isotropic consolidation stresses of 140–340 kN m^{-2} were applied to bracket field overburden stresses. Test results are summarised in Table 2 and plotted in Figure 3.

Table 2: Triaxial test parameters for three core samples from Bramley Drive (after Mills and Moon, 2016)

parameter	symbol	unit	S1	S2	S3	strength parameters
effective confining stress	σ_c	kN m^{-2}	140	240	340	
saturation parameter	B	%	95	98	98	
axial strain at failure	ε_f	%	1.9	3.2	2.0	
deviator stress at failure	q_r	kN m^{-2}	179	246	299	
strain softening		%	14	20	50	
failure mechanism			W	S	S-W	
peak effective cohesion	c'_p	kN m^{-2}				26
residual effective cohesion	c'_r	kN m^{-2}				24
peak effective friction angle	ϕ'_p	°				31
residual effective friction angle	ϕ'_r	°				26

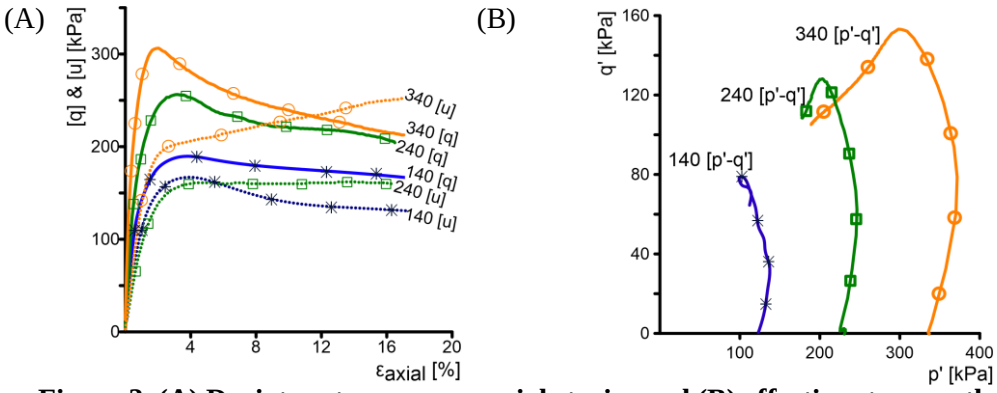

Figure 3. (A) Deviator stress versus axial strain, and (B) effective stress path plots for static triaxial tests (from Mills and Moon, 2016)

Samples failed at axial strains of 3.2 % or less, and exhibited significant strain softening post-failure as expected for sensitive soils. Pore water pressures climbed sharply on application of axial stress, then dropped or plateaued post-failure in the samples tested at lower effective confining stresses (σ_c = 140 & 240 kN m^{-2}), but continued to increase after failure in the sample at the highest confining stress (σ_c = 340 kN m^{-2}). Effective stress path plots show contractive behaviour, particularly at the higher confining stresses.

Strength parameters derived from these tests are included in Table 2. The values are in keeping with commonly reported values for the strength of halloysite-rich soils (Table 1) and show relatively low cohesion and high friction angle in undisturbed (peak) conditions. Residual cohesion is similar to the undisturbed value, and the friction angle undergoes only a small change post-failure. Strain softening of effective cohesion values and friction angles is thus limited, indicating that pore water pressure changes post-failure are key to the significant strain softening observed.

Following strength testing, thin section description and computerised x-ray tomography (CT) of the failed cores were undertaken to examine the fracture surfaces developed during stress application. Thin sections were prepared by cutting surfaces oriented vertically on the failed core; these were air-dried slowly under ambient laboratory conditions, and impregnated with resin

before following normal thin section preparation procedures. Small (10 mm inside diameter) core samples were taken normal to the macroscopic shear surface for micro-CT scans which were undertaken using a Bruker Skyscan 2000 Micro-CT at the University of Auckland.

Thin section samples (tested at 240 and 340 kN m^{-2}) show multiple principal shear zones evidenced by zones of particle reorientation up to 1.0 mm wide that have distinct boundaries with the surrounding matrix material (Figure 4A). The shear zones are continuous across the full length of the thin sections, and commonly show branching and coalescence, most notably around weathered zones or particle concentrations. As well, minor shears that are not continuous are commonly observed. A portion of the micro-CT scan image (sample tested at 355 kN m^{-2} effective stress) is shown in Figure 4B. A matrix of clays is indicated in green, dense particles are red colours, and shear zones are highlighted with pale green, black and pink annotations. All angles are measured with respect to the angle of the macroscopic principal shear (PDS) identified on the failed core. Two small shear zones 0.05–0.1 mm thick and spaced 2–3 mm apart are apparent in the core. These are most closely oriented to the direction expected for Reidel R shears, and are linked by antithetic R' shears. Reorientation of particles within these shear zones is not apparent, but the clay matrix within the shears is notably denser than in the surrounding matrix.

Overall, we observe brittle failure occurring along multiple shear zones oriented approximately as expected for Riedel shears, with some antithetic (R') shears observed linking the principal shear zones. Clay minerals are densified in the shear zones compared with the matrix density, and larger grains are reoriented to parallel the shear zone.

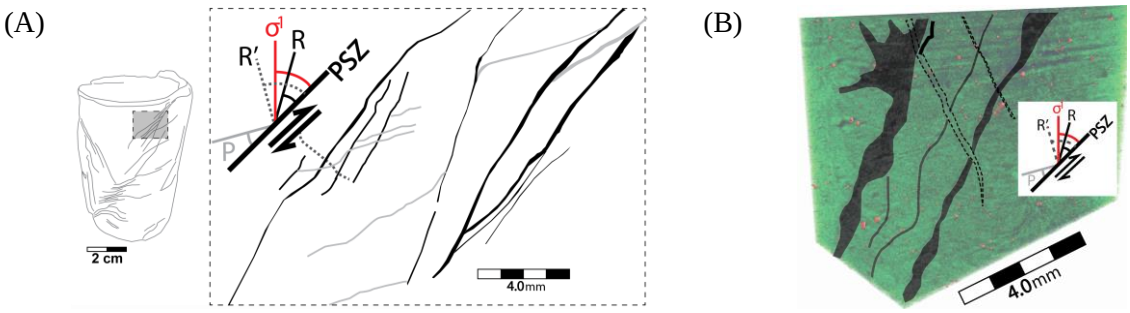

Figure 4. Thin section (A) and microCT section (B) of failure surfaces (from Mills, 2016).

5 CYCLIC RESPONSE

Cyclic triaxial testing on samples from the same location as those used for the static testing was undertaken at Bremen University, Germany. Thin-walled samplers of 36 mm internal diameter were pushed into the sampling platform; samples were wrapped and shipped to Germany in their samplers. Cyclic testing was undertaken following DIN 18137-2:2011-04 (2011). Samples were isotropically consolidated to 240 kN m^{-2} effective stress to match the estimated *in situ* consolidation stress at 19 m depth. After consolidation a combination of average shear stress (τ_{av}) and cyclic shear stress (τ_{cyc}) was applied in order to assess the combined effects of static and cyclic loads on the shear strain development and shear strength.

Figure 5A shows the test results for one sample tested at with high average shear stress of τ_{av}=75 kN m^{-2} and low cyclic shear stress of τ_{cyc}=30 kN m^{-2}, meaning that the sample remains in compression throughout the test. Notable is that the hysteresis loops remain relatively unaffected by loading cycles for most of the test, then the sample fails suddenly over a few cycles (failure in this case is defined as 5 % single amplitude axial strain). Pore water pressure rises sharply as the stress is initially increased, then remains high throughout the test. By contrast, Figure 5B shows the results of a test run with average shear stress of τ_{av}=40 kN m^{-2} and cyclic stress of τ_{cyc}=60 kN m^{-2} (ie. the sample experienced extension for part of each loading cycle). Both samples described develop compressional strain and increased pore water pressure throughout, but in the second test

the hysteresis loops develop a much more distorted shape (decreased stiffness), especially in the extensional regime, as the sample approaches failure; post-failure the pore water pressure increases and the stiffness decreases markedly.

The sudden increase in axial strain and the decrease in stiffness observed in the cyclic triaxial tests is in keeping with the sensitive nature of the soils where brittle failure and considerable post-failure strain softening are observed in the static compression testing presented above. The development of pore water pressure during loading is inferred to play a significant role in the development of failure in these materials.

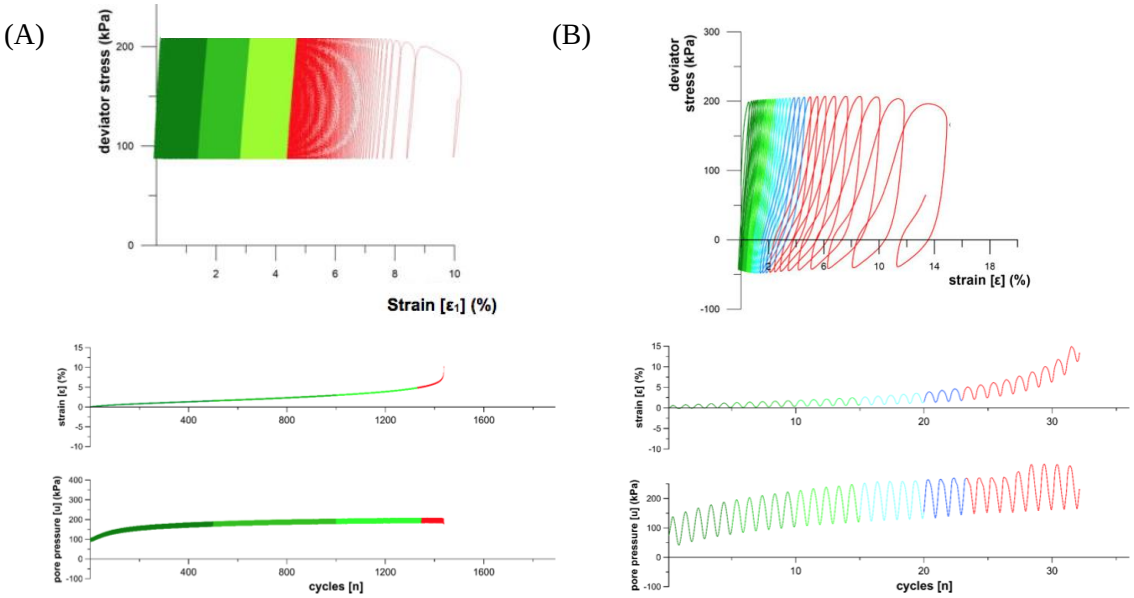

Figure 5. Cyclic triaxial test results for two samples. (A) 75 kN m^{-2} average applied stress, 30 kN m^{-2} cyclic stress; (B) 40 kN m^{-2} applied average stress, 60 kN m^{-2} cyclic stress (from Mills, 2016)

6 CONCLUSION

Sensitive soils have been known to pose a landslide hazard at Omokoroa and in the wider Bay of Plenty for some time. These sensitive soils create flow-slides with long runout, and failures that regress back into the slope over long time intervals. Recognition of halloysite as the key clay mineral in the Pahoia Tephra sequence that hosts the failure surface of these flow-slides allows us to predict and understand the basic physical characteristics of the soils; most notably inactive clay minerals with high liquidity indexes which are characteristic features of sensitive soils globally. Remoulded halloysite samples are also known to have distinctive responses to pH, and cation type and concentration (Theng and Wells, 1995). These responses allow for the possibility of slope improvement by means of cation manipulation, an avenue being investigated by Robertson *et al*. (this volume), but any treatment needs to be targeted to known characteristics of halloysite.

In static strength testing the materials exhibit brittle failure at ~ 3 % strain with well developed principal shear surfaces showing a densified clay mineral matrix and particle realignment. A contractive response is exemplified by considerable strain softening after failure, and pore water pressures that rise sharply with applied stress and remain high post-failure. Cyclic strength testing indicates considerable resistance to cyclic stresses, but when failure does occur it happens very suddenly, with samples exhibiting complete breakdown over a small number of loading cycles, a reflection of the sensitivity of the soil.

By looking more deeply at the structure of the clay minerals, identifying mushroom-cap shaped halloysite spheroids as dominant in the most sensitive soil layers allows us to recognise the nature of the framework of the soil, and hence infer mechanisms for breakdown of the structure. Little cohesion or friction softening is recognised in static triaxial testing; this follows from the nature of the clay minerals – spheres will not inherently realign as might be expected with platy minerals, their friction will be similar before and after; cohesion will presumably be lost, but limited cohesion exists in the undisturbed condition due to only weak attractive forces being able to develop between the outer and broken segments of the mushroom caps. We infer that excess pore pressure gradients initiate the separation of mushroom caps, leading to brittle shear surface evolution. Dramatic particle rearrangement on detachment of the weakly bonded spheroids leads to release of further pore water along the shear zone, enhancing pressure gradients and hence propagation of failure progressively to form discrete shear surfaces.

7 ACKNOWLEDGEMENTS

We thank Deutsche Forschungsgemeinschaft (DFG) via the Integrated Coastal Zone and Shelf Sea Research Training Group INTERCOAST for funding, and for scholarship support for MOK, Callaghan Innovation, the University of Waikato, and MBIE for scholarship support for PRM. Helen Turner at the University of Waikato and Dane Gerneke at the University of Auckland are thanked for SEM imaging and microCT scanning.

REFERENCES

Cunningham, M.J., Lowe, D.J., Wyatt, J.B., Moon, V.G., Churchman, G.J. (2016). Discovery of halloysite books in altered silicic Quaternary tephras, northern New Zealand. *Clay Minerals* 51, 351-372

Gulliver C. P. & Houghton B. F. (1980). *Omokoroa Point land stability investigation.* Report prepared by Tonkin & Taylor for Tauranga County Council (New Zealand).

Gylland, A. S., H. Rueslåtten, H. P. Jostad,. S. Nordal. (2013). Microstructural observations of shear zones in sensitive clay. *Engineering Geology* 163: 75-88.

Kluger, M. O., Moon, V. G., Kreiter, S., Lowe, D. J., Churchman, G., Hepp, D. A., Seibel, D., Jorat, M. E. & Mörz, T. 2017. A new attraction-detachment model for explaining flow sliding in clay-rich tephras. *Geology*, 42, 131-134.

Mills, P. R. (2016). *Failure mechanisms in sensitive volcanic soils in the Tauranga Region, New Zealand*. Unpublished MSc thesis, University of Waikato.

Mills, P. & Moon, V. (2016). Static failure mechanisms in sensitive volcanic soils in the Tauranga Region, New Zealand. In: Neeson, F. C., Lacey, D., Buxton, D. & Storie, L., eds. *11th Australia and New Zealand Young Geotechnical Professionals Conference,* 2016 Queenstown, New Zealand. New Zealand Geotechnical Society.

Moon, V. (2016). Halloysite behaving badly: geomechanics and slope behaviour of halloysite-rich soils. *Clay minerals*, 51(3), 517-528.

Robertson, T., Moon, V. G., Lowe, D. J. (this volume). Is there a potassium-based solution to sensitive soil slipping within the Bay of Plenty?

Smalley L. J., Ross C. W. & Whitton J. S., 1980. Clays from New Zealand support the inactive particle theory of soil sensitivity. *Nature*, 288, 576−577.

Theng B. K. G. & Wells N., 1995. The flow characteristics of halloysite suspensions. *Clay Minerals*, 30, 99-106.

Wesley L. 1973. Some basic engineering properties of halloysite and allophane clays in Java, Indonesia. *Géotechnique*, 23, 471−494.

Soil type identification and fines content estimation using the Screw Driving Sounding (SDS) data

S Y Mirjafari M
Department of Civil and Environmental Engineering, University of Auckland, NZ.
y.mirjafari@auckland.ac.nz (Corresponding author)

R P Orense
Department of Civil and Environmental Engineering, University of Auckland, NZ.
r.orense@auckland.ac.nz

N Suemasa
Department of Urban and Civil Engineering, Tokyo City University, Japan.
nsuemasa@tcu.ac.jp

Keywords: SDS, soil classification, in-situ, fines content.

ABSTRACT

Identification of ground conditions is a very important step before starting to build any geotechnical structure. Geotechnical investigations are performed to determine the soils conditions and to evaluate the cost-effectiveness and design of a proposed engineering construction. Fines contents (*FC*) in sandy soils also play an important role in the engineering design of geotechnical structures, particularly in areas prone to earthquakes. The Screw Driving Sounding (SDS) is a new in-situ test in which a machine drills a screw point into the ground in several loading steps while the attached rod is continuously rotated. At the same time, a number of parameters, such as torque, load and speed of penetration are logged at every rotation of the rod. Because this machine can continuously measure these parameters, an interpreted overview of the soil profile throughout the depth of penetration can be obtained. In this study, a large number of tests were conducted adjacent to boreholes in New Zealand. An attempt was made to correlate the SDS parameters to the soil type as described in the boring logs. In addition, samples from several SDS sites were obtained and sieve analyses were performed in order to formulate a relationship between the fines content and the SDS parameters. From the results, charts were developed to show how soil can be classified and fines content can be estimated using the SDS data. As a simple, fast and economical test, the SDS method can be a reliable alternative in-situ test for soil characterisation.

1 INTRODUCTION

Adequate information about ground conditions is very important for analyses, design and construction of geotechnical systems. Recently, the use of in-situ soil testing has increased in geotechnical engineering practice mainly due to the development of field testing procedures, better understanding of soil behaviour, and identification of the drawbacks and limitations of some laboratory testing (Eslami & Gholami 2006). Standard penetration test (SPT) and cone penetration test (CPT) are the most common in-situ tests around the world due to their capability in accurately characterising soils. Other field tests which are being used in geotechnical practice, such as dynamic cone penetration test (DCP), Swedish weight sounding (SWS), flat dilatometer (DMT), pressure meter test (PMT), vane shear test (VST) and Piezo-cone (CPTu), are less popular than SPT and CPT. Each of these tests applies specific loading pattern to identify the corresponding soil properties, such as strength and/or stiffness (Mayne, 1988). In order to perform some in-situ tests, such as the SPT, PMT and VST, boreholes are required; however, to conduct CPT, CPTu, SWS and DMT, no boreholes are needed. The SDS machine has been recently

designed and developed in Japan to reduce the drawbacks of SWS, as well as to include a method of measuring the friction on the rod. The machine previously used for the SWS test has been modified and improved so that it is suitable for the SDS test. In this method, a rod is drilled into the ground in several loading steps at the same time that the rod is continuously turned. An empirical relationship has been developed between the soil parameters and the SDS data (e.g. Tanaka et al., 2012; Maeda et al., 2015); In this study, based on the results of the SDS tests which were conducted adjacent to boreholes in different soil types around New Zealand, a soil classification graph is presented and it is shown that how the soil type can be identified using the SDS data. Furthermore by performing sieve analysis on the samples obtained from the boreholes, a correlation is developed for obtaining fines content directly from the SDS parameter. The SDS test is fast, small in size and relatively cheap compared to other in-situ testing methods and these advantages make it a good alternative for soil characterisation.

2 SCREW DRIVING SOUNDING TEST

2.1 SDS test procedure

A monotonic loading system is used in the SDS test and the number of load steps is set to 7. The rod is continuously turned at a constant rate of 25 rpm while the test is going on. The load steps are 0.25, 0.38, 0.50, 0.63, 0.75, 0.88, 1.0 kN in this order, and the load is increased at every rotation of the rod. The parameters measured in the test are: maximum torque (T_{max}), average torque (T_{avg}), minimum torque on the rod (T_{min}), penetration length (L), penetration velocity (V) and number of rotations of rod (N). These data are measured on the completion of each revolution of the rod. In SDS, the rod is automatically moved up by one centimetre after each 25cm penetration and then rotated to measure the rod friction. Due to the effects of rod friction on the measured torque and load during penetration, the amount of measured load and torque required for penetration is greater than that required at the screw point. The rod friction can be divided into a vertical component (W_f) and a horizontal component (T_f) as the rod rotates and penetrates into the ground. The corrected torque (T) and corrected load (W) are defined as follows:

$$T = T_a - T_f \quad (1)$$

$$W = W_a - W_f \quad (2)$$

Where W_a and T_a are the total applied load and applied torque by the SDS machine, respectively. The procedure of calculating W_f and T_f is explained by Tanaka et al. (2012).

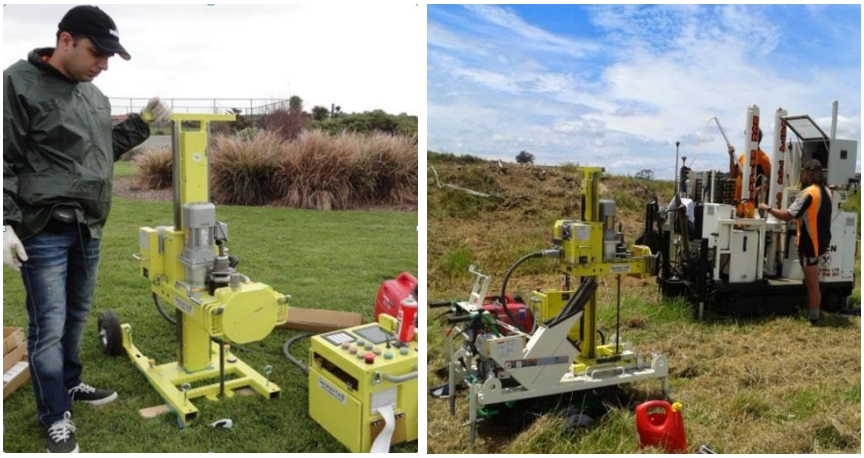

(a) (b)

Figure 1 Screw driving sounding (SDS) equipment: (a) SDS machine during operation; (b) SDS machine mounted on a crawler side-by-side with a CPT rig.

Figure 1(a) illustrates the small-scale SDS machine during operation while Figure 1(b) shows the machine on top of a crawler (which was designed to ease the transportation of the machine) and CPT rig side by side. As shown in the figure, SDS does not need large space for operation (especially without crawler) and is much smaller in scale than the smallest CPT rig. The SDS machine can be disassembled for ease in transport and the whole SDS machine on top of the crawler can be placed inside a van. Except gravelly soils, the SDS test can be performed in most of the soil types and the maximum depth of penetration depends on the type of the soil which cause the rod friction and difficulty of penetration.

2.2 Definition of SDS parameters

Figure 2 shows typical SDS results. The test was conducted along Avonside Drive in Christchurch, New Zealand. The SDS results illustrate the corrected load, corrected torque and the speed of penetration at every 25 cm. Data points are connected to each other by lines.

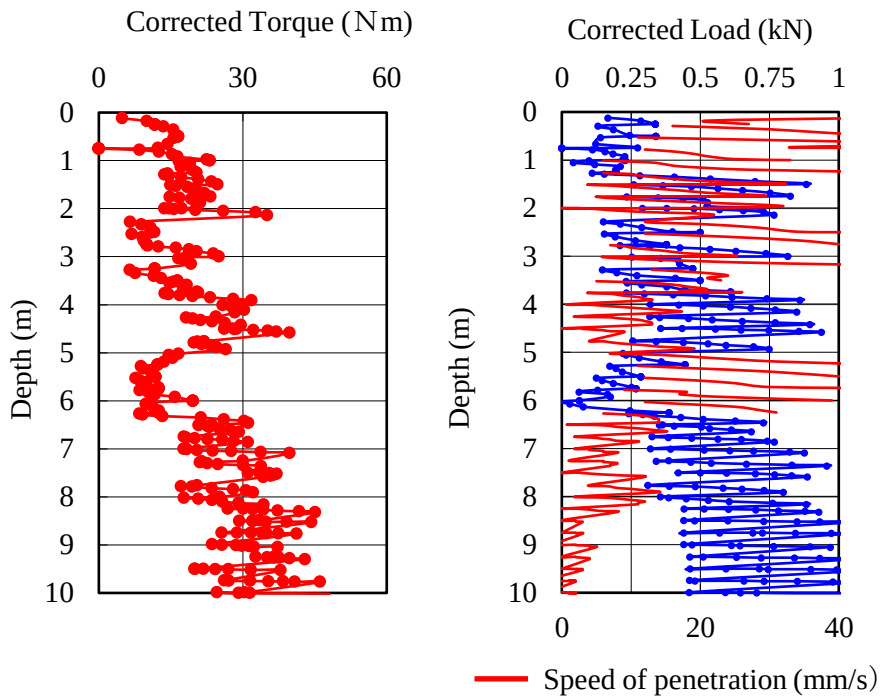

Figure 2 SDS results (torque, load and velocity).

By processing the raw data obtained from the SDS tests more, helpful information for soil characterisation can be obtained. Based on the plasticity theory, Suemesa et al. (2005) defined the coefficient of plastic potential, c_p is as follows:

$$c_p = \frac{N_{SD}D}{\pi T/WD} \tag{3}$$

Where $N_{SD}D$ is the normalized half-turns and is obtained by multiplying the number of half-turns for every 25 cm of penetration (N_{SD}) by the outer diameter of the screw point (D)., T and W are, corrected torque and corrected load, respectively. c_p is a parameter that indicates the difficulty of penetration. Based on the large set of data base in Japan, c_p is highly dependent on the types of soils (Tanaka et al. 2012). Figure 3 shows the changes of $N_{sd}D$, $\pi T/WD$ and c_p along a soil profile.

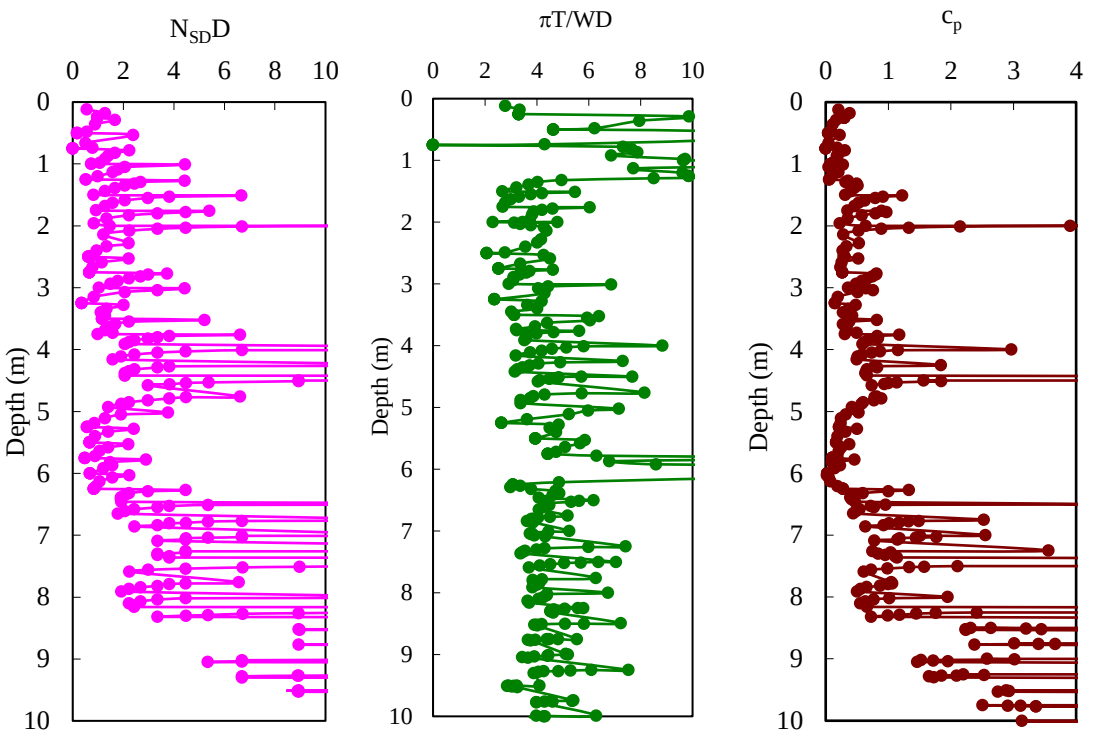

Figure 2 Additional information from test

3 SOIL CLASSIFICATION CHART

Overall, SDS tests were performed at 164 sites in New Zealand (74 in Christchurch, 56 in Auckland and 34 in Wellington). These tests were conducted adjacent to boreholes and therefore the soil types within a given layer are known. Boreholes were done after 2011 Christchurch earthquake and prior to the SDS tests and the data were obtained from New Zealand geotechnical data base (NZGD, 2016). Various SDS parameters (expressed in terms of measured torque, load, energy, etc.) were investigated to examine which of these best correlate with the appropriate soil types. The following parameters were considered:

$$\text{Ave}\delta T = \frac{1}{n}\sum_{n=1}^{6} T_{n+1} - T_n \tag{4}$$

$$c_p'' = \frac{1}{n}\sum_{i=1}^{n}\left(\frac{N_{SD}D}{\pi T/WD}\right)_i \tag{5}$$

where δT is the change in torque, T, at each step of loading, i; n is the number of load step; c_p" is the modified coefficient of plastic potential; N_{SD} is the number of normalised half-turns; W is the applied load; and D is the cross-sectional diameter of the screw point. The soil classification chart obtained based on the NZ soil database is shown in Figure 4. The horizontal axis is *Ave* δT which related to the grain size of soil is high in frictional soils due to their drained behaviour and low in cohesive soils due to the undrained behaviour (Mirjafari, 2016). The vertical axis is c_p" which represents the difficulty of penetration.

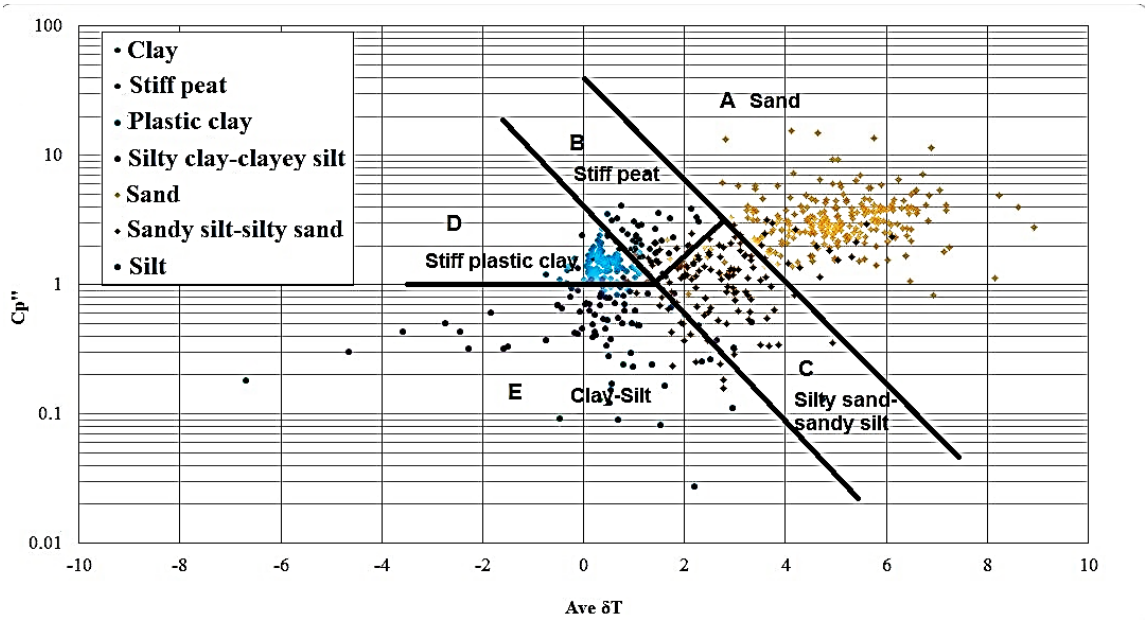

Figure 4 SDS-based soil classification chart for New Zealand soil

Note that the boundary lines were drawn visually to separate data such that points representing similar soil types are grouped together. Data points in region A are sandy soils which, because of their frictional nature, are expected to have higher *Ave(δT)* and c_p" values compared to the other soil types. Based on borehole data analysis, sands on the left part of the region are finer than those on the right part. In addition, as c_p" is an indication of the difficulty in penetration, the upper part of region A would be denser than those on the lower part. Region B is for stiff peat, which can be found in South Auckland; peat is considered as *c-ϕ* soil and it is reasonable that it is positioned to the right side of Regions D and E, both of which represent cohesive soils. Region C represents sandy silt and silty sands. Soils at the bottom left of region B contain more silt than sand; therefore, this region can be considered as a transition zone from frictional behaviour to frictionless (cohesive) one. Soils in region D are highly-plastic stiff clays which have *AveδT* values < 1 and $1 < c_p" < 2$. Finally, region E belongs to clayey silt, silty-clay, silt and clay. Note that the available borehole data for clayey soils were scarce and more analysis are planned to separate clay and silt. However, it is expected that the upper part of this region would represent stiff clay or silt while the lower part would be for soft clay.

4 COMPARISON BETWEEN SDS AND CPT FOR SOIL CLASSIFICATION

The SDS-based soil classification is compared to the CPT-based one; for this purpose, the CPT soil behaviour type classification used in this study is based on the Robertson (2010) soil behaviour type chart. Tables 1 and 2 show a comparison of the results of soil classification using SDS, CPT and boreholes for two randomly selected sites, one located in Avonside Drive (Christchurch) and another in Ihumatao Road (Auckland), respectively. As can be seen in Tables 1 and 2, the results obtained from SDS test are very accurate and almost similar to those shown in the borehole description.

A very good example of the advantage of SDS is the ability to recognise peat behaviour. In Table 2, SDS accurately predicted the peat soil while CPT found it as silty sand. Because of its high compressibility, peat can be a very problematic material for any construction.

Table 1 Soil classification using SDS, CPT and BH data (Avonside Drive, Christchurch).

CPT Soil description	SDS Soil description	Soil description	Depth (cm)
-	-	Fill: Fine sand, dry, poorly graded	0-80
Silty sand- Sandy silt	Sandy Silt Silty Sand	Sandy silt, Moist, low plasticity, sand is fine	80-275
Sand and Silty sand	Sandy Silt Silty Sand	Fine sand with trace silt, wet, poorly graded	275-300
Silty sand-Sandy silt	Sandy Silt Silty Sand	Sandy silt, moist, low plasticity, sand is fine	300-350
Silty sand-Sandy silt	Sandy Silt Silty Sand	Fine sand with trace silt, Wet, poorly graded	350-375
Sand and Silty sand	Sand		375-470
Sand and Silty sand	Sand	Fine to medium sand with trace silt, wet, well graded	470-525
Silty sand	Sand		525-600
Silty sand- Sand	Sand		600-750

Table 2 Soil classification using SDS, CPT and BH data (Ihumatao Road, Auckland).

CPT Soil description	SDS Soil description	Soil description	Depth (cm)
-	-	Fill	0-150
Clayey silt to silty	Stiff plastic clay	Clayey silt-Silty clay	150-300
Clayey silt to silty	Stiff plastic clay	Silty clay-very plastic	300-350
Clayey silt to silty	Sandy Silt Silty Sand	Silty fine sand	350-400
Sandy Silt Silty Sand	Sandy Silt Silty Sand	Clayey silt-Silty clay	400-450
Sand	Sandy Silt Silty Sand	Silty sand	450-600
Sandy Silt Silty Sand	Silty clay-clayey silt	Silty clay	600-650
Sandy Silt Silty Sand	Sandy Silt Silty Sand	Fine sand –some clay	650-700
Sandy Silt Silty Sand	Silty clay-clayey silt	Silt-some clay	700-750
Sandy Silt Silty Sand	Stiff Peat	Peat-very stiff	750-1000

5 ESTIMATION OF FINES CONTENT

Fines content (*FC*) in sandy soils plays an important role in the engineering design of geotechnical structures, particularly when the area is prone to earthquakes. The amount of *FC* significantly influences the liquefaction potential of soil. In engineering practice, it is very common to estimate the *FC* using the CPT data, as this test has become the most common field test for the design of structures. However, recently it was found that the CPT soil behaviour type often appears to overestimate the fines content within a soil (Van T Venn, 2015). In the previous section, it was shown that the SDS machine can identify the soil type with a high degree of accuracy that is even

better than with the CPT in some soils. Hence, an attempt was made to formulate a relationship between the fines content and the SDS parameter, as an alternative to CPT. As mentioned earlier, *AveδT* relates to the grain size of soils. Hence a relationship between fines content (*FC*) and *AveδT* parameter was sought.

For this purpose, samples from 6 different sites in Christchurch were provided by the Earthquake Commission (EQC) and sieve analysis was performed on 115 samples. The particle size distribution for the samples was obtained by the method of wet sieving described by NZS 4402.2.8 (1986). Soil characterisation using sieve analysis yielded fines content (*FC*), defined as the percentage by weight passing through a 63μm sieve. All the data were compiled and Figure 5 shows how *AveδT* changes as *FC* increases. It can be seen that there is a good correlation between *FC* and *AveδT* where the coefficient of correlation is 0.792.

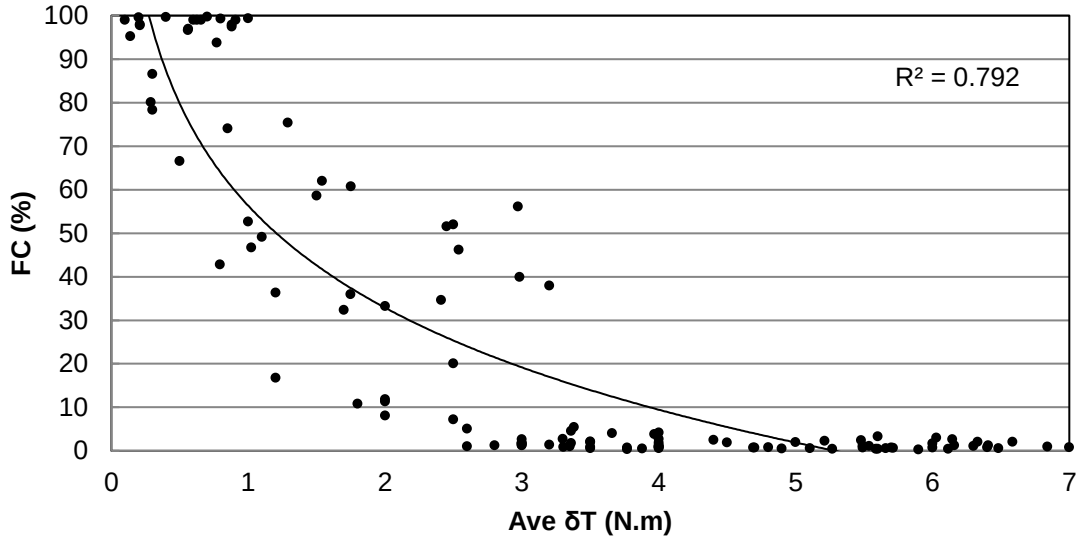

Figure 5 Estimation of fines content using SDS parameter.

The equation for the line is:

$$\mathrm{FC} = -33.81 \ln\left(\mathrm{Ave}\ \delta\mathrm{T}\right) + 56.32 \tag{6}$$

As can be seen from the figure, a high value of *AveδT* parameter (i.e *AveδT*>3 Nm) represents clean sand and, for the *AveδT* values less than 3 Nm, soil would contain fines. Although the graph shows a good correlation between *FC* and *AveδT*, more tests need to be performed, especially for soils with *AveδT* values of less than 3 Nm (including silty sand, sandy silt, clayey sand and sandy clay). It should be noted that the plasticity of fines was not taken into consideration in the plot. Further investigation needs to be done to evaluate the applicability of the proposed method if it is being used for soils in areas different from Christchurch. Currently more tests are being conducted to improve the developed plot.

6 CONCLUSIONS

A total of 164 tests in the three cities of Christchurch, Wellington and Auckland were conducted adjacent to available CPT/SPT locations. A new soil classification chart was generated based on New Zealand soil. A variety of soil types was included in the graph such as sand and silty sand available in Christchurch and Wellington, and peat or clayey soil existing in Auckland. The soil classification graph was validated by evaluating its accuracy in classifying the soil at two sites in Auckland and Christchurch. It was shown that SDS can predict the soil type with a high degree

of accuracy. To find a relationship between *FC* and SDS parameters, 115 sieve analyses were performed on samples taken from 6 sites in Christchurch. A correlation between $Ave\delta T$ and *FC* was formulated that can estimate *FC* directly using SDS parameter ($Ave\delta T$). In comparison with other methods, SDS is simpler and it does not need a large space to conduct the test, and by measuring a variety of parameters continuously including torque, load, and speed of penetration it can give a clear image of the soil profile.

REFERENCES

Eslami, A. and M. Gholami (2006) Analytical Model for the Ultimate Bearing Capacity of Foundations from Cone Resistance. *Scientia Iranica,* 13(3): 223-233.

Maeda, Y., Yamato, S., Sugano, Y., Sakai, G., Suemasa, N., Tanaka, N., (2015) Evaluation of Soil Liquefaction Potential by Screw Driving Sounding Test in Residential Areas. *6th International Conference on Earthquake Geotechnical Engineering*, 1-4 November 2015, Christchurch, New Zealand.

Mayne, P. W. Christopher, B. R, and De Jong, J. (1988) *Manual on Subsurface Investigations*, Washington, D.C.: American Association of State Highway and Transportation Officials.

Mirjafari, S. Y. (2016) Soil Characterization using Screw Driving Sounding (SDS) data, *Ph.D. Thesis*, University of Auckland.

New Zealand Geotechnical Database (2016). https:// www.nzgd.org.nz. Retrieved Feb 2016.

Robertson, P.K. (2010) Soil behaviour type from the CPT: an update. *2nd International Symposium on Cone Penetration Testing, CPT'10*, Huntington Beach, CA, USA. www.cpt10.com.

Standards Association of New Zealand (1986) *Methods of Testing Soils for Civil Engineering Purposes* Part 2.8: Determination of the Particle-Size Distribution. NZS 4402.2.8.

Suemasa N, Shinkai K, Suzawa T & Tamura M. (2005) A plasticity model for Swedish Weight Sounding test, *4th Japan-Philippines Workshop on Safety and Stability of Infrastructure against Environmental Impacts*, University of Philippines, 169-177.

Tanaka T, Suemasa N & Ikegame A. (2012). Classification of strata using Screwdriver Sounding test., *Proc. 22nd International Offshore and Polar Engineering*, Conference Rhodes, Greece.

Van T Veen, L. H. (2015). CPT Prediction of Soil Behaviour Type, Liquefaction Potential and Ground Settlement in North-West Christchurch, *M.Sc Thesis*, University of Canterbury.

Development of detailed liquefaction case histories from the 1987 Edgecumbe Earthquake

N Mellsop
Tonkin + Taylor, Auckland
nmellsop@tonkintaylor.co.nz (Corresponding author)

S Bastin
QuakeCoRE, University of Canterbury, Christchurch
s.bastin@canterbury.ac.nz

L Wotherspoon
University of Auckland, Auckland
l.wotherspoon@auckland.ac.nz

S van Ballegooy
Tonkin + Taylor, Auckland
svanballegooy@tonkintaylor.co.nz

Keywords: liquefaction, case histories, Edgecumbe earthquake

ABSTRACT

Liquefaction and associated lateral spreading during the 1987 M_w 6.5 Edgecumbe earthquake caused severe damage within parts of the Whakatane township. Liquefaction primarily manifested proximal to the Whakatane River in areas underlain by recent fluvial and marine sediments. The development of ground motion intensity and groundwater models for the Whakatane region for the Edgecumbe earthquake enabled CPT based liquefaction assessments to be applied using an extensive CPT dataset. Liquefaction assessments undertaken using the median PGA model and median groundwater model were found to closely correspond with the observed severity of liquefaction manifestation at sites known to have surface manifestation. However, significant over prediction of manifestation severity was evident in the Central Business District (CBD) under these conditions. Sensitivity analyses of the PGA and groundwater models were not able to account for these issues, with reduction in PGA and lowering of water table providing some improvement in areas without manifestation while at the same time providing underestimates in areas with manifestation. Overall, the findings suggest that standard CPT based methods of liquefaction assessment may be causing conservative predictions in the Whakatane CBD; further research is required to examine potential factors behind the inconsistent predictions.

1 INTRODUCTION

Earthquake-induced liquefaction and associated lateral spreading pose a significant hazard to the built environment. It is critical that liquefaction hazards are able to be adequately assessed so that the hazard can be effectively managed and the associated impacts minimized. The simplified liquefaction triggering procedures for assessing liquefaction hazards have been derived from liquefaction case histories collected following large earthquakes (e.g. Idriss and Boulanger, 2008 and Boulanger and Idriss, 2014). Cases where liquefaction is predicted by the simplified procedures, yet was not observed, provide important insights into the limitations of the current assessment methodologies, including their applicability in various soil types.

The 1987 M_W 6.5 Edgecumbe earthquake caused localised liquefaction and lateral spreading in parts of the Rangitaki Plains in the Bay of Plenty, New Zealand. Liquefaction and lateral spreading resulted in severe damage to infrastructure and lifelines, including NZ$10 million worth of damage to flood control and drainage schemes within the region (Pender & Robertson, 1987; Christensen, 1995; Dowrick & Rhoades, 1990; Berrill, et al., 2001). The township of Whakatane experienced localized liquefaction and lateral spreading proximal to the Whakatane River, however no liquefaction was reported within the in the Central Business District (CBD).

In this paper, the extents of liquefaction manifestation within Whakatane for the Edgecumbe earthquake as collated from historical photographs, technical reports, and publications are presented. The collated extents are then compared with the predicted liquefaction severity estimated from the extensive CPT dataset collated for the Whakatane township using modelled peak ground accelerations (PGA) and the depth to groundwater at the time of the earthquake. Three peak ground acceleration models and three groundwater models were developed for the Whakatane region to account for the uncertainty in these variables during the earthquake (a median, lower estimate and upper estimate).

2 LIQUEFACTION OBSERVATIONS

Observations of liquefaction related land damage, including sand ejecta and lateral spreading associated with the Edgecumbe earthquake sequence, were compiled from technical reports, publications, and historical photographs (i.e. Pender & Roberson (1987), Franks et al. (1989) and Jennings et al. (1988)). The records were digitally compiled and presented geospatially for the purpose of this research (Figure 1). The accuracy in location and extent of the observations varies significantly as a function of the method of observations. For example, observations transcribed from aerial photographs onto hand drawn maps are significantly more innacurate than ejecta locations that have been digitised through precise descriptions of where samples have been taken (Such as in Pender & Robertson, (1987)) and near field photographs where landmarks are visible. Because of the above two categories have been chosen to distinguish between the confidence in the location of liquefaction manifestation, these being “Liquefaction Manifestation Confirmed” and “Possible Liquefaction Manifestation”.

The most severe liquefaction manifestation in Whakatane occurred in point-bar deposits within the inside bends of the Whakatane River, particularly the James Street Loop and the Netball Courts, and in paleo-channel deposits along the western side of the Landing Road Bridge (SH2). It is noted that there was no evidence of liquefaction having occurred throughout the Central Business District (CBD). Areas of liquefaction manifestation in Whakatane are summarised in Figure 1.

3 PEAK GROUND ACCELERATION MODEL DEVELOPMENT

The ground motion characteristics of the Edgecumbe earthquake were recorded by four strong motions stations (SMSs) within approximately 100 km of the causative fault plane, however there were no SMSs located within Whakatane. The closest SMS was Matahina Dam, which was approximately 11 km from the fault plane recorded a geometric mean PGA of 0.26g, while the western edge of Whakatane was approximately 9 km from the fault plane.

In order to estimate the Peak Ground Accelerations (PGAs) in Whakatane a number of ground motion models (GMMs) were assessed. From these, the Bradley (2013) GMM was chosen as the recorded PGA was well approximated by the 79th percentile of the Bradley GMM at each SMS location. Using this recorded PGA data, this percentile was then assumed to represent the median PGA for the Edgecumbe earthquake and the inter-event uncertainty was removed. To represent the uncertainty in the PGA only the intra-event standard deviation was used. This approach was

taken as in the absence of any recorded data the combined inter- and intra-event uncertainty would result in a wide distribution of potential PGA values in Whakatane. By assigning a modified median representative of this event, the uncertainty reduces and is expected to be more representative of the actual PGA experienced in Whakatane.

The 15th and 85th percentile of the new probability distributions were used to represent upper and lower estimates of the PGA across the region. To provide another assessment of the accuracy of this model, the median PGA models was converted to equivalent MMI using the PGA-MMI relationships of Wald et al. (1999). The resulting MMI values were shown to correlate well with the reported MMI values across Whakatane. From this model a geospatial representation of the PGA across Whakatane was developed, with contours representing the respective PGA estimates presented in Figures 1-3.

4 GROUNDWATER MODEL DEVELOPMENT

Groundwater at the time of the Edgecumbe earthquake was modelled using a kriging interpolation method to develop a groundwater elevation surface between depth to groundwater at monitoring wells and river levels. The groundwater elevation surface was subsequently subtracted from a digital elevation model (DEM) to build a model of groundwater depth. River level data from 1956 to present from monitoring stations was used to derive a river level model at 50 m increments along the river assuming a constant gradient between the recording stations. Using groundwater data available from a range of sources, a correlation was identified indicating that groundwater is governed by the river levels. The groundwater data from more recent investigations were subsequently adjusted to levels expected during the Edgecumbe earthquake based on the river levels at the time of the earthquake. The standard deviation of the correlation between the river levels and groundwater levels was used to create upper and lower depth to groundwater estimates. Two standard deviations were added for the upper estimate of the depth to groundwater, while two standard deviations were subtracted for the lower estimate of the depth to groundwater. A more comprehensive description of the development of the groundwater models is discussed by Mellsop (2017).

5 LIQUEFACTION ASSESSMENT

The factor of safety against liquefaction was evaluated with depth at each sounding location using the Boulanger & Idriss (2014) liquefaction triggering methodology to evaluate the likelihood of liquefaction. The soil's fines content (FC) was estimated using the default Boulanger and Idriss (2014) FC-I_c correlation with the C_{FC} fitting parameter set to zero. The cyclic resistance ratio (CRR) curves for a probability of liquefaction (P_L) of 15% were adopted for the liquefaction triggering analyses. Soil layers with I_c values greater than 2.6 were considered plastic in behaviour to liquefy (Robertson and Wride, 1998).

Predicted land damage was subsequently calculated for each CPT using the Liquefaction Severity Number (LSN) (van Ballegooy, et al., 2014) and Liquefaction Potential Index (LPI) (Iwasaki, et al., 1984) liquefaction manifestation severity parameters. Previous studies have shown a good correlation between the LSN and LPI with observed liquefaction manifestation (Juang, et al., 2005a; Juang, et al., 2005b; Toprak & Holzer, 2003; Maurer, et al., 2014; van Ballegooy, et al., 2014). These studies generally find that LSNs greater than 16 and LPIs greater than 5 coincide with minor to moderate liquefaction manifestation, while LSNs and LPIs greater than 26 and 15, respectively align with moderate to severe liquefaction manifestation. It is important to acknowledge that the LPI and LSN are not intended to consider lateral spreading, and therefore may not account for the liquefaction severity observed proximal to the Whakatane River. However, the collated reports indicate sand boils formed in the flat land adjacent to the lateral spread sites and thus should correspond with LSNs and LPIs higher than 16 and 5 respectively.

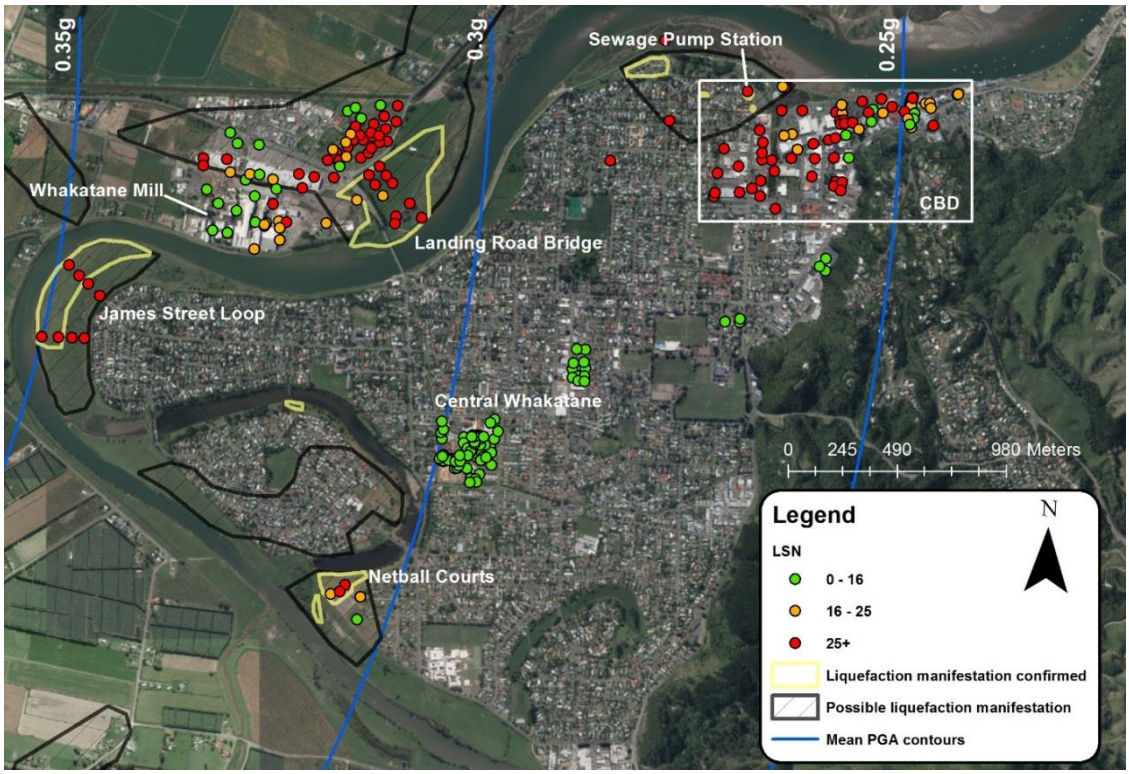

Figure 1: Map of CPT-based LSN values across Whakatane resulting from the liquefaction assessment undertaken using the median PGA model and median groundwater model.

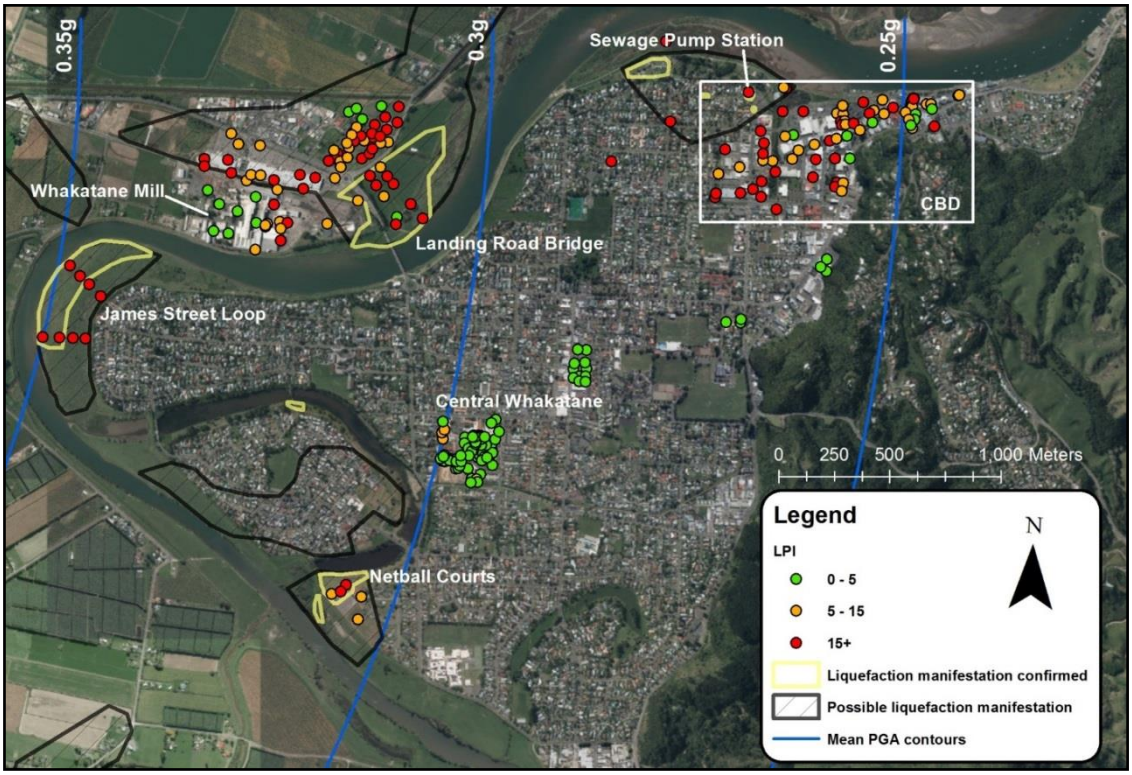

Figure 2: Map of CPT-based LPI values across Whakatane resulting from the liquefaction assessment undertaken using the median PGA model and median groundwater model.

The resultant LSN and LPI calculated using the median PGA and groundwater models are presented in Figure 1 and Figure 2, respectively. The mapped extent of liquefaction manifestation is summarised in these figures with the contours of the PGA model for each. Each point in these figures corresponds to a single CPT sounding and the corresponding predicted manifestation severity (green=none, orange=minor-moderate, red=moderate-severe). High LSN and LPI values are generally observed within "liquefaction manifestation confirmed" zones and thus correlate well with the observations. Outside of the CBD in areas with no observed manifestation the estimated LPI and LSN values matched the observed values. However, high LSN and LPI values were predicted within the CBD area in which no liquefaction was observed during the Edgecumbe earthquake. Some of this discrepancy in the CBD may be due to incorrect categorisation of the CPT as a consequence of insufficient historical data. However, given the large number of CPTs, it is more likely that the liquefaction assessment is over predicting the manifestation severity.

The lower estimate PGA and groundwater elevation models produced LSN and LPI that better fit the absence of liquefaction manifestation within the CBD, albeit there were still cases, particularly in the south-west of the CBD in which the severity is still over-predicted when using LSN. Additionally, the use of the lower-bound models led to under-prediction of the liquefaction manifestation severity in the areas where manifestation has been confirmed (Landings Rd and Netball Courts). A summary of the LPI values using these two lower estimate models is presented in Figure 3, demonstrating improved correlation with observed manifestation in the CBD, but again underprediction of manifestation severity at Landings Rd and the Netball Courts. The under-prediction of the liquefaction severity at sites where the damage was well-documented indicates that the LSN and LPI produced from the median PGA and groundwater models it likely a better representation of the local conditions in the township at the time of the earthquake.

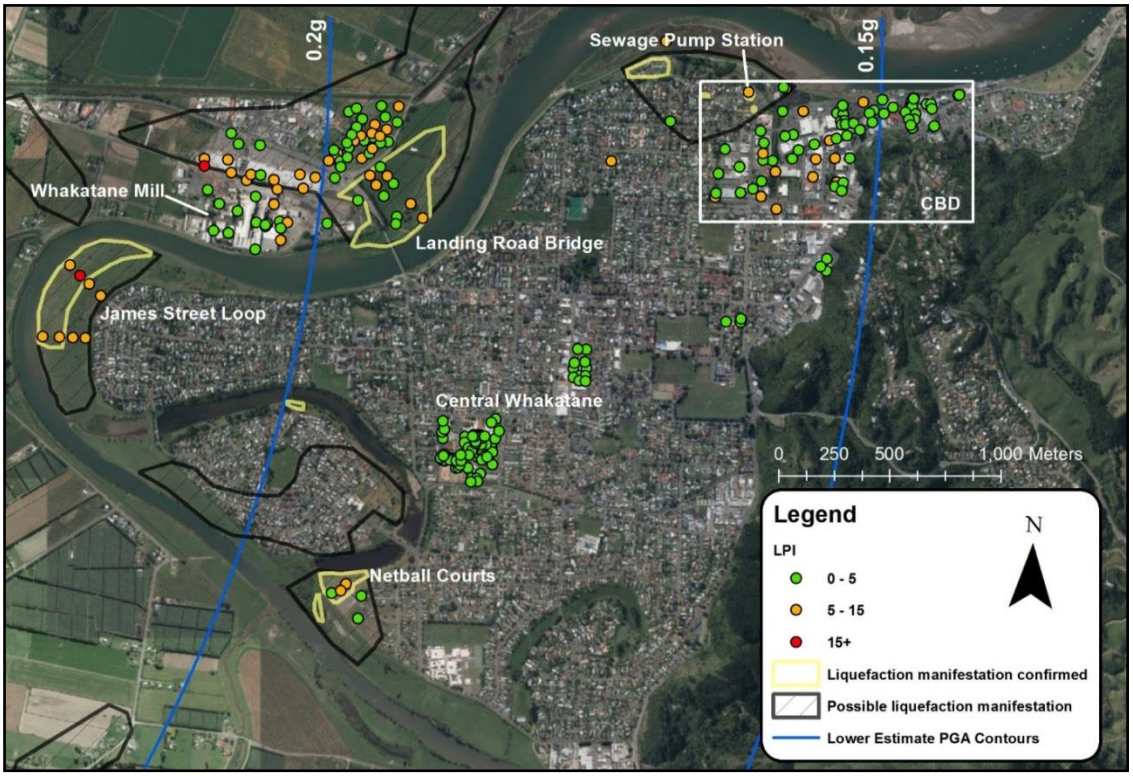

Figure 3: Map of CPT-based LPI values across Whakatane resulting from the liquefaction assessment undertaken using the lower estimate PGA model and lower estimate groundwater model.

Trenching work conducted at sites within the CBD in which liquefaction was predicted but where manifestation was not observed revealed stratigraphy that did not contain liquefaction features,

further confirming that liquefaction was unlikely to have triggered at these sites. Results of the trenching work are presented by Bastin et al. (2017) and indicate that some of the inconsistencies at these false positive sites may result from the inability of the CPT to discern fine scale inter-layering of sands and silts, and/or the presence of pumice which are not accounted for in the simplified methodologies. These factors, along with other potential mitigating factors such as the difference between measured and actual ground-water depths due to partial saturation are the focus of more in-depth assessment of a selection of case study sites summarised by Mellsop (2017).

6 CONCLUSIONS

A back calculated liquefaction assessment has been undertaken for Whakatane during the Edgecumbe earthquake using a large Cone Penetration Test (CPT) dataset and standard CPT-based liquefaction assessment methods. By performing the liquefaction assessment with varying PGA and groundwater models, the influence of these variables on predicted liquefaction manifestation severity has been considered. Liquefaction assessments undertaken using the median PGA model and median groundwater model were found to correlate well with the severity of liquefaction manifestation at those sites that are known to have surface manifestation. However, under these conditions significant over-prediction of manifestation severity was evident in the Central Business District (CBD).

Using the lower estimate PGA and groundwater models, LSN values accurately captured the liquefaction manifestation severity at sites with surface manifestation, but again resulted in over-prediction in the CBD. LPI results from these lower estimate models under-predicted liquefaction manifestation during the Edgecumbe earthquake where manifestation was observed, and still resulted in some minor over prediction in the CBD. Overall, the findings suggest that standard CPT based methods of liquefaction assessment may be producing conservative estimates of liquefaction manifestation severity in the Whakatane CBD, and further research is needed to improve these approaches.

7 ACKNOWLEDGEMENTS

We thank the Whakatane District Council for providing access to the study sites and for the supply of historical data and data related to the development of the groundwater model. We thank local engineering firms for the supply of historical geotechnical investigation information. This work was funded by QuakeCoRE – New Zealand Centre for Earthquake Resilience, with additional support from the Ministry of Business, Innovation and Employment (MBIE) and the Earthquake Commission. This is QuakeCoRE paper number 0200.

REFERENCES

Bastin, S., van Ballegooy, S., Mellsop, N. & Wotherspoon, L. (2017) Liquefaction case histories from Whakatane, New Zealand as a result of the 1987 Edgecumbe Earthquake –– Insights from an extensive CPT dataset and paleo-liquefaction trenching. *PBD III Earthquake Geotechnical Engineering*. Vancouver, CA.

Berrill, J., Christensen, S., Kennan, R. & Pettinga, J. (2001) Case study of lateral spreading forces on a piled foundation. *Geotechnique*. 51(6), pp. 501-517.

Bradley, B. A. (2013) A New Zealand-Specific Pseudospectral Acceleration Ground-Motion Prediction Equation for Active Shallow Crustal Earthquakes Based on Foreign

Models. *Bulletin of the Seismological Society of America*. 103(3), pp. 1801-1822.

Boulanger, R. W. & Idriss, I. M. (2014) *CPT and SPT Based Liquefaction Triggering Procedures*. Report No. UCD/CGM-14/01, Davis, California: Center for Geotechnical Modeling.

Christensen, S. A. (1995) *Liquefaction of Cohesionless Soils in the March 2, 1987 Edgecumbe Earthquake, Bay of Plenty, New Zealand and Other Earthquakes*. Christchurch: University of Canterbury.

Dowrick, D. J. (1988) Edgecumbe Earthquake - Some Notes on its Source, Ground Motions, and Damage in Relation to Safety. *Bulletin of the New Zealand Society for Earthquake Engineering*. 21(3), pp. 198-203.

Dowrick, D. & Rhoades, D. (1990) Damage ratios for domestic buildings in the 1987 Edgecumbe earthquake. *Bulletin of the New Zealand National Society for Earthquake Engineering*. 23(2), pp. 137-149.

Franks, C. A., (1989) Ground damage and seismic response resulting from the 1987 Edgcumbe Earthquake, New Zealand. *New Zealand Journal of Geology and Geophysics*. Volume 32, pp. 135-144.

Idriss, I. M. & Boulanger, R. W. (2008) *Soil liquefaction during earthquakes*. Monograph MNO-12, Oakland, CA.

Iwasaki, T., Arakawa, T. & Tokida, K. (1984) Simplified Procedures for assessing soil liquefaction during earthquakes. *International Journal of Soil Dynamics and Earthquake Engineering*. 3(1), pp. 49-58.

Jennings, D. N., Edwards, M. C. & Franks, C. R. (1988) *Some Observations of Sand Liquefaction in the 2 March 1987 Edgecumbe (New Zealand) Earthquake*. Sydney.

Juang, C. H., Yang, S. H., Yuan, H. & Fang, S. Y. (2005a) Liquefaction in the Chi-Chi earthquake - effect of fines and capping non-liquefiable layers. *Soil and Foundations*. Volume 45, pp. 89-101.

Juang, C. H. et al. (2005b) Estimating severity of liquefaction-induced damage near foundations. *Soil Dynamics and Earthquakes*. Volume 25, pp. 403-411.

Maurer, B. W., Green, R. A., Cubrinovski, M. & Bradley, B. A. (2014) Evaluation of the Liquefaction Potential Index for Assessing Liquefaction Hazard in Christchurch, New Zealand. *ASCE Journal of Geotechnical and Geoenvironmental Engineering*. 140(7).

Mellsop, N. (2017) Liquefaction case histories from the 1987 Edgcumbe earthquake – Insights from an extensive CPT dataset, direct push cross hole shear and compression wave velocity (V_sV_p) testing and paleo-liquefaction trenching. *ME Thesis*, University of Auckland.

Pender, M. J. & Robertson, T. W. (1987) Edgecumbe Earthquake: Reconnaissance Report. *Bulletin of the New Zealand Society for Earthquake Engineering*. 20(3), pp. 201-249.

Toprak, S. & Holzer, T. L. (2003) Liquefaction potential index: field assessment. *Journal of Geotechincal and Geoenvironmental Engineering*. 129(4), pp. 315-322.

van Ballegooy, S. et al. (2014) Assessment of Liquefaction-Induced Land Damage for Residential Christchurch. *Earthquake Spectra*. 30(1), pp. 31-55.

Wald, D. J., Quitoriano, V., Heaton, T. H. & Kanamori, H. (1999) Relationship between Peak Ground Acceleration, Peak Ground Velocity, and Modified Mercalli Intensity in Calafornia. *Earthquake Spectra*. 15(3), pp. 557-564.

Dynamic Site Characterisation of the Nelson-Tasman Region

R McMahon
Beca NZ Ltd. (formerly University of Auckland)
rmcm343@aucklanduni.ac.nz (Corresponding author)

L Wotherspoon
Faculty of Engineering, University of Auckland, NZ
l.wotherspoon@auckland.ac.nz

Keywords: Site characterisation, geophysical testing, Nelson and Tasman

ABSTRACT

This paper presents a study being undertaken to characterise the subsurface across Nelson and Tasman using active source surface wave testing, ambient wave field (passive) and H/V spectral ratio methods. Deep soil and gravels deposits are present in this area which may lead to amplification of ground shaking and basin effects. However, there is currently little information available on the dynamic properties of the deposits across the Nelson-Tasman region, and the potential site amplification effects. Existing subsoil information has been used to constrain the shear wave velocity profiles at a number of sites developed from surface wave testing, highlighting the high shear wave velocities in the regional gravel deposits. H/V spectral ratio measurements were employed in order to characterise the wider basin structure. However, based on current data and knowledge of the deeper regional geology, it is likely that there is often no strong impedance contrast at the bottom of the basin due to the significant depth and high shear wave velocity of dense claybound gravels overlying the bedrock. This means that H/V spectral ratio measurements may only be able to characterise the response of profiles above shallow impedance contrasts, not the overall soil profile.

1 INTRODUCTION

The Nelson-Tasman region is the north-western section of the South Island of New Zealand. The main centre, Nelson city, has a population of 46,000 and when combined with the wider Tasman area the region has a combined population of nearly 90,000 (Immigration NZ, 2016). The Nelson-Tasman region has two large shallow bays – Tasman Bay and Golden Bay, with a mountainous interior. Urban development is limited both spatially and in density, with only a small number of multi-story buildings present in the city business district. Nelson-Tasman Region is considered a 'moderately' seismic area, due to the proximity to the Alpine Fault and the local Waimea-Flaxmore Fault System.

Nelson-Tasman region is a rugged mountainous area formed of very hard rocks, some of which are among the oldest in New Zealand (GNS, 2016). The area comprises rugged, recently deglaciated Tasman Mountains in the west and the lower Richmond Range and other ranges in the east separated by the low-lying Moutere Depression. In the southeast, the Wairau valley separates the Richmond Range from the southern Nelson area and is characterised by relatively shallow water depths (Rattenbury et al., 1998).

The steep rocky mountain ranges that enclose the region have supplied huge volumes of gravel to the lower lying areas. Over time, the relatively flat areas of Nelson and Richmond have been formed on outwash gravels. There have also been a number of areas reclaimed in recent years with the use of hardfill and domestic rubbish to extend the natural foreshore area Figure 1.

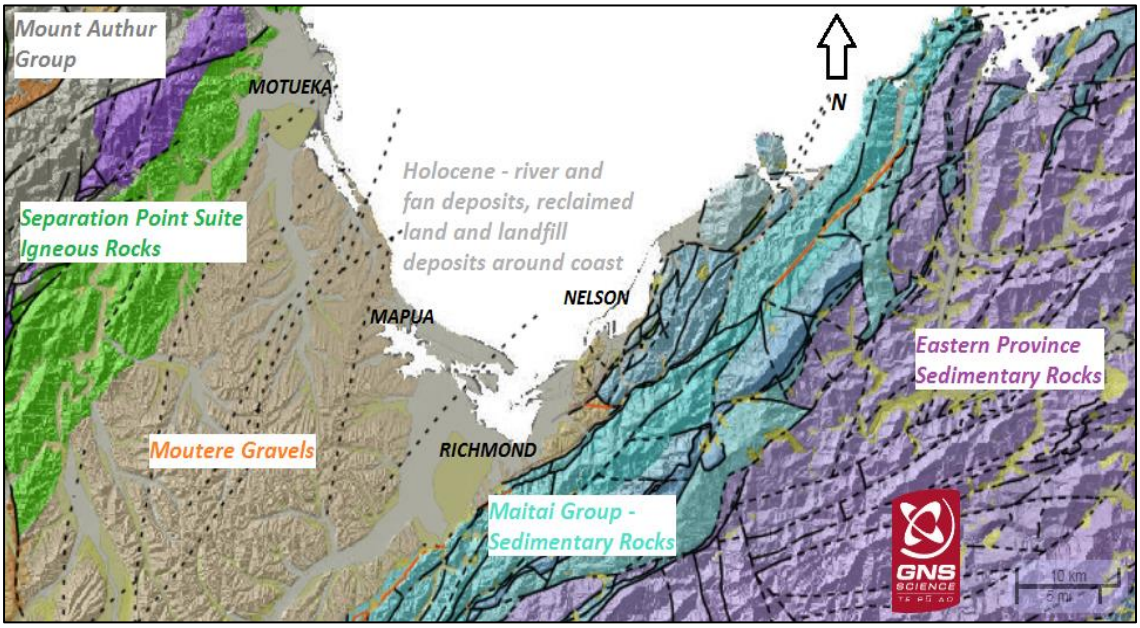

Figure 1: Overview of the Nelson-Tasman Region Geology (modified from Nelson Urban Area Geological Map, 1:250 000, New Zealand Geological Survey (2014) http://data.gns.cri.nz/geology/).

A large proportion of Nelson-Tasman is underlain by a very deep basin of dense gravel. The most prominent formations are the Moutere Gravels (Tasman) and Port Hills Gravels (Nelson) which are of a similar age and structure.

In Nelson city, the Port Hills Gravels are up to 500 m thick, and consist of granitic conglomerate grading upwards into conglomerate composed of clasts of volcanic Permian/Triassic rocks largely derived from the east of the Waimea Fault. Port Hills Gravel is comprised of heterogeneous clay and silt bound gravel with lenses of sandstone and occasional lignite seams and is intersected by a number of faults (Westerson, 2007).

The Moutere depression and surrounding areas of Tasman are generally underlain by Moutere Gravels. According to seismic reflection studies and interpretation of regional geology the Moutere Gravels extend thousands of meters below the ground surface, and are very dense (Lihou, 1992). Slightly weathered, well rounded quartzfeldspathic sandstone clasts in a brown weathered muddy sand matrix comprise the bulk of the Moutere Gravel. In the Moutere depression, an extensive area of Moutere Gravel is preserved. The gravels are described as uniform yellow-brown, clay-bound gravel, with deeply weathered clasts is almost entirely of Torlesse-derived sandstone and semi-schist (Rattenbury et al., 1998).

Although regional seismic reflection has provided an overview of the structure of the subsurface, there is very little knowledge of the dynamic characteristics of the regional deposits described previously. The primary aim for this study is to provide guidance and information on dynamic site parameters and seismic site classification in the Nelson Tasman region by developing shear wave velocity-depth relationships for regional deposits. Mapping of inferred NZS1170.5 (Standards New Zealand, 2004) site classes based on testing and analysis will also provide useful high-level guidance for seismic design.

The Nelson-Tasman site characterisation study is aimed at collecting information for site characterisation purposes using geophysical and traditional geotechnical techniques. Outputs will include site period estimates derived from H/V spectral ratio measurements and shear wave velocity profiles for a number of sites across the region.

2 DATA COLLECTION METHODOLOGY

A range of methods were used to collect data for the purposes of this project. This included collation of available traditional subsurface information as well as active-source and passive-source geophysical testing as detailed below. The processing and interpretation of the collected information was completed using best-practice methods.

2.1 Factual Geotechnical Database

Available subsurface data and geotechnical information was compiled to develop a reference dataset which would then be used to constrain and interpret the geophysical data collected. The use of factual geotechnical information as a means of constraining test data is an essential part of the geophysical site characterisation process.

2.2 Surface Wave Testing Methodology

Both active-source and passive-source surface wave testing methods were utilised to develop shear wave velocity profiles across the region. In this paper field investigation data was collected using a linear array for active source testing and a two-dimensional L array for passive source testing. Active source testing was performed using 24 geophones at 2 m spacing, with at least three separate source locations from the first receiver in the array (e.g. 5, 10, 20 m) to account for the effect of offset distance on the dispersion curve data, and from each end of the array to account for lateral heterogeneity. L-array testing was carried out using 24 geophones at 5 m spacing, creating an "L" shape with lengths of 60 m and 55 m. While not presented here, additional passive source surface wave testing has been carried out using circular arrays of broadband seismometers with diameters ranging from 50 m to 200 m. This will enable the characterisation of the shear wave velocity profile to much greater depths (up to 200 m).

Dispersion data from each array were combined to form composite dispersion curves for each processing method. The Rayleigh-wave dispersion data was inverted using a multi-mode inversion along with the neighbourhood algorithm in Geopsy (Wathelet, 2008). To provide the best representation of the shear wave velocity profile at each site layering characteristics from subsurface investigation data was used to constrain the surface wave inversion parameters. This is a key step in the development of profiles that are representative of the actual site conditions, as without this constraint there will be an increase in the uncertainty of shear wave velocity profiles that are developed (Wood et al., 2015). Rather than providing a single, deterministic Vs profile for each site, these inversions provide a suite of profiles that fit the experimental data equally well.

2.3 H/V Spectral Ratio Methodology

To estimate the site period (T_0) at each location, the ratios of the horizontal-to-vertical Fourier amplitude spectra (FAS) of recorded ambient noise were used (i.e., H/V spectral ratios) (Nakamura, 1989). Broadband 3-component seismometers (Nanometrics Trillium Compact, 20 second period) were used at individual test locations at sites including council owned parks and road-reserves. The seismometers were either embedded in the ground and packed securely into place, or placed on a levelling cradle used to ensure the sensor has a firm connection with the ground. H/V data were processed using the software Geopsy (www.geopsy.org). Time windows that were overly noisy were removed, with the remaining windows used to develop the spectral average at each location. The geometric mean of the horizontal-component Fourier spectra were used to develop the H/V spectral ratios, and a Konno & Ohmachi (1998) smoothing function with a smoothing constant of b=40 was applied. The H/V spectral ratios from a range of time window lengths were compared during processing to determine the influence of window lengths on the estimated spectral peak(s) and to estimate the uncertainty associated with the spectral peak(s).

The data presented in this paper used a window length of 100 seconds with no overlap and a 5% cosine taper.

The H/V spectral peak(/s) from ambient noise recordings in this region were expected to correspond to: (1) the site period for the entire soil profile down to basement rock (a significant impedance contrast); or (2) the site period of shallow sandy soils above a shallow impedance contrasts.

2.4 Site Classification Metrics

In this paper we present the shear wave velocity profile and direct site period measurements. The site period (T_0) is the fundamental period of vibration of the overall soil profile above bedrock at a particular location. In the most simple sense, this can be related to the shear wave velocity by the equation below (the quarter wavelength method):

$$T_0 = \frac{4H}{V_{s,avg}}$$

where:
H is the thickness of the soil deposit above bedrock or above the identified impedance contrast at a given site.
V s, avg is the time averaged shear wave velocity profile calculated using the following equation

$$V_{s,avg} = \frac{\sum_i h_i}{\sum_i \frac{h_i}{V_{si}}}$$

where h_i is the thickness of the soil layer (i) and V_{si} is the shear wave velocity of layer (i). A more rigorous estimate of the site period can be made using the small strain transfer function between the bottom and top of the profile, with the maximum peak in the transfer function corresponding to the site period (e.g. Kramer, 1996).

3 RESULTS

Four sites have been selected to illustrate the type of outputs that this project will deliver for a number of sites across the region. The four locations are (with simplified mapped geology according to Rattenbury et al. (1998)): Tahunanui Fields (Tahunanui sands, underlain by Port Hills gravels), Greenmeadows Park (Stoke Fan Gravels underlain by Port Hills Gravels), Saxton's Fields (Stoke Fan Gravels, underlain by Moutere Gravels) and Ben Cooper Park (Stoke Fan Gravels, underlain by Moutere Gravels).

The map in Figure 2 shows the relative locations of the example sites, and also provides a summary of H/V spectral ratio data recorded using broadband seismometers. The peak frequency (i.e. inverse of fundamental period) is relatively clear for most of the sites, but it is noted that there is a relatively weak peak measured at Greenmeadows Park, with a H/V ratio of around 2. At Ben Cooper Park two close peaks are identified. All peaks are less than 0.3 seconds, suggesting that they represent the response of a shallow soil profile rather than the overall profile to bedrock.

For each shear wave velocity test location, 1000 theoretical shear wave velocity profiles were derived which best represented the measured dispersion curve. The 1000 best shear wave velocity profiles for each site have been plotted with depth in Figure 3 and 4. At each site, the 'Lowest Misfit Profile' is the shear wave velocity profile from the inversion process that best fits the experimental data and is shown in bold on each plot. A typical trend at each site is an increase in the range of shear wave velocities as depth increases.

As indicated previously, the period identified by the H/V spectral ratio method likely corresponds to the response of a shallow soil profile above an impedance contrast. Using the shear wave velocity profiles, we are able to identify potential shallow impedance contrasts and calculate the

site period using the two methods described previously. The impedance contrast depth adopted for each site and the resulting site period for the quarter wavelength, transfer function and H/V spectral ratio method are reported in Table 1.

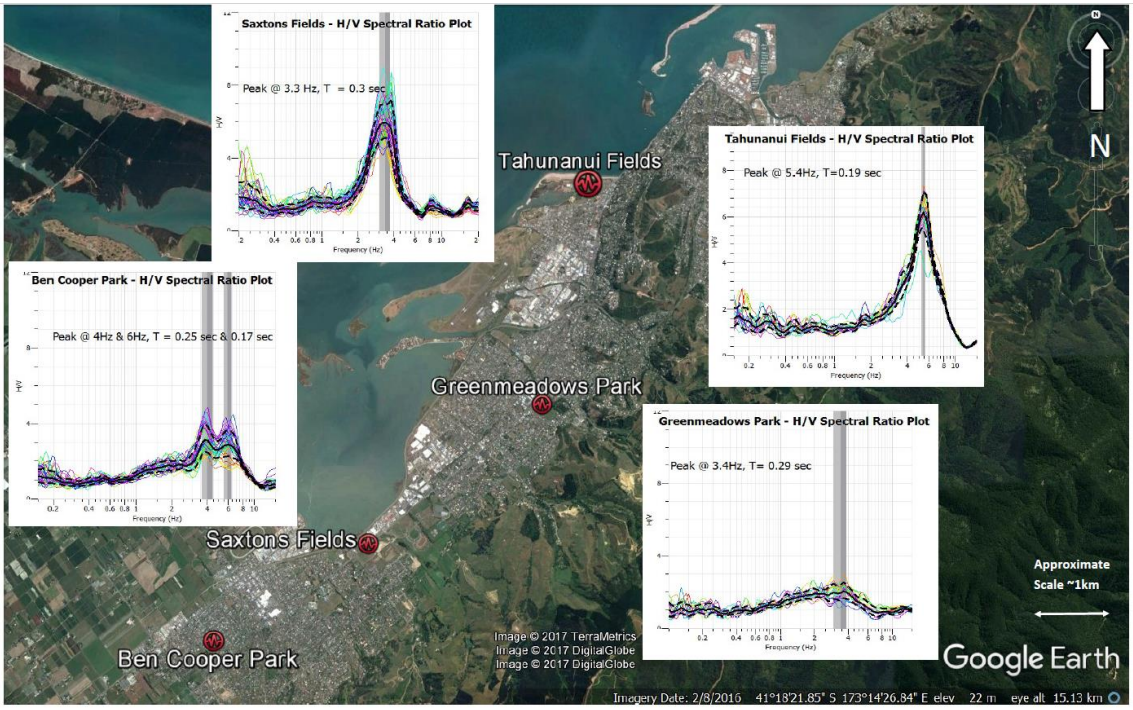

Figure 2: Locations Nelson-Tasman sites considered for comparison

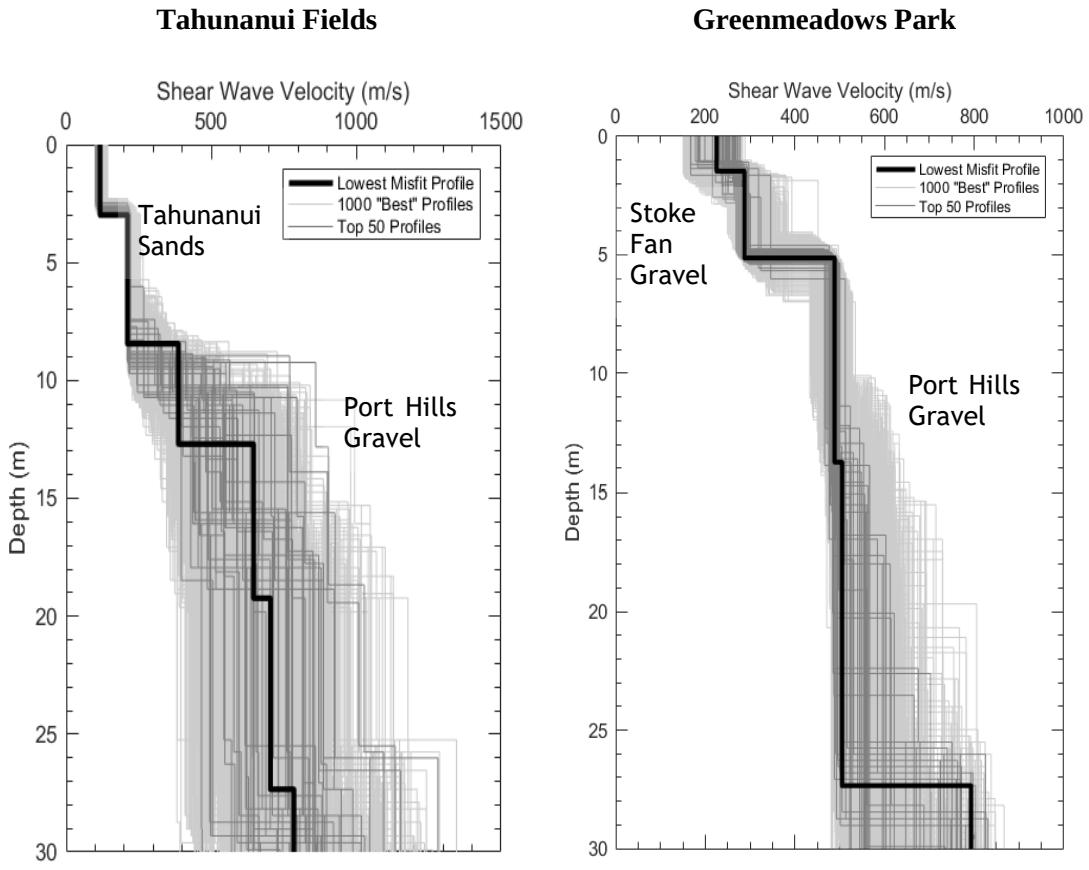

Figure 3: Shear-wave velocity top 1000 profiles ('best-fit' profile shown on bold) and transfer functions for each site, derived from 'best fit' Vs profile

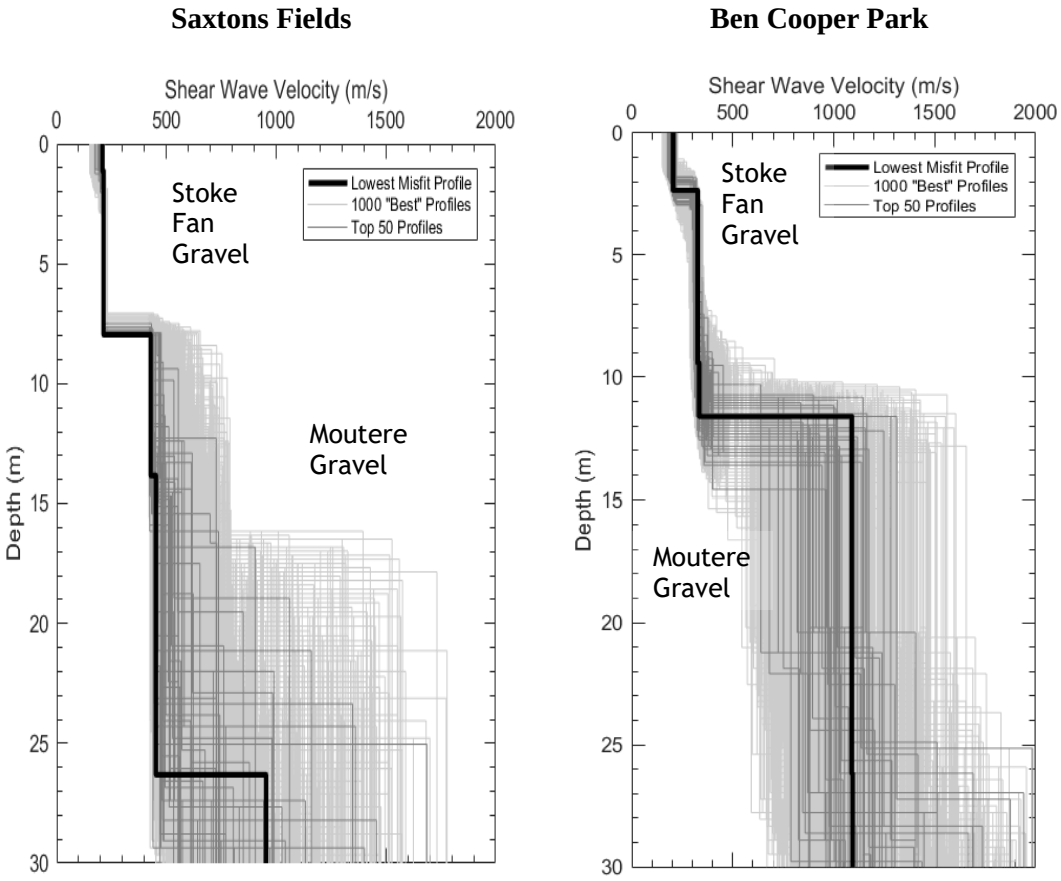

Figure 4: Shear-wave velocity top 1000 profiles ('best-fit' profile shown on bold) and transfer functions for each site, derived from 'best fit' Vs profile

Table 1: Site Period Method Comparison for Nelson-Tasman Sites Analysed

Site Name	Depth to impedance contrast	Transfer Function Method	Quarter Wavelength Method	H/V Spectral Ratio Method
Tahunanui Fields	13 m	0.19 sec	0.20 sec	0.19 sec
Greenmeadows Park	23 m	0.23 sec	0.24 sec	0.29 sec
Saxton Fields	26 m	0.25 sec	0.28 sec	0.30 sec
Ben Cooper Park	12 m	0.14 sec	0.15 sec	0.17 sec & 0.25 sec

The estimates of the shallow profile period for each site using the three different methods show some variation, but in general there is good agreement between methods. As the shear wave velocity profiles show an increase with depth the simple quarter wavelength method provides a fairly good representation of the shallow profile period. This is most significant for Greenmeadows Park and Saxton Fields, possibly because the depth to the inferred impedance contrast is deeper than that identified at Tahunanui Fields and Ben Cooper Park. The increase in measured shear wave velocity is also more gradual with a weaker impedance contrast at Greenmeadows and Saxton Fields, making it more difficult for the applied methods to clearly define the period of the shallow profile for a given site. Analysis of the passive source circular array test data will help to constrain these effects.

4 DISCUSSION

Compared to testing completed in other regions across New Zealand with broadband seismometers the measured H/V spectral ratio peaks had significantly shorter period and less clearly defined. It is inferred that this is due to the lack of strong impedance contrast at basement depth in the Nelson-Tasman geology, and seems to be supported by the large velocities measured in the clay bound gravel deposits.

The shear wave velocities derived from the inversion process are in the order of 600 – 1200 m/s for Moutere Gravels and Port Hills Gravels at shallow depths of around 15 m to 20 m below ground level. Such high shear wave velocity is normally associated with bedrock with an Unconfined Compressive Strength (UCS) of more than 1 MPa. A shear wave velocity of 800 – 1200 m/s is reported by the 'Caltrans/NEHRP soil profile types' (Wair et al. 2012) to be within the considered range of Vs30 for rock. The Moutere Gravels and Port Hills Gravels are generally a clay bound gravel, are very dense and stiff, but are unlikely to be a cemented conglomerate rock until around 30 m below ground level for Port Hills Gravel or more than 100 m depth for Moutere Gravels (Wopereis, 2017). Therefore, some revision of what we consider to be 'rock' in the guidelines for assessing seismic site class may need to be considered, particularly for regions such as Nelson-Tasman which have very deep and dense gravel deposits.

5 CONCLUSION

The information presented in this paper summarises the data from four considered sites across the Nelson-Tasman region. Discrepancies shown between the resulting site period estimates are likely to be partly caused by the lack of strong impedance contrast in the region. Consideration of the definition of 'seismic bedrock' (i.e. the defined rock underlying a surficial soil profile) needs to be explored further for sites with deep gravel basins overlying deep rock.

6 ACKNOWLEDGEMENTS

We acknowledge the financial support from QuakeCoRE and the EQC/NZSEE Ivan Skinner Award. This is QuakeCoRE publication number 0199. The authors acknowledge Nelson City Council, Tasman District Council and local consultants for the in kind support they have provided to this project. We thank Joseph Barratt, James Tyson and Kevin Foster for their field work assistance and Seokho Jeong for his processing and technical assistance as part of QuakeCoRE Technology Platform 2.

REFERENCES

GNS. (2016) *GNS Science.* 02 01 2016. www.gns.cri.nz/Home/Our-Science/Earth-Science/Regional-Geology/The-Geology-of-New-Zealand.

Immigration NZ (2016). Nelson-Tasman. *New Zealand Now.* 29 01 2016. https://www.newzealandnow.govt.nz/regions-nz/nelson-tasman.

Konno, K, & T Omachi. (1998) Ground-motion Characteristics estimated from spectral ratio between horizontal and vertical components of microtremor. *Bulletin of the Seismological Society of America*, 228-241.

Kramer, S. L. (1996) *Geotechnical Earthquake Engineering.* Upper Saddle River: Prentice-Hall.

Lihou, J. (1992) Reinterpretation of seismic reflection data from the Moutere Depression, Nelson region, South Island, New Zealand. *New Zealand Journal of Geology and Geophysics*, 477-490.

Nakamura, Y. (1989) A method for dynamic chatacteristics estimation of subsurface using microtremor on the ground surface. *Quarterly Report of the Railway Technical Research Institute 30(1),* 25-33.

Rattenbury et al. (1998) *Geology of the Nelson Area.* Lower Hutt: Graphic Press & Packaging Ltd.

Standards New Zealand. (2004) *Structural Design Actions, Part 5: Earthquake Actions – New Zealand*, NZS1170.5:2004 Incorporating Ammendment No.1, Wellington.

Wair et al. (2012) *Guidelines for Estimation of Shear Wave Veclocity Profiles.* California: Pacific Earthquake Engineering Research Center.

Wathelet, M. (2008) An improved neighbourhoof algorithm: parameter conditions and dynamic scaling. *Geophysical Research Letters*.

Westerson, J. (2007) *Fill Compaction Criteria for Port Hills Gravel Formation Soil, Nelson.* Christchurch: University of Canterbury.

Wood et al. (2015) Influence of a priori subsurface layering data on the development of realistic shear wave velocity profiles from surface wave inversion. *6th International Conference on Earthquake Geotechnical Engineering*.

Wopereis, P. (2017) Personal Communication.

Wotherspoon et al. (2015) The horizontal-to-vertical spectral ratio technique: Application and Limitations. *NZ Geomechanics News, Issue 89, ISSN 011-6851,* 90-93.

Evaluating soil and landscape models to predict liquefaction susceptibility in the Hinuera Formation, Hamilton Basin

A. M. McKay
School of Science, University of Waikato, Private Bag 3105, Hamilton 3240, NZ
aleeshamckay@gmail.com **(corresponding author)**

D. J. Lowe
School of Science, University of Waikato, Private Bag 3105, Hamilton 3240, NZ
david.lowe@waikato.ac.nz

V. G. Moon
School of Science, University of Waikato, Private Bag 3105, Hamilton 3240, NZ
vicki.moon@waikato.ac.nz

Key words: liquefaction, Hinuera Formation

ABSTRACT

Cone Penetration Tests (CPT) derived from the Hamilton section of the Waikato Expressway were analysed within CLiq™ software. The derived Liquefaction Potential Index (LPI) from each CPT was then combined with LIDAR, pedological and geological maps for statistical analysis. A soil model that incorporates the conditions of modern soil development with these derived LPI values was developed as a preliminary assessment tool for liquefaction potential within Hamilton Basin soils. The model shows that liquefaction is more likely to occur on interfluvial areas where there is little topographical relief. Pedological soils with high organic component are also a likely indicator of high liquefaction susceptibility.

1 INTRODUCTION

Liquefaction is the process by which an increase in pore water pressure occurs from seismic stressors, resulting in loss of shear strength and resultant fluid-like behaviour of the affected soil (Obermeier, 2009). The ideal conditions for such an event include relatively recent (Holocene to Late Pleistocene) sediments that are cohesionless, dominated by coarse silt to fine sand, loosely packed, with a shallow water table (Eslami, Mola-Abasi, & Shourijeh, 2014; Owen & Moretti, 2011; Robertson & Wride, 1998). Within the Hamilton Basin, the Hinuera Formation comprises extensive Late Pleistocene (c. 22 to 17 cal ka) volcanogenic (mainly rhyolitic) alluvium dominated by unconsolidated and highly variable sediments, including pumiceous, ranging from cross-stratified gravelly or slightly gravelly sands, sandy gravels, and silts that show marked changes in lithology both vertically and horizontally over short distances (Hume, Sherwood, & Nelson, 1975). The Hinuera Formation has the potential to liquefy in the event of an earthquake because its physical properties in many places meet the criteria mentioned above. Paleoliquefaction features have occurred within the Hinuera Formation (Clayton & Johnson, 2013; Kleyburg, 2015). Pedological soils (at the land surface, usually to ~1 m depth) tend to reflect underlying characteristics of their parent materials in terms of texture, drainage, and water table level, these features being encompassed by 'soil family' for this particular study. A soil family is the fourth category in the New Zealand Soil Classification (NZSC) (Webb, 2011), with families being defined on the basis of physical properties, not genesis. These characteristics are also those which control the susceptibility, or otherwise, of subsurface materials to liquefaction. This paper investigates the thesis (following Kleyburg et al., 2015) that the mapped pedological soils on the surface of the Hinuera Formation provide a means of predicting the likely liquefaction susceptibility of a site.

2 METHODS

2.1 Site selection and data acquisition

The Hamilton Basin was chosen as the area of study because of the hazard a liquefaction event would pose to its many residents. The data were selected on the basis of availability from the New Zealand Geotechnical Database (NZGD), which provided a record of the initial CPT testing carried out before development began on the Hamilton section of the Waikato Expressway. LIDAR data were sourced from Waikato Regional Council. The pedological soil map was provided by Waikato Regional Council with the permission of Landcare Research. A total of 216 CPT data points were available in NZGD over a distance of ~18.5 km from Horsham Downs (north of Hamilton) to Tamahere (south of Hamilton).

2.2 CLiq™ analysis

Raw CPT data were entered into CLiq™ software to obtain the predicted Liquefaction Potential Index (LPI) developed by Iwasaki *et al.* in 1978 for assessing liquefaction potential based on the depth of the liquefiable layer in relation to ground surface as well as its thickness and its computed factor of safety (FS) (Toprak & Holzer, 2003). LPI is classified within CLiq™ as either low (<5), moderate (5-15) or high (>15) potential based on the Robertson and Wride (NCEER 1998, 2009) calculation method for three separate depths of 3 m, 5 m and 10 m. Liquefaction potential (derived from LPI) was considered at a depth of 3 m as shallow liquefaction will be the most damaging in general, yet shallower materials are unlikely to liquefy due to lack of normal stress (Luo, Wang, & Li, 2013). A maximum depth of 10 m was considered because liquefaction deeper than this is likely to extend to the ground surface only for very large proximal earthquakes (Huang & Yu, 2013). The parameters used to compute LPI were derived from multiple sources. Input parameters included: horizontal peak ground acceleration (pga); earthquake moment magnitude (M_w); water table depth; and fines content. Horizontal pga was computed as 0.38 (g) using a_h = ZRC where Z (Hazard factor) = 0.16, R (Return period factor) = 1.8, and C (Site response factor) = 1.33 (NZ Transport Agency, 2014 & Technical Committee BD-006-04-11, 2004). A magnitude M_w = 7 event was assumed as worse-case selected from ranges of 5.5-7 M_w suggested for the Kerepehi Fault (Persaud et al., 2016; Wallace, Hamling, Holden, Villamor, & Williams, 2016). There is a relatively wide range within the literature regarding ground water table depth within the Hamilton Basin, with values as low as 0.6 m and as high as 4 m recorded in the field area. To account for water table level variation a depth of 1 m was used following the examples of Opus (2014) and (Ministry of Business Innovation and Employment, 2017; Opus, 2014) Fines content was also included in analysis as the finer component of a soil has a significant influence on liquefaction potential (Thevanayagam, 2000).

2.3 Data analysis

Data were compiled in Excel into a uniform format that could be easily imported into the software that would carry out analysis. The Excel spreadsheet consisted of each CPT having an appropriate label, alongside GPS coordinates, and the specific cumulative LPI values for 3, 5, and 10 m depths derived from the raw results of CLiq™. Factors of slope, elevation (derived from LIDAR DEM data), and soil families and associated soil siblings (defined by other physical properties and recorded using numbers) from S-map (Lilburne *et al*., 2011; Landcare Research, 2016) were included in the spreadsheet that was then imported into STATISTICA™. Soil families, identified by a geographical name with suffix *f*, are defined by the nature of soil profile material to 100 cm depth, parent rock (if present), dominant texture class to 60 cm depth, and permeability of the slowest horizon within 100 cm depth (Webb & Lilburne, 2011).

Parameters of LPI, slope, elevation, soil family and soil sibling were put into STATISTICA software to determine the most influential factors to liquefaction. Regressive Exhaustive CHAID (chi-square automatic interaction detection) was developed to identify and categorise parameters that are of higher influence to LPI where liquefaction potential was input as the predictive value (dependent variable), with slope, elevation and soil texture then input as continuous variables and soil family as a categorical variable (independent variables). The resultant graph then displays each independent variable as separate classes (low, moderate and high liquefaction potential)

based on their associated LPI. Due to limited data availability some soil families only had one CPT test undertaken within them and therefore only one recorded LPI value. These families were not included within the analysis as only one LPI value could not faithfully represent the liquefaction potential for that particular family. GIS (Geographical Information Systems) was then used to depict the results from the statistical analysis in terms of liquefaction susceptibility.

3 RESULTS

3.1 CLiq^{TM} analysis

Liquefaction susceptibility, displayed as data points to the west of Hamilton City, show an increasing cumulative susceptibility with an increase in depth (Figure 1). At 3 m depth susceptibility is low (119 sites) to moderate (97 sites) with the majority of sites being considered as having a low susceptibility to liquefaction (LPI <5). At greater depths susceptibility can be seen to range from low to high with 10 m depths being dominated by high liquefaction susceptibility. When referring to Figure 1A, areas of moderate susceptibility appear more concentrated toward the southern end of the field area; within Figure 1B, high susceptibility appears within the middle/lower region of the field area also.

Figure 2 illustrates eight individual CLiq^{TM} output traces (3 m depth), with colours (see key) representing normalized Soil Behaviour Type (SBTn) and the yellow line indicating what the recorded soil behaviour was at each particular depth. These eight profiles were chosen because they illustrate how variation in soil behaviour can affect the resultant liquefaction potential, with each profile illustrating a different degree of LPI (from no liquefaction to moderate-high potential liquefaction occurrence). Profiles were derived from upper (northern), middle, and lower (southern) sections of the field area to give an accurate representation of entire data set.

Those that are of no to low susceptibility (Figure 2A & B) have a soil behaviour that is nearer to that of a granular soil or in contrast has a soil behaviour that is too-fines rich, typically >2.6 I_c (soil behaviour type index). As soil behaviour moves into more silt/sand textures susceptibility increases. The main difference that can be seen between those that read low moderate compared with those of high moderate is the influence of an increased fines content toward the top of the profile reaching a soil behaviour value of I_c ~2.6-3. Moderate susceptibility profiles show a similar pattern but do not exceed I_c=3, having a higher proportion of clay dominated fines.

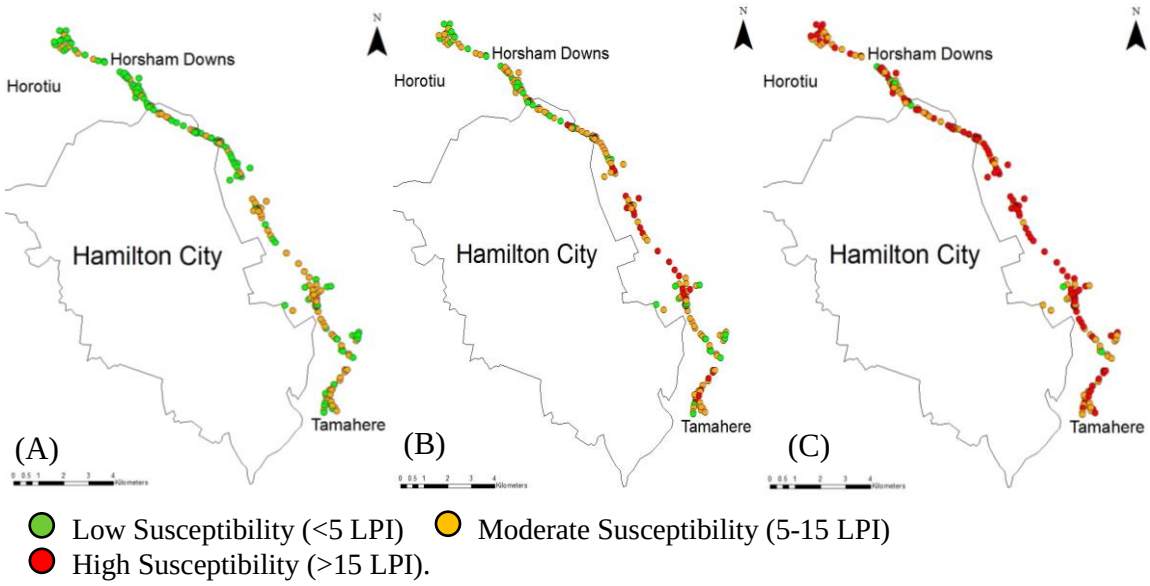

Figure 1. Field area (Hamilton city with Waikato Expressway Hamilton Section under construction to the east). Data points represent CPT sites and subsequent LPI based on Robertson and Wride (NCEER 1998, 2009) calculation method. (A) 3 m depth, (B) 5m depth, (C) 10 m depth.

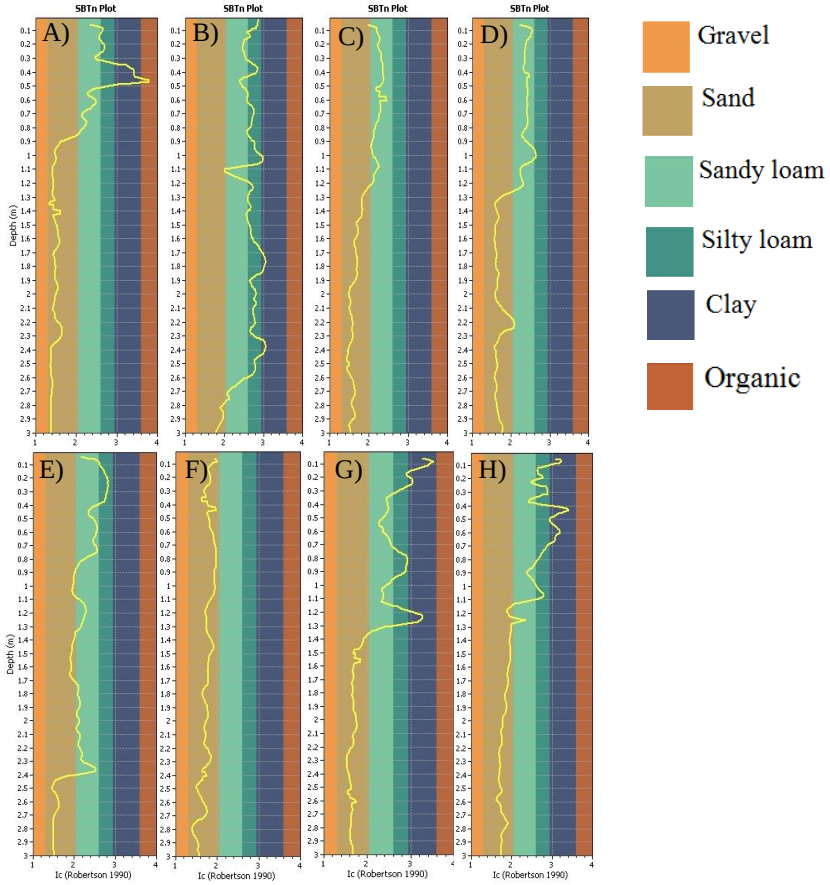

Figure 2. SBTn plots showing changes in proposed soil behaviour from 0.1- 3 m with each profile illustrating a different LPI value (Fig 2A-0, Fig2B-0.5, Fig2C-1.8, Fig2D-3.5, Fig2E-5.1, Fig2F-6.5, Fig2G-8.8 & Fig2H-11.28).

3.2 Statistical analysis

The results of the Exhaustive CHAID analysis can be seen in Figure 3. Of the independent variables, soil family, slope, elevation and sibling number, it can be seen that soil family is the most influential (dependent variable) when it comes to predicting liquefaction potential (shown in Figure 3 at 3 m depth but also shown at 5 m and 10 m depth when analysed). The soil families can be classified into three classes of liquefaction potential, low, medium and high. Pukehina*f*, Moeatoa*f*, Kohuratahi*f*, Kainui*f*, and Rotokauri*f* families are classified as low LPI (mean value of 3.72); Otorohanga*f*, Matakana*f*, and Te Puninga*f* families as medium LPI (mean value of 5.3); and Utuhina*f* and Kaipaki*f* families as high LPI (mean value of 7.57). Note, however, there is a relatively high variance within each LPI class (between 5–8), reflecting the variability within the soil families. With the exception of the high susceptibility node (ID 4–7.5 LPI) which terminates at soil family, the second most influential factor is elevation (Figure 3 has been 'pruned' for simplification and so does not show further splits based on less influential independent variables). For lower susceptibility soils (ID 2) elevation is, on average, higher than moderate susceptibility (ID 3) at approximately 36–38 m and 24–29 m, respectively. It is apparent from the data that liquefaction potential is at its highest when topography is less complex with little to no relief.

It can be seen within Figure 4, that on average, the susceptibility class predominantly ranges from low (green) to low-moderate (orange) with high-moderate values being confined to the Northeast of Hamilton City. The three main topographical features that can be identified on the surface of the Hinuera Formation are small ridges (mounds) up to a few metres in height, channels (paleo and current), and the interfluve zones (flat areas with little topographical relief). From Figure 4 it is apparent that when the topography becomes more complex the susceptibility is seen to

decrease, such as in the drainage channels as well as along the low ridges. The areas that are displaying moderate to high susceptibilities are mainly within the interfluvial zone where ground is near to level.

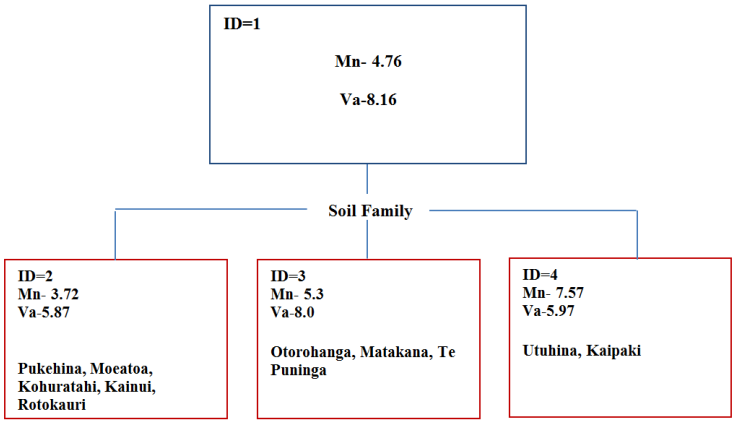

Figure 3. Exhaustive CHAID analysis at 3 m depths with ID 2 including Pukehina, Moeatoa, Kohuratahi, Kainui, Rotokauri families; ID 3 Otorohanga, Matakana, Te Puninga families; and ID 4, Utuhina, Kaipaki families. In the boxes, the mean LPI (Mn) and variance (Va) are shown.

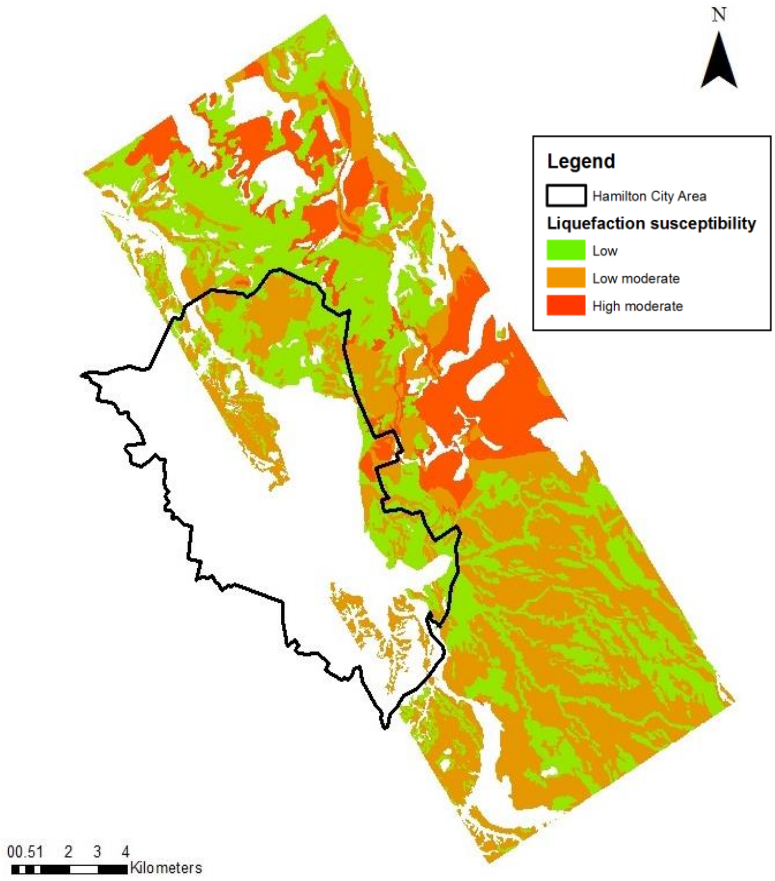

Figure 4. Generalised liquefaction susceptibility map of the Hamilton Basin based on STATISTICA analysis. Green= low susceptibility, Orange= low-moderate susceptibility and Red=high-moderate susceptibility.

4 DISCUSSION

Because of its alluvial origin, the Hinuera Formation is extremely diverse spatially in texture and sedimentary structure, and hence shows considerable lateral and vertical variability in liquefaction susceptibility. Typical stratigraphies show sand-dominated materials at the base, with an increase in fines content towards the upper profile. This upward decrease in grain size is expected when deposition is of alluvial origin, in particular a river channel that has changed course many times, as the grain size and pattern is indicative of flow dynamics with larger, more granular (clean sand) material being deposited where energy is at its highest (upstream or at depth), while finer grains are typically deposited closer to channel termination where shallowing occurs as a result of decreasing energy by decreasing gradient downstream (Nichols. G, 2009). This pattern of increasing fines within the upper profile is evident in the CPT data, however, the degree of fines does vary with some profiles showing more clay-dominated behaviors. Variability in LPI is likely due to differences in sand/silt/clay ratios so that mixed textures (silty sand/sandy silt) show a higher degree of liquefaction potential relative to profiles with predominantly sand (granular) or fines (clayey silt/silty clay) textures which generate lower LPI values.

It is important to take the soil behaviour derived from CLiq^{TM} as simply a guide and not a definitive conclusion, as it merely reflects the way the soil behaves in response to penetration with no empirical evidence from the texture itself. In addition, CLiq^{TM} may underestimate the degree of plasticity within soil (Robertson & Wride, 1998) as well as the crushability of pumiceous material, hence overestimating LPI due to lower computed soil resistance which is particularly important in the field area (Opus, 2013). In sites with sandy soil near to granular in nature (Figures 2A-D), low susceptibility is likely a result of increased cementation and grain size. The textures in Figures 2E-H appear closer to the sandy silt (I_c>2) boundary where it is likely to have a relative proportion of fines but still be sand dominated with limited plasticity. The predicted moderate LPI value would support the idea that an increase in fines is likely to increase liquefaction susceptibility (Ibrahim, 2014; Thevanayagam, 2000). The presence of a clay cap is also a factor that likely influences the predicted LPI values although this is not considered within CLiq^{TM} so empirical site specific information will be required to supplement this conclusion.

Statistical analysis showed that there may be a relationship between soil family and the underlying sediment (Hinuera Formation) that is subject to liquefaction. We postulate that factors and properties that influence pedological soil formation, such as water table level, soil texture, and topographic position, are similar vectors to those that influence liquefaction susceptibility. Both Utuhina and Kaipaki are organic soils formed on peat in permanently wet conditions (i.e., with high water tables) underlain by inorganic sand- and silt-rich alluvium. In our analysis, the Utuhina and Kaipaki soil families consistently have LPI values within the high-moderate range at all depths. Another significant factor of these soil families is that peat formation is indicative of a low relief (flat to gently undulating) because basin peat formation needs a level or slightly concave topography to sustain a saturated and therefore anoxic condition for partial organic matter decay (Dargie et al., 2017). A high water table is a prerequisite for liquefaction, and organic surface soils reflect this water table level as well as sand/silt mixtures being most likely to liquefy as shown by Cliq^{TM} analysis with the diverse nature of an alluvial system typically having these textures. While the organic soils or peats themselves are unlikely to liquefy, the underlying materials (Hinuera Formation) are potentially highly susceptible. The Hinuera Formation is the dominant alluvial deposit within the Hamilton Basin with more recent alluvial sediments only being found in close proximity to the Waikato River. Those soil families that were classified as having lower susceptibilities on average were more of a mixed texture and lacked that dominant organic component, suggesting lower water tables due to better drainage conditions, or a more complex topography. It can therefore be suggested the origin and texture of pedological soils (at the land surface) can indicate the physical conditions of the materials below and, in turn, provide a simple first-pass predictor of liquefaction susceptibility at a site. It is important to remember, however, that soil family attributes simply act as a guide to aid decision making on whether the site should be investigated further. Pedological soil is unlikely to liquefy itself due to it being at or near the surface and therefore lacking sufficient overburden for pore pressure build up under

seismic stress.

With these observations it is possible that areas of potential significant liquefaction occurrence can now be identified in advance. Low-relief topography is a requirement for liquefaction occurrence, with the Hinuera Formation being the dominant soil parent material of the alluvial plains of the Hamilton Basin. Therefore, organic soils, such as Kaipaki*f*, underlain by Hinuera Formation, warrant further liquefaction testing based on the conclusions derived from our statistical analyses. This idea is further supported in Figure 4 with the higher liquefaction potential occurring on areas of lower relief and less complex topography, the areas in red being directly correlated to areas of localized peat bog formation. Liquefaction susceptibility is seen to decrease in drainage channels and on top of low ridges, and to increase on the flat interfluve areas. Drainage channels underlain mainly by coarser deposits that reflect high-energy river flow and hence are well drained. In contrast, decreased liquefaction potential on ridges is likely a result of increased overburden pressure as well as increased drainage due to slope gradient (Owen & Moretti, 2011).

5 CONCLUSION

We show that soil family, a pedological map class, provides a good initial indication of the physical conditions of the underlying liquefiable soil and therefore in turn liquefaction potential of land on the plains within the Hamilton Basin. Although the pedological soils will not, in themselves, liquefy in general, their modes of formation mean that they represent the underlying parent materials, water table levels, and local depositional environment. These characteristics are the key to generating soils that have high liquefaction potential, and hence the soil developed on a given lithology and topography will indicate the likely susceptibility of underlying sediments to liquefaction. From our analysis, it is suggested that the soil reflects liquefaction susceptibility to about 5 m depth; below this, changes in the lithologies are inevitable given the nature of alluvial fan deposition. As shallow liquefaction is likely to be the most damaging, the depths reflected in the soil profile will be those of greatest interest for many applications. For our study area, we recognize increased liquefaction potential in interfluve areas compared with channels or low ridges, and especially high potential in areas of low surface relief where peat bogs have formed. As soils and the pattern of liquefaction susceptibility are spatially highly variable, we appreciate that this division provides a general idea of the patterns of liquefaction susceptibility over a wide area: lateral variability means that specific sites may be different. The guide developed here does not replace site-specific investigation, but may help in targeting areas deserving more detailed assessment.

6 ACKNOWLEDGEMENTS

The authors thank Waikato Regional Council for funding support for AMM and provision of LIDAR data, and Gavin Alexander for helpful comments.

REFERENCES

Clayton, P., & Johnson, J. (2013) Liquefaction Resistance and Possible Aging Effects in Selected Pleistocene Soils of the Upper North Island. In: Chin, C.Y. (ed). *Proc. 19th NZGS Geotechnical Symposium*, November 2013, Queenstown.

Dargie, G. C., Lewis, S. L., Lawson, I. T., Mitchard, E. T., Page, S. E., Bocko, Y. E., & Ifo, S. A. (2017) Age, extent and carbon storage of the central Congo Basin peatland complex. *Nature*.

Edbrooke, S.W. (compiler) 2005 *Geology of the Waikato area*. Institute of Geological and Nuclear Sciences 1:250,000 geological map 4. 68pp. + map sheet. IGNS, Lower Hutt.

Hewitt, A.E. (2010) *New Zealand Soil Classification 3rd ed*. Manaaki Whenua Press, Lincoln, 136pp.

Huang, Y., & Yu, M. (2013) Review of soil liquefaction characteristics during major earthquakes of the twenty-first century. *Natural Hazards*, 65(3), 2375-2384.

Hume, T. M., Sherwood, A. M., & Nelson, C. S. (1975) Alluvial Sedimentology of the Upper Pleistocene Hinuera Formation, Hamilton Basin, New Zealand. *Journal of the Royal Society of New Zealand*, 5(4), 421-462.

Kleyburg, M.A., Moon, V.G., Lowe, D.J., Nelson, C.S. (2015) Paleoliquefaction in Late Pleistocene alluvial sediments in Hauraki and Hamilton basins, and implications for paleoseismicity. *Proceedings, 12th ANZ Conference on Geomechanics*, 22-25 February, 2015, Wellington, pp. 524-531.

Landcare Research (2016) *S-map online: the digital soil map for New Zealand* (https://smap.landcareresearch.co.nz/)

Lilburne, L.R., Webb, T.H., Hewitt, A.E., Lynn, I.H., de Pauw, B. (2011) S-map database manual. *Landcare Research Report LC478*, 61 pp.

Luo, Q., Wang, C. Y., & Li, X. W. (2013) Experimental Study on Silt Liquefaction Characteristics of Different Fines Content. In *Applied Mechanics and Materials* (Vol. 353, pp. 2323-2326). Trans Tech Publications.

New Zealand Geotechnical Society (2016) Earthquake geotechnical engineering practice. MODULE 1: Overview of the guidelines.

NZ Transport Agency (2014) The NZ Transport Agency's Bridge manual. Site Stability, Foundations, Earthworks and Retaining Walls: 6-7.

Obermeier, S. F. (1996) Use of Liquefaction-Induced Features for Paleoseismic Analysis. *Engineering Geology*, 44(1-4), 1-76.

Obermeier, S. F. (2009) Using Liquefaction Induced and Other Soft Sediment Features for Paleoseismic Analysis. *International Geophysics*, 95, 497-564.

Opus. (2013) Ruakura Development: Stage 1 Geotechnical Investigation. Retrieved from New Zealand: http://www.epa.govt.nz/resource-management/NSP000034.

Opus (2014) Waikato Expressway: Hamilton Section, Ruakura Interchange: Assessment of Water Effects. Retrieved from Hamilton New Zealand: http://www.hamilton.govt.nz/ourcouncil/councilpublications/operativedistrictplan/Documents/Ruakura%20Interchange/2H%20FINAL%20Stormwater%20Report.pdf.

Owen, G., & Moretti, M. (2011) Identifying Triggers for Liquefaction-Induced Soft-Sediment Deformation in Sands. *Sedimentary Geology*, 235(3), 141-147.

Persaud, M., Villamor, P., Berryman, K., Ries, W., Cousins, J., Litchfield, N., & Alloway, B. (2016) The Kerepehi Fault, Hauraki Rift, North Island, New Zealand: active fault characterisation and hazard. *New Zealand Journal of Geology and Geophysics*, 59(1), 117-135.

Robertson, P., & Wride, C. (1998) Evaluating Cyclic Liquefaction Potential using the Cone Penetration Test. *Canadian Geotechnical Journal*, 35(3), 442-459.

Technical Committee BD-006-04-11. (2004) New Zealand Standard, *Structural Design Actions, Part 5: Earthquake actions*.

Thevanayagam, S. (2000) Liquefaction potential and undrained fragility of silty soils. *Proceedings of the 12th World Conference Earthquake Engineering*, Wellington, New Zealand.

Toprak, S., & Holzer, T. L. (2003) Liquefaction potential index: field assessment. *Journal of Geotechnical and Geoenvironmental Engineering*, 129(4), 315-322.

Wallace, L. M., Hamling, I., Holden, C., Villamor, P., & Williams, C. (2016) Introduction to NZJGG special issue in honour of John Beavan's scientific contributions.

Webb, T. H., Lilburne, L.R. (2011) Criteria for defining the soil family and soil sibling – the fourth and fifth categories of the New Zealand Soil Classification. *Landcare Research Science Series No. 3 (2nd ed)*. 38pp.

Pre-excavation grouting for groundwater ingress control in tunneling – Auckland, New Zealand.

R McCarrison
WSP, Auckland, NZ
mccarrisonr@pbworld.com

ABSTRACT

Water ingress into a mined tunnel can be an issue – not just for construction but also for depressurisation and the potential consequential surface settlement. The Waterview Connection in Auckland has twin ~14.5m diameter TBM tunnels linked by 16 mined cross passages. Each cross passage is under 15m long, placed at ± 150m centres en route with excavation works predominantly through the East Coast Bay Formation geology.

Based on geotechnical investigations and probe hole drilling, some cross passages were known to have a high risk of strong water ingress. Furthermore, the TBM passage in the first tunnel had encountered zones where Earth Pressure Balance (EPB) methodology was essential to limit groundwater inflows which would otherwise have exceeded permitted limits. These limits addressed the risks associated with drawdown and settlement effects at the surface, and the risk of hydraulic connection to the Oakley Creek where it crossed the alignment.

This paper outlines the unique challenges and design for dealing with high groundwater inflow in the East Coast Bays Formation, the construction methodology used in a segmental lined tunnel and efficacy of the pre excavation grouting used where necessary in some of the cross passages. An effective seal was achieved through the pre-excavation permeation grouting.

1 BACKGROUND INFORMATION

The Waterview Connection is a New Zealand Transport Authority (NZTA) motorway construction project that completes the Auckland western ring route linking State Highway (SH) 20 to SH16 by way of a 3 lane dual carriageway motorway in Auckland, New Zealand. The project includes a tunnel section consisting of 2 tunnels, 2.4 kilometres long running in a north south direction (Figure 1).

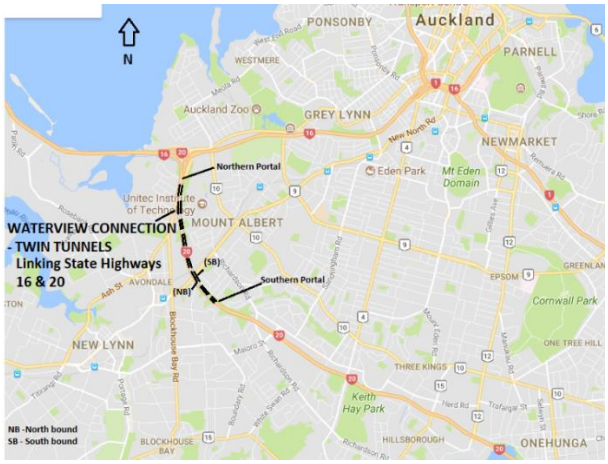

Figure 1 - Map of Auckland with the new Waterview Connection route.

The tunnels are connected by sixteen mined cross passages, each having an internal span of 5.2m and being 6.0m in height. At each of the cross passage entrances, concrete segments were replaced with steel segments to form a steel frame after opening (Figure 2).

Figure 2 - Cross Passage steel segment entrance along the south bound tunnel.

The mainline tunnels and cross passages were designed as undrained structures to prevent groundwater drawdown in the permanent condition. The tunnel alignment passes under areas of residential and commercial land including a live rail track and petrol station at the surface roughly 30m-40m above the crown. This undrained approach, preventing groundwater drawdown, was used to reduce the possible consequential surface settlement and associated damage to these sensitivities.

Prior to commencement of the cross passage excavation works, observations and investigation testing identified some of the cross passages were likely to encounter high groundwater inflows of greater than 20l/sec that could, if not controlled, result in groundwater drawdown. One of the key objectives of the pre excavation grouting was to maintain the undrained condition during cross passage construction. It was important to be able to control flows during construction not only to manage drawdown impacts but also for the safety of the crew executing out the excavation works.

2 GEOLOGY/HYDROLOGY

The project site is located within the Waitemata basin where the geology generally comprises of a thick sequence of interbedded extremely weak to weak siltstones and sandstones (East Coast Bays Formation (ECBF)) and locally interbedded coarser grained volcaniclastic sandstones (Parnell Grit Member) which are part of the Waitemata Group.

After an extensive borehole investigation prior to construction commencing, the geotechnical information revealed the Waterview tunnel alignment was positioned to drive through the ECBF and the Parnell Grit member sequence that had undergone faulting and folding during the tectonic uplift of the Waitemata basin (Figure 3). The presence of the faults crossing the proposed alignment are generally discrete zones of displacement rather than large zones of fractured rock. This embedded sequence is typical within the Auckland city geology.

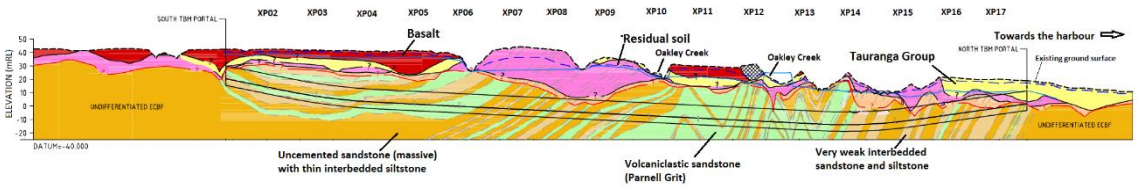

Figure 3 - Geological long section (Southbound tunnel)

The groundwater levels measured along the alignment were typical of the regional groundwater table, typically falling from RL 42m near the southern portal and discharging towards the harbour in the north at a gradient of around 4% and locally discharging to Oakley Creek (see Figure 3). Ground water flows through the Waitemata Group rock are dominantly defect controlled through

fractures and bedding planes. Minor flow can be expected through the matrix of coarser sandstone beds (Parnell Grit member).

During the design stage, the majority of cross passages were thought to be excavated through "typical", low hydraulic conductivity rock (K_h =3 x 10^{-7} m/s) with low storativity. Analyses indicated inflows were likely to be negligible (<1 l/s when the entire cross passage is open and dewatered).

In the tunnel section between cross passages XP11 and XP14, higher strength coarser grained rock (higher percentages of Parnell Grit) was intercepted, resulting in an increased overall hydraulic conductivity (K_h = 10^{-5} m/s).

Pumping tests within this area indicated sustained discharges of 5 l/s and peak discharges of up to 20 l/s may be possible during excavation. The design assessment indicated such flows were likely to cause drawdown and possibly consolidation settlement at the ground surface and therefore pre excavation grouting would be required.

3 CROSS PASSAGE INVESTIGATION

3.1 First tunnel

An initial summary of ground conditions and groundwater behaviors was compiled from the first tunnel. This summary included rock permeability and likely groundwater inflow conditions as the TBM passed each cross passage. The initial summary is provided in Table 1 below.

Table 1: Summary of ground conditions encountered from the first tunnel (Southbound)

Permeability /Inflow	Cross Passage (XP)	Ground Conditions	Additional Notes:
Very low to low permeability (<5L/s) from discrete fractures	2, 3, 4, 5, 6, 7, 8, 9, 15, 16, 17	Very weak to weak sandstone with thin interbedded siltstone beds. Beds typically 0.5m to 2m thick. UCS of 5 (MPa). XP16 & encountered extremely weak to very weak sandstone.	Drawdowns noted in response to various TBM operations, minor to negligible inflows. XP8 - possibility of discrete fracture flows.
Moderate permeability (5 - 10 L/s)	10, 11, 14	Very weak to weak sandstone with interbedded siltstone beds (0.3 - 3m thick), UCS 1-20 (MPa).	XP10 - fault logged in face during cutter head intervention with minor inflows noted. Moderate to high inflows possible. Likely to encounter higher percentage of Parnell Grit.
High permeability inflows (>30l/s)	12, 13	XP12 – Weak siltstone massive with closely spaced joints. UCS of 5 (MPa). XP13 - Weak coarse grained sandstone interbedded with Parnell Grit. Beds typically 1m to 2m thick. UCS 5-25 (MPa).	Likely to dewater and recover quickly but pumped volumes will remain high throughout drained period. Cutter-head intervention (6m south XP12) was abandoned due to face instability.

This initial summary of ground conditions encountered during the construction of the first tunnel, showed cross passages XP12 and XP13 would likely require groundwater control with the possibility of further ground treatment at cross passages XP10, XP11 and XP14.

3.2 Probe drilling

Probe drilling was used to verify and assess the geological and hydrogeological conditions ahead of each cross passage excavation. After completion of the first (southbound) tunnel, probe holes were drilled through the steel openings at each cross passage.

The probe drilling investigation completed at least 2 probe holes at each cross passage, and ground class, support type for construction and groundwater inflow measurements were investigated and reported.

Drilling was carried out using a horizontal rotary drill rig to a length of 10m. The core was logged and groundwater inflow measurements were taken during and 24 hours after drilling completion. Figure 4 presents the monitoring results from the inflows recorded during probe hole drilling.

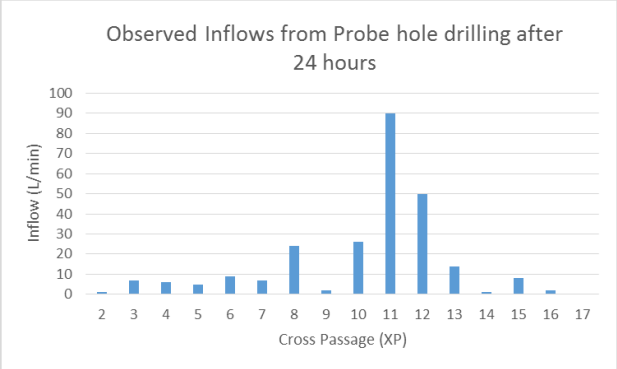

Figure 4: Summary of Groundwater Inflows from Probe Drilling

The groundwater inflow results identified cross passages XP08, X10, XP11, and XP12 required pre-excavation grouting due to groundwater inflows exceeding the allowable threshold of 27 l/min sustained flow after 24 hours from a 10m probe hole.

Further analysis of the results was undertaken by the project's hydrogeologist using the analytical method of Heuer (1995). The analysis calculated a rock mass permeability of between 5 x 10^{-7} m/s for XP 8 and 1 x 10^{-5} m/s for XP11 and XP12. The estimated peak inflow range during excavation was calculated to be of between 5-10 l/sec for XP 08 and up to 50 – 80 l/sec for cross passages XP11 and XP12.

Further monitoring of groundwater flows was undertaken during the canopy installation. The canopy tubes were installed around the crown of the cross passage in a semicircular profile, then grouted. Between the time of the install and grouting, high groundwater inflows were observed, similar to the high flows measured from the probe drilling. Cross passage XP12 had some of the highest flows (>20 l/sec) until the canopy tube was either capped or grouted.

4 GROUTING DESIGN AND METHODOLOGY

Pre-excavation grouting was seen as a necessary method of reducing inflows for cross passages XP8, 10, 11 and 12. The main objective was reducing inflows to levels below resource consent levels i.e less than 27 l/min per 10m length of probe hole sustained over 24 hours.

4.1 Drilling

The pre excavation grouting involved drilling horizontal boreholes (65mm in diameter) slightly inclined to avoid overlap and to maximise the area grouted.

4.1.1 Drilling Sequence

The typical arrangement of grout holes is shown in Figure 5. The grout holes were divided into 3 categories:

- Primary holes - The primary holes (typically 10 holes) were drilled through 70mm ports which already existed in the main tunnel concrete lining segments for further grouting purposes related to the mainline tunnel lining.
- Secondary holes - The secondary holes (typically 11 holes but additional holes were drilled for cross passage XP12) were drilled around the steel opening perimeter through either 100mm diameter steel nipples or through existing port holes in the steel cross passage segments.
- Tertiary holes - The tertiary holes (9 x 240mm diameter steel nipples installed in the cross passage opening segments) were initially drilled as test holes to measure groundwater inflows after completion of the initial grouting works. These holes were the final group to be grouted unless the previous holes grouted (i.e. primary holes) had provided sufficient reduction in water ingress.

All drilling and grouting works were completed from the south bound tunnel. A 300mm exclusion zone from the north bound tunnel and a 5^0 drill deviation was designed to minimise the risk of borehole and tunnel intersections.

The drill rig consisted of a compressed air operated drill with a minimum working pressure of 100 psi and flow volume of 350 cfm. The drill mast was mounted onto an excavator with an elevated platform for access. The boreholes were drilled using a drag bit with water as the flushing medium. As excessive groundwater was expected, allowance was made for an air operated diaphragm pump.
Once drilled, each hole had a valve installed that was kept closed unless flow measurements were to be taken.

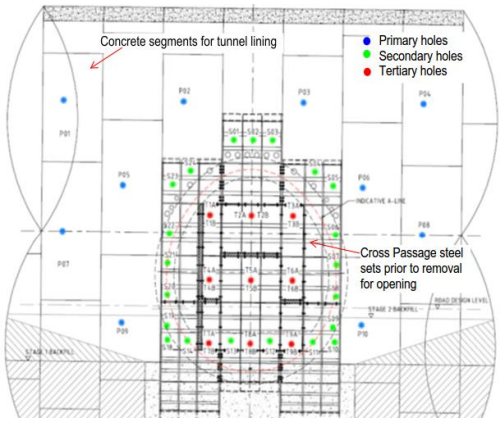

Figure 5 - Typical arrangement of grout holes at Cross Passages XP11 & XP12. (No secondary holes were drilled for XP08 & XP10.)

4.2 GROUTING

4.2.1 Grouting Material

The cement used for injection grouting was required to meet the requirements of AS 3972 - 1997 for Type GP cement. An initial series of tests were performed on the grout prior to its use for pressure grouting in the holes. Grout properties monitored using a bleed test, with a maximum bleed at 90 minutes of 2%, density test (mud balance) and viscosity test (marsh flow cone test). A high early strength (HE) cement with grout aid and super plasticiser mix was used.

4.2.2 Grouting equipment

Equipment for the cement grouting was specified to include:

- High speed colloidal grout mixer capable of mixing grouts with water/cement (w/c) ratios between 0.3 - 3.0.
- Grout agitator capable of keeping grout at ratios between 0.3 and 3.0 in suspension.
- Grout pump - capable of pumping at a range of 10 - 30 l/min reducing to 0 - 2 l/min at PMax. A valve type pump (piston pump) was used.

- Flow meter and pressure gauges for air, water and grout supply lines, packers and fittings to supply a continuous flow of grout and an accurate pressure control.

4.3 Initial Trial

Prior to any grout testing procedure at each of the targeted cross passages, strain gauges were installed on mounting blocks welded onto the cross passage openings. Convergence prisms were set up for convergence monitoring of the tunnel lining.

Under the Standard Operating Procedure as part of the design requirements, a water pressure test to stimulate grouting pressures on the tunnel lining was attempted in a drilled tertiary hole (T1) at XP12. This trial was abandoned due to the sub-contractor being unable to increase or even reach pressure as the water pumped through the hole kept dissipating into the ground resulting in no pressure build up. The trial test was then continued with grout consisting of a 1.5 w/c ratio and no additives.

The drilled hole for the trial was 11.4m in length with a 5^0 inclination through the steel segment of the cross passage opening. The drill hole is stopped 200mm from the north bound tunnel to determine the full effect of the grouting method and maximum pressure limits.
The hole was then plugged with an inflated packer at the opening. Pressure grouting initially commenced to an average pressure of 5 bar with a grout take of 50 litres. As the grouting progressed the pressure was increased by 1 bar increments as 0.5 bar increments were not possible with the design of the piston pump.

During testing, the pressure was increased to 6 bar and then up to an average 7 bar (max 8.5 bar) with grout takes of 40 and 15 litres respectively. The test was stopped at this point, based on the total volume of grout being equal to three times the hole volume. Immediately after testing, the hole was flushed with water with the surrounding holes left open.

The results of the strain gauges and convergence monitoring were assessed throughout the full trial to determine if any significant strain was induced in the tunnel lining. Grouting pressures were maintained during the trial in 10 min pressure increments, as best the pump could provide for. This allowed the data logger of the strain gauges to update in a 5 min cycle. At the end of the trial the monitoring observed very minimal to no movement from all gauges (Figure 6) and prisms. This allowed grouting to proceed, beginning with XP12, with daily convergence, strain gauge, and surface monitoring ongoing.

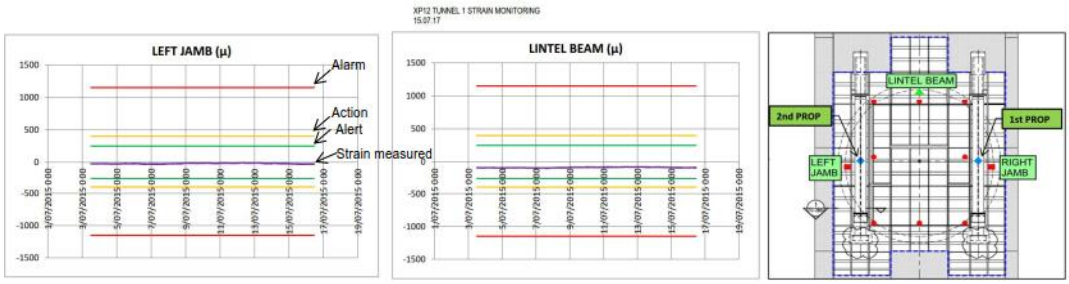

Figure 6 - Strain gauge monitoring on the tunnel lining during the grout trial.

4.4 Cross Passage Grouting Sequence

The primary holes of XP12 were initially drilled and grouted. During grouting, nearby holes were monitored for interconnections and pressure release. Even with the slight incline, some of the nearby holes interconnected. After completion of the primary grouting, several of the tertiary holes were drilled and the inflow measured. These measurements gave an indication of whether further grouting was necessary.

In all the targeted cross passages, both the primary and tertiary holes were grouted. Additional holes around the steel opening (secondary holes) were drilled and grouted at XP11 and 12 prior to proceeding to the tertiary holes (within the excavated area).

5 RESULTS OF GROUTING PERFORMANCE

After completion of grouting at each stage (primary, secondary, tertiary) several of the tertiary holes were either uncapped or drilled to measure groundwater inflows. Figure 7 presents the measured inflows from the monitoring holes during grouting procedure as it progressed in towards the excavation zone.

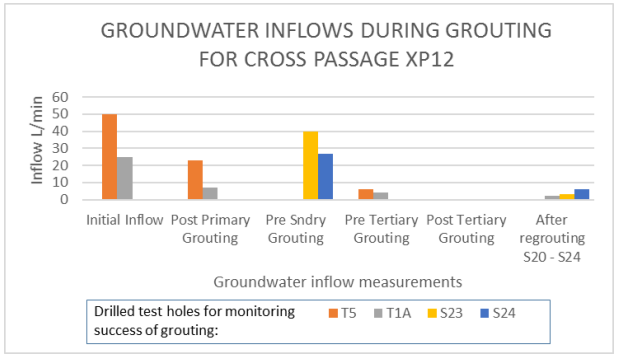

Figure 7 – Cross Passage XP12 groundwater inflow measurements at each stage.

During the grouting process, measurements of initial groundwater inflows and subsequent grout volumes were recorded for each hole. The results for cross passages XP10 and XP12 are presented in the following figures.

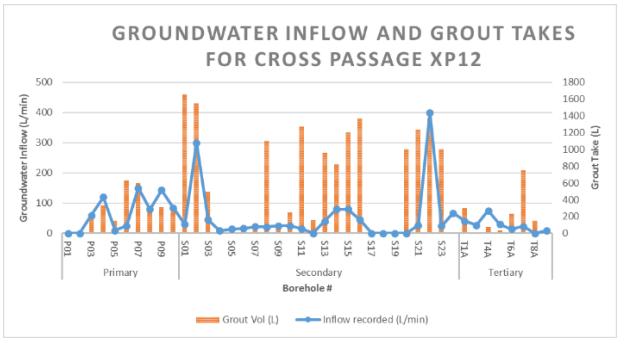

Figure 8 - Initial groundwater inflow and subsequent grout takes for XP12.

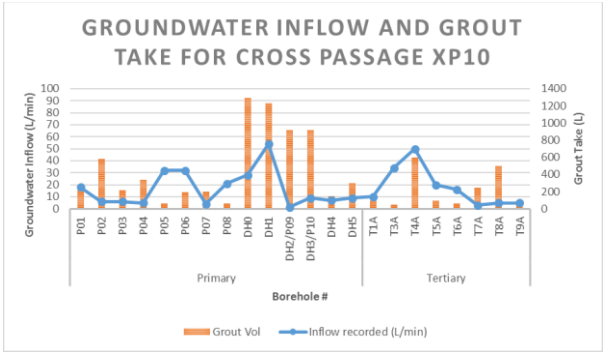

Figure 9 - Initial groundwater inflow and subsequent grout takes for XP10

The results presented in Figures 8 and 9 generally show large grout takes correlating with high inflows. This also gave the indication there were possible distinct zones, possibly related to highly fractured zones or zones of interbedded Parnell Grit. Where holes measured lower flows but high

grout takes there was generally an interconnection with adjacent holes which registered increased pressure very quickly if not instantly.

6 POST GROUTING – CROSS PASSAGE EXCAVATION

Logging during excavation of cross passages XP8, XP10 – XP12 noted the following ground conditions and groundwater inflows:

- Dripping from joints or canopy tubes as excavation progressed. Generally estimated to be less than 5 l/min over the full excavated face (XP8, XP10, XP11, & XP 12).
- XP12, from the first advance, mapping of the excavated face recorded highly fractured massive siltstone, with indistinct bedding. Groundwater inflows were recorded as damp (<5 l/min)
- XP11 encountered a fault zone within approximately the second and third advance. Groundwater inflows were recorded as damp (<1 l/min).
- XP08 and XP10 encountered Parnell Grit with groundwater inflows recorded as damp with minor seepage from crown around the canopy tubes.

7 CONCLUSION

- Groundwater inflows during cross passage excavation were successfully reduced to manageable levels due to the pre-excavation grouting methodology adopted.
- The investigation and observational methods used to determine where pre excavation grouting would be required, was a successful program in itself.
- Grout pressures of up to 8.5 bar were able to successfully infill the joints and fractures with grout, while having no detrimental effects on the mainline tunnel lining.
- Grout pressures and volumes established in the initial trial managed to successfully reduce groundwater inflow volumes during excavation.
- High grout volumes generally correlated to holes measuring high groundwater inflows.
- High inflows recorded at cross passages XP12 and XP11 encountered highly fractured zones during cross passage excavation.

8 ACKNOWLEDGEMENTS

The author gratefully acknowledges the Waterview Well Connected Alliance team, (the designers and the construction team) who put a lot of time and effort into providing the right information and construction knowledge for these works to happen. The support and contributions of Evan Giles and Wataru Okada of WSP are also gratefully acknowledged.

REFERENCES

Bowskill, A. & Harrison, C. (2014) High-pressure Fissure Grouting for Drill and Blast Tunnelling, Ambuklao, Philippines. *Proceedings of the 15th Australian Tunnelling conference, 2014. – Underground Space – Solutions for the Future. Sydney, Australia.*

Heuer, R.E. (1995) Estimating rock tunnel inflow, *Proceedings of the Rapid Excavation and tunnelling Conference, June 18-21, 1995, San Francisco, California.*

Houlsby, A.C. (1990) *Construction and design of cement grouting – A guide to grouting in rock foundations,* John Wiley & Sons, Inc, New York.

Mahajan, R & Okada, W. (2017) Design of Mined Cross Passages for Waterview Project Auckland (NZ): Comparison between Predicted vs Actual Performance. *Proceedings of the World Tunnel Congress 2017 – Surface challenges – Underground solutions. Bergen, Norway*.

Spies, P., Burden, J. and Hanke, S. 2014. The Waterview Connection Project – Progress to date, *Proceedings of the 15th Australian Tunnelling Conference, 2014. – Underground Space – Solutions for the Future. Sydney, Australia.*

Warner, J. (2004) *Practical handbook of grouting*, John Wiley & Sons, Inc, New Jersey

Mason, D., Brabhaharan, P. & Saul, G. (2017)
Performance of road networks in the 2016 Kaikōura earthquake: Observations on ground damage and outage effects. *Proc. 20th NZGS Geotechnical Symposium.* Eds. GJ Alexander & CY Chin, Napier

Performance of road networks in the 2016 Kaikōura earthquake: observations on ground damage and outage effects

D Mason, P Brabhaharan & G Saul
Opus International Consultants Ltd
Doug.Mason@opus.co.nz (Corresponding author)

Keywords: Earthquake hazards; Road networks, Fault rupture; Landslides; Embankments; Retaining walls; Bridges

ABSTRACT

The 14 November 2016 M_w 7.8 Kaikōura earthquake triggered thousands of large landslides and caused severe disruption to the state highway and local road network in the North Canterbury and Marlborough regions. Damage to the network included landslides, debris flows, rock falls, failure of retaining walls, and slumping of embankments, including minor damage from liquefaction and lateral spreading. Landslides and embankment failures caused the most damage and disruption to the transportation infrastructure, particularly where the cumulative effect of large landslides along narrow road corridors through steep inaccessible terrain lead to restricted access for plant and equipment and consequently resulted in very long road outage times. Surface fault rupture also caused closure of the roads, but access was quickly reinstated by formation of ramps or repairs to the pavement. Failures of low height cut slopes were able to be cleared quickly and only caused short term closure of the road. Extensive slumping of low height embankments commonly reduced the available lane width but the damage was quickly reinstated by temporary repairs of the damaged sections. Damage to some bridges occurred in the earthquake, but most bridges were able to be opened quickly with restrictions or bypassed with alternative crossings. Settlement at bridge abutments was widespread and in some cases prevented access over the bridges until temporary ramps could be formed.

1 INTRODUCTION

Road networks provide a vital lifelines function to society, and their availability is critical for emergency response and recovery after major hazard events. A severe magnitude 7.8 earthquake struck 15 km north-east of Culverden in the South Island of New Zealand, at 12:02 am on Monday 14th November 2016. This was followed by numerous aftershocks. At least 21 faults ruptured on and offshore of the north-east of the South Island of New Zealand. The ruptures began on The Humps Fault near Culverden and continued north-eastwards for ~180 km (Stirling *et al*., 2017).

The earthquake caused widespread damage across the northeast of the South Island. In particular, fault rupture, strong ground shaking, and co-seismic landslides severely damaged road networks, including State Highway 1 (SH1) between Ward and Cheviot and other local roads in the Kaikōura and Marlborough districts. This paper provides a summary of the observed ground damage along the road networks in North Canterbury and Marlborough, and the impacts these had on availability of access during the immediate phase of emergency response.

2 GROUND SHAKING

The ground motions were recorded by Geonet seismographs in the upper South Island, with the largest horizontal peak ground accelerations being recorded at the Ward Fire Station (1.27g) and the largest vertical ground acceleration being recorded in Te Mara Farm in Waiau (3.22g),

although this record may have been contaminated by other effects (Kaiser *et al*., 2017). The relative magnitudes of the accelerations and the MM intensities are shown in Figure 1.

Ground shaking was strongest in the epicentral region near Culverden, and to the northeast between Kekerengu and Seddon. The strong shaking near Ward is possibly due to the southwest-to-northeast earthquake rupture sequence directed towards this part of the South Island (Kaiser *et al*., 2017). The ground shaking attenuated rapidly towards the south, with minimal shaking south of Amberley (57 km south of epicentre).

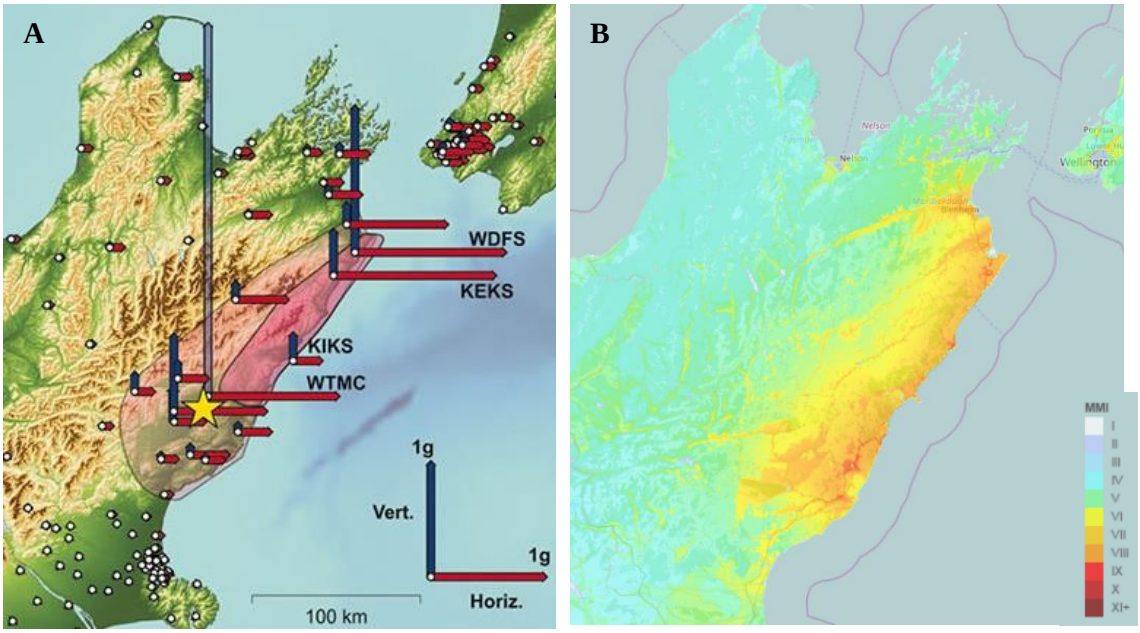

Figure 1. (A) Ground accelerations in the Kaikōura earthquake, with the extent of mapped landslides in the pink shaded areas (Source: https://www.gns.cri.nz/Home/News-and-Events/Media-Releases/strongest-ground-shaking-in-NZ. (B) Modified Mercalli Intensity of shaking in the Kaikōura earthquake (Source: http://shakemap.geonet.org.nz/mapping/2016p858000.html

3 ROAD CLOSURES

The state highway network in the upper South Island is shown in Figure 2. Immediately following the earthquake, SH1 was closed between Waipara and Wairau River township, and SH7 (including SH7A) was closed between Waipara and Springs Junction. Local roads were also closed, cutting off access to Kaikōura, Hanmer, and other smaller settlements in the region. By the end of 14 November, SH1 had reopened from Waipara to Cheviot and SH7 between Waipara and Springs Junction (Davies *et al*., 2017).

NZ Transport Agency contractors began to clear SH1 to Kaikōura from the south on 15 November, and army convoys began travelling on Route 70 in the first few days after the earthquake to deliver essential supplies to Kaikōura. Access for the convoys was subject to daily geotechnical inspection of the road conditions and geohazards. By 18 November, SH1 was open between Blenheim and Ward, and there was controlled access along SH1 between Cheviot and Goose Bay. SH1 between Ward and Clarence was opened on 12 December and between Cheviot and Kaikōura on 21 December (Davies *et al*., 2017).

SH1 between Clarence and Mangamaunu remains closed at the time of writing (August 2017) due to ongoing slip clearance and road repair works.

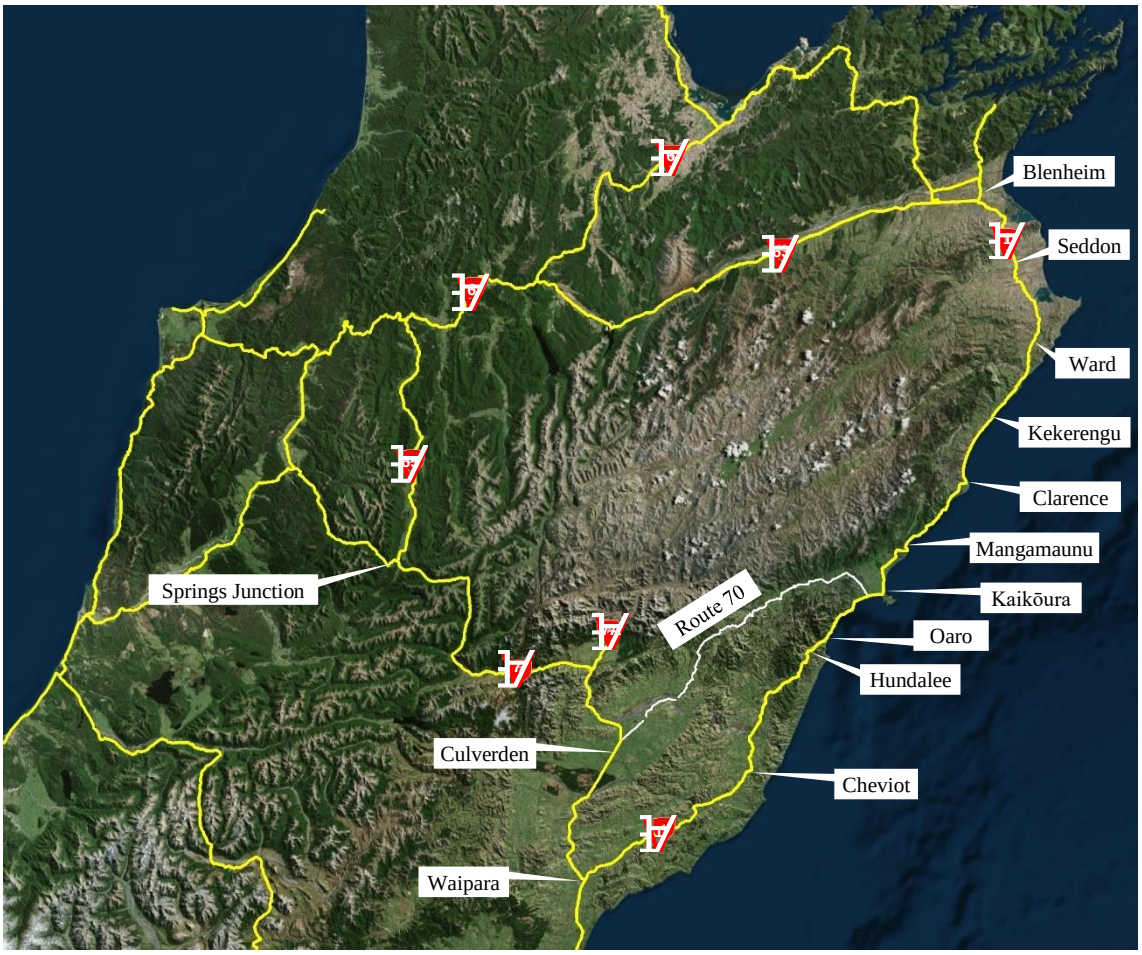

Figure 2. Map of the regional state highway network in the upper South Island

4 GROUND DAMAGE EFFECTS ON ROADS

Widespread severe ground damage resulted from the earthquake, and was the major cause for the road closures. The following effects from the earthquake were observed during the immediate post-earthquake response in November 2016 as the principal causes of road closure:

- Fault rupture
- Landslides, cut slope failures and rock fall
- Embankment damage (including lateral spreading)
- Retaining wall damage
- Damage to bridges

4.1 Fault rupture

Surface fault rupture during the earthquake caused disruption to the road network in a number of places (Stirling *et al*., 2017). The extent of damage from fault rupture ranged from limited or small scale (<0.5 m) deformation of the road to large vertical displacement of 2-4 metres of the road surface. The most severe damage was caused by rupture of the Kekerengu and Papatea faults across SH1, where the damage was impassable and the road therefore was closed (Figure 3).

The outage time was limited, however, as access tracks were formed across the fault scarps by bulldozers within 1-2 days of the earthquake. Access across other fault scarps that had displaced the road was also quickly reinstated by forming gravel ramps over the faults.

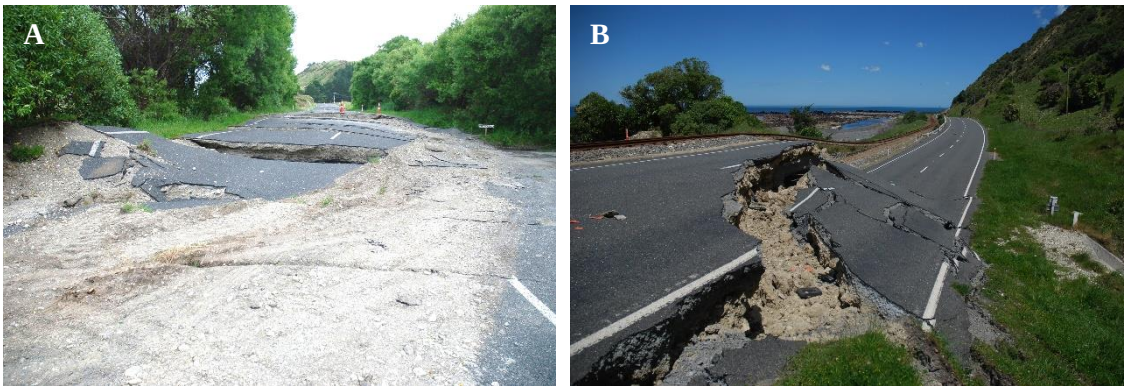

Figure 3. Examples of major damage to SH1 from fault rupture. (A) Rupture of the Kekerengu Fault near Tirohanga; ~2 m vertical displacement. (B) Rupture of the Papatea Fault at Mounsey Creek, Waipapa Bay; ~3-4 m vertical displacement.

4.2 Slope failures

Slope failures were the principal form of ground damage that caused prolonged closure of SH1 and other local roads. The types of slope failures along the roads and their impacts on road availability and outage times were influenced by the topography and road form.

4.2.1 Cut slope failures

Extensive cut slopes had been formed along SH1 between Ward and Okiwi Bay (south of Clarence) and between Oaro and Hundalee. These cut slopes were formed predominantly in weak Tertiary sedimentary rocks, overburden colluvium and alluvial terraces (Rattenbury *et al*., 2006). Cut slope angles ranged from about 45° to over 60°, and were predominantly of only modest heights of up to 20 m. These cut slopes suffered extensively from relatively shallow failures in the overburden and rock (Figure 4), particularly along SH1 between Ward and Clarence where nearly every cut slope had failed regardless of their height. This performance is considered likely to be due to the very high ground accelerations over 1 g recorded in this area (Figure 1).

Failure of cuttings was dominated by shallow translational sliding and wedge failures in the upper half of the cuttings, particularly in the Ward to Clarence area. This was likely due to topographical amplification of ground shaking and the presence of more dilated soil and rock masses in the upper parts of the cuts. Run-out from the failures of the upper half of the slope covered the lower half of the cuttings and encroached into the road depending on the height of these cuttings (Figure 4).

Figure 4. Examples of cut slope failures along SH1. (A) Failure of low height cutting in weak Tertiary siltstone, with accumulation of debris over the lower part of the slope. (B) Failure of cutting in indurated greywacke bedrock with encroachment of debris onto the road.

Given the limited height of these cuttings, the slip debris generally affected the shoulder and one half of the road, and where it affected both lanes, they were able to be partially cleared quickly to create at least one lane access.

Higher cut slopes in indurated greywacke bedrock, predominantly at the lower flanks of high hillsides were present along SH1 between Okiwi Bay and Mangamaunu (north of Kaikoura) and from Peketa to Goose Bay (south of Kaikoura). These cut slopes also suffered from extensive failures, predominantly shallow rock slides and wedge failures (Figure 4). However, the effects of cut slope failures in steep greywacke terrain were often insignificant in comparison to the larger failures of the natural hillslopes.

4.2.2 Landslides on natural slopes

Landslides on natural hillsides along the highway caused most of the prolonged road closures in the Kaikōura earthquake event. Along SH1, these landslides occurred predominantly between Okiwi Bay and Mangamaunu (north of Kaikōura) and from Peketa to Goose Bay (south of Kaikōura). Most of these landslides were soil and rock debris avalanches formed in both the overburden deposits as well as fractured and weathered rock. These failures mainly originated from the upper parts of the hillslopes, but given their size covered the lower slopes and completely buried the road below (Figure 5A). Topographical amplification and the presence of overburden and weathered and dilated rocks in the upper slopes are considered likely to have contributed to failure of the upper slopes.

Some large block slides also affected almost the full height of the slope and led to displacement of the slide mass onto the road below (Figure 5B). Defect-controlled rock slides were also observed in some areas, for example on Route 70 failure occurred by sliding on outward-dipping bedding planes in Tertiary sandstone (Figure 5C).

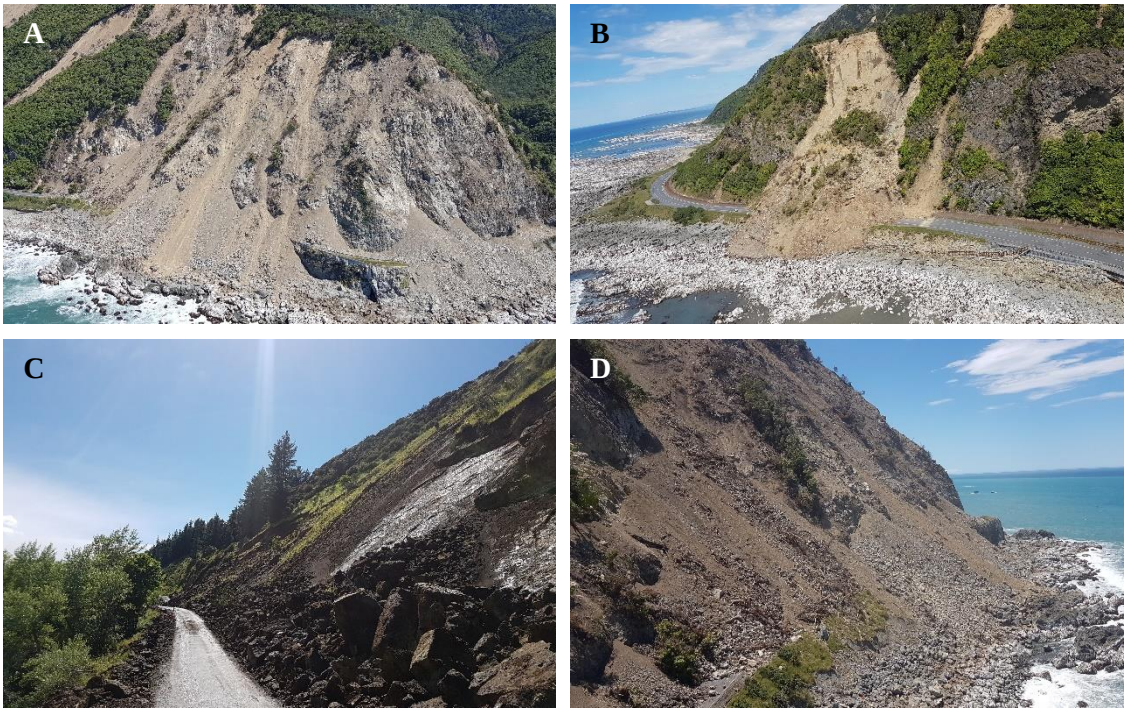

Figure 5. Examples of landslides on natural slopes. (A) Rock slides and debris avalanches originating at the tops of hillslopes and burying the road at the base of the slope. (B) Large block slide inundating the road. (C) Defect-controlled rock slide. (D) Complete burial of road by debris with large volumes of debris remaining on slope above.

These landslides were very damaging to the state highway and local roads, as they deposited large quantities rock and soil debris onto the road, and often large volumes of displaced debris with loose rock also remaining perched on the slopes posing ongoing safety hazards (Figure 5D), and led to long periods of outage where the road was closed. The section of SH1 between Clarence and Mangamaunu remains closed at the time of writing ~9 months after the earthquake while large landslides are cleared and the slopes stabilised.

4.2.3 Rock falls

Rock falls were observed along sections of highway where large landslides had occurred, as well as in areas without large scale failures. Rock falls often originated from cut slopes or steep bluffs above cuttings. Limited areas of rock slope stabilisation measures had been installed along the Kaikōura coast in the ~10-15 years before the earthquake, and these measures (generally consisting of rock bolts and mesh) generally performed well.

The potential for ongoing rock fall where the slopes have been loosened by the earthquake posed ongoing safety hazards to road users, and hence affected the ability to fully open roads for traffic without mitigation measures such as containers or earth bunds in place.

4.3 Embankments

Extensive damage was caused to earth embankments on SH1, particularly between Ward and Clarence and between Oaro and Cheviot, and on the inland Route 70. The predominant types of damage included cracking and deformation of the road surface, displacement and settlement of embankments, and displacement and failures of embankment slopes (e.g. Figure 6A). Damage to embankments in the Hundalees was often associated with reactivation of pre-existing landslide features, as well as settlement or displacement of the road where it crossed infilled gullies in the Tertiary mudstone bedrock (Figure 6B).

These features resulted in significant damage to the road, resulting in difficult access for the initial emergency response. However, the consequence was relatively minor, as slow access for 4WD vehicles was still available along the road, and the damage was quickly reinstated by repairs to the pavement and resurfacing of the damaged sections.

Localised sections of road embankment failure on SH1 and Route 70 were also closed or significantly damaged due to lateral spreading in recent alluvial/swampy deposits adjacent to waterways.

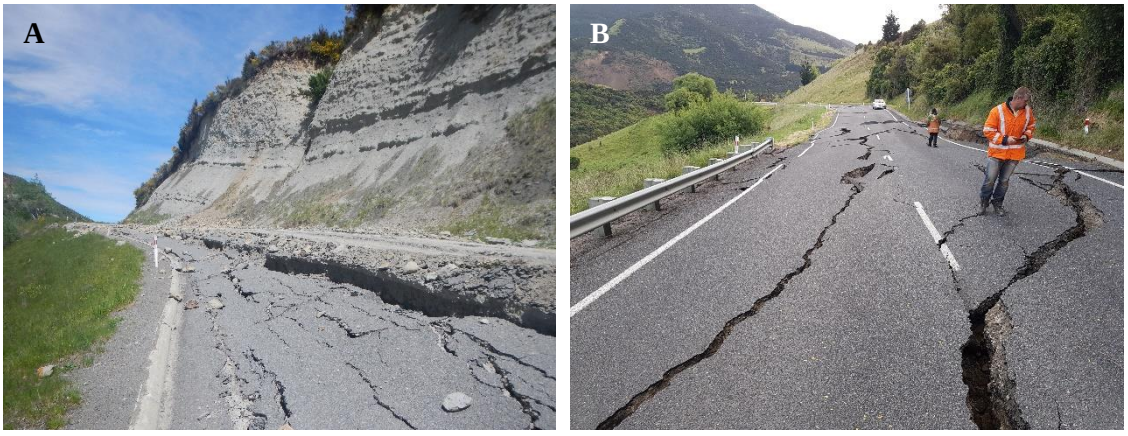

Figure 6. Examples of damage to embankments. (A) Large vertical settlement and spreading of an embankment slope on Route 70. (B) Displacement of SH1 embankment across an infilled gully in the Hundalees.

4.4 Retaining walls

Retaining wall structures which were tied back generally performed well, including gabion basket walls and timber pole walls up to 3 m to 5 m retained height. Gravity retaining structures generally performed poorly. These structures predominantly comprised gabion basket walls ranging in height from 1 m to 3 m height. Failure of the gabion basket walls was generally due to overturning, with a number of instances of translation observed. Pavement cracking and loss of shoulder support to the carriageway typically occurred at walls which exhibited this type of failure, with more severe damage to the wall or underslips resulting in loss of one lane (Figure 7).

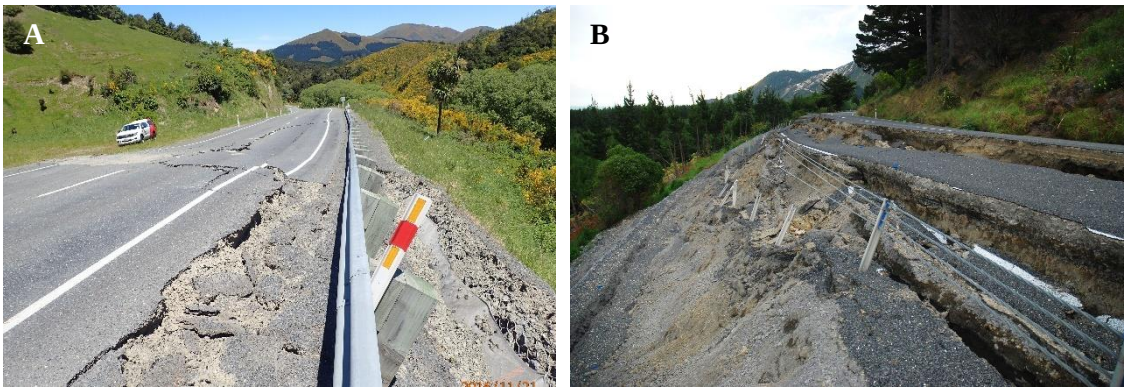

Figure 7. Examples of failure of gabion basket retaining walls. (A) Overturning failure. (B) Translational failure due to underslip.

4.5 Bridges

Many bridges suffered minor to moderate structural damage, predominantly pier plastic hinging, due to high ground shaking intensity (Palermo *et al*., 2017). Settlement at bridge abutments was widespread and in some cases prevented access over the bridges until fill or asphaltic concrete was used to form small ramps onto the bridges (Figure 8). Despite the widespread damage to bridges across the North Canterbury and Marlborough regions, most of the bridges were open for emergency access. Notable exceptions were the state highway overbridge over the railway lines at Oaro, which was able to be bypassed with a temporary level crossing, and the Wandle River bridge on Route 70, which was replaced by a bailey bridge.

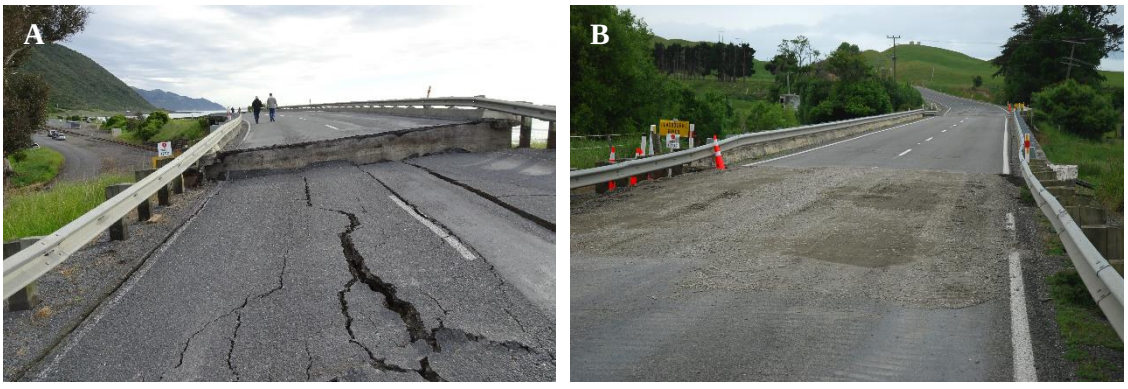

Figure 8. Examples of damage to bridges affecting road access. (A) The state highway overbridge at Oaro was closed due to >0.5 m of settlement at the approaches. (B) Access across bridges with less severe settlement was able to be quickly reinstated with temporary ramps.

5 CONCLUSIONS

The damage caused by the earthquake to the road networks provides valuable lessons on the impacts of large earthquakes on road performance and the duration of outage following such an event.

Landslides and embankment failures caused the most damage and disruption to the transportation infrastructure in the 2016 Kaikōura earthquake. Failures of low height cut slopes were able to be cleared quickly and only caused short term closure of the road, whereas landslides on high hillslopes extending 50 m to 100 m or more caused extensive damage and prolonged the closure. The unstable nature of the debris and the presence of disrupted rock masses along the slopes above the roadway made reconstruction efforts more difficult and involved a much longer duration for clearing of debris with sluicing, roped access scaling and careful formation of access to clear debris safely. Therefore the outage periods were much longer, such as on the coastal section of SH1 between Clarence and Mangamaunu.

Extensive slumping occurred of low height embankments between Ward and Clarence, and Oaro and Cheviot. This commonly reduced the available road or lane width but the overall consequence was relatively minor, as slow access for 4WD vehicles was still available along the roads and the damage was quickly reinstated by temporary repairs of the damaged sections. Similarly, surface fault rupture caused closure of the roads, but access was quickly reinstated by formation of ramps or repairs to the pavement.

Damage to some bridges occurred in the earthquake, but most bridges were able to be opened quickly with restrictions or bypassed with alternative crossings. Settlement at bridge abutments was widespread and in some cases prevented access over the bridges until fill or asphaltic concrete was used to form small ramps onto the bridges.

6 ACKNOWLEDGEMENTS

We wish to thank the team of geologists and engineers who were involved in the immediate emergency response for the road networks in North Canterbury and Marlborough for their urgent response and exceptional effort. The permission of NZTA and Marlborough Roads to publish the paper is also gratefully acknowledged.

REFERENCES

Davies, A., Sadashiva, V., Aghababaei, M., Barnhill, D., Costello, S. *et al.* (2017) Transport infrastructure performance and management in the South Island of New Zealand, during the first 100 days following the 2016 M_w 7.8 "Kaikōura" earthquake. *Bulletin of the New Zealand Society for Earthquake Engineering 50* (2): 271-299.

Kaiser, A., Balfour, N., Fry, B., Holden, C., Litchfield, N. *et al*. (2017) The 2016 Kaikōura, New Zealand, earthquake: Preliminary seismological report. *Seismological Research Letters 88* (3): 727-739.

Palermo, A., Liu, R., Rais, A., McHaffie, B., Andisheh, K. *et al*. (2017) Performance of road bridges during the 14 November 2016 Kaikōura earthquake. *Bulletin of the New Zealand Society of Earthquake Engineering 50* (2): 253-270.

Rattenbury, M., Townsend, D., Johnston, M. (2006) *Geology of the Kaikoura area.* Institute of Geological and Nuclear Sciences 1:250 000 geological map 13. 1 sheet + 70p. Lower Hutt, New Zealand. GNS Science.

Stirling, M., Litchfield, N., Villamor, P., Van Dissen, R., Nicol, A. *et al*. (2017) The M_w 7.8 2016 Kaikōura earthquake: Surface fault rupture and seismic hazard context. *Bulletin of the New Zealand Society for Earthquake Engineering 50* (2): 73-84.

State Highway 5 Tumunui tomo - a case of road resilience to piping in the Rotorua-Taupo area

P Martins
Beca Ltd, Tauranga, NZ
pedro.martins@beca.com (Corresponding author)

D Van Toan
Beca Ltd, Auckland, NZ
dovan.toan@beca.com

Keywords: piping erosion, tomo, road resilience, Rotorua-Taupo

ABSTRACT

On 23 June 2016, following a heavy rain event, a section of SH5 at the locality of Tumunui, about 18km south of Rotorua, was closed due to flooding. When the water recessed a little, significant damage to the road and adjacent properties was revealed. The New Zealand Transport Agency - Bay of Plenty East Network Outcomes Contract (BoPE NOC) is the road asset management contract covering the damaged section of SH5. Due to the immediate risk to road users arising from the event, the geotechnical incident response procedure of the BoPE NOC was triggered. Based on the geotechnical investigation undertaken it was concluded that the damage sustained by SH5 at Tumunui was due to reactivation of a naturally occurring internal erosion process that had been developing across the area since at least the 1970's. The process is intrinsically associated with the geomorphic context of the site and the underlying geology. Following the event, a risk assessment was undertaken and concluded that with management controls in place it was possible to keep the road partially open to traffic. Medium and long term remedial options were investigated to reopen the road to full traffic. A geogrid-reinforced soil raft was preferred due to its quick implementation even in wet weather, and relatively low cost. Three and a half months after the rain event, the road was fully reopened to traffic. Ongoing monitoring indicates that minimal settlement has occurred since completion of the works.

1 INTRODUCTION

State Highway 5 (SH5) is a regional strategic highway extending from SH1 at Tirau, in the Waikato, to SH2 just north of Napier. In the early hours of 23 June 2016, following a heavy rain event, a section of SH5 at Tumunui, about 18km south of Rotorua, was closed due to extensive flooding. A couple of hours later the rain eased and the water receded, revealing significant damage to the road and adjacent properties.

The New Zealand Transport Agency - Bay of Plenty East Network Outcomes Contract (BoPE NOC) is the road asset management contract covering the damaged section of SH5. Due to the imminent risk to road users arising from the event, the geotechnical incident response procedure of the BoPE NOC was triggered to better assess the risk and to develop mitigation strategies.

2 THEORETICAL BACKGROUND – PIPING AND TOMOS

Dispersion followed by internal erosion is the process causing the loss of soils due to entrainment by groundwater flow. Water seeping through the ground carries clay size particles followed by transport of the silt/sand particles leaving a cavity. Regressive erosion develops from downstream

to upstream until it reaches the ground surface and a continuous pipe is formed. At this point, the flow rate, and hence the erosion potential, increases dramatically. As the pipe grows, the soil cover gets thinner. At a certain point the roof of the pipe becomes too thin to form a competent arch and collapses, forming a sinkhole. Tomo is the Maori word for sinkhole and is a very common feature in the central North Island due to the extensive occurrence of ash and pumice soils.

3 GEOTECHNICAL EMERGENCY RESPONSE

3.1 Site Walkover

A site walkover was carried out on the same day to assess the damage to the road and to develop an initial understanding of the geological process that caused the damage. It was observed that a 12m long section of the road, bound by cracks extending across the whole width of the pavement, had dropped about 30mm (Figure 1). Aligned with the dropped road section, tomos had developed in paddocks in the properties on both sides of the road. To the west, a 10m wide tomo had extended for more than 100m, terminating as a natural tunnel into a hill (Figure 2). Groundwater was observed at the base of the new tomos, flowing from east to west and then "disappearing" into the tunnel.

An inspection of the existing surface drainage system identified that the swales and culverts were too high to drain the water that ponds in the paddocks adjacent to the road (Figure 3).

3.2 Desk Study

A review of rainfall data confirmed a that heavy rain event occurred just before the new tomos appeared on the west side of the road. Between 6am on 22/06/2016 and 6am on 23/06/2016, the Okaro farm rain gauge (7km away from the site) recorded 110mm of rain with a peak intensity of 26mm/hr (Bay of Plenty Regional Council, 2016).

Lidar elevation data available for the region indicated that the Tumunui area is an enclosed depression, consisting of a catchment of about 270ha (Bay Explorer, 2016). Geologically, this depression corresponds to a volcanic vent of approximately 27ka, as indicated in the *Geology of the Okataina Volcanic Centre* (Nairn, 2002).

The lowest point of the Tumunui depression is located on the east side of SH5, which means that the only possible exit for all surface water in the catchment to the west of the highway is via groundwater flow, including a natural underground pipe/tunnel network, as the road embankment creates a damming effect and the surface drainage system is ineffective (refer Section 2.1).

A review of historical aerial photos revealed that a gully has existed on the east side of the site since the mid 1970's at least (older photos were not reviewed). Small circular sinkholes started to appear on the west side after 2006. The fact that these sinkholes align well with the currently developed tomos, could suggest that some sub-vertical geological structure is influencing the development of the piping process.

Although a number of active faults are present in the wider Rotorua region associated with the Taupo Rift Zone, in the Tumunui area in particular, no active faults are known to exist, as indicated in Figure 4 (New Zealand Active Faults Database, 2016). In addition, whilst the vast majority of the active faults in the region are NE-SW oriented, in Tumunui the orientation of the gully on the east side of the road and the recently developed tomos is closer to E-W. Therefore it is considered unlikely that the piping process affecting SH5 is associated with active faults.

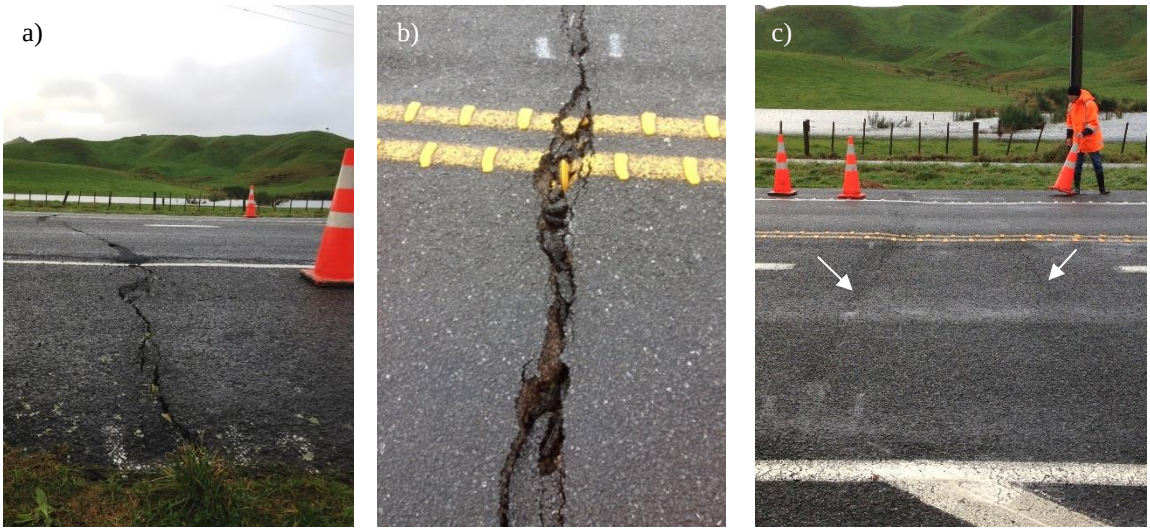

Figure 1: Observed damage to the road. a) North crack; b) Detail of the north crack; c) South cracks, as indicated by the arrows.

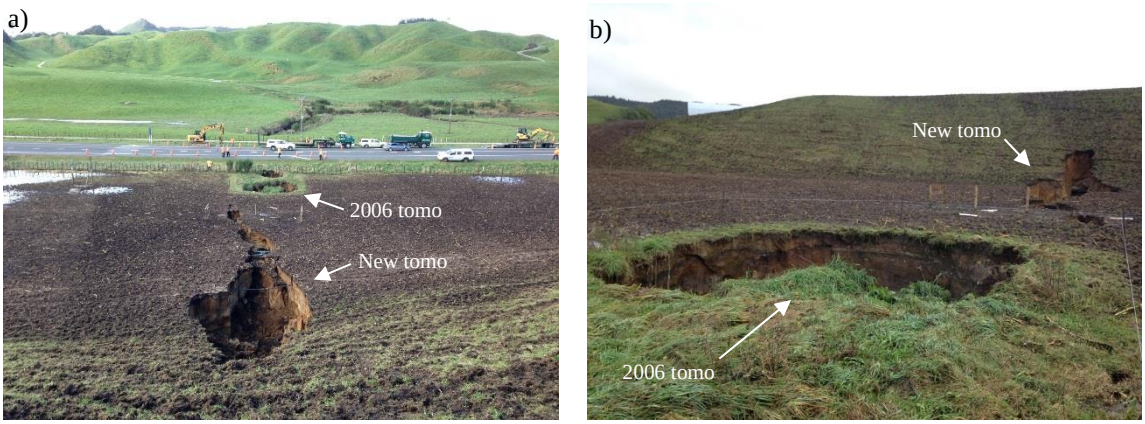

Figure 2: Sinkholes/tomos developed in the adjacent properties. a) Looking east from the hill towards the road. b) Looking west from the road towards the hill.

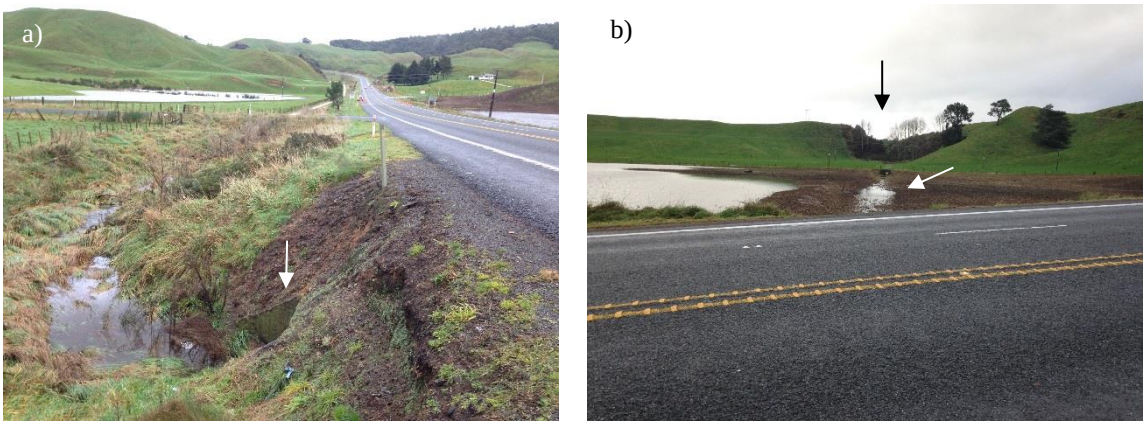

Figure 3: The existing surface drainage is too high to drain water ponding in the area. a) Culvert (as indicated by arrow) supposed to drain water from ditch on the east side of the road to swale on west side. b) Swale (white arrow) supposed to drain water to gully downstream (black arrow).

Figure 4: Active faults in the Tumunui area (New Zealand Active Faults Database, 2016). White ellipse indicates section of road affected by tomos.

3.3 Ground Investigation

Based on the information gathered from the desk study and the observations from the site walkover, a conceptual ground model was developed. To confirm some key aspects of the model and inform the development of remedial options, limited geotechnical investigations were carried out at the site. These investigations consisted of:

- One trial trench, about 15m long, 1m wide and 4.5m deep.
- Three large diameter machine auger holes (450mm diameter), to up to 12m depth.

The position of these investigations at the site is indicated in Figure 5.

In addition to the investigations mentioned above, about a year before the piping event affected the road, 14 Cone Penetration Tests (CPTs) to up to 10m depth were carried out by Pattle Delamore Partners Ltd (PDP) for First Gas Ltd (First Gas) on the adjacent property to the west of the site. The location of these CPTs, as well as some representative results are indicated in Figure 6.

3.4 Ground Model and Understanding of the Piping Process

Based on the information obtained from the site walkover, the desk study and the ground investigation, a ground model for the site was developed. A cross-section illustrating the ground model is shown in Figure 7. The key findings from the investigation are discussed below.

Previous tomos occurred at the site in the past, as indicated by the existence of naturally infilled voids with an upright conical shape, extending from the surface to about 7m depth.

A layer of loose, clean, fine to coarse pumiceous sands was found typically between 4m and 7m depth. When the trial trench was being excavated, even though the groundwater level was nearly at the ground surface because of flooding, the excavation was progressing relatively dry through the topmost layer of fine soils. Once the excavation entered the loose pumiceous sands, water immediately started gushing into the trench. This indicated that the loose pumiceous sands are permeable and can conduct significant amounts of groundwater.

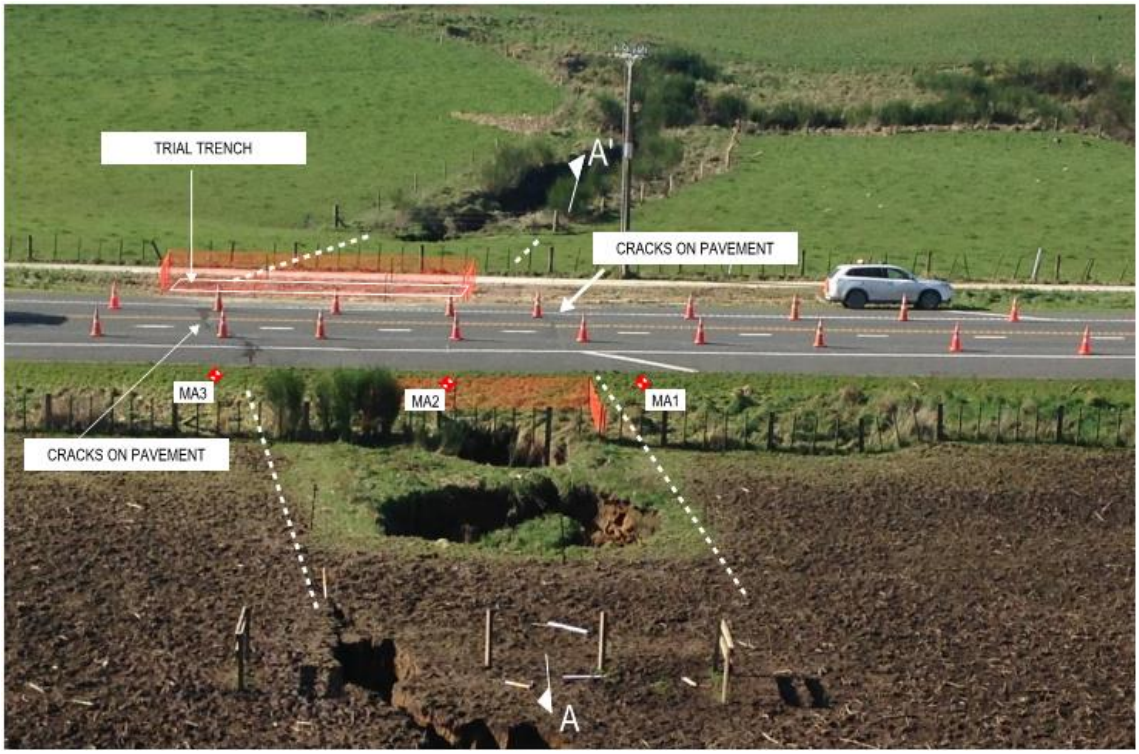

Figure 5: Location of ground investigations. Dashed lines indicate position of cracks observed. Section line A-A' is also indicated.

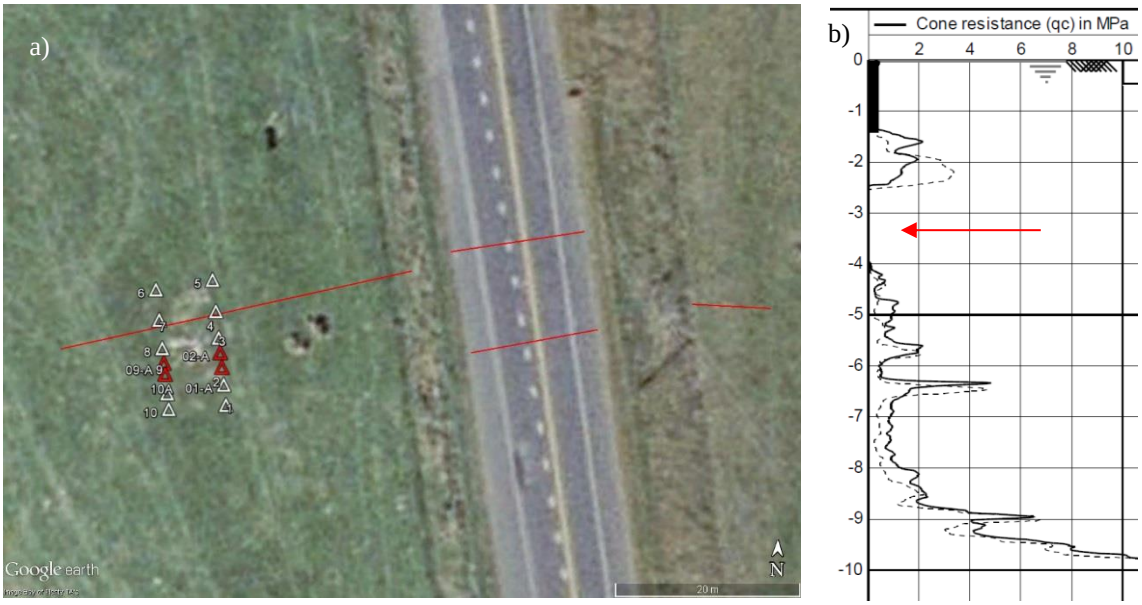

Figure 6: CPTs on adjacent property to the west. a) Test locations: red triangles indicate location of potential voids. Red lines indicate position of cracks observed. b) CPTs where potential voids were intercepted, as indicated by red arrow.

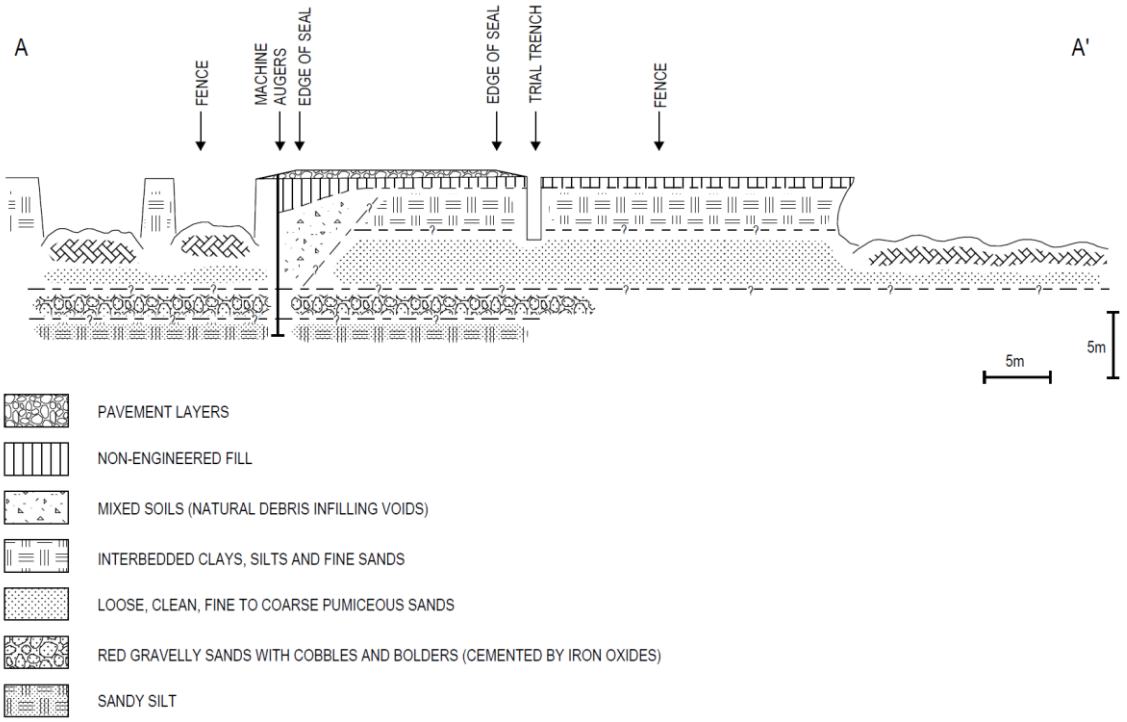

Figure 7: Section A-A' illustrating the ground model for the site.

Another point noted was that the depth of the loose pumice sands matched with the base of the gully to the east of the road. Also, the position of these sands coincided with the depths of the potential voids detected by the CPTs.

Below the loose pumiceous sands, a 1m thick layer of dark red gravelly sands with some cobbles and small boulders, partially cemented by iron oxides was encountered.

Based on the key points described above, it was concluded that the layer of loose pumiceous sands was the main zone were the piping (silt/sand transport) process was developing, and that the top of the layer marked the roof of the piping system. It was considered that the underlying cemented gravelly sands with cobbles and boulders would likely mark the base of the system.

The width of the piping zone was interpreted to be likely around 12m, as marked by the cracks on the pavement. It was also concluded that the piping was well developed under the road and downstream (i.e. to the west).

Lastly, it was concluded that the cover above the tomo was up to 4m thick and the shallow soils were unable to naturally bridge a tomo of the intepreted size.

4 RISK MANAGEMENT STRATEGY

Based on the understanding of the internal erosion piping process described above, it was concluded that the section of road between the two cracks (about 12m long) subsided and needed to be replaced by a suitable solution. As a result, immediate measures were put in place to manage the risk to road users and options for the long term repair of the road were investigated.

4.1 Short term

Following discussions between all parties involved with the BoPE NOC, it was decided to put the following measures in place to manage the risk to road users:

- 24/7 Temporary traffic management consisting of single lane stop-go operation to enforce a 30km/h temporary speed limit and close the road if conditions deteriorated.
- Overweight vehicles diverted from the site.
- Three times daily monitoring of pavement cracks (width and drop).
- Monitoring of weather conditions: road to be closed when there was heavy rain.
- Flood-lighting to improve visibility for night traffic.

4.2 Medium and Long Term

Temporary and long term remedial options were discussed with the BoPE NOC team, with the main philosophy being to interfere as little as possible with the existing underground water flow system. Any blockages to the natural drainage path would cause groundwater to find an alternate path, which could lead to the development of new tomos, introducing new unknown risks.

The preferred option was a medium-term solution consisting of a geogrid-reinforced soil raft, able of spanning the voids whilst providing enough robustness to avoid sudden collapse should the cavities enlarge as the erosion progresses.

The final design of the geogrid-reinforced soil raft was carried out based on BS 8006-1:2010. A long section of the raft is illustrated in Figure 8.

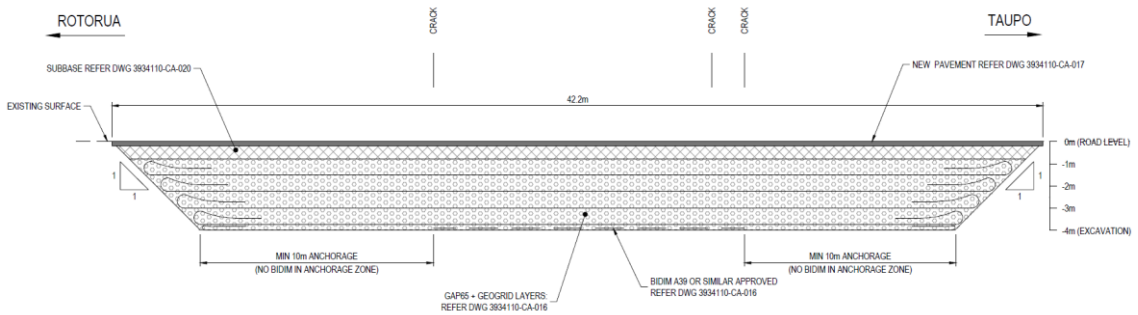

Figure 8: Long section of the geogrid-reinforced soil raft.

5 CONSTRUCTION

During construction, the anticipated ground model was generally confirmed and no significant voids or cavities were encountered in the excavation to 4m depth. Some small cavities up to 200mm long and 20mm wide were observed along a set of widely spaced subvertical fractures oriented at around N75E, as illustrated in Figure 9.

These subvertical fractures were only observed within the 12m wide zone delimited by the north and south cracks in the pavement. The north and south cracks themselves were found to be surface traces of the subvertical fractures, and could be traced along the full height of the east and west walls of the excavation. No displacements were observed across any fractures at the site.

6 POST-CONSTRUCTION MONITORING

On completion of the remedial works, a settlement monitoring program was put in place. The purpose of the monitoring was to track the performance of the reinforced soil raft and to identify early signs of potential larger ground movements due to progressive development of the underground tomo system. The program is still ongoing and, after more than 250 days, the maximum measured settlement is 7mm, which can be considered negligible for the soil raft.

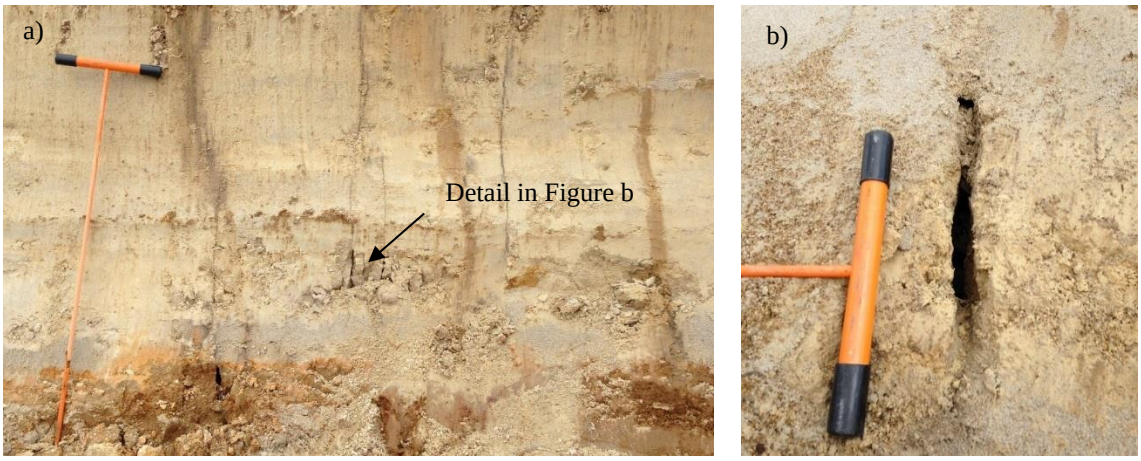

Figure 9: Small-scale piping along subvertical fractures on the west wall of the excavation.

7 CONCLUSIONS

The damage sustained by SH5 at Tumunui after the heavy rain event that occurred on 23 June was due to reactivation of a naturally occurring internal erosion process that had been developing across the area since for a long time. The process is intrinsically associated with the geomorphic context of the site and the underlying geology.

Following the event, a risk assessment was undertaken and concluded that with controls in place it was possible to keep the road partially open to traffic. Medium and long term remedial options were investigated to fully reopen the road. A geogrid-reinforced soil raft solution was preferred due to its quick implementation even in wet weather, and relatively low cost.

Three and a half months after the rain event, the road was fully reopened to traffic. Ongoing monitoring indicates that minimal settlement has occurred since completion of the works.

The key highlights of the project were: (i) The remediation measures were delivered in a good timeframe, considering the extent and seriousness of the natural hazard involved; (ii) A large earthworks solution was delivered over the wet season; (iii) There was relatively little disruption to road users, with the road partially open all the time.

8 ACKNOWLEDGEMENTS

The authors gratefully acknowledge the permission of the NZ Transport Agency and Higgins Group Holdings Ltd to publish the results of the work conducted for the BoPE NOC in Tumunui. The authors also thank First Gas and Pattle Delamore Partners for kindly providing the results of the CPTs. Lastly, the authors acknowledge Beca for the institutional support to prepare this paper.

REFERENCES

Bay Explorer (2016) Bay of Plenty Regional Council web based GIS. Accessed 27 June 2016, http://geospatial.boprc.govt.nz/Html5Viewer/Index.html?viewer=bayexplorer

Bay of Plenty Regional Council (2016) Telemetry Data for Rainfall. Accessed 27 June 2016, http://monitoring.boprc.govt.nz/MonitoredSites/cgi-bin/hydwebserver.cgi/catchments/details?catchment=21

BS 8006-1:2010 *Code of practice for strengthened/reinforced soils and other fills.*

Nairn, I.A. (2002) *Geology of the Okataina Volcanic Centre*, scale 1:50,000. Lower Hutt: Institute of Geological & Nuclear Sciences.

New Zealand Active Faults Database (2016) Accessed 27 June 2016, <http://data.gns.cri.nz/af/>

A design approach to residual rockfall hazard of drapery systems: example from Clifton Hill, Sumner

C Lambert
Golder Associates (NZ) Limited, Christchurch, NZ.
clambert@golder.co.nz (Corresponding author)

T McMorran
Golder Associates (NZ) Limited, Christchurch, NZ.
tmcmorran@golder.co.nz

A Giacomini, K Thoeni
The University of Newcastle, Newcastle, Australia.
anna.giacomini@newcastle.edu.au
klaus.thoeni@newcastle.edu.au

Keywords: Rockfall, double-twisted hexagonal drape, residual hazard, DEM modelling

ABSTRACT

Unsecured draperies are routinely used as a rockfall mitigation system. These systems do not completely eliminate the rockfall hazard and are typically classified as passive structures aiming primarily at controlling rockfall motions by constraining them towards the slope. Rockfall hazard is seldom completely eliminated, therefore requiring another line of defence such as a catch ditch or a berm.
This paper presents a new approach that was implemented on Sumner Road at Clifton Hill in Christchurch to quantify the efficiency of the drapery to control the motions of potential rock falls, therefore optimising the design requirements for the catch ditch at the base of the slope. A discrete element model (DEM) was previously developed to specifically simulate the interaction between falling blocks and draperies. Results of 3D rockfall trajectory simulations were used to characterise the influence of block size, shape and fall height on the efficiency of a drapery to reduce the impact kinetic energy and constraint the bottom impact location. Simplified relationships were derived and used to estimate the rebounds at the base of the slope and subsequently design the catch ditch.

1 INTRODUCTION

During the 2010 - 2011 Canterbury Earthquake Sequence, rockfall occurred from a cliff at Clifton Hill, Sumner, affecting the adjacent Main Road. A preliminary assessment indicated an unacceptably high on-going risk of rockfall affecting road users. Shipping containers were placed as a temporary rockfall risk mitigation measure to protect road users. However, Christchurch City Council wishes to remove the shipping containers while introducing effective long term mitigation measures to address the rockfall hazard. Placement of a double twisted wire mesh unsecured drape over the full height of the cliff is proposed as a primary mitigation measure.

Unsecured drapery, i.e. only anchored along the top (Muhunthan et al., 2005), addresses rockfall that originates from the covered area. Although the system can provide some resistance to rockfalls where the mesh is in contact with the slope, it allows for blocks to fall between the slope and the mesh, controlling its descent into a catchment area at the base of the slope. It intends at reducing and confining the risk rather than eliminating it. It is therefore essential for designers to

understand the level of risk reduction that is achieved to ensure that appropriate secondary control measures are implemented wherever necessary.
Based on observed performance of unsecured draperies installed in North America, Muhunthan et al. (2005) developed design guidance providing design and installation recommendations. However, to the authors' knowledge, no guidance is available on catchment requirement at the toe or on the risk reduction achieved by an unsecured drapery.

To this date, few studies have attempted to quantify the performance of draperies. Giacomini et al. (2012) performed a series of rockfall field experiments behind unsecured drapery using stereo paired high speed video cameras to record the trajectories. These tests provided the first insight on the level of energy reduction or confinement that can be achieved; however, they were limited to a single slope with no variation of block shape or size. Muhunthan et al. (2005) developed a finite element model of a drapery to investigate static load distribution across the system but did not perform any rockfall trajectory simulation. Bertrand et al. (2008) proposed a discrete element model (DEM) of a double-twisted hexagonal mesh but the model was intended at modelling the dynamic response of gabion baskets. Subsequently, Thoeni et al. (2013, 2014) enhanced the DEM model to successfully simulate three-dimensional rockfall trajectories behind a drapery therefore providing a promising tool to quantify the efficiency of the system at reducing and confining the rockfall risk.

This papers describes a simplified approach developed to quantify the risk reduction achieved by the proposed drapery at Clifton Hill. The general performance of draperies as observed by Giacomini et al. (2012) is first summarised. Results of a sensitivity analysis performed using the model from Thoeni et al. (2014) are presented. The sensitivity analysis included block shape, block size and surface irregularities. General empirical relations to estimate minimum catchment width and energy reduction were derived for a 30 m high slope. These relations were then used to demonstrate the suitability of the secondary control measures implemented at the toe of the slope.

2 PERFORMANCE OF DRAPERIES

2.1 Field experiment

Giacomini et al. (2012) investigated the performance of double-twisted hexagonal wire drapes as a rockfall mitigation system. In situ rockfall experiments were conducted at a mine site to assess the effectiveness of drapery mesh in reducing the rockfall hazard. Two series of tests were carried out by releasing concrete blocks from the top of a highwall, in a meshed and a neighbouring unmeshed area with similar topography and geological characteristics. The blocks falls were recorded and their trajectories were reconstructed via stereo-photogrammetry. These trajectories were then used to infer the motion characteristics of velocity, energy and restitution coefficients (Figure 1).

The comparison between tests with and without drapery clearly highlighted the effect of the protective structure on the block trajectories and impact energies (Table 1). The confining function effect, quantified as the maximum deflection from the slope, was reduced by approximately 70% on average. This confining of the trajectory resulted in an increased number of impacts along the 40 m high slope (2 – 3 impacts without drapery and 4 – 5 with a drapery) and shallower impact angles.

As expected the presence of a drapery tends to reduce the translational velocity of falling blocks. The maximum translational velocity along the fall tends to be reduced to approximately 60% of its counterpart on a similar undraped slope. While the reduction in velocity achieved by the presence of a drape is significant, the maximum velocities observed along a fall largely exceed residual exit velocities sometimes assumed by practitioners (Lambert et al. 2016).

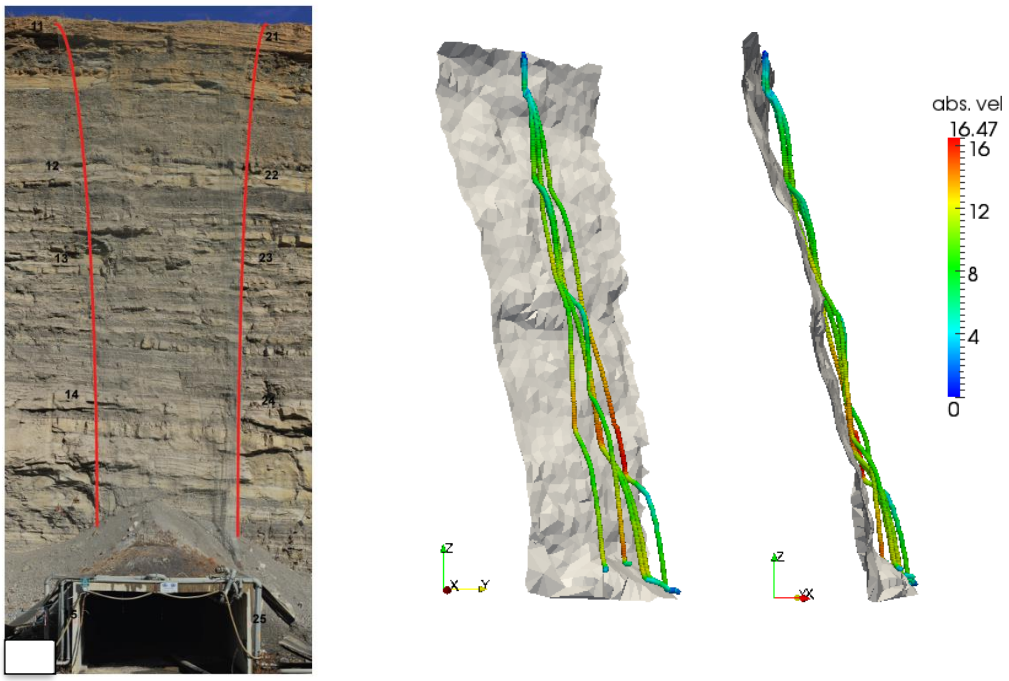

(a) (b)

Figure 1. Rockfall field testing of a drapery system: (a) underground entry portal with a 4 panel wide drapery system and (b) boulder trajectories reconstructed from stereo pairs of high speed video cameras (from Giacomini et al., 2012)

In the presence of a drape, the energy dissipated along the fall can be attributed to two distinct mechanisms: energy dissipated upon impacting the slope, traditionally captured by the use of restitution coefficients and frictional dissipation through block / mesh interaction. The confining of the trajectory results in an increased number of dissipative events. This is however partially overcome by the change in impact angle. Indeed, shallower impact angles results in higher normal restitution coefficient (Wyllie, 2014) and therefore lower energy dissipation upon each impact.

An interesting aspect during a rock fall is the coupling upon impact between tangential velocity and rotational velocity (Preh et al. 2015) resulting in a transfer of kinetic energy from translational to rotational kinetic energy (and vice versa). Experiments by Giacomini et al. (2012) captured this transfer for each impact. It was also observed that the drape was very efficient at dissipating the rotational energy between two successive impacts (between 20% and 80% of the rotational energy dissipated between two consecutive impacts), preventing a gradual increase of the rotational velocity along the fall. Accounting for both translational and rotational kinetic energies, it was observed that overall the block / drape interaction resulted in an average energy dissipation of 0.12 kJ per meter of fall.

Table 1. Comparison of rockfall characteristics between draped and undraped slopes

	Maximum mesh deflection (m)		**Maximum translational velocity (m/s)**	
	Draped	Undraped	Draped	Undraped
Avg	1.6	5.6	15.0	26.5
St dev	0.3	3.4	0.9	1.7
Max	2.1	10.1	16.5	28.4
95th %tile	2.1	9.8	16.2	28.4

2.2 Discrete element model of a double-twisted hexagonal drape system

Thoeni et al. (2013, 2014) proposed a novel approach for the simulation of rockfalls behind drapery systems which can be used to accurately assess the residual rockfall hazard involved with such systems. Based on classical discrete element method, the model offers the ability to account for all the relevant interactions during a rockfall event, i.e. block – slope, block – drapery and slope – drapery (Figure 2). The block is represented by a rigid assembly of spheres. The slope is represented by triangular elements and the drapery is represented by spherical particle which interact remotely. All components of the model are rigorously calibrated and validated against laboratory experiments (Thoeni et al., 2013) and can accurately predict block trajectories and block velocities for rockfall analysis without and with drapery (Thoeni et al., 2014).

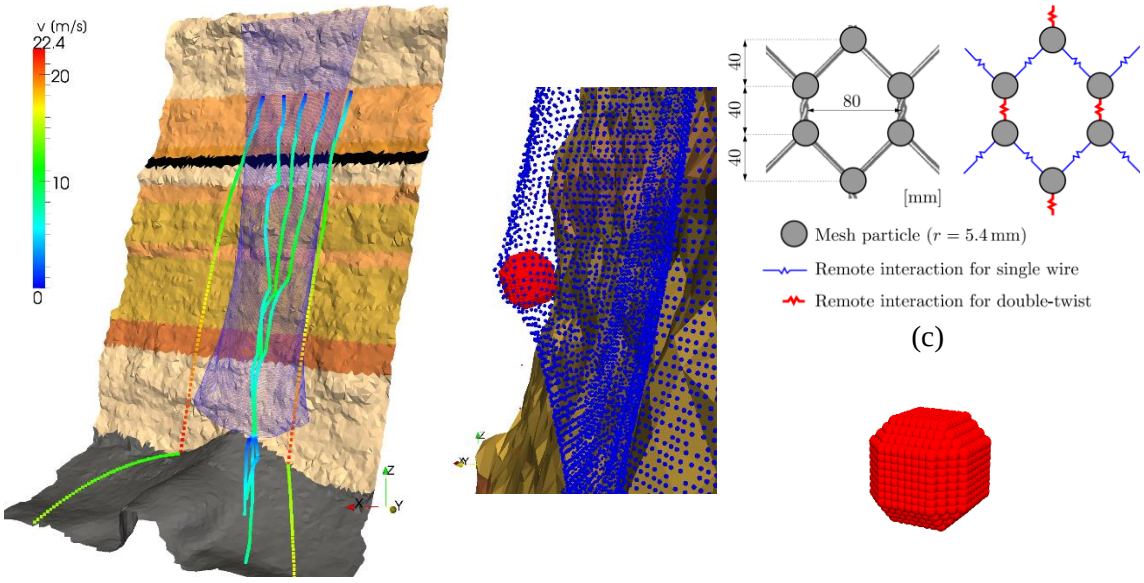

Figure 2. Three dimensional Discrete Element Model for rockfall trajectory analysis behind drapery systems: (a) Full scale model; (b) close-up view of block - drape interaction; (c) DEM model of drape with remote particle interaction; (d) model of ETAG 027 concrete block

2.3 Sensitivity analysis

While site specific modelling should be performed for a quantitative assessment of the residual hazard, such analysis can be time consuming and is not practical at an early stage of a project. In an attempt to derive preliminary design recommendations, a sensitivity analysis was performed. Nine different blocks were considered as a combination of three different shapes (sphere, cube and elongated cube) and three characteristic dimensions (0.2 m, 0.4 m and 0.8 m) resulting in the mass ranging from 10.1 kg (0.2 m sphere) to 2.5 t (0.8 m elongated cube).

A standard slope geometry used in the parameter study was based on the highwall section presented in Thoeni et al. (2014) with a total slope height of 45 m and an average slope angle of approximately 75°. Some modifications to the slope morphology were introduced to investigate a range of slope surface irregularities that may locally reduce the efficiency of the drapery due to a reduced slope mesh contact. Ledges at different heights (15 m and 30 m) with different depths (0.5m to 2.0 m) were introduced to generate different slope scenarios (Figure 3). Three of each blocks were then released from three positions at the same elevation on the slope. Block trajectories during the fall were recorded, from which kinetic energy, and bouncing distance from the slope, were derived. The energy and block deflection after a 30 m fall were analysed.

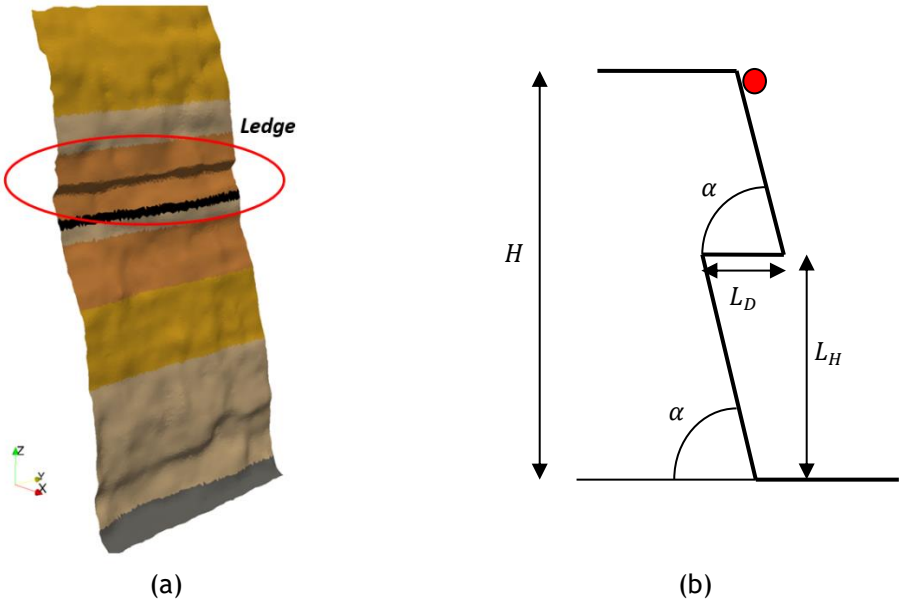

Figure 3. (a) Example of artificially modified geometry for rockfall trajectory study; (b) surface irregularity scenario considered in the analysis

Translational kinetic energy is presented as a function of block mass in
Figure **4**a. Results suggest block mass is the primary controlling factor and that block shape and slope morphology only have a secondary influence. Conservation of energy implies that the maximum energy that can be achieved by a falling block is equal to its initial potential energy (m×g×30). The efficiency of the drapery can be expressed as the ratio of impact energy to initial potential energy (E_{kin}/E_{pot}), i.e. a high ratio correspond to a low efficiency (i.e. a high proportion of the potential energy is transferred into kinetic energy).
Figure **4**b suggests that the efficiency as energy reduction can be minimal for large blocks (500 kg or above).

An upper bound bottom impact energy trend line can be estimated as:

$$E_{kin} = C_k \times m^{\alpha} \quad (2)$$

where C_k = 125, α = 1.15 and the mass is expressed in kg.

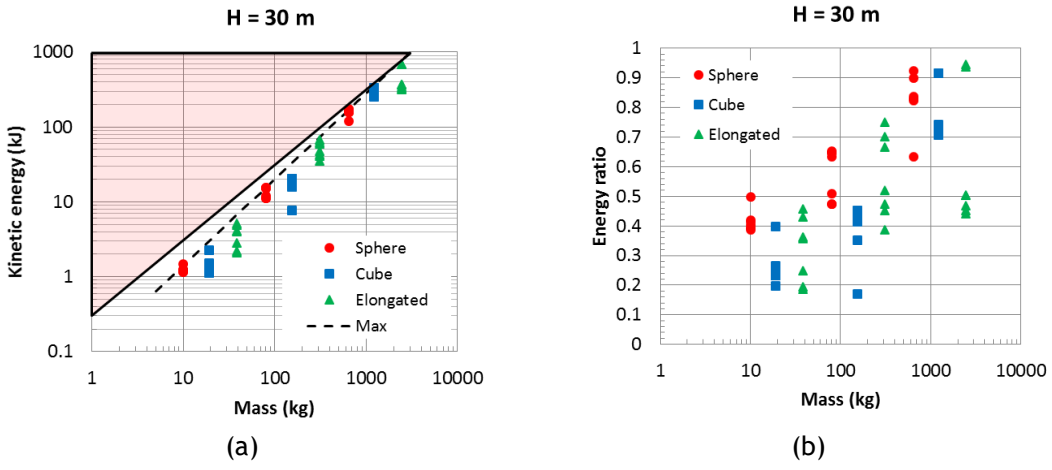

Figure 4. (a) Translational kinetic energy as a function of mass for all combinations of block shapes, sizes and slope morphologies; (b) energy dissipation ratio

As discussed previously, a key aspect in the performance of a drapery lies in its ability to confine trajectories and therefore bottom impact locations close to the toe of the slope. The requirement for a minimum bottom catch width was therefore assessed from the observed deflection (Figure 5). While deflection appears generally greater when a ledge is present on the slope, no obvious trend can be derived with the location or the depth of ledge. However, results suggest again block mass is broadly the primary controlling factor, above block shape or slope irregularities. The catch width tends to increase with mass. An upper bound envelope for the minimum catch width can be expressed with the following equation:

$$d_{\max} = C_d + \beta \cdot \log m \quad (3)$$

where: $C_d = 0.5$ and $\beta = 1.6$

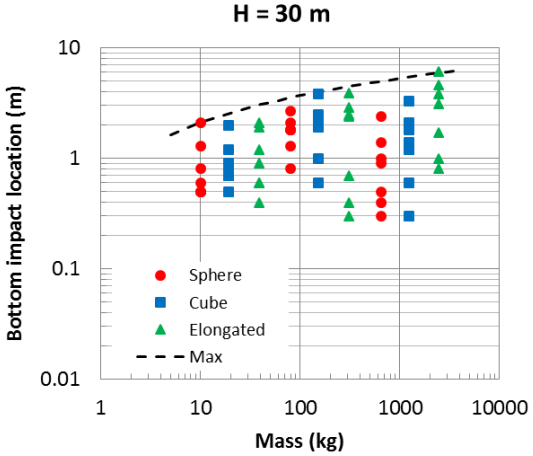

Figure 5. Horizontal bounce as a function of mass for all combinations of block sizes, shapes and slope morphologies

3 ROCKFALL PROTECTION AT CLIFTON HILL

3.1 Clifton Hill

The cliff at Clifton Hill comprises a 20 m to 30 m high steep rock slope exposing interlayered basalt lava flows and volcanic breccia with rare thin epiclastic horizons (
Figure **6**). The crest of the cliff exposes a layer of loess in the order of two metres thickness.

Rock blocks up to about 1 m in maximum dimension fell from the slope during the earthquakes and while most of the debris did not land on the road, some blocks in the area where the separation between the road and the toe of the cliff is at a minimum, landed on the city-bound lane.

Analysis of the cliff as part of the detailed design concluded that the likelihood of large scale cliff collapse failure of the cliff at this location is acceptably low and that the main geo-hazard to road users is the rockfall of discrete blocks of rock. Therefore, as part of the long term mitigation measures to address the rockfall hazard after removal of the shipping containers, it was proposed to install a double twist mesh drape over a length of about 100 m of cliff face extending the full height of the cliff (
Figure **6**).

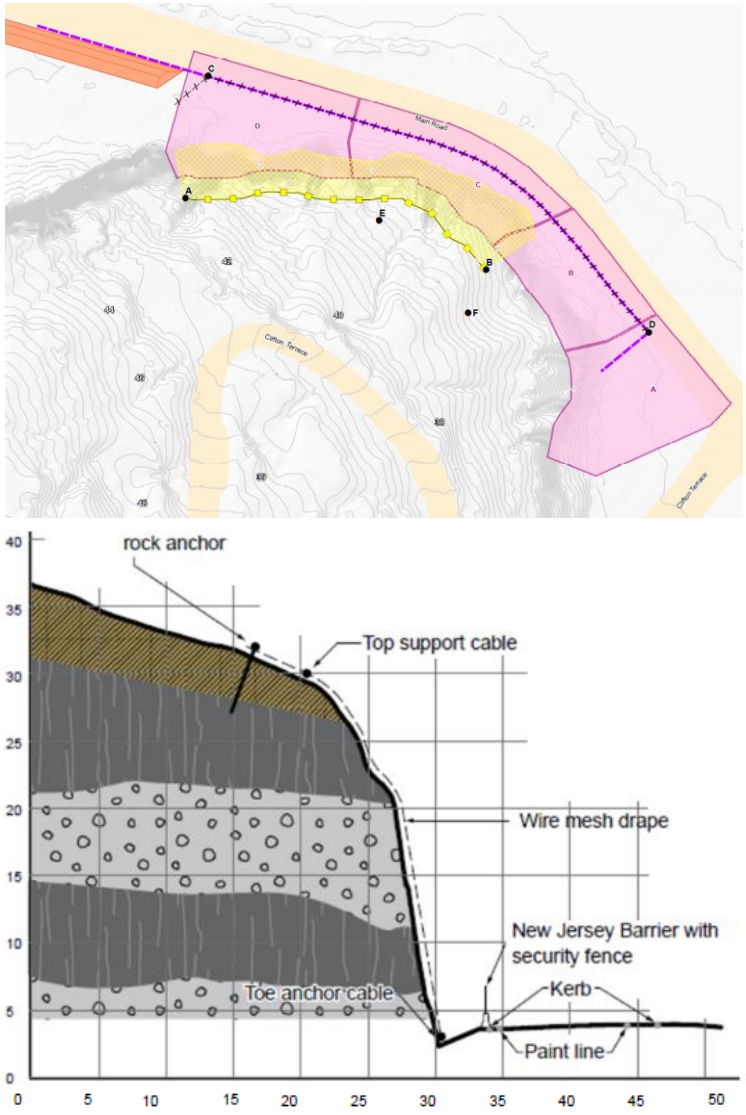

Figure 6. Clifton Hill rockfall mitigation: (top) Site plan with approximate extend of double twist wire mesh; (bottom) Typical cross section with proposed rockfall protection

3.2 Residual hazard

Due to the geometrical similarities (slope angle, height and irregularities) between Clifton Hill and the slope profiles used Section 2.3, impact energy and catchment width requirement were derived using equation (2) and (3) respectively. A design rock block for the rockfall hazard assessment of 500 kg was considered, corresponding to the maximum size of potentially unstable block. Indeed, larger blocks were either bolted to the slope or scaled prior to the installation of the drape. For the 500 kg design block, bottom impact energy is expected to be in the order of 160 kN whereas a minimum catch width of 4.8 m is required.

A minimum 5 m wide catchment area was therefore designed with a 1V:6H back slope covered with a loose granular cushioning material to absorb the kinetic energy of blocks potentially falling between the drape and the slope. Assuming normal and tangential restitution coefficients of 0.15 and 0.6 respectively (Giacomini et al., 2012), the maximum subsequent bounce height and resulting kinetic energy at the base of the slope are expected to be in the order of 0.7 m and 7 kJ. A 0.9 m high segmental concrete barrier was therefore installed adjacent to the road to provide additional rockfall protection.

4 CONCLUSIONS

This paper provides some insights on the performance of unsecured drapery systems. Based on field experiments and numerical analysis, the efficiency is discussed both in terms of kinetic energy reduction and trajectory confinement. The influence of block shape, block mass and slope irregularities was investigated using a DEM model. Results show that boulder mass is the most important aspect to consider when assessing the efficiency of a drapery and the residual hazard at the bottom both in terms of magnitude and areal extent.

Unsecured drapery systems are more efficient at reducing impact energy for smaller blocks than larger blocks. It was found that a 10 kg boulder may have its kinetic energy reduced to less than 50% its potential energy. Energy dissipation was observed to be minimal for blocks larger 500 kg. In addition, it was found that, as mass increases, the confining effect is reduced, from 2 m or less for a 10 kg boulder to up to 6 m for a 2,500 kg boulder. Two empirical relationships were derived to provide estimates the residual impact energy at the base of the slope and the minimum catch width requirement. An example of application is presented to illustrate how these relationships can be used to verify the suitability of additional measures to mitigate the residual hazard.

Ideally, site specific modelling should be performed to analyse the residual hazard associated with the installation of a drape, especially if slope characteristics differ from those presented in this study, i.e. 75° slope angle and a 30 m vertical drop or if the surface irregularities present on the slope fall outside of the range of scenarios covered in the sensitivity analysis.

REFERENCES

Bertrand, D. et al (2008) *Discrete element method (DEM) numerical modelling of double-twisted hexagonal mesh.* Canadian Geotechnical Journal, vol. 45: 1104-1117.

Giacomini, A. et al (2012) *Experimental study on rockfall drapery systems for open pit highwalls.* International Journal of Rock Mechanics and Mining Sciences, vol. 56, pp. 171–181.

Lambert, C. et al (2016) *Rockfall mitigation measures and design scenarios at the base of highwalls.* Proceedings of the 1st Asia Pacific Slope Stability in Mining conference. ACG Publishers.

Muhunthan, B. et al (2005) *Design guidelines for wire mesh/cable net slope protection.* Washington State Transport Center Report WA-RD 612.2.

Pierson, L.A. et al (2001) *Rockfall catchment area design guide*. Oregon Department of Transportation – Research Group. Report SPR-3(032).

Preh, A. et al (2015) *Stochastic analysis of rock fall dynamics on quarry slopes.* International Journal of Rock Mechanics and Mining Sciences, vol. 80, pp. 57-66.

Thoeni, K. et al (2013) *Discrete modelling of hexagonal wire meshes with a stochastically distorted contact model.* Computers and Geotechnics, vol. 49, pp. 158–169.

Thoeni, K. et al (2014) *A 3D Discrete Element Modelling Approach for Rockfall Analysis with Drapery Systems.* International Journal of Rock Mechanics and Mining Sciences, vol. 68, pp. 107–119.

Wyllie, D.C. (2014) *Calibration of Rock Fall Modeling Parameters*. International Journal of Rock Mechanics and Mining Sciences, vol. 67: 170–180.

Geological Inputs into the Waipori Dams Stability Review

L A King
Riley Consultants Ltd, Christchurch, NZ
lking@riley.co.nz

T Fritz
Trustpower Ltd, Tauranga, NZ
thomas.fritz@trustpower.co.nz

Keywords: Waipori, concrete arch dam, geological appraisal, geological mapping, dam stability

ABSTRACT

Three concrete arch dams (Mahinerangi Dam, Waipori Nos. 2 and 4) and one gravity weir (Waipori No.3) of varying ages provide the impoundments for the Waipori Hydro-electric Scheme. Findings of a comprehensive dam safety review carried out in 2012 indicated some knowledge shortcomings when assessing the stability of the No.2 and No.4 structures. It was proposed to fill these knowledge gaps by carrying out a multi-staged assessment of the two structures comprising a comprehensive desk study and gap analysis; fieldwork comprising detailed engineering geological mapping and intrusive geological investigation; determination of analysis parameters, and assessment of kinematically feasible failure modes to inform a Finite Element Method model build and analysis.

Whilst regulatory requirements are entirely different today to when the dams were initially constructed (1914 and 1956) and given that records of construction are minimal, this project demonstrates the importance of carrying out thorough reviews of historical records where they exist, prior to launching into deep and expensive site investigation. The reviews turned up several important documents which reduced site investigation inputs later and aided in building a clearer understanding of the history of work at the sites.

Geological mapping was a key element to understanding risk at the sites in a geologically complex setting, more so than intrusive investigation, which was carried out primarily to gain samples for strength testing. Geological mapping and traditional geological analysis tools such as aerial photo interpretation, stereonets and assessment of rock quality from boreholes have been critical for provision of rock mass properties and determination of potential kinematically feasible failure mechanisms of these ageing assets. The first stages of work have provided valuable inputs into the forthcoming finite element analysis (FEA).

1 INTRODUCTION

In the late 1990s, Trustpower's generation portfolio grew significantly through the purchase of a range of hydro generation facilities across New Zealand. These facilities had a diverse range of historical ownership and asset management methodologies. Trustpower's current dam portfolio contains 47 large dams (as defined by the New Zealand Building Act), with a variety of dam types and an age range from less than 10 to over 100 years. The dams are located in a wide variety of geological, seismological and hydrological settings. This level of diversity has always presented a challenge for dam safety and deficiency management.

Over the years dam safety regulations have been progressively promoted in New Zealand, however, there remains no specific dam safety regulatory framework in New Zealand. Rather dam safety is often addressed indirectly through the Resource Management Act (RMA 1991). In the absence of a specific regulatory framework, dam safety management is largely industry led

with guidance provided via the New Zealand Society on Large Dams (NZSOLD) Dam Safety Guidelines 2015.

1.1 Dam Safety Deficiency Management Programme

Since the late 1990s, Trustpower has needed to adopt a range of methodologies to manage dam safety and associated deficiencies. Trustpower developed its current approach in late 2014, which uses a Maturity Matrix approach. All structures and processes are broken down into manageable sub-categories and rated on a scale from Rating 1 ("Desirable") to Rating 7 ("Deficient"). This includes known deficiencies and areas of uncertainty. Two of those structures which were identified as having uncertainty regarding stability were the Waipori No 2 Dam and Waipori No 4 Dam, which are the subject of this paper.

1.2 The Project

Trustpower's 2012 Comprehensive Dam Safety Review identified uncertainties for both No. 2 and No. 4 dams with regard to their stability under earthquake loads. Trustpower initiated a project to establish if there is a deficiency. In order to confirm this, a modern day Finite Element Analysis (FEA) needs to be conducted including analysis for static, flood and seismic loadings. This paper discusses the steps that needed to be carried out in order to gain relevant information on the ageing dams prior to creating the model with a focus on the geological inputs required.

2 BACKGROUND

The Waipori Scheme comprises four dam or weir structures of varying ages. This paper focuses on Dam Nos. 2 and 4.

2.1 No.2 Dam

No.2 Dam is an 18.6 m high, concrete gravity arch weir. Having no spillway, the dam was designed to overtop and has a crest length of 52 m. Construction of the original dam is believed to have been completed in 1914. Following intrusive investigation into concrete strength carried out from 1969 to 1971 the dam was subsequently raised by 0.9m in 1963 and a further 1.2m in 1970 and strengthened with grouting and installation of anchors within the dam from 1973 to 1988.

2.2 No.4 Dam

Built in 1956, the No.4 dam is a concrete arch structure with a gravity spillway. It is 18.6 m high and has a crest length of 76.2 m. During a flood event in 1977 the right wing-wall of the spillway collapsed and was subsequently replaced. Otherwise, the dam stands as it was originally constructed.

2.3 Existing Information and Knowledge Gaps

It was recognised early in the project that information on the dams themselves was scarce and not collated in one location. This led to the first stage of the project being an assessment of existing records to determine knowledge gaps. Information was sourced from a variety of locations including the Waipori station, Dunedin City Council and Calibre Consultants Ltd in Dunedin (formally Duffill, Watts and King (DWK) the consultants for the scheme throughout the 1970s to 1990s).

The desk study phase of the project collated known information, but also uncovered useful documents in archived locations. These documents included historical photographs from construction, earlier geological mapping, in particular detail at No.4 dam, plans and sections for the dams, and an early Finite Element Analysis of No.2 and No.4 Dams carried out in 1992 by DWK.

While formerly unknown drawings had been found providing additional information on the foundation level of No.4, it was recognised that detailed as-built information was still missing for both structures, as well as any site observations recorded during construction. DWK carried out an assessment of concrete strength of No.2 dam for the 1970s to 1980s strengthening programme but present day assessment of concrete strength had been based on visual assessments only since that time for No.2 Dam, and only ever based on visual assessments for No.4 Dam. Additionally, there was no information at all on the founding material of No.2 Dam. While a 'geological appreciation study' was carried out in 1986 for No.4 Dam there was no determination of rock mass characteristics or intrusive geotechnical investigation at either structure.

In order for a modern day FEA to be carried out these knowledge gaps were required to be addressed.

3 SITE INVESTIGATION

3.1 Geological Appreciation

Overview

Bedrock in the area is known to comprise Haast Schist (Bishop & Turnbull 1996), exposed in mid-Cretaceous times by uplift on north to north-west trending faults. Subsequent erosion has resulted in the formation of a peneplain, which created gentle topography that has since been altered by post-peneplain faulting and folding. Haast schist in the region had been mapped as Textural Zone IIIA (Bishop and Turnbull, 1996). From site mapping it was determined that characteristics of the bedrock included well foliated quartzo-feldspathic schist with prominent quartz segregations parallel to foliation. Quartz veins that cross-cut foliation are notable by their absence. Pelitic (fine-grained) schist is dominant throughout the area, individual mica grains are fine sand sized discernible through hand-lens. Lineation in the form of rodding and bedding foliation intersections are evident. Using a re-appraisal of the Haast Schist Textural Zones (Turnbull et al, 2001), Haast Schist in the Waipori Hydro-Scheme area is considered to be Textural Zone III, defined on the basis of mica grain size and foliation penetration. Engineering projects throughout the region carried out within Haast Schist have faced difficulties as this material is known for well-defined foliation parallel shears that can result in large complex deep seated landslides and cause problems for slopes, cuts and structure foundations. The best known of these projects is likely to be the Clyde Dam construction.

Surficial deposits on gentler slopes comprise colluvium with schist derived quartz rich alluvial sediments found in some areas within the valley floor.

Two prominent faults are identified in the wider Waipori area (Bishop & Turnbull 1996). Both faults are classed as inactive by GNS Science (Bishop & Turnbull, 1996). The North Eastern Fault trends broadly north to south, traversing the eastern end of the Mahinerangi Reservoir, east of No.2 Dam and crossing the Waipori River approximately 400 m downstream of No.2 Dam (Bishop & Turnbull 1996). The McNamara Fault trends east to west along the Waipori Valley mapped to be passing 200 m south of the right abutment of No.4 Dam. Overall, the seismic risk in the area is relatively low in the New Zealand context.

No.2 Dam Geological Mapping

The No.2 dam is accessed via a gravel road that drops from the peneplain into the gorge. The road cut, the platform for the No.1 water supply tunnel and construction of the dam itself have resulted in excellent exposure of schist bedrock on both abutments down to foundation level. For geological mapping purposes the left abutment was accessed using safety ropes.

Exposed rock was consistent, noted to be moderately weathered, moderately strong with a fracture preference parallel to foliation. Foliation is well-developed and predominantly south dipping 30 to 40 degrees. Quartz segregations are typically 10 to 30 mm thick and comprise 20 to 30 % of the rock mass.

Surfaces are controlled by foliation and jointing. In addition to the joint set parallel to foliation there are three more dominant joint sets identified consistently in the area of the No.2 Dam.

No.4 Dam Geological Mapping

An earlier geological map (MacFarlane, 1986) uncovered in the desk study phase formed the basis of geological mapping at No.4 Dam.

On the left abutment of the dam, the schist is of good quality, moderately weathered, moderately strong with quartz segregations up to 50 mm thick, though typically less than 20 mm. Foliation attitude on the left abutment dips 20 to 30 degrees to east to north-east. By contrast, the right abutment is highly disturbed with numerous shear zones present, varying in character but with distinctly fissile rock mass sheared to fine to coarse, platy, angular gravel. Foliation orientation within shear zones is variable though broadly parallel to sub-parallel with the orientation of the McNamara Fault, with micro-folds (Figure 1) evident within some zones. The disturbed nature of bedrock on the right abutment is attributed to the proximity of the McNamara Fault which was mapped (MacFarlane 1986) as passing approximately 200 m to the south of the dam. Recently a new track has been cut on the river right of the No.4 reservoir, which exposes the fault. The zone of deformation is approximately 70 m in width at this location (consistent with the earlier DSIR report), highly disturbed, with a lack of distinct fabric. Material in the fault zone is predominantly extremely weak and when logged as a soil material is assessed to be moderately dense, light greyish brown sandy angular gravel. There are zones (up to 2 m diameter) of dark bluish-grey, highly plastic silty clay within localised pockets within the overall fault zone. Shear and crushed zones were noted up to 300 m on either side of the 70 m wide fault zone, including on the right abutment of the No.4 Dam. The fault appears to be high angle and downthrown on the southern side, indicative of a reverse thrust fault.

Figure 1: Micro-folds within shear zones in Haast Schist at No.4 Dam

3.2 Intrusive Investigation

No.2 Dam

Due to the consistency observed in outcrops around No.2 Dam, the intrusive investigation was limited to one borehole to assess the impact of weathering on the exposure and to obtain a sample for core testing. The borehole was drilled near the right abutment of the dam to a depth of 27 m. A distinct weathering profile was observed where at a depth of 7.1 m a clear colour change was noted and the rock changed from slightly weathered to fresh. Rock Quality Designation (RQD) in recovered core was 80 % consistent with geological mapping.

No.4 Dam

From mapping, a distinct change in rock mass quality was noted from the right abutment to the left. Previous mapping (MacFarlane, 1986) hypothesised the presence of a fault or shear zone within the dam foundation due to a change in foliation attitude from the left to right abutment and indeed the presence of the gorge in this location. However, the mapping carried out as part of

this project (and the original maps of MacFarlane) did not support a change in overall foliation attitude and rather indicate that the outcrop on the right abutment was highly disturbed likely due to the proximity of the McNamara Fault.

Although mapping provided more information there was still some uncertainty on the condition of the dam foundation at depth. Therefore, four boreholes were carried out to assess the change in rock mass and material properties across the footprint of the dam. As Trustpower wished to continue generation as much as possible throughout this time, the three vertical bores (BH4-2 to BH4-4) were drilled (20 m into the foundation) from a floating barge adjacent to the upstream face of the dam. The fourth borehole (BH4-1) was drilled from scaffolding on the upstream side of the right abutment, and inclined at 60 degrees into the right abutment using PQ triple tube coring to improve recovery of the fractured rock mass.

Other than the upper 10 m of BH4-1, core recovery was generally good, exceeding 90 %. The upper 10 m of BH4-1 had total core recovery of only 61 %. There was no apparent correlation of RQD other than that generally the upper 10 m of each borehole were more fractured than the remainder of the borehole. Results are skewed across the dam footprint by a change in core diameter as the size was reduced to HQ in better quality rock. An improvement of rock mass quality was also noted from right to left across the dam. The weathering profile is deeper on the dam abutments (up to 13 m) than in the reservoir base where only the upper 2 m to 3 m of rock was weathered. Dark orange brown staining is evident on many joints within the weathered zone indicative of water flow.

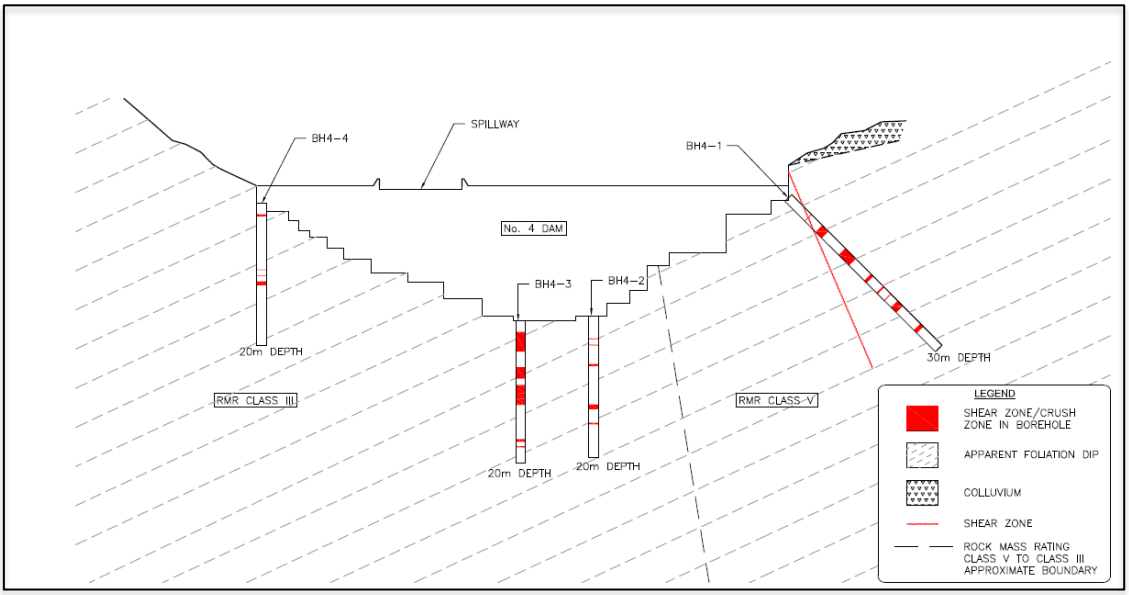

Figure 3: Cross Section of No.4 Dam showing encountered shear/crush zones.

Many crushed and sheared zones were noted on the borehole logs as shown in Figure 3. While it is possible that shear zones could daylight in the dam foundation (as proposed by MacFarlane 1986), in light of the recent investigation it was considered unlikely that one large crush or fault zone exists within the dam foundation, rather a number of smaller shears likely attributed to the proximity of the McNamara Fault.

Concrete Coring

An additional knowledge gap identified in the review relates to the strength of the concrete. Therefore, ten 140 mm diameter concrete core samples were obtained from the downstream face of each dam. Core samples were gathered by horizontally drilling into the downstream face of the dams using rope access contractors. Samples were obtained from intact concrete and across lift joints, as well as in areas known to have been grouted in the No.2 Dam strengthening works.

3.3 Laboratory Testing

Typical laboratory characterisation tests were carried out on both foundation rock and concrete cored from the dams. Additionally, elastic modulus testing and splitting tensile tests were conducted on the concrete, including tensile strength across construction lift joints.

Concrete Testing
Compressive strength, density and elastic modulus results were consistent with international studies on concrete strengths in dams greater than 30 years of age. All results showed concrete used in the older No.2 dam is generally of better quality than that tested from No.4 dam.

Splitting tensile strengths were converted to direct tensile strength using two methods, which gave consistent results of 1.5 MPa for No.2 Dam and 1.3 MPa for No.4 Dam. Test results over lift joints, where core was received at the laboratory intact and able to be tested, gave low tensile strengths. Due to the amount of broken sample a tensile strength of 0 MPa was used for lift joints.

Bedrock Testing
Density of the tested schist was consistent across the two dams with 27 kN/m^3 at No.2 Dam and 28 kN/m^3 at No.4 Dam. Unconfined Compressive Tests for intact rock strength ranged from 39 MPa to 60 MPa, with the mean being 51 MPa. The lower values correlated with rock sampled from the right abutment of No.4 Dam.

4 ASSIGNMENT OF MATERAL PROPERTIES FOR FEA

Material properties for the concrete within the dams were derived from site specific laboratory testing. For bedrock, however, it is not as simple as using the rock material parameters from laboratory testing, as testing was only undertaken on intact core samples and the results are not representative of the rock mass.

Hoek Brown failure criterion were derived for the right abutment of No.4 dam, however, this methodology was not considered appropriate for the remainder of the sites where foliation is dominant and foliation parallel joints sets tend to occur. Therefore, the Rock Mass Rating (RMR) System (Bieniawski, 1989) was utilised to take into account rock mass characteristics including defect spacing and orientation, Table 1 shows results.

Table 1: Rock Mass Rating (after Bieniawski, 1989)

Site	Strength	Drill Core Quality	Defect Spacing	Defect Condition	Groundwater	Orientation Adjustment	Rock Class
No.2 Left Abutment	7	17	15	25	15	-50	Class IV Poor
No.2 Foundation	7	17	15	25	7	-7	Class II Good
No.2 Right Abutment	7	17	15	25	4	0	Class II Good
No.4 Left Abutment	7	3	8	25	10	-5	Class III Fair
No.4 Foundation	7	3	5	30	10	-7	Class III Fair
No.4 Right Abutment	4	3	5	20	4	-25	Class V Very Poor

Using this system, the main areas of concern were highlighted as being the right abutment of No.4 Dam and the left abutment of No.2 dam.

5 FAILURE MODE ASSESSMENT

The investigations carried out at both dams have allowed the geological model to be verified, along with characterising the dam foundations and the dams themselves. Another input required was to determine kinematically feasible potential failure modes at the dams to determine if there are any potential failure planes or interfaces that needed to be specially considered as part of the FEA. A check on failure modes was carried out per NZSOLD Guidelines Section 6.92.

Failure via basal shear was discounted at both structures. Arch dams transfer load predominantly into the dam abutments and therefore basal sliding was not seen as a likely failure mechanism. Additionally, there is an absence of low angle defects to act as a slide plane at both sites.

Stereograph interpretation and use of the programme SWEDGE by Rocscience were used to determine wedge failure potential at the dams. This was also determined to be a low risk at both sites, generally due to quite favourably orientated foliation and joint sets.

A potential sliding failure mechanism was identified for the left abutment of the No.2 Dam. Historical photos of No.2 dam shows there does not appear to have been movement on this abutment since completion of construction (Figure 4a), however, it is noted that since raising the dam, water does now flow over the left abutment during dam overtopping events (Figure 4b). FEA analysis should assess the risk of block failure in this location and any impact this might have on abutment and dam stability.

Figure 4a: Historical photo of No.2 Dam, showing potential slide block, arrow indicates foliation plane and dashed line indicates potential block of instability (date unknown).

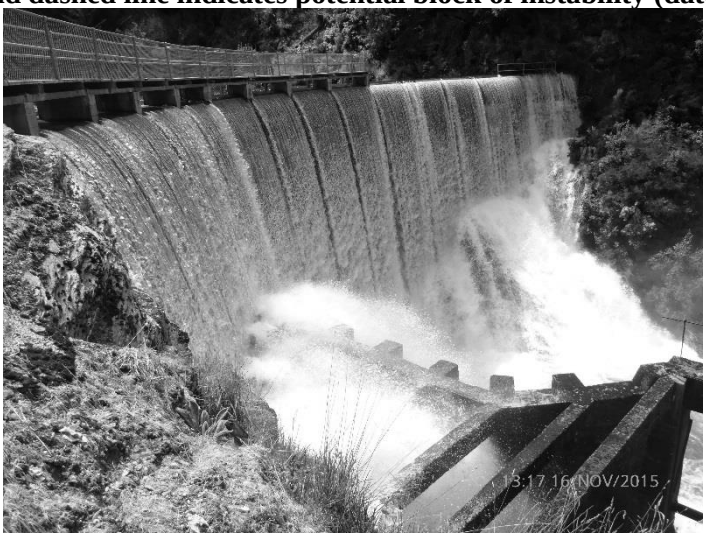

Figure 4b: Present day overtopping event at No.2 Dam (taken from downstream of right abutment, November 2015).

For the No.4 dam, the rock mass on the right abutment is highly jointed and sheared, and it is kinematically possible that a failure could develop through the jointed rock mass.

6 CONCLUSION

It can be a difficult and costly exercise to obtain the necessary inputs for modern day Finite Element Analysis in order to determine if ageing infrastructure meets today's standards for safety and stability. In the Waipori No.2 and No.4 Dam assessments, a review of available historical documentation and detailed geological mapping were both critical to carrying out an efficient and targeted intrusive geotechnical investigation. While investigation was still required to gain knowledge of rock and concrete strengths the main benefit of the intrusive investigation was providing ground truthing to the geological model in areas that could not be mapped (for example the reservoir foundation).

The definition of rock mass properties as a whole rather than just assessing intact rock strength will lead to more realistic inputs into the FEA. An assessment of kinematically possible failure modes using simple stereonet analysis allows advanced modellers to know which areas are of concern and which parts of their models they need to take a step further.

This study confirms that basic geological mapping and geological tools such as aerial photo interpretation, stereonet analysis and review of historical photos are still an important consideration in the world of 3D laser scans and complex modern day FEA. The outputs from advanced models will only be as good as the inputs gathered from basic site characterisation using traditional techniques.

7 ACKNOWLEDGEMENTS

We would like to acknowledge out client, Trustpower Ltd who has allowed the project to be showcased and also Don Tate at Riley Consultants Ltd for providing review.

REFERENCES

Bienawski, Z., (1989) *Engineering Rock Mass Classifications: A Complete Manual for Engineers and Geologists in Mining, Civil and Petroleum Engineering.* New York: Wiley-Interscience.

Bishop, D.G., Turnbull, I.M. (compilers) (1996) *Geology of the Dunedin Area.* Institute of Geological and Nuclear Sciences, 1:250,000 geological map 21. Lower Hutt, New Zealand.

MacFarlane, D. (1986) *Geology of the Waipori No.4 Dam and Site Area*. Department of Scientific and Industrial Research.

Turnbull, I.M., Mortimer, N. and Craw, D. (2001) *Textural zones in the Haast Schist – a reappraisel*, New Zealand Journal of Geology and Geophysics, 44:1, 171-183.

Underlying failure mechanism and spatial extent of the Omoto Slip, Greymouth, New Zealand

H G B Jenkinson
Faculty of Geology, University of Canterbury, NZ.
hgj18@uclive.ac.nz (Corresponding author)

D H Bell
Senior Lecturer in Engineering & Mining Geology, University of Canterbury, NZ.
david.bell@canterbury.ac.nz

Keywords: Slope Stability, Mass wasting, Rotational failure, MID

ABSTRACT

The underlying failure mechanism at the Omoto Slip is translational soil creep of the 5-30 m thick colluvium cover over the Kaiata Mudstone bedrock erosional surface that extends across the entire Omoto slope area. This is driven by major evacuative failures at the toe of the slope. These rotational failures occur during 1 in 20+ year flooding events due to the elevated lower water table increasing hydraulic pressures, creating buoyancy and decreasing the frictional strength of the colluvium. Flooding instigates translational creep along the bedrock erosional surface due to the removal of toe material moving the slope away from equilibrium geometry causing secondary rotational failures and creep to occur. These are assisted by the highly active and variable perched aquifer system within the colluvium that responds to intense rainfall runoff only. The detachment mechanism for the rafted limestone blocks from Peter Ridge are planar and wedge sliding or direct toppling. Large scale failures and high rates of movement are concentrated at McKendries Corner. The large spatial area and random locations of these failures create issues when trying to increase stability across the site. However, the most effective mitigation measure is surface drainage. The site's current system needs maintenance and repairs to ensure efficiency. Riprap scour protection along the edge of the Grey River is also suggested.

1 INTRODUCTION

The Omotomoto (Omoto) Slip, 2 km east of Greymouth has been detrimental to State Highway 7 (SH7) and the KiwiRail Midland Line (MID) that traverse it at the base since 1894. The situation is inherently complex with an approximate lateral limit of 2.5 km (Figure 1). The slip comprises of colluvium, limestone scree and large discrete (> 40,000 m^3) rafted limestone blocks. Movements are governed by the hydrological system, driven by the highly variable rainfall patterns of the Westland region that affect river levels and surface runoff. The following authors; McLean & Read, 1975; Galloway, 1977; Mansergh, 1977 a & b; Paterson, 1984; Mclean, 1987; Leung, 1988; Paterson, 1989 a & b; Golder Associates (NZ) Ltd, 2002; Justice, 2012; ENGEO, 2015, have summarized the site during geotechnical investigations and stability works. However, these are primarily focused on the small portion of the area that failed at that specific time. The mechanism and trigger for these individual failures is well understood. However, there are contradicting statements on the major underlying basal failure mechanism that covers the greater site, whether it is a deep seated rotational failure or translational creep. The presence and effect of the rafted limestone blocks is also poorly understood. Furthermore, previous field maps convey conflicting spatial extents with no evidence for the portrayed head scarp.

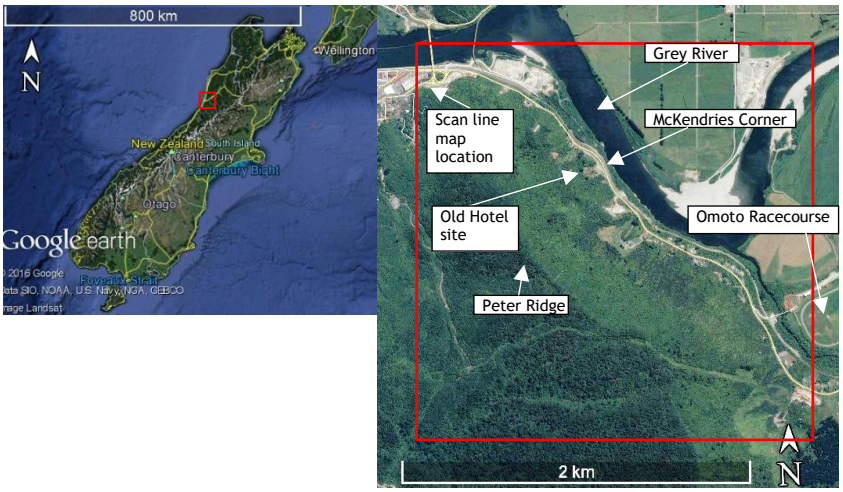

Figure 1: Red square representing the study area, approximately 5.25 km^2. Images retrieved from Google Earth.

2 RESEARCH METHODOLOGY

2.1 Literature Research and Desktop study

A systematic literature review and desktop study was undertaken to understand the geological evolution and history of the Omoto Slip. Reviewing previous geotechnical reports and literature in a chronological order provided an insight into how the understanding of the slip has evolved over time, highlighting contradictions between authors which create uncertainties in the current understanding.

2.2 Engineering Geology/Geomorphic Mapping

Initial mapping was undertaken by stereographic imagery analysis, accompanied with high resolution aerial photography and LiDAR data supplied by the West Coast Regional Council (WCRC). Critically reviewing current maps derived by Suggate, 1953; Mclean & Read, 1975; Mansergh, 1977a; Mclean, 1987; Leung, 1988; Paterson, 1989a; Golder Associates (NZ) Ltd, 2002; Justice, 2012; ENGEO, 2015, enabled cross checking and validation. The first-edition map compiled is thus a rendition of past mapping, assisted with remote mapping techniques that were not available in previous efforts. This stage identified where in-depth field mapping should then be focused. A geological compass, map board with mylar and a handheld GPS was used. The final map is presented as Figure 2. This map was digitally complied using Inkscape drawing software to ensure high resolution and usability.

2.3 Rafted Limestone Blocks

The detachment mechanism for the large Cobden Limestone blocks across the site was assessed in the stereographic computer program "DIPS" by Rocscience. A scan line map was drafted, accompanied by recording all structure in a 1 m^2 area on the mapped rock face. The structure observed and recorded was then assessed for kinematic feasibility for all failure styles. This analysis is portrayed on Figure 4.

2.4 Engineering Geology Block Models

Block models are a fundamental tool for portraying critical geological and geotechnical characteristics and parameters in one, salient 3D diagram. The 3D nature allows for a spatial and temporal insight into the controls and links between the geomorphic, geotechnical and subsurface geological structure allowing for the interpretation and understanding of an engineering geology

phenomenon, such as a landslide (Figure 3). Conversely, aerial photography and 2D maps do not have the ability to tie these links together, creating a disconnection between surface expression, processes and subsurface structure, leading to confusion of the situation (Parry et al. 2014).

3 RESULTS

3.1 Literature review and desktop study

3.1.1 History of the Omoto Slip

The Omoto site is inherently complex with variable rates and scales of slope instability within the area. Five large evacuative failures have occurred since 1894 causing damage and delays to both SH7 and the MID; 1913, 1954, twice in 1972 and once in 1984 (Justice, 2012). Smaller scale failures and soil creep have occurred in-between, causing continued deflection to both life lines. The major failures are attributed to high flood stage levels of the Grey River and intense rainfall runoff in the local catchment, although, Golder Associates (NZ) Ltd (2002), suggest failures in 1954 and once in 1972 were related to earthworks. The failures across the site have led to many geotechnical studies and investigations, with major work re-aligning SH7 and the MID though McKendries Corner. However, failures and creep continue to disrupt this segment, with a permanent speed limit of 10 km/hr between 209.45 km to 209.7 km rail markers on the MID and 80 km/hr on SH7.

3.1.2 Geology

The tectonic regime from the convergent Alpine Fault system has folded and faulted Mesozoic Torlesse composite terrane units into a series of anticline and synclines. The north-south trending Brunner Anticline has a west dipping limb in the Cobden Limestone Member of the Nile Group (nc) which is underlain conformably by the Port Elizabeth Member of the Kaiata Mudstone Formation (rkp) (Nathan, 1978) (Figure 2). Bedding is typically dipping at 25-30° W, creating a scarp slope on the eastern slope (Mansergh, 1977b). The Omoto site is blanketed by 5 – 30 m of colluvium composed of limestone screes, rafted limestone blocks and weathered mudstone over lying the 15° erosional surface of the Kaiata Mudstone bedrock (McLean, 1987). Reports suggest the underlying failure mechanism of the Omoto Slip could be either a deep seated rotational failure (Suggate, 1953; Mansergh, 1977a) or a shallow translational failure (Paterson, 1984 &1989a; Justice, 2012).

3.1.3 Hydrology and hydrogeology

Failures throughout the Omoto area are governed by the complex hydrogeological system present. Two water tables have been identified by (Mclean 1987; Paterson 1989 a; Justice, 2012). 1) The lower is directly related to the Grey River. Christensen, Throssell, & Ferg (2012) conducted a hydrological assessment of the Grey River in 2012. Flood stage heights of 4, 5 and 7 m above sea level have return periods of 2.33, 5 and 100 years respectively. There is no tidal effect on this water table. 2) The upper, a perched aquifer system within the colluvium, confined by the Kaiata Mudstone bedrock. The highly heterogenous hydraulic conductivities over the site created by multiple scree deposits, boulders and rafted limestone blocks allow fast water ingress into the low permeably mudstone derived colluvium (Justice, 2012).

3.2 Spatial extent

Remote and field mapping identified there is no head scarp at the base of the Peter Ridge, indicating the slip is in fact comprised of multiple rotational failures within the colluvium that is also translating along the erosional surface, which is not bound to a lateral limit (Figure 2 & 3). Previous literature and field mapping confirm scale and rates of movement are concentrated in the centre portion of the segment at McKendries Corner.

3.3 Failure mechanism

3.3.1 Omoto Slip

Two types of failure have been observed from reviewing literature and field observations. The underlying failure style across the entire site is translational soil creep (mass wasting) along the Kaiata Mudstone erosional surface. This includes the rafted limestone blocks and colluvium material. Secondary failures are defined as rotational, limited to the colluvium material (Figure 3). There is no feasible evidence for a large deep seated rotational failure to be extending into the Kaiata bedrock due to the scarp slope bedding geometry.

3.3.2 Limestone blocks

Kinematic analysis in the program DIPS identified there are three styles of joint controlled failures that can occur in the Cobden Limestone (Figure 4). Planar sliding, direct toppling and wedge failure can all feasibly occur, acting as the failure mechanism for the detachment of the >40,000 m^3 limestone blocks that are scattered across the McKendries Corner zone of the site. These blocks have tumbled or slid into the current location.

4 DISCUSSION

4.1 Spatial extent

The spatial extent of the Omoto Slip cannot be clearly defined due to the absence of a head scarp. Failures are observed to occur over the entire slope from the limestone/mudstone contact near the Grey River bridge to the Omoto Racecourse, where the two life lines move away from the slope. Therefore, the entire slope is unstable with rates of movement and the scale of failures increasing at McKendries Corner. This is thought to be governed by the limestone blocks and associated discontinuities that are promoting surface water to pool and percolate into the colluvium. Areas either side of McKendries Corner which do not have these limestone blocks and hummocky surface expression do not portray the same scale and rates of movement. A defined scarp has not been drawn onto Figure 3 in this study. Instead, a red box indicates the area where the greatest creep rates, scale and reoccurrence of failures is occurring.

4.2 Failure mechanism

4.2.1 Omoto Slip

The presence of the Grey River at the immediate base of the slope is the primary trigger for slope movements by undercutting and eroding toe material. Additionally, during a major flooding event (> 1 in 20 yr) the lower water table contributes to failures due to increased pore water pressures, creating uplift and buoyancy in the toe. Reduction in shear resistance also occurs and as the water recedes the rapid draw down causes large evacuative failures to occur. Thus, the slope falls away from equilibrium geometry, which causes translational creep and secondary rotational failures in the upper areas of colluvium as it moves back towards equilibrium state. These secondary failures are assisted by the upper water table which responds to intense rainfall events and subsequent water ingress. Limestone scree and rafted blocks allow for high permeability, while colluvium derived directly from the Kaiata Mudstone bedrock does not. Creep is identified to occur continuously, however the rates are exacerbated when a large evacuative failure occurs at the toe. A protection and or support structure along the western bank of the Grey River may assist in mitigating these failures, reducing creep rates. Surface run off is removed from the lower areas of the slope via concrete channels and culverts. This system was observed to be overgrown, full of rubbish and debris and in places damaged causing the system to fail.

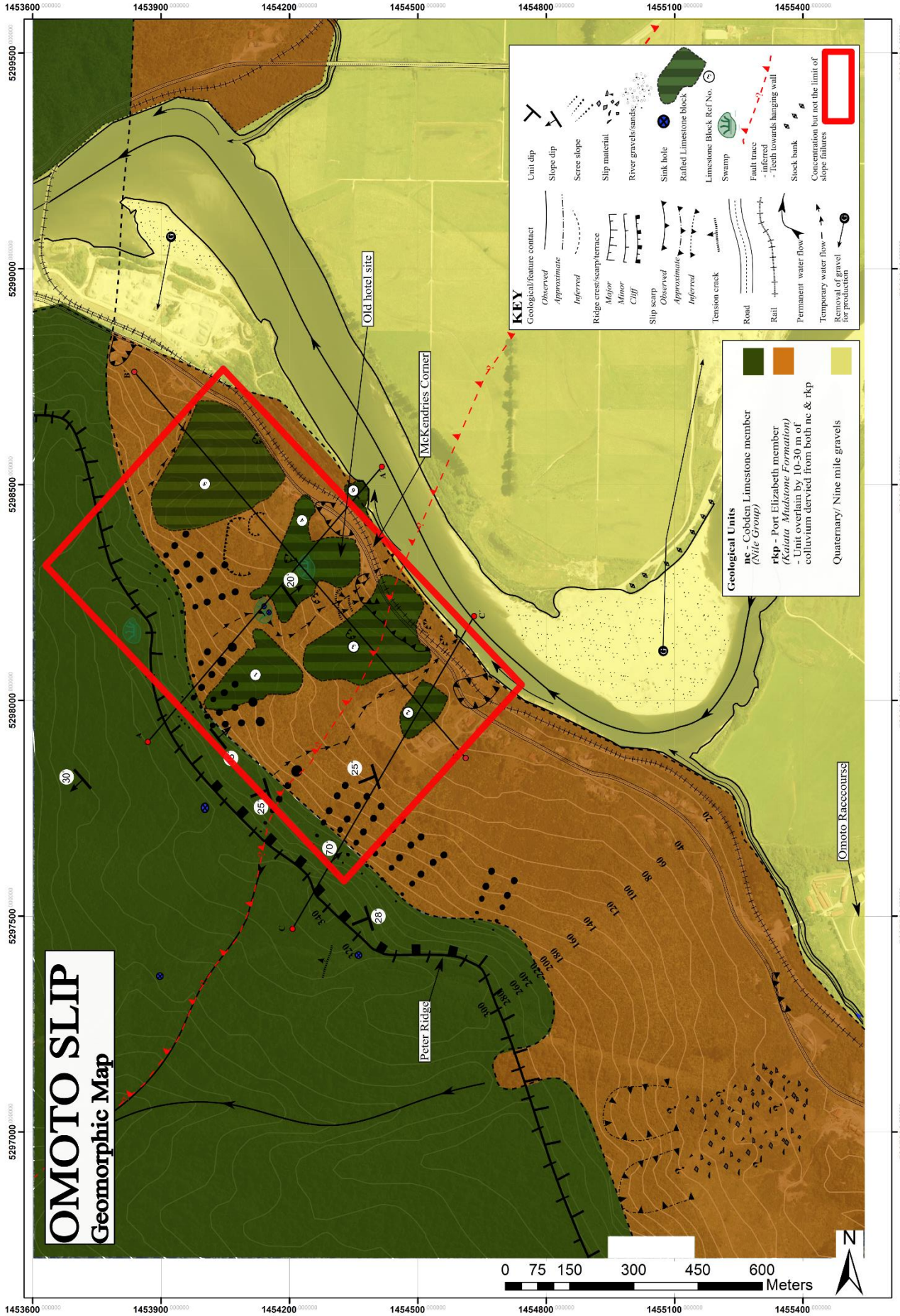

Figure 2: Geomorphic map of the Omoto area

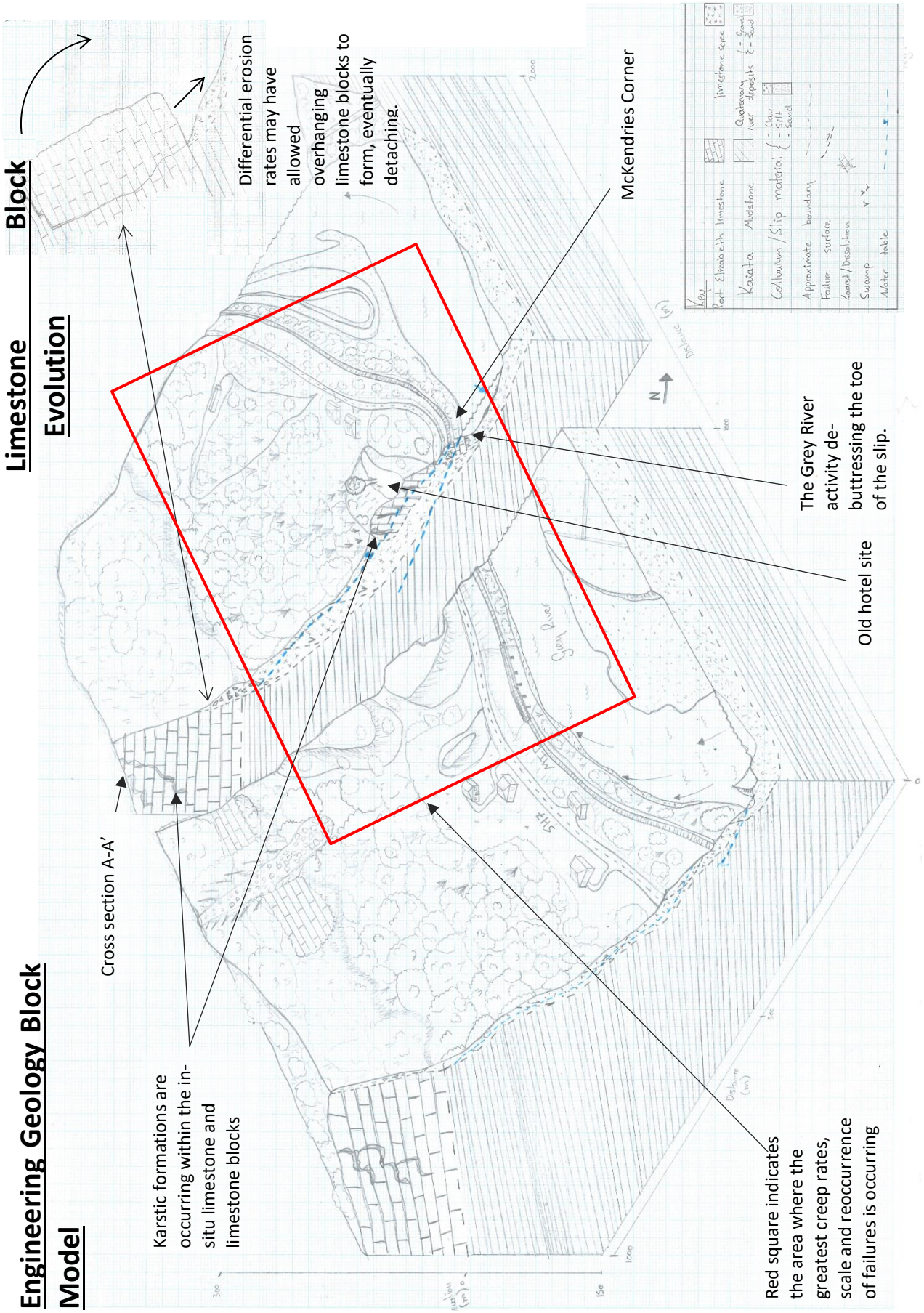

Figure 3: Schematic engineering geology block model portraying the Omoto slip in 3D

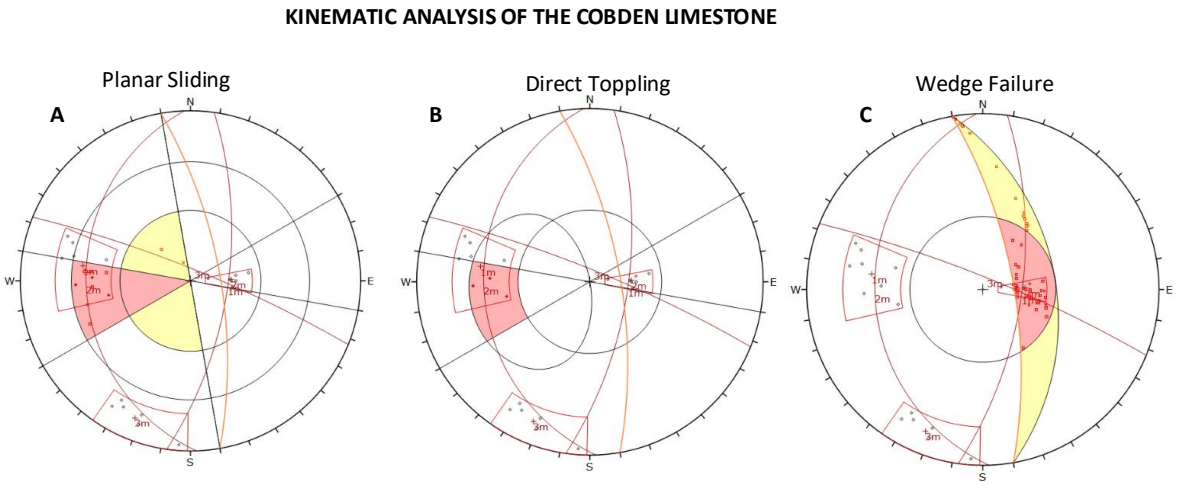

Figure 4: Kinematic feasibility analysis for the detachment of the rafted limestone blocks

4.2.2 Limestone Blocks

There are multiple stages in the formation 40,000 m^3 to 1,750,000 m^3 limestone blocks. The differential erosion rates between the Cobden Limestone and Kaiata Mudstone could allow for a large overhang to form. With only some of the beds showing close to moderate spaced discontinuities it is possible that beds showing no jointing structure on available outcrops, in fact have joints at very wide intervals (15-25 m) which have formed perpendicular to the principal stress created by the regional tectonic regime (Gonzalez de Vallejo & Ferrer, 2011). With the assistance of karst processes and internal weathering it becomes feasible for these large limestone blocks to detach via planar/wedge failure or direct toppling off the Peter Ridge face (Figure 3 & 4). Furthermore, Mansergh (1977 a) suggests rafted limestone blocks 2 and 5 portray disorientated bedding while the others portray similar orientations to in situ, indicating some have tumbled down slope, while others have simply slid to the current location.

5 CONCLUSION

The multi-component situation at the Omoto Slip is driven by primary large scale evacuative failures at the base of the slope which in turn, causes the rest of the slope to move back to an equilibrium state via creep and secondary rotational movements (mass wasting). The hydrological and hydrogeological systems present are the driving factor for the instability, thus they need to be managed successfully. Field investigations revealed there is no defined head scarp, nor any indication of it terminating at the fringes, indicating the site is bound within the colluvium mass which is translating along the erosional surface of the Kaiata Mudstone. Major failures are concentrated at McKendries Corner due to the presence of the large discrete limestone blocks with smaller scale failures occurring at either side. These large rafted blocks are detaching from the Peter Ridge via planar and wedge sliding or direct toppling. Some have toppled down slope, while others have slid along and within the colluvium surface, confirmed by the current bedding orientations. The multi-component hydrological and hydrogeological system present is the governing factor for the two failure mechanisms present. Understanding and mitigating the effect this system has on the geotechnical characteristics of the soils and rocks present is imperative to increasing stability across the site. Mitigation efforts should be focused on repairing and maintaining the existing drainage system that is not effective in its current state. Further efforts could be implementing riprap scour protection and or buttress for protecting the toe of the slip.

REFERENCES

Christensen, K., Throssell, B., & Ferg, D. (2012). *Hydrology for Omoto Landslide Assessment*. Wellington: Pattle Delamore Partners.

ENGEO. (2015). McKendries Corner Slope Movement, Omoto Landslide, Midland Railway line. Christchurch: *Geoscience*.

Galloway, J. H. (1977). *Omoto Half Bridge Greymouth*. Christchurch: Ministry of Works and Development.

Golder Associates (NZ) Ltd. (2002). *Geotechnical Assessment of SH 7 Kaiata to McKendries Realignment of I&R*. Greymouth: Golder Associates NZ.

Gonzalez de Vallejo, L., & Ferrer, M. (2011). *Geological Engineering*. London: CRC Press.

Justice, R. (2012). *Risk management strategy Omoto landslide Midland line 208-10 km*, draft for comment. Geoscience Consulting.

Leung, P. (1988). SH 7: *Omoto Slip Investigations Geotechnical Study*. Works and Development Services Corporation.

Mansergh, G. D. (1977 a). *Slope stability in the Omotu Slip*. Wellington: NZ Geological Survey.

Mansergh, G. D. (1977 b). *Omoto Slip NZMS 1-S44*. Christchurch: NZ Geological Survey.

McLean, J. D. (1987). SH7 *Greymouth, Omoto Slip Investigations*. Engineering Geology. Christchurch: NZ Geological Survey.

McLean, J. D., & Read, S. A. (1975). *Proposed housing development, Omoto, Greymouth geological report*. Wellington: NZ Geological survey.

Nathan, S. (1978). *Geology of the Greymouth area 1:63,360*. Wellington: Institute of Geological & Nuclear Sciences Limited.

Parry, S., Baynes, F. J., Culshaw, M. G., Eggers, M., Keaton, J. F., Lentfer, K., . . . Paul, D. (2014). Engineering geological models: an introduction: IAEG commission 25. *Bulletin of Engineering Geology and the Environment*, 73(3), 689-706. doi:10.1007/s10064-014-0576-x

Paterson, B. (1989b). *Omoto Slip Drilling*. Christchurch: Department of Scientific and Industrial Research.

Paterson, B. R. (1984). *Engineering Geological Immediate report 84/031: Investigation of Recent Movement of Omoto Slip, Greymouth.* New Zealand Geological Survey.

Paterson, B. R. (1989a). *SH7 Omoto Slip, McKendries Corner*, Greymouth Engineering Geological Investigations. Wellington: NZ Geological survey.

Suggate, R. P. (1953). Sheet 44 - *Landslips on the Greymouth-Omoto Railway and road*. NZ Geological Survey.

Typical values of the CPT cone factor, N_{kt}, in Auckland clays

M Holtrigter, A Thorp & R D Barnes
Ground Investigation Limited, Auckland, NZ
marco@g-i.co.nz (Corresponding author)

Keywords: Cone penetration test, CPT, dilatometer, DMT, cone factor, N_{kt},

ABSTRACT

The near surface geology of the Auckland area generally comprises alluvial soils, volcanic tuff/ash and/or residual soils. These soils may be expected to display different engineering characteristics given their different geological origins. The soils are mostly cohesive and the undrained shear strength, s_u, is of geotechnical interest. The cone penetration test (CPT) allows an estimate of s_u to be made via application of bearing capacity theory using a cone factor, N_{kt}. Typically, N_{kt} varies from 10 to 18, depending on the soil type, so it is often necessary to compare with a reference test to determine the N_{kt} factor that is appropriate for the soil type on a site-specific basis. In this study, we have undertaken flat dilatometer tests (DMT) next to CPT tests at various sites in Auckland with the DMT acting as the reference test. In this way, typical N_{kt} factors for the different geological units have been suggested.

1 INTRODUCTION

The undrained shear strength of a cohesive soil can be estimated using the cone penetration test (CPT). This is usually done by utilising a cone factor, N_{kt}. The N_{kt} value is generally not known and can vary over a large range depending on geology and soil type. This often leaves the geotechnical engineer having to guess what N_{kt} value to use, if there are no reference tests to help establish a site specific correlation. The purpose of this study is to help provide an indication of what N_{kt} values may be applicable to the different soil types in Auckland by using the DMT test as a reference test.

In this study, the authors have selected 50 side-by-side CPT and DMT tests from various sites of various geological units across Auckland. The results have been compared to help determine suitable N_{kt} values.

2 BRIEF GEOLOGY OF AUCKLAND SOILS

The geology of Auckland is shown on the GNS Geological Map and described in the associated booklet (Kermode, 1992). In general terms, the near surface soils in the Auckland area are predominately cohesive (silts and clays) but have been formed by different geological processes. The most recent deposits (Holocene) are marine sediments in the harbours and under reclaimed land, and localised areas of stream and flood plain alluvium. A large proportion of the surface geology of Auckland is alluvium of the Tauranga Group (mostly Pleistocene), which comprise mostly firm to stiff silts and clays, but also contains Pumice material from the Taupo Volcanic Zone as well as significant deposits of peat in places. More recent volcanic deposits from the Auckland Volcanic Field provide a coverage of tuff and ash (as well as Basalt lava flows and scoria) over parts of Auckland. The tuff and ash have generally weathered to form soft to very stiff sandy or silty clays. The volcanic soils can be interbedded or interspersed with the sedimentary alluvial deposits. The Waitemata Group sandstones and siltstones (Miocene), which

underlie most of the Auckland area, form a mantle of residual soil (silts and clays, some sand) over a deep weathering profile. The Waitemata Group residual soils often present at, or near the surface. To the east of Auckland, uplifted Greywacke (Mesozoic) through the line of the Hunua ranges, is exposed in Waiheke and Motutapu Islands of the Hauraki Gulf, weathering to clays at the surface.

Although the near surface soils are mostly clay-like, they vary in plasticity and silt content, are sandy in places, are usually layered and almost always non-homogeneous. This adds a further complication to the varying geological origins, which provide different clay minerology and (macro and micro) structural effects. This makes establishing correlations to geotechnical soil parameters difficult and standard correlations that are based on well behaved 'text book' soils may not be applicable.

3 UNDRAINED SHEAR STRENGTH

The undrained shear strength, s_u, is not a unique soil property. It varies depending on the mode of failure, the stress state of the soil, anisotropic effects and rate of failure. Furthermore, in situ tests may not necessarily be fully drained, as may be the case for silty soils, and so not truly represent undrained shear strength.

Kamei (1996) showed that anisotropy is a significant factor by comparison of isotropic consolidated triaxial tests (CIU) with K_0 (coefficient of earth pressure at rest) consolidated triaxial tests (CK_0U). Figure 1 shows that the CK_0C tests give lower undrained shear strengths than the CIU tests, both in compression and extension. This figure also shows that tests in extension are significantly less than tests in compression, which illustrates variation due to mode of failure. Mayne (2016) also illustrated the effect of failure mode on s_u, as illustrated in Figure 2. There may be a factor of 6 between the highest and lowest measured undrained shear strengths – of the same soil! The figure also illustrates the hierarchy of s_u from highest to lowest, being: field vane test, triaxial compression, direct simple shear (DSS) and triaxial extension.

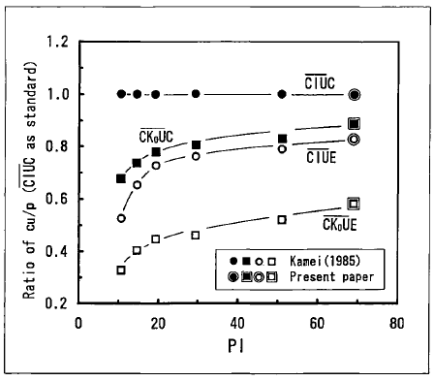

Figure 1: s_u variation between isotropic and K_0 consolidated triaxial tests (Kamei, 1996)

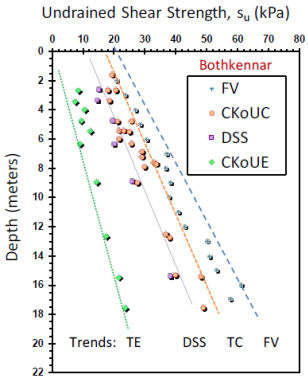

Figure 2: s_u variation between tests of different failure mode (Mayne, 2016)

This presents a problem as to which test to use as a reference test when correlating to another test, in this case, the CPT. Mayne (2016) suggests that the DSS mode is most appropriate. This mode presents s_u results that fall more-or-less mid-way between the other test modes and thus provides an 'average' result. It is also the mode that best relates to the SHANSEP method (Stress History and Normalised Soil Engineering Properties) (Ladd et al 1977) and theory of critical state soil mechanics (Wroth, 1984). The DSS represents the simplest form of shearing.

By the SHANSEP method (Ladd et al. 1977):

$$s_u = 0.22.OCR^{0.8} \quad (1)$$

where

σ'_{vo} = the effective overburden pressure and OCR = overconsolidation ratio.

The terms 0.22 and 0.8 in equation (1) are averaged values of a narrow range of variables determined experimentally. A similar relationship can be derived theoretically using critical state soil mechanics (CSSM) (Wroth, 1984):

$$s_u = ½ \sin\phi'.\sigma'_{vo}.OCR^{\Lambda} \quad (2)$$

where

ϕ' = effective angle of friction and $\Lambda = 1 – c_s/c_c$.

and

c_s and c_c = swelling and compression index, respectively

Both the SHANSEP method and the CSSM methods are related to the DSS mode of undrained shear strength.

3.1 Undrained shear strength from CPT

The undrained shear strength of clays can be estimated from CPT results using the following equation (Lunne et al.):

$$s_u = q_{net}/N_{kt} \quad (3)$$

where

q_{net} = net cone resistance ($q_c – \sigma_{vo}$) and N_{kt} = cone factor

Equation (3) is a direct application of bearing capacity theory, where N_{kt} is then the bearing capacity factor for the cone. N_{kt} is determined empirically, usually by correlation to a reference test. Typically, N_{kt} is between 10 and 18, with an average of 14 (Robertson and Cabal, 2015).

There are other methods of estimating s_u, such as by using effective cone resistance, by using excess pore water pressure, by cavity expansion, or by critical state soil mechanics (Mayne, 2016). However, equation (3) is the most common method.

3.2 Undrained shear strength from DMT

A correlation for undrained shear strength from DMT was established by Marchetti (1980), via the relationship with OCR:

$$OCR = (0.5.K_D)^{1.56} \quad (4)$$

Where

K_D = horizontal stress index (strongly correlated to K_0)

By applying the SHANSEP method, represented by equation (1), the relationship for s_u becomes:

$$s_u = 0.22.(0.5.K_D)^{1.25} \quad (5)$$

This relationship has been found to provide a reliable estimation of undrained shear strength by numerous researchers (e.g. Lacasse & Lunne, 1988 and Powell & Uglow, 1988). However, most research has been in soft to firm normally to moderately overconsolidated sedimentary clays. Marchetti (2015) stressed that equation (5) is applicable only to 'text book' clays.

4 SIDE-BY-SIDE CPT AND DMT RESULTS

25 sets of CPT-DMT sounding pairs have been selected for this study from the Ground Investigation Ltd's database. These have been supplemented by borehole information from the New Zealand Geotechnical database to assist with identifying geological units. The approximate locations where the tests were performed are shown on Figure 3. The pairs were selected based on distance between tests (less than 10m), availability of nearby borehole information and uniformity of ground conditions between tests. It was difficult to find tests that met the last criteria as most of the sites display layered soils and lateral variation.

Figure 3: Approximate locations of test sites used in this study

The data was separated into groups according to geology. The geological units chosen being; Marine Sediments; Peat; Alluvium; Volcanic soils; Residual Waitemata Group soils and; Residual Waipapa Group soils (Greywacke). Some cleaning of the data was carried out by way of depth shifts and removal of anomalies, such as inconsistent spikes in data. The data was then plotted on graphs of q_{net} vs CPT_{DMT}. These are shown on Figure 4 for the various geological units.

4.1 Marine Sediments/Intertidal Mud

There are only two data sets of Marine Sediments used in this study. These are from the tidal mudflats adjacent to the SH16 causeway on Auckland's northwestern motorway. The plot on Figure 4(a) suggests an N_{kt} of 6 with a strong correlation. The soils here are normally or very slightly overconsolidated sedimentary soils and so should behave as a 'text book' soil and so the

DMT derived s_u should be reliable. The $N_{kt} = 6$ seems low considering the typical range, however, Lunne et al. (1997) showed that N_{kt} decreases with increasing B_q (normalised pore pressure ratio). In very sensitive fine-grained soils, where B_q is around 1.0, the N_{kt} can be as low as 6. The CPT plots from this data set show B_q at 1.0 or slightly higher (indicating sensitive soil). In this instance, $N_{kt} = 6$ appears correct. This validates to some extent the use of the DMT as a reference test. It also highlights the need to consider the porewater pressure response and the need for good

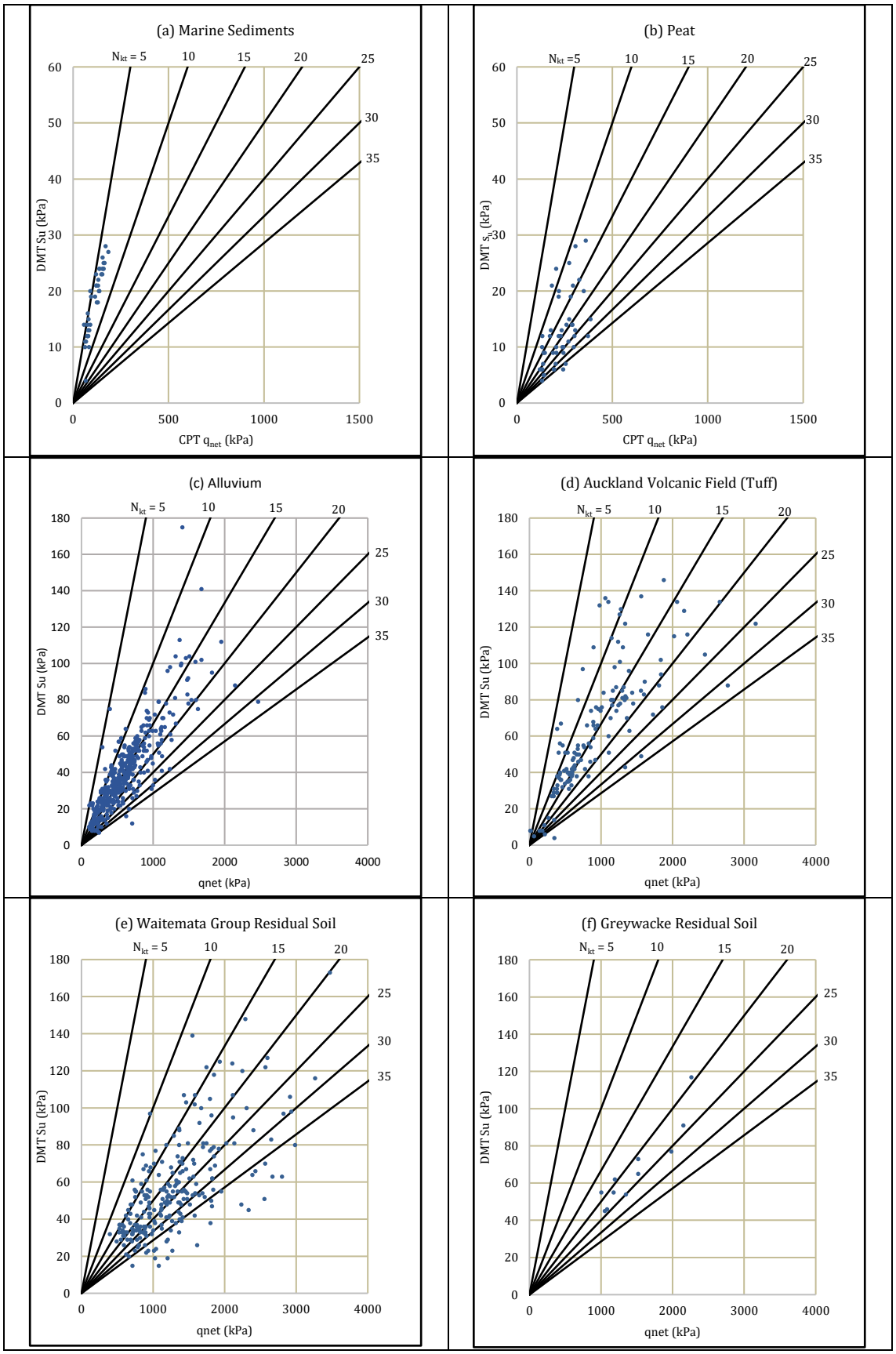

Figure 4: Plots of DMT derived s_u vs. CPT q_{net}

u_2 readings in soft clays. Alternative methods of determining s_u by excess porewater pressure or by effective cone resistance should also be considered in these soft deposits.

Figure 5(a) shows a depth plot of DMT derived s_u overlain with the s_u derived from an adjacent CPT using N_{kt} = 6. The marine sediment/mud is underlain by older alluvial materials, to which Nkt = 15 appears to be applicable (see Section 4.3 below).

4.2 Peat

There is one DMT-CPT pair in peat soil. At this site, the peat is mostly amorphous, tending to organic clay in places and with some fibrous material. Figure 4(b) shows the resulting plot of DMT s_u and CPT q_{net}. There is considerable natural variability in this material and, therefore, it is difficult to get an exact match between the CPT and DMT data. Hence the plot shows a reasonable scatter. However, an average value of N_{kt} = 15 could be taken from that plot. When the DMT su is plotted with depth along with the CPT su derived from N_{kt} = 15, as shown in Figure 5(b) there is reasonable agreement considering the variability of the soil.

4.3 Alluvium

The data for the Alluvium set is mostly in the Puketoka Formation of the Tauranga Group, but may also include some more recent (Holocene) alluvium. The results of 11 side-by-side DMT and CPT tests in alluvial deposits are shown on Figure 4(c). There is reasonable scatter, much of which is likely the result of material variability between the tests. Most data falls within the range N_{kt} = 10 to 20, which is the typical range for most soils. Regression of this data gives a N_{kt} = approx.15. Using this value and applying it to one of the CPT/DMT pairs shows good agreement (Figure 5c). These alluvial deposits appear to behave as expected and N_{kt} = 15 is likely to be appropriate for these soils as a general value.

4.4 Volcanic Tuff/Ash

Figure 4(d) shows some scatter but the average again appears to be around N_{kt} = 15 for this data set (three CPT/DMT pairs). Using N_{kt} = 15, shows good reasonable agreement between CPT and DMT derived s_u values on the depth plot in Figure 5(d). This value (N_{kt} = 15) appears to work well for this particular data set, but the same value may not be applicable for all volcanic clays in Auckland. There is likely to be a large amount of variability in this material and so caution should be taken when assigning a N_{kt} value in these soils. Site specific correlation may be required. It should also be noted that the DMT s_u correlations using the standard Marchetti (1980) correlations based on SHANSEP may not be applicable for these soils. Another reference test may be required for a site specific correlation.

4.5 Waitemata and Waipapa Group Residual Soils

There are 7 data sets in the Waitemata Group but only one in the Greywacke residual soils. Both these geological units show a similar trend in the DMT s_u vs. q_{net} plots on Figures 4(e) and 4(f) with N_{kt} tending to the higher end, averaging between 20 and 25. There is considerable scatter in the Waitemata Group soils, most of which may be attributable to the natural variation and layered nature of the material. A depth plot of the Waitemata Group materials in shown on Figure 5(e) showing DMT derived s_u values with those derived from CPT using an N_{kt} = 25. This seems high and may be a reflection of the DMT derived s_u values possibly not being applicable to these residual soils. Further research will be required to establish the DMT-s_u correlations in these soils.

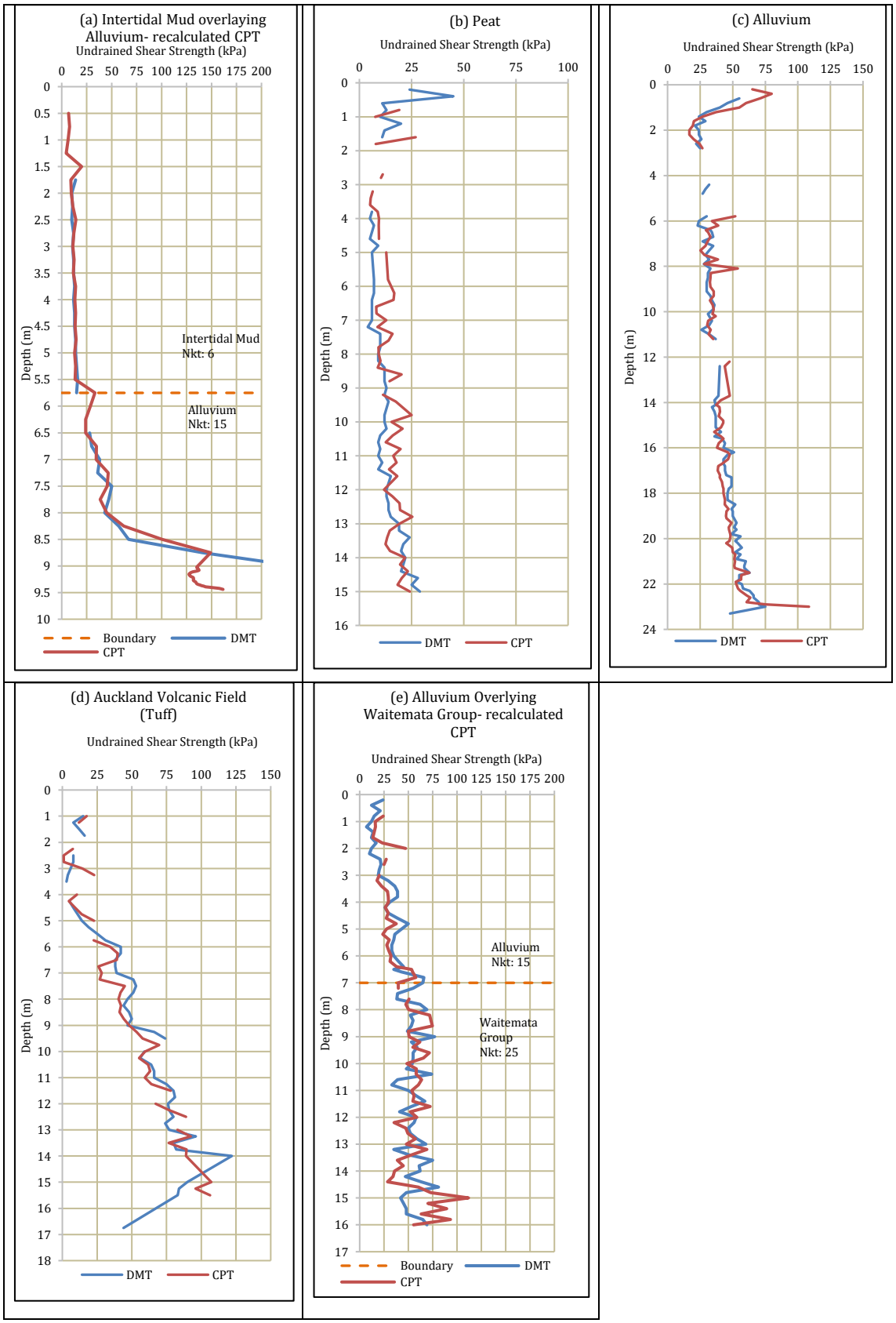

Figure 5: Depth plots of DMT and CPT derived s_u values

5 CONCLUSIONS

The undrained shear strength, s_u, derived from side-by-side CPT and DMT tests over a range of Auckland clays have been compared to determine typical N_{kt} values for the various geological units. In this approach, the DMT is used as the reference test to which the CPT is compared. It appears that a N_{kt} value of 15 is a good fit in general for the Alluvial clays. In this study, N_{kt} = 15 also appears to work well for amorphous peats and volcanic soils, however, caution should be applied in these materials and site-specific correlation is advised. In marine intertidal muds, an N_{kt} = 6 appears to be applicable, but will be dependent on the normalised pore pressure. Good pore pressure response, u_2, in the CPT test is important to allow a more comprehensive assessment of s_u in soft clays. In the residual Waitemata Group soils, N_{kt} values appear high (around 25) using the approach of this paper. It is possible that the standard DMT-s_u correlations may not be applicable in these soils. Until correlations have been developed, site-specific correlation with another reference test is suggested to determine N_{kt} in these residual soils.

REFERENCES

Kamei, T. (1996) Undrained shear strength and interrelationships among CIUC, CKoUC, CIUE and CKoUE tests. *Geoscience Rept*. Shimane Univ., 15, p.137-145.

Kermode, L.O. (1992) Geology of the Auckland urban area. Scale 1:50,000. *Institute of Geological & Nuclear Sciences geological map 2. 1 sheet + 63p.* Institute of Geological and Nuclear Sciences Ltd, Lower Hutt, New Zealand.

Lacasse, S. and Lunne, T. (1988) Calibration of dilatometer correlations. *Proceedings ISOPT-1*. Orlando FL. Vol. 1: p.539-548.

Ladd, C.C., Foott, R., Ishihara, K., Schlosser, F. and Poulos, H.G. (1977) Stress deformation and strength characteristics. *Proceedings 9th ICSMFE*. Tokyo, Vol. 2: p. 421-494.

Lunne, T., Robertson, P.K. and Powell, J.J.M. (1997) *The cone penetration test in geotechnical practice*. EF Spon/Blackie Academic, Routledge Publishing, New York. P. 64.

Marchetti, S. (1980) In situ tests by flat dilatometer. *ASCE Jnl GED*. Vol. 106, No. GT3, Mar: p. 299-321.

Marchetti, S. (2015) Keynote lecture: Updates to the TC16 DMT Report. *DMT-15 Conf*. Rome

Mayne, P.W. (2016) Invited Keynote: Evaluating effective stress parameters and undrained shear strength of soft-firm clays from CPT and DMT. *In Pursuit of Best Practices – Proc. 5th Intl. Conf. on Geotechnical & Geophysical Site Characterisation*. ISC-5, Jupiters Resort, Gold Coast, Australian Geomechnics Society. Vol. 1: p.19-40.

Powell, J.J.M. and Uglow, I.M. (1988) The interpretation of the Marchetti dilatometer test in UK clays. ICE Proc. Conf. Penetration Testing in the UK. Univ. of Birmingham, July, Paper No. 34: p.269-273.

Robertson, P.K. and Cabal, K.L. (2015) Guide to Cone Penetration Testing for Geotechnical Engineering. *Gregg Drilling & Testing, Inc*. 6th Edition

Wroth, C.P. (1984) The interpretation of in situ soil tests. *Geotechniqu* 34(4): p. 449-489.

The Casagrande plasticity chart – does it help or hinder the NZGS soil classification process?

K J Hind
Tonkin & Taylor Ltd, Auckland, NZ.
khind@tonkintaylor.co.nz (Corresponding author)

Keywords: Casagrande, plasticity chart, soil classification

ABSTRACT

A routine part of any geotechnical investigation is the classification of the recovered soils. In New Zealand this should be undertaken in the field in accordance with the New Zealand Geotechnical Society's guidelines. There is a general expectation that laboratory-based methods should both verify and enhance those classifications obtained in the field, yet it is not uncommon for the two to differ significantly. Field and laboratory data for fine-grained inorganic soils from across Auckland have provided an insight into the nature, magnitude and likely origins of these differences. It is demonstrated that field logging and the plasticity chart commonly assign the same materials to different soil groups. This appears to originate from the majority of soils being fundamentally plastic in nature yet displaying physical properties noticeably different from that expected for a clay due to the significant non-clay fraction. Furthermore the plasticity chart cannot be used to classify soils in accordance with the New Zealand taxonomy. As a result intermediate soil classifications incompatible with the plasticity chart are typically assigned in the field. Recommendations are given with respect to developing a stand-alone New Zealand-specific classification system and the use of both field and laboratory data.

1 INTRODUCTION

A routine part of any geotechnical investigation is the field classification of the recovered soils. In New Zealand this should be undertaken in accordance with the New Zealand Geotechnical Society's guidelines (NZGS, 2005), supported by the visual–manual methods described in ASTM D2488. Laboratory testing in support of the field determinations is typically undertaken on only a very small proportion of the total available material. In the case of fine-grained soils, the Casagrande plasticity chart may be used in conjunction with the Atterberg Limit tests to distinguish basic soil types.

There is a general expectation that laboratory-based methods should both verify and enhance those soil descriptions and classifications obtained in the field. Yet it is not uncommon for the two to differ significantly. This is particularly true for Auckland's fine-grained soils, where the same material may be assigned by the two methodologies to entirely different soil groups. An expectation of convergence can encourage some practitioners to modify field logs to better reflect the laboratory data in the belief that the field classifications are somehow erroneous. Yet a close examination of NZGS (2005) and the Unified Soil Classification System (USCS) indicates that it is taxonomical differences, and not user error, that are the primary reason for the different outcomes. Rather than forcing a convergence, it is better to recognise that field and laboratory classifications are separate non-equivalent processes.

This paper uses a database of some of Auckland's fine-grained inorganic soils to investigate the nature, magnitude and likely origin of the differences that can be observed between field-based and laboratory-based classifications. In particular it evaluates whether use of the Casagrande plasticity chart is helping or hindering the soil classification process for Auckland's soils.

2 THE CLASSIFICATION OF FINE-GRAINED SOILS

Fine-grained soils are comprised of varying proportions of clay, silt, sand and organic matter, together with a typically minor quantity of coarser material. Early soil taxonomy was developed largely for agricultural purposes, with soil groups defined by the relative abundance of their constituent particles (Casagrande, 1948). Attempts were made to adopt these systems for geotechnical purposes, however it was evident by the mid-20th Century that the engineering behaviour of fine-grained soils was poorly correlated with grain size. Arthur Casagrande argued that plasticity was the most important characteristic of fine-grained soils and that this, rather than grain size, should be the basis of a new soil classification system to be used for engineering purposes (Casagrande, 1948). Initially developed as part of the Allied effort during WWII, Casagrande's Airfield Classification System (ACS) would eventually become the Unified Soil Classification System (USCS), the parent of many modern engineering-oriented soil classification systems including NZGS (2005), AS 1726 and BS 5930.

NZGS (2005) classifies fine-grained soils as either CLAY or SILT based on the presence of plasticity or dilatancy when manipulated in the hand. Intermediate or hybrid soil names are assigned to those soils that exhibit distinct physical characteristics associated with a subordinate fraction. Examples given in NZGS (2005) include Sandy CLAY, Silty CLAY and Clayey SILT. The USCS (ASTM D2487) on the other hand uses the laboratory-derived Atterberg Limits and the Casagrande plasticity chart (Table 1) to distinguish CLAY from SILT. Clays generally plot above the plasticity chart's A-Line, whereas silts generally plot below it. Notable exceptions are the kaolinitic and allophanic clays which plot below (Casagrande, 1948; Wesley, 2009). The USCS does not use intermediate soil names in the same manner as NZGS (2005), although the term Silty CLAY is used for the very narrow zone in the lower corner of the plasticity chart where two soil groups overlap. ASTM D2488 provides some guidance on the field description of fine-grained soils, however the USCS is fundamentally a laboratory-based process.

It is important to note that the terms clay and silt refer to the clay-like and silt-like characteristics of a soil rather than grain size. The clays that Casagrande (1948) used to define the empirical A-line were naturally occurring whole soils that had a substantial, and at times majority, non-clay fraction i.e. a majority clay content is not a prerequisit for a soil to plot above the A-Line. Although NZGS (2005) states that it is based on the USCS (ASTM D2487), there are a number of fundamental differences between the two including the following:

- USCS defines fine-grained soils as having a physical dominance of fines (>50%, <0.075mm), whereas NZGS (2005) requires only a 35% fines content (<0.060mm) for a soil to be classified as fine-grained.
- Soil group boundaries are clearly defined in USCS, whereas in NZGS (2005) they are not. The former is based directly on the Atterberg Limits, whereas the latter are based primarily on perceived material behaviour (e.g. CLAY or SILT) with some recognition of composition (e.g. Sandy CLAY).
- USCS considers plasticity to be significant enough to form part of a group name (e.g. Lean Clay, Fat Clay), whereas NZGS (2005) has plasticity only as a qualifying term in the description and not in the classification itself (e.g. CLAY. High plasticity).
- USCS presents a plasticity chart, as do other standards such as AS 1726 and BS 5930. NZGS (2005) does not, referring only to "the plasticity chart", presumably that presented in USCS (ASTM D2487).

The lower fines content threshold used in NZGS (2005) is an acknowledgment that some soils exhibit the fine-grained characteristics even though coarse-grained material is physically more abundant. This difference means that clayey or silty soils with a 50 to 65% sand content will be classified as coarse-grained according to the USCS, but fine-grained according to NZGS (2005). Casagrande (1948) would not have included such soils in the development of the plasticity chart.

Table 1: USCS – inorganic fine-grained soils component only (ASTM D2487, ASTM D2488 and Casagrande, 1948)

Liquid Limit	Plasticity Index relative to A-line	Soil class and plasticity	Code
Liquid Limit <50% (L)	On or above	**Lean Clay** Inorganic clays, sandy clays, silty clays, lean clays. Low to medium plasticity, no or slow dilatancy.	CL
	Below	**Silt** Inorganic silts and very fine sands, rock flour, silty or clayey fine sands. Slight plasticity to non-plastic, slow to rapid dilatancy.	ML
Liquid Limit >50% (H)	On or above	**Fat Clay** Inorganic clays, fat clays. High plasticity, no dilatancy.	CH
	Below	**Elastic Silt** Micaceous or diatomaceous fine sandy and silty soils, elastic silts. Low to medium plasticity, no to slow dilatancy.	MH
Liquid Limit <30% (L) Plasticity Index 4 to 7%	Not applicable	**Silty Clay** Mixed zone where both CL and ML soils plot	CL-ML

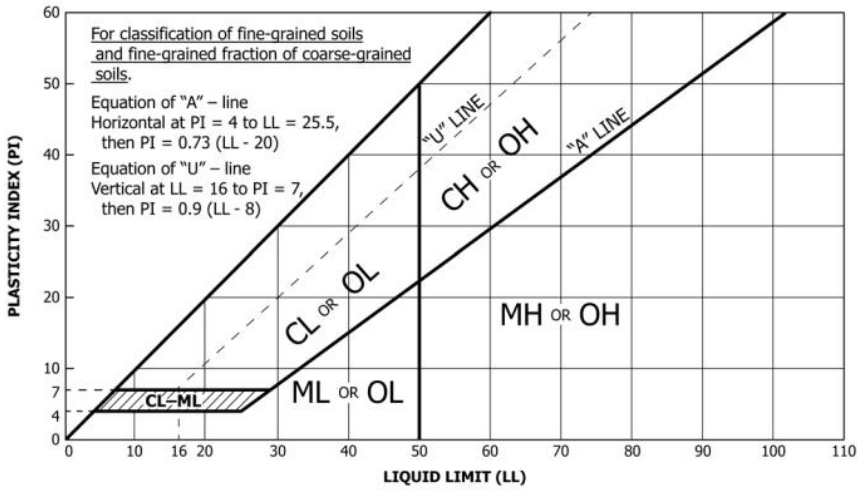

It is not clear from a reading of NZGS (2005) whether intermediate soil names represent a continuum between CLAY and SILT or whether they are subsets of them. For example, does a Clayey SILT first have to satisfy the dilatancy requirement of SILT before "Clayey" is added in recognition of some minor cohesive component, or can it be a term applied to a plastic clay-silt mixture in which silt is clearly dominant but dilatancy is not a characteristic? The former would likely plot below the A-Line whereas the latter would likely plot above it. As a "low plasticity Clayey SILT" (with no reference to dilatancy) is presented as an example classification in NZGS (2005), it would appear that the soils are considered to be a continuum.

3 THE IMPORTANCE OF SOIL PLASTICITY

Plasticity is the putty-like property of a cohesive soil that allows it to be remoulded without rupture. Because higher plasticity soils exhibit this characteristic over a much wider range of moisture contents than do low plasticity soils, the Atterberg Limits are typically the basis on which plasticity determinations are made. Some classification systems define plasticity solely on the basis of liquid limit (e.g. AS 1726 and BS 5930) whereas others take into account both the

liquid and plastic limits in the form of the plasticity index (e.g. Sowers, 1979). NZGS (2005) does not define plasticity with respect to a measurable parameter, referring instead to a soil's dry strength and ability to be remoulded.

NZGS (2005) defines plasticity as being either low or high, yet it is very common in New Zealand for the terms "moderate" or "medium" plasticity to be used in field descriptions. AS 1726 has long used such a three tier plasticity classification and its plasticity chart has commonly been used in New Zealand. Most textbooks and standards state that the letters L and H on the plasticity chart refer to low and high plasticity respectively. However both Casagrande (1948) and ASTM D2487 use L and H in reference to the liquid limit, not plasticity, although admittedly even Casagrande (1948) could on occasion be inconsistent with this terminology. It should be noted that medium plasticity is used within USCS (ASTM D2488) and Casagrande (1948) (see Table 1). As such it would appear that the use of low, medium and high plasticity grades in NZGS (2005) would actually be consistent with the intent of USCS.

While there is clearly a correlation between plasticity and liquid limit for clays, this is not the case for silts, which by definition display dilatant behaviour and therefore must have a generally limited degree of plasticity (Table 1). The literature typically describe silts as being dilatant yet USCS (ASTM D2487) defines elastic silts as having "no to slow" dilatancy, and both AS 1726 and BS 5930 allow for high plasticity silts. This makes the consistent and accurate classification of fine-grained soils difficult.

4 THE NATURE OF AUCKLAND SOILS

In simplified terms the soils of Auckland consist of residually weathered Miocene flysh (Waitemata Group), Pliocene to Recent alluvium (Tauranga Group) and weathered Quaternary basaltic pyroclastics (Auckland Volcanic Field). Although significant areas of the Auckland Isthmus have a thin or partial covering of weathered volcanic ash, these soils represent only a small minority of the field and laboratory data available. To aid interpretation, the database has been limited to the fine-grained soils from the Waitemata Group and the Tauranga Group. Organic soils and fills have also been excluded. The database consists of 124 samples for which both Atterberg limit and hydrometer data are available. Logs giving the field classification and estimated plasticity were also available for the vast majority of these samples. Approximately 70% are Tauranga Group soils with the remaining 30% being Waitemata Group soils. All samples come from projects undertaken within the Auckland urban area.

The textural composition of the soils is summarised in Figure 1. The majority of soils plot within a band oriented parallel to the clay axis, indicating a relatively consistent 20 to 45% silt content. Both the clay and sand contents are significantly more variable than silt. Relatively few samples show a substantial dominance of one component over the others. The mean clay, silt and sand contents of the database is 34%, 37% and 29% respectively. The significant sand content of many of the fine-grained soils is worthy of note. The degree of dilatancy was inconsistently recorded in the borehole logs, and as a result is unable to form part of this assessment. The vast majority of the database (85%) has at least 15% clay (Figure 1), the approximate level where cohesive characteristics might be expected.

The field-derived soil classifications (Table 2) are dominated by SILT, with 69% of the soils being classified as either SILT, Clayey SILT or Sandy SILT. Only 6% of the database was classified in the field as CLAY, all of which were also described as being highly plastic. This indicates that a low to medium plasticity state is interpreted in the field as being due to the presence of silt rather than clay with a lower activity.

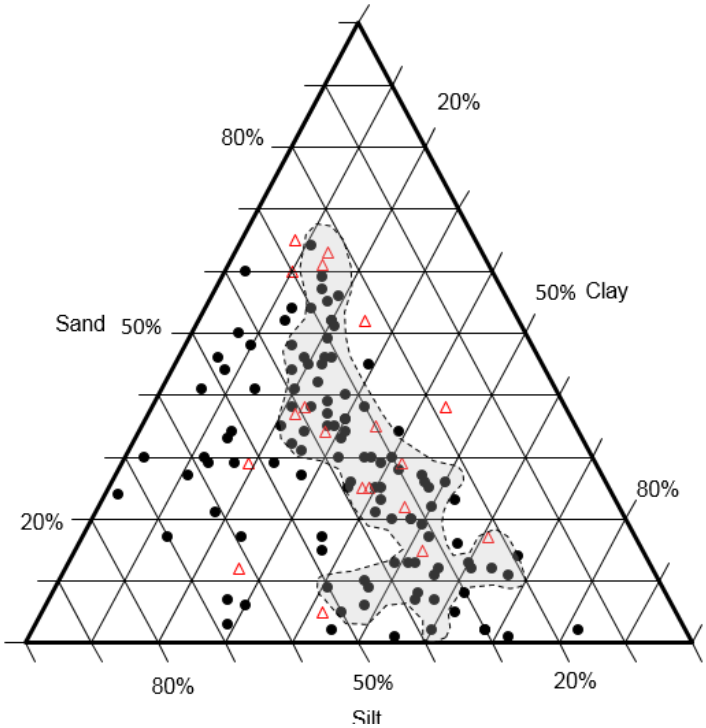

Figure 1: Textural plot of soils used in this study. Contour encloses 4 or more data points per 10% triangle. Circles plot above the A-Line, triangles below.

All samples in the database have been classified according to the USCS (ASTM D2487) plasticity chart (Figure 2 and Table 3). Two significant observations can be made. Firstly, the two systems give fundamentally different results in the majority of cases, with classifications determined by the plasticity chart being dominated by CLAY (82%) whereas field classifications, as we have already seen, are dominated by SILT (69%). Secondly, those soils that plot above the A-Line cannot be distinguished on the basis of their composition from those that plot below (Figure 1). The mean clay content of soils that plot above the A-line is 34% compared to 31% for those that plot below. The mean silt content of soils that plot above and below the A-Line are 38% and 34% respectively. Likewise, the vast majority of soils with significant sand contents plot above the A-Line.

Table 2: Summary of field classifications (NZGS, 2005)

Sample Group	No. of Samples	Clay (%)	Silty Clay (%)	Clayey Silt (%)	Silt (%)	Sandy Silt (%)
All samples	113	6	25	32	21	16
Waitemata Group	37	5	19	27	25	24
Tauranga Group	76	7	30	33	13	17
Low plasticity	42	0	0	7	11	14
Moderate plasticity	26	0	6	13	2	3
High plasticity	32	6	18	11	5	5

Note: not all laboratory samples had corresponding field plasticity descriptions

Table 3: Summary of laboratory classifications (USCS, ASTM D2487)

Geology	No. of Samples	CL (%)	CH (%)	ML (%)	MH (%)	CL-ML (%)
All	124	16	66	2	15	1
Waitemata Group	39	10	74	3	13	0
Tauranga Group	85	19	63	1	16	1

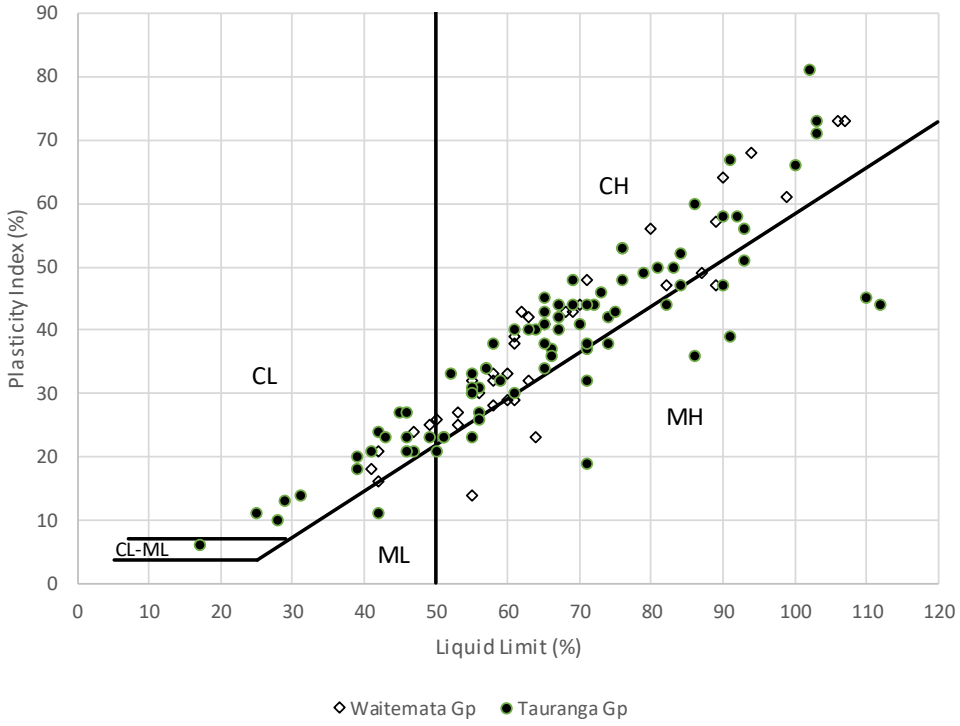

Figure 2: Plasticity chart for all samples

The NZGS (2005) soil groups do not form distinct fields within the plasticity chart but overlap along the length of the A-Line (Figure 3). It might be expected that as the silt fraction becomes significantly greater than the clay fraction, soils would be observed plotting below the A-Line, however there is no evidence of this occurring for Auckland's soils. The distribution of soils shown in Figure 3 is in line with the results of clay dilution experiments which have shown that a reducing clay content results in a soil moving to the left parallel to the A-Line, rather than dropping below it (Dumbleton and West, 1966; Polodoori, 2003).

The data supports the author's experience that even though Auckland's fine-grained soils are typically plastic enough to plot above the A-Line, they have a sufficient silt and sand component to noticeably depart in their physical properties from what can be considered a typical clay. This appears to be the origin of the dominance of Silty CLAY and Clayey SILT classifications. The plotting of so many soils logged as SILT above the A-Line does raise the question as to whether dilatancy is being taken into account sufficiently when such determinations are being made. Potentially many of these soils should be Clayey SILT or possibly even Silty CLAY.

5 A ROLE FOR THE PLASTICITY CHART WITH NZGS (2005)

With the NZGS (2005) soil groups not being based on the Atterberg Limits, it is apparent that the plasticity chart cannot fulfil the same classification role that is does in the USCS. Not only can NZGS (2005) soil names such as Clayey SILT not be derived from the plasticity chart, there is no means by which USCS soil groups derived from it can be converted into NZGS (2005) equivalents.

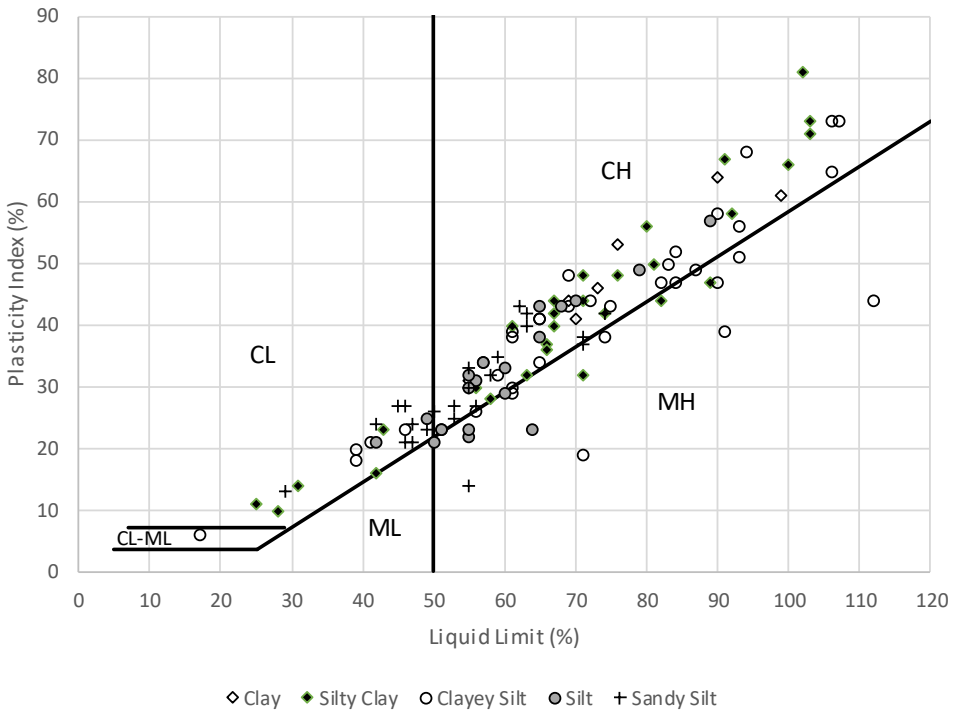

Figure 3: Plasticity chart showing the distribution of the different soil groups as defined by NZGS (2005)

NZGS (2005) suggests that if laboratory data is available, the plasticity chart can be used to distinguish clays from silts in the manner of USCS (ASTM D2487). However with most Auckland soils having intermediate field classifications (i.e. Silty CLAY and Clayey SILT), the plasticity chart can only be a half measure in terms of the classification process. Also, as has been demonstrated, the plasticity chart often does not correlate at all well with the field determinations. A choice of which to believe subsequently results.

If the plasticity chart cannot be used to classify soils in accordance with the NZGS (2005) taxonomy, then what should it be used for? The general rule still holds true that soils which plot below the A-line have more favourable engineering characteristics than those that plot above it (Wesley, 2009). As such the plasticity chart is a means of identifying potentially problematic geotechnical characteristics. Casagrande (1948) originally used the plasticity chart to characterise a soil's potential for compressibility. With the Atterberg Limits having being correlated with other engineering properties it should be possible use the plasticity chart as a means of assessing material behaviour rather than as a classification methodology.

6 CONCLUSIONS

The Casagrande plasticity chart has been used for more than 70 years to classify fine-grained soils in accordance with the USCS. New Zealand's soil classification system (NZGS, 2005) is largely field-based, however the plasticity chart remains part of the assessment process when laboratory data is available. Although NZGS (2005) is largely a derivative of the USCS, the plasticity chart is unable to classify soils according to the NZGS (2005) taxonomy because it effectively uses a continuum of soil groups incompatible with the binary system used in USCS (ASTM D2487). An assessment of soil data from across Auckland has shown that the field and laboratory-based systems typically classify fine-grained soils very differently. The majority are classified in the field as SILT, whereas these same soils are classified by the plasticity chart as CLAY. It would appear that the departure in behaviour of many of these soils from what would be considered

typical of clay is resulting in plastic soils being classified as silts or silt-clay mixtures. Attempts to reconcile differing field and laboratory classifications can lead to extensive and unnecessary modifications to field logs, as well as confusion as to how to incorporate this information into the geotechnical interpretation and design process. In a number of respects therefore, the plasticity chart is not assisting and is potentially hindering the classification process. As a means of addressing these issues, it is recommended that the NZGS guideline document be revised to present the following:

- A stand-alone classification system fully independent of the USCS (ASTM D2487).
- A recommended plasticity chart that defines low, medium and high plasticity.
- A definition as to whether soil groups form a continuum between CLAY and SILT or whether they are subsets of them. In particular, the dilatancy or plasticity characteristics of soils such as Clayey SILT should be clearly defined.
- Guidance on the use and interpretation of the plasticity chart, although this is outside of the description and classification process for which NZGS (2005) was developed.

REFERENCES

Standards Australia, AS 1726-2017. Geotechnical site investigations

British Standard, BS 5930:2015. Code of practice for site investigations

ASTM D2487-06.Standard Practice for Classification of Soils for Engineering Purposes (unified Soil Classification System)

ASTM D2488-09a. Standard Practice for Description and Identification of Soils (Visual-Manual Procedure)

Casagrande, A. Classification and identification of soils. Transactions, ASCE, vol.113, 901-930.

Dumbleton, M.J. and West, G. (1966). Some factors affecting the relation between the clay minerals in soils and their plasticity. *Clay Minerals*, No. 6, 179-193

New Zealand Geotechnical Society (2005). *Field description of soil and rock. Guideline for the field classification and description of soil and rock for engineering purposes*. New Zealand Geotechnical Society Inc.

Polidori, E. (2003) Proposal for a new plasticity chart. *Geotechnique*, vol 53, No. 4, 397-406.

Sowers, G.F. (1979). *Introductory soil mechanics and foundations: geotechnical engineering*, 4th edition. Macmillan, New York.

Wesley, L. (2009) *Fundamentals of soil mechanics for sedimentary and residual soils*. John Wiley & Sons.

Tunnelling through volcaniclastic grit; monitoring and management of groundwater effects on the Waterview Connection Project

S J France
Beca Ltd, Auckland, NZ.
sian.france@beac.com (Corresponding author)

Keywords: groundwater, drawdown, tunnelling, volcaniclastic grit, Waterview Connection

ABSTRACT

The NZ Transport Agency's Waterview Connection project involves the construction of 5 km of motorway to complete Auckland's Western Ring Route. Half of this new link is twin 14.5 m diameter tunnels constructed by Tunnel Boring Machine with 16 sequentially excavated cross-passages. Over most of the tunnelled length the excavation is through weak interbedded sandstones and mudstones; however, a 150 m long zone of moderately strong volcaniclastic grit was identified during site investigations.

This zone was characterised by steeply dipping, fractured and faulted, higher permeability rock which might allow a direct groundwater-surface water connection to overlying Oakley Creek, and increased the risk of drawdown in overlying contaminated and compressible soils. This zone was identified as one of the highest risk areas in terms of potential adverse effects resulting from groundwater drawdown and ground settlement.

Monitoring during drained maintenance stops recorded inflows to the tunnel excavation of up to 30 L/s with near instantaneous drawdown at distances of almost 200 m, and, air bubbles in the creek coincident with the TBM location confirming the connection between groundwater and surface water. Visual inspections and instrumented monitoring were used to regularly inform drive parameters and negligible adverse effects were recorded as a result of the drawdown during tunnelling. Pre-excavation fissure grouting was undertaken ahead of cross-passage excavations to limit groundwater inflows and drawdown, and monitoring confirmed the effectiveness of this technique in these materials. These proactive mitigation measures meant that negligible adverse effects were recorded as a result of the drawdown.

1 PROJECT INTRODUCTION

The Waterview Connection project involves the construction of 5 km of 6-lane motorway through and beneath Auckland's western suburbs, linking two existing State Highways to complete a motorway ring route around the city. Half of this new link will be in tunnels and the remaining half comprises surface highways and approach trenches (Figure 1).

The segmentally lined mainline tunnels were constructed using a 14.5 m diameter Earth Pressure Balance Tunnel Boring Machine ("the TBM"). The mainline tunnels are linked by 16 sequentially excavated, nominally 6 m diameter cross-passages.

2 GEOLOGICAL CONDITIONS AND IMPLICATIONS FOR TUNNELING AND EXCAVATION

2.1 Geological Setting

The project is located in the western-central suburbs of Auckland, with the tunnel alignment broadly following the incised valley of Oakley Creek, between the Mt Albert (Owairaka) Volcano to the east and the Great North Road/Blockhouse Bay Ridge to the west (Figure 1).

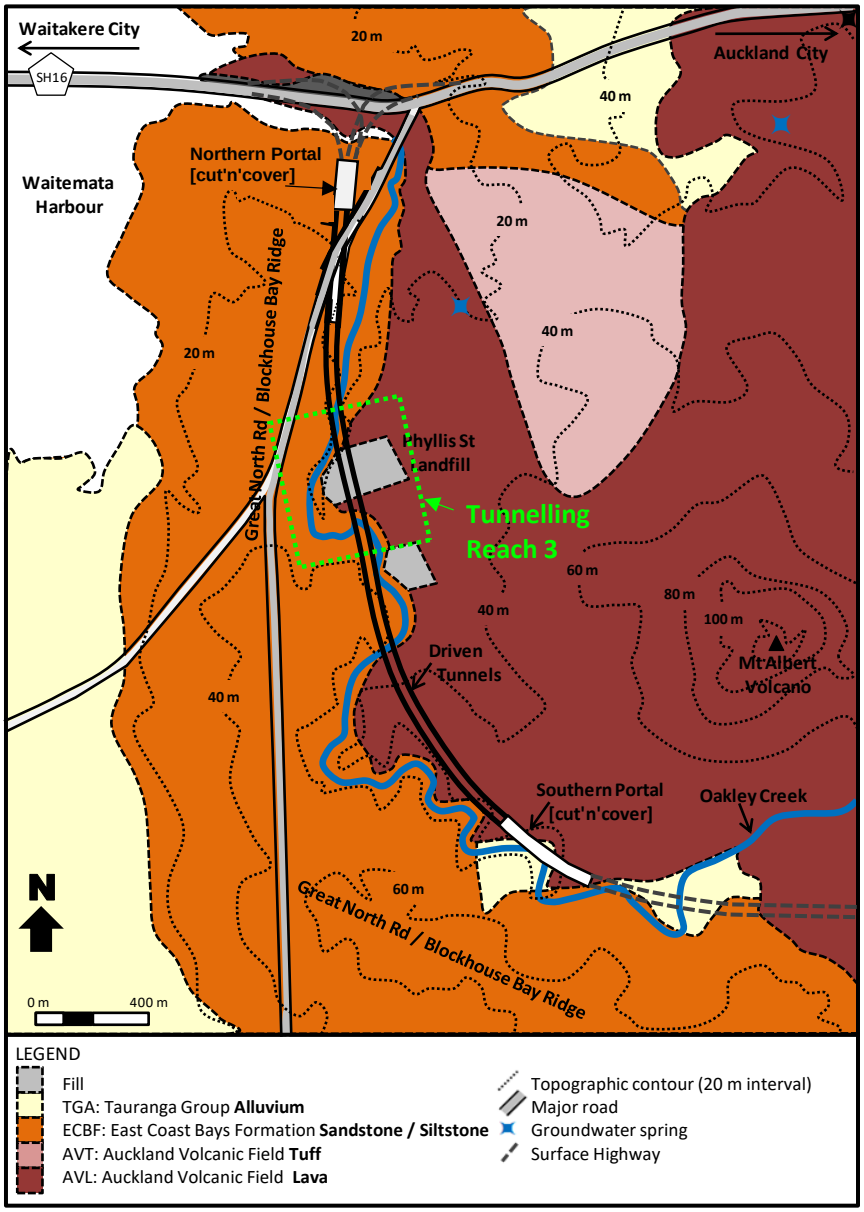

Figure 1: Location map for the project (modified after France et al, 2011)

Tertiary age, weak sandstones and mudstones of the East Coast Bays Formation (ECBF), form the bedrock in the project area and outcrop in the Great North Road / Blockhouse Bay Road Ridge and locally within Oakley Creek. Compressible Tauranga Group alluvium fills the paleo-valley of Oakley Creek and is encountered within the present-day valley of Oakley Creek and beneath the basaltic lava flows to the east of the Creek.

Mt Albert (Owairaka) Volcano erupted onto a now buried paleo-ridge of ECBF and lava flows in-filled the paleo-valley to the north, west and south. The current position of Oakley Creek roughly follows the western edge of the lava flows. Uncontrolled back-filling of historic quarries within the basaltic lava flows has resulted in pockets of landfill adjacent to the Creek.

2.2 Characterisation of Geological Conditions for Tunnelling

The Well-Connected Alliance developed a 3D geological model from the geotechnical investigation data (over 500 locations) and used it to generate geological long and cross sections to assess tunnelling conditions. Six tunnelling reaches were identified based on predominant lithology, hydrogeology and geological structure. Over most of the tunnelled length (5 reaches) the tunnelling and cross passage excavation is through typical, weak ECBF.

However, within the ECBF are lenses of a stronger, coarse grained volcaniclastic grit (commonly referred to as Parnell Grit). Reach 3 comprises 500 m of interbedded weak ECBF and lenses of the stronger grit, but with a central ~150 m long zone in which the tunnel excavation was wholly within the grit. The rock in this zone was also characterised by steeply dipping joints and folded bedding.

2.3 Characterisation of the Grit in Reach 3

In total 155 in-situ (slug, packer or pumping) tests were undertaken in the East Coast Bays Formation over the wider project area. The geometric mean and median of all tests is approximately 3 x 10^{-7} m/s, typical of ECBF, with 85 % of all test results falling in the range of 1 x 10^{-8} m/s to 5 x 10^{-6} m/s (Figure 2).

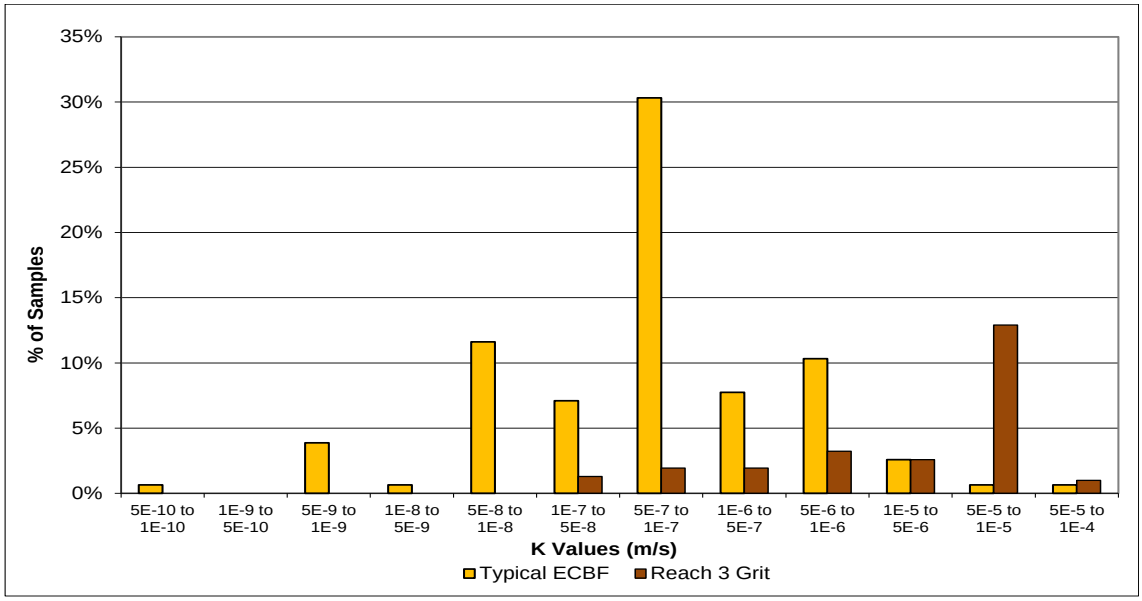

Figure 2: Permeability test results from typical ECBF and Reach 3 grit

Whilst a broad trend between permeability and rock strength was identified, review of spatial trends indicated that the highest permeability values were associated with the steeply dipping, openly jointed volcaniclastic grit beds located within Reach 3.

The 41 No. in-situ tests undertaken in Reach 3 indicated permeability values of up to 1 x 10^{-4} m/s (Figure 2). Pumping tests indicated peak flows (from a 250 mm diameter well) of up to 16 l/s and sustained flows of almost 10 l/s. Recorded drawdown during the pumping testing indicated a clear SW-NE structural control on the extent of drawdown and the potential for drawdown to extend to distances of up to 500 m.

The locations of tests that indicated high permeability, the observed structural control on drawdown and indications of boundary features in the pumping test all coincide with the mapped extent of thick, channel filling grit (Figure 3).

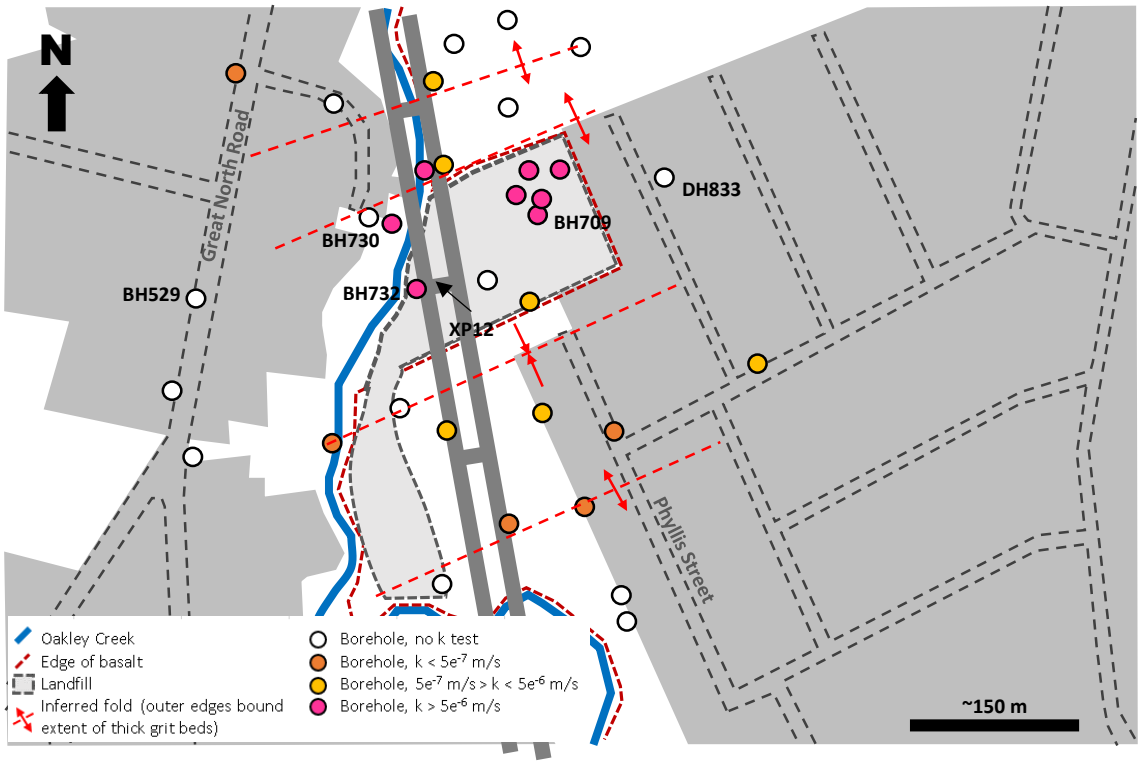

Figure 3: Inferred extent of high permeability (k) grit within Reach 3 (labelled boreholes are referred to in text or subsequent figures)

2.4 Implications for Tunnelling and Excavation

Defects recorded in boreholes and surface lineaments suggest that Oakley Creek likely follows larger scale geological structures, whilst geological mapping of the creek identified that the steeply dipping grit beds observed at the depth of the tunnel extend to the surface, potentially allowing a direct groundwater-surface water connection to the overlying creek.

Additionally, land-use at the surface of Reach 3 comprises sports fields (Phyllis Reserve) that have been created on a former landfill with no basal liner. Hence any drawdown from tunnelling or excavation could result in contaminant migration, whilst settlement at the surface could allow cracking of the landfill cap and / or ponding of surface water that might result in increased leachate generation.

Reach 3 was therefore identified as one of the highest risk areas in terms of potential adverse effects resulting from groundwater drawdown and ground settlement. The use of an EPB-TBM that could be operated in a closed and pressurised mode, was expected to limit the potential for groundwater inflows and drawdown during tunnelling. However, open drained stops were required for planned maintenance of tail brushes, changing of cutting tools etcetera, and one such stop was proposed to be undertaken immediately prior to entering Reach 3 to allow optimal TBM operation through this zone.

Further, the cross passages were sequentially excavated, and an enlarged (~9 m diameter) cross passage (XP12) was required in Reach 3 to form the tunnel's low point sump. It was identified during the early stages of the project that pre-excavation fissure grouting would be required at XP12 (and several other cross passages) to ensure safe working conditions and reduce groundwater inflows during excavation.

3 GROUNDWATER EFFECTS DURING TUNNELLING AND EXCAVATION

3.1 Drained Maintenance Stop

Immediately prior to entering the highest risk zone, the TBM was stopped for a planned period of maintenance and replacement of the tail brushes, a critical tool for maintaining face pressure and reducing groundwater inflows during tunnelling. The TBM was stopped on 15th July 2014 and immediate peak groundwater inflows of 30 l/s occurred at the tunnel face, though these rapidly reduced over a few days to ~10 l/s which was then maintained for the 2 week duration of the stop.

Instantaneous drawdown of 18.5 m was recorded in the nearest piezometer (BH732) located 35 m from the face of the TBM, with drawdown approaching near steady state conditions and a maximum 26.3 m drawdown at the end of the two week stop.

As with the earlier pumping testing, a clear structural control on drawdown was observed, with a near-instant response in groundwater level recorded at distances of more than 200 m away, including at BH529 located on the opposite side of Oakley Creek (i.e. across what might often be considered a "groundwater divide", Figure 4 and Figure 7).

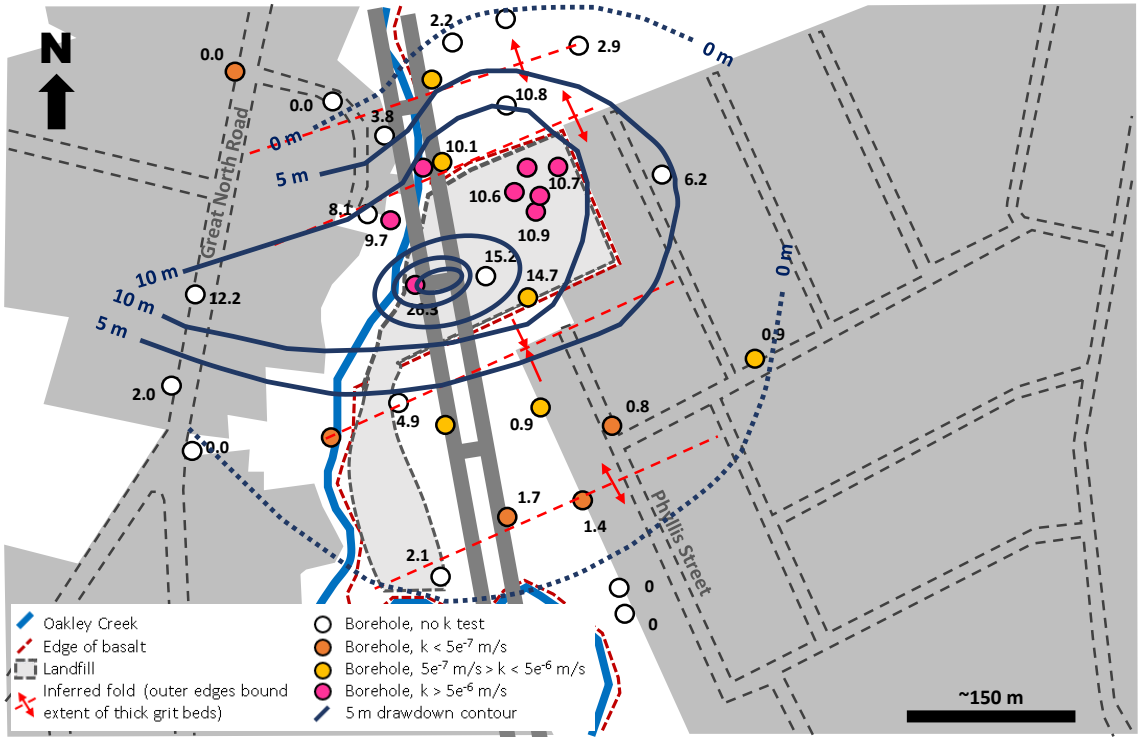

Figure 4: Extent of drawdown at end of drained maintenance stop (boreholes are labelled on Figure 3)

Recovery of groundwater levels was equally rapid, with most piezometers recovering to 50 % to 85 % of their pre-strop water levels within 7 days, and all fully recovering within 2 months. The only exception being BH529, which some 3 years later has still not fully recovered with an apparent permanent drawdown of 5 m relative to pre-tunnelling conditions.

3.2 TBM Tunnelling Induced Effects on Groundwater and Surface Water

Generally, where tunnelling was undertaken in both the typical ECBF and the more permeable volcaniclastic grit, and with a closed and pressurised face, there was negligible recorded drawdown of the groundwater level.

In some areas, where there was a concern over mechanical ground movements at the surface, the TBM was operated at a higher face pressure in order to allow optimal performance (and hence speed) through the area of concern, while also limiting mechanical movements and groundwater inflows. Reach 3 was identified as one such area as a result of the large groundwater inflows during the maintenance stop, the occurrence of contaminated land fill at the surface, and the close proximity of buildings (with known weather-tightness issues) within 30 m of the tunnel alignment.

As this was also an area of potential connection between groundwater and surface water, twice-daily visual inspections of the creek were undertaken, in addition to continuous stream gauging, in order to visually assess if any irregularities in flow were occurring. During one of these inspections air bubbles were noted rising from the creek bed (Figure 5), coincident with the TBM location, confirming the connection between groundwater and surface water.

Figure 5: Photo of air bubbles observed in Oakley Creek during tunnelling and map showing TBM location at time

The TBM face pressure was slowly lowered until the bubbles reduced to an acceptable level, whilst still maintaining minimal groundwater inflows to the face or drawdown in adjacent piezometers. Daily monitoring of piezometers in the immediate area was then used as a check against the TBM drive parameters (that were set early in the design phase) to confirm the optimal operational pressure.

3.3 Cross-passage XP12 Excavation

Prior to cross passage excavation, narrow (76 mm) diameter probe-holes were undertaken from the completed south-bound tunnel, to confirm geological conditions and allow measurements of groundwater inflows to determine if pre-excavation grouting was required. The recorded inflows to the probe-holes indicated that peak inflows to the larger cross passage excavation of 30 l/s to 80 l/s might occur, with sustainable flows of 10 – 20 l/s (i.e. comparable to that observed during the maintenance stop).

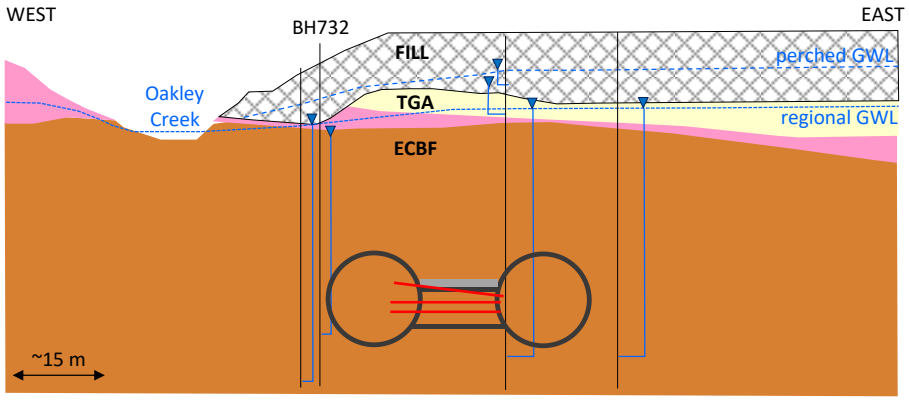

Figure 6: Geological cross section through XP12 (grey line indicates canopy tube, red line indicates probe drilling). NB: ECBF comprises grit (steeply dipping out of page).

During probe-hole drilling, and canopy tube drilling, immediate drawdowns of up to 1.5 m were observed in the ECBF at a distance of 14 m from probe-holes (BH732, Figure 7), with detectable drawdown (0.5 m) recorded at a distance of more than 200 m (DH833 and BH529).

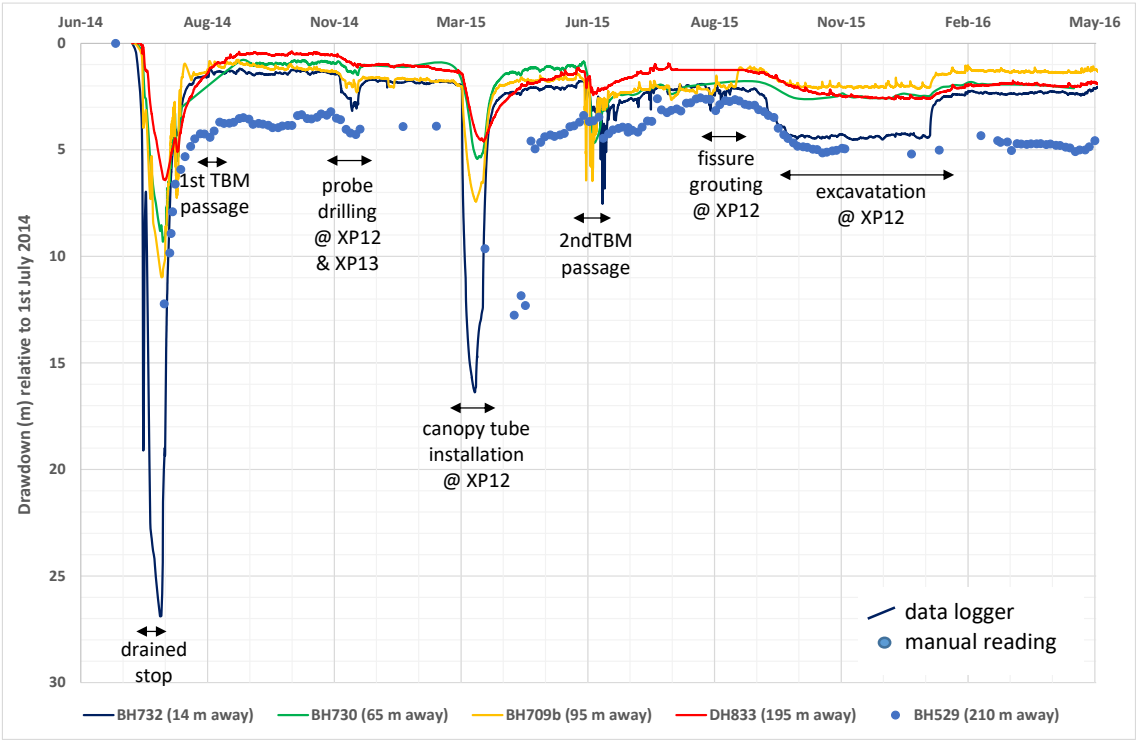

Figure 7: Observed drawdown at select monitoring locations in Reach 3 (distances are relative to outer edges of XP12)

A cementitious grout, targeting larger aperture joints was selected (Maclean et al, 2017) with grouting carried out by a specialist grouting contractor, through grout ports pre-installed in the segmental lining. Having observed the connection between TBM pressure at depth and Oakley Creek, care was taken to limit grouting pressures to reduce the risk of grout being ejected at the surface, with visual inspections of the creek and piezometer monitoring undertaken to confirm.

The cross passages were excavated in a series of short advances with spraying of shotcrete for temporary support. Prior to shotcreting the excavated face was logged by an Engineering Geologist and a visual estimation of seepage was made. Pre-excavation grouting was observed to be highly effective in reducing groundwater inflows. At XP12, groundwater was mainly observed as isolated seepage from occasional joints with the flow estimated to be less than l/s.

The grouting was also effective in limiting the magnitude of drawdown at distance (Figure 6), which, for the 9 m diameter excavation (open and dewatered for 5 months), was not significantly greater, and in some cases was less (BH709b) than observed during short term drilling and testing of the probe-holes. The magnitude of drawdown was also less than observed during the drained maintenance stop and flow gauging of Oakley Creek confirmed no impacts on creek flows.

4 CONCLUSIONS

Site investigations and observations from tunnelling through a discrete zone of moderately strong, jointed volcaniclastic grit, identify that significant groundwater flows and groundwater drawdown can propagate rapidly through the high permeability, but low storativity joints and fractures that often accompany these materials. The extent of drawdown was strongly structurally controlled, with drawdown occurring preferentially in a SW-NE direction, at distances of greater than 200 m and beneath the opposite side of Oakley Creek.

Although no impact on base flows in Oakley Creek was noted, connection to the creek was confirmed by the propagation of air bubbles to the surface. Visual inspections and instrumented monitoring were used to regularly inform TBM drive and grouting parameters to reduce the effects at the surface.

Peak groundwater inflows of 30 l/s and sustained inflows of 10 l/s occurred in open excavations through the grit. However, monitoring confirms that fissure grouting was successful in significantly reducing groundwater inflows and controlling the magnitude of drawdown at distance.

The monitoring results confirm the need for monitoring, and proactive management of groundwater effects, when grit is encountered in deep excavations or tunnelling projects.

5 ACKNOWLEDGEMENTS

The writer would like to thank the NZ Transport Agency and its Well-Connected Alliance partners for permission to publish details of the project, and also Ann Williams for her review of this paper.

REFERENCES

France, S.J., Williams, A. & Cammack, E. (2011) Western Ring Route – Waterview Connection Driven Tunnel: Assessment of Groundwater Effects. *Proceedings of the 14th Australasian Tunnelling Conference*. The Press, London.

Maclean, H.J., Cartwright, S. and Giauque, A. (2017) *Fissure grouting and rock defect characterisation for the Waterview cross passage tunnels*. in prep.

Measuring the vertical and lateral swelling pressure of expansive residual soils using a K_0 triaxial cell

H Elsaidy
Department of Civil and Environmental Engineering, The University of Auckland, NZ.
hels811@aucklanduni.ac.nz (Corresponding author)

W M Yan
Department of Civil and Environmental Engineering, The University of Auckland, NZ.
r.yan@auckland.ac.nz

M J Pender
Department of Civil and Environmental Engineering, The University of Auckland, NZ.
m.pender@auckland.ac.nz

Keywords: swelling soils, lateral stress, oedometer, wetting

ABSTRACT

Expansive soil has been well recognised as a problematic soil due to its swelling and shrinkage behaviour during wetting and drying cycles. The swelling pressure developed upon wetting is often investigated by placing an initially unsaturated soil specimen into an oedometric cell modified to restrain the specimen's volume change. Water is then added to the specimen and the increase in vertical stress due to wetting is then measured. In this study a K_0 triaxial cell, originally designed for saturated soil testing, is modified and used to investigate the development of swelling pressure. The cell allows not only vertical but also radial stresses to be measured during the wetting process. An initially unsaturated residual soil specimen is assembled into the K_0 cell where wetting of the specimen is allowed from the bottom drainage line. Allowing neither vertical nor radial strain during the wetting, vertical and radial swelling stresses developed during the process were recorded. Important experimental issues related to the tests are discussed aiming to improve the result quality.

1 INTRODUCTION

An expansive soil swells upon wetting and shrinks when subject to drying. This type of geomaterial has been well recognised as problematic. Lightly loaded structures built on expansive soils heaved when subject to wetting (Jennings & Kerrich, 1962; Fredlund & Rahardjo, 1991). Pender (1996) reported that retaining walls supporting expansive soils could tilt noticeably when subject to seasonal wetting and drying. In extreme cases, the walls could even collapse upon prolonged raining (Thomas, 2008; Ozer et al. 2012). Furthermore, deformation caused by soil swelling was identified as an important failure mechanism in expansive soil slopes (Ng et al. 2003; Qi & Vanapalli 2016). Conventionally, swelling pressure is often evaluated using oedometric cells while specimens are inundated under constant volume. It is anticipated that swelling stress measured using this approach would have been underestimated due to side friction of the oedometric ring (Al-Shamrani & Dhowian, 2003; ASTM D4546-03). This paper presents a modified triaxial cell which allows wetting of soil specimen under K_0 condition. Preliminary results are presented and important experimental issues related to the testing are highlighted and discussed.

2 STUDIED SOIL

Block soil samples were retrieved from a site near Newmarket, Auckland. The orange-brown residual soil is a weathering product of sandstones belonging to the East Coast Bays Formation (Kermode 1992). Natural water content of the soil was 60±2%. Table 1 summarises index properties of the soil obtained in accordance with NZS 4402:1986. The soil contains significant amount of clay fraction, exhibits a high liquid limit, and is referred to as CH according to USCS. The soil is considered to be highly expansive based on its liquid limit, plasticity index and activity according to Chen (2012) and van der Merwe (1964). X-ray diffraction (XRD) and X-ray fluorescence (XRF) analyses were carried out to determine the mineralogy of the studied soils. The soil was found to contain 64% quartz, 21% montmorillonite, 12% goethite and 3% of oxides with various cations.

Table 1: Index properties of the studied soil

Index	
Specific gravity	2.64
Silt fraction	12%
Clay fraction	88%
Liquid limit	114%
Plastic limit	48%
Shrinkage limit	23%
Activity	0.75

3 TEST EQUIPMENT AND SPECIMEN PREPARATION

3.1 Oedometer

Soil specimen in the oedometer cell has diameter and height of 76 mm and 19 mm respectively. The oedometer ring with specimen was carefully placed into the cell. Then, a vertical stress of 25 kPa was applied. The specimen was inundated under constant volume and the development of vertical swelling stress was recorded. It was found that the change of swelling pressure became negligible 24 hours after the inundation.

3.2 Triaxial Cell

A K_0 triaxial cell (Campanella & Vaid 1972; Hettiaratchi et al., 1992; Meyer, 1997) was used to investigate the development of vertical and radial swelling pressures of an initially unsaturated triaxial specimen when subject to wetting. The specimen has dimensions of 120 mm height and 60 mm in diameter. Upper drainage line of the specimen was connected to an open-end burette tube partially filled with water maintaining at atmospheric pressure. Saturation of the specimen could be easily visualised when the out-coming fluid changed from air bubbles to yellowish water containing fines of the studied soil. The K_0 triaxial cell has a rigid chamber wall. By restraining the flow of cell fluid, a K_0 condition could be imposed onto the specimen. By measuring the pressure of the cell fluid, the change of radial stress of the specimen could be monitored. Vertical deformation of the specimen was not allowed and the development of vertical swelling pressure was recorded by an internal load cell.

After the specimen had been assembled into the triaxial cell, vertical and radial pressures of 25 kPa and 10 kPa respectively were applied to the specimen. A small back pressure was then applied at the bottom drainage line which aimed to wet the specimen from bottom to top. Fig. 1 shows a schematic diagram and a photo of the setup of K_0 triaxial cell. Note that all the K_0 triaxial wetting tests were carried out at a temperature-controlled room with temperature varying within 1 °C.

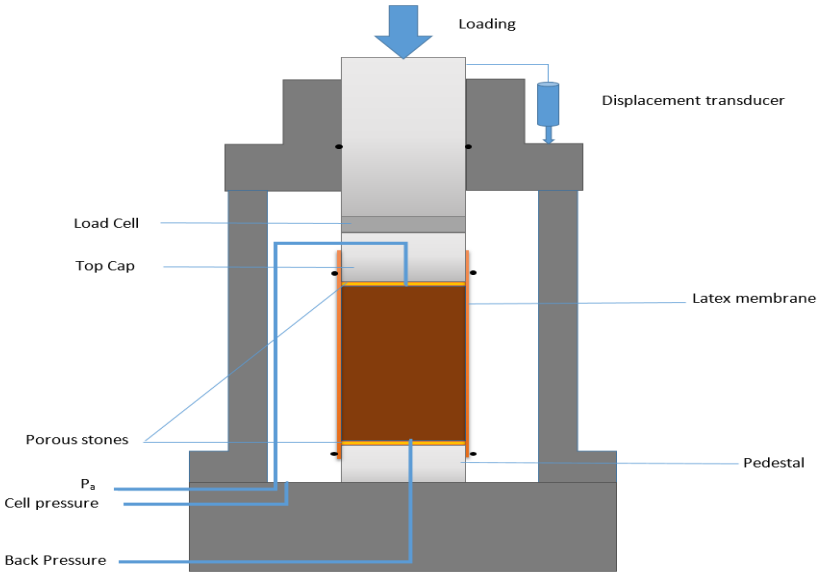

(a)

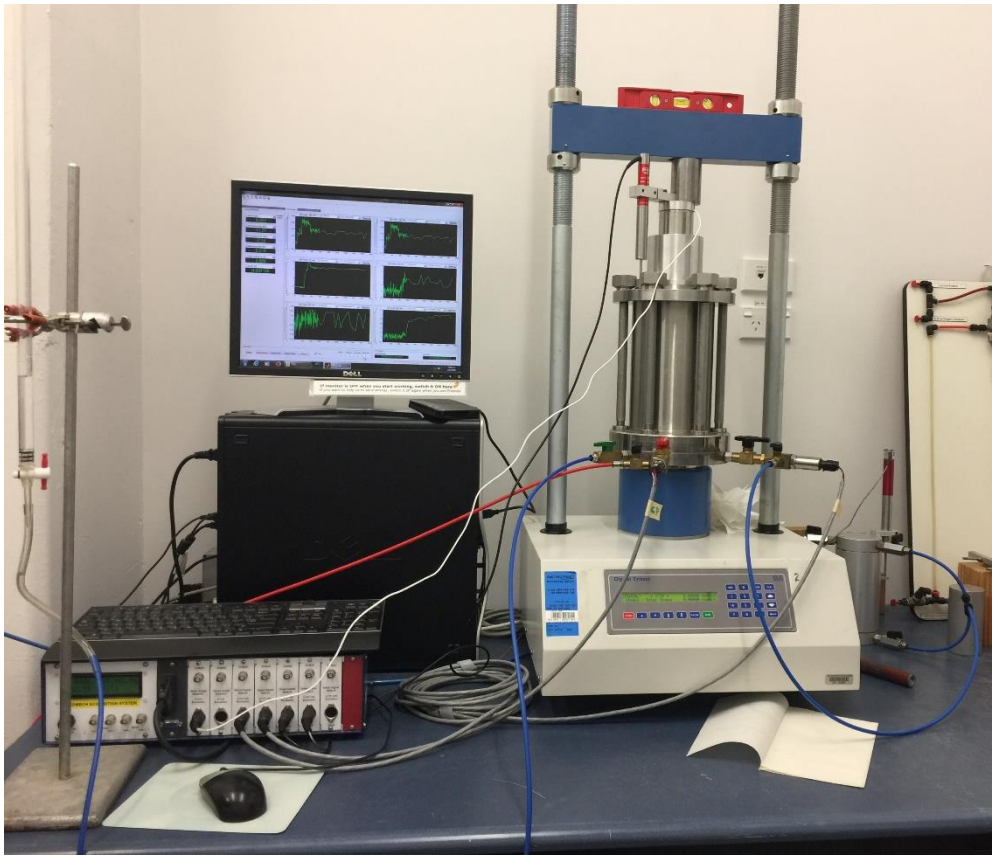

(b)

Figure 1: Setup of the K_0 triaxial cell: (a) schematic diagram; (b) photo

3.3 Specimen Preparation

This paper only presents preliminary results obtained from compacted specimens. Soil was compacted at 22% water content in a standard proctor compaction mould to a target density of 1.6 Mg/m^3. Each proctor sample was then trimmed into two specimens; one for oedometer and another one for K_0 triaxial testing.

4 RESULTS

4.1 Swelling in oedometric cell

Constant volume oedometer test provided a relatively simple experimental means to evaluate the development of vertical swelling pressure. Fig. 2 shows the test result. It was found that the vertical swelling pressure was rapidly developed within the first 3 hours and became essentially stable after 10 hours. The oedometer specimen showed a final vertical swelling pressure of about 370 kPa upon inundation.

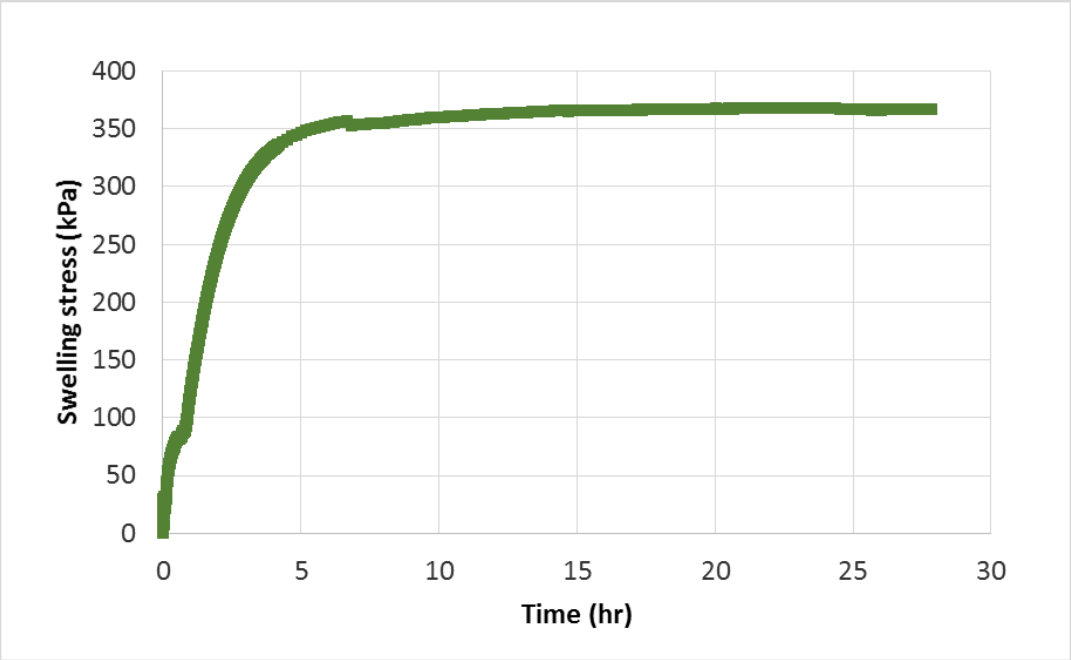

Figure 2: Development of vertical swelling pressure in constant volume oedometer testing

4.2 Swelling in K_0 cell

Two wetting tests, denoted by K1 and K2, were conducted in the K_0 triaxial cell. Fig. 3 shows the development of vertical and radial swelling pressure with time. It can be seen that both vertical and radial stresses in K1 developed very slowly during the first 5 hours yet the rate increased noticeably afterwards. It is because the back pressure first adopted in K1 was too small to wet the specimen effectively. The back pressure was then increased to 7 kPa to improve the effectiveness of soil wetting. Since then a more noticeable increase in both the vertical and radial stresses can be seen. The test was terminated after 6 days of testing though a mild increasing in the vertical swelling stress was observed. It was because K1 only served as a preliminary test to investigate the effect of back pressure on the rate of wetting. In K2, a 7 kPa back pressure was applied since the beginning of the test and the development of swelling pressure resembled a better trend and a faster rate as compared to K1. Test K2 was terminated after 3.5 days as both the vertical and radial swelling stresses became essentially steady. Besides, water was found coming out from the top drainage line which appeared to be indicting that the soil has reached a very high degree of saturation. At the end of the K2, the increase in vertical and radial stress due to wetting induced swelling was about 500 kPa and 100 kPa, respectively. The vertical swelling stress was larger than that obtained using the oedometer (which was 370 kPa). It is anticipated that friction along the oedometer ring may account for the difference in vertical swelling stress.

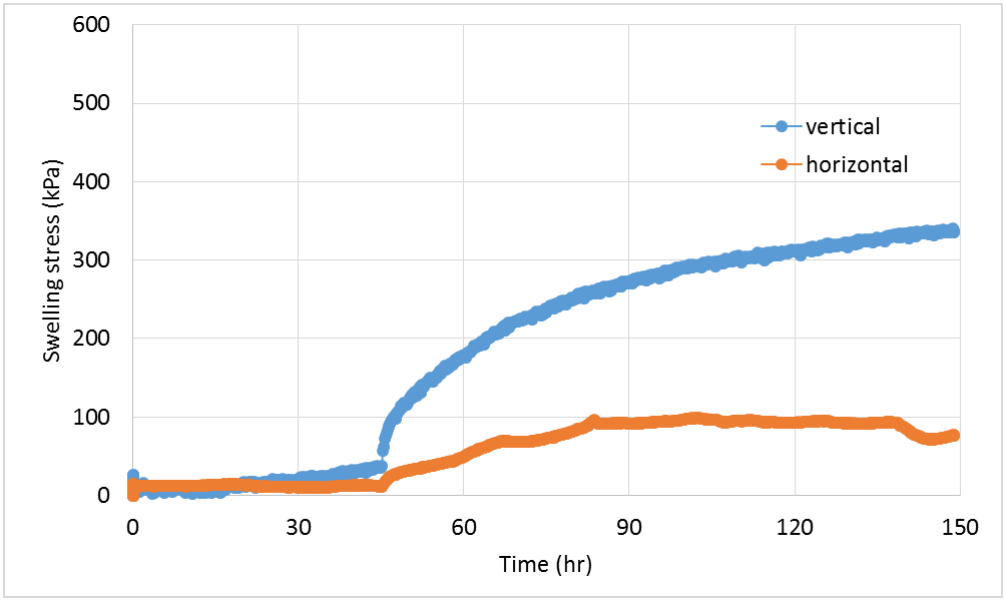

(a)

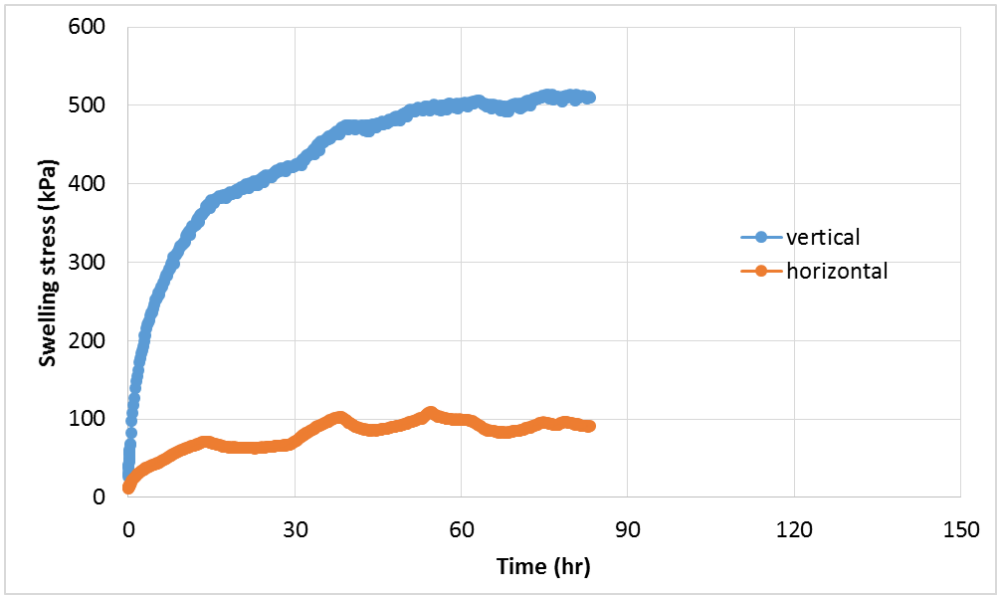

(b)

Figure 3: Development of vertical and radial swelling pressure in the K_0 triaxial cell: (a) Test K1; (b) Test K2

4.3 Observations and lessons learned

At the end of the K2 test, the specimen was cut into 3 slices representing soils at the top, middle and bottom of the specimen. Oven drying of the slices provided clear evidence that the water content at the end of the wetting test varied along the height of the specimen. Soil at the upper part of the specimen was not yet fully saturated. Indeed, fully saturating the specimen was not a trivial task and required a good control of back pressure and time. Furthermore, whether the cell chamber has been fully filled up with de-aired water or not is crucial to the determination of swelling pressure. Even a small air void inside the cell fluid chamber allows a specimen to increase its volume upon wetting and therefore gives noticeably lower swelling pressures. To sum up, the swelling pressures reported in K1 and K2 should have underestimated the swelling pressure that the soil can actually develop.

5 CONCLUSIONS

Experimental studies were undertaken to investigate the development of swelling pressure of a residual soil found in Auckland when subject to wetting. Key findings of the studies were:

- The proposed K_0 triaxial setup can be used to investigate the development of swelling pressure in both vertical and radial directions when an initially unsaturated soil is subject to wetting.
- Higher vertical swelling stress was reported from the K_0 triaxial cell as compared to results obtained based on conventionally used oedometer setup. Side friction along the oedometer ring probably attributed to the difference.
- The swelling pressures reported in the two preliminary K_0 triaxial tests should have been underestimated due to the difficulties in fully saturating the soil and the cell fluid chamber of the K_0 triaxial cell.

REFERENCES

Al-Shamrani, M.A. & Dhowian, A.W. (2003). Experimental study of lateral restraint effects on the potential heave of expansive soils. *Engineering Geology*, 69(1), 63-81.

ASTM (2003). Standard Test Methods for One-Dimensional Swell or Collapse of Soils, D4546-03, ASTM International, West Conshohocken, PA.

Campanella, R.G., & Vaid, Y.P. (1972). A simple K_0 triaxial cell. *Canadian Geotechnical Journal*, 9(3), 249-260.

Chen, F.H. (2012). *Foundations on expansive soils*. Elsevier.

Fredlund, D.G. & Rahardjo, H. (1991). Stress state variable approach to the prediction of heave. I*nternational Workshop on Clay Swelling and Expansive Soils*, Cornell University, Ithaca, New York, USA, 12-16.

Hettiaratchi, D.R.P., O'Sullivan, M.F. & Campbell, D.J. (1992). A constant cell volume triaxial testing technique for evaluating critical state parameters of unsaturated soils. *European Journal of Soil Science*, 43(4), 791-806.

Jennings, J.E.B. & Kerrich, J.E. (1962). The heaving of buildings and the associated economic consequences, with particular reference to the Orange Free State Goldfields, *The Civil Engineer in South Africa*, 4(11), 221-248.

Kermode, L.O. (1992). Geology of the Auckland urban area. Institute of Geological & Nuclear Sciences Ltd, Lower Hutt, New Zealand

Meyer, V. (1997). *Stress-strain and strength properties of an Auckland residual soil*. Doctoral Thesis. The University of Auckland, New Zealand.

Ng, C.W.W., Zhan, L.T., Bao, C.G., Fredlund, D.G. & Gong, B.W. (2003). Performance of an unsaturated expansive soil slope subjected to artificial rainfall infiltration. *Géotechnique*, 53(2), 143-157.

Ozer, M., Ulusay, R. & Isik, N. (2012). Evaluation of damage to light structures erected on a fill material rich in expansive soil. *Bulletin of Engineering Geology and the Environment*, 71(1), 21-36.

Pender, M.J. (1996). Aspects of Geotechnical Behaviour of Some NZ Materials. *Proceedings of the 7th Australia New Zealand Conference on Geomechanics: Geomechanics in a Changing World*. Adelaide, Australia. 21-39.

Qi, S. & Vanapalli, S.K. (2016). Influence of swelling behavior on the stability of an infinite unsaturated expansive soil slope. *Computers and Geotechnics*, 76(6), 154-169.

Thomas, M.G. (2008). *Impact of lateral swell pressure on retaining structure design using expansive cohesive backfill*. Master Thesis, University of Texas, Arlington, USA.

Van Der Merwe, D.H. (1964) The prediction of heave from the plasticity index and percentage clay fraction of soil. *South African Institute of Civil Engineers*, 6, 103-107.

Dellow, S., Massey, C.I., McColl, S.T., Townsend, D.B., Villeneuve, M. (2017)
Landslides caused by the 14 November 2016 Kaikoura earthquake, South Island, New Zealand
Proc. 20th NZGS Geotechnical Symposium. Eds. GJ Alexander & CY Chin, Napier

Landslides caused by the 14 November 2016 Kaikoura earthquake, South Island, New Zealand

S Dellow
GNS Science, Lower Hutt, NZ
s.dellow@gns.cri.nz (Corresponding Author)

C I Massey
GNS Science, Lower Hutt, NZ
c.massey@gns.cri.nz

S T McColl
Massey University
sammccoll@gmail.com

D B Townsend
GNS Science, Lower Hutt, NZ
d.townsend@gns.cri.nz

M Villeneuve
University of Canterbury
marlene.villeneuve@canterbury.ac.nz

Keywords: Kaikoura, earthquake, landslide, inventory, map

ABSTRACT

At 12.03 am local time on 14th November 2016 (UTC: 11.03 am 13th November 2016) a shallow, magnitude 7.8 earthquake struck near Waiau in North Canterbury, NZ. Strong ground shaking affected the North Canterbury and Marlborough regions of the South Island, causing widespread damage to buildings and infrastructure across these sparsely populated areas. Mid-rise (8-15 story) buildings in Wellington were also damaged. The most visible consequence of the strong ground shaking was widespread landslides. The area affected by landslides is sparsely populated, only a few dwellings were impacted and there were no recorded deaths due to landslides.

Tens of thousands of landslides were generated over 10,000 km^2 of North Canterbury and Marlborough, with the most intense landslide damage concentrated in 3500 km^2 around the areas of fault rupture. Landslides caused major disruption with all road and rail links to Kaikoura being severed. Several parts of State Highway 1 and the South Island main trunk railway between Ward in Marlborough and Oaro in North Canterbury were closed due to landslides.

The mapped landslide distribution reflects the complexity of the earthquake ruptures. The landslides are distributed across an elongated area consistent with the area affected by fault ruptures and intense ground shaking. The largest landslides triggered by the earthquake are located either on or adjacent to faults that ruptured to the ground surface. Initial results from our landslide investigations suggest that predictive models relying only on ground-shaking estimates may underestimate the number and size of the larger landslides that occurred.

1 INTRODUCTION

The Kaikoura Mw7.8 earthquake struck at 12.03 am local time on 14th November 2016 (UTC: 11.03 am 13th November 2016) - a shallow (15 km) magnitude 7.8 earthquake (Mw), with an epicentre located near Waiau in North Canterbury (Kaiser et al, 2017), and strongly shook the

North Canterbury and Marlborough regions of NZ. The strong ground shaking caused damage to buildings and infrastructure across the northeast of the South Island. A consequence of the strong ground shaking was widespread landslides. Given the sparsely populated area affected by landslides, only a few homes were impacted and no deaths from landslides occurred.

GeoNet, the geohazards monitoring programme run by GNS Science and funded by EQC, responds to major landslide events in New Zealand using a set of well-established criteria (Dellow 2001, McSaveney et al. 2010). The Mw7.8 Kaikoura earthquake met several of these criteria, including the presence of consequential hazards in the form of landslide dams and direct damage in excess of $1 M. The landslide response in the first week involved developing an awareness of where landslides had occurred and their relative size and spatial density. Response activities quickly evolved into two work-streams. One work-stream focussed on developing the processes and acquiring data in order to compile a world-class landslide inventory. The other work-stream focussed on landslide dams (landslides blocking rivers and streams and impounding bodies of water) and became an evolving process: from a search task, to a rapid assessment of hazard and examining high hazard dams for consequent risks, and then undertaking more detailed work to survey the most dangerous dams so the consequences of a very rapid (catastrophic) failure could be modelled and used by authorities to monitor and manage the risks.

Compiling landslide inventories from events that generate thousands to tens of thousands of landslides has evolved over the last sixteen years. The challenge is record critical information, especially on location and size, as accurately as possible using the best available source data. This ensures any subsequent work to understand and mitigate future hazards and risks from landslides has a good empirical evidence base. This work is important because it provides the basis for providing advice on longer term measures to manage the risks from landslide hazards, such as rules and regulations in district plans implementing risk reduction measures.

2 KAIKOURA LANDSLIDE INVENTORY

A landslide inventory is being compiled to capture the spatial distribution of landslides triggered by the Kaikoura earthquake, to provide information for recovery activities and to provide a high quality dataset for future research. The inventory captures information on: landslide type (material type and style of movement), landslide magnitude (areal size, and volume where possible), runout (distance the debris travels down slope), activity (whether pre-existing), connection and/or interaction with rivers (e.g. occlusions, blockages, buffered), and method of mapping and source of the data, along with the person who digitised and attributed the landslide (Table 1). Capturing the landslide data is an ongoing process as new information becomes available (e.g. satellite images, LiDAR survey data). Once the inventory has been completed it will be uploaded to the NZ landslide database maintained by GNS Science (http://data.gns.cri.nz/landslides).

The compilation of the landslide inventory has or will utilize the following data sources:

- Satellite imagery including: WorldView- 2 (WV2) 2.4 m resolution (multispectral bands). Imagery date: 22 November 2016; WorldView- 3 (WV3) 1.4 m resolution (multispectral bands). Imagery date: 25 November 2016; GeoEye (GE) 2 m resolution. Imagery date: 15 November 2016.
- Low level aerial oblique photographs are also being used to help define the landslides. These photographs (many thousands) have been captured by the landslide reconnaissance team and others post-earthquake, mainly from helicopters. The photographs are georeferenced using a GPS flight track-log, and they cover most of the area affected by landslides.
- Pre- and post-earthquake orthorectified aerial photographs (captured by Aerial Surveys Limited and commissioned by LINZ), 0.3 m resolution.
- Post-earthquake digital elevation models derived from airborne LiDAR.
- Post-earthquake digital surface models derived from stereo satellite imagery (NSF RAPID project).

- Pre- and post-earthquake digital surface models derived from the aerial photographs.

The WV2 and WV3 images (provided by Digital Globe) have been processed by GNS Science. These have moderate positional accuracy and in some mountainous areas the images have been orthorectified using a low-resolution digital surface model. The same images have been processed by EAGLE Technology and these have better relief stretch but poor positional accuracy. The images from the different data sources do not cover the entire area affected by landslides, but together they cover all of the main area affected.

Table 1: Landslide source area attribute table.

Fields	*ObjectID*	Source ID	Primary material	Secondary material
Explanation	*Auto*	A unique number for each digitiser's working copy of the database. Each source area should have a unique number. Number does not have to be unique to the whole database, as 'Originator' field will be used to differentiate duplicate id numbers.	The main material type that failed. This is not the geology or description of the origin of the material, but rather related to the material properties and their genesis (origin) which influence the failure and runout behavior. If it cannot be easily assessed use the 'undifferentiated' term.	If there is a second material type involved which appears to have had a significant influence on the failure or runout mechanics, then can include a second material type. If only one major material type, just leave this field as 'Null'.
Examples		1000.	Rock, clay, mud, coarse clastic (e.g. non-plastic silt, sand, gravel and boulders), peat, ice, undifferentiated.	Same options as primary material.

Landslide style	Activity/history	Connectivity	Comment	Method & Confidence
The movement mechanism of the landslide.	Indicates whether landslide appears to be a first-time failure or a reactivation of a previous movement.	This describes the relationship of the landslide debris to streams/rivers or major drainage lines.	Additional notes or clarifications.	Initial mapping method (i.e. imagery etc.) used to digitize the landslide, and confidence in the mapping.
Fall, topple, slide (can differentiate into rotational, planar, wedge), flow (can differentiate into avalanche, dry flow, flowslide, earthflow), slope deformation, or creep. Use 'undifferentiated' if you cannot tell which style of movement.	First-time failure, reactivated, retrogressed.	Uncoupled (i.e. sediment has remained on the slope); Coupled (at least some of the sediment has entered a drainage line (including active floodplain, but **not** including well-vegetated terraces); Blocked (any evidence of blockage even if blockage has since breached).		For each of the methods (Satellite, Orthophoto, Oblique photo, Ground visit, or Multiple [i.e. some combination of these methods]), specify the confidence of the mapping by either 'High' or 'Low'. 'Low' confidence may indicate strong uncertainty in the landslide boundary, uncertainty in the type of landslide mapped, or uncertainty in co-seismic occurrence (in Kaikoura EQ sequence). 'High' confidence can be used if you are fairly confident on the mapping.

Shape Area	*Length*	*Geology*	Originator
Auto generated	*Auto generated*	*Will auto generate from QMAP data later*	Who digitized the landslide
			C. Massey

In addition to the satellite imagery, low level aerial oblique photographs are also being used to help define the landslides. They are made available to the mapping team via a geodatabase structure in ESRI ArcMap. The national LINZ 8 m resolution digital elevation model (DEM) covers the entire area affected by landslides and is also being used for the mapping. In addition, a 1 m resolution DEM generated from pre-earthquake LiDAR covers a small coastal strip, but is still useful where applicable. The USGS landslide program team and members of the Landslide GEER (Geotechnical Extreme Events Reconnaissance) team have also contributed their data. These data have been used to generate the initial landslide inventory but this only includes larger landslides and only covers some of the main area affected by landslides. The process for compiling the definitive landslide inventory for the 14 November 2016 M7.8 Kaikoura Earthquake is described below.

To ensure a consistent methodology for capturing landslide information, several feature classes in an ArcGIS geodatabase have been set up, with fields containing drop down (restricted) lists for capturing the key landslide information. After scientists have mapped their respective areas, the data is collated and sent to various parties. A sample of each area is checked by another mapper. Following this, further samples of the mapped data have been targeted for field verification.

For each landslide, the following is being collected:
Polygons:

1. Extent of source area (polygon). Note that as best as possible, this should define the whole source area (not just the exposed source area), and may therefore overlap with the landslide debris.
2. Extent of landslide debris. If debris trails from multiple source areas merge, then the polygons also need to merge.

Points:

3. Landslide crown: A point at the top of the landslide crown/headscarp (highest point).
4. Debris Toe: A point at the distal end of debris tail (lowest down slope point).

Lines:

5. Surface deformation: evidence of surficial cracking (scarps), bulging or other deformation indicating mass movement not captured within the landslide polygon areas. These are potential sites of water ingress during later rainstorm events that may destabilize the slope.

For each landslide, all of these features are linked by a common number assigned to the ‘SourceID’ field within each feature class. If there are multiple source areas linked to one debris trail, each Source ID number is added into the ‘SourceID’ field in the landslide debris attribute table, separated by a comma.

For each landslide source area polygon, as much information as possible is entered into the attribute table (Table 1). There are drop down lists for landslide type information (material type and movement style/mechanism), which are based on the Hungr et al. (2014) classification. There are potentially other terms that can be added later that are not included in the classification. There are also a few landslide types that are rare (such as peat failures) but that have been included for completeness. For the debris trail polygon feature class, and the crown and debris toe points, only the SourceID is used to link to the landslide source area.

In addition to discrete landslides, linear slope deformation indicators (i.e. evidence of incipient failures, such as scarps, anti-scarps, or cracks that occur outside of the landslide polygons), can be mapped using a Surface Deformation feature class. These linear features are attributed with the type of surface deformation (from the ‘Type’ dropdown list). Work areas that cannot be mapped (e.g. due to cloud cover or very poor image quality) are also identified. For these areas, a polygon shapefile (e.g. named ‘obscured areas’) is created that outlines the obscured areas. These areas may be mapped at a later date if suitable imagery becomes available.

3 DISCUSSION

The 14 November 2016 Mw7.8 Kaikoura earthquake generated thousands of landslides and 196 landslide dams. Landslides affected a total area of about 10,000 km^2 with the majority concentrated in a smaller area of about 3,600 km^2. During the Kaikoura earthquake at least 23 faults ruptured to the ground surface or sea floor (Langridge et al., 2017). The observed landslide types correlate to two main types of geologically and geotechnically distinct materials, Neogene sedimentary rocks, and Triassic to Cretaceous Torlesse greywacke (Massey et al., in prep). The largest landslides triggered by the earthquake are located on or adjacent to faults that ruptured to the ground surface and are distributed across a broad area of intense ground shaking rather than clustered around the earthquake epicentre, and their locations appear to have a strong structural geological control (Rattenbury et al., 2006). This suggests that event-triggered populations of large landslides could be used to map surface-fault rupture for previous historical earthquakes in New Zealand (e.g. 17 June 1929 M7.8 Murchison earthquake; Hancox et al., 2002).

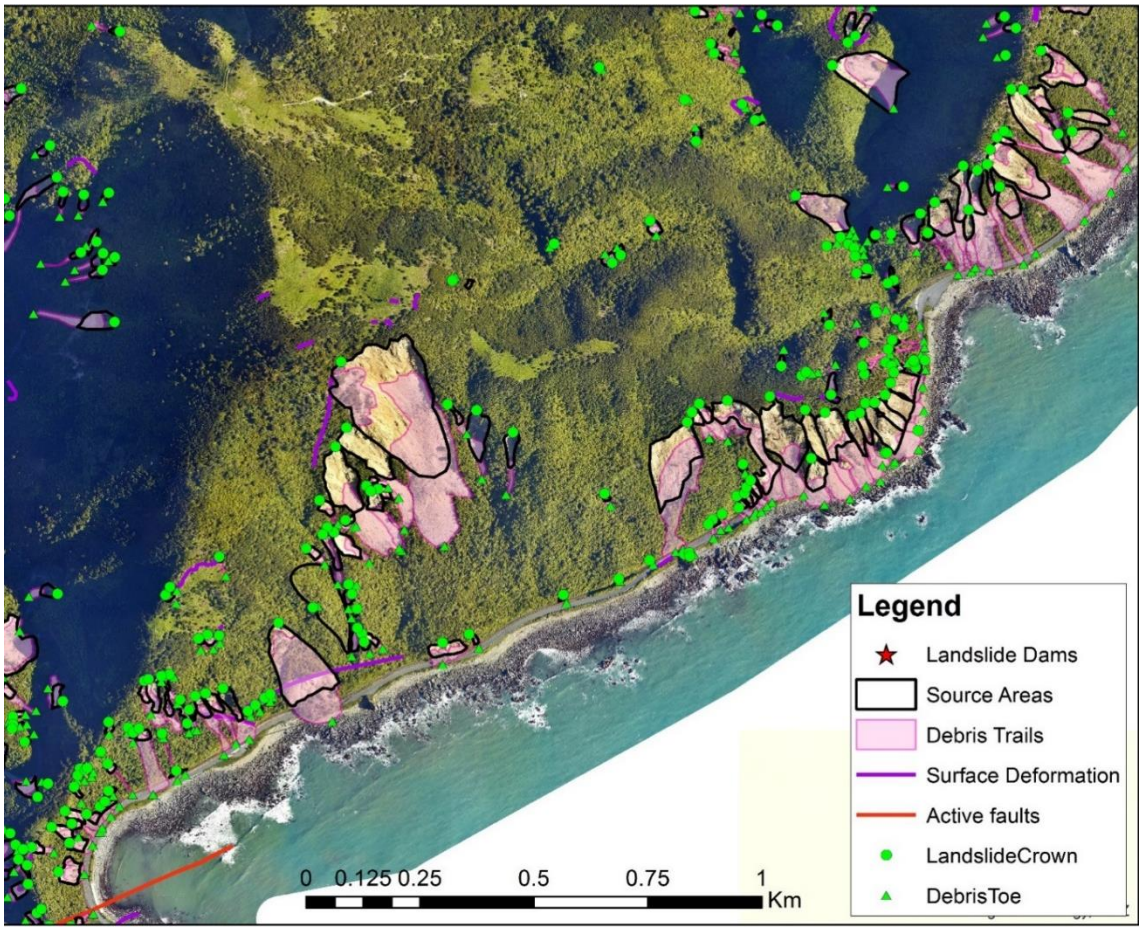

Figure 1: An example of landslide inventory mapping on the coast north of Kaikoura. The large landslides in the centre left of the photo did not reach the foot of the slope during the initial failure and the debris is a hazard that will remobilize in an aftershock or rainstorm and will present an ongoing risk to road and rail users if mitigation measures are not implemented.

The majority of landslides occurred predominantly in two geologically and geotechnically distinct materials, namely: weak to moderately strong (5-50 MPa) Neogene sedimentary rocks (limestones, sandstones and siltstones), and moderately strong to very strong (20-100 MPa) Triassic to Cretaceous Torlesse "basement" rocks (sandstones and argillite). The most frequently occurring landslide types, adopting the scheme of Hungr et al. (2014), correlate to these materials, where reactivated, rock planar and rotational slides tend to be the dominant landslide type in the

Neogene sedimentary rocks, and first time rock and debris avalanches with strong structural geological controls, were the dominant landslide type in the basement materials.

A noticeable feature of this earthquake is the number of valley blocking landslides it generated, which was partly due to the steep slopes and confined valleys in the area, and to the widely distributed strong ground shaking. More than 200 significant valley-blocking landslides triggered by this event have been mapped. The largest has an approximate volume of 23(±2) M m^3 and at least some of the debris from this travelled about 2.7 km down slope where it formed a dam blocking the Hapuku River. There are at least three other mapped valley-blocking landslides with volumes ranging from 2 M to 8 M m^3. Another noticeable aspect of this event is the large number of landslides that occurred on the steep coastal cliffs between Ward, in southern Marlborough, and Oaro, north of Christchurch (Figure 2).

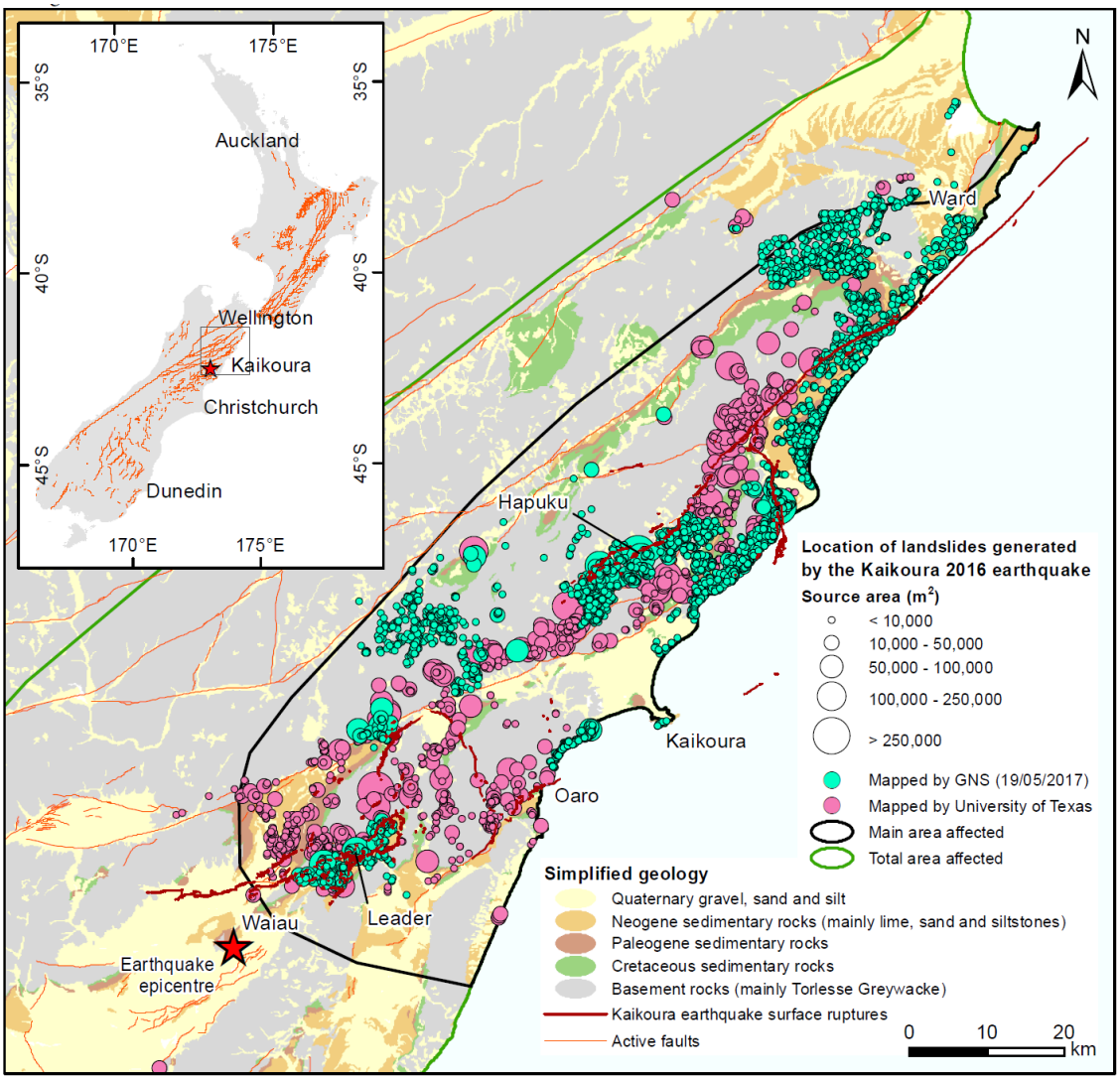

Figure 2: The landslide inventory for the 14 November 2016 Mw7.8 Kaikoura earthquake as at 19 May 2017. The active fault ruptures caused by the earthquake are shown as black lines.

The area affected by landslides is relatively remote with few people living there, and so only a few homes were impacted by landslides; there were no recorded deaths due to landslides. Landslides along the coast, however, caused the closure of State Highway (SH) 1 and the North Line of the South Island Main Trunk Railway, preventing people and goods from entering or leaving the town of Kaikoura, which had a permanent population of about 3,550 people (and seasonally expands due to tourists). These closures led the responsible government agencies to prioritise opening the 'Inland Route 70' to Kaikoura to allow the passage of people, food and

water. At the time of writing, the northern section of SH1 from Kaikoura and the North Line of the South Island Main Trunk Railway are both still closed, eight months after the earthquake. The long-term stability of the cracked slopes and the valley-blocking landslide dams during future strong earthquakes and significant rain events are an ongoing concern to the central and local government agencies responsible for rebuilding homes and infrastructure. The number of dams that are of concern is reducing with rainstorm events (particularly in early April 2017) resulting in breaching of four of the dams of greatest concern. Although the direct threat of debris flood hazards from rapid dam breaching is reducing, the longer-term effects of sediment aggradation as landslide debris moves downstream from the steeper in-land slopes to the sea is another 'cascading' hazard that could pose a risk to agriculture, aquaculture and infrastructure. For example, these cascading hazards will increase river aggradation which will widen river beds, increase bank erosion and consequently increase both the magnitude and frequency of flooding.

The mapped landslide distribution from the Mw7.8 Kaikoura earthquake suggests a complex interaction among earthquake ground shaking, geology and topographic slope angle, which drives the occurrence of the largest landslides generated by this event. Past efforts to explain the spatial variability in co-seismic landslide size and concentration typically rely on comparisons with earthquake magnitude and mechanism, epicentral distance, seismic observations such as peak ground acceleration, peak ground velocity, and engineering parameters such as Arias Intensity and other proxies for ground shaking intensity such as proximity to mapped faults. These factors are then combined with topographic slope angle and geologic information to generate event-based statistical or deterministic models used to explain the distribution of landslide frequency and area or volume. However, most event-based models fail to adequately describe the occurrence of the few relatively large-volume landslides generated by a given earthquake, and in plots of landslide frequency and volume, these landslides are typically outliers. This limits the usefulness of such models for assessing the hazard and geomorphic impacts associated with large co-seismic landslides. A high quality landslide inventory and detailed engineering geological mapping of the largest landslides will allow the interaction between large landslide occurrence and surface fault rupture to be investigated and how the localised release of energy, along with structural geological and material controls and slope morphology interact to initiate large landslides.

The data will be useful for recognizing immediate hazards (potential for failures/reactivations), outburst floods (dam breaches), short- to longer-term potential for debris flow and valley floor aggradation impacts, sediment budgets for catchments, and for assessing landslide causes (i.e. relationships with topography, geology, fault structures, shaking). One of the main uses of this data will be to assess how slopes performed in particular rock and soil (material) types during the earthquake. This data will be especially useful for those similar-sized slopes in Wellington, where much of the city is formed in similar materials (greywacke sandstones and argillite) to those forming the slopes in the, albeit more mountainous, Kaikoura region. Such data will allow us to better constrain the response of the Wellington slopes to strong shaking, e.g. a Wellington Fault earthquake.

4 CONCLUSIONS

Tens of thousands of landslides were generated over 10,000 km^2 of North Canterbury and Marlborough as a consequence of the 14 November 2016, Mw7.8 Kaikoura Earthquake. The most intense landslide damage was concentrated in 3500 km^2 around the areas of fault rupture. Given the sparsely populated area affected by landslides, only a few homes were impacted and there were no recorded deaths due to landslides. Landslides caused major disruption with all road and rail links with Kaikoura being severed. State Highway 1 (the main road link in the South Island of New Zealand) and the South Island main trunk railway between Ward in Marlborough and Oaro in North Canterbury, were closed because of landslides.

Landslide inventory work after a major natural hazard event is an evolving process. Information is required immediately but creating high-quality empirical landslide inventories takes time and

underpins the development of plans and policies to mitigate and manage the risks from slope instability. High-quality empirical landslide inventories are crucial as a baseline dataset against which to quantify changing hazards as rainstorms and aftershocks further alter the landscape. A high-quality landslide inventory will provide a basis for understanding the longer-term impacts of this earthquakes as sediment is washed from slopes and through fluvial systems where bridges and flood protection schemes are at risk of being overwhelmed.

5 ACKNOWLEDGEMENTS

The work described in this paper is the result of the efforts of many people. In the interests of space three people heavily involved in the initial response are named as authors, but that in no way reflects or diminishes the contributions made by the following people. From GNS Science, Lower Hutt NZ: G Archibald, J Begg, Z Bruce, J Carey, F Della Pasqua, M Hill, K Jones, B Lyndsell, B Lukovic, M Rattenbury, S Read, B Rosser, C Singeisen, P Villamor. From GNS Science, Dunedin, NZ: P Glassey. From the University of Canterbury, Christchurch, NZ: J Davidson. From the United States Geological Survey, Menlo Park, California: J Godt, R Jibson, K Allstadt, F Rengers. From the University of Washington, Seattle, USA: J Wartman. From the University of Texas, Austin, USA: E Rathje, M Little. From the University of California, Berkeley, USA: N Sitar. From the University of Michigan, Ann Arbor, USA: A Adda. From the Elixis Group Ltd., Athens, Greece: J Manousakis. The authors also thank the paper reviewers for their comments. And of course this work would not have been possible without the skill and dedication of the helicopter pilots from Precision Helicopters; Christchurch Helicopters; and Advanced Flight Ltd.

REFERENCES

Dellow G.D. 2001 GeoNet landslide response. *New Zealand Geomechanics News* 62: 31-35.

Hancox, G.T.; Perrin, N.D.; Dellow, G.D. 2002 Recent studies of historical earthquake-induced landsliding, ground damage, and MM intensity in New Zealand. *Bulletin of the New Zealand Society for Earthquake Engineering*, 35(2): 59-

Hungr, O., Leroueil, S., Picarelli, L., 2014. The Varnes classification of landslide types, an update. Review article. *Landslides*. April 2014. Volume 11. Issue 2, pp 167-194.

Langridge, R.M.; Litchfield, N.J.; Van Dissen, R.J.; Ries, W.F. 2017 A summary of fault ruptures and slip from the November 14th 2016 Kaikoura earthquake. p. 32 In: Kelly, K.; Christophersen, A.; Rhoades, D.A.; Gerstenberger, M.C.; Wang, T.; Harte, D.S.; Hammond, K.A.T. *10th International Workshop on Statistical Seismology*, 20 - 24 February 2017, Wellington, New Zealand. Programme and abstracts. Lower Hutt, N.Z.: GNS Science. GNS Science miscellaneous series 101

McSaveney MJ, Massey CI, Dellow GD 2010 Landslide response and monitoring: The New Zealand GeoNet experience. p. 443-450 (paper 053) IN: Williams, A.L.; Pinches, G.M.; Chin, C.Y.; McMorran, T.J.; Massey, C.I. (eds) Geologically active: delegate papers *11th Congress of the International Association for Engineering Geology and the Environment*, Auckland, Aotearoa, 5-10 September 2010. Boca Raton, Fla: CRC Press.

Rattenbury, M.S.; Townsend, D.; Johnston, M.R. (compilers) 2006: Geology of the Kaikoura area: scale 1:250,000 geological map. Lower Hutt: GNS Science. Institute of Geological & Nuclear Sciences 1:250,000 geological map 13. 70 p. + 1 folded map.

Dellow, S., Massey, C.I. & Cox, S.C. (2017)
Response and initial risk management of landslide dams caused by the 14 November 2016 Kaikoura Earthquake, South Island, New Zealand *Proc. 20th NZGS Geotechnical Symposium.* Eds. GJ Alexander & CY Chin, Napier

Response and initial risk management of landslide dams caused by the 14 November 2016 Kaikoura earthquake, South Island, New Zealand

S Dellow
GNS Science, Lower Hutt, NZ
s.dellow@gns.cri.nz (Corresponding Author)

C I Massey
GNS Science, Lower Hutt, NZ
c.massey@gns.cri.nz

S C Cox
GNS Science, Dunedin, NZ
s.cox@gns.cri.nz

Keywords: Kaikoura, earthquake, landslide, dams, risk, management

ABSTRACT

At 12.03 am local time on 14th November 2016 (UTC: 11.03 am 13th November 2016) a shallow magnitude 7.8 earthquake, with an epicentre located near Waiau in North Canterbury, struck the North Canterbury and Marlborough regions of NZ. The most visible consequence of the strong ground shaking was widespread landslides. A feature of the landslides from this earthquake is the large number (196) of drainage blocking landslides it generated. This was partly due to the steep and confined slopes in the area and the widely distributed strong ground shaking.

The majority of the landslide dams occurred in two geological and geotechnically distinct materials: weak sedimentary rocks (sandstones and siltstones) where first-time and reactivated rock-slides were the dominant landslide type, and; strong sedimentary rocks (greywacke and limestones) where first-time rock and debris avalanches dominated. This gave rise to two quite distinct end-member landslide dam types, large rock block slides comprised a few large blocks, and rock and debris avalanches comprised of coarse angular gravels.

Identifying the location and size of landslide dams was a priority in the post-earthquake response because of the potential public safety risks. Once dams had been located the hazard of catastrophic failure (likelihood) was assessed. Those with a higher likelihood of catastrophic failure had the consequences (risks) from failure identified. Those with a higher likelihood of failure and substantive risks were examined in more detail using field mapping and terrestrial laser scanning. These data were used to model the catastrophic failure scenarios to determine the scale of the risk so that appropriate countermeasures could be put in place to alleviate the risks.

1 INTRODUCTION

The Kaikoura Mw7.8 earthquake struck at 12.03 am local time on 14th November 2016 (UTC: 11.03 am 13th November 2016) - a shallow (15 km) magnitude 7.8 earthquake (Mw), with an epicentre located near Waiau in North Canterbury (Kaiser et al, 2017), and strongly shook the North Canterbury and Marlborough regions of NZ (Figure 1). The strong ground shaking caused widespread damage to buildings and infrastructure across the sparsely populated areas of the northeast of the South Island. The most visible consequence of the strong ground shaking was widespread landslides (Figure 1). Given the sparsely populated area affected by landslides, only a few homes were impacted and there were no recorded deaths due to landslides.

GeoNet, the geohazards monitoring programme funded by the New Zealand Earthquake Commission and run by GNS Science, has a requirement to respond to major landslide events in New Zealand using a set of established criteria (Dellow 2001, McSaveney et al. 2010). The M_W7.8 Kaikoura earthquake met several of these criteria, including the presence of consequential hazard in the form of landslide dams and direct damage in excess of $1M. The landslide reconnaissance effort the first day after the earthquake quickly determined that landslide dams represented on ongoing hazard and risk to earthquake response activities. Immediate plans were made to search for, photograph and attribute all the landslide dams. Following on from this, a process for evaluating the hazard of dam failure and the risks or consequences of failure was developed. This process quickly identified landslide dams with the highest hazards and greatest risks allowing emergency managers to focus efforts to develop mitigation plans. The dams with the greatest risks, to people or road networks, were selected for additional work to acquire survey-quality data to model rapid dam failure to further inform mitigation strategies.

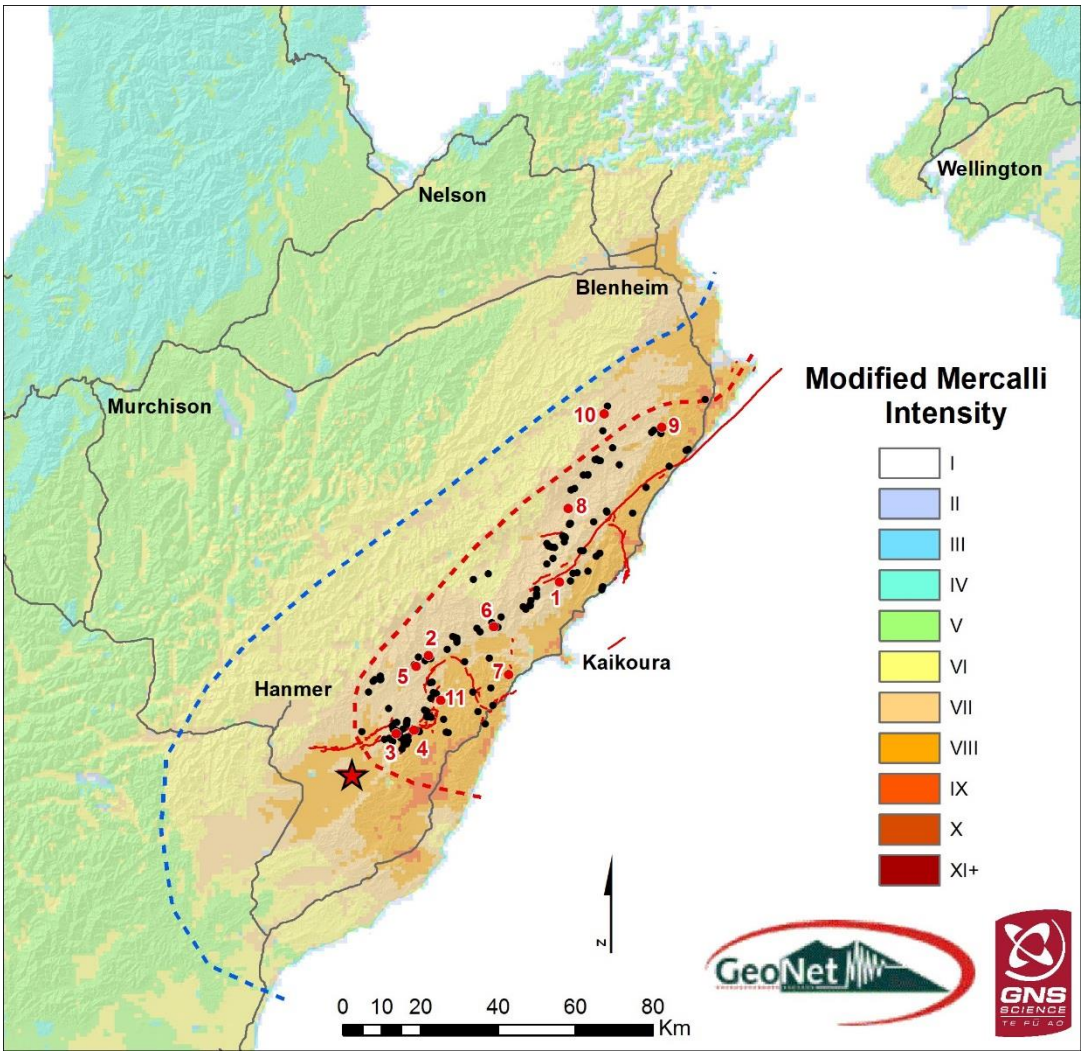

Figure 1: The 14th November 2016 M_W7.8 Kaikoura Earthquake. The epicentre is shown by the red star. The colours depict the MM Shaking Intensity, with MM VIII in the worst affected areas with isolated pockets of MM IX where deep soils are present. The areas of light to moderate landslide damage (area between the blue dashed and red dashed lines), and severe landslide damage (area inside the red dashed line) are shown. Fault rupture during the earthquake is shown as solid red lines (Litchfield et al, 2017). The landslide dams are by a black dot, or for the dams assessed having the highest failure hazard and consequential risks a numbered red dot: 1: Hapuku; 2: Conway; 3: Stanton; 4. Leader; 5. Towy; 6. Linton; 7. Ote Makura (Goose Bay); 8. Clarence; 9. Waima/Ure; 10: Medway; 11. Gelt. (Map credits: MMI: Nick Horspool).

2 LANDSLIDE RECONNAISSANCE

As the Kaikoura earthquake occurred in the middle of the night, aerial reconnaissance of the damage could not start until daylight. The first helicopter from Wellington left at daybreak (6.00 am) and identified the first slope failures caused by the earthquake on the western side of Cape Campbell. Further south the large landslides completely blocking State Highway 1 and the railway line were seen. While flying along the Hope Fault, which is at the southeast foot of the Seaward Kaikoura Range, several of the rivers crossing the range front were flown upstream, particularly if river flows were absent or the water was discoloured. This revealed landslide damming in several river valleys with water slowly impounding behind the landslide dams.

No reports of people trapped or missing were received (a priority for emergency services) indicating that it was unlikely any potential victims had been buried by rock falls and slides along State Highway 1 north and south of Kaikoura. This allowed the response to shift focus to potential public safety risks. The key concern with respect to public safety was finding and assessing the landslide dams because of the potential for rapid failure of the dams resulting in a flood wave travelling down the river valleys without warning and presenting a risk to life and property. This was further highlighted by Environment Canterbury reporting on and dealing with the landslide dam in the Clarence River that failed about 4.00 pm on the afternoon of the 14 November 2016, some 16 hours after the earthquake.

A plan to systematically search for, and assess landslide dams was developed and implemented. The first task of the landslide reconnaissance effort was to determine the extent of the area to be searched for landslide dams. Within three days of the earthquake it was determined that the approximate bounds of the landslide damage extended from the Waiau River in the south, from the coast to inland at Hanmer Springs, and from Hanmer Springs to the Clarence Acheron confluence, north along the Acheron until Wards Pass before following the Awatere River to the coast (the area within the red dashed line on Figure 1).

3 LANDSLIDE DAMS

The assessment of, landslide dams after the 14th November 2016 M_W7.8 Kaikoura Earthquake is still in progress (as of July 2017). The process started with delineating the area that needed to be searched to find landslides that had blocked river and stream valleys, forming landslide dams. This first step required defining the search area (Figure 1). Once the search area had been defined, and in reality this was an iterative process, a systematic search was undertaken starting with the areas where the strongest shaking was reported and where lives and/or property might be at risk from rapid failure of the landslide dams.

On the 14 November 2016 a landslide dam blocking the Clarence River was quickly identified. By 4.00 pm on the 14 November 2016 this landslide dam had overtopped and breached, sending a rapidly attenuating flood-wave down the Clarence River. The early identification and reporting of this dam to Environment Canterbury, the government agency responsible for managing floods in Canterbury's rivers, allowed a warning to be issued to residents of the Clarence Valley. As more landslide dams were recognised in the first week after the earthquake a general warning to the public was issued to stay away from rivers and streams because of the possible risk of rapid failure of landslide dams sending a flood-wave down valleys without warning. The systematic search for landslide dams eventually identified 196 drainage blocking or drainage constricting landslides in the area affected by landslides (Figure 1). This figure includes landslides that diverted river and stream courses over low-lying river terraces as well as landslides that completely blocked valleys to a depth of sometimes tens of metres. The rational was that areas of identified instability could potentially fail again during strong aftershocks or high intensity rainfall events, and having a list of sites where the exiting instability could result in a more substantial blockage was deemed prudent.

Initially all catchments were searched systematically by helicopter reconnaissance flights and any constrictions located by GPS, photographed and recorded in a GIS. At the start we reported daily observations to MCDEM using map coordinates, but these had potential for misunderstanding and miscommunication. Once the nearest altitude contour was adopted with the catchment name, we had a unique identifier that enabled consistent reporting, communication, classification of photographs and follow-up investigations. Landslides were initially triaged daily, with their hazard classified into high, medium, low, unlikely and yet to develop. For those involved in the first week this typically involved 6-8 hours of flying per day, followed by 5-6 hours of data plotting and photo assessment, then 1-2 hours writing reports and recommendations for MCDEM. It was an intensive phase of work that utilised many people and left all weary.

Using the estimated values for the key variables for each dam, the hazard of the dam failing suddenly and sending a flood-wave downstream was made. This included identifying rivers and streams where multiple dams were present and where the flood could become a cumulative event. From this exercise a list of about thirty landslide dams was compiled where a breach hazard was present. This list of dams was then assessed for potential downstream risks, i.e. where people or property were potentially at risk from the rapid failure of a dam, taking into account the likely rapid attenuation of the flood-wave. This initially reduced the list to 12 dams (the process is a fluid one and remains so – some dams have overtopped and breached, some have breached by piping failure, others have been added to or removed from the list as better data has come to hand). Where the hazard or risk was assessed as high, either because of a large volume of impounded water, or people or critical assets (e.g. road bridges) in the path of a flood caused by rapid failure of the landslide dam further work was undertaken. A team of geologists and geomorphologists from the United States Geological Survey, including landslide specialists was then asked to review the landslide dam assessments and visited the key dams in the field. This peer review of the initial work carried out by the GeoNet landslide reconnaissance team confirmed the initial field assessments.

A process was then started to survey the dams in priority order based on risk, with life safety issues given the highest priority. The life safety issues identified included both occupied buildings (including a campground) and risks to road-users. Seven dams were identified as posing potential life safety risks, and additional data was collected so that rapid or catastrophic failure of the landslide dam could be modelled and the results used to inform those agencies tasked with managing public safety. Initially this started with experienced engineering geologists and geotechnical engineers providing visual estimation of the key parameters. However, it quickly became apparent there was variation in the way people interpreted observations and interpreted risk, so a process to obtain more rigorous data by surveying the dams and acquiring good topographic data for the potential flow-paths downstream of the dams was instigated. A terrestrial laser scanner was used to acquire initial scans of the landslides. However, it has taken longer to get LiDAR topographic data which is the preferred dataset for modelling the flow-paths. As each dataset has been acquired, the models have been re-run. This has consistently shown the initial visual estimates were conservative.

Two types of landslide dams are recognised based on the geological source material as mapped by Rattenbury et al (2006), namely: weak (5-20 MPa) Neogene sedimentary rocks (sandstones and siltstones), and moderately strong to very strong (20-100 MPa) Carboniferous to Cretaceous Torlesse 'basement' greywacke (sandstone) and argillite (mudstone) rock, but also includes some Neogene limestones. The most frequently occurring landslide types, adopting the scheme of Hungr et al. (2014), correlate to these materials, where reactivated rock planar and rotational slides tend to be the dominant landslide type in the Neogene sedimentary rocks. First time rock and debris avalanches with strong structural geological controls, were the dominant landslide type in the basement materials. This led to two quite distinct types of landslide dam. The weak rocks failed as large block slides and slumps and, compared to the strong rock dams, were relatively impervious (Figure 2). In contrast, the landslide dams formed from strong source rocks were effectively piles of porous angular gravels where piping of water flows through the dam is readily

apparent (Figure 3). The source material for these landslides is Torlesse Greywacke which typically forms disrupted rock slides because of the closely jointed and fractured nature of the source rock mass. The resulting debris can be described as an angular gravel and is highly permeable. As a result, the large greywacke-derived landslide dams developed flows through the permeable material forming the dam under normal flow conditions. On the 6 April 2017, ex-Tropical Cyclone Debbie passed over the area dumping 100-150 mm of rain in 24-hours for the first time since the earthquake. As a consequence of this rainfall several of the greywacke dams finally overtopped and breached, effectively removing the landslide barrier and potential hazard.

How these two very different styles of landslide dam perform over the coming months and years is of interest as it will inform landslide dam assessment after future earthquakes. As of the 12th July 2017 only one of the large, strong source rock dams remain (on the Hapuku), the others having breached during annual flood flows generated by heavy rainfall in early April 2017. The large weak rock dams on the Stanton and Leader rivers are either still intact (Stanton River) or partially intact (Leader River).

Figure 2: Landslide dam on the Leader River shortly after the earthquake. The landslide is a slump/block slide in a siltstone and is typical of the large landslides in weak Neogene rocks. The dam overtopped and partially breached in February 2017 (Photo credit: Environment Canterbury).

In one case, the landslide dam in the upper reaches of the Hapuku River, the terrestrial laser scanning process has been repeated three times. The change model was derived from two scans, the first taken on 15 December 2016 and the second on 28 March 2017 (Figure 4) and shows the landslide dam was slowly deforming. The crest of the dam was lowered by a nearly one metre over a period of nearly four months, and the front of the dam shows erosion and scour from piping flows with deposition downslope. Subsequent to the second scan, the dam overtopped on 6 April 2017 with the formation of an overflow channel and further erosion of the downstream face.

4 DISCUSSION

A noticeable feature of this earthquake is the number of drainage blocking landslides it generated, which was partly due to the steep and confined slopes in the area and to the widely distributed

strong ground shaking. 196 drainage blocking landslides triggered by this event have been mapped. The largest has an approximate volume of 12(±2) M m^3 and the debris from this travelled about 2.7 km down slope where it formed a dam blocking the Hapuku River. There are at least three other mapped drainage blocking landslides with volumes ranging from 2M to 8M m^3.

The largest landslides triggered by the Kaikoura earthquake are located either on or adjacent to faults that ruptured to the ground surface, are distributed across a broad area of intense ground shaking are not clustered around the earthquake epicentre, and their location appears to have a strong structural geological control (Figure 1). The mapped landslide distribution from the M_W7.8 Kaikoura earthquake, therefore suggests a complex interaction among earthquake ground shaking, geology, and topographic slope angle, which drives the occurrence of the largest landslides generated by this event. Many of the very large landslides that formed drainage blocking dams are also associated with fault rupture through or close to the source area. It is the potential for these large landslide dams to fail rapidly that represents the longer-term hazard after an earthquake. The large landslide dams on the Leader River, Stanton River and Hapuku River were identified as potential hazards in November 2016 and remain hazardous as of July 2017.

Figure 3: The greywacke-derived landslide dam in the upper reaches of the Conway River in the Seaward Kaikoura Ranges. This large dam developed flows through the permeable material of the dam under normal flow conditions (Photo 3A: J. Mitchell, 22/11/2016). On the 6 April 2017, 100-150 mm of rain fell in 24-hours and as a consequence this dam overtopped and breached, removing the landslide barrier and potential hazard. (Photo 3B: D. Townsend, 7/4/2017).

Monitoring and observations of landslide dams over a period of several months shows these features change. The change can be gradual as in the case of the settlement of the debris forming the dam across the Hapuku River or rapid as in the case of dams breaching. Rainstorms are an obvious driver of rapid change to landslide dams. A hazard that has slowly emerged is where large landslides occurred high in catchments. The inflow of water has been very slow and it has taken several months for lake filling to reach a point where it needs to be monitored regularly. An

example is the landslide dam on the Bourne Stream, a tributary of the Waiau River, 5 km east of Waiau. This lake was still 4 metres below crest level as of July 2017.

The long-term stability of the cracked slopes and the drainage blocking landslide 'dams' during future strong earthquakes and significant rain events are an ongoing concern to the central and local government agencies responsible for rebuilding homes and infrastructure. A particular concern are the debris flood hazards that occur when some of the landslide dams breach. Several of these dams are located upstream from people and critical infrastructure such as road bridges, which might be at risk if the hazard were to occur. However, the number of dams that are of concern is reducing with rainstorm events (particularly in early April) resulting in breaching of four of the dams of greatest concern. Although the direct threat of debris flood hazards from rapid dam breaching is reducing the longer-term effects of sediment aggradation as the debris moves downstream from the steeper in-land slopes to the sea is another 'cascading' hazard that could pose a risk to agriculture, aquaculture and infrastructure. For example, these cascading hazards will increase river aggradation which will widen river beds, increase bank erosion and consequently increase both the magnitude and frequency of flooding.

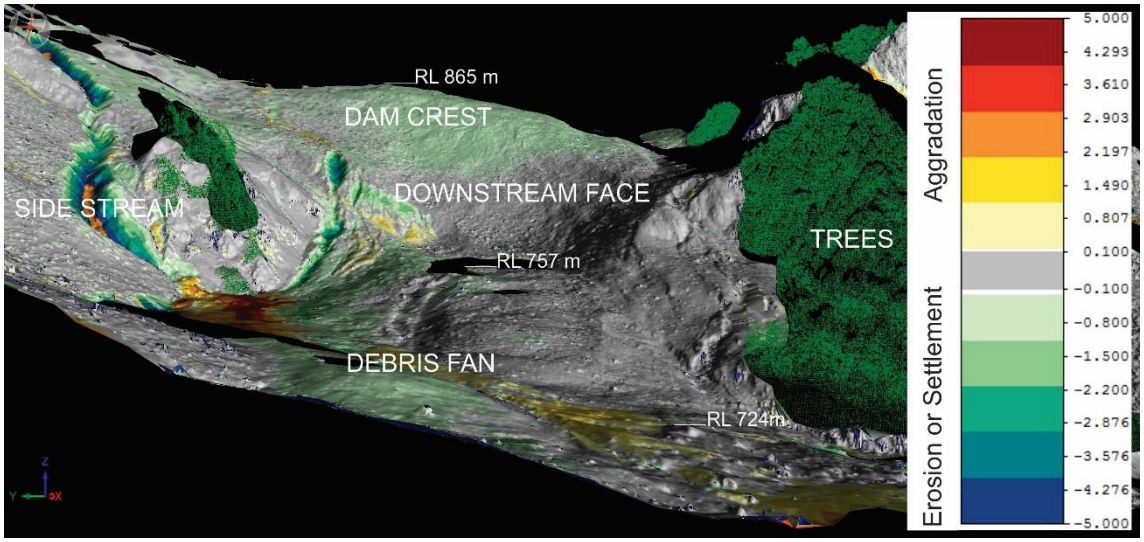

Figure 4: A change model of the downstream face of the Hapuku landslide dam. It shows cool colours in areas of settlement and erosion (greens and blues) and warm colours (oranges and yellows) in areas of aggradation. Dark green is woody vegetation. (Image processing carried out by Garth Archibald, GNS Science).

5 CONCLUSIONS

196 landslide dams or significant drainage constrictions were created as a result of this earthquake. Most have been assessed as having a low probability of failing in a way that will cause a hazard or present a risk to people or property as a consequence of rapid failure. However, at least a dozen, were identified as potentially hazardous with seven having clearly identified risks to people and property should they fail rapidly. Work to monitor and revise landslide dam hazard and risk assessments was ongoing for many months after the earthquake and in some cases continues (as of July 2017). The assessment of hazards and risks posed by the landslide dams informed the development of long-term management plans to mitigate the hazards and manage the residual risk. However, natural events have also played a hand with four of the seven dams assessed as having the highest risk having already breached before or during rainstorms in April 2017. These breached dams no longer pose a direct risk, but the longer term behaviour of the landslide source areas and the large volume of landslide debris now in the river systems still needs to be determined.

6 ACKNOWLEDGEMENTS

The work described in this paper is the result of the efforts of many people. In the interests of space three people involved in the initial response are named as authors, but that in no way reflects or diminishes the contributions made by the following people. From GNS Science, Lower Hutt NZ: G Archibald, J Begg, Z Bruce, J Carey, F Della Pasqua, M Hill, K Jones, B Lyndsell, B Lukovic, M Rattenbury, S Read, B Rosser, C Singeisen, D Townsend, P Villamor. From GNS Science, Dunedin, NZ: P Glassey. From the University of Canterbury, Christchurch, NZ: J Davidson, M Villeneuve. From Massey University, Palmerston North, NZ: S McColl. From Environment Canterbury, Christchurch, NZ: M Schoenfeld, N Griffiths, S McCracken, C Margetts. From Golder Associates, Christchurch, NZ: J Bensing. From Aurecon, Christchurch, NZ: Jan Kupec. From Emergency Management Ltd, Wellington NZ: Jon Mitchell. From the United States Geological Survey, Menlo Park, California: J Godt, R Jibson, K Allstadt, F Rengers. From the University of Washington, Seattle, USA: J Wartman. From the University of Texas, Austin, USA: E Rathje, M Little. From the University of California, Berkeley, USA: N Sitar. From the University of Michigan, Ann Arbor, USA: A Adda. From the Elixis Group Ltd., Athens, Greece: J Manousakis. And of course this work would not have been possible without the skill and dedication of the helicopter pilots from Precision Helicopters; Christchurch Helicopters; and Advanced Flight Ltd.

REFERENCES

Dellow G.D. 2001 GeoNet landslide response. New Zealand Geomechanics News 62: 31-35.

Hungr, O., Leroueil, S., Picarelli, L., 2014. The Varnes classification of landslide types, an update. Review article. *Landslides*. April 2014. Volume 11. Issue 2, pp 167-194.

Kaiser, A.E.; Balfour, N.; Fry, B.; Holden, C.; Litchfield, N.J.; Gerstenberger, M.C.; D'Anastasio, E.; Horspool, N.A.; McVerry, G.H.; Ristau, J.; Bannister, S.C.; Christophersen, A.; Clark, K.J.; Power, W.L.; Rhoades, D.A.; Massey, C.I.; Hamling, I.J.; Wallace, L.M.; Mountjoy, J.; Kaneko, Y.; Benites, R.A.; Van Houtte, C.; Dellow, G.D.; Wotherspoon, L.; Elwood, K.; Gledhill, K.R. 2017 The 2016 Kaikoura, New Zealand, earthquake: preliminary seismological report. *Seismological Research Letters, 88(3):* 1-13; doi: 10.1785/0220170018

Litchfield, N., Villamor, P., Van Dissen, R.J., Nicol, A., Pettinga, J., Barnes, P., Langridge, R., Little, T., Barrell, D., Mountjoy,J., Ries, W., Rowland, J., Fenton, C., Stirling, M., Cochran, U., and the surface rupture mapping team. Submitted. Surface fault ruptures of the Mw 7.8 2016 Kaikōura Earthquake demonstrate complexity at a plate boundary transition zone. Geology.

McSaveney MJ, Massey CI, Dellow GD 2010 Landslide response and monitoring: The New Zealand GeoNet experience. p. 443-450 (paper 053) IN: Williams, A.L.; Pinches, G.M.; Chin, C.Y.; McMorran, T.J.; Massey, C.I. (eds) Geologically active: delegate papers *11th Congress of the International Association for Engineering Geology and the Environment*, Auckland, Aotearoa, 5-10 September 2010. Boca Raton, Fla: CRC Press.

Rattenbury, M.S.; Townsend, D.; Johnston, M.R. (compilers) 2006: Geology of the Kaikoura area: scale 1:250,000 geological map. Lower Hutt: GNS Science. Institute of Geological & Nuclear Sciences 1:250,000 geological map 13. 70 p. + 1 folded map.

South British House – A collaborative approach for the seismic upgrade of a building

K L de Graaf
Beca, Tauranga, NZ
kim.degraaf@beca.com (Corresponding author)

H Wahab
Beca, Tauranga, NZ
harry.wahab@beca.com

Keywords: seismic assessment, liquefaction, numerical modelling, Plaxis2D

ABSTRACT

This paper describes the geotechnical aspects of a collaborative seismic assessment and foundation strengthening design for an existing building in the Tauranga CBD. The reinforced concrete 6 storey high structure is supported on concrete piles founded on potentially liquefiable volcanic soils. Initial assessments concluded that the building seismic rating was governed by the foundations, limited by piles bearing on liquefiable soils. Both CPT based and shear wave velocity based methods were used to assess the liquefaction potential at the site. The data indicated that the site was susceptible to liquefaction at a moderate level of shaking, and that the zones of liquefaction differed across the building footprint. The detailed seismic assessment concluded that ground effects were a limiting factor for the building's seismic performance and foundation strengthening would be required. The assessment and design of the foundation strengthening scheme required numerical analyses to model the soil-structure interaction effects. Two independent numerical models, one structural the other geotechnical, were run in parallel. Close collaboration between the geotechnical and structural engineers enabled the independent models to converge allowing the strengthening design to be based on a robust analysis. A key feature of the foundation strengthening design was an emphasis on controlling building (and therefore soil) deformation under seismic loading. This meant that pile settlement tolerances under the ULS seismic conditions could be relaxed from that normally associated with conventional designs.

1 INTRODUCTION

The seismic assessment of buildings in New Zealand requires collaboration between structural and geotechnical engineers to ensure that both the building superstructure and local site conditions are adequately considered. Where the site conditions are difficult, such as liquefiable ground, or the superstructure unusual, such as an asymmetric structure, numerical modelling can be a useful tool to determine the effects of soil-structure interaction. The resulting soil-structure interaction effects can then be communicated between geotechnical and structural engineers to produce the best possible outcome for the building owner.

Such a process has been undertaken for South British House in Tauranga. South British House is a six storey high rectangular shaped building located on a near-level site at 35 Grey Street in the Tauranga CBD. The building was constructed circa 1978, and consists of a reinforced concrete-framed and shear walled dual system supported on concrete piles. The building is founded on potentially liquefiable volcanic soils and was classified as earthquake prone by an Initial Evaluation Procedure (IEP) completed in 2012. Design records and limited pile testing suggested that many of the piles supporting the structure were founded within the potentially liquefiable soils.

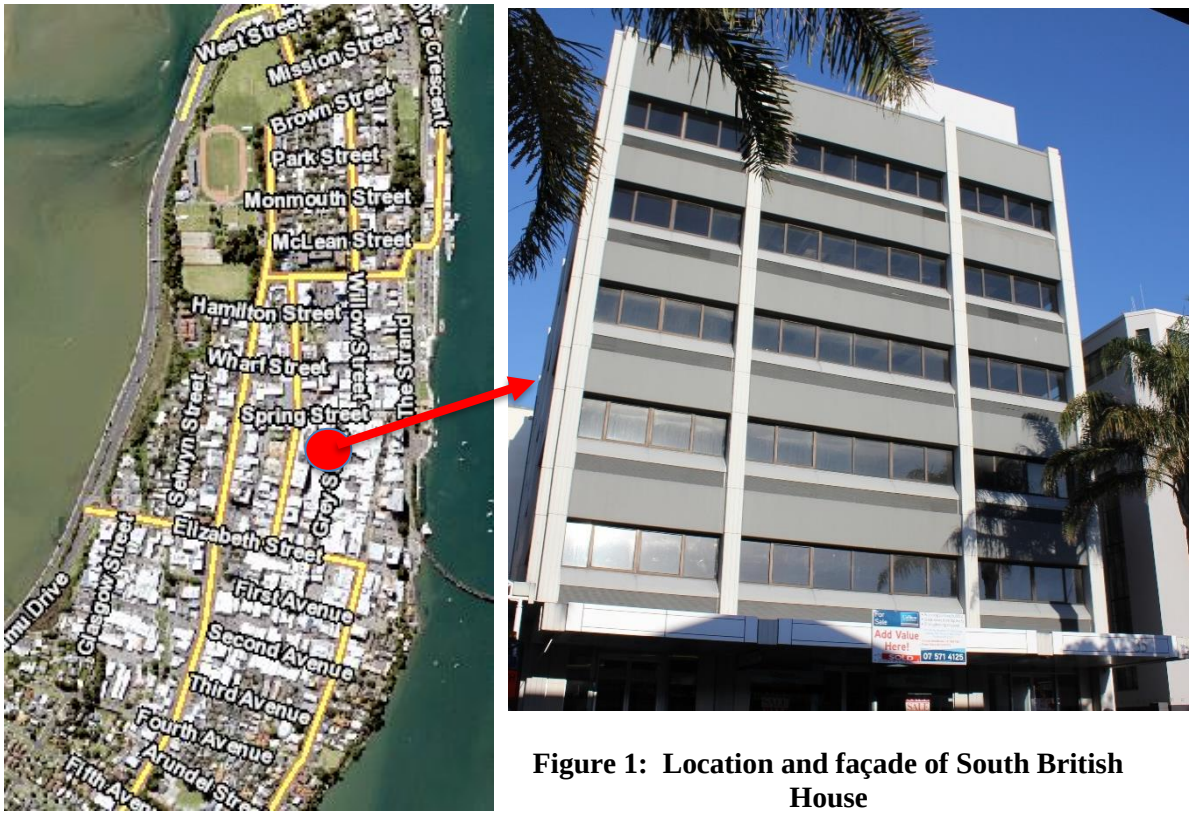

Figure 1: Location and façade of South British House

The building owner wished to strengthen the building to a minimum of 67% of the New Building Standard (67%NBS). A low percentage NBS rating based on the IEP combined with liquefiable ground conditions suggested extensive strengthening of both the substructure and superstructure would be required. In addition there were a number of challenges, including:

- Uncertainty surrounding the existing pile depths (there were no as-built records), although limited testing indicated there was variability in the lengths;
- An asymmetric structural system;
- The building is located within a constrained site (see Figure 1) surrounded by other buildings, an alley way and Grey Street. The majority of any foundation works would need to be carried out from within the building, i.e. with limited headroom;
- The presence of a significant underground service (11kV cable) running under the rear of the building which presented a significant constraint to investigation, design and construction;
- The Client's preference that the existing tenants at the front of the building on the ground floor should be able to remain during the works.

2 GEOTECHNICAL CONSIDERATIONS

The initial geotechnical investigations were conducted in 2013 and indicated significant risks of liquefaction to depths of at least 20m below ground level (bgl). These initial investigations consisted of Cone Penetration Testing (CPT) and machine boreholes. The soils identified during this testing included the Matua Subgroup, a material that can have a large amount of pumiceous content. More recently, the geotechnical community has become aware of the limitations of CPT based liquefaction assessments in the Matua Subgroup due to the potential for crushing of this pumice content (for example Orense et al, 2012). Therefore, additional geotechnical

investigations were undertaken to better understand the liquefaction hazard by considering the low strain properties the materials being investigated.

This additional testing was undertaken in 2015 during the detailed seismic assessment process and consisted of seismic CPT (sCPT), hand auger boreholes and laboratory testing. These investigations were carried out in the alley to the south of the building and also internally.

Internal investigations by sCPT proved to be challenging owing to the electromagnetic 'noise' from the 11kV cable and difficulty with generating a signal through the ground floor slab. The latter was overcome by cutting slots through the floor slab to allow the surface wave generator to be in direct contact with the ground. The former was overcome by performing the testing at night when the cable could be turned off.

2.1 Soil Profile

The soil profile was collated from both series of investigations and was found to comprise fill and undifferentiated volcanic ashes overlying silty sands and sandy silts of the Matua Subgroup, with groundwater at around 2.5m bgl (refer Figure 2). The Matua Subgroup soils are of Pleistocene age (c. 1.8 Ma to 10,000 years) and can be highly variable in their distribution. The Matua Subgroup soils encountered included a succession of loose to medium dense silty sands and sandy silts, and medium dense to very dense sands.

An infilled valley / channel feature was encountered under Grey Street that consisted of mostly cohesive Holocene Alluvium. Some differences in the soil profile in the transverse direction were also found with the infilled valley feature appearing to narrow towards the north.

2.2 Liquefaction Assessment

Liquefaction analyses utilised conventional CPT methods (Boulanger & Idriss, 2014) combined with shear wave velocity methods (Kayen et al., 2013, 2015). The assessment of the Matua Subgroup included consideration of the shear wave velocity measurements in relation to the theoretical limit of the onset of liquefaction due to the age of the materials. The overall assessment indicated that a thin 0.5m layer just beneath the water table is likely to liquefy, along with a 3m thick layer from between 5 and 8m bgl across the site. The denser Matua Subgroup was regarded as less likely to liquefy at the seismic shaking levels being considered.

This initial liquefaction assessment was conducted with the magnitude and Peak Ground Acceleration (PGA) determined following NZS1170.5:2004. Following the updated recommendations from MBIE/NZGS Module 3 (2016), the PGA and magnitude were amended to that outlined in the NZTA Bridge Manual (2016), and resulted in the thin 0.5m layer as not being susceptible to liquefaction. Therefore the crust thickness across the site was able to be increased.

Regardless, extensive liquefaction is indicated at a PGA of 0.12-0.14g in the deeper 5-8m bgl layer, which would lead to a loss of bearing support to the piles founded within or close to the liquefied soils, resulting in step-change behaviour as outlined by Clayton et al (2014).

2.3 Pile Investigations

The original building drawings indicate that the structure was founded on piles formed as 2 pile or 3 pile groups, with some individual piles. The drawings do not indicate a required depth of founding for the piles and as-built information is not available. Low strain pile integrity testing was initially undertaken in 2013 and focussed on the building piles located along the alley and the building frontage on Grey Street. This initial testing suggested that the piles tested along Grey Street were founded at approximately 15-16m bgl and those along the alley at 5-6m bgl.

Other methods to confirm the pile depths were considered destructive, and as the piles were to be retained, it was decided to complete the low strain pile integrity testing on the remainder of the piles. This concluded that with the exception of the Grey Street piles, all piles were founded at approximately 5-6m bgl, and thus founded on or within a liquefiable layer (Figure 2). The testing

was not conclusive for two piles located on the northern side, possibly shorter than anticipated, and this was considered during our analysis.

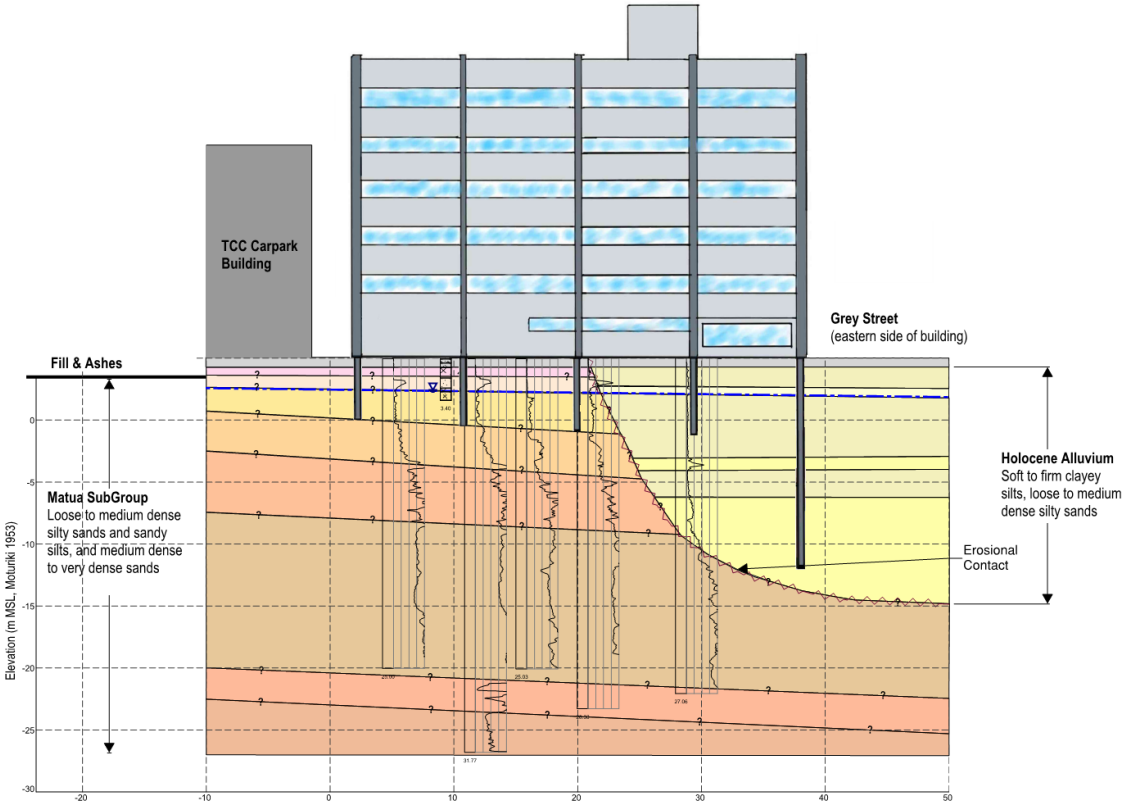

Figure 2: Soil profile and pile lengths southern side (Lavin et al, 2016)

2.4 Detailed Seismic Assessment

A detailed seismic assessment of the existing building was completed following the recommendations provided in the New Zealand Society for Earthquake Engineering (NZSEE) guideline document (NZSEE, 2006 including amendments 1, 2, 3 and 4).

The assessment concluded a seismic rating for the building of 55%NBS (IL2), as determined using the NZSEE guidelines. The rating was limited by the potential loss of pile bearing support resulting from the anticipated onset of liquefaction in the founding soils at 55% of the Ultimate Limit State (ULS) seismic loading (approximately 0.14g).

3 NUMERICAL MODELLING OF STRENGTHENING OPTIONS

A number of potential foundation strengthening solutions were considered, including:

- Reinforced concrete raft foundation tied into existing ground beams and pile caps.
- Formation of a soil raft by jet grouting under the building.
- Bored piles around the perimeter of the building with ground beams tied into the existing pile caps.
- Multiple screw or micro-piles each side of existing piles tied into the existing foundations by way of reinforced concrete pile caps.

Given that the liquefiable layers are influential in the movement of the building during seismic shaking, it was identified that there was a need for geotechnical and structural collaboration in order to appropriately consider the effects of the soil-structure interaction.

Preliminary geotechnical finite element models (FEM) of the problem were analysed using Plaxis2D Classic (2012). The initial results of soil behaviour were then provided to the structural engineers in the form of moduli of subgrade reaction or soil springs, to consider the effects of the various strengthening options on the building superstructure in eTABs. Results from eTABs were then incorporated back into the Plaxis2D model to update the soil response. In this manner, several iterations of modelling were performed.

3.1 Plaxis2D Model

Plaxis2D modelling was undertaken in order to understand the effects of the liquefiable layers on the existing foundations and superstructure, and the proposed new foundations. The variability in the soil profile across the building indicated less liquefiable material was present on the northern side of the building with a variable crust thickness above this. The axisymmetric design of the building also caused variability in the stiffness of the building from the north to the south and therefore the seismic loads that would be incurred across the building foundations. Thus both soil profiles were modelled to consider the three-dimensional effects on the building.

The modelling was not concerned with the response of the ground due to seismic shaking, rather the effects of loss of bearing, tilting and settlement on the superstructure. From the initial geotechnical model, structural engineers returned likely loading scenarios under static and seismic conditions across the footprint of the building and through the piles (refer to Lavin et al (2016)). These loads were included in the Plaxis2D model as point and uniformly distributed loads (UDL) at piles and across ground beams, respectively. The sensitivity of the depth of embedment of the existing piles, from the pile integrity testing, was considered during the modelling with variations in depths for the piles on the north-east side of the building and toward Grey Street.

The liquefied materials within the soil profiles on the northern and southern side were represented by a Mohr-Coulomb material with a reduced Young's Modulus and undrained shear strength. The stiffness of the liquefied soils was varied from 3-5% of the original values as sensitivity runs, following Cubrinovski et al (2006), and the undrained shear strength amended to a liquefied shear strength following Olson & Stark (2002).

3.2 Modelling Outcomes

The Plaxis2D modelling considered the proposed foundation options; including the existing foundation, a raft foundation, a raft with additional piles and a raft with ground improvement. All cases were considered for both the northern and southern sides of the building to understand the impact of the change in the soil profile beneath the building.

As anticipated, both the northern and southern sides of the building showed tilting toward the west under the existing piles when liquefied layers were included. The raft foundation with and without ground improvement also failed to reduce the differential settlements.

The inclusion of additional piles, in the centre and western areas of the building, which are founded well beneath the liquefiable layers, was found to provide a robust solution with resilience of the foundations to liquefaction (Figures 3 and 4). The soil movements resulting from this solution were considered manageable for the superstructure when included in the eTABs structural model.

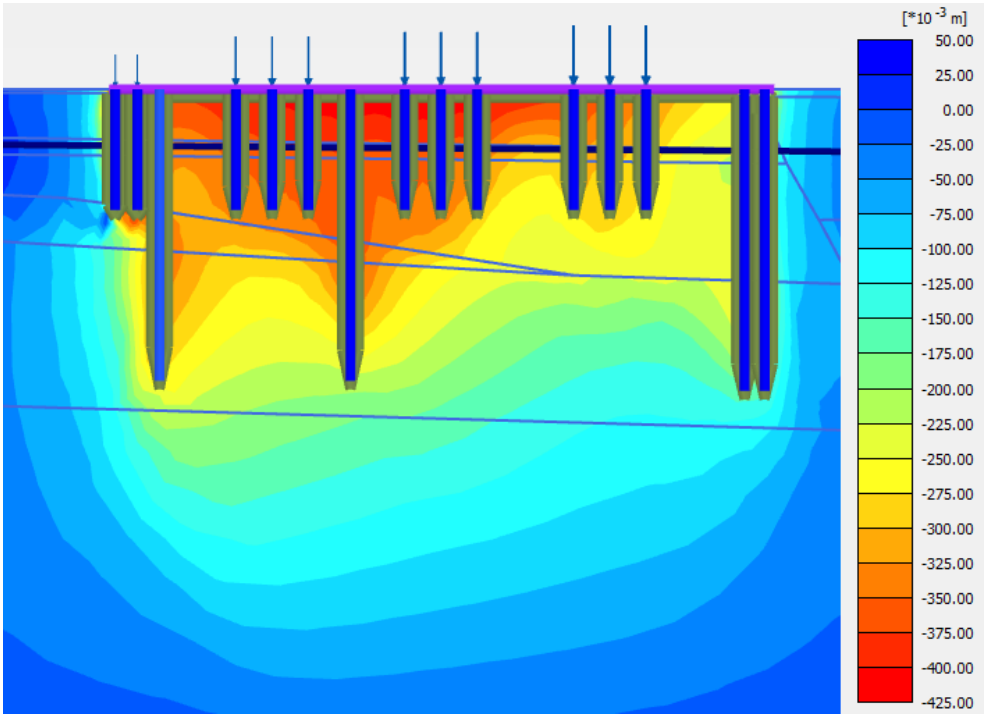

Figure 3: Plaxis2D analysis vertical settlements on northern side

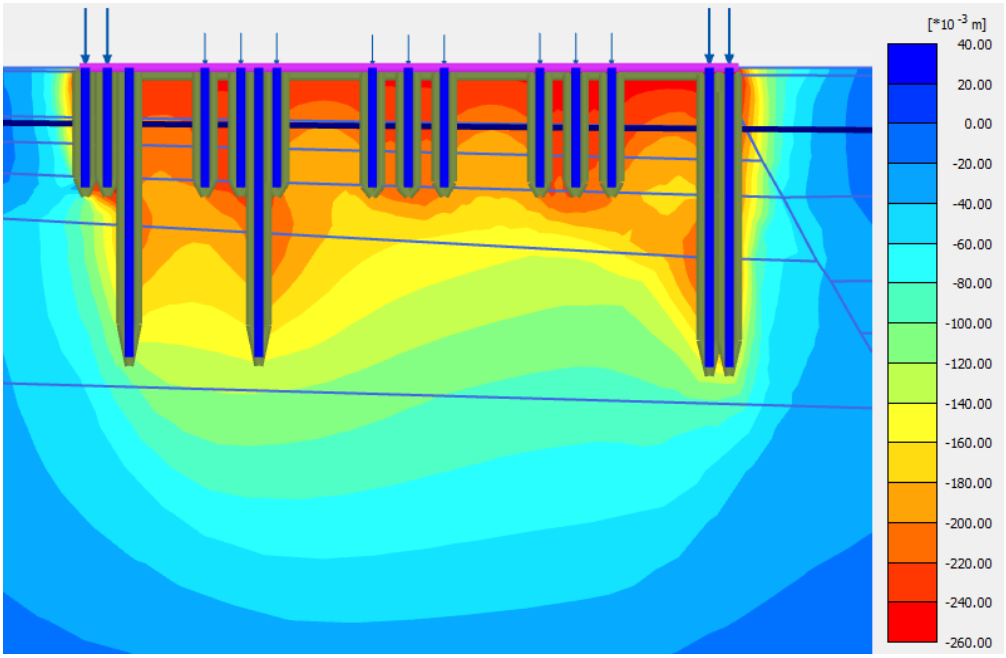

Figure 4: Plaxis2D analysis vertical settlements on southern side

4 FOUNDATION DESIGN

The results of the joint numerical modelling indicated that additional piles would be required under seismic conditions to support the building. This result, in combination with the constrained space around and within the building, lead to a foundation strengthening design using screw piles, with a substantial structural raft foundation beside the shear wall on the northern side of the building.

A key feature of the foundation strengthening design was an emphasis on controlling the building and associated soil deformations under seismic loading. Due to this, pile settlement tolerances under the ULS seismic conditions could be relaxed from that normally associated with conventional designs, as building serviceability was not the governing factor. This allowed the screw piles to be designed for greater deflections.

As Tauranga soils are inherently variable, the pile designer installed three screw piles to the south of the building to undertake pile testing. This testing allowed the pile designer to be confident that the depths of embedment and pile sizing would be adequate to provide the required support to the building during seismic events. The ultimate load and deflection results were incorporated back into the eTABs model to further improve the foundation and superstructure design.

5 CONSTRUCTION

Safety in design reviews of the construction process outlined difficulties in opening multiple sections of ground around the columns, with likely reduction in support for the pile caps and therefore the building, if a seismic event happened during construction. Due to this and the site constraints, screw piling has been undertaken in stages.

Initial screw piling began in late 2016 (Figure 6) with the raft foundation adjacent to the shear wall completed in June 2017. It is anticipated that construction of the foundations will be completed by the end of August 2017.

Figure 6: Stage 1 installation of screw piles (Lavin et al, 2016)

6 CONCLUSIONS

The seismic assessment of a six storey building in the Tauranga CBD has resulted in an increased %NBS and reduced cost to the building owner for retrofit, due to a collaborative approach between geotechnical and structural engineers, and the pile designer.

Initial evaluations of the South British House building suggested that it was earthquake prone and would require substantial foundation and superstructure remedial works. Additional investigations to characterise the behaviour of the Matua Subgroup led to a reduction in the likely depths of material susceptible to liquefaction, however pile bearing was still affected.

The collaborative approach between the structural and geotechnical engineers, and later the pile designer, involved the sharing of numerical modelling results and pile testing results. The

incorporation of the various results into the numerical models resulted in a robust retrofit design that could be carried out within a restricted site.

7 ACKNOWLEDGEMENTS

We would like to acknowledge Steve McLennan, Kamil Kazimoglu, Craig Lavin, Harris Maragkos and our many colleagues who have assisted with this work.

REFERENCES

Boulanger, R. W., and Idriss, I. M. (2014). *CPT and SPT based liquefaction triggering procedures.* Report No. UCD/CGM-14/01, Center for Geotechnical Modeling, Department of Civil and Environmental Engineering, University of California, Davis.

Clayton, P., Kam, W.Y., and Beer, A. (2014). Interaction of geotechnical and structural engineering for the seismic assessment of existing buildings. *Proc. Annual Conference NZSEE 2014*, Wellington.

Cubrinovski, M., Kokusho, T., and Ishihara, K. (2006). Interpretation from large-scale shake table tests on piles undergoing lateral spreading in liquefied soils. *Soil Dynamics and Earthquake Engineering*, 26: 275-286.

Kayen, R., Moss, R. E., Thompson, E. M., Seed, R. B. Cetin, K. O. Kiureghian, A. D. Tanaka, Y. and Tokimatsu, K. (2013). Shear-wave velocity-based probabilistic and deterministic assessment of seismic soil liquefaction potential. *Journal of Geotechnical and Geoenvironmental Engineering*, 139:407-419.

Kayen, R., Moss, R. E., Thompson, E. M., Seed, R. B. Cetin, K. O. Kiureghian, A. D. Tanaka, Y. and Tokimatsu, K.(2015). Erratum for "Shear-wave velocity-based probabilistic and deterministic assessment of seismic soil liquefaction potential." *Journal of Geotechnical and Geoenvironmental Engineering*, 141(9):1-1.

Lavin, C., Wahab, H., de Graaf, K., and Maragkos, H. (2017). South British House – seismic upgrade of a building founded on liquefiable soils. *Proc. Annual Conference NZSEE 2017*, Wellington.

MBIE/NZGS. (2016). Module 3: Identification, assessment and mitigation of liquefaction hazards. *Earthquake Geotechnical Engineering Practice*. May 2016.

NZSEE. (2006). *Assessment and improvement of the structural performance of buildings in earthquakes* (including amendments 1, 2, 3 and 4). New Zealand Soc. for Earthquake Eng. (NZSEE), Wellington, New Zealand.

NZS1170.5. (2004). *Structural Design Actions, Part 5: Earthquake Actions*. Wellington, New Zealand, Standards New Zealand.

NZTA. (2016). *Bridge Manual* (SP/M/022). Third Edition, Amendment 2, NZ Transport Agency. New Zealand: NZ Transport Agency.

Olson, S.M., and Stark, T.D. (2002). Liquefied strength ratio from liquefaction flow failure case histories. *Canadian Geotechnical Journal*, 39: 629-647.

Orense, R.P., Pender, M.J., and O'Sullivan, A.S. (2012). *Liquefaction Characteristics of Pumice Sands*. Final Report of EQC Project 10/589.

Plaxis. (2012). Plaxis2D Classic.

Improving site specific modified driving formulae using high frequency displacement monitoring

R Damen
Brian Perry Civil, Auckland, NZ
ronaldd@fcc.co.nz (Corresponding author)

D Denes
Foundation Specialists Group, Melbourne, Australia
ddenes@foundationspecialists.com.au

Keywords: high strain dynamic testing, PDA, driving formulae

ABSTRACT

Results from high strain dynamic pile testing (PDA) of impact driven piles are frequently correlated to pile driving sets and temporary compression, to obtain site specific modifications of driving formulae. An accurate record of driving set and temporary compression is required to obtain meaningful correlations. Traditionally, pile sets and temporary compression are measured manually on the pile during pile driving. The development of high frequency displacement monitoring has enabled more accurate measurement of set and temporary compression. Data obtained using high frequency displacement monitoring of closed ended piles has revealed differences between the apparent set at around 200 milliseconds and the final set at around 1 second. Incorporation of this data into the signal matching process and the subsequent correlations with driving formulae resulted in a more consistent match. Recommendations are made to improve correlations with pile driving formulae.

1 BACKGROUND

Deep foundations are constructed to transfer loads from a superstructure into the subsoil. In order to minimise the risk of failure of the foundation elements, design methods take into account the uncertainty of the load and the resistance. Pile testing can reduce the uncertainty of the pile-soil resistance behaviour.

AS2159-2009 and Verification Method B1/VM4 both assign a lower value for the geotechnical strength reduction factor (ϕ_g) if the risk rating of a project is higher, and allow for an increase of ϕ_g if pile testing (such as static load testing or high strain dynamic testing) is conducted.

However, pile testing is limited by time and budget constraints, and it is highly unlikely that all piles on a project will be verified using pile testing methods. Static load testing can only reasonably be done on one or at most a few piles (Rausche et al., 2008) and high strain dynamic testing is generally limited to 5-15% of the number of piles (Seidel, 2015a). Therefore, alternative methods are required to ensure that the geotechnical behaviour of the remaining piles is within acceptable tolerances.

This may be done by simply comparing installation records of non-tested piles to installation records of tested piles and ensuring that non-tested piles have been driven to similar or harder conditions. In general practice, dynamic formulae, such as the Hiley formula (Hiley, 1930) are often used. For example, the Auckland Structural Group Piling Specification (2002) recommends its use, and it is accepted by AS2159-2009 as an appropriate method for pile load verification, providing the appropriate ϕ_g is used. The use of generic dynamic formulae has been the subject

of academic debate from as early as 1941 (American Society of Civil Engineers, 1941) and has continued to date (Allin, 2015). Allin recommends to use wave equation analyses instead of generic dynamic formulae for the assessment of untested piles. In wave equation analyses, predictions of driving behaviour are made using more detailed information on pile, hammer and soil interaction, thus providing more site specific relations between driving and geotechnical strength, when based on site-specific input. However, these more detailed analyses still use the set (permanent displacement per hammer blow) and an assumed driving energy to obtain R_{ug} from the wave equation predictions.

Auckland Structural Group (2002) states that the Hiley formula has its accuracy improved when adjusted for site-specific data. Seidel (2015a) proposes the use of site specific dynamic formulae, which are to be calibrated based on test data. This same approach would also be applicable to calibrating the results of wave equation analyses. In both cases, a relatively simple criterion for on-site verification of the geotechnical strength of untested piles can be provided, whilst incorporating test results. This paper will focus on the calibration of dynamic formulae, as these are most commonly used in New Zealand practice.

Both Allin (2015) and Seidel (2015b) emphasize the high variability in energy transfer from impact hammers and caution for the sensitivity of driving formulae and wave equation analyses to this parameter. Energy correlations that use a co-efficient of restitution to incorporate the energy loss associated with the impact between the hammer and pile should be used with caution. Given the sensitivity of driving formulae to this parameter, either measurements of energy in the pile should be used, or an energy efficiency factor should be applied based on measured data.

2 HIGH STRAIN DYNAMIC TESTING

High strain dynamic testing is a pile testing procedure that uses strain gauges and accelerometers attached to the pile to evaluate force and velocity of a driven pile. The test is commonly conducted using an impact pile driving hammer. The impact causes a stress wave that travels down the pile, moving the pile relative to the surrounding soil. The mobilised soil resistance at the shaft of the pile reflects compression waves back up the pile. Depending on the soil type at the pile toe, a tension wave or compression wave is reflected upwards. The cumulative effect is an upward travelling force wave that can be inferred from the force and velocity, and which is indicative of the total dynamic resistance of the pile. Additionally, the measurements provide information on the total amount of energy transferred into the pile.

The inferred resistance obtained from the measurements includes the dynamic resistance of the pile-soil interface. In order to infer the geotechnical ultimate strength (R_{ug}) against static loading, this dynamic component must be eliminated. A field estimate can be made by applying an overall damping factor, such as the Case damping factor J_c (Hussein & Likins, 1991). Further accuracy is obtained by conducting a process called signal matching, in which the measured signal is compared to a signal that is generated by a wave equation model. An iterative process is applied to adapt the model to match the measured signal to an acceptable level. A match quality number is computed based on the mismatch of computed and measured signals, as an objective measure of the match quality, independent of a visual or personal assessment (PDI, 2014). A lower match quality number indicates a better match. There is no unique solution to signal matching, and non-credible soil-pile models may result is a good match quality.

The dynamic testing equipment measures the maximum displacement of the pile using accelerometers, but does not distinguish between temporary compression and set. It is recommended that the set determined from actual measurements is used as input in the signal matching process, to improve the match quality (PDI, 2014). However, it should be noted that the

estimated geotechnical ultimate strength from signal matching is not very sensitive to the set input (PDI, 2014).

3 SITE SPECIFIC DYNAMIC FORMULA

The geotechnical strength resulting from the signal matching process can be used as input for the calibration of dynamic formulae for untested piles. Each pile test will provide at least one correlation between set and geotechnical strength. It is important to realise that this is relative to the energy imparted by the hammer.

Temporary compression of the pile is used as a proxy of hammer energy and dynamic soil response in the Hiley formula. Alternatively, the measured peak velocity of the pile can provide an indication of energy imparted. A third method to provide an indication of imparted energy is observing the maximum displacement (set plus temporary compression), as piles founding in similar stratigraphy at similar penetrations should have similar maximum displacement values, even if the sets are different.

The most basic approach to obtain a site specific dynamic formula is to eliminate the dynamic component from the formula. One method, developed by Seidel, applies a Dynamic Reduction Factor (DRF) to correlate the geotechnical strength derived from dynamic formulae ($R_{ug,DF}$) to the geotechnical strength obtained from signal matching ($R_{ug,SM}$) for tested piles. This relationship is shown in its simplest form in Equations 1 and 2.

The DRF is derived for all test piles, as follows:

$$DRF = \frac{R_{ug,DF,test\ pile}}{R_{ug,SM,test\ pile}} \quad (1)$$

It is subsequently applied to non-tested piles:

$$R_{ug,non\ tested\ pile} = \frac{R_{ug,DF,non\ tested\ pile}}{DRF} \quad (2)$$

Dynamic formulae typically predict driving resistance, which is a combination of static and dynamic resistance. The DRF approach aims to eliminate the dynamic resistance component, based on site specific tests. Since dynamic effects are a function of pile velocity, the DRF is not a unique value, but will be dependent on set if applied to piles driven in similar conditions (same size, maximum displacement, penetration and energy applied). In order to determine the relationship between DRF and set multiple tests are required at various sets, with the same input energy.

It should be noted that modified driving formulae are only to be used for piles driven to similar conditions and driving behaviour. This may require the development of multiple driving formulae for one project.

4 HIGH FREQUENCY DISPLACEMENT MONITORING

High frequency displacement monitoring was developed to enhance the quality of set and temporary compression measurements, using optical sensors and high power light emitting diodes (LED) in combination with reflectors on the pile. The Pile Driving Monitor (PDM), developed by Advanced Foundation Technologies, was used in the case described in this paper. The PDM has a sampling rate of 4,000Hz, and can be used at an offset distance of 6 to 20m from the pile (Advanced Foundation Technologies, 2015).

High frequency displacement monitoring can replace the traditional manual set card and provides a significantly higher level of detail (see Figure 1), as this eliminates the associated errors caused by human influence.

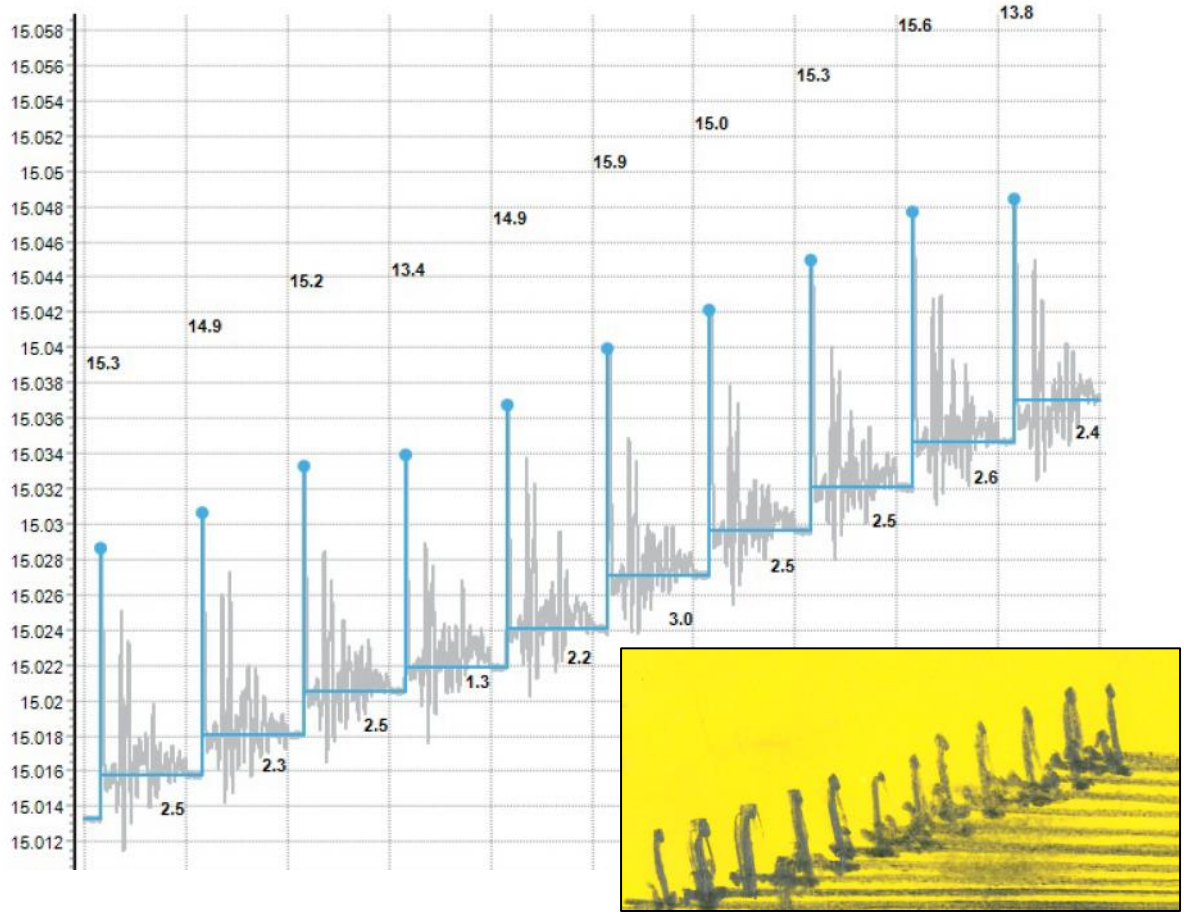

Figure 1: Manual set card results vs PDM results

The high frequency of the measurements provides more insight in the pile movement during driving, as is illustrated in Figure 2. In the record shown, a secondary movement is visible, which is caused by hammer rebound. Also, the lifting of the hammer can be distinguished, leading to a small upwards movement of the pile, as the mass is lifted off the pile.

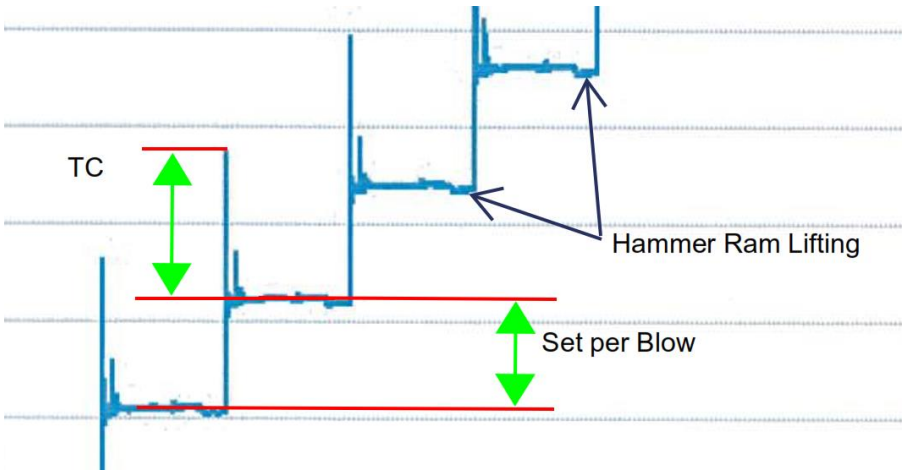

Figure 2: PDM record showing detailed pile movement

5 OBSERVATIONS OF SET RECORDING

The authors have conducted tests using high strain dynamic testing in conjunction with high frequency displacement monitoring. In several of these tests, the use of high frequency displacement monitoring has revealed a difference between the "short term set" at several hundreds of milliseconds after impact and the "long term set" at higher time increments. Figure 3 illustrates this with the short term set (3.8mm) occurring between t = 0ms and t = 400ms and the long term set (1.2mm) occurring at t > 400ms.

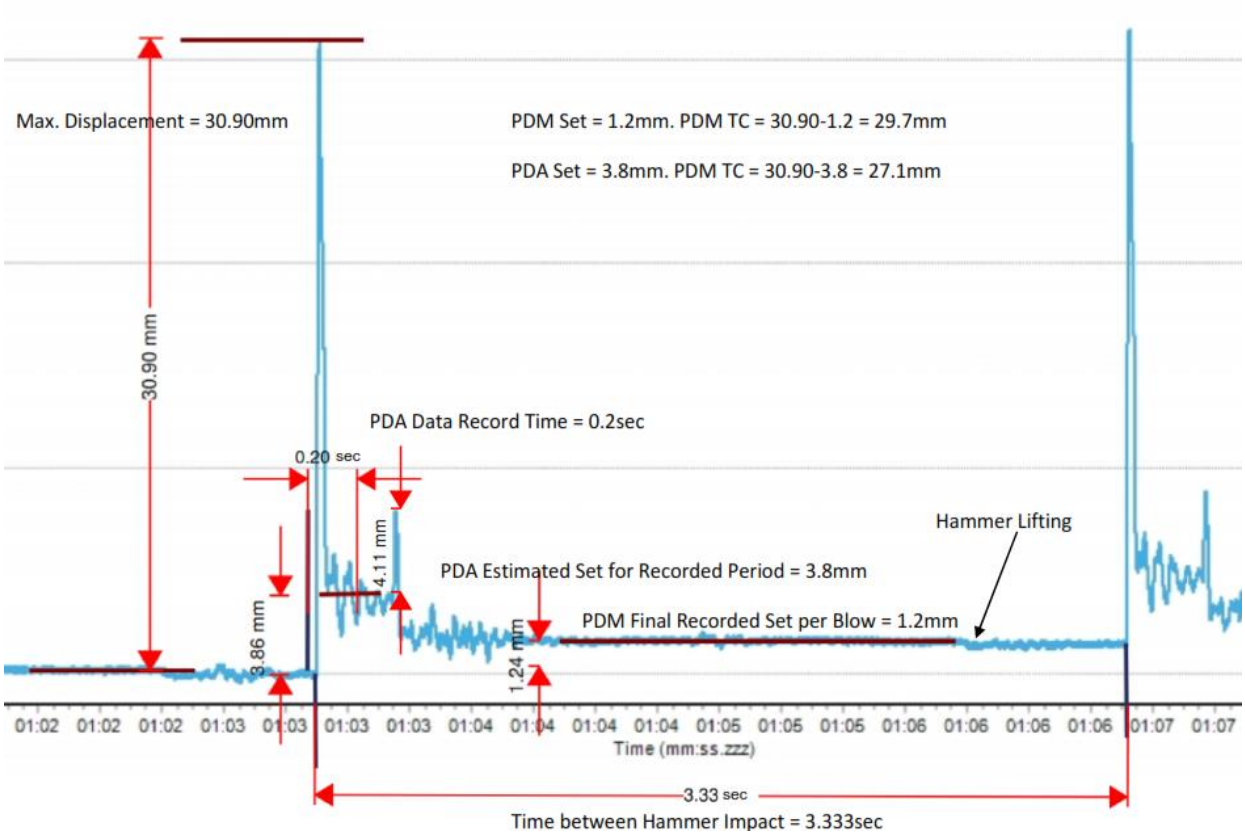

Figure 3: Short term vs long term set as recorded by PDM (Pile C27-EOD)

As discussed above, the match quality of the signal matching process used in dynamic testing is improved by the input of a measured set. Since the dynamic testing equipment records data for a relative short duration (up to 200ms as a default), the appropriate input for this would be the short term set. The set that would normally be recorded in a manual set card would be the long term set, as manual measurements are not sensitive enough to record the set at 200ms. Dynamic formulae would also incorporate the long term set.

Table 1 shows the sensitivity of both the signal matching and the (generic) Hiley formula for short and long term sets, based on the data shown in Figure 3, as well as a derived DRF.

Table 1: Sensitivity to short term and long term set (pile C27-EOD)

Set type	t (ms)	Set (mm/blow)	Temporary Compression (mm)	Signal Matching R_{ug} (kN)	Signal Match Quality	Hiley R_{ug} (kN)	DRF (-)
Short Term	200	3.8	27.1	5000	2.91	8,602	1.72
Long Term	>400	1.2	29.7	5000	3.07	7,885	1.57

It can be seen from Table 1 that the signal matching process is not sensitive to the set. The match quality is slightly improved by using the correct short term set instead of the long term set. The geotechnical strength determined from the Hiley formula is however very sensitive to the set input.

Problems may arise when the displacement data from the high strain dynamic test shows a mismatch with the manually recorded set on site. If a better match is found with the short term set, it is the experience of the authors that practitioners assume the manually measured set to be incorrect and the mismatch due to inaccuracies in the method. As the presented data from high strain displacement monitoring shows, differences in observed set may be due to the time duration of measurements. This understanding is important to ensure that signal matching and field measurements are correctly correlated. Using high strain displacement monitoring can aid in the elimination of manual inaccuracies and a better understanding of actual displacement over time.

6 CONCLUSION

The use of high frequency displacement monitoring provides detailed information on the movement of a pile, thus providing more insight into the development of set and temporary displacements than manual set cards. It also provides a much higher accuracy and operator independency when measuring set and temporary compression, both of which are key input parameters of the commonly used Hiley formula. Additionally, measured pile velocities can serve as a proxy for energy input, when correlated with high strain dynamic testing.

The use of high frequency displacement monitoring revealed differences between the short term set and long term set. Signal matching of one dynamic test pile was conducted using both the short term and long term set. Incorporating the short term set in the signal matching process did not lead to changes in the estimated ultimate geotechnical strength. The signal match quality was slightly improved. The long term set should always be used as input of formulae. The short term set should only be used for the signal matching process.

From the initial analysis, the geotechnical strength estimates of the signal matching do not seem sensitive to the set input. The authors intend to conduct further analyses on a greater data set to confirm this finding.

REFERENCES

Advanced Foundation Technologies (2015) *Pile Driving Monitor, Because Every Pile Is Important, General Specifications.* Melbourne, Australia.

Allin, R., Likins, G. and Honeycutt, J. (2015) Pile driving formulas revisited. *Proceedings of the International Foundations Congress and Equipment Expo 2015.* San Antonio, Texas. Eds. M. Iskander et al.

American Society of Civil Engineers (1941) Pile driving formulas. Progress report of the committee on the bearing value of pile foundations. *Proceedings of the American Society of Civil Engineers*. Vol. 67, No. 5, pp853-866.

Auckland Structural Group (2002) *Auckland Structural Group Piling Specification*. Auckland, New Zealand.

Hiley, A. (1930) Pile-driving calculations with notes on driving forces, and ground resistance. *The Journal of the Institution of Structural Engineers*. pp 246-259 (part 1, July) and pp278-288 (part 2, August)

Hussein, M.H. and Likins, G.E. (1991) Static Pile Capacity by Dynamic Methods. *First Geotechnical Engineering Conference.* Cairo, Egypt. Eds. J. Al-Qahirah, K. al-Handasah. https://www.pile.com/wp-content/uploads/2017/03/StaticPile CapacityByDynamicMethods.pdf.

Seidel, J.P. (2015a) Overview of the Role of Testing and Monitoring in the Verification of Driven Pile Foundations. *Proceedings on the 12th Australia New Zealand Conference on Geomechanics (ANZ2015).* Wellington. Ed. G. Ramsay. pp389-396.

Seidel, J.P. (2015b) Enhanced Use of Dynamic Pile Testing in Foundation Engineering. *Proceedings on the 12th Australia New Zealand Conference on Geomechanics (ANZ2015).* Wellington. Ed. G. Ramsay. pp397-404.

The use of remote high strain dynamic testing and high frequency displacement monitoring to improve safety and quality – case study LPC admin and operations building

R Damen
Brian Perry Civil, Auckland, NZ
ronaldd@fcc.co.nz (Corresponding author)

M D Larisch
Brian Perry Civil, Auckland, NZ
martinla@fcc.co.nz

Keywords: health and safety, high strain dynamic testing, PDA, driven piles

ABSTRACT

The foundation of the Administration and Operations Building of Lyttelton Port of Christchurch (LPC) required the installation of 81 driven steel piles, of which 8 were tested using high strain dynamic testing (PDA). The majority of these high strain dynamic tests were conducted remotely, with the testing engineer operating from Auckland. Remote testing reduced turnaround time on the testing, enhanced quality of data collection and reduced safety hazards for the testing engineer.

Measurements of driving set and temporary compression were conducted using high frequency displacement monitoring. In contrast to the traditional manual set card, measurements could be taken from outside the exclusion zone, which provided significant reduction of hazards to the site crew. Due to the high frequency of the monitoring, the quality of the measurements and reporting was also greatly improved.

1 BACKGROUND

The foundation of the new Administration and Operations Building for Lyttelton Port of Christchurch (LPC) comprises 81 driven steel H-piles (76 No. 310UC158 and 5 No. 400HCC252, all steel grade 300SO), which were installed by Brian Perry Civil (BPC). The design for the foundation was done by Golder Associates (hereafter referred to as the Engineer). The building itself consists of 3 stories, with a footprint of approximately 1800 m^2.

Geotechnical investigation was limited, with 2 CPTs and 2 boreholes completed. Shear wave velocity tests were conducted in 2 locations. The site is located in a land reclamation site, which was previously used for timber storage. Reclamation fill is present from ground level to a depth of approximately 9 to 18 m below ground level, underlain by 7 to 12 m of estuarine deposits and loess colluvium. The fill was expected to comprise of sandy and silty gravel with the presence of cobbles and boulders. Bedrock consists of weathered to fresh basalt of the Port Hills Volcanics (Dismuke, 2016). Piles were to be founded in the weathered bedrock. The uncontrolled fill layer overlying the site was of particular concern with regards to the pile driving process. In order to limit the risk of premature pile refusal and localised pile damage due to obstructions, all 81 pile locations were pre-augered to a depth of 14 to 18 m using a Soilmec SR-30 with a 450 mm CFA auger. During the pre-augering, no spoil was removed from the pile locations.

Piles were pitched and vibrated to refusal using an ICE 23RF resonance free vibratory hammer and subsequently impact driven to target levels using a BSP HH9 hydraulic hammer.

2 HIGH STRAIN DYNAMIC TESTING

High strain dynamic testing is a pile testing procedure that uses strain gauges and accelerometers attached to the pile to evaluate force and velocity of a driven pile. The test is commonly conducted using an impact pile driving hammer. The impact causes a stress wave that travels down the pile, moving the pile relative to the surrounding soil. The mobilised soil resistance at the shaft of the pile reflects compression waves back up the pile. Depending on the soil type at the pile toe, a tension wave or compression wave is reflected upwards. The cumulative effect is an upward travelling force wave that can be inferred from the force and velocity, and which is indicative of the total dynamic resistance of the pile. Additionally, the measurements provide information on the total amount of energy transferred into the pile, which, combined with information on the potential energy of the hammer, can be translated into hammer efficiency. Also, maximum average driving stresses at the location of the gauges can be calculated and large defects in the pile shaft may be identified.

Proprietary testing systems include the Pile Driving Analyzer (PDA) by Pile Dynamics and the PDR by Allnamics.

The inferred resistance obtained from the measurements includes the dynamic resistance of the pile-soil interface. In order to infer the geotechnical ultimate strength (R_{ug}) against static loading, this dynamic component must be eliminated. A field estimate can be made by applying an overall damping factor, such as the Case damping factor J_c (Hussein & Likins, 1991). Further accuracy is obtained by conducting a process called signal matching, in which the measured signal is compared to a signal that is generated by a wave equation model. An iterative process is applied to adapt the model to match the measured signal to an acceptable level. There is no unique solution, and non-credible soil-pile models may result is a good match quality. Therefore, it is essential that the signal matching process is conducted by a skilled and experienced engineer, and is based on a credible soil model (Rausche et al., 2008; Seidel, 2015). Proprietary software to conduct this signal matching process includes CAPWAP by Pile Dynamics and AllWave-DLT by Allnamics.

In the LPC project, high strain dynamic testing was specified by the Engineer as a means of quality assurance for the pile foundation. 10% testing (8 No. piles) was required, with test pile locations specified by the Engineer. Testing was conducted using an 8G PDA, with 2 piezo-electric strain gauges and 2 accelerometers per pile. Signal matching was conducted by a third party using CAPWAP.

The objective of the test was to verify that the piles had obtained the required geotechnical ultimate strength (R_{ug}) and were embedded at least 0.5 m into a competent bearing strata (i.e. weathered rock). The required minimum R_{ug} for the 310UC158 piles was 2,100 kN and required R_{ug} for the 400HCC252 piles was 5,000 kN. This was based on a geotechnical reduction factor (ϕ_g) of 0.48 in accordance with AS2159-2009. Figure 1 summarises the ultimate geotechnical strength obtained from signal matching in relation to the driving sets.

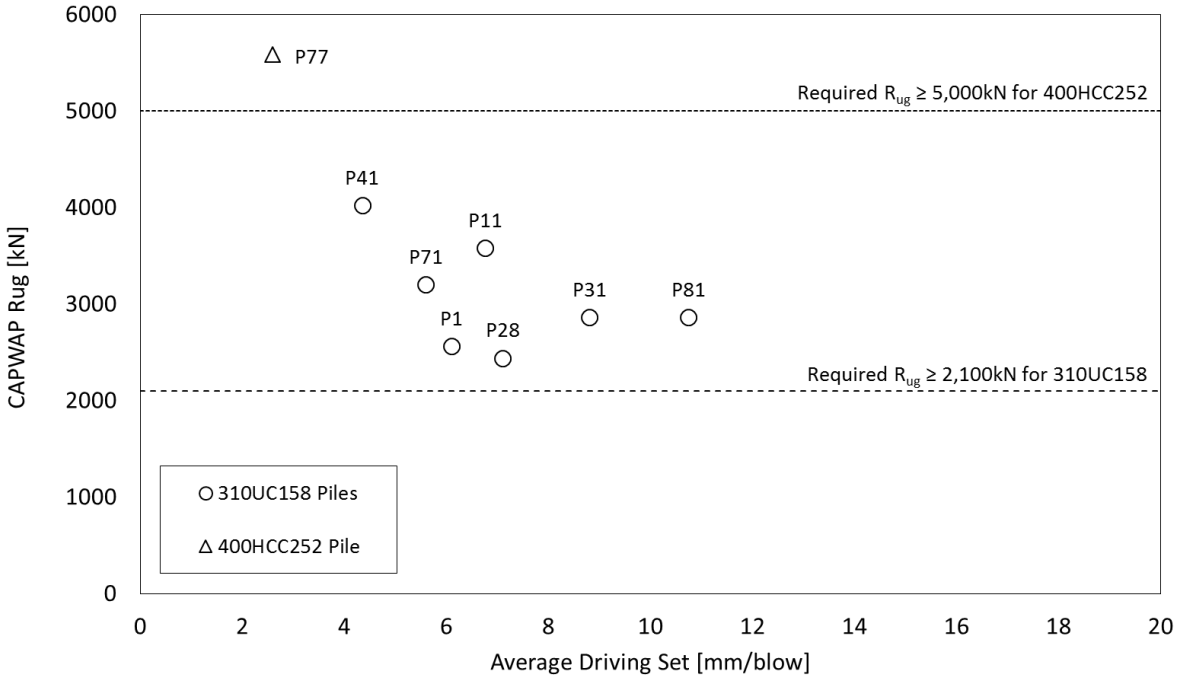

Figure 1: Geotechnical ultimate strength from signal matching vs average driving set

In addition to determining the ultimate geotechnical strength of the piles, the high strain dynamic testing was used by the contractor to also monitor driving stresses and verify pile integrity for the full duration of impact driving of the first pile (pile P81). As can be seen in Figure 2, the driving stresses were well below the allowed 90% of the steel grade (i.e. 270 MPa), in accordance with AS2159:2009.

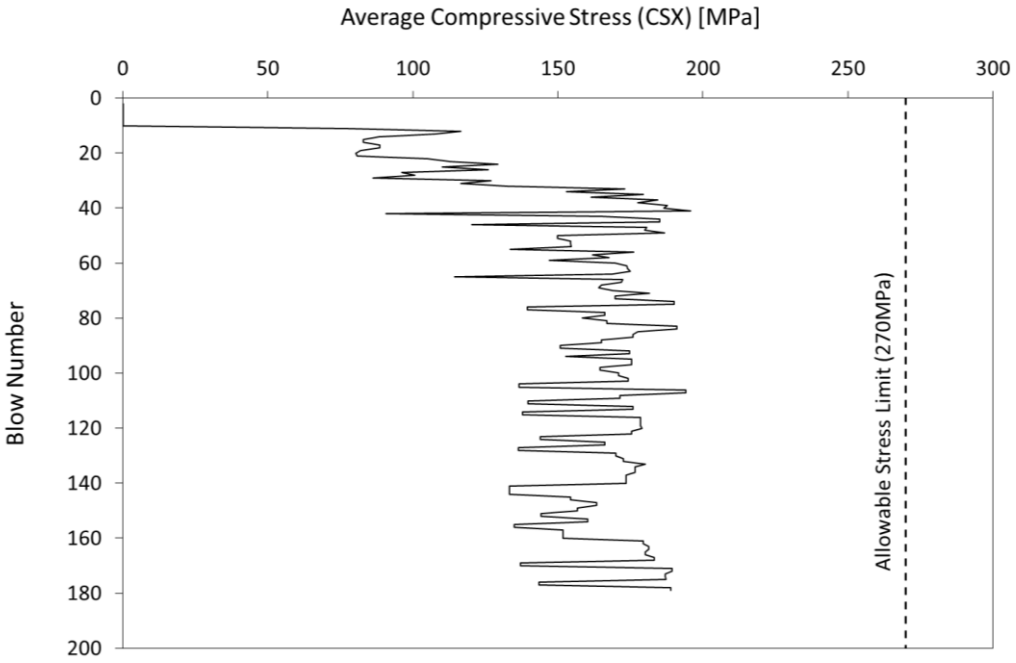

Figure 2: Average Compressive Stress (CSX) vs Blow Number pile P81

3 REMOTE TESTING

High strain dynamic testing requires a skilled and experienced engineer to conduct and monitor the test and subsequently conduct the signal matching process (Rausche et al., 2008).

Traditionally, a skilled testing engineer would mobilise to the construction site for each test, which results in potential down time of the piling operation on site, inefficient use of the testing engineer's time and higher cost. Alternatively, tests could be bundled to reduce the number of site visits by the testing engineer. However, this may not align with the optimum piling sequence, as test piles are generally geographically spread over the site.

The 8G PDA system that is used by BPC has remote capability, which allows remote access to the system. This capability was utilised by BPC for the first time in New Zealand on this project.

During driving of the first pile, the testing engineer mobilised to site and trained the site engineer to correctly prepare the pile, connect gauges and set up the system. The first test was conducted by the testing engineer onsite. All following tests were conducted remotely, with the Auckland-based testing engineer accessing the PDA system through an internet connection.

Pile testing was conducted satisfactorily using this method. Most notably, the turnaround time for testing could be reduced significantly. Generally, at the start of the week the site engineer and testing engineer discussed over the phone which selected test piles were due for testing. Testing windows were agreed upon, ensuring the testing engineer's availability and were narrowed down on the actual test day. Actual pile testing took less than one hour on average to conduct.

This approach provided significant flexibility to the site crew to adapt the testing schedule to the piling operation on site. For example, pile tests could be easily rescheduled when the installation of test piles was delayed due to breakdown of hired plant.

4 HIGH FREQUENCY DISPLACEMENT MONITORING

A key input parameter to driven pile verification is the driving set, or permanent displacement per hammer blow. Furthermore, the temporary compression is generally recorded, which is indicative of the dynamic effects in the pile and is used in dynamic formulae, such as the Hiley formula (Hiley, 1930; Auckland Structural Group, 2002).

Traditionally, the only method to record the temporary compression, was by means of a manual set card, in which a pencil or chalk is physically held by person to the pile (or to a paper attached to the pile) during pile driving. Often an inclined spirit level is used to provide a more or less stable reference level. The result can then be measured. This method is commonly applied for 10 impact blows, and results are subsequently averaged. Figure 3 shows an example of a manual set card.

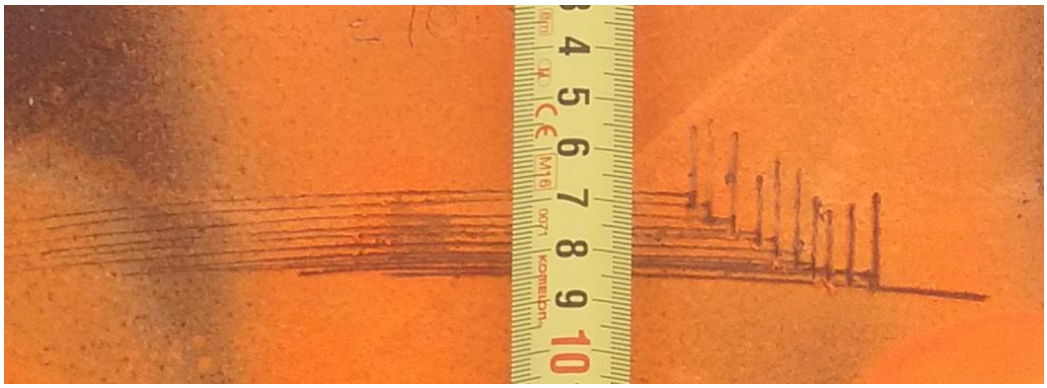

Figure 3: Example of manual set card on steel pile

The obvious disadvantage of this method is the high safety risk, since it requires a person to be in close proximity to the pile during the driving process. The method requires significant skill and experience of the person recording and is therefore highly operator dependent, which potentially impacts the quality of the measurements. Temporary ground displacements around the pile may also affect the measurement.

High frequency displacement monitoring was developed to enhance the quality of set and temporary compression measurements, using optical sensors and high power light emitting diodes (LED) in combination with reflectors on the pile. The Pile Driving Monitor (PDM), developed by Advanced Foundation Technologies, was used on this project. The PDM has a sampling rate of 4,000 Hz, and can be used at an offset distance of 6 to 20 m from the pile (Advanced Foundation Technologies, 2015).

BPC used the PDM (Model G2) to replace manual set cards on all piles of this project. The main reason to use the PDM on this project was the obvious benefit to occupational safety. The device enabled the site engineer to measure set and temporary compression, whilst being well outside the exclusion zone (see Figure 4).

Figure 4: PDM set up outside exclusion zone

Additional benefits are the increased accuracy of the measurements and the operator independency of the method. An example of the PDM results as reported to the client is shown in Figure 5.

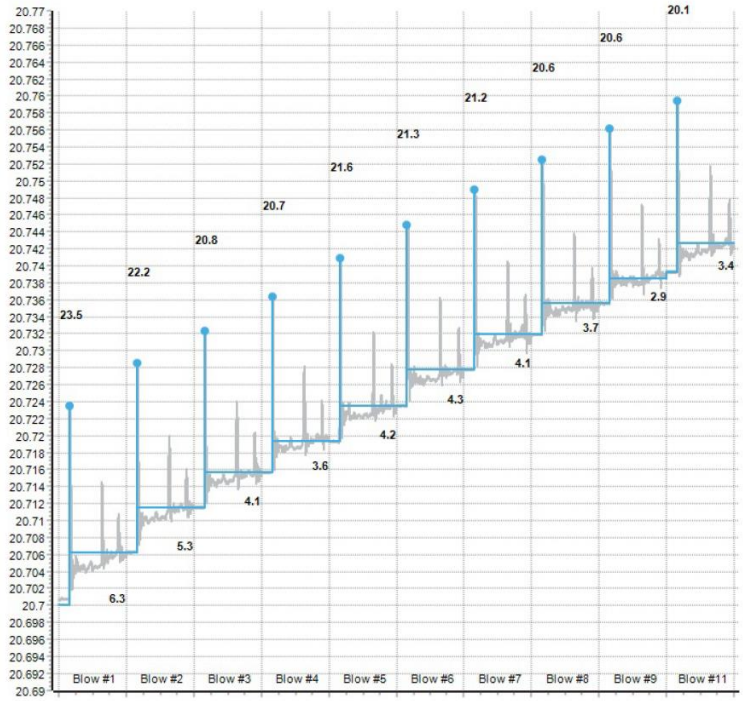

Figure 5: PDM generated set card

PDM training was provided by the testing engineer to the site engineer, in addition to PDA training. The site engineer was able to conduct all PDM tests, with minor remote support from the testing engineer.

Lessons learned included avoiding exposure to heat, as the PDM and accompanying tablet quickly overheated when exposed to sunlight for longer durations (30 minutes). Furthermore, enabling a clear line of vision for the PDM to the pile proved challenging as piling proceeded and the site became more congested. Offset distance is a key input parameter and results are sensitive to this input. Therefore, three measurements were made of offset distance using a laser distance gauge (Ryobi RLM30).

5 CONCLUSION

High strain dynamic testing demonstrated that all piles were driven to the required ultimate geotechnical strength (R_{ug}). Driving stresses were found to be well within the limits specified by AS2159:2009, and no indication of overstressing or pile damage was observed.

The application of remote testing provided significant flexibility to adapt pile testing to the piling operations. Additionally, turnaround times were reduced.

The replacement of manual set cards by high frequency displacement monitoring led to health and safety benefits, in conjunction with higher quality and operator independent set and temporary compression records.

REFERENCES

Advanced Foundation Technologies (2015) *Pile Driving Monitor, Because Every Pile Is Important, General Specifications.* Melbourne, Australia.

Auckland Structural Group (2002) *Auckland Structural Group Piling Specification*. Auckland, New Zealand.

Dismuke, J. (2016) *Pile Foundation Design, Lyttelton Port of Christchurch: Operations and Administration Building (Rev 1).* Golder Associates (NZ) Ltd, Christchurch.

Hiley, A. (1930) Pile-driving calculations with notes on driving forces, and ground resistance. *The Journal of the Institution of Structural Engineers.* pp 246-259 (part 1, July) and pp278-288 (part 2, August)

Hussein, M.H. and Likins, G.E. (1991) Static Pile Capacity by Dynamic Methods. *First Geotechnical Engineering Conference.* Cairo, Egypt. Eds. J. Al-Qahirah, K. al-Handasah. https://www.pile.com/wp-content/uploads/2017/03/StaticPile CapacityByDynamicMethods.pdf.

Rausche, F., Nagy, M. and Likins, J. (2008) Mastering the art of pile testing. *Proceedings of the 8th International Conference on the Application of Stresswave Theory to Piles.* Lisbon, Portugal. Ed. J.A. dos Santos. pp19-32.

Seidel, J.P. (2015) Overview of the Role of Testing and Monitoring in the Verification of Driven Pile Foundations. *Proceedings on the 12th Australia New Zealand Conference on Geomechanics (ANZ2015).* Wellington. Ed. G. Ramsay. pp389-396.

Case study in the use of shear wave velocity techniques to investigate liquefaction potential of Waikato soils for the Hamilton section of the Waikato expressway

P J Clayton
Beca Infrastructure, Auckland, NZ.
philip.clayton@beca.com (Corresponding author)

I Yong
Beca Infrastructure, Auckland, NZ.
irene.yongz@beca.com

L Wotherspoon
University of Auckland, Auckland, NZ.
l.wotherspoon@auckland.ac.nz

Keywords: pumice, shearwave velocity, aging, liquefaction, MEVR.

ABSTRACT

The four-lane, 21.8 kilometre long, Hamilton Section of the Waikato Expressway is the largest roading project undertaken in this region's history and one of the larger projects currently being undertaken in New Zealand. Many of the seventeen expressway bridges in the Hamilton Section are underlain by saturated Pleistocene sandy alluvial soils. Conventional CPT/SPT penetration resistance based methods generally indicate a liquefaction potential for these soils that extends to considerable depth. Some researchers have however suggested that conventional penetrometer based methods may overestimate the liquefaction potential in these soils due to their age and pumice content. In recognition of this effect liquefaction assessment on this project has been undertaken utilising shear wave velocity as the primary indicator of liquefaction triggering and for the derivation of liquefied shear strength. Recognising the less well developed state of both the acquisition of shear wave data and the associated liquefaction assessment methodology the design team undertook a number of measures to validate data and approaches. Side by side downhole/crosshole tests provide the opportunity to consider the repeatability of Vs testing as well as side by side CPT, DMT and shear wave measurements (crosshole and downhole) as well as paleoliquefaction investigation (discussed in companion paper – Clayton et al,, (2017)) provide the opportunity to compare and contrast the liquefaction potential indicated by these various methods in these specific soils.

1 INTRODUCTION

The City Edge Alliance (The Alliance) has been commissioned to undertake detailed design for the 21.8 kilometre long Hamilton Section of the Waikato Expressway in the North island of New Zealand. The Alliance is made up of the New Zealand Transport Agency, Fletcher Construction, Higgins, Beca and Coffey. The Alliance approach was adopted to maximise the potential for full integration of the traditional roles of client, designer and constructor for the benefit of the project, enabling a collective approach and risk sharing. Within the geotechnical sphere of the project, this has been further enhanced through a Geotechnical Steering Group with representatives from the designer, constructor and client. This Group enabled consideration of 'best for project' approaches and thereby the ability to look at approaches and methods that would not normally occur within more traditional contracts.

Much of the route passes through a geomorphic region known as the Hamilton Lowlands which is characterised by late Pleistocene alluvial sandy deposits and a relatively high water table. Conventional penetrometer based liquefaction assessment within these soils indicate a liquefaction potential that extends to considerable depth, however recent research into the effect of aging and particle crushing suggest that the liquefaction risk may be overestimated by such methods. This paper compares the assessed liquefaction potential based on CPT, downhole and crosshole shear wave velocity methods. Measured to estimated velocity ratio (MEVR) is used to discuss possible reasons for the differences between liquefaction resistance indicated by penetrometer and Vs based methods in these soils.

2 BACKGROUND

A number of researchers have noted that conventional penetrometer based liquefaction assessment methods can over predict liquefaction triggering in some soils (Orense, 2013). The over prediction has been attributed to the effects of particle crushing and/or aging.

2.1 Particle Crushing

Particle crushing has been reported during CPT testing in pumiceous soils (Wesley et al., 1998). Where significant crushing occurs during penetrometer testing the relative density may be underestimated and hence liquefaction potential overestimated.

2.2 Age Effects

Over time granular soils tend to gain strength through a number of mechanisms. Creep between particles may lead to a denser state of packing and/or cementation may develop. A number of researchers (Andrus et al. 2009) have noted that the cementation that develops may arise from a number of mechanisms, some of which are relatively weak. It is thought that these comparatively weaker bonds may contribute to liquefaction resistance but may not be fully recognised by large strain penetrometer based methods leading to an underestimation of the liquefaction potential of older soils by penetrometer based methods.

2.3 Role of Shear Wave Based Liquefaction Assessment

Methods based on shear wave velocity have been suggested as being more appropriate for liquefaction assessment in the aged and/or pumiceous soils of the Waikato as small strain methods do not subject the soil to stresses high enough to result in significant particle crushing or disruption of weaker bonds (Clayton & Johnson 2013). While considered more appropriate, shear wave velocity based methods are not as well developed as penetrometer based methods and the project team had concerns about the reliability of shear wave velocity (Vs) measurement methods. To address concerns about the reliability of Vs measurement paired tests were undertaken at 10 locations along the route in a range of ground conditions including stiff silts/dense sands of the Piako Group and relatively loose sands of the Hinuera Formation utilising a number of different methods including crosshole, downhole true interval and (a lesser number of) downhole pseudo interval. Results were also compared to those of a paleoliquefaction study, which is the subject of a companion paper (Clayton et al., 2017)

3 GEOLOGY, GROUNDWATER AND SEISMICITY

Refer to companion paper (Clayton et al., 2017) for details of geology/soil conditions, ground water and seismicity within the study area.

4 METHODS OF ASSESSMENT

4.1 CPT Testing

Cone Penetrometer Tests (CPT) were regularly undertaken along the route with multiple tests at each bridge abutment. CPT were utilised to refine stratigraphy, inform saturation and groundwater level in highly permeable soils, and to provide correlation to fines content and soil behaviour index (Ic). The latter utilised specific correlations for some units (Wong & Clayton, 2017). Where paired testing was undertaken, using a combination of co-located CPT, seismic dilatometer (sDMT), Crosshole Seismic Tests (CST), these tests were undertaken around 2m apart in a triangular formation to avoid disturbance related effects.

4.2 Shear wave velocity

Shear wave velocity testing was undertaken utilising a variety of methods including seismic cone penetrometer (sCPT), sDMT & CST methods. For this study the sDMT tests utilised a true interval approach utilising two geophones/accelerometers located 0.5m apart and a surface source (sledgehammer striking timber sleeper). Stacking was undertaken where low signal to noise (S/N) ratio occurred. Internal validation was undertaken by comparing left hand and right hand polarised tests. Tests were typically undertaken at 0.5m intervals vertically. Direct-push crosshole tests (CST) (Wotherspoon et al., 2015) were also undertaken. A source and a receiver sensor were advanced separately into the ground to the same depth using standard CPT rods and two small-scale cone penetrometer rigs. At each depth testing was performed using a hammer impact source applied to the top of the source rod, with at least three separate tests performed at each depth and stacked to increase signal-to-noise ratio.

5 INTERPRETATION METHODOLOGY

The interpretation methodology adopted for this comparison is summarised below in Table 1

Table 1 interpretation methodology

Test Method	Methodology for susceptibility	Methodology for Triggering assessment	Methodology for Liquefied shear strength
CPT	Based on Ic with Ic cutoff calibrated to Atterburg tests on samples from paired borehole. Refer to Young and Clayton (2017).	Following approach published by Boulanger and Idriss (2014).Fines content correlated to Ic with calibration using laboratory grading tests on paired borehole samples.	Following approach published by Idriss and Boulanger (2014).
All Vs methods	Based on Ic from paired CPT with calibrated Ic Cutoff as per CPT based assessment.	Based on Kayen et al. (2013) Fines content correlated to Ic from paired CPT, calibrated as per CPT based assessment.	Based on Ozener (2012)

6 ANALYSIS RESULTS

6.1 Profile comparisons

Comparisons have been undertaken between different measured Vs profiles and Vs correlated to CPT qc. Refer example plot in Figure 1a. To illustrate the consequence of variations in Vs, liquefaction potential and liquefied shear strength have also been determined (sDMT & CST)

utilising methodology published by researchers (Kayen et al. 2013) and (Ozener 2012). For comparison analysis direct from CPT (Idriss and Boulanger 2014) is also presented. Refer Figures 1b&c.

Figures 1a, 1b&1c: Plot of measured and estimated (correlated) shear wave velocity vs depth, FOSliq vs depth and liquefied shear strength vs depth.

6.2 Soil Unit Comparisons

A convenient way of identifying if particle crushing or aging effects (or other mechanisms affecting liquefaction potential) are present is through the use of measured Vs to estimated Vs as a velocity ratio (MEVR) (Andrus et al., 2009; Clayton & Johnson, 2013). Comparison has been undertaken by calculating MEVR using a ratio of Vs(CPT) correlated from CPT - Andrus and Stokoe (1994) and measured Vs, and then compiling the results from ten sites where side by side tests were undertaken, refer Fig 2a.

$$Vs = sqrt\ Gmax/mass\ density$$

Gmax = 1634(qc)^0.25(sigv')^0.375

Ratio have also been prepared for liquefaction factor of safety (FOSliq) based on CPT (FOSliq(CPT)) / FOSliq(Vs), refer fig 2b).

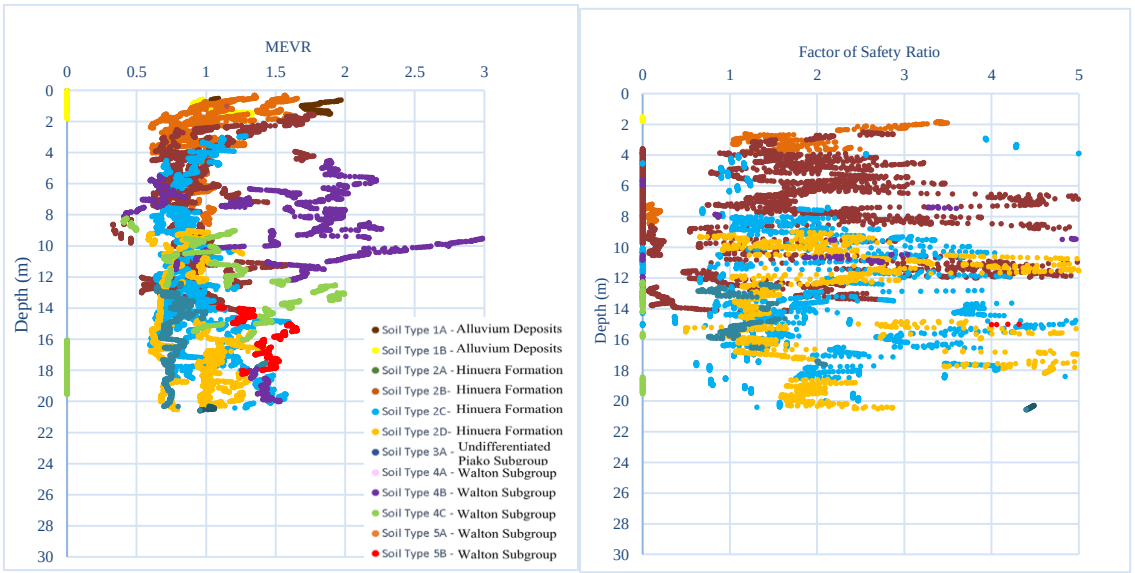

Figure 2a & 2b: Shear wave MEVR and FOSliq ratio vs Depth

In order to investigate the MEVR of soils which have different pumice contents and different age since deposition we have selected specific soil units for comparison:

- Hinuera Formation soils (Unit 2a-d) are relatively young (circa 26Ka) alluvial deposits that may contain a significant proportion of rhyolitic glass (pumice). Figure 3a presents MEVR vs depth for Hinuera Formation deposits.

- Walton Subgroup (sandy) soils (Unit 4c & 5b) are older (0.34 to 1.8Ma) alluvial and pyroclastic flow deposits. Figure 3b presents MEVR vs depth for selected (sandy) Walton Group deposits.

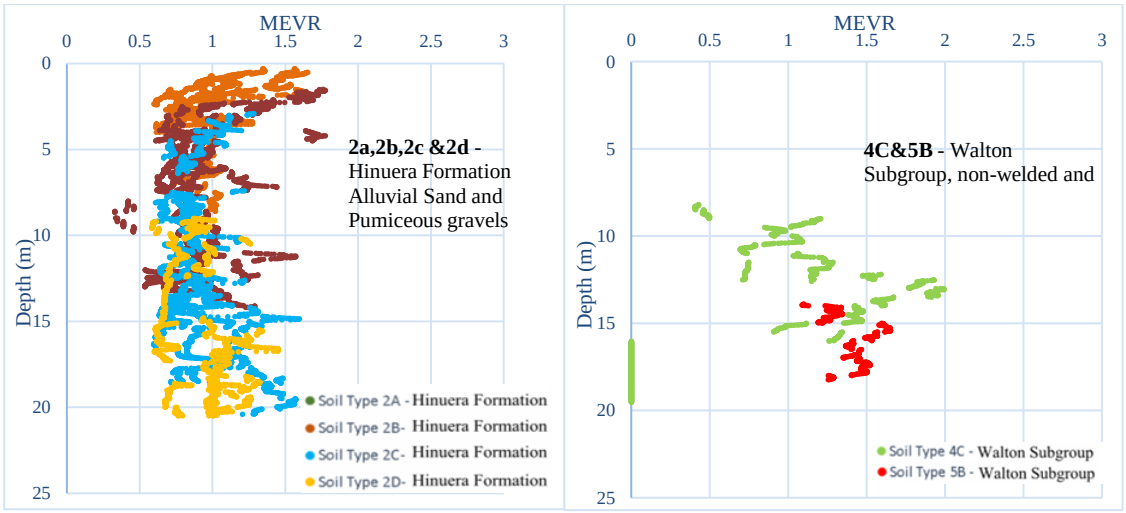

Figure 3a & 3b: Shear wave velocity MEVR vs Depth (selected soils)

7 DISCUSSION

7.1 Comparison of downhole and crosshole methods.

Comparisons have been undertaken of CST and sDMT measurements of Vs in a range of soil conditions. Test results were found to be generally consistent, with a reasonable agreement between methods. Within the majority of the soils, the ratio between Vs from CST and Vs from sDMT has a median of (0.87-0.98) indicating minimal bias and a comparatively small standard deviation (0.12-0.21). This finding supports the ongoing use of downhole methods for the determination of Vs for low-moderate risk projects on sites without complex stratigraphy, although the reliability of results should be evaluated and discrepancies further investigated or discarded in situations such as the following:

- Where paired polarised results or results of different analysis methods diverge significantly.

- Where results are benchmarked against other methods such as CPT and significant unexplainable discrepancies are identified.

Refer to further discussion on this subject in the paper by Wahab and Clayton (2017).

7.2 Comparison of FOSliq and SUliq

Comparisons have been undertaken between CST, sDMT and CPT for FOSliq and Suliq for each of the paired test locations.

7.2.1 Comparisons between CST, sDMT and CPT for FOSliq

The following general observations can be made:

- The variation between FOSliq between CST, sDMT & CPT is greater than the variation in Vs noted in 6.1. This can be attributed to the nonlinearity of CRR with respect to Vs, particularly at higher Vs.

- There appears to be a mismatch between the correlated Vs from CPT and the calculated FOSliq. Where MEVR =1, FOSliq from Vs is > FOSliq from CPT.

7.2.2 Comparisons between CST, sDMT and CPT for Suliq.

The following general observations can be made:

- The variation in Suliq between CST, sDMT & CPT is relatively small in comparison to for FOSliq, although in the case presented many of the data points derived from Vs would be irrelevant form an engineering point of view as FOSliq>1.0

7.3 Comparison between Vs and CPT

Comparisons have also been undertaken to investigate how variations between measured and correlated Vs (MEVR) vary between soil types, possible explanations for this variance are provided.

7.3.1 Hinuera Formation MEVR

Fig 2a presents MEVR from CST and CPT vs depth. The MEVR plot shows three zones:

An upper zone (surface to 3m) where the MEVR is in the range of 0.8 to 1.5. This appears to indicate the presence of a consistent 'crust' of high velocity material not recognised by the CPT. This zone, potentially significant for the design of lightweight structures may result from a number of possible mechanisms including negative pore pressure in the capillary zone or weak cementation e.g. 'limonite' in aerobic zone.

An intermediate zone where the MEVR remains relatively constant at around 0.8 to 0.9. A MEVR of 1.0 indicates an ideal Vs to CPTqc correlation, however with the correlation used in this study (reference) the MEVR of young, shallow sandy soil deposits typically yield a MEVR in the 0.8 to 0.9 range and in fact a MEVR ratio in these soils (and for the correlation used) of 0.8 to 0.9 corresponds to a FOSliq ratio of around 1.

A deeper zone (10m to 20m) where the MEVR increases from around 0.9 to 1.5. The high MEVR in this zone may result from a number of possible mechanisms including:

- Particle crushing during CPT probing. Noting that crushing is more likely under greater confinement at depth.
- Older deposits at depth. Considered less likely as the Hinuera formation deposits are relatively young and were emplaced relatively rapidly with deeper deposits not significantly older.

7.3.2 Walton Subgroup MEVR.

Fig 3b presents MEVR from CST and CPT vs depth. The MEVR plot shows a range of 0.7 to 2.0 throughout but typically between 1.2 and 1.7. This relatively high MEVR may result from a number of possible mechanisms including:

- Aging effects - The Walton Subgroup has an age of 0.34 to1.8Ma. Based on Andrus et al, (2009) this age might be expected to correlate to a MEVR of approximately 1.35 to 1.45 which is comparable to that observed.

- Particle crushing – Pumice is present within soil units 4C and 5B, but in no higher concentrations that the Hinuera Unit 2 deposits discussed in 6.3.1 above, but which show a significantly lower MEVR.

8 CONCLUSIONS

As part of the geotechnical investigation for the Hamilton section of the Waikato Expressway a number of co-located crosshole (CST) and downhole (sDMT) shear wave velocity tests were undertaken. The CST were undertaken to support the adoption of shear wave velocity based liquefaction potential and liquefied shear strength assessment in the commonly pumiceous soils present along the alignment. A paleoliquefaction study was also undertaken as part of the validation of this approach, this study is documented separately in a companion paper. Having ten co-located sets of CPT, CST & sDMT provided an opportunity to undertake a number of comparisons. Initially we compared crosshole and downhole tests and found that results were generally in good agreement which supports the ongoing use of downhole test methods for low to moderate risk projects. The study then compared the Vs data from the CST to correlated Vs from the co-located CPT, generating MEVR (measured to estimated velocity ratio) for individual soil layers. Interpretation of the MEVR within the pumiceous comparatively young (circa 26ka) Hinuera Formation has lead to the following conclusions:

- Within the Hinuera formation there appears to be a near surface zone or crust with elevated MEVR. This zone is unlikely to differ significantly in composition from underlying soils, partial crushing is therefore unlikely and the theory of superposition rules out aging effects. Postulated causes include weak cementation (e.g. limonite) related to unsaturated weathering or negative pore pressure within the partially saturated zone.

- Below the near surface zone to a depth of around 10m MEVR is low suggesting that particle crushing or aging effects are negligible in this zone. FOSliq by Vs and CPT are similar in this zone.

- Below a depth of around 10m MEVR increases. A possible explanation of this observation is particle crushing increasing with the level of confinement. The age difference between mid and lower Hinuera formation is considered unlikely to justify the observed increase in MEVR.

The apparent potential for particle crushing at greater depths supports the use of shear wave velocity based liquefaction assessment in these soils. The high MEVR within the significantly older Walton Subgroup (0.34 to 1.8Ma) supports a conclusion that aging effects may be significant for these soils and that the use of either an age correction factor with penetrometer methods or where suitable data is available, direct shear wave velocity based liquefaction assessment.

9 ACKNOWLEDGEMENTS

The authors wish to thank the New Zealand Transport Agency for their permission to publish this paper and in particular the valuable contributions from Stuart Finlan. The authors would also like to acknowledge The City Edge Alliance, the Project Geotechnical Steering Group, Beca

colleagues and the significant contribution by Dylan Bai and Jamie Chen, who are currently studying for a Bachelor's of Engineering (Honours), at the University of Auckland.

REFERENCES

Andrus, R., Hayati, H., and Mohanan, N. (2009). *Correcting Liquefaction Resistance for Aged Sands Using Measured to Estimated Velocity Ratio*. J. Geotech. Geoenviron. Eng., 135(6), 735–744.

Boulanger, R. W., and Idriss, I. M. (2014). *CPT and SPT based liquefaction triggering procedures.* Report No. UCD/CGM-14/01, Center for Geotechnical Modeling, Department of Civil and Environmental Engineering, University of California, Davis, CA, 134 pp.

Kayen, R., Moss R., Thompson E., Seed R., Cetin K., Der Kiureghian A., Tanaka Y., Tokimatsu, K. (2013). Shearwave velocity–based probabilistic and deterministic assessment of seismic soil liquefaction potential. *J. Geotech. Geoenviron. Eng*., 139(3): 407–419.

Clayton, P.J., Yong, I., Green, R.A., Bastin, S.H., (2017). Case study in the use of paleoliquefaction techniques to investigate liquefaction potential of Waikato soils for the Hamilton section of the Waikato expressway *Proceedings 29th NZGS Geotechnical Symposium.* Eds. GJ Alexander & CY Chin, Napier.

Clayton, P.J., Johnson,J.,T., (2013) Liquefaction Resistance and Possible Aging Effects in Selected Pleistocene Soils of the Upper North Island *Proc. 19th NZGS Geotechnical Symposium*, Queenstown.

Orense, R.P., Pender, M.J., (2013) Liquefaction characteristics of crushable pumice sand, *Proceeding of the 18th International Conference on Soil Mechanics and Geotechnical Engineering.* 2–6 September, Paris. pp 1559–1562

Özener, P., (2012). Estimation of residual shear strength ratios of liquefied soil deposits from shear wave velocity. *Earthquake Engineering and Engineering Vibration*, 10.1007/s11803-012-0134-0, 461-484. Pender et al. (2013);

Wesley L.D., Meyer V. & Pender M.J. 1998. Cone penetrometer tests in pumice sand. *NZ Geomechanics News*, June 1998, 57-61.

Wotherspoon LM, Cox BR, Stokoe II KH, Ashfield DJ, Phillips RA (2015): Utilizing direction-push crosshole testing to assess the effectiveness of soil stiffening caused by installation of stone columns and Rammed Aggregate Piers, *6th International Conference on Earthquake Geotechnical Engineering*, 1-4 November 2015, Christchurch, New Zealand

Yong, I., Clayton, P.J., (2017). Application of soil specific correction factors for liquefaction assessment: case study in Waikato soils for the Hamilton section of the Waikato expressway. *Proceedings 29th NZGS Geotechnical Symposium.* Eds. GJ Alexander & CY Chin, Napier.

Case study in the use of paleoliquefaction techniques to investigate liquefaction potential of Waikato soils for the Hamilton section of the Waikato expressway

P J Clayton
Beca Ltd, Auckland, NZ.
philip.clayton@beca.com (Corresponding author)

S C Tilsley
Beca Ltd, Auckland, NZ.
susan.tilsley@beca.com

S H Bastin
QuakeCoRE, Christchurch, NZ.
sarah.bastin@canterbury.ac.nz

R A Green
Department of Civil and Environmental Engineering, Virginia Tech, Blacksburg, VA, USA.
rugreen@vt.edu

Keywords: pumice, volcanic glass, paleoliquefaction, aging, liquefaction.

ABSTRACT

The four-lane, 21.8-km long, Hamilton Section of the Waikato Expressway is the largest road project undertaken in the Waikato region's history and one of the larger highway projects currently being undertaken in New Zealand. Many of the seventeen expressway bridges in the Hamilton Section are underlain by saturated Pleistocene silty and sandy alluvial soils that have considerable pumice and volcanic glass content. Conventional penetration based methods generally indicate that the potential for liquefaction for these soils extends to considerable depth. However, some researchers have suggested that conventional penetrometer-based methods may overestimate the liquefaction potential in these soils due to the pumice and volcanic glass fragments' tendency to crush during penetration testing and the penetration-based liquefaction evaluation procedures' lack of accounting for aging effects on liquefaction resistance.

To investigate these effects and to inform design, the liquefaction hazard was also assessed using small strain shear wave velocity (Vs) based procedure (discussed in companion paper – Clayton et.al 2017) and a paleoliquefaction study was performed. The paleoliquefaction investigation was comprised of the excavation of seven trenches at sites proximal to the expressway where liquefaction is anticipated. Detailed logging of features encountered in the trenches accompanied by C14 dating of samples was undertaken to document and determine approximate ages of paleoliquefaction features. Observations from the paleoliquefaction study were more consistent with predictions for the Vs-based liquefaction evaluation than they were with those penetration-based method and indicate that the penetration-based methods overestimate the liquefaction potential of the study sites.

1 INTRODUCTION

The City Edge Alliance (The Alliance) has been commissioned to undertake detailed design for the 21.8-km long Hamilton Section of the Waikato Expressway on the North Island of New Zealand. The Alliance is made up of the New Zealand Transport Agency, Fletcher Construction, Higgins, Beca and Coffey. The Alliance approach was adopted to maximise the potential for full

integration of the traditional roles of client, designer and constructor for the benefit of the project, enabling a collective approach and risk sharing. Within the geotechnical sphere of the project, this has been further enhanced through a Geotechnical Steering Group with representatives from the designer, constructor and client. This Group enabled consideration of 'best for project' approaches and thereby the ability to look at approaches and methods that would not normally occur within more traditional contracts.

Much of the route passes through a geographic region known as the Hamilton Lowlands which is characterised by late Pleistocene alluvial silt and sand deposits with a high pumice and volcanic glass content and a relatively high water table. Liquefaction assessments performed using conventional penetrometer-based procedures (i.e., Standard Penetration Test, SPT, and Cone Penetration Test, CPT, based procedures) indicate that the potential for liquefaction extends to considerable depth at many of the seventeen expressway bridges within this section. However, the penetration-based procedures are thought to over predict the liquefaction potential of these deposits because of the tendency for the pumice and volcanic glass fragments to crush during in-situ testing, resulting in an underestimation of soil density and liquefaction resistance. Additionally, the penetration tests are inherently large strain and, thus, are not sensitive to aging effects that increase the liquefaction resistance of the deposits (e.g., Orense and Pender, 2013). Accordingly, alternative assessment procedures were used to evaluate the liquefaction potential of sites along the Hamilton Section of the expressway, to include using small strain shear wave velocity (Vs) based procedures and performing a paleoliquefaction study to look for evidence of liquefaction during previous events.

This paper documents the methodology and results of the paleoliquefaction investigation undertaken and compares the observations with the liquefaction potential assessed using both CPT- and Vs-based evaluation procedures. Reference should also be made to a companion paper (Clayton et al., 2017) that reports the results of the Vs-based liquefaction assessment undertaken for this same project.

2 BACKGROUND

2.1 Penetration-based liquefaction evaluation

A number of researchers have noted that conventional penetrometer-based (e.g., SPT- and CPT-based) liquefaction assessment methods can over predict liquefaction triggering potential in some soils (e.g., Orense and Pender, 2013). The over prediction has been attributed to the effects of particle crushing and/or aging, among other factors.

Particle crushing has been reported during CPT testing in carbonate and pumiceous soils. Where significant crushing occurs during penetration testing, the relative density and, hence, liquefaction potential are underestimated. Additionally, over time granular soils tend to gain strength through a number of mechanisms, referred to as 'aging'. Creep between particles may lead to a more stable packing and/or cementation may develop. These effects increase the liquefaction resistance of soils, but may not be fully recognised by large strain penetration-based liquefaction evaluation methods. Methods based on Vs have been suggested as being more appropriate for liquefaction assessment of crushable soils and older deposits. This is because the small strain nature of Vs testing does not result in particle crushing and is capable of directly recognising age related effects. While considered more appropriate in these soils, Vs-based liquefaction evaluation procedures are not as 'mature' as penetration-based methods, and therefore, it was decided to validate Vs-based assessments by also undertaking paleoliquefaction investigations.

2.2 Paleoliquefaction study

Liquefaction features are often preserved in the geologic record where host-sediments are remain largely intact. These features, termed paleoliquefaction features, are commonly comprised of sub-

vertical dikes and/or injection structures, in which sand dikes or sills intrude through subsequent layers and cross-cut the surrounding stratigraphy.

By examining the presence and/or absence of paleoliquefaction features against liquefaction potential based on in-situ test results, we have sought to demonstrate the reliability of our proposed approach to liquefaction assessment and the inherent conservatism of penetration-based liquefaction assessment methods in the Waikato soils of rhyolitic volcanic origin. Towards this end, paleoliquefaction investigations have been undertaken at seven locations along the alignment of the Hamilton Section of the Waikato Expressway.

3 GEOLOGY AND SOIL COMPOSITION

3.1 Geology

The published Geological and Nuclear Science (GNS Science) 1:250,000 scale geology map of the Waikato area (Edbrooke, 2005) shows the lowlands within the Hamilton area as being underlain primarily by alluvial fan deposits of the Hinuera Formation, Piako Subgroup. These alluvial sediments infilled the Hamilton basin mostly in two episodes between about 17,000 to 50,000 years ago. Holocene (~12,000 years ago to present) volcanic ashfall, peat bogs, and lake deposits locally overlie the Hinuera Formation. Refer to Fig 1.

The selected sites for the paleoliquefaction investigations are all situated within the younger soils of the Hinuera Formation inferred to post-date the Oruanui Eruption (26,500y BP).

3.2 Soil Composition

Most of the primary soils underlying this section of the Expressway are comprised of fluvially deposited rhyolitic soils sourced from volcanic events within the Taupo Volcanic Zone, located approximately 100 km southeast of Hamilton. The soils are comprised of significant amounts of volcanic glass, pumice, and other rhyolitic gravels, as well as crystalline minerals of quartz, feldspar (plagioclase), oxides (magnetite), pyroxenes (hypersthene, augite), amphibole (hornblende), and mica (biotite) (Hume et al., 1975). The grains are typically angular with a limited amount of rounding.

4 SEISMICITY

The seismicity of the Expressway alignment has been investigated by GNS Science as part of the preparation of the Site Specific Seismic Study (SSHA) for the wider Waikato Expressway Project (Buxton et al., 2010). Table 1 summarises the characteristics of the known faults near the project area. The SSHA presents interpretation of the seismic hazard along the route combining the contribution of known faults and unknown fault potential to derive a probabilistic earthquake shaking hazard expressed in terms of a design acceleration for a range of return periods. These are summarised in Table 2 for structures of high importance (IL3).

Table 1: Known faults contributing to the project area seismic hazard (Buxton et al., 2010)

Fault Segment	Approx. Dist. to Hamilton Section (km)	Maximum Estimated Magnitude (M_w)	Inferred Recurrence Interval (yrs)
Kerepehi South	22	6.6	3,400
Kerepehi Central	27	6.9	5,400
Kerepehi North	48	6.8	8,900
Kerepehi Offshore	75	7.2	20,000
Wairoa North	85	6.7	13,000

Table 2: Design acceleration and representative magnitudes for Ultimate Limit State (ULS) and Maximum Credible Earthquake (MCE) motions (Stirling et al., 2010)

Design Case	Design Acceleration (g)	Representative Magnitude (M_w)	Return Period (yrs)	Equivalent number of events*
ULS	0.29	5.9	2,500	~10
MCE	0.39	6.9	~20,000	~1
*Design return period compared to the time since deposition of the soils investigated (Hinuera Formation, post Kawakawa/Oruanui ash 26,500y BP)				

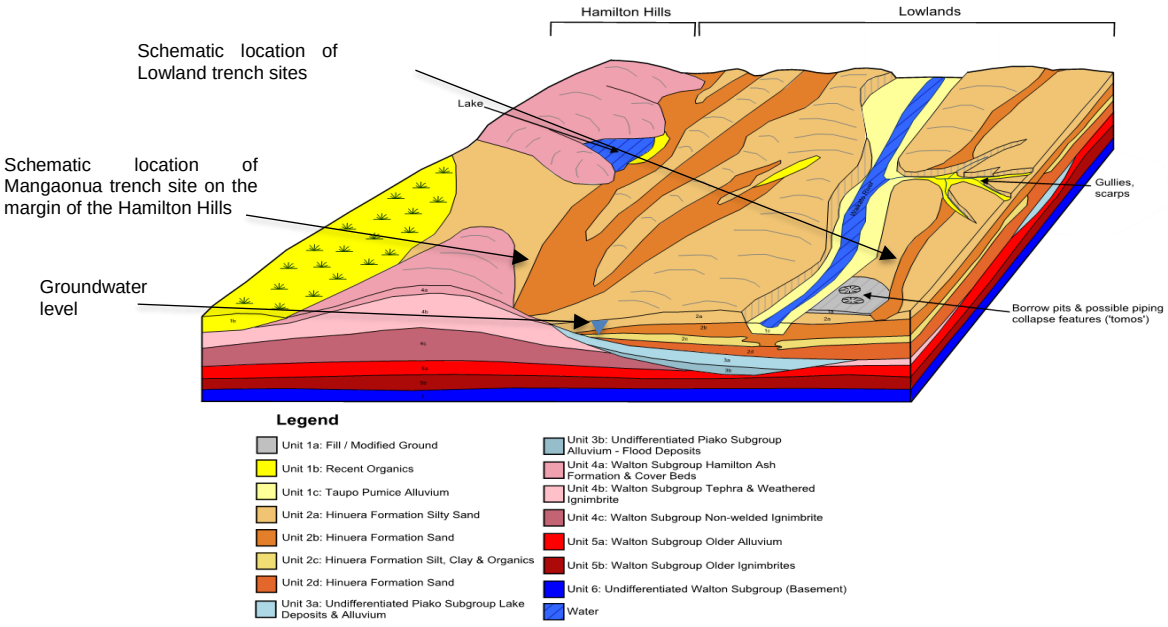

Figure 1: A Schematic block diagram showing the two geological terrains Hamilton Hills and Lowlands (modified from Lowe, 2010)

5 GROUNDWATER

Groundwater levels were investigated through a range of methods, including observations during drilling and CPT testing, monitoring of piezometers, and through seismic compression wave studies. For liquefaction assessment we have assumed that the groundwater conditions at the time of investigation are representative. However for paleoliquefaction correlations, we note that it groundwater is likely to have been higher in the past, down cutting has occurred over the last 20,000 yrs. Thus the liquefaction hazard would have been higher historically and if the soils haven't liquefied in the past, then they are unlikely to in the current groundwater conditions.

6 LIQUEFACTION POTENTIAL BY IN-SITU METHODS

Liquefaction potential was evaluated using the CPT-based and Vs-based simplified procedures proposed by Boulanger & Idriss (2014) (B&I14) and Kayen et.al (2013), respectively. In the analyses, we assumed that soils having a CPT Soil Behaviour Type Index (Ic) less than or equal to 2.6 were liquefiable and soils having Ic > 2.6 to be not susceptible (Robertson & Wride, 1998). The analyses considered Cyclic Resistance Ratios (CRR) corresponding to both 15% probability of liquefaction (in line with the standard deterministic approach to liquefaction assessment for

design) and 50% probability of liquefaction (for direct comparison to observed effects). The difference between the results from using the CRR curves corresponding to the two probabilities of liquefaction was not found to be significant where liquefaction potential was low.

7 PALEOLIQUEFACTION INVESTIGATION

As part of the paleoliquefaction investigation, seven trenches were excavated to depths varying between 1.0 to 1.5 m and detailed logging undertaken (Fig. 2). Some adjacent deeper pits were excavated to assess groundwater levels. Six of the selected trench sites were predicted to have a high liquefaction potential based on investigated material properties and elevated groundwater levels. An additional site, at Mangaonua, was selected where geomorphic evidence suggested possible paleo-lateral spreading. Detailed trench logs of soil, groundwater, and soil structures have been prepared, however due to space limitations observations are summarised in Table 3.

Table 3: Summary of observations from the paleoliquefaction trenching study

Investigation Point	Summary of findings	Paleo-liquefaction Features
Trench 1 – Resolution	Interbedded sands and silts of the Hinuera Formation encountered. Groundwater at 1.75 m in adjacent test pit. Near the southern end of the trench a possible paleoliquefaction feature comprising a steep to subvertical dyke like intrusion was encountered. It is unclear whether this is a paleoliquefaction feature or a synsedimentary structure. No extensional features, consistent with lateral spreading or large cyclic ground movements were observed.	Feature assessed as having a low probability of being related to paleo-liquefaction.
Trench 2 – Puketaha 1	Interbedded sands and silts and organic soils of the late Hinuera Formation, overlain by swampy deposits. Groundwater at 2.0m	None observed.
Trench 3 - Puketaha 2	The western section is comprised of clay rich Hamilton Ash Formation dipping down slope to the south-east with on-lapping Hinuera Formation from the east. The Hinuera Formation comprises silt overlying clean sand with discontinuous moderately thin lenses of clayey silt and organic rich silt. No groundwater noted.	None observed.
Trench 4 - Puketaha 3	Hinuera Formation comprises interbedded silt and well graded clean sand in thick beds, with very thin basal lenses of coarse pumice sand/fine gravel. Groundwater seepage from perched horizons approximately 1.5m below ground level (bgl). Groundwater at 2.1m bgl in adjacent test pit. Two sand filled dykes encountered were interpreted as paleoliquefaction features arising from the liquefaction of the immediately underlying sandy bed. Homogenous infill suggests a single event. Features do not penetrate into the base of the thick organic rich topsoil. No extensional features, consistent with lateral spreading or large cyclic ground movements were observed. Features observed appeared to be locally sourced, no significant thoroughgoing dykes were identified indicative of ejecta arising from significant depth. Refer Figure 2.	Multiple small features observed.
Trench 5 – Ruakura	This trench extends from a small terrace and to lower lying ground. Hinuera Formation soils comprised of a moderately thick topsoil overlying interbedded thick silty sand /silt and clean pumiceous sand/gravel encountered. No groundwater noted.	None observed.
Trench 6 – Mangaonua	Hinuera Formation soils comprising very thin to moderately thinly interbedded sand and silt encountered. Further excavation adjacent to trench confirmed evidence of previous sand mining, which is likely to have formed observed “terracing” of the river bank, rather than extensional movement. No groundwater noted.	None observed.
Trench 7 – Matangi Rd	Hinuera Formation soils comprising interbedded silt, sandy silt and well graded clean sands encountered. No groundwater noted.	None observed.

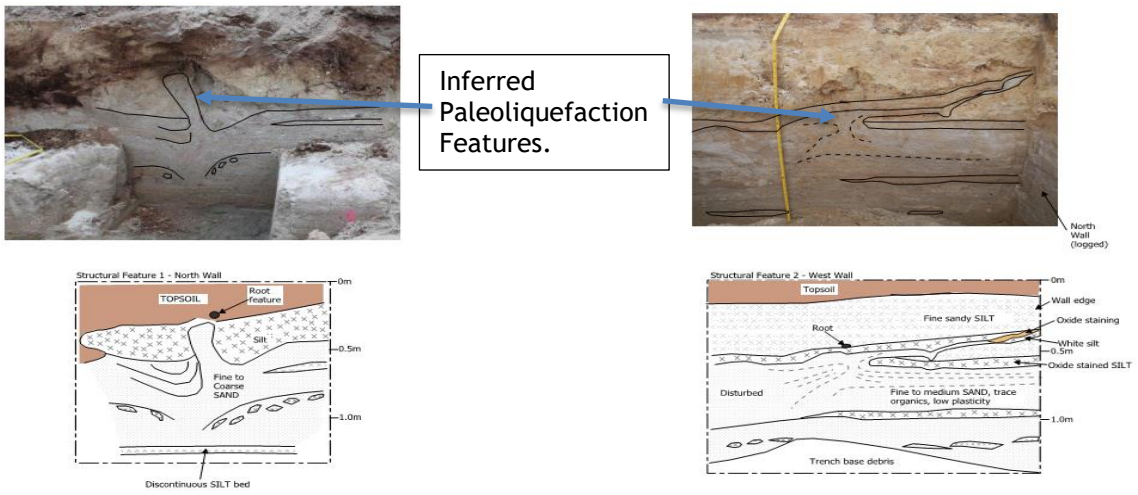

Figure 2: Sketches taken of paleoliquefaction features identified in the Puketaha trench.

Laboratory radiocarbon dating of organic samples was undertaken by Waikato University to obtain approximate age of the formation of materials overlying the paleoliquefaction feature in the north wall of Puketaha Trench 3. Two samples were successfully dated, shown in brackets below corrected for isotopic fractionation and reported in years before present (BP):

- A 2000 year (2065 +/- 20 BP) date from a charcoal deposit at 200 mm depth. The charcoal underlies a thin tephra (inferred to have originated as part of the Hatepe eruption of the Taupo Volcano around 1800 years ago). This charcoal deposit (and overlying tephra) do not appear to have been penetrated by the dyke.

- A 6000 year (5788 +/- 20 BP) date from a charcoal deposit at 700 mm depth. This charcoal deposit does not appear to have been penetrated by the dyke.

Accordingly, the liquefaction episode that resulted in the formation of the dyke is inferred to have occurred more than 6,000 years ago. In the last 6,000 years, two Ultimate Limit State (ULS) events are expected to have occurred and there is no evidence found for liquefaction in this time period.

8 COMPARISON OF METHODS AND DISCUSSION

A comparison of the liquefaction assessment results from various in-situ test methods and the observations from the paleoliquefaction study are presented in Fig. 3. For the purpose of interpreting the findings we have grouped the test locations into two areas on the basis of inferred liquefaction hazard and current groundwater depth. The northern section (Resolution, Puketaha 1, 2 & 3, Ruakura), where the groundwater depth is typically shallow, and a southern section (Mangaonua, Matangi) where the groundwater depth is currently deep. The southern areas were still investigated because CPT data indicated the significant thickness of potentially liquefiable material at depth which could have given rise to lateral spreading and slope regression to deeply incised gullies, however such features were not evident in the investigation locations.

Paleoliquefaction features were anticipated within the five locations investigated in the northern section where relatively high groundwater levels are present, in particular where this occurs within Hinuera Formation deposits. However, evidence of liquefaction was found only in the site (Puketaha 3), which had the highest assessed liquefaction potential of all sites. At Puketaha 3 liquefiable soils are indicated to be present to a significant depth by all in-situ investigation methods. The paleoliquefaction investigation identified two features within a 25-m long, up to 2-

m deep trench (Fig 2). The features observed were relatively small in section (<100 mm across) and blind (terminating below the topsoil), did not show evidence of repeated events, and propagated in a sinuous manner suggesting that this event was unlikely to have been associated with significant lateral spreading. Evidence of widespread, deeper seated liquefaction, such as large thoroughgoing ejecta dykes, were not identified. The features are estimated to be between 6,000 and 26,500 years old.

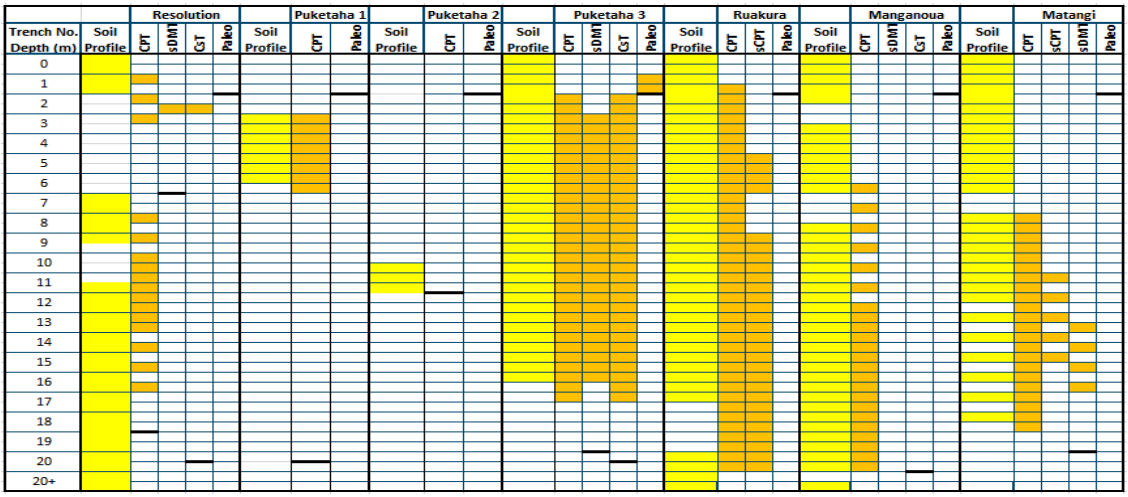

Key: Yellow – sand in borehole samples, Orange -liquefaction potential, blank – no liquefaction potential, black line – base depth of investigation; CPT – Cone Penetration Test, sCPT – Seismic Cone Penetration Test, sDMT – Seismic Dilatometer Test, CsT –Cross Hole Seismic Test, Paleo – Paleoliquefaction trench

Figure 3: Comparison of results from CPT- and Vs-based liquefaction assessment and interpretation from the paleoliquefaction trenching study.

CPT-based liquefaction assessments indicate the potential for liquefaction throughout the majority of sand units within the northern section. Vs-based methods indicate limited shallow liquefaction throughout the northern section, with the exception of Puketaha 3. At Puketaha 3 Vs-based methods indicate liquefaction from the water table to ~10 m for the ULS (2500 y return) shaking and to ~17 m for the MCE (20,000y return). Interpretation of paleoliquefaction evidence suggests that at Puketaha 3 liquefaction occurred sometime between 6,000 y and 26,500 y ago. The observed features were likely formed during a single event, with liquefaction occurring in soils at a relatively shallow depth and did not result in significant lateral spreading. The absence of large thoroughgoing ejecta dykes is considered evidence that widespread, deeper seated liquefaction, such as that indicated by CPT and Vs-based methods has not occurred at this site.

9 CONCLUSIONS

When compared to hard grained soils, deposits containing pumice have been widely reported in the geotechnical literature to have a higher resistance to liquefaction than indicated when assessed utilising penetrometer (CPT, SPT) based methods. A number of respected sources, including NZGS (NZGS. 2010), have suggested the use of Vs-based methods for triggering assessment in these soils. However, because Vs-based methods are not as mature as penetrometer based methods, The Alliance opted to undertake a paleoliquefaction study as part of the investigation of liquefaction hazard. The goal of this effort was to provide independent and site specific validation that the use of Vs-based methods provide a reliable assessment of liquefaction potential in these soils. The results of the paleoliquefaction investigation confirms the liquefaction hazard in the Hamilton Lowlands, where expected in the alluvial sands with high groundwater. Based on the comparison undertaken as part of this study, Vs-based methods were found to be more consistent (albeit still conservative) with the findings of the paleoliquefaction investigation. More detail on

the comparison between CPT and shear wave velocity testing is provided in a companion paper (Clayton et al., 2017).

10 ACKNOWLEDGEMENTS

The authors wish to thank the New Zealand Transport Agency for their permission to publish this paper and in particular the valuable contributions from Stuart Finlan. The authors would also like to acknowledge The City Edge Alliance, the Project Geotechnical Steering Group and Beca colleagues Jacqui Coleman and Alicia Newton who contributed to this project.

REFERENCES

Boulanger, R.W. & Idriss, I.M. (2014) *CPT and SPT based liquefaction triggering procedures*. Report No. UCD/CGM-14/01, Center for Geotechnical Modeling, Department of Civil and Environmental Engineering, University of California, Davis, CA,.

Buxton, R. et al. (2010) *Seismic hazard maps and spectra for Waikato Expressway*. GNS Science Consultancy Report 2010/206, 35 p.

Clayton, P.J. et al. (2017) Case study in the use of shear wave velocity techniques to investigate liquefaction potential of Waikato soils for the Hamilton section of the Waikato expressway. *Proc. 20th NZGS Geotechnical Symposium* (G.J. Alexander & C.Y. Chin, eds.), 23-26 Nov 2017, Napier, New Zealand.

Edbrooke, S.W. (compiler) (2005) Geology of the Waikato area: scale 1:250,000. Lower Hutt: Institute of Geological & Nuclear Sciences. Institute of Geological & Nuclear Sciences 1:250,000 geological map 4. 68 p. + 1 folded map;

Hume et al. (1975) Alluvial sedimentology of the Upper Pleistocene Hinuera Formation, Hamilton Basin, New Zealand. Journal of the Royal Society of New Zealand 5: p 421- 462 Ishihara, K. (1985) Stability of natural deposits during earthquakes. *Proc. 11th International Conference on Soil Mechanics and Foundation Engineering*, A.A. Balkema, Rotterdam, 1, 321-376.

Ishihara, K. (1985) Stability of natural deposits during earthquakes. *Proceedings, 11th International Conference on Soil Mechanics and Foundation Engineering.* San Francisco.

Kayen, R. et al. (2013) Shearwave velocity–based probabilistic and deterministic assessment of seismic soil liquefaction potential. *J. Geotech. Geoenviron. Eng.*, 139(3).

Lowe, D. J. et al (2010). Introduction to the landscapes and soils of the Hamilton Basin. *In Soil and Earth Sciences Occasional Publication No. 3.* [Guidebook for Pre-conference North Island, New Zealand 'Volcanoes to Oceans' field tour].

NZGS, 2010. *Geotechnical earthquake engineering practice, Module 1 – Guideline for the identification, assessment and mitigation of liquefaction hazards*. New Zealand Geotechnical Society, July 2010.

Orense, R. & Pender, M. (2013) Liquefaction characteristics of crushable pumice sand. *Proc. 18th Intern. Conf. on Soil Mechanics and Geotechnical Engineering*, Paris, France.

Robertson, P.K. & Wride, C.E. (1998) Evaluating cyclic liquefaction potential using the cone penetration test. *Canadian Geotechnical Journal,* 35(3), 442-459.

Selection of suitable ground improvement techniques: Lessons learnt from the Mackays to Peka Peka expressway, New Zealand

PJ Clayton
Beca Ltd, Auckland, NZ.
philip.clayton@beca.com (Corresponding author)

TM Pervan
Brian Perry Civil, Auckland, NZ.
timp@fcc.co.nz

Keywords: Ground Improvement, liquefaction, vibro-compaction, in-situ mixing, undercut and replacement, vibro-replacement.

ABSTRACT

Assessment and mitigation of potential liquefaction is a critical requirement for successful infrastructure design in seismically active regions of New Zealand. This paper highlights several important lessons learnt from the design and construction of ground improvements to mitigate the effects of liquefaction on the MacKays to Peka Peka Expressway. Learnings are presented on the design and construction challenges of implementing four ground improvement techniques: Undercut and replacement, in-situ mixing, vibro-densification, and vibro-replacement with particular reference to improvement of fine, poorly graded dune sands. The findings lead to a number of lessons learnt for the project team, the most significant being that widely adopted, empirically based correlations for 'improveability' of sands based on fines content/plasticity and soil behaviour indices, may be unreliable when applied to soils with high uniformity, sphericity and porosity.

1 INTRODUCTION

A new expressway has recently been completed along the Kāpiti Coast near Wellington, New Zealand. The 18km long, four lane MacKays to Peka Peka (M2PP) Expressway was designed and built by an Alliance, made up of Fletcher, Beca, Higgins and the New Zealand Transport Agency (NZTA).

The M2PP Expressway includes fifteen road bridges and three cycle, walkway and bridleway bridges. It forms part of the Wellington Northern Corridor, and opened earlier this year. The Wellington Northern Corridor runs from Levin to Wellington Airport and is one of seven Roads of National Significance (RoNs) that the New Zealand Government has identified as essential state highways that support economic growth. After a major earthquake, the expressway is to form part of a life-line route to provide providing access to the City of Wellington.

2 MATERIALS

2.1 Geological Setting

The expressway route crosses the coastal plain to the west of the Tararua Ranges, in an area that has been shaped by repeated cycles of glaciation that have occurred in the past two million years. Much of the route is underlain by potentially liquefiable dune sands and silts interspersed by peat (Coe & Alexander, 2012). Loose to medium dense Holocene sands and underlying Pleistocene sands are present under most bridge abutments. Ground water was located near surface across much of the 18km long expressway.

3 DESIGN REQUIREMENTS

3.1 Seismic Loading

The lower North Island of New Zealand is a seismically active region, producing large magnitude earthquake events. Although no major active faults are mapped passing directly through the expressway site, the high shaking hazard results in design peak ground accelerations of up to 0.98g in a 1/2500-year ultimate limit state (ULS) design event. Many of the bridge sites were underlain by materials susceptible to widespread liquefaction or cyclic softening under earthquakes of 1 in 100 years and higher.

3.2 Ground Improvement Design Philosophy

Ground improvement was primarily utilised to control seismically induced displacements of bridge abutments to around 150-200mm under ULS seismic events. These displacements were considered to represent a reasonable limit for the steel H piles that supported the bridge abutments. The extent of the required ground improvement area was determined from seismic slope stability analyses, with typically around 30m x 50m plan area of ground improvement beneath each abutment. A simplified diagram illustrating the analyses undertaken for sizing the ground improvement is presented in Figure 1.

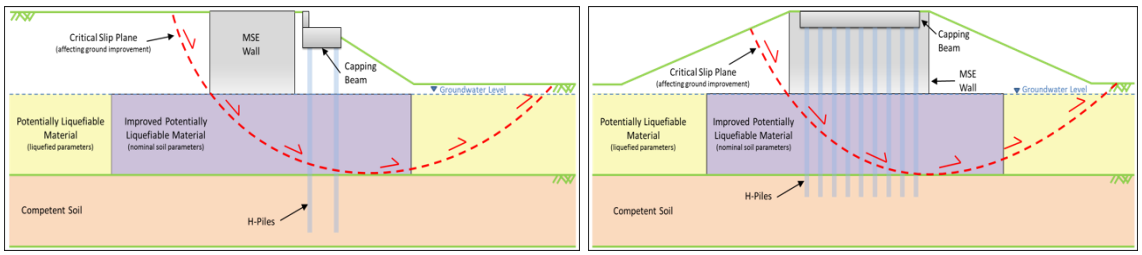

Figure 1 Longitudinal and transverse seismic displacement assessments (not to scale).

4 PRELIMINARY GROUND IMPROVEMENT DESIGN

4.1 Proposed Methods

The selection of ground improvement techniques during the initial design phase was based on anticipated equipment availability, cost and ground conditions. Preliminary design assumed a combination of the following techniques, presented below in order of increasing cost:

- Excavate and replace;
- Vibro-compaction (vibroflot);
- Vibro-replacement (stone columns);
- Insitu soil/cement lattice structures.

4.2 Initial Selection Process

4.2.1 Excavate and Replace

Excavate and replace options were proposed for areas where peat, unsuitable fine-grained soil or shallow zones of liquefiable soil underlay the footprint of bridge abutments. Excavation to depths of up to 5m below the water table were considered. Proposed backfill material comprised either imported hard fill or Holocene dune sand, with the latter being preferred on cost and environmental considerations. Where conventional earthworks compaction techniques were not expected to sufficiently compact the replaced material, such below the water table, vibro-densificaton was proposed.

4.2.2 Vibro-Desification

Vibro-densification was proposed as a method for in-situ improvement of clean sands and sand fill used to backfill undercut areas. Densification was to be validated utilising cone penetration tests (CPTs) undertaken between improvement points. These results were then to be compared against design curves of CPT penetration resistance (qt) versus depth to achieve the desired liquefaction resistance.

4.2.3 Vibro-Replacement

Vibro compacted gravel (stone) columns were proposed as the principal ground improvement method to densify deeper in-situ sand deposits. Based on historical experience and published research, the upper limit for most effective densification was assumed to be a friction ratio of 1.0 or a soil behaviour index (Ic) of approximately 2.0. Column spacing for planning purposes was developed based on the methodology published by Barksdale and Bacchus (1983). Densification was to be validated in the same manner as for vibro-densification, conservatively ignoring the beneficial effects of shear stiffening and improved drainage.

4.2.4 In-situ soil/cement lattice

For ground improvement on sites containing soils that were not anticipated to respond to vibro replacement methods, such as soils containing a significant proportion of fine grained material or plastic interbeds, ground improvement by stress redistribution was proposed. This method improves the resistance of soil through the introduction of stiff elements that limit overall strains to a point where liquefaction is inhibited. The initial lattice design assumed in-situ cement / soil mixed orthogonal panels (or diaphragms), constructed vertically through potentially liquefiable soils at 5m centres each way. The design approach was based on the stress redistribution method as described by Baez & Martin (1994), modified by the recommendations of OTREC (2013) after Ngyugen et al. (2012) to account for strain incompatibility.

5 GROUND IMPROVEMENT TRIALS

5.1 Excavate and Replace with Vibro-Compaction

At the Paetawa Drain Bridge, near the northern end of the project, site investigation had identified organic deposits extending down to 5m below the water table. A design was developed that involved excavating the peat and its replacement with compacted sand fill, followed by vibro-compaction of any low density areas. De-watering was not used due to the extensive peat deposits and large area of replacement and high water table. Figure 2 illustrates the typical working conditions.

Figure 2 Excavate and replace at the Paetawa Bridge Site.

CPT testing undertaken following backfill (using only conventional earthworks methods) indicated that further densification was required below the groundwater table and particularly within a continuous zone at the interface between insitu and replaced material.

Vibro compaction field trials were then undertaken on the fill using a range of probe sizes. The field trials demonstrated that regardless of the equipment used, the loose sand fill below the ground water level could not be compacted to meet the design criteria. Site observations indicated that the sand fill introduced from ground level failed to migrate down towards the probe tip, instead remaining in suspension. Post-trial CPTs indicated virtually no improvement below the water table using vibro-densification methods.

Following this unsuccessful trail, vibro-compaction was abandoned. Dynamic compaction was subsequently used to densify the undercut backfill material at the Paetawa Drain Bridge (Robins & Pervan, 2017).

5.2 Vibro-Replacement (Waikanae River Bridge)

The new Waikanae River Bridge was underlain mostly by dense to very dense Pleistocene sand and gravel interbedded with Pleistocene silt. Pre-treatment CPTs identified a 3m to 4m layer of medium dense sands at around 6-8m depth that were potentially liquefiable under ULS Conditions. Vibro-replacement (stone columns) was specified across each abutment footprint area of about 2500m2, to a depth varying between 6m and 8m. The wet, top feed method was selected by the construction team based on the availability of suitable working and water recycling space.

A 25% replacement ratio was initially proposed, based on work by Baez & Martin after Barcsdale and Bacchus, and Priebe. The initial design assumed using a small vibroflot probe to form a 600mm nominal diameter column. This was later changed to a larger probe to assist penetration through the dense upper sand layer, subsequently increasing the nominal column diameter to 800mm.

Figure 3 Photos from the Waikanae River Bridge stone column trials.

A stone (65/40) ballast sourced from the nearby Otaki River was used for the column aggregate construction. Trial areas were setup in a corner of the improvement block for three separate area replacement ratios (21%, 25% and 32%). The results of CPT testing midway between the columns found that the area ratio had to be increased to the maximum trialled area replacement ratio of 32% (1.5m triangular grid pattern) to achieve the required level of densification.

Further interpretation confirmed that the treatment generally resulted in adequate densification to the targeted sand layers. Some variability was present with limited improvement through interbedded silt layers, as well as evidence of strength degradation in already dense sand layers (some examples of these issues are presented in figure 4).

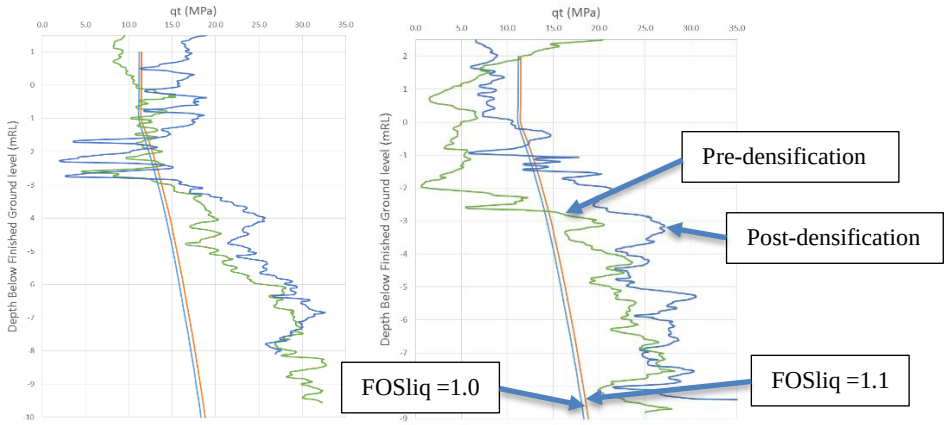

Figure 4 Example pre (green) vs post (blue) CPT comparisons and design lines.

5.3 Insitu Soil Mixing

The first bridge site requiring lattice ground improvement was the Otaihanga Road Overbridge. The soils underlying the Otaihanga Bridge consisted of Holocene dune sands with thin silt interbeds to depths of around 4.5m. A lattice design was adopted for ground improvement based on the designer's past observations of poor performance of vibro-replacement techniques on interbedded sites. Development of the lattice design called for laboratory trials to confirm cement binder contents and field trials to confirm mixing efficiency.

The design lattices consisted of 5m x 5m cells with a wall thickness of 500mm. To mitigate liquefaction, the lattice material was required to have a shear stiffness of approximately 400kPa, or an equivalent unconfined compressive strength (UCS) of 1,200kPa. The proposed construction methodology involved 750mm diameter insitu soil mixed columns that interlocked at 550mm centres to provide a continuous wall thickness. The intention was to construct the columns using a low pressure, wet mixing method from a rotary drill rig with a mixing blade attachment.

Laboratory testing was undertaken to determine the cement binder content and water to cement (W/C) ratio that would achieve the required design shear strength and stiffness. Sand samples from depths of 2m and 4m were split into batches and wet mixed with 6%, 9%, 12% and 20% cement content by weight and W/C ratios between 1 and 1.5.

UCS testing highlighted a generally poor response to the cement binder and a significant difference in interpreted shear strengths between different deposits of Holocene dune sands. Typically sand from 2m depth achieved a maximum UCS of about 100kPa, while the samples tested from 4m depth exceeded 1,500 kPa for similar cement contents.

Based on the highly variable results and the higher than expected binder content required to generate reasonable results, the soil mixed column methodology was converted to an interlocking concrete option utilising a CFA piling rig employing batched low strength concrete delivered to the site.

6 DISCUSSION

6.1 Excavate, Replace and Vibro-Densification

A thin (<500mm) loose/soft layer was at times identified at the interface between fill and in-situ ground, where excavate and replace ground improvement had been undertaken below the water table. The team initially assumed that this was an inclusion of unsuitable material overlooked in the excavation process, however more detailed investigation identified that these layers typically appeared to be loosened in-situ soils from just below the cut line. Possible explanations include:

- Upward ground water flow through the base of the excavation disturbing the sand;
- Physical disturbance by toothed buckets on soil immediately below the cut line.

Wellpoint de-watering was found to resolve the above issues, confirming the upwards groundwater flow as the culprit, although this approach resulted in significant additional physical effects and compliance costs on a large scale.

Considering the fines (silt/clay) content and CPT soil behaviour Index (Ic) in isolation the sand fill material could have been expected to respond well to vibro-compaction, however this was clearly not the case in practice. In the Authors view there are a number of reasons for the poor performance that are all related to the geological origin of the material. The sand fill utilised on the M2PP project was predominantly a dune or aeolian deposit, further sorted by the wind into deposits of uniform sized fine sand and in the process of transportation the grains had become rounded.

The M2PP deposits have typically 1% passing the 0.063mm sieve and 80% passing the 0.15mm sieve with a uniformity coefficient of 1.49. The sand also had a high sphericity typically of 0.5-0.9 and regularity of 0.5-0.6. These factors affect the packing and thus the achievable density and strength (mechanical interlock) and porosity. In Figure 5 the Holocene dune sand grading curve is compared to the range of particle sizes for which vibro-compaction should be effective (CIRIA Report C572 2002). The Authors have concluded that the particle shape and uniformity are also important factors to consider in assessing the potential for sand to respond to vibro-methods.

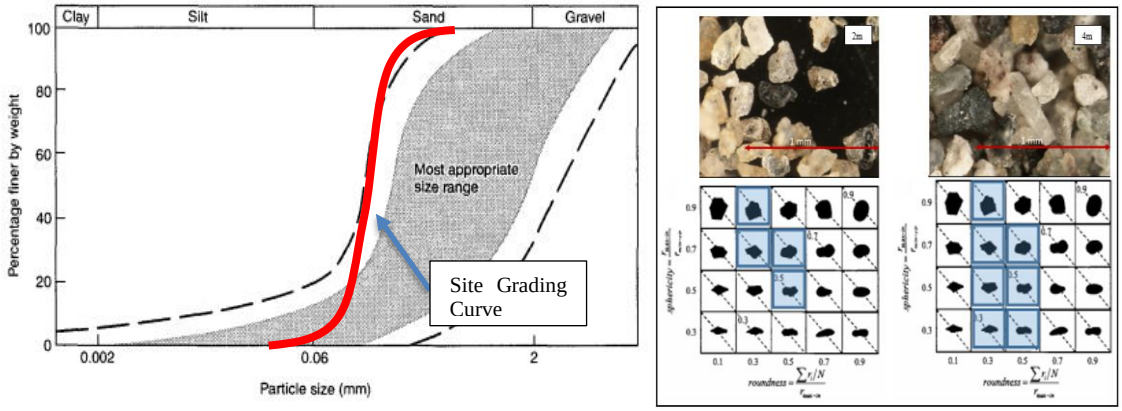

Figure 5 Holocene dune sand macro photography, grain shape assessment and grading curve compared to the range of particle sizes for which vibro compaction should be effective (modified from CIRIA Report C572 2002).

6.2 Vibro-Replacement (Stone Column)

The observations from the vibro-densification trials were partially reflected in the Vibro-replacement trails. Area replacement ratios of 21%, 25%, 33% and 35% were trialled with CPT soundings taken immediately prior to treatment and seven days following treatment. Densification was not as effective as expected and a very high replacement ratio was required to achieve satisfactory densification in the medium dense sands. Replacement ratios of 21% and 25% showed little to no densification improvement and a replacement ratio of 33% showed reasonable improvement. An increase to a 35% replacement ratio did not yield any further improvement.

Another notable, but not entirely unexpected response, was that sands in the vicinity of silt interbeds did not appear to improve. These zones, typically not more than 500mm thick, associated with thin (<100mm) and laterally discontinuous silt layers could not be improved to meet the minimum qt values. These were considered unlikely to compromise the overall performance of the ground improvement in a ULS event.

The authors concluded that published guidance on target replacement ratios, such as the work from Baez (1995) and Priebe (1995), does not provide a reliable indication of effective replacement ratios in these soils, and that this was due to their uniform grading and sphericity.

6.3 In-situ Mixing

Laboratory soil/cement mixing trials were completed on two sand samples taken at 2m and 4m depth. The geologic origins of these sands is thought to be similar (dune deposits) however their characteristics differ somewhat and this is reflected in their response to the use of a cement binder. Table 1 summaries the difference in soil characteristics between the two samples.

Table 1 Comparison of sand properties from Otaihanga Road Overpass

Origin	Otaihanga 2m depth	Otaihanga 4m depth
Description	Fine quartzose dune sand	Fine quartzose dune sand
Grading	Generally within the 0.1 to 0.2mm size range, 15% fines.	Generally within the 0.1 to 0.2mm size range, 2% fines
Cu	1.8 (may not fully reflect the uniformity in the sand due to presence of fines)	1.5
Sphericity	0.5-0.9	0.3-0.9
Regularity	0.5-0.6	0.3-0.6
Dry Density	1.33 t/m3 (compacted)	1.51 t/m3 (compacted)
Porosity	50%	44%
UCS at 6%	45 kPa	150 kPa
UCS at 9%	50 kPa	380 kPa
UCS at 12%	50 kPa	800 kPa
UCS at 20%	50 kPa	1500 kPa

The generally poor test results meant that the in-situ mixing method was non-viable with cement contents of more than 20% and high variability in results. These results were considered to be affected by the high uniformity of the sand which in turn, resulted in a high void ratio which appears to have prevented efficient cementation. Work completed by Consoli et al. (2012) demonstrating the variation of unconfined compressive strength (qu) with porosity of cemented soils appears to be consistent with the range of UCS results achieved with both the 2m and 4m samples (refer figure 6).

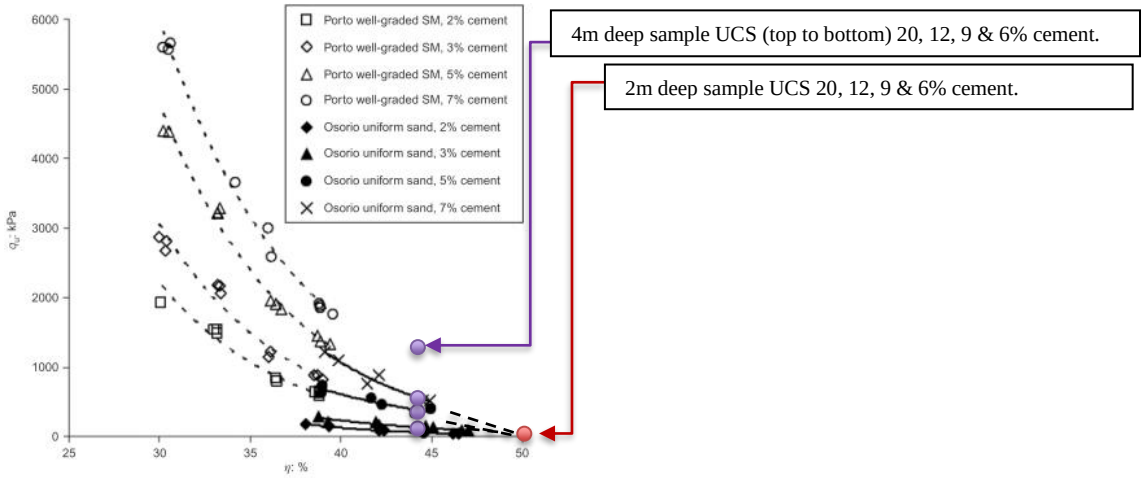

Figure 6 Variation of UCS (qu) for cemented soils with porosity (modified from Consoli et al. 2012) compared with the UCS results from Otaihanga sand samples.

The authors concluded that while the grading and composition of the sands are similar, the effect of porosity can have a significant impact on engineering behaviour of artificially cemented soils.

7 CONCLUSIONS

A number of different ground improvement methods were trialled in saturated dune sands and found to be unsuccessful or requiring the utilisation of very high area ratios to achieve the desired level of improvement.

The sands to be improved were notable in that the grains were fine, uniform and comparatively spherical. As a consequence these sands were found to be more difficult to compact or to cement than would have been expected if assessing simply based on fines content or CPT soil behaviour Index. Vibro-compaction was found to be unsuccessful, vibro-repacement provided limited success, requiring very high area ratio and cement stabilisation was not consistent even at very high binder contents

These findings lead to a number of lessons learnt for the project team, the most significant being that widely adopted, empirically based correlations for 'improveability' of sands based on fines content/plasticity and soil behaviour indices, may be unreliable when applied to soils with high uniformity, sphericity and porosity.

8 ACKNOWLEDGEMENTS

The authors would like to thank the MacKays to Peka Peka Expressway Alliance, Nick Wharmby (formally Brian Perry Civil) and David Chadwick (Keller GE Australia). The authors would also like to thank the New Zealand Transport Agency who granted permission to publish this paper.

REFERENCES

Barksdale, R.D. and Bachus, R.C., (1983) *Design and Construction of Stone Columns, Volume I*. Report No FHWA/RD-83/026, Federal Highway Administration, Washington, D.C.

Baez, J. I. & Martin, G. R. (1993) Advances in the Design of Vibro Systems for the Improvement of Liquefaction Resistance. *Proceedings of the 7th Annual Symposium of Ground Improvement.*

CIRIA Report C572. (2002) *Treated ground: engineering properties and performance*. CIRIA London.

Coe, L. J., and Alexander, G. J., (2012) MacKays to Peka Peka Expressway: Road Embankment Construction on Peat Deposits. *Proceedings of the 11th Australia and New Zealand Conference on Geomechanics* (ANZ 2012).

Consoli, N.C., Rosa, D.A., Cruz, R.C. and Rosa, A.D. (2011) Water content, porosity and cement content as parameters controlling strength of artificially cemented silty soil. *Eng. Geol*., 122(3-4), 328-333.

Consoli, N.C., Fonseca, A.V., Silva, S. R., Cruz, R.C. and Fontini, A. (2012) Parameters controlling stiffness and strength of artificially cemented soils. *Geotechnique*, No. 2, 177-183.

Mitchell, J. (1981) *Soil Improvement – State of the art report. Session 12*. Amelioration des Sols.

Ngyugen, T.V., Rayamajhi, D., Ashford, S.A., Boulanger, R.W., Lu, J., Elgamal, A. & Shao, L. (2012) Effect of DSM grids on shear stress distribution in liquefiable soil. *ASCE Geo Congress Conference*, Oakland, California, March 25-29.

OTREC (Oregon Transportation Research and Education Consortium) (2013) *Reducing Seismic Risk to Highway Mobility: Assessment and Design Examples for Pile Foundations Affected by Lateral Spreading*. Oregon Dept. of Transportation.

Priebe, H.J. (1995) *The Design of Vibro Replacement*. *Ground Engineering*, Technical Paper GT 07-13 E, 1995.

Development of a magnetic tracking system for monitoring ground movements during geohazards: some preliminary results

X Y Chen and R P Orense
Department of Civil and Environmental Engineering, University of Auckland, NZ
xche753@aucklanduni.ac.nz (Corresponding author)

Keywords: soil movement, ground deformation, geohazard, monitoring, magnetic trackers

ABSTRACT

In the study of geotechnical hazards, such as soil liquefaction and landslide, the analysis of soil movements or soil particle movements is always one of the major preoccupations. An efficient soil movement sensing technique requires the tracking of different parts of a soil mass in order to develop an overall displacement field for the purpose of examining the mechanism involved and to establish a precise early warning system. A magnetic tracker system is therefore proposed with permanent magnets as trackers and magnetometers as receivers. When permanent magnets, deployed in soil to serve as excitation sources, move with a soil body during a geotechnical event, they generate static magnetic fields whose flux densities are related to the positions and orientations of the magnets. Magnetometers are used as receivers to detect the generated magnetic fields, which can be further used in calculating the magnets' locations and orientations based on appropriate algorithms. Due to the fact that soil has magnetic permeability very similar to that of non-ferromagnetic materials, such as air and water, it cannot influence the static magnetic field generated by magnets; therefore high accuracy can be guaranteed within a limited sensing range. This paper presents some of the results of preliminary works on the use of magnetic sensing technology for ground deformation detection.

1 INTRODUCTION

Identification of possible failure mechanisms and assessment of potential damage associated with earthquake hazards are important ingredients in mitigating their impacts to the built environment (Orense 2003). Understanding "why" and "how" these hazards will occur can help engineers and public policy makers design safer structures and sites for the society. On the other hand, there is also a need to assess the temporal development of failure, i.e. to evaluate "when" ground failures will occur and their progress, so that countermeasures and necessary operations to reduce damage can be effectively implemented. One way to achieve this is through monitoring and alarm systems.

Monitoring ground deformations is a vital component of many early warning systems that have been established. Such systems require continuous recording of soil movements, so that if the monitored movement reaches a pre-set threshold, precaution of failure (such as warning or alarm) is generally issued. Moreover, accurate tracing of the exact movements of soil particles can shed further understanding of the mechanism of the seismic hazard and the consequent countermeasure techniques. For example, understanding the mechanism of subsurface ground deformations induced by soil liquefaction could provide better insight on the mechanism(s) involved in the process for better design of underground structures.

Although significant progress concerning soil liquefaction has been achieved through a large number of high quality field investigations, almost all of the findings so far relate to the displacements observed on the ground surface, i.e. the cause of and the mechanism behind seismically-induced ground surface deformation remains unknown. Delicately designed

laboratory tests can simulate this very well, but because of the opaqueness of the soil grains, the exact particle movements within a soil model is difficult to quantify. For this reason, other methods of monitoring subsurface deformation that can withstand underground condition (presence of soil cover, saturated soil environment, etc.) need to be developed.

In general, movement sensing can be categorise into two groups: positioning sensing and displacement sensing (Nyce 2004). In positioning sensing, the distance between a reference point and the present location of the target is measured. For example, in landslide monitoring, an extensometer can be used to measure changes in the length of a slope; a long wire and a fixed pole is necessary to measure the distance between the pole and the target location. Although a non-contact extensometer may not need long wires to measure distance, fixed points are still indispensable. Conversely, in displacement sensing, the distance between the current location and the previously recorded location is measured. For example, an inertial navigation system (INS) is a relative measurement which does not rely on external fixed point. Akeila et al. (2007; 2010) used smart pebbles embedded with a strap-down INS system to monitor riverbed sediment transport. Although these smart pebbles can also be applied in soils to record information related to acceleration and applied forces, the most important displacement information is beyond capture. To circumvent this, the exact position of a target in three-dimensional space can be calculated mathematically by integrating the accelerations and rotations about the three axes; however, since the data are error-prone, the integration processes lead to errors that grow with time (Paik 1996). A Global Positioning System (GPS)-aided INS can be applied in the smart pebble to increase the level of accuracy and reliability as well as the information update rate. However, as the targets of interest are usually buried, which means the signals of smart pebble underground need to penetrate the depth of soil without being blocked, the strength of the signal may not be strong enough to guarantee the accuracy.

In order to overcome the shortcomings described above, a novel way of monitoring ground deformations is examined. In this paper, the technology whereby soil movement can be obtained from a magnetic sensing technique is introduced. Firstly, the algorithm developed to define the location and orientation of the magnets is discussed and its validation using a numerical model is presented. Finally, the results of simple physical model tests are presented as a way of illustrating the capability of the proposed technique.

2 MAGNETIC SENSOR SYSTEMS

2.1 Background

Magnetic sensor system is a type of position sensing technique with an obvious advantage of non-contact operation. When a permanent magnet (acting as magnetic tracer) is deployed within the subsoil, it will generate a magnetic field which can be detected by magnetometers (magnetic field sensors) above the ground. The magnetic strength and direction at a certain target point in the ground give information about the relative distance between the target point and the magnetic tracer. As soil moves during an earthquake and/or liquefaction, the magnetic tracer will move along with the soil particles (provided they have similar density). In this way, the movements of the soil particles can be traced by the movements of the magnetic tracer.

The position as well as the direction information can be derived by detecting the magnetic flux density (B with the unit of Tesla) around the magnetic dipole. Schlageter et al. (2001) developed a system capable of tracking a permanent magnet with a 2D-array of 16 cylindrical Hall sensors. Hu et al. (2006) investigated the use of magnet-based localization in wireless capsule endoscopic technique. Also, because soil has magnetic permeability very similar to that of non-ferromagnetic materials, such as air and water, it cannot influence the static magnetic field generated by magnets. Therefore, it is possible to locate a magnetic tracker buried in soil with high accuracy. When the magnetic tracker is deployed in soil, it will generate a magnetic field which can be detected by

magnetometers. The magnetic flux density at a certain target point in the space gives information about the relative distance between that target point and the magnetic tracker. As soil moves due to geohazards, the magnetic tracker will move along with the soil particles. In this way, the movements of the soil particles can be illustrated by the movements of the magnetic tracker.

There are some advantages of the magnetic tracer technique compared to other existing techniques: (1) there is no way to block a magnetic field, so this tracing technique has the potential to be well-applied underground; (2) the feasibility of accurate tracing is largely dependent on the strength produced by the magnetic tracer; so if the strength of a permanent magnet mixed with soil particles can be strong enough, the size of the tracer can be as small as a normal permanent magnet due to the fact that no other circuits or devices are required (unlike the smart pebble); although in order to enhance the field strength of a tracer, an electromagnet with batteries can be installed together as a tracer.

2.2 Formulation of Algorithm

The first step in the research concerning the establishment of the magnetic sensor system is to come up with an algorithm to calculate the location information about a tracker (or multiple trackers) from data collected by magnetometers. Each set of data collected by a magnetometer at a specific point is comprised of three-axis magnetic flux densities. The proposed algorithm can calculate the coordinate point (*x*, *y*, *z*), using the magnetic flux densities.

The proposed magnetic sensor system comprises permanent magnets as trackers, and magnetometers as receivers to detect the magnetic flux densities generated by the trackers. Trackers are buried in soils and magnetometers are arranged outside the soil body of interest. Collected data is sent to a computer and then analysed through proper algorithm to determine the locations of the trackers. The relationship between the magnetic flux density at a spatial point and the location of the point is illustrated by:

$$\vec{B} = \frac{\mu_0 m}{4\pi r^3}(2cos\theta\hat{r} + sin\theta\hat{\theta}) \tag{1}$$

$$\vec{B} = \overrightarrow{B_x} + \overrightarrow{B_y} = 3\frac{\mu_0 m}{4\pi r^3} sin\theta cos\theta \cdot \hat{x} + \frac{\mu_0 m}{4\pi r^3}(3cos^2\theta - 1) \cdot \hat{y} \tag{2}$$

where m is the magnetic moment of the dipole whose unit is $A \cdot m^2$; μ_0 is the permeability of a vacuum (free space), and B is measured in Tesla. The values of r and θ provide the information of the location of the magnetic tracker in polar coordinates. $\hat{r}$ and $\hat{\theta}$ are unit vectors shown in Figure 1. Although the above equations are easy to understand, it is difficult to develop an effective algorithm based on the above equations because during any movement, the direction of the tracker or the direction of the magnetic moment is not constant.

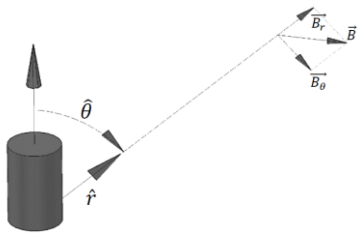

Figure 1. Schematic of the magnetic flux density generated by a magnetic dipole

In reality, the magnetic flux density at a spatial point is not only dependent on the relative distance from the magnet, but also dependent on the orientation of the magnet (the magnetization direction). To solve the location (*x*, *y*, *z*) and the orientation (*m*, *n*, *p*) of a tracker, 6 independent equations are required. However, considering that the size of the tracker is much smaller than the distance between the tracker and the magnetometers and the tracker is either a disc magnet or an

electromagnetic coil, spinning around the axis of the magnetization direction will not change the spatial distributions of the magnetic flux densities. Hence, the magnetic positioning in this case is actually a 5-D positioning because, in addition to 3 unknowns related with location, there are only 2 more unknowns required to indicate the orientation. As a result, it is more convenient to change the above equations into the following ones including a unit vector $\overrightarrow{M_0}$ indicating the direction of the magnetic dipole:

$$\overrightarrow{B_i} = B_T \left(\frac{3(\overrightarrow{M_0} \cdot \overrightarrow{R_i}) \cdot \overrightarrow{R_i}}{R_i^5} - \frac{\overrightarrow{M_0}}{R_i^3} \right) \tag{3}$$

$$R_i = \sqrt{(x_i - a)^2 + (y_i - b)^2 + (z_i - c)^2} \tag{4}$$

$$\overrightarrow{R_i} = (x_i - a, y_i - b, z_i - c) \tag{5}$$

$$\overrightarrow{M_0} = (m, n, p) \tag{6}$$

where B_T is a constant parameter related to the magnet being used; $\overrightarrow{B_i}$ is the magnetic flux density detected by magnetometer i, where the location of the magnetometer i is indicated by (x_i, y_i, z_i); (m, n, p) denotes the magnetization direction of the magnet with $m^2 + n^2 + p^2 = 1$; and (a, b, c) is the location of interest. The schematic of the magnetic sensor system is shown in Figure 2. In order to develop the algorithm required, Equation (3) can be expanded as:

$$B_{xi} = B_T \left(\frac{3[m(x_i - a) + n(y_i - b) + p(z_i - c)] \cdot (x_i - a)}{R_i^5} - \frac{m}{R_i^3} \right) \tag{7}$$

$$B_{yi} = B_T \left(\frac{3[m(x_i - a) + n(y_i - b) + p(z_i - c)] \cdot (y_i - b)}{R_i^5} - \frac{n}{R_i^3} \right) \tag{8}$$

$$B_{zi} = B_T \left(\frac{3[m(x_i - a) + n(y_i - b) + p(z_i - c)] \cdot (z_i - c)}{R_i^5} - \frac{p}{R_i^3} \right) \tag{9}$$

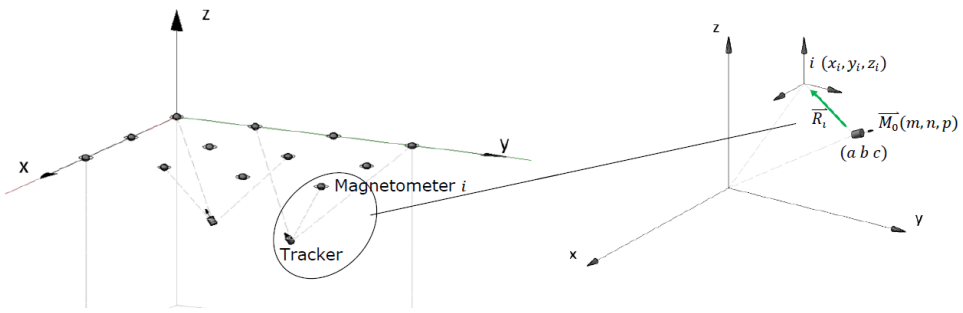

Figure 2. Schematic of the magnetic sensor system in the global coordinate frame.

where B_{xi}, B_{yi} and B_{zi} are the *x*, *y* and z components of $\overrightarrow{B_i}$ respectively. An effective algorithm should be able to solve the equations for the position of the tracker (a, b, c) and the orientation (m, n, p) using the inputs of B_{xi}, B_{yi} and B_{zi}, and also with the known position of the magnetometer (x_i, y_i, z_i). In order to solve the above high-order nonlinear equations, a Levenberg-Marquardt (L-M) algorithm (Levenberg 1944; Marquardt 1963) and a linear algorithm are used (Hu et al., 2006). Due to space limitation, the appropriate equations for these algorithms are not presented here; however, both linear and L-M algorithms can be coded easily in MATLAB.

3 VALIDATION OF ALGORITHM

In order to test the algorithm without data derived from real physical tests, Finite Element Method Magnetics (FEMM) (Meeker, 2015) was used to generate the magnetic flux density from a permanent magnet (10 mm ϕ, 10 mm high, 52 MGOe Neodymium magnet). In FEMM, a permanent magnet is modelled as a volume of ferromagnetic material surrounded by a thin sheet of current. Assuming the locations and directions of magnetization of the permanent magnet change as shown by the white arrows in Figure 3, the two-axis magnetic flux densities are recorded at the location of the receiver each time it moves. White noise is then added to the recorded flux densities to simulate the real ones captured by a magnetometer. As shown in the figure, the movement of the tracker is assumed as

$$x(i) = 0.3 + 0.05 * i \qquad i = 1,2,3 \ldots, 20 \qquad (10)$$

$$y(i) = sin(\pi/2 * 1.0026 * x(i)\text{^}2 - 3/20) + 0.3 - 1.6 \qquad i = 1,2,3 \ldots, 20 \qquad (11)$$

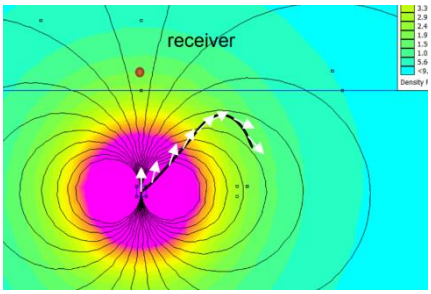

Figure 3. Magnetic flux densities generated by FEMM as assumed inputs

The algorithm developed is tested in the MATLAB program in a 2-D scenario, which uses magnetic flux density B_{xi}, B_{yi} and B_{zi} generated by FEMM with some additional white noise. As shown in Figure 4, the more magnetometers being used, the more accurate the location would be, and even with only one magnetometer, the algorithm can provide acceptable results. However, when using the L-M method to solve non-linear high order equations, a starting point or an initial guess is required to begin iteration, and if the initial guess has large error, the algorithm may fail to give correct global minimizer due to the fact that there are too many local minimizers.

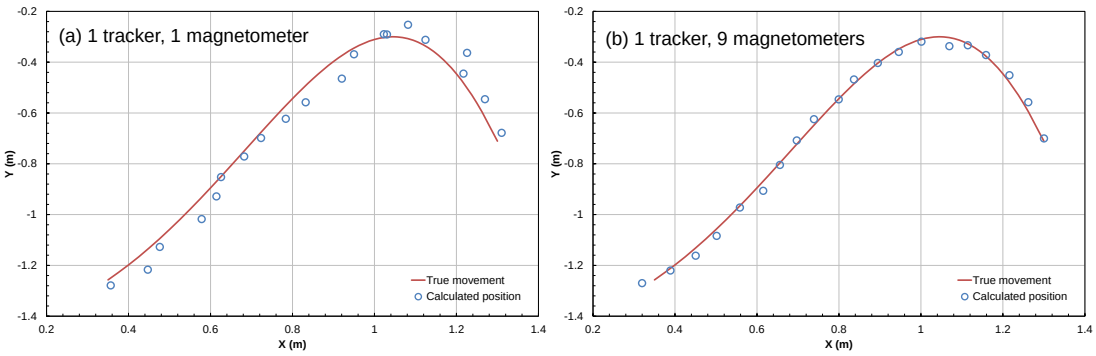

Figure 4. (a) L-M method tested with 1 magnetometer and one tracker; (b) L-M method tested with 9 magnetometers and one tracker.

The linear algorithm is also tested in the MATLAB program in a 3-D scenario. For the linear method, at least 6 magnetometers are required for tracking 1 magnet in space. Compared to the L-M method, an advantage is that there is no need for an initial guess to be set. However, the number of magnetometers required increases as the number of trackers increases. Moreover, the linear algorithm cannot be used in 2-D scenario, because the coplanar assumption is automatically satisfied in 2-D. Due to space limitation, the validation for linear algorithm through FEMM is not shown here.

4 VALIDATION THROUGH PHYSICAL MODEL TESTS

Preliminary physical tests are conducted in two sequential steps. In the first step, the magnetometers are calibrated in a real sensor array system before using to collect data. Secondly, the combination of the linear algorithm and the Levenberg-Marquardt algorithm is tested.

4.1 Calibrations of magnetometers

A magnetometer is a type of sensor that measures the strength and orientation of local magnetic flux density. Due to the fact that magnetic measurements are subjected to hard and soft iron distortions, all readings from the three axes of a magnetometer should be calibrated before use. Hard-iron distortions are produced by nearby materials, such as a permanent magnet or a piece of magnetized iron, that generate a magnetic field superimposed on the earth's magnetic field. Therefore hard-iron distortions usually result in a permanent bias in the sensor readings. On the other hand, soft-iron distortions are created when there are ferromagnetic materials nearby, which are not necessarily the sources of magnetic fields but will influence or distort local magnetic field.

However, in magnetic localization of a magnetic tracker, it is the change of the detected magnetic field that can be used to calculate the relative locations of the tracker. Consequently, it is only necessary to find out the gains (or sensitivities) of all the three axes of each magnetometer. For example, in the *x*-axis readings of Magnetometer No. *i*, the relationship of the sampled data and the location information, as well as the orientation information, can be represented by Equation (12):

$$B_{xi} = Kx\left(\frac{3[m(x_i-a)+n(y_i-b)+p(z_i-c)]\cdot(x_i-a)}{R_i^5} - \frac{m}{R_i^3}\right) \tag{12}$$

where B_{xi} is the sampled data by *x* axis from Magnetometer No. i, while Kx is the sensitivity of that axis. Other parameters are same with those in Equations (3) to (9). In order to acquire the sensitivity of *x* axis of magnetometer No. *i*, a permanent magnet is moved along the magnetometer *x* axis on the line where *y* and *z* components are 0, such that $x_i = y_i = z_i = b = c = 0$ and $n = p = 0, m = 1$. During calibration, sampled data B_{xi} and displacements between magnet and magnetometer (a) are recorded. Therefore, sensitivity Kx is derived as:

$$Kx = \frac{B_{xi}\cdot(-a)^3}{2} \tag{13}$$

For higher accuracy, 11 samples are taken for calibration of each axis. For each magnetometer used, the sensitivities in *x*-, *y*-, and *z*-directions were evaluated.

4.2 Test results

After proper calibrations, 9 magnetometers were arranged in an array, as shown in Figure 5. In the first series of tests, in order to verify the feasibility and to evaluate the errors of calculation, a laser sensor is used to detect the displacement of a permanent magnet moving linearly. In the first trial, the permanent magnet was set lying down so that the orientation is parallel to the direction of movement, i.e. the orientation remains constant at around (0, -1, 0). In the second trial, the magnet was maintained upright such that its movement was perpendicular to its orientation, which is (0, 0, 1). In the second series of tests, the movement of the permanent magnet undergoing pendulum movement was investigated. In all cases, the magnetometers sampled data every 0.1 sec. Note that due to the limited effective range of the laser sensor, the total displacement of the permanent magnet (the tracker) in the first series of test was limited to 20 cm. Figure 6(a) shows the results detected from magnetometer array compared to that using laser sensor for the first trial, while the results for the second trial are shown in Figure 6(b).

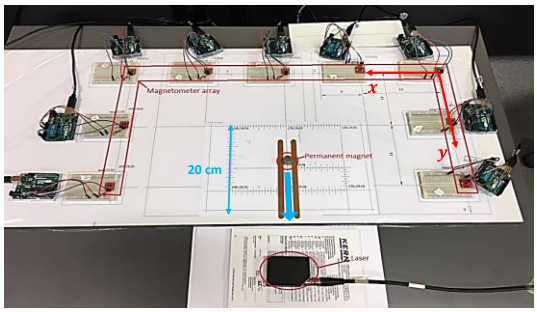

Figure 5. Sensor layout in the first model test.

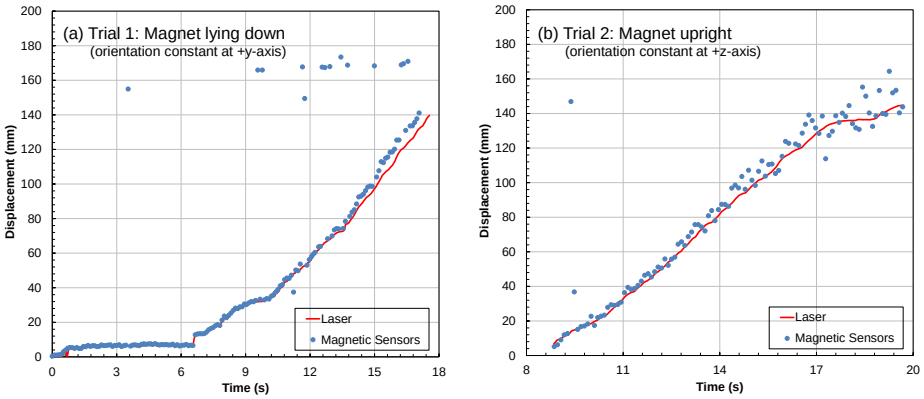

Figure 6. Comparison of movement from sensors and laser: (a) Trial 1; and (b) Trial 2

It can be seen from the results that the magnetic sensing system detected the position of the moving magnet quite accurately. The difference between the results is that when the magnet remained upright, the vertical components of magnetic flux densities at the locations of the magnetometers were dominant as compared to the horizontal components, because the magnet was moving on the same plane where those magnetometers were located. As a result, for all the 27 sets of data input (i.e. 3 for each magnetometer), only 9 (all the *z*-axis) of them have the great impact on the calculation.

The second test was conducted with the magnet wrapped by a piece of cloth and allowed to swing, like a pendulum. The experimental set-up is shown in Figure 7(a). The high speed spinning of the magnet was prevented and it swung generally along the *x* axis. Figure 7(b) shows the three axis projections of its movement versus time. The results show that the algorithm developed generally tracked the sinusoidal movement of the magnet very well in the *x* direction. Since the movement was not really confined to along *x*-axis only, similar sinusoidal movement, albeit with smaller amplitude, can be observed on the *y*-axis. Along *z*-axis, movement was generally negligible.

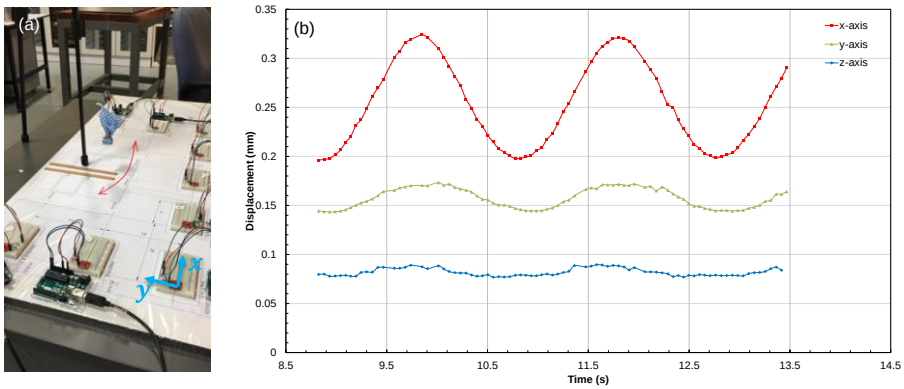

Figure 7. Pendulum test: (a) experimental set-up; (b) results

5 CONCLUDING REMARKS

The feasibility of using a magnetometer array to locate a magnetic tracker (e.g. a permanent magnet) is proved to be possible, as illustrated by the simple physical model tests. Future improvements of the accuracy of the magnetometer array can be achieved by: 1) further calibration such as magnetometer position adjustment and magnetometer orientation adjustment; and 2) rearranging the magnetometers to reach an optimized arrangement, in which the potentials of all three axes of those magnetometers can be exploited to the hilt. Moreover, it is planned in the future to perform small-scale laboratory tests where the permanent magnet will be buried in moving ground, simulating landslides and/or lateral flow of liquefied soil.

6 ACKNOWLEDGMENT

The authors would like to acknowledge the assistance of staff of the Dept. of Electrical and Computer Engineering, University of Auckland, particularly Dr Dariusz Kacprzak for providing guidance in understanding FEMM and Rob Champion, for the assembly of the magnetometers.

REFERENCES

Akeila, E., Salcic, Z., Kularatna, N., Melville, B. and Dwivedi, A. (2007) Testing and calibration of smart pebble for river bed sediment transport monitoring. *Proceedings of IEEE Sensors*, Art. No. 4388624, 1201-1204.

Akeila, E., Salcic, Z. & Swain A. (2010) Smart pebble for monitoring riverbed sediment transport. *Sensors Journal, IEEE,* 10(11), 1705-1717.

Hu, C., Meng, MQ-H. & Mandal, M. (2006) Efficient linear algorithm for magnetic localization and orientation in capsule endoscopy. *2005 IEEE Engineering in Medicine and Biology 27th Annual Conference*.

Levenberg, K. (1944) A method for the solution of certain non-linear problems in least squares. *Quarterly of Applied Mathematics* 2.2: 164-168.

Marquardt, D. W. (1963) An algorithm for least-squares estimation of nonlinear parameters. *Journ. Society for Industrial and Applied Mathematics* 11(2): 431-441.

Meeker, D. (2015) Finite Element Method Magnetic, *User's Manual* Vers 4.2.

Nyce, D.S. (2004) *Linear Position Sensors: Theory and Application*. John Wiley & Sons.

Orense, R.P. (2003) *Geotechnical Hazards: Nature, Assessment and Mitigation*, University of the Philippines Press, 510pp.

Paik, H.J. (1996) Superconducting accelerometers, gravitational-wave transducers, and gravity gradiometers. *SQUID Sensors: Fundamentals, Fabrication and Applications* (H. Weinstock, Ed.) Kluwer, 569–598.

Schlageter, V., Besse, P.-A. , Popovic, R.S. & Kucera, P. (2001) Tracking system with five degrees of freedom using a 2D-array of Hall sensors and a permanent magnet. *Sensors and Actuators A: Physical*, 92(1): 37-42.

Cappellaro, C., Cubrinovski, M., Chiaro, G., Stringer, M.E., Bray, J.D. & Riemer, M.F. (2017)
Undrained cyclic direct simple shear testing of Christchurch sandy soils
Proc. 20th NZGS Geotechnical Symposium. Eds. GJ Alexander & CY Chin, Napier

Undrained cyclic direct simple shear testing of Christchurch sandy soils

C Cappellaro, M Cubrinovski, G Chiaro, M E Stringer
Department of Civil and Natural Resources Engineering, University of Canterbury, NZ
claudio.cappellaro@pg.canterbury.ac.nz (Corresponding author)

J D Bray, M F Riemer
Department of Civil and Environmental Engineering, University of California, Berkeley, US

Keywords: liquefaction, cyclic direct simple shear, water sedimentation, sandy soil.

ABSTRACT

The earthquakes that hit the region of Canterbury, New Zealand, in 2010-2011 resulted in severe damage to buildings and infrastructure due to widespread liquefaction of natural clean sand and silty sand deposits of fluvial origin. Despite the significant hazard posed by earthquake-induced liquefaction to New Zealand communities and economy, the undrained cyclic behaviour of silty sands remains poorly understood, with few laboratory data available to support developments in research and design methodologies.

For these reasons, a comprehensive laboratory testing programme on Christchurch soils has been undertaken at the University of Canterbury since 2006. After the 2010-2011 Canterbury Earthquake Sequence, these research efforts have been extended to include both broad field and experimental investigations, in collaboration with the University of California, Berkeley. Within this context, this paper describes the preliminary results from a series of undrained cyclic Direct Simple Shear (DSS) tests performed on specimens prepared with a natural clean sand retrieved from Christchurch, as part of a broader testing programme which will be extended to include also silty sands and stratified silt-sand specimens. Test specimens are reconstituted with the water sedimentation method. In comparison to other deposition methods, this technique allows the preparation of specimens with soil fabric and soil structural features, such as segregation and layering, which are more representative of the characteristics of natural fluvial deposits like those typically encountered in Christchurch. Analysis of experimental data provides the first evidence on how the DSS response of these soils is affected by the magnitude of the imposed cyclic loading and by soil density.

1 INTRODUCTION

1.1 Current research context on the liquefaction behaviour of sandy soils

Earthquake-triggered soil liquefaction is the temporary reduction in soil strength and stiffness accompanying the build-up of excess pore water pressures induced by seismic stress waves propagating through the ground. Early studies on soil liquefaction essentially focused on loose clean sands (i.e. sands with less than 5% fines or particles smaller than 75 μm), as the first well-documented case histories reported liquefaction in this type of soils (Seed, 1979). Later evidence, however, added a significant number of case histories of liquefaction, lateral spreading and flow failure in fines-containing soils (Cubrinovski & Ishihara, 2000), including the phenomena observed within the urban area of Christchurch in 2010-2011 (Cubrinovski et al., 2011). This leads to the necessity to establish a reliable basis for liquefaction evaluations of silty sands, rather than always referring to idealized clean sands.

Fabric, i.e. the arrangement of soil grains in the packing (skeleton), and structural features such as soil layering (micro- and macro-structure) are the outcome of the formation processes of natural soil deposits, and are unique to the depositional environment. The liquefaction strength of cohesionless soils has been shown to be strongly influenced by fabric (Ladd, 1977; Mulilis et al., 1977) and layered structure (Verdugo et al., 1995). In order to capture these effects, ideally one should test undisturbed specimens collected from the field. However, sampling of cohesionless soils without significant disturbance is a difficult task. This is the main reason why research in the past has often made use of reconstituted specimens prepared in the laboratory. Obviously, in order to get a better picture of the liquefaction behaviour of natural soil deposits, one has to produce in the laboratory a fabric similar to that encountered in the field. There exist several specimen reconstitution techniques, each one of them resulting in a different fabric. Among them, moist tamping has been widely used by researchers as it allows to easily prepare either loose or dense specimens. Fabric obtained with moist tamping, however, is not representative of the fabric of natural soils. Although it is more difficult to employ than moist tamping, the water sedimentation technique is considered to result in a fabric more closely resembling that of fluvial soil deposits (Vaid & Sivathayalan, 2000).

Previous research performed at the University of Canterbury includes undrained cyclic and monotonic triaxial tests of fines-containing sandy soils from Christchurch. Rees (2010) focused on specimens with various fines contents reconstituted by moist tamping, while Taylor (2015) presented comparisons between undisturbed and moist-tamped reconstituted specimens for another set of Christchurch soils. Additional data on undisturbed specimens of Christchurch soils are presented by Stringer et al. (2015) and Beyzaei et al. (2015).

This study is a continuation of these efforts. Its aim is to highlight how fabric and layered structure influence the undrained cyclic response of sandy soils from Christchurch in Direct Simple Shear (DSS) conditions. This will be achieved by performing comparative tests on undisturbed specimens, collected with the Gel-Push and Dames & Moore samplers, and on specimens of the same soils prepared in the laboratory using the technique of water sedimentation. In this paper, experimental results for DSS tests on specimens of a clean sand sourced from Christchurch reconstituted at different relative densities are presented. Given the extensive research performed in the past on the undrained cyclic response of clean sands, this test series represents the most relevant reference benchmark for the analysis of subsequent tests on fines-containing sands.

1.2 Features of cyclic DSS for liquefaction studies

Past laboratory studies on the undrained cyclic behaviour of cohesionless soils have made extensive use of the triaxial device because of its relative simplicity in use and its more common availability in research facilities compared to other testing apparatuses. However, level-ground free-field response induced by earthquake shaking involves a simple shear mode of deformation which is reproduced more rigorously in a Direct Simple Shear test. The conversion of triaxial test data to simple shear mode of deformation, as encountered in level-ground free-field conditions, has traditionally been expressed in terms of the cyclic stress ratio (CSR) using equation (1):

$$CSR = [\tau/\sigma'_v]_{field} = (1 + 2\cdot K_0)/3\cdot[|q|/(2\cdot\sigma'_c)]_{TX} \quad (1)$$

where the effective stresses terms herein employed are consistent with the total stresses shown in Figure 1. The actual relationship for the liquefaction resistances between triaxial and simple shear conditions is a complex function depending on factors such as tested soil, amplitude of imposed cyclic stresses, and soil fabric, among others, which are not captured by equation (1) (Tatsuoka et al., 1986). One of the main reasons for this discrepancy is that the stresses imposed on a triaxial test specimen are very different from the stresses induced by earthquakes to soils in level-ground free-field deposits. DSS testing was conceived as a means to overcome this shortcoming of triaxial testing.

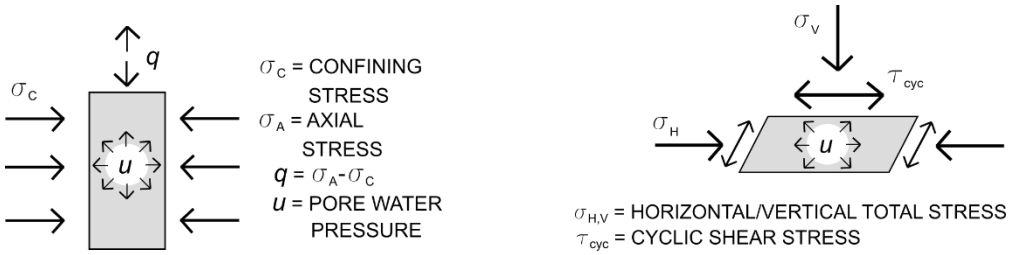

Figure 1: Triaxial (left) and idealized simple shear (right) cyclic loading conditions.

Ideal undrained DSS loading conditions correspond to a planar state of strain: a soil element undergoes shear strains in the vertical plane while subjected to shear stresses in the horizontal plane; constant height and constant volume are enforced during the shearing process. Implementation of the simple shear conditions in the practice presents several technical difficulties (see for example Boulanger, 1990). This has resulted, over the years, in the development of a variety of testing procedures and designs of testing apparatuses. Tested specimens can have rectangular or circular cross-section. Circular specimens can be laterally confined by means of a wire-reinforced membrane (NGI-type devices), by a stack of rigid rings (SGI-type devices), or by wrapping the specimen within a plain latex membrane and applying a lateral pressure, analogously to a triaxial test. The design of the loading system must minimize rocking of the horizontal faces of the specimen, which stems from the significant non-uniformity in the states of stress and strain across the specimen. Also, in order to overcome potential scale effects, tested specimens should have a large diameter-to-height ratio (≥ 4), as opposed to triaxial specimens. This may result in a specimen with a relatively small height, which in turn may pose difficulties in accurately estimating the relative density of the specimen, an issue that has been encountered in this study.

This experimental study makes use of a custom-designed DSS device built at the University of California, Berkeley (Figure 2). Tested specimens are cylindrical in shape, 61 mm in diameter and 15 mm in height, and wrapped within a plain latex membrane. The device is provided with a pressure chamber, where compressed air is used to apply confining stresses to the specimen, and makes use of a back pressure for saturation. The upper and lower faces of the specimen are in contact with two porous stones fitted in the recesses of two aluminium caps. These provide a means to realize a firm connection between the specimen and the horizontal and vertical loading systems. The bottom cap is clamped to a sliding table mounted on track bearings and connected to a servo-controlled pneumatic actuator. The top cap is connected, via an analogous sliding block on track bearings, to a manually-controlled pneumatic actuator. The systems of track bearings are designed to minimize rocking of the top cap and friction. A set of transducers is employed to measure and record vertical and horizontal loads and displacements, pore water pressure, and volume change.

2 EXPERIMENTAL SETUP

2.1 Test material

The tests presented in this paper were performed on a sand retrieved from a site in the Red Zone of Christchurch. Relevant index properties for this sand are listed in Figure 3. As the amount of soil available to prepare reconstituted specimens was limited, the same batch of soil had to be reused multiple times in the testing. In order to assess the amount of fine particles lost during the water sedimentation process and testing procedures, grain size analyses were performed at the beginning of this DSS testing series, and every time all the soil available from this batch had been used for preparing a specimen. Each repetition comprised a dry sieve analysis, carried out on two samples, and a Laser Diffraction Analysis performed on four samples.

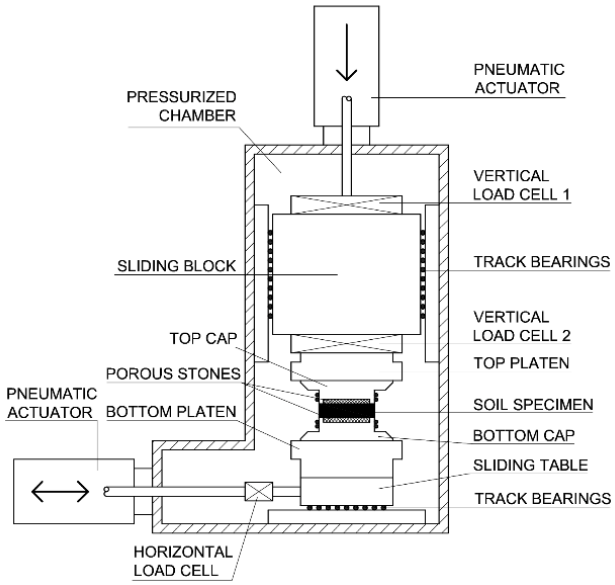

Figure 2: Schematic plot of the DSS device (modified, after Boulanger, 1990)

Figure 3 shows the particle size distribution curves obtained from the Laser Diffraction Analysis. Although the water sedimentation process seems to result in some changes in the particle size distribution with respect to the original soil, the magnitude of these alterations can be treated as negligible for the purposes of the present study.

2.2 Testing procedure

Test specimens were prepared using the water sedimentation technique. With this method, dry soil was poured (using a funnel and a rubber hose) into a mould filled with water, yielding a specimen in a loose state. In this study, the typical relative density for the sand obtained by this procedure was about 50%. The top surface of the specimen was then levelled with a spatula, and the top cap was carefully positioned on it. For the preparation of denser specimens, subsequent densification was achieved by positioning additional weights on the top cap and using a mallet to impose small vibrations for a pre-determined amount of time to the table on which the mould was resting. By varying the mass of the weights and the duration of the vibration process, target relative densities of about 60% and 70% were achieved. A vacuum of 25 kPa was then applied to the specimen.

Saturation was performed by first percolating carbon dioxide through the specimen for at least 30 minutes, followed by percolation of de-aired water, and finally by pressurizing the pore water in the specimen to at least 200 kPa. Post-consolidation B-values ranged between 0.92 and 0.97.

Specimens were consolidated anisotropically to to σ'_v = 100 kPa, with a ratio $K = \sigma'_h/\sigma'_v = 0.5$. Imposing this stress ratio gives an approximate condition of one-dimensional consolidation, as was verified by the negligible average consolidation radial strains.

Before shearing, the vertical piston is clamped in position to enforce a constant height condition, and undrained conditions are then imposed by closing the drainage valve. A sinusoidal shear load waveform of pre-determined amplitude is applied to the specimen by the servo-control system at a frequency of 0.05 Hz. The cyclic shearing phase takes place at constant total horizontal stress, $\sigma_h = \sigma_{\text{cell pressure}}$.

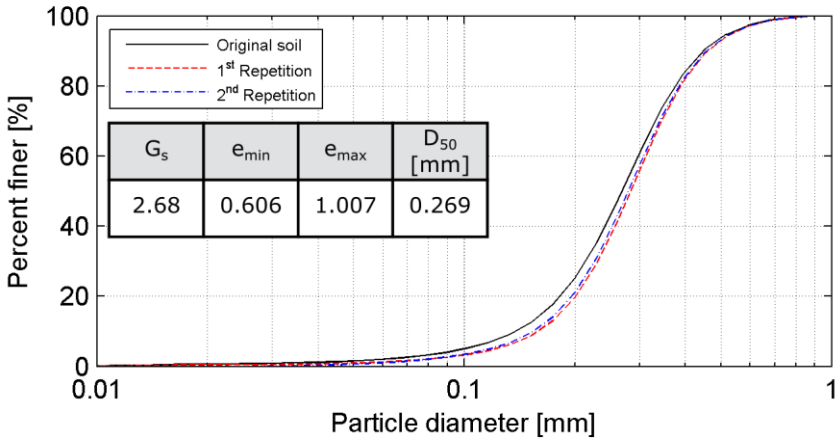

Figure 3: Index properties and particle size distribution curves from Laser Diffraction Analysis for test sand

3 PRESENTATION AND DISCUSSION OF TEST RESULTS

Figure 4 shows results from three cyclic DSS tests run at similar levels of cyclic shear stress on specimens prepared at the three target relative densities. Plotted on the left are the effective stress paths in the τ- σ'_v space, while on the right is portrayed the shear stress-shear strain response of the specimens, which exhibits the typical hysteresis loops. The repeated shearing actions imposed on the specimens generate excess pore water pressure which results in a decrease in the vertical effective stress, σ'_v. This is accompanied by a loss of stiffness which in turn leads to a progressive development of shear strains. A characteristic feature of the hysteresis loops of the DSS tests herein described is their symmetric shape, unlike those obtained from cyclic triaxial tests (see for example Rees, 2010, and Taylor, 2015).

The three specimens exhibit a different response to cyclic loading depending on their relative density: the looser the specimen, the higher its tendency to contract is, which under undrained conditions means that higher pressures are generated during each loading cycle in the pore water. Thus, a loose specimen liquefies more rapidly than a dense specimen, producing very large strains in a small number of loading cycles. This is a well-established pattern for the behaviour of clean sands. Figure 4 shows that under CSR = 0.25-0.26, the number of cycles required to produce a double amplitude shear strain of 7.5% was N_c = 3, 10 and 17 cycles for the specimens with relative densities at D_R = 50%, 61% and 68%, respectively.

Figure 5 summarizes the experimental results from all tests performed so far in terms of number of cycles necessary to develop 7.5% double amplitude (DA, i.e. peak-to-peak) shear strain against imposed CSR. The effect of relative density on the liquefaction resistance is evident in the figure, where higher CSR values are needed to produce liquefaction at a given number of cycles for denser specimens. Fifteen DSS tests have been performed so far, but the experimental testing is still ongoing. An additional small number of tests on the same material is required to obtain a sufficient number of data points for each density bin between 1-3 and 30-50 cycles to liquefaction, as this is the range of interest for most of the earthquake geotechnical engineering applications.

Plotted in Figure 5 are the experimental Liquefaction Resistance Curves for Christchurch sand at relative densities of 50% and 60%, and for Monterey #0/30 sand specimens prepared by moist tamping at 60% relative density (Cappellaro & Cubrinovski, 2016). This curve represents a useful reference because several studies on the undrained behaviour of coarse-grained soils described in the literature employed Monterey sand as test material. The Liquefaction Resistance Curves defined in accordance with Boulanger & Idriss (2014) for values q_{c1Ncs} = 100, 120 and 140 of the

normalized cone tip resistance in clean sand are also shown for comparison. The q_{c1Ncs}-based curves are the standard tool for the ordinary assessment of liquefaction hazard, and are derived from the boundary between liquefaction-no liquefaction case histories recorded at different sites during past earthquakes. In this sense, they represent a lower limit to the resistance to liquefaction of sands. The procedure to compute the q_{c1Ncs}-based curves plotted in Figure 5 is detailed in Cubrinovski et al. (2017); q_{c1Ncs} values have been converted to equivalent relative densities D_R using the relationship indicated by Idriss & Boulanger (2008).

Figure 5 shows that the liquefaction resistance recorded in the DSS tests for water sedimented Christchurch sand specimens (red curves) is higher than the q_{c1Ncs}-based resistance (dashed lines) for similar values of relative density. This difference can be ascribed to the conservativeness in the definition of the liquefaction-no liquefaction boundary from which the q_{c1Ncs}-based strengths are derived. On the other hand, Monterey sand exhibited a significantly lower liquefaction resistance, possibly because the fabric attained by this sand when moist tamped is particularly unstable in comparison to fabrics encountered in natural soil deposits.

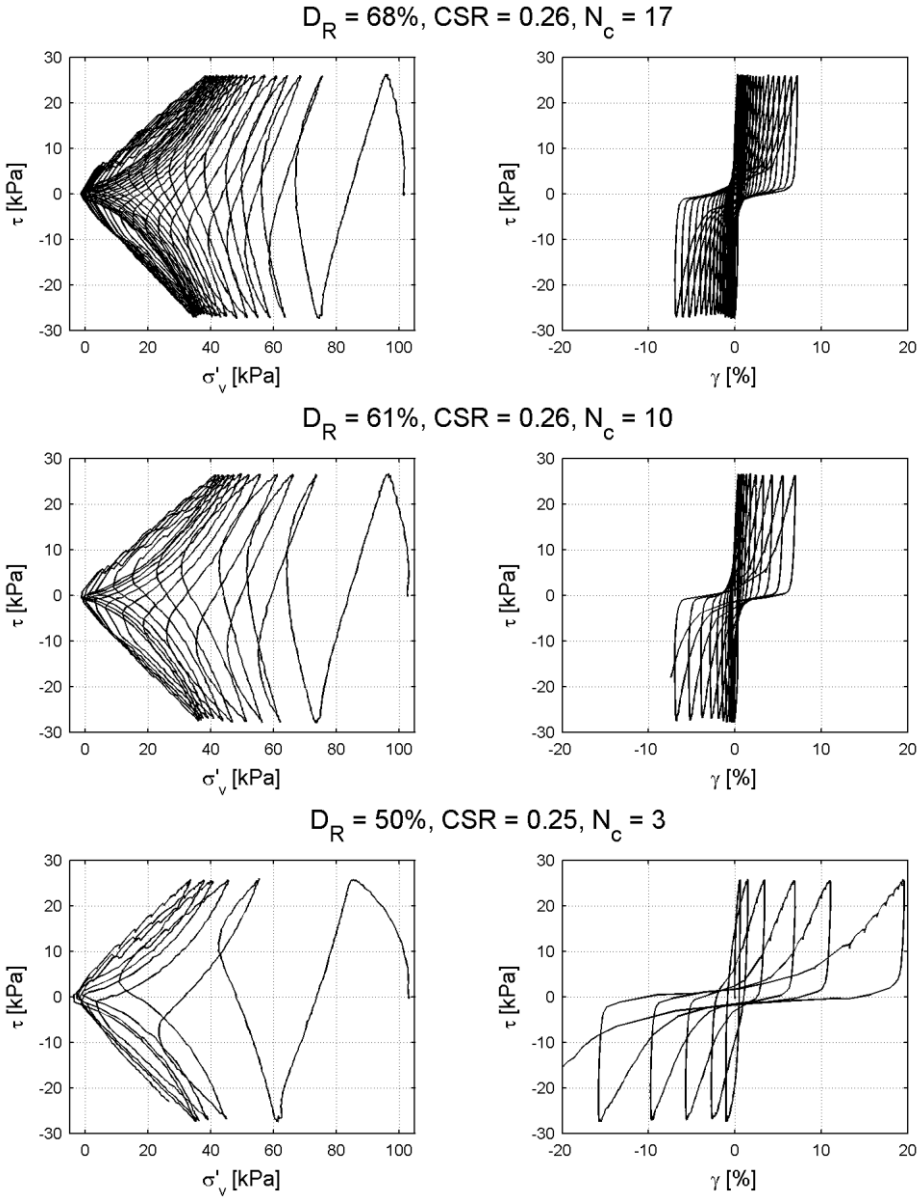

Figure 4: Stress paths and stress-strain curves for cyclic DSS tests on specimens of Christchurch sand prepared by water sedimentation at different relative densities

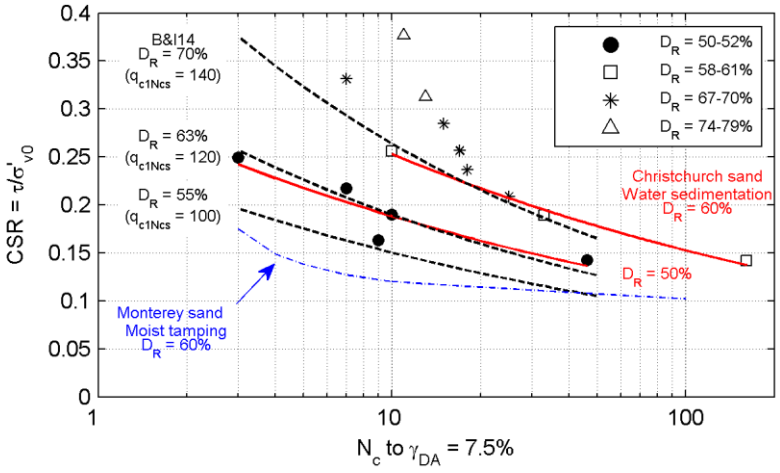

Figure 5: Number of cycles against CSR for 7.5% DA shear strain in DSS for Christchurch sand (red lines) and Monterey #0/30 sand (blue line), and from q_{c1Ncs} relationships by Boulanger & Idriss (2014) (dashed black lines)

The DSS dataset for D_R = 70% is still incomplete, but available data for specimens subjected to high CSR suggests a deviation from the trend portrayed by the q_{c1Ncs}-based curves, with a sharp increase in slope for less than 15 loading cycles. The reasons behind this discrepancy will be investigated following the completion of the present test series.

4 CONCLUSIONS

A series of cyclic DSS tests on specimens of a clean sand from Christchurch was performed as part of a study on the liquefaction behaviour of Christchurch natural soils. The tests provide reference behaviour for clean sand at relative density of 50%, 60% and 70% using cyclic DSS tests. Future developments include the performance of a small number of additional tests on the same material, so as to develop a robust dataset on the cyclic response of Christchurch clean sands and provide a reference benchmark liquefaction resistance which will be used in a comparative evaluation of subsequent tests on reconstituted and undisturbed specimens of fines-containing sands.

5 ACKNOWLEDGEMENTS

The authors would like to acknowledge the support provided by the Earthquake Commission (EQC) and the Natural Hazards Research Platform (NHRP). The help and assistance provided by the lab technicians at the University of Canterbury, Mr Siale Faitotonu, Ms Nicole van de Weerd and Mr Michael Weavers, is gratefully acknowledged. The first author wishes also to thank the support provided by the UC Doctoral Scholarship.

REFERENCES

Beyzaei, C. Z et al. (2015) Liquefaction Resistance of Silty Soils at the Riccarton Road Site, Christchurch, New Zealand. *Proc. 6th ICEGE*, Christchurch, New Zealand, Paper No 616.

Boulanger, R. W. (1990) *Liquefaction Behaviour of Saturated Cohesionless Soils Subjected to Uni-Directional and Bi-Directional Static and Cyclic Simple Shear Stresses.* PhD Thesis, University of California, Berkeley.

Boulanger, R.W. & Idriss, I.M. (2014) *CPT and SPT Based Liquefaction Triggering Procedures.* Report No. UCD/CGM-14/01, Center for Geotechnical Modeling, Department of Civil and Environmental Engineering, University of California, Davis.

Cappellaro, C. & Cubrinovski, M. (2016) The Undrained Cyclic Response of Monterey Sand in Direct Simple Shear. *Proc. 11YGPC*, Queenstown, New Zealand.

Cubrinovski, M. et al. (2011) Geotechnical aspects of the 22 February 2011 Christchurch Earthquake. *Bulletin of the New Zealand Society of Earthquake Engineering*, 44(4), 205–26.

Cubrinovski, M. et al. (2017) System response of liquefiable deposits. *Proc. PBDIII*, Vancouver, Canada.

Cubrinovski, M. & Ishihara, K. (2000) Flow Potential of Sandy Soils with Different Grain Compositions. *Soils and Foundations*, 40(4), 103-119.

Idriss, I.M. & Boulanger R.W. (2008) *Soil liquefaction during earthquakes.* Monograph MNO-12. Oakland, CA: Earthquake Engineering Research Institute; 261.

Ladd, R. D. (1977) Specimen Preparation and Cyclic Stability of Sands. *Journal of the Geotechnical Engineering Division*, 103(6), 535-547.

Mulilis, J. P. et al. (1977) Effects of Sample Preparation on Sand Liquefaction. *Journal of the Geotechnical Engineering Division*, 103(2), 91-108.

Rees, S. (2010) *Effects of Fines on the Undrained Behaviour of Christchurch Sandy Soils*. PhD Thesis, University of Canterbury, Christchurch, New Zealand.

Seed, H. B. (1979) Soil Liquefaction and Cyclic Mobility Evaluation for Level Ground during Earthquakes. *Journal of the Geotechnical Engineering Division*, 105(2), 201-255.

Stringer, M. et al. (2015) Liquefaction Characteristics of Christchurch Silty Soils: Gainsborough Reserve. *Proc. 6th ICEGE*, Christchurch, New Zealand, Paper No 726.

Tatsuoka, F. et al. (1986) Cyclic Undrained Triaxial and Torsional Shear Strength of Sands for Different Sample Preparation Methods. *Soils and Foundations*, 26(3), 23-41.

Taylor, M. (2015) *The Geotechnical Characterization of Christchurch Sands for Advanced Soil Modelling*. PhD Thesis, University of Canterbury, Christchurch, New Zealand.

Vaid, Y. P. & Sivathayalan, S. (2000) Fundamental Factors Affecting Liquefaction Susceptibility of Sands. *Canadian Geotechnical Journal*, 37, 592-606.

Verdugo, R. et al. (1995) Initial Soil Structure and Steady State Strength. *1st International Conference on Earthquake Geotechnical Engineering*, K. Ishihara, ed., Tokyo, Japan, 209-214.

Puketutu Island Rehabilitation Project – Engineering of a Biosolids Monofill Facility

J. Burr
CH2M Beca Ltd., Auckland, NZ.
James.Burr@beca.com (Corresponding author)

C. Grimes
CH2M Beca Ltd., Auckland, NZ.
Chris.Grimes@beca.com

C. Male
Watercare Services Limited, Auckland, NZ.
Caleb.Male@water.co.nz

Keywords: Liner, Settlement, Stability, Biosolids, Uncontrolled Fill, Wet Bins

ABSTRACT

Watercare Services Limited (WSL) operate a very large municipal wastewater treatment plant at Mangere, Auckland. A by-product of the treatment process is the creation of a stabilised biosolid. Through a review of operations an opportunity was identified to rehabilitate a retired quarry on the adjacent Puketutu Island site, both improving the Islands environment and reducing the cost and transport burden to take this material to commercial landfill. The new facility, referred to as the Puketutu Island Rehabilitation Project, is a modern fully lined monofill facility located in a central volcanic cone that has been historically quarried out and partially backfilled.

CH2M Beca Ltd. were engaged to prepare the detailed design and construction management of the first two phases of the facility and this paper presents some of the challenges faced in preparing those designs and the subsequent construction.

The nature of this past site use created some design challenges for construction within the consented footprint. This included backfilling of large ponds, rock blasting, a large landslip, and known and unknown wet bin locations. The facility was designed to a similar standard as a landfill, with full liner, leachate collection and biosiolds affected stormwater capture.

A 3D geological model was created to better understand the complex underlying geology. Some interesting aspects include the design of the embankments using the variable materials on site and underlain by existing uncontrolled fill and wet bins to achieve stability under a 1/2500 AEP earthquake, confirming liner integrity, staging of the project while maintaining a fully operational facility, and construction of internal access roads to allow the biosolids to be placed in cells by the tractor/trailer units. Additionally, it was necessary for the construction to be able to take place year round to meet the project timeframes.

1 INTRODUCTION

Puketutu Island is located in the Manukau Harbour in Auckland, New Zealand. It is approximately 195 hectares in total and has a central volcanic cone with associated ash deposits (tuff) and lava flows (basalt) around the island perimeter. Within the footprint of the Puketutu Island Rehabilitation Project Monofill Facility, extensive quarrying and clean fill operations have occurred over the past five-decades.

The project involves rehabilitating part of the quarried areas of the island with biosolids to create a landform that is consistent with the remaining geology of the island. The landform will comprise an outer embankment within which the biosolids will be placed in order to create an elevated central landform. The Island will eventually become a regional park, with parts of the island being opened to the public as soon as practicable.

The main objectives of this rehabilitation project, which form the basis from which the design philosophy and rehabilitation project have been developed, included providing a sustainable and economic use of biosolids from the population served by WSL, incorporating design features that manage any potential impacts on the environment and be considerate of any cultural or social implications.

The first two phases (referred to as Phase 1, but split into two sub phases of 1A, 1B and 1C – see Figure 1) of design, discussed in this paper, have been peer reviewed and approved by Auckland Council to ensure that the key elements of the consented concept design have been maintained and equivalence proven when changes to the concept have been implemented.

The resource consent process was completed prior to Beca's involvement; therefore any changes to the consented design needed to go through a thorough peer review process to prove equivalence and gain acceptance.

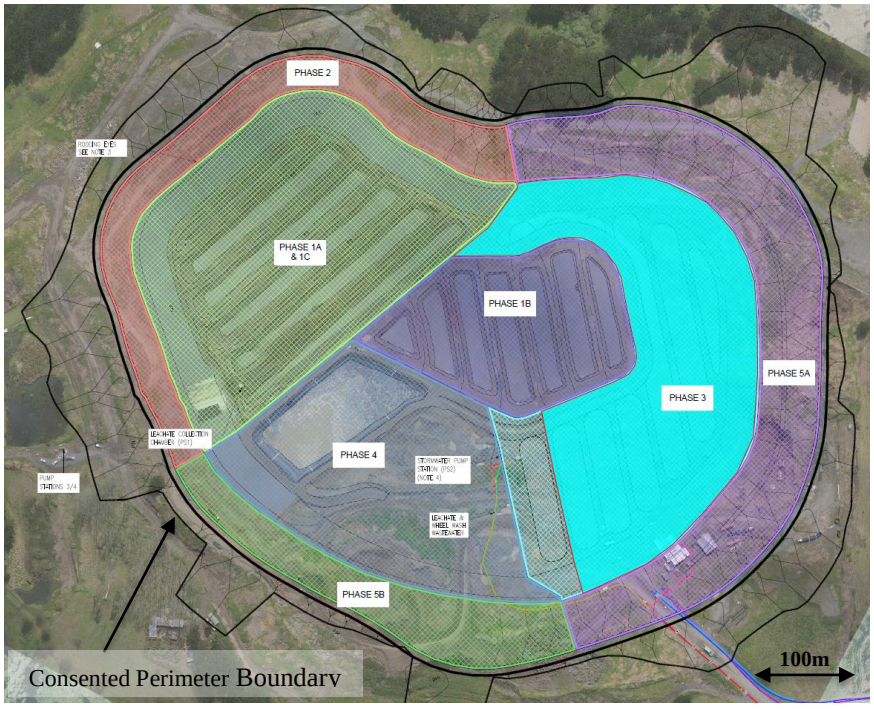

Figure 1: Phase 1 Layout

2 DESIGN DETAILS

The core geotechnical analyses completed for the design of the facility included slope stability analyses (for short term, long term, seismic and during construction), settlement analyses, liner design and groundwater modelling.

Figure 2 shows a typical leapfrog geological cross section; running approximately E-W across the site.

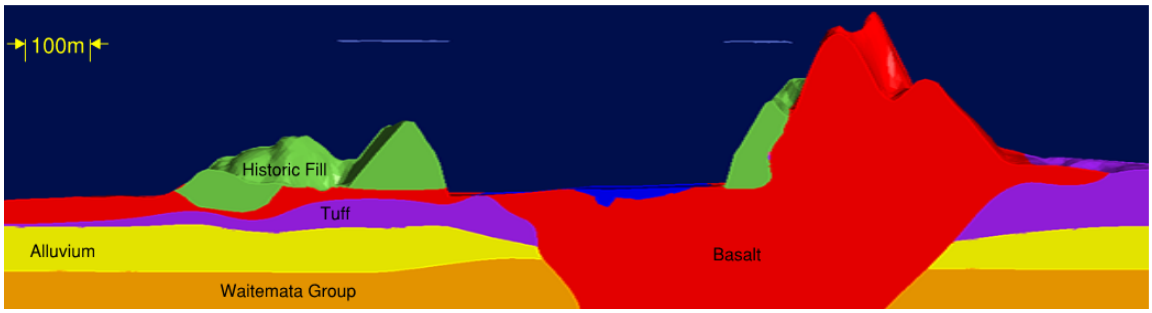

Figure 2: Geological Section E-W across the site (5x vertical exaggeration)

2.1 Site Layout

The overall facility has been designed with external perimeter embankment slopes no steeper than 4H:1V and internal perimeter embankment slopes of 3H:1V with a mid-height bench.

Internal haul roads have been designed with a top width of 6.5m, 1H:1V side slopes and at a spacing of typically 30m to suit the maximum reach of the biosolids placement operating equipment. The maximum lift height (between cells) is 2m; which are constructed in a "Christmas tree" pattern with geogrids placed at the base of each lift.

Perimeter haul roads have been designed so that a 12.5m long truck can manoeuvre safely around curves in either direction. These roads have internal 1:1 side slopes, 1.5:1 external side slopes, and both reinforced with geogrids. It is important to note that these are temporary embankments located only on the floor of the facility which are designed for short term conditions and should not be confused with the permanent flatter perimeter embankment slopes of the overall consented facility.

A typical layout of the biosolids placement on the facility floor is shown in Figure 3.

The staging of these roads (and other site infrastructure) enabled the full facility to be constructed in stages but still be fully functional without disruption to operations in the future.

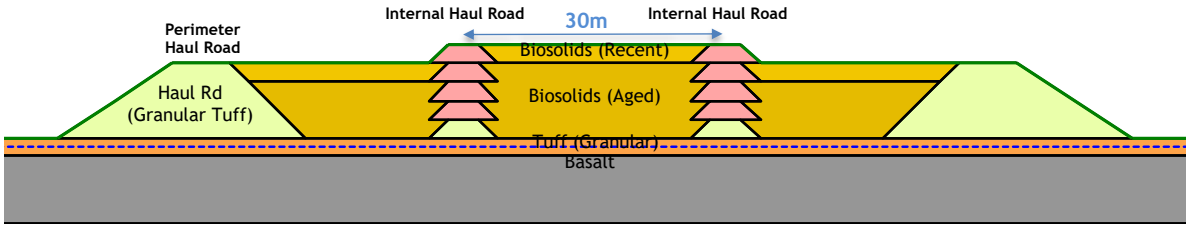

Figure 3 –Biosolids Placement on Facility Floor

2.2 Materials

Numerous investigations (approx. 170 boreholes) have been undertaken at the site since 1997 with targeted investigations for this design completed since 2007. A 3D geological model (using Leapfrog) was created to better understand the complex underlying geology (including historic fill) and this enabled us to investigate specific areas of concern during detailed design (for example, to compare and cut critical cross sections for the settlement/stability analyses).

The key materials used in the detailed design analyses, as identified from the investigations, are biosolids, granular tuff/basalt (used for haul road construction and floor foundation materials),

historic fill, imported fill (clay liner) and other soils that are present occasionally throughout the site with varying thicknesses (Scoria, Alluvium and Waitemata group soils).

A review of the historical geotechnical investigations and laboratory testing (Kayser 2012) were used to assess material parameters for these soils and the biosolids.

2.3 Seismic Design

The facility has been designed for both SLS and ULS events, with differing performance criteria for the internal haul roads and perimeter embankments.

The peak ground accelerations (PGAs) for the project have been derived from NZS1170.5:2004. The project site was classed as soil class C.

The consequences of failure of the structure are considered to be high, with 'very great' environmental consequences (Table 3.1 AS/NZ1170.0:2002). The biosolids facility is not considered to be a post-disaster facility (Table 3.2) and as such, has been assigned an Importance Level of 3. The required design working life of the haul road bunds was 25 years; which based on Table 3.3 in AS/NZ1170.0:2002, corresponds to a ULS event annual probability of exceedance (APE) of 1 in 500 years and an SLS APE of 1 in 25 years. For the final facility perimeter embankments, a required design working life was 100 years, which corresponds to a ULS APE of 1 in 2500 years and an SLS APE of 1 in 25 years. A 20mm maximum displacement criteria was adopted for the seismic design of the perimeter slopes, with no failure anticipated to breach the liner.

We have also considered the appropriate earthquake loads for landfills as this monofill has some design similarities to those facilities. Guidance from the EPA (1995) requires the seismic design of landfills be undertaken for an earthquake having a 90% probability of non-exceedance in 250 years (approximate return interval of 2500 years). This indicates that the ULS design earthquake derived from AS/NZ1170.0:2002 for this facility is appropriate.

3 DESIGN CHALLENGES

A number of key elements provided design challenges; these included backfilling deep ponds, rock blasting, uncontrolled fill, historic wet bins, perimeter embankments, a landslip, and an alternative lining system.

Some of the challenges were due to a differing detailed design elements versus the consented concept design (i.e. requirement to prove as equivalent or better), while others were due to the uncertainties around past site use (i.e. uncontrolled fill and wet bins).

3.1 Backfilling Deep Ponds

Two large ponds (up to 7m deep with one below sea level) had been formed on the floor footprint during quarrying activities and needed to be backfilled during Phase 1.

The construction challenges included dewatering the ponds which sit within highly permeable basalt and tuff zones at pumping rates below the consented limits and then backfilling, both safely and practically through water. Not all water could be pumped in isolated areas (typically a few meters of water remained) during backfilling due to the very high recharge rates. Only one of the two ponds was able to be fully pumped and backfilled in dry conditions.

The design challenge with this backfilling method was to ensure that base settlement was controlled so that no damage to the liner system (in particular liner strain) would occur. In addition, placement of rock, soil and geotextiles needed to be controlled to ensure that filter compatibility (i.e. a graded fill approach adopted based on Fell et al 2005) was achieved from soil/rock layering and that groundwater could flow between the layers to avoid pore pressure build up on the base of the liner.

To minimize the risk of backfilling in the deeper partially saturated pond, Beca developed a methodology with the contractor to ensure the backfilling could be completed safely and to ensure it would meet the required design outcome. A graded fill approach was adopted, which also included the use of sacrificial risers to continue pumping during backfill and incorporation of geotextiles to bridge over the pond backfill rock blinding layer before placement of the hard fill to subgrade level. Additionally, the ponds were backfilled well in advance of the liner being placed, which allowed monitoring of the base above the pond infills for defects prior to the placement of the liner system.

3.2 Rock Blasting

Historic fill was removed from the floor below design subgrade level and replaced with compacted hard fill (tuff) prior to constructing the liner system. However, at some locations basalt was encountered above the design subgrade level. The basalt was too strong to be excavated by ripping, therefore rock blasting was required in isolated areas.

In order to avoid sharp contacts below the floor lining system, which could cause large differential settlements (and therefore high liner strain, see section 3.5), 4H:1V slopes were formed if within 2m of the subgrade design level (reduced to 3H:1V if below 2m). “Dental concrete” was also used as required to provide a smoother finish. Plaxis analyses was completed to assess the settlement and liner strains on the site floor and establish the construction criteria.

3.3 Uncontrolled Fill

Historically the site operated as a basalt rock quarry and then as a managed fill site. However, historic fill was placed in an uncontrolled manner and investigations indicate that the quality and strength is variable throughout the site.

The uncontrolled fill was historically placed to form the majority of the embankments around the site, therefore the design allowed for this fill to remain in place, which is discussed further in the embankment design section below.

This uncontrolled fill, which needed to be cut to form the designed facility layout, was able to be reused where drying was possible to achieve a reasonable quality of material as discussed in section 3.6.

3.4 Wet Bins

There are wet bins (i.e. soft compressible soil with Su<25kPa) located within the historic fill, formed by end tipping of saturated/uncompacted fill by the quarry operator during winter placement. These zones have been identified based on past site experience and from review of historical air photos. However, it is acknowledged that there is a risk that wet bins exist at additional locations across the site, not identified.

In order to minimize this risk of wet bins for the embankment design, we modelled large “soft” zones in our settlement analyses (with $C_c/(1+e_0)$=12% using Plaxis). These simulated a weak zone located within the final perimeter embankment and quantify the impact on the lining system, in

terms of total settlement, differential settlement and more importantly liner strain. This option also provided a safer design for construction because the contractor was not required to complete temporary works for the removal of the soft soil while working on the existing quarry slopes, which were steeper than the designed slopes.

Ongoing review of boreholes and test pits indicate that large soft wet zones may not exist today or may not be as bad as modelled, even at locations where previous site activities indicated that they may exist. There were isolated soft, wet layers identified within the borehole logs, but not as thick as modelled in our analysis.

3.5 Embankment Design

The perimeter embankment has been designed to tie into the overall consented surface, plus leave the historic uncontrolled fill and wet bins in place, while providing a practical and stable platform for the construction of the liner and the placement of the biosolids.

It has been designed to be constructed in two stages with an internal mid-height bench between stages to allow the liner to be joined on a horizontal surface. However, the first phase also analysed the ultimate profiles, which allowed for the completion of the embankments in future construction phases, and for some flexibility in the construction process.

It was necessary for the construction of the facility to be able to take place year round to meet the project timeframes. Therefore, the design allowed for the uncontrolled fill and wet bins to remain in place, resulting in less earthworks and less area exposed. Slightly conservative parameters (i.e. Su=25kPa, c'=3kPa and Φ'=25° with sensitivity checks completed as part of the probabilistic analyses discussed below) were adopted to enable this; however, it avoided the need for double handling of the fill and the cost, plus adverse environmental effects of importing/exporting large quantities of fill to/from the Island.

A key feature in the design, which enabled the historic fill to remain in place, was the construction of a 10m wide material replacement zone (MRZ) on the internal face of the perimeter embankment. The MRZ provided confidence in the strength and behaviour of this upper/outer layer by re-using the historic fill, but controlling the quality and compaction effort required during constriction. The MRZ has been designed to perform several functions, including:

- Improve stability of the slope, particularly against shallow failures,
- Provide a bridging or rafting layer over areas of softer/weaker soils (i.e. wet bins), particularly in relation to differential settlements and liner strain, and
- Provide a layer of known cohesive soil to act as a diffusive layer for the liner (liner system discussed later).

Tensile strain on the liner was estimated as < 0.7% for all cases on side slopes with "soft zones" and on the floor where sharp contacts with basalt was encountered. The estimated strains are much lower than the typical strains of 5% for a GCL and 2% for a CCL (LaGatta et el, 1997).

Probabilistic analysis was undertaken (in Slope/W) to assess the sensitivity of embankment stability (for static, seismic and r_u scenarios) to changes in soil strength parameters, which was very important given the variability of the uncontrolled historic fill placed around the site. They show that the design is robust for static and seismic scenarios, but the stability is sensitive to r_u; therefore, vibrating wire piezometers were installed and monitored (with trigger levels identified) during construction.

3.6 Landslip

A landslip occurred within the historic fill placed to the east of the Phase 1 area, but within the future extent of the facility (currently being designed). The cause has been contributed to a previous site activity of end tipping clean fill behind a narrow bund (essentially creating a dam) at the site, similar to the wet bins discussed previously. It is understood that this material was likely placed wet, was exposed and ponded water added to the trigger of the bund breach and slope flow failure.

Investigations have been completed to determine the vertical extent of the failure. A methodology has been developed for the safe removal of the slip material for future expansion of the site. It has been confirmed that all slip material will need to be removed for future expansion in that area.

3.7 Lining System

The lining system for both the floor and side slopes were revised from the consented design. The alternative liners were peer reviewed and accepted as having 'equivalent chemical and hydraulic containment'.

The alternative lining systems reduced the amount of controlled clay fill required to be imported to site and allowed for year round construction at the site. Note that the Phase 1 floor and first 30m (i.e. 10m vertical) up the side slopes was successfully constructed over a two week window in August over winter.

The consent application liner comprised a 900mm thick clay liner on the side slopes and a 600mm thick clay liner overlain by a 1.5mm flexible membrane liner (FML) on the floor. The clay liner specified a permeability of not more than $1x10^{-9}$ m/s)

There was a change to the consent conditions to permit alternatives with equivalent containment. The liner for the floor was changed to 300 mm thick cohesive subsoil layer overlain by a geosynthetic clay liner (GCL), and then an FML. The liner for the perimeter embankment internal side slopes consists of a 450 mm thick cohesive subsoil layer, overlain by a GCL and then an FML. The cohesive subsoil layer specified a permeability $<1 \times 10^{-8}$ m/s.

These alternative lining systems can be constructed in short periods over winter to meet the project requirements, while maintaining equivalence to the consented design.

4 FUTURE SITE DEVELOPMENT/EXPANSION

The facility has been designed and constructed for up to 5 years of biosolids placement. However, there is a requirement for up to 30 more years of placement at the site; which requires the facility to expand both laterally and vertically. Although the overall facility has been designed and generally accepted, future phases will require the same peer review and council acceptance on a phase by phase basis.

5 CONCLUSION

There were design and construction challenges encountered during the first phase to allow up to 5 years of biosolids placement. And although additional design packages are required for the subsequent design phases to expand the facility for the full 35 year storage space required, the bulk of the geotechnical driven design elements has been completed. This is because many of the key challenge solutions, which are common across the entire site, have been peer reviewed and

agreed with the consenting authorities. The most significant challenges and the solutions included:

- *Perimeter Embankment Design*: The design considered the variable conditions around the full consented facility, not just the Phase 1 footprint. It allowed for historically placed uncontrolled fill and wet bins to remain in place, but still meet the consented design criteria. Leaving them in place also meant there was less earthworks involved and less area exposed, which was favourable for year round construction.
- *Internal Haul Roads:* The biggest challenge for design/construction of the internal haul roads was the backfilling of the deep ponds and rock blasting on the facility floor. It required design to ensure that the liner constructed above would not be damaged due to the construction of the floor subgrade and planning to ensure it could be completed safely by the contractor. Also, by designing the haul roads using a granular hard fill, construction could continue over the winter and the facility could remain operational year round.
- *Alternative Lining Systems:* It was necessary for the construction to be able to take place year round to meet the project timeframes. So the alternative lining system (equivalent to the consented) provided an opportunity that could be constructed in short periods over winter.

6 ACKNOWLEDGEMENTS

Too many people have been involved in Phase 1 of the project to name individually; however there were a few people that we would like to acknowledge for their contributions, including:

- David Anstiss for his involvement with the project since 2012, with his main inputs on the design of the lining system and assessment of the uncontrolled fill quality, as well as ongoing construction inspections/advice.
- WSL project and operations teams for on-going input and collaboration during the initial design and construction phases.
- Ron Boyle of WSL, for providing feedback on this paper and giving permission to publish it.

REFERENCES

AS/NZ1170.0 (2002) *NZ Standard 1170.0:2002 Structural design actions – Part 0: General Principles*: Standards New Zealand.

EPA (1995). RCRA Subtitle D (258) *Seismic Design Guidance for Municipal Solid Waste Landfill Facilities*. Environmental Protection Agency. April 1995.

Fell et al., (2005) *Geotechnical Engineering for Dams (Chapter 9 – Filter Compatibility).* Balkema Publishers. 2005.

LaGatta, M.D., Boardman, B.T., Cooley, B.H., Daniel, D.E. (1997) *Geosynthetic Clay Liners Subjected to Differential Settlement*. Journal of Geotechnical and Geoenvironmental Engineering, 123, No. 5, 402-410.

Kayser, C. (2012) *The Geotechnical and Environmental Properties of Amended Biosolid*. Department of Civil and Environmental Engineering. The University of Auckland.

NZS 1170.5 (2004) *NZ Standard 1170.5:2004 Structural design actions – Part 5: Earthquake actions – New Zealand*. Standards New Zealand.

Development of 3D models of slope failure during Canterbury earthquake sequence

I R Brown
Ian R Brown Associates Ltd, and TAGA Engineering Software Ltd, Wellington, NZ
ian@irba.co.nz (Corresponding author)

C J Skinner
Ian R Brown Associates Ltd, Wellington, NZ
callum@irba.co.nz

Keywords: 3D slope model, 3D limit equilibrium analysis, slope stability, seismic displacement

ABSTRACT

Christchurch City and its surrounds experienced a series of damaging earthquakes in 2010 and 2011. During the 22 February 2011 earthquake, extensive cracking and movement of the ground occurred in some areas of the Port Hills. We have used a geological modelling package, Leapfrog3D®, to build 3D models of three of the well documented landslide areas. The surfaces that were developed in Leapfrog3D® have been used in TSLOPE, a new slope stability package, to investigate the 3D effects on slope stability. An objective of our study was to develop a number of slope models that could be used to calibrate computational methods used to predict seismic displacements, and to make these available to other researchers.

1 INTRODUCTION

We have been involved with the development of a slope stability analysis system, TSLOPE, that works with a full 3D model of the slope (TAGAsoft, 2017). As we continue to use the program on different slope problems, we have become aware of the limitations of slope stability analysis using 2D models. In some cases the 2D results are very conservative compared with 3D, and in others they are slightly non-conservative.

It is not always clear where the difference between 3D and 2D results will lie ahead of carrying out comparative analyses. An important part of our software development effort has been to model well documented slope failures and carry out 3D and equivalent 2D analyses.

Following the 22 February 2011 earthquake, extensive cracking and movement of the ground occurred in some areas of the Port Hills, Christchurch City. Eight of these slope failures were very well documented in a series of reports prepared for Christchurch City Council by GNS Science. The report on each area provides all the geotechnical data that were gathered during field investigations, as well as 2D numerical slope stability modelling results.

The Corresponding author mentored a student at University of Canterbury who carried out a 3D slope stability analysis of the Clifton Terrace area (Wilson, 2016), one of the eight areas studied by GNS Science. Following Wilson's work, we have adopted the methodology he used and built our own model for the Clifton Terrace area.

2 METHODOLOGY

There are various software systems that can be used to create digital slope models, however, we have found Leapfrog3D® (ARANZ Geo, 2017) to be a user friendly and appropriate system to create and edit geologic 3D models. The models we built used publicly available data as shown in Table 1. Christchurch City Council provided the LiDAR[1] data, and the New Zealand Geotechnical Database was used to source drillhole data.

For the model of the Clifton Terrace area, we were able to reproduce the slope model shown in Massey *et al*. (2014a). The other areas we modelled were Deans Head (Massey *et al*., 2014b) and Maffeys Road (Della Pasqua *et al.* 2014). The focus of this paper is on Clifton Terrace, however we will also present the Deans Head model as that serves as an example of the difficulty in building a 3D model when data has not been collected with that as an end objective.

Table 1: Data used to create 3D slope models.

Data	Description	Source	Date	Use
LiDAR digital elevation data	Post 13 June 2011 earthquake LiDAR survey; re-sampled to 1 m grid.	NZ Aerial Mapping	July - August 2011	Used to create 3D ground surface for model.
Drillhole logs	Results from logging drillholes carried out at or near the site of interest.	Tonkin and Taylor Ltd	2012	Used to create 3D surface of geologic units.
Drillhole logs	Results from logging drillholes carried out at or near the site of interest.	Aurecon NZ Ltd	2013	Used to create 3D surface of geologic units.
Geotechnical properties	Results from laboratory and field analysis	GNS Science	2014	Used to in models for material properties to constrain failure surfaces/units.
Engineering geologic map	Engineering geologic map constructed by GNS Science	GNS Science	2014	Used to project significant faults onto the model, geologic unit contacts, ensure drillholes were accurately placed and ensure 2D cross-sections were consistent.

2.1 3D Modelling Approach

The 3D model for each slope project was built with the following workflow in Leapfrog3D®

- the LiDAR data set was imported and used to build a terrain model;
- the engineering geologic map was georeferenced and draped over the terrain model;
- the terrain model was clipped to only underlie the map extent;
- the drillhole locations and lithology were loaded;

- lithologies were grouped into three units based on engineering properties:

[1] LiDAR - Light Detection and Ranging, a remote sensing method that uses light in the form of a pulsed laser to measure distance from the instrument to a reflecting surface.

  - loess (loess and mixed fill);
  - weathered mixed colluvium; and
  - volcanics (breccia, basalt and ash).
- the contact between the volcanics and loess was digitised from the draped map to constrain the surface modelling of the geologic units;
  - the aerial extent of the loess unit was constrained by the map, and drill holes were used to model loess depth;
  - the weathered mixed colluvium was not mapped at surface so was modelled from drillholes to pinch out at the contact between loess and volcanics;
  - top of the volcanics was modelled from the drill holes and the mapped contact;
- a tension crack was modelled using the structural disc function in Leapfrog3D®, these were placed along the trend of most intense tension cracking as mapped;
- all modelled surfaces were clipped so that they did not overlap or extend into space; and
- each surface component of the model was then individually exported as a .obj file for loading into TSLOPE.

2.2 Clifton Terrace

The Clifton Terrace model is shown in perspective view in Figure 1. This shows the GNS Science engineering geology map draped on the model. The black dots are drill hole locations, the yellow discs are orientation markers that also define the tension crack location. GNS cross section locations are shown by the black lines that cross the model.

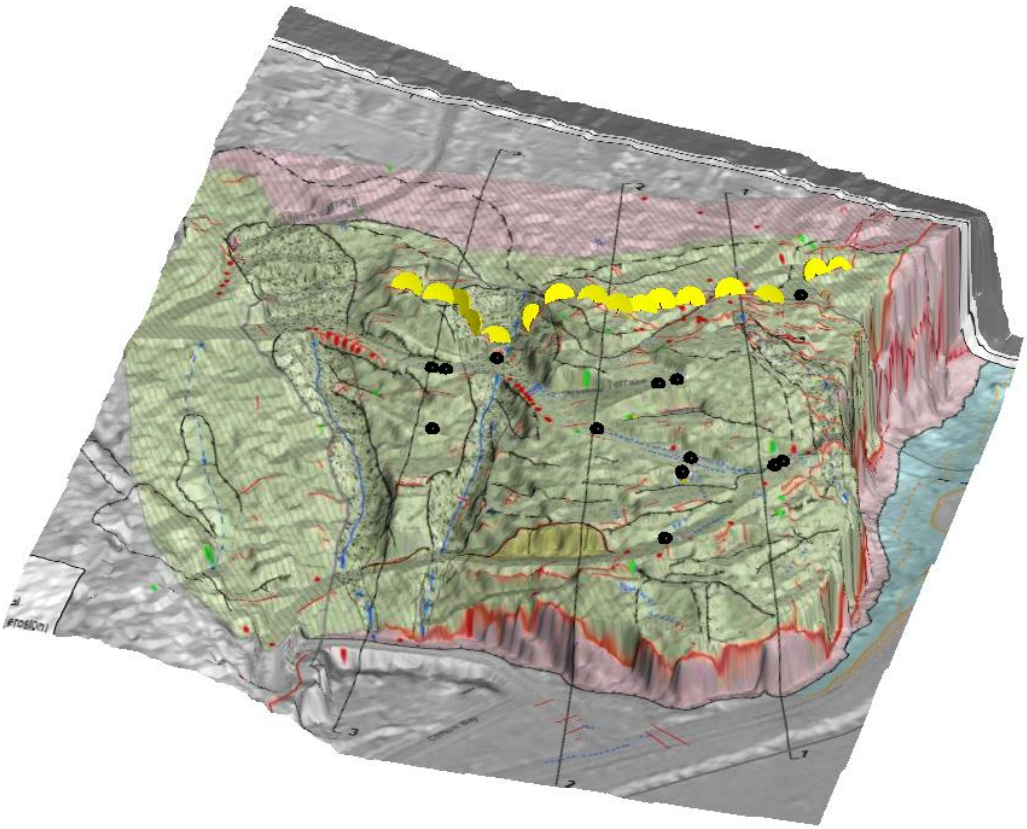

Figure 1. Clifton Terrace model – perspective view

A section through the 3D model is shown in Figure 2, where the cylinders are drill holes, colour coded by lithology, with a modelled surface showing the tension crack (yellow).

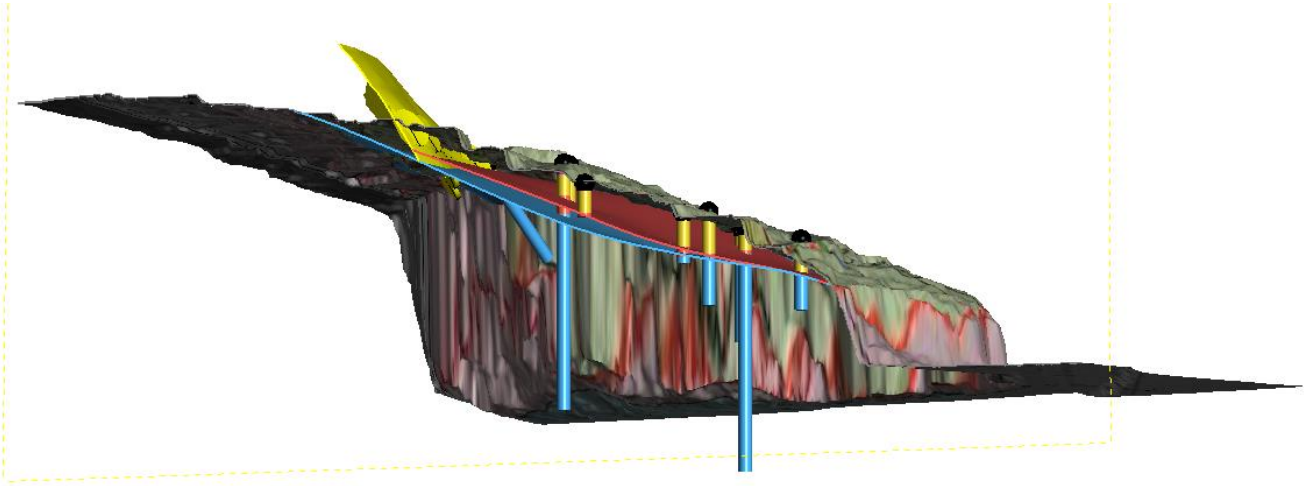

Figure 2. Clifton Terrace model – section through 3D model

2.3 Deans Head

Figures 3 and 4 show perspective and section views of the Deans Head model. The drill holes used to construct this model were located more or less on a line, close to one of the section lines used by GNS Science. This meant that there was little useful data out of the plane of the section that could be used to define the surfaces away from the slope and the line of drill holes.

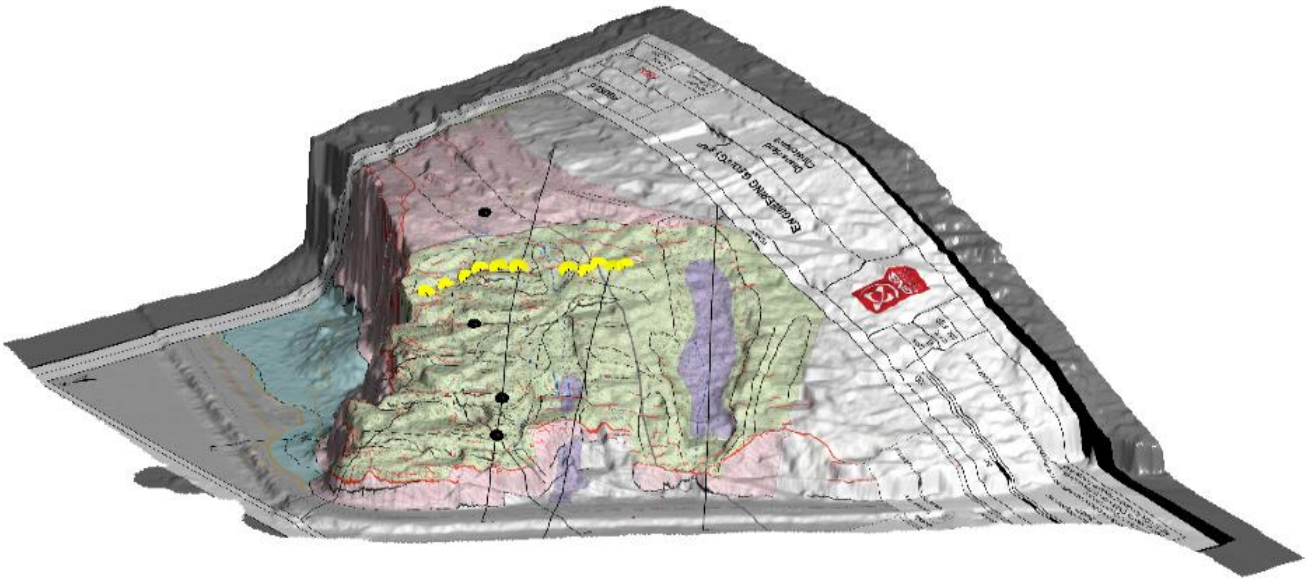

Figure 3. Deans Head model – perspective view

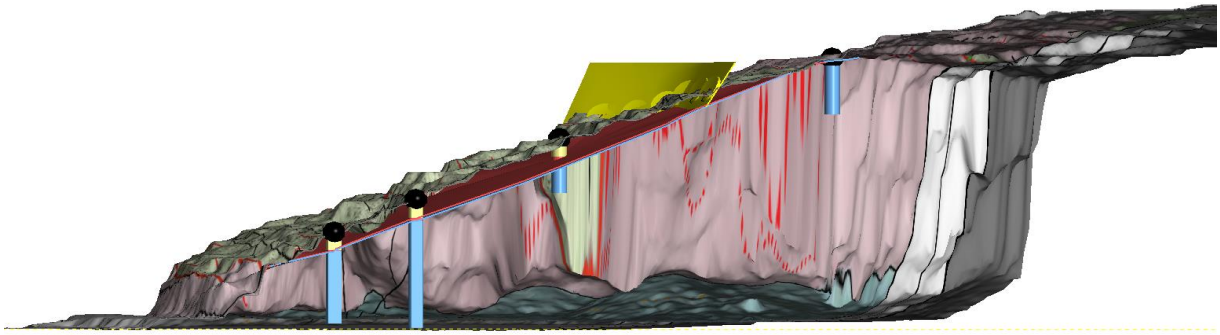

Figure 4. Deans Head model – section through 3D model

2.4 Slope Stability Analysis

The individual surfaces modelled with Leapfrog® along with the georeferenced GNS map were loaded in TSLOPE to form a project for each of the three sites. We represented the slope stratigraphy as Layers, with a surface defining the top of each layer. The three layers were assigned appropriate material properties; for the analyses that we present in this paper, we used the values shown in Table 2.

Table 2: Geotechnical material parameters

Lithology	Unit Weight (kN/m^3)	Cohesion c' (kPa)	Friction ϕ' (degrees)
Loess	17	10	30
Weathered mixed colluvium	17	0	21
Volcanics	18	110	30

TSLOPE's 3D analysis requires a 3D surface to be defined as the basal failure surface. For each of the slopes we used the surface at top of the colluvium (the interface between loess and colluvium), and the surface at the base of the colluvium. A groundwater surface was also transferred from Leapfrog3D®.

Each model was then analysed in 3D using Spencer's method (Spencer, 1967), a limit equilibrium analysis method that fully satisfies force and moment equilibrium. Similar overall factors of safety were also obtained using the Ordinary Method of Columns which is used to obtain the starting estimate of the factor of safety for Spencer's Method. The models were also analysed in 2D along the same cross-sections used by GNS Science.

We present the results obtained for our Clifton Terrace slope model to illustrate the differences between 3D and 2D analyses.

A 3D slope case with the failure surface at the top of the colluvium is shown in Figure 5. TSLOPE discretises the slope into vertical columns; the active columns are the dark coloured columns. Figure 5 shows the factor of safety (FS) computed by Spencer's method and the bearing of the sliding direction.

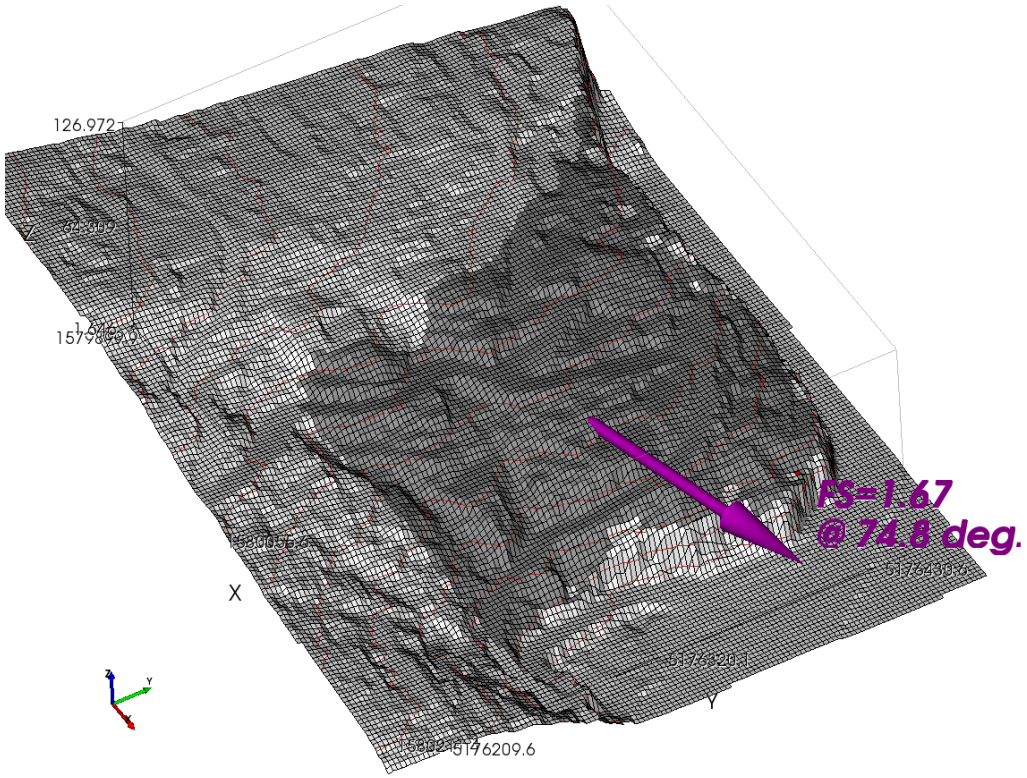

Figure 5. Clifton Terrace TSLOPE 3D model.

TSLOPE also uses a 3D formulation of the Ordinary Method of Slices, known as the Ordinary Method of Columns (OMC). This assumes no inter column transfer of forces, and the factor of safety is defined as the sum of the resisting forces divided by the sum of the driving forces. We can then investigate the distribution of the local factor of safety (OMC Local FS) as shown in Figure 6. This allows visualisation of the columns that are resisting sliding (green colours) and those that are not (red colours).

We used the Clifton Terrace TSLOPE model to build two 3D slope cases, and two 2D slope cases. The results of the analyses are summarised in Table 3.

Table 3: TSLOPE results

Slope case	2D Factor of safety	2D Yield acceleration	3D Factor of safety	3D Yield acceleration
Failure surface at top of colluvium	1.53	0.150g	1.67	0.201g
Failure surface at base of colluvium	0.94		1.24	0.074g

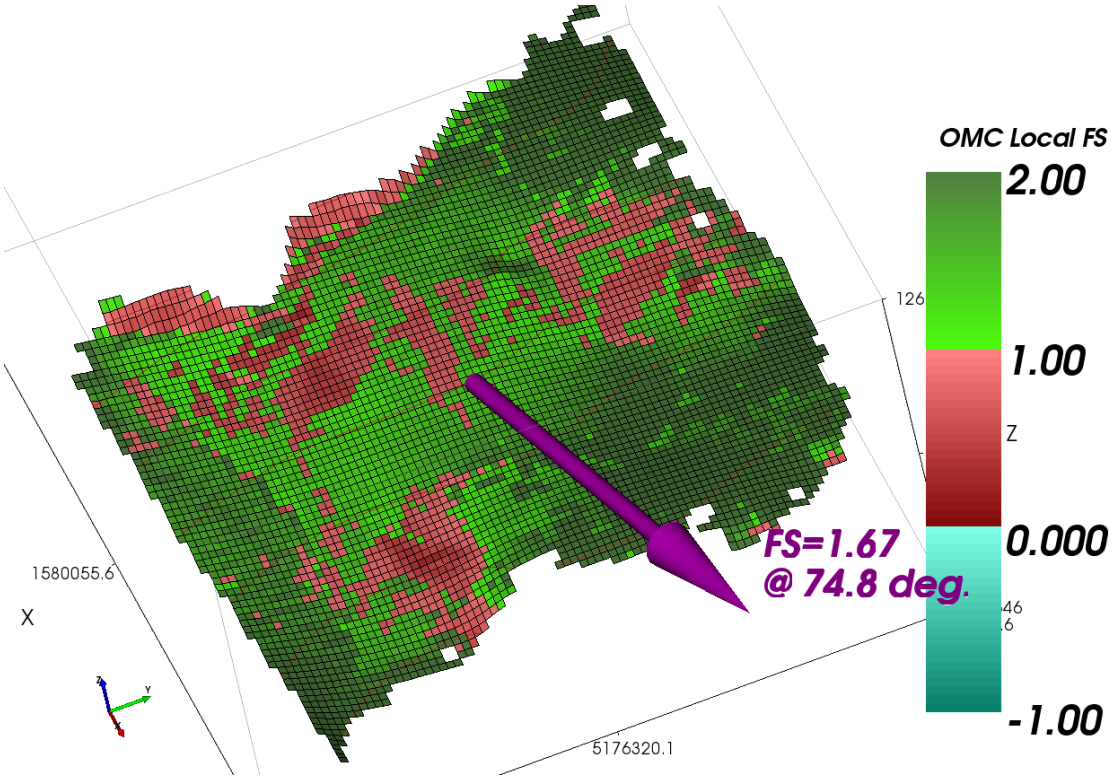

Figure 6. Clifton Terrace TSLOPE failure surface at top of colluvium

3 DISCUSSION

Table 3 shows that there is a difference between factors of safety calculated using 2D and 3D formulations of Spencer's method. For these slope cases, the 2D factors of safety are lower, suggesting that the variable shape of the failure surface relative to the ground surface provides resistance to sliding that cannot be taken into account with a 2D analysis.

This also impacts on the calculation of a yield acceleration, applying the standard pseudo-static approach commonly used in limit equilibrium analyses.

Similar differences between 2D and 3D results were obtained from the Deans Head and Maffeys Road models.

We also noted some small differences in the sections used for 2D analysis, and those presented by GNS Science at the same location. We expect that these differences are because our sections were produced from a 3D model, whereas "hand estimated" sections may not reflect out of plane data points and the influence that they have on the projection of a surface.

The data available for the Deans Head model may also reflect the 2D approach that is commonly used for slope problems. In this case, the few drill holes were aligned in the line of the section used for stability analysis. This meant that there were few data out of the 2D plane that we could use to constrain the modelled surfaces.

4 CONCLUSIONS

The Leapfrog3D® models that we have prepared for the Clifton Terrace, Deans Head, and Maffeys Road areas of Christchurch Port Hills complement the earlier work by GNS Science. These

models have provided detailed 3D surfaces that were required as input to TSLOPE projects for each area. The analyses we have carried out of the slopes confirmed that 3D effects are important when considering slope stability.

The Leapfrog3D® models are available to use for calibration and validation of computational methods used to predict seismic displacements. We are happy to share these models with other researchers.

5 ACKNOWLEDGMENTS

ARANZ Geo Ltd, developers of Leapfrog3D® provided assistance with the use of their 3D modelling software. Mr Peter Wood of TAGA Engineering Software Ltd assisted us with application of TSLOPE. Dr Chris Massey of GNS Science reviewed the 3D geological models. Mr Jonathan Wilson made the initial 3D model of the Clifton Terrace area. Mr Peter Kingsbury at Christchurch City Council provided support for this study.

REFERENCES

ARANZ Geo (2017) *Leapfrog3D®* http://www.leapfrog3d.com ARANZ Geo Ltd

Della Pasqua, F., Massey, C.I., Lukovic, B., Ries, W., Archibald, G., Heron, D. (2014) *Canterbury Earthquakes 2010/11 Port Hills Slope Stability: Risk assessment for Maffeys Road. GNS* Science Consultancy Report 2014/79.

Massey, C.I., Della Pasqua, F., Lukovic, B., Yetton, M.D., Archibald, G., Ries, W. (2014a) *Canterbury Earthquakes 2010/11 Port Hills Slope Stability: Risk assessment for Clifton Terrace*. GNS Science Consultancy Report 2014/76.

Massey, C.I., Della Pasqua, F., Taig, T., Lukovic, B., Ries, W., Heron, D. (2014b) *Canterbury Earthquakes 2010/11 Port Hills Slope Stability: Risk assessment for Deans Head*. GNS Science Consultancy Report 2014/77.

Spencer, E. (1967) *A method of analysis of the stability of embankments assuming parallel inter-slice forces*. Geotechnique 17: p11-26.

TAGAsoft (2017) *TSLOPE* https://tagasoft.com/tslope-technical-information/ TAGA Engineering Software Ltd

Wilson, J.J. (2016) A three dimensional slope stability analysis of the Clifton Terrace mass movement area, Christchurch. *Unpublished research report for Professional Master of Engineering Geology*, University of Canterbury.

Bevan, D.J., Brook, M.S., Tunnicliffe, J., Richards, N.P. & Prebble, W.M. (2017)
Use of UAV/Structure-from-Motion (SfM) for engineering geological landslide mapping
Proc. 20th NZGS Geotechnical Symposium. Eds. GJ Alexander & CY Chin, Napier

Use of UAV mounted /Structure-from-Motion (SfM) data capture for engineering geological landslide mapping

D J Bevan, M S Brook, J Tunnicliffe, N P Richards
School of Environment, University of Auckland, NZ.
m.brook@auckland.ac.nz (Corresponding author)

W M Prebble
Beca, Auckland, NZ

Keywords: UAV, structure-from-motion, landslide, mapping

ABSTRACT

Accurate, high-resolution topographic models are fundamentally important for detailed engineering geological mapping. Nevertheless, high economic costs of topographic data collection are often exacerbated by remoteness of field sites, rendering cheaper, more portable surveying platforms (i.e. terrestrial laser scanning or GPS) impractical. An alternative is Structure-from-Motion (SfM) photogrammetry, which allows for rapid, high-resolution modelling of terrain, comparable in resolution to LiDAR (~0.1 m), but at a fraction of the cost. Utilising SfM in conjunction with Unmanned Aerial Vehicles (UAVs) as means of a low-altitude survey platform, this allows for rapid collection of terrain imagery, with a minimum of ground-control-points. The imagery is then used as a basis for construction of high-resolution engineering geological maps in a 3D space. SfM generates high-resolution topography and co-registered texture (colour) from an unstructured set of overlapping photos taken from varying viewpoints and known camera orientations. The techniques were applied to the coastal landslide at Ohuka (Port Waikato), and the Kepa Road landslide, Auckland. Both of these slope failures are complex, with head and lateral scarps delineating the extent of failure, and irregular surface topography indicative of more recent slope failures in the form of flows, slips and compressional features. The SfM imagery captured the wide range of engineering geological features in a high degree of detail as 3D digital elevation models. In addition, sequential studies can be used for 4D landslide assessments. Hence, the SfM application represents an effective, financially viable alternative to traditional topographic surveying and LiDAR, particularly for practical application in remote, inaccessible regions.

1 INTRODUCTION

Landslide monitoring requires continued assessment of the extent, rate of displacement, surface topography, and detection of fissure structures that could be related to fracture processes. Measurements of vertical and horizontal displacements improve the understanding of landslide mechanisms. Digital Elevation Models (DEMs) are indispensable information sources in such engineering geological assessments of landslides, and modern remote sensing technologies have greatly facilitated the creation of DEMs for landslide monitoring and hazard mitigation. Measurements at high spatial resolution and sub-meter accuracy are required for the investigation at local scales (*c*. 1:10,000), where topographic information is often acquired from airborne or terrestrial photogrammetry or laser scanning. Over the last decade, Light-Detection and Ranging (LiDAR) has been utilised in a wide number of sites and environments to provide high resolution (<0.5 m) surface representations because of its ability to penetrate vegetation and to acquire dense, precise point-clouds (James et al., 2017). Nevertheless, costs of LiDAR equipment and deployment remain rather high, so frequent repeat acquisitions to provide high temporal resolution are, therefore, not always feasible.

1.1 Unmanned Aerial Vehicles (UAVs)

A more cost-effective approach to development of high resolution DEMs for landslide mapping and monitoring is to utilize Unmanned Aerial Vehicles (UAVs) as a platform for data capture. Indeed, the use of UAVs for landslide mapping has emerged in recent years and is evolving due to technological developments such as autopilot systems, quality digital cameras, miniature GPS, and advances in lightweight carbon fibre airframes. Recent developments in UAV technology provide exciting new opportunities for data capture to support ultra-high resolution (1–20 cm resolution) mapping and monitoring. Key advantages of UAV-mounted cameras for landslide mapping include their superior spatial resolution, the capacity to fly on-demand at critical times, and their capability of carrying multiple sensors (Lucieer et al., 2014).

1.2 Structure-from-Motion (SfM)

In addition to advances in UAV technology outlined above, recent advances in photogrammetric image processing and computer vision have resulted in the Structure-from-Motion (SfM) technique. In contrast to traditional photogrammetry, SfM uses algorithms to identify matching features in a series of overlapping digital images and calculates camera location and orientation from the differential positions of multiple matched features. From these calculations, overlapping imagery is then used to reconstruct a "sparse" or "coarse" 3D point cloud model of the photographed object or surface or scene. This 3D model from the SfM method is usually refined to a finer resolution using Multi-View Stereo (MVS) methods, thereby completing the full SfM-MVS workflow (Carrivick *et al*., 2016). The technique was originally designed for 3D reconstructions of building facades (Koutsoudis *et al*., 2014), but is now often used in geomorphology and landslide mapping e.g., Lucieer *et al.*, 2014).

1.3 Aims

The aim of this paper is to apply the UAV-SfM image acquisition and processing technology to the engineering geological mapping of two landslides: (1) Kepa Road Landslide on the margins of Orakei Basin, Auckland; and (2) Ohuka Landslide, 14 km south of Port Waikato (Figure 1). In addition, we contextualise the effectiveness of our results with other published studies that have also proven the utility of UAVs combined with SfM for landslide mapping and monitoring.

2 STUDY AREAS

2.1 Kepa Road Landslide, Orakei Basin, Auckland

The Kepa Road Landslide is within the Pourewa Landslide Zone, which includes four major prehistoric landslides (Brook et al., 2017a): Ngapipi Road Landslide, Kepa Road Landslide, St Josephs Landslide, and Pourewa Landslide. Kepa Road Landslide is the only landslide of the four, which is thought to remain unstable. The landslide is located on the north-eastern bank of the Orakei Basin in Auckland, 4.5 km east of Auckland CBD (Figure 1). It is 300 m wide, and extends 200 m from toe-to-headscarp horizontally, and 50 m vertically. Previous work (Franklin, 1999) reported the original failure was probably a translational block-slide, displacing ~2 million m^3 of lithified tuff rock between 7-10 ka. The initial translational failure was likely due to: (1) a favourably-oriented extremely weak layer of residual clay at the top of the East Coast Bays Formation (ECBF); (2) high pore-water pressure at the top of the clay and the base of the overlying tuff, decreasing shear strength; (3) removal of the toe-slope by fluvial activity and Holocene marine transgression. Since the original slide, a range of secondary slope failures have occurred within the landslide complex, periodically reactivated in response to rainfall-induced pore-water pressure fluctuations, and are typically confined to the upper soil layers. The Orakei Basin is one of the volcanoes of the Late Quaternary Auckland Volcanic Field, which erupted about 85,000 yrs BP phreato-magmatically, resulting in a central crater surrounded by a tuff ring

(Nemeth et al., 2012). The tuff ring is generally stable except for the northeast side because of its steep slope, underlain by Miocene Waitemata Group East Coast Bays Formation.

2.2 Ohuka Landslide, Waikato coast

The Ohuka Landslide (Brook et al., 2017b) is a coastal mass movement complex located on the west coast of the North Island, 14 km south of Port Waikato (Figure. 1). It extends for 500 m along the coast, is 200 m from toe-to-headscarp, with the top of the headscarp 84 m above the toe. Toward the base of the mass movement is the 1 Ma Kidnappers Tephra, and the slope is assumed to either have failed initially as a block slide or rotational slump facilitated by a residual clay seam during the mid-Holocene (Chappell, 1964; Arthurs, 2011). The lowermost units are Early Miocene (23-16 Ma) in age and contain layers of mudstone with low angles of internal friction and peak/residual shear strengths that can facilitate planar failure.

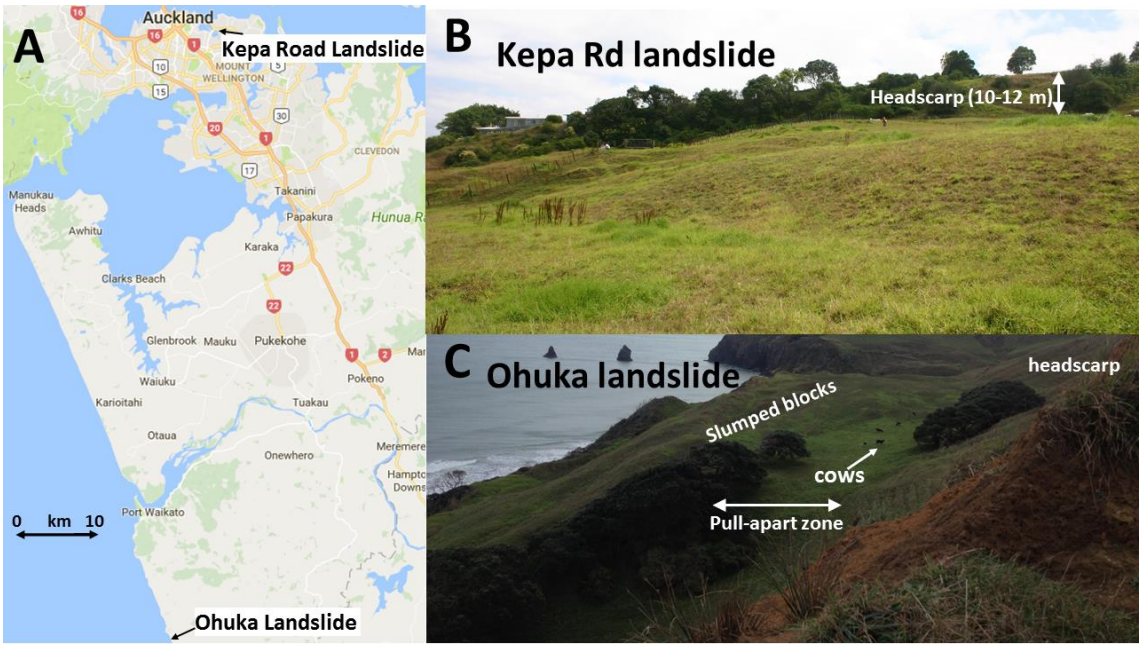

Figure 1: (A) Location of Kepa Road Landslide in Orakei Basin, Auckland, and Ohuka Landslide, Port Waikato coast; (B) Kepa Road Landslide; (C) Ohuka Landslide

3 METHODS

A Dà-Jiāng Innovations (DJI) Inspire 1 drone (Figure 2) equipped with a Zenmuse X3 camera was used to acquire datasets of 200-300 overlapping aerial photographs at each landslide. Up to 20 ground control points (GCP's; plastic mats and man-made features) were geo-located with a real-time kinematic global positioning system (RTK-GPS).

Figure 2: DJI Inspire 1 UAV taking off near a black and white GCP (Ohuka Landslide).

The acquisition-processing workflow is summarised in Figure 3. The image datasets were input into Agisoft Photoscan version 1.2.6 to construct full-colour orthophoto, DEM, and 3D models. First, in Photoscan each image was individually inspected for image quality where blurry images were removed from the dataset. Camera positions were loaded from the photo exchangeable image file data and calibrated with camera parameters during an "alignment" process with NZTM2000.

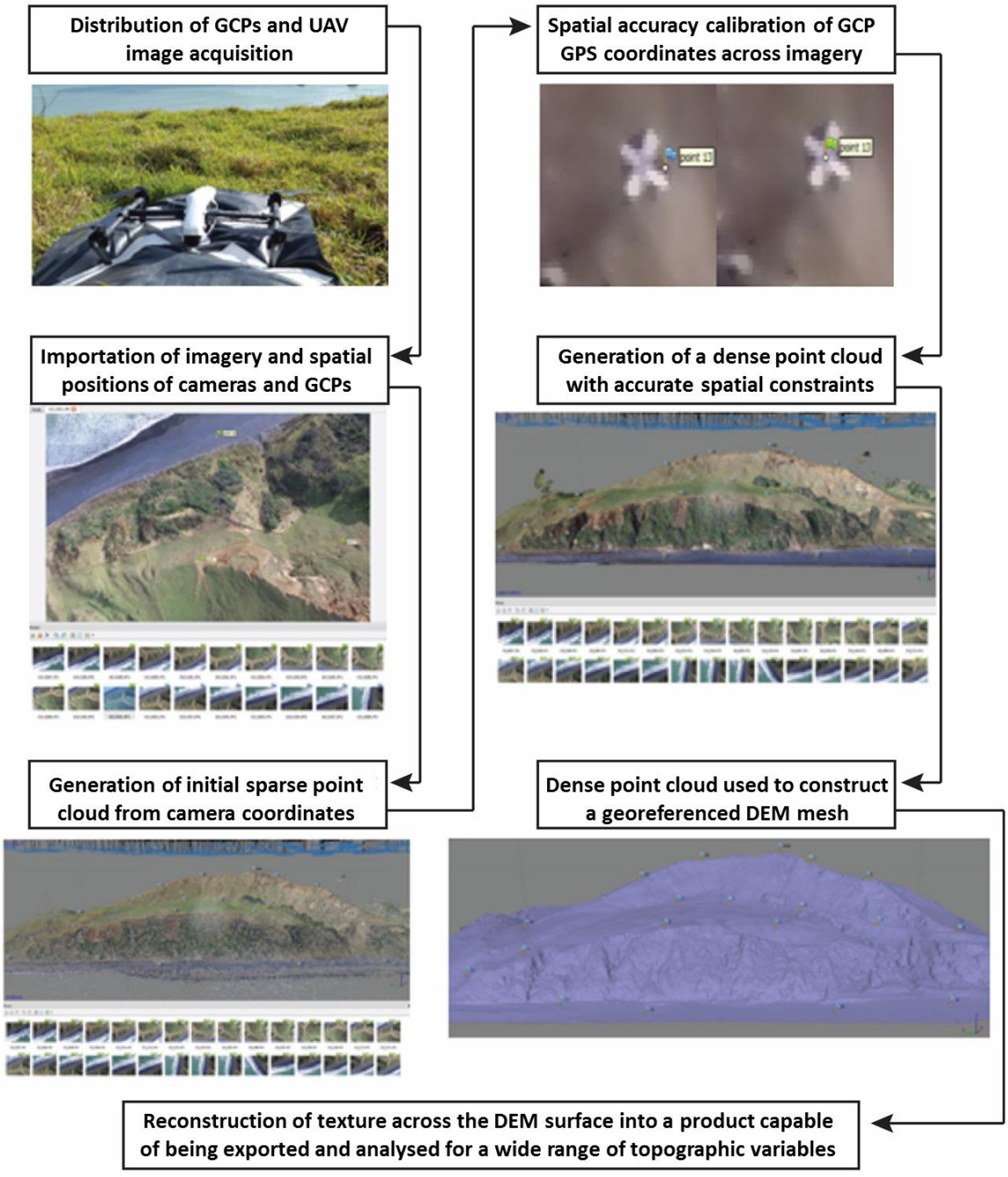

Figure 3: UAV-SfM data acquisition and processing workflow

The camera alignment process matches points between overlapping imagery and estimates the camera positions for each photo to construct a sparse point-cloud model. The following settings were selected for the camera alignment process: very high accuracy, reference pair preselection, 40,000 key point limit and a 10,000 tie point limit (e.g., Agisoft, 2016).

4 RESULTS AND DISCUSSION

The processed orthomosaics and shaded relief maps are shown in Figures 4 and 5, for Kepa Road Landslide and Ohuka Landslide, respectively. As can be seen from the surface models, the key engineering geomorphological features are clearly visible.

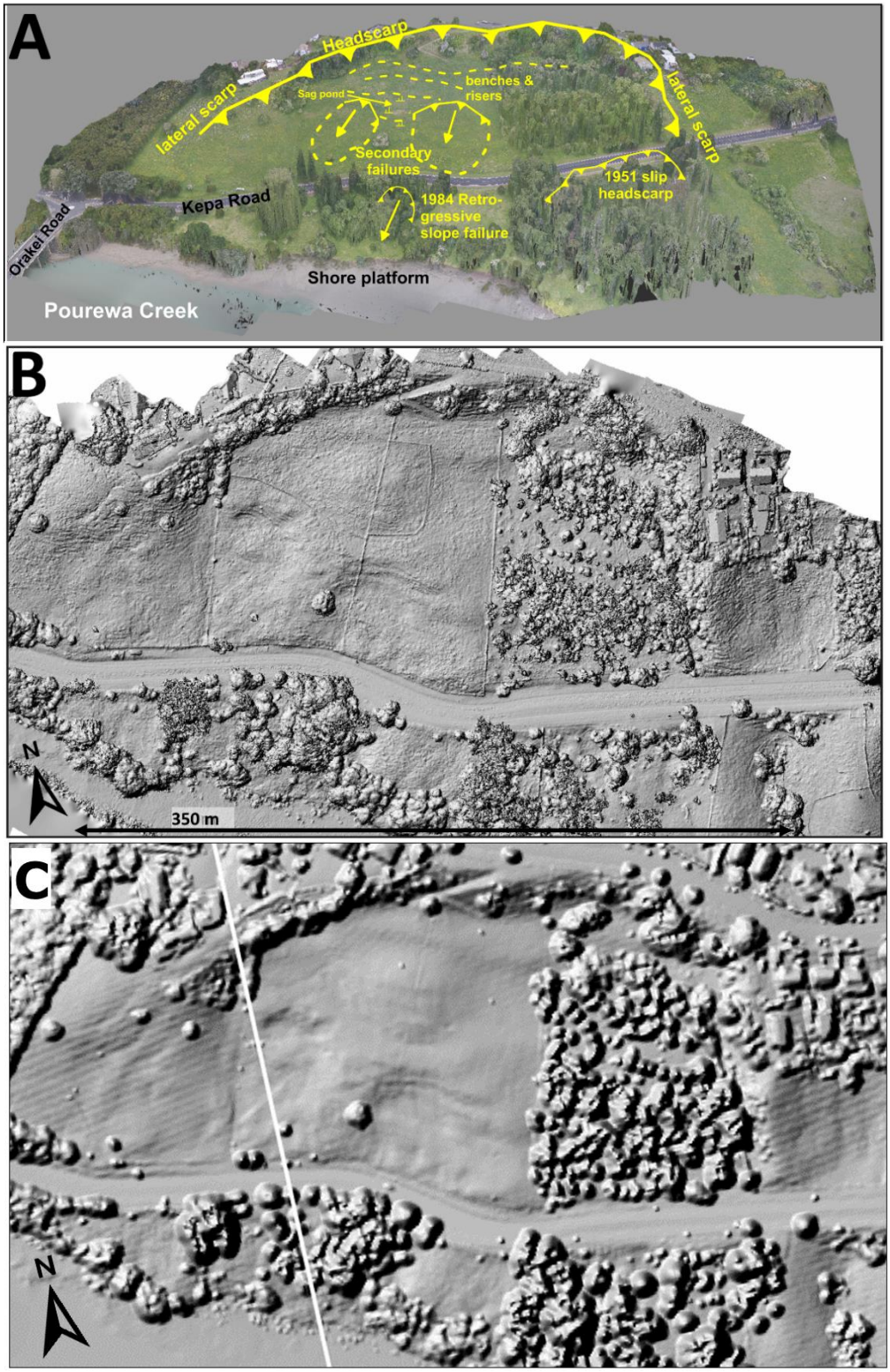

Figure 4: Kepa Road Landslide models: (A) UAV-SfM oblique georeferenced orthomosaic (250 images) and (B) shaded relief model; (C) LiDAR 1 m digital surface model (DSM; courtesy of Auckland Council, 2013)

Microtopography is further enhanced on the grey-scale shaded relief models, which are comparable with typical LiDAR data (only available here for Kepa Road Landslide). At the Kepa Road Landslide, the key engineering geological features visible on the UAV-SfM image and shaded relief map include features of both the original failure, and more recent 20th/21st century slope reactivation. The prominent arcuate headscarp marks the upslope extent of the landslide, and the lateral scarps along both margins are from the original failure.

More recent landslide reactivation is indicated by the depressions in the centre left marking a sag pond, as well as undulating benches and risers (Figure 4). A recent LiDAR 1 m digital surface model (DSM) is shown for comparison in Figure 4C. As can be seen from the models, topographic expression on the quickly (1 hour on site) and cheaply acquired UAV-SfM model is superior to that of the LiDAR shaded relief DSM (Auckland Council, 2013).

Likewise, the UAV-SfM model of Ohuka Landslide (Figure 5) also shows the key engineering geological features in detail. In particular, landslide features include a large arcuate scarp, flanked by gullies, which indicate the lateral boundaries of initial slope failure. Other topographic features include a ~200 m wide bench with several uphill-facing scarps, pull-apart zones, and surface flows from ongoing reactivation. The series of uphill-facing scarps is indicative of several slump blocks rather than a singular large-scale slump block.

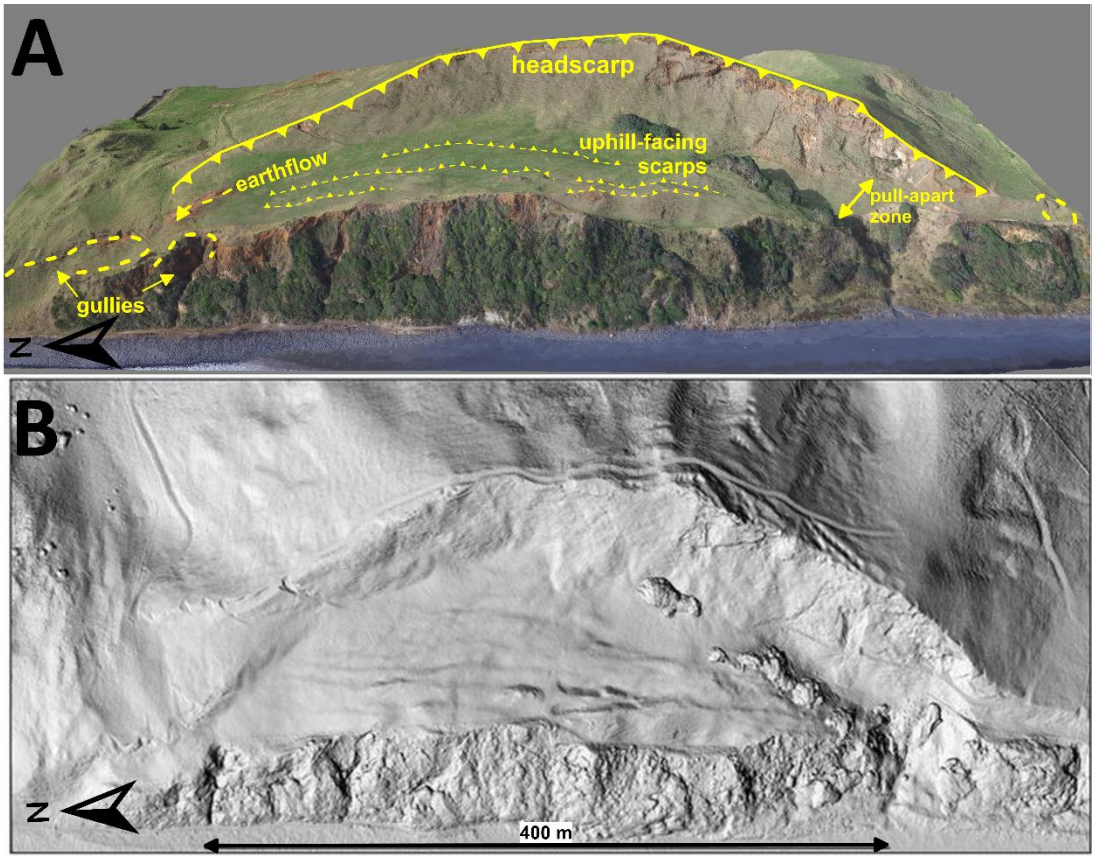

Figure 5: Ohuka Landslide UAV-SfM derived data: (A) oblique georeferenced orthomosaic (270 images); (B) shaded relief model

To summarise, this study presents a mapping workflow for landslides based on UAV imagery and SfM algorithms at two sites on the North Island. This allowed the possibility of detailed mapping of engineering geological landforms at a range of spatial scales. As the above examples demonstrate, the apparent logistical and cost advantages of SfM (limited hardware needs and portability) are, at least in part, offset by processing times compared to 'data-ready' methods such

as LiDAR, terrestrial laser scanning (TLS) or GPS. In addition, a number of sources of uncertainty can be identified using UAV-SfM approach. Different illumination conditions during image acquisition are a source of uncertainty, including direction of solar illumination and shadowing and diffuse light. This can be somewhat overcome by positioning of GCPs (Westoby et al., 2012).

5 CONCLUSIONS

The examples of the two landslides outlined here were ideally suited to the application of the SfM technique. Minimal vegetation coverage and relatively complex, heterogeneous topography at both the intermediate and micro-scales allows the extraction of suitable amounts of keypoint descriptors for consistent, dense point-cloud coverage. Our results are part of a longer-term 4D monitoring program, using multi-temporal UAV-acquired imagery and SfM algorithms for 3D surface reconstructions, combined with subsurface geophysical investigations. This allows for accurate monitoring of landslides, using feature tracking correlation and DEM differencing (i.e. 4D).

REFERENCES

Agisoft, (2016) *Agisoft PhotoScan User Manual*. Professional Edition, Version 1.2.

Arthurs, J. (2011) *The nature of sensitivity in rhyolitic pyroclastic soils from New Zealand*. PhD thesis, University of Auckland.

Auckland Council, (2013) LiDAR data. Retrieved from: https://data.linz.govt.nz/layer/3405-auckland-lidar-1m-dem-2013/

Brook, M.S. et al (2017a) Assessing reactivation of the Pourewa Landslide Zone, Auckland, New Zealand, using Structure-from-Motion, LiDAR, and geophysics. *Geophysical Research Abstracts* Vol. 19, EGU2017-10816, Vienna, Austria.

Brook, M.S. et al (2017b) Structure-from-Motion (SfM) and Electrical Resistivity Tomography (ERT) evaluation of the Ohuka landslide, North Island, New Zealand. *Geophysical Research Abstracts* Vol. 19, EGU2017-10807, Vienna, Austria.

Carrivick, J. et al. (2016) *Structure from Motion in the Geosciences*. Wiley, Chichester.

Chappell, J. (1964) *Quaternary geology of South-west Auckland and North Taranaki coast*. MSc thesis, University of Auckland.

Franklin, J.T. (1999) *Geology of the Orakei Basin*. MSc thesis, University of Auckland.

James, M.R. et al. (2017) Optimising UAV topographic surveys processed with structure-from-motion: Ground control quality, quantity and bundle adjustment. *Geomorphology* 280: 51-66.

Kousoudis, A. et al. (2014) Multi-image 3D reconstruction data evaluation. *Journal of Cultural Heritage* 15(1): 73-79.

Lucieer, A. et al. (2014) Mapping landslide displacements using Structure from Motion (SfM) and image correlation of multi-temporal UAV photography. *Progress in Physical Geography* 38(1): 97-116.

Nemeth, K et al. (2012) Amplified hazard of small-volume monogenetic eruptions due to environmental controls, Orakei Basin, Auckland Volcanic Field, New Zealand. *Bulletin of Volcanology* 74(9): 2121-2137.

Westoby, M. et al. (2012) 'structure-from-motion' photogrammetry: A low-cost, effective tool for geoscience applications. *Geomorphology* 179: 300-314.

Brabhaharan, P., Mason D. & Gkeli, E. (2017)
Resilience based Design Approach for Cut Slopes along Transportation Routes
Proc. 20th NZGS Geotechnical Symposium. Eds. GJ Alexander & CY Chin, Napier

Resilience based Design Approach for Cut Slopes along Transportation Routes

P Brabhaharan
Opus International Consultants, Wellington, NZ
brabha@opus.co.nz (Corresponding author)

D Mason
Opus International Consultants, Wellington, NZ
doug.mason@opus.co.nz

E Gkeli
Opus International Consultants, Wellington, NZ
eleni.gkeli@opus.co.nz

Keywords: cut slopes, earthquake design, resilience, transportation routes

ABSTRACT

It is recognised that earthquake design of high cut slopes in hilly to mountainous terrain is important to ensure that the next generation of transportation routes have adequate resilience to provide access to communities following an earthquake event. There is very little guidance in New Zealand or worldwide on the seismic design of cut slopes. Research and development of guidelines for the seismic design of high cut slopes was carried out by Opus for the New Zealand Transport Agency. The guidelines propose a new performance based approach where the need for resilience underpins the design. The design loadings and approach are based on the importance of the route and the resilience expectations for that link, given the national resilience context. A new Resilience Importance Category (RIC) is proposed to guide the design approach. The guidance addresses a number of critical issues in the seismic design of cut slopes, such as selection of topographic amplification factors, the use of pseudo-static ground accelerations for design, and mechanisms of slope instability. The new principle of resilience based design has a focus on achieving resilience of access for communities, through consideration of the performance of cut slopes in earthquakes, and also the likely time taken for restoration of access. The proposed approach to account for topographical amplification effects is based on the research to date as well as specific numerical analyses, and could be refined as further research information comes available.

1 INTRODUCTION

New Zealand has rugged and mountainous terrain and major transportation routes are often associated with high cut slopes. It has been always recognised that the resilience of transportation routes in New Zealand greatly depends on the performance of these high cut slopes in earthquakes. This has been distinctively demonstrated in the 14 November 2016 M7.8 Kaikoura earthquake event, by the significant cut failures and landslips that caused one of the primary road and railway transportation corridors in the South Island to close for many months (Figure 1).

Currently there is very little guidance available for the earthquake design of high cut slopes either in New Zealand or internationally. The potential for topographical amplification of earthquake shaking, and the observation of the large landslides that have affected transportation routes in earthquake events has raised the awareness of the need for research and development of guidelines for the seismic design of high cut slopes. The New Zealand Transport Agency engaged Opus International Consultants to carry out this research and the development of guidance.

The research objectives included review of the performance of high cut slopes in recent worldwide earthquakes, consideration of the influences of the distinctive aspects of New Zealand's seismicity and topography, review of relevant recent research on topographical effects from New Zealand and overseas and limited numerical analyses on characteristic topographies in New Zealand, review of current design practice in New Zealand and overseas and development of guidelines for the earthquake design of high cut slopes in New Zealand. The New Zealand topography and Seismicity as well as the existing design guidance were presented by Brabhaharan et al 2015. This paper will focus on the other aspects of the research and the development of the design guidelines.

Figure 1: Landsliding on State Highway 1 from 2016 M7.8 Kaikoura Earthquake

2 OVERVIEW OF RESEARCH FINDINGS

2.1 Lessons from past earthquakes

A review of co-seismic landsliding and performance of slopes during historical New Zealand and worldwide earthquakes was carried out as part of the research. The main findings were:

- Small or large failures in steep unsupported cuts can be triggered by earthquakes leading to MM6 or greater shaking.
- Significant or widespread landsliding occurs when earthquake shaking exceeds MM 7-8 (peak ground accelerations of 0.1g to 0.5g).
- Landslides tend to be concentrated on the hanging wall side of the fault in reverse/thrust fault earthquakes. Thrust faults appear to give rise to greater shaking for a larger distance from the fault, and hence more landslides.
- Earthquake induced landslides are predominantly small (~10^3 m^3) to large (~10^5 m^3) disrupted falls, slides, and avalanches of rock, debris, and soil. Common failure mechanisms involve translational sliding at the interface between bedrock and the overlying soil/regolith, or sliding and release along defects in bedrock.
- Steeper slopes are more prone to landsliding, but the slope angles appear to depend on the local geology, terrain and climatic conditions. Slopes steeper than 40° to 50°

underlain by young (Miocene or younger) sedimentary rocks, have been observed to be particularly prone to large types of landslides.

- Landslides in much gentler slopes in volcanic soils have been observed in the April 2016 Kumamoto earthquakes in Japan (Brabhaharan, 2017).
- Steep slopes in competent bedrock with few joints exhibit low to moderate risk of widespread failure and are prone to more localised shallow rock slides and rock falls. Steep slopes (>45^o - 50^o) in well jointed strong rocks are prone to larger and more damaging primarily defect-controlled failures as also recently observed in Kaikoura.
- Earthquake induced slope failures appear to predominate in the upper parts of slopes, and this may be related to the topographic effects as well as weaker ground conditions.
- Antecedent rainfall and climate appears to have a strong influence on the extent of landsliding in earthquakes, for example in the 2016 Kumamoto earthquakes.
- Slopes can be weakened but not fail during strong earthquake shaking. Post-event rainfall or aftershocks have been observed to trigger widespread failures (e.g. 1999 Chi-Chi earthquake, 2016 Kaikoura earthquake followed by the April 2017 cyclones).
- Similar post- event behaviour was observed in the 2016 Kaikoura Earthquake where both areas near the epicentre and in Wellington were affected by the earthquake. A severe rainfall in Wellington event two days after the earthquake triggered numerous slips around the city that caused closure of roads for a day to a week and damage to many residential properties on slopes.
- Slope stabilisation measures such as rock bolts, anchors and shotcrete appear to have been effective against earthquake induced landsliding, but design records appear to have not been available or researched to confirm and understand their effectiveness.

Historical seismicity in New Zealand shows that shallow M 5 and 6 or greater earthquakes that trigger damaging landslides are more likely in northwest Nelson, the central Southern Alps, Fiordland, Marlborough, Kaikoura, Wellington, Wairarapa, Hawke's Bay, and East Cape areas. Central North Island, Auckland, Central Otago and Southland areas have a lower hazard.

A critical point to be considered in developing the earthquake design methodology of large cuttings from the study of past earthquake induced landslides, are the cumulative effects of a sequence of earthquakes and storms following the main event. Although ground shaking during the main event may not always trigger immediate brittle failure in all the cases, it produces systematic preferential tensile fracturing in the rock and zones of deformed material. These incipient failure zones have degraded properties relative to the pre-earthquake conditions, and that in turn can generate geological and topographical amplification effects in subsequent earthquakes, leading to large scale slope failure in aftershocks and storms.

2.2 Topography effects and numerical analysis

Research into topographic effects has been carried out over the last 15-25 years, and has indicated the complexity of the subject with a wide variety of topographies, geology and seismicity having important effects. The main conclusions of past research is that topography has a clear effect on ground shaking in steep terrain. Ground accelerations appear to be amplified at the crest of the slope, and possibly attenuated at the mid height and at the toe of the slope and also deeper into the hill. Topographic effects are frequency dependent, but amplification also depends on a number of other factors, e.g. the incident angle of the seismic waves, the geometry of the slope, the surrounding morphology (e.g. multiple ridges), the geology etc. Numerical modelling indicates topographic amplification factors which are on the order of 1 to 1.5 or perhaps up to 3, whereas experimental observations indicate much greater topographical amplifications, say up to 10.

Limited numerical analyses were carried out as part of this research to provide a better insight into the variation of ground acceleration along the height of the slope. Understanding the performance of the common New Zealand, and particularly lower North Island topographies, i.e.

ridge and terrace like slopes was the focus of this recent research. The slopes were assumed to consist of rock, to avoid high complexity and multi-factored influences in the model. Strain softening of material or appropriate properties of rock under dynamic loading were not part of this study. Limited analyses were also carried out to examine the effects of a weaker layer overlying bedrock on the slopes, either a soil overburden layer or highly weathered rock.

The conclusions from the analyses for New Zealand conditions are in general agreement with the observations drawn from the literature review, which are summarised below:

- For the terrace topography the amplification effect is found to be mostly influenced by the frequency of the excitation and the slope height, when the slope consists of rock. The amplification effect at the upper part of the slope is negligible for the small frequencies when the slope consists of rock but amplification factors of the order of 1.2 and 1.4 are indicated for higher frequencies. Amplification factors become significant for normalised slope height $H/\lambda > 0.1$ and maximum for $H/\lambda \approx 0.2$, which is in general agreement with the conclusions of the literature review (where H is the height of the slope and λ the wavelength).
- For the ridge topography, the amplification of the top of the ridge topography is about 30% higher than that of the corresponding terrace-like slope, i.e. with the same height and inclination. The amplification factors at the crest do not seem to have a consistent trend (e.g. increase or decrease) with frequency but appear to be predominantly influenced by the relationship of the geometry of the ridge (height and width of top and base) to the wavelength.
- De-amplification of the seismic ground motions is observed at the toe of the slope, at mid-slope height and inside the slope for the terrace topography. Complex, alternating patterns of amplification and de-amplification on different parts of the ridge slope varying with the wavelength of the seismic excitation were observed in our analyses, and also indicated from our research from literature.
- Amplification is significantly pronounced by the presence of weaker overburden soil material or highly weathered rock overlying unweathered or slightly weathered bedrock, with amplification factors exceeding 10 for both topographies.
- Amplification factors comparable to those at the crest, are observed on the ground surface at a distance of 20 m behind the crest for the high frequency excitations in the terrace topography. Literature review indicates that free field conditions behind the crest are usually observed at a distance of the order of (2 to 8) H, where H is the height of the slope, but this was not tested in our analyses.
- Vertical accelerations were examined for the ridge topography only as part of this research. The vertical accelerations observed for the bedrock case and the case with HW rock overlying bedrock were of the order of 0.6 g – 0.8 g, while for the case with soil overburden were much higher. The variation of vertical acceleration does not seem to vary consistently with frequency, but appears to be increasing at the higher frequencies.
- Amplification of seismic acceleration was observed at the crest of the cut slope in the case of a ridge with a cut excavated at its toe. The amplification factors show a tendency to increase as the irregularity becomes more pronounced, i.e. for steeper cut slope angles in relation to the natural slope angle.

3 DEVELOPMENT OF DESIGN GUIDELINES IN NEW ZEALAND

3.1 Resilience Concept

Resilience is the ability of an entity to recover readily and return to its original form from adversity. Brabhaharan et al (2006) adapt this concept of resilience for application to transportation networks as conceptually illustrated in Figure 2.

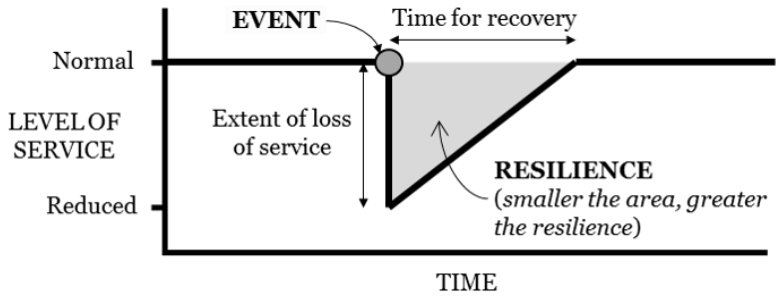

Figure 2: Characterisation scheme for New Zealand topography

Road networks provide a vital lifelines function to society, and their availability is critical for emergency response and recovery after major natural events. In this context, the concept of resilience of road transportation lifelines is dependent on their vulnerability to a loss of quality or serviceability, and the time taken to bring them back into original usage state after the reduction or loss of access, as illustrated in Figure 2. The smaller the shaded area, the more resilient is the lifeline. The greater the area, the poorer is the performance.

To achieve a more resilient society, we need to go beyond our focus on life safety from earthquakes, and consider the resilience of the built environment. This requires focus on how a loss of functionality can be minimised, as well as achieving a form that is conducive to quick return to functionality (Brabhaharan, 2013).

3.2 Design Guidelines framework

The design guidelines framework was developed on the basis of the key findings of the research in conjunction with the resilience concept explained in the previous section. The objective is to design cut slopes for resilience with low vulnerability to failures and subsequent closure of the route. This will be achieved by minimising the size and nature of failures, thus enabling the functionality of the transportation route to be restored quickly.

3.2.1 Importance Level Category (ILC)

The first step in the design guidelines is the classification of cut slopes to enable selection of appropriate levels of earthquake shaking and adopt an appropriate design approach for cut slopes. This enables cut slopes to be designed in accordance with the resilience expectations for the transportation facility it affects; and use a level of design which is consistent with the importance of the transportation route, as well as the criticality of the cut slope for the performance of the route. Four Importance Levels (IL) are defined, IL1 to IL4, as defined in AS/NZS 1170.0 and supplemented by the Bridge Manual for highways and arterial roads. The aim of this selection has been to use the existing importance level framework in the New Zealand standards and Bridge Manual. Further, the anomaly as to how cut slopes are currently considered in the Bridge Manual is attempted to be addressed.

3.2.2 Resilience Importance Category (RIC)

Resilience Importance Categories have been developed to provide for incorporating the local context and resilience expectations into the design process. The resilience importance category (RIC) of cut slopes take into consideration the Importance Level of the transportation route as well as the resilience expectations of the section of route from a regional network context. This recognises that sections of the transportation network may have a higher resilience importance because of the nature of the regional network, its resilience and the availability or lack of alternative routes in the event of incidents. Five categories, RIC I – RIC V are developed in the proposed framework. It is envisaged that the transportation authority would consider the regional

context and select the Resilience Importance Category to be used in the design of cut slopes for a particular transportation corridor.

3.2.3 Design Approach

A four-level design approach is proposed, to suit the design importance level and Resilience Importance Category (RIC) of cut slopes, as follows:

- Design Approach 1 – is a simplified design approach suitable for use by practitioners for simple relatively low height cut slopes of relatively low importance.
- Design Approach 2 – is a standard design approach for use where performance is important for continued functionality on relatively moderate height cut slopes in simple geotechnical conditions.
- Design Approach 3 – use where performance is important for continued functionality, with relatively high cut slopes and moderately complex geotechnical conditions.
- Design Approach 4 – use where performance is critically important for continued functionality, very high cut slopes, or in complex geotechnical conditions.

A fundamental difference of the design approach given compared to that stipulated in AS/NZS 1170 is that the design is for resilience rather than life safety alone. Cut slopes most commonly affect the functionality of transportation routes, although they can also be critical to life safety in some circumstances. The selection of the Design Approach is based on the Resilience Importance Categories, the height of the slope and the geotechnical conditions.

3.2.4 Peak ground accelerations and topography effects

The peak ground accelerations for design are selected based on the Bridge Manual (NZTA, 2014), which provides peak ground accelerations that are not weighted by their relevant magnitudes. The peak ground accelerations selected based on the Bridge Manual represent free-field accelerations before any topographical effects are taken into consideration. Spectral accelerations may be considered if there is a dominant period for the site.

The numerical analyses and evidence from observations in earthquakes clearly indicate that topographical amplification is present and highest at the crest of slopes. The amplification further down the slope at mid height or below is much lower, or even de-amplification may be encountered. The evidence of slope failures from earthquakes also suggest that slope failures are predominant at the top of slopes, both ridges and terraces. It is also clear that the ground accelerations whether amplified by topography or not, are likely to be different along the height of slopes and the peak acceleration is not expected to be encountered at the same point in time during an earthquake along the height of the slope.

Therefore, a lower average acceleration is appropriate for pseudo-static design when large failure mechanisms are considered. Topographical amplification factors to use in design are given in the proposed design framework, based on up to date research and current knowledge. Understanding and quantifying topographical amplification is an area of recent research and development, and there is more research required to develop a good understanding of the issues.

There is an anomaly in the current Bridge Manual in that it provides for different hazard levels for different types of structures – bridge, retaining wall, embankments and cut slopes – on transportation routes with a selected importance level. For example for an important transportation route, a bridge or retaining wall is designed for a 2500 year return period earthquake, while the cut slopes on the same route (regardless of height) are designed for earthquakes with return period of 500 years, i.e. $1/5^{th}$ of the return period used for bridges. High embankments are designed for a 1,000 year return period. The hazard levels for cut slopes proposed in this design framework are higher than currently provided for in the Bridge Manual.

This is proposed to ensure appropriate design of cut slopes, consistent with the hazard levels for bridges, to avoid the formation of new transportation routes that have poor resilience.

3.3 Performance Criteria

In the earthquake design of cut slopes, it would be important to set appropriate performance criteria, to:

- Achieve a level of performance that is consistent with the resilience objectives set for the transportation route / project
- Achieve an economical solution.

Unlike made structures such as bridges and earth structures (e.g. embankments), cut slopes are mostly formed in natural materials with their inherent variability and in situ ground characteristics. Smaller failures, such as small wedge failures in rock, are difficult to prevent, unless a significant expenditure is incurred to protect / stabilise the slope against such small failures. A resilience based design would be suitable, i.e. consideration of the effect of any failures on the level of service or performance of the transportation route, but also of the time it would take to restore the level of service or access. It would be more economical to accept such small failures in large events, but design the cut slope to avoid or minimise the risk of large scale failures that would affect the performance of the route. For example, small failures that affect only the shoulder and can be quickly reinstated, can be accepted as it would have only a small effect on resilience. However, large failures that could close the road, and for long period of time, should be designed against.

Safety of the users of transportation routes and other people is an important consideration in addition to resilience of access. The cut slopes should be designed to ensure safety, i.e. small failures that do not impact on safety may be accepted, and larger failures or mechanisms that impact on safety, should be carefully considered and designed for. One of the mechanisms, rock fall, can affect safety and should be considered in the design under normal conditions, in storm events as well as earthquake events. This may require rock fall protection measures to be implemented, particularly to allow use of the route to be restored.

Earth structures can be designed for allowing a limited amount of displacement in earthquakes, because the limited displacement occurs when the resistance against instability is exceeded during an earthquake of a short duration. This approach is suited to ductile earth structures such as embankments and reinforced soil walls, and to a lesser extent to natural soils, where there is confidence that the displacement will not be associated with a reduction or loss of the resistance to instability. The displacement behaviour of natural soils need to be understood to ensure that they can accommodate limited displacements without an associated loss of strength. Large strain strength properties should be used in assessing displacements of slopes in earthquakes.

Rocks are generally brittle, and displacement leads to breakage through intact rock through en echelon type failures, and this leads to a permanent loss in the strength of the rock mass.
Cracks associated with displacements in rock and soil materials can also allow infiltration of surface water, leading to a reduction in stability, and failure of slopes in storm or rainfall events after the earthquake. Such failures have been observed in a number of earthquakes including in the recent 2016 Kaikoura earthquake. Therefore, this needs to be considered in limiting any displacements and associated cracking of ground particularly above cut slopes. Therefore in considering rock slopes, design based on acceptance of displacements should be avoided, or acceptable displacements are limited to very small values.

4 CONCLUSIONS

Past earthquakes have caused extensive slope failures in both natural and cut slopes. These have been observed in steep slopes of greater than 40 to 50 degrees in both rocks and soils, but have

also been observed in much gentler slopes in volcanic soils. Topographical amplification and the weaker or weathered materials at the upper part of slopes appear to play a significant role in earthquake induced slope failures observed in high slopes. Numerical analyses to represent New Zealand conditions were carried out, and indicate the potential for significant topographical amplifications of 1.5 to 3 or more, and the potential for amplification at the upper part of cut slopes formed in the toe of natural hill slopes.

The proposed design approach in this guidance, uses a novel resilience based approach to cut slope design, and addresses significant gaps in current design guidance for cut slopes. This takes into consideration the resilience context of new cut slopes in the regional context of the transportation route, and a design approach based on the criticality of the cutting. A resilience based acceptance of small failures that do not impact on safety or route availability for significant periods, and design to minimise the risk of larger failures than can compromise resilience of the route and can lead to closure for long periods is proposed. A displacement based design approach is also proposed to allow displacements in soils with a more ductile behaviour, but avoiding or limiting displacements to very small values in rocks with brittle behaviour.

5 ACKNOWLEDGEMENTS

We acknowledge the commissioning of this research by the NZ Transport Agency and their encouragement to publicise the findings through technical papers such as this one.

REFERENCES

Australian / New Zealand Standards (2002). Structural design actions - Part 0: General principles. June 2002.

Brabhaharan, P (2006). Recent Advances in Improving the Resilience of Road Networks. *Annual Conference of the New Zealand Society for Earthquake Engineering.* Napier, 10-12 March 2006.

Brabhaharan, P. (pers com) (2016). Comments following the Learning from Earthquakes mission to Japan to observe damage from the Kumamoto Earthquakes in April 2016.

Brabhaharan P., Mason D., Gkeli E. (2015). Research into Seismic Design and Performance of High Cut Slopes in New Zealand, *6th International Conference on Earthquake Geotechnical Engineering*, 1-4 November 2015, Christchurch, New Zealand.

Brabhaharan, P, Mason, D and Gkeli, E (2017). *Seismic design and performance of high cut slopes*. NZ Transport Agency research report 613. Opus International Consultants. February 2017.

Hancox, G. (2015). *Performance of slopes in past New Zealand earthquakes: Literature review and lessons learned from historical earthquakes.* GNS Science Report CR2015/04. Prepared by Hancox, G.T. as part of the Opus led research into the seismic performance and design of high cut slopes, March 2015, 66 p.

New Zealand Transport Agency (2014). *Bridge Manual*. Third edition. Wellington, New Zealand.

New Zealand Standards (2004). *Structural Design Actions.* Part 5: Earthquake Actions, New Zealand. December 2004.

Opus International Consultants (2012). *Wellington Region Road Network Earthquake Resilience Study*. Risk Study Report. Prepared by Brabhaharan, P and Mason, D for the NZ Transport Agency, Wellington City Council, Hutt City Council, Upper Hutt City Council, Porirua City Council and Kapiti Coast District Council. Report No 2012-21. August 2012.

Case study – seismic design and soil-structure interaction of a critical wharf facility in soft soils

H J Bowen
Tonkin & Taylor Ltd, Christchurch, NZ
hbowen@tonkintaylor.co.nz (Corresponding author)

S D Rees
Tonkin & Taylor Ltd, Christchurch, NZ
srees@tonkintaylor.co.nz

Keywords: performance based design, earthquake engineering, dynamic analysis

ABSTRACT

A case study of performance based seismic design (PBD) for a critical wharf facility is presented and compared to conventional design methods. The Oil Wharf at the Lyttelton Port is a critical infrastructure link for New Zealand's South Island. The wharf suffered extensive damage due to the Canterbury earthquakes and is to be replaced with a new structure. The design of a replacement wharf utilised PBD principles throughout every aspect of the project, including probabilistic seismic hazard assessment, selection of design ground motions, nonlinear site response analyses and nonlinear, dynamic deformation and soil structure interaction analyses.

The site is located on soft marine sediments only four kilometres from the epicentre of the M6.3 22 February 2011 Christchurch earthquake. A unique strong motion dataset is available at the site; a seismograph on soft soil is located 100m away and another on rock is located 900m away. Site response analysis using the recorded rock ground motions as input was able to match the recorded soft soil ground motions over a range of earthquake sizes. Site response analyses were then used to derive the design spectra for structural design.

Nonlinear deformation analyses (NDAs) were able to replicate key displacement mechanisms observed in the Canterbury earthquakes. Predicted displacements matched the surveyed slope deformation data which enabled real world validation of the analyses results. A series of NDAs were performed to design the new wharf structure. Performance based design resulted in significant construction cost savings for the design of the new wharf structure when compared to conventional design methods.

1 INTRODUCTION

Lyttelton Port of Christchurch (LPC) has experienced many large earthquakes and thousands of aftershocks during the 2010-2011 Canterbury Earthquake sequence. Consequently, LPC and their consultants and contractors have a very clear understanding of Performance Based Design as they have observed the actual performance of their land and structures through a wide range of earthquake magnitudes.

An example of one of their damaged structures is the Oil Berth, which is a critical facility that supplies oil, petrol, LPG and bitumen to New Zealand's South Island. The Oil Berth suffered extensive damage in the 2010-2011 Canterbury Earthquake sequence.

A replacement wharf has been designed which will replace the existing wharf. This paper describes the performance-based design of the replacement wharf, including the following key aspects:

- Utilising the extensive post-earthquake observations (including survey measurements, structural inspections, strong motion data) to benchmark geotechnical analysis and design
- Design to the performance based ASCE 61-14 code for the Seismic Design for Piers and Wharves using advanced methods for site response analysis, seismic hazard assessment and dynamic non-linear deformation and soil structure interaction analysis

A comparison between the performance based design approach and conventional design is presented.

2 LYTTELTON PORT OIL BERTH

The Oil Berth is located in Lyttelton Harbour, New Zealand. The existing wharf structure comprises a wharf supported on timber piles, pipelines, a reinforced concrete seawall, mooring bollards and thrust blocks. Fender blocks are supported on four 600mm diameter steel encased concrete piles.

A new oil wharf, 63.3m long by 15m wide is proposed. The proposed wharf has a 0.8m thick reinforced concrete deck and is supported on 39 no. 1.2m diameter steel encased concrete piles. A 36.5m long by 6m wide access jetty will link the wharf with the shore, which will incorporate a 0.8m thick reinforced concrete deck.

The site is situated on reclaimed land that overlies harbour deposits consisting of soft to stiff silts with medium dense to very dense sands from approximately 40 m depth and volcanic boulders and rock at approximately 50 m depth. The reclamation process involved construction of a breakwater by end dumping quarried basalt gravel on top of the natural marine deposits. Progressive slope failures were reported during construction. Reclamation of land behind the breakwater was then carried out with hydraulic fill dredged from the harbour bed.

Figure 1: Lyttelton Port showing a vessel moored at the existing Oil Berth

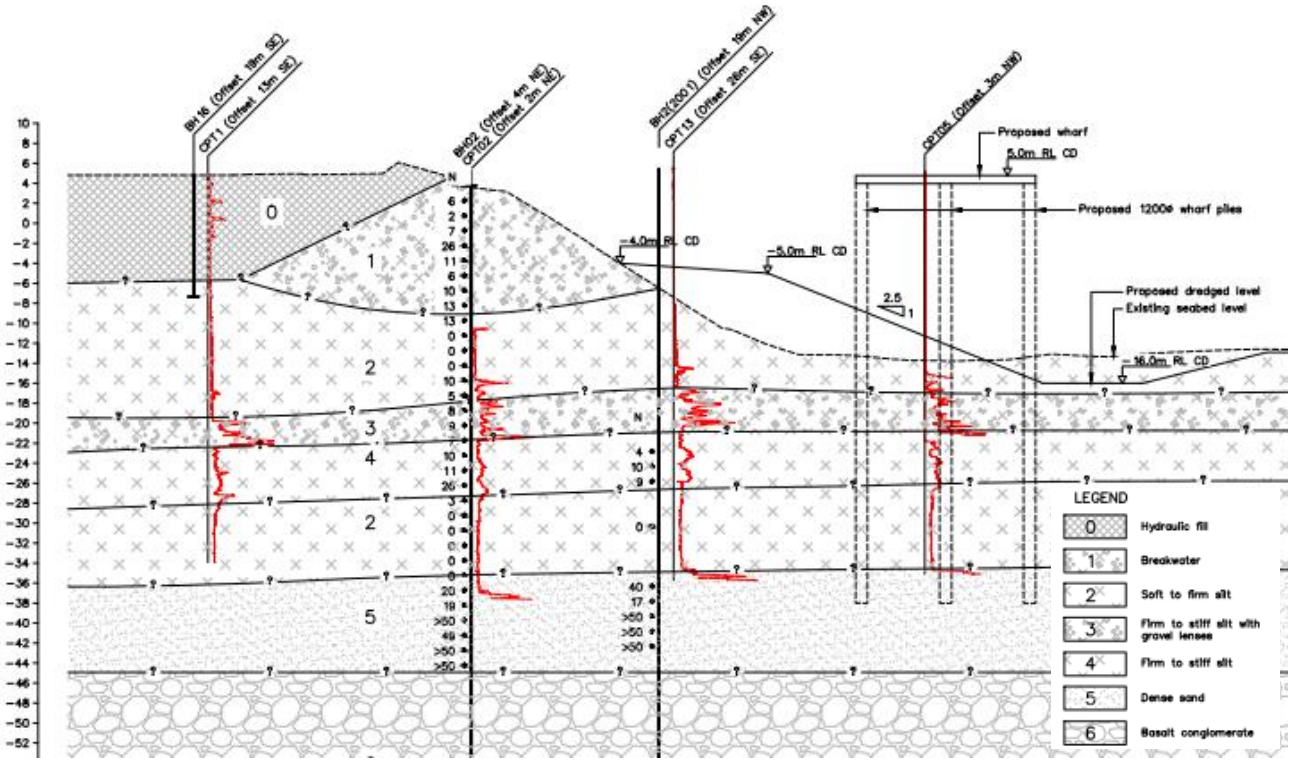

Figure 2: Geotechnical cross section through proposed Oil Berth

3 DESIGN METHODOLOGY

3.1 Performance requirements

The replacement Oil Berth is designated as a 'High' Design Classification in terms of the ASCE Standard 61-14 Seismic Design of Piers and Wharves. This is because the Oil Berth is deemed essential to the region's economy and post-event recovery. As such the wharf and associated breakwater slope must be designed to provide the following performance requirements:

- Long term static factor of safety greater than 1.5
- Post- earthquake static factor of safety greater than 1.1
- Minimal damage in a 75 year return period earthquake
- Controlled and repairable damage in a 475 year return period earthquake
- Life safety protection in a 2500 year return period earthquake

At the Oil Berth site there are many geotechnical challenges in achieving these requirements, including weak natural soils, potentially variable fill material, poor existing slope performance and an increase in slope height through dredging. In addition the existing Oil Berth must be kept operational during construction.

3.2 Design outline

Four key steps were carried out in the geotechnical design of the Oil Berth:

1. Site specific seismic hazard assessment. This was completed using a Probabilistic Seismic Hazard Analysis (PSHA). The main motivations for carrying out the PSHA were to better quantify the aftershock hazard following the 2010-2011 Canterbury Earthquakes and to better characterise the 2500 year return period event. The PSHA resulting in a significant reduction in seismic hazard compared to code values.

Table 1: Seismic design cases as per ASCE 61-14

Design case	Ground motion probability of exceedance	Peak Horizontal Ground Surface Acceleration (PGA_H)		Required performance level
		NZS 1170.5 (Class D)	Site-specific seismic hazard assessment	
OLE Operating level earthquake	50% in 50 years (72-year return period)	0.18g	0.153g	Minimal damage
CLE Contingency level earthquake	10% in 50 years (475- year return period)	0.35g	0.330g	Controlled and repairable damage
DE Design earthquake	2% in 50 years (2500- year return period)	0.63g	0.500g	Life safety protection

2. Ground motion selection using the Generalised Conditional Intensity Measure (GCIM) approach. Ground motion selection and analysis was desired to take advantage of the recorded rock and soft soil time histories available from the Canterbury earthquakes. The selected ground motions are summarised in Table 2. Both the East-West and North-South components of the ground motions were used.
3. Non-linear site response analysis to determine the appropriate design spectra for seismic assessment of the wharf structure. This step was undertaken at this site because the site investigation results indicated Site Subsoil Class E in terms of NZS1170.5 and Site Class F in terms of ASCE 7 (2005). Site response analysis therefore enabled a reduction in seismic demand from NZS 1170.5 and met the requirements of ASCE 61-14 which requires a site response analysis for Site Class F sites.
4. Dynamic non-linear deformation analysis (NDA) was undertaken to assess lateral loadings on the piles, soil-structure interaction and the pile pinning effects on the breakwater slope. Inertial loading from the wharf superstructure and kinematic loading caused by lateral ground deformations was considered simultaneously.

The third and fourth tasks are described in more detail in the following sections.

4 NON-LINEAR SITE RESPONSE ANALYSIS

The dynamic response of soil deposits beneath a site has a significant influence on the ground motion hazard of engineered structures. During seismic shaking, bedrock motions have the potential to be both amplified and/or damped when travelling through surficial soils, ultimately affecting the resulting seismic forces which are imparted on structures at the surface. These effects depend on the ground profile, the physical characteristics of each soil layer and the strength and direction of shaking.

1D site response analyses were undertaken using a non-linear method (DMOD2000). The analysis methodology was verified through back analyses of the recorded rock ground motions at GNS monitoring station LPCC. The input from the calibration model was able to match the recorded soft soil ground motions at GNS seismograph station LPOC over a range of earthquake sizes.

Equivalent linear methods (e.g. SHAKE2000) were unable to capture the response of the soft soils to strong ground shaking.

Table 2: Summary of selected seismic ground motions

Ground motion source	Earthquake magnitude (Mw)	Distance of record source from fault rupture (km)	Ground Vs30 at record source (m/s)
LPCC 4/9/10	7.1	22.1	780
LPCC 22/2/11	6.2	7.1	780
LPCC 13/6/11	6.0	5.8	780
LPCC 23/12/11	5.9	12.4	780
Chi Chi, Taiwan 1999 TCU076	6.2	14.7	615
Kobe, Japan 1995 Nishi-Akashi	6.9	7.1	609
Kocaeli, Turkey 1999 Gebze	7.5	10.9	792

Once the back analysis could demonstrate satisfactory results forward analysis was undertaken to verify that the PSHA spectra for surface soils was appropriate given the soft soils at the site.

The assessed site specific response spectra have been calculated as the mean spectra from a suite of 28 ground motion analyses (based on the seven earthquake records which are summarised in Table 3). Figure 2 shows the spectral accelerations from the site response analysis compared to the PSHA spectra curves for the CLE design events.

The main conclusions from the site response analysis are:

1 The natural soil period is approximately 0.7 to 1.3 seconds depending on the level of shaking, as evaluated by comparing the ratio of ground response spectra to rock outcrop spectra. Given that the period of the wharf structure is estimated to be around 2.0 seconds we consider that the use of the PSHA spectra curve in Figure 2 is appropriate for the site.

2 For long spectral periods (T>~1s) the site response analysis indicates a spectra significantly less than the PSHA curves using Vs30=180m/s. However, there may be physical processes at long periods (i.e. surface waves, topography or basin effects) that are present at the site but unable to be captured within the 1D analysis. Therefore it was considered that using the lower spectral acceleration values from the site response analysis (as shown in Figure 3) was not appropriate for structural design.

5 DYNAMIC TIME HISTORY ANALYSIS

The analysis methodology used to assess the slope stability and evaluate the seismic slope displacements comprised three steps:

1. The model parameters were evaluated using correlations with the site investigation data.
2. Back analysis of the land performance which was observed during the Canterbury earthquakes.
3. Dynamic forward analysis using the ground motions presented in Table 2 scaled to the appropriate OLE, CLE and DE events.

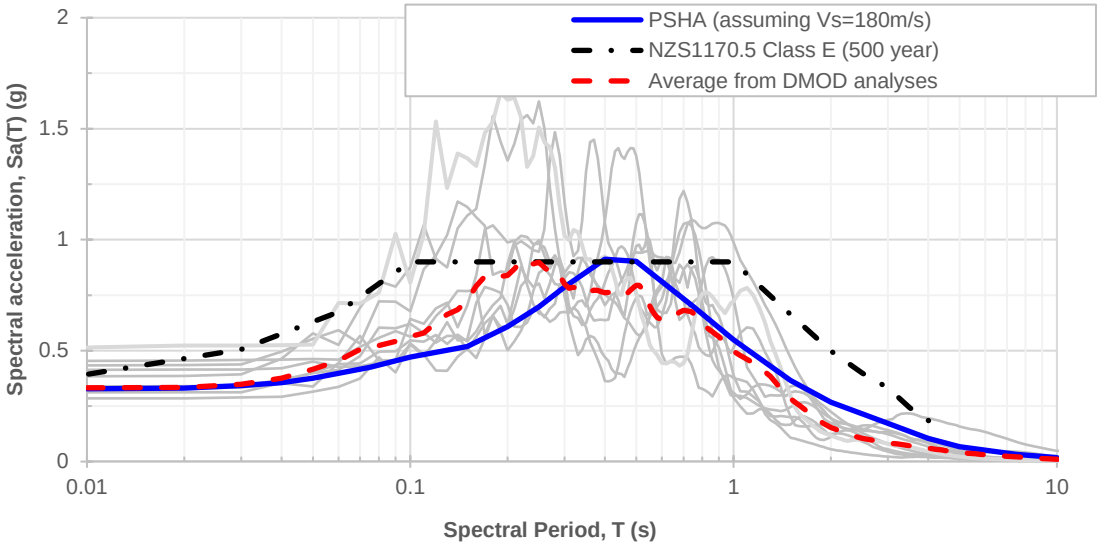

Figure 3: Response spectra plot for the CLE event showing the results from the PSHA (blue line), code spectra from NZS1170.5 (black line) and average spectra from the DMOD analyses (red line). The light grey lines are the spectra from individual DMOD analyses.

5.1 Geotechnical model

The harbour deposits were subdivided into five layers, with a further division in 'seaward' and 'landward' soil layers to account for the difference in strength due to consolidation of the landward soils under the weight of the hydraulic fill and breakwater.

The undrained shear strength profiles for the harbour deposits were derived from the CPT results using an Nk factor equal to 12. Nk = 12 was used based on correlation with shear vane testing.

In the dynamic model, the HS Small constitutive model was used for all materials, except the hydraulic fill, dense sand and rock layers, to account for stiffness degradation under large strains and to incorporate hysteric damping effects. The HS small model stiffness and damping parameters were derived using a combination of shear wave velocity data, CPT results, machine-drilled borehole data, and triaxial and oedometer laboratory testing of harbour deposits at Cashin Quay.

5.2 Back analysis

A back analysis of the slope was undertaken using the slope movement data which was collected following the Canterbury earthquakes. The purpose of the back analysis was to validate the PLAXIS slope stability model and geotechnical parameters.

The back analysis and calibration of the dynamic PLAXIS model was performed using the earthquake record from the GNS LPCC seismograph station was used as a bedrock motion. The magnitude and distribution of vertical and horizontal seismic displacements predicted by the model were compared to post earthquake survey measurements.

Table 4 summarise the results from the dynamic analysis. The model was able to provide a reasonable match with the model displacements within ten percent of the observed displacements. This provided confidence in the methodology to enable forward analysis incorporating the revised slope profile and the addition of the wharf piles.

Table 3: Back analysis of seawall displacement during the Canterbury earthquakes – comparison between measured values and dynamic PLAXIS model results

Parameter	4 September 2010 earthquake	22 February 2011 earthquake
Measured horizontal displacement at seawall	0.26m	0.4m
Horizontal displacement from dynamic PLAXIS model at seawall	0.23m	0.37m

5.3 Forward analysis

The earthquake records presented in Table 3 were used as a bedrock motion in a dynamic PLAXIS model. A total of 42 dynamic analyses were undertaken, using both the North-South and East-West components of all seven earthquake records scaled to the OLE, CLE and DE levels of shaking. The model was used to directly estimate the magnitude and distribution of vertical and horizontal seismic displacements.

Figure 6 shows the wharf horizontal displacements for the CLE design case. The largest cyclic displacements were observed in the Kocaeli EW and NS records which included significant forward directivity effects. ASCE 61-14 allows that the mean value be used for design if more than seven time history records have been used. The mean maximum horizontal wharf displacement from all the analyses was 0.21m and the mean displacement at the end of the shaking was 0.14m. These values were used in design of the wharf piles.

5.4 Comparison with conventional pseudo-static analysis

A conventional analysis was also completed with a pseudo static PLAXIS analysis to determine the yield acceleration of the slope. The yield acceleration, as well as the peak ground accelerations from the PSHA were then used as inputs into a sliding block analysis (Jibson 2007) to estimate the peak horizontal seismic slope displacements. This method indicated the yield acceleration of the proposed slope (including fill buttress) to be approximately ac = 0.090, which resulted in an estimated displacements much larger than the dynamic analysis. Table 5 provides a comparison between the estimated wharf displacements between the pseudo-static and dynamic analyses.

The magnitude of slope displacement has a direct influence of the soil loading on the piles. Prior to the dynamic analysis being undertaken the pile casings needed to have a steel thickness of 24mm to meet the requirements of ASCE 61-14. Through adopting the slope displacement values from the dynamic analysis the pile casing thickness was able to be reduced to 16mm while still meeting the ASCE6 61-14 requirements. This resulted in a project cost saving of NZD$600,000.

Table 4: Comparison between dynamic and pseudo-static analysis

Design case	Mean maximum horizontal wharf displacement		Percentage increase from dynamic to pseudo static
	Dynamic analysis	Pseudo static analysis	
CLE	0.21m	0.27m	30%
DE	0.44m	0.66m	50%

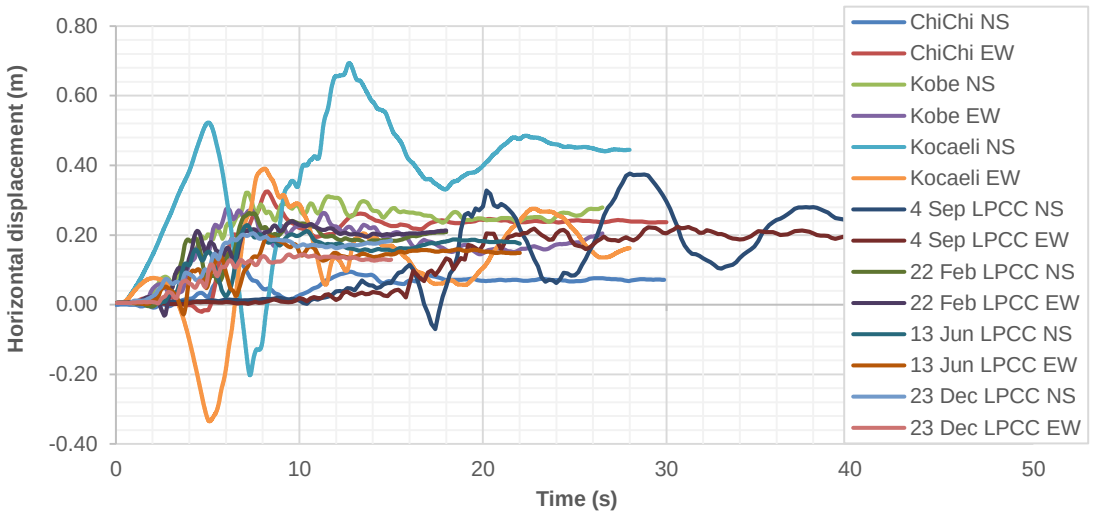

Figure 4: Wharf horizontal displacement versus time plots from the PLAXIS dynamic analysis for all fourteen earthquake cases scaled to the Contingency Level Earthquake (475 year return period)

6 CONCLUSIONS

This paper presents a case study where advanced analysis was undertaken in every step of the project; (1) characterisation of seismic hazard, (2) selection of ground motions for analysis, (3) assessment of the dynamic soil response at the site, and (4) analysis of soil-structure interaction. Advanced analyses were suited to this particular project due to the soft soils at the site and the high seismic design standard required for the proposed wharf.

The advanced analysis resulted in significant reductions in seismic actions on the wharf structure. This resulted in significant reductions in construction cost which were well in excess of the cost of the analysis.

REFERENCES

ASCE/COPRI (2014) Seismic Design of Piers and Wharves ASCE/COPRI 61-14. American Society of Civil Engineers

Jibson R.W. (2007) *Regression models for estimating coseismic landslide displacement*. Engineering Geology Vol 91, Issues 2-4, pp. 209-218.

NZS 1170.5 (2004). Structural design actions. Part 5: Earthquake actions – New Zealand. Standards New Zealand.

Bastin, S.H., van Ballegooy, S., & Wotherspoon, L. (2017)
Cross-Checking Liquefaction Hazard Assessments with Liquefaction Observations from New Zealand Earthquakes and Paleo-liquefaction Trenching
Proc. 20th NZGS Geotechnical Symposium. Eds. GJ Alexander & CY Chin, Napier

Cross-Checking Liquefaction Hazard Assessments with Liquefaction Observations from New Zealand Earthquakes and Paleo-liquefaction Trenching

S H Bastin
QuakeCoRE, University of Canterbury, Christchurch, New Zealand.
Sarah.bastin@canterbury.ac.nz (Corresponding author)

S van Ballegooy
Tonkin + Taylor Ltd, Auckland, NZ
svanballegooy@tonkintaylor.co.nz

L Wotherspoon
University of Auckland, Auckland
l.wotherspoon@auckland.ac.nz

Keywords: liquefaction hazard assessments, historical liquefaction extents, geomorphic mapping, paleo-liquefaction, trenching

ABSTRACT

Liquefaction has been reported following upwards of 13 recent and historical earthquakes in New Zealand. Collating reports outlining the extents of liquefaction manifestation following these events provides insights into the distributions of sediments with low cyclic resistances to liquefaction, and enables liquefaction hazard assessments to be cross-examined. Collated reports following the 1987 Edgecumbe earthquake indicate that localized liquefaction manifestations occurred proximal to the Whakatane River in Whakatane. However, analysis of an extensive geotechnical dataset using back-calculated peak ground accelerations and depth to ground water models show that the simplified methodologies predict widespread and severe liquefaction for much of Whakatane. Comparison of observed and predicted manifestations with local geomorphic variability indicates areas of inconsistent prediction occur within the distal flood-plain, while manifestations are accurately predicted within point-bar and paleo-channel deposits. Paleo-liquefaction trenching confirms an absence of liquefaction features in areas where liquefaction was predicted yet not observed, and provides a methodology by which predicted liquefaction extents can be moderated. This paper highlights the potential applications of incorporating historical extents of liquefaction manifestation, with geomorphic mapping, and paleo-liquefaction trenching into liquefaction hazard assessments.

1 INTRODUCTION

Liquefaction and associated lateral spreading poses a significant hazard to the built environment, as highlighted following the 2010-2011 Canterbury Earthquake Sequence (CES), and 2016 Kaikoura earthquake (Quigley, 2017; GEER, 2017). Liquefaction during the CES heightened awareness of the consequences of liquefaction to the built environment and associated financial losses. As a result, revisions to the Resource Management Act (1991) have been proposed which will require councils to better understand natural hazards in their area, including producing relevant hazard maps as part of their planning requirements. Liquefaction hazard maps are typically derived from the identification of low lying Quaternary aged alluvial deposits from geological maps, then further refined using simplified CPT- and SPT-based liquefaction triggering procedures on available geotechnical data. Historical cases of liquefaction are often not considered in the development of these maps, nor are the resultant maps cross-checked with observed performances from historical earthquakes.

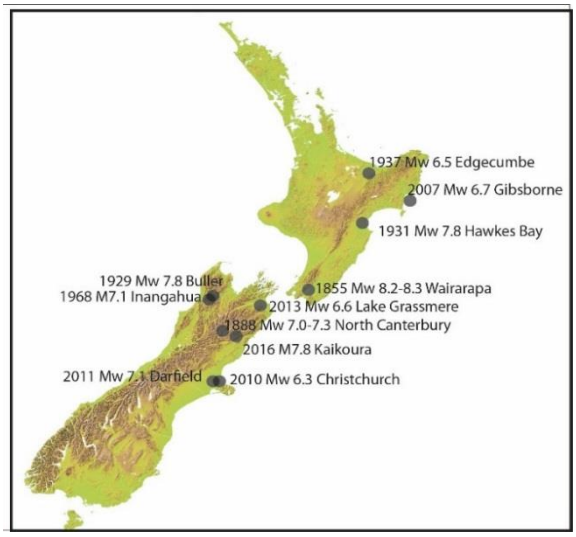

Figure 1: Historical earthquakes known to have triggered liquefaction in New Zealand.

Historical records indicate that upwards of 13 earthquakes have triggered liquefaction within parts of New Zealand prior to the CES, resulting in damage to the built environment (indicated in Figure 1; e.g. Fairless and Berrill, 1984). Much of the post-event literature indicates that localized liquefaction occurred proximal to waterways during these events, however recent liquefaction hazard assessments suggests that soils with low cyclic resistances to liquefaction are widespread throughout the urban centres in New Zealand. Recent studies following the 2010-2011 Canterbury earthquake sequence (CES) have shown inconsistencies between the predicted and observed extents of liquefaction manifestation (i.e. van Ballegooy, 2016). Many of the areas of over-prediction have been shown to correspond with silty back-swamps distal the rivers within the region (Beyzaei et al., 2017). The potential over-prediction of liquefaction hazards may result in unnecessary restrictions on land development and retrofitting of existing infrastructure, and may direct efforts away from areas that are truly susceptible to liquefaction.

Records of ‘ground cracking’ and ‘quick sand’ are present throughout local newspaper articles, and archives following large earthquakes in New Zealand, while maps outlining liquefaction manifestations are scattered throughout publications and technical reports following more recent events (e.g. Figures 2 & 3). Collation of the historical records enables extents of liquefaction manifestation to be approximated, and thus the distribution of sediments susceptible to liquefaction during future events to be determined. The New Zealand geotechnical database (NZGD) enables liquefaction analyses to be conducted on a regional basis. The extents of liquefaction manifestation predicted by the simplified liquefaction methodologies for a given earthquake shaking intensity may therefore be predicted for a given region. Comparison of predicted extents of liquefaction manifestation, with that observed from historical earthquakes, provides an independent methodology by which liquefaction hazard assessments may be validated. In addition, comparison of predicted and observed extents of liquefaction with geomorphic maps provides insights into areas where liquefaction typically manifests, and areas where over-prediction tends to occur. The presence and/or absence of liquefaction features may additionally be cross-examined through paleo-liquefaction trenching investigations.

This paper presents an overview of the potential applications of using historical observations of liquefaction manifestation, geomorphic mapping, and trenching in assessing liquefaction hazards using examples from Whakatane following the 1987 Edgecumbe earthquake.

"Fissures opened parallel with the water front for chains back; the wharf warped slightly; the railway-lines twisted; and the long straight of the break-water mole showed gentle swings from side to side and up and down as the embankment settled unevenly on the uncompacted estuarine deposits".

Figure 2: Example of a historical record referring to the occurrence of liquefaction following the 1929 Murchison earthquake (Collated from Carr (2004)).

Figure 3: Historical photographs outlining the occurrence of liquefaction in Whakatane following the 1987 Edgecumbe earthquake (Collated from Christensen (1995)).

2 COLLATING HISTORICAL ACCOUNTS OF LIQUEFACTION

Reports of earthquake-induced damage to land, infrastructure, and contents are present in letters, photographs, and diaries held within local archives across New Zealand. In some cases the reports are scattered with references to 'boils', 'fissuring', 'flooding' and other features indicating the occurrence of liquefaction (Figure 2). The presence or absence of ejecta, cracking, and/or flooding in post-event photography and reports provides key liquefaction and non-liquefaction case history sites (e.g. Figure 3). The resultant manifestations may be inferred across the surrounding geomorphological setting to provide a more comprehensive overview of the likely liquefaction manifestations. For more recent earthquakes, such as the 1987 Edgecumbe earthquake, reports of liquefaction manifestation are present in post-event publications and technical reports, and may be supplemented by local residents who are often able to recall specific localities. Combining all available resources enables the extents of liquefaction manifestations to be constrained for recent and historical events in New Zealand. Work to collate observational records into an online GIS-based database are ongoing and will result in a published dataset outlining liquefaction and non-liquefaction case history sites.

Collation of technical reports, journal papers, and historical photographs, along with local residents observations indicates that localized ejecta and lateral spreading occurred proximal to the Whakatane River in Whakatane following the 1987 Edgecumbe earthquake (indicated in Figure 4; i.e. Pender and Robertson, 1987; Christensen, 1995). No manifestation was observed within the Central Business District (CBD) nor in the suburbs distal to the river (Figure 4).

3 COMPARISON OF OBSERVED AND PREDICTED LIQUEFACTION MANIFESTATION

Collated liquefaction and non-liquefaction case history sites provides a means by which the results of the simplified liquefaction triggering procedures and associated liquefaction hazard assessments may be cross-checked. The extents of liquefaction manifestation predicted for a given earthquake may be back-calculated using event-specific peak ground accelerations and depth to groundwater models. The results may be compared with that observed to identify areas of consistent and inconsistent prediction. As peak ground accelerations and depth to groundwater data are not typically available for historical events, these values must be estimated. The methodology used to derive peak ground acceleration (PGA) and depth to groundwater models for Whakatane at the time of the Edgecumbe earthquake is summarized in Mellsop et al. (2017; these proceedings), and Bastin et al. (2017).

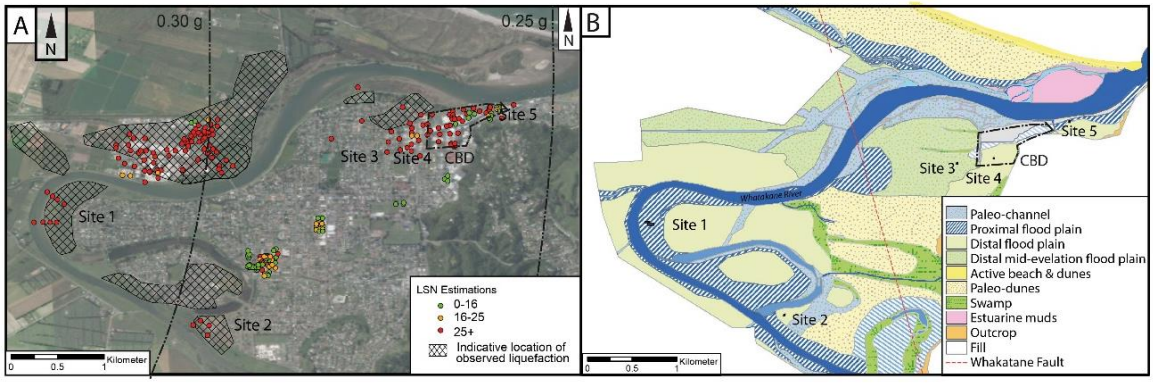

Figure 4: A) LSN predicted from simplified analyses using median peak ground acceleration and depth to ground water models and plotted with median PGA (dotted lines) and recorded extents of liquefaction (hatched areas). B) Geomorphic map with the location of trenches indicated.

Work undertaken using median modelled PGA and depth to groundwater derived for the Edgecumbe earthquake indicates that widespread and severe liquefaction (LSN 25+) is predicted for much of Whakatane (Figure 4; see Mellsop et al. (2017) for a detailed discussion). The LSN is shown to over-predict the severity of liquefaction manifestation within the Central Business District (CBD) compared to that inferred from the historical reports (Figure 4). Sensitivity analysis undertaken using lower-bound estimated PGA and depth to groundwater model additionally over-predicted the occurrence of liquefaction manifestation in the CBD however, under-predicted the severity of liquefaction at sites where liquefaction was well documented. The manifestations predicted using the median PGA and depth to groundwater models are therefore considered to best fit the post-event observational record of liquefaction.

4 COMPARISON OF OBSERVED LIQUEFACTION WITH GEOMORPHOLOGY

Geomorphic mapping provides insights into the settings where liquefaction was predicted and manifested and settings where liquefaction was predicted by the simplified liquefaction triggering methodologies yet was not observed. Geomorphic maps may be produced from analysis of topographic variability across an area, coupled with basic river morphologies, positions of historical river channels, and a review of available literature. The resultant observations provide insights into the paleo-depositional settings and likely subsurface sediment types within an area.

Geomorphic maps of Whakatane indicate that the township is primarily situated upon the low-elevation (0 to 3 m above sea level (a.s.l)) flood plain of the meandering Whakatane River. The area is locally truncated by higher elevation (2 to 10 m a.s.l) paleo-beach ridges associated with shoreline regression and coastline progression following the ~6,500 year before present highstand. The area is underlain by alluvial sands, silts, and granules deposited by the Whakatane River, and near-shore marine sands and silts associated with coastal regression (Figs. 1 & 2; Nairn and Beanland, 1989). Shoreline progradation of up to 10 km is inferred following the Whakatane (1850 y BP) and Kaharoa (800 y BP) pyroclastic eruptions in the Taupo Volcanic Zone (TVZ). In addition, up to 1.5 m of sediment accumulation is inferred within the active flood-plain of the Whakatane River following the 1886 Tarawera eruption (Christensen, 1995). Paleo-channels and ox-bow lakes associated with cut-off meander bends of the Whakatane River are present to the south-west and west of the township and recognizable as topographic depressions and swamp-land (Figure 4; Christensen, 1995). Tidal mud flats present near the mouth of the Whakatane River were infilled with rock tailings in the early 1900's as part of reclamation for development of the CBD (Figure 4B) (WDC archives). Swamps within the distal flood-plain were additionally infilled during the development of the township.

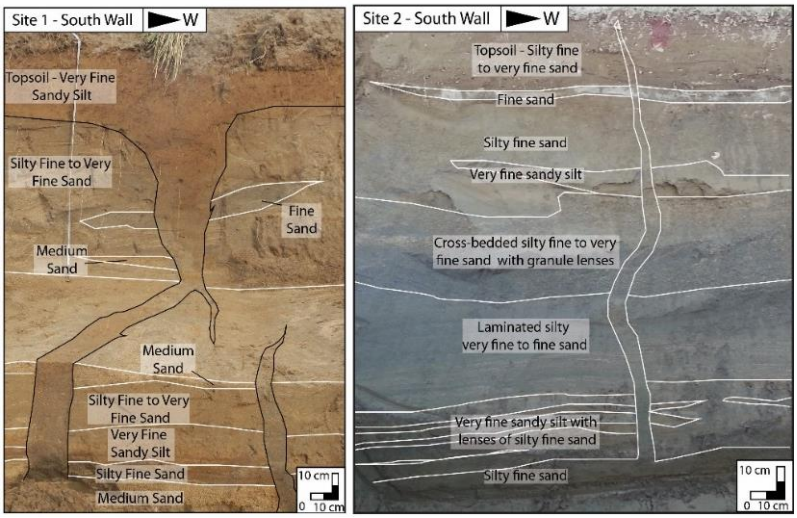

Figure 5: Interpreted field photographs of liquefaction features formed during the Edgecumbe earthquake as observed at Sites 1 and during trenching.

Areas of reported liquefaction manifestation following the Edgecumbe earthquake are shown to correspond with the inside banks of meander bends and paleo-channels of the Whakatane River (Figure 4B). These areas are likely underlain by thick successions of recent, fluvial deposited, and loosely consolidated fine to medium sands and granules, including sediments deposited following the Tarawera eruption. In contrast, no liquefaction manifested in the areas distal to the river which comprise paleo-dunes and the distal flood-plain (Figure 4). Sedimentation within the distal flood-plain is limited to large bank-overtopping flood events and thus the area generally comprises thinly inter-layered over-bank deposits of silts and fine sands. As a result, the near surface (>10 m) sediments are likely to be comparably older (>500 y BP) than those deposited proximal to the active river channel.

5 GROUND TRUTHING LIQUEFACTION EXTENTS THROUGH TRENCHING

Inconsistencies between the predicted and observed extents of liquefaction manifestation within Whakatane highlights potential shortcomings of the simplified liquefaction triggering methodologies and associated manifestation severity parameters. These inconsistencies have significant implications for liquefaction hazard assessments in the region, and across similar geologic settings in New Zealand. Paleo-liquefaction trenching provides an alternative methodology by which the occurrence or non-occurrence of liquefaction may be examined, and the associated liquefaction hazard may be cross-checked.

Paleo-liquefaction trenching in Whakatane enabled the observed and predicted extents of liquefaction to be 'ground-truthed' and the presence of pre-Edgecumbe liquefaction features to be examined. Trenching was conducted at sites where liquefaction was predicted by the simplified methodologies and was observed (Sites 1 and 2), and sites where liquefaction was predicted by the simplified methodologies yet was not observed (Sites 3 - 5). Trenches were orientated perpendicular to the closest bank of the Whakatane River which gave the best chance of intersecting lateral spreading features, and were excavated to maximum lengths possible at the selected sites (indicated in Figure 4).

Trenching at sites within the low-elevation flood-plain of the Whakatane River which are known to have liquefied during the Edgecumbe earthquake (Sites 1 and 2), revealed approximately 20 to 40 cm wide lateral spreading fissures that cross-cut the fluvial stratigraphy. The features generally increase in width with depth indicating that they formed by the upwards ejection of liquefied sediment (Figure 5). The margins of the features exhibited limited re-working (i.e. bioturbation of contacts) indicating that they most likely formed during the Edgecumbe earthquake. No

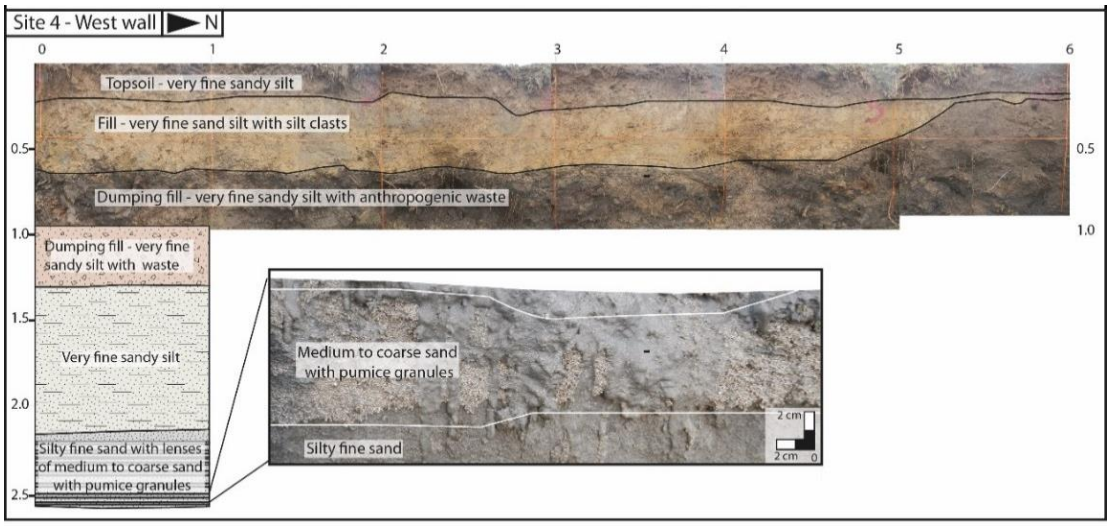

Figure 6: Interpreted photo log of the trench at Site 4 where liquefaction was predicted for the Edgecumbe earthquake by the simplified methodologies yet was not observed.

evidence for pre-1987 liquefaction was observed in the trenches, indicating that the sediments had most likely not liquefied since their deposition and prior to the Edgecumbe earthquake. The exposed stratigraphy comprises laminated silty fine sand and fine sandy silt with lenses of fine sand that are cross-cut by channelized lenses of cross-bedded medium sand with granules of pumice. The stratigraphy is interpreted to represent recent fluvial deposits of the Whakatane River associated with its avulsion to its present location and associated point-bar deposits. The upper 1.5 m of sediment likely reflects active deposition following the 1886 Tarawera eruption.

In comparison, no liquefaction features were observed during trenching at sites where liquefaction was predicted by the simplified methodologies yet was not observed (Sites 3-5). The absence of liquefaction features further confirms that liquefaction did not manifest at these sites during the Edgecumbe earthquake (Figure 6). The exposed stratigraphy comprises anthropogenic fill associated with development of the township, and is underlain by silts with inter-layered lenses of fine sand and medium to coarse sand with granules of pumice (Figure 6). The stratigraphy is generally consistent with the positions of the sites in the distal flood-plain of the Whakatane River, and are interpreted as over-bank flood deposits. It is considered unlikely that significant sediment accumulation occurred at these sites following the 1886 Tarawera eruption.

Potential reasoning for the inconsistencies between the predicted and observed manifestations of liquefaction are the subject of ongoing research. One of the more noticeable variations between the sites is the inferred variability in soil ages between Sites 1-2, and Sites 3-5, which has been shown to influence liquefaction potential (e.g. Hayati et.al. (2008)). Additional factors potentially influencing liquefaction triggering at the site include variability in measured and actual ground-water depths, the inability of the CPT to distinguish thin inter-layering of sands and silts in distal back-swamps, which has been shown to minimize liquefaction triggering (Beyzaei et al., 2017), and the presence of pumice granules for which the simplified methodologies are not developed (Orense et al. 2012).

6 POTENTIAL APPLICATIONS TO LIQUEFACTION HAZARD ASSESSMENTS

Collated reports indicate that liquefaction manifestation occurred within recent paleo-channel and point-bar deposits in Whakatane during the 1987 Edgecumbe earthquake which comprise loose and unconsolidated fine sand with lenses of silt, and medium to coarse sand with pumice granules. The upper 1.5 m of the soil profile is considered likely to have been deposited in the last 150 years (i.e. post Tarawera), and the under-lying strata is likely geologically young. No manifestations were observed within the distal flood plain of the Whakatane River, despite the simplified methodologies predicting widespread and severe liquefaction manifestations. Trenching indicates

these areas are underlain by silts with inter-layered lenses of fine sand and medium to coarse sand with granules of pumice which are interpreted to be comparably older (>150 years) than those exposed at Sites 1 and 2. Similar spatial trends in liquefaction manifestations are indicated in post-event literature following other recent and historical earthquakes within New Zealand. Descriptions often indicate that fissuring and sand-boils formed in areas proximal to waterways (i.e. Figure 2), while no records of liquefaction manifestation are generally reported to the rivers.

The recorded extents of liquefaction manifestation indicates that young, unconsolidated point-bar and paleo-channel deposits are highly susceptible to liquefaction, and thus are likely to liquefy during future events. The extents of liquefaction manifestations during future events generating similar PGA are considered likely to be similar to that of previous events. However, no inferences can be made for events generating higher PGA. The historical extents may therefore be used to approximate liquefaction hazards for future events generating similar ground accelerations. Geomorphic mapping may additionally be employed to identify areas potentially underlain by sediments with low cyclic resistances to liquefaction in areas where geotechnical testing data is lacking. The presence or absence of liquefaction features at given site may be 'ground-truthed' through paleo-liquefaction trenching. Combining historical extents of liquefaction, geomorphic mapping, and paleo-liquefaction trenching enables the assigned liquefaction hazard to be cross-examined for a given area, and provides a methodology by which predicted liquefaction extents can be moderated.

7 CONCLUSIONS

Liquefaction manifestations have been reported following upwards of thirteen recent and historical earthquakes in New Zealand. Collation of historical records outlining extents of liquefaction manifestation provide an independent methodology by which liquefaction hazard assessments may be 'cross-checked', and key liquefaction and non-liquefaction case history sites established. The extents of liquefaction manifestations predicted for a given earthquake may be derived from simplified analysis of existing geotechnical datasets using back-calculated PGA and depth to ground water models. Comparison of predicted manifestations with that observed, enables areas of consistent and inconsistent prediction to be identified. The presence or absence of liquefaction features in these areas may be confirmed through paleo-liquefaction trenching.

Collation of historical records of liquefaction manifestation within Whakatane following the 1987 Edgecumbe earthquake indicates that liquefaction occurred proximal to the Whakatane River. Comparison of the collated extents of liquefaction manifestation with that predicted from the simplified methodologies using back-calculated PGA and depth to ground water models indicates areas of inconsistent prediction occur distal to the Whakatane River. Geomorphic mapping indicates that liquefaction manifestations occurred with recent point-bar and paleo-channel deposits. Trenching confirms the presence of liquefaction features in areas where it was reported, and an absence of features in areas where liquefaction was predicted yet not observed. Potential reasoning for the inconsistent predictions include variability in the depositional setting, age of the deposits, thin-scale inter-layering present within the distal flood-plain, and/or the presence of pumice. The results highlight the potential applications of incorporating historical extents of liquefaction, geomorphic mapping, and paleo-liquefaction trenching into the development of liquefaction hazard assessments.

8 ACKNOWLEDGEMENTS

We thank the Whakatane District Council for their assistance with their project, specifically Jeff Farrell. This project was supported by QuakeCoRE, a New Zealand Tertiary Education Commission-funded Centre. This is QuakeCoRE publication number 0202. Additional support came from the Ministry of Building, Innovation and Employment.

REFERENCES

Bastin, S., van Ballegooy, S., Mellsop, N., Wotherspoon, L. (2017) Liquefaction case histories from Whakatane, New Zealand as a result of the 1987 Edgecumbe Earthquake - Insights from an extensive CPT dataset and paleo-liquefaction trenching, *3rd International Conference on Performance-based Design in Earthquake Geotechnical Engineering (PBD-III)* Vancouver, BC, Canada, July 16-19.

Beyzaei, C.Z., Bray, J.D., van Ballegooy, S., Cubrinovski, M., Bastin S. (2017) Swamp Depositional Environment Effects on Liquefaction Performance in Christchurch, New Zealand", *3rd International Conference on Performance-based Design in Earthquake Geotechnical Engineering (PBD-III)* Vancouver, BC, Canada, July 16-19.

Carr, K.M. (2004) Liquefaction case histories from the West Coast of the South Island, New Zealand, Unpublished MSc thesis. University of Canterbury, Christchurch, New Zealand.

Christensen, S.A. (1995) Liquefaction of cohesionless soils in the March 2, 1987 Edgecumbe Earthquake, Bay of Plenty, New Zealand, and other earthquakes, *Masters Thesis*, University of Canterbury, Christchurch, New Zealand.

Fairless, G.J.; Berrill, J.B. (1984) Liquefaction during historic earthquakes in New Zealand. *Bulletin of the New Zealand National Society for Earthquake Engineering*, 17(4): 280-291.

GEER 2017. Geotechnical Reconnaissance of the 2016 Mw 7.8 Kaikoura, New Zealand Earthquake. Version 1: November 8, 2011, *Report of the National Science Foundation – Sponsored Geotechnical Extreme Events Reconnaissance* (GEER) Team.

Hayati, H., Andrus, R.D., Gassman, S.L., Hasek, M., Camp, W.M., Talwani, P. (2007) Characterizing the liquefaction resistance of Aged Soils, *Geotechnical Earthquake Engineering and Soil Dynamics Congress IV*, Sacramento, United States, p 1-10.

Mellsop, N., Bastin, S., Wotherspoon, L., van Ballegooy, S. (2017) Development of detailed liquefaction case histories from the 1987 Edgecumbe Earthquake, *New Zealand Geotechnical Symposium*, Napier, New Zealand, November 2017.

Nairn, I.A., & Beanland, S. (1989) Geological setting of the 1987 Edgecumbe earthquake, New Zealand. *New Zealand journal of Geology and Geophysics*, 32: 1-13.

Orense, R.P., Pender, M.J. and O'Sullivan, A. (2012) *Liquefaction Characteristics of Pumice Sands*, EQC Project 10/289 Final Report, 123pp

Pender, M.J. & Robertson (eds), 1987. Edgecumbe earthquake; reconnaissance report, *Bulletin of the New Zealand National Society for Earthquake Engineering*, 20(3): 201-248.

Quigley, M., Hughes, M., Bradley, B., van Ballegooy, S., Reid, C., Morgenroth, J., Horton, T., Duffy, B., and Pettinga, J. (2016) The 2010-2011 Canterbury earthquake sequence: Environmental effects, seismic triggering thresholds and geologic legacy, *Tectonophysics* 672–673: 228–274.

RMA, (1991). *Resource Management Act*, Ministry for the Environment, New Zealand.

Stringer, M.E., Bastin, S., McGann, C.R., Cappellaro, C., El Kortbawi, M., McMahon, R., Wotherspoon, L.M., Green, R.A., Aricheta, J., Davis, R., McGlynn, L., Hargraves, S., van Ballegooy, S., Cubrinovski, M., Bradley, B.A., Bellagamba, X., Foster, K., Lai, C., Ashfield, D., Baki, A., Zekkos, A., Lee, R., Ntritsos, N. (2017) Geotechnical aspects of the 2016 Kaikoura Earthquake on the South Island of New Zealand, *Bulletin of the New Zealand Society for Earthquake Engineering*, 50(2): 117-141.

van Ballegooy, S., Malan, P., Lacrosse, V., Jacka, M., Cubrinovski, M., Bray, J. D., Cowan, H. (2014) Assessment of liquefaction-induced land damage for residential Christchurch. *Earthquake Spectra*, February 2014, 30 (1), 31-55.

Characterisation of in situ soils based on the resilient soil modulus obtained using Light Weight Deflectometer (LWD)

N Barounis
Cook Costello, Christchurch, New Zealand.
nickbarounis@coco.co.nz

T Smith
Cook Costello, Christchurch, New Zealand.
tomsmith@coco.co.nz (Corresponding author)

Keywords: LWD, static plate load test, resilient modulus Evd, static modulus Ev1 and Ev2

ABSTRACT

The Light Weight Deflectometer (LWD) is a portable device that measures the onsite dynamic or resilient modulus (Evd) of subgrade soils and pavements. The LWD, which has been used extensively in Europe and the United States, has become popular for assessing the stiffness of embankments, structural fills and other earth structures. It assesses the bearing capacity, the stiffness and the compaction degree of soils that have a maximum grain size of 63mm. The LWD assessment considers the stiffness (or compressibility) characteristics of the materials under testing to a depth of 600mm below plate level. The paper presents available correlations between Evd with the static soil modulus Ev obtained from static plate load tests. It also presents how Evd can be linked with CBR and thus be useful for pavement design, but also with the subgrade reaction modulus K of the assessed soils. It also discusses the fundamental principles behind the testing along with the benefits that may arise from its use on specific applications. Such applications include the design and construction monitoring of gravel rafts, the design of pavements, engineered and non-engineered fills, landfills, MSE walls, pipelines and services, evaluation of ground improvement effectiveness and soil stiffness mapping.

1 INTRODUCTION

The Light Weight Deflectometer (LWD) is a portable device that measures the onsite dynamic or resilient modulus (Evd) of subgrade soils and pavements. It is suitable for cohesionless, cohesive and mixed types of soils with a maximum grain size of 63mm. It can be used on natural subgrade and subsoils, unbound base layers, granular layers, soil stabilised with lime or other additives. The LWD test method has been gaining in popularity following its use in European countries and the USA for over 30 years. The test method was originally designed to measure the resilient modulus (Evd) of an in-situ material which indicates the material's stiffness. The LWD can be perceived as an on-site simulation of a laboratory cyclic triaxial test for unbound or bound materials. The tested soil volume by the LWD is 300mm in diameter and 600mm in depth. Numerous standards have been developed for the LWD and allow the characterisation of various materials based on Evd, which can facilitate the estimation of bearing capacity and the compaction degree of engineered fills. This is extremely beneficial for infrastructure design and testing as it allows a fundamental engineering property (Evd) to be measured and used in the design and construction process.

The resilient modulus (Evd) represents the elastic response of the soil specimen after many cycles of loading. Cyclic triaxial tests, used for measuring the resilient modulus (Evd) of untreated base/sub-base materials, are expensive and difficult to execute in New Zealand. This has caused

the measurement of such an important geotechnical parameter to often be ignored during the design and construction process of infrastructure in New Zealand. The LWD test method therefore offers a great alternative for measuring the onsite resilient modulus, at a fraction of the laboratory cost. It should be noted that CBR characterises a soil based on its failure to penetration; this is an indirect measure of soil strength. In contrast to resilient modulus, CBR is not a fundamental material property. However, the use of CBR is well justified in the geotechnical community as it is widely accepted for pavement design.

2 LWD TEST METHOD, STANDARDS AND APPARATUS

2.1 LWD test method and standards

The principle of this test was developed in 1981. The test simulates a truck with a 10ton axle weight travelling on a road at 80km per hour. A steel plate of 300mm diameter is placed on the soil to be tested. A 10kg weight drops from a height of 72 cm onto the plate. The load pulse creates a soil pressure of 100kPa under the plate. The approximate duration of the load pulse is around 17ms and it is created by means of engineered springs located above the plate. An acceleration sensor is arranged on the load plate. The generated acceleration signal is recorded. From single and double integration of the acceleration signal, the velocity and the displacement (settlement) of the plate is calculated.

From this simple test method the recorded values can be used for determining:

- Resilient or dynamic soil modulus (Evd)
- Bearing capacity
- Dynamic spring stiffness (Kvd)
- Degree of compaction and compaction quality control

The resilient modulus Evd is given in MPa by the equation:

$$Evd = \frac{22.5}{s} \quad (1)$$

where s is the measured plate settlement in mm.

The specifications for the LWD apparatus are defined in both ASTM E2835-11 and ZTVE-StB 09 and conform to strict equipment production criteria. The apparatus is also required to be calibrated on an annual basis by an accredited calibration institute.

Numerous international standards have been produced following the inception of the LWD as a test procedure. The two main internationally accepted test methods are:

- ASTM E2835-11: American Standard Test Method for Measuring Deflections using a Portable Impulse Plate Load Test Device
- ZTVE-StB 09: German Engineering Code for Soil and Rock in Road Construction

While these test methods are the most widely accepted in industry, many other standards have been produced to complement more specific design codes and procedures. Some other available international standards on LWD include:

- TP BF-StB B 8.3 version 2012: German Engineering Code for Soil and Rock in Road Construction
- ZTV E-StB 09: German additional terms of contract and rules for earthwork in road construction
- ZTV T-StB 95: German additional terms of contract and rules for subbases in earthworks
- ZTV A-StB 97: German additional terms of contract and rules for excavation in traffic access

- RVS 08.03.04 March 2008: Austrian regulation - Compaction test by means of dynamic plate load test
- RIL 836, Deutsche Bahn AG: Guideline for the use of the Light Drop-Weight Tester in railway construction
- UNE 103807-2:2008: Spanish regulation - Plate Load Test by means of the Light Drop Weight Tester-Part 2
- TB 10102-2004, J338-2004: Chinese regulation - Standard for soil testing in railway construction

The number of standards available shows that the test procedure is widely accepted and utilised for a diverse range of engineering applications throughout the globe. This also provides a simple platform for the integration of the LWD into New Zealand design and construction procedures through the utilisation of these existing standards.

2.2 Description of LWD apparatus

There are numerous, well designed and robust LWD equipment apparatus available internationally (Zorn ZFG 2000, Keros LWD, Dynatest 3031 LWD, HMP LFG Pro). Figure 1 shows a schematic view of the LWD apparatus. This equipment is small and portable, allowing it to be easily transported and utilised on a construction site by one technician.

The apparatus is controlled during testing by means of an electronic recorder that provides a step by step guidance to the operator during the testing process. This removes the potential for any measurement errors.

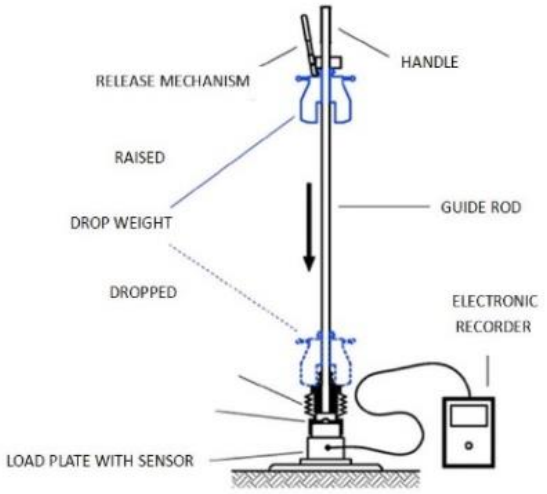

Figure 1: Components of the Light Weight Deflectometer (LWD) as per ASTM E2835-11

Following the test procedure, the electronic recorder on the apparatus provides an instant graphical and tabular display of the results which are then stored on the device for download. The apparatus also includes a GPS and a built-in printer that can instantly print the results onsite for quality assurance records.

3 GENERAL APPLICATIONS FOR LWD

The use of the LWD test method in New Zealand is a natural progression by utilisation of 'best practice' test methods as they become more widely recognised and accepted in the civil and

geotechnical engineering industries. This, combined with the many benefits of the test method, is likely to benefit the following sectors:

- Site investigations for projects where the bearing capacity and settlement of shallow foundations is a key consideration
- Highways and Bridges: Design and construction monitoring of highway pavements and their subgrades, highway embankments, reinforced earth structures and MSE walls, backfills, granular fills behind abutments and retaining walls
- Earthworks and Land Development: earthworks of any type, trenches and services, landfills and backfilled areas, quality assurance testing for quarries and aggregates, compressibility of ground on derelict or contaminated land, quality assurance for temporary works, site feasibility and suitability assessment, subdivisions
- Geotechnical Engineering: gravel rafts, structural fills, compaction control of treated and untreated soils, foundation soils, evaluation of ground improvement effectiveness, soil stiffness mapping
- Civil Works and Infrastructure: canals, airports and airfields, pipe and services trenches, marine works

4 CHARACTERISATION OF IN SITU SOILS BASED ON LWD

4.1 Estimation of CBR and static modulus Ev

The LWD can assist in the characterisation of in situ soils using correlations to other well accepted test methods. The dynamic soil modulus (Evd) obtained using LWD, is well correlated with the static soil modulus (Ev1), obtained by static plate load tests (PLT), for both cohesive and cohesionless soils (refer to Figure 2). As the PLT is well correlated with CBR, the LWD can also assist in the characterisation of soils for use in pavement design.

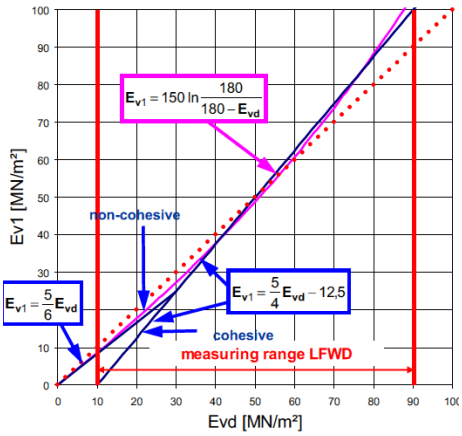

Figure 2: General correlation between Evd and Ev1 for cohesionless and cohesive soils

There is a plethora of comparative tests between dynamic (LWD) and static plate load tests (PLT) for both cohesive and granular soils (Adam and Kopf, 2004). These correlations relate Ev1 measured by static PLT, with Evd measured by LWD. A useful note that can be made for the relationship between Evd and Ev1 shown in Figure 2 for cohesionless or cohesive soils is the following:

When Evd ≤ 50MPa, Evd > Ev1 and when Evd ≥ 50MPa, Ev1 > Evd (2)

Another correlation suggested in the Austrian standard RVS 08.03.04 (2008), suggests the following correlations:

When $Ev1 \geq 25MPa$, $Evd = 10 + 0.8\ Ev1$ (3)

and when $Ev1 < 25MPa$, $Evd = 1.2\ Ev1$ (4)

When conducting static plate load tests with a 762mm diameter plate, the CBR value can be estimated from the following equation (IAN 73/06, 2009):

$$CBR\ (\%) = 6.1 \times 10^{-8} \times (K_{762})^{1.733} \quad (5)$$

where K_{762} is the modulus of subgrade reaction (kN/m^3) for the 762mm plate. K_{762} is defined as the stress σ (in kPa) that causes 1.25mm settlement, divided by 0.00125m.

$$K_{762} = \frac{\sigma}{1.25x10^{-3}} \quad \text{in kN/m}^3 \quad (6)$$

Thus, by conducting LWD testing with a 300mm diameter plate, the CBR value can be estimated with the following procedure:

- Evd can be converted to Ev1 depending on the soil material by using equations 3 or 4 and/or the correlation presented in Figure 2 above.
- Convert the Ev1 to a spring stiffness K_{300} for a plate width B of 300mm by using the equation (Bowles, 1997):

  $$K_{300} = \frac{Ev1}{B\ (1-\nu^2)} \quad (7)$$

  Where ν is the Poisson's ratio of the tested material.

- Convert the K_{300} to a K_{762} by using the conversion factor shown in Figure 3. For converting from a 300mm plate to a 762mm plate, the factor is 0.44. Thus:

  $$K_{762} = 0.44\ K_{300} \quad (8)$$

- For estimating CBR, use equation 5 above by substituting the value for K_{762} obtained from the previous step.

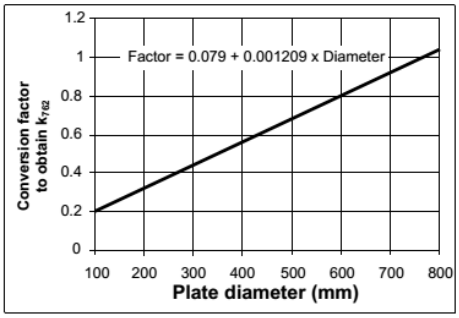

Figure 3: Conversion factor for smaller plate sizes (IAN 73/06, 2009)

The above suggests that by measuring the resilient modulus (Evd) on site, the static modulus (Ev1) and the CBR can also be estimated and thus the soil or the site can be characterised. The above correlations can be invaluable as the design engineer is then in a position to facilitate static settlement calculations for shallow foundations or to assess the capacity of a subgrade for accommodating a pavement.

4.2 General purpose characterisation of natural soils

An effort is made to compile a rough soil characterisation scheme for general use for cohesionless and cohesive soils. The intention of this effort is to classify naturally formed in-situ soils before being treated or compacted. The proposed scheme is shown in Tables 1 and 2. This characterisation scheme is completely uncoupled from compaction criteria which are presented in the next paragraph.
The soil characterisation scheme is based on the following:

- The modulus values provided by Bowles (1997), which correspond to Ev1 values
- The relative density of sands and the state of their packing as assessed by SPT
- The consistency of clays based on their undrained cohesion C_u
- By applying linear interpolation for the intermediate values for the above parameters and for Evd
- By considering Figure 2 and equations 2, 3 and 4

Variation is expected as this scheme is not based on the exact grain sizes present in the soil and their mass percentage.

Table 1: Soil characterisation scheme for cohesionless soils

Cohesionless soils	Very loose	Loose	Medium dense	Dense	Very dense
Evd (MPa)	0-12	12-24	24-34	34-50	50-90
Ev1 (MPa)	0-10	10-20	20-30	30-50	50-100

Table 2: Soil characterisation scheme for cohesive soils

Cohesive soils	Very soft	Soft	Firm	Stiff	Very stiff	Hard
Evd (MPa)	0-22	22-30	30-36	36-43	43-50	50-90
Ev1 (MPa)	0-15	15-25	25-33	33-41	41-50	50-100

Subgrade testing undertaken using LWD yielded various Evd values for different soil types. Table 3 provides examples of Evd values for a number of soil types measured in Christchurch, New Zealand. Tables 1 and 2 above can then be used to classify these soils based on their description and Evd measured using LWD.

Table 3: Example Evd values for various soils measured using LWD

Soil Type	Evd (MPa)	Soil characterisation
TOPSOIL (cohesive)	5	Very Soft
Clayey SILT (cohesive)	8 – 14	Very Soft
SILT (cohesionless)	17 - 27	Loose to Medium Dense
AP40 compacted GRAVEL (wet)	18 - 34	Loose to Medium Dense
AP40 compacted GRAVEL (moist – dry)	40 - 64	Dense to Very Dense

4.3 Compaction assessment based on modulus criteria

Table 4 presents target values for Evd and the reload modulus Ev2 for cohesionless soils extracted from the German standard ZTVE-StB 09. The reload modulus Ev2 is obtained by a static plate load test when the soil is first incrementally loaded to measure Ev1, then incrementally unloaded to zero stress and then incrementally reloaded to the same stress level as for when Ev1 was assessed. For well compacted soils, the ratio of Ev2 over Ev1 (Ev2/Ev1) is greater than one and usually smaller than 2.6. The classification of these soils is relying on the German soil classification system DIN 18196 and is somewhat similar to the U.S.C.S. classification system.

Table 4: Modulus based compaction criteria for Evd and EV2 (ZTVE-StB 09)

Soil group	Evd (MPa)	Ev2 (MPa)	Compaction degree (%)
GW, GI, GE (gravels)	≥50	≥100	≥100
SW, SI, SE (sands)	≥40	≥80	≥98

5 BENEFITS FROM THE USE OF LWD

5.1 Potential benefits to New Zealand construction and economy

The LWD has become an internationally recognised test method for many areas of construction following its use in Europe and the United States over the last 30 years. The major benefits of using the LWD from a practical perspective are:

- It relies on sound principles of geotechnical engineering
- It is fast, portable and easily operated by one technician
- It produces repeatable results and is cost effective
- The geotechnical parameters measured allow a more robust performance based approach to be adopted in the design and construction monitoring phases

Additionally, specific benefits for New Zealand can potentially be the following:

- It is environmentally safe and does not have the safety and transport issues of a nuclear density meter (NDM)
- It offers a 600mm investigation depth below plate level (Adam and Kopf, 2004) which is substantially deeper than other well established methods. This 600mm thickness can be the same uniform soil layer or a composite section made of subgrade, subbase and base materials.
- Compared to NDM, it provides a more reliable assessment tool when checking materials coarser than 40mm for assessing degree of compaction; CETANZ Technical Guide TG3 recommends caution when interpreting test results from NDM for granular materials coarser than 40mm
- Assessment of the soil modulus as per AS/NZS 2566.1:1988 when flexible pipes are installed in trenches, becomes more straightforward for both designers and contractors, leaving less room for disputes over construction quality acceptance
- Looking at several of the more common test methods utilised in New Zealand practice (Clegg hammer, CPT, DCP/Scala penetrometer, shear vane, CBR), it is clear that none of them actually measure the soil modulus

If CBR tests are also conducted in conjunction with LWD, then a correlation between Evd and CBR can be established. Currently, there is significant discussion and research occurring in the American geotechnical community on the development of modulus-based construction specification for acceptance of compacted geomaterials (NCHRP 10-84, 2014). However, modulus-based construction specifications are already well-established and accepted in European practice as presented in paragraph 4.3.

5.2 Potential cost savings for highway projects

The LWD was used for assessing the stabilisation process of the founding aggregates on the A556 improvement scheme in Cheshire, UK (Ground Engineering, 2016). The ground conditions along the route were very challenging and variable with CBR values as low as 1.5%. The finished pavement was required to meet Foundation Class II with greater than 100MPa modulus as per Highways England's Interim Advice Note 73/06. One of the main tests used for demonstrating compliance with the design was LWD. The performance based design required a mean Evd modulus of 50MPa for the geogrid reinforced capping layer. By achieving this requirement for

the capping layer, it was ensured that the Foundation Class II (100MPa) was achieved on the finished pavement surface. It was found that surface moduli of up to 700MPa were achieved using this construction and quality assurance methodology. The contractor and the designer succeeded to save £2M ($NZD3.5M) when compared to soil excavation and replacement. From the above example, it can be concluded that more efficient designs and hence cost savings could be achieved if New Zealand Standards are introduced on the use and interpretation of LWD.

6 CONCLUSIONS

The Light Weight Deflectometer (LWD) is an internationally recognised and utilised test method that has been gaining in popularity following its use in European countries (for example, Germany and UK on a performance design basis) and the USA for over 30 years. However, its utilisation in New Zealand for both design and construction has been limited to date for various reasons. With modern and robust test equipment now available, and internationally accepted standards readily available, utilisation of the LWD in New Zealand is likely to become more prolific.

The LWD provides many advantages over other in-situ and laboratory test methods by quickly and easily measuring the resilient modulus (Evd), and allowing it to be easily incorporated into the design process or utilised at the construction monitoring phase.

Utilisation of the LWD in the design and construction process allows the creation of a performance based design with a more robust construction monitoring process. This in-turn creates more resilient infrastructure through the use of performance based acceptance criteria. The LWD equipment also reduces construction timeframes due to its portability, speed of testing and ease-of-use for technicians.

REFERENCES

ASTM E2835-11 (2015). *Standard Test Method for Measuring Deflections using a Portable Impulse Plate Load Test Device*. American Society of Testing and Materials, USA.

Adam, D. and Kopf, F. (2004). Operational devices for compaction optimization and quality control (Continuous Compaction Control & Light Falling Weight Device). *Proceedings of the International Seminar on Geotechnics in Pavement and Railway Design and Construction* Gomes Correia and Loizos (eds), Millpress, Rotterdam.

Bowles, J.E. (1997). *Foundation analysis and design, 5th Edition*. New York: McGraw-Hill.
Ground Engineering (2016). Stabilising influence. Issue October 2016, pp.20-24.

German Earthworks and Foundation Engineering Task Force (2009). *Supplementary Technical Terms and Conditions of Contract and Guidelines for Earthworks in Road Construction* ZTVE-StB 09.

Interim Advice Note 73/06, Revision 1 (2009). *Design guidance for road pavement foundations (Draft HD25)*. Standards for Highways, UK.

National Cooperative Highway Research Program NCHRP Project 10-84 (2014*). Modulus-based construction specification for compaction of earthwork and unbound aggregate.*

The engineering and durability properties of polystyrene injected concrete (PIC) and its performance as a shallow ground improvement

N Barounis
Cook Costello, Christchurch, New Zealand.
nickbarounis@coco.co.nz

T Smith
Cook Costello, Christchurch, New Zealand.
tomsmith@coco.co.nz (Corresponding author)

Keywords: Lightweight Aggregate Concrete (LWAC), Polystyrene Injected Concrete (PIC), shallow ground improvement, durability, Static Plate Load Test (PLT), Light Weight Deflectometer (LWD)

ABSTRACT

Polystyrene injected concrete (PIC) is a type of lightweight concrete that internationally has a number of different applications, ranging from thermal insulation to shallow ground improvement (PIC Raft). Due to the lightweight character of this material, several benefits arise from its use in buildings and infrastructure. The engineering community has significant understanding of the strength characteristics for PIC. However, less is known about the durability characteristics of this material. The intention of this paper is to provide some insight into the durability of PIC in conjunction with its onsite engineering performance under static and dynamic loading when used as a shallow ground improvement method. This paper presents the engineering properties that have been measured on site and in the laboratory. The onsite engineering properties have been assessed by means of static plate load testing (PLT) and light weight deflectometer (LWD) undertaken on a 4m^2 trial PIC pad that was constructed at a low soil modulus site in Christchurch. Laboratory results of the engineering and durability properties are also presented which were undertaken with the respective AS/NZS standards. These test methods include: unconfined compressive strength (UCS) testing, breaking load testing, moisture content, ambient density, dry density, cold and boiling water absorption and hydraulic permeability. The testing also included cycles of soaking and drying PIC specimens in sodium chloride and sodium sulphate solutions. This was carried out to model PIC's resistance to salt attack, as well as degradation from chlorides and sulphates. A discussion of both the onsite and the laboratory performance of PIC is presented with useful observations that were carried out.

1 INTRODUCTION

Lightweight Aggregate Concretes (LWAC) are available in a wide range of densities, strengths and sizes (Chandra and Berntsson, 2002) and are used internationally for a wide variety of applications. Polystyrene Injected Concrete (PIC), a type of LWAC, consists of cement, water and aggregates, including lightweight recycled polystyrene (referred to as EPS). EPS is a low strength but lightweight material that provides lightweight properties to the PIC, while also recycling a material that cannot be disposed of due to its inability to break down. As a result, PIC has a lower compressive strength and modulus than standard concrete but has a lower density and higher modulus than common soils or engineered fills. These properties are considered advantageous for a number of applications.

Lightweight aggregate concretes (LWAC) have been utilised for applications that include:

- Lightweight precast panels for cladding applications; the thermal properties of EPS provide significant insulation performance
- Lightweight backfill for retaining structures; LWAC produce lower lateral earth pressures compared to normal soils
- Void filling applications e.g. decommissioning of underground storage tanks or filling underfloor voids
- Stabilisation of subgrades for roading applications
- Raft type shallow ground improvement under shallow foundations

While PIC has had limited use in New Zealand to date, it's utilisation as a shallow ground improvement method has begun to gain traction following the recent earthquake events (Canterbury and Kaikoura) that have impacted infrastructure significantly.

The design mixture used for testing utilised an 850 kg/m^3 mixture designed by Axis Policon Ltd. The testing carried out was commissioned by Axis Policon Ltd., in order to better understand the performance characteristics of their PIC Raft shallow ground improvement product.

2 ENGINEERING PROPERTIES – PIC SHALLOW GROUND IMPROVEMENT TRIAL

Testing was undertaken at a site in Christchurch to better understand the engineering properties and performance of PIC when utilised as a shallow ground improvement method. Testing was carried out firstly on the untreated subgrade material (Silt, non-plastic), to obtain the performance characteristics of the in-situ soil. Controlled construction of a 4m^2 PIC Raft (see Figure 1) was then carried out in order to allow testing of the strength and deformation characteristics of the PIC Raft and to gauge the level of "improvement" that had occurred at the site.

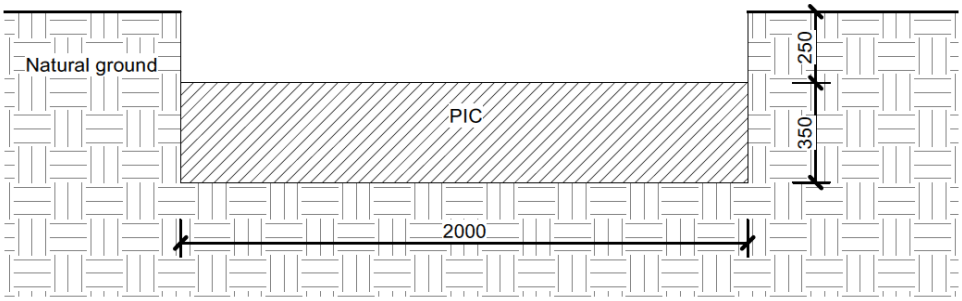

Figure 1: Schematic cross section of the 4m^2 trial PIC raft constructed for testing of the engineering properties of PIC when utilised as a shallow ground improvement method

The testing carried out involved the use of:
- Static Plate Load Testing (PLT)
- Light Weight Deflectometer (LWD) testing
- Unconfined Compressive Strength (UCS) testing

These tests were chosen to allow comparison of the pre and post static and dynamic performance of the treated areas and to gauge the increase in strength and stiffness of the PIC Raft over time.

For testing purposes, the stripped ground testing was carried out at 250mm below ground level (bgl) in order to gauge the in-situ soil strength and deformability. The proposed treatment area was then excavated to 600mm bgl before placing the 350mm PIC.

2.1 Static Plate Load Test (PLT)

Static PLT's were undertaken on both the stripped ground surface (250mm bgl) and the finished level of the PIC Raft following 28 days of curing. These tests were carried out to show the improvement in the static soil modulus (Ev) of the treated area following the addition of a 350mm thick PIC Raft ground improvement.

The testing was carried out using a 300mm diameter static plate load apparatus, the dimensions of which are consistent with foundation sizes utilised in NZS 3604. The test procedure followed the German standard for plate load testing (DIN 18 134), with digital acquisition of data, which involves loading the soil to 500 kPa in 7 increments whilst measuring the settlement of the plate, before unloading the soil in 3 increments. The soil is then reloaded in 5 increments to 450 kPa whilst measuring the settlement of the plate to obtain the reloading characteristics of the soil. The plate was placed having direct and full contact on the surface of the test area.

The use of the German standard for static PLT (DIN 18 134) was chosen to allow the calculation of static soil modulus ratios at the site. This allowed the initial static soil modulus (Ev1) and the compacted static soil modulus (Ev2) to be obtained and then compared. Ev1 essentially gives the in-situ static soil modulus while Ev2 gives the maximum static soil modulus that is able to be obtained by the soil following being loaded under 500 kPa of pressure. The modulus ratio therefore shows how close a soil is to being "acceptably compacted."

The static PLT's undertaken at the test site showed that the introduction of a 350mm thick PIC Raft as a shallow ground improvement method reduced the immediate static settlements experienced at the treated area under 500 kPa loading from 8.16mm to 0.20mm (97.5% reduction). As shown in Table 1 below, this was accompanied by an increase in the static soil modulus of the treated area from 14.15MPa to 561.47MPa (3970% increase).

Table 1: Soil modulus (E_v) values from static plate load tests for pre and post PIC Raft placement

	Ev1 (MPa)	Ev2 (MPa)	Ev2/Ev1
Stripped Ground Static Plate Load Test	14.15	37.06	2.62
28 Day Static Plate Load Test	561.47	839.89	1.5
Increase in Static Soil Modulus Following Placement of PIC Raft	3970%	2270%	

By substituting the 14.15MPa silt with the 350mm PIC Raft ground improvement, the modulus ratio of the site reduced from 2.62 to 1.50. The introduction of the PIC Raft at the site therefore significantly reduced the level of settlement that could be expected at the treated area under static loading.

2.2 Light Weight Deflectometer (LWD)

LWD tests, like the static PLT, were undertaken on both the stripped ground surface (250mm bgl) and the finished level of the PIC Raft following 28 days of curing. These tests were carried out to show the improvement in the dynamic soil modulus (Evd) of the treated area following the addition of a 350mm thick PIC Raft.

The testing was carried out using a 300mm diameter plate and LWD apparatus. The test procedure followed the ASTM E2835-11 standard which involves dynamically loading the soil to 100 kPa whilst measuring the settlement of the plate. This dynamic test is carried out three times before taking the average settlement of the plate under 100 kPa of dynamic loading. This then allows the

dynamic soil modulus to be obtained from the results measured. Figure 2 below shows an example of the LWD apparatus used for the dynamic soil modulus testing.

The LWD testing undertaken showed that the introduction of a 350mm thick PIC Raft increased the average dynamic soil modulus from approximately 26MPa to 185MPa (see Table 2). This is an increase of approximately 700% between pre and post improvement.

Table 2: Dynamic soil modulus (Evd) values from LWD tests for pre and post PIC Raft shallow ground improvement

	Evd (MPa)	Evd (MPa)
Stripped Ground Light Weight Deflectometer Test	27.21	25.45
28 Day Light Weight Deflectometer Test	190.68	178.57
Increase in Dynamic Modulus	701%	702%

Figure 2: LWD equipment in use on PIC Raft shallow ground improvement

2.3 Unconfined Compressive Strength (UCS)

UCS tests were undertaken on samples obtained from the PIC Raft at the test site. These tests were carried out at regular intervals during the curing of the PIC Raft to show the improvement in the UCS with time. The testing was limited to 28 days as this is the accepted curing time where concrete is expected to reach its maximum strength (>99%).

The testing was carried out using 100mm diameter and 200mm long core samples drilled from the test site after 7, 14 and 28 days of curing. The test procedure followed NZS 4402:1986, Test 6.3.1 and consisted of measuring the strain (change in length) of the core sample as it is loaded in the UCS apparatus. The samples are continually loaded until they "fail" (rupture) and the maximum stress exerted on the samples is recorded as the peak strength. Figure 3 below shows the peak UCS values for the different samples collected during the curing process.

As shown in Figure 3, the strength of the PIC raft is over 1.0 MPa after 7 days of curing. The strength of the PIC raft continues to increase until a peak measured strength of nearly 3.5 MPa after 28 days of curing. This shows a significant increase in strength of the PIC raft over 28 days to a maximum strength that is approximately 40% greater than the design strength of 2.5 MPa. The Young's modulus measured during the UCS testing also showed an increase from 912.6MPa after 7 days to 1516.5MPa after 28 days (66% increase).

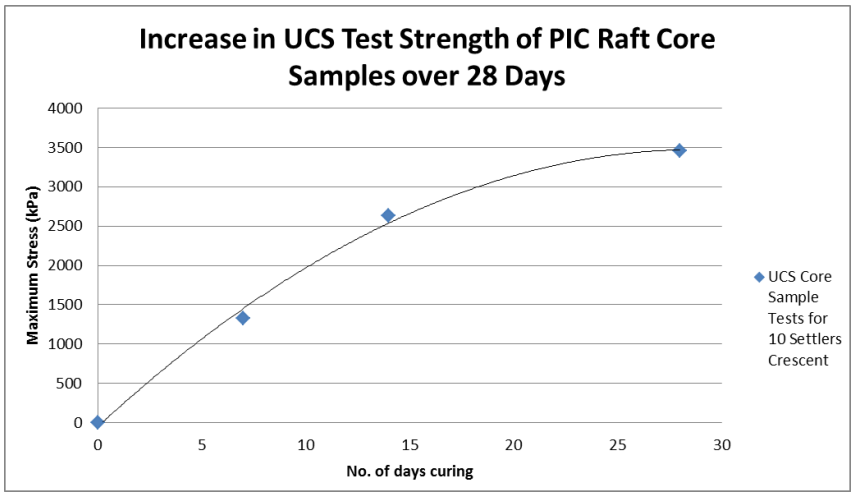

Figure 3: Development in unconfined compressive strength of PIC Raft over 28 days of curing

3 DURABILITY PROPERTIES OF PIC RAFT

For PIC Raft to comply with the requirements addressed in the New Zealand Building Code (NZBC), the design of the PIC Raft needs to consider:

- New Zealand Building code B1/VM4-Foundations
  - The strength of PIC must be such that it provides the required stability to a building
- New Zealand Building Code B2-Durability
  - Laboratory testing of PIC Raft properties and durability performance
  - Performance of materials similar to that of PIC Raft (i.e. concrete)
  - Any limitations to the use of PIC Raft that may cause it not to comply with the requirements of the NZBC

As the strength requirements were obtained during the onsite strength and stiffness testing regime, the durability assessment focused on the durability requirements as set out in the B2-Durability document of the NZBC. As outlined in B2 of the Building Code, the requirement to ensure structural stability of the building and the difficulty of access and replacement of the building element (PIC Raft) require PIC Raft to be durable enough for a 50 year design life.

The durability of standard concrete for structural use (i.e. concrete having a strength between 20MPa and 50MPa) is well covered and addressed in the NZS 3101 standard (2006). In this document, the durability depends on the exposure environment at the given geographic location within New Zealand. Following this, the required concrete mix is then designed accordingly. However, the durability of PIC is outside the scope of NZS 3101.

The intention of the durability assessment was to demonstrate that PIC complies with the NZBC requirements by proof of performance according to Verification Method B2/VM1 based on comparisons to the performance of similar materials (B2/VM1, 1.3 Similar Materials) and successful performance in a set of different laboratory tests (B2/VM1, 1.2 Laboratory Testing).

3.1 Durability Characteristics of Similar Materials

As per B2/VM1 (1.3, Similar materials), an assessment of PIC Raft was undertaken to draw comparisons to concrete. Concrete (as defined by NZS 3101-2006) is “a mixture of Portland cement or any other hydraulic cement, sand, coarse aggregate and water”. PIC Raft is a

lightweight concrete design, with the only change to the design of the PIC Raft material from standard concrete being the removal of some heavyweight aggregates and replacement with EPS. PIC Raft is therefore almost identical to concrete (as described by NZS 3101, 2006), with the only exception being the substitution of some coarse aggregates for lightweight EPS aggregates. Given this similarity, the performance of current concrete materials in New Zealand can be used as a guideline for the performance of PIC Raft.

The concrete mix used in the PIC Raft is supplied by well-established concrete suppliers in New Zealand who produce concrete mixes that comply with all the necessary standards.

Some of these standards include:

- NZS 3101:2006; Concrete Structures Standard
- NZS 3104:1991; Specification for Concrete Production
- NZS 3109:1997; Concrete Construction
- NZS 3111:1986; Methods of Test for Water and Aggregate for Concrete
- NZS 3112.1:1986; Specification for Methods of Test for Concrete; Tests relating to fresh concrete
- NZS 3112:1986; Specification for Methods of Test for Concrete

Due to this, the material can be assumed to have similar durability performance characteristics to that of standard concrete and other cement based materials (cement paste, grout etc.).

3.2 Laboratory Testing of PIC Raft Durability Properties

An assessment of PIC Raft's likely placement conditions found that it is likely to be subject to a number of degradation mechanisms throughout the design life of the material.

The degradation mechanisms that PIC Raft could be subjected to include:

- Sulphate and chloride attack (corrosive soils, chemical contamination, salt water etc.). This type of degradation would cause breakdown of the cementitious structure of the material over time.
- Salt attack (coastal/marine environments). This would cause cracking and spalling of the material under repeated cycles of saturation by a salt solution.
- Freeze/thaw degradation (cold environments, subjected to numerous freeze/thaw cycles). As with salt attack, this mechanism would cause cracking and spalling of the material under repeated freezing cycles.
- Petroleum based degradation of EPS. EPS is likely to undergo breakdown of the material if subjected to direct contact with petroleum based products. Durability from petroleum is not covered in this report as it is well documented internationally.

The test methods utilised were aimed at assessing the performance of PIC Raft when subjected to the likely mechanisms of degradation mentioned above. The test methods also assessed the properties of PIC Raft, to gauge the materials resistance to these types of degradation.

The type of tests undertaken, the results of the testing and the respective standards followed are presented in Figure 4.

PIC - Lightweight Concrete Raft

Durability Testing Summary

Properties	Typical Values	Units	Relevant Test Method
Density			
Dry Density	765	kg/m^3	AS/NZS 4456.8
Ambient Density	842.5	kg/m^3	AS/NZS 4456.8
Moisture Content			
As percentage of dry density	9.9	%	AS/NZS 4456.8
As percentage of ambient density	8.9	%	AS/NZS 4456.8
Water Absorption Properties			
Cold water immersion absorption	16.4	%	AS/NZS 4456.14
Boiling water immersion absorption	43.6	%	AS/NZS 4456.14
Permeability to Water			
Permeability	$1.39x10^{-8}$	m/s	AS/NZS 4456.16
Determining Resistance to Salt Attack			
Loss of mass after 40 cycles (Chloride)	0.06	g	AS/NZS 4456.10
Percentage loss of mass after 40 cycles (Chloride)	0.24	%	
Loss of mass after 40 cycles (Sulphate)	0.12	g	AS/NZS 4456.10
Percentage loss of mass after 40 cycles (Sulphate)	0.47	%	
Breaking Load			
Breaking load	2.7	kN	AS/NZS 4456.5

Figure 4: Summary of durability testing of PIC Raft samples

The resistance to salt attack test was chosen utilising both the sodium sulphate and sodium chloride methods in order to model the performance of the PIC Raft under sulphate, chloride and salt attack as well as freeze-thaw degradation mechanisms.

When comparing the results collected during the laboratory testing to the respective standard, it was found that the PIC Raft material performed well. All testing passed the requirements of the relevant standards and results indicated that PIC Raft can be assumed to meet the durability requirements for 50 year design life under ideal conditions, provided the limitations of the material are considered.

The limitations to application of PIC Raft can be considered as follows:

- Due the lightweight properties of the PIC Raft and the bulk density of the material (850 kg/m^3) being less than that of water (1000 kg/m^3), there is the potential for buoyancy effects to occur if PIC Raft is used under the water table or at a level where potential water table rise could impact the PIC Raft:
  - PIC Raft should be placed above the water table to remove the potential for buoyancy forces acting on the PIC Raft.
- Although PIC Raft performed well in the resistance to salt attack testing, one of the test samples showed minor spalling from the sodium sulphate solution testing. Given this:
  - It is recommended that pH testing be undertaken on suspicious sites to confirm that a low pH (acidic) soil is not present. If a low pH is encountered, sulphate testing of the soil should then be undertaken to assess the potential of sulphate attack at the site. If excessive sulphates are encountered, a Damp Proof Membrane (DPM) or similar material should be placed at the base of the excavation in order to isolate PIC Raft from contacting sulphate rich soils.
- Given EPS's poor durability when contacted with petroleum products or subjected to excessive and prolonged heat exposure (causing breakdown of the EPS material):
  - PIC Raft should not be utilised where there is potential for the material to come in contact with petroleum based products or be subjected to excessive and prolonged heat (i.e. fire).

4 CONCLUSIONS

Polystyrene Injected Concrete (PIC) Raft is used as a shallow ground improvement material under foundations where unfavourable soil conditions are encountered. PIC Raft essentially consists of cement, water and aggregates including lightweight recycled polystyrene (EPS).

By conducting in situ and laboratory tests, the engineering and durability properties of PIC have been assessed in order to better understand its performance as a shallow ground improvement method.

In situ static Plate Load Testing (PLT) and dynamic Lightweight Deflectometer (LWD) indicated that the introduction of a 350mm thick PIC raft under a 300mm wide plate (designed to replicate a typical NZS 3604 type foundation) producing a static stress of 500kPa and a dynamic stress of 100kPa:

- Reduced the immediate static settlement of the plate at the test site by 97.5%
- Increased the static soil modulus of the treated area from 14.15MPa to 561.47MPa
- Increased the average dynamic soil modulus of the treated area from approximately 26MPa to 185MPa

Laboratory UCS testing showed that the strength of the PIC raft continued to increase until a peak measured strength of nearly 3.5 MPa after 28 days of curing. The Young's modulus measured during the UCS testing also showed an increase from 912.6MPa after 7 days to 1516.5MPa after 28 days.

PIC Raft provides structural stability to a building and, being placed under a building's foundation, it is also difficult to replace. As per section B2 of the NZBC, this requires PIC Raft to be durable (i.e. not break down, degrade or lose strength etc.) for a period of 50 years.

Following assessment of PIC Raft's durability including laboratory testing, an assessment of similar materials and interpretation of the likely performance characteristics, PIC Raft was found to meet the durability requirements for 50 year design life under ideal conditions, subject to the following conditions of use:

- PIC Raft should be placed above the water table
- It is recommended that pH testing be undertaken on sites suspected to contain a low pH (acidic) soil, sulphate rich soil or any other suspicious soil chemistry
- PIC Raft should not be utilised where there is potential for the material to come in contact with petroleum based products or be subjected to excessive and prolonged heat (i.e. fire)

REFERENCES

American Society of Testing and Materials (ASTM) E2835-11 (2015). *Standard Test Method for Measuring Deflections using a Portable Impulse Plate Load Test Device*. West Conshohocken, PA, U.S.A.

Chandra, S. and Berntsson, L. (2002). *Lightweight Aggregate Concrete, Science, Technology and Applications.* Noyes Publications, New York, U.S.A.

DIN 18134 (2012). *Soil Testing Procedures and Testing Equipment –Plate load test.* English translation of DIN 18134:2012-04.

New Zealand Standard (2006). *Concrete Structures Standard NZS 3101:Part1:2006*. Standards Council, Wellington, New Zealand.

Estimation of the static vertical subgrade reaction modulus k_s from CPT for flexible shallow foundations on cohesionless soils

N Barounis
Cook Costello, Christchurch, New Zealand
nickbarounis@coco.co.nz (Corresponding author)

J Philpot
Cook Costello, Christchurch, New Zealand
johnnyp@coco.co.nz

Keywords: CPT, SPT, static vertical subgrade reaction modulus, flexible foundation, equivalent spring stiffness $K_{eq20\%}$, foundation influence depth, 20% rule, plate load test, Scott's method

ABSTRACT

In this paper, an integrated methodology is introduced for estimating the static vertical subgrade reaction modulus from CPT for shallow foundations on cohesionless soils. The proposed methodology relies on fundamental concepts of soil mechanics and foundation engineering applicable to flexible foundations. The methodology returns similar values to the SPT correlation proposed by Scott (Scott, 1981). As a result, it produces values that are in alignment with the traditional SPT approach. The proposed methodology can be used in conjunction with other methods for low risk projects. The methodology is applied to four sites in Christchurch, New Zealand and the results are assessed.

1 INTRODUCTION

As an initial step for facilitating the earthquake-resistant design of a building and its foundations, the static spring stiffness, or static vertical subgrade reaction modulus, on the surface of an assumed homogeneous half-space is typically evaluated for the given site. Then, by applying numerous dynamic modification factors to the static spring stiffness (ASCE, 41-13 or Gazetas, 1991), the dynamic spring stiffness can be evaluated. Dynamic modification factors are applied to account for the frequency of the excitation force, the embedment of the foundation and the foundation shape. The most fundamental step in this process for the structural engineer, is to determine if the foundation system under analysis is rigid or flexible. Many references are available for facilitating this step (refer to ASCE 41-13, 2014 or ACI 336). Thus, the estimation of the static spring stiffness is an important step in undertaking both static and earthquake resistant design of foundations. This paper is focused only on the static spring stiffness of flexible foundation systems.
The static vertical subgrade reaction modulus k_s is a conceptual relationship, which is defined as the soil pressure exerted σ divided by the deflection δ (Bowles, 1997).

$$k_s = \sigma / \delta \tag{1}$$

The static vertical subgrade reaction modulus is not an actual engineering property of the soil, such as Poisson's ratio, as it varies with the width and shape of the foundation (Terzaghi, 1955). The principle underlying the definition of k_s is the resistance a soil layer provides as some deflection is imposed to it due to the applied stress, analogous to a spring shortening at some imposed load. In structural engineering applications, k_s is used to model the soil stiffness in the vertical plane when soil-foundation-structure interaction considerations are included in the structural analysis. Typically, as best practice suggests, structural engineers adopt k_s values

recommended by a geotechnical engineer. The structural engineer further tests the sensitivity of the model for k_s values ranging between 0.5 k_s and 2.0 k_s (ACI 336, 2002). The geotechnical engineer needs to assess the k_s range for the particular situation. These values are also to be accompanied by ultimate foundation capacity estimations.

A methodology for the estimation of k_s for sands from the Cone Penetration Test (CPT), as an alternative to the conventional correlation to plate load test from the SPT, was proposed by Barounis et al. in 2013. From recent research on the applicability of the method (Barounis and Armaos, 2016), it was demonstrated that the k_s values produced by the proposed CPT method are stiffer than the values produced from the conventional SPT method proposed by Scott (Scott, 1981). The stiffer springs from CPT are conservative for the seismic response of the structure, while the softer springs from SPT are conservative for foundation deformation and their effects to the superstructure.

This paper presents an integrated methodology for the estimation of k_s values for flexible shallow foundations on cohesionless soils. The methodology produces similar values to the SPT method proposed by Scott for the k_1 of a 300mm plate. The final foundation value K_F is similar to the value produced by conventional SPT methods.

For a detailed explanation of the background theory to the method, please refer to previous papers from Barounis et al. (2013, 2015, 2016 and 2017) on this topic.

2 INTEGRATED METHODOLOGY FOR ESTIMATING THE MODULUS OF SUBGRADE REACTION K_S

2.1 Fundamental assumptions, advantages and theoretical basis of the methodology

The fundamental assumptions and theoretical basis for the proposed methodology and its advantages are the following:

- The method is applicable to cohesionless soils, only when tested with a CPT that measures penetration resistance at 10 or 20mm increments with a 35.7mm diameter cone.
- The theory of springs in series is assumed, modified to consider the configuration of soil layers. This means that the equivalent spring stiffness K_{eq} can be estimated by using the proposed methodology.
- The range of SPT N_{60} values is limited to between 0 and 50 blows. No extrapolation over 50 blows shall be adopted in any case. Thus, an SPT N_{60} of 50 is considered to be effective refusal.
- This upper bound value of SPT produces a maximum $K_{SPT(0.3)}$ value of 90MN/m^3. Thus, any k_s values produced using this method for the actual foundation cannot exceed 90MN/m^3.
- If values larger than 90MN/m^3 need to be adopted, either for the 300mm plate, or for the actual foundation, then actual plate load tests and further site investigations will need to be performed to prove that the subgrade modulus exceeds this value.
- The corresponding q_c value of any soil with I_c between 1.00 and 2.60 is related to SPT N_{60} according to the correlation by Jefferies and Davies, as shown in Figure 8. This figure shows that for increasing I_c values (increasing fines content) at effective SPT refusal, the corresponding q_c value reduces from 33.6MPa for I_c=1.00 to 18.7MPa for I_c=2.60. As the fines content increases and for a given N_{60} value, the cone resistance and the spring stiffness reduces, along with the soil stiffness E_s (refer Figure 8).

- The method is applicable for circular, square, continuous or rectangular shallow foundations, founded at any shallow depth in the ground including at the ground surface. The equivalent modulus K_{eq} for any foundation shape is estimated based on the simplified formulae provided by Poulos and Davies (Xiao, 2015) that computes the vertical stress distribution beneath the centre of the foundation.
- By using the Poulos and Davies (Xiao, 2015) formulae, essentially a weighting factor is applied to every 10mm or 20mm long spring. Hence, the soils nearer the foundation become more critical to the overall response than the soils substantially deeper, or outside the pressure bulb of the foundation.
- The method considers an influence depth under any foundation configuration to be the depth at which the vertical stress increase from the foundation becomes equal to 20% of the vertical effective stress (20% rule).
- The method is sensitive to stiffness inversions, i.e. very dense soils overlying very loose soils. The methodology is also sensitive when denser soils are present at some depth from the foundation (within the 20% influence depth). In general, the methodology produces good results, even for highly stratified soils or for sandwiched layers of contrasting stiffness.

The methodology is presented in Table 1. Detailed explanations for each step of the methodology are given in the subsequent paragraphs.

Table 1: Methodology for estimating the spring stiffness of flexible foundations from CPT

Step #	Equation	Units	Notes
1	For 10mm increment: $K_{CPT}=100q_c$ For 20mm increment: $K_{CPT}=50q_c$	MN/m^3	CPT spring stiffness
2	$K_{CPT\ (0.3)}=0.119K_{CPT}$	MN/m^3	Conversion to 300mm plate spring stiffness
3	$K_{CPT\ (SPT0.3)}= K_{CPT(0.3)} / CF$ where for 10mm increment: $CF=5.67-1.23Ic$ and for 20mm increment: $CF=2.83-0.61Ic$	MN/m^3	Conversion to a similar SPT spring stiffness for a 300mm plate as per Scott's correlation, $K_{SPT\ (0.3)}=1.8N_{60}$
4	$K_{eq20\%} = \frac{\sum_{i=1}^{n} Iz_i K_i}{\sum_{i=1}^{n} Iz_i}$	MN/m^3	Equivalent spring stiffness for a 300mm plate considering an influence depth as per the 20% rule that corresponds to the foundation geometry under analysis
5	$K_F=K_{eq}$ x $(m+0.5)/(1.5m)$ where m = L/B	MN/m^3	Shape correction for the given foundation geometry under analysis

2.1.1 1st Step: Estimation of K_{CPT} stiffness

In this first step, the spring stiffness of the 10mm long soil element is estimated. As per equation 1, the spring stiffness is the cone resistance q_c divided by the displacement. For a CPT with 35.7mm diameter and a 10mm incremental penetration:

$$K_{CPT}=100q_c[MN/m^3] \quad (2)$$

This conversion is applied for every q_c measurement until the final CPT depth.

2.1.2 2nd Step: Estimation of the 300mm plate by conversion from Step 1

In this step, a conversion takes place from the CPT spring to the equivalent 300mm diameter plate spring. This is undertaken according to the formula proposed by ACI (ACI 336, 2002) and Bowles (Bowles, 1997), which relies on principles earlier presented by Terzaghi (1955):

$$K_{CPT(0.3)}=K_{CPT}x(D_{CPT}/300)=K_{CPT}x(35.7/300)=0.119K_{CPT} \quad (3)$$

This is consistent with the subgrade reaction modulus theory as a greater loaded area produces lower subgrade reaction values (Terzaghi, 1955 and Bowles, 1997).

2.1.3 3rd Step: Conversion to a similar SPT spring stiffness value depending on I_c by means of CF

Jefferies and Davies (1993) have linked the relationship between q_c and SPT N_{60} with the soil behaviour type index I_c. The I_c is defined by Robertson and Wride (Robertson, 2015). The relation is the following:

$$\frac{\frac{qt}{pa}}{N60}=8.5\left(1-\frac{I_c}{4.6}\right) \quad (4)$$

Where $q_t=q_c$ for cohesionless soils and p_a=atmospheric pressure.

By substituting I_c values between 1.00 and 2.60 that correspond to the range of cohesionless soils, p_a of 101kPa, and SPT N_{60} from 0 to 50 as per the assumptions in section 2.1, the relation is depicted in Figure 8.

By dividing the $K_{CPT(0.3)}$ with $K_{SPT(0.3)}$, the stiffness ratio of the CPT spring for the 300mm plate is compared to the SPT spring for the same 300mm plate. We can define this ratio as the Conversion Factor CF:

$$CF=\frac{KCPT(0.3)}{KSPT(0.3)}=\frac{100\ qc\ 0.119}{1.8\ N60}=\frac{11.9\ qc}{1.8\ N60}=6.61\frac{qc}{N60} \quad (5)$$

and by solving equation (4) for q_c and substituting in (5) we have:

$$CF=\frac{KCPT(0.3)}{KSPT(0.3)}=6.61\frac{qc}{N60}=\frac{6.61\ 8.5\left(1-\frac{Ic}{4.6}\right)\ N60\ 0.101}{N60}\approx 5.67-1.23I_c \quad (6)$$

Similarly, for a 20mm increment:

$$CF=2.83-0.61I_c \quad (7)$$

This means that CF is dependent on I_c. If we apply the CF to the $K_{CPT(0.3)}$, then it returns similar spring stiffness for a 300mm plate diameter according to Scott (1981). By using the symbol $K_{CPT(SPT0.3)}$ for the SPT spring stiffness produced by the CPT approach, the equation becomes:

$$K_{CPT(SPT0.3)}=\frac{KCPT(0.3)}{CF} \quad (8)$$

The value of CF can be taken from equations 6 or 7 depending on the increment used.

2.1.4 4th Step: Equivalent spring stiffness $\underline{K_{eq}}$ for a 300mm plate

The general theory of springs suggests that the equivalent spring stiffness K_{eq} of an infinite chain of springs is given by the formula:

$$K_{eq}=\frac{k1\ k2\ k3.....ki}{k1+k2+k3+\cdots ki}=\frac{\prod_{k=1}^{i} k}{\sum_{k=1}^{i} k} \quad (9)$$

It must be recognised that equation 9 is insensitive to the configuration of soil layers. In other words, the equivalent spring stiffness would return the same value regardless of the sequence with which the soil layers are configured. The assumptions underlying this formula maybe appropriate to be used in structural mechanics; however, it does not accurately capture the soil and foundation behaviour, especially when looser soils are located near the foundation level, or when very dense soils are located at some depth below the foundation, but within the 20% influence bulb. Also, from a numerical perspective, it is impossible for common software to compute the product of 100 individual springs per 1m of CPT. For these reasons, it is proposed to model and capture any layer configuration by using the Boussinesq theory in accordance with the simplified formulae proposed by Poulos and Davies (1974) as presented in Xiao (Xiao, 2015). In essence, the Boussinesq method is used to apply a weighting factor to every K_{CPT} spring within the influence bulb of the foundation. As depth increases, the associated spring stiffness value becomes less significant for the foundation behaviour. Thus, denser deeper soils may not provide substantial stiffness to the foundation, or looser deeper soils may soften the spring substantially. The weighting factor is the well-known influence factor I_z, which takes the value of 1.0 at the foundation depth and diminishes to values that tend to zero with increasing depth.
The proposed formula has the following form:

$$K_{eq20\%}=\frac{\sum_{i=1}^{n} Iz_i K_i}{\sum_{i=1}^{n} Iz_i} \quad (10)$$

Where Iz_i is the influence factor that corresponds to a spring stiffness K_i at depth z_i as per the following equations (Xiao, 2015):

Circular foundation: $\Delta\sigma z= (q-\sigma'_0)\ Iz_i = (q-\sigma'_0)\ [1-(\frac{1}{1+\left(\frac{B}{2z}\right)^2})^{1.50}]$ (11)

Square foundation: $\Delta\sigma z = (q-\sigma'_0)\ Iz_i = (q-\sigma'_0)\ [1-(\frac{1}{1+(\frac{B}{2z})^2})^{1.76}]$ (12)

Continuous foundation: $\Delta\sigma z = (q-\sigma'_0)\ Iz_i = (q-\sigma'_0)\ [1-(\frac{1}{1+(\frac{B}{2z})^2})^{2.60}]$ (13)

Rectangular foundation: $\Delta\sigma z = (q-\sigma'_0)\ Iz_i = (q-\sigma'_0)\ [1-(\frac{1}{1+(\frac{B}{2z})^{\left(1.38+\frac{0.62B}{L}\right)}})^{2.60-0.84B/L}]$ (14)

where B, L and z are respectively the width, length and depth below the foundation in metres, and $(q-\sigma'_0)$ is the net applied foundation pressure in kPa. Equation 10 is applied to the depth z at which the stress increase from the net applied pressure equals 20% of the vertical effective stress.

2.1.5 5th Step: Correction for shape of foundation

In this step, the final foundation spring stiffness value K_F is estimated. From the four previous steps, a similar spring stiffness value to the SPT approach has been established. The application of a correction factor for the shape of the foundation with length L and breadth B will also result in a similar corrected spring as for the SPT approach. The shape correction factors are presented in Table 2. The K_F is determined from the equation:

$$K_F=S_F\,K_{eq20\%} \quad (15)$$

Table 2: Shape correction factors for actual foundation shapes

Foundation shape	Shape correction factor, S_F
Circular	1.0
Continuous	$(m+0.5)/(1.5m)$, m=L/B, tends to 0.67 when L/B≥5
Square	1.0
Rectangular	$(m+0.5)/(1.5m)$, m=L/B

3 EXAMPLE CALCULATIONS: FOUR SANDY SITES IN CHRISTCHURCH

The proposed methodology has been applied on four different sandy sites in Christchurch, New Zealand. The foundation shape, dimensions, applied pressures and other key information are presented in Table 3.

Table 3: Foundation shape dimensions and applied pressures

Site	Foundation Shape	Length (m)	Breadth (m)	Depth (m)	Applied Pressure (kPa)	GWT Depth (m)	Influence Depth {20% Rule} (m)
1	Rectangular	10	5	0	50	0.6	5.16
2	Continuous	10	2	0	50	1.0	3.02
3	Square	5	5	0	50	1.2	3.44
4	Circular	N/A	5	0	50	1.0	3.36

The SBTn plots for all four sites are shown in Figures 1-4 below.

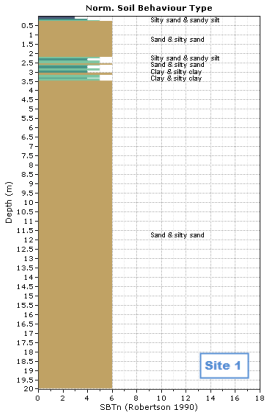

Figure 1: SBTn Site 1 – Rectangular

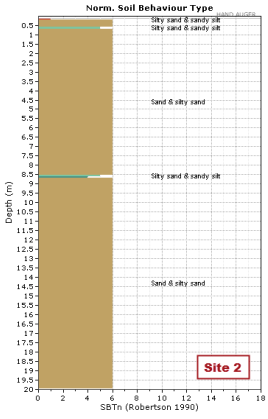

Figure 2: SBTn Site 2 – Continuous

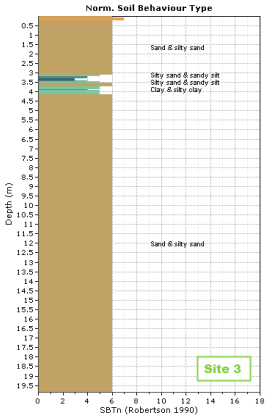

Figure 3: SBTn Site 3 – Square

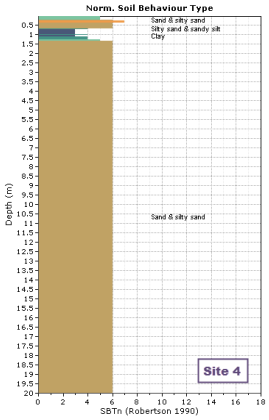

Figure 4: SBTn Site 4 – Circular

The summary of results from the proposed method is presented in Figures 5-7.

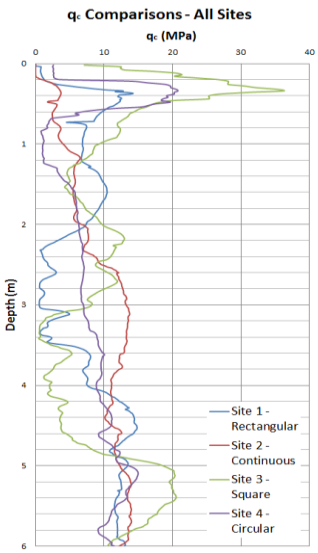

Figure 5: Comparison of q_c across all four sites

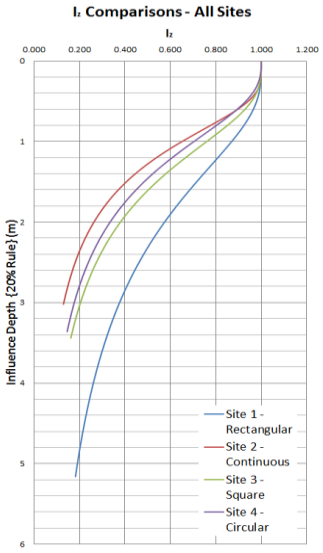

Figure 6: Comparison of influence depths (20% rule) across all four sites

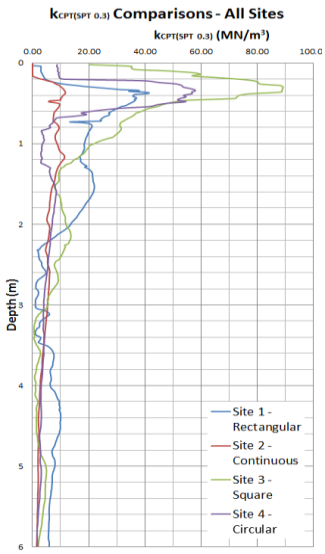

Figure 7: Comparison of $K_{CPT\ (SPT\ 0.3)}$ values across all four sites

The results of the proposed methodology for the four sites and their agreement with Scott's approach are presented in Table 4. The bar above the N_{60} and q_c values in Table 4 indicates that these are depth weighted values as per Poulos and Davies (1974). These values are equivalent N_{60} and q_c for the influenced soil layers as a whole. These are also plotted in Figure 8 indicating the values are consistent with the soil types encountered at all four sites.

Table 4: Results of the proposed methodologies for four sites in Christchurch

Site	$K_{eq,\ 20\%}$ (MN/m³)	K_F (MN/m³)	$\overline{N}_{60}$	$\overline{q}_c$ (MPa)	$\frac{\overline{q}_c}{\overline{N}_{60}}$	$K_{eq,\ Scott}$ (MN/m³)	$K_{F,\ Scott}$ (MN/m³)
1	21.44	17.86	12	6.84	0.57	21.44	17.87
2	13.60	9.97	8	4.21	0.56	13.60	9.97
3	39.09	39.09	22	13.01	0.60	39.09	39.09
4	21.68	21.68	12	6.89	0.57	21.69	21.69

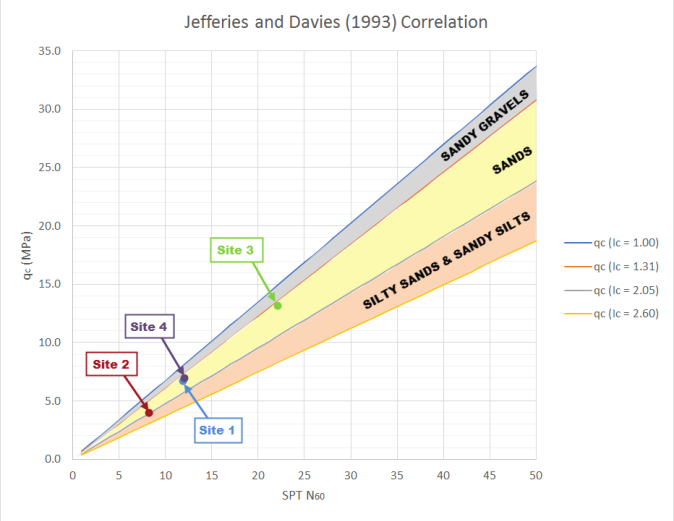

Figure 8: Relation between q_c and N_{60} for I_c between 1.00 and 2.60 with depth weighted values plotted for all four sites

4 CONCLUSIONS

An integrated method for the estimation of static spring stiffness from CPT has been presented for flexible shallow foundations on cohesionless soils. The method can be applied to estimate the equivalent spring stiffness $K_{eq20\%}$ for a flexible shallow foundation and then subsequently estimate the K_F value for the actual foundation size and shape. The method can only be applied for SPT values ranging from 0 to 50, corresponding to a q_c that depends on I_c. For facilitating a Winkler foundation type of analysis applicable to flexible foundation systems, ultimate foundation capacity estimations also need to be undertaken by a geotechnical engineer as per well-established available methodologies. The methodology is expected to return similar values, in alignment with the SPT approach as per Scott (1981). However, more research, that includes sensitivity analysis for the proposed methodology, needs to be undertaken to verify the method returns reliable spring values for all possible soil configurations. For assessing K_F, one should not rely on one method. A number of methods should be applied, of which this could be one.

REFERENCES

ACI Committee 336 (2002) *Suggested Design Procedures for Combined Footings and Mats*. Detroit: American Concrete Institute.

ASCE Standard ASCE/SEI 41-13 (2014) *Seismic Evaluation and Retrofit of Existing Buildings*. American Society of Civil Engineers.

Barounis, N. and Armaos, P. (2016) Sensitivity analysis of the vertical modulus of subgrade reaction, as estimated from CPT for the design of foundations and for comparison with values from SPT for a site in Christchurch. *NZSEE 2016 Conference, Reducing Risk-Raising Resilience*, 1-3 April 2016, Christchurch, New Zealand.

Barounis, N. and McMahon, P. (2015) Estimation of vertical subgrade reaction modulus for sands from CPT investigations. *16th European Conference of Soil Mechanics and Geotechnical Engineering*, 13-17 September 2015. Edinburgh: UK.

Barounis, N., Saul, G., Lally, D. (2013) Estimation of vertical subgrade reaction coefficient from CPT investigations: applications in Christchurch. *Proceedings 19th NZGS Geotechnical Symposium*, 2013, Queenstown.

Barounis, N. and Philpot, J. (2017) Estimation of the vertical subgrade reaction modulus k_s from CPT for shallow foundations on cohesionless soils. *NZSEE 2017 Conference, Next Generation of Low Damage and Resilient Structures*, 27-29 April, Wellington, New Zealand.

Bowles, J.E. (1997) *Foundation analysis and design*, 5th Edition. New York: McGraw-Hill.

Gazetas G. (1991) Formulas and charts for impedances of surface and embedded foundations. *Journal of Geotechnical Engineering*, ASCE, 113(5), 458-475.

Poulos, H.G and Davis, E.H. (1974) *Elastic solutions for soil and rock mechanics.* John Wiley, New York.

Robertson, P. K. and Cabal, K.L. (2015) *Guide to cone penetration testing, 6th Edition*. Gregg Drilling.

Scott, R.F. (1981) *Foundation analysis*. Prentice Hall, Englewood Cliffs, NJ.

Terzaghi, K. (1955) Evaluation of Coefficients of Subgrade Reaction. *Geotechnique*, Volume 5, Issue 4, 01 December 1955, pages 297-326.

Xiao, M. (2015) *Geotechnical Engineering Design*. John Wiley and Sons, Ltd., UK.

Estimation of in-situ water content, void ratio, dry unit weight and porosity using CPT for saturated sands

N Barounis
Cook Costello, Christchurch, New Zealand
nickbarounis@coco.co.nz (Corresponding author)

J Philpot
Cook Costello, Christchurch, New Zealand
johnnyp@coco.co.nz

Keywords: CPT, bulk unit weight, specific gravity, water content, void ratio, dry unit weight, porosity, sands, saturation, ground water level

ABSTRACT

The CPT is used extensively for site characterization, soil profiling, determination of groundwater conditions and the estimation of geotechnical parameters. The geotechnical parameters that can be estimated by using the CPT include bulk unit weight, shear strength and stiffness, among many others. Best practice suggests the CPT is to be used in combination with laboratory testing, when the budget and timeframes allow for such testing to be undertaken. For typical structures of Importance Level 2, such testing is not undertaken due to a restricted budget. Typical soil classification tests, such as water content, bulk unit weight, sieve analysis and plasticity index, are not commonly performed for such projects. However, such tests are considered to be essential for the geotechnical engineer, who typically needs to adopt a number of parameters, relying solely on CPT information. Important parameters, that are often overlooked, are the water content, void ratio, dry unit weight and porosity. These parameters are important for characterizing the soil behavior, in both static and dynamic conditions.

This paper proposes a methodology for estimating the in-situ water content, void ratio, dry unit weight and porosity from CPT for saturated sandy soils. The methodology involves published work on estimating unit weight from CPT by Robertson (2010), combined with concepts of fundamental soil mechanics. The proposed methodology is applied on a predominantly sandy site in Christchurch, New Zealand and compared against laboratory results for the same site. Comments and conclusions are made on the usefulness and applicability of the proposed methodology along with recommendations for future applications.

1 INTRODUCTION

The CPT is a well-established strain-controlled undrained failure test that is typically performed by pushing a 35.7 mm diameter penetrometer, with a conical tip and an apex angle of 60°, vertically into the ground at a penetration rate of approximately 20 mm/s. The tip resistance stress of the cone q_c and the sleeve friction resistance f_s (both in MPa), are recorded versus the testing depth. Typically, q_c is recorded against an incremental penetration of 10 mm. Other cone sizes and geometries are also available for pushing through dense gravels and deep soils.

The CPT is used extensively for delineating soil stratigraphy and estimating geotechnical parameters including bulk unit weight, relative density, cohesion, angle of friction and shear modulus (Robertson, 2015) for a wide range of soils. The correlations for geotechnical parameters from CPT are semi-empirical and vary in both reliability and applicability (Robertson, 2015). CPT is also a well-established test for evaluating the liquefaction potential (Robertson, 2015).

This paper presents an alternative method for estimating water content, void ratio, dry unit weight and porosity based on the well-established correlation by Robertson (2010). Based on this correlation, the bulk unit weight (γ) of each soil layer is estimated depending on the recorded q_t (cone resistance corrected for pore water effects) and f_s.

The correlation for the bulk unit weight is expressed by the following equation (Robertson, 2010):

$$\gamma/\gamma_w = 0.27\ [\log R_f] + 0.36\ [\log(q_t/p_a)] + 1.236 \quad (1)$$

R_f = friction ratio = (f_s/q_t) 100 %
γ_w = unit weight of water, in same units as γ (kN/m^3)
p_a = atmospheric pressure, in same units as q_t (MPa or kPa)

Prediction of the soil behaviour is achieved by means of the normalised Soil Behaviour Type (SBTn) (Robertson, 2015) for soils ranging from clays and silts to sands and gravels. Thus, a soil profile to the final testing depth can be inferred, accompanied by the corresponding unit weight. This procedure enables the geotechnical engineer to produce a continuous estimate of the total overburden stress. By delineating the location of the groundwater table, effective overburden stress can be also estimated.
In the absence of laboratory test results for any given project, the water content, void ratio, dry unit weight and porosity are four important parameters that are usually overlooked. These parameters are important for characterizing the soil behavior, in both static and dynamic conditions.
In this paper, a simple methodology is proposed for estimating the in-situ water content, void ratio, dry unit weight and porosity from CPT. The theoretical background, limitations and advantages of the proposed methodology are discussed in the next paragraphs.

2 THEORETICAL BACKGROUND OF THE PROPOSED METHOD

2.1 Soil phase relationships and limitations

The proposed method has the following important limitations:

- It is only applicable for inorganic soils: clays, silts, sands, gravels and their mixtures, for which the G_s values can be reliably assumed, or determined. Organic soils, fill material and peats are excluded from applying the proposed method. Typical SBT_n values that the method may be applicable to vary between 3 and 9 (as per Robertson, 2015).
- It is only applicable for saturated soils below groundwater level, or in other words when the saturation degree S_r equals 1. This is an assumption, as there may be a zone of partial saturation immediately below the water table where the saturation degree may be slightly below 100%; however, this assumption is considered to be appropriate for use in a simplified analysis. For the method to return reliable results, the location of the groundwater level needs to be determined at any given site during testing. Best practice suggests the groundwater level to be measured by the CPT (u2 pore pressure or dissipation tests) and/or by water level observation in boreholes, wells or standpipes. Where the budget allows, P-wave geophysical methods could be incorporated to more accurately locate the depth at which full saturation occurs and make the applicability of the proposed method more reliable. The method shall not be applied to soils located above the ground water level.
- This paper applies the proposed method to a sandy site due to the relatively high level of confidence in the assumed G_s value of 2.65 for sands. The method may be extended to other inorganic soils; however, it is recommended that the assumptions underlying the method are calibrated for different inorganic soil types. The intention is to undertake further research for the methodology to be extended to include saturated inorganic fine-

grained soils at a later stage. The supporting theory of the proposed method is based on classical soil mechanics (Bowles, 1997).

For any inorganic soil, there are five parameters that need to be determined (e, w, G_s, S_r, γ). From these five parameters, G_s can be assumed (or determined in the laboratory), and S_r is known to be equal to 1 below a certain depth, as explained above when the soil is saturated. The bulk unit weight γ can be estimated by the correlation shown in equation 1 by Robertson. Thus, there are only two unknowns to be determined: w and e.
The water content w (%), saturation degree S_r, void ratio e and the specific gravity G_s of the soil solids are interrelated by the following relationship:

$$e = \frac{w\, G_s}{S_r} \tag{2}$$

which, for saturated conditions (S_r=1), simplifies to:

$$e = w\, G_s \tag{3}$$

A G_s value of 2.65 is typically assumed for sandy soils.
For determining w and e, another relationship needs to be developed in conjunction with equation (3). Equation (4) relates the void ratio e with the dry unit weight and specific gravity:

$$e = \frac{G_s\, \gamma_w}{\gamma_d} - 1 \tag{4}$$

Where, γ_w = unit weight of water (9.81 kN/m^3).
For any inorganic soil, the relationship between dry unit weight γ_d (kN/m^3), the water content and its bulk unit weight γ (kN/m^3) is defined by equation (5):

$$\gamma_d = \frac{\gamma}{1+w} \tag{5}$$

By combining equations (3), (4) and (5), the following relationship is determined:

$$w\, Gs = \frac{Gs\, \gamma_w}{\left(\frac{\gamma}{1+w}\right)} - 1 \tag{6}$$

In equation (6), the only unknown is the water content w. In essence, equation (6) requires that the left hand side, which expresses the full saturation of the soil, must be in equilibrium with the right hand side, which expresses the water content-bulk unit weight relationship when G_s is known. The solution for the water content at saturation (Sr=1) then is:

$$w = \frac{Gs\, \gamma_w - \gamma}{Gs\, \gamma - Gs\, \gamma_w} \tag{7}$$

Thus, for a known γ, obtained from CPT, and an appropriate assumed (or determined) value for G_s, depending on the soil type, there is a unique value for the water content w that satisfies equation (7). The void ratio and dry unit weight can then be derived from equations (3) and (5), respectively.
The porosity n can subsequently be estimated with the following relationship:

$$n = \frac{e}{1+e} \tag{8}$$

The method is summarised in three steps in Figure 1.

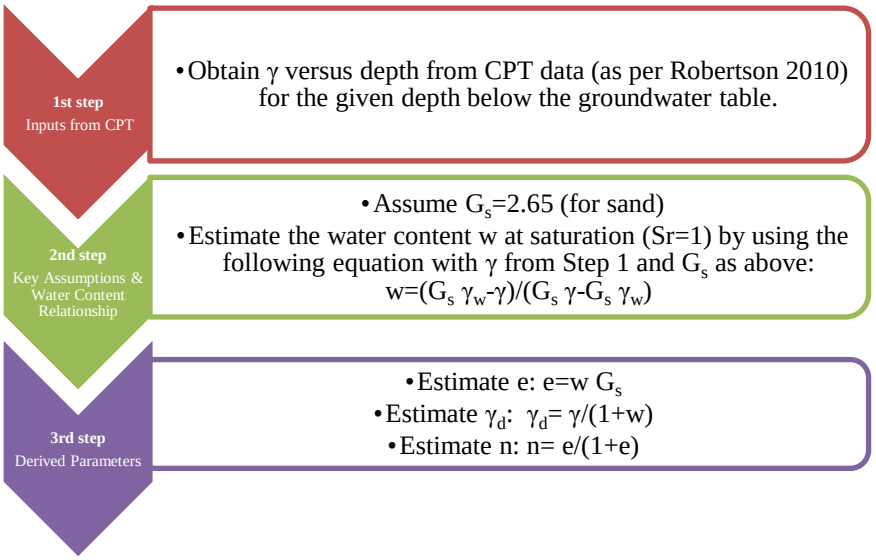

Figure 1: Summary of proposed methodology for sands estimating w, e, γ_d and n

2.2 Advantages of the proposed method

The proposed method is simple and can be implemented for projects where there is a relatively shallow water table and the G_s values can be reliably assumed (or determined), particularly when laboratory tests are not included in the scope of the site investigations due to cost constraints. Where there is available budget for laboratory tests, the results from the proposed method can be checked against the laboratory results. The method can delineate against depth w, e, γ_d and n, and produce graphs similar to those shown in Figures 2-7, presented in Section 4 of this paper. The graphs for each of the estimated parameters begin at the depth where the groundwater surface was inferred at the given site.

3 TYPICAL VALUES FOR DIFFERENT TYPES OF SANDY SOIL

Typical values (Das, 2004) for water content, void ratio and dry unit weight for some cohesionless soils are presented in Table 1.

Table 1: Typical water content, void ratio and dry unit weight values for some cohesionless soils

Type of soil	Void ratio, e	Water content (%), w	Dry unit weight, γ_d (kN/m^3)
Loose uniform sand	0.80	30	14.5
Dense uniform sand	0.45	16	18.0
Loose angular-grained silty sand	0.65	25	16.0
Dense angular-grained silty sand	0.40	15	19.0

4 APPLICATION FOR A CHRISTCHURCH SITE WITH SANDY SOILS

For applying the proposed methodology, a CPT was downloaded from the New Zealand Geotechnical Database. Key requirements for selecting the CPT were that:

- The site was known to have a relatively shallow groundwater table;
- The testing was undertaken on a sandy site in Christchurch, New Zealand;
- The CPT was undertaken in close proximity to a borehole, where soil samples have been taken to the laboratory to evaluate the water content;
- The number of soil samples taken at the site was adequate to compare the proposed CPT method and the laboratory testing and to draw some conclusions on the applicability of the method.

For simplicity, a specific gravity G_s of 2.65 was adopted throughout the entire depth of the CPT, as the soil profile is predominantly sands and silty sands between 4.4 to 19.5m depth. This may not be an appropriate assumption for some of the fine-grained soil layers in the upper 4.4m of the soil profile. The GWT depth was estimated to be 3m below ground level. Six graphs have been presented:

- q_c versus depth
- Normalised SBTn versus depth
- Water content versus depth, showing the comparison between CPT method and laboratory testing
- Void ratio versus depth
- Bulk and dry unit weights versus depth
- Porosity versus depth

4.1 Borehole and sampling results

A summary of borehole and laboratory testing results are presented in Tables 2 and 3.

Table 2: Borehole summary

Depth (m)	Soil description	Representative SPT N values
0.0 – 2.6	Sandy GRAVEL (no recovery between 0.2-2.0m)	22
2.6 – 4.4	SILT	4
4.4 – 5.0	Silty SAND	20
5.0 – 19.5	SAND	13-29 (Avg. = 22)
19.5 – 20.0	SILT	14

Table 3: Laboratory results summary (for sandy soils)

Depth (m)	Fines content passing 75μm (%)	Water content (%)
6.0	5.69	23.0
9.0	5.81	25.6
12.0	6.22	24.2
15.0	4.95	22.4

4.2 CPT results

CPT results and estimated parameters from the proposed methodology are presented in Figures 2-7 below.

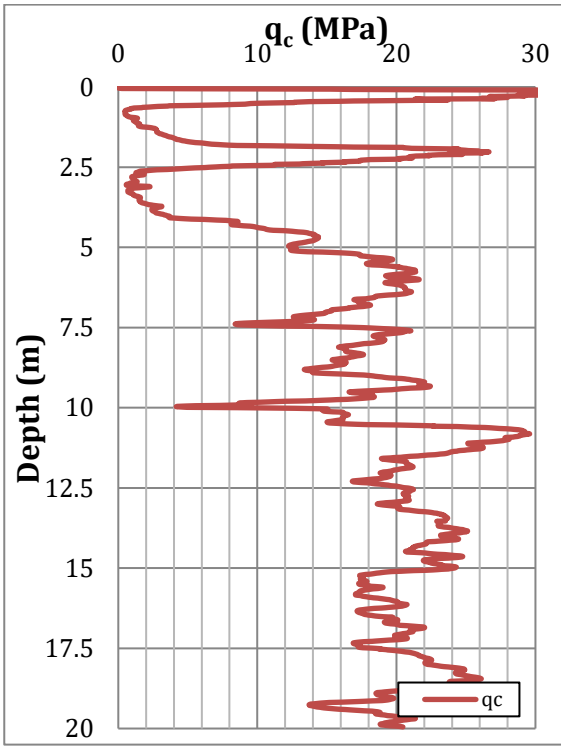

Figure 2: q_c plot

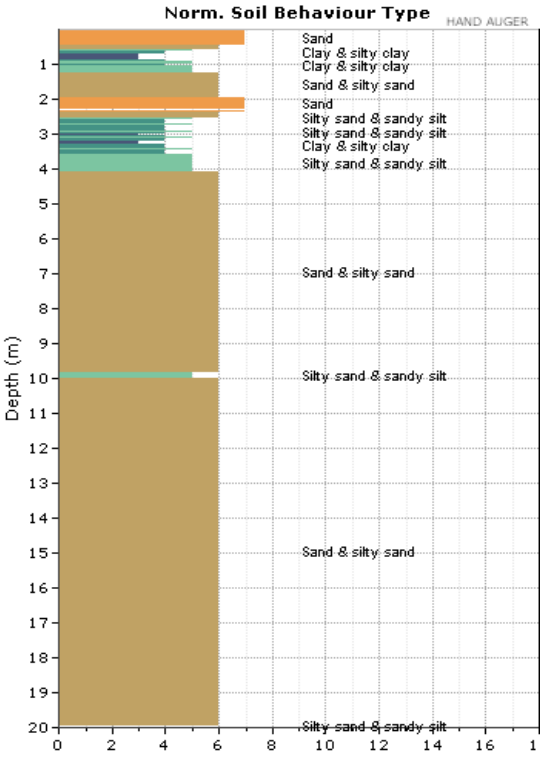

Figure 3: SBTn plot

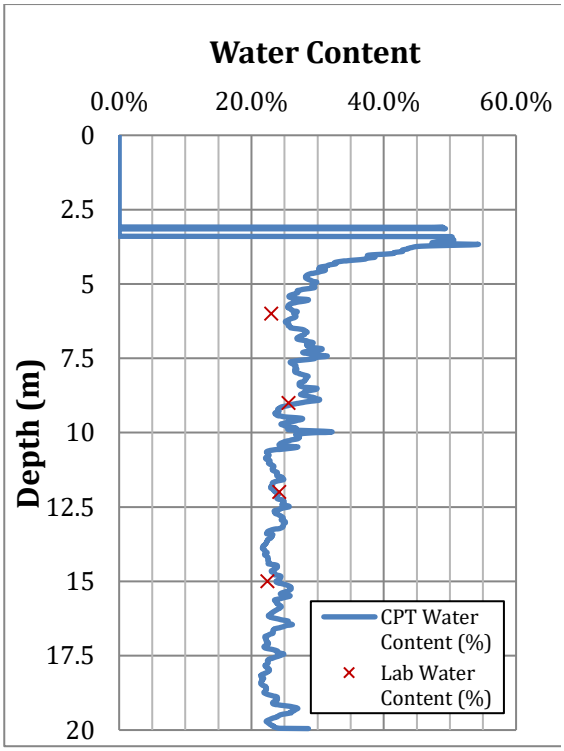

Figure 4: Water content comparison

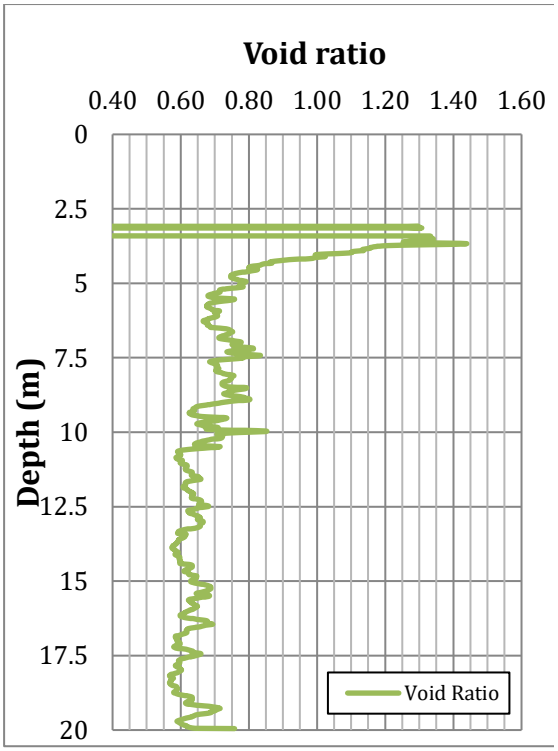

Figure 5: Void ratio

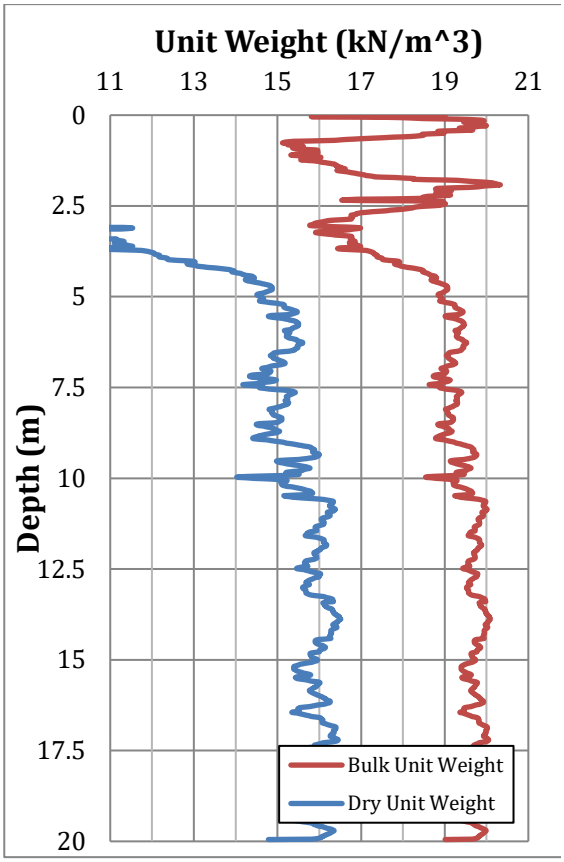

Figure 6: Bulk and dry unit weights

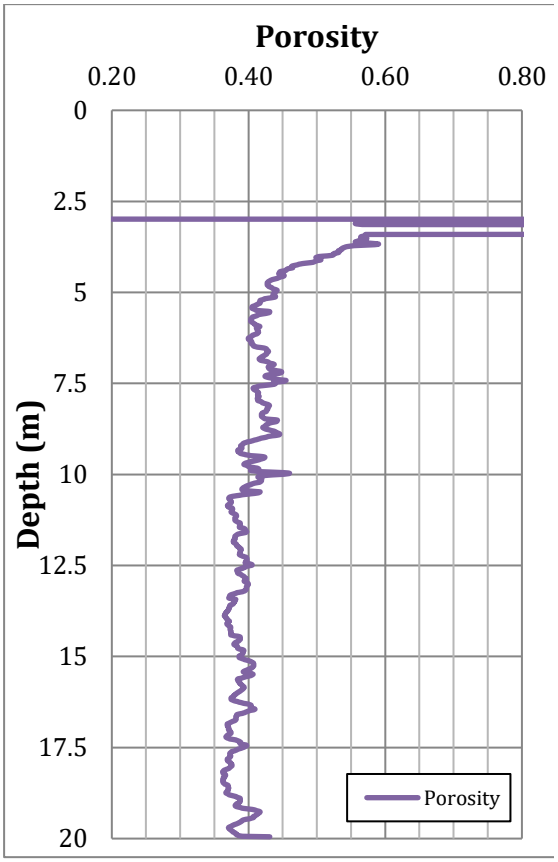

Figure 7: Porosity

4.3 Summary

The qc (Figure 2) and SBTn (Figure 3) plots have been included to provide the reader with an understanding of the raw CPT results and soil behaviour type interpretations, which indicate that the soil predominantly consists of sands and silty sands below 4m depth. This is consistent with the borehole results.

Figure 4 shows a comparison between the CPT method for estimating water content and laboratory testing results. From this graph, it can be seen that there is a close agreement in the values returned by the two methods. This result indicates that the proposed CPT method, based on Robertson's unit weight correlation, is accurately estimating the water content for the soil conditions encountered at this site. It can also be concluded that high quality results have been obtained from the laboratory.

Figures 5, 6 and 7 present the estimated void ratio, dry unit weight and porosity, respectively. The plots for these parameters indicate the values produced by the CPT method are consistent with typical values for the soil conditions encountered at the site, in accordance with Table 1. As these parameters have been derived based on the same assumptions as the water content, it is inferred that these estimated parameters have a similar degree of accuracy associated with them.

Table 4 shows a comparison between the laboratory water content values and the CPT estimates at the four sampling depths. An absolute difference in water content of between 0.5-3.5% (average difference of 1.8%) is considered to be an encouraging result.

Table 4: Comparison between laboratory and CPT results

Sample Depth (m)	Laboratory water content w (%)	Estimated water content from CPT w (%)	Absolute difference between measured and estimated w (%)
6	23.0	26.5	3.5
9	25.6	27.3	1.7
12	24.2	23.7	0.5
15	22.4	23.7	1.3

5 CONCLUSIONS

Based on fundamental principles of soil mechanics and the well-established published correlation for estimating bulk unit weight from CPT by Robertson (2010), and for saturated conditions with an appropriate G_s value, it is possible to estimate versus depth the:

- Water content
- Void ratio
- Dry unit weight
- Porosity

The proposed methodology can only be applied to inorganic and saturated soils. This means that the proposed methodology is applicable to coastal areas and other regions where the groundwater is typically near the ground surface. The proposed methodology was applied to a sandy site in Christchurch, New Zealand, which yielded typical results for the soil conditions encountered and showed close agreement with the laboratory testing results for the same site. It is intended to extend the methodology to estimate these soil parameters in fine-grained soils.

For projects where both CPT and laboratory testing have been undertaken, the CPT method can also be utilised as a quality control measure for the results obtained. If the underlying assumptions for the CPT method are satisfied and are sufficiently accurate for the soil conditions present at the site, there should be relatively close agreement between the CPT-estimated water content and the laboratory water content results.

The four above estimated parameters can be plotted versus depth and could be used for facilitating numerical analysis with FEM and alternative methods for estimating the following:

- Assessment of shear wave velocity
- Assessment of soil natural frequency or period
- Assessment of small-strain shear modulus
- Assessment of relative density and state of packing for cohesionless soils
- Assessment of soil permeability
- Assessment of soil groutability
- Assessment of collapse potential of soil

Further research needs to be undertaken for comparing the estimated parameters from the proposed method against the measured laboratory results for a greater number of sites.

REFERENCES

Bowles, J.E. (1997). *Foundation analysis and design*, 5th Edition. New York: McGraw-Hill.

Das, B. M. (2004).*Principles of foundation engineering.* Brooks/Cole, Thomson Learning, U.S.A.

Robertson, P. K. and Cabal, K.L. (2010). *Estimating soil unit weight from CPT*. Second International Symposium on Cone Penetration Testing, Huntington Beach, CA, USA.

Robertson, P. K. and Cabal, K.L. (2015). *Guide to cone penetration testing,* 6th Edition. Gregg Drilling.

Review on recent developments in alkali-activated materials

S H Bahmani and R P Orense
Department of Civil & Environmental Engineering, University of Auckland, Auckland, NZ
sbah010@aucklanduni.ac.nz (Corresponding author)

Keywords: alkali-activated, cementitious, waste glass, environment, industrial

ABSTRACT

Recently, there is significant increase in globalisation in industrial areas especially in developed countries. Thus, their waste by-products become a major challenge because of the large quantities involved and the scarcity of disposal space. Industrial waste by-products and the use of traditional cementitious binders (e.g. lime, cement, and gypsum) in geotechnical applications are facing many challenges due to high greenhouse gas emissions, intensive use of energy and depletion of natural resources. In addition, most of the traditional binders are not readily acceptable due to stringent occupational health and safety issues as well as threats to the soil and groundwater environment. To address these challenges, new binders using industrial waste-by products are being investigated. Among these, alkaline activation is one of the most interesting methods being developed; it has equal or better performance than cement-based binders, but with lower environmental issues and costs. This paper reviews the key developments in alkali-activated materials since 2011, with a particular focus on advances in characterisation techniques, structural understanding, binder precursors, activation approaches, design and processing, and reaction mechanism. Finally, the paper proposes further research and development topics and suggests steps forward to enhance the potential application of these materials for ground improvement.

1 INTRODUCTION

Loss of soil stiffness and strength due to liquefaction and consequent large ground deformation has caused extensive structural damage and economic losses in urban areas during major earthquakes. Therefore, wide ranges of remedial measures have been developed for treating or improving soils against liquefaction. These include densification, solidification, pore pressure relief, lowering ground water table, and restraint of shear deformation. Moreover, cementitious materials like cement have been widely utilised in different mitigation techniques such as compacting grouting, deep soil mixing, and jet grouting (Srbulov, 2009). These chemical admixtures are often used as an additive to improve the strength and stiffness of soils (Tatsuoka et al., 1995). However, the improvement in shear strength using traditional additives is often associated with decreased plasticity and enhanced brittleness attributed to pozzolanic hardening. Cement industry not only accounts for around 5-7% of global carbon dioxide emissions and environmental footprint such as global warming and soil ecotoxicity, but also has setting time challenge. One potential replacement for cementitious materials is alkali-activated materials (AAMs) which seem to yield similar mechanical properties like cementitious materials (Provis, 2014). Alkali activation is the generic term which is applied to the reaction of a solid aluminosilicate (termed the 'precursor') under alkaline conditions (induced by the 'alkali activator'), to produce a hardened binder, which is based on a combination of hydrous alkali-aluminosilicate and/or alkali-alkali earth-aluminosilicate phases (Provis et al., 2015). Additional terminology often used to refer to these materials includes 'geopolymer' nomenclature that is used largely to describe low-calcium alkali-activated aluminosilicate binders. The defining characteristic of a geopolymer is that the binding phase comprises an alkali aluminosilicate gel, with aluminium and silicon linked in a three-dimensional tetrahedral gel framework that is relatively resistant to dissolution in water (Palomo et al., 2014). According to a recent definition

by Provis (2014), alkali activated materials are produced through the reaction of an aluminosilicate, normally supplied in powder form as an industrial by-product or other inexpensive materials, with an alkaline activator which is usually a concentrated aqueous solution of alkali hydroxide, silicate, carbonate or sulphate. In recent years, geopolymer has attracted considerable attention among these binders because of its compressive strength, low permeability, good chemical resistance and excellent fire resistance behaviour (Provis, 2017). Because of these advantageous properties, geopolymer is a promising alternative to cementitious materials in addressing various geotechnical problems and waste immobilization solutions for the industries. The aim of the current paper is to review and highlight the key recent scientific enhancements in the development, characterisation, processing and environmental assessment of AAMs.

2 ALKALINE ACTIVATION AND GEOTECHNICAL APPLICATIONS

It is noticeable that using alkaline activation in geotechnical applications is still at the early stage of development. However, Table 1 summarises the existing literature about utilising alkali-activated binder for the purpose of ground improvement. In very limited attempts, some geotechnical researchers investigated the effectiveness of precursors, including fly ash (FA), metakaolin, blast furnace slag (GGBS), palm oil fuel ash (POFA) and red gypsum (RG), with soft soil in the presence of a predesigned concentrated aqueous alkaline hydroxide or silicate solution. In this respect, Cristelo et al. (2013) address the effectiveness of alkali-activated low-calcium and high-calcium FA as silica and alumina amorphous sources. Based mostly on the microstructural analysis, these authors demonstrated that a binding gel (either N–A–S–H and/or C–A–S–H) is developed inside the soil voids, helping to form more compact microstructures and, as a consequence, improved compressive strength. Moreover, the authors reported that the short-term strength gain of the stabilised soil is faster when high-calcium FA was used as a precursor. Sargent et al. (2013) carried out a research work to study the feasibility of using some alkali-activated by-products, such as GGBS, FA and RG, on some geotechnical properties of soft soil. Based on the test results, they concluded that alkali-activated GGBS, GGBS–FA and GGBS–RG exhibited significant strength regarding the untreated soil. Pourakbar et al. (2015) reported that the addition of highly alkaline solutes, including NaOH and KOH, increased the strength of the treated soil samples. According to this study, curing time and the water content of soil were also shown to have a significant strengthening effect on the treated soil.

Table 1: Summary of alkali-activated binders for ground improvement

Source binder	Alkali-activator	Conclusions	Reference
Low-calcium fly ash; High-calcium fly ash	Sodium hydroxide and sodium silicate	The alkali-activated binder is a successful method of deep soil stabilisation. Also, alkaline activation method is a simple process and it does not involve any sophisticated or costly procedures. In the case of fly ash (source binder) with various calcium contents, a lower percentage of calcium in the silica and alumina source has a positive effect on mechanical performance of treated soil through long curing time.	Cristelo et al. (2013)
Fly ash; Red gypsum	Sodium hydroxide and sodium silicate	Alkali-activated fly ash and red gypsum exhibited higher strengths and much higher brittleness in comparison with untreated soil.	Sargent et al. (2013)
Palm oil fuel ash	Sodium hydroxide; Potassium hydroxide	The strength of the soil treated by alkaline activation process mainly depends on four factors: (1) the quantity of source binder; (2) the kind of alkali activator; (3) the natural water content of host soil; and (4) the curing condition.	Pourakbar et al. (2015)

3 ADVANCES IN CHARACTERISATION

3.1 Nanostructural Characterisation

The nanostructure of AAMs is strongly dependent on the available calcium content of precursors; a high-calcium system such as alkali-activated blast furnace slag is dominated by a calcium aluminosilicate hydrate (C–A–S–H) gel with a to bermorite-like structure (Provis et al., 2014), while low-calcium systems such as those based on meta-kaolin or fly ash tend to generate an alkali aluminosilicate (N–A–S–H) gel with a highly cross-linked, disordered pseudo-zeolitic structure (Richardson et al., 1994). These gels can coexist in binders based on blends of high-calcium and low-calcium precursors (Davidovits, 2005; Provis, 2014). Fourier transform infrared (FTIR) spectroscopy is a key technique for the analysis of AAMs, particularly for low-calcium systems where it can probe the connectivity within Si–O– (Si, Al) frameworks via shifts in the peak corresponding to the asymmetric stretch of that bond (Provis, 2014). The gel theory of an initial Al-rich binder gel ("Gel 1") forming at the first hours, and then evolving to a more Si-rich structure ("Gel 2"), which was developed from ex-situ analysis of the gel evolution (Provis et al., 2015) has been refined. Note that FTIR spectroscopy (see Figure 1) detects bond vibrations rather than the actual nuclei. The 'Gel 1' stage involves a high degree of formation of Si–O–Al bonds relative to the bulk Si/Al ratio, because the formation of cross-links involving Al atoms joining between Si sites is rapid. This leads to a gel, which has a relatively high concentration of Si–O–Al bonds (Richardson et al., 1994).

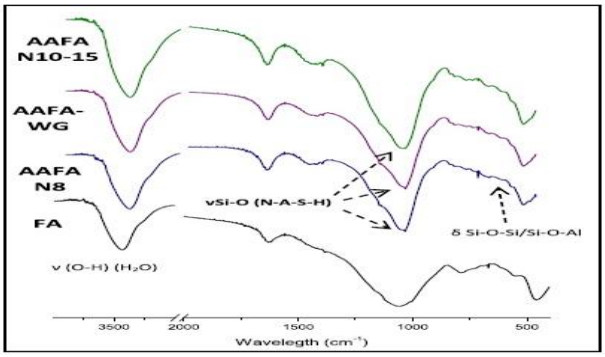

Figure 1: FTIR spectra for fly ash and alkali-activated fly ash pastes (adapted from Richardson et al. 1994)

3.2 Microstructural Characterisation

Recent developments in the understanding of microstructural and the C–A–S–H gel in alkali-activated binders have been focused on the construction of a realistic structural description of the silicate chain structures in the AAM gel, which can differ significantly from those formed in the C–S–H produced by Portland cement hydration (Provis, 2014). As can be seen from the Figure 2, this is mainly attributed to the low Ca/Si ratio and high Al content of the gel produced by alkali activation of binder, which opens the possibility of cross-linking between the dreierketten chains of the tobermorite-like gel (Pelisser et al., 2013). The most widely used tool for microstructural analysis of AAMs is scanning electron microscopy (SEM), energy-dispersive spectroscopy (EDS), and transmission electron microscopy (TEM). The C-S-H was found to be intermixed on an intimate scale with an Mg/Al-rich phase, presumably hydrotalcite. Another key tool which is gaining popularity and interest is tomography. This can be applied on both nanometre (Provis, 2014) and micrometre (Provis et al., 2015) length scales using X-rays.

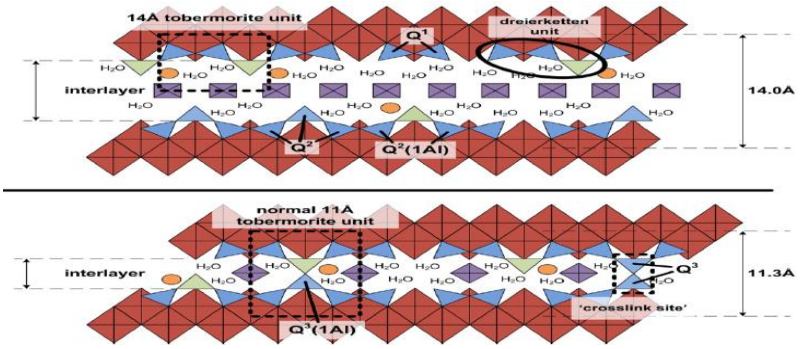

Figure 2: Schematic of structural features, silicate and aluminate, cross-linking (adapted from Provis et al. 2014).

4 ADVANCES IN BINDER DEVELOPMENT

Early studies and applications of AAMs mainly used precursors, such as blast furnace slag, and fly ash. The chemical and physical characteristics of these precursors are well described in the literature (e.g. Provis, 2014; 2017).

4.1 Waste Glass

The recycling of waste glasses from consumer utilisation and industrial processes poses a major problem for municipalities worldwide. Puertas and Torres-Carrasco (2014) investigated the properties and microstructure of alkali-activated glass fibre waste using NaOH and KOH solution as activators. The mortar samples showed compressive strengths of up to 77MPa after three days when NaOH solution was used as activator (Figure 3). Puertas and Torres-Carrasco (2014) used metakaolin (MK) to replace a part of the glass powder in order to introduce Al and also to stabilise alkali ions in the system. Compressive strength of the mortars increased with additional aluminium sources is common in the alkali activation of waste glasses, as commercial glass systems contain sufficient Al to produce a stable AAM. Bajare et al. (2014) investigated the use of a combination of aluminium recycling, calcined kaolin clay, and lead–silica glass (LSG) from recycled fluorescent lamps, to prepare foamed alkali activated binders. The residual aluminium metal in the dross generates hydrogen when reacting with NaOH activator, with a total porosity of 82–83%. An interesting point of novelty in this work was the use of a waste material as a new binder in alkaline activation methods (Pascual et al., 2014).

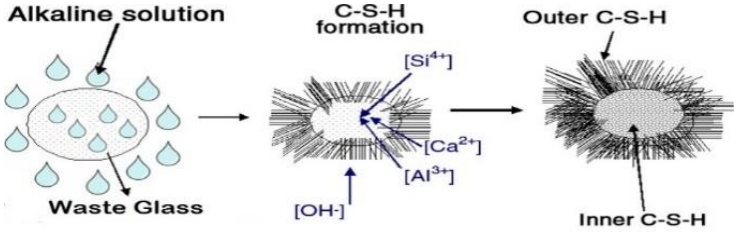

Figure 3: Reaction mechanism in an alkaline-activated recycled glass (adapted from Palomo et al. 2014).

5 COMPARISON WITH CEMENTITIOUS MATERIALS

5.1 Production Process

There does not appear to be a strong need to develop new process facilities in the short term to enable the production of alkali-activated materials. Mixing and using alkali-activated materials can generally be achieved using the same technology as used in Portland cement products, potentially with slight modifications to optimise the input of mixing energy and the dosing of the activator (Provis, 2014). The capital costs of a plant producing alkali-activated materials will therefore be significantly lower than that of a plant producing Portland cement. An increase in the scale of sodium hydroxide production to support million-tonne-scale production of alkali-activated binders will require more capital-intensive facilities, but the activator only comprises 5–10% of the total mass of the binder (Provis, 2017).

5.2 Material Processing and Application

Mix design of alkali-activated materials can broadly follow similar heuristics to those used for Portland cement products, particularly in terms of applications, but the binder must be designed and optimized on a case-by-case basis: the precursors available at each location will differ in chemistry, mineralogy and fineness, and will be combined with activators which are selected depending on both technical and commercial parameters (Jamieson et al., 2015). There is not yet a universal mix design procedure which can be applied to alkali-activated binders, due to the differences in chemistry, mineralogy and particle characteristics between different precursor sources, so optimisation of mixes needs to be carried out for each new precursor that is sourced (Provis, 2017). Accurate quality monitoring and control of the characteristics of precursors, which are sourced as wastes or by-products from other industries, is also essential to the successful production of alkali-activated products. Alkali-activated slag cements tend to harden rather rapidly, and in some cases, retarders are used to regulate the setting rates (Richardson et al., 1994). Probably the main challenge related to processing and application of alkali-activated materials in construction at present is the difficulty associated with developing or sourcing effective admixtures for rheology control in these systems (Provis, 2014).

6 SIMPLIFIED ENVIRONMENTAL ASSESSMENT

In any given production situation, factors such as the mix design, source and dose of the activator, transport requirements for aggregates and precursors, and energy mix used in production of all components (electricity, nuclear), must all be specified for each particular mix design, location and application. When comparing with Portland cement-based products, a comparable baseline for a particular location and application must also be specified (Habert & Ouellet-Plamondon, 2016). For these reasons, it is clearly impossible to provide a single value to globally describe the environmental savings which may be achieved through the use of alkali-activated materials in place of conventional cement and concrete (Provis, 2017; Provis et al., 2005). A recent detailed discussion of life-cycle analysis (LCA) of alkali-activated binder systems has been provided by Habert & Ouellet-Plamondon (2016). The importance of reliable inventory data, which has not always been the case, particularly for activator components (Pelisser et al., 2013), for instance, mortar based on blast furnace slag, activated by Na_2CO_3 and containing a high volume of granular limestone, CO_2 and energy savings as high as 97% have been calculated (Provis, 2014). Habert and Ouellet-Plamondon (2016) used LCA methodology to analyse the environmental impacts of AAM concretes made with fly ash, blast furnace slag and metakaolin using published results. A calculation based on an average of 49 published mix designs indicated that fly ash-based AAM mixtures released 45% less CO_2 than an average Portland cement concrete (McLellan et al., 2011). Figure 4 exemplifies the importance of the activator in the emission calculations for several fly ash-based AAM formulations.

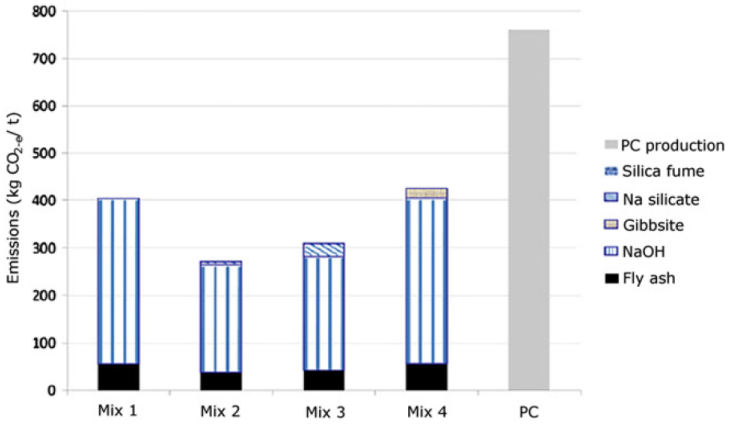

Figure 4: Calculated CO_2-equivalent emissions of four different fly ash-based AAMs paste mix designs using typical Australian data (adapted from McLellan et al. 2011).

7 DISCUSSION

One of the main advantages of alkali-activated methods can constitute interesting materials to fully eliminate traditional cementitious binder (i.e. cement and lime) usage in geotechnical projects. That is, alkaline activation binder is generally a synthetic alkali aluminosilicate material that is produced from the reaction of a solid aluminosilicate with a pre-designed concentrated aqueous alkaline hydroxide or silicate solution. There are many factors that influence the process of alkaline activation. Moreover, production of cementitious materials not only accounts for around 5-7% of global carbon dioxide emission and contribute to environmental footprint such as global warming and soil ecotoxicity, but also has setting time challenge. Another advantage of alkaline activation is the development of new binders using industrial waste by-products (geopolymer binders) with equal or better performance than cement-based binders for geotechnical applications, but with lower environmental issues and costs. Various source materials including natural clay, aluminosilicate minerals and agro-industrial by-products can be utilised through alkaline activation technique. Also, the recycling of industrial by-products, such as waste glasses from consumer utilisation and industrial processes, poses a major problem for New Zealand. In addition, since the strength of AAMs demands low energy consumption, environmentally-friendly nature of the process, and excellent engineering properties, alkali-activated binders are fast emerging as materials of choice for highly-demanding geotechnical engineering applications. Moreover, another advantage of AAMs is that the cost of production of alkali-activated binders is, in general, a closely-held trade secret and is fundamentally dependent on the degree of control of the materials supply chain which is held by the material. Industrial waste by-products, such as fly ash and slag, may be purchased at a cheaper price compared to that of Portland cement.

Despite the enhancement of AAMs using industrial by-products for geotechnical applications, there has been a concern for their adoption because of potential environmental impact. Hence, one of the major weaknesses of AAMs and activators is that they are not readily acceptable due to stringent occupational health and safety issues as well as threats to the soil environment, such as increased alkalinity (pH 11-12). Also, alkaline activation methods have difficulty in terms of field handling. There is limited study on activation of industrial wastes for geotechnical applications, such as soil stabilisation or ground improvement. Apart from extensive developments of using alkali-activated binder in civil engineering framework, using this technology in geotechnical applications is still at the early stage of development and, hence, need comprehensive research works in order to become technically and economically viable.

8 CONCLUSIONS

Based on the discussions, it is concluded that alkaline activation method has considerable potential to be used as a new method in geotechnical applications. The development and optimisation of alkali-activated binder formulations from an increasingly diverse range of waste-derived precursors has become the focus of efforts of many research teams worldwide, often with a focus on locally available or problematic materials. In New Zealand, the amount of glass available and utilisation of domestic recycled glass is a main challenge. So far, alkaline activation is the most promising method to develop new binders using recycled glass as compared to cement, with its lower environmental issues and costs. However, there are still a number of areas which require attention, from both scientific and technological perspectives, particularly the control of setting time and rheology. Hence, appropriate and meaningful testing and description of both advanced processing methodologies and environmental sustainability is essential in ensuring the future role of alkali activated binder systems in the geotechnical applications. Some key aspects that require detailed research attention include:

- experimental investigation of the effectiveness of the AAMs with different alkaline solution molarity on geotechnical parameters of soils;
- detailed definition of the links between the physico-chemical properties of precursors, and selected activators;
- investigation of appropriate method(s) for the characterisation of AAMs for ground improvement techniques;
- seeking of new information through the use of analytical tools such as Raman spectroscopy, confocal microscopy, and X-ray photoelectron spectroscopy, which have been under-utilised, or not used at all, in the study of AAMs;
- assessment of cyclic behaviour of the AAM-treated soils under seismic loading;
- study of the microstructural and mineralogical phases of soils before and after treatment with AAMs; and
- derivation of constitutive model for incorporation in user-friendly numerical (FEM) code.

REFERENCES

Bajare, D., Bumanis, G., & Korjakins, A. (2014) New porous material made from industrial and municipal waste for building application. *Materials Science, 20*(3), 333-338.

Cristelo, N., Glendinning, S., Fernandes, L., & Pinto, A. T. (2013) Effects of alkaline-activated fly ash and Portland cement on soft soil stabilisation. *Acta Geotechnica, 8*(4), 395-405.

Davidovits, J. (2005) Geopolymer, green chemistry and sustainable development solutions: *Proceedings of the World Congress Geopolymer*. Geopolymer Institute.

Habert, G., & Ouellet-Plamondon, C. (2016) Recent update on the environmental impact of geopolymers. *RILEM technical Letters, 1*, 17-23.

Jamieson, E., McLellan, B., Van Riessen, A., & Nikraz, H. (2015) Comparison of embodied energies of ordinary Portland Cement with Bayer-derived geopolymer products. *Journal of Cleaner Production, 99*, 112-118.

McLellan, B. C., Williams, R. P., Lay, J., Van Riessen, A., & Corder, G. D. (2011) Costs and carbon emissions for geopolymer pastes in comparison to ordinary Portland cement. *Journal of Cleaner Production, 19*(9), 1080-1090.

Palomo, A., Krivenko, P., Garcia-Lodeiro, I., Kavalerova, E., Maltseva, O., & Fernández-Jiménez, A. (2014) A review on alkaline activation: new analytical perspectives. *Materiales de Construcción, 64*(315), 022.

Pascual, A. B., Tognonvi, M. T., & Tagnit-Hamou, A. (2014) Waste glass powder-based alkali-activated mortar. *Int. J. Res. Eng. Technol, 3*(13), 32-36.

Pelisser, F., Guerrino, E., Menger, M., Michel, M., & Labrincha, J. (2013) Micromechanical characterization of metakaolin-based geopolymers. *Construction and Building Materials, 49*, 547-553.

Pourakbar, S., Asadi, A., Huat, B., & Fasihnikoutalab, M. H. (2015) Soil stabilization with alkali-activated agro-waste. *Environmental Geotechnics, 2*(6), 359-370.

Provis, J. L. (2014) Geopolymers and other alkali activated materials: why, how, and what? *Materials and Structures, 47*(1-2), 11-25.

Provis, J. L. (2017) Alkali-activated materials. *Cement and Concrete Research (*available online). doi:10.1016/j.cemconres.2017.02.009

Provis, J. L., Lukey, G. C., & van Deventer, J. S. (2005) Do geopolymers actually contain nanocrystalline zeolites? A reexamination of existing results. *Chemistry of Materials, 17*(12), 3075-3085.

Provis, J. L., Fernández-Jiménez, A., Kamseu, E., Leonelli, C., & Palomo, A. (2014). Binder chemistry–low-calcium alkali-activated materials alkali activated materials. *State-of-the-Art Report, RILEM TC 224-AAM*, Springer, 93-123.

Provis, J. L., Palomo, A., & Shi, C. (2015) Advances in understanding alkali-activated materials. *Cement and Concrete Research, 78*, 110-125.

Puertas, F., & Torres-Carrasco, M. (2014) Use of glass waste as an activator in the preparation of alkali-activated slag. Mechanical strength and paste characterisation. *Cement and Concrete Research, 57*, 95-104.

Richardson, I., Brough, A., Groves, G., & Dobson, C. (1994) The characterization of hardened alkali-activated blast-furnace slag pastes and the nature of the calcium silicate hydrate (CSH) phase. *Cement and Concrete Research, 24*(5), 813-829.

Sargent, P., Hughes, P. N., Rouainia, M., & White, M. L. (2013) The use of alkali activated waste binders in enhancing the mechanical properties and durability of soft alluvial soils. *Engineering Geology, 152*(1), 96-108.

Srbulov, M. (2009) Comments on some frequent liquefaction potential mitigation measures. *Geotechnical Earthquake Engineering*, 203-209.

Tatsuoka, F., Lo Presti, D., & Kohata, Y. (1995) Deformation characteristics of soils and soft rocks under monotonic and cyclic loads and their relationships. *Proceedings of International Conference on Recent Advances in Geotechnical Earthquake Engineering and Soil Dynamics,11(1),* 851-879.

Tools and methods to manage groundwater and settlement effects from the construction of an expressway on peat deposits

T Avanidou
Beca Ltd, Christchurch, NZ
Dora.avanidou@beca.com (Corresponding author)

G J Alexander
Beca Ltd, Auckland, NZ
Gavin.alexander@beca.com

Keywords: peat, groundwater, settlement, monitoring

ABSTRACT

The Mackays to Peka Peka Expressway is part of the Wellington Northern Corridor, identified as a Road of National Significance for New Zealand. The Expressway runs in close proximity to several wetlands of significant ecological and cultural value with unique fauna and flora, and to transport infrastructure and residential buildings built over peat deposits. Approximately 50% of the Expressway earthwork footprint is underlain by peat deposits that are typically 0.5m to 8.0m thick and are characterised as very soft, highly organic and compressible. Groundwater in the peat deposits is shallow and is directly connected to nearby wetlands. Expressway construction required either removal of the peat beneath its footprint or preloading and surcharging of it, to manage long term settlement. Both approaches involve significant potential alteration to the near surface groundwater system.

A comprehensive groundwater monitoring and settlement monitoring programme was established prior to construction commencing, with some 110 piezometers to record natural variations in groundwater levels and 100 settlement monitoring points. In order to differentiate construction effects from normal seasonal variations, a statistical approach was developed for setting both high and low trigger levels for the 22 telemetered piezometers located in and around five sensitive wetlands. Recorded groundwater levels and settlement have generally remained within the consented levels. Some exceedances were recorded however a pragmatic approach to monitoring and management of these exceedances allowed works to continue with minimal disruption and no adverse environmental effects.

1 INTRODUCTION

The MacKays to Peka Peka (M2PP) Expressway Project is one of eight sections that make up the Wellington Northern Corridor, identified as one of the 'Roads of National Significance' (RoNS). The Expressway consists of approximately 18km of four lane median-divided Expressway from the Raumati Straights in the south through to Peka Peka in the north (Figure 1). The Expressway runs in close proximity to several wetlands of significant ecological and cultural value, transport infrastructure and residential buildings built over peat deposits. Groundwater in the peat deposits is shallow and is directly connected to nearby wetlands. The Expressway is predominately on embankments, rising up to 10m high at crossing points. Expressway construction activities required embankment construction with localised preload and surcharge or excavation and replacement of peat below the groundwater table to manage long term settlement (Figure 2).

Additionally construction of stormwater devices for treatment, conveyance and attenuation of run-off, and short-term groundwater take for construction water supply, have the potential to

change groundwater level and might result in ground settlement, or changes to water levels in existing wetlands, ecological systems or water supplies.

Figure 1: Project Location and Extents

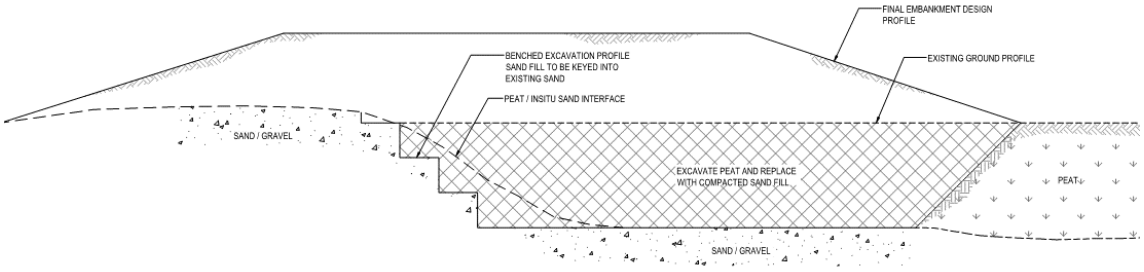

Figure 2: Typical cross section: Peat undercut for embankment on peat and sand

During the project consenting process an assessment of groundwater effects (France and Anderson, 2012) was undertaken, in order to assess potential changes to the existing groundwater regime as a result of the Expressway construction and operation. The effects on groundwater were assessed by the development of regional and area-specific 2- and 3-dimensional computer groundwater models, calibrated to water level monitoring data, and taking into consideration the modelling work carried out in the past. The associated Groundwater Management Plan (GMP)

(Williams, 2013) defined the best practicable options for groundwater monitoring and management practices and procedures to minimize impact on the environment. Furthermore an assessment of ground settlement effects (Coe, 2012) was also undertaken associated with the construction and operation of the Expressway and the expected effects of the settlements on existing buildings, services and transport infrastructure. The Settlements Effects Monitoring Plan (SEMP) (Ainsworth, 2013) defined the settlement monitoring procedure and measures to manage ground settlements associated with the Expressway.

2 GEOLOGICAL AND HYDROGEOLOGICAL SETTING

The Expressway route is bounded, in the east, by the Tararua Ranges. These are steep greywacke hills which have formed by tectonic activity along NESW oriented faults such as the Ohariu fault (which runs along the base of the hills). The Expressway crosses the coastal plain west of the Ranges, an area which has been further shaped by repeated cycles of glaciation that have occurred in the past two million years. During the glacial cycles, sea levels were approximately 120m lower than present, as water was locked in ice-sheets and glaciers. The Tararua Ranges held valley glaciers during these times and physical weathering of rock, combined with sea level fall, contributed to severe erosion in the Ranges generating alluvial fans. These processes, in combination with longshore drift, formed large coastal plains. With each large scale tectonic movement, the rivers altered course and slowly migrated north and south across the alluvial fans depositing gravels, sands and silts. Episodic flood events resulted in finer materials (silts and clays) being deposited further away from the river channels, and in between such events, areas of peat developed in low lying areas between dunes. Sand dunes inter-finger with the peat deposits and rise up to 20 m in elevation along the coast.

The groundwater regime consists of unconfined aquifers in the Holocene sand and peat deposits above a series of unconfined aquifers in the Pleistocene sand and alluvium layers. The alignment passes through the Waikanae Groundwater Zone (WGZ), one of six broad groundwater management zones on the Kāpiti Coast. The key aquifer horizons within the WGZ are the deep Waimea Aquifer and Parata Aquifers, from which the Kapiti Coast District Council (KCDC) production wells abstract water for public water supply. Domestic wells in the area generally abstract water from the shallow Pleistocene and Holocene Sands.

A large number of wetlands occur within the WGZ. Wetlands and lagoons have typically formed in the low lying areas between dunes where peat has been deposited and where the groundwater level is very close to the surface. Wetlands are generally thought to be points of groundwater "discharge" with flows largely sustained by shallow groundwater (Gyopari, 2002). However there is also evidence that some wetlands within the Kapiti Coast are "recharge" wetlands fed by rainfall and run-off perching on the low permeability peat (Allen, 2010). Data collected and modelling carried out as part of this project confirms that both types of wetland occur, depending on the particular conditions at each site.

3 MONITORING

3.1 Groundwater Monitoring

A comprehensive groundwater monitoring programme was established prior to construction commencing, with some 110 piezometers (Figure 3) monitored monthly for at least one year to record natural variations in groundwater levels.

This baseline data has been used to identify natural seasonal groundwater level variations and to set alert and action levels (Figure 4). The groundwater alert level was set at the lowest recorded level (preconstruction) minus the predicted drawdown reduced by 25% or 200mm. A further

100mm was allowed for the action trigger level. Similarly high trigger levels have been set to check against surface ponding. All piezometers were measured monthly, with monitoring frequency increased to twice weekly in active construction areas.

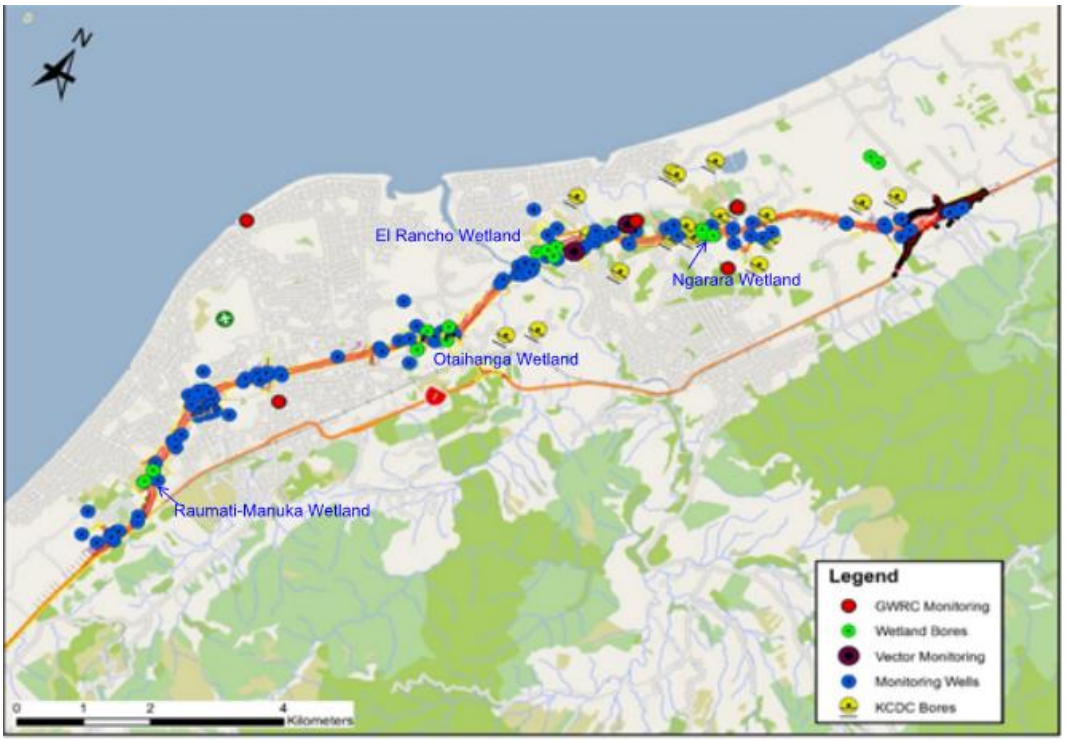

Figure 3: Overview map of groundwater level monitoring

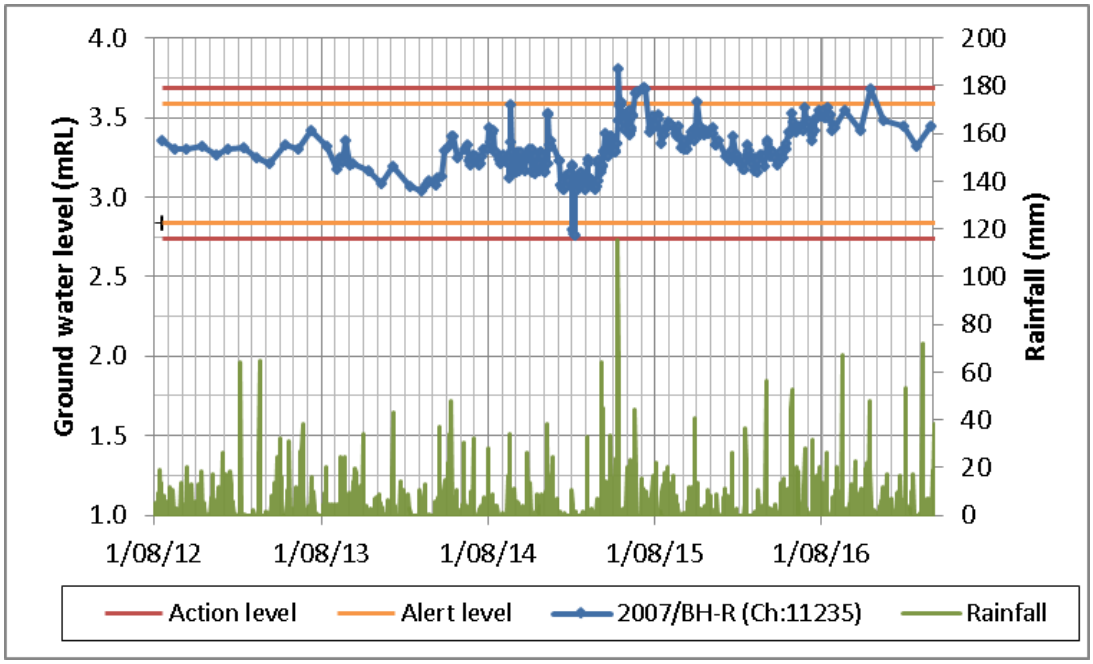

Figure 4: Groundwater levels measured in piezometer 2007/BH-R plotted against trigger levels and rainfall data

Five wetlands: Raumati Manuka, Otaihanga Northern & Southern, El Rancho and Ngarara were identified as "sensitive" for this project and 22 telemetered piezometers were installed to monitor the groundwater levels in these areas (Figure 3). As mentioned above the Kāpiti Coast wetlands

were formed in different ways according to the local ground and groundwater conditions and the water level in some will naturally vary more than in others. The baseline monitoring data was reviewed to identify likely hydrogeological behaviour of each wetland.
In Raumati-Manuka and Otaihanga wetlands groundwater level data indicates a downwards gradient, suggesting that rainfall is held up on the near-surface peaty soils, but slowly infiltrates through them to recharge the underlying sands and gravels. The El Rancho wetland is complex and the northern part of the wetland exhibits a downward gradient and the southern part exhibits a downward gradient with recharge to the underlying soils during the winter months, but is fed by the underlying aquifer during the summer months. In the Ngarara wetland groundwater both recharges and drains the aquifer beneath it. Because even small changes in groundwater level outside the normal seasonal variation may have a deleterious effect on a wetland and the limited number of measurements that were available for the establishment and understanding of the normal wetland water levels, a statistical approach was developed for calculating both high and low trigger levels.

Using data from telemetered piezometers screened in the same shallow aquifers outside the project area and monitored by the Regional Council for many years, the "expected" water level was calculated for each project piezometer based on a multiple linear regression analysis for each reading. A variation of the expected value increased by the margin of error of the 80% confidence prediction interval outside the expected water level triggers an alert for the monitoring bore (Figure 5).

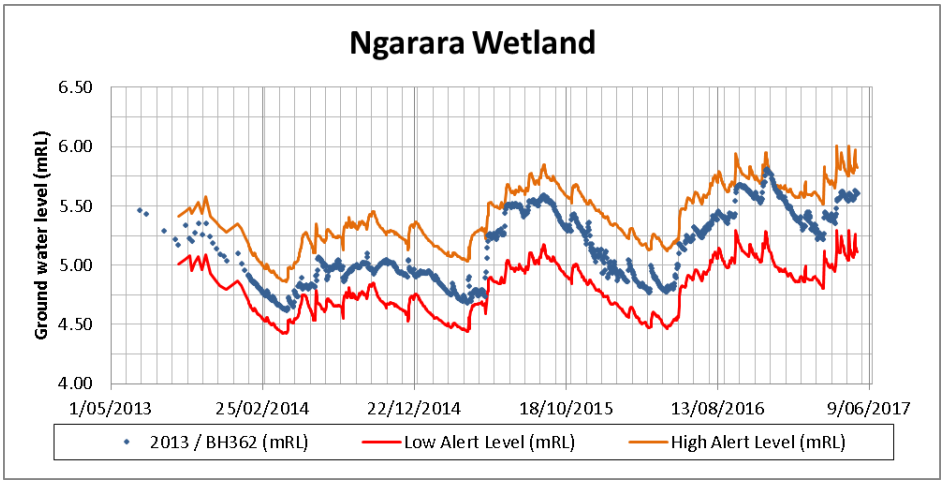

Figure 5: Groundwater levels plotted against statistically calculated trigger levels

This statistical approach was also employed to check exceedances in piezometers that were in active construction zones (earthworks within 200m) but where the works were not anticipated to influence the groundwater levels. The monitoring data demonstrated that the statistically calculated triggers take into consideration district-wide changes in groundwater levels and more clearly distinguish natural effects such as weather patterns (a low trigger level alert during dry summer months) from those resulting from construction activities (pumping during excavation) than triggers set as a standard difference as illustrated in Figures 6a and 6b. This approach allowed for minimum disruption to the construction works from unwarranted alert or alarm readings, and no adverse environmental effects.

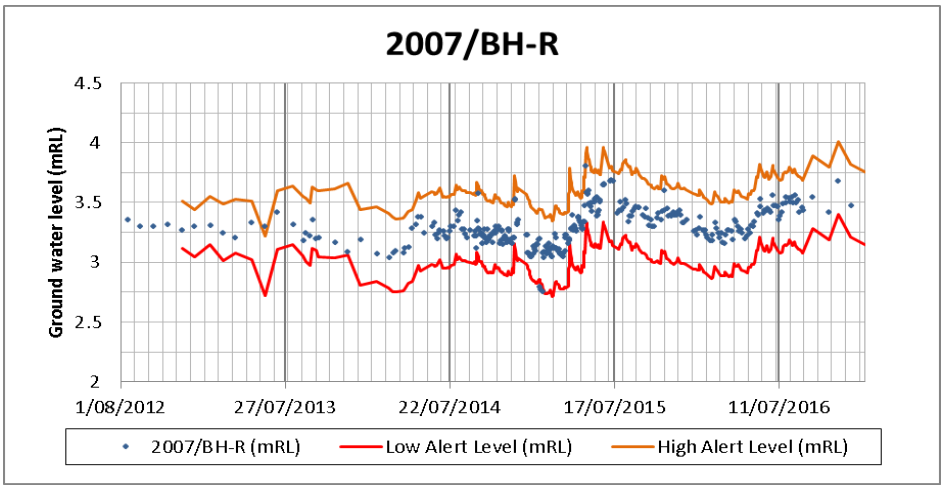

Figure 6a: Observed Water Levels in piezometer 2007/BH-R plotted against statistical trigger levels calculated based on regional data

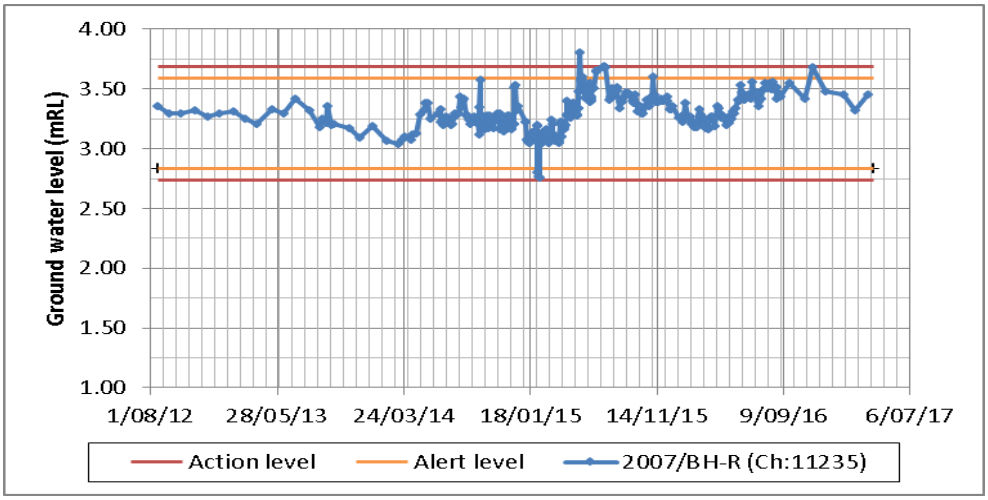

Figure 6b: Observed Water Levels in piezometer 2007/BH-R plotted against constant trigger levels

3.2 Settlement Monitoring

Consolidation settlements from embankment construction (preload and surcharge and groundwater lowering from excavation and replacement of peat) have been analysed in 13 cross sections along the length of the expressway. The location of one of the cross sections analysed is shown in Figure 7. Figure 8 presents the predicted combined settlement for that location and Figure 9 the monitoring results from one of the marks in that section.

Approximately 100 survey marks along the length of the expressway were installed and regularly monitored to provide information to compare to the settlement estimates. Monitoring marks were placed as far as practical to match with cross sections that have been used for the settlement estimates and extended out from the Expressway where settlements were expected to be greater than 12.5mm. Marks were also placed at specific stormwater features where groundwater drawdown of more than 0.1m was predicted and they coincided with groundwater level monitoring piezometers in selected locations. The marks were installed and monitored for vertical movement with 13 sets of baseline values taken during the year prior to the Expressway construction commencing. The lowest preconstruction value was used as the base value to calculate differences in vertical movement (where positive movement indicates settlement). The trigger level for each mark was set equal or lower than the expected/ estimated settlement at that location (Figure 9).

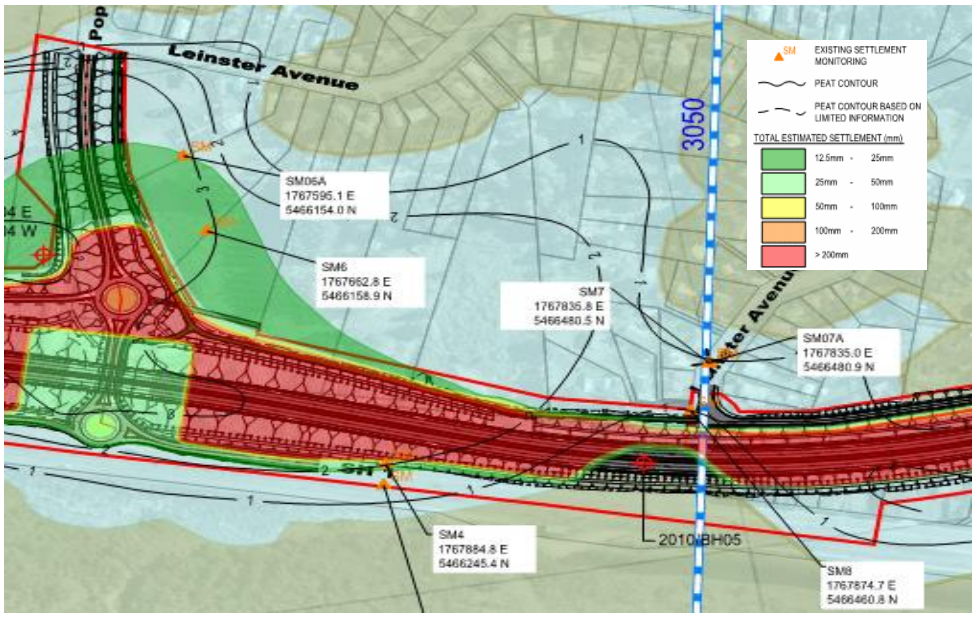

Figure 7: Settlement Markers in Cross Section 3050

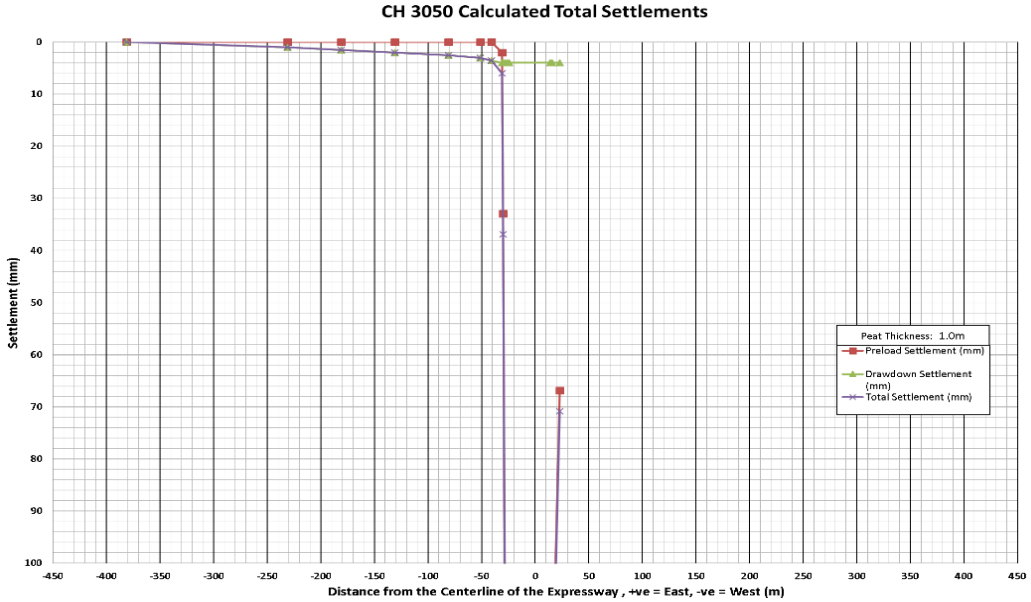

Figure 8: Predicted settlement at Cross section 3050

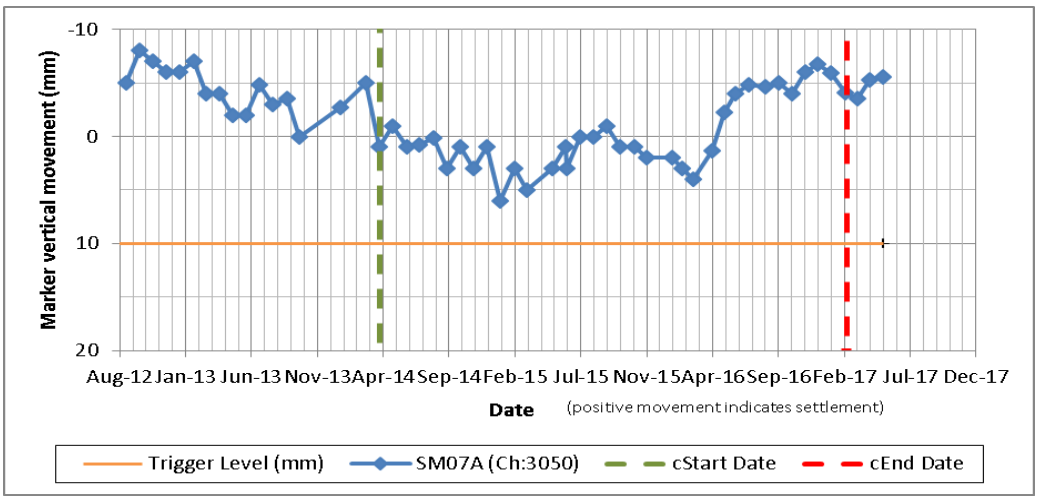

Figure 9: SM07A mark vertical movement (cross section 3050)

Monitoring frequency following the establishment of the baseline was reduced to quarterly and increased to monthly when active construction started (earthworks commenced within 200m of a particular location). When pavement construction was completed the monitoring is reduced to quarterly for 6 months and to half yearly for two years following that. The predicted settlements were generally less than 25mm beyond the edge of the earthworks. In areas of thicker peat deposits, the predicted settlement was in the order of 25 to 50mm up to 20m from the earthworks footprint, reducing to less than 25mmm beyond this. Monitoring data generally were within the magnitude and range of predicted settlements (Figures 8 and 9). Two exceedances were recorded (i.e. monitoring results indicated movement outside the expected range) and additional monitoring was undertaken and an assessment of effect of this movement was undertaken.

4 CONCLUSIONS

A comprehensive groundwater monitoring and settlement monitoring programme was established prior to construction commencing. In order to differentiate construction effects from normal seasonal variations, a statistical approach was developed. Recorded groundwater levels and settlement have generally remained within the consented levels. Some exceedances were recorded however a pragmatic approach to monitoring and management of these exceedances allowed works to continue with minimal disruption and no adverse environmental effects.

The monitoring data demonstrate that the statistically calculated triggers take into consideration district-wide changes in groundwater levels and more clearly distinguish natural effects such as weather patterns from those resulting from construction activities than triggers set as a standard difference.

5 ACKNOWLEDGEMENTS

The authors would like to thank the Mackays to Peka Peka Expressway Alliance, and in particularly the NZ Transport Agency, for permission to publish this paper.

REFERENCES

Ainsworth, P. (2013) Settlements Effects Management Plan (SEMP), *MacKays to PekaPeka Expressway Project Construction Environmental Management Plan (CEMP).*

Allen, C. (2010) *Hydrological characteristics of the Te Hapua wetland complex: The potential influence of groundwater level, bore abstraction and climate change on wetland surface water levels*. Unpublished MSc thesis

Coe, L. (2012) Assessment of Ground Settlement Effects: Technical Report 35, Volume 3, *MacKays to PekaPeka Expressway Project AEE*.

France, S. & Anderson, M (2012) Assessment of Groundwater Effects: Technical Report 21, Volume 3, *MacKays to PekaPeka Expressway Project AEE.*

Gyopari M. (2002) *Te Harakeke Wetland, Kapiti Coast, Hydrological Study Final Report*, Report prepared for the Wellington Regional Council.

Williams, A. (2013) Groundwater Management Plan (GMP), *MacKays to PekaPeka Expressway Project Construction Environmental Management Plan (CEMP).*

Dynamic behaviour of undisturbed natural pumiceous soils

M B Asadi, M S Asadi, R P Orense & M J Pender
Department of Civil and Environmental Engineering, University of Auckland, New Zealand.
masa093@aucklanduni.ac.nz (Corresponding author)

Keywords: Natural pumiceous soil, earthquake, dynamic behaviour, liquefaction resistance, maximum shear modulus

ABSTRACT

The maximum shear modulus and liquefaction resistance of soils are fundamental input parameters in the non-linear dynamic analyses of soil structures. This paper focuses on the dynamic behaviour of natural pumiceous soils, which originated from a series of volcanic eruptions centred in the Taupo and Rotorua regions and then mixed with other materials during re-working and then re-deposition. They are highly crushable, compressible and lightweight due to the vesicular nature and presence of internal voids in the pumice particles, making them problematic from an engineering point of view. The test specimens were obtained from a site near Rangiriri, Waikato using a block sampling method. Cyclic undrained triaxial tests were conducted on specimens using triaxial apparatus equipped with bender elements. The maximum shear modulus of the pumiceous materials was assessed by considering the effect of confining pressure. Moreover, the liquefaction resistance curves from cyclic loading tests were measured and compared with those of reconstituted hard-grained Toyoura sand. In addition, to distinguish the crushable volcanic soils from the hard-grained sands, image analyses on both pumice and Toyoura sand particles using scanning electron microscopy were performed.

1 INTRODUCTION

It is well-known that earthquakes can have disastrous effects on infrastructure, buildings and society. One reason for earthquake damage is related to soil failure under seismic loading. For instance, widespread liquefaction was one of the main causes of damage following the 2010-2011 Canterbury Earthquake Sequence in New Zealand (Cubrinovski et al. 2010; 2011). Consequently, understanding the geotechnical characteristics and seismic behaviour of various local soils is important for the purpose of designing earthquake resistant structures.

Volcanic soils, including pumiceous sands, are found in several areas of the North Island. They originated from a series of volcanic eruptions centred in the Taupo and Rotorua region, called the Taupo Volcanic Zone (Pender et al. 2006). By the power of explosion and airborne transport which were followed by erosion and river transport, the pumice materials were distributed and mixed with other materials in the Waikato Basin. As a consequence of infrastructure development in the region, many engineering projects frequently encounter pumiceous materials, so there is a need to understand how these deposits behave under seismic loading. Pumice is characterised by a number of distinctive properties. Pumice particles are highly crushable, compressible and lightweight as a result of the vesicular nature and the presence of internal voids (Orense et al. 2012). Due to these features, it is found that pumice deposits are problematic from an engineering point of view. Another important characteristic of pumice is its unique appearance (Figure 1) with the particles having high angularity that enables them to have very high angles of internal friction (Asadi et al. 2015; Asadi et al. 2016; Kikkawa et al. 2013). Although some studies have investigated the dynamic properties and cyclic behaviour of crushable soils such as carbonate sand and commercially-available pumice, little is known about the seismic response of natural pumiceous deposits which are a mixture of pumice with other constituents.

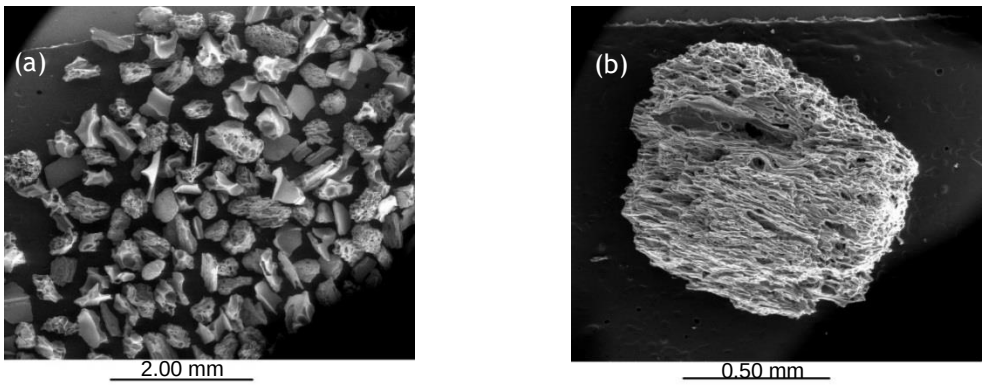

Figure 1: (a) Scanning electron microscope of pumiceous materials; and (b) pumice particle with complex surface texture

The maximum shear modulus (G_{max}) and liquefaction resistance are fundamental parameters required in non-linear dynamic analysis of soil, such as foundation design, settlement prediction, soil improvement and liquefaction assessment. In this paper, bender element and cyclic triaxial tests were employed to calculate G_{max} and liquefaction resistance of natural pumiceous soils, respectively.

2 MATERIAL USED AND TEST PROGRAMME

2.1 Site location and sampling methodology

The samples used were undisturbed pumiceous deposits from a site near Rangiriri, Waikato (see Figure 2). In order to get reasonable results from laboratory tests, it is necessary to have high-quality undisturbed samples because soil fabric, age and stress history play an important role in the dynamic behaviour of soils (Ishihara 1993). Thus, for this study, a small block sampling method was implemented to obtain undisturbed pumiceous soil samples. After excavating the ground to reach the target depth of 4.0 - 4.5m, a hydraulic jack was used to push 200 mm diameter and 200 mm high sampling tubes which were fitted with low angle cutting shoe into the ground. The tubes were then dug out of the ground, and both ends were levelled and sealed with rubber discs between the soil and caps to preserve the natural water content of soil samples.

2.2 Specimen preparation and triaxial test set up

After obtaining the undisturbed block samples, the materials were transported to the laboratory in Auckland. In the laboratory, a hydraulic jack was used to extrude the undisturbed soil samples from the sampling tube. Then, this was followed by cutting them into four pieces using a bandsaw, and subsequent trimming using a soil lathe to obtain specimens with target size of 126 mm high and 63 mm diameter. Moreover, for the purpose of comparison, another set of tests were performed on Toyoura sand which is known as a hard-grained, sub-angular material and commonly used in laboratory tests in Japan. The reconstituted Toyoura sand specimens for the triaxial tests were prepared by the moist tamping method, with the target specimen size of 63mm diameter and 126mm high. Prior to the sample preparation, the soil materials were mixed with water (approximately 20% of soil weight) to form uniformly moist samples. Then the specimens were prepared in a split mould with the membrane in place to achieve different target initial relative density. After the samples reached the target height, the top cap was positioned and the membrane sealed with O-rings, then the split mould was removed. Next, the specimens were saturated by subjecting them to back pressure of 600 kPa. B-values greater than 0.95 ensured that all the specimens were fully saturated. Then, the specimens were isotropically consolidated at the target effective confining pressures. The index properties of the materials

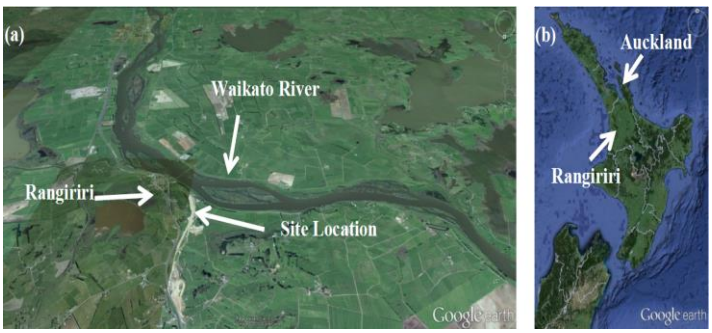

Figure 2: (a) Site location south-east of Rangiriri; and (b) location of Rangiriri, Waikato

Table 1: Index properties of natural pumiceous soils and Toyoura sand (some data after Orense et al. 2012)

Material	G_s	e_{max}	e_{min}	D_{50}	C_u	F_c (%)	PI
Natural pumice soil	2.50	1.81	1.03	0.12	7.8	35	10
Toyoura sand	2.65	0.89	0.61	0.19	1.23	0	0
Pumice-A	1.95	2.58	1.76	1.15	2.5	0	0

tested are illustrated in Table 1. The Japanese standard method (JGS 2000) was adopted to measure the index properties of the materials. Note that the pumiceous soils have a lower G_s and larger void ratio range than Toyoura sand.

2.3 Bender element test

The bender element test is a non-destructive dynamic method developed by Shirley and Hampton (1978). This test enables the measurement of shear wave velocity, V_s, of soil in laboratory by the following equation:

$$V_s = L/t \tag{1}$$

where L is distance between tip-to-tip of bender elements and t is the travel time of wave propagation. Then, based on theory of wave propagation in elastic media, the maximum shear modulus of soil is measured by Equation (2):

$$G_{max} = \rho V_s^2 \tag{2}$$

where ρ is the bulk density of soil. The bender element system employed consisted of a FG110 synthesized function generator and a TDS 2024C digital oscilloscope for generating waves and recording the generator and receiver signals for post data analysis, respectively. In bender element data analysis, the peak-to-peak arrival time was chosen to determine travel time, owing to the consistency, clarity and simplicity of this method as compared to other approaches.

2.4 Cyclic triaxial tests

After consolidating the specimens with an effective confining pressure of 100 kPa, a servo-hydraulic loading frame applied the cyclic loading during the tests. All the specimens were

subjected to a sinusoidal cyclic axial load with a frequency of 0.1 Hz under undrained condition. After the double amplitude axial strain reached 5%, the cyclic loading application was stopped. Furthermore, the axial load, displacement, cell pressure and back pressure were electronically recorded through a data acquisition system with a 16 bit A/D conversion into a computer for analysis.

2.5 Particle shape index

In order to distinguish the pumiceous sands from the other types of hard-grained soil particles, 2D scanning electron microscope (SEM) images were taken on different particle sizes of pumice soils and Toyoura sand at their most stable configuration. Subsequently, the methodology of Kikkawa et al. (2013) was followed to analyse the SEM images and quantify the soil particle shape characteristics through roundness coefficient (R_c), aspect ratio (A_r) and angular coefficient (A_c), which are defined as follows:

$$R_c=L^2/4\pi A \tag{3}$$

$$A_r=b/a \tag{4}$$

$$A_c=|R_c - 1 + A_r^2/(2A_r)| \tag{5}$$

In the above equations, L is the perimeter, A is the surface area, while a and b are the dimensions of the particles along the minor and major axes, respectively. Each of the aforementioned parameters (R_c, A_r and A_c) indicates an important feature of a soil particle. For instance, if the value of R_c is equal to one, the particle is circular and if it exceeds unity, the shape would change to ellipsoidal. Furthermore, if $A_r > 1$, the soil particle is more elongated. A higher value of A_c illustrates a more angular particle surface. While the interaction between particles within the triaxial specimen is essentially 3D, these 2D indices can very well characterize the shape of the particles. The average image analysing results are summarized in Table 2 and it is evident that the particle shape indices of natural pumiceous sand are considerably different from those of Toyoura sand. For example, the value of R_c for natural pumiceous soils is approximately 1.5 times higher than that of Toyoura sand. Furthermore, the average A_r value for natural pumice soil is 1.812, compared to 1.483 for Toyoura sand. The A_c value of the natural pumiceous soils is about 5 times higher than that of Toyoura sand.

Table 2: Particle shape indices of pumice sand and Toyoura sand

Soil Type	Number of analysed soil particle images	Average R_c	Average A_r	Average A_c
Natural pumice soil	98	1.703	1.812	0.521
Toyoura sand	50	1.258	1.483	0.179

3 TEST RESULTS

3.1 Effect of confining pressure on maximum shear modulus of pumiceous soils

It has long been established that the maximum shear modulus (G_{max}) of sandy soils is significantly influenced by effective confining pressure (σ'_c) and void ratio (e) (Kokusho 1980). In order to investigate the effect of confining pressure on the G_{max} of undisturbed natural pumiceous soils, several series of bender element tests at different levels of σ'_c (ranging from 50 to 600 kPa) were performed on a single specimen. Furthermore, for the purpose of comparison similar tests conducted on the reconstituted hard-grained Toyoura sand and some results after

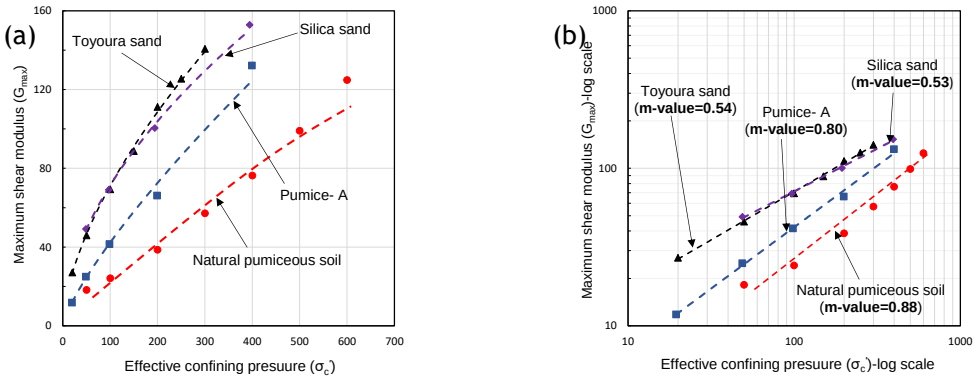

Figure 3: Confining pressure effect on G_{max} of pumiceous soils and hard-grained sands in: (a) normal scale; and (b) log-log scale

Orense et al. (2013) on pure pumice (pumice-A sand) and hard-grained silica sand were collected and compared with natural pumiceous soils.

Figure 3 presents the G_{max} - σ'_c relationship for undisturbed pumiceous material and compared with Toyoura sand, Silica sand and Pumice-A sand. As evident from the graph, the G_{max} of natural pumiceous soil is considerably lower than that of Toyoura sand, Silica sand and Pumice-A sand at all levels of σ'_c. In addition, Figure 3b illustrates that the dependence of G_{max} for natural pumiceous soil on σ'_c is significantly more pronounced when compared to other soils. For instance, in the well-known $G_{max} \propto \sigma'^{m}_c$ relationship, the m value, representing the slope of the best-fit line through the data points, is 0.88 for undisturbed natural pumiceous soil and almost similar to that of Pumice-A sand with m=0.80. However, the m value for hard-grained Toyoura sand and silica sand are significantly lower, with values of 0.54 and 0.53, respectively.

The substantial differences in G_{max} as well as in G_{max}- σ'_c relation for natural pumiceous soil and hard-grained soils (i.e. Toyoura and Silica sands) can be explained by soil particle morphology and the crushability feature of pumice particles. Therefore, the lower value of G_{max} for natural pumiceous soil compared to hard-grained materials could be owing to the distinctive pumice particle characteristics such as porosity, lower unit weight and brittle feature (Wesley 2001; Orense et al. 2012). Furthermore, Figure 4 indicates that the shear wave velocity (V_s) of natural pumiceous soil is lower than that of Toyoura sand. It is well-known that the V_s propagation in soft soil deposits is considerably lower than in stiff soils and, consequently, using a lower value of V_s and unit weight for natural pumiceous soil in Equation (2) would result in lower G_{max} for pumiceous soil when compared to Toyoura sand.

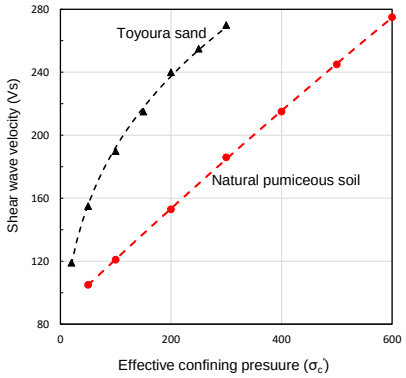

Figure 4: Effect of confining pressure on shear wave velocity of natural pumiceous soil compared to hard-grained Toyoura sand.

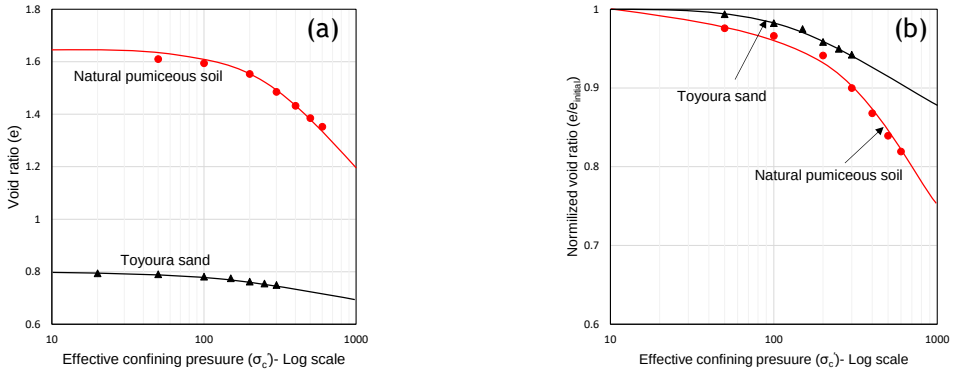

Figure 5: (a) Change in void ratio with respect to confining pressure on single specimen; and (b) normalized void ratio variation with σ'_c for undisturbed natural pumiceous soil and Toyoura sand.

On the other hand, the higher G_{max}-σ'_c dependence of pumiceous soils compared to hard-grained sand can be explained by a better contact area between pumice particles, higher angularity and manifestation of particle crushing. As the isotropic consolidation test results on the tested materials shown in Figure 5 indicate, the natural pumiceous soil illustrates higher decrease in void ratio with respect to the increase in σ'_c during the test compared to Toyoura sand. In order to indicate the changes in void ratio during consolidation test more clearly, the void ratios at all levels of σ'_c were normalized by the initial void ratio ($e_{initial}$) in Figure 5b. The plots indicate that the increment in contact area between pumice particles is more than that of Toyoura sand at each level of consolidation pressure, resulting in a higher m value. Moreover, Cho et al. (2006) investigated that as the soil particles tend to be more angular and elongated, the m value would increase. Along this line, the higher angularity and elongation of natural pumiceous soil, which are shown in Table 2, could be an additional reason for higher m value for natural pumiceous soil compared to Toyoura sand. In addition, the higher angularity and elongation of pumice particles would help the soil assembly to have better interaction (interlocking) with each other and, as a result, have better contact area as σ'_c increases, leading to a higher rate of increase in G_{max} than occurs for hard-grained sand.

3.2 Liquefaction resistance

Figure 6a compared the liquefaction resistance of undisturbed natural pumiceous deposits (D_r=50%) with commercially-available pumice sands. It is noted that the undisturbed pumiceous deposits are more resistant to liquefaction compared to reconstituted commercially-available pumice. This can be explained partially by the contribution of soil fabric and stress history on the liquefaction resistance of the soil, although the effect of other factors (such as difference in fines content and composition) may also be significant.

From Figure 6b, it can be seen that the pumiceous materials are less susceptible to liquefaction compared to Toyoura sand. For example, if the cyclic resistance is defined in terms of the cyclic stress ratio (CSR) corresponding to 15 cycles, then dense Toyoura sand (D_r=90%) has liquefaction resistance almost half of that of undisturbed pumiceous materials (D_r=50%). The higher liquefaction resistance of pumiceous soils compared to Toyoura sand is partly due to the consequences of particle crushing during the cyclic test and rearrangement of the soil skeleton resulting in a more stable soil structure (Asadi et al. 2017). More tests are planned to confirm this phenomenon. It is worth mentioning that Yamawaki et al. (2002) noted that as the values of R_c and A_r of various geomaterials increase, the liquefaction resistance would also increase. In the same vein, the higher angularity of pumiceous soils may be a reason for their high liquefaction resistance when compared to Toyoura sand.

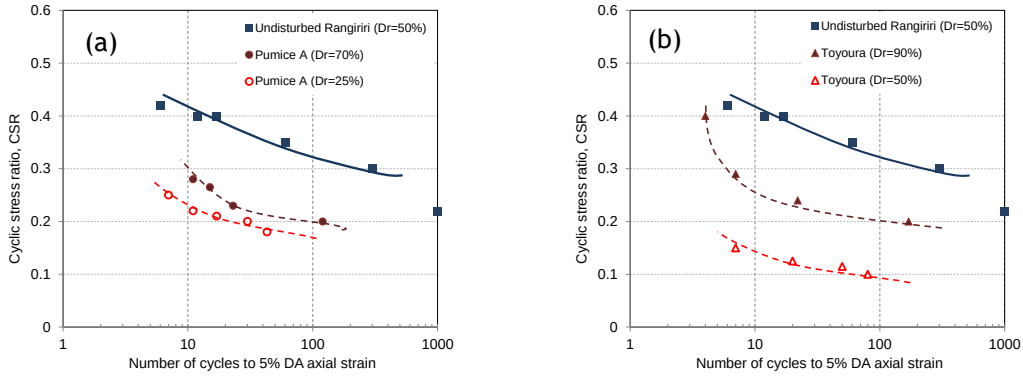

Figure 6: Comparison of cyclic resistance curves of undisturbed pumiceous material with (a) commercially-available pumice; and (b) Toyoura sand (some data after Orense et al. 2012).

4 CONCLUSIONS

In order to investigate the dynamic properties of pumiceous soils from the Waikato basin in the North Island, New Zealand, several series of bender element tests and undrained cyclic triaxial tests were performed on undisturbed pumiceous soils. Similar tests were also conducted on reconstituted hard-grained Toyoura sand. Moreover, to distinguish the pumice particles from hard-grained sand, SEM images of the soil particles were analysed to illustrate the differences. The following are the major conclusions of this study:

- The effect of confining pressure on the maximum shear modulus of natural pumiceous soil was more significant compared to non-crushable soil.
- The maximum shear modulus of natural pumiceous soil was substantially lower than hard-grained Toyoura sand.
- The liquefaction resistance of undisturbed natural pumiceous materials (D_r=50%) was found to be 1.6 times higher than that of medium dense pumice sand (D_r=70%) and almost twice that of dense Toyoura sand (D_r=90%).

REFERENCES

Asadi, M. S., Orense, R. P., & Pender, M. J. (2015) Undrained cyclic strength of undisturbed pumiceous deposits. *Proc. 12th Australia New Zealand Conference on Geomechanics*, Wellington, 8pp.

Asadi, M. B., Asadi M. S., Pender, M. J. & Orense, R. P. (2016) Dynamic properties and undrained cyclic behaviour of undisturbed pumiceous soil. *New Zealand Society for Earthquake Engineering Conference*, Christchurch.

Asadi, M. S., Asadi, M. B., Orense, R. P., & Pender, M. J. (2017) Undrained cyclic and post-liquefaction behaviour of natural pumiceous soils. *3rd International Conference on Performance-based Design in Earthquake Geotechnical Engineering (PBD-III),* Canada.

Cho, G.C., Dodds, J. & Santamarina, J.C (2006) Particle shape effects on packing density, stiffness and strength: natural and crushed sands. *J Geotech Geoenviron Eng*; 132(5):591-602

Cubrinovski, M., Green, RA., Allen, J., Ashford, S., Bowman, E., Bradley, B., Cox, B., Hutchinson, T., Kavazanjian, E., Orense, R., Pender, M., Quigley, M. & Wotherspoon, L. (2010). Geotechnical reconnaissance of the 2010 Darfield (Canterbury) earthquake. *Bulletin of the New Zealand Society for Earthquake Engineering*, 43(4), 243-320.

Cubrinovski, M., Bradley, B.A., Wotherspoon, L., Green, R., Bray, J., Wood, C., Pender, M., Allen, J., Bradshaw, A., Rix, G., Taylor, M., Robinson, K., Henderson, D., Giorgini, S., Ma, K., Winkley, A. & Zupan, J. (2011) Geotechnical Aspects of the 22 February 2011 Christchurch earthquake. *Bulletin of the New Zealand Society of Earthquake Engineering*, 44(4), 181-194.

Ishihara, K. (1993) Liquefaction and flow failure during earthquakes. *Geotechnique, 43*(3), 351-415.

Japanese Geotechnical Society, JGS. (2000) *Soil Test Procedure and Commentaries*, Revised 1st Ed Tokyo (in Japanese).

Kikkawa, N., Orense, R. P., & Pender, M. J. (2013) Observations on microstructure of pumice particles using computed tomography. *Canadian Geotechnical Journal*, 50(11), 1109-1117.

Kokusho, T. (1980) Cyclic triaxial test of dynamic soil properties for wide strain range. *Soils and Foundations*, *20*(2), 45-60.

Orense, R. P., Pender, M. J., Hyodo, M. & Nakata, Y. (2013) Micro-mechanical properties of crushable pumice sands. *Geotechnique Letters, 3*(APRIL/JUN), 67-71.

Orense, R. P., Pender, M. J., & O'Sullivan, A. (2012) Liquefaction characteristics of pumice sands. *Report No. EQC 10/589*, University of Auckland, New Zealand.

Pender, M. J., Wesley, L. D., Larkin, T. J., & Pranjoto, S. (2006) Geotechnical properties of a pumice sand. *Soils and Foundations*, 46(1), 69-81.

Yamawaki, D., Hyodo, M., Nakata, Y., Murata, H., Yoshimoto, N., & Matsuoka, N. (2002) Effect of particle shape on shear behaviour of sand. *Proc., 37th Japan National Conference on Geotechnical Engineering* (in Japanese).

Shirley, D. J. & Hampton, L. D. (1978). Shear-wave measurements in laboratory sediments. *Journal of the Acoustical Society of America, 63*(2), 607-613.

Wesley, L. D. (2001). Determination of specific gravity and void ratio of pumice materials. *Geotechnical Testing Journal*, 24(4), 418-422.

Case study: Geotechnical design of bored piles in rock for the Kawarau Falls Bridge

A S Awad
Coffey Services (NZ), Christchurch
andrew.awad@coffey.com

I Antonopoulos
Coffey Services (NZ), Christchurch
ioannis.antonopoulos@coffey.com

M Sadeghian
Faculty of Engineering, Qazvin International University, Iran
mahdisadeghian36@gmail.com

Keywords: Piles, Queenstown, bridge, schist, elastic continuum method

ABSTRACT

The two-lane bridge on State Highway 6 (SH6) at Kawarau Falls near Queenstown is scheduled to open in the second half of 2017. Designed to withstand a 1/ 2500 hazard level earthquake, the new bridge will provide better access into the Queenstown area and better account for closures and traffic congestion than the existing iconic bridge.

The Structural Designers adopted a two-group pile system for the bridge abutments and five monopile piers to support the deck spanning across the Kawarau River. Given the large loading demands and the anisotropic schist bedrock, the lateral pile performance governed the geotechnical design of the rock socket conditions.

The Elastic Continuum Method (ECM) was utilised for the pile-rock analysis. In this paper, the authors outline their design approach and compare their results with those derived from the Finite Element Method (FEM). The authors discuss the merits and limitations of each method and provide a framework for lateral pile analysis work.

1 PROJECT INTRODUCTION

Queenstown is important to the New Zealand tourism industry and its local population also continues to grow. Over 8,000 vehicles per day cross the existing iconic single-lane Kawarau Falls Bridge which was originally built in 1926 as a dam structure to help with the recovering gold in river below the lake. To alleviate traffic congestion, the New Zealand Transport Agency (NZTA) proposed a new 250 m long and 14 m wide two-lane bridge to replace the existing bridge as the main carriageway.

A two-group pile system was adopted for the north and south abutments and five monopile piers were adopted to support the deck spanning across the Kawarau River. The piers were embedded directly into rock whereas the abutment piles were embedded in lake sediments and glacial till and socketed in rock. The minimum rock socket depths were 5 m for the abutment piles and 7 m for the piers. For Pier 2 (P2) a minimum 8 m rock socket was recommended as this pier had the longest free head length (approximately 17 m). For brevity, the analysis presented in this paper is for P2 only.

2 GEOLOGICAL AND SEISMIC SETTING

Queenstown and the surrounding Wakatipu Valley are underlain by schist of the Caples and Rakaia Terranes. The schist is actively being folded, faulted and eroded in response to regional compression and strain distributed across the mid to lower South Island. Geologists suggest that much of the fault activity and uplift in the area has occurred over the past five million years, and that the ongoing high-stress folding is reflected in the ruggedness of the local mountain ranges.

Repeated glaciations have carved deep troughs into the landscape, with Lake Wakatipu occupying the largest trough in the area. Lake Wakatipu covers an area of approximately 290 km^2 and is over 370 m deep. Furthermore, during the last glacial (Otira) period, the glacial lake covered a much larger area and was significantly deeper.

There is a schist rock outcrop in the middle of the Kawarau River. However, the steeply dipping folded rock meant that that the top of rock elevation varied at each pile location.

The nearby mapped active faults – the Alpine Fault, Nevis Fault and Cardrona Fault – are all capable of producing earthquakes with moment magnitudes (M_w) greater than 7. According to a recent seismic hazard study undertaken by the Otago Regional Council for the Queenstown Lakes District, the primary seismic hazard facing the region is an Alpine Fault earthquake; which is predicted to have a 30% probability of rupturing in the next 50 years.

A 1/ 2500-year return period design peak ground acceleration (α_{max}) of 0.83 g was adopted for the site Class B (Rock) conditions.

3 GEOTECHNICAL PROPERTIES OF SCHIST BEDROCK

The schist bedrock is technically referred to as a 'quartzofeldspathic grey schist and green schist'. It is moderately weathered to unweathered along the pile socket depths. By observing the retrieved core specimen, the platy structure of the rock allows for it to break more readily in the lateral direction (parallel with the schistosity) than in the vertical direction.

The index properties of the schist are outlined below in Table 1 and a photo of the retrieved specimen is shown in Figure 1.

Table 1: Schist Index Properties

Property	Value
Unit weight, γ	27.5 kN/m^3
Intact unconfined uniaxial compressive strength, σ_{ci}	20 – 40 MPa
Rock quality designation (RQD)	10 – 95 %
Intact rock modulus, E_i	7 – 14 GPa
Rock mass modulus, E_m	2.9 GPa
Rock mass modulus parallel with schistosity, E_{m1}	0.6 – 3.7 GPa
Rock mass modulus perpendicular to schistosity, E_{m2}	1.9 – 4.7 GPa
Rock mass rating (RMR)	26 - 50
Geological strength index (GSI)	21 – 45

The rock mass shear strength was estimated using the Hoek and Brown failure criterion (edition 2002).

Figure 1: Photo of typical retrieved core specimen showing foliation patterns

4 PILE DESIGN METHODOLOGY & RESULTS

4.1 Choice of ECM over p-y curves method

The geotechnical analysis of the bridge foundations was carried out using the ECM (by means of in-house Coffey software), as presented in Poulos & Davis (1980). The pile is modelled as a thin elastic strip and the geotechnical layers are modelled as a continuous medium and are assumed to have an elastic stress-strain behaviour. Therefore, the load-deformation pile response output is for small-strain ground behaviour. This method adopts a simplified boundary element approach by limiting the axial and lateral ground pressures to ultimate values specified by the Designer.

The ground reaction-pile displacement (p-y curves) analysis method is the most widely used method for laterally loaded pile design. The ground reaction–pile displacement response is represented by a series of independent bi-linear springs so that at each depth the ground reaction is a non-linear function of lateral pile displacement. This non-linear relationship is represented by the differential equation proposed by Hetenyi (1946):

$$EI.\ d^4y/dx^4 + P_x.d^2y/dx^2 - p - W = 0 \qquad (1)$$

Where: EI = pile flexural stiffness, P = axial load on pile, p = lateral ground reaction (per unit length), w = distributed load along length of pile. The integration of this original formula then produces profiles for shear (V), bending moment (M), bending slope (S) and lateral displacement (y).

Over the years, full-scale lateral load tests on various types of soils have led to established p-y curves being adopted for soil but only a limited number of load tests have been carried out for rock strata. The most commonly used p-y curve rock is the one proposed by Reese (1997) for bored piles in 'weak rock' (σ_{ci} = 0.5 – 5 MPa). Although this approach is commonly used within the industry, it was not adopted as the primary lateral pile design methodology for the Kawarau Falls Bridge due to its limitations and sources of uncertainty.

These sources of uncertainty are:

- It is based on intact rock strength (σ_{ci}) and does not account for rock mass strength, which is important given the schist anisotropy.
- It is based on a limited number of full-scale load tests – one carried out on a brittle coral limestone in Florida and another carried out on sandstone in California. And further, these load tests were for 1.2 m and 2.25 m diameter piles. In reality, the lateral ground reaction depends on the size (diameter) of the foundation.
- It represents an elastoplastic deformation behaviour. The schist rock at Queenstown, being a harder material, is expected to have a more brittle and bi-linear deformation behaviour.

The theoretical advantage of the ECM over the p-y curves method for rock is that the p-y curves method is cruder due to the spacing between the lateral springs acting on the pile.

4.2 Geotechnical strength reduction factor

The geotechnical strength reduction factor (Φg) for pile foundations was derived using the risk-based methodology set out in the Australian piling standard (AS2159-2009) and was calculated to have a value of 0.52.

4.3 Modelling of the pile free length

The free length of the monopiles was modelled as a "virtual layer" (i.e. minimal stiffness values input [E = 0.001 MPa]) because the ECM software program requires input parameters for every layer along the pile length.

4.4 Modelling of pile head and pile toe conditions

As there is no true free head or fixed head condition, both head conditions were modelled to provide a displacement range for the structural modelling to account for. To adopt a reasonable rock socket depth, the toe condition was not fixed against rotation but was fixed against translation (i.e. pinned). Poulos (1972) suggests the pinned toe condition be adopted to model a pile bearing on (but not socketed into) rock. Poulos (1972) initially proposed modelling a rock socketed pile by completely fixing the toe against rotation and displacement. However, for this particular design case, the pinned toe model was adopted to ensure that the stiffness of the surrounding rock was suppressing the pile rotations and bringing the system to equilibrium.

4.5 Analysis of P2

The input parameters for P2 are outlined in Table 2.

Table 2: P2 Analysis Input Parameters

Property	Value
Vertical load at pile head	22.03 MN
Horizontal load at pile head	0.6 MN
Moment at pile head	10.3 MN.m
Concrete pile modulus, E_{pile}	28 GPa
Overall rock mass modulus, E_m	1.9 GPa
Schist skin friction pressure, f_s	0.9 MPa
Schist end bearing pressure, f_b	21.5 MPa
Schist lateral yield pressure, P_y	5.4 MPa (for upper 1.5 m) 10.7 MPa (for the rest)

To account for the anisotropic behavior in relation to lateral pile performance;

- A lower bound E_m value was adopted for design.
- A reduced lateral yield pressure value within the top 1.5 m of rock was adopted due to the increased likelihood of failure along pre-existing fractures at low overburden pressures.

The results of the maximum pile actions for both the fixed head and free head conditions is presented in Table 3.

Table 3: P2 Maximum Pile Actions

Pile Action	Fixed Head	Free Head
Bending moment (MN.m)	6	20
Lateral displacement (mm)	12	120
Shear force (MN)	1	5

5 EVALUATION – COMPARING ECM WITH FEM

To further evaluate the use of the ECM, the authors comparatively assessed the P2 pile response using a Mohr-Coulomb constitutive model with 3D FEM software. In addition to the elastic properties of the pile and rock, using the FEM software required the rock shear strength properties and unit weights of the rock and the pile be input into the model. A concrete unit weight of 25 kN/m3 was assumed for the pile.

The meshed 3D model showing a free head pile embedded into the ground is shown in Figure 3 and the comparative assessment of the results is shown in Figure 4.

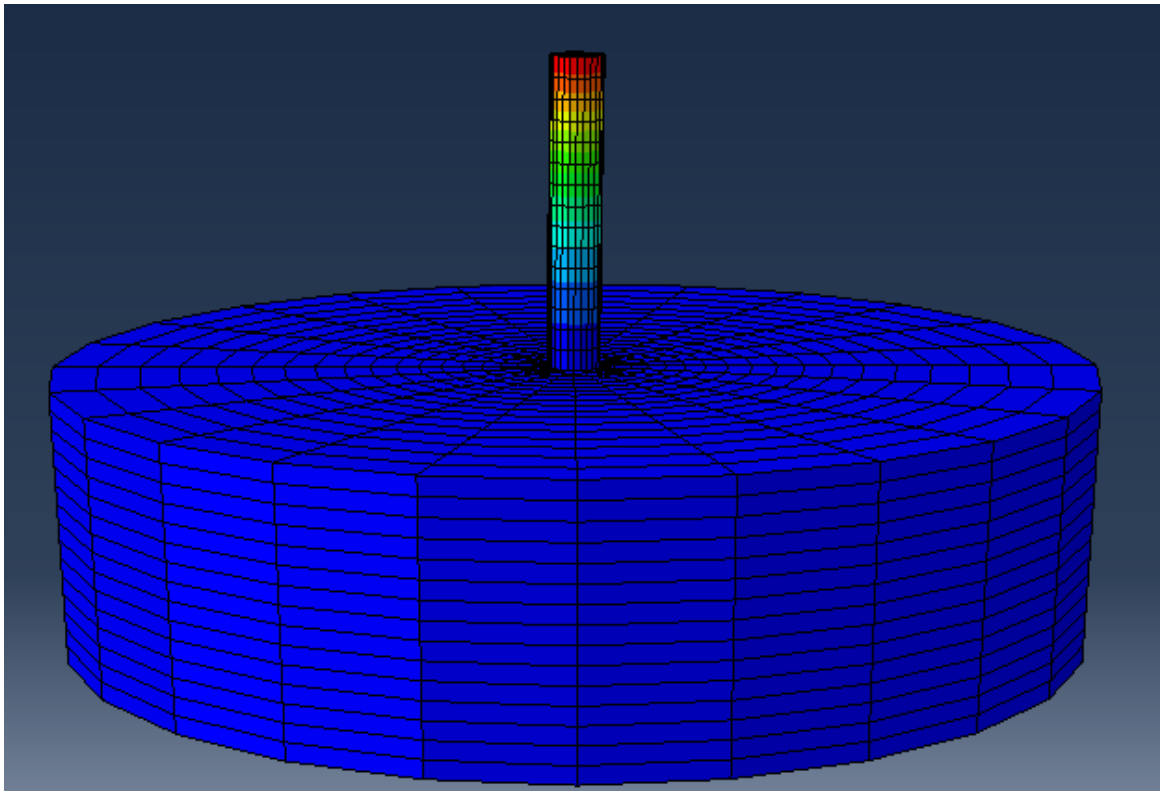

Figure 3: P2 meshed model and for free head pile socketed in rock

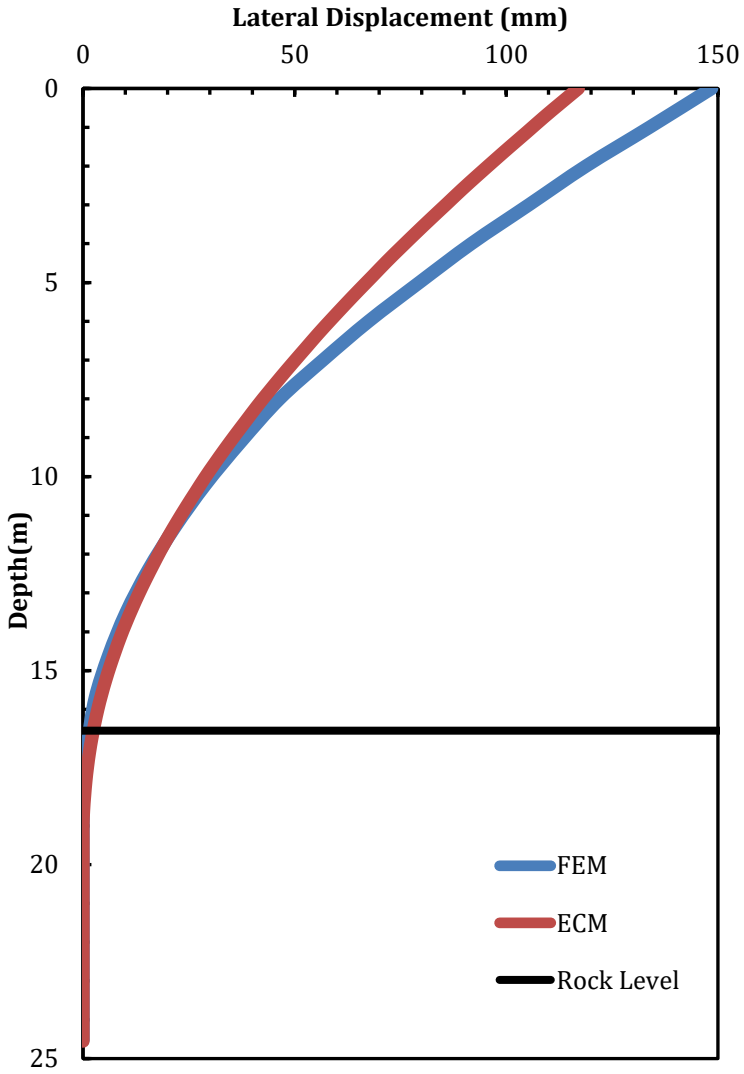

Figure 4: Comparison of ECM with FEM for P2

The results in Figure 4 show that the pile-rock interaction along the rock socket length are almost identical and that the differences between the 1D and 3D analyses along the free head length lie within reasonable limits.

The ECM and FEM are similar in that both methods consider the geotechnical and structural failure of the piles. While they do not account for all the structural details (e.g. the presence and configuration of pile reinforcement), they do provide a reasonable assessment of how the structural element interacts with the surrounding ground. The limitation of FEM, in this particular case, is that it could only model a free head condition because no other superstructure element was constructed in the model to restrain the head movement. However, this limitation also demonstrates an advantage of FEM in that if the ground-structure interaction was modelled for the entire superstructure rather (as opposed to being limited to a single pile element), this would better indicate the actual pile actions at each location. However, the use of the ECM to model a single pile element with both head conditions is a quicker process.

6 DESIGN PROCESS RECOMMENDATIONS

Given the complex pile-rock interaction, an iterative collaborative process between Geotechnical and Structural Engineers is needed throughout the design process for laterally loaded piles. It is recommend that preliminary geotechnical modelling be carried out on trial design lengths, pile diameters, rock socket lengths, etc. Based on the subgrade reaction profile, the Geotechnical Engineers then provide lateral spring values for the Structural Engineers to model the superstructure (and revise loads where necessary). The iterative process is repeated until both the geotechnical and structural models provide comparable pile displacement behaviour (e.g. values within a 10% range) where the pile structural capacity and the geotechnical capacity of the ground have not been exceeded.

7 CONCLUSIONS

Given the complex pile-rock interaction, an iterative collaborative process between Geotechnical and Structural Engineers is needed throughout the design process for laterally loaded piles. Based on this case study, the authors consider that utilising the ECM for piles socketed in rock provides reasonable results when the applied lateral ground pressures are not exceeding the given lateral yield pressure. Further, the results of the ECM are comparable with those of the FEM. Alternatively, more full-scale field load tests on various rock types are recommended and the subsequent p -y curve parameters should be related to the rock mass properties, not only intact rock properties.

8 ACKNOWLEGEMENTS

The authors wish to acknowledge the NZTA and McConnell Dowell Contractors.

REFERENCES

Awad, A., and Searle, J. (2016) Liquefaction potential of the micaceous lake sediments in the Queenstown area, *Proceedings from the ANZ 11th Young Geotechnical Professional Conference*, Queenstown, New Zealand.

Hetenyi, M. (1946) *Beams on elastic foundation*. Ann Arbor: The University of Michigan Press.

Hoek, E., C. Carranza-Torres, and B. Corkum (2002) Hoek–Brown Failure Criterion—2002 Edition, *Proceedings, North American Rock Mechanics Society Meeting*, July 8–10, 2002, Toronto, ON, Canada.

Otago Regional Council. (2015) *Seismic Hazard in Queenstown Lakes District*: Study Report.

National Corporate Highway Research Program, NCHRP Synthesis 360. (2006) *Rock-Socketed Shafts for Highway Structure Foundations*, Transportation Research Board of National Academics, Washington D.C.

Poulos, H.G. and Davis, E.H. (1980) *Pile foundation analysis and design*, John Wiley, New York.

Poulos, H.G. (1972) Behaviour of Laterally Loaded Piles: III Socketed Piles, *Journal of the Soil Mechanics and Foundations Division*, Vol. 98, No. SM4, pp. 341–360.

Reese & Van Impe (2011) *Single Piles and Pile Groups under Lateral Loading* (2nd Edition), CRC Press – Taylor and Francis Group, Netherlands.

Reese, L.C. (1997) Analysis of Laterally Loaded Piles in Weak Rock, *Journal of Geotechnical and Geoenvironmental Engineering*, Vol. 123, No. 11, pp. 1010–1017.

Standards Australia (2009) *Piling – Design and Installation*, AS 2159-2009 (Incorporating Amendment No. 1), Standards Australia, Sydney, Australia.

Turnbull, I.M.(compiler). (2000) *Geology of the Wakatipu Area*, Institute of Geological & Nuclear Sciences 1:250000 geological map 18. 1 sheet + 72 p. Institute of Geological & Nuclear Sciences Limited, Lower Hutt, New Zealand.

Defining importance levels for the design of retaining walls

K R Anderson
AECOM NZ Ltd, Auckland, NZ
kevin.anderson2@aecom.com (Corresponding author)

Keywords: retaining wall, importance level, safety, design standard

ABSTRACT

Retaining wall design does not typically differentiate between levels of importance, particularly for static design. Walls that are more important, for example supporting importance level four buildings, are often designed to the same safety margins as relatively unimportant walls. Indeed, it can be argued that using more sophisticated analysis and more geotechnical data for more important walls, that the overall level of safety may be lower than less important walls which typically require only routine and inherently more conservative methods.

Importance levels are commonly used in the design of buildings, as required by the Building Act 2004 and associated Building Regulations 1992. However, they are not typically used for retaining wall design except for in some limited load cases such as to determine seismic earth pressures. Whilst the design of retaining walls is subject to the requirements of the Act and Regulations, the importance levels definitions are intended for buildings and are not easily interpreted for retaining wall design. This paper provides a review of local and international practice in defining differing levels of importance to retaining wall and recommends a method of interpretation for New Zealand practice.

1 INTRODUCTION

The design of retaining walls does not typically differentiate on the importance of the wall. For example a wall supporting the foundations of a building required for post-disaster functions may be designed to the same level of safety as a relatively less important wall, such as a wall supporting a cut above a low use private road. The consequences of failure of these examples are significantly different. Should the more important wall be required to be designed to a higher standard?

Walls with higher consequences of failure are often designed with better information, such as higher quality geotechnical investigations and well defined geometry, and with more sophisticated methods of analysis. Whilst this improves the understanding of wall behaviour and reduces the uncertainties relating to failure, it is more likely that the wall design is optimised and value engineered, which may result in smaller margins of error against failure. The risk of failure is studied in reliability and probabilistic methods of analysis, but is more implicit in the more common deterministic methods of analysis. Retaining wall design is often governed by static design, particularly in low seismic hazard areas and for flexible walls where displacement in earthquakes can be tolerated, therefore the importance level classification makes little difference to the design of many retaining walls.

Importance levels are used to a limited extent in some aspects of geotechnical engineering. These are probably best understood when evaluating seismic hazard, where less likely but higher consequence earthquakes are considered in the design. This is typically simplified to a return period factor, where a higher factor (and therefore stronger ground motions) is used for more important structures.

Established standards such as the Building Regulations (MBIE, 1992), NZS1170 (Standards NZ, 2002) and Bridge Manual (NZ Transport Agency, 2016) provide some guidance on importance levels. These are typically for buildings and critical infrastructure. Therefore, interpretation is required for typical retaining walls.

2 EXISTING STANDARDS

2.1 Building Regulations

All building work in New Zealand, including retaining walls, must comply with the Building Act, Building Regulations and Building Code. Retaining walls would usually be classified as an ancillary building, i.e. not used for human habitation (Regulations, Clause 8). This classification allows exemption from some provisions such as amenity, but structural and safety aspects must still be complied with. Clause A3 of the Regulations sets out building importance levels. Whilst the clause describes building use and occupation, interpretation can be made for retaining wall design.

Table 1: Importance Level as defined by the Regulations (amended)

Importance Level	Description of building type
1	Buildings posing low risk to human life or the environment, or a low economic cost should the building fail. These are typically small non-habitable buildings, such as sheds, barns, and the like, that are not normally occupied, though they may have occupants from time to time. Examples: • Ancillary building not for human habitation • Minor storage facilities
2	Buildings posing normal risk to human life or the environment, or a normal economic cost, should the building fail. These are typical residential, commercial, and industrial buildings.
3	Buildings of a higher level of societal benefit or importance or with higher levels of risk significant factors to building occupants. These buildings have increased performance requirements because they may house large numbers of people, vulnerable populations or occupants with other risk factors or fulfil a role of increased importance to the local community of society in general Examples: • Where >300 people congregate in one area • Primary or secondary school or daycare (capacity > 250), college or adult education facilities (capacity >500) • Health care facilities (capacity >50) but not having surgery or emergency treatment • Jails and detention facilities • Any other building with >5,000 capacity • Power generating facilities, potable water and wastewater treatment facilities, and other public utilities facilities not designated as post-disaster
4	Buildings that are essential to post-disaster recovery or associated with hazardous facilities. Examples: • Hospitals and other health care facilities having surgery or emergency treatment • Fire, rescue, and police stations • Emergency shelters, preparedness, operation centres and response • Power generating stations and other utilities required as emergency backup facilities for importance level 3 structures

2.2 Building Code Clause B1 Verification Method VM4

The verification method B1/VM4 Foundations (MBIE, 2016) provides a design method by which compliance with the Building Code may be verified. It is very commonly used and referenced when designing retaining walls in New Zealand. The method does not provide any guidance on determining importance levels.

2.3 AS/NZS1170.0:2002 Structural design actions, Part 0: General principles

NZS1170.0 specifies general procedures and criteria for the structural design of a building or structure. It is a widely used reference for design in New Zealand. The importance level is reflected in the acceptance of the probability of exceeding a limit state. This is determined using the annual probability of exceedance for actions. A 10% probability of exceedance in the life of the structure is commonly accepted, therefore 1/500 for earthquakes. This probabilistic approach is only used for the highly variable environmental actions, for example wind, earthquakes and snow. Other actions are determined deterministically including dead, live and earth pressure loads. Therefore, in some aspects, structural design does not differentiate between buildings of different importance.

2.4 NZTA Bridge Manual

The Bridge Manual (NZTA, 2016) sets out criteria for the design of bridges, culverts, earthworks and retaining walls. The manual is used for NZTA's state highways but other organisations often reference it, for example local council road controlling authorities. Similar to NZS1170, the manual follows limit state principles adopting a statistical approached to deriving loads. Specific guidance for importance levels is provided for retaining wall design. As NZTA's state highway network is typically of relatively high importance due to the high consequences of failure, use of the manual for private development and less important assets would generally be considered quite conservative.

Table 2: Importance level for retaining walls as defined by the bridge manual (from NZTA, 2016, amended)

Importance Level	Route security (typically supports road)	Protection to adjacent property (typically above road)
1	Not primary lifeline route and height <5m or area <50m^2 No-exit or loop rural roads and serving population <50 Where failure would not affect the use of the road	Failure would not significantly endanger adjacent property
2	Primary lifeline route and height <5m or area <100m^2 Not primary lifeline route and height >5m or area >50m^2	NZS1170.0 Table 3.2 Consequences >$1.3M
3	Primary lifeline route and height >5m or area >100m^2	NZS1170.0 Table 3.2
4	Critical to post-disaster recovery (for example where failure would close important roads)	Post disaster function NZS1170.0 Table 3.2
• Retaining walls associated with bridges determined based on that bridge • Retaining walls not defined above to be IL2 • Determination of height includes consideration of backslope		

2.5 AS4678-2002 Earth retaining structures

The standard sets out requirements and recommendations relating to the design and construction of structures required to retain soil, rock and other materials. The standard is widely used in New Zealand. Walls are classified as shown in the following table. The classification is used to vary some aspects of the design, for example lesser live load surcharge and less conservative strength

reduction factors may be used for the lower classification walls. The standard also provides recommendations for different levels of construction monitoring. The principles of the approach in the standard are interesting, however the system is rather limited as most walls will be in the middle classification which would cover several importance levels in the NZ Building Regulations/NZS1170.0 system. The partial factors that vary for the classification are not necessarily critical to the design, therefore, there may be little difference in safety.

Table 3: Structure classification for retaining walls as defined by AS4678-2002 (amended)

Classification	Description	Examples
A	Low consequence for loss of human life, or small or moderate economic, social or environmental consequences	Where failure would result in minimal damage and loss of access. Areas rarely visited by people. Walls on private property supporting gardens.
B	Medium consequence for loss of human life, or considerable economic, social or environmental consequences	Where failure would result in moderate damage and loss of access. Walls supporting or above normal structures. Walls supporting minor roads. Walls above public spaces. Walls >1.5m height.
C	High consequence for loss of human life, or very great economic, social or environmental consequences	Where failure would result in significant damage or loss of life. Walls supporting, or supporting or above access for, structures identified for post-disaster recovery.

2.6 Other international guidance

Eurocode 7 Geotechnical Design (BS EN 1997-1:2004) includes a three tier categorisation system which is based on the complexity of the structure. For example, Category 1 is for small and simple structure and Category 3 is for large or unusual structures or those in high seismic areas. The system does not require safer structures through mandated partial safety factors.

BS8006:1995 Code of practice for strengthened/reinforced soils and other fills included a partial load factor depending on the ramifications of failure. Three categories were defined. The system is similar to AS4678-2002.

Hong Kong's Geoguide 7 Guide to Soil Nail Design and Construction (GEO, 2008) describes a three tier system where the consequences to life and economy are to be considered with higher safety required for the more important structures. There can be quite a significant different (1.4 compared to >1.0) in the required safety between the most and least important structures.

3 POTENTIAL ISSUES WITH CURRENT PRACTICE

Two related potential issues have been identified with the determination and application of importance levels in the design of retaining walls in typical projects in New Zealand. These are inconsistency and the lack of relevance.

3.1 Inconsistent use of importance levels

There is a wide range of importance levels (IL) that can be applied to retaining wall design, particularly for private development. Many designers adopt an IL equivalent to typical buildings, i.e. IL2. However, the IL for a typical 5m high wall could be IL1, IL2 or IL3 based on the definition in the Regulations, a typical building or Bridge Manual respectively. The decision between these would largely be dependent on the subjective interpretation by the designer.

An example of where inappropriate selection of the importance level could occur is where a retaining wall is very close to a more important structure, for example a building with a post-disaster function which is therefore classified as importance level four. Collapse of the retaining wall could result in disruption to that building by blocking access or even cause significant structure damage. The Bridge Manual, however, requires that such "associated" structures be classified with equivalent importance as the more important structure.

3.2 Lack of relevance of the importance level in retaining wall design

It could be expected that more important structures be designed to be safer. However, if the only actions that increase due to a higher importance classification are not critical to the design, then there is no difference in safety of these structures. Research has indicated that earthquake design is not critical for many types of retaining wall where the design acceleration is less than 0.4g (Atik & Sitar, 2010). The following table indicates that for a typical flexible retaining wall there are few locations where the seismic hazard is high enough to be critical to the design.

Another comparison would be to consider the decrease in load factor for static design (F_E = 1.5) to seismic design (E_u = 1.0). As earth pressure is usually the critical action, it would need to increase by 50% due to earthquake acceleration even before other behaviours are considered like tolerable wall displacement. The coefficient of earthquake active lateral pressure (DK_{AE}) only exceeds 0.5 in very strong earthquakes.

Table 4: Comparison between return period factors and load factors

Importance Level	Return period factor (Annual probability of exceedance)	Hazard factor for k_h > 0.4g	Locations
1	R = 0.5 (1/100)	C0,1000 > 0.65	None
2	R = 1.0 (1/500)	C0,1000 = 0.58	Arthur's Pass and Otira
3	R = 1.3 (1/1000)	C0,1000 = 0.44	Woodville/Masterton/Wellington The north and west South Island (NW of Cheviot/Te Anau)
Assuming 50 year design life, Site subsoil class C, wall displacement factor 0.5			

4 RECOMMENDED DEFINITION AND USE OF IMPORTANCE LEVELS

The fundamental issue with considering the use of importance levels is whether it is desirable that more important retaining walls be safer than walls where the consequences of failure are less significant. If it is desirable, then it is necessary that importance levels are used to differentiate for all critical failure mechanisms, not only seismic actions as current practice. This could be achieved by applying partial safety factors based on importance level. These could be load factors or strength reduction factors, or both.

The importance levels defined by the Building Regulations are considered appropriate for use for retaining walls. The interpretation is critical. Too many walls are defined with an unnecessarily high importance level. Compared to buildings, which are usually occupied, failure of a typical retaining wall is unlikely to result in fatalities or high economic cost. Even locations such as high use car parks or city centre footpaths rarely have people standing at locations where failure would pose them an extreme risk.

It is also unnecessary to directly relate importance level to wall geometry such as area, or more significantly to height, rather than using a risk based approach. It is more likely that large walls are more important for other reasons, such as their failure could damage a nearby building.

However, a 10m high wall supporting a car park is not necessarily as important as a smaller wall supporting the foundations of a building.

The following table provides recommended guidance for determining importance levels for retaining wall design.

Table 5: Recommended definition of importance levels for retaining walls

Importance Level	Risk to human life and environment should the retaining wall fail	Comment
1	Low	Most retaining walls
2	Normal	Typically supporting, or above, area commonly occupied
3	High	Typically supporting or above area commonly occupied by a large number of people or where failure would have significant consequences to society
4	Very high	Retaining wall required for post-disaster function or associated with hazardous facilities

Notes:

1. Where failure of a retaining wall would pose a significant risk to a structure of higher importance level (i.e. the retaining wall is an associated structure), then the same importance level as that structure to be used. This includes where a retaining wall supports, or is above, access or emergency egress from that building.
2. For clients and asset owners that have specific requirements (for example NZTA), their definition of importance level to be used.
3. Risk of failure should be compared to a building of the same importance level.

Increasingly conservative safety factors are recommended based on importance level. This would require more important walls to be safer. The following factors have been derived from similar retaining wall standards used internationally and extrapolated to the New Zealand importance level system.

Table 6: Recommended safety factors for retaining walls considering importance level

Importance Level	Global factor of safety for static design	Load factor for static design	Strength reduction factor
1	1.4	1.0	1.00
2	1.5	1.1	0.95
3	1.6	1.2	0.90
4	1.7	1.3	0.85

Notes:

1. Global factors of safety are typically used for deep seated slope stability failure mechanisms. These should also be applied to associated slopes, for example retaining wall backslopes.
2. Load factor to be additional to those typically used for actions. For example for IL3, equation 6-4 of the NZGS Module 6 becomes $E_{d,dst} = 1.2 * [1.2G + 1.5 F_E + 0.4Q]$ for the gravity design case.
3. Strength reduction factor to be additional to those typically used when assessing resistance and capacity.

5 IMPLICATIONS IN PRACTICE

The improved definition of importance levels would allow a more rational basis for retaining wall design. There would be a clear difference between retaining walls where the consequences of

failure are relatively minor compared to walls where failure would be significant. The use of specific safety factors would require more important walls to be safer for all failure mechanisms.

It is possible that the cost of more important retaining walls would increase. However, improved use of project based strength reduction factors (for example those defined in the piling standard AS2159-2009) and improved understanding of risk based design would result in more appropriate solutions. It is also likely that better definitions of less important walls combined with less conservative safety factors would result in more economic solutions for many retaining walls.

6 CONCLUSION

The existing use of importance levels in retaining walls design is inconsistent due to the lack of definition for how to interpret building standards. What guidance is available tends to be for assets of high importance and community value, for example state highways required for lifelines in post-disaster circumstances. Design practice only typically uses importance levels for seismic design which is often not critical to the design of walls, therefore the use of importance levels of little relevance to the final design outcomes. A specific design standard or guideline would likely improve the consistency and quality of retaining wall design.

The philosophy and intent of importance levels is potentially very useful. It would be straightforward to require more important walls to be designed to be safer. There are some examples internationally of additional requirements, for example for safer partial factors to be used. It is logical that walls required for post-disaster functions and where the consequences of failure are more significant that the probability of failure would be much lower.

Importance levels can easily be defined by the risk of failure. Most retaining walls have a relatively low risk compared to buildings, therefore most walls should be importance level one. Where the consequences are higher, for example where failure may result in significant damage to a building, then higher importance levels should be used. It is not necessary to define importance levels based on height or other parameters.

It is recommended that more conservative safety factors be used for more important walls. Specific partial factors have been suggested in this paper ranging from 1.4 to 1.7 for global stability, 1.0 to 1.3 for load factors and 1.0 to 0.85 for strength reduction factors. Use of such factors would result in a significant difference in safety between high and low importance retaining walls.

REFERENCES

AS2159-2009 Piling – Design and installation, Standards Australia

AS4678-2002 Earth retaining structures, Standards Australia

AS/NZS1170.0:2002 Structural design actions, Part 0: General principles, Standards NZ

Atik, L.A. & Sitar, N.S. (2010), Seismic earth pressure on cantilever retaining structures, ASCE *Journal of Geotechnical and Geoenvironmental Engineering*

BS8006:1995 Code of Practice for Strengthened/reinforced Soils and Other Fills, British Standards Institute

BS EN 1997-1:2004 Eurocode 7 Geotechnical Design, British Standards Institute

Geotechnical Engineering Office (2008), *Geoguide 7 Guide to Soil Nail Design and Construction*, Civil Engineering and Development Department, The Government of the Hong Kong Special Administrative Region

Ministry of Business, Innovation and Employment (2016), *Acceptable Solutions and Verification Methods for NZ Building Code Clause B1 Structure*

NZ Geotechnical Society & Ministry of Business, Innovation and Employment (2017), *Earthquake geotechnical engineering practice, module 6: earthquake resistant retaining wall design*

NZ Government (2004), *Building Act*

NZ Government (1992), *Building Regulations*, SR1992/150, administered by Ministry of Business, Innovation and Employment

NZS1170.5:2004 Structural design actions, Part 5: Earthquake actions – New Zealand, Standards NZ

NZTA, 2016, *Bridge Manual*, SP/M/022, 3rd edition

New Plymouth CBD Site Subsoil Class: Results from ground investigation

G J Alexander, C Y Chin, C Kayser & J Bradshaw
Beca Ltd, Auckland, NZ
Gavin.alexander@beca.com (Corresponding author)

Keywords: New Plymouth, Site Subsoil Class, NZS 1170.5

ABSTRACT

The geological profile of a site and hence the determination of a site subsoil class can have a significant influence on the selection of a design peak ground acceleration (PGA) as derived from NZS 1170.5 (2004). At the New Plymouth Central Business District (CBD), various practitioners have historically held different views of the site subsoil class. These have been presented as being either Class C or D. This has come about when the underlying Quaternary Lahars or the Late Miocene-Pliocene sedimentary Matemateaonga Formation have been considered as bedrock.

Results of ground investigations comprising three deep cored boreholes put down in the CBD, unconfined compressive strength testing and shear wave velocity testing are presented. An assessment of the site subsoil class based on a strict interpretation from NZS 1170.5 (2004) is presented in this paper. The results show that neither the Lahars nor the Matemateaonga Formation meet the criteria of bedrock in accordance with NZS 1170.5 (2004). This means that the site in the CBD should have a subsoil class of Class D based on a strict interpretation of NZS 1170.5 (2004, Amendment 1, 2016). These findings may have implications on the selection of site subsoil class for other parts of New Zealand which are underlain by weak and variably cemented rock, and wider debate is encouraged.

1 INTRODUCTION

Beca was commissioned by the New Plymouth District Council (NPDC) to undertake ground investigation over a period from January 2016 to August 2016 in the New Plymouth Central Business District. The Ministry of Business, Innovation and Employment (MBIE) provided funding for the shear wave velocity testing component of the investigation. The purpose of the investigation was to obtain data to assist with the assessment of the site subsoil classification in terms of NZS 1170.5 (2004).

The scope of works included the drilling of three deep cored boreholes up to 162.5m depth to determine the depth to and nature of rock, and the stiffness of the Laharic deposits above. Unconfined compressive strength (UCS) testing of recovered core samples were undertaken and PVC access tubes were installed to allow for shear wave velocity testing.

The boreholes were drilled at three Council owned sites within the New Plymouth CBD (as shown on Figure 1 and described in Table 1).

2 GEOLOGY OF THE NEW PLYMOUTH CBD

The relevant published geological map for the area, Geology of the Taranaki Area (Townsend et al. 2008) shows the New Plymouth CBD to be underlain by Quaternary Beach Deposits overlying Undifferentiated Quaternary Lahars which are in turn underlain by Late Miocene - Pliocene sedimentary rock (Matemateaonga Formation).

The Quaternary beach deposits typically comprise planar to cross-bedded sands, and may include gravel and boulders. The undifferentiated Quaternary Lahars comprise gravelly sand, with cobbles and boulders of andesite, while generally competent and suitable for founding structures, the origin of this material implies that it is laterally and vertically discontinuous. The Matemateaonga Formation consists of muddy sandstone, with beds of siltstone, mudstone, limestone or shellbeds, and locally coal and conglomerate.

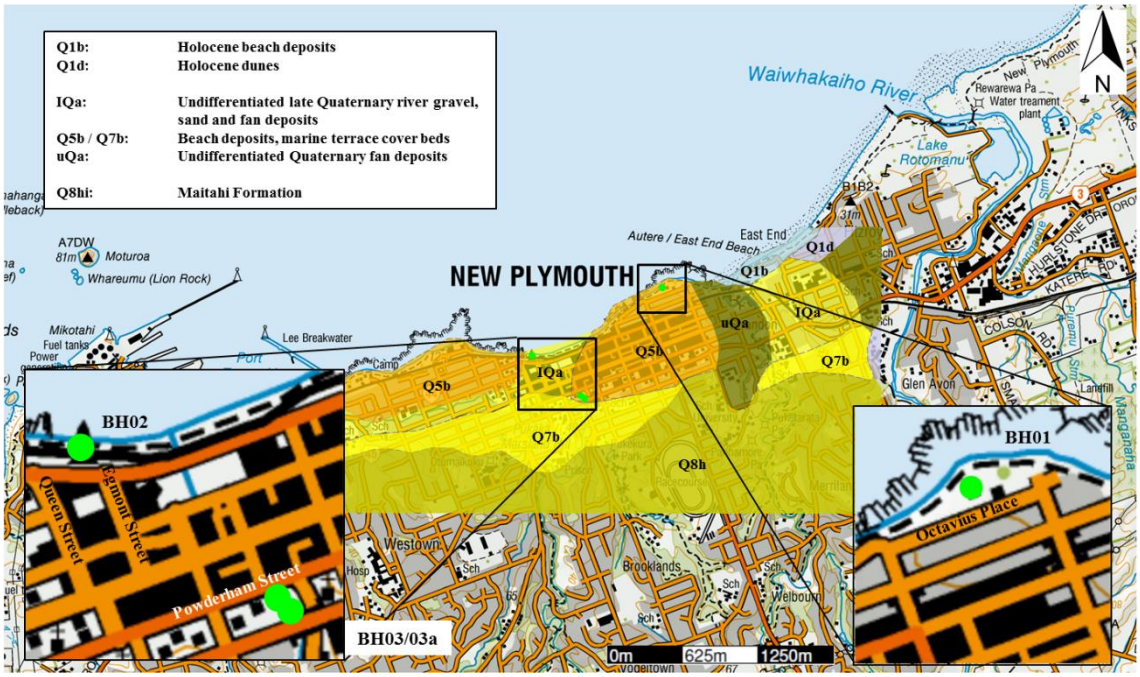

Figure 1: Borehole locations, NZ topo50 Gridless Maps (Land Information New Zealand (LINZ)) and geological layers as per Townsend et al. (2008)

3 RESULTS OF GROUND INVESTIGATION

3.1 Borehole Drilling

Machine boreholes were drilled at 3 CBD locations, triple tube cored (to 'H' size) to depths of between 92.0m and 162.5m. The upper soil profile included ~5m thickness of andesitic ash (cohesive), overlying Quaternary beach deposit sands (~8.5m thick, found at the coastal BH01 only), overlying gravelly sandy undifferentiated Quaternary lahar deposits (~22m to 31m thick), with muddy sandstone/mudstone rock of the Matemateaonga Formation beginning at 33m to 45m depth. BH03 also included uncemented marine sand between the lahars and Matemateaonga Formation rock (~8.5m thick).

Target drilling depths of 110m to 130m were proposed, to drill sufficiently beyond the expected rock interface to prove strong/cemented intact rock. However, rock strengths and cementation remained variable with depth.

Core samples of sandstone/mudstone of varying strengths and depths were collected from all three boreholes for UCS testing.

3.2 Shear Wave Velocity Testing

Shear wave velocity testing was initially proposed to be undertaken at 1.0m intervals, in two directions in each borehole. However, a number of borehole obstructions and equipment damage occurred during testing which prevented the tests to be completed to the full depth of Boreholes

1 and 3. Testing was initially undertaken in June 2016, and re-testing in August 2016. A summary of the shear wave testing undertaken is shown in Table 1 below.

Table 1 – Summary of Shear Wave Testing

Bore ID	Location	Depth (m)	Direction (s)	Test depth achieved (m)	Comments
BH01	Mt Bryan (near Octavius Place)	162.5	N-S E-W	136.0 94.0	Shear wave probe was accidentally dropped at 136m and the cable damaged, preventing further testing.
BH02	Wind Wand (Egmont St)	92.0 (88.0)	N-S E-W	88.0 88.0	The borehole was drilled to 92m, however the PVC tube was installed to 88m due to drilling complications.
BH03	Carrington St carpark	131.0	N-S E-W	108.0 119.0	Testing encountered an obstruction at 119m depth.

Comparisons of measured shear wave velocities in two directions for a given borehole were carried out. Results of shear wave velocity profiles, soil and rock profile together with UCS test results at respective depths are summarised in Figure 2, Figure 3 and Figure 4.

Except for some differences in BH02 at -39.5mRL and in BH03 at -15mRL and -65mRL, the shear wave velocity measurements in two axes for each borehole were generally close to each other. The average of the differences of shear velocity expressed as a percentage for the two axes down each borehole ranged from -3% to 5% for the three boreholes.

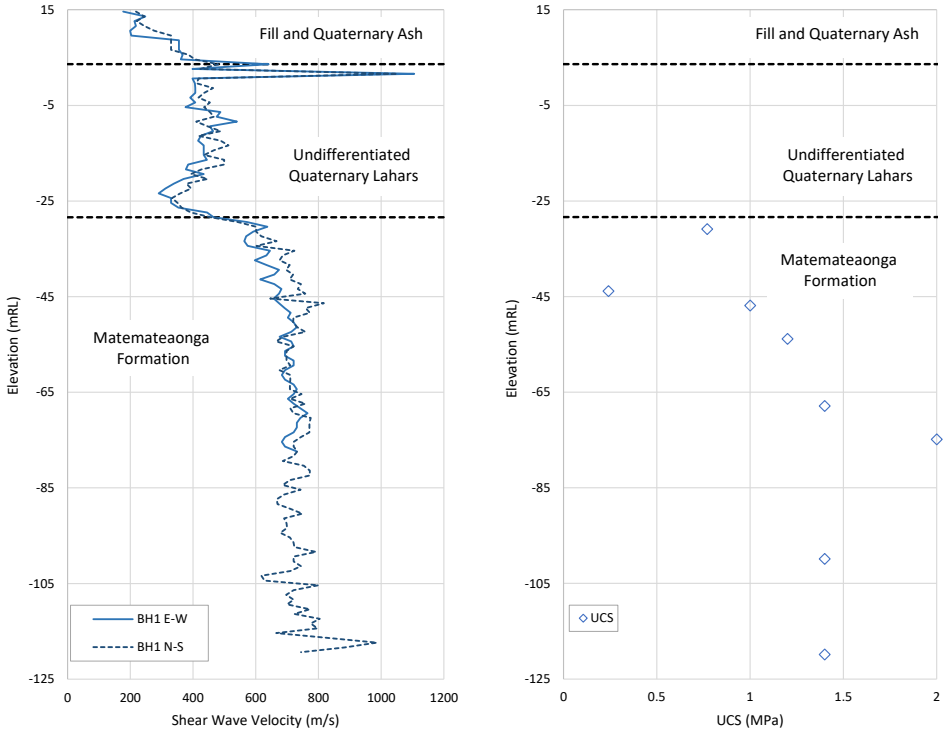

Figure 2: Shear wave velocity profile and relevant UCS results for BH01

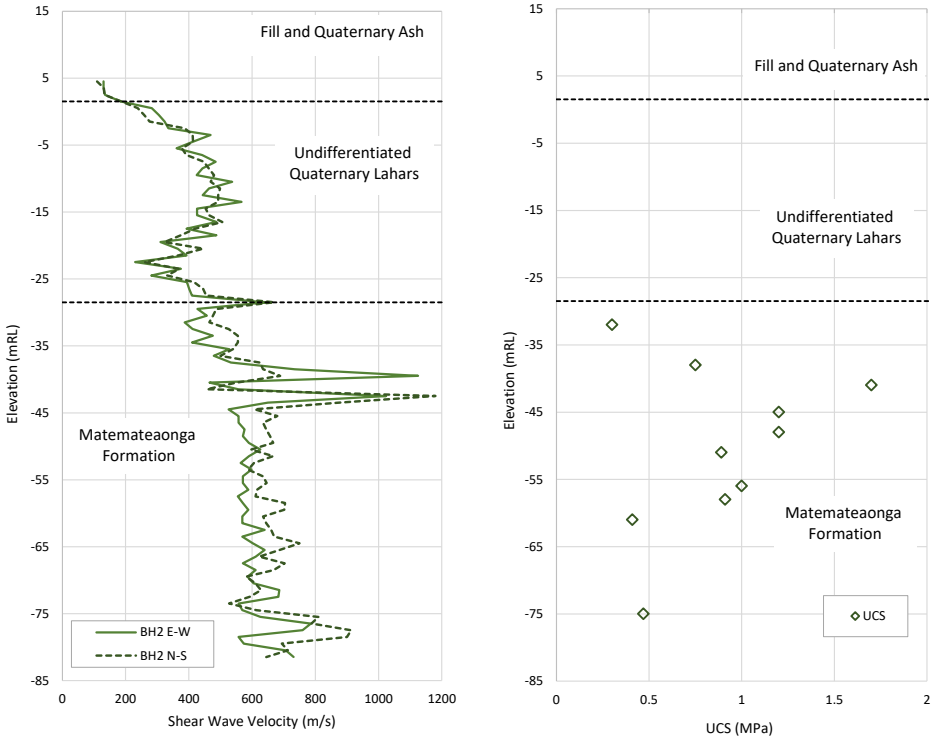

Figure 3: Shear wave velocity profile and relevant UCS results for BH02

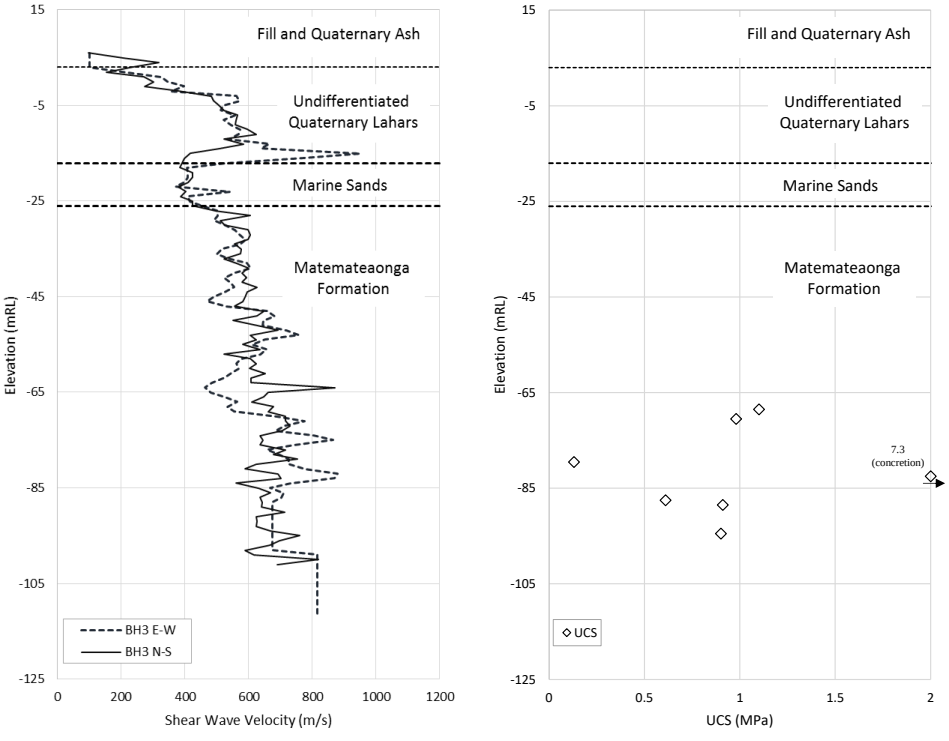

Figure 4: Shear wave velocity profile and relevant UCS results for BH03

4 ASSESSMENT OF SITE SOIL-CLASS

NZS 1170.5 Clause 3.1.3.1 (Amendment 1, September 2016) specifies a number of methods to assess the site class in the following order of preference:

(a) Measurements of shear-wave travel times or shear-wave velocities;
(b) Shear-wave velocities obtained by inversion of geophysical measurements, where the inversions are constrained by information from site profiles developed from geotechnical logging at the site or nearby;
(c) Shear-wave velocities calculated from empirical correlations for the relevant soil materials;
(d) Borelogs including measurement of geotechnical properties;
(e) Evaluation of site periods from Nakamura (horizontal/vertical) spectral ratios or from recorded earthquake motions;
(f) Borelogs with descriptors but no geotechnical measurements; or
(g) Surface geology and estimates of the depth to underlying rock.

For sites with layered soils, NZS 1170.5 (Clause 3.1.3.7) allows the natural period of the site to be estimated by summing the contributions to the natural period of each layer. The contribution of each layer may be estimated by multiplying 0.6s by the ratio of the layer's thickness to that for its soil type in Table 3.2 of NZS 1170.5 (2004). However, Larkin and Van Houtte (2014) provide evidence that the NZS 1170.5 method calculates smaller (and unconservative) site periods when compared with other established methods such as closed form solutions (e.g., Dobry & Madera in Madera (1971) as reported in Larkin and Van Houtte (2014)) or lumped mass solutions. Given the soil layering observed in this site, the closed form solution (Dobry & Madera) was adopted for the determination of site period.

5 FINDINGS

Descriptions of the Matemateaonga formation below are confined spatially to the locations of the boreholes and results should not be extrapolated beyond these locations.

5.1 Strict Interpretation of NZS 1170.5

The Matemateaonga formation encountered in the three boreholes comprised alternating layers of extremely weak to weak, moderately to slightly weathered mudstone, extremely weak to very weak, moderately to slightly weathered sandstone, and layers of uncemented dense, fine to medium sand at interspersed depths in all three boreholes. NZS 1170.5 (2004) defines rock as having:

- A compressive strength between 1MPa and 50MPa; and
- An average shear-wave velocity over the top 30m greater than 360m/s; and
- Not underlain by materials having a compressive strength less than 0.8MPa or a shear wave velocity less than 300m/s.

The following were observed from the investigations:-

- UCS of the Matemateaonga formation ranged generally between 0.24MPa to 2.1MPa, with one rock sample identified as a concretion tested at 7.3MPa. This range falls outside (less than) the 1MPa minimum threshold to be considered as a rock.
- Rock with interbedded sand layers is expected to have different spectra from rock without sand layers. The Commentary to NZS 1170.5 with respect to the definition of rock clarifies that "…the spectra and peak ground accelerations for the soil sites that were formerly combined with rock sites were statistically significantly different from rock spectra, and similar to spectra from other shallow soils." It further states that "Very

> stiff or very dense soils or gravels that may have shear-wave velocities in this range are excluded on the basis of the studies referred to earlier."

Based on the above findings and on carrying out a strict interpretation from the definitions in NZS 1170.5 (2004) with respect to rock strength and soil inter-layering, we conclude that the Matemateaonga formation should not be considered as bedrock.

5.2 Interpretation from Site Period

Using shear wave velocity measurements obtained from this study, calculations of site periods were undertaken based on Dobry & Madera (as reported in Larkin & Van Houtte (2014)). Assuming that the maximum depth of the Matemateaonga Formation was equal to the proven depth of 136m BGL and that bedrock is immediately below 136m bgl, calculated site periods based on maximum and minimum measured shear wave velocities ranged from 0.73s to 0.94s respectively. Based on averaged shear wave velocities from all borehole measurements, the calculated site period was 0.82s.

As the Matemateaonga Formation is understood to be deeper than 136m bgl, the site period is therefore expected to be greater than the above. Given that the calculated site period exceeds 0.6s, it can be concluded that the site subsoil class should be Class D.

6 CONCLUSIONS

The above study concludes that based on a strict interpretation of NZS 1170.5 (2004) for the area tested, the site should have a subsoil class of Class D. This conclusion hinges on whether the Matemateaonga Formation should be classed as a rock. On the basis of its low strength (< 1MPa in many instances) and soil inter-layering, this Formation falls outside of the interpretation of rock as provided by NZS 1170.5 (2004). In addition, calculated site periods from measured shear wave velocities exceed the 0.6s threshold which defines the site subsoil class as Class D.

This conclusion has implications for other areas in New Zealand which are underlain by weak and variably cemented rock. It is, perhaps, timely that the current formal definition of rock for site subsoil class determination is debated and a revised set of criteria developed.

7 ACKNOWLEDGEMENTS

The authors would like to thank Peter Scantlebury (NPDC) for approval to prepare this paper and Mike Stannard and Adrian Bennett (MBIE Building System Performance Branch) for supporting this project by funding the shear wave testing work.

REFERENCES

Larkin, T. and Van Houtte, C. (2014) *Determination of Site Period for NZS 1170.5:2004*. Bulletin of the New Zealand Society for Earthquake Engineering, 47(1): 28-40.

Madera, G.A. (1971) *Fundamental period and amplification of peak acceleration in layered systems*. Research Report R70-37, Department of Civil Engineering, MIT, Cambridge, Massachusetts.

NZS 1170.5 (2004) *New Zealand Standard 1170.5: Structural Design Actions. Part 5: Earthquake Actions – New Zealand*. Standards New Zealand, Wellington, 88pp.

Townsend, D., Vonk, A., Kamp, P.J.J. (compilers) 2008: *Geology of the Taranaki Area: scale 1:250,000*. Lower Hutt: GNS Science. Institute of Geological & Nuclear Sciences 1:250,000 geological map 7. 77 p. + 1 folded map. New Zealand.